PROCEEDINGS OF EIGHTH CONFERENCE

ON

COASTAL ENGINEERING

MEXICO CITY, MEXICO

NOVEMBER 1962

Edited by

J W JOHNSON

Professor of Hydraulic Engineering

UNIVERSITY OF CALIFORNIA

BERKELEY

PUBLISHED BY

COUNCIL ON WAVE RESEARCH

THE ENGINEERING FOUNDATION

1963

COUNCIL ON WAVE RESEARCH
Building 159
Richmond Field Station
University of California
Richmond, California

Lithographed in the United States of America

ACKNOWLEDGMENTS

This conference was sponsored jointly by the Council on Wave Research, Berkeley, California, and the Instituto Politecnico Nacional and the Secretaria de Marina of Mexico Appreciation is expressed to the Secretaria de Marina for aerial photographs supplied to illustrate the cover and section title pages of this publication

The following engineers from Mexico served as the organizing committee for the conference.

Presidente Honorario·	Ing Eugenio Mendez
Presidente·	Ing Armando Aguilera Dorantes
Secretario General·	Ing Rafael Vazquez de la Cerda
Vice Presidentes	Ing Roberto Bustamante Ahumada Ing Roberto Vera Strathman Ing Jose Rodriguez Cabo
Vocal Ejecutivo·	Ing Humberto Cos Maldonado
Vocal Secretario.	Ing Carlos Cuevas Inostrosa
Comision de Asuntos Tecnicos.	Ing Pablo Bistrain Ing Daniel Cervantes Castro
Segundo Vocal de Coordinacion	Ing Ruben Flores Garcia
Vocal Tesorero·	Sr Hector M Paz Puglia
Primer Vocal de Relaciones:	Dr Juan Manuel Ortiz de Zarate
Segundo Vocal de Relaciones·	Ing Luis Gonzalez Leon
Vocal de Coordinacion	Sr Francisco Jose Berzunza Valdez

CONTENTS

CONTENTS

CONTENTS

CONTENTS

CONTENTS

INTRODUCTION

REMARKS AT THE OPENING SESSION OF THE EIGHTH INTERNATIONAL CONFERENCE ON COASTAL ENGINEERING, I

Admiral C. G. Manuel Zermaño Araico
Secretario de Marina
Mexico

It is with deep satisfaction that I am privileged to extend a cordial welcome to all attending this Eighth International Conference on Coastal Engineering. The first Conference was held in California in 1950; at the last, which took place in the Hague in 1960, it was agreed that Mexico be given the Chair for the Conference which opens today. For Mexico, a country with extended coastlines, it is deeply significant that this Conference is being held in its territory. The world's greatest scientists in the field are represented here. For this reason, the Ministries of Education and of the Navy, through the Instituto Politecnico Nacional and the Secretaria de Marina, respectively, are honored in sponsoring the Conference, and are certain that results obtained here will highly favor the rapid development of this fundamental branch of Engineering.

Twenty-seven countries, including Mexico, are represented at this Conference. As at previous meetings, discussion will include all aspects of Maritime Engineering: winds, hurricanes, tides and surges, currents, conveyance and sediments, formation and erosion of coasts, protection works, sea walls, construction and maintenance of harbors, as well as technical instruments and scientific methods used in investigations in this field. The theoretical problems embodied in the construction of a port, including maintenance, conditions for navigation and efficient operation are also to be discussed.

Engineering has as its goal the solving of problems created by Nature to the ultimate benefit of humanity. As far back as 1828, we find this concept in the definition registered in the Charter of England's Institution of Civil Engineers, where it is expressed that "Engineering is the art of directing Nature's forces for man's use and convenience." This definition has its utmost meaning in Maritime Engineering. We all know of the fabulous potential of phenomena arising at sea, and of the sea's incalculable nutritive wealth and resources. If this potential could be made to benefit man, his basic needs might be fulfilled: man, merely from the fact of his human condition, deserves to enjoy a more dignified and just life.

Maritime Engineering, of all the branches of civil engineering, offers and deserves a high scientific ranking due to the complex problems that the water element presents in its application. The solution of these problems demands highly specialized personnel, thoroughly trained in the diverse technical aspects involved in the execution of these works under hostile conditions. Therefore, these Conferences are of relevant significance inasmuch as they bring together men of science, men who by constant study and effort have dedicated their lives to their profession, in the basic task of cooperating to build a better world so that humanity may advance a step further in its present struggle to benefit from an integral and rational utilization of the ocean's resources.

All cultural gains achieved by man in his thousands of years of uninterrupted activity should be under his exclusive command. This view was expressed by the President of Mexico, Licenciado Adolfo López Mateos, in his speech delivered at Manila on October 22, 1962, upon being bestowed an Honoris Causa Doctorate by the University of the Philippines: "The greater the danger that unrestrained science ignores the values of ethics, the greater our effort should be to limit it to the service of humanity itself. It is not a matter of undermining its progress; on the contrary, it is a matter of harmonzing scientific improvements to a level parallel to man who today, as before, should be the measure of science."

This principle has invariable validity since man, as a thinker and performer, is a being created only once within a determined length of time and space and he should not remain at the edge of or behind his works. Should this happen, he would be an unconscious automaton, falling fatally under the command of the machine. Human endeavor is always governed by the intensity of our thought and our good will, making man the actor and the author of his own history. Consequently, if man determines to serve humanity, his acts will be manifested as commendable and unselfish. Opposed to this are those who pretend to use technical and scientific achievements to subjugate and oppress mankind. These people find destruction the only means of culminating their adverse ambitions, thereby placing humanity in the grave danger of remaining in the middle of its life path or exposed to total destruction.

This scientific knowledge, anti-dogmatic by nature, should be outside the struggle of ideologies and should project itself against sectarian passions, in order that its benefits protect all men. Every new discovery should be made known beyond all national frontiers, in order to speed progress and to safeguard the future of the human species. Priority should be given to the basic problems encountered, not to utopian schemes that bring about the loss of resources and lives, occurring when the stability of the established international order is

violated.

In the present day and age we cannot afford to divert and waste the creative efforts of science in inventing and manufacturing elements detrimental to man. It is more imperative to employ the considerable econom ic resources that are spent on such endeavors in raising standards of living and hastening social development. All the countries of the world should unite in their efforts to fight against such common enemies as unhealthy environment, ignorance and misery, traditional calamities of humanity. All creative genius and human effort should be directed to win these battles and not those which result in the destruction of man, by his own hand or by the machines he has built in the legitimate aspiration of progress.

Furthermore, in spite of the amazing scientific developments of the present era, we must consider that there is much more in store for us in the future. We can practically foresee man's conquest of other planets, after he has penetrated the mysteries of all substance and the disintegration of its elements. There are still unexplored regions in our planet, not only on the earth, but in the depths of the ocean. These mysteries are a permanent challenge to the scientist faced with the task of unveiling them, in order to obtain the benefits that are necessary to safeguard a better future and to insure happiness to all men on earth.

As specifically regards this Congress, it is appropriate to point out that we are concerned with learning more about the ocean that surrounds us and that greatly influences us because of its capital importance If we consider that everything in life is oscillatory, as the earth moves in its orbit within the planetary system, we must conclude that there are other earthly and cosmic phenomena that are beyond our control. Consequently, at best we can only aspire, through technical and scientific knowledge, to properly direct these phenomena from being detrimental toward production of benefits that effect the destiny of mankind.

Because of the elevated aims of the outstanding personalities that participate in them, the events at this Congress enrich the scientific and cultural level of all men, without discrimination of origin or political affiliation and irrespective of the boundaries or coastline of the countries to which they belong. Because the destiny of humanity is the same for all it should be a common purpose to control the fury of the elements that may destroy instead of benefiting mankind. To this end, we must take ad vantage of technical and scientific improvements, as well as the instruments of universal culture, which constitute the richest inheritance accumulated by man in his historical encounters.

The conquest of the ocean may be an efficient vehicle to strengthei

the ties of solidarity of which all men should be a part. Besides being the most important source of food storage and inexhaustible source of energy available at the present time, the ocean is actually a symbolic bridge that unites the various regions of the globe. Its total and proper use could very well end exploitation of man, by himself and by his own subjugation to any foreign power, be it political or economical.

Mexico welcomes you most heartily. Our country has an inviolable vocation for freedom, democracy and social justice. The spiritual image that has configurated the course of its history remains unalterable and we take pride in having the Constitution of the Republic as our most perfect social product. During the Administration of President López Mateos this important instrument has become the basic policy of national harmony and a useful element in human survival, for it postulates peace and universal harmony, as well as auto-determination and non-intervention in the internal affairs of other states.

We have much to learn from you about the integral realization of the Maritime Development Program of President Mateos, whose program aims to take wise advantage of the resources available from this country's ten thousand kilometers of coastline, representing 71% of its perimeter. This figure also represents an equivalent proportion of the extension of the oceans and the earth underneath, inasmuch as the vast water spaces occupy approximately 73% of the surface of the total world. This gives us an exact and clear idea of the potentialities of Mexico in this respect.

Despite the fact that the basic pillars of the National Maritime Development Program have been established, there are still greater goals to be reached, particularly the development of the Mexican Merchant Marine and the harbor works that are planned. These goals depend greatly on the general progress of the country and, consequently, on the appropriations invested in these projects according to the increase observed in economic activities.

In addition to the reasons stated above, we consider the realization of this VIII Conference on Coastal Engineering of great importance to the whole world, and most particularly to Mexico, because of the invaluable opportunity we have to learn from it. It gives us the opportunity to participate with our maritime resources in the solution of the problems of humanity. As we welcome you fraternally and firmly assure you of the success of this Conference, we wish to take this opportunity to sincerely congratulate you for your generous efforts in contributing your knowledge to the supreme aims of man. We extend our best wishes for your personal welfare and happiness.

Mexico City, November 5, 1962

REMARKS AT THE OPENING SESSION OF THE EIGHTH INTERNATIONAL CONFERENCE ON COASTAL ENGINEERING, II

Morrough P. O'Brien
Professor of Engineering Emeritus
University of California
Berkeley

The Council on Wave Research was pleased and honored by the invitation of the Secretaria de Marina to hold this VIIIth International Congress on Coastal Engineering in Mexico City. We look forward to a program of interesting and instructive papers and to a week of sight-seeing and entertainment in this beautiful and exciting city.

For the information of those attending their first Congress on Coastal Engineering, I should explain briefly the functions and organization of the Council on Wave Research. The first of these Congresses was held in Long Beach, California, in 1950 under the auspices of the University of California. There was at that time no permanent organization with the responsibility for focusing attention on this area of scientific and technical work or for arranging subsequent meetings. At the suggestion of the late Professor Boris A. Bakhmeteff, the Engineering Foundation, an agency of the American engineering societies, formed the Council on Wave Research to promote research in the sciences related to coastal engineering and to hold occasional congresses and conferences for the purpose of making the results of both scientific research and professional experience available to practicing engineers. The proceedings of these congresses are published and are available from the Secretary.

Coastal Engineering is a specialized and relatively minor branch of the engineering profession, if judged in terms of the number of engineers and scientists involved or in terms of annual expenditures for construction. However, the importance of the shore areas to recreation and to commerce is already considerable and is growing steadily. Industrial societies generate an intense concentration of population in the metropolitan centers and these city-dwellers must have relief at times from the crowding and the pressures which such living entails. Of all forms of recreation possible, the combination of activities which the seashore affords seems to have the most universal appeal - and these opportunities can be made available to people of all classes at relatively small expense in proportion to the numbers served. This situation has caused increasing attention

to the preservation and the improvement of coastal areas for recreational use. In the United States, the Congress recognized the need for special attention to the problems of the shoreline, established the Beach Erosion Board to carry on research and to promote cooperation between the Federal government and local governments in studies and works intended to preserve the shoreline "for the healthful recreation of the people."

Coastal engineering is a branch of the profession in which judgment based on experience plays a major role. Admittedly, there has been an advance in our quantitative understanding of the forces controlling shoreline phenomena, and this Congress represents an advance in this respect; however, after the scientific and technical principles have been applied to each particular shoreline problem, there always remains an element of uncertainty to which judgment must be applied. An engineer develops judgment in part through his own observation and experience but he must also add vicariously to his basis for judgment through studying the experiences of others. To this end, the proceedings of these Congresses have included a number of "case histories" of coastal engineering projects, usually dealing with the engineering work in the geographical area in which the meeting is held. We look forward to the meetings of this Congress for a view of the coastal phenomena and particular projects of Mexico.

There is one peculiarity of coastal engineering which I should emphasize. Laymen - and many engineers without experience in the field - are more prone to theorize about, and hold strong opinions about, local coastal problems and their cure than about any other branch of engineering with which I am acquainted. Engineers experienced in construction on land tend to underestimate the tremendous and relentless capacity of the sea to crush, undermine, corrode, or otherwise destroy man-made structures - and they tend to minimize the cumulative effect of slow gradual change induced by relatively minor works constructed at the shoreline. The coastal engineer himself must be conservative in applying theoretical results or experience elsewhere to specific local problems. The antidote for this common malady is knowledge and experience - and a proper respect for the power of the sea.

A final comment - not directly related to the work of this Congress but one possibly appropriate from an engineer who has spent his professional life in a rapidly expanding section of the United States - is that Mexico impresses me as being on the verge of a rapid industrial activity. I am a newcomer to your country and do not presume to have detailed knowledge but I have seen enough to be convinced that Mexico has built - and is building - the essential solid base in power, trans-

portation, irrigation, water supply, communications, and all the elements of the infrastructure of an industrial society - and in the important related area of higher education - for an upsurge of productive activity which will yield in the decades immediately ahead a substantial increase in the prosperity of your people and your country. It is exciting and inspiring for an engineer to watch this stage of a nation's growth - one in which engineering works play so fundamental a role.

We are grateful to many individuals - the members of the organizing committee, the authors of the papers, and many others who have made this Congress possible. We are honored that the President of the Republic, Adolfo Lopez Mateos, is participating at this opening session. We are deeply grateful to you, sir, for the opportunity to hold this Congress in your beautiful country.

TAMPICO

PART 1
THEORETICAL AND OBSERVED BASIC OCEANOGRAPHIC DATA

TUXPAN

CHAPTER 1

APPROXIMATE ESTIMATIONS OF CORRELATION COEFFICIENT BETWEEN WAVE HEIGHT AND PERIOD OF SHALLOW WATER WIND WAVES

Takeshi Ijima
Chief Research Engineer
Harbor Technics Research Institute
Ministry of Transportation, Yokosuka, Japan

INTRODUCTION

From the fact that the marginal frequency distributions for wave height and period of complex sea waves both follow the Rayleigh type distribution and approximately exists a linear relationship between wave height and period, Bretschneider(1959) derived wave height and energy spectra of wave period, introducing the summation function of wave height. Then he estimated the correlation coefficient r between height and period of waves as a function of non-dimensional fetch f ($= g\bar{F}/U^2$). However, his estimation seems not theoretical but empirical, being derived mainly from qulitative considerations and observed data. In this paper, the author tries to derive theoretically the equation for r as a function of f, assuming the classical energy equation for significant wave is applicable to the individual wave in complex sea. Moreover, extending the same method, he intends to estimate the coefficient for shallow water waves as a function of f and non-dimensional depth d ($= gD/U^2$).

As the results, coefficient r for deep water waves consists fairly well with that of Bretschneider and comparing with the author's observed data, the one for shallow water waves seems to be resonable.

DERIVATION OF CORRELATION COEFFICIENT FOR DEEP WATER WAVES

After Bretschneider, the marginal frequency distributions for both wave height and period of complex sea follow the Rayleigh type distribution and in terms of correlation coefficient r between them, the energy spectra (H^2 spectra) of period T is given as follows:

$$S_{H^2}(T) = \frac{4a^2(\bar{H})^2\left[1-r+ar\left(\frac{T}{\bar{T}}\right)^2\right]^2}{1+\left(\frac{4}{\pi}-1\right)r^2}\cdot\frac{T^3}{(\bar{T})^4}\cdot e^{-\frac{\pi a^2}{4}\left(\frac{T}{\bar{T}}\right)^4} \qquad (1)$$

where $a = 0.927$, H and T are height and period of individual wave, and $\bar{H}$ and $\bar{T}$ are mean height and period of successive waves in any observation period (usually in twenty minutes). Integration of (1) with T from zero to infinity gives mean square wave height proportional to the potential energy of waves.

$$\int_0^\infty S_{H^2}(T)\,dT = \overline{H^2} = \frac{4}{\pi}(\bar{H})^2 \qquad (2)$$

(1) is available for both deep and shallow water waves, and significant wave height $H_{1/3}$ and period $T_{1/3}$ are related to mean height H and period $\bar{T}$, respectivelly, through r as follows:

$$H_{1/3} = 1.60\,\bar{H}, \qquad T_{1/3} = \bar{T}\sqrt{1+0.60\gamma} \tag{3}$$

After Bretschneider's fetch graph(1958) for deep water waves, significant wave height and period are approximately expressed by the following equations in terms of non-dimensional fetch f in the range of $1 < f < 2\times10^4$.

$$\frac{gH_{1/3}}{U^2} = 0.0040\left(\frac{gF}{U^2}\right)^{0.40} \tag{4}$$

$$\frac{gT_{1/3}}{2\pi U} = 0.085\left(\frac{gF}{U^2}\right)^{0.26} \tag{5}$$

where U is wind velocity, g the acceleration of gravity, F the fetch length. Therefore, when the coefficient r is given by f, wave spectra for deep water waves are fully determined by (1) in terms of f through (3) (4) and (5).

As for r, Bretschneider assumed as follows:
(i) $r = 0$ for the upper limit of f,
(ii) $r = 1.0$ for the lower limit of f,
(iii) r decreases gradually from the lower limit to the upper limit of f,
And moreover, from observed data of r for $f = 10^2 \sim 10^3$, he empirically estimated r as a function of f. His estimations are, however, not yet ultimately determined but to be revised by the future accumulation of observed data.

The author tries to estimate the coefficient r using the energy equation and the relationships (4) and (5) in the region of $1 < f < 10^4$ in which wave velocity is smaller than wind velocity.

In the case of significant wave, the transmitted wave energy P is equal to $\frac{E}{2}C$, where E is the total energy per wave length as given by $\frac{1}{8}\rho g H^2$ and C is wave velocity. In steady state, the space rate of change of P is equal to the supplied energy R_T plus R_N from wind to waves, where R_T and R_N are amount of energy supplied by tangential and normal stresses of wind, respectively. Accordingly, the energy equation becomes

$$\frac{dP}{dF} = R_T + R_N \tag{6}$$

where $P = \frac{\rho g^2}{32\pi}H^2T$, and after Sverdrup and Munk (1947),

$$R_T = E\cdot A\cdot g\cdot\left(\frac{C}{U}\right)^{-3}\cdot\frac{1}{U} = E\,A\,g\,\frac{U^2}{C^3} \tag{7}$$

$$R_N = E\cdot A\cdot g\,\frac{U^2}{C^3}\cdot\alpha\cdot\left(1+\frac{C}{U}\right)^2 \tag{8}$$

where $E = \frac{1}{8}\rho g H^2$, $A = 2\gamma^2\frac{\rho'}{\rho}$, $\alpha = \frac{S}{2\gamma^2}$, and ρ, ρ' are densities of water

and air, γ^2 the friction coefficient of wind over sea surface, and s the sheltering coefficient after Jeffreys. Sverdrup and Munk suggested $A \fallingdotseq 6.5 \times 10^{-6}$ and $\alpha = 2.5$.

(6) (7) and (8) are available to the significant wave and now we assume that they are also applicable to the individual wave. Thus from (6), taking the averages for all the successive waves in any time interval, we obtain

$$\overline{\left[\frac{dP}{dF}\right]} = \overline{R}_T + \overline{R}_N \tag{9}$$

where $\overline{\left[\frac{dP}{dF}\right]}$ is replaced by $\frac{d\overline{P}}{dF}$.

Using (1), $\overline{P}$ is written as follows:

$$\begin{aligned}\overline{P} &= \frac{\rho g^2}{32\pi}\overline{H^2 T} = \frac{\rho g^2}{32\pi}\int_0^\infty S_{H^2}(T)\cdot T\cdot dT \\ &= \frac{\rho g^2}{32\pi}\frac{4\alpha^2(\overline{H}\chi\overline{T})}{1+(\frac{4}{\pi}-1)\gamma^2}\int_0^\infty (1-\gamma+a\gamma\zeta^2)^2\zeta^4 e^{-\frac{\pi a^2}{4}\zeta^4} d\zeta \\ &= \frac{\rho g^2}{8\pi^2}\cdot\frac{1+0.2899\gamma+0.3039\gamma^2}{1+0.273\gamma^2}\cdot(\overline{H})^2\cdot\overline{T}\end{aligned} \tag{10}$$

Now putting

$$h = \frac{g\overline{H}}{U^2}\ , \qquad t = \frac{g\overline{T}}{2\pi U}\ , \qquad f = \frac{gF}{U^2} \tag{11}$$

then

$$\frac{d\overline{P}}{dF} = \frac{g}{U^2}\cdot\frac{d\overline{P}}{df}\ , \qquad (\overline{H})^2\overline{T} = \frac{2\pi U^5}{g^3}\cdot h^2 t \tag{12}$$

and from (3) (4) and (5),

$$h = 0.0025\, f^{0.40}\ , \qquad t = \frac{0.085}{\sqrt{1+0.60\gamma}}\, f^{0.26} \tag{13}$$

Hence

$$\frac{d\overline{P}}{dF} = 53.12\,\frac{d}{df}\left[(1-0.0125\gamma+0.0791\gamma^2)\cdot f^{1.06}\right]\frac{\rho U^3}{4\pi}\times 10^{-8} \tag{14}$$

On the other hand, from (7) and (8),

$$\overline{R}_T = \frac{\pi^3\alpha\rho A U^2}{g}\cdot\overline{\left[\frac{H^2}{T^3}\right]} \tag{15}$$

$$\overline{R_N} = \frac{\pi^3 \alpha \rho A U^2}{g} \left\{ \left[\frac{\overline{H^2}}{T^3} \right] - \frac{g}{\pi U} \left[\frac{\overline{H^2}}{T^2} \right] + \frac{g^2}{4\pi^2 U^2} \left[\frac{\overline{H^2}}{T} \right] \right\}$$

Similar to $\frac{d\bar{P}}{dt}$, $\overline{R_T}$ and $\overline{R_N}$ are written in terms of f and r as follows:

$$\overline{R_T} \fallingdotseq 0.437 A (1 - 0.337\gamma - 0.707\gamma^2) \cdot f^{0.02} \cdot \rho U^3 \times 10^{-2} \tag{16}$$

$$\overline{R_N} = \alpha A \left\{ 0.437 (1 - 0.337\gamma) f^{0.02} \times 10^{-2} - 0.394 (1 - 0.127\gamma) f^{0.28} \times 10^{-3} + 0.125 (1 - 0.029\gamma) f^{0.54} \times 10^{-4} \right\} \cdot \rho U^3 \tag{17}$$

Neglecting higher order terms than γ^2 and substituting (9) with (14) (16) and (17), the energy equation is obtained in terms of r and f as follows:

$$\frac{d}{df} \left\{ (1 - 0.012\gamma) f^{1.06} \right\} = 0.103 A (1 + \alpha)(1 - 0.337\gamma) f^{0.02} - 0.00947 A \cdot \alpha (1 - 0.127\gamma) f^{0.28} \times 10^{5} + 0.00031 A \alpha (1 - 0.029\gamma) f^{0.54} \times 10^{4} \tag{18}$$

or putting $A' = A \times 10^6$, $A'(1+\alpha) = m$ and $A'\alpha = n$, (18) becomes

$$\frac{d}{df} \left\{ (1 - 0.012\gamma) f^{1.06} \right\} = 0.103 m (1 - 0.337\gamma) f^{0.02} - 0.00947 n (1 - 0.127\gamma) f^{0.28} + 0.00031 n (1 - 0.029\gamma) f^{0.54} \tag{18'}$$

where the third term in the right hand side is neglisibly smaller than the second term in the region of f considered, and also 0.012r in the left hand side is small compared with 1. Hence, to the first order approximation, (18') becomes

$$1.06 f^{0.04} = 0.103 m (1 - 0.337\gamma) - 0.00947 n (1 - 0.127\gamma) f^{0.26} \tag{19}$$

from which r is obtained as follows:

$$\gamma = \frac{10.3 m - 0.947 f^{0.26} - 106 f^{0.04}}{34.7 m - 0.120 n f^{0.26}} \tag{20}$$

Thus for $m > 0$, $n > 0$, r is a steadily decreasing function of f.

When $A' = 6.5$, $\alpha = 2.5$, that is, $m = 22.8$, $n = 16.2$, $|r|$ becomes greater than 1.0, which is clearly unreasonable. Therefore, m and n should be selected reasonably.

According to Bretschneider's estimation, r is nearly equal to 0.9 for $f = 1$. Taking this condition into (20), m and n are related by the next equation.

$$m = 0.117\,n + 14.76 \tag{21}$$

And for $n = 0$, 1, and 2, r are calculated from (21) and (20), of which the results are shown in Figure 1.

From the figure, it is found that Bretschneider's estimation is the best fit for $n = 0$. When n is zero, m becomes 14.76 and $A' = 14.76$, $\alpha = 0$, which means that supply of energy from wind to waves is mainly done by tangential stress and the friction coefficient γ^2 becomes twice the one given by Munk. Such a result is somewhat different from actual phenomena, but its tendency is near to the facts that the sheltering coefficient may be much smaller than the one proposed by Jeffreys and also γ^2 may become appreciably larger than 0.0026 in some cases.

Accordingly, taking $m = 14.76$, $n = 0$, the first order approximation of r becomes

$$r = 2.97 - 2.07\, f^{0.04} \tag{22}$$

And the second order approximation is obtained from (18') as follows:

$$r = 2.97 - 2.00\, f^{0.04} - 0.053\, f^{0.08} \tag{23}$$

which consists fairly well with Bretschneider's estimation in the range of $1 < f < 10^4$. Therefore, it might be not so unreasonable to assume that the energy equation for significant wave is applicable to the individual wave and in the range of f considered the energy supply by normal stress of wind may be possibly neglected for our estimation.

ESTIMATIONS OF CORRELATION COEFFICIENT FOR SHALLOW WATER WAVES

As previously described in deep water, the correlation coefficient r gradually decreases from 1.0 to 0 with increasing f, that is, with the developement of waves. While, in shallow water, Bretschneider suggested that by the effect of bottom friction the coefficient r decreases more remarkably and possibly tends to negative, that is, r variates from + 1.0 to — 1.0 with increasing f and decreasing d (non-dimensional water depth as given by gD/U^2, where D is water depth). From the assumption of Rayleigh distribution for wave height and period, however, r cannot tend to — 1.0 but get to about $-0.6 \sim -0.7$ as its minimum limiting value. (Bretschneider did not show this limiting value.)

Following to the above descriptions, we assume for r in shallow water wind waves as follows:

(i) r decreases with the developement of waves,

(ii) r becomes possibly negative but cannot get to smaller than — 0.7.

DEVELOPEMENT OF SHALLOW WATER WIND WAVES

Now consider the case of constant water depth D. The shallow water significant wave height H_S, period T_S, fetch length F, and water depth D are expressed non-dimensionally as follows:

$$h_S = \frac{gH_S}{U^2}, \quad t_S = \frac{gT_S}{2\pi U}, \quad f = \frac{gF}{U^2}, \quad d = \frac{gD}{U^2} \tag{24}$$

Bretschneider has shown the relations of h_S, f and d from his observations and calculations of wave height change by bottom friction, of which the result is shown in Figure 15C on Page 28d of Technical Report No.4 entitled " Shore Protection Planning and Design ", issued from Beach Erosion Board. Figure 2 in this paper is made from that Figure 15C, excepting the curves for t_S v.s. f.

It is seen from Figure 2 that for any fixed d, h_S increases with f initially along the same curve as for deep water waves and from certain point of f (say f_t) it begins to deviate and at the other point of f (say f_u) attains a steady constant state. The value of h_S at point f_t (say h_t) is expressed from the Figure 15C of Bretschneider as follows:

$$h_t = 0.0840\, d^{0.72} \tag{25}$$

On the other hand, h_t is the same for deep water waves at f_t. Thus from (4), f_t is given as follows:

$$f_t = 2.020\, d^{1.8} \tag{26}$$

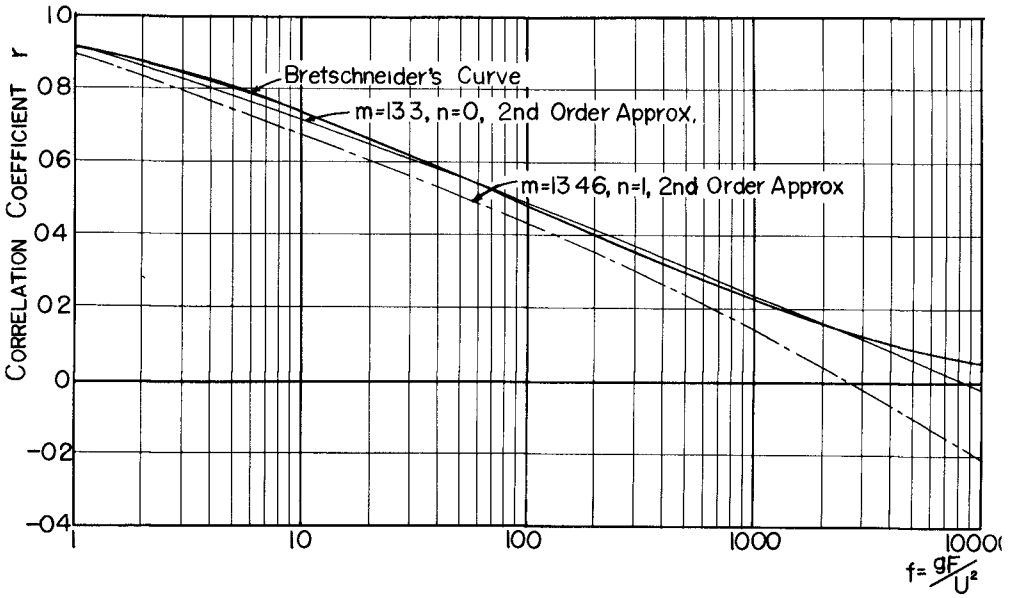

Fig. 1. Relation between correlation coefficient and non-dimensional fetch for deep water waves.

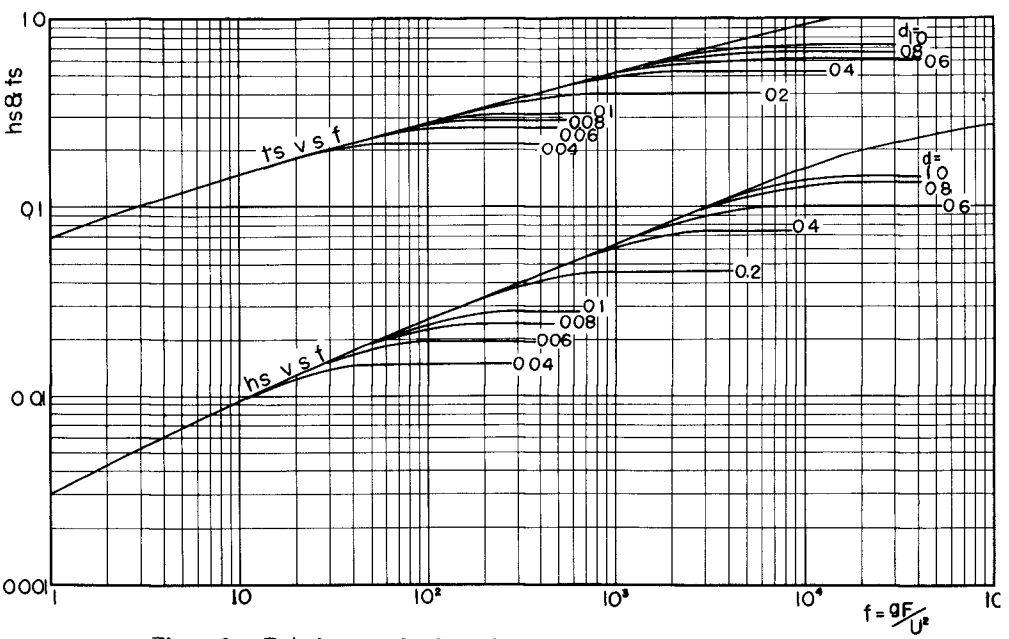

Fig. 2. Fetch graph for deep and shallow water waves.

Similarly the value of h_s at point f_u (say h_u) is obtained from that Bretschneider's Figure.

$$h_u = 0.143\, d^{0.72} \tag{27}$$

and

$$f_u = 14940\, d^{1.8} \tag{28}$$

As for wave period, Bretschneider gave no curve. Hence we derive the relation of t_s and f from the following considerations.

Similar to wave height h_s, there must be f_t , bellow which t_s is the same as that of deep water waves, and f_u, above which t_s becomes steadily constant, and also f_t and f_u are the same as those for wave height h_s. That is, both wave height and period begin to deviate from the curves of deep water waves at point f_t and get to constant at f_u.

The value of t_s at point f_t (say t_t) is obtained by substituting (5) with (26).

$$t_t = 0.615\, d^{0.468} \tag{29}$$

Theoretically, the effect of bottom friction begins to appear when wave length becomes twice the water depth. The value of t_s satisfying this condition (say $t_{t'}$) is

$$t_{t'} = \left(\frac{d}{\pi}\right)^{0.5} = 0.564\, d^{0.5} \tag{30}$$

From (5), the corresponding f (say $f_{t'}$) is

$$f_{t'} = 1445\, d^{1.92} \tag{31}$$

Hence, in the region of $0 < d < 10$, $t_{t'}$ is smaller than t_t and theoretically the effect of friction appears even when $f < f_t$.

After Bretschneider(1960), significant wave period T_S is not too critical and it is conveniently represented by wave height H_S as follows:

$$T_S = 3.86\sqrt{H_S} \tag{32}$$

where T_S is in seconds, H_S in meters. Assuming that this relationship is applicable to the region of $f > f_u$,

$$t_u = 1.924\, h_u^{0.50} \tag{33}$$

or from (27) $$t_u = 0.728\, d^{0.36} \tag{34}$$

Thus period t_s at f_f and f_u are given by (29) and (34).

Accordingly, it is easy for us to draw smooth curves of t_s v.s. f on the fetch graph, which are tangent to those of deep water waves at f_t and asymptotically tend to the constant value at f_u. Figure 2 is thus obtained.

ENERGY EQUATION FOR SHALLOW WATER WIND WAVES

For the steady state of shallow water wind waves being affected by bottom friction, the energy equation becomes as follows corresponding to (9).

$$\frac{d\overline{P}}{dF} = \overline{R_T} + \overline{R_N} - \overline{D_f} \tag{35}$$

where $\overline{D_f}$ is the loss of energy by bottom friction, averaged for successive waves in any observed period.

The transmitted wave energy P is as follows:

$$P = \frac{\rho g^2 H^2 T}{32\pi} \cdot \tanh\frac{2\pi D}{L}\left(1 + \frac{\frac{4\pi D}{L}}{\sinh\frac{4\pi D}{L}}\right) \tag{36}$$

where D is water depth and L is wave length.

Putting

$$F_1 = \frac{1}{2}\tanh\frac{2\pi D}{L}\left(1 + \frac{\frac{4\pi D}{L}}{\sinh\frac{4\pi D}{L}}\right) \tag{37}$$

then F_1 is a function of D/L_o. (L_o is the deep water wave length of period T as given $gT^2/2\pi$.)

Putting $\bar{h} = g\bar{H}/U^2$, and $\bar{t} = g\bar{T}/2\pi U$, from (36) and (37),

$$\overline{P} = \frac{\rho g^2}{16\pi}\left[\overline{H^2 T \cdot F_1\left(\frac{2\pi D}{gT^2}\right)}\right] = \frac{\rho g^2}{16\pi}\int_0^\infty S_{H^2}(T)\cdot T\, F_1\left(\frac{2\pi D}{gT^2}\right) dT$$

$$= \frac{\rho g^2}{16\pi}\,\frac{3.434}{1+0.273\gamma^2}(\bar{H})^2\bar{T}\int_0^\infty (1+\gamma+0.927\gamma\tau^2)^2\tau^4 e^{-0.695\tau^4} F_1\left(\frac{2\pi D}{gT^2}\,\frac{1}{\tau^2}\right) d\tau$$

$$= \frac{\rho U^5}{8g}\cdot\frac{3.434}{1+0.273\gamma^2}(\bar{h})^2\bar{t}\int_0^\infty (1-\gamma+0.927\gamma\tau^2)^2\tau^4 e^{-0.695\tau^4} F_1\left(\frac{d}{2\pi(\bar{t})^2}\,\frac{1}{\tau^2}\right) d\tau \tag{38}$$

Thus

$$\frac{d\overline{P}}{dF} = \frac{3.434\rho U^3}{8}\,\frac{d}{df}\left\{\frac{(\bar{h})^2\cdot\bar{t}}{1+0.273\gamma^2}\int_0^\infty (1-\gamma+0.927\gamma\tau^2)^2\tau^4 e^{-0.695\tau^4} F_1\left(\frac{d}{2\pi(\bar{t})^2}\cdot\frac{1}{\tau^2}\right) d\tau\right\} \tag{39}$$

From (3), $\bar{h} = hs/1.6$, $\bar{t} = ts/\sqrt{1+0.6r}$, and (39) is written as

$$\frac{d\bar{P}}{dF} = 0.1677 \frac{d}{df}\left\{(1-0.30\gamma-0.138\gamma^2)\, h_s^2\, t_s\, A\left(\frac{d}{2\pi(\bar{t})^2}, \gamma\right)\right\} \rho U^3 \qquad (40)$$

where

$$A\left(\frac{d}{2\pi(\bar{t})^2}, \gamma\right) = \int_0^\infty (1-\gamma+0.927\gamma\tau^2)^2 \tau^4 e^{-0.675\tau^4} F_1\left(\frac{d}{2\pi(\bar{t})^2}\cdot\frac{1}{\tau^2}\right) d\tau \qquad (41)$$

$\bar{R}_T$ and $\bar{R}_N$ are energy supplied from wind by tangential and normal stresses, and similar to the case of deep water waves, $\bar{R}_N$ is considered to be neglisible to $\bar{R}_T$. As for R_T in shallow water waves, Kishi(1955) proposed the next equation for significant wave.

$$R_T = E\, A_S\, f\left(\frac{U^2}{C^3}\right) \frac{1}{2}\left[1 + \left(\tanh\frac{2\pi D}{L}\right)^2\right]$$

$$= \frac{\pi^3 A_S}{2g} \rho U^2 \frac{H^2}{T^3}\left[\coth\frac{2\pi D}{L} + \left(\coth\frac{2\pi D}{L}\right)^3\right] \qquad (42)$$

where A_S corresponds to A for deep water waves, and its magnitude is considered to be in the order of $(10 \sim 20) \times 10^{-6}$.

Putting

$$F_2 = \coth\frac{2\pi D}{L} + \left(\coth\frac{2\pi D}{L}\right)^3 \qquad (43)$$

F_2 is also a function of D/L_0 $(= 2\pi D/gT^2)$.

From (42)

$$\bar{R}_T = \frac{\pi^3 A_S \rho U^3}{2g}\left[\frac{H^2}{T^3}\left(\coth\frac{2\pi D}{L} + \coth^3\frac{2\pi D}{L}\right)\right]$$

$$= \frac{\pi^3 A_S \rho U^3}{2g}\cdot\frac{3.434}{1+0.273\gamma^2}\cdot\frac{(\bar{H})^2}{(\bar{T})^3}\int_0^\infty (1-\gamma+0.927\gamma\tau^2)^2 e^{-0.675\tau^4} F_2\left(\frac{2\pi D}{g(\bar{T})^2}\cdot\frac{1}{\tau^2}\right) d\tau$$

$$= 0.0838\, A_S\,(1+0.90\gamma-0.138\gamma^2)\frac{h_s^2}{t_s^3}\cdot B\left(\frac{d}{2\pi(\bar{t})^2}, \gamma\right)\rho U^3 \qquad (44)$$

where

$$B\left(\frac{d}{2\pi(\bar{t})^2}, \gamma\right) = \int_0^\infty (1-\gamma+0.927\gamma\tau^2)^2 \cdot e^{-0.675\tau^4} F_2\left(\frac{d}{2\pi(\bar{t})^2}\frac{1}{\tau^2}\right) d\tau \qquad (45)$$

Loss of energy by bottom friction D_f is given after Putnum and Johnson(1949).

$$D_f = \frac{4}{3}\pi^2 \rho \cdot k \cdot \frac{H^3}{T^3\left(\sinh\frac{2\pi D}{L}\right)^3} \qquad (46)$$

where k is the coefficient of friction, which is about $0.01 \sim 0.02$ after Bretschneider. Assuming that (46) is still available to the individual wave, $\overline{D_f}$ becomes

$$\overline{D_f} = \frac{4}{3}\pi^2 \rho k \overline{\left[\frac{H^3}{T^3\left(\sinh\frac{2\pi D}{L}\right)^3}\right]} = \frac{4}{3}\pi^2 \rho k \int_0^\infty S_{H^3}(T) \frac{dT}{T^3\left(\sinh\frac{2\pi D}{L}\right)^3} \quad (47)$$

where $S_{H^3}(T)$ is the H^3 spectra of T, which shall be obtained using correlation coefficient r as follows:

$$S_{H^3}(T) = \frac{6a^2(\bar{H})^3\left[1-r+ar\left(\frac{T}{\bar{T}}\right)^2\right]^3}{1+\left(\frac{12}{\pi}-3\right)r^2+\left(2-\frac{6}{\pi}\right)r^3} \frac{T^3}{(\bar{T})^4} e^{-\frac{\pi a^2}{4}\left(\frac{T}{\bar{T}}\right)^4}$$

$$= \frac{5.156(\bar{H})^3\left[1-r+0.927\left(\frac{T}{\bar{T}}\right)^2\right]^3}{1+0.820r^2+0.090r^2} \frac{T^3}{(\bar{T})^4} e^{-0.675\left(\frac{T}{\bar{T}}\right)^4} \quad (48)$$

Hence, putting

$$F_3 = \frac{1}{\left(\sinh\frac{2\pi D}{L}\right)^3} \quad (49)$$

F_3 is also a function of D/L_0 $(= 2\pi D/gT^2)$.

Putting

$$\alpha' = \frac{4}{3}\pi^2 k = 13.15\,k \quad (50)$$

α' shall be in order of $0.1 \sim 0.2$.

From (47) and (48), $\overline{D_f}$ becomes as follows:

$$\overline{D_f} = \frac{5.156\,\alpha' \rho}{1+0.820r+0.090r^2} \frac{(\bar{H})^3}{(\bar{T})^3} \cdot \int_0^\infty (1-r+0.927r\tau^2)^3 e^{-0.675\tau^4} F_3\left(\frac{2\pi D}{g(\bar{T})^2\tau^2}\right) d\tau$$

$$= 0.005082\alpha'(1+0.90r-0.685r^2) \cdot \frac{h_s^3}{t_s^3} \cdot C\left(\frac{d}{2\pi(\bar{t})^2}, r\right) \cdot \rho U^3 \quad (51)$$

where

$$C\left(\frac{d}{2\pi(\bar{t})^2}, r\right) = \int_0^\infty (1+r+0.927r\tau^2)^3 e^{-0.675\tau^4} F_3\left(\frac{d}{2\pi(\bar{t})^2}\frac{1}{\tau^2}\right) d\tau \quad (52)$$

Hence, substituting (35) with (40) (44) and (51), putting $\overline{R_N} = 0$, and neglecting higher order terms than r^2, energy equation becomes

$$0.1677\frac{d}{df}\left\{(1-0.30\gamma)\,h_s^2\cdot t_s\cdot A\left(\frac{d}{2\pi(\bar{t})^2},\gamma\right)\right\}$$

$$=0.0838A_s(1+0.90\gamma)\frac{h_s^2}{t_s^3}B\left(\frac{d}{2\pi(\bar{t})^2},\gamma\right)-0.005082\alpha'(1+0.90\gamma)\frac{h_s^3}{t_s^3}C\left(\frac{d}{2\pi(\bar{t})^2},\gamma\right) \quad (53)$$

where A, B and C are functions of r, $\bar{t}$ and d, and expressed as polynomials of r as follows:

$$A\left(\frac{d}{2\pi(\bar{t})^2},\gamma\right)=a_0\left(\frac{d}{2\pi(\bar{t})^2}\right)+a_1\left(\frac{d}{2\pi(\bar{t})^2}\right)\gamma+a_2\left(\frac{d}{2\pi(\bar{t})^2}\right)\gamma^2$$

$$B\left(\frac{d}{2\pi(\bar{t})^2},\gamma\right)=b_0\left(\frac{d}{2\pi(\bar{t})^2}\right)+b_1\left(\frac{d}{2\pi(\bar{t})^2}\right)\gamma+b_2\left(\frac{d}{2\pi(\bar{t})^2}\right)\gamma^2 \quad (54)$$

$$C\left(\frac{d}{2\pi(\bar{t})^2},\gamma\right)=C_0\left(\frac{d}{2\pi(\bar{t})^2}\right)+C_1\left(\frac{d}{2\pi(\bar{t})^2}\right)\gamma+C_2\left(\frac{d}{2\pi(\bar{t})^2}\right)\gamma^2+C_3\left(\frac{d}{2\pi(\bar{t})^2}\right)\gamma^3$$

where a, b, c, etc. have the following form,

$$\int_0^\infty \tau^n F_m\left(\frac{d}{2\pi(\bar{t})^2}\cdot\frac{1}{\tau^2}\right)e^{-0.675\tau^4}d\tau,\quad \begin{pmatrix} m=1,2,3 \\ n=0,2,4,6,8\end{pmatrix}$$

which are numerically integrable. In practices, d varies from 0.02 to 1.0 and $\bar{t}$ from 0.1 to 0.8. From numerical calculations for d = 0.04, 0.06, 0.08, 0.1, 0.2, 0.4, 0.6, 0.8 and 1.0, it is known that a_0, a_1, a_2 and b_0, b_1, b_2 are all the same order of magnitude, and at any given d, their variations for the change of $\bar{t}$ are small. c_0, c_1, c_2 and c_3 are all the same order of magnitude and for any given d, they are all increasing functions of $\bar{t}$, and their rates of increase for the change of $\bar{t}$ are remarkably large.

Due to the above fact, higher order terms than r^2 can be neglected to the first approximation. For convenience of calculations, a_0, a_1, b_0, b_1 are expanded in terms of $\bar{t}$ for each d. As an example, for d = 0.06, $\bar{t}$ changes from about 0.15 to 0.25 and they are expressed in this region as follows:

$$a_0=0.067+1.28\bar{t}-2.8(\bar{t})^2,\qquad a_1=0.013+1.074\bar{t}-2.96(\bar{t})^2$$

$$b_0=2.26-5.2\bar{t}+20(\bar{t})^2,\qquad b_1=-2.275+0.15\bar{t}+(\bar{t})^2$$

Replacing $\bar{t}$ by $t_s/\sqrt{1+0.6r}$, and neglecting higher order terms than r^2, we obtain for d = 0.06,

$$A\left(\frac{d}{2\pi(\bar{t})^2},\gamma\right)=(0.067+1.28t_s-2.8t_s^2)+\gamma(0.013+0.690t_s-1.28t_s^2)$$

APPROXIMATE ESTIMATIONS OF CORRELATION COEFFICIENT BETWEEN WAVE HEIGHT AND PERIOD OF SHALLOW WATER WIND WAVES

$$B\left(\frac{d}{2\pi(\bar{t})^2},\gamma\right) = (2.26-5.2t_s+20t_s^2)+\gamma(-2.275+1.71t_s-11.0t_s^2)$$

Similar expressions are obtained for other d.

c_0, c_1 cannot be expressed by quadratics of $\bar{t}$, c_1/c_0 is expressed as quadratics of $\bar{t}$ approximately and because of $\bar{t} \fallingdotseq (1-0.3r)t_S$, we obtain to the first order approximation as follows:

$$C_0(\bar{t}) \fallingdotseq C_0(t_S) - 0.3\gamma t_S C_0'(t_S) = C_0(t_S)\left(1-0.3\gamma t_S \frac{C_0'}{C_0}\right)$$

where c_0'/c_0 is presented approximately in quadratics of t_S. As an example, for $d = 0.06$,

$$\frac{C_1}{C_0} = 6.30-38.2\,t_S+68\,t_S^2, \quad \frac{C_0'}{C_0} = 215.5-1505\,t_S+2900\,t_S^2$$

Hence,

$$C\left(\frac{d}{2\pi(\bar{t})^2},\gamma\right) = C_0(t_S)\left(1-0.3\gamma t_S\frac{C_0'}{C_0}\right)\left(1+\frac{C_1}{C_0}\gamma\right)$$
$$= C_0(t_S)\left\{1+\gamma(6.30-102.85\,t_S+519.5\,t_S^2-870\,t_S^3)\right\}$$

Similarly, for other d, A, B, and C in (53) are presented as rational expressions in terms of r and t_S.

Thus for $d = 0.06$, (53) becomes

$$\frac{d}{df}\left[\left\{(0.01124+0.215t_S-0.470t_S^2)+\gamma(-0.0021+0.0513t_S-0.0738t_S^2)h_S^2 t_S\right\}\right.$$
$$= A_S\left\{(0.1894-0.436t_S+1.676t_S^2)+\gamma(-0.0202-0.2489t_S+0.587t_S^2)\frac{h_S^2}{t_S^3}\right.$$
$$\left.-\alpha'\left\{(0.005082+\gamma(0.03659-0.5227t_S+2.640t_S^2-4.421t_S^3)\right\}C_0(t_S)\cdot\frac{h_S^3}{t_S^3}\right. \qquad (55)$$

which is an example of the approximately expressed energy equation for shallow water waves.

In (55), the second term in the left hand side is neglisibly small compared with the first term for $|r|<1$ and $t_S<1$. Therefore, (55) becomes

$$\gamma\left[\alpha'(0.03659-0.5227t_S+2.640t_S^2-4.421t_S^3)C_0(t_S)\cdot h_S-(-0.02020-0.2489t_S+0.589t_S^2)\right.$$
$$\left.\times A_S\right] = A_S(0.1894-0.436t_S+1.676t_S^2)-0.005082\alpha' C_0(t_S)h_S$$
$$-\frac{t_S^3}{h_S^2}\frac{d}{df}\left\{(0.01124+0.215t_S-0.470t_S^2)h_S^2 t_S\right\} \qquad (56)$$

from which r is calculated for given t_S and h_S, that is, for given f.

In the above energy equation, A_S and α' are not yet given. As for A_S, it is reasonably assumed to be nearly equal to A for deep water

waves. Hence we take here $A_S = 15 \times 10^{-6}$. As for α', it should be in order of $0.1 \sim 0.2$ and be selected as reasonably as possible. For the purpose of it, we tried rough calculations of r for each d, putting $\alpha' =$ 0.1, 0.15, 0.20, 0.25, and 0.30.

When $\alpha' = 0.1$ and 0.15, r increases with increase of f for $d = 0.04 \sim 1.0$, which is contradictory to the asumed properties of r. When 0.20, 0.25, and 0.30, r has the tendency of decrease with increasing f for all d, which becomes more and more remarkably for larger values of α' and when $\alpha' = 0.30$, r decreases beyond -0.7, the assumed lower limit of r. Hence $\alpha' = 0.30$ is too large. In conclusions, the value of α' suitable for the assumed properties of r should be in the range of 0.20 $\sim$ 0.25, which means from (50) that the coefficient of friction is to be about $0.015 \sim 0.019$. Therefore we take $A_S = 15 \times 10^{-6}$, and $\alpha' = 0.20$.

(61) will be correct enough near $r = 0$, but apart from it, it will become erroneous, and it is not always enough to use only (61) in order to obtain r. Accordingly, we proceed as follows:

(i) When $f < f_t$, $\overline{D_f}$ becomes much smaller than $\overline{R_T}$ and r should tend to that of deep water waves. From (44) and (51),

$$\frac{\overline{D_f}}{\overline{R_T}} = 0.0606 \frac{\alpha'}{A_S} \frac{C\left(\frac{d}{2\pi(\bar{t})^2}, r\right)}{B\left(\frac{d}{2\pi(\bar{t})^2}, r\right)} = 0.000808 \frac{C_0(\bar{t}) + C_1(\bar{t})\, r}{b_0(\bar{t}) + b_1(\bar{t})\, r} \cdot h_S \tag{57}$$

from which the value of f satisfying the condition $\overline{D_f} < 0.02\overline{R_T}$ (say f_o) is calculated for each d, and at f_o, r should be nearly equal to that of deep water waves. After calculations, f_o is obtained approximately as a function of d as follows:

$$f_o = 1000\, d^{1.80} \tag{58}$$

which is shown in Figure 3. Compared with (26), f_o is about a half of f_t and still smaller than f_t'(31). This may be because of the existence of longer individual wave than the significant wave.

(ii) When $f_u > f > f_t$, taking $A_S = 15 \times 10^{-6}$, $\alpha' = 0.2$, the value of f where r becomes zero (say $f_{(r=o)}$) is obtained for each d from (56), of which the result is as follows:

$$f_{(r=o)} = 1060\, d^{1.30} \tag{59}$$

which is shown in Figure 3.

(iii) When $f > f_u$, $d\overline{P}/dF$ becomes zero and $\overline{R_T} = \overline{D_f}$. And then r should be constant. Such a constant value of r is obtained from (57), putting $\overline{D_f} = \overline{R_T}$, and is shown in Figure 4 as a function of d.

APPROXIMATE ESTIMATIONS OF CORRELATION COEFFICIENT BETWEEN WAVE HEIGHT AND PERIOD OF SHALLOW WATER WIND WAVES

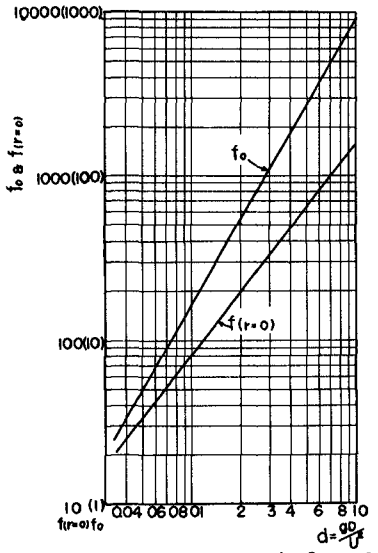

Fig. 3. f_o and $f_{(r=o)}$ for d.

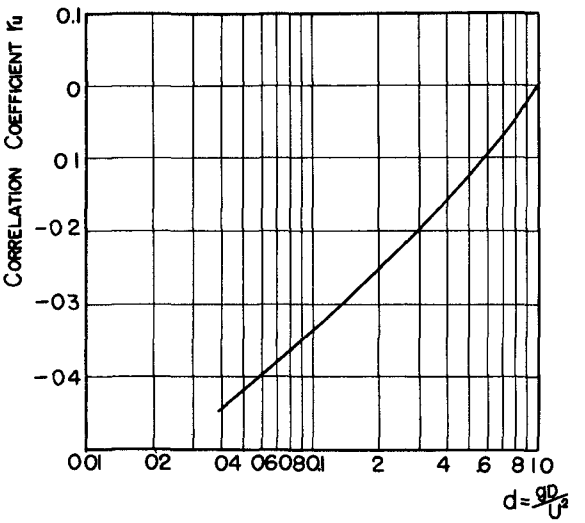

Fig. 4. Correlation coefficient for d.

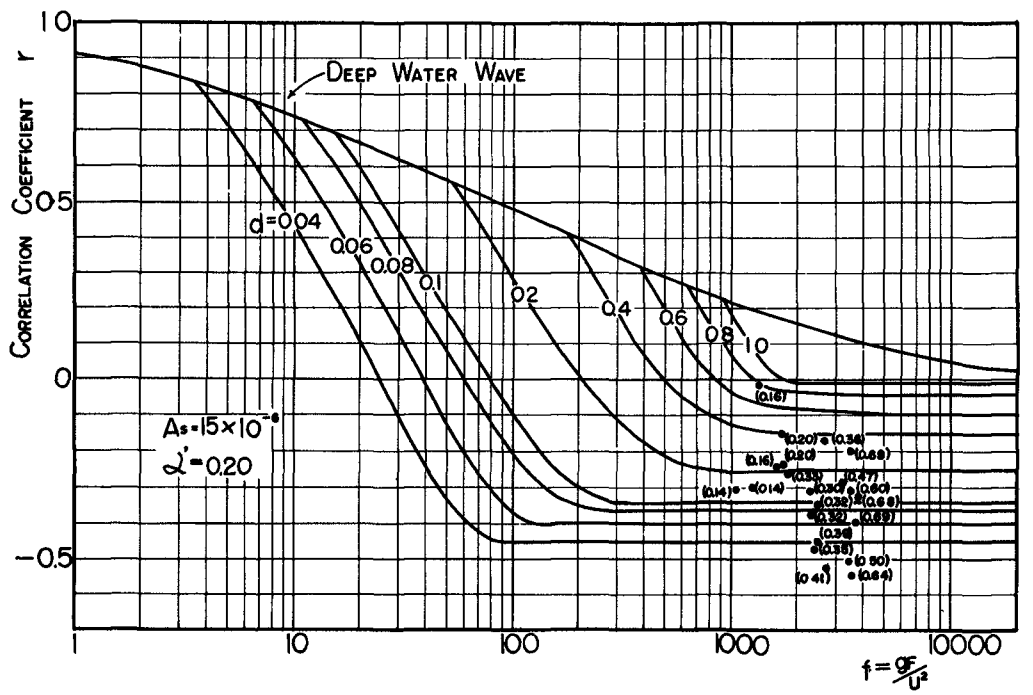

Fig. 5. Relationship between correlation coefficient and non-dimensional fetch for shallow water waves.

As mentioned aboved, at $f = f_0$, r begins to deviate from the value of r for deep water waves, and then gets to zero at $f_{(\gamma=0)}$, and still continuously decreases down to the ultimate, constant value. Figure 5 shows the curves of r thus obtained for each d.

SOME RESULTS OF OBSERVATIONS

The above- mentioned r for shallow water waves should be verified by a lot of observation data. Wave observations are now carried on near the Port of IzumiOotsu on the east coast of Oosaka Bay by means of under-water-preesure type wave-meters, and correlation coefficients are calculated from records at the depth of -2.20 meters below L.W.L., of which some results are plotted in Figure 5. Up to date, the amount of data is not satisfactory but the above-estimated tendency of r is seen from the Figure in some degree.

CONCLUSIONS

(I) In the case of deep water waves, asumming that the energy supplied by normal stress from wind is neglisible to that by tangential stress and energy equation by significant wave is available to the individual wave, and taking $A = 2\gamma^2\rho'/\rho = 15 \times 10^{-6}$, the correlation coefficient r for wave height and period is presented in terms of f in the region of $1 < f < 10^4$ approximately as follows:

$$\gamma = 2.97 - 2.00 f^{0.04} - 0.053 f^{0.08}$$

(II) In the case of shallow water waves, asumming similarly to the case of deep water waves and taking the coefficient of bottom friction as $0.015 \sim 0.019$, the correlation coefficient r is given as a function of d and f, as shown in Figure 5. r decreases more rapidly than that of deep water waves and gets to a certain negative value for each d.

The above-mentioned estimation is, however, only derived by approximate calculations with simple assumptions and so it should be necessarily verified by future investigations.

REFERENCES

Bretschneider, C.L.(1959):" Wave Variability and Wave Spectra for Wind Generated Gravity Waves." Tech. Memo. No.118, B.E.B.

Bretschneider, C.L.(1958):" Revisions in Wave Forecasting: Deep and Shallow Water." Proc. Sixth Con. on Coast. Eng.

Sverdrup H.U. and W.H.Munk(1947):" Wind Sea and Swell, Theory of Relations for Forecasting." H.O.Pub. No.601, U.S.Navy

Bretschneider, C.L.(1960): Letter to the author.

Kishi, T.(1955):"On Nearshore Waves." Proc. Second Con. Coast. Eng. Japan

Putnum, J.A. and J.W.Johnson(1949):" The Dissipation of Wave Energy Loss by Bottom Friction." Trans. A. G. U. Vol.30, No.1

CHAPTER 2

MODIFICATION OF WAVE SPECTRA ON THE CONTINENTAL SHELF AND IN THE SURF ZONE

Charles L. Bretschneider, Ph. D.
Senior Staff
National Engineering Science Co.
Washington 6, D. C.

ABSTRACT

This paper discusses the problem pertaining to the modification of the wave spectrum over the continental shelf. Modification factors include bottom friction, percolation, refraction, breaking waves, ocean currents, and regeneration of wind waves in shallow water, among other factors. A formulation of the problem is presented but no general solution is made, primarily because of lack of basic data. Several special solutions are presented based on reasonable assumptions. The case for a steep continental shelf with parallel bottom contours and wave crests parallel to the coast and for which bottom friction is neglected has been investigated. For this case it is found that the predominant period shifts toward longer periods. The implication is, for example, that the significant periods observed along the U. S. Pacific coast are longer than those which would be observed several miles westward over deep water.

The case for a gentle continental shelf with parallel bottom contours and wave crests parallel to the coast and for which bottom friction is important has also been investigated. For this case it is found that the predominant period shifts toward shorter periods as the water depth decreases. The implication is, for example, that the significant periods observed in the shallow water over the continental shelf are shorter than those which would be observed beyond the continental slope. In very shallow water, because shoaling becomes important, a secondary peak appears at higher periods.

The joint distribution of wave heights and wave periods is required in order to determine the most probable maximum breaking wave, which can be of lesser height than the most probable maximum non-breaking wave. In very shallow water the most probable maximum breaking wave which first occurs would be governed by the breaking depth criteria, whereas in deeper water wave steepness can also be a governing factor. It can be expected that in very shallow water the period of the most probable maximum breaking wave should be longer than the significant period; and for deeper water the period of the most probable maximum breaking wave can be less than the significant period.

COASTAL ENGINEERING

INTRODUCTION

During the last decade, a great number of studies has been carried out on wave forecasting and wave spectrum in deep water. Despite this fact, a great deal remains to be accomplished in this field.

One of the most important steps to be taken next is the study of the modification of the wave spectrum upon its arrival on the continental shelf and in the surf zone.

When the waves generated by a storm in deep water off the continental shelf are propagated as swell over the continental shelf, they are modified by bottom friction, percolation, refraction, shoaling and whitecaps As an overall effect, the waves composing the spectrum are damped due to the dissipation of wave energy. As a consequence, this damping involves a deformation of the wave spectrum with the result that the wave heights of the spectrum can no longer be defined by the special type Gamma function distribution such as the Rayleigh distribution.

Upon arrival in the surfing zone, each component of the spectrum breaks at a different water depth in the surfing zone. The distribution of breaking depth and the probability and distribution of the angle of breaking wave crest with the shoreline depend upon the wave spectrum characteristics arriving in the surfing zone and the change in the angle of the wave crest with the shoreline due to refraction effects.

GENERAL CONSIDERATIONS ON THE MODIFICATION OF THE WAVE SPECTRUM

The significant wave method for dealing with the transformation of surface waves as they are propagated into shallow water, taking bottom friction, percolation and refraction into account, has been presented by Bretschneider and Reid[9]*. Instead of assuming a uniform wave train, it is assumed that the significant period of the wave is invariant. This implies essentially that there is no selective attenuation or selective amplification of the wave spectrum. The functions characterizing the dissipation of energy used in the above reference are the same as those introduced by Putnam and Johnson[1], and hence, all assumptions pertaining to these dissipation functions have been incorporated in the work by Bretschneider and Reid.

The significant wave method has been extended by Bretschneider[6] to forecasting wind waves in shallow water, taking into account wave energy loss due to bottom friction. This method is semi-empirical and has been correlated with wind and wave data from Lake Okeechobee, Florida.

---

* Numbers indicate references listed at end of paper.

These forecasting relationships for shallow water of constant depth are comparable to similar relationships obtained by Thijsse[8] by an entirely different method. The relationships given by Bretschneider[6] as well as those given by Thijsse[8], have certain practical applications.

The attenuation of energy by bottom friction over the continental shelf for waves of long period can be explained qualitatively as due to the fact that the long waves effectively "feel" bottom sooner than the short period waves and consequently are subjected to frictional dissipation over a greater distance. In a complex wave group this selective attenuation could produce, under certain conditions, a shift in the peak of the power spectrum towards lower periods as the waves travel towards shore. There is some evidence to support this in the shallow, flat Atchafalaya Bay region of the Gulf of Mexico where a smaller significant period has been observed inshore compared with simultaneous measurements offshore, as reported by Bretschneider[6]. However, this is not conclusive since distortion of the power spectrum with a consequent change of significant period can also result when no energy is lost, as Pierson, et al, have shown [10] on the basis that each component of the spectrum has a different shoaling and refraction factor. However, shoaling and/or refraction can cause a shift either to higher or lower significant period depending on the actual conditions.

In general, however, it is believed that the predominant period of the period spectrum will shift to lower periods because of wave energy loss due to bottom friction. This is an opposite effect to what is known about the increase in predominant period due to increase in fetch length and wind duration. On the other hand, in deep water the predominant wave period increases with distance from decaying swell, but decreases with time at any particular decay distance. Pierson and Marks[11] have also demonstrated a shift in the predominant period of the sub-surface pressure spectrum, in which case the predominant period increases with depth.

A SUMMARY OF EXISTING KNOWLEDGE ON WAVE DAMPING EFFECTS

Most of the theoretical studies on wave damping have been carried out for regular wave trains: Boussinesq[17], Lamb[18], Basset[19], Hough[20], Biesel[21], Keulegan[3], Putnam and Johnson[1], Miche[25], Reid and Bretschneider[9], among others.

From a theoretical point of view, two methods exist to attack the problem. The first method -- the analytical method -- consists of solving directly the basic differential equations -- momentum, continuity taking into account a friction term. This method presents the advantage of giving not only the damping but also the deformation of wave motion due to friction forces. This is more important for long waves in shallow

water and becomes essential at the limit for tidal waves in an estuary, for example.

For the problem under study, an approximate method -- the energ method -- is simpler and as accurate. It consists of determining the wave motion independent of the friction forces and neglecting the convective inertia. As a consequence the wave profile is symmetrical. This approximation is valid because the decay of wave amplitude over a wave length is very small.

The damping effect is simply defined as a decay in wave height calculated from energy consideration: the loss of energy over a given leng is equal to variation of the wave energy.

The theory for modification of wave height (assuming significant wave as a wave train) due to bottom friction, percolation and refraction has been presented in detail, particularly by Bretschneider and Reid[9]. Shoaling does not represent a loss in wave energy but this modification is included as a transformation process. It will suffice at present only to summarize the theory here. The theory is based on waves of small steepness. For steady state conditions, the rate at which the total power is altered per unit distance along one of the wave rays is given by

$$\frac{d(Pb)}{dx} = -(D_f + D_p)\, b \qquad \ldots (1)$$

where x is the distance measured along the wave ray in the direction of propagation of waves (see Figure 1). P represents the energy propagated per unit time through a vertical area of depth d and unit width (normal to the wave ray) averaged over one wave length. The average power (or energy transfer per unit time) between two wave rays of horizontal spacing b is consequently Pb. Under steady conditions, this power would remain constant for given wave rays in the absence of dissipation, reflection, breaking and lateral dispersion of energy. However, in the presence of bottom friction and/or percolation, the value of Pb decreases slowly from one wave to the next in shallow water.

In equation (1) D_f and D_p are functions characterizing the dissipation of energy from bottom friction and percolation, respectively. The problem is to evaluate these functions. The bottom friction effect can be calculated theoretically when the flow is laminar. However, this flow is more often turbulent than laminar. This necessitates experiments or field observations. Laboratory studies on wave energy loss have been made by Keulegan[3], Savage[4], Ippen and Kulin[5], and others. (In fact, Keulegan, Ippen and Kulin considered the case of solitary waves, the results of which might be applicable to the surf zone.)

This leads to a more general discussion of the boundary layer problem and inception of turbulence in unsteady motion.

First, it is assumed that a wave motion is well defined by a velocity potential function. Hence the flow is irrotational, i.e. without

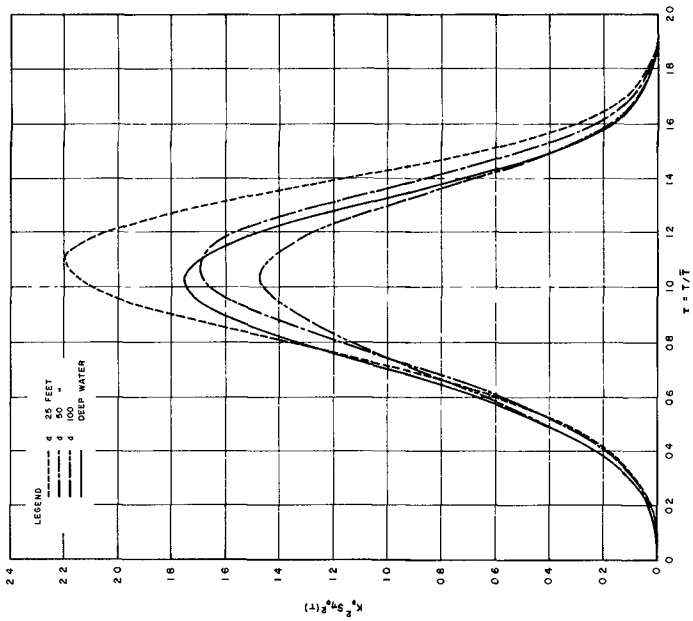

Fig. 2. Modification of wave spectrum due to shoaling.

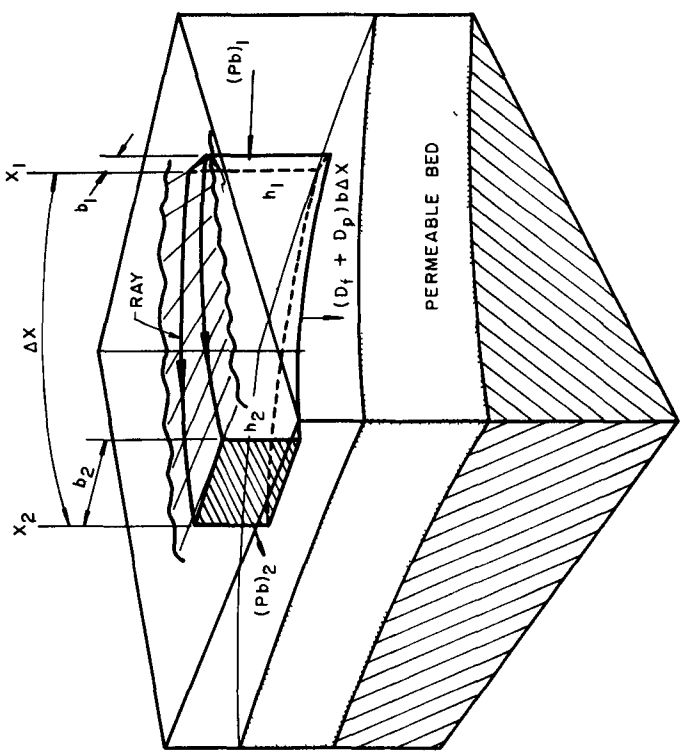

Fig. 1. Schematic of energy transfer.

friction.

$$\mu \nabla^2 \vec{V} = \mu \nabla^2 \operatorname{grad} \varphi = \mu \operatorname{grad} \nabla^2 \varphi = 0 \quad \ldots (2)$$

However, it often happens that a current, such as tidal current or longshore current, is superimposed on the wave motion. This current may be the cause of instability and turbulence. By causing turbulence throughout the mass of water within the wave motion, there is an action on the internal damping mechanism of the wave spectrum, independent from the turbulence due to whitecaps.

Under this irrotational wave motion, there is the boundary layer where the flow is strongly rotational. Without whitecaps, it is in the boundary layer that the greatest part of wave energy is lost.

In the case of viscous flow, the periodic motion in the boundary layer on a smooth plane is relatively well known.

The thickness of the boundary layer δ is proportional to $[\nu T]^{1/2}$, that is, δ increases with the wave period. δ is of the order of magnitude of a few millimeters. The shearing stress τ is proportional to $\mu \cdot u_b / \delta$ where u_b is the bottom velocity. The damping effect due to the loss of energy in the boundary layer may also be calculated. It is found that the wave height decreases exponentially with distance. This decay is independent from the absolute value of H.

However, for some Reynolds' numbers the flow in the boundary layer becomes unstable and turbulent. The stability of such unsteady motion has not been investigated by theory. Some experiments (Collins[22]) show that the boundary layer becomes turbulent for a Reynolds' number

$$\frac{u_b \delta}{\nu} = \left(\frac{\pi}{\nu T}\right)^{1/2} \frac{H}{\sinh md} > 160 \quad \ldots (3)$$

$m = \frac{2\pi}{L}$; H = wave height.

On a rough boundary the inception of turbulence and the damping depend also upon the relative roughness ε / δ . Hence, on a sandy bottom ripples have an effect on the wave damping. The thickness of the boundary layer is unknown but also grows as T increases. It often happens that the turbulence issued from the bottom is damped quickly throughout the mass of water. Hence, a turbulent boundary layer under a laminar wave motion is possible. A cloud of sand in suspension can be seen only a few inches above the ripples.

The shearing stress is then proportional to the square of the bottom velocity.

$$\tau = \rho f u_b |u_b| \qquad \ldots (4)$$

where f is a friction coefficient which varies with the relative roughness and a Reynolds' number. u_b is the bottom velocity at the top of the boundary layer. u_b can be defined from the velocity potential defining the wave motion.

In relatively deep water δ is very small by comparison with the depth d . Hence,

$$u_b = u \cong u_d = \left.\frac{\partial \varphi}{\partial x}\right|_{z=-d} \qquad \ldots (5)$$

Using such assumptions, Putnam and Johnson have found that the wave energy D_f dissipated per unit area at the bottom per unit time (averaged over a wave length) is given by:

$$D_f = \frac{4}{3}\pi^2 \frac{\rho f H^3}{L^3 \left(\sinh \frac{2\pi d}{L}\right)^3} \qquad \ldots (6)$$

and the variation of wave height varies hyperbolically with distance and depends upon the absolute value of H .

Biesel[23] and Putnam[2] have also examined the oscillatory percolation of water through a permeable sea bed, associated with sinusoidal waves of small amplitude in the overlying water. According to Putnam, the amount of energy D_p dissipated by viscous forces in the permeable bed per unit area of the bottom per unit time (averaged over a wave length) is given by:

$$D_f = \frac{\pi g^2}{\nu} \frac{\rho K H^2}{L \left(\cosh \frac{2\pi d}{L}\right)^2} \qquad \ldots (7)$$

for a permeable bed whose depth is greater than 0. 3 L. In the above equation, K equals the permeability coefficient of Darcy's law. The other symbols have previously been explained. (It should be noted that Reid and Kajura[12] have shown that equation (7) is in error by a factor of 4 ; i. e. equation (7) should be preceded by 1/4.)

Using D_f and D_p as given by the above expression, the differential equation (1) has been formulated by Bretschneider and Reid[9] and certain special solutions have been obtained. The general solution is obtained in part by numerical integration of the functions characterizing the dissipation of energy.

One of the most important requirements is a knowledge of the friction coefficient f and this presents a number of difficulties.

First, the difference between an exponential damping in laminar flow or a hyperbolic damping in turbulent flow is so small that both solutions could be considered as possible. However, for long waves in very shallow water, the boundary layer becomes thicker and the velocity distribution in the vertical plane is influenced very much by the bottom friction effect. Moreover, the theoretical value for u_b equals $u = \frac{\partial \eta}{\partial x} = f(x,t)$ whatever the value of z.

From this point of view, long waves in shallow water can be considered almost as a succession of steady flows. The velocity distribution in a vertical plane is close to the velocity distribution for steady flow. At the limit, the tidal motion in an estuary is defined on such an assumption.

The friction coefficient f can then be expressed as a function of the Chezy coefficient C_h or the Manning coefficient n:

$$f = \frac{g}{C_h^2} \quad , \quad C_h = \frac{1.486}{n} d^{1/6} \qquad \ldots (8)$$

From laboratory data on short waves, Bagnold[14] has obtained the following formula for the friction coefficient:

$$f = .074 (R/p)^{-0.75} \qquad \ldots (9)$$

where R is half the total horizontal displacement of particle velocity at the bottom, and p is the horizontal distance between the sand ripple crests at the bottom.

SOME CONSIDERATIONS ON THE MODIFICATION OF WAVE SPECTRUM

It is of interest to anticipate the influence on the wave spectrum due to various modification factors. In this respect an example is given assuming that in deep water the root mean square wave height and the mean wave period are given respectively by $H_r = 30$ feet and $T = 12$ seconds. In the following example the deep water wave spectrum equation given by Bretschneider[13] will be used although similar manipulations could be applied to the spectra equations given by Neumann[30] and Darbyshire[31 & 32] among others.

For the case of deep water, the wave period spectrum given by Bretschneider[1] is:

$$S\eta_o^2(\tau) = K_1 \tau^3 e^{-B_1\tau^{-4}} \quad \ldots (10)$$

in which case the wave frequency spectrum is

$$S\eta_o^2(\nu) = K_2 \nu^{-5} e^{-B_2\nu^{-4}} \quad \ldots (11)$$

In the above equations $S\eta_o^2(\tau)$ and $S\eta_o^2(\nu)$ respectively represent the sum of the squares of the wave height as a function of wave period and wave frequency. The symbols used are:

$$\eta_o^2 = H_o^2/\overline{H_o^2}, \quad \tau = T/\overline{T}, \quad \nu = \omega/\overline{\omega}$$

where $\omega = 2\pi/T$, $\overline{H^2}$ is the average of the squared wave heights, $\overline{T}$ is the average of the wave periods, $\overline{\omega}$ is the average of the wave frequencies, and K_1, K_2, B_1 and B_2 are constants. The subscript o is used to denote deep water wave spectrum.

As the spectrum is propagated across the continental shelf, unaffected by winds, the modifications that can take place are: (1) wave energy loss due to bottom friction, (2) wave energy loss due to percolation in a permeable sea bed, (3) shoaling, and (4) refraction. In addition, wave energy can be lost due to whitecaps, ocean and tidal currents, longshore currents, etc.

It will be convenient to define a modification factor K^2, which includes the above considerations, and which naturally will vary with wave period, water depth, bottom conditions, etc., such that the wave spectrum in shallow water becomes

$$S\eta^2(\tau) = K^2 S\eta_o^2(\tau) \quad \ldots (12)$$

or in terms of frequency

$$S\eta^2(\nu) = K^2 S\eta_o^2(\nu) \quad \ldots (13)$$

If the continental shelf is steep, such as off the Pacific Coast of the United States, wave energy loss due to bottom friction and percolation will be negligible. If the wave crests are parallel to parallel bottom contours, refraction will be absent, and if no waves break, then the modification will be due entirely to shoaling, whence $K = K_s$. K_s is the

shoaling factor and is a function only of h/L where h is the water depth and L the wave length, corresponding to the appropriate wave period (or wave frequency) of the spectrum. Based on $T = 12$ seconds the shoaling coefficients were determined for various wave periods and water depths, and applied to equation (10). The results are shown in Figure 2. I is interesting to note the shift in the predominant wave period. In deep water the predominant period is equal to $1.027 \times 12 = 12.3$ seconds and at a depth of 25 feet becomes $1.1 \times 12 = 13.2$ seconds. The same computations could have been performed for the frequency spectrum, but the period spectrum seems to illustrate the shift in period more clearly.

If the wave spectrum is propagated across the continental shelf off the East Coast or Gulf Coast, then bottom friction becomes important. Considering only bottom friction (without shoaling) $K = K_f$, and equation (10) or (11) becomes an equivalent deep water wave spectrum. Considering a bottom of constant slope and assuming a constant friction factor, K_f was determined for various water depths for $f/m = 7.6$, f being the bottom friction factor and m the bottom slope. The results of these computations are shown in Figure 3. It is interesting to note now that the predominant wave period has shifted to the lower wave periods. That is, the predominant wave period is 12.3 seconds in deep water and about 9.0 seconds in a depth of 25 feet. The same sort of shift to lower wave periods can also occur by the breaking of the longer period waves, which also can have an effect on the high frequency components of the spectrum.

A wave recorder would naturally record the shoaled waves, the deduced spectrum of which would not be in accordance with Figure 3. Applying the shoaling coefficients to Figure 3 results in the squared wave height spectrum such as would be obtained from a wave recorder. The results of these computations are shown in Figure 4. It can be seen from Figure 4 that the shift in the predominant wave period is also toward lower wave periods, but not so pronounced as in Figure 3. For the 25-foot water depth, the combined effect of shoaling and bottom friction introduces an additional predominant period.

Corresponding frequency spectrum for the combined effect of shoaling and bottom friction is given in Figure 5.

THE MAXIMUM POSSIBLE WAVE AND THE MAXIMUM PROBABLE WAVE

The maximum possible wave is governed by the breaking wave criteria, whereas the maximum probable wave represents a statistical probability.

A great number of studies has been carried out by defining the breaking conditions of a regular wave. The most significant formulas are those proposed by:

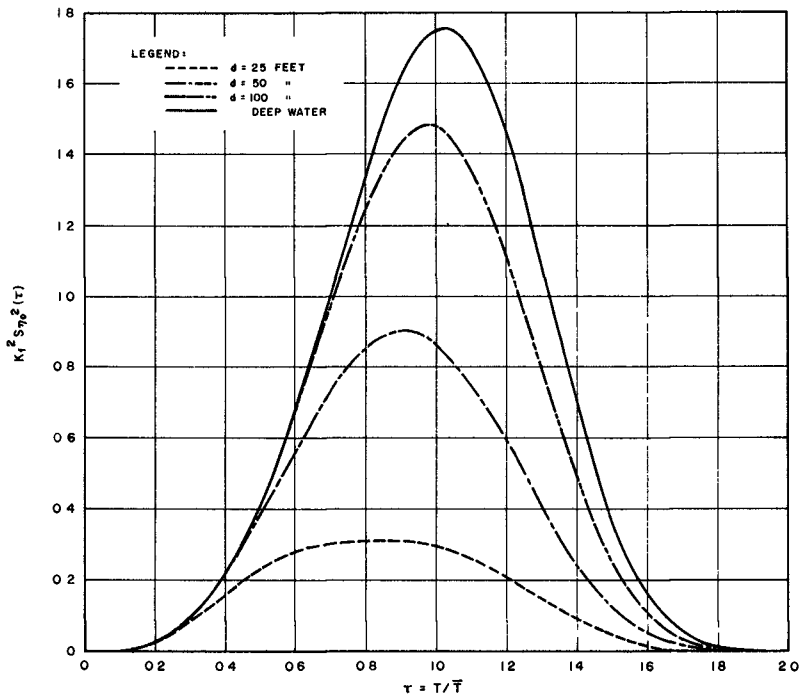

Fig. 3. Modification of period spectrum due to bottom friction (f/m = 7.6).

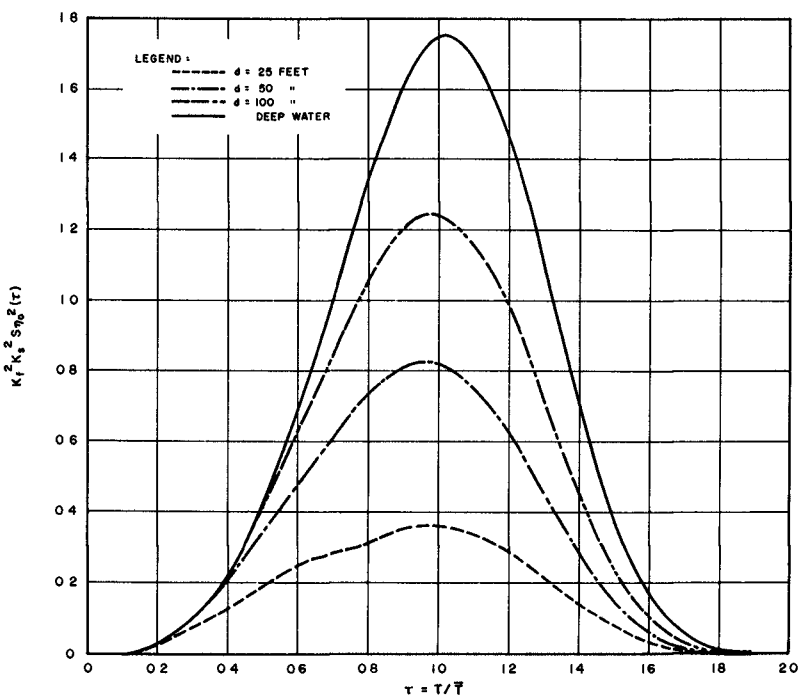

Fig. 4. Modification of period spectrum due to shoaling and bottom friction (f/m = 7.6).

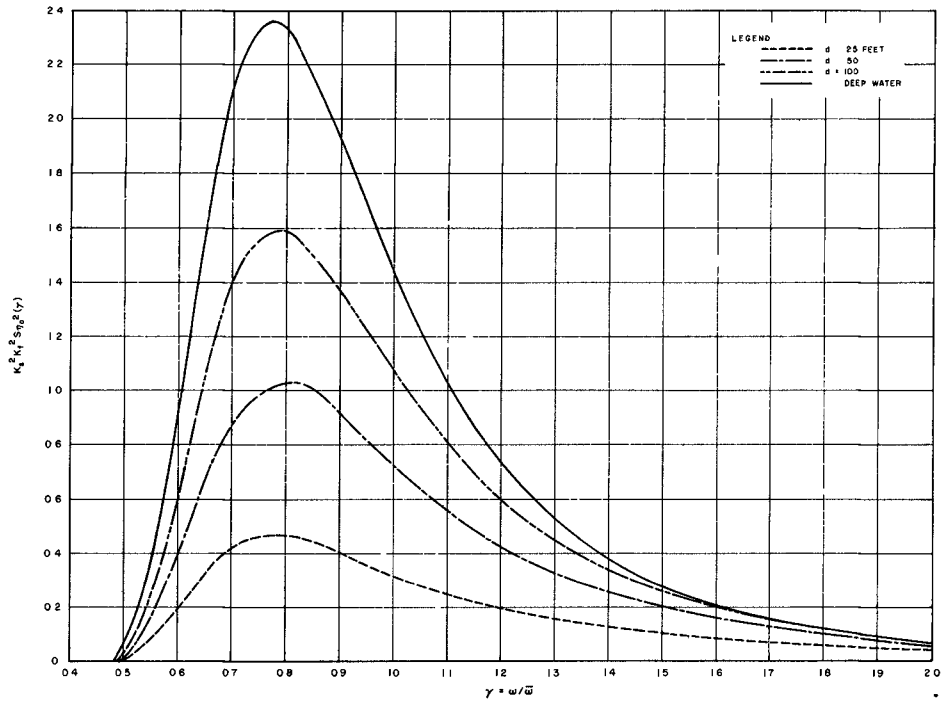

Fig. 5. Modification of frequency spectrum due to shoaling and bottom friction (f/m = 7.6).

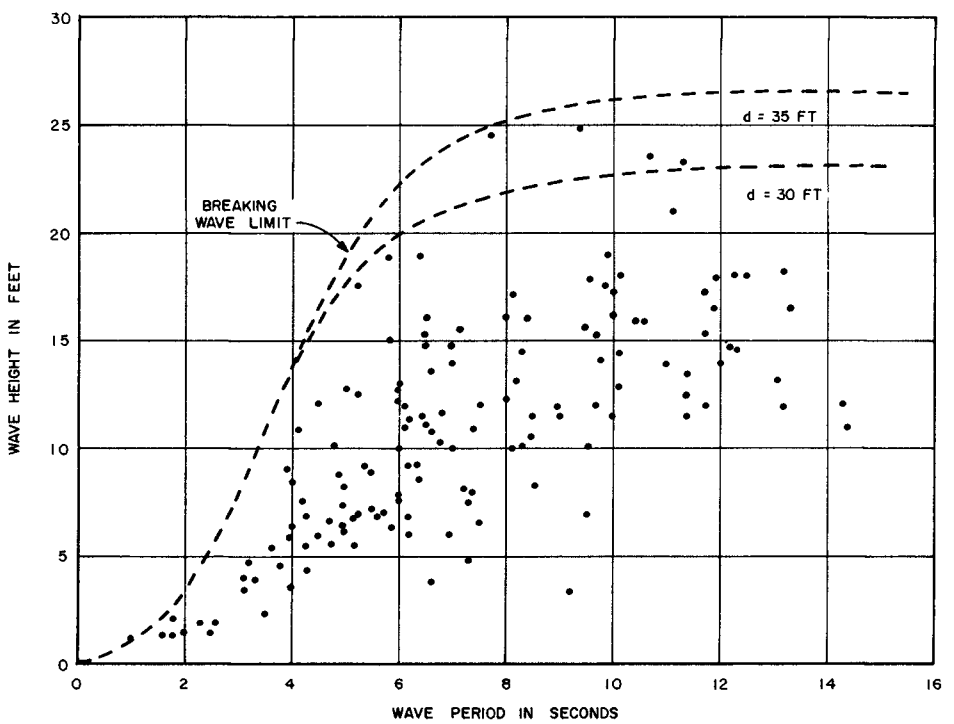

Fig. 6. Wave heights and periods, Hurricane Audrey, June 27, 1957.

Stokes[27] in deep water: $\frac{H}{L} = 0.14$ . . . (14

Miche[26] for any depth: $\frac{H}{L} = 0.14 \operatorname{Tanh} \frac{2\pi d}{L}$ . . . (15

Munk[28] and others for solitary waves, valid for long waves in very shallow water: $\frac{H}{L} = 0.78$ . . . (1

Experiments by Danel[29] have shown the limit of validity of the Miche theory. Bretschneider[24] has presented, by empirical interpolation, practical graphs valid for any case. Le Méhauté[15] has analyzed the case of a wave breaking at an angle with the shoreline at a first order of approximation, in which case the angle of wave crest in deep water is related to the angle of breaking wave crest in shallow water.

Based on the assumptions of a narrow (linear) wave spectrum, Longuet-Higgins[16] derived the Rayleigh distribution for ocean wave heights. For a long record the asymptotic solution for the most probable maximum wave height is given by:

$$H_{max} = .707\ H_S \left(\ln N \right)^{1/2} \quad \ldots (17$$

where H_{max} is the most probable maximum wave height,

H_S is the significant wave height, and

N is the total number of waves.

The above formula is intended to apply when N is large (say 100 to 1000) and for near-steady state conditions. This formula is based on linear assumptions and should therefore be used with caution for very steep waves or for waves in very shallow water, where breaking occurs.

It is desirable to define a most probable maximum breaking wave, which would be given by the intersection of the breaking index criteria and the joint probability distribution of wave heights and periods. Figure 6 is an example of the joint distribution of wave heights and periods obtained in the Gulf of Mexico during Hurricane Audrey in 1957. The data were obtained by the California Company and analyzed at the Beach Erosion Board. The breaking criteria is shown by the dashed lines for two water depths covering the possible range of total water depth, including storm surge and tide.

It is apparent (but not too clearly demonstrated in figure 6) that there can be a most probable maximum breaking wave height which is smaller than the most probable maximum wave height.

The data given in figure 6 have been analyzed by a very quick method for determining the distributions shown in figure 7. The upper graph (6a) represents the histogram or distribution of periods. The other two graphs (6b and 6c) are related to the period spectrum. The solid blocks are for periods grouped 1-3, 3-5, etc. and the dashed blocks are for periods grouped 0-2, 2-4, 4-6, etc. A careful look at both figures 6 and 7 seems to indicate that a detailed spectrum analysis would result in a spectrum having at least two well-defined peaks, one at about six seconds and the other at about ten seconds. The ten-second peak probably results from the fact that the shoaling coefficient for water depths 30 to 35 feet is greater for the ten-second wave than for the six-second wave.

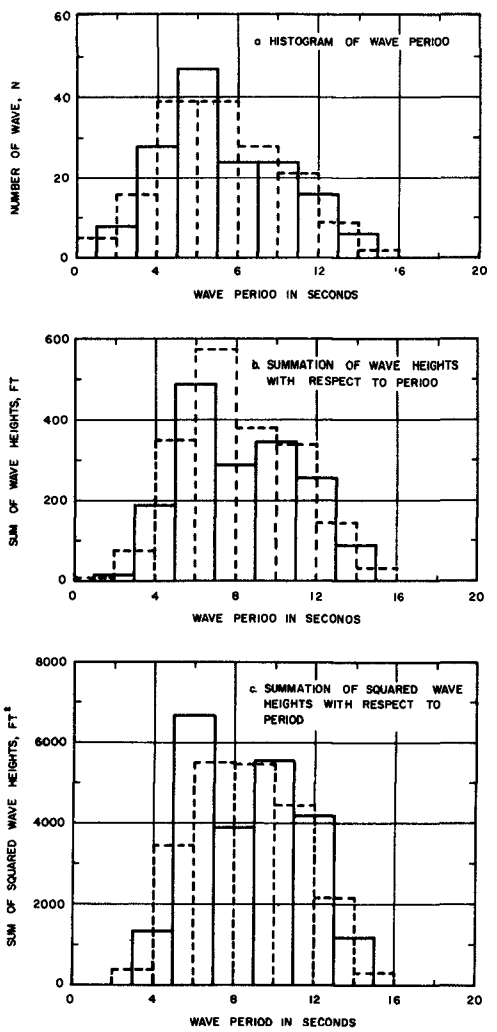

Fig. 7. Results of wave data, Hurricane Audrey, 1957.

The peak at six seconds probably occurs because bottom friction has not been important for the short period waves, and also the regeneration of waves is more rapid for the shorter periods than for the longer period waves. This phenomenon of a double peak is expected from the considerations given in figure 4. In fact, the peak at $\tau = 0.6$ (figure 4) would be much higher if the wind effect had been included.

SUMMARY AND CONCLUSIONS

There can be a most probable maximum breaking wave which is equal to or less than the height of the most probable maximum wave. This should be considered in selecting the design wave. For example, for a particular design storm, the most probable maximum wave might be H = 22 feet and T = 9 seconds for d = 30 feet. This is a non-breaking wave. For the same spectrum there can be a 20-foot, 6-second wave which is a breaking wave. As another example, for another particular design storm, the most probable maximum wave might be H = 23 feet and T = 12 seconds for d = 30 feet. This is a breaking wave. However, for the same spectrum there can also be a 23-foot, 14-second wave which is also a breaker.

ACKNOWLEDGEMENTS

Appreciation is extended to the National Engineering Science Co. for making available time and personnel for the preparation of this paper. In particular, appreciation is given to Dr. Le Méhauté for his ideas and views on wave damping. Finally, appreciation is given to the California Company, New Orleans, La., for permission to use the wave data on joint distribution shown in figure 6.

REFERENCES

1. Putnam, J. A. and J. W. Johnson (1949). "The Dissipation of Wave Energy by Bottom Friction." Transactions, Amer. Geophys. Union, Vol. 30, No. 1, pp. 67-74.

2. Putnam, J. A. (1949). "Loss of Wave Energy due to Percolation in a Permeable Sea Bottom." Transactions, Amer. Geophys. Union, Vol. 30, Nl. 3, pp. 349-356.

3. Keulegan, G. H. (1948). "Gradual Damping of Solitary Waves." Jour. Res., Nat. Bur. Standards, Vol. 40, pp. 487-498.

4. Savage, R. P. (1953) "Laboratory Study of Wave Energy Losses by Bottom Friction and Percolation." Tech Mmeo No. 31, Beach Erosion Board, Dept. of the Army Corps of Engineers, 25 pp.

5. Ippen, A. I. and G. Kulin (1957). "The Effect of Boundary Resistance on Solitary Waves." La Houille Blanche, Jul-Aug., No. 3, p. 901.

6. Bretschneider, C. L. (1954). "Field Investigation of Wave Energy Loss in Shallow Water Ocean Waves." Tech Memo No. 46, Beach Erosion Board, Dept. of the Army Corps of Engineers, 21 pp. and appendices.

7. Bretschneider, C. L. (1954). "Generation of Wind Waves Over a Shallow Bottom." Tech Memo No. 51, Beach Erosion Board, Dept. of the Army Corps of Engineers.

8. Thijsse, J. Th. and J. B. Schijf. (1949). "Report on Waves." 17th International Navigation Congress, Section II, Communication 4, Lisbon.

9. Bretschneider, C. L. and R. O. Reid (1954). "Changes in Wave Height due to Bottom Firction, Percolation and Refraction." Tech Memo No. 45, Beach Erosion Board, Dept. of the Army Corps of Engineers, 36 pp.

10. Pierson, W. J., J. J. Tuttel and J. A. Woolley (1953). "The Theory of the Refraction of a Short-Crested Gaussian Sea Surface with Application to the Northern New Jersey Coast." Proceedings, IIId Conference on Coastal Engineering, pp. 86-108.

11. Pierson, W. J. and W. Marks (1952). "The Power Spectrum Analysis of Ocean-Wave Records." Transactions, Amer. Geophys Union, Vol. 33, pp. 834-844.

12. Reid, R. O. and K. Kajura (1957). "On the Damping of Gravity Waves Over a Permeable Sea Bed." Transactions, Amer. Geophy Union, Vol. 38, No. 5, pp. 662-666.

13. Bretschneider, C. L. (1959). "Wave Variability and Wave Spectra for Wind-Generated Gravity Waves." Tech Memo No. 118, Beach Erosion Board, U. S. Army Corps of Engineers, 192 pp.

14. Bagnold, R. A. (1947). "Sand Movement by Waves; Some Small-Scale Experiments with Sand of Very Low Density." Jour. Institute of Civil Engineering, Vol. 27, pp. 447-469.

15. Le Méhauté, B. (1961). "A Theoretical Study of a Wave Breaking at an Angle with the Shoreline." Trans., Amer. Geophys. Union, Vol. 66, No. 2.

16. Longuet-Higgins, M. S. (1952). "On the Statistical Distribution of the Heights of Sea Waves." Jour., Marine Research, Vol XI, No. 3, pp. 345-366.

17. Boussinesq. Essais sur la theorie de eaux courantes.

18. Lamb, H. Hydrodynamics. Sixth Ed., 1932, p. 625

19. Basset. (1888). Hydrodynamique.

20. Hough (1877). Proceedings, London Math. Soc., Vol. XXVIII, p. 264.

21. Biesel, F. (1949). Notule hydraulique, La Houille Blanche, Sep-Oct.

22. Collins, G. (1961). "Effect on Mass Transport of the Onset of Turbulence at the Bed Under Periodic Gravity Waves." ASME-EIC, Hydraulics Conference, Montreal, Paper No. 61, EIC-8.

23. Biésel, F. (1949). A Mortissement des houles par permeabilite de nd., I. A. H. R., Grenoble, Sep.

24. Bretschneider, C. (1960). "Selection of Design Wave for Offshore Structures." Trans., ASCE, Paper No. 3026.

25. Miche, R. (1954). "Train d'ondes oceaniques." COEC, Ministere defense nationale, No. 135.

26. Miche, M. (1954). "Undulatory Motion of the Sea in Constant or Decreasing Depth." Wave Research Laboratory, Berkeley, Calif., Series 3, Issue 363, June.

27. Stokes, G. G. (1847). "On the Theory of Oscillatory Waves."

28. Munk, W. (1949). "The Solitary Wave Theory and Its Application to Surf Problems." Annals, N. Y. Academy of Sciences, Vol. 51, Art. 3, May.

29. Danel, P. (1951). "On the Limiting Clapotis." Gravity Waves, U. S. Dept. of Commerce, Nat. Bureau of Standards, Circular 521.

30. Neumann, G. (1952). "On Ocean Wave Spectra and a New Method of Forecasting Wind-Generated Sea." Beach Erosion Board Tech Memo No. 43, U. S. Army Corps of Engineers, 42 pp.

31. Darbyshire, J. (1952). "The Generation of Waves by Wind." Proc., Royal Society, A 215, pp. 299-328.

32. Darbyshire, J. (1955). "An Investigation of Storm Waves in the North Atlantic Ocean." Proc., Royal Society, A 230, pp. 299-328.

CHAPTER 3

THE SURFACE WAVE IN A TWO-DIMENSIONAL VORTEX LAYER

Tokuichi Hamada
Port and Harbour Technical
Research Institute, Japan

ABSTRACTS

Progressive surface wave in a two-dimensional vortex layer is theoretically treated. Dynamical equations and free surface conditions are shown by using the two-dimensional stream functions of wave and vortex.

Then the perturbation equations are given by assuming that the ratio of length scale of vortices and wave is fairly small. The first approximate solution of wave has a usual form of an irrotational progressive wave. Vortices are assumed to be steady and to have simplified Fourier-Stieltjes form. Then the interaction of this primary wave and the vortices are examined. To satisfy the free surface contition of the second order, existent waves are formed. In the second order term of the free surface elevation, these secondary waves offset the effect of the above mentioned interaction, and so the surface profile of the primary wave is not altered by the existence of inner vortices of high frequency.

Some pictures of irregular surface waves in a turbulent flow are shown to verify this property.

DERIVATION OF PERTURBATION EQUATIONS

We use the two-dimensional co-ordinate system. x-axis is taken horizontally at the still water surface, y-axis is vertically upwards. The depth of water is assumed to be infinite and the motion is considered inviscid.

Then we suppose the motion is consisted both of the surface gravity wave and vortices in a steady uniform current and we assume that the motion of surface wave can be linearized. In the following equations suffix 1 is concerned to vortices and suffix 2 to wave, and u_0 is the horizontal velocity of steady uniform current.

Equations of motion are

$$\frac{\partial u_1}{\partial t}+\frac{\partial u_2}{\partial t}+(u_0+u_1+u_2)\frac{\partial}{\partial x}(u_1+u_2)+(v_1+v_2)\frac{\partial}{\partial y}(u_1+u_2) = -\frac{1}{\rho}\frac{\partial p}{\partial x} \qquad (1)$$

$$\frac{\partial v_1}{\partial t} + \frac{\partial v_2}{\partial t} + (u_0 + u_1 + u_2)\frac{\partial}{\partial x}(v_1 + v_2) + (v_1 + v_2)\frac{\partial}{\partial y}(v_1 + v_2) = -g - \frac{1}{\rho}\frac{\partial p}{\partial y} \tag{2}$$

(1) and (2) are linearized as to u_2, v_2, and

$$\frac{\partial u_1}{\partial t} + \frac{\partial u_2}{\partial t} + (u_0 + u_1 + u_2)\frac{\partial u_1}{\partial x} + (u_0 + u_1)\frac{\partial u_2}{\partial x} + (v_1 + v_2)\frac{\partial u_1}{\partial y} + v_1\frac{\partial u_2}{\partial y} = -\frac{1}{\rho}\frac{\partial p}{\partial x} \tag{3}$$

$$\frac{\partial v_1}{\partial t} + \frac{\partial v_2}{\partial t} + (u_0 + u_1 + u_2)\frac{\partial v_1}{\partial x} + (u_0 + u_1)\frac{\partial v_2}{\partial x} + (v_1 + v_2)\frac{\partial v_1}{\partial y} + v_1\frac{\partial v_2}{\partial y} = -g - \frac{1}{\rho}\frac{\partial p}{\partial y} \tag{4}$$

In incompressible fluid, the equation of continuity is

$$\frac{\partial u_1}{\partial x} + \frac{\partial u_2}{\partial x} + \frac{\partial v_1}{\partial y} + \frac{\partial v_2}{\partial y} = 0 \tag{5}$$

Here we put the following boundary condition of v_1 at $y=0$

$$v_1 = 0 \qquad \text{at } y=0 \tag{6}$$

and so $$\frac{\partial v_1}{\partial t} = \frac{\partial v_1}{\partial x} = 0 \qquad \text{at } y=0 \tag{7}$$

Kinematical boundary condition at surface is

$$\frac{\partial \eta}{\partial t} + (u_0 + u_1 + u_2)\frac{\partial \eta}{\partial x} = v_1 + v_2 \qquad \text{at } y = \eta \tag{8}$$

This is linearized as to surface wave, and using (6)

$$\frac{\partial \eta}{\partial t} + (u_0 + u_1)\frac{\partial \eta}{\partial x} = v_2 \qquad \text{at } y=0 \tag{9}$$

Dynamical boundary condition at surface is

$$\frac{\partial p}{\partial t} + u_0\frac{\partial p}{\partial x} + u_1\frac{\partial p}{\partial x} + u_2\frac{\partial p}{\partial x} + v_1\frac{\partial p}{\partial y} + v_2\frac{\partial p}{\partial y} = 0 \qquad \text{at } y = \eta \tag{10}$$

Multiplying (3) by u_2, and linearizing as to u_2, v_2, (11) is obtained

$$u_2\frac{\partial u_1}{\partial t} + (u_0 + u_1)u_2\frac{\partial u_1}{\partial x} + v_1 u_2\frac{\partial u_1}{\partial y} = -\frac{1}{\rho}u_2\frac{\partial p}{\partial x} \tag{11}$$

Multiplying (4) by v_2 and linearizing as to u_2, v_2, (12) is obtained

$$v_2\frac{\partial v_1}{\partial t} + (u_0 + u_1)v_2\frac{\partial v_1}{\partial x} + v_1 v_2\frac{\partial v_1}{\partial y} = -v_2 g - \frac{1}{\rho}v_2\frac{\partial p}{\partial y} \tag{12}$$

Inserting (11), (12) into (10),

$$\frac{\partial p}{\partial t} + u_0\frac{\partial p}{\partial x} + u_1\frac{\partial p}{\partial x} + v_1\frac{\partial p}{\partial y} - \rho u_2\frac{\partial u_1}{\partial t} - \rho(u_0 + u_1)u_2\frac{\partial u_1}{\partial x} - \rho v_1 u_2\frac{\partial u_1}{\partial y} - \rho v_2\frac{\partial v_1}{\partial t} - \rho(u_0 + u_1)v_2\frac{\partial v_1}{\partial x} - \rho v_1 v_2\frac{\partial v_1}{\partial y} - \rho v_2 g = 0 \qquad \text{at } y=0 \tag{13}$$

Using (6) and (7), (13) is simplified as

$$\frac{\partial p}{\partial t} + u_0\frac{\partial p}{\partial x} + u_1\frac{\partial p}{\partial x} - \rho u_2\frac{\partial u_1}{\partial t} - \rho(u_0+u_1)u_2\frac{\partial u_1}{\partial x}$$
$$-\rho v_2 g = 0 \qquad \text{at } y=0 \quad (14)$$

We use stream functions ψ_1 , ψ_2 and difine them as

$$u_1 = -\frac{\partial \psi_1}{\partial y}\ , \ u_2 = -\frac{\partial \psi_2}{\partial y}\ , \ v_1 = \frac{\partial \psi_1}{\partial x}\ , \ v_2 = \frac{\partial \psi_2}{\partial x} \qquad (15)$$

The equation of continuity (5) is clearly satisfied by (15). The vorticity of vortex motion is

$$\zeta_1 = \frac{\partial v_1}{\partial x} - \frac{\partial u_1}{\partial y} = \left(\frac{\partial^2}{\partial x^2} + \frac{\partial^2}{\partial y^2}\right)\psi_1 \qquad (16)$$

The vorticity of surface wave is

$$\zeta_2 = \frac{\partial v_2}{\partial x} - \frac{\partial u_2}{\partial y} = \left(\frac{\partial^2}{\partial x^2} + \frac{\partial^2}{\partial y^2}\right)\psi_2 \qquad (17)$$

If surface wave does not exist, it becomes $\psi_2 = 0$ and in the present inviscid condition

$$\frac{\partial}{\partial t}\left\{\frac{\partial^2\psi_1}{\partial x^2} + \frac{\partial^2\psi_1}{\partial y^2}\right\} + \left(u_0 - \frac{\partial \psi_1}{\partial y}\right)\frac{\partial}{\partial x}\left\{\frac{\partial^2\psi_1}{\partial x^2} + \frac{\partial^2\psi_1}{\partial y^2}\right\}$$
$$+ \frac{\partial \psi_1}{\partial x}\frac{\partial}{\partial y}\left\{\frac{\partial^2\psi_1}{\partial x^2} + \frac{\partial^2\psi_1}{\partial y^2}\right\} = 0 \qquad (18)$$

If ψ_2 exists and it is a function of x, y, t, we cannot deduce (18) from the motion of $\psi_1 + \psi_2$, and we assume that the condition (18) is maintained even in this case. In other words, we assume that the vorticity (16) of vortex motion is steady and it is not influenced by the existence of surface wave. From (3), (4), eliminating pressure p and using ψ_1 , ψ_2 of (15) we obtain the equation concerned to the vorticity of the motion of $\psi_1 + \psi_2$. Subtracting (18) from the equation, we have

$$\frac{\partial}{\partial t}\left(\frac{\partial^2\psi_2}{\partial x^2} + \frac{\partial^2\psi_2}{\partial y^2}\right) + \left(u_0 - \frac{\partial \psi_1}{\partial y}\right)\frac{\partial}{\partial x}\left(\frac{\partial^2\psi_2}{\partial x^2} + \frac{\partial^2\psi_2}{\partial y^2}\right)$$
$$+ \frac{\partial \psi_1}{\partial x}\frac{\partial}{\partial y}\left(\frac{\partial^2\psi_2}{\partial x^2} + \frac{\partial^2\psi_2}{\partial y^2}\right) - \frac{\partial}{\partial x}\left(\frac{\partial^2\psi_1}{\partial x^2} + \frac{\partial^2\psi_1}{\partial y^2}\right)\cdot\frac{\partial \psi_2}{\partial y}$$
$$+ \frac{\partial}{\partial y}\left(\frac{\partial^2\psi_1}{\partial x^2} + \frac{\partial^2\psi_1}{\partial y^2}\right)\cdot\frac{\partial \psi_2}{\partial x} = 0 \qquad (19)$$

Here we suppose the primary surface wave and its period, length and celerity are given by T_2, L_2 and C_2 ($L_2 = C_2T_2$) and stillmore the length L_1 is taken as a representative length of ψ_1 . By making use of these representative values, we set the following dimensionless values. They are $\psi_1 = C_2L_1\psi_1'$, $\psi_2 = C_2L_2\psi_2'$, $\eta = L_2\eta'$, $p = L_2\rho g p'$, $t = T_2t'$, $x = L_2x'$, $y = L_2y'$ and $u_0 = C_2u_0'$.

Using these values, equation (19) and surface conditions (9) and (14) are transformed to dimensionless.

$$\frac{\partial}{\partial t'}\left(\frac{\partial^2\psi_2'}{\partial x'^2}+\frac{\partial^2\psi_2'}{\partial y'^2}\right)+\left(u_0'-\frac{L_1}{L_2}\frac{\partial\psi_1'}{\partial y'}\right)\frac{\partial}{\partial x'}\left(\frac{\partial^2\psi_2'}{\partial x'^2}+\frac{\partial^2\psi_2'}{\partial y'^2}\right)$$
$$+\frac{L_1}{L_2}\frac{\partial\psi_1'}{\partial x'}\frac{\partial}{\partial y'}\left(\frac{\partial^2\psi_2'}{\partial x'^2}+\frac{\partial^2\psi_2'}{\partial y'^2}\right)-\frac{L_1}{L_2}\frac{\partial}{\partial x'}\left(\frac{\partial^2\psi_1'}{\partial x'^2}+\frac{\partial^2\psi_1'}{\partial y'^2}\right)\cdot\frac{\partial\psi_2'}{\partial y'}$$
$$+\frac{L_1}{L_2}\frac{\partial}{\partial y'}\left(\frac{\partial^2\psi_1'}{\partial x'^2}+\frac{\partial^2\psi_1'}{\partial y'^2}\right)\cdot\frac{\partial\psi_2'}{\partial x'}=0 \qquad (20)$$

$$\frac{\partial\eta'}{\partial t'}+\left(u_0'-\frac{L_1}{L_2}\frac{\partial\psi_1'}{\partial y'}\right)\frac{\partial\eta'}{\partial x'}=\frac{\partial\psi_2'}{\partial x'} \qquad \text{at } y'=0 \quad (21)$$

$$g\frac{\partial p'}{\partial t'}+u_0'g\frac{\partial p'}{\partial x'}-\frac{L_1}{L_2}g\frac{\partial\psi_1'}{\partial y'}\frac{\partial p'}{\partial x'}-\frac{L_1}{L_2}\frac{C_2}{T_2}\frac{\partial\psi_2'}{\partial y'}\frac{\partial^2\psi_1'}{\partial y'\partial t'}$$
$$-\frac{C_2}{T_2}\left(u_0'-\frac{L_1}{L_2}\frac{\partial\psi_1'}{\partial y'}\right)\frac{\partial\psi_2'}{\partial y'}\frac{L_1}{L_2}\frac{\partial^2\psi_1'}{\partial x'\partial y'}-g\frac{\partial\psi_2'}{\partial x'}=0 \qquad \text{at } y'=0 \quad (22)$$

We put $L_1/L_2=\alpha$, $C_2/T_2=\beta$, and $\beta/g=\gamma$ has clearly order of 10^0, but α can be taken arbitrary. Here we consider the case in which L_1 is fairly small compared with L_2, and so $\alpha<1$. We use the method of perturbation concerned to α. ψ_2', η', p' can be expanded as

$$\left.\begin{aligned}\psi_2'&=\psi_{20}'+\alpha\psi_{21}'+\alpha^2\psi_{22}'+\alpha^3\psi_{23}'+\cdots\\ \eta'&=\eta_0'+\alpha\eta_1'+\alpha^2\eta_2'+\alpha^3\eta_3'+\cdots\\ p'&=p_0'+\alpha p_1'+\alpha^2 p_2'+\alpha^3 p_3'+\cdots\end{aligned}\right\} \qquad (23)$$

Inserting (23) into (20), (21) and (22) and comparing terms of same power of α, the following perturbed equations may be obtained.

From (20)

$$\frac{\partial}{\partial t'}\nabla^2\psi_{20}'+u_0'\frac{\partial}{\partial x'}\nabla^2\psi_{20}'=0 \qquad (24\text{-}1)$$

$$\frac{\partial}{\partial t'}\nabla^2\psi_{21}'+u_0'\frac{\partial}{\partial x'}\nabla^2\psi_{21}'-\frac{\partial\psi_1'}{\partial y'}\frac{\partial}{\partial x'}\nabla^2\psi_{20}'+\frac{\partial\psi_1'}{\partial x'}\frac{\partial}{\partial y'}\nabla^2\psi_{20}'$$
$$-\frac{\partial}{\partial x'}\nabla^2\psi_1'\cdot\frac{\partial\psi_{20}'}{\partial y'}+\frac{\partial}{\partial y'}\nabla^2\psi_1'\cdot\frac{\partial\psi_{20}'}{\partial x'}=0 \qquad (24\text{-}2)$$

$$\frac{\partial}{\partial t'}\nabla^2\psi_{22}'+u_0'\frac{\partial}{\partial x'}\nabla^2\psi_{22}'-\frac{\partial\psi_1'}{\partial y'}\frac{\partial}{\partial x'}\nabla^2\psi_{21}'+\frac{\partial\psi_1'}{\partial x'}\frac{\partial}{\partial y'}\nabla^2\psi_{21}'$$
$$-\frac{\partial}{\partial x'}\nabla^2\psi_1'\cdot\frac{\partial\psi_{21}'}{\partial y'}+\frac{\partial}{\partial y'}\nabla^2\psi_1'\cdot\frac{\partial\psi_{21}'}{\partial x'}=0 \qquad (24\text{-}3)$$

Here $\nabla^2=\dfrac{\partial^2}{\partial x'^2}+\dfrac{\partial^2}{\partial y'^2}$

From (21), at $y'=0$

$$\frac{\partial\eta_0'}{\partial t'}+u_0'\frac{\partial\eta_0'}{\partial x'}=\frac{\partial\psi_{20}'}{\partial x'} \qquad (25\text{-}1)$$

$$\frac{\partial \eta_1'}{\partial t'} + u_0' \frac{\partial \eta_1'}{\partial x'} - \frac{\partial \psi_1'}{\partial y'} \frac{\partial \eta_0'}{\partial x'} = \frac{\partial \psi_{21}'}{\partial x'} \tag{25-2}$$

$$\frac{\partial \eta_2'}{\partial t'} + u_0' \frac{\partial \eta_2'}{\partial x'} - \frac{\partial \psi_1'}{\partial y'} \frac{\partial \eta_1'}{\partial x'} = \frac{\partial \psi_{22}'}{\partial x'} \tag{25-3}$$

From (22), at $y'=0$

$$\frac{\partial p_0'}{\partial t'} + u_0' \frac{\partial p_0'}{\partial x'} - \frac{\partial \psi_{20}'}{\partial x'} = 0 \tag{26-1}$$

$$\frac{\partial p_1'}{\partial t'} + u_0' \frac{\partial p_1'}{\partial x'} - \frac{\partial \psi_1'}{\partial y'} \frac{\partial p_0'}{\partial x'} - \gamma \frac{\partial^2 \psi_1'}{\partial y' \partial t'} \frac{\partial \psi_{20}'}{\partial y'} - \gamma u_0' \frac{\partial \psi_{20}'}{\partial y'} \frac{\partial^2 \psi_1'}{\partial x' \partial y'} - \frac{\partial \psi_{21}'}{\partial x'} = 0 \tag{26-2}$$

$$\frac{\partial p_2'}{\partial t'} + u_0' \frac{\partial p_2'}{\partial x'} - \frac{\partial \psi_1'}{\partial y'} \frac{\partial p_1'}{\partial x'} - \gamma \frac{\partial^2 \psi_1'}{\partial y' \partial t'} \frac{\partial \psi_{21}'}{\partial y'} - \gamma u_0' \frac{\partial \psi_{21}'}{\partial y'} \frac{\partial^2 \psi_1'}{\partial x' \partial y'} + \gamma \frac{\partial \psi_1'}{\partial y'} \frac{\partial \psi_{20}'}{\partial y'} - \frac{\partial \psi_{22}'}{\partial x'} = 0 \tag{26-3}$$

Besides these perturbed equations, we need equation of motion in x (or y) direction to determine p', and we may use the equation of motion in x direction. Its perturbed form is

$$-\frac{\partial^2 \psi_{20}'}{\partial t' \partial y'} - u_0' \frac{\partial^2 \psi_{20}'}{\partial x' \partial y'} + \frac{1}{\gamma} \frac{\partial p_0'}{\partial x'} = 0 \tag{27-1}$$

$$-\frac{\partial^2 \psi_1'}{\partial t' \partial y'} - \frac{\partial^2 \psi_{21}'}{\partial t' \partial y'} - u_0' \frac{\partial^2 \psi_1'}{\partial x' \partial y'} + \frac{\partial \psi_{20}'}{\partial y'} \frac{\partial^2 \psi_1'}{\partial x' \partial y'} - u_0' \frac{\partial^2 \psi_{21}'}{\partial x' \partial y'} + \frac{\partial \psi_1'}{\partial y'} \frac{\partial^2 \psi_{20}'}{\partial x' \partial y'} - \frac{\partial \psi_{20}'}{\partial x'} \frac{\partial^2 \psi_1'}{\partial y'^2} - \frac{\partial \psi_1'}{\partial x'} \frac{\partial^2 \psi_{20}'}{\partial y'^2} + \frac{1}{\gamma} \frac{\partial p_1'}{\partial x'} = 0 \tag{27-2}$$

$$-\frac{\partial^2 \psi_{22}'}{\partial t' \partial y'} + \frac{\partial \psi_1'}{\partial y'} \frac{\partial^2 \psi_1'}{\partial x' \partial y'} + \frac{\partial \psi_{21}'}{\partial y'} \frac{\partial^2 \psi_1'}{\partial x' \partial y'} - u_0' \frac{\partial^2 \psi_{22}'}{\partial x' \partial y'} + \frac{\partial \psi_1'}{\partial y'} \frac{\partial^2 \psi_{21}'}{\partial x' \partial y'} - \frac{\partial \psi_1'}{\partial x'} \frac{\partial^2 \psi_1'}{\partial y'^2} - \frac{\partial \psi_{21}'}{\partial x'} \frac{\partial^2 \psi_1'}{\partial y'^2} - \frac{\partial \psi_1'}{\partial x'} \frac{\partial^2 \psi_{21}'}{\partial y'^2} + \frac{1}{\gamma} \frac{\partial p_2'}{\partial x'} = 0 \tag{27-3}$$

By making use of (24), (25), (26), (27), we may proceed to higher order approximation of ψ_2' for given ψ_1'.

THE SURFACE WAVE IN A TWO-DIMENSIONAL VORTEX LAYER

THE FIRST AND SECOND APPROXIMATION

(1) The first approximation

We put ψ_{20}', η_0', p_0' as follows.

$$\psi_{20}' = \varphi_{20}'(y')\, e^{i2\pi(x'-t')} \tag{28-1}$$

$$\eta_0' = A_0'\, e^{i2\pi(x'-t')} \tag{28-2}$$

$$p_0' = D_0'(y')\, e^{i2\pi(x'-t')} - y' \tag{28-3}$$

From (28-1)

$$\nabla^2\psi_{20}' = \left\{-4\pi^2\varphi_{20}'(y') + \frac{\partial^2\varphi_{20}'(y')}{\partial y'^2}\right\} e^{i2\pi(x'-t')}$$

Inserting this into (24-1)

$$\left\{-4\pi^2\varphi_{20}'(y') + \frac{\partial^2\varphi_{20}'(y')}{\partial y'^2}\right\}(u_0' - 1) = 0$$

In general, u_0' -1 is not zero, and so

$$\frac{\partial^2\varphi_{20}'(y')}{\partial y'^2} - 4\pi^2\varphi_{20}'(y') = 0 \tag{29}$$

Here $\psi_{20}' \to 0$ is physically demanded at $y' \to -\infty$.
From (29)

$$\varphi_{20}'(y') = B_{20}'\, e^{2\pi y'} \tag{30}$$

From (29) $\nabla^2\psi_{20}' = 0$. This means the motion given by ψ_{20}' is irrotational. Then inserting (28-2) and (30) into surface condition (25-1)

$$B_{20}' = A_0'(u_0' - 1) \tag{31}$$

$D_0'(y')$ in (28-3) may be determined by (27-1)

$$D_0'(y') = 2\pi\gamma A_0'(u_0' - 1)^2\, e^{2\pi y'} \tag{32}$$

γ is determined by the surface dynamical condition (26-1).

$$\gamma = \frac{1}{2\pi(u_0' - 1)^2} \tag{33}$$

By these computations, (28-1), (28-2), (28-3) may be rewritten

$$\psi_{20}' = A_0'(u_0' - 1)\, e^{2\pi y' + i2\pi(x'-t')} \tag{34-1}$$

$$\eta_0' = A_0' e^{i2\pi(x'-t')} \tag{34-2}$$

$$p_0' = A_0' e^{2\pi y' + i2\pi(x'-t')} - y' \tag{34-3}$$

We use the real part of these expressions.

(2) The second approximation

We select the simplest expression of ψ_1, which satisfies both the vorticity equation (18) and surface conditions (6), (7). Naming such ψ_1 as ψ_{10}, we put its representative component as follows.

$$\psi_{10} = -\frac{u_{100}}{k_1}\cos k_3(x-u_0t)\sin k_3 y \tag{35}$$

Here $k_1 = \frac{2\pi}{L_1}$, $k_3 = \frac{2\pi}{L_3}$, $\frac{L_1}{L_2} = \alpha$, $\frac{L_3}{L_2} = \alpha'$

and so

$$u_{10} = \frac{u_{100}}{k_1} k_3 \cos k_3(x-u_0t)\cos k_3 y$$

$$v_{10} = \frac{u_{100}}{k_1} k_3 \sin k_3(x-u_0t)\sin k_3 y$$

$$\zeta_{10} = \frac{\partial v_{10}}{\partial x} - \frac{\partial u_{10}}{\partial y} = \frac{2u_{100}}{k_1} k_3^2 \cos k_3(x-u_0t)\sin k_3 y$$

Therefore ψ_{10} satisfies (18).

ψ_{10} is transformed to

$$\psi_{10} = -\frac{C_2 L_1 u_{100}'}{2\pi}\cos\frac{2\pi}{\frac{L_3}{L_2}}(x'-u_0't')\sin\frac{2\pi}{\frac{L_3}{L_2}}y'$$

and its dimensionless form is

$$\psi_{10}' = -\frac{u_{100}'}{2\pi}\cos\frac{2\pi}{\alpha'}(x'-u_0't')\sin\frac{2\pi}{\alpha'}y'$$

$$= -\frac{u_{100}'}{2\pi}\cos k'(x'-u_0't')\sin k'y'$$

$$\left(\frac{2\pi}{\alpha'} = k'\right)$$

The general expression of ψ_{10}' is

$$\psi_{10}' = \int_{-\infty}^{\infty} -\frac{du_{100}'(k')}{8\pi i}(\operatorname{sgn} k')\, e^{-ik'u_0't'} e^{ik'(x'+y')}$$

$$+\int_{-\infty}^{\infty}\frac{du_{100}'(k')}{8\pi i}(\operatorname{sgn} k')\, e^{-ik'u_0't'} e^{ik'(x'-y')} \tag{36}$$

Here uncorrelated increment $d\mathcal{U}'_{100}(k')$ satisfies $d\mathcal{U}'_{100}(k') = \overline{d\mathcal{U}'_{100}(-k')}$ (bar indicates the complex conjugate), and its argument is related to x' variable. The form of spectrum given by ψ'_{10} must not be inconsistent with the method of perturbed derivation in the preceding paragraph.

From (36)

$$u'_{10} = -\frac{\partial \psi'_{10}}{\partial y'} = \int_{-\infty}^{\infty} \frac{d\mathcal{U}'_{100}(k')}{8\pi} k' (\operatorname{sgn} k') e^{-ik'U'_0 t'} e^{ik'(x'+y')} + \int_{-\infty}^{\infty} \frac{d\mathcal{U}'_{100}(k')}{8\pi} k' (\operatorname{sgn} k') e^{-ik'U'_0 t'} e^{ik'(x'-y')} \tag{37}$$

$$v'_{10} = \frac{\partial \psi'_{10}}{\partial x'} = \int_{-\infty}^{\infty} -\frac{d\mathcal{U}'_{100}(k')}{8\pi} k' (\operatorname{sgn} k') e^{-ik'U'_0 t'} e^{ik'(x'+y')} + \int_{-\infty}^{\infty} \frac{d\mathcal{U}'_{100}(k')}{8\pi} k' (\operatorname{sgn} k') e^{-ik'U'_0 t'} e^{ik'(x'-y')} \tag{38}$$

$$\zeta'_{10} = \nabla^2 \psi'_{10} = \int_{-\infty}^{\infty} \frac{d\mathcal{U}'_{100}(k')}{4\pi i} k'^2 (\operatorname{sgn} k') e^{-ik'U'_0 t'} e^{ik'(x'+y')} - \int_{-\infty}^{\infty} \frac{d\mathcal{U}'_{100}(k')}{4\pi i} k'^2 (\operatorname{sgn} k') e^{-ik'U'_0 t'} e^{ik'(x'-y')} \tag{39}$$

(putting $2\pi = k'_0 (k'_0 > 0)$)

From (34-1), (34-2) and (34-3)

$$\psi'_{20} = \frac{A'_0 (U'_0 - 1)}{2} e^{k'_0 y'} \left\{ e^{ik'_0 (x'-t')} + e^{-ik'_0 (x'-t')} \right\} \tag{40}$$

$$\eta'_0 = \frac{A'_0}{2} \left\{ e^{ik'_0 (x'-t')} + e^{-ik'_0 (x'-t')} \right\} \tag{41}$$

$$p'_0 = \frac{A'_0}{2} e^{k'_0 y'} \left\{ e^{ik'_0 (x'-t')} + e^{-ik'_0 (x'-t')} \right\} - y' \tag{42}$$

By making use of (24-2) and $\nabla^2 \psi'_{20} = 0$,

$$\frac{\partial}{\partial t'} \nabla^2 \psi'_{21} + U'_0 \frac{\partial}{\partial x'} \nabla^2 \psi'_{21} - \frac{\partial}{\partial x'} \nabla^2 \psi'_1 \cdot \frac{\partial \psi'_{20}}{\partial y'} + \frac{\partial}{\partial y'} \nabla^2 \psi'_1 \cdot \frac{\partial \psi'_{20}}{\partial x'} = 0 \tag{43}$$

Inserting $\nabla^2 \psi'_1$, ψ'_{20} given by (39), (40) into (43), $\nabla^2 \psi'_{21} \left(= \zeta'_{21} \right)$ may be expressed by

$$\zeta'_{21} = \int_{-\infty}^{\infty} \frac{\sqrt{2} A'_0 d\mathcal{U}'_{100}(k') (\operatorname{sgn} k')}{8\pi} k'^3 \left[e^{i\left(\frac{5}{4}\pi + 2n\pi\right)} e^{(k'_0 + ik')y'} \cdot e^{i(k'_0 + k')x'} e^{-i(k'_0 + k'U'_0)t'} + e^{i\left(\frac{3}{4}\pi + 2n\pi\right)} e^{(k'_0 + ik')y'} \right.$$

$$\cdot e^{-i(k_0'-k')x'} e^{-i(k'u_0'-k_0')t'} + e^{i(\frac{3}{4}\pi+2n\pi)} e^{(k_0'-ik')y'}$$
$$\cdot e^{i(k_0'+k')x'} e^{-i(k_0'+k'u_0')t'} + e^{i(\frac{5}{4}\pi+2n\pi)} e^{(k_0'-ik')y'}$$
$$\cdot e^{-i(k_0'-k')x'} e^{-i(k'u_0'-k_0')t'}\Big] \qquad (44)$$

Homogeneous equation $\nabla^2\psi_{21}' = 0$ has a following form of solution

$$\psi_{21}'^{(0)} = \sum A_{\beta'}'(t')\, e^{\pm i\beta'x'+\beta'y'} \qquad (45)$$

here $\mathbb{R}(\beta') > 0$,

The general solution of ψ_{21}' is

$$\psi_{21}' = \sum_{\mathbb{R}(\beta')>0} A_{\beta'}'(t')\, e^{\pm i\beta'x'+\beta'y'}$$
$$+\int_{-\infty}^{\infty} \frac{\sqrt{2}\,A_0'\,d\mathcal{U}_{100}'(k')(\operatorname{sgn}k')}{16\pi} k'^2\Big[\frac{1}{ik_0'-k'-k_0'} e^{i(\frac{5}{4}\pi+2n\pi)}$$
$$\cdot e^{(k_0'+ik')y'} e^{i(k_0'+k')x'} e^{-i(k_0'+k'u_0')t'} + \frac{1}{ik_0'-k'+k_0'}$$
$$\cdot e^{i(\frac{3}{4}\pi+2n\pi)} e^{(k_0'+ik')y'} e^{-i(k_0'-k')x'} e^{-i(k'u_0'-k_0')t'}$$
$$+\frac{1}{-ik_0'-k'-k_0'} e^{i(\frac{3}{4}\pi+2n\pi)} e^{(k_0'-ik')y'} e^{i(k_0'+k')x'}$$
$$\cdot e^{-i(k_0'+k'u_0')t'} + \frac{1}{-ik_0'-k'+k_0'} e^{i(\frac{5}{4}\pi+2n\pi)}$$
$$\cdot e^{(k_0'-ik')y'} e^{-i(k_0'-k')x'} e^{-i(k'u_0'-k_0')t'}\Big] \qquad (46)$$

Using (46), p_1' may be expressed from (27-2).

$$p_1' = \gamma \sum_{\mathbb{R}(\beta')>0} \Big\{\frac{1}{\pm i}\frac{\partial A_{\beta'}'(t')}{\partial t'} + \beta'u_0' A_{\beta'}'(t')\Big\} e^{\pm i\beta'x'+\beta'y'}$$
$$+\int_{-\infty}^{\infty} \gamma \frac{A_0'\,d\mathcal{U}_{100}'(k')(\operatorname{sgn}k')}{8\pi}(u_0'-1)k'k_0'^2\Big[\frac{-1}{ik_0'-k'-k_0'} e^{i(k_0'+k')x'}$$
$$\cdot e^{(k_0'+ik')y'} e^{-i(k'u_0'+k_0')t'} + \frac{1}{ik_0'-k'+k_0'} e^{i(k'-k_0')x'} e^{(k_0'+ik')y'}$$
$$\cdot e^{-i(k'u_0'-k_0')t'} - \frac{1}{-ik_0'-k'-k_0'} e^{i(k_0'+k')x'} e^{(k_0'-ik')y'} e^{-i(k'u_0'+k_0')t'}$$
$$+\frac{1}{-ik_0'-k'+k_0'} e^{i(k'-k_0')x'} e^{(k_0'-ik')y'} e^{-i(k'u_0'-k_0')t'}\Big] \qquad (47)$$

$A'_{\beta'}(t')$ is determined by the surface dynamical condition (26-2), when we insert ψ'_{21} , p'_1 represented by (46), (47) into (26-2). After some computations, the final forms of ψ'_{21} , p'_1 are

$$\psi'_{21} = \int_{-\infty}^{\infty} A_1(k') e^{i(k'_0+k')x'} e^{|k'_0+k'|y'} e^{-i(k'u'_0+k'_0)t'}$$
$$+ \int_{-\infty}^{\infty} A_2(k') e^{i(k'-k'_0)x'} e^{|k'-k'_0|y'} e^{-i(k'u'_0-k'_0)t'} + \int_{-\infty}^{\infty} \frac{A'_0 du'_{100}(k')(\operatorname{sgn} k')}{16\pi} k'^2$$
$$\cdot \left[\frac{-1-i}{ik'_0-k'-k'_0} e^{i(k'_0+k')x'} e^{(k'_0+ik')y'} e^{-i(k'_0+k'u'_0)t'} + \frac{-1+i}{ik'_0-k'+k'_0} \right.$$
$$\cdot e^{i(k'-k'_0)x'} e^{(k'_0+ik')y'} e^{-i(k'u'_0-k'_0)t'} + \frac{-1+i}{-ik'_0-k'-k'_0} e^{i(k'_0+k')x'}$$
$$\cdot e^{(k'_0-ik')y'} e^{-i(k'_0+k'u'_0)t'} + \frac{-1-i}{-ik'_0-k'+k'_0} e^{i(k'-k'_0)x'} e^{(k'_0-ik')y'}$$
$$\left. \cdot e^{-i(k'u'_0-k'_0)t'} \right] \qquad (48)$$

$$p'_1 = -\gamma \int_{-\infty}^{\infty} \left\{ \{\operatorname{sgn}(k'_0+k')\}(k'u'_0+k'_0) - |k'_0+k'|u'_0 \right\} A_1(k')$$
$$\cdot e^{i(k'_0+k')x'} e^{|k'_0+k'|y'} e^{-i(k'u'_0+k'_0)t'}$$
$$- \gamma \int_{-\infty}^{\infty} \left\{ \{\operatorname{sgn}(k'-k'_0)\}(k'u'_0-k'_0) - |k'-k'_0|u'_0 \right\} A_2(k') e^{i(k'-k'_0)x'}$$
$$\cdot e^{|k'-k'_0|y'} e^{-i(k'u'_0-k'_0)t'} + \int_{-\infty}^{\infty} \gamma \frac{A'_0 du'_{100}(k')(\operatorname{sgn} k')}{8\pi} (u'_0-1) k' k'^2_0$$
$$\cdot \left[\frac{-1}{ik'_0-k'-k'_0} e^{i(k'_0+k')x'} e^{(k'_0+ik')y'} e^{-i(k'u'_0+k'_0)t'} \right.$$
$$+ \frac{1}{ik'_0-k'+k'_0} e^{i(k'-k'_0)x'} e^{(k'_0+ik')y'} e^{-i(k'u'_0-k'_0)t'} - \frac{1}{-ik'_0-k'-k'_0}$$
$$\cdot e^{i(k'_0+k')x'} e^{(k'_0-ik')y'} e^{-i(k'u'_0+k'_0)t'} + \frac{1}{-ik'_0-k'+k'_0}$$
$$\left. \cdot e^{i(k'-k'_0)x'} e^{(k'_0-ik')y'} e^{-i(k'u'_0-k'_0)t'} \right] \qquad (49)$$

Here

$$A_1(k')=-\frac{A_0'du_{100}'(k')(\operatorname{sgn}k')}{8\pi}\frac{2\gamma(u_0'-1)^2k'k_0'^3(k'+k_0')+k'(2k_0'^3+2k_0'^2k'-k'^3)}{(2k_0'^2+2k_0'k'+k'^2)\left[\{\operatorname{sgn}(k'+k_0')\}\frac{k_0'^2}{2\pi}-(k_0'+k')\right]} \tag{50}$$

$$A_2(k')=-\frac{A_0'du_{100}'(k')(\operatorname{sgn}k')}{8\pi}\frac{2\gamma(u_0'-1)^2k'k_0'^3(k'-k_0')-k'(2k_0'^3-2k'k_0'^2+k'^3)}{(2k_0'^2-2k_0'k'+k'^2)\left[\{\operatorname{sgn}(k'-k_0')\}\frac{k_0'^2}{2\pi}-(k'-k_0')\right]} \tag{51}$$

The first and the second integrals of (48) indicate the irrotational surface waves which are determined by the surface dynamical condition (26-2), and their celerities are quite different from those derived by usual surface dynamical conditions.

Inserting (48) into (25-2),

$$\eta_1'=\int_{-\infty}^{\infty}\left[\frac{A_0'du_{100}'(k')}{k_0'(u_0'-1)8\pi}(\operatorname{sgn}k')k'\frac{k'^3-2k'k_0'^2-2k_0'^3}{k'^2+2k'k_0'+2k_0'^2}\right.$$

$$\left.+\frac{A_1(k')(k_0'+k')}{k'(u_0'-1)}\right]e^{i(k_0'+k')x'}e^{-i(k'u_0'+k_0')t'}$$

$$-\int_{-\infty}^{\infty}\left[\frac{A_0'du_{100}'(k')}{k_0'(u_0'-1)8\pi}(\operatorname{sgn}k')k'\frac{k'^3-2k'k_0'^2+2k_0'^3}{2k_0'^2-2k_0'k'+k'^2}+\frac{A_2(k')(k'-k_0')}{k_0'(u_0'-1)}\right]$$

$$\cdot e^{i(k'-k_0')x'}e^{-i(k'u_0'-k_0')t'} \tag{52}$$

The expansion of η' in (23) indicates that $\alpha\eta_1'$ may be considered as the approximate expression of surface irregularity of wave profile due to the interaction with vortex motion.

NUMERICAL COMPUTATION OF η_1'

In the two integrals of (52), the first terms show the surface irregularities caused by the direct interaction between primary wave and the vortex motion. The second terms are contributed by the second order dynamical condition of surface. Of cource they are closely connected with each other. Stillmore $|du_{100}'(k')|$ should be sufficiently small when $|k'|$ is large, not to disturb the method of perturbation.

To know the essential property of η_1' in (52), numerical computations are shown in Table-1. We summarize the first term in the first integral of (52) as $A_0'du_{100}'(k')m_1$, the second term in the same integral as $A_0'du_{100}'(k')m_2$, the first term in the second integral of (52) as $A_0'du_{100}'(k')n_1$, and

Table 1

u_0'	k'	m_1	m_2	m_1+m_2	$\frac{m_1}{m_2}$	n_1	n_2	n_1+n_2	$\frac{n_1}{n_2}$
	4π	-0.14286	-0.42857	-0.57143	+0.33333	-2.1429	∞	∞	0
	6π	-1.19748	+0.92437	-0.27311	-1.2955	-4.9286	+8.1429	+3.2143	-0.60526
	10π	-5.45367	+5.84942	+0.39575	-0.93234	-12.2899	+15.2661	+2.9762	-0.80504
	20π	-28.6300	+30.7844	+2.1544	-0.93000	-42.7700	+47.2343	+4.4643	-0.90549
	100π	-857.156	+873.586	+16.430	-0.98118	-928.556	+947.161	+18.605	-0.98036
+0.3	200π	-3500.01	+3534.31	+34.30	-0.99035	-3642.84	+3679.29	+36.45	-0.99010
	-4π	+2.1429	∞	∞	0	+0.14286	+0.42857	+0.57143	+0.33333
	-6π	+4.9286	-8.1429	-3.2143	-0.60526	+1.19748	-0.92437	+0.27311	-1.2955
	-10π	+12.2899	-15.2661	-2.9762	-0.80504	+5.45367	-5.84942	-0.39575	-0.93235
	-20π	+42.7700	-47.2343	-4.4643	-0.90549	+28.6300	-30.7844	-2.1544	-0.93002
	-100π	+928.556	-947.161	-18.605	-0.98036	+857.156	-873.586	-16.430	-0.98119
	-200π	+3642.84	-3679.29	-36.45	-0.99010	+3500.01	-3534.31	-34.30	-0.99030
	4π	-0.07692	-0.23077	-0.30769	+0.33333	-2.15385	∞	∞	0
	6π	-0.64480	+0.49774	-0.14706	-1.2955	-2.65385	+4.38462	+1.7308	-0.60526
	10π	-2.93659	+3.14968	+0.21309	-0.93234	-6.61765	+8.22023	+1.6026	-0.80504
	20π	-15.4162	+16.5762	+1.1600	-0.93000	-23.0300	+25.4338	+2.4038	-0.90549
	100π	-461.546	+470.392	+8.846	-0.98117	-499.992	+510.010	+10.018	-0.98036
-0.3	200π	-1884.63	+1903.09	+18.46	-0.99030	-1961.53	+1981.15	+19.62	-0.99010
	-4π	+1.15385	∞	∞	0	+0.07692	+0.23077	+0.30769	+0.33333
	-6π	+2.65385	-4.38462	-1.7308	-0.60526	+0.64480	-0.49774	+0.14706	-1.2955
	-10π	+6.61765	-8.22023	-1.6026	-0.80504	+2.93659	-3.14968	-0.21309	-0.93235
	-20π	+23.0300	-25.4338	-2.4038	-0.90549	+15.4162	-16.5762	-1.1600	-0.93002
	-100π	+499.992	-510.010	-10.018	-0.98036	+461.546	-470.392	-8.846	-0.98119
	-200π	+1961.53	-1981.15	-19.62	-0.99010	+1884.63	-1903.09	-18.46	-0.99030
	4π	-0.1	-0.3	-0.4	+0.33333	-1.5	∞	∞	0
	6π	-0.83824	+0.64706	-0.19118	-1.2955	-3.45	+5.70	+2.25	-0.60526
	10π	-3.8176	+4.0946	+0.2770	-0.93235	-8.6029	+10.6863	+2.0834	-0.80504
	20π	-20.041	+21.549	+1.508	-0.93002	-29.939	+33.064	+3.125	-0.90549
	100π	-600.01	+611.51	+11.50	-0.98119	-649.99	+663.01	+13.02	-0.98036
$u_0'=0$	200π	-2450.0	+2474.0	+24.0	-0.99030	-2550.0	+2575.5	+25.50	-0.99010
	-4π	+1.5	∞	∞	0	+0.1	+0.3	+0.4	+0.33333
	-6π	+3.45	-5.70	-2.25	-0.60526	+0.83824	-0.64706	+0.19118	-1.2955
	-10π	+8.6029	-10.6863	-2.0834	-0.80504	+3.8176	-4.0946	-0.2770	-0.93235
	-20π	+29.939	-33.064	-3.125	-0.90549	+20.041	-21.549	-1.5080	-0.93002
	-100π	+649.989	-663.013	-13.024	-0.98036	+600.01	-611.51	-11.50	-0.98119
	-200π	+2550.0	-2575.5	-25.50	-0.99010	+2450.0	-2474.0	-24.0	-0.99030

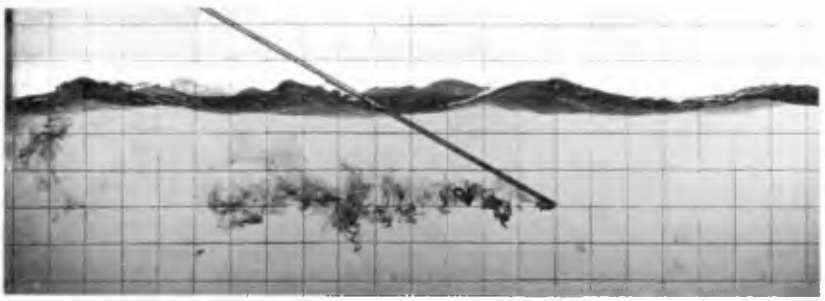

Wind wave in a turbulent flow under direct wind action.
Photo 1

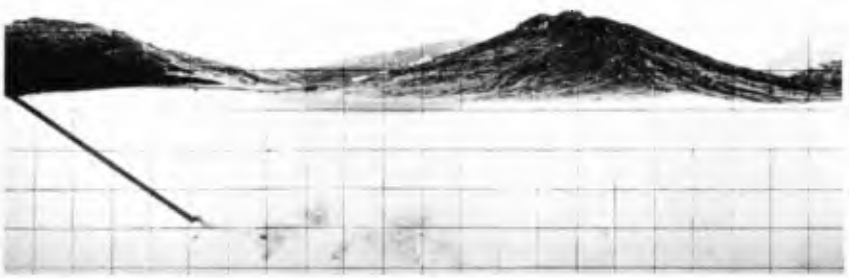

Wind wave in a turbulent flow under direct wind action.
Photo 2

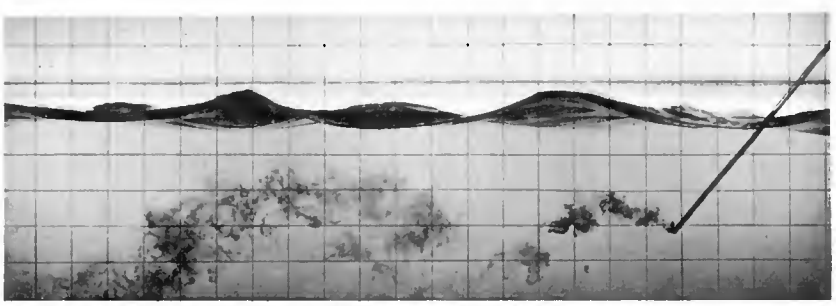

Wind generated wave in a turbulent flow under calm air.
Photo 3

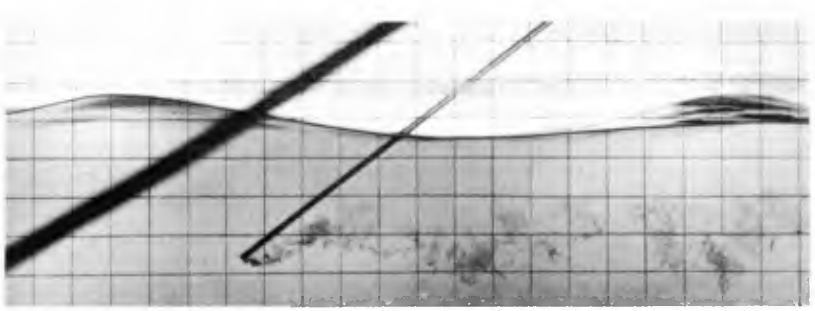

Wind generated wave in a turbulent flow under calm air.
Photo 4

the second term in the same integral as $A_0' d u_{100}'(k') n_2$. In the table the numerical values of m_1 , m_2 , n_1 and n_2 for k' ($|k'| > k_0'$) are shown. We take the numerical value of u_0' as 0.3, 0, −0.3, and this selection may cover the proper range of u_0' . The table shows η_1' is a real process and m_2, n_2 each offsets m_1, n_1 except cases of $k' = 4\pi, -4\pi$. Refering to the expression ψ_{21}' in (48), $k' = 4\pi (= 2k_0')$ and $-4\pi (= -2k_0')$ are very special cases, and we follow the numerical cases of $|k'| \geqq 6\pi$.

PHOTOGRAPHIC EXAMPLES

From the above-mentioned computations we generally expect that surface waves have almost smooth surface even if they coexist with the vortex motion of moderate strength. This is caused by the condition of constant pressure at the direct wave surface. If the surface pressure is disturbed by wind in the different condition, the surface profile of waves may be also different. To examine this problem experimentally, the surface profiles of wind generated waves in turbulent flows are photographed. Photo-1, 2, 3, 4 are their examples. Photo-1, 2 show the waves under direct wind action. (Averaged wind velocity 1,100cm/sec.) In Photo-1, the direction of water current consists with the direction of wave propagation and in Photo-2, they are opposite each other. We can observe surface irregularities. To understand properly these irregularities, of course, the term including the effect of surface tension should be considered in the surface dynamical condition. Photo-3, 4 show the waves under calm air. In Photo-3, the direction of water current coincides with the direction of wave propagation and in Photo-4 they are inverse. The velocity of water flow is from 13cm/sec to 26cm/sec, and its turbulent condition is shown by dye injected to water. The surfaces of waves are very smooth.

REFERENCES

Phillips, O. M. (1959). The scattering of gravity waves by turbulence: Journal of Fluid Mechanics, Vol. 5.

Phillips, O. M. (1961). A note on the turbulence generated by gravity waves: Journal of Geophysical Research, Vol. 66.

CHAPTER 4

AN APPROXIMATION OF THE WAVE RUN-UP FREQUENCY DISTRIBUTION

By

Thorndike Saville, Jr.
U.S. Army Beach Erosion Board
Washington, D. C.

The distribution of wave steepness (H/T^2) for fully developed sea is obtained from Bretschneider's joint distribution of wave height and wave period. This steepness distribution is used with standard wave run-up curves to develop a frequency curve of wave run-up. Use of this run-up distribution curve will permit more accurate estimation of the variability in wave run-up for design cases, and particularly the percent of time in which run-ups will exceed that predicted for the significant wave. The distribution may also be used with normal overtopping procedures to determine more accurate estimates of overtopping quantities.

Wave run-up may be defined as the vertical height above mean water level to which water from a breaking wave will rise on a structure face. Accurate design data on the height of wave run-up is needed for determination of design crest elevations of protective structures subject to wave action such as seawalls, beach fills, surge barriers, and dams. Such structures are normally designed to prevent wave overtopping with consequent flooding on the landward side and, if of an earth type, possible failure by rearface erosion.

Because of the importance of wave run-up elevations in determining structure heights and freeboards, a great deal of work has been done in the past six years in an attempt to relate wave run-up to incident wave characteristics, and slope or structure characteristics. Compilations based largely on laboratory experimental work have been made and have resulted in curves similar to those shown in Figure 1 which is reprinted[1]* from the U. S. Beach Erosion Board Technical Report No. 4. Such curves most frequently have related the dimensionless ratio of relative run-up (R/H_o) to incident wave steepness in deep water (H_o/T^2), as a function of structure type or slope. (H_o is the equivalent deep water wave height.) The curves shown in Figure 1 are of this type, and pertain to structures having a depth of water greater than three wave heights at the toe of the structure; this depth limitation in effect means that the wave breaks directly on the structure. The curves shown in Figure 1 are a portion of a set of five separate figures, covering different structure depths (d/H_o). All are published in Beach Erosion Board Technical Report Number 4.[1]

These curves were derived primarily from small scale laboratory tests. Further laboratory tests with much larger waves (heights two to five feet) have shown that a scale effect exists for some conditions.

*Numbers in parentheses indicate references listed at end of report.

AN APPROXIMATION OF THE WAVE RUN-UP FREQUENCY DISTRIBUTION

TABLE I

JOINT DISTRIBUTION OF H AND T FOR ZERO CORRELATION
Number of Waves Per 1,000 Consecutive Waves for Various Ranges in Height and Period

Range in Relative Height $H/\overline{H}$	RANGE IN RELATIVE PERIOD $T/\overline{T}$											
	0-0.2	0.2-0.4	0.4-0.6	0.6-0.8	0.8-1.0	1.0-1.2	1.2-1.4	1.4-1.6	1.6-1.8	1.8-2.0	0-2.0	Cumulative
0-0.2	0.03	0.50	2.05	4.86	7.68	8.09	5.31	1.92	0.34	0.03	30.81	30.81
0.2-0.4	0.10	1.41	5.81	13.78	21.76	23.92	15.05	5.44	0.98	0.07	88.32	119.13
0.4-0.6	0.14	2.06	8.54	20.23	31.95	33.65	22.10	7.99	1.44	0.11	128.21	247.34
0.6-0.8	0.16	2.40	9.91	23.48	37.08	39.06	25.65	9.27	1.67	0.12	148.80	396.14
0.8-1.0	0.16	2.40	9.92	23.51	37.13	39.11	25.69	9.28	1.67	0.12	148.99	545.13
1.0-1.2	0.15	2.14	8.87	21.02	33.19	34.97	22.96	8.30	1.49	0.11	133.20	678.33
1.2-1.4	0.12	1.74	7.21	17.07	26.96	28.40	18.65	6.74	1.21	0.09	108.19	786.52
1.4-1.6	0.09	1.30	5.37	12.72	20.09	21.16	13.90	5.02	0.90	0.07	80.62	867.14
1.6-1.8	0.06	0.90	3.72	8.82	13.93	14.67	9.64	3.48	0.63	0.05	55.90	923.04
1.8-2.0	0.03	0.48	1.99	4.72	7.45	7.85	5.15	1.86	0.33	0.03	29.89	952.93
2.0-2.2	0.03	0.42	1.72	4.09	6.45	6.80	4.47	1.61	0.29	0.02	25.90	978.83
2.2-2.4	0.01	0.18	0.76	1.80	2.84	2.99	1.97	0.71	0.13	0.01	11.40	990.23
2.4-2.6	0.01	0.09	0.39	0.93	1.47	1.55	1.02	0.37	0.07		5.90	996.13
2.6-2.8		0.04	0.18	0.43	0.67	0.71	0.47	0.17	0.03		2.70	998.83
0-3.0	1.09	16.06	66.44	157.46	248.65	262.93	172.03	62.16	11.18	0.83		
Cumulative	1.09	17.15	83.59	241.05	489.70	752.63	924.66	986.82	998.00	998.83		

(Bretschneider – 1959)

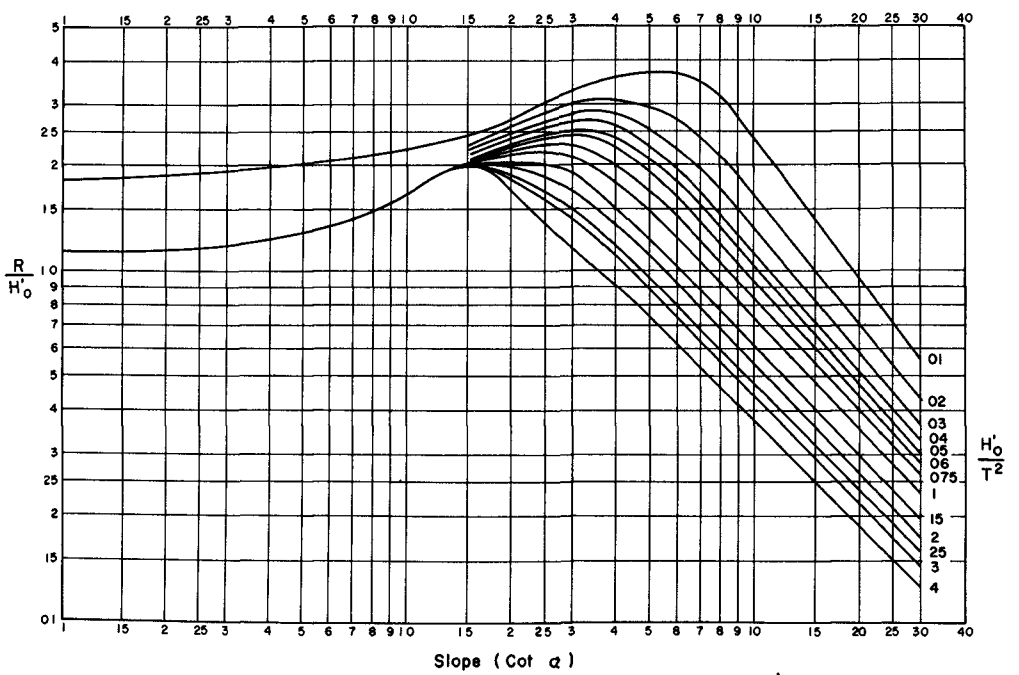

FIGURE I WAVE RUN-UP FOR SPECIFIC VALUES OF $\frac{H'_o}{T^2}$ $\left(\frac{d}{H'_o} > 3\right)$

Methods of taking this scale effect into account are also discussed in Technical Report Number 4,[1] and will not be further covered here. Use of these curves with appropriate scale correction appears to give quite accurate determinations of wave run-up for smooth structures, if the waves are of the same type as generated in the laboratory. These laboratory waves are simple repetitive waves, with each successive wave being essentially identical to the one preceding and following it.

Unfortunately, waves in nature are not generally of this type. In nature, no two waves are exactly alike, each successive wave being different from the preceding and following ones by a greater or lesser amount. The difference in successive waves is apparent in both height and period (or length). Consequently, there is some question as to the method in which the laboratory-derived run-up curves should be applied to actual wave conditions in nature. Practice in the past has been to apply these curves using the so called significant wave, which is a hypothetical wave having statistically described characteristics. Its height is defined as the average height of the upper one-third of the waves in the wave train, and its period is the average period of these higher waves. If the waves in a wave train are grouped according to their various heights, a statistical distribution is essentially the same regardless of the actual magnitude of the heights, or the state of generation or decay of the wave train. The significant wave, representing the average of the higher one-third of the waves, is exceeded by only thirteen percent of the waves in the wave train. If this wave height is used for design run-up considerations, the run-up obtained will be exceeded by only a small percentage of the waves, and damage is unlikely to occur. Experience has proved this assumption generally valid.

In the few cases where the importance of completely preventing wave overtopping of a structure is quite crucial, normal practice has been to compute a spectrum of wave run-ups using these same run-up curves and obtaining a range of wave steepness values based on the varying height values and a constant significant period assumed applicable to all of the higher waves. It is recognized that such computations are in error, but it has been assumed that the error would be relatively slight and of little importance.

Several years ago, however, a joint distribution of wave height and period was described by Bretschneider[2] for the particular case of fully developed sea - that is the case where the wind has been blowing long enough over a great enough distance to generate waves which are in a steady state condition. The fully developed sea condition is that for the case when the correlation coefficient between wave height and wave period (or length) is zero.

This correlation coefficient has been defined as

$$r(\eta,\lambda) = \frac{\overline{\eta\lambda} - 1}{\left[\left(\overline{\eta^2} - 1\right)\left(\overline{\lambda^2} - 1\right)\right]^{\frac{1}{2}}}$$

where $\eta = \frac{H}{\overline{H}}$

and $\lambda = \frac{L}{\overline{L}} = \frac{T^2}{\overline{T^2}}$

The bar indicates average values and H, L, and T, are, respectively, the wave height, length, and period. For the special case of zero correlation, the probability of both a particular value of height and length occurring simultaneously may be given non-dimensionally as

$$p(\eta,\lambda) = p(\eta) \cdot p(\lambda)$$

Utilizing this equation and the expressions for the individual height and length distribution functions, Bretschneider[2] derives a cumulative joint distribution for height and length as

$$P(\eta,\lambda) = \left[1 - e^{-\frac{\pi\eta^2}{4}}\right]\left[1 - e^{-\frac{\pi\lambda^2}{4}}\right]$$

which may be put in terms of period as

$$P(\eta,\tau) = \left[1 - e^{-\frac{\pi\eta^2}{4}}\right]\left[1 - e^{-.675\,\tau^4}\right]$$

where $\tau = \frac{T}{\overline{T}}$

This equation gives the percent of waves (P) having simultaneous values of relative height (η) and relative period (τ) equal to or less than stated values.

With this equation, Bretschneider has obtained a table showing the percentage of waves in a consecutive wave train that would be expected to occur having various values of relative height ($\eta = H/\overline{H}$) and period

($\tau = T/\overline{T}$ [2]). These values may be used to obtain an approximate frequency tabulation of relative wave steepness by taking values of η/τ^2 since

$$\frac{\eta}{\tau^2} = \frac{\frac{H}{\overline{H}}}{\left(\frac{T}{\overline{T}}\right)^2} = \frac{H}{T^2} \Big/ \frac{\overline{H}}{(\overline{T})^2}$$

This has been done, assuming that the mid-value of η and τ for each η and τ range is approximately appropriate to the frequency tabulated. The resulting curve is shown in Figure 2.

Now the average wave steepness $\overline{\left(\frac{H}{T^2}\right)} = \frac{\pi}{2} \frac{\overline{H}}{\overline{T^2}}$ for fully developed sea [3], and

$$\overline{T^2} = 1.079\ (\overline{T})^2$$

so that for fully developed sea

$$\overline{\left(\frac{H}{T^2}\right)} = \frac{\pi}{2} \frac{\overline{H}}{1.079\ (\overline{T})^2} = 1.456\ \frac{\overline{H}}{(\overline{T})^2}$$

As the frequency curve for steepness in terms of $\overline{H}/(\overline{T})^2$ has already been obtained, a frequency curve in terms of average steepness $\overline{(H/T^2)}$ can now also be obtained. This has been done, and the frequency curve of relative steepness (for fully developed sea) is shown also in Figure 2.

However, for design cases it is more frequently the significant height and period which is available, particularly if wave characteristics are obtained on a hindcasting basis. The steepness distribution in terms of significant wave parameters would therefore also be of use. They may be easily obtained since, as has been shown by Longuet-Higgins [4]

$$H_{1/3} = 1.60\ \overline{H}$$

and, according to Bretschneider, for fully developed sea (zero correlation)

$$T_{1/3} = \overline{T}$$

Then substituting above,

$$\frac{H_{1/3}}{T_{1/3}^2} = 1.6\ \frac{\overline{H}}{(\overline{T})^2} = 1.10\ \overline{\left(\frac{H}{T^2}\right)}$$

This curve is shown in Figure 2. It represents the distribution of wave steepness for a fully developed sea as a ratio of the steepness of the significant wave.

The limiting wave steepness in deep water as given by Reid and Bretschneider[5] from Michell's work[6] is $H/T^2 = 0.88$. However, in the frequency distribution shown, values of steepness as great as 250 times the average steepness were derived. Even with a relatively low value for the average wave steepness, these values would still considerably exceed the limiting value of 0.88. These waves must then be breaking and represent the proportion of waves that at any one instant are exceeding the critical steepness and breaking either as relatively small whitecaps or, less frequently, as relatively large breakers.

An estimate of the relative amount of these breaking waves would be interesting, and is readily available if the average steepness can be obtained. For the case of fully developed sea, the steepness of the significant wave ($H_{1/3}/T^2_{1/3}$) is about 0.06.[2] With this steepness value, and the steepness distribution as shown in Figure 2, a value of about 0.17% is derived as the approximate proportion of waves in a fully developed sea which are breaking at any one particular time.

However, the case of a truly fully developed sea seldom if ever occurs in nature, requiring as it does relatively unattainable durations and fetches. The case of more practical interest is that of the normal storm generating area, in which the steepness of the significant wave is more nearly equal to 0.22 (the value most frequently used for design purposes). (This value corresponds to an average steepness of 0.20). If one assumes that the Bretschneider relationship for joint distribution of height and period for fully developed sea is approximately valid also for this condition, then a value of about 2.2% is obtained as the approximate proportion of waves in a normal generating area which are in the process of breaking at any particular time. This estimate would seem of the right order of magnitude, although no specific observations of this measure appear to be available to check its validation.

Actually the Bretschneider joint distribution is for a zero correlation between wave height and period. For the more normal generating area zero correlation does not occur, but the actual correlation of approximately 0.2 is not far removed. The true distribution would be skewed somewhat toward the long period values, but the approximation of the Bretschneider distribution would still appear reasonable (see his Figure 7.2 for example[2]), particularly when the general accuracy of the distributions as a whole is considered. Consequently a rough estimate of the proportion of whitecaps and breaking waves in a generating area can reasonably be made as about 2% or a little more.

Using this steepness distribution and the run-up curve given in Figure 1, a distribution of individual relative run-ups may be derived. This distribution has been obtained for the more interesting case of a generating area where $H_{1/3}/T^2_{1/3} = 0.22$ and is shown in Figure 3. Again, the assumption is made that the Bretschneider joint distribution is also approximately valid for the normal generating case. Figure 3a shows the distribution of individual relative run-ups; that is, the run-ups as related to the height of the particular wave associated with that particular run-up. Figure 3b shows this distribution normalized by division by the relative run-up of the significant wave, also as a function of slope.

The distribution shown in Figure 3 is of interest, but of still greater interest would be the distribution of run-up alone, or of run-up as a ratio of the run-up of the significant wave. Figure 3b shows this relation, but as a ratio to the wave height distribution ($H/H_{1/3}$). Despite the fact that the height distribution[4] is known it appears impossible to accurately obtain the $R/R_{1/3}$ distribution directly from these two known distributions since all three are definitely interrelated.

However, the initial steepness distribution obtained can also be tabulated (from Bretschneider's table) to give percentage values of occurrence of particular steepnesses as associated with particular relative heights ($H/\bar{H}$) and periods ($T/\bar{T}$). Such a table is initially in normalized form, $(H/T^2)/(\overline{H/T^2})$, but may be put in terms of particular steepnesses if a particular value of $\overline{(H/T^2)}$ is assumed. (Note that assumption of a particular value of $\overline{(H/T^2)}$ is tantamount to assumption of a particular value of $H_{1/3}/T^2_{1/3}$). Once this value has been assumed, a similar table for relative run-up (R/H) may be derived from Figure 1 using these steepness values; this table will show the percentage values of occurrence of relative run-up as associated with particular relative heights ($H/\bar{H}$) and periods ($T/\bar{T}$). Each relative run-up (R/H) may then be multiplied by the value of relative height ($H/\bar{H}$) associated with it to obtain a table showing a percentage distribution of $R/\bar{H}$ - that is, run-up as a ratio to the average height of the wave train considered.

These values of $R/\bar{H}$ may then be accumulated to give a frequency diagram. Since $H_{1/3} = 1.6\ \bar{H}$, a frequency diagram of $R/H_{1/3}$ may in turn be obtained from this diagram. The desired frequency distribution $R/R_{1/3}$ may be obtained by dividing this $R/H_{1/3}$ distribution by the known value of $R_{1/3}/H_{1/3}$ associated with the significant wave steepness ($H_{1/3}/T^2_{1/3}$) assumed above in obtaining the original non-normalized steepness distribution table.

This process has been carried out for two slopes (1 on 6 and 1 on 2-1/4) using the steepness distribution for fully developed sea (i.e., $H_{1/3}/T^2_{1/3} = 0.06$) and four slopes (1 on 6, 1 on 3, 1 on 2-1/4, and 1 on 1-1/2) assuming a significant wave steepness $H_{1/3}/T^2_{1/3} = 0.22$, as applicable to most normal generating areas. The latter case again

AN APPROXIMATION OF THE WAVE RUN-UP FREQUENCY DISTRIBUTION

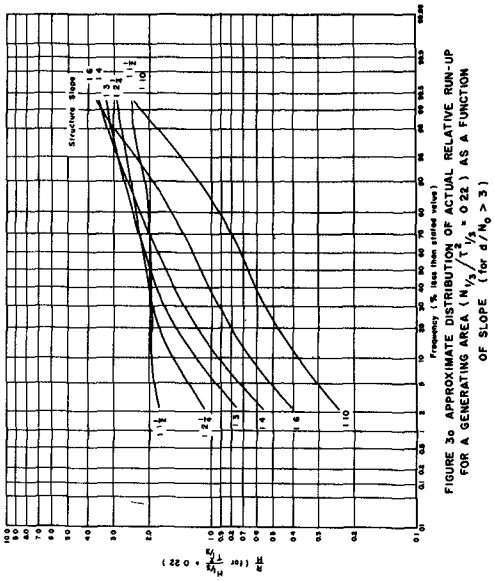

FIGURE 3a APPROXIMATE DISTRIBUTION OF ACTUAL RELATIVE RUN-UP FOR A GENERATING AREA ($N_{1/3}/T^2_{1/3} = 0.22$) AS A FUNCTION OF SLOPE (for $d/N_0 > 3$)

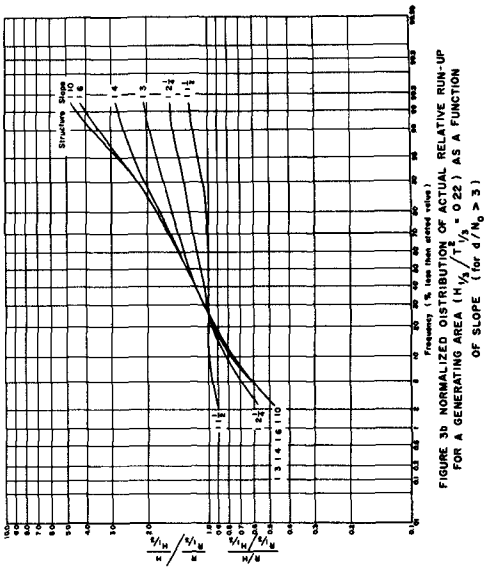

FIGURE 3b NORMALIZED DISTRIBUTION OF ACTUAL RELATIVE RUN-UP FOR A GENERATING AREA ($H_{1/3}/T^2_{1/3} = 0.22$) AS A FUNCTION OF SLOPE (for $d/N_0 > 3$)

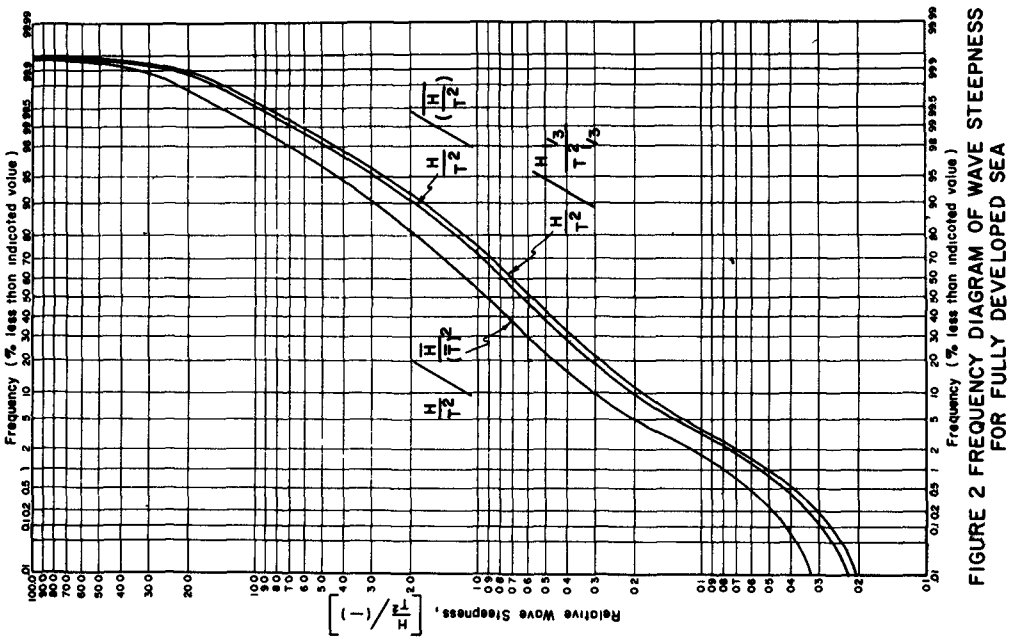

FIGURE 2 FREQUENCY DIAGRAM OF WAVE STEEPNESS FOR FULLY DEVELOPED SEA

assumes that the Bretschneider distribution for fully developed sea is also approximately valid for such generating areas.

These distribution curves are shown in Figure 4. They all lie quite close to one another, particularly in the higher run-up ranges which are of most interest. Of especial importance is the fact that the distributions derived for the two wave steepnesses (0.06 and 0.22) are very nearly exactly identical for each of the two slopes determined.

That portion of the distribution curves for lower values of $R/R_{1/3}$ is somewhat less exactly determined, probably because of the relatively large proportionate ranges of $H/\overline{H}$ and $T/\overline{T}$ used to obtain these values. This use resulted in a noticeable stair-step plot of the lower end of the distribution, and the curves are drawn as dashed in this region. For the higher values however the plotted points showed very little scatter, and a fairly exact curve may be drawn. The determination of the distribution of the lower values is primarily of academic interest since, of course, it is the distribution of values higher than $R_{1/3}$ which is of paramount practical engineering design value.

The distribution curves for these four slopes are very nearly the same, and within the limits of approximation implied by the method of their obtention, may be considered to be the same. The outer limits of these curves are shown in Figure 5 to describe the band of frequencies determined. An average line has been drawn within this band as a single approximate run-up distribution to be used for all slopes - for waves still in the generating area, and for structure depths, d/H, greater than 3. This curve is suprisingly close to the distribution curve for wave heights, which is also shown in Figure 5. In fact, within the approximations and assumptions used in obtaining the run-up distribution curve, the run-up distribution is probably equally well represented by the height distribution curve - at least in the area of engineering interest which is generally for the run-ups in excess of $R_{1/3}$. And usage of the height distribution which is relatively widely known probably facilitates general application. From either curve, it is seen that about 13% of the run-ups exceed the run-up of the significant wave, that about 1% of the run-ups will be 1.5 times $R_{1/3}$, and that about 1 in 1000 will be 2 times $R_{1/3}$.

Use of the distribution shown in Figure 5 results in appreciably higher values of run-up (approximately twice the increase in run-up above $R_{1/3}$) for any particular frequency value than use of the earlier approximation involving run-ups computed on the basis of steepness values obtained from the height distribution and a constant significant period. It is felt, however, to give a more accurate estimate of what actually occurs in nature.

AN APPROXIMATION OF THE WAVE RUN-UP FREQUENCY DISTRIBUTION

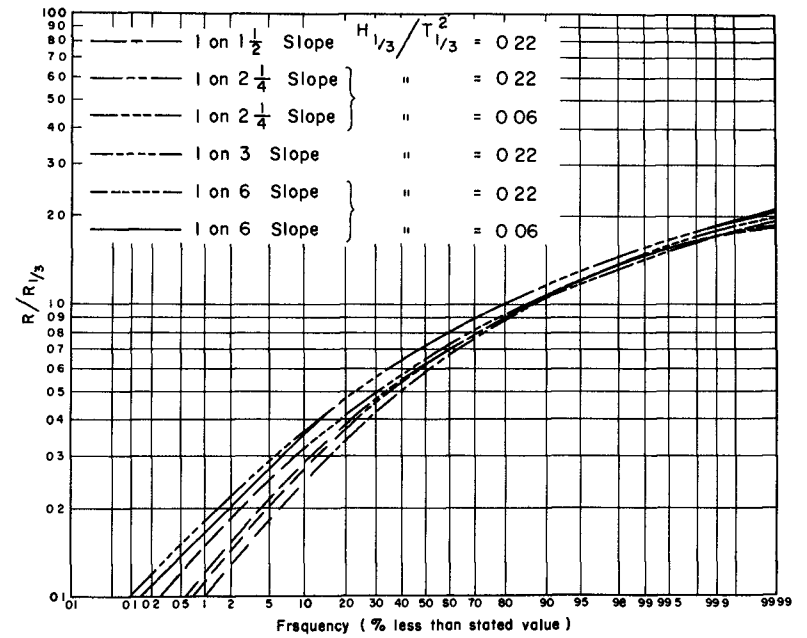

FIGURE 4 FREQUENCY DISTRIBUTION OF WAVE RUN-UP FOR ANY PARTICULAR WAVE TRAIN AS A FUNCTION OF STRUCTURE SLOPE
(for waves still in the generating area and structure depth $d/H_0 > 3$)

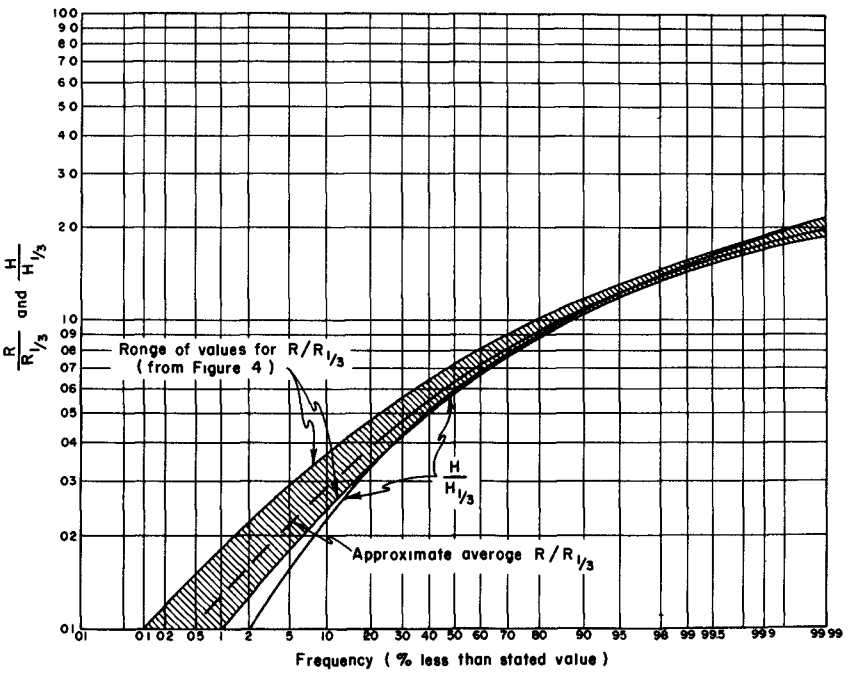

FIGURE 5 FREQUENCY DISTRIBUTION OF WAVE RUN-UP
(for waves still in the generating area and structure depth $d/H_0 > 3$)

Derivation of the run-up distribution has been only for relative structure depths, d/H, greater than 3. However, the same process can be carried through for other relative structure depths, and this work is now underway.

Actual validation of such a run-up distribution must await considerably improved field observations, or test in a wave flume which can generate a complex wave train having the statistical properties of actual ocean waves. Such a generator is now under design for one of the Beach Erosion Board wave flumes, and it is hoped its later use will permit more exact empirical test of this run-up distribution. It is quite possible, for example, that the run-up of a particular wave in an actual wave train depends more on the wave height or run-up of the immediately preceding wave, than on its own steepness. But until observations permit accurate checking, the run-up distribution presented herein is felt to be a more realistic estimate than earlier methods.

ACKNOWLEDGEMENTS

The analysis presented herein was made in connection with the general research program of the U. S. Army Engineer Beach Erosion Board and supported by Beach Erosion Development Study funds and by the Civil Works Investigations program of the U. S. Army Corps of Engineers. Permission of the Chief of Engineers to publish this information is appreciated. Grateful acknowledgement is also made to Dr. Churchill Eisenhart of the U. S. National Bureau of Standards who when an impasse was reached in an attempt to obtain the run-up distribution from Figure 3, suggested that it could nevertheless be obtained directly from the joint distribution of wave height and period and the run-up curves.

REFERENCES

1. U. S. Army Engineer Beach Erosion Board: "Shore Protection Planning and Design", Technical Report Number 4, Beach Erosion Board, Washington, D. C., 1961 (revised).

2. Bretschneider, Charles L: "Wave Variability and Wave Spectra for Wind-Generated Gravity Waves", Technical Memorandum Number 118, U. S. Beach Erosion Board, Washington, D. C., 1959.

3. Bretschneider, Charles L.: "Revisions in Wave Forecasting: Deep and Shallow Water", Proceedings of the Sixth Conference on Coastal Engineering, Council on Wave Research, Engineering Foundation, 1958.

4. Longuet-Higgins, M.S.: "On the Statistical Distribution of the Height of Sea Waves" , Journal of Marine Research, V.11, n.3, 1952

5. Reid, R. O. and C. L. Bretschneider: "Surface Waves and Offshore Structures", Technical Report, Texas A&M Research Foundation, October 1953.

6. Michell, J. H.: "On the Highest Waves in Water", Philosophical Magazine, V.36, n.5, 1893.

CHAPTER 5

TRANSFORMATION, BREAKING AND RUN-UP OF A LONG WAVE OF FINITE HEIGHT

Tsutomu Kishi
Faculty of Engineering, Hokkaido University
Sapporo, Japan

INTRODUCTION

On studying the transformation, breaking and run-up of a relatively steep wave of a short period, the theory for waves of permanent type has given us many fruitful results. However, the theory gradually loses its applicability as a wave becomes flat, since a considerable deformation of the wave profile is inevitable in its propagation.

In § 1, a discussion concerning the transformation of a long wave in a channel of variable section is presented based on the non-linear shallow water theory. Approximate solutions obtained by G. B. Whitham's method (1958) are shown. Further, some brief considerations are given to the effects of bottom friction on wave transformation.

In § 2, breaking of a long wave is discussed. Breakings on a uniformly sloping beach and on a beach of parabolic profile are considered and the effects of beach profile on breaking are clarified.

Finally in § 3, experimental results on wave run-up over 1/30 slope are described in comparing with the Kaplan's results.

1. TRANSFORMATION OF A LONG WAVE OF FINITE HEIGHT.

1. 1. TRANSFORMATION IN SHOALING WATER.

When the effects of bottom friction is neglected, the conservation equations of mass and momentum in the non-linear shallow-water theory are

$$[v^*(\eta^* + h^*)]_{x^*} = -\eta^*_{t^*} \tag{1-1}$$

and

$$v^*_{t^*} + v^* v^*_{x^*} = -g^* \eta^*_{x^*} \tag{1-2}$$

where the symbols η^*, h^*, and x^* are defined in Figure 1, v^* is velocity, t^* is time, and g^* is the gravitational acceleration. The asterisks denote dimensional quantities. The following dimensionless variables are introduced for the sake of simplicity :

TRANSFORMATION, BREAKING AND RUN-UP OF A LONG WAVE OF FINITE HEIGHT

$$x = x^*/l_o^* \quad , \quad h = h^*/h_o^* \quad , \quad \eta = \eta^*/h_o^*$$
$$v = v^*/v_o^* \quad , \quad t = t^*/t_o^*$$

where l_o^* = distance from the origin to the shoreline
h_o^* = water depth at the origin
$t_o^* = l_o^*/(g^* h_o^*)^{1/2}$, $v_o^* = (g^* h_o^*)^{1/2}$

Let the depth be given by $h = h(x)$, the basic equations are as follows when these dimensionless variables are substituted :

$$[v(h+\eta)]_x = -\eta_t \tag{1-3}$$

$$v_t + vv_x = -\eta_x \tag{1-4}$$

The characteristic equations to be derived from these hyperbolic equations are

$$dx/dt = v + c \tag{1-5}$$

$$d(v + 2c) + dt = 0 \tag{1-6}$$

$$dx/dt = v - c \tag{1-7}$$

$$d(v - 2c) + dt = 0 \tag{1-8}$$

where $c^2 = h + \eta$

Next, a compressive wave propagating shoreward will be considered. It is well known that a compressive wave continues to deform its profile in its propagation and eventually breaks by the curling of the wave front. And from the physical point of view, the wave is considered to form a bore after breaking. In this meaning the theory of a bore in shoaling water given by H. B. Keller, D. A. Lavine, and G. B. Whitham (1960) would give some informations on the transformation of a deformed long wave.

Suppose that particle velocity and propagation velocity of a wave in shoaling water are related to surface elevation by the following expressions:

$$v = 2\sqrt{h}\,(\sqrt{1+M} - 1) \tag{1-9}$$

$$C = \sqrt{h}\,\sqrt{1+M} \tag{1-10}$$

where $M = \eta / h$

Since the above relations are precise solutions for the case of a uniform depth, they must also be approximately applied in shoaling water, provided the change of water depth within the distance between the wave front and the crest is not large. It is of interest to compare the transformation of a wave governed by the above relations with that of a bore, since the above relations differ a little from the bore conditions as are shown in the following relations :

$$v'/v \cong (1+M-\frac{15}{32}M^2)$$

$$c'/c \cong (1+\frac{1}{4}M-\frac{1}{32}M^2)$$

where v' is the particle velocity just behind the bore and c' is the propagation velocity of a bore.

Substitution of Eq.(1-5) into Eq.(1-6) leads to

$$d(v+2c) - dh/(v+c) = 0 \tag{1-11}$$

And substitution of Eqs.(1-9) and (1-10) into Eq.(1-11) yields the differential equation concerning M as a function of h :

$$\frac{1}{h}\frac{dh}{dM} = -\frac{2\{3\sqrt{1+M}-2\}}{\{\sqrt{1+M}-1\}\{6\sqrt{1+M}-1\}\sqrt{1+M}} \tag{1-12}$$

When M is small, Eq.(1-12) is approximately equivalent to

$$dh/h = -\frac{4}{5}\,dM/M \tag{1-13}$$

Therefore, $$M \propto h^{-5/4}\ ,\quad \eta \propto h^{-1/4} \tag{1-14}$$

This is a well known relation for waves of small height.

Integration of Eq.(1-12) gives

$$h = A_0\,(\sqrt{1+M}-1)^{-4/5}\,(6\sqrt{1+M}-1)^{-6/5} \tag{1-15}$$

Where A_0 is an integration constant to be determined by a boundary condition.

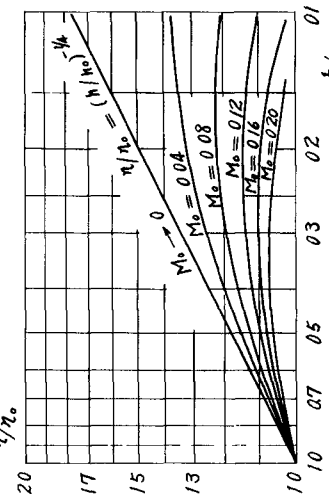

Fig. 3. Relation between (η/η_0) and (h/h_0) for a bore in shoaling water (by H. B. Keller, D.A. Levine and G.B.Whitham).

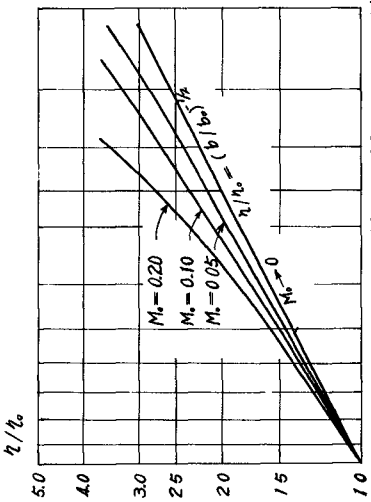

Fig. 4. Relation between (η/η_0) and (b/b_0) for a long wave in a channel of variable width.

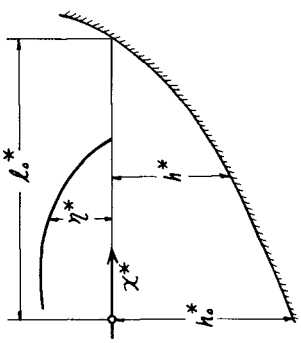

Fig. 1. Definition sketch of a long wave on a sloping beach.

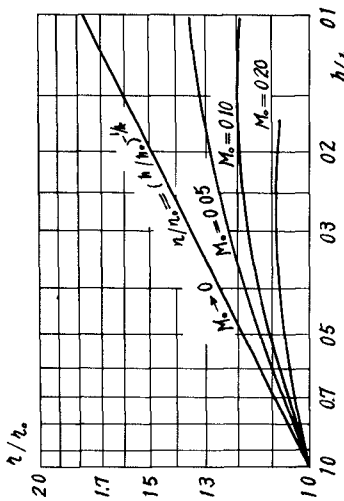

Fig. 2. Relation between (η/η_0) and h/h_0 for a long wave in shoaling water.

Under the boundary condition $M = M_0$ at $h = 1$, Eq.(1-15) becomes

$$h = \left(\frac{\sqrt{1+M_0} - 1}{\sqrt{1+M} - 1}\right)^{4/5} \left(\frac{6\sqrt{1+M_0} - 1}{6\sqrt{1+M} - 1}\right)^{6/5} \tag{1-16}$$

Turning to the details of the relation given by Eq.(1-12), it will be seen that M increases monotonically as h decreases when $M > 0$. However, this manner of variation does not exist in the height η. The maximum of η occurs when

$$d\eta / dh = M + h\, dM/dh = 0 \tag{1-17}$$

Substitution of Eq.(1-12) into Eq.(1-17) gives

$$M = 7/9 \quad , \quad \text{or} \quad \eta_{max} = 0.778\, h \tag{1-18}$$

The relation between (η/η_0) and (h/h_0) obtained from Eq.(1-16) is illustrated in Figure 2. For the purpose of comparison the corresponding relation for a bore obtained by H. B. Keller, D. A. Lavine and G. B. Whitham (1960) is illustrated in Figure 3.

In the above analysis two interesting features are found, one of them being that the rate of amplification of wave height in decreasing depth decreases as the relative wave height increases and the other being the existence of the maximum of wave height.

1. 2. TRANSFORMATION IN A CHANNEL OF VARIABLE WIDTH.

Suppose a channel has a variable width and a uniform depth and let the dimensionless channel width be given by $b = b(x)$. Dimensionless variables are defined as follows :

$$b = B^*/h_0^* \,, \quad \eta = \eta^*/h_0^* \,, \quad x = x^*/h_0^*$$

$$u = u^*/u_0^* \,, \quad \text{and} \quad t = t^*/t_0^*$$

where $B^* =$ width of channel, $h_0^* =$ uniform water depth

and $v_0^* = (g^* h_0^*)^{1/2}$, $t_0^* = (h_0^*/g^*)^{1/2}$

The positive characteristic equations of the conservation equations of mass and momentum, in the dimensionless form, are

$$dx/dt = v + c \tag{1-19}$$

$$d(v+2c) + vc\,(b_x/b)\,dt = 0 \tag{1-20}$$

By the combination of the above two equations, one has

$$d(v+2c) + \frac{vc}{v+c}\,\frac{db}{b} = 0 \tag{1-21}$$

When $h = 1$ is considered, substitution of Eqs.(1-9) and (1-10) into Eq.(1-21) yields

$$\frac{db}{b} = -\frac{3\sqrt{1+\eta} - 2}{(1+\eta)(\sqrt{1+\eta} - 1)}\,d\eta \tag{1-22}$$

When η is small, Eq.(1-22) is approximately

$$\frac{db}{b} = -2\,\frac{d\eta}{\eta} \tag{1-23}$$

which gives $$\eta \propto b^{-1/2} \tag{1-24}$$

This is the well known relation for waves of small height. Under the boundary condition $\eta = \eta_0$ at $b = b_0$, Eq.(1-22) becomes

$$\frac{b}{b_0} = \left(\frac{1+M}{1+M_0}\right)^2 \left(\frac{\sqrt{1+M} - 1}{\sqrt{1+M_0} - 1}\right)^{-2} \tag{1-25}$$

The relation between (η/η_0) and (b/b_0) obtained from Eq.(1-25) is illustrated in Figure 4. The wave transformation in a channel of variable width shows different character from the preceding case of variable depth. The rate of amplification of wave height in converging channel continuously increases as the relative height of wave increases.

1. 3. EFFECTS OF BOTTOM FRICTION ON WAVE TRANSFORMATION.

The conservation equation of momentum which accounts for the effects of bottom friction is given by

$$v^*_{t^*} + v^* v^*_{x^*} = -g^* \eta^*_{x^*} - k'(v^{*2}/h^* + \eta^*) \tag{1-26}$$

where $k' = g^*/C_e^{*2}$ and C_e^* = Chézy's roughness factor

By using the same dimensionless variables as in 1.1 the positive characteristic equations of conservation equations of mass and momentum on a uniformly sloping beach, $h = 1 - x$, can be given by

$$dx/dt = v + c \tag{1-27}$$

$$d(v+2c) + \{1 + k(v/c)^2\}\, dt = 0 \tag{1-28}$$

where $k = k'/S$, and S = beach slope.

Substitution of Eqs.(1-9) and (1-10) into the equation which is obtained by combining the above two equations leads to

$$\frac{1}{h}\frac{dh}{dN} = -\frac{4N^2(3N-2)}{N^2(6N^2-1)(N^2-1) - 4k(N-1)^2} \tag{1-29}$$

where $N = \sqrt{1+M}$

Provided the terms smaller than $(N-1)^3$ can be neglected, Eq.(1-29) approximately integrates to

$$h \cong A_0 \varepsilon^{-4/5}\left(\alpha\varepsilon + \frac{5}{4}\right)^{\beta} \exp\left(-\frac{7}{2}\varepsilon\right) \tag{1-30-1}$$

where $\varepsilon = N - 1$

$$\alpha = 4 - k$$

$$\beta = \frac{1}{\alpha}\left(5 - \frac{35}{4\alpha} - \frac{4\alpha}{5}\right)$$

In a special case of $\alpha = 0$, $k = 4$ the above relation can be reduced to

$$h \cong A_0 \varepsilon^{-4/5} \exp\left\{-2\varepsilon\left(\frac{7}{5}\varepsilon + 2\right)\right\} \tag{1-30-2}$$

In the case of a uniform depth the attenuation of wave height will be expressed by

$$d(v+2c) + k'(v/c)^2 \frac{dx}{v+c} = 0 \tag{1-31}$$

Where $k' = g^*/c_e^{*2}$ and the dimensionless variables are similar to those in 1. 2. Substitution of Eqs.(1-9) and (1-10) into Eq.(1-31) gives

$$dx = -\frac{\sqrt{1+\eta}\,(3\sqrt{1+\eta}-2)}{2k'(\sqrt{1+\eta}-1)^2}\,d\eta \qquad (1\text{-}32)$$

which can be integrated as

$$x = \frac{1}{k'}\left[\left(\frac{1}{N-1}-\frac{1}{N_0-1}\right)-5\log\left(\frac{N-1}{N_0-1}\right)-4(N-N_0)-\frac{3}{2}(N^2-N_0^2)\right] \qquad (1\text{-}33)$$

where $N=\sqrt{1+\eta}$ and N_0 is N at $x=0$

As an example, attenuation of long wave under the condition $k'=0.01$ is illustrated in Figure 5. However, the value of roughness factor, $k'=0.01$ is only an example and experimental studies are necessary to discuss further.

2. BREAKING OF A LONG WAVE IN SHOALING WATER.

A long wave continues to deform due to the difference of its local propagation velocity and eventually breaks by the curling of its front. From the mathematical point of view, breaking points are expressed by an envelope of interesections of characteristic curves. In the following a wave which has a non-zero slope at the wave front and propagates shoreward into quiescent water is considered.

At first, a uniformly sloping beach with a depth of $h^* = S(l_0^* - x^*)$ will be considered, here S is the beach slope. It takes a dimensionless form of

$$h = 1 - x \qquad (2\text{-}1)$$

Considering a characteristic curve $dx/dt = v+c$, which starts from the origin at time $t=\tau$, one has the following equation from the relation given by Eq.(1-6) :

$$C(t) = C(\tau) - \frac{1}{2}(t-\tau) - \frac{1}{2}\{v(t)-v(\tau)\} \qquad (2\text{-}2)$$

Then, the positive characteristic curve is

$$dx/dt = v+C = C(\tau) - \frac{1}{2}(t-\tau) + \frac{1}{2}\{v(t)+v(\tau)\} \qquad (2\text{-}3)$$

By the combination of Eqs.(1-9) and (1-14), the particle velocity at time t along the above characteristic curve can be given approximately by

$$v(t) \cong \eta(\tau) h^{-3/4} - \frac{1}{4}\eta^2(\tau) h^{-2} \tag{2-4}$$

Substituting Eq.(2-4) into Eq.(2-3) and considering Eq.(2-1) one has

$$\frac{dx}{dt} = (1+\sigma)^{1/2} - \frac{1}{2}(t-\tau) + \sigma\left\{1 + \frac{3}{8}x + \frac{21}{64}x^2 + \frac{77}{256}x^3 + \cdots\right\} - \sigma^2\left\{\frac{1}{4} + \frac{1}{4}x + \frac{3}{8}x^2 + \frac{1}{2}x^3 + \cdots\right\} \tag{2-5}$$

where $\sigma = \eta(\tau)$ and $c(\tau) = (1+\sigma)^{1/2}$

It is assumed that the solution of Eq.(2-5) is expressed as a power series of σ

$$x = x_0 + \sigma x_1 + \sigma^2 x_2 + \cdots \tag{2-6}$$

The intersections of characteristic curves are obtained from

$$\frac{\partial x}{\partial \tau} = \frac{\partial x_0}{\partial \tau} + \sigma\frac{\partial x_1}{\partial \tau} + \frac{\partial \sigma}{\partial \tau}x_1 + \cdots = 0 \tag{2-7}$$

The initial breaking point is given by putting $\tau = 0$ and $\sigma = 0$ in Eq.(2-7). Thus, the initial breaking point is determined from the first two terms of the right hand side of Eq.(2-6).

Substituting Eq.(2-6) into Eq.(2-5) and considering the initial condition, $x = 0$ when $t = \tau$, one has

$$\left.\begin{aligned} x_0 &= (t-\tau) - \frac{1}{4}(t-\tau)^2 \\ x_1 &= 1.500000(t-\tau) + 0.187500(t-\tau)^2 \\ &\quad + 0.078125(t-\tau)^3 + 0.034180(t-\tau)^4 \\ &\quad + 0.015381(t-\tau)^5 + \cdots \end{aligned}\right\} \tag{2-8}$$

With the substitution of Eq.(2-8) into Eq.(2-7) a relation to give the initial breaking time t_b is obtained.

$$-1 + \frac{1}{2}t_b + m\,t_b\,(1.500000 + 0.187500\,t_b + 0.078125\,t_b^2 + 0.034180\,t_b^3 + 0.015381\,t_b^4 + \cdots) = 0 \tag{2-9}$$

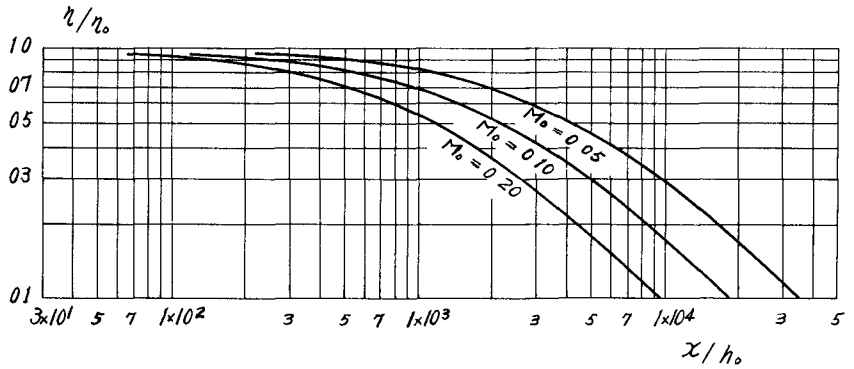

Fig.5. Attenuation of a long wave in a channel of uniform depth with roughness factor k' = 0.01.

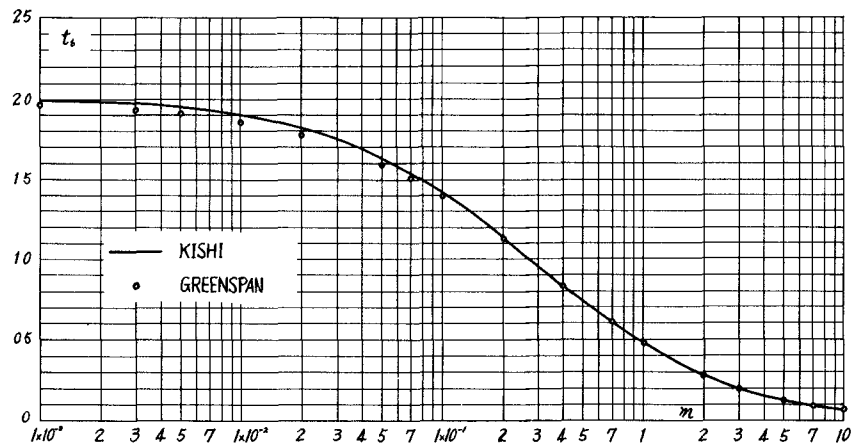

Fig. 6. Breaking time t_b as a function of initial slope m for a uniformly sloping beach.

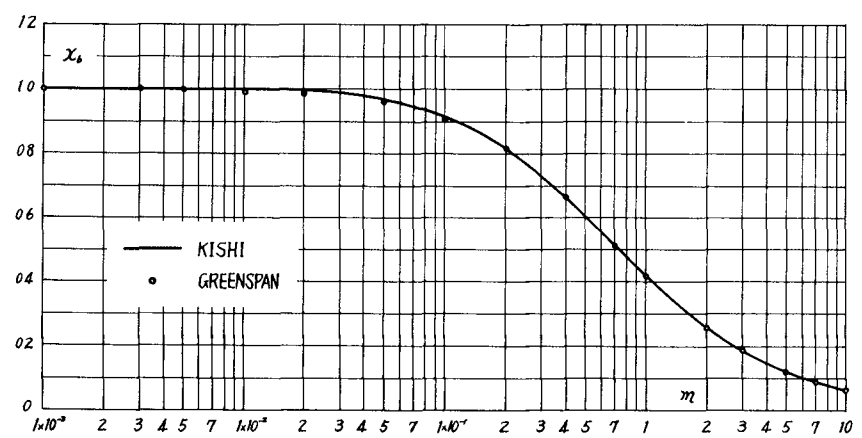

Fig. 7. Breaking position x_b as a function of initial slope m for a uniformly sloping beach.

where $m = \left(\frac{\partial \sigma}{\partial \tau}\right)_{\sigma=0} = -\left(\frac{\partial \sigma}{\partial x}\right)_{\sigma=0}$ *

The corresponding breaking point x_b can be found by $x_b = x_0(t_b)$, since $\tau = 0$ and $\sigma = 0$:

$$x_b = t_b - \frac{1}{4} t_b^2 \qquad (2\text{-}10)$$

The curves of t_b and x_b as a function of initial slope m are shown in Figure 6 and 7, respectively. For the purpose of comparison, the corresponding values obtained by H. P. Greenspan (1958) are plotted in the figure which shows a good agreement with the present theory.

The above theory gives an explanation about the effects of beach slope on wave breaking. Provided the wave is sinusoidal, the relation between the initial slope m and the wave steepness can be given by

$$m = (\pi / S)(H_i / L_i)$$

where H_i = wave height at the origin

L_i = wave length at the origin

S = beach slope

Thus, the breaking position is determined for the given values of beach slope and wave steepness. And the transformation of wave height between the origin and the breaking position is assumed to satisfy the following relation (the analysis in § 1 considers only a compressive wave or elevation, and a rarefaction wave or depression is not considered) :

$$H_b / H_i \cong (1 - x_b)^{-1/4}$$

Then graphs showing the relation between H_b/H_i and H_i/L_i are obtained for the given values of beach slope.

However, the above graphs are not the relations between deep water and the breaking position. Then a relation between the deep water and the origin is also of interest to be calculated. In the present calculations relative depth at the origin h_i/L_i is assumed to be 0.044 . Provided the small amplitude theory is applied, the relations between the deep water and the origin are

$$H_b / H_0 = 1.4 \, (H_b / H_i)$$

$$H_0 / T^2 = 5.12 \, (H_0 / L_0) = H_i / L_i$$

---

* At the origin $(C)_{\sigma=0} = 1$

Results of the present calculations are compared with the experimental curves given by H. W. Iversen (1952) in Figure 8. It would be seen from the figure that the present theory gives an explanation about the effects of beach slope on wave breaking, although some assumptions are included in this calculations.

Next, a consideration on the effects of bottom profiles on wave breaking will be given. For an example, let the depth $h=(1-x)$ be replaced by

$$h = 1 - x^2 \tag{2-11}$$

The positive characteristic equations are

$$dx/dt = v + c \tag{2-12}$$

$$d(v + 2c) + 2x\,dt = 0 \tag{2-13}$$

Eq.(2-13) can be written as

$$v(t) + 2c(t) = v(\tau) + 2c(\tau) - 2\int_\tau^t x\,dt$$

$$\text{or} \qquad c(t) = c(\tau) - \frac{1}{2}\left\{v(t) - v(\tau)\right\} - \int_\tau^t x\,dt \tag{2-14}$$

Combination of Eqs.(2-13) and (2-14) gives the following equation of characteristic curve which can be derived by the same reduction described in the first example :

$$\frac{dx}{dt} = (1+\sigma)^{1/2} - \int_\tau^t x\,dt + \sigma\left\{1 + \frac{3}{8}x^2 + \frac{21}{64}x^4 + \frac{77}{256}x^6 + \cdots\right\} - \sigma^2\left\{\frac{1}{4} + \frac{1}{4}x^2 + \frac{3}{8}x^4 + \frac{1}{2}x^6 + \cdots\right\} \tag{2-15}$$

Assuming that the solution of Eq.(2-15) is given by a power series of σ such as Eq.(2-6), the function x_0 , x_1 , ... can be determined successively.

$$\frac{dx_0}{dt} = 1 - \int_\tau^t x_0\,dt \tag{2-16}$$

$$\frac{dx_1}{dt} = \frac{3}{2} - \int_\tau^t x_1\,dt + \frac{3}{8}x_0^2 + \frac{21}{64}x_0^4 + \frac{77}{256}x_0^6 + \cdots \tag{2-17}$$

Since the initial condition is $x = o$ when $t = \tau$, the solution of Eq.(2-16) which satisfies the initial condition is assumed to have the form

$$x_o = \sum_{h=o}^{\infty} a_{2h+1} (t-\tau)^{2n+1} \tag{2-18}$$

where a_n is a constant to be determined from Eq.(2-16). Substitution of Eq.(2-18) into Eq.(2-16) yields

$$x_o = (t-\tau) - \frac{1}{6}(t-\tau)^3 + \frac{1}{120}(t-\tau)^5 - \frac{1}{5,040}(t-\tau)^7 + \cdots$$

$$\text{or} \quad x_o = (t-\tau) - 0.16667(t-\tau)^3 + 0.008333(t-\tau)^5 - 0.000198(t-\tau)^7 + \cdots \tag{2-19}$$

In the same way, one has

$$x_1 = 1.500000(t-\tau) - 0.125000(t-\tau)^3 + 0.046875(t-\tau)^5 + 0.012984(t-\tau)^7 + \cdots \tag{2-20}$$

Thus, the initial breaking time t_b and position x_b are given by Eqs.(2-21) and (2-22), respectively.

$$-1 + 0.500000\, t_b^2 - 0.041667\, t_b^4 + 0.001389\, t_b^6 + m t_b (1.500000 - 0.125000\, t_b^2 + 0.046875\, t_b^4 + 0.012984\, t_b^6 + \cdots) = 0 \tag{2-21}$$

$$x_b = t_b - 0.166667\, t_b^3 + 0.008333\, t_b^5 - 0.000198\, t_b^7 + \cdots \tag{2-22}$$

The curves of t_b and x_b as a function of the initial slope m are shown in Figure 9. Then, two values of water depth at the breaking position which are obtained on the uniformly sloping beach and the parabolic beach, respectively, are compared in Figure 10. As will be seen from the figure, breaking of a long wave is affected by the beach profile. This may be a reason why a large scattering is found in connecting the breakers of very flat waves with the deep water waves.

3. EXPERIMENTS ON THE RUN-UP HEIGHT OF A LONG WAVE OVER A UNIFORMLY SLOPING BEACH.

The author carried out some preliminary experiments on the run-up height of a long wave with the aim of investigating the hydraulic behaviours of Tsunami which runs up a beach. Few data exist about the run-up characters

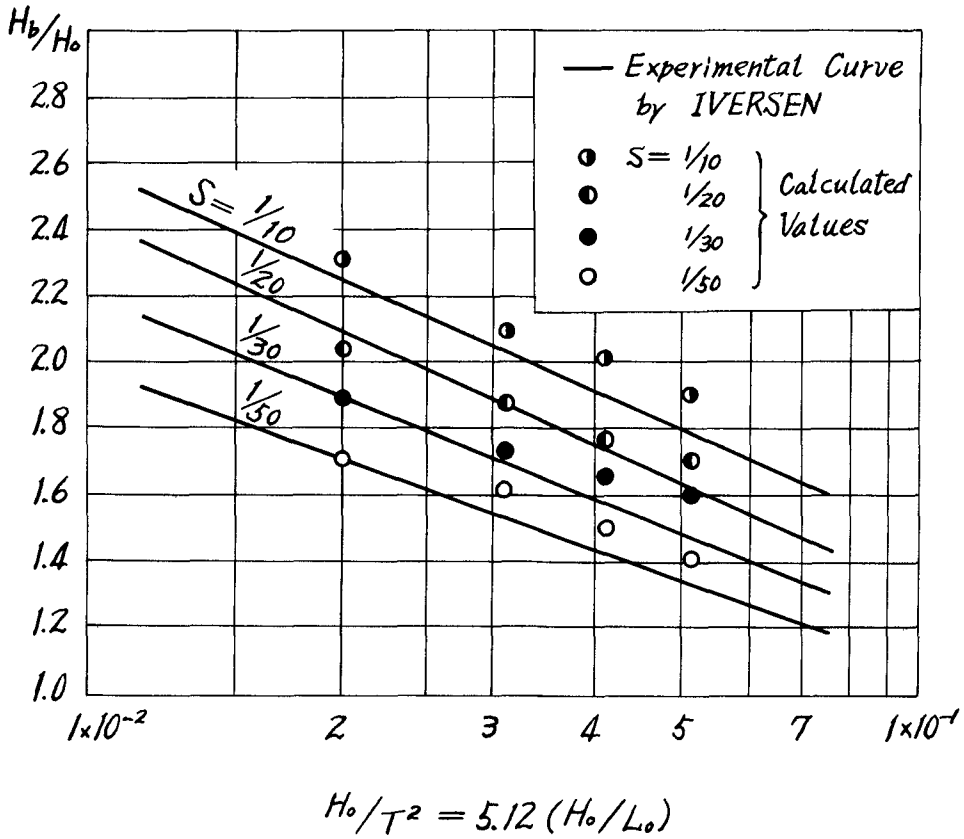

Fig. 8. Effects of beach slope on wave breaking.

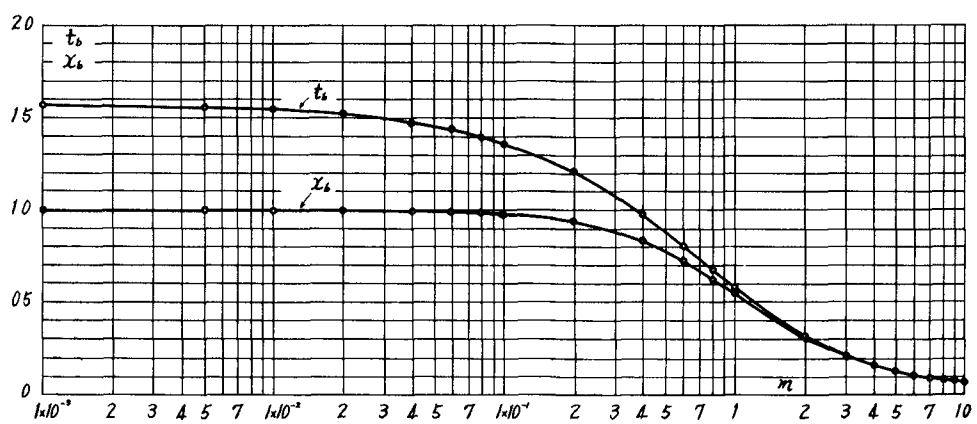

Fig. 9. Breaking time t_b and position x_b as a function of initial slope m for a beach with parabolic profile.

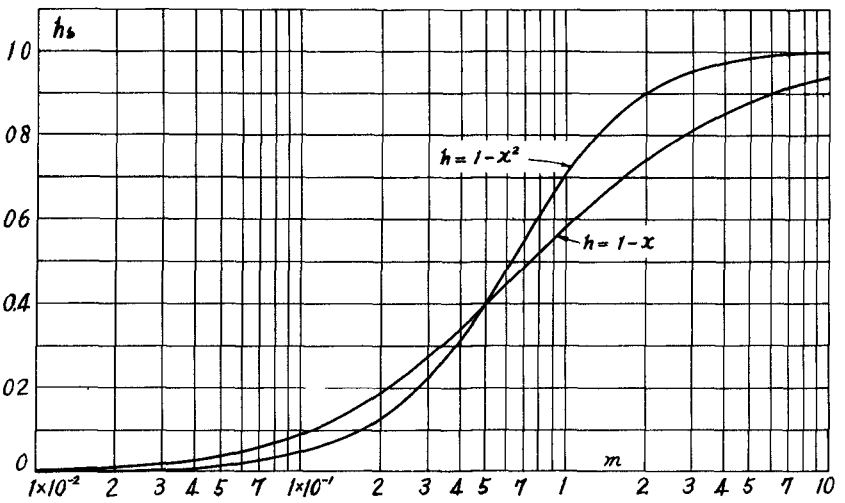

Fig. 10. Effects of beach profile on wave breaking.

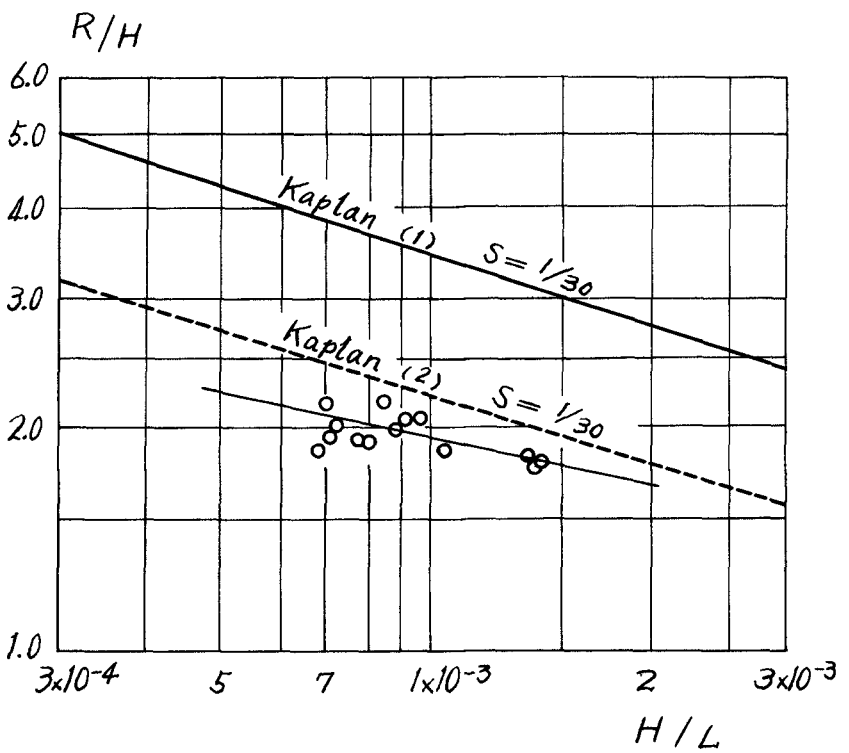

Fig. 11. Run-up of a long wave on 1/30 slope.

of very flat waves as Tsunami which usually has a period of several ten minutes.

Experiments were carried on in a wave tank of 14cm width installed with a pneumatic wave generator at one end and a beach of 1/30 slope at the other end. Water depth at the foot of the slope was 9cm. Three kinds of wave periods, 10sec, 15sec, and 20sec were given by adjusting the rotating speed of a rotary valve. Values of wave steepness at the foot of the beach were varied from 7×10^{-4} to 1.4×10^{-3}.

Relation between the relative run-up height and the wave steepness is shown in Figure 11. In the figure, R is the run-up height above S.W.L., H and L are wave height and wave length at the foot of the slope, respectively. For the purpose of comparison, the experimental curve obtained by K. Kaplan (1952) is indicated on the same figure. Kaplan's relation is

$$R/H = 0.381\,(H/L)^{-0.316} \quad \text{for 1 on 30 slope} \qquad (3\text{-}1)$$

Since a solitary wave was used in Kaplan's experiments, two curves are shown ; the one is the curve in full-line on which the height of solitary wave is replaced by the height of the long wave and the other is the curve in broken line on which the height of solitary wave is replaced by the half wave height of the long wave.

The author's results are fairly close with the latter curve, though the points in the present experiments stand somewhat below. A little inconsistency of the two experiments is presumably due to the difference of hydraulic characters between a long wave and a solitary wave. However, the author would like to reserve further discussions in this respect, since the scale of the experiments was too small to investigate the details.

4. CONCLUSION

1) By the use of approximate expressions for particle velocity and propagation velocity, a relation of wave transformation in shoaling water is derived. The rate of amplification of wave height in decreasing depth decreases as the relative wave height increases. And the maximum height of wave crest appears when $\eta = 0.778h$.

2) A compressive wave is considered to form a bore after its breaking. A relation on the transformation of a bore in shoaling water has been presented by H. B. Keller, D. A. Lavine and G. B. Whitham. For the purpose of comparison, two relations of transformation for a long wave and a bore are shown in Figure 2 and Figure 3, respectively.

3) Further, a relation of wave transformation in a channel of variable width is derived. The rate of amplification of wave height in converging width increases as the relative wave height increases.

4) Brief descriptions about the effects of bottom friction on wave transformation are given in section 3, § 1.

5) An approximate method to calculate the wave deformation is presented. As an example, the initial breaking time and position for uniformly sloping beach are calculated. The author's results show good agreement with the Greenspan's precise solution. Next, the initial breaking time and position for a beach of parabolic profile are calculated. The effects of beach profile on wave breaking are clarified.

6) The fact that the breaker height is affected by beach slope for a very flat wave has been shown in the Iversen's experiments. An explanation of the above fact is given on the basis of theoretical breaking conditions.

7) Experimental results on wave run-up of a long wave for 1/30 slope are described. An experimental relation between the relative run-up height and the wave steepness is presented. The relation is fairly close with the Kaplan's curve provided the height of the solitary wave is replaced by the half wave height of the long wave, though the points in the present experiments stand somewhat below.

REFERENCES

Whitham, G. B. (1958). On the propagation of shock waves through regions of non-uniform area or flow, Journal of Fluid Mechanics, Vol.4, Part 4.

Keller, H. B., Levine, D. A., and Whitham, G. B. (1960). Motion of a bore over a sloping beach, Journal of Fluid Mechanics, Vol.7, Part 2.

Greenspan, H. P. (1958). On the breaking of water waves of finite amplitude on a sloping beach, Journal of Fluid Mechanics, Vol.4, Part 3.

Iversen, H. W. (1952). Waves and Breakers in shoaling water, Proc. of 3rd Conferenoe on Coastal Engineering.

Kaplan, K. (1956). Proc. of A. S. C. E., Vol.82, Journal of the Waterways and Harbors Division, No. WW 3.

CHAPTER 6

ON NON-SATURATED BREAKERS AND THE WAVE RUN-UP

Bernard Le Méhauté, D. Sc.
Senior Staff
National Engineering Science Co.
Washington 6, D. C.

ABSTRACT

Some theoretical results pertaining to the physical behavior of gravity waves on a sloped plane are presented. The notion of "saturated" breakers and "non-saturated" breakers which follow the breaking index curve is introduced. Criteria for different kinds of breaking and successive breaking of waves are presented. Some considerations on the wave run-up are deduced.

Then a critical analysis of the method of characteristics is presented, with some possible refinements. Path curvature effect is taken into account and the problem of waves climbing on a dry bed is solved. Criteria for determining saturated and non-saturated breakers and the wave run-up by the method of characteristics are proposed.

INTRODUCTION

It is commonly admitted that breakers on a beach can be separated into spilling breakers on a very flat slope and plunging breakers on a steeper slope. (Plunging breakers are sometimes called surging breakers on a very steep slope.) This separation of breakers into these two (or three) categories is based on visual observations rather than on some hydrodynamical criterium. However, the essential hydrodynamical characteristics of these breakers are recalled.

The profile of a spilling breaker remains, for the most part, almost symmetrical and the wave breaks by curling over slightly at the crest (Figure 1). As long as the foam of the breaker is small by comparison with the "bulk" water, which happens on a very gentle slope, the wave presents roughly the main characteristics of a solitary wave, even after breaking inception. But due to the spilling breaker a given amount of energy is

dissipated in such a way that the wave crest follows the breaking index curve defined by $H = 0.78\, d$. Then the spilling breaker is transformed into a bore when the slope becomes steeper. When the slope is steep before breaking inception, the wave profile first losts its symmetrical shape, then a plunging breaking wave generates a bore directly.

In the following an attempt is made to analytically investigate these described phenomena. As usual two methods exist. The first method -- the energy method -- is only approximate but gives a great amount of information from relatively simple calculations. The second method -- the analytical method -- is more accurate but requires tedious computations for each particular case. Then it will be seen that the method of characteristics requires some refinements for analyzing the surf motion.

THE ENERGY METHOD

The energy method of investigation consists of first determining the wave motion on a horizontal bottom independent of the friction forces. This work has already been accomplished. Then the wave motion is assumed to keep its essential characteristics on a sloped bottom with friction forces with only a simple change in wave height (and wave length). This method is valid provided the bottom slope is gentle enough. Then the cnoidal wave theory or the solitary wave theory is used for very shallow water.

Even after the inception of breaking the essential characteristics of the motion of "bulk" water will be assumed to be also those of a solitary wave. In practice these assumptions are valid for swell waves which give rise to slightly spilling breakers on a very gentle beach. The case under study is presented schematically in figure 1a. Such assumptions do not hold true for steep waves (sea waves) on steep beaches which give rise to plunging breakers, or even when the foam of a spilling breaker becomes too important.

Then it will be written that the variation of transmitted wave energy over a length dx, namely $\frac{d(EC)}{dx}$, is equal to the rate at which this energy is destroyed: $-\frac{dE}{dt}$ which is written:

$$\frac{d(EC)}{dx} = -\frac{dE}{dt}$$

Now the problem arises of how to evaluate EC. Because of the great simplicity of the solitary wave theory one assumes that the wave characteristics are those of a solitary wave, even if the energy is distributed otherwise over a "wave length".

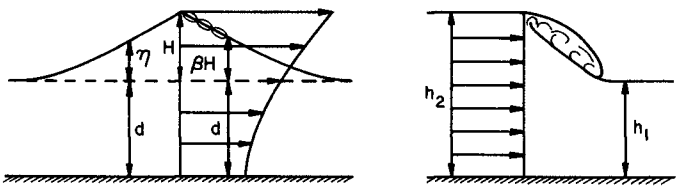

a. SPILLING BREAKER b BORE

Fig. 1

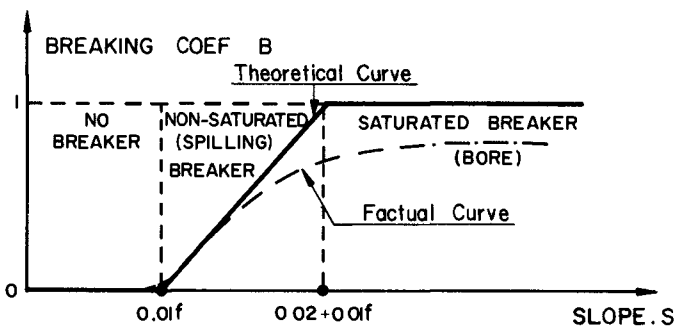

Fig. 2

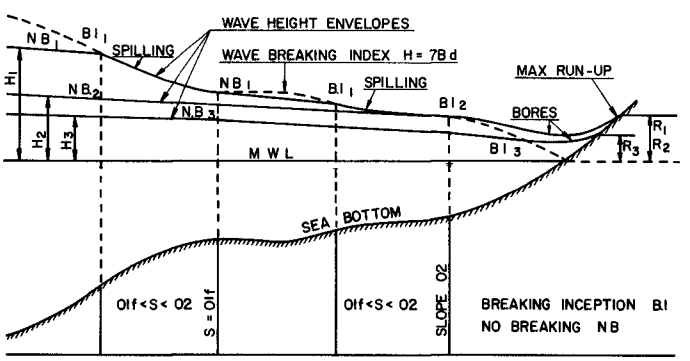

Fig. 3

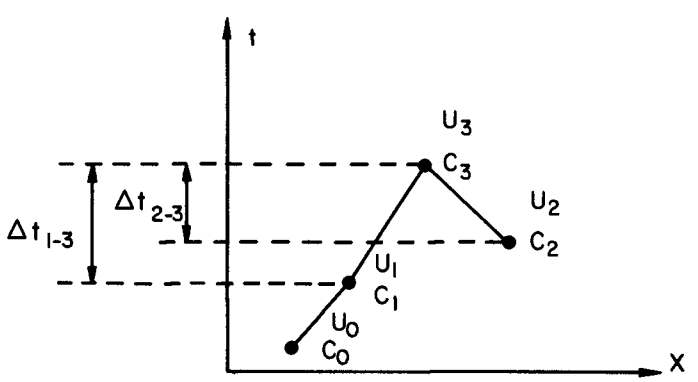

Fig. 4

Then it is known (Munk[1]*):

$$\frac{d(EC)}{dx} = \frac{8}{3\sqrt{3}} \rho g \frac{d}{dx}\left(H^{3/2} d^{3/2} C\right) \qquad \ldots (1)$$

where $C = g(d + H)^{1/2}$.

The rate at which the energy is lost is due to bottom friction $\left.\frac{dE}{dt}\right|_b$ and to spilling breaker $\left.\frac{dE}{dt}\right|_s$. Hence:

$$\frac{d(EC)}{dx} = -\left[\left.\frac{dE}{dt}\right|_b + \left.\frac{dE}{dt}\right|_s\right] \qquad \ldots (2)$$

A number of studies has been carried out on the damping of solitary waves due to viscous bottom friction. However, despite the difficult encountered in evaluating a friction coefficient, it is more realistic for practical purposes to assume the motion to be turbulent. Then the unit shear τ is quadratic: $\tau = \rho f u^2$ where f is a friction coefficient and u the horizontal velocity.

$$\left.\frac{dE}{dt}\right|_b = \int_{-\infty}^{\infty} \tau u \, dx$$

Then by inserting some classical relationships from the solitary wave theory

$$u = C\frac{\eta}{d}, \qquad \eta = \frac{H}{\cosh^2 \alpha}$$

where

$$\alpha = \frac{\sqrt{3}}{2}\left(\frac{H}{d}\right)^{1/2} \frac{x - Ct}{d}$$

it is found that

$$\left.\frac{dE}{dt}\right|_b = \frac{2}{\sqrt{3}} \rho f C^3 \left(\frac{H}{d}\right)^{3/2} H \int_{-\infty}^{\infty} \frac{d\alpha}{\cosh^6 \alpha}$$

By use of the guddermannian of α it is found that the integral is equal to 16/15. Hence, finally

$$\left.\frac{dE}{dt}\right|_b = \frac{32}{15\sqrt{3}} \rho f \frac{H^{3/2} C^3}{d^{3/2}} \qquad \ldots (3)$$

---

* Numbers refer to references listed at end of paper.

ON NON-SATURATED BREAKERS AND THE WAVE RUN-UP

In a very first approximation, f can be taken to be equal to g/C_h^2 where C_h is the Chezy coefficient and n is the Manning coefficient.

$$f = \frac{g}{C_h^2} = \frac{g\,n^2}{(1486)^2\, d^{1/3}} = 14.6\,\frac{n^2}{d^{1/3}} \qquad \ldots (4)$$

This assumption involves that the vertical velocity distribution due to bottom friction in a solitary wave appears as that of a succession of steady flows. In practice such an assumption is really valid for periodic, very long waves in shallow water, which themselves are considered as a succession of solitary waves.

The rate of loss of energy due to a spilling breaker is very similar to that of a tidal bore (which is a shock wave). In the case of a shock wave it is known that (see figure 1b) (Stoker[2]):

$$\frac{dE}{dt} = \rho g Q \frac{(h_2 - h_1)^3}{4 h_1 h_2} \qquad \ldots (5)$$

where h_1 and h_2 are the depths before and after the front of the bore, respectively, and Q is the discharge due to the moving bore. It is recalled that the above formula is based on the assumption that the vertical distribution of the horizontal velocity u is uniform.

In the case under study the spilling breaker is due to the fact that the horizontal velocity at the crest becomes greater than the wave celerity C. By analogy (see figure 1a) $h_2 = d + H$ and $h_1 = d + \beta H$ where β is always smaller than unity and can be zero at the limit. The vertical velocity distribution, and consequently the discharge, is directly related to the average horizontal velocity. Hence the discharge could be written:

$$Q = (d+H)u_2 - (d+\beta H)u_1 = C\frac{H}{d}\left[d + H - \beta(d+\beta H)\right]$$

Inserting these values into equation (5) and defining B as follows:

$$\left.\frac{dE}{dt}\right|_s = \rho g C \frac{H}{d}\left[d+H-\beta(d+\beta H)\right]\frac{H^3(1-\beta)^3}{4(d+H)(d+\beta H)} = \rho g B \frac{C H^4}{4 d^2} \qquad (6)$$

B will be called the "breaking coefficient". The breaking coefficient B is the ratio of the rate of energy dissipated by the spilling breaker to the rate of energy which could be dissipated by a bore of front height equal to the height of the solitary wave which generated it. B = 0 corresponds to no breaking (β = 1). A small value for B corresponds to a little

spilling breaking near the crest (β close to unity). It is a partial breaking or a non-saturated breaker. It is difficult to ascertain the maximum value for B by the energy method. However, it is certain that B cannot be larger than unit ($\beta = 0$). Then there is total breaking and the breaker is a saturated breaker. Further consideration will be given to the physical meaning of B later in this paper.

Now, by introducing equalities (1), (3) and (5) into equation (2), it is found that

$$\frac{d}{dx}\left[H^{3/2}\, d^{3/2}\, C\right] = -\left[\frac{4}{5}\,\frac{f}{g}\,\frac{H^{5/2}}{d^{3/2}} + \frac{3\sqrt{2}}{32}\,\frac{B\,C\,H^{4}}{d^{2}}\right] \quad \ldots \quad (7)$$

which gives after division by $H^{3/2}d^{3/2}C$, integration between a small interval $\Delta x = x_2 - x_1$, and since $e^{-ax} \cong 1 - ax$

$$H_2 = H_1 \left(\frac{d_1}{d_2}\right)\left(\frac{C_1}{C_2}\right)^{2/3}\left[1 - \frac{8}{15}\,\frac{f\,H_1\,C_1^{2}\,\Delta x}{g\,d_{1\text{-}3}^{3}} - \frac{\sqrt{2}}{16}\,\frac{B\,H_1^{5/2}\,\Delta x}{d_{1\text{-}2}^{7/2}}\right] \quad \ldots \quad (8)$$

When all friction effects are neglected (f = 0) and there is no breaking (B = 0), the classical law

$$\frac{H_2}{H_1} = \frac{d_1}{d_2}\left(\frac{d_1 + H_1}{d_2 + H_2}\right)^{1/3} \cong \left(\frac{d_1}{d_2}\right)^{4/3} \quad \ldots \quad (9)$$

is easily recognized. It is known that such a law is not too well verified experimentally. The variation of wave height with distance depends, in fact, on the relative depth $\frac{d_1 + d_2}{d_b}$ where d_b is the depth of breaking[1] and the slope (Ippen and Kulin[5]). This has thrown some doubt on the validity of using the solitary wave theory for analyzing the wave motion on a slope. It is also known that equation (9) should be replaced by the Green Law $\frac{H_2}{H_1} = \left(\frac{d_1}{d_2}\right)^{1/4}$ or again by $\frac{H_2}{H_1} = \left(\frac{d_1 + H_1}{d_2 + H_2}\right)^{1/4}$

Despite these limitations, the physical interpretation of this study will be based on equations (7) and (8) because the spilling breaker effect tends to replace the variation of wave height by a simple $H = 0.78\, d$. When $H < 0.78\, d$, there is no breaking and the breaking coefficient $B = 0$. Then $C = [\, g\,(d + H)\,]^{1/2}$. Moreover, assuming H is small by comparison with d ,

$$H_2 = H_1 \left(\frac{d_1}{d_2}\right)^{4/3} \left[1 - \frac{8}{15} \frac{f H_1 \Delta x}{d_{1\text{-}2}^2}\right] \qquad \ldots (10)$$

It is interesting to note that in the case of long periodic waves, a calculation based on similar assumptions gives

$$H_2 = H_1 \left(\frac{d_1}{d_2}\right)^{1/4} \left[1 - \frac{2}{3\pi} \frac{f H_1 \Delta x}{d_{1\text{-}2}^2}\right]$$

When $H_b = 0.78\, d_b$, there is inception of breaking and the breaking coefficient B becomes > 0. In the case of a small spilling breaker, C keeps its value $C = [g(d + H)]^{1/2}$ Then, replacing these values for H and C in equation (7):

$$\frac{d}{dx}\left(d^{7/2}\right) = 1.1 \frac{f}{g} d^{5/2} + 0.07\, B\, d^{5/2}$$

i.e. the slope $S = \frac{d}{dx}(d) = 0.01\, f + 0.02\, B$ or within the known limits:

$$0 \leqslant B = 50S - 0.5 f < 1 \qquad \ldots (11)$$

It is seen that the breaking coefficient B increases with the slope: the steeper the slope, the greater the rate at which the energy is dissipated by the spilling breaker.

It may occur that due to bottom friction B always retains a zero value despite the shoaling when $S < 0.01\, f$ as is easily seen from equation (11). (This result can also be found directly from equation (7) when replacing H by 0.78d and equating B with zero.)

Inserting the value (4) for f, a criterium for damping without breaking is proposed:

$$S < \frac{14.6\, n^2}{100\, d^{1/3}}$$

i.e. with the Manning coefficient $n = 0.02$

$$S < \frac{6.10^{-5}}{d^{1/3}} \qquad \text{(d in feet)} \qquad \ldots (12)$$

On the other hand, it has been seen that B cannot exceed unity. This happens when $S = 0.02 + 0.01\, f \cong 0.02$. When $S = 0.02$, then the breaker is "saturated." Figure 2 illustrates these considerations.

Now a complete physical interpretation can be drawn from the previous considerations. If the slope is always smaller than $6.10^{-5}/d^{1/3}$,

then the wave height is completely damped by bottom friction. There is no breaking and no run-up. This occurrence is very rare.

On a steeper slope, there is a maximum amount of wave energy that a solitary wave can transmit towards the shoreline over a given depth. This maximum energy is reached when $H = 0.78\ d$. If the amoun of energy passing through a given plane tends to be larger than this maximum value, a spilling breaker will dissipate the difference. This is on a relatively gentle slope and is a non-saturated breaker, in which case the wave height is directly related only to the depth. Then the run-up is negligible.

Considering the usual range of variation of the bottom slope S and a possible range of variation for f , a reason for successive wave breaking due to change of slope and depth is found and its criterium established.

In fact other reasons also exist for successive wave breaking. First, by effect of "hydraulic hysteresis" or inertia for the free turbulenc due to the breaker being damped, more wave energy is spent by a breaker than indicated by equation (11). Then another non-breaking wave could be reformed, even if equation (12) is not fully satisfied.

Moreover, successive breaking may also be due to the superimposition of crests of irregular waves for which the following formula is proposed: (Le Méhauté[3])

$$\sum^{n} \left(\frac{H}{L}\right)^2 = \frac{0.02}{n} \sum^{n} \tanh^2 \frac{2\pi d}{L}$$

(It is interesting to note that this formula gives good results whatever the wave direction: two-dimensional irregular waves, clapotis, short-crested waves.) However, since in very shallow water all waves tend to travel to a constant velocity, the above criterium is valid more for the whitecaps at sea than in the vicinity of the shoreline.

Now the case of total breaking is considered.

It is seen, also, that there is a limiting amount of energy which could be dissipated by a breaker over a given length. Hence, when the slope becomes steeper and steeper, the regulating effect of the spilling breaker reaches its limit when $B = 1$. Then the breaking index curve is surpassed by the height of the front bore. There is run-up. The words "saturated" and "non-saturated" breakers are now defined, explained and justified.

ON NON-SATURATED BREAKERS AND THE WAVE RUN-UP

A very important conclusion is also drawn: On a beach having its curvature upwards, the maximum possible wave run-up is given by the wave which breaks at a depth where the slope is equal to 0.02. It is known that if d_b is the depth over that slope, the corresponding wave height is $H_b = 0.78\, d_b$. Any wave having a greater height breaks sooner, dissipating its energy following the breaking index curve up to the plane where the slope becomes larger than 0.02.

In fact the theoretical value 0.02 for the critical slope (corresponding to $B = 1$) may be replaced by a more factual and conservative value 0.01. The exact determination of this value requires further investigation by the method of characteristics.

The results of this section are summarized in figure 3 by three typical cases. It must be noted that the run-up in cases I and II is the same despite their different deep water wave heights.

ON THE METHOD OF CHARACTERISTICS

First the usual presentation of the method of characteristics is recalled. Then it will be seen that the application of this method to the problem under study requires a number of modifications and refinements.

It seems that the first application of the method of characteristics to the problem of a wave breaking over a beach was due to Stoker[2]. (Other references are given by Ho and Meyer.[4]) In fact the same method has been applied for a long time in studying tidal motion and bore formation in estuaries. In both cases the vertical velocity distribution is assumed to be uniform and the pressure distribution hydrostatic. Moreover, the friction forces (neglected by Stoker) take great importance in the study of tidal motion in estuaries. Then the two basic equations are:

momentum: $$\frac{\partial u}{\partial t} + u\frac{\partial u}{\partial x} = -g\frac{\partial \eta}{\partial x} - g\frac{u|u|}{C_h^2(d+\eta)}$$

continuity: $$\frac{\partial \eta}{\partial t} = -\frac{\partial u(d+\eta)}{\partial x}$$

where u is the average horizontal velocity along OX, η the elevation of the free surface above the still water level, $(d+\eta)$ the depth, and C_h the Chezy coefficient.

Defining the quantity $c = [g(d+\eta)]^{1/2}$ it is found after some transformation that

$$\left\{\frac{\partial}{\partial t} + (u \mp c)\frac{\partial}{\partial x}\right\}(u \mp 2c) = G$$

where $G = -gS - \frac{g}{C_h^2} \frac{u|u|}{(d+y)}$

i.e. $\frac{d}{dt}(u + 2c) = G$ along $\frac{dx}{dt} = u + c$

$\frac{d}{dt}(u - 2c) = G$ along $\frac{dx}{dt} = u - c$

It is recalled that G is considered as a constant over a small interval Δ t.

Then, by knowing u and c at two points defined by their position x and time t (figure 4), it is possible to calculate the location of a third point by drawing the lines of slope $1/u_1 + c_1$ and $1/u_2 - c_2$ in a (t,x) diagram and to calculate u_3 and c_3 from the equations:

$$\begin{cases} u_3 + 2c_3 = u_1 + 2c_1 + G\,\Delta t_{1-3} \\ u_3 - 2c_3 = u_2 - 2c_2 + G\,\Delta t_{2-3} \end{cases}$$

Hence, this powerful method permits the complete analysis of the wave motion as a function of time and space. However, as it is presently used, it has some limitations. One of them is rightly pointed out by Stoker:

The method of characteristics gives a marked steepening of the wave front and a very unsymmetrical shape for the wave at breaking. In a word, the method of characteristics gives directly a bore or saturated breaker while it is well observed that spilling breakers remain almost symmetrical in shape.

The case of a solitary wave on a horizontal bottom without friction is of particular interest because it is known that a solitary wave must travel without deformation. When this problem is treated by the method of characteristics, the wave profile becomes quickly deformed and even generates a bore, despite the fact that the bottom is horizontal. This discrepancy is due to the fact that the flow curvature, particularly important near the crest of a wave, is neglected in the method of characteristics while the profile of a solitary wave is obtained by integrating the continuity and momentum equations in which a term for the flow curvature has been introduced. It is because of this term that the pressure distribution in a solitary wave is actually smaller than the hydrostatic pressure and much smaller (40%) under a near breaking wave crest.

This term is presented in many books. It is therefore judged unnecessary to reproduce the calculations here. It is sufficient to know that it is obtained by considering that the vertical component of velocity is

assumed to be linearly distributed from the bottom to the free surface. This is a very realistic assumption. It is also assumed that the bottom slope has a negligible effect on the path curvature. This assumption holds true only for a gentle slope near the wave crest. But, if these conditions are not satisfied, the path curvature correction becomes small, in any case, by comparison with other terms such as ($-g\,S$). Hence a more complex calculation of the path curvature effect taking account of the bottom slope would be easy to perform but not worthwhile for practical purposes.

Then the momentum equation is written

$$\frac{\partial u}{\partial t} + u\,\frac{\partial u}{\partial x} = -\,g\,\frac{\partial \eta}{\partial x} - g\,\frac{u|u|}{C_h^2\,(d+\eta)} - \frac{d+\eta}{3}\,\frac{\partial^3 \eta}{\partial t^2\,\partial x}$$

Hence the only modification introduced by the flow curvature in the method of characteristics is to give G the value

$$G = -\,gS - \frac{g\,u|u|}{C_h^2\,(d+\eta)} - \frac{d+\eta}{3}\,\frac{\partial^3 \eta}{\partial t^2\,\partial x}$$

This expression can easily be expressed as a function of u and c for each point of the x, t diagram along the characteristics since according to the continuity equation and the definition for c

$$G = -\,gS - \frac{g^2}{C_h^2}\left(\frac{u}{c}\right)^2 + \frac{c^2}{3g^2}\,\frac{\partial^3 (u\,c^2)}{\partial t\,\partial x^2}$$

Hence the previous values for G, G_1 and G_2 will be corrected by terms ΔG_1 and ΔG_2 .

For more generality it is of great interest to work with dimensionless terms. Defining $C_* = [\,g\,d_1\,]^{1/2}$ where d_1 is an arbitrary depth

$$U = \frac{u}{C_*}\ ,\quad C = \frac{c}{C_*}\ ,\quad X = \frac{x}{d_1}\ ,\quad T = \frac{C_*\,t}{d_1}$$

The basic equations become

$$\frac{d}{dT}\,(U \mp 2C) = G_* = -\,S - \frac{g}{C_h^2}\left(\frac{U}{C}\right)^2 + \frac{C^2}{3}\,\frac{\partial^3 (UC^2)}{\partial X^2\,\partial T}$$

along $U \pm C = \frac{dX}{dT}$.

In view of determining the maximum possible run-up, it is seen from the first part of this study that the most convenient input is the profile of a limit solitary wave where the slope tends to become steeper than 0.01. Then d_1 can be taken as the depth at that particular location. It is at this location that the breaking index curve is no longer followed. The breaker is close to being saturated. The relative maximum possible wave run-up, $\frac{R_{Max}}{0.78\, d_1} = \frac{R_{max}}{H_{Max}}$, will appear as a function of the slope only. Such a method of calculation often permits reduction of the number of calculations required. Consequently the cumulative errors are reduced in such a way that the final result is even better than that which would be given by starting directly from an input defined by a non-breaking wave in deep water. Also, as long as the wave travels on a slope smaller than 1/10, the curvature term has a non-negligible influence in computing the run-up.

Now another deficiency of the method of characteristics and its solution are analyzed. First it is recalled that there is bore formation when two characteristics of the same family cross each other. Then two values for c, and consequently for v, are obtained. It means physical that the wave breaks and forms a tidal bore.

Actually, as pointed out in the first section of this paper, a spillin breaker appears prior to bore formation. It has been seen resulting in a loss of energy, which is not taken into account by the method of character istics. This is due to the fact that the method of characteristics is based on the assumption that the vertical velocity distribution is uniform while the spilling breaker is due to the local high particle velocity near the cres

The method of characteristics can be corrected in order to take account of this important phenomenon. It is sufficient to impose to v or H, and consequently to c, a maximum value prior to the bore formation. This maximum value for H will be $0.78d$, for example. Then $c_{max} = [1.78\, gd]^{1/2}$.

Such computations define the area for non-saturated breakers. Then, again, when two characteristics of the same family cross each othe the bore appears and the non-saturated spilling breakers are transformed into saturated breakers. It is evident that on a steep slope this intermedi process of calculation does not appear.

Now the succeeding steps of the computations are given.

U and C can always be determined on the low side of the bore, say U_d and C_d. Along the bore line defined by $\frac{dX}{dT} = V$, where V is the speed of the bore, three unknowns must be determined: V itself, and U C on the high side of the bore, namely U_u and C_u. These three unknowns are determined from the momentum equation and the continuity equation for shock waves, and by the U + C line which crosses the V line on the high side of the bore from a point o (U_o, C_o). (Its construction may require some interpolation.) Hence, the system of equations to be solved is:

$$C_u^2 - C_d^2 = 2 C_d^2 [V - U_d][U_u - U_d]$$

$$U_u C_u^2 - U_d C_d^2 = V [C_u^2 - C_d^2]$$

$$U_u + 2 C_u = U_o + 2 C_o + G_* \Delta T_{o-u}$$

The solution of this system is given by the following set of equations:

$$\frac{X^4 - 1}{\sqrt{2} X [1 + X^2]^{1/2}} + 2X = K$$

where

$$X = \frac{C_u}{C_d} \quad , \quad K = \frac{U_o + 2 C_o - U_d + G_* \Delta T_{o-u}}{C_d}$$

which permits calculation of C_u. Then U_u is obtained directly and

$$V = U_d + \frac{C_u}{C_d} \left[\frac{C_u^2 + C_d^2}{2} \right]^{1/2}$$

Now the characteristics on the high side of the bore are easily determined from the obtained values for U_u and C_u.

When the depth tends to zero, $C_d \longrightarrow 0$. Then it has been said that the above formula for V loses its physical meaning because V

tends to infinity. In fact it is pointed out that V can never exceed $U_u + C_u$. First, the wave elements have a tendency to catch up the front of the bore at a speed U + C. Then the energy at the front of the bore is dissipated by turbulence as it is in a shock wave. Hence C_u decreases up to the point where V given by the above formula equals $U_u + C_u$. The above equation for the bore is always valid but then C_u also tends to zero when C_d tends to zero, i.e. near the shoreline. It is a "depression wave." (But U retains a value different from zero.) Then the set of equations becomes:

$$V = U_u + C_u = U_d + \frac{C_u}{C_d}\left[\frac{C_u^2 + C_d^2}{2}\right]^{1/2}$$

and also, since the characteristics for V become

$$V = \frac{dx}{dT} = U_u + C_u \quad , \quad U_u + 2C_u = (U_u + 2C_u)_o + G\,\Delta T_{ou-u}$$

index o indicating the previous values on the V line. This set of equation can easily be solved from the equations for C_u:

$$C_u^4 - AC_u^2 + BC_u - C = 0$$

where $A = C_d^2$

$$B = 4\left\{(U_u + 2C_u)_o + G\Delta T - U_d\right\}C_d^2$$

$$C = 2\left\{(U_u + 2C_u)_o + G\Delta T - U_d\right\}^2$$

Then the calculation of U_u and $V = U_u + C_u$ is obtained easily for the following step.

It is seen that the shock wave disappears at the shoreline and that it is an edge of water which climbs on the beach. Hydrodynamically speaking, it is not a bore (nor a shock wave) which climbs on a dry bed, but a "depression wave." In fact it is true that the extreme edge of water is cut and the front of the water is roughly at a 60° angle with the vertical, presenting the aspect of a bore. At this extreme edge C always equals zero since then $\eta = -d$ and $V = U$. The maximum wave run-up is obtained when U also tends to zero.

The same mathematical process can be applied for studying the wave due to the breaking of a dam: V can never exceed U + C in shallow water and U on a dry bed.

CONCLUSION

New concepts such as saturated and non-saturated breakers and corresponding criteria have been established. It has been demonstrated that spilling breakers follow the breaking index curve as long as the bottom slope is not steeper than 0.02, at which point the breaker becomes saturated. Hence the maximum possible wave run-up is given by the wave which breaks over this slope. If the wave is higher it will dissipate its energy sooner and will finally give the same run-up. Because of this result, application of the method of characteristics in deeper water is without use. The input of the method of characteristics can be taken as a limit solitary wave where the slope is 0.02 or 0.01 by safety. Starting the method of characteristics on a gentler slope in deeper water will give more error due to the cumulative effect of errors.

It has been shown that on a slope smaller than 1/10, the path curvature has an important effect on wave deformation, which cannot be neglected The correcting term to be included in the method of characteristics has been established. It has also been shown that the dissipation of energy at the crest of a spilling breaker (without shock wave) has to be taken into account by imposing a maximum value for C.

Finally the method of computing the bore in shallow water and the climb of the water on a dry beach has been established. It has been demonstrated that the bore or shock wave stops at the shoreline and it is a "depression wave" or edge of water which climbs on the beach.

It can be concluded that the wave run-up (and associated problems such as waves due to the breaking of a dam) can now be completely solved by theory, whatever the complexity of the slope.

A computing program presently under development should permit investigation of the wave spectrum run-up taking into account the interaction of one wave on the following wave.

ACKNOWLEDGEMENTS

This study, initiated while the writer was at Queen's University, under the sponsorship of the National Research Council of Ottawa, was completed at the National Engineering Science Co. The writer is very indebted to Prof. R. J. Kennedy and Dr. C. L. Bretschneider for their encouragement and fruitful discussions. The author also wishes to express his deep gratitude to Dr. J. Freeman who gave him so much information on the method of characteristics and who must be credited for finding that V can never exceed $U + C$.

REFERENCES

1. Munk, W. H. "The Solitary Wave Theory and Its Application to Surf Problems." Annals, N. Y. Academy of Sciences, Vol. 51, Art. 3, p. 376

2. Stoker, J. J. Water Waves. Interscience Publishers, N. Y., N. Y.

3. Le Méhauté, B. (1961) "A Theoretical Study of a Wave Breaking at an Angle with a Shoreline." Journal of Geophysical Research, Vol. 66, No. 2, p. 495

4. Ho, D. V. and R. E. Meyer (1962). Climb of a Bore on a Beach. Office of Naval Research, U. S. Navy, Tech Report No. 47.

5. Ippen, A. T. and G. Kulin. (1954) "The Shoaling and Breaking of a Solitary Wave." Vth Coastal Engineering Conference, Proceedings, Grenoble, p. 27.

6. Keulegan, G. H. "Gradual Damping of a Solitary Wave." Journal of Research, Nat. Bureau of Standards, Vol. 40, No. 6, p. 487

7. Iverson, H. W. (1951) "Laboratory Study of Breakers." Gravity Waves. Nat. Bureau of Standards Circular 521.

CHAPTER 7

EFFECT OF ENTRANCE ON SEICHE MOTION IN OCEAN PORTS

Nikhilesh Roy
Assistant Professor, Civil Engineering Department
Indian Institute of Technology, Kharagpur, India.

ABSTRACT

The seiche motion induced in a partially open harbour is uniquely determined by the standing wave pattern formed in the outside ocean. The variable location and size of the coupling makes the problem essentially three-dimensional. Existing potential theory has been extended, for the case of a simple rectangular port, to simulate ocean conditions by approximating the open ocean by another rectangular basin of large size. The theoretical problem then reduces to solving the Neuman problem for the two-dimensional Helmholtz equation $\nabla^2 F + K^2 F = 0$ for a polygonal contour. The finite dimensional approximation of an infinite domain is, however, unsatisfactory at least from the analytical point of view. This difficulty has been removed, in this paper, by using elliptic-cylindrical co-ordinates for the semi-infinite domain in which the perturbation potential has been expanded in terms periodic Mathieu functions. These theoretical developments have been verified by a series of numerical calculations and experimental studies,

INTRODUCTION

The phenomenon of long period standing wave is variously termed as surge, seiche motion, or simply seiche. When resonance occurs in the induced motion in the port, the amplitude of motion is magnified, sometimes greatly, and although the height of surge may be smaller than that of storm waves, the horizontal water motion is usually large. Since a ship is small compared to the wave length of a seiche motion, it may be expected to move in space with water motion unless rigidly restrained. Although this type of wave motion and consequent damages to ship were first observed in the Pacific coast of the U.S.A. (1), recent reports (2,3) indicate that such motion exists in many coastal regions of the world and has been a source of serious concern to harbour authorities at these places.

Because of the extremely small steepness of the seiche waves, a standing wave pattern exists offshore of any coast line that receives such waves. If this coast line is now broken to accomodate an entrance to a port, a part of the incident wave is transmitted inside and suffers multiple reflections at the harbour boundaries. Depending on the boundary geometry, a forced oscillation results which, if losses are neglected, is in phase with the outside motion.

The free surface pattern is dominated by the nearest free oscillation mode of the harbour assumed closed on all sides. The two-dimensional picture of the open sea also undergoes a local deformation around the harbour mouth which dies out with increasing distance at a rate depending upon the ratio of the entrance width to the wave length. The oscillations inside and outside of the port should, therefore, be considered parts of the same motion. Mathematically, this means that the potential of motion should be that of standing wave both inside and outside of the port, the analytic continuity of the two functions being maintained through the harbour mouth.

The theoretical treatment when the open sea is approximated by a finite basin is relatively simple and was developed by Apte'(4) and recently extended by Ippen and Raichlen(In both cases an experimental model was selected to represent ocean conditions near the harbour mouth as each investigator thought appropriate. This model, which in the case of Raichlen was more representative of the prototype situation, was then analysed theoretically under certain restrictive conditions.

On the other hand, until Miles and Munk(6) published their work, there was no analytical solution available for the open sea case. Their approach was, however, somewhat different as they assumed the harbour to oscillate freely and, due to the presence of the entrance opening, radiate energy toward the open sea. This radiated energy is radially diffused in the open expanse and lost to the harbour itself thus limiting the maximum amplification of the harbour system at resonance. As a result, the potential of motion inside the port was that of standing wave and that outside, of a standing wave and progressive wave. However, in computing the resonant wave number, only the real part of the open sea potential was considered.

The present studies were undertaken when neither the work of Raichlen nor that of Miles and Munk were published. Even then, there are material differences in the work described here and those referred above. Figures 1 and 2 show the relative position of the port, the outer sea and a channel of variable length that connects the two. In fig.1, the outer sea has been assumed finite while fig.2 shows this basin to be infinite in extent. The arrangement shown in these figures are more general than those considered previously because, in any physical situation, the harbour does not begin immediately shoreward of the sea. In fact, ports with 'narrow' approach channels of finite length are not rare in nature.

In the present studies only waves with crests parallel to the coast line have been considered. The outer boundary of the finite open sea is constituted by a virtual wall at an antinodal line that is sufficiently away from the harbour mouth to be appreciably distorted by the presence of the opening. For the semi-infinite open sea, it is necessary to consider, in addition to the two-dimensional standing wave potential, a perturbation potential which possesses a finite gradient at the harbour mouth, a zero gradient at the rest of the coast line and disappears at large distances from the mouth. Such a solution is available if we use elliptic-cylindrical co-ordinates and expand the perturbation potential of the open sea in terms of periodic angular and radial Mathieu functions, the angular functions forming an orthogonal set. It may be remarked here that the Hankel function expansion proposed by Miles is convenient only as long as the harbour entrance is 'narrow'. Besides, the variational principle used in their analysis can not predict the complete response curve and the form of the proposed entrance velocity distribution function leads to an arbitrary entrance velocity and consequently an arbitrary amplitude of motion at resonance although, the power amplification is finite.

Perhaps, this brief review will be incomplete without a reference to the valuable work done by Biesel and Le Me'haute'(7,8) in this field.But, their approach, was, essentially, two-dimensional, the harbour entrance being treated as a localised obstruction in the passage of progressive waves. It is apparent that such an approach can take care of the width of the opening but not its location in the seward side of the port which, as will be shown later, plays an important role in those oscillations of the harbour that are primarily transversal. Unfortunately, transversal oscillations have not received much attention so far although, such motions are not at all unusual in harbours.

THEORETICAL STUDIES

THE MODEL

In the figures 1 and 2 the domains of the port, canal, and the sea are denoted D_p, D_c and D_s respectively, the domain D_s being placed symmetrically with respect to the domain D_p. The basins are of constant depth h and the boundary walls are assumed vertical. The axes of reference are Oxyz, the Oxy plane coinciding with the mean water level in the basins, and the axis Oz is directed vertically upwards so that $z = -h$ denotes the bottom of the basins. It may be noted that the side GFKJ represents the totally reflecting coast line which extends, in the case of semi-infinite outer domain, to infinity in the positive & negative x - direction.

The desired standing wave pattern in the closed domain D_s is produced by a wave train incident at the other end of the long, narrow wave canal shown at extreme right of figure 1 The analysis presented in the following pages can be utilised to show that this arrangement produces negligible disturbance.

BASIC THEORY

The flow is assumed irrotational. As the wave steepness is very small, the exact linear surface wave theory can be used to solve this three dimensional-problem.

The velocity potential satisfying the Laplace, free surface and the bottom surface conditions can be written, assuming simple harmonic oscillation, as :

$$\phi_{Pot} = -\frac{g\,T}{2\pi}.\mathrm{Cos}\,\frac{2\pi t}{T}\cdot\frac{\mathrm{Cosh}\,K\,(z+h)}{\mathrm{Cosh}\,K\,h}\,F(x,y) \quad \ldots\ldots \quad (1)$$

Where T is the period of the generating wave, and F(x,y) satisfies the differential equation :

$$\nabla^2 F + K^2 F = 0 \quad \ldots\ldots \quad (2)$$

K is related to the period by the equation

$$\left(\frac{2\pi}{T}\right)^2 = g\,K\,\tanh\,K\,h \quad \ldots\ldots \quad (3)$$

In addition to (2), F satisfies the condition

$$\frac{\partial F}{\partial n} = 0 \quad \ldots \quad \ldots\ldots \quad (4)$$

along the vertical walls of the port, where n is the direction of the outward drawn normal to the boundary of the basins. Along the two parts of the boundary occupied by the left and right end of the communicating canal we can write

$$\text{(i)}\quad \frac{\partial F_p}{\partial n} = -\frac{\partial F_c}{\partial n} \quad \text{for} \quad y = 0$$

$$\text{i.e.}\ \frac{\partial F_p}{\partial y} = \frac{F_c}{\partial y} = V^s(x) \ \text{for} \ y = 0 \quad \ldots \quad (5)$$

and

$$\text{(ii)}\quad \frac{\partial F_c}{\partial n} = -\frac{\partial F_s}{\partial n}, \quad \text{for} \quad y = -L$$

$$\text{i.e.}\quad \frac{\partial F_c}{\partial y} = \frac{\partial F_s}{\partial y} = G^s(x), \text{for } y = -L, \quad \ldots \quad (6)$$

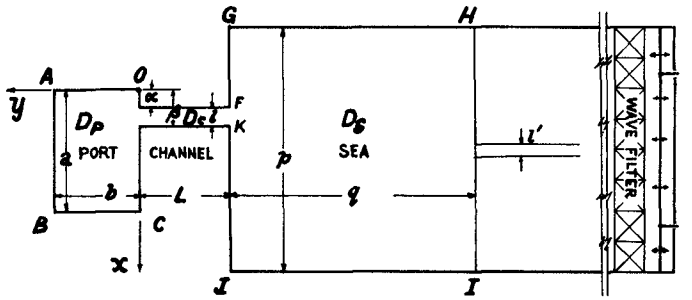

Fig. 1. Rectangular harbour and approach channel connected to a finite wave basin.

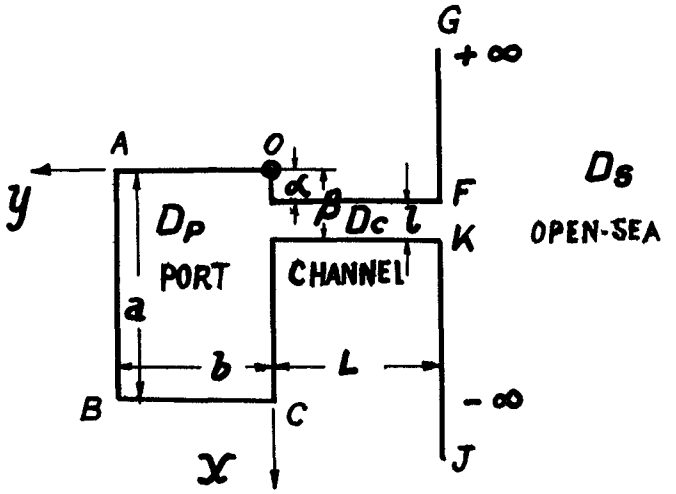

Fig. 2. Rectangular harbour and approach channel connected to an open sea.

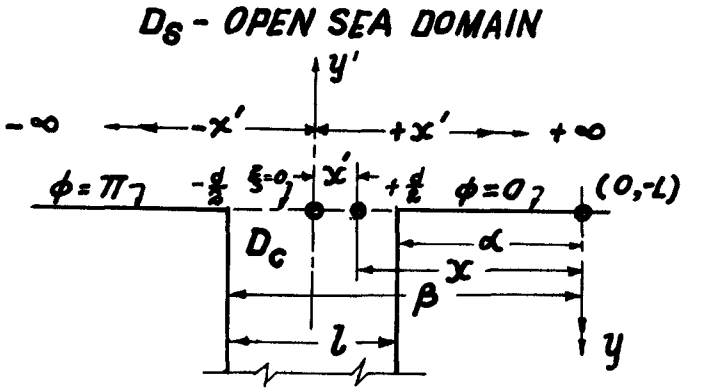

Fig. 3. Co-ordinate system used in the open sea analysis.

where the subscripts of F are the domain subscripts, The two auxiliary functions $V^s(x)$ and $G^s(x)$ are defined by the following fourier series representation

$$V^s(x) = \sum_{m=0}^{\infty} U_m \cos\frac{m\pi x}{a} = \sum_{k=0}^{\infty} f_k \cos\frac{k\pi(x-\alpha)}{l}, \quad \begin{matrix} 0 & 0<x<\alpha \\ 1 & \alpha\leq x\leq\beta \\ 0 & \beta<x<a \end{matrix} \qquad (7)$$

$$G^s(x) = \sum_{i=0}^{\infty} V_i \cos\frac{i\pi(x+c)}{p} = \sum_{k=0}^{\infty} g_k \cos\frac{k\pi(x-\alpha)}{l}, \quad \begin{matrix} 0 & -c<x<\alpha \\ 1 & \alpha\leq x\leq\beta \\ 0 & \beta<x<a+c \end{matrix} \qquad (8)$$

Again the equality of water level at the common sections gives us;

$$F_p = F_c \quad \text{for } y = 0, \qquad \ldots (9)$$

$$\text{and} \quad F_c = F_s \quad \text{for } y = -L, \qquad \ldots (10)$$

ANALYTICAL DEVELOPMENT

The Helmholtz equation, eqn (2), is solved forthe various basins by expanding the F functions in terms of the eigen functions of these separate basins assumed closed. Only those frequencies of excitation are considered here which give"resonance"in the domains D_p and D_s individually. This gives

$$K^2 = \pi^2\left(\frac{m_o^2}{a^2} + \frac{n_o^2}{b^2}\right) = \pi^2\left(\frac{i_o^2}{p^2} + \frac{J_o^2}{q^2}\right) \qquad \ldots (11)$$

where m_o, n_o and i_o, j_o represents the number of nodal lines parallel to the corresponding sides of the two basins. However, the general development is valid for other frequencies as well.

We now write the F functions for the various domains noting that these, when substituted in eqn.(1), give the corresponding velocity potentials

(i) Domain D_p

$$F_p(x,y) = \sum_{m=0}^{m<\frac{ak}{\pi}} U_m \cos\frac{m\pi x}{a}\cdot\frac{\cos\phi_m(y-b)}{\phi_m \sin\phi_m b} +$$

$$+R_{mo}\cos\frac{m_o\pi x}{a}\cdot\cos\frac{n_o\pi y}{b} = \sum_{m>ak/\pi}^{\infty} U_m \cos\frac{m\pi x}{a}\cdot\frac{\cosh\phi'_m(y-b)}{\phi'_m \sinh\phi'_m b} \qquad \ldots (12)$$

(ii) Domain D_c :

$$F_c(x,y) = \sum_{k=0}^{k<\frac{lK}{\pi}} \frac{\cos \frac{k\pi(x-\alpha)}{l}}{\phi_k \sin \phi_k L} \left\{ - f_k \cos \phi_k (y+L) + \right.$$

$$\left. + g_k \cos \phi_k y \right\} + \sum_{k>lK/\pi}^{\infty} \frac{\cos \frac{k\pi(x-\alpha)}{l}}{\phi'_k \sinh \phi'_k L} \left\{ + f_k \cosh \phi'_k (y+L) - g_k \cosh \right.$$

$$\left. \phi'_k y \right\} \qquad \ldots \qquad (13)$$

(iii) Domain D_s :

$$F_s(x,y) = -\sum_{i=0}^{i<\frac{pK}{\pi}} V_i \cos \frac{i\pi(x+c)}{p} \cdot \frac{\cos \phi_i (y+L+q)}{\phi_i \sin \phi_i q} +$$

$$P_{i_o} \cos \frac{i_o \pi (x+c)}{p} \cos \frac{J_o \pi y}{q} + \sum_{i>pK/\pi}^{\infty} V_i \cos \frac{i\pi(x+c)}{p} \cdot$$

$$\cdot \frac{\cosh \phi'_i (y+L+q)}{\phi'_i \sinh \phi_i q} \qquad \ldots \quad (14)$$

Where

$$\phi_m = \left(K^2 - \frac{m^2\pi^2}{a^2}\right)^{\frac{1}{2}}; \quad \phi'_m = \left(\frac{m^2\pi^2}{a^2} - K^2\right)^{\frac{1}{2}}$$

$$\phi_k = \left(K^2 - \frac{k^2\pi^2}{l^2}\right)^{\frac{1}{2}}; \quad \phi'_k = \left(\frac{k^2\pi^2}{l^2} - K^2\right)^{\frac{1}{2}}$$

$$\phi_i = \left(K^2 - \frac{i^2\pi^2}{p^2}\right)^{\frac{1}{2}}; \quad \phi'_i = \left(\frac{i^2\pi^2}{p^2} - K^2\right)^{\frac{1}{2}}$$

These expressions satisfy the partial derivative equations (5) and (6) with the help of first definitions of the auxiliary functions given in equations (7) and (8).

It may be noted that the various Fourier coefficients are yet unknown. The coefficients f_k and g_k are determined by applying the matching conditions prescribed in equations (9) and (10).

Analytic continuity of the velocity potential at the left end of the coupling canal (y = 0) gives, then,

$$\sum_{k=0}^{\infty} f_k A_k \cos\frac{k\pi(x-\alpha)}{l} - \sum_{k=0}^{\infty} g_k B_k \cdot \cos\frac{k\pi(x-\alpha)}{l} = \sum_{m=0}^{\infty\,\prime} U_m A_m \cos\frac{m\pi x}{a} + R_{mo}\cos\frac{m_o\pi x}{a} \quad \ldots\ldots \quad (15)$$

Where, the dashed summation sign indicates that the m_o th term has been omitted in the infinite series in m, and

$$A_m = \frac{\cot \phi_m b}{\phi_m}, \quad m < \frac{a K}{\pi}$$

$$= \frac{-\coth \phi'_m b}{\phi'_m}, \quad m > \frac{a K}{\pi} \quad \ldots\ldots \quad (16a)$$

$$A_k = -\frac{\cot \phi_k L}{\phi_k}\ ;\ B_k = -\frac{\operatorname{Cosec} \phi_k L}{\phi_k}\ ;\ k < \frac{l K}{\pi}$$

$$= +\frac{\coth \phi'_k L}{\phi'_k}\ ;\ = +\frac{\operatorname{Cosech} \phi'_k L}{\phi'_k}\ ;\ k > \frac{l K}{\pi} \quad \ldots\ldots \quad (16b)$$

Both, the series in equation (18) are uniformly and absolutely convergent in the interval $\alpha \leq x \leq \beta$. Hence, we can multiply both sides of the equation by $\cos\frac{r\pi(x-\alpha)}{l}$, $r = 0,1,2, \ldots, \infty$ and integrate, term by term, within that interval to obtain;

$$f_r N_r A_r - g_r N_r B_r = \sum_{m=0}^{\infty\,\prime} U_m A_m M_{mr} + R_{mo} M_{mor} \quad \ldots\ldots \quad (17)$$

$$r = 0,1,2, \ldots, \infty$$

Where, $N_0 = 1$ and $N_r = \frac{1}{2}$ for $r \geq 1$

$$\text{and } M_{mr} = \int_{\alpha}^{\beta} \text{Cos } \frac{m\pi x}{a} \cdot \text{Cos } \frac{r\pi(x-\alpha)}{l} \cdot dx \quad \ldots\ldots (18)$$

Similarly, the analytic continuity at the right end of the canal ($y = -L$) gives,

$$\sum_{k=0}^{\infty} f_k B_k \text{ Cos } \frac{K\pi(x-\alpha)}{l} - \sum_{k=0}^{\infty} g_k A_K \text{ Cos } \frac{k\pi(x-\alpha)}{l}$$

$$= \sum_{i=0}^{\infty}{}' V_i A_i \text{ Cos } \frac{i\pi(x+c)}{p} + P_{io} \text{ Cos } \frac{i_o\pi(x+c)}{p} \quad \ldots\ldots (19)$$

Where,

$$A_i = -\frac{\text{Cot } \phi_i b}{\phi}, \quad i < \frac{pK}{\pi}$$

$$= \frac{\text{Coth } \phi_i' b}{\phi_i'}, \quad i > \frac{pK}{\pi}$$

and the dashed summation sign indicates again, that the i_oth term has been omitted in the infinite series in i.

Proceeding as before, we get :

$$f_r N_r B_r - g_r N_r A_r = \sum_{i=0}^{\infty}{}' V_i A_i M_{ir} + P_{io} M_{i_o r}$$

$$r = 0,1,2,3, \ldots\ldots\infty \quad \ldots\ldots (20)$$

where $N_o = 1$ and $N_r = 1/2$ for $r \geq 1$
Replacing U_m and V_i in terms of f_k and g_k, respectively from equns (7) and (8), we can rewrite equations (17) and (20) as below :

$$f_r N_r A_r - g_r N_r B_r = \sum_{k=0}^{\infty} f_k \sum_{m=0}^{\infty}{}' A_m' M_{mk} M_{mr} + R_{mo} M_{mor} \quad \ldots(21a)$$

$$r, k = 0,1,2, \ldots\ldots,\infty$$

and

$$f_r N_r B_r - g_r N_r A_r = \sum_{k=0}^{\infty} g_k \sum_{i=0}^{\infty}{}' A_i' M_{ik} M_{ir} + P_{io} M_{i_o r} \quad \ldots(21b)$$

$$r, k = 0,1,2, \ldots\ldots,\infty$$

Where, $A'_m = \frac{1}{a} A_m$, for $m = 0$; $A'_i = \frac{1}{p} A_i$, for $i = 0$

$= \frac{2}{a} A_m$ for $m \geq 1$; $= \frac{2}{p} A_i$, for $i \geq 1$

and $M_{mk} = \int_{\alpha}^{\beta} \text{Cos} \frac{m\pi x}{a} \cdot \text{Cos} \frac{k\pi(x-\alpha)}{l} \cdot dx$

$M_{ik} = \int_{\alpha}^{\beta} \text{Cos} \frac{i\pi(x+c)}{p} \cdot \text{Cos} \frac{k\pi(x+\alpha)}{l} \cdot dx$

Similarly, M_{mr} and M_{ir}.
Writing equations (21) in matrix form

$$\begin{aligned} [D_{rk}] + [\Lambda_{rk}]\ (g_k) + P_{io}\ (Mi_o r) &= [\lambda_{rk}]\ (f_k) \\ [B_{rk}] - [\Lambda_{rk}]\ (f_k) + Rm_o\ (Mm_o r) &= -[\lambda_{rk}]\ (g_k) \end{aligned} \quad \ldots\ldots(22)$$

$k, r = 0,1,2, \ldots\ldots\infty$

Where, $[\Lambda_{rk}]$ and $[\lambda_{rk}]$ are diagonal matrices whose diagonal elements are given by $N_o A_o$, $N_1 A_1$,....etc. and $N_o B_o$, $N_1 B_1$ ...etc., respectively. Further, the elements of the matrices $[B_{rk}]$ and $[D_{rk}]$ are given by

$$B_{oo} = \frac{l^2}{a} A_o + \sum_{m=1}^{\infty}{}' A'_m M_{mo} M_{mo}; \quad k = r = o$$

$$B_{ok} = B_{ko} = \sum_{m=1}^{\infty}{}' A'_m M_{mk} M_{mo}; \quad r = o; \quad k \geq 1 \quad \ldots\ldots (23)$$

$$B_{rk} = B_{kr} = \sum_{m=1}^{\infty}{}' A'_m M_{mr} M_{mk}; \quad r, k \geq 1$$

and

$$D_{oo} = \frac{l^2}{p} A_o + \sum_{i=1}^{\infty}{}' A'_i M_{io} M_{io}; \quad k = r = o$$

$$D_{ok} = D_{ko} = \sum_{i=1}^{\infty}{}' A'_i M_{ik} M_{io}; \quad r = o, k \geq 1 \quad \ldots (24)$$

$$D_{rk} = D_{kr} = \sum_{i=1}^{\infty}{}' A'_i M_{ik} M_{ir}; \quad k, r \geq 1$$

Denoting $[D_{rk}] + [\Lambda_{rk}]$ by $[D'_{rk}]$ and $[B_{rk}] - [\Lambda_{rk}]$ by $[B'_{rk}]$ equations (25) is simplified to read :

$$\begin{aligned} [D'_{rk}]\ (g_k) + P_{i_o}\ (M_{i_o r} &= [\lambda_{rk}]\ (f_k) \\ [B'_{rk}]\ (f_k) + R_{mo}\ (M_{m_o r}) &= -[\lambda_{rk}]\ (g_k) \end{aligned} \quad \ldots \quad (25)$$

$$r = o, 1, 2, \ldots \infty.$$
$$k = o, 1, 2, \ldots \infty.$$

The matrix equation (28) can now be solved for either (g_k) or (f_k) directly. But, we would like to solve for f_k s since the Oscillations inside the port are of immediate interest to us. Further, it may be noted that the general solution should not involve inversion of the diagonal matrix $[\lambda_{rk}]$ as its elements, for $r \neq k > \frac{1}{\pi} K$, tend rapidly to zero as L, the length of the Canal, increases. Eqn, (28) is therefore, reduced as below.

$$[S_{rk}]\ (fk) = R_{mo}\ (M_{m_o r}) - P_{i_o}\ (E_r) \quad \ldots \quad (26)$$

$$r \neq k = 0, 1, 2, \ldots \infty$$

where $[S_{rk}] = [G_{rk}] - [B'_{rk}]$

$$[G_{rk}] = -[\lambda_{rk}]\,[D'^{-1}_{kr}]\,[\lambda_{rk}]$$

and $(E_r) = [\lambda_{rk}]\,[D'^{-1}_{kr}]\,(M_{i_o r})$

Solving the matrix equation (29)

$$(f_k) = R_{mo}\,[S^{-1}_{kr}]\,(M_{m_o r}) - P_{i_o}\,[S^{-I}_{kr}]\,(E_r) \quad \ldots \quad (27a)$$

$$(g_k) = [D'^{-1}_{kr}][\lambda_{rk}]\,(f_k) - P_{i_o}\,[D'_{kr}]\,(M_{i_o r}) \quad \ldots \quad (27b)$$

These operations give f_k s and g_k s in terms of R_{mo} and P_{i_o}, the principal "resonant" amplitudes in the report and sea respectively. We note at this stage that to simulate the ocean condition at the domain D_s, we must take $i_o = o$, so that P_{i_o} is P_o and $M_{i_o r}$ is M_{or}.

To solve R_{mo} explicitty in terms of P_o one must now apply the " resonant " condition (8) in the port, viz.

$$\sum_{k=0}^{\infty} f_k\ M_{mok} = o \quad \ldots \quad (28)$$

Using this value of R_{mo} in equ. (27a) f_ks can be obtained in terms of P_o and the "resonant" motion everywhere

in the port becomes known interms of the undisturbed amplitude (P_0) of the incident clapotis at the sea outside.

We next investigate the case when the domain D_s becomes semi-infinite (Fig.2). The previous developments for the port and the canal remain unchanged. Only the potential ϕ_s, for the outer domain, should be established anew and matched at the right end (y = -L) of the communicating canal with the local value of the velocity potential ϕ_c.

A solution for the perturbed potential function in the open sea (domain D_s) can be simply obtained by an extension of a method first outlined by Morse and Rubenstain (9) for diffraction of electro-magnatic waves by ribbons and slits. The method was later used by Carr and Stelzriede (10) in solving the problem of diffraction of straight crested water waves by a finite gap in a breakwater. Using this method the function $F_s(x,y)$ is obtained partly in elliptic-cylindrical co-ordinates (ξ ,ϕ) and partly rectilinear co-ordinates (x,y); the co-ordinate systems are shown in fig.3 which is an enlarged view of the right end of the coupling canal.

The various co-ordinates shown are related as below -

$$\begin{aligned} x' &= -x, \quad y' = -y + L \\ x' &= (d/2) \cosh \xi \cos \phi \\ y' &= (d/2) \operatorname{Sinh} \xi \sin \phi \\ z' &= z \end{aligned} \qquad \ldots \quad (29)$$

For constant z, lines of constant ξ and ϕ become, respectively, confocal ellipses and hyperbolas of focal length, d. When $\phi = 0$ and $\phi = \pi$, the hyperbolas degenerate into a straight line with a gap of width d, the gap itself being given by $\xi = 0$, $0 < \phi < \pi$, the degenerate ellipse.

We define the function $F_s(x,y)$ in the following manner:

$$F_s(x,y) = \Psi(x,y) + P_0 \cos Ky \qquad \ldots \quad (30)$$

In equation (33) the second term on the right satisfies the field equation, eqn (2), has a zero gradient at the coast line including the gap, and gives when introduced in eqn (1), the potential of principal oscillation mode, i.e. of clapotis, at sea outside. It is, therefore, necessary to find a $\Psi(x,y)$, such that it satisfies equation (2), possess-es a zero gradient at the two coastlines, disappear at infinty and remain finite in the region of the gap. We call this function the "perturbation" function and the corresponding potential, the perturbation potential. It is for this function that the elliptic - cylindrical co-ordinates are useful.

Introducing the co-ordinates of equation (29), the complete solution for the perturbation function $\Psi(\xi, \phi)$ that is periodic in ϕ, can be written interms of even and odd angular and radial Mathieu functions (11)

$$\Psi(\xi,\phi) = Re\left[\sum_{m=0}^{\infty} \frac{V_m}{N_m} S_{em}(s,\phi)\ J_{em}(s,\xi) - i\, N_{e,m}(s,\xi)\right. \quad \ldots (31)$$

$$\left. + \sum_{m=0}^{\infty} \frac{V'_m}{N'_m} S_{o,m}(s,\phi)\ J_{om}(s,\xi) - i\, N_{o,m}(s,\xi)\right]$$

Where $S = \left(\frac{\pi d}{\lambda}\right)^2 = \left(\frac{d}{2} \cdot K\right)^2$

The arbitrary coefficients (to be specialize later) V_m, and V'_m may be imaginary and N_m and N'_m are the normalizing factors. This representation of the complex perturbation function gives rise to a perturbation potential individual terms of which represents outward travelling waves that disappear at large distances from the opening. Since only the even function solution satisfy the boundary condition of zero gradient at solid boundaries, we have finally, for the standing waves perturbation function,

$$\Psi(\xi,\phi) = Re\left[\sum_{m=0}^{\infty} \frac{V_m}{N_m} S_{e,m}(s,\phi)\ J_{e,m}(s,\xi) - i\, N_{e,m}(s,\xi)\right] \quad \ldots (32)$$

where R_e means the real part.

The coefficients V_m are determined by satisfying the boundary condition of equation (6) and we get :

$$V_m = -\frac{2i}{N'_{e,m}(s,0)} \sum_{k=0}^{\infty} g_k\ C_{mk} \quad \ldots\ (33)$$

where $i = \sqrt{-1}$ and

$$C_{mk} = \frac{d}{2} \int_0^{\pi} \mathrm{Cos}\, \frac{k\pi(x-\alpha)}{l} \cdot S_{e,m}(s,\phi) \cdot \mathrm{Sin}\, \phi \cdot d\phi \quad \ldots\ (34)$$

Introducing equn (33) in (32) and putting the resulting expression for $\Psi(\xi,\phi)$ in eqn (30), we get

$$F_s(x,y) = P_o \cos Ky - 2\sum_{k=0}^{\infty} g_k \sum_{m=0}^{\infty} \frac{C_{mk}}{N_m} \cdot S_{e,m}(s,\phi) \cdot \frac{N_{e,m}(s,\xi)}{N'_{e,m}(s,o)} \quad \ldots (35)$$

Equation (39) replaces, then eqn (17) of the finite outer domain case. The right hand side of eqn (22) is similarly replaced by the new series.

$$F_s(x,L) = P_o + 2\sum_{k=o}^{\infty} g_k \sum_{m=o}^{\infty} \frac{C_{mk}}{N_m} \cdot \frac{f_{e,m}}{\left(g_{e,m}^2\right)} S_{e,m}(s, \phi) \quad .. (36)$$

Where $f_{e,m}$ and $g_{e,m}$ are the joining factors tabulated in Tables relating to Mathieu Functions (11*). Further developments proceed in a manner similar to that used in the finite domain case.

The new R.H.S. of eqn (24b) $= \sum_{k=o}^{\infty} g_k \sum_{m=o}^{\infty} B_m C_{mk} C_{mr} + P_{ol}\delta$ or

$$= \sum_{k=o}^{\infty} g_k \; D_{rk} + P_{ol}\delta \text{ or } \quad \ldots \quad (37)$$

$$k, r = 0,1,2 \ldots\ldots,\infty$$

where, $$B_m = \frac{2}{N_m} \cdot \frac{f_{e,m}}{g_{e,m}^2}$$

δ_{or} is a Kronecker delta $= \frac{1}{1} M_{or}$, and $\quad \ldots\ldots (38)$

$$D_{rk} = \sum_{m=o}^{\infty} B_m C_{mk} C_{mr}, \; k, r = 0,1,2, \ldots,\infty$$

The matrix equation (22) is then unchanged except for the fact that we must take $i_o = 0$ and that the elements of the matrix $[D_{rk}]$ should be calculated from equation (38) and not from equation (24). Further developments are identical with the steps leading to the equations (25) thru' (28) which gives the desired solution.

For narrow harbour mouths (1 K $\ll$1), the preceding development for the open sea case reduces to that given by Miles and Munk. For instance, if we use the entrance velocity distribution function, $\phi_1(x)$, proposed by Miles and Munk and adopt their scheme of normalisation for this function then, in the expression for D(k), a term †

$(1^2/2) \sum_{m=o}^{\infty} (C_m^2/N_m)\,(1/g_{e,m}) \exp(-i\,\gamma_m)$ is obtained instead of the term $\left[(-1/2)i + (1/\pi)\ln(8/\gamma\, 1\, K)\right]$ derived by them.

In these expressions,

γ = 1.78 ..., the Euler's constant,

γ_m = - Cot $(f_{e,m})$,

and $C_m = \int_0^{\pi} \phi_1(x).\ S_{e,m}(s, \phi).\ \text{Sin}\ \phi.\ d\phi$

It can now be readily shown that as (1 K) tends to $\ll 1$,

$$(1^2/2) \sum_{m=0}^{\infty} (C_m^2/N_m\ g_{e,m}) \exp(-i\gamma_m) \rightarrow (1/\pi) \ln(4.49/1\ K) - (1/2)i$$
$$\simeq (1/\pi)\ \ln(8/\gamma 1\ K) - (1/2)i$$

indicating the identity of the two approaches for narrow harbour mouths.

NUMERICAL EXAMPLE

The dimensions (Refer fig.1) used for the analysis, that are invariant for the various cases studied, are

a = 12, b = 7, p = 24, q = 24.18

and $l = \beta - \alpha = 2$

The wave period was selected to produce one of the normal modes in each basin, assumed closed. For the port, this was taken to be the case when $m_o = n_o = 1$ and the length of the outer basin was adjusted to make $i_o = 0$ and $J_o = 4$, so that the following relationship results :

$$K^2_{m_o n_o} = \left(\frac{1}{12^2} + \frac{1}{7^2}\right) = K^2_{i_o j_o} = \left(0 + \frac{4^2}{q^2}\right)$$

from which :

$K_{m_o n_o} = K_{i_o j_o} = 0.5196$

$\lambda = 12.09$, and

$q = 24.18$

Surface profiles have not been calculated in detail; but the values of the function $F_p(x,y)$ have been computed at the four corner points viz.(o,o), (a,o), (o,b) and (a,b) of the port.

Two effects have been studied. In the first, the length of the communicating canal (L) has been taken as zero, and the entrance location varied as indicated in table I. The same table also shows, for each entrance location, the values of $F_p(x,y)$ for (a) a finite sized outer domain D_s and (b) a semi-infinite outer domain.

In the second study only one location of the coupling canal, viz, $\alpha = 2$, $\beta = 4$, has been used and the length of the canal L varied to make $L = 0, \frac{1}{2}, 1, 2, 2.1, 4$, and $12.09 = \lambda$. Table II gives the results of these computations. The results for $L = \lambda$ were obtained by suitably modifying eqn(16) and prescribing an additional condition, that of "resonance", inside the channel.

The coefficients A_m, A_i and the integrals M_{mk}, M_{mr} and M_{ik}, M_{ir} have been computed with $m = 0 - 48$, $i = 0 - 72$ and $r = k = 0 - 4$. For the Open Sea case, the coefficients B_m and the integrals C_{mk}, C_{mr} are computed with $m = 0-6$ and $r = k = 0 - 4$. The convergence of some of the terms were slow and although a formal proof of convergence could not be given, these calculations amply demonstrated that the various series proposed in the analysis do indeed converge absolutely.

EXPERIMENTS

The results of the numerical example were verified experimentally in a 7 ft. wide concrete channel using the arrangement shown in fig.1. The desired agitation in the finite dimensional sea (GHIJ) was brought in by a narrow communicating channel located at the center of the side IH. Although, this experimental arrangement deviated somewhat from the mathematical model used in the analysis, an involved mathematical formulation of the actual experimental set up showed the difference to be exceedingly small as long as $(l'K/\pi) \ll 1$.

The water depth and wave length used throughout the experiments were 9 in. and 36.27 in., respectively. The geometrical dimensions of the model were, therefore, three-times the values, in inches, used in the numerical example. The wave was produced by a simple flap type wave generator driven by a variable speed drive. The wave heights were measured, initially, by means of parallel-wire resistance gauges when the wave generator drive consisted of a variable speed D.C. motor. Later, for better speed control, a constant speed A.C. motor with mechanical speed variation arrangement was installed and it was found that ordinary point gauges could be used with better accuracy. The results of experimental verification, for one corner of the port, are presented in figures 4 and 5.

DISCUSSION OF RESULTS

It can be seen, from table 1, that the location of the entrance has a marked effect on the agitation inside the port. But, the difference in the results for the assumption of (a) a finite outer domain, and (b) an open sea is

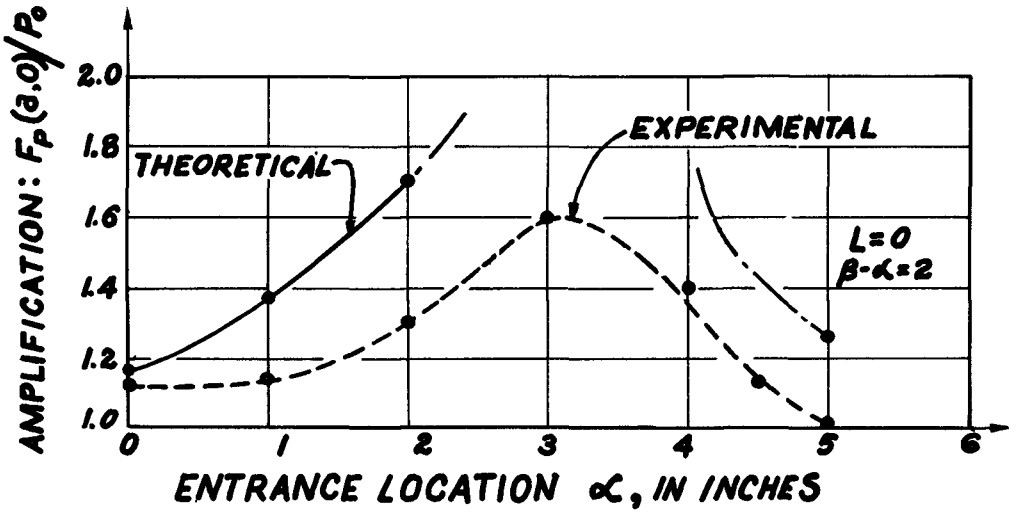

Fig. 4. Comparison of theoretical and experimental amplification factor for corner (a,0) of harbour.

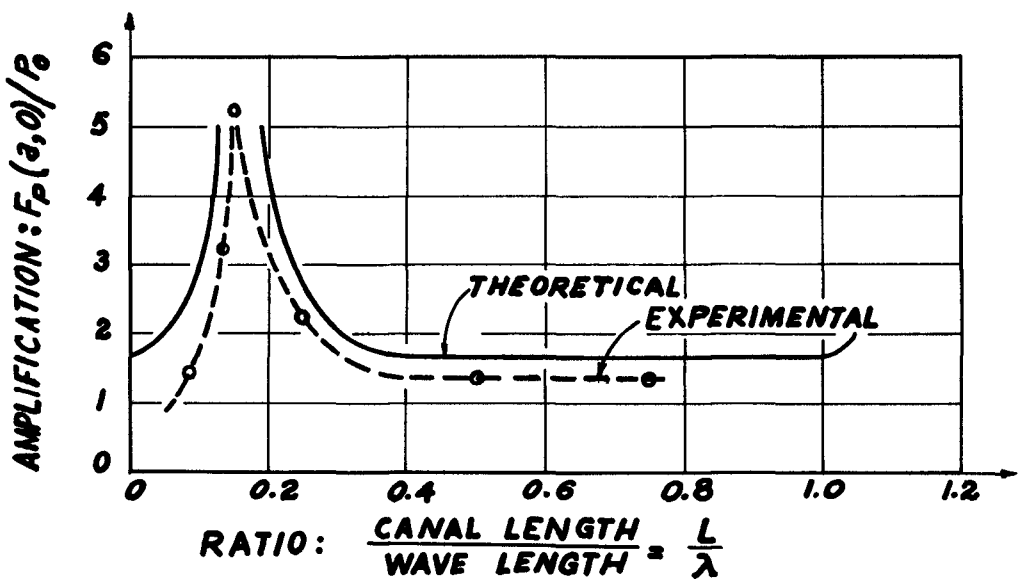

Fig. 5. Comparison of theoretical and experimental amplification factor at corner (a,0) of harbour for variation in channel length.

negligible even though the finite outer domain is only of moderate size. The quantitative agreement between the experimental and theoretical data presented in fig.4 is rather poor. This is, probably, due to the large hydraulic losses that were associated with the highly adjustable model used in the experiments.

Table II shows that as the length of the coupling canal is increased from zero, the agitation inside the port increases rapidly, attains a peak in the neighbourhood of L = 2, and decreases as rapidly thereafter. When the length of the canal is in the vicinity of the critical length, very large changes in amplitude take place for only slight changes in the canal length. This resulted in somewhat unstable operation in this region. The experiments also failed to realize (see fig.5) the large amplitude oscillations indicated by the analysis. Similar disagreement between peaks theoretically predicted and actually observed in the laboratory has been reported by LeMehaute and Raichlen. Although a large part of the observed discrepancy is due to the neglect of dissipative forces in the analysis, breakdown of the linear wave theory at such large amplitudes of oscillation may be no less important a reason. In fact, for approach channel lengths approaching the critical value, the oscillation modes became remarkably deformed in the regions of high amplitude.

The studies reported here are only exploratory in nature, as complete response curves have not been determined. These are in progress. It is possible, even then, to make certain general observations in the light of existing knowledge. For instance, the observed influence of entrance location is due to the presence of a transversal mode of oscillation. Naturally, this influence will be less pronounced for oscillations that are primarily longitudinal. Again, a complete response curve will probably show that the maximum agitation at specified places occur at different frequencies, although their magnitudes may only depend on the width of the harbour mouth. It is, therefore meaningless to attempt to segregrate areas in the harbour as 'quiet' or 'disturbed' zones or specify entrance locations that are particularly desirable unless, the power spectral density of the excitation exterior to the harbour is peaked over only a narrow band width of frequency. The exterior spectrum is, usually, a function of the topographical features of the neighbouring coastline and continental shelf and in some localities the spectrum is indeed peaked at frequencies typical of harbour seiches.

The case with an approach channel interposed between the harbour and the open sea has a special significance as, in almost all harbours, the entrance itself has a dimension of length. For a given wave number and harbour geometry, the effect of varying the length of this approach channel is merely to change the phase of the incident wave at the

TABLE - I
(Effect of entrance location on harbour agitation)

No.	Entrance Location		Outer Sea	$F_p(0,0)$	$F_p(a,0)$	$F_p(0,b)$	$F_p(a,b)$
	α	β					
1	0	2	Finite	1.03	-1.16	-1.15	1.06
			Open	1.02	-1.15	-1.14	1.05
2	1	3	Finite	1.09	-1.39	-1.38	1.12
			Open	1.06	-1.39	-1.37	1.10
3	2	4	Finite	1.12	-1.68	-1.64	1.17
			Open	1.12	-1.67	-1.64	1.17
4	5	7	Finite	-.85	- .85	- .69	- .69
			Open	-.98	- .98	- .80	- .80

Note : All magnitudes are in terms of P_o.
Length of approach channel, L=0.

TABLE - II
(Effect of channel length on harbour agitation)

No.	Outer Sea & Entrance	Approach Channel Length, L.	$F_p(0,0)$	$F_p(0,b)$	$F_p(a,0)$	$F_p(a,b)$
1		0	1.12	-1.68	-1.64	-1.17
2	Finite	$\frac{1}{2}$	1.37	-1.96	-1.93	1.41
3	Outer Sea	1	1.83	-2.62	-2.58	1.89
4		2	13.35	-19.14	-18.84	13.80
5	Entrance Location	2.1	40.95	-58.47	-57.50	42.26
6	α = 2	4	-1.26	1.81	1.78	-1.30
7	β = 4	12.09	1.18	- 1.67	- 1.66	1.20

Note : All magnitudes are in terms of P_o.

harbour mouth. In fact, the 'spiked' response characteristics observed in some of the M.I.T. experiments clearly demonstrate the need for considering the phase of the incident wave as an additional independent variable in seiche studies. This will be especially important for harbours that project out of the general run of the coast line.

CONCLUSIONS

As the number of cases studied, numerically as well as experimentally, is small only few definite conclusions can be drawn. These are :

(i) For the case studied, the proposed open sea solution is in very good agreement with the solution obtained by approximating the open sea by a finite sized. rectangular basin.

(ii) The agitation inside a rectangular port is greatly dependent on the entrance location as long as the mode of water motion has primarily transversal oscillation component.

(iii) For a given excitation and harbour geometry, there exists a critical length of approach channel which produces maximum agitation inside the harbour basin.

REFERENCES

1. Knapp, R.T., and Vanoni, V.A. Wave and surge study for the Naval Operating Base, Terminal Island, Calif : Hydro. Lab. Pub. No.55, Calif. Inst. of Tech.,Jan., 1945.

2. Decon, Russel, and Palmer, Origin and effects of long period waves in ports : Communication 1, Section II, XIXth Internatl. Navg. Congress, London, July, 1957.

3. Wilson, B.W. Origin and effects of long period waves in ports : Communication 1, Sect.II, XIXth Internatl. Navg. Congress, London, July, 1957.

4. Apte, A.S. Recherches theoriques at experimentales sur les mouvements des liquide peasants avec surface libre. Publ. Scientifiques Et Techniques Du Ministere De L'Air No.338, Paris 1957.

5. Ippen, A.T. and Raichlen, F. Wave induced oscillations in harbors : The problem of coupling of highly reflective basins : Hydro. Lab. No.49, Massachusetts Inst. of Tech., May, 1962.

6. Miles, J. and Munk, W. Harbor Paradox : Proc. A.S.C.E., Vol.87, No.WW 3, pp 111-130. Aug., 1961.

REFERENCES (CONTD)

7. Biesel, F. and Le Me'haute', B, Mouvements de resonance a deux dimensions dans une enceinte sous l' action d 'onde incidents : La Houille Blanche, July - August,1956.

8. Le Me'haute' B. Theory of wave agitation in a harbor : Proc. A.S.C.E., Volume 87, No.HY2, pp 31 - 50, March, 1961.

9. Morse, P.M. and Rubenstein, P.J. The diffraction of waves by ribbons and by slits : Physical Review, Vol.54, Dec., 1938.

10. Carr, J.H. and Stelzriede, M.E. Diffraction of water waves by breakwaters : Gravity Waves, N.B.S. Circular No.521, Nov., 1952.

11. Tables Relating to Mathieu Functions, prepared by the Computation Laboratory, N.B.S., Columbia University Press, 1951.

CHAPTER 8

INVESTIGATION OF SEICHE ACTIVITY IN WEST COAST HARBORS

Glen E. Ellis and Joseph L. Collins
Research Scientists, Defense Research Laboratory
The University of Texas, Austin, Texas

INTRODUCTION

The seiche activity in several West Coast harbors has been investigated during the past two years. This investigation has been oriented mainly as an experimental problem in which a new oceanographic instrument, the solion infrasonic hydrophone,[1] is used to detect bottom pressure fluctuations over a range of 5 sec to 1800 sec periods.

A limited theoretical consideration of this problem is presented in an attempt to correlate the seiche phenomenon to the harbor geometry.

The data presented in this paper are for San Diego Bay and Long Beach Harbor. These data were recorded on magnetic tape and returned to the laboratory for analysis. This analysis consists of prewhitening the data with bandpass filters and then computing the power spectra by the method of Blackman and Tukey.[2,3]

A short discussion is presented to relate the use of this type of data to the study of two harbor engineering problems, ship mooring and close quarter navigation.

RECORDING INSTRUMENT

The bottom pressure fluctuations were detected with a solion infrasonic hydrophone.[4] This hydrophone consists of a hydroacoustic high-pass filter in combination with a solion linear differential pressure transducer. The linear response of the hydrophone is in excess of 200:1 (46 dB) and the pressure threshold is comparable to other bottom pressure transducers.[5] Stability of the solion is excellent over long periods of time.

The hydrophone bandpass is relatively flat, with -3 dB period response points at approximately 5 sec and 800 sec periods. Falloff beyond the -3 dB points approaches -6 dB per octave. The output signals of the hydrophone, which are proportional to the pressure signal, were recorded on magnetic tape for analysis over the range of 5 sec to 1800 sec periods.[6] All of the pressure recordings were of 6 to 8 hours duration.

INVESTIGATION OF SEICHE ACTIVITY IN WEST COAST HARBORS

DATA

Bottom pressure fluctuations were recorded at three locations in San Diego Bay, California. Figure 1 shows the location at which the recordings were made in relation to the open sea. It does not, however, show that part of the bay which extends to the southeast and terminates in broad mud flats. The pertinent environmental conditions that existed during each recording period is given in Table I.

Bottom pressure fluctuations were measured at two locations in the area of San Pedro Bay, California. The recording locations were in the Long Beach Middle Harbor and the Long Beach Outer Harbor. A map of the San Pedro Bay area is shown in Fig. 2. Table II gives the pertinent environmental conditions that existed during each recording period.

ANALYSIS TECHNIQUE

The frequency analysis of a time series such as an ocean wave record can readily be accomplished by computing its power spectrum. The practical computation of the power spectrum of such a time series is given in detail by Blackman and Tukey.[7] This method of computing power spectra has been applied to surface wave records by Pierson and Marks and to bottom pressure records by Timme and Stinson.[8]

This method of attack is based upon Weiner's theorem,[9] which states that the auto-covariance function of a time series X(t) is the Fourier transform of its smoothed power spectrum. If we define the auto-covariance function by the relation

$$C(\tau) = \lim_{T\to\infty} 1/T \int_{-T/2}^{T/2} X(t) \cdot X(t+\tau)\, dt , \qquad (1)$$

where τ is a time delay, then it is related to the smoothed power spectrum P(f) by the relation

$$C(\tau) = \int_{-\infty}^{+\infty} P(f)\, e^{2\pi i f \tau}\, df , \qquad (2)$$

where

$$P(f) = \lim_{T\to\infty} 1/T \left| \int_{-T/2}^{T/2} X(t)\, e^{-2\pi i f t}\, dt \right|^2 . \qquad (3)$$

The auto-correlation function will be designated as the normalized auto-covariance function, given as

$$\phi(\tau) = C(\tau)/C(o) . \qquad (4)$$

Table I. Environmental Conditions During Bottom Pressure Measurements

Location	Date	Water Depth(ft)	Wind Speed(mph)	Wind Direction	Sea State
Pier Alpha	23 Apr 1960	40	5-15 Gusty	Northwest	1
	24 Jan 1961	40	Calm	--	0-1
	25 Oct 1961	40	Calm	--	0-1
Ballast Point	28 Apr 1960	45	10-20 Gusty	East	1-2
	25 Jan 1961	45	Calm	--	0-1
	26 Oct 1961	45	0-10	Northwest	1
Broadway Street Pier	27 Apr 1960	36	5-10	Northeast changing to Southwest	1
	27 Oct 1961	36	0-10	Southwest	1

Table II. Environmental Conditions During Bottom Pressure Measurements

Location	Date	Water Depth(ft)	Wind Speed(mph)	Wind Direction	Sea State
Middle Harbor	23 Aug 1960	45	6-15 Gusty	Southwest	1
	17 Jan 1961	45	Calm	--	Storm the previous week off coast of Northern California
	23 Oct 1961	45	Calm	--	0
Outer Harbor	25 Aug 1960	40	5-15	Southeast	1
	19 Jan 1961	40	10-15 Gusty	North	Storm the previous week off coast of Northern California

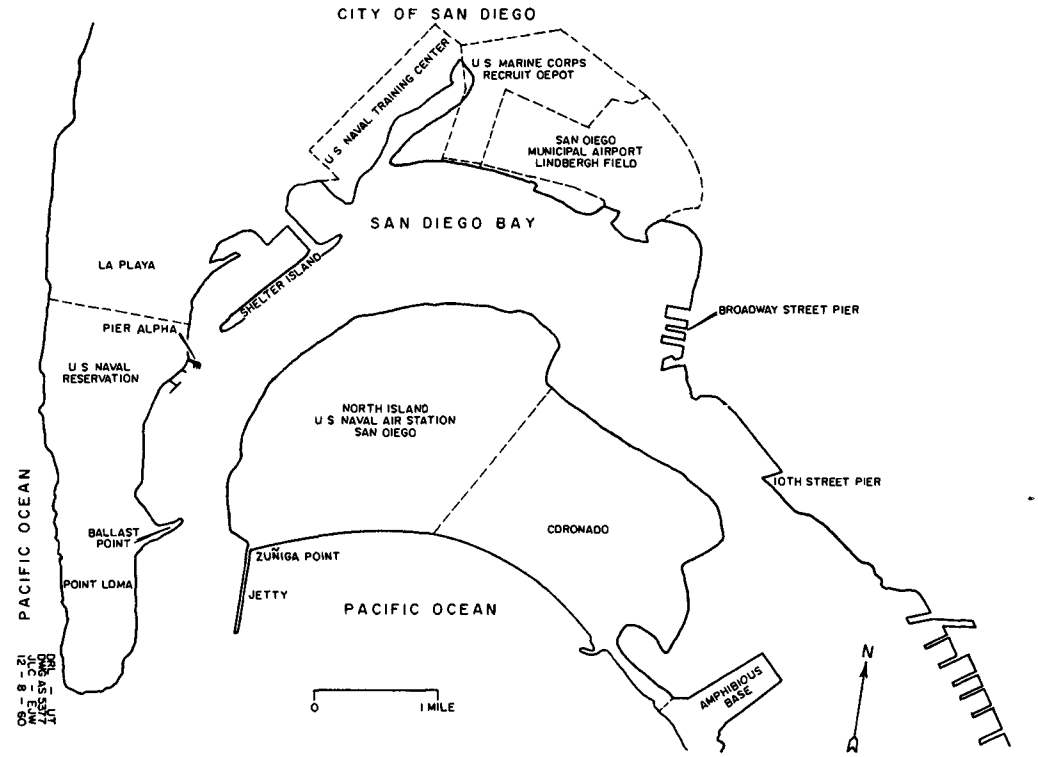

Fig. 1. Map of San Diego Bay.

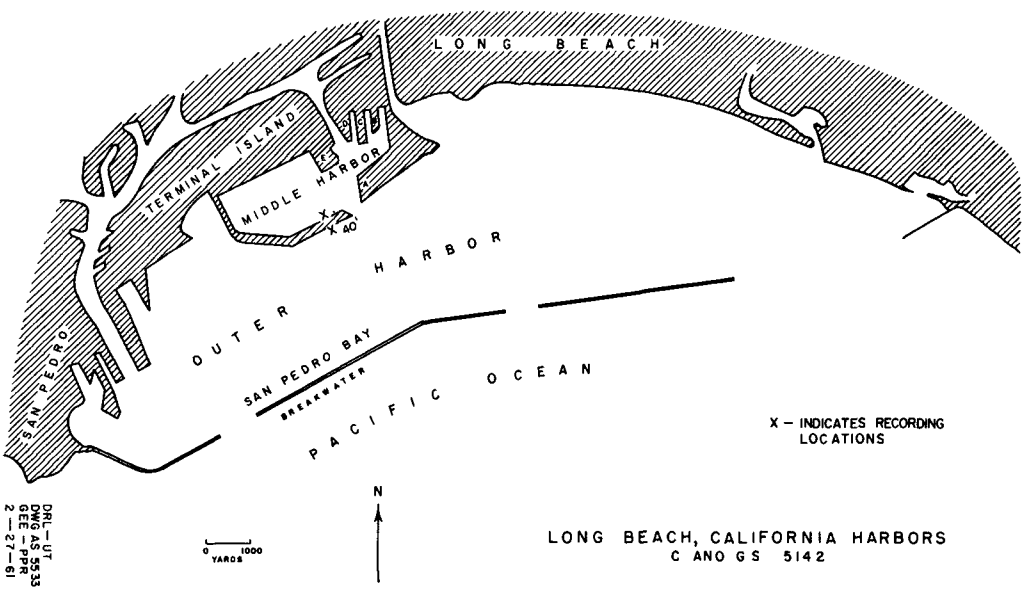

Fig. 2. Map of Long Beach Harbors and San Pedro Bay.

The recorded pressure data were brought back to the laboratory for pre-processing with the low frequency analyzer, which consists mainly of a set of eight octave bandpass analog filters.[9] This method of pre-whitening the data was chosen, since the length of the record is limited, to give greater resolution in the final power spectrum.

A set of power spectral estimates was computed for the resulting noise record from each filter. The power spectral estimates corresponding to the frequencies between the -3 dB points for each filter were combined to give a reasonable estimate of the power spectrum over the entire range of interest. Since the number of data points varies for each filter band, the maximum and minimum 80 percent confidence intervals, based upon the chi square distribution, are indicated on each figure.

In this paper, the magnitude of the power density is presented only as relative values. This was felt acceptable since all of the interpretation will be made on the frequency or period content of the spectra.

DISCUSSION

The seiche of a harbor can be excited by various mechanisms. Sudden changes in barometric pressure, a change in the wind, or seismic activity is capable of exciting standing wave oscillations in basins. One of the main mechanisms for exciting seiche activity in harbors, however, is the motion of external waves at the harbor mouth. These driving forces could be wave motions generated either at sea or in a closely coupled, partially enclosed body of water. External waves can excite both resonant and nonresonant types of motion. For resonant motions there does not exist a velocity component normal to the plane of the harbor entrance, whereas the nonresonant motion is directly affected by a normal velocity component other than zero at the entrance. McNown has completed model studies of various harbors with idealized shapes which verify that both types of motions can exist.[10]

The seiche in the harbor will appear as a periodic signal in the bottom pressure background recordings. This periodic signal may readily be detected by the method of power spectra analysis. A periodic signal will appear as a peak in the spectra, with the period corresponding to this peak being the period of the signal. If there are several different modes of the seiche present in the time series, then each mode will appear as a spectral peak at the period characterizing that mode of oscillation.

An examination of the spectra presented shows that the period content of each harbor is approximately constant regardless of the time of year and the different environmental conditions. It is assumed, therefore, that the spectra are a representation of the true background conditions in each harbor.

INVESTIGATION OF SEICHE ACTIVITY IN WEST COAST HARBORS

SAN DIEGO BAY

From the spectra analysis of the bottom pressure data recorded at Pier Alpha (Fig. 3) and Ballast Point (Fig. 4) the power density of swell activity is shown by a prominent peak at 15 sec. The magnitude of this peak has diminished considerably in the spectrum at Broadway Pier (Fig. 5). This is to be expected since Broadway Pier is further removed from the ocean or the driving force than either Pier Alpha or Ballast Point. A prominent peak in the spectra for Broadway Pier, which appears in the 6.5 sec region, probably corresponds to local wind-generated wave activity.

All of the spectra show a prominent peak in the region of 1300-1500 sec. This is attributed to a seiche propagating along the length of the harbor, since this spectral peak does not vary its period appreciably with location.

The spectra of the bottom pressure data recorded at Pier Alpha show a prominent peak in the 160-170 sec region. This is attributed to a transverse seiche in the vicinity of Pier Alpha. There are various other peaks in the spectra that have not been accounted for at this time.

The characteristics of a seiche have been shown to be directly dependent upon the geometry of the containing basin.[11] For a rectangular basin with both ends either closed or open, the period is given by the relation

$$T_m = 2L/[m/gh] \ , \ m = 1,2,3,\ldots, \tag{5}$$

where L is the length and h the depth of the basin. For a rectangular basin with one end closed and one end open, Eq. (5) becomes

$$T_m = 4L/[m/gh] \ , \ m = 1,3,5,\ldots. \tag{6}$$

If a two-dimensional consideration is made of a rectangular basin, the relation for the period is

$$T_{m,n} = 2(gh)^{-1/2} \left[m^2/L^2 + n^2/B^2\right]^{-1/2} \ , \ \begin{matrix} m = 0,1,2,\ldots, \\ n = 0,1,2,\ldots, \end{matrix} \tag{7}$$

where B is the width of the basin.

Equations (5) and (6) were used to calculate the possible modes of the longitudinal oscillations for San Diego Bay. The results of these calculations are given in Table III.

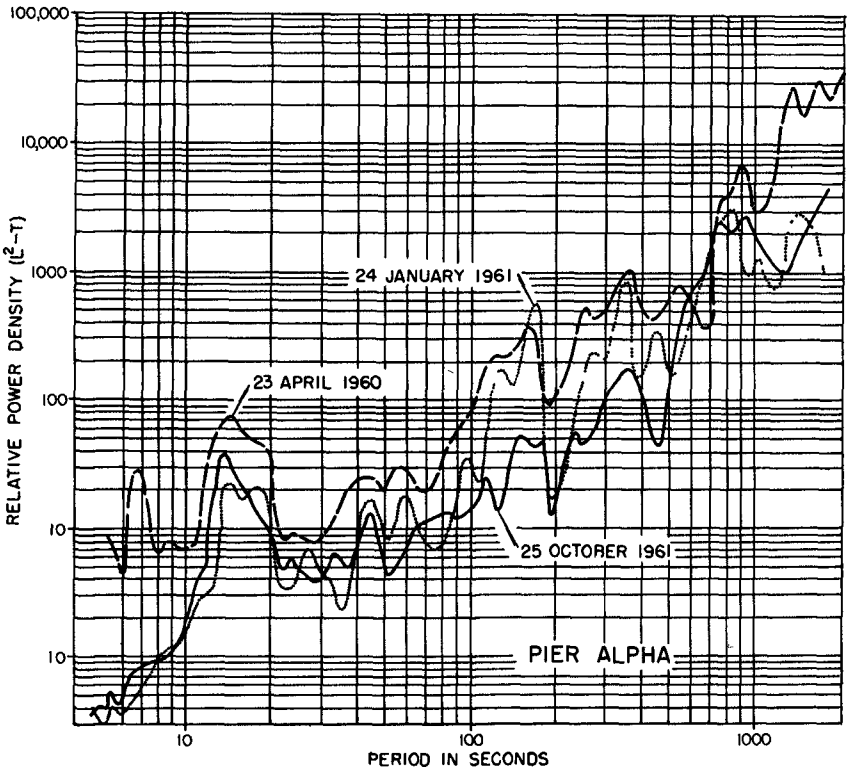

Fig. 3. Relative power spectra for Pier Alpha, San Diego Bay.

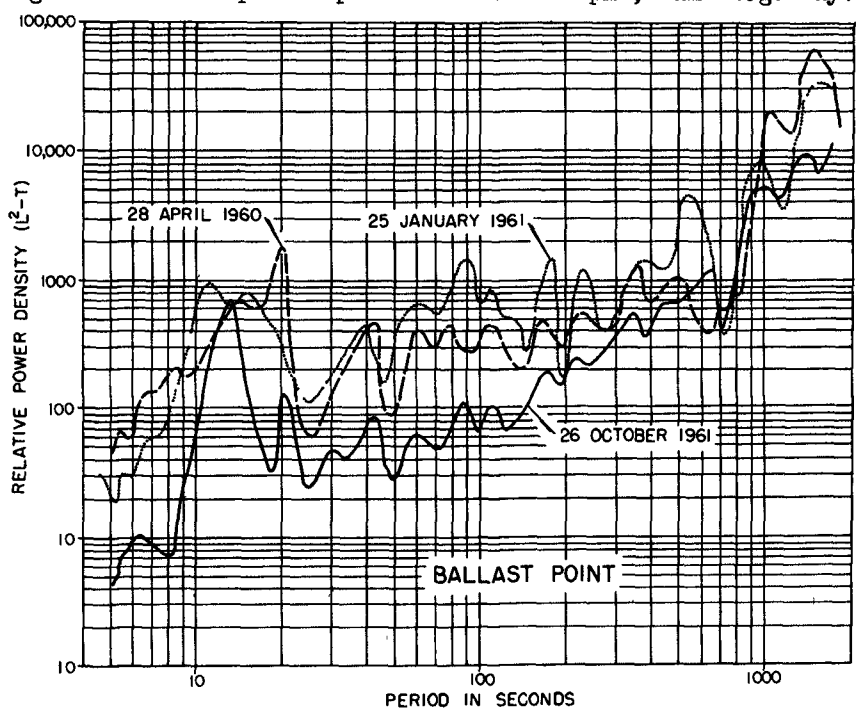

Fig. 4. Relative power spectra for Ballast Point, San Diego Bay.

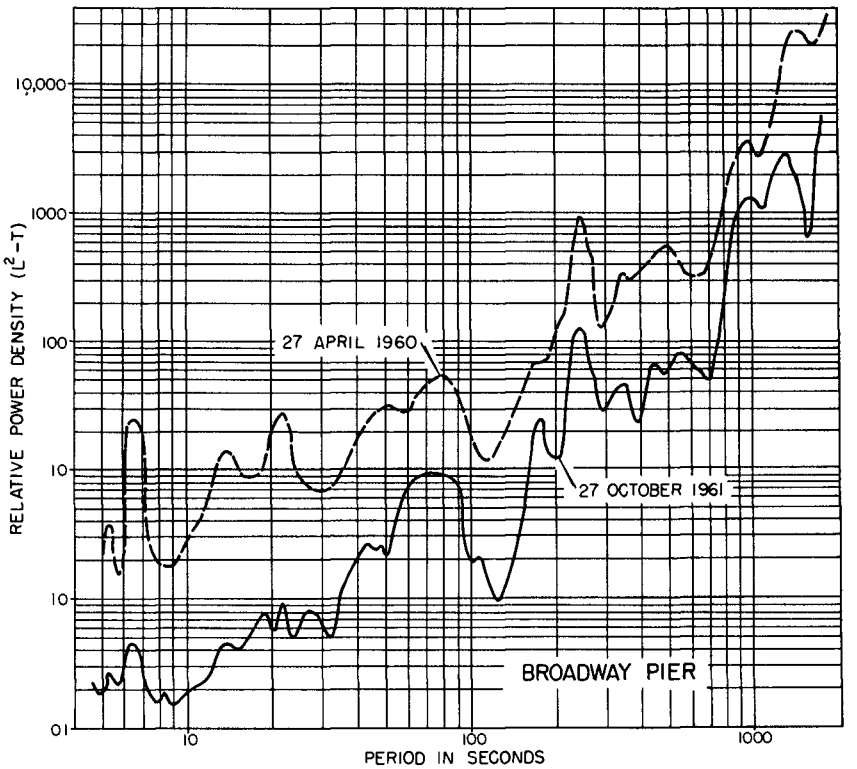

Fig. 5. Relative power spectra for Broadway Pier, San Diego Bay.

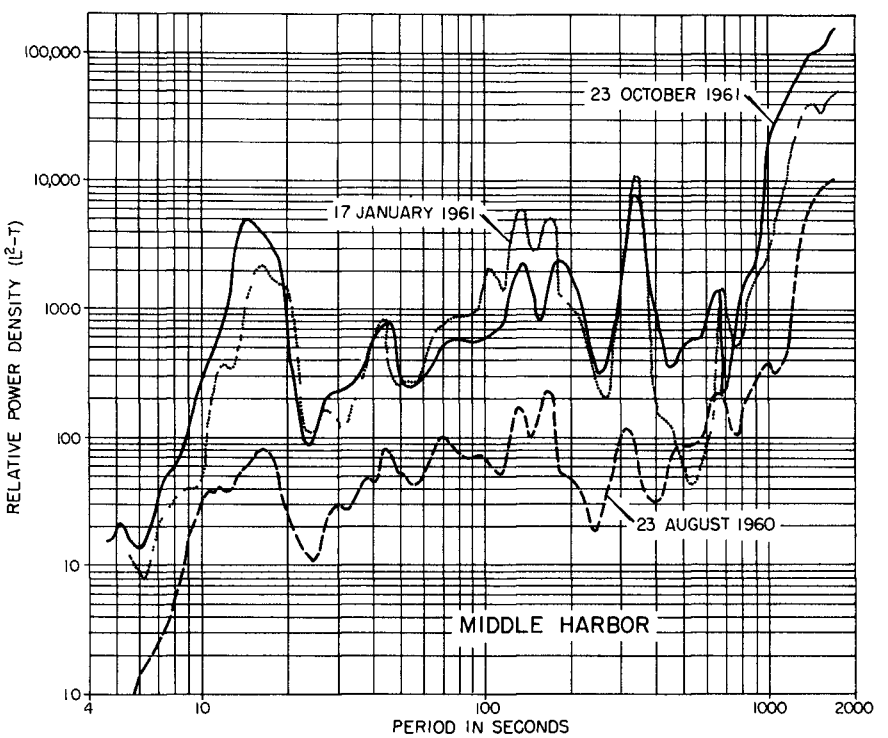

Fig. 6. Relative power spectra for Long Beach Middle Harbor.

Table III. Calculated Periods of Possible Modes of Oscillation Based Upon the Average Length and Depth of San Diego Bay

m	Period given by Eq. (5) in sec	Period given by Eq. (6) in sec	Mode of Oscillation
1	2900	5800	First
2	1450	--	Second
3	966	1933	Third
4	725	--	Fourth
5	580	1160	Fifth

The broad mud flats at the southeast end of the bay will approximate a wave absorber for the long period standing waves associated with this type of oscillation. The standing wave phenomenon would, therefore, be analogous to that taking place in an organ pipe with both ends open. Equation (5) would then govern the longitudinal seiche in the bay, and the peak in the power spectra at 1450 sec could be explained as being due to the second mode or second harmonic seiche activity. This would be an oscillation with a mode of vertical displacement at the entrance to the bay, at the terminating end of the bay, and in the vicinity of the 10th Street Pier. Present analysis does not extend to the 3000 sec period region, and the predicted 2900 sec period oscillation cannot be confirmed.

The spectra of the pressure data recorded at Pier Alpha show a prominent peak in the 160-170 sec region. This may possibly be a local oscillation across the bay in the vicinity of Pier Alpha. Calculations using Eq. (5) have been made by taking various sections across the bay. This gives a mean value for the period of the fundamental mode of the oscillation to be 160 sec.

The relative power spectra of Broadway Pier (Fig. 5) show a peak at 240 sec. This may be a transverse seiche in the neighborhood of Broadway Pier. By using Eq. (5) the fundamental period of a seiche of this type is found to be 494 sec, with a second harmonic of 247 sec.

LONG BEACH HARBORS

Figure 6 shows the relative power spectra of the bottom pressure data recorded in the middle harbor. There is a peak at 16.5 sec which corresponds to the swell activity in the harbor. There are three other definite peaks at 135 sec, 170 sec, and in the 320 to 340 sec region. All of the spectra show a rising trend around 1500 sec. The spectral peak in the 320 to 340 sec region is the second mode or harmonic of the longitudinal oscillation. This would give a possible fundamental mode of 640 to 680 sec, which also corresponds to a peak in the spectra. The peak in the spectra at 170 sec is probably composed of several modes,

the most prominent of which is the fundamental of an oscillation across the width of the basin. The fourth harmonic of the longitudinal mode may also be excited.

Carr has shown by model studies of the middle harbor that the fundamental of the longitudinal oscillation has a period of 720 sec.[12] He found, however, that the resonance of the basin to the second harmonic of 360 sec produces an oscillation of higher amplitude than the fundamental. Carr also measured, from model studies, an oscillation across the harbor with a period of 180 sec. The periods of these oscillations determined by the model studies differ from the periods determined by power spectrum analysis by approximately 10 percent. Experimental errors readily account for this difference.

Calculations of the periods of the possible modes for the middle harbor have been made by using Eqs. (5) and (7). According to this theory, using mean dimensions in Eq. (5), the period of the fundamental mode of the longitudinal seiche is 652 sec. The second harmonic or mode would have a period of 326 sec, and the fourth harmonic or mode would have a period of 163 sec. The calculated period for the fundamental mode of the oscillation across the harbor is 244 sec. If Eq. (7) is used--that is, if the basin is given a two-dimensional consideration--the period $T_{1,2}$ is found to be 185 sec.

The spectra of the middle harbor show a rising trend around the 1500 sec region. This trend also appears in the spectra of the bottom pressure records of the outer harbor (Fig. 7). The period of the third harmonic of a longitudinal seiche in the outer harbor was found, by using Eq. (6), to be 1420 sec. This would give a fundamental mode of 4263 sec, which would be out of the bandpass of the recording hydrophone. The fifth harmonic, as calculated according to this theory, would be 825 sec. This type of motion in the outer harbor would readily account for the peak in the spectra of the middle harbor at 1500 sec.

On examination of the spectra from both harbors, it is seen that several peaks of the same period occur in each. This may be attributed to the nonresonant phenomena stimulated by the waves in the outer harbor. A "second generation" solion infrasonic hydrophone with a flat period response beyond 5000 sec is being constructed to help investigate this phenomenon.

APPLICATION OF RESULTS

The seiche phenomenon that occurs in harbors presents various problems to ship mooring and to close quarter navigation, such as docking. A better knowledge of the spectra of the harbor would give some insight to the solution of such problems.

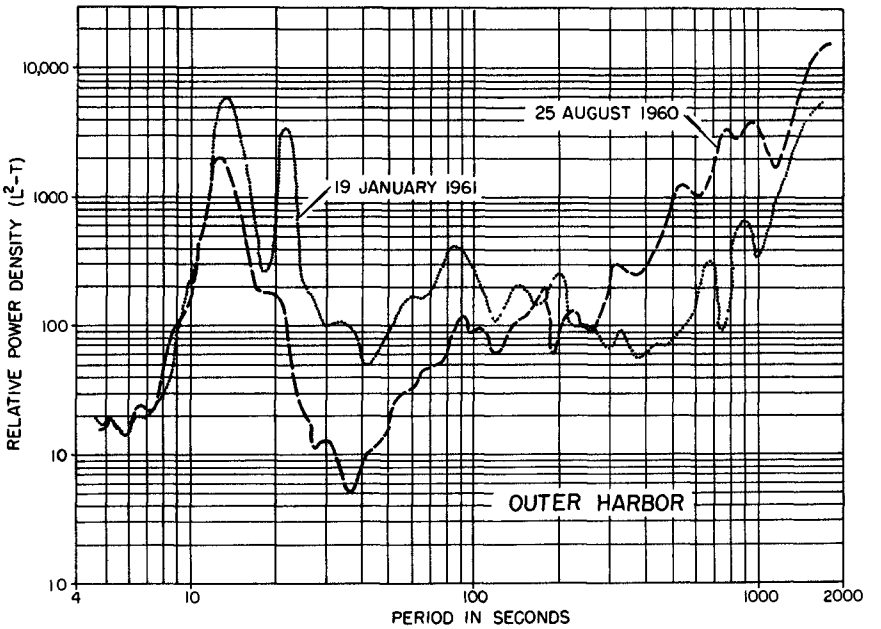

Fig. 7. Relative power spectra for Long Beach outer harbor.

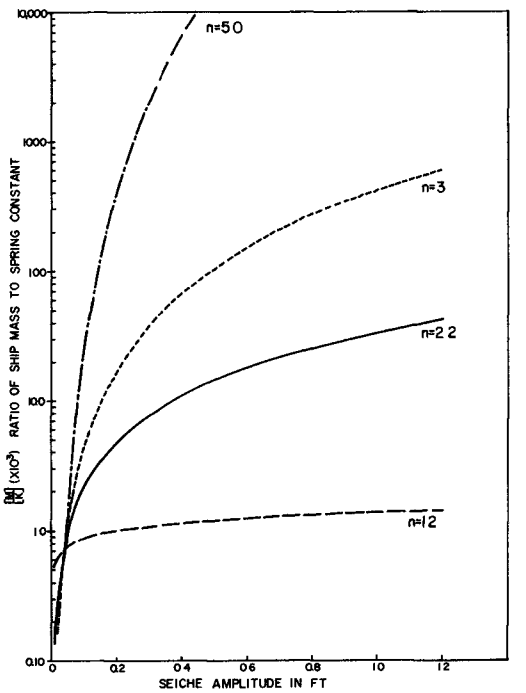

Fig. 8. Relation between the ratio of the mass of the ship to the spring constant and the seiche amplitude for resonant conditions.

INVESTIGATION OF SEICHE ACTIVITY IN WEST COAST HARBORS

The problem of a ship moored in the direction parallel to the dock face has been described by Wilson[13] using the analogy of a spring-mass vibratory system. The resonant period of a moored ship is given by the relation

$$T_n = 2\pi \sqrt{\frac{M}{K}} \left[\frac{MgA^2}{Kd} \right]^{\frac{1-n}{2(n+1)}} \qquad (8)$$

where M is the mass of the ship, K is the spring constant for all lines collectively, g is the acceleration due to gravity, d is the depth of the water at the mooring, and n is the numerical exponent expressing the non-linear load-movement behavior of the representative mooring line. When the resonant period of the moored ship corresponds to the fundamental period or one of the harmonic periods of the seiche, then ship damage can occur. Figure 8 shows a graph of the ratio of the ship mass to the spring constant versus the amplitude of the seiche. This family of curves is governed by Eq. (8) at resonant conditions. That is, the period T_n of the ship is chosen to be equal to 170 sec, the period of the transverse seiche at Pier Alpha, San Diego Bay. The value of n may be determined by measurement of the particular ship.[14] One could then determine the resonant spring constant of a given ship for a particular amplitude of the seiche, enabling the ship to be moored in such a manner as to avoid resonance.

The problem of close quarter navigation has been evident at Broadway Pier in San Diego Bay. While docking ships the pilots find that a current will flow in one direction at one time, but in the opposite direction at another time. This may well be due to the long period seiche along the length of the harbor or the shorter period seiche across the bay in the neighborhood of Broadway Pier. A greater knowledge of the spectra of the harbor would allow a prediction of the magnitude and direction of the current during a particular time interval.

ACKNOWLEDGMENTS

This work was sponsored by the Department of the Navy, Bureau of Naval Weapons, and the Office of Naval Research.

REFERENCES

1. Collins, J. L. and Ellis, G. E. (In preparation). Measurement of Seiche Activity in San Diego Bay

2. Ibid

3. Blackman, R. B. and Tukey, J. W. (1958). The Measurement of Power Spectra: Dover Publications, Inc., New York

4. Collins and Ellis, op. cit.

5. Snodgrass, F. (1958). Shore-Based Recorder of Low Frequency Ocean Waves: Trans. Am. Geophys. Un., Vol. 39

6. Collins and Ellis, op. cit.

7. Blackman and Tukey, op. cit.

8. Timme, R. C. and Stinson, F. A. (1955). Preliminary Investigation on Predicting Properties of Bottom-Pressure Fluctuations: Hydrographic Office, U. S. Navy, TR-14

9. Goldman, S. (1954). Information Theory: p. 241, Prentice-Hall, Inc. New York

10. McNown, J. S. (1952). Waves and Seiches in Idealized Ports: Gravit Waves, Nat'l Bur. Stds. Cir. 521, p. 153

11. Defant, A. (1961). Physical Oceanography: Vol. II, Ch. VI, Pergamo Press, New York

12. Carr, J. H. (1952). Long-Period Waves or Surges in Harbors: Am. Soc. Civil Engrs., Vol. 78, Sep. 123

13. Wilson, B. W. (1950). Ship Response to Range Action in Harbor Basins: Proc. Am. Soc. Civ. Engrs., Vol. 76, Sep. 41

14. O'Brien, J. T. (1955). Forces on Moored Ships Due to Wave Action: Proc. First Conf. on Ships and Waves, Ch. 32, Council on Wave Research and Society of Naval Architects and Marine Engineers

CHAPTER 9

THE ANALYSIS OF HARBOR AND ESTUARY SYSTEMS

J. A. Harder
College of Engineering
University of California
Berkeley, California

INTRODUCTION

It is one of the paradoxes of our age that hydraulic engineering is concerned with problems that in many ways exceed in difficulty those encountered in the more glamorous fields of science. One measure of this situation is that classical mathematics, which is a powerful tool when applied to simple systems, has proved to be a rather impotent aid in hydraulic calculations, except when the geometry is simple. Harbor and estuary systems are usually associated with complex geometry, and thus we ordinarily cannot depend on mathematics to give general solutions. Instead of solving the hydraulic equations of flow in the complex geometry, we have sought to reconstruct the geometry of the prototype in a reduced scale, by means of models, and by assuming that the equations governing the full-size and reduced-scale systems are the same, to find specific solutions through direct measurements in the latter.

Because of scale effects, the hydraulic model is not perfect, but it does reproduce the complex geometry and some of the complexities of three dimensional flows in the prototype. These cannot at present be described mathematically, and where they are important a properly constructed and adjusted hydraulic model is our most powerful tool in the investigation of estuarial problems, and is likely to remain so.

However, hydraulic models are very expensive, especially if they are built to a reasonably large scale, so it behooves us to be sure that we have not overlooked other, perhaps less powerful, methods when we are confronted with a particular problem. Within the past decade two methods have been developed that will eventually replace hydraulic models for tidal flow and river flood routing investigations. One is based on the use of digital computers to numerically integrate the differential equations of open channel flow; the realization of this method by a digital computer program for a particular system has been called a "mathematical model". The second is based on the use of analog elements that behave with respect to electrical current in the same way as the prototype behaves with respect to flows of water. When an assembly of such elements is adjusted to duplicate the behavior of a hydraulic system in a way similar to the way a hydraulic model is adjusted during its verification period, the result may be called an analog model.

THE MATHEMATICAL BASIS OF TIDAL FLOW CALCULATIONS

Each of the two methods depends on a mathematical description of the flow in open channels that was already well developed at the turn of the century, and which has formed the basis for many hand calculation methods during the past fifty years. One of the earliest practical applications was by Parsons(1) who published in 1918 a history of the construction of the Cape Cod Canal in Massachusetts and incidentally presented an excellent summary of the theory of tidal hydraulics, a subject that had at that time not been treated in hydraulic texts, together with his careful measurements of the tides and currents in the canal for comparison with theory. He brought to the attention of his American colleagues the classical work of Sir George Biddell Airy of Cambridge, on "Tides and Waves" (2). Parsons recognized the limitations of using linear friction (an assumption that leads to a simple solution of the equations) and recalled the methods being used in the computation of surge tank behavior, where the equations are the same and where a useful concept of linearized friction was being employed. In this concept the friction is described by a term that depends linearly on the velocity, but which has a coefficient that makes the total energy dissipated over a complete tidal cycle the same as would be the case if square-law friction had been assumed. He credited this idea to Prasil(3) and Dubs(4).

When the geometry is simple, as in the case of artificial canal, analytic solutions based on linearized friction are often all that are needed These are well described by Einstein and Fuchs(5) and by Dronkers and Schoenfeld(6). The latter also describe some approximate analytic methods for predicting higher harmonics due to non-linear friction. These methods require both a good mathematical and physical insight on the part of the computor and considerable tedious calculation. In contrast the "brute force" methods of direct integration of the differential equations, either along characteristics or in a properly chosen rectangular grid, can be programmed for digital computers, and it is likely that this will be the future trend. These numerical methods are described in references (5) and (6) and by Stoker(7).

SCHEMATIZATION AND VERIFICATION

As we consider the attractions of turning the tedious work of computation over to a computer or an analog model, we should anticipate an additional difficulty, that of schematization. This is not a difficulty inherent in any method, but arises from the complexity of the geometry. In both the mathematical integration methods and the analog model methods the system of waterways must be divided into short reaches within which we can assume that the channel properties can be averaged into a representative set of values. We must assign values of friction factor for each

reach; these values must be guesses, for we normally cannot establish steady flow in an estuary and measure the water surface slope due to friction acting alone. This incidentally is a familiar task to operators of hydraulic models. In any computation or analog model approach, however, there are additional assumptions that must be made about the contribution that each part of a given cross section makes to the inertia. The division of a cross section into a main part that contributes inertia and a shoal part that contributes only to storage is illustrated in Figure 1.

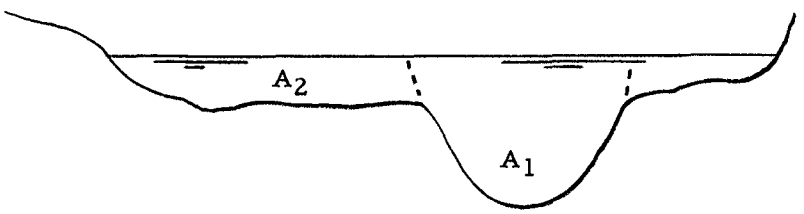

Figure 1. Irregular cross section in an estuary

In a compact but irregular cross section theory tells us that the shallow water wave velocity should be $\sqrt{gA/B}$, where A is the cross sectional area and B is the water surface width. The shoal areas do not contribute completely to the area A, however, but are often the scene of sluggish and sometimes reverse currents. Thus, in an investigation of tide wave motion in San Francisco Bay we found that the active cross section, A_1, could be considerably less than half of the total, and that a workable general rule was that we could assume that areas shallower than ten feet did not contribute to the inertia; however, it was still necessary to check this assump tion.

Fortunately, friction had only a small effect on the velocity of propagation and a principal effect on the attenuation, so we could adjust our assumptions of inertia to achieve the correct wave speed, and the friction to achieve the correct attenuation. Thus, in contrast to the verification procedure for hydraulic models, where only the friction ordinarily needs adjusting, both friction and inertia must be adjusted in an analog model. This is, of course, equally true for a computational model.

Figure 2 shows superimposed on a map of the San Francisco Bay-Sacramento-San Joaquin Delta System the network of analog elements employed in a study of tidal flows there. The system contained analog elements, of which twenty were supplied with square-law resistors developed in the Hydraulics Laboratory at the University of California Berkeley. Figure 3 shows the result of a verification run. Both the tidal amplitude and phase were obtained for a large number of stations along the hundred-mile course leading from the Golden Gate outlet and the Pacific Ocean to the City of Sacramento. These measurements are shown by circled points. The results of measurements on the analog model are shown as small triangles. At all stations except the last, at Sacramento, the difference between the readings is within the error of measurement. This work was reported on in greater detail in reference (8). It was performed under contract for the California Department of Water Resources.

RELATIVE MERITS OF ANALOG AND MATHEMATICAL MODELS

In estimating the relative advantages of mathematical models and analog models, one can say that the digital computer is inherently capable of the greater precision. It will be found, however, that accuracy will depend in each instance on the completeness of the verification process. Here the much higher speed of the analog is an advantage, for it can go through thousands of tidal cycles per second, and any adjustments to the inertial elements or the friction is reflected almost instantaneously in the results (a graphical presentation on an oscilloscope screen). When using a digital computer one must wait for a complete new solution to evaluate the effect of each change in a coefficient, and even on the fastest machines this may take many minutes. When both the friction and the inertia must be adjusted for as many as one hundred elements, and due to interactions this must be repeated many times, the temptation to stop short of the best adjustment must be great. We have found that it takes several weeks of intermittent work to adjust a moderate size analog, even when the results of a given adjustment are immediately visible to the operator.

A limitation of the analog, that may be of importance in some instances, is that it is impractical to include all of the terms in the hydraulic equations. For example, total hydraulic head may be accounted for, but the velocity head may not be separated out. Two-dimensional flows require additional hardware to bring the velocity vector to the same direction as the loss vector, etc. None of these has proved insurmountable, though they may suggest that once the principal values of inertia and friction are determined on an analog a greater refinement may be possible using a digital computer, with these as starting values. Some experience is essential here, however, to avoid the beginner's mistake of asking for a far greater accuracy in the computations than is warranted by the variability of the data used in the verification procedure.

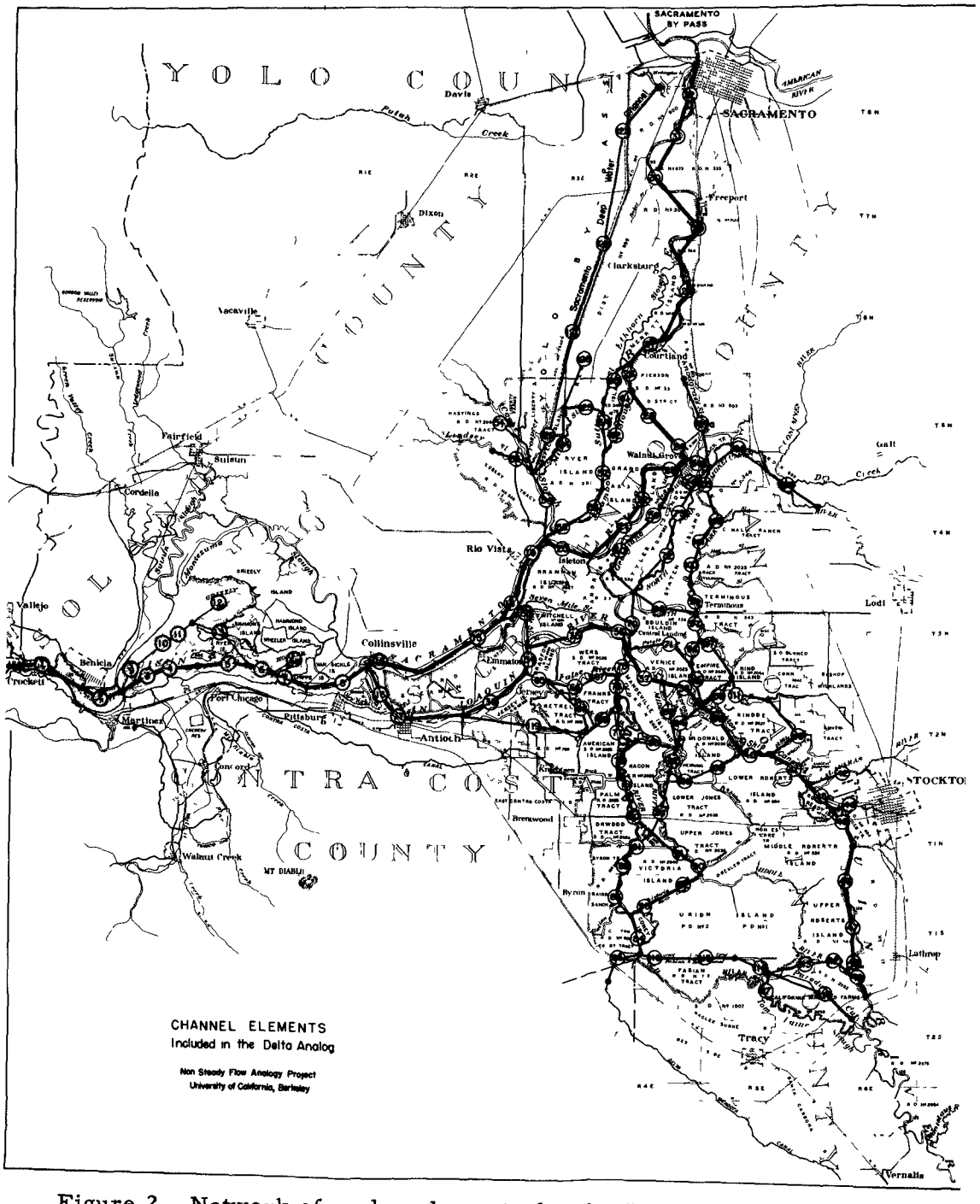

Figure 2. Network of analog elements for the Sacramento-San Joaquin Delta Analog

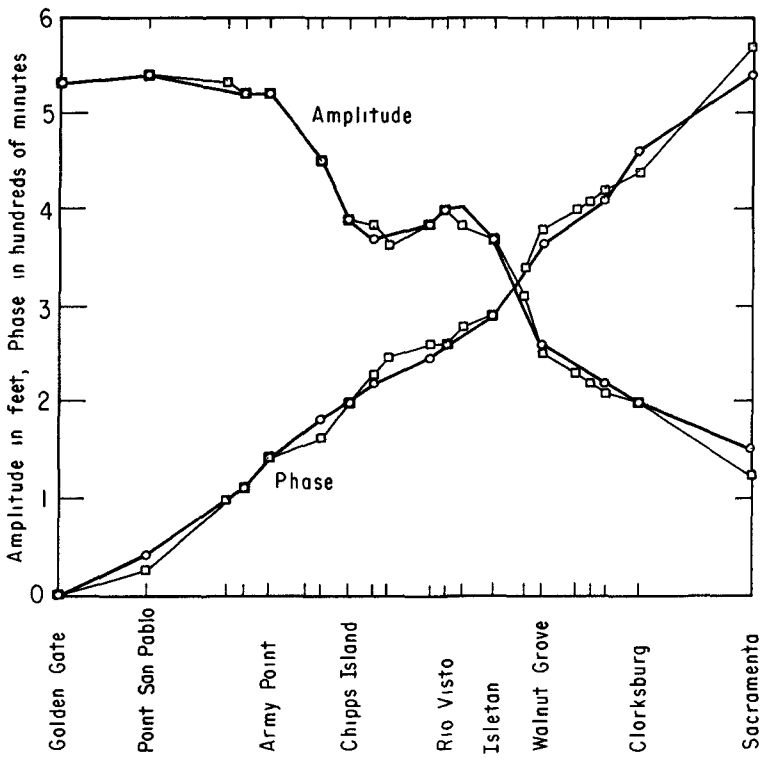

Figure 3. Prototype vs. analog measurements in the Delta

PRESENT AND FUTURE TRENDS

Salinity intrusions into estuaries would seem to be an appropriate subject for a digital computer application. The approach might be to try to solve the convected diffusion equation by numerical integration. The operative equation is:

$$\frac{\partial \phi}{\partial t} = K \frac{\partial^2 \phi}{\partial x^2} - u \frac{\partial \phi}{\partial x}$$

where ϕ is the salinity, K is the diffusivity coefficient, and u is the velocity with which the salinity would be convected downstream in the absen of diffusion. Practically, this would have to be solved with the boundary conditions of u as a function of time at the upper end and ϕ as a constant at the ocean outlet. The production of a set of K's for the reaches that would lead to a duplication of the time history and profile of salinity, as between the prototype during a particular period and the mathematical model, would constitute a partial verification. It would only be partial because there is a strong possibility that K is not only a function of distance along the estuary, but of u and possibly ϕ.

Thus, if the diffusivity depends on the salinity and the local velocity, or velocity gradients, we are no longer very sure that a duplication in one case would lead to a duplication for another. Furthermore, we are really not even sure that the equation itself is a good description of the process of salinity intrusion. What then is possible? To gain a little perspective on this problem, let us step back and ask what information is available. If a considerable body of historical data is available for values of ϕ and u, we may be able to form a connection between them that will serve as a predictor. If the relationship is a linear one, even though there is a time lag the solution is reasonably well assured. That the connection can be made if the relationship is non-linear is also possible under some circumstances as shown by Jacoby(9). The proof is involved, but an idea of the power of the method is apparent in the following example drawn with slight modification from Jacoby's doctoral dissertation.

Assume that we have a basin connected to the sea by a canal and that a long series of measurements are available of both the tidal fluctuations in the sea and in the basin. We do not know the size of the basin, the length of the canal, or the friction, or anything at all about the physica system. However, we know that it is non-linear because the friction depends on the square of the velocity.

We built such a system out of electronic components in our laboratory, and set about trying to make enough measurements to enable us to fully predict the behavior of the system, without knowing how it was put together. Since we were assuming a natural system, we did not allow ourselves the luxury of applying steady flows, etc., to the system, as this would be impossible in most natural systems. We did apply a random signal in the place of the ocean tide, and made simultaneous measurements of the tide inside the simulated basin. A typical section of the record obtained is given in Figure 4.

From approximately 10,000 data points (more than was necessary in all probability) we were able to derive 28 predicting coefficients. More coefficients would have improved the predictions, but would also have increased the amount of the computations, which already required about 45 minutes on a 704 computer.

With the predictor equation developed, we applied a pure sine wave to the input of the simulated system and measured it plus the output. A comparison between the predicted and the observed output is given in Figure 5. Notice that the correct amplitude and time delay are predicted. More remarkable is the fact that the correct degree of flattening of the wave crests is predicted. This flattening of the crests might be expected on the basis of square law friction in the connecting channel.

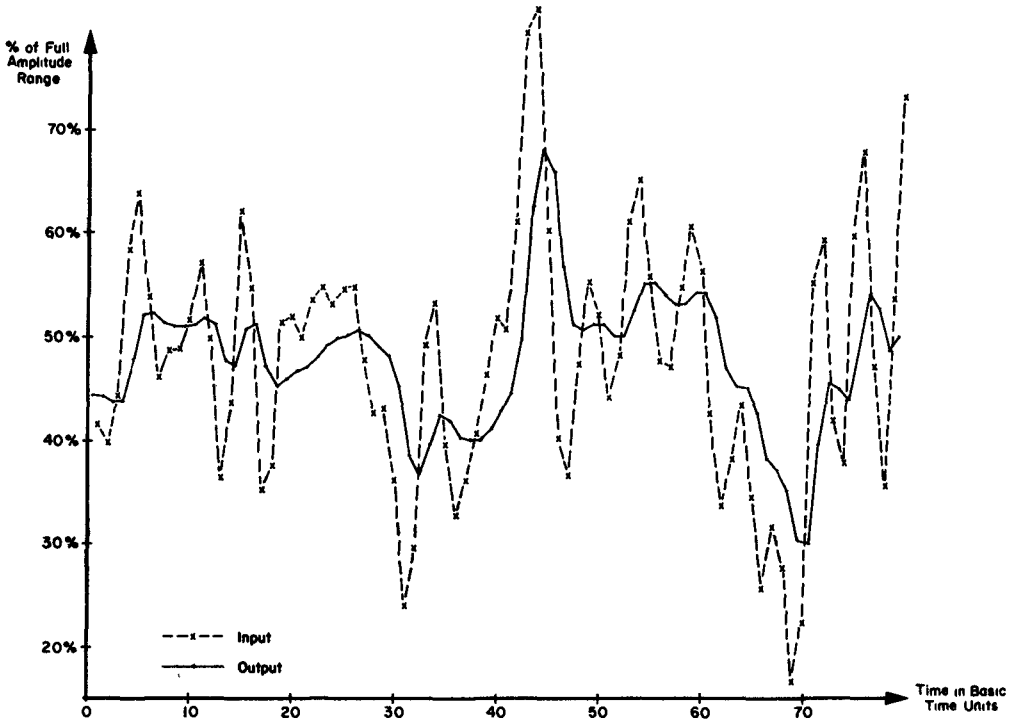

Figure 4. Typical section of input and output records

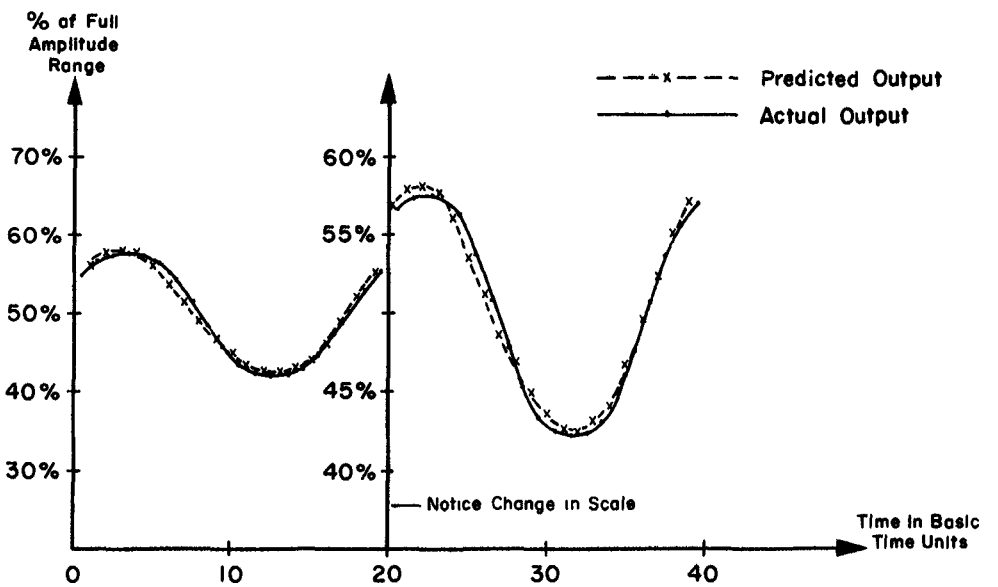

Figure 5. Comparison between predicted and measured output from the experimental system

This example should not be taken too literally -- there is little likelihood that this method would be the best one to use in the problem as given, for the simple reason that we would ordinarily be able to start with a knowledge of the basin and channel dimensions and be able to make predictions on the basis of far less data. In a more abstract sense, though, this example illustrates how other problems can be attacked. The method needs further improvement, in the direction of making the most efficient use of the data available in constructing the predictor, but it constitutes an important advance in our analysis of engineering systems. It also illustrates the powerful methods that have been made feasible by the digital computer, and that we need not be forever limited to using the computer merely to mechanize methods already developed.

REFERENCES

(1) Parsons, W. B., The Cape Cod Canal, Transactions, ASCE, v. 82, p. 1 (1918).

(2) Airy, G. B., Tides and Waves, in Encyclopedia Metropolitana (1845).

(3) Prasil, F., Wasserschloss Probleme, Schweizerische Bauzeitung, v. 52, n. 21.

(4) Dubs, R., and Bataillard, V., Allgemeine Theorie uber die veranderlische Bewegung des Wassers in Leitungen, pp. 219-221, Berlin (1909).

(5) Einstein, H. A., and Fuchs, R. A., Computation of Tides and Tidal Currents -- United States Practice, Proceedings, ASCE, v. 81, n. 715, June 1955.

(6) Dronkers, J. J., and Schoenfeld, J. C., Tidal Computations in Water, Rijkswaterstaat Communications No. 1, Rijkswaterstaat, The Hague (1959).

(7) Stoker, J. J., Water Waves, Interscience Publishers, New York (1957).

(8) Einstein, H. A., and Harder, J. A., Electric Analog Model of a Tidal Estuary, Transactions, ASCE, Paper 3277 (1961).

(9) Jacoby, S., Analysis of Some Nonlinear Hydraulic Systems, Ph. D. Thesis, U. of California, Berkeley, 1962.

CHAPTER 10

ON DETERMINATION OF THE TIDAL HARMONIC CONSTANTS AND TIDE PREDICTION FOR THE MEXICAN PORTS

Pedro Lezama
Instituto de Geofísica, U.N.A.M.
and
Centro de Investigación y de Estudios Avanzados
del Instituto Politécnico Nacional

ABSTRACT*

1) A canonical computation of the tidal harmonic constants for some of the Mexican ports is obtained.

2) Following Doodson's Tide Generating Potential, the determination of the node factors $f_i(t)$ and the angle $u_i(t)$ for a period of twenty years (1950 - 1970) is obtained by electronic computation.

3) The I.B.M. 650 electronic computer's program for the height of tide is given, and this program is applied to the values of high and low water at any day and time of the year.

4) A graphical and numerical comparison for the height of the tide is shown.

5) The determination of the port establishment for some Mexican ports is obtained.

---

*Because of the length of this paper, only the above abstract can be presented in this publication.

Oaxaca Coast

Part 2
COASTAL SEDIMENT PROBLEMS

Michoacan Coast

CHAPTER 11

FLUME EXPERIMENTS ON SAND TRANSPORT BY WAVES AND CURRENTS

Douglas L. Inman
Scripps Institution of Oceanography,
University of California, La Jolla, California

and

Anthony J. Bowen
Hydraulics Research Station, Wallingford, England

ABSTRACT

Measurements were made of the sand transport (solid discharge) caused by waves and currents traveling over a horizontal sand bed in water 50 cm deep. The waves had heights of 15 cm, and periods of 1.4 and 2.0 sec. The sand transport was measured first in the presence of waves only, then in the presence of waves superimposed on currents. The currents flowed in the direction of wave travel, with steady uniform velocities of 2, 4, and 6 cm/sec.

Since sand moves to and fro under the influence of waves, sand traps were placed flush with the surface at either end of the bed. The net sand transport was determined by subtracting the amount of sand trapped at the upwave end of the bed, from that trapped at the downwave end.

The total amount of sand caught in both traps was greatest with waves of 2.0 sec period, while the net sand transport was greatest with waves of 1.4 sec period. Super position of waves on currents of 2 cm/sec produced a two-fold increase in the sand transport for both wave types. Surprisingly, faster currents of 4 and 6 cm/sec caused the discharge to decrease somewhat.

Estimates of the power expended by waves was obtained from the decrement in wave height as the wave traveled over the sand bed. The decrement in wave height was found to be about 10^{-3} per unit of distance traveled. Certain calculations show that about one tenth of the total power expended by the waves was used in transporting sediment.

INTRODUCTION

Surface waves traveling in shallow water over a horizontal bed of sand usually produce a net transport of sand in the direction of wave travel. As a working hypothesis it was assumed that the wave motion made the sand available for transport, so that any current near the bed would produce a net transport of sand. The purpose of this experiment was to test the hypothesis by measuring the transport rates of sand under

Contribution from the Scripps Institution of Oceanography, University of California, San Diego.

several types of waves and for a variety of superimposed currents.

The purpose of the superimposed current was to simulate conditions prevailing along natural beaches. Longuet-Higgins (1953) and Russell and Osorio (1958) have shown theoretically and practically that, in a flume, the wave-induced drift velocity is downwave near the surface and bed but upwave in the center. However experiments on real beaches, Shepard and Inman (1950), have shown that the drift velocity is onshore at all depths; the system being kept in equilibrium by the rip currents spaced along the beach. To obtain a model of the conditions which prevail between the rip currents it was considered necessary to superimpose a current upon the wave system in the flume. The current velocities superimposed were of the same order of magnitude as the wave-induced drift velocities, i.e., several cm/sec.

It is assumed that a portion of the wave power is expended on the granular bed by the to and fro motion of the water over the bed, and that this power places the sand grains in motion and supports their weight above the bed. If the back and forth motions are equal, then there should be no net transport of grains and the wave power is simply expended in to and fro motion of the sand. Since the grains are supported above the bed by the wave stresses, the presence of a current should produce a transport in the direction of the current. A relation of this sort for wave induced transport was formulated by Bagnold (in press, eq. 10).

$$i_\Theta = K\omega \frac{u_\Theta}{u_m} \quad \ldots\ldots\ldots\ldots (1)$$

where i_Θ is the dynamic transport rate of sand (i.e., immersed weight per unit time and per unit width of bed) which results when wave stress (ω/u_m) places sand available for transport in the presence of a current u_Θ, and K is a dimensionless coefficient of proportionality. In a sense K is a measure of efficiency, which conceivably could have values exceeding unity. In this relation, ω is the decrement in transmitted power of the waves attributable to bed drag, and u_m is the maximum horizontal component of the orbital velocity near the bed.

The dynamic transport rate i_Θ is equal to g'mU where $g' = \frac{\rho_s - \rho}{\rho_s} g$ is a factor converting the dry mass transport rate per unit width mU into immersed weight transport, g is the acceleration of gravity, m is the mass of sediment load over unit area of bed which is transported at velocity U and ρ and ρ_s are the density of the liquid and solid grains respectively. Thus the dry mass transport rate of sand in grams per cm width of wave crest per second becomes

$$j = mU = K\omega \frac{u_\Theta}{u_m} \frac{1}{g'} \quad \ldots\ldots\ldots (2)$$

where u_Θ is a steady current flowing near the bed in the direction of wave travel.

Longuet-Higgins and Stewart (1960) show that when a train of gravity waves of height H, ride upon a steady current $\bar{u}$, the whole power transmitted forward across any vertical plane normal to the motion is given by

$$P = ECn + E\bar{u} + \tfrac{1}{2}\rho h \bar{u}^3 + S_x\bar{u} \quad \ldots\ldots (3)$$

where $E = \frac{1}{8}\rho g H^2$ is the mean energy density of the waves per unit surface area, Cn is the group velocity of waves in still water of depth h, and S_x is the radiation stress defined below. The first two terms represent the bodily transport of wave energy by the group velocity and the stream velocity, while the third term represents the transport by the stream of its own kinetic energy. The last term represents the work done due to the interaction of waves and currents and is equal to

$$S_x = E\left[2n - \tfrac{1}{2}\right] \quad \ldots\ldots\ldots\ldots \quad (4)$$

where n is the ratio of the wave group velocity Cn to the wave phase velocity C.

The decrement in wave power per unit of bed area, ω, is equal to dP/dx, which for waves propagating in water of constant depth and hence at constant velocity, becomes

$$\omega = \frac{dP}{dx} = \tfrac{1}{4}\rho g H \frac{dH}{dx}\left[Cn + U\left(2n + \tfrac{1}{2}\right)\right] \quad . \quad (5)$$

where the third term in equation (3) is assumed to be negligible. If there is no current, then the relation becomes $\omega = \frac{1}{4}\rho g H \frac{dH}{dx} Cn$.

An estimate of the decrement in transmitted power ω can be obtained from relation (5) if the decrement in wave height per unit of distance traveled, dH/dx, is known. A primary objective of these experiments was to obtain experimental values of dH/dx over rippled and smooth bed.

It was observed that the distribution in wave height was approximately exponential in form and could be represented by

$$H = H_1 e^{-ax} \quad \ldots\ldots\ldots\ldots \quad (6)$$

where H is the wave height at some distance x downwave from an incident wave of height H_1, and "a" is a wave attenuation coefficient with units of x^{-1}. Differentiation of this relation gives the decrement in wave height as dH/dx = -aH. In the analysis of the experimental data in a smooth channel it was assumed that the total attenuation coefficient, a, was the sum of the attenuations due to viscous effects on the smooth wall (a_1) and smooth bottom (a_2). In the presence of a sand bed it was assumed that the total attenuation coefficient was the sum of a_1 and the attenuation due to the rippled sand bottom a_3, i.e., in the absence of a smooth bed $a = a_1 + a_2$ and in the presence of a rippled bed $a = a_1 + a_3$.

In the case of waves traveling in a channel bounded by a smooth bed and side walls, the motion in the boundary layers should be laminar. It would be expected that viscous stresses in the thin laminar layer near the solid boundary would account for most of the energy dissipation. A calculation by Hunt (1952) making plausible assumptions, gives the relation for the theoretical wave attenuation coefficient as

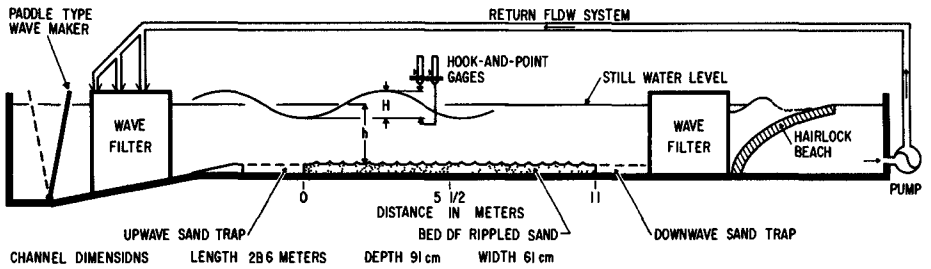

Fig. 1. Schematic diagram of the wave channel.

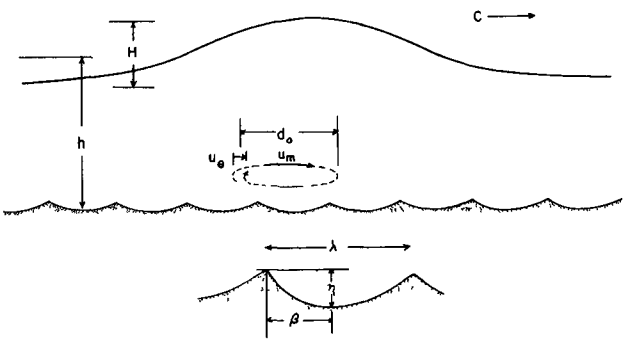

Fig. 2. Schematic diagram of wave and bed features.

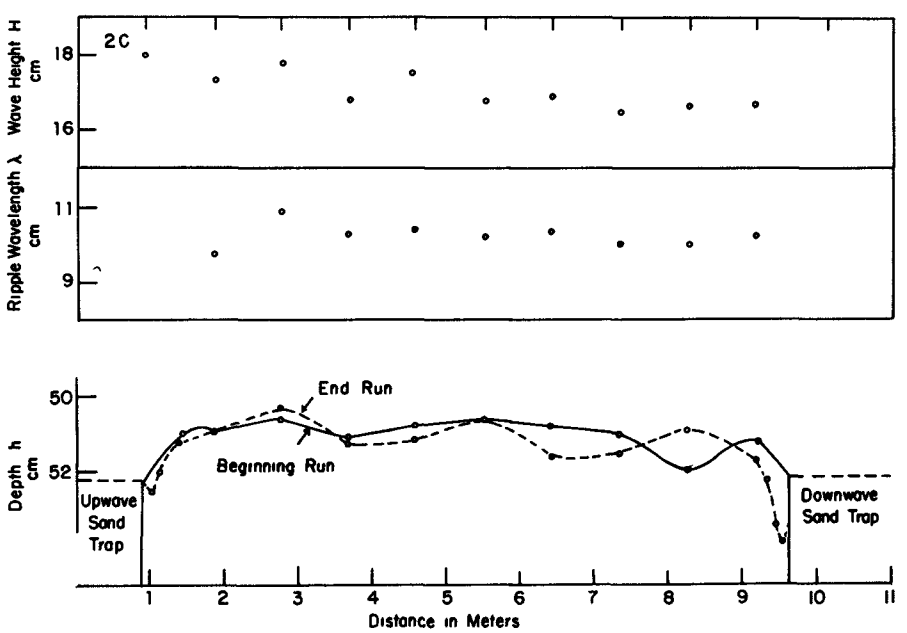

Fig. 3. Comparison of bed profiles, Run 2C.

$$a_o = \frac{k}{b}\left[\frac{\nu T}{\pi}\right]^{\frac{1}{2}}\left[\frac{kb + \sinh 2kh}{2kh + \sinh 2kh}\right] \quad \ldots\ldots (7)$$

where $k = 2\pi/L$ is the wave number, b is the width of the channel, ν is the kinetic viscosity, and h is the still water depth.

EQUIPMENT

The experiments were performed in the "94-foot wave channel" at the Hydraulic Research Station of the Department of Scientific and Industrial Research, Wallingford, England. Waves are generated in the deep end of the concrete channel by a paddle-type wave maker, and propagate into a uniform section of channel, 21 meters long by 91 cm deep and 61 cm wide (Figure 1). An inclined beach, consisting of a three inch thick porous "hair-lock" mat, was placed at the downwave end of the channel to absorb the energy of the waves and minimize their reflection. To decrease wave harmonics, filters consisting of eight vertical, slightly wavy sections of perforated metal were situated near the wave maker and the hair-lock beach. When desired, a steady current of 2 to 6 cm/sec was generated by pumping water from behind the porous beach and re-introducing the flow into the channel at the deep end between the wave paddle and the filter. Three flexible canvas hoses permitted re-introduction of flow with a minimum distortion of wave form.

An eleven meter long sand bed was placed in the central, horizontal portion of the channel, beginning about ten meters downwave from the wave maker. All measurements of wave height and velocity were made in this section of the channel. The wave channel had a glass wall midway along the sand bed, and centered around measurement station 5.5 meters. Measurement of the orbital trajectory of wave motion was made through the glass wall by observation of successive positions of neutrally buoyant particles in the water. Details of the trajectories were obtained by study of motion pictures of the particles. Velocity profiles, in the case of steady flow in the absence of waves, were obtained by use of a mini flow meter developed at the Hydraulic Research Station. Profiles of the rippled sand bed were obtained through the glass wall, and the rate of ripple advance determined by comparing successive ripple profiles.

A physical measure of the transport of sand was obtained from sand traps placed at the upwave and downwave ends of the sand bed. The traps consisted of perforated steel sheets placed flush with the level of the troughs of the sand ripples in the bed. The perforations consisted of slots ½ inch long by 1/16 inch wide and spaced 1/8 inch apart, arranged so that the ratio of solid to whole area was 0.77. The slots paralleled the orbital motion of the waves, and it was intended that sand carried over the traps by the wave motion, would fall through the slots and be retained in the void between the metal sheet and the cement floor of the channel.

Bed Material

The bed material consisted of quartz sand having a median diameter

of about 0.2 millimeters. Mechanical analysis of the sand by sieves gave a median diameter of 0.19 mm while that by settling tube gave 0.22 mm. Both analyses gave a grain size distribution with a standard deviation σ_ϕ. of about 0.35ϕ, where $\sigma_\phi = \log_2 [D_{16}/D_{84}]$ and D_{16} and D_{84} are the 16th and 84th percentile diameters of cumulative size distribution curve (Inman, 1952, table 1). The sand had a solid grain density ρ_s of 2.65 gm/cm^3 and a "dry" bulk density ρ_s' of 1.47 gm/cm^3, giving a volume concentration of 0.55.

EXPERIMENTAL PROCEDURE

Before each experiment the sand bed was smoothed by dragging a screen over the surface to obtain a uniform sand bed of about 4 cm thickness. Waves were then generated over the bed until the resulting sand ripples on the bed attained a constant and uniform height and length and a steady rate of advance. The wave maker was then stopped, water drained from the channel and the traps emptied of sand. Care was taken to replace any sand scoured from around the sand trap and to re-form the sand bordering the traps to a level such that the ripple troughs were approximately flush with the top of the perforated sheet forming the trap. The profile of the bed (measured to the ripple troughs) was then obtained and the channel refilled with water, ready for the experimental observation. A comparison of the bed profiles before and after Run 2C is shown in Figure 3.

The raw data from each experimental run is listed in Table 1. During each run, wave height profiles were obtained by hook-and-pointer gages over the 11 meter length of sand bed (Figures 5 and 6). Wave phase velocity, C, and wave period, T, were measured with a stop watch. The tabulated phase velocity has been reduced by the amount of the steady flow $\bar{u}$ upon which the wave train was riding. The volume discharge per unit time, Q, of the circulating water was measured with a manometer which gave the pressure difference across an orifice plate placed in the return-flow pipe; $\bar{u}$ was then given by Q/bh.

The orbital diameter of the wave motion near the bed, d_o, and the wave induced current over the bed, u_θ, were obtained by observing the trajectories of neutrally buoyant particles, called "Bagnold particles". These particles were made from a mixture of wax and lead stearate and had a median diameter of about 2 mm. Motion pictures were taken of their movement when close to the bed so that, by examining a series of frames, a diagram was obtained which showed the movement of water above the ripples during the passage of a wave, Figure 7. In most cases the orbital measurements apply to a zone about one half ripple wavelength above the bed, as the particle motion adjacent to the bed was too complex to obtain systematic measurements. The orbital diameter d_o is the mean of the horizontal components of upwave and downwave particle displacements, averaged over many wave cycles. The wave-drift current, u_θ, is the rate of drift of particles averaged over many wavelengths and includes drift induced by the steady current $\bar{u}$.

In the course of each run, fluorescent tracer grains were injected into the regime of sediment suspension above the bed. Twenty-one injections were made at 30 sec. intervals and the final tracer distribution in the

Table 1. Measurement over a rippled sand bed.

QUANTITY	SYMBOL	UNITS \ RUN	1A	1B	1C	1D	2A	2B	2C	2D
Superposed flow	$\bar{u}$	cm/sec	0	2	4	6	0	2	4	6
Wave period	T	sec	1 4	1 4	1 4	1 4	2 0	2 0	2 0	2 0
Wave height	H	cm	15 7	15 3	15 1	15 4	16 5	16 5	16 8	16 8
Still water depth	h	cm	50 1	50 5	50 1	50 4	50 0	51 0	49 9	50 8
Wave phase velocity	C	cm/sec	180	183	187	184	206	209	205	209
Wavelength	L = CT	cm	254	258	264	259	412	418	410	416
Orbital diameter near bed	d_o	cm	9 8	9 4	9 6	9 6	19 2	18 5	18 6	18 2
Orbital velocity near bed	$u_m=\frac{\pi d_o}{T}$	cm/sec	21 8	21 0	21 4	21 4	30 1	29 1	29 2	28 6
Wave-drift current near bed	u_s	cm/sec	0 85	1 21	1 50	2 93	0 92	2 14	1 36	1 97
Water temperature		°C	8	7	6½	8½	15	11	6	7
Running time	Δt	min	98	62	50	70	44	44½	34	42
Downwave sand trap, dry wt		kg	4 76	4 54	3 83	2 93	3 68	5 28	2 56	3 23
Upwave sand trap, dry wt		kg	0 71	0 62	0 43	0 57	4 00	4 17	3 44	3 64
Ripple wavelength	λ	cm	6 5	6 5	6 5	6 4	10 8	10 2	10 6	10 3
Ripple height	η	cm	1 1	1 0	1 0	1 0	1 5	1 6	1 5	1 6
Ripple symmetry	β/λ		48	44	47	45	44	48	44	38
Rate of ripple advance	U_r	$10^{-3}\frac{cm}{sec}$	2 7	3 0	3 6	2 8	0 6	2 1	-2 5	-1 5
Wave height decrement	$\frac{\Delta H}{\Delta x}$	10^{-3}	1 64	1 46	1 55	1 73	1 00	1 00	1 22	1 33
Attenuation coefficient	a	$10^{-4}cm^{-1}$	1 02	0 93	0 99	1 17	0 60	0 61	0 72	0 78

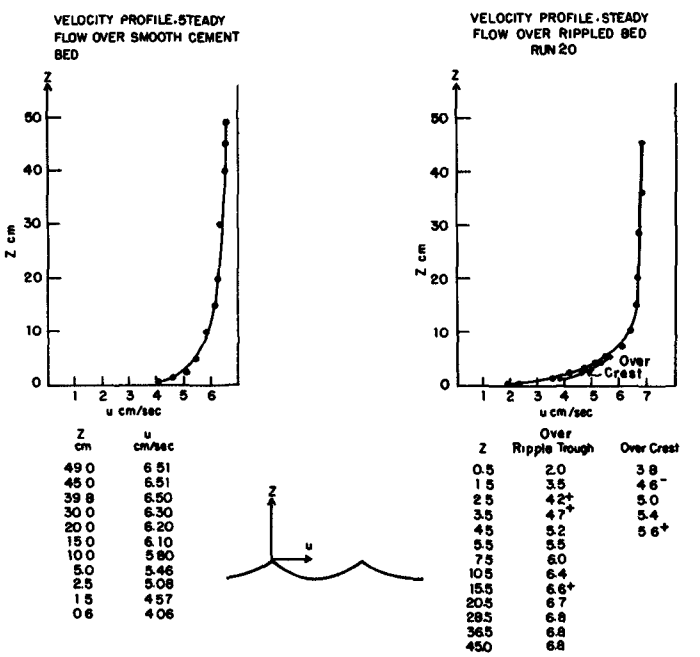

Z cm	u cm/sec
49 0	6 51
45 0	6.51
39 8	6.50
30 0	6.30
20 0	6.20
15 0	6.10
10 0	5 80
5.0	5.46
2.5	5.08
1 5	4 57
0 6	4 06

Z	Over Ripple Trough	Over Crest
0.5	2.0	3 8
1 5	3.5	4 6⁻
2 5	4 2+	5.0
3.5	4 7+	5.4
4 5	5.2	5 6+
5.5	5.5	
7 5	6.0	
10 5	6.4	
15.5	6.6+	
20.5	6 7	
28.5	6.8	
36.5	6.8	
450	6.8	

Fig. 4. Velocity profile for steady flow over smooth and rippled bed.

ripples is shown in Figure 8, for an experiment in which the ripple velocity was downwave. Methods to determine the rate of sediment transport are being developed and further interpretation of the tracer data may then be possible.

At the end of a run the flume was drained carefully, each trap was emptied and its sand content dried and weighed. Due to the decreases in wave height down the flume, the conditions above the two traps are not similar. A correction was made by assuming the transport into a trap was dependent on the power expended on the bed in that area. Putnam and Johnson (1949) suggest that the power expended on unit area of the bed can be approximated by taking the product of the bed stress, $c\rho u_m^2$ and the orbital velocity, u_m.

Then assuming trap content proportional to the power expended and hence to $c\rho u_m^3$, the content is proportional to u_m^3. The results given by the traps were corrected to give the quantity of sand which would have been caught if the traps had been subject to the wave conditions in the middle of the flume.

Four experiments were made in which the sand bed was replaced by a bed of smooth concrete. In each case the profile of the wave height was measured and the wave attenuation was assumed to be exponential (Eq. 6). Although the profile measured was confused due to the presence of standing waves, the general decrease in wave height closely approximated the expected exponential decrease and the value of the attenuation coefficient could be determined accurately.

Standing waves of wavelength approximately $\frac{1}{2}L$ were found in the wave height profile for every experiment whether over a sand or concrete bed. Ursell, Dean and Yu (1960) have thoroughly investigated this phenomenon which is due to the partial reflection of the propagating wave from the beach. No way was found to reduce the reflection coefficient to a value at which the standing waves would be of negligible amplitude.

In the early stages of a run the wave height at any given point varied due to the formation of the sand ripples on the bed which initially was smooth.

DISCUSSION

The attenuation coefficient for waves propagating in a smooth flume has been considered theoretically by Hunt (1952), Eq. 7, however the case of superimposed current was not considered. A comparison between the experimental and theoretical attenuation could only be made for runs 1A and 2A over a smooth concrete bed, Table 2. It can be seen that there was very good agreement between the measured values of attenuation of coefficient, $a_1 + a_2$ and the theoretical values, a_o. Theory also shows that, for the particular dimensions of channel used, the attenuation due to the walls alone was approximately $a_1 = 0.7\, a_o$, and that due to the smooth bed was $a_2 = 0.3\, a_o$. The wave attenuation due solely to the rippled bed should then be given by

$$a_3 = a - a_1 = a - 0.7(a_1 + a_2)$$

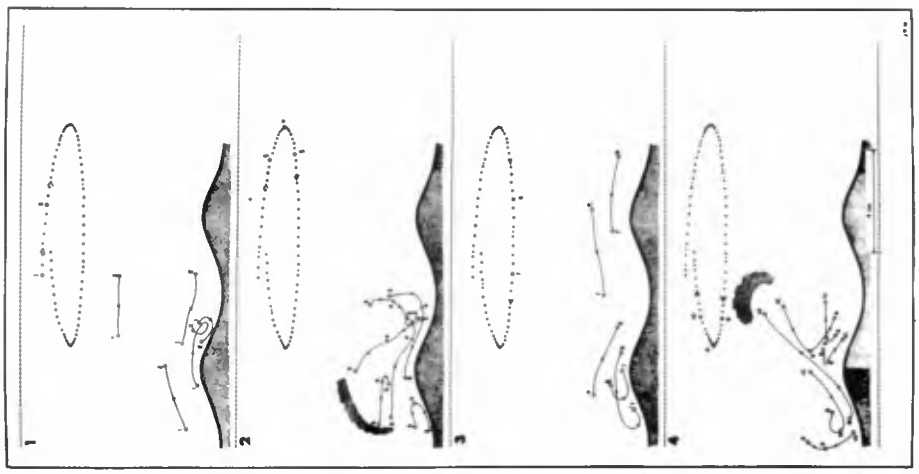

Fig. 7. Particle trajectories over a rippled bed.

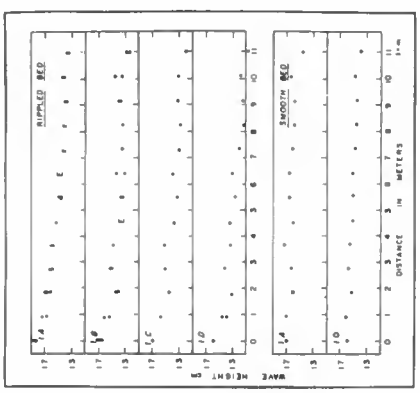

Fig. 5. Wave height profile for Run 1A - D.

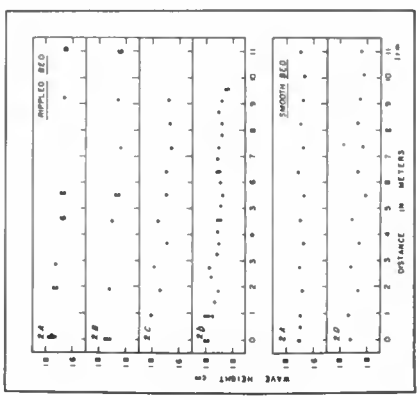

Fig. 6. Wave height profile for Run 2A - D.

The values of a_3 in Table 3 wer obtained using this correction. The value of a_3 was greatest for the runs with a short period, 1A - D, by an amount consistent with the attenuation being a "per wave" function.

Figure 7 shows the water movement over the ripple during the passage of a wave in run 1A. The water moving over a ripple crest during the forward semi-orbit generated a vortex in the lee of the ripple (1, 1-2). As the water decelerated, the system became unstable and the vortex, no longer restrained, dispersed rapidly. It was lifted up over the ripple by the combination of its own vorticity and the initial acceleration of the backward semi-orbit. This process removed sediment from above the downwave face of the ripple and dispersed it as a cloudy suspension moving upwave (2, 3-4-5). During the second half of the orbit a vortex was generated upwave from the ripple (3, 6-7) and then dispersed, its sediment content being thrown into suspension downwave from the ripple (4, 8-9-10). Material is thus placed in suspension, with some initial velocity, at two distinct periods during an orbit. If the motion were otherwise symmetrica the dirft velocity, u_θ, should then be the factor determining the directioı and magnitude of the sediment transport.

For runs 1A and 2A, which had no superimposed flow, the ripples were fairly symmetrical, but there was a considerable difference between the maximum height of the suspended sediment during the passage of a wave crest and that during the passage of a trough; the height being greater under a crest. The difference in height was approximately equal to the vertical orbital displacement.

The effect of the increase of $\bar{u}$ was to reduce further the symmetry of the system by increasing the effective orbital velocity downwave and decreasing it upwave. This resulted in a flattening of the upwave face of the ripple and the steepening of the downwave face. The vortex generated on the downwave face then became by far the stronger and hence much of the material placed in suspension had an upwave initial velocity. This mechanism was the cause of the negative ripple velocities found in runs 2 C, D and its general effect was to prevent an increase in u_θ necessarily increasing the sediment transport. It can be seen that for runs 1D and 2C the transport was less than for 1C and 2B despite an increase in $\bar{u}$. This can only be a temporary reversal as it is obvious that if $\bar{u}$ were considerably increased it would come to be more important than the wave motion and the transport would then be in the direction of the superimposed flow. Hence the increase in transport from 2C to 2D is not unexpected. However, the very high value of u_θ for run 2B was unexpected and unaccountable; otherwise the values of u_θ increased steadily for increasing $\bar{u}$, Figure 9.

Table 3 shows the values of the corrected transport rate of sand, j, the decrement in transmitted power of the waves attributable to bed drag, ω, and the coefficient of proportionality K as defined in Equation 2. For both series of experiments K was constant for increasing $\bar{u}$ as long as j increased also, i.e. as long as the system stayed reasonably symmetrical. However, when the system was subjected to periodic movements which were both strong and asymmetric, the basic assumptions of the energy theory were invalidated and the derived value of K decreased considerably.

Table 2. Measurement over a smooth concrete bed.

Wave height decrement	$\frac{\Delta H}{\Delta x}$	10^{-3}	0.50			0.64	0.29			0.55
Attenuation coefficient	a_1+a_2	$10^{-4}cm^{-1}$	0.30			0.40	0.17			0.33
Theoretical attenuation coefficient	a_o	$10^{-4}cm^{-1}$	0.28				0.18			

Table 3. Computations.

QUANTITY	SYMBOL	RUN / UNITS	1A	1B	1C	1D	2A	2B	2C	2D
Corrected downwave sand trap		$10^{-2}\frac{gm/sec}{cm\ width}$	1.38	2.12	2.29	1.42	2.41	3.08	2.24	2.16
Corrected upwave sand trap		$10^{-2}\frac{gm/sec}{cm\ width}$	0.18	0.20	0.17	0.17	2.06	2.24	2.35	1.98
Rate of sand transport	J	$10^{-2}\frac{gm/sec}{cm\ width}$	1.20	1.92	2.12	1.25	0.35	0.84	-0.11	0.18
Attenuation coefficient	a_3	$10^{-4}cm^{-1}$	0.81	0.70	0.74	0.89	0.48	0.46	0.53	0.55
Wave height decrement	$[\Delta H/\Delta X]_3$	10^{-3}	1.30	1.30	1.30	1.30	0.80	0.80	0.80	0.80
	$\frac{1}{4}gH(\Delta H/\Delta X)_3 Cn$	gm/sec^3	645	640	645	630	560	570	570	575
	$\frac{1}{4}gH(\Delta H/\Delta X)_3\bar{u}(2n+\frac{1}{2})$	gm/sec^3	--	19	37	55	--	14	29	43
Decrement in wave power	ω	gm/sec^3	645	659	682	685	560	584	599	618
Coefficient of proportionality	$K = \frac{1}{\omega}\frac{u_m}{u_o}$	---	0.29	0.30	0.27	0.08	0.12	0.12	-0.01	0.03
Transport by ripple advance	$0.37\rho_s'\lambda\eta\psi$	$10^{-2}\frac{gm/sec}{cm\ width}$	1.05	1.07	1.28	0.98	0.53	1.85	-2.15	-1.35

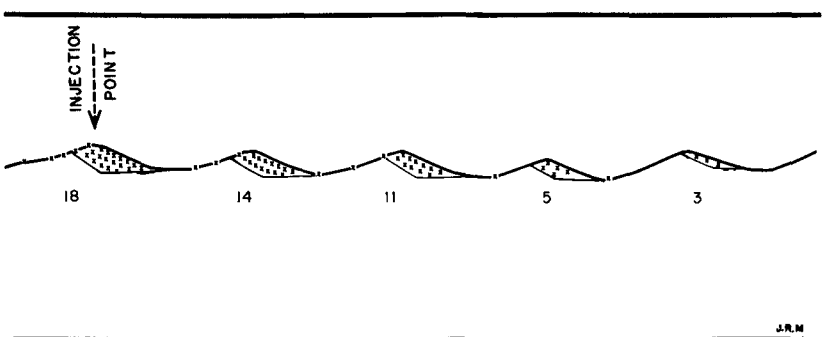

Fig. 8. Entrapment of tracer in ripple crest.

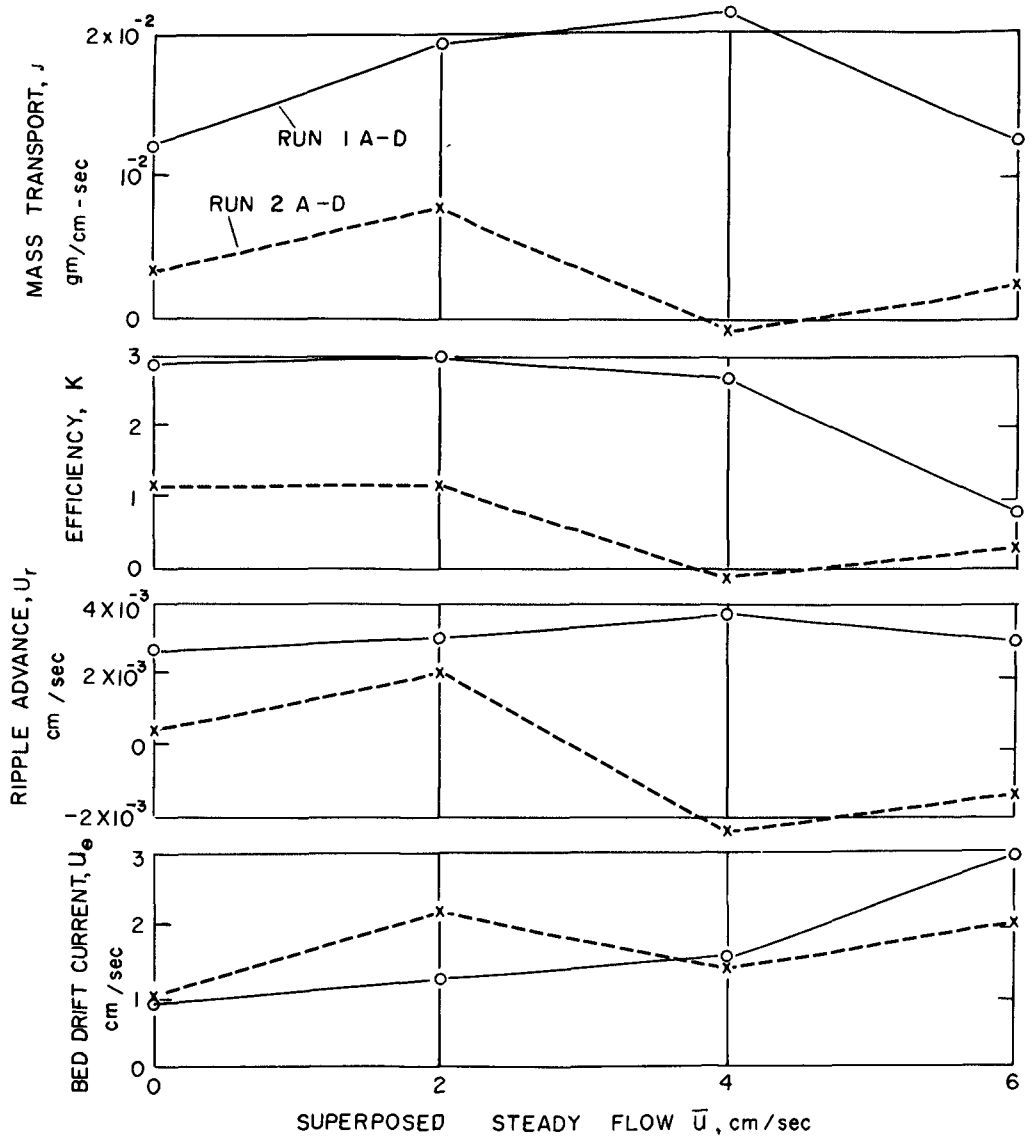

Fig. 9. Summary comparisons of transport properties of Runs 1 & 2.

It was determined that the area within the ripple profile was given by $0.37\lambda\eta$. The product of the mass of sand in a ripple and the rate of ripple advance $0.37\lambda\eta\rho_s \cdot U_r$ gave a transport expression which varied in much the same way as the measured sand transport.

FUTURE INVESTIGATIONS

This work comprises a pilot study and the conclusions drawn should be considered as tentative. The experiments should be repeated using a wider range of wave type, different sizes of bed sand, and wider, but controlled, conditions of liquid viscosity. It would be instructive to evaluate the transport relations when the orbital diameter greatly exceeds the ripple wavelength, causing the ripples to vanish and the bed to become smooth. Such a smooth bed is common near natural surf zones, and should be in better agreement with the model (Eq. 1).

Very little practical work has been done on the interaction between waves and currents, especially in the investigation of the behaviour of the boundary layer. For example, it is not known whether the superposition of wave motion on steady flow aids the spread of the turbulent boundary layer or inhibits it; or if the behaviour of the system depends on whether waves or currents are generated first. It would also be interesting to have complete vertical velocity profiles of the combined system, particularly for flow over ripples. It might then become possible to make a more direct comparison between the bahaviour of a beach and that of a model.

CONCLUSIONS

For low values of $\bar{u}$ a consistent relationship was found between the energy loss of the waves and the work done in transporting the sediment over the bed, the values of the coefficient, K, being 0.29 for run 1 and 0.12 for run 2. Further increase in $\bar{u}$ created a complex movement above the ripples which was periodic but asymmetric; the phase-dependent phenomena then had a greater effect on the system than that of the drift velocity. Under these conditions the theoretical assumptions were no longer valid and any calculated value of K was very small.

ACKNOWLEDGMENTS

The experimental work was performed at the Hydraulics Research Station, Wallingford, England, while the senior author was a Guggenheim Fellow. The authors are indebted to R. A. Bagnold for furnishing the guiding principles leading to this study. We wish to acknowledge the contributions of members of the Hydraulics Research Station staff; R. C. H. Russell, S. Yalin and H. Anwar for their many helpful suggestions during the course of the investigation; D. E. Newman for developing the tracers and an injection technique, and A. Lovegreen for modifying the experimental apparatus.

REFERENCES

Bagnold, R. A. (in press). Mechanics of marine sedimentation: The Sea, Ideas and Observations. (ed. by M. Hill, W. Munk, E. Goldberg and C. Iselin). Interscience Publishers.

Hunt, J. N. (1952). Viscous damping of waves over an inclined bed in a channel of finite width: La Houille Blanche, vol. 7, pp. 836-842.

Inman, D. L. (1952). Measures for describing the size distribution of sediments: Jour. Sed. Pet., vol. 22, pp. 125-148.

Longuet-Higgins, M. S. (1953). Mass transport in water waves: Phil. Trans. Royal Society, London, Series A, vol. 245, pp. 535-581.

Longuet-Higgins, M. S. and Stewart, R. W. (1960). Changes in the form of short gravity waves on long waves and tidal currents: Jour. Fluid Mechanics, vol. 8, pp. 565-583.

Putnam, J. A. and Johnson, J. W. (1949). The dissipation of wave energy by bottom friction: Trans. Amer. Geophys. Union, vol. 30, pp. 67-74

Russell, R. C. H. and Osorio, J. D. C. (1958). An experimental investigation of drift profiles in a closed channel: Proc. Sixth Conference Coastal Engineering, pp. 171-183.

Shepard, F. P. and Inman, D. L. (1950). Nearshore water circulation related to bottom topography and wave refraction: Trans. Amer. Geophys. Union, vol. 3, pp. 196-212.

Ursell, F.; Dean, R. G.; and Yu, Y. S. (1960). Forced small amplitude water waves: a comparison of theory and experiment: Jour. Fluid Mechanics, vol. 7, pp. 33-52.

CHAPTER 12

SIMILARITY IN SEDIMENT TRANSPORT DUE TO WAVES

S. Yalin, Dozent, Dr.-Ing.,
and
R. C. H. Russell, M.A., A.M.I.C.E., A.M.I.Mech.E.
Hydraulics Research Station, Wallingford, England.

ABSTRACT

The paper concerns the movement by waves of cohesionless sediment lying on a horizontal bed. In particular it concerns the number of dimensionless parameters that are necessary to define the 2-phase motion at the bed; the specification of which would enable perfect similarity to be obtained.

It is shown that in general four dimensionless parameters are necessary; but that when the motion of the water at the bed can be adequately defined by an orbit length (a) and a period (T), the two-phase motion can be described by the numerical value of three dimensionless parameters. This condition is satisfied when the wave-height is low, because then the orbital motion at the bed is sinusoidal and the drift velocity is negligible.

Model and prototype experiments were conducted in a wave channel, using low waves, in which the scale for depth of water and for wavelengths was $\frac{3}{10}$. The dependent parameters, three of which are sufficient to verify similarity of all aspects of the phenomenon were chosen to be ripple height, ripple length and transport of sediment. The identity of the dimensionless numbers signifying the ripple height, ripple length and transport in model and prototype, shown in Figs. 8, 9 and 11, is proof that similarity had been obtained.

1) DEFINITION OF THE TWO-PHASE PHENOMENON, CHARACTERISTIC PARAMETERS

Consider two-dimensional progressive wave motion of a real fluid with a finite depth (i.e. $h < L/2$) over a horizontal and cohesionless movable bed (Fig. 1). If the motion of the fluid is able to produce the movement of the bed material then both motions depending reciprocally each on the other together constitute an inseparable mechanical whole - a "two-phase phenomenon".

We assume that the following geometrical properties (independent of the absolute size) are specified:

(i) the form of the waves (i.e. we assume that the function $y/H = \varphi(x/L)$ has a certain definite form; where the x-axis travels on the still surface of the fluid with the velocity of wave propagation C).

(ii) the form of the particle - size distribution curve of the bed material.

(iii) the form of the particles of the bed material.

In this case the two-phase phenomenon in the vicinity of the bed is completely defined by specifying the following 7 independent quantities (characteristic parameters)

ρ	density of fluid	physical properties of fluid
ν	kinematic viscosity	
D	any typical diameter of bed material (e.g. D_{50}, D_{max} etc.)	properties of bed material
γ_s	specific weight of the bed material in fluid	
a_b	the orbit length at the bed*)	mechanical properties of the fluid motion at the bed
T	period	
w_b	the drift velocity at the bed	

(1)

Hence any mechanical quantity A related to the two-phase pnenomenon in the vicinity of the bed (regardless of whether A is a property of the fluid motion or of the motion of the bed material) must be a certain function of the characteristic parameters (1)

$$A = f_A(\rho, \nu, D, \gamma_s, T, a_b, w_b) \qquad (2)$$

The subscript A in f_A indicates that the form of the above function varies as A, the quantity under investigation, varies.

---

*) "at the bed" means "at the region just above the boundary layer". Since the distributions of a and w with depth both tend to be vertical as they approach the boundary layer more precise definition of location is not necessary.

SIMILARITY IN SEDIMENT TRANSPORT DUE TO WAVES

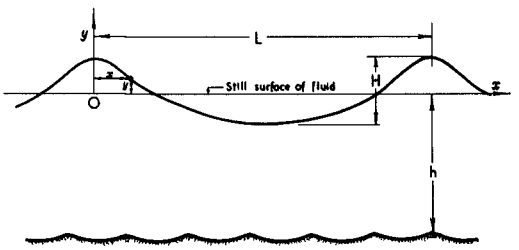

Fig. 1

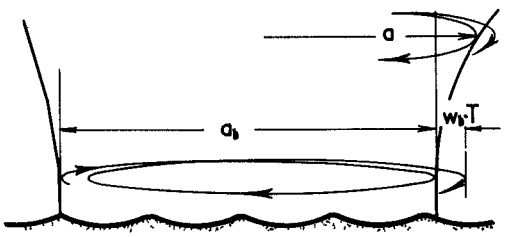

Fig. 2

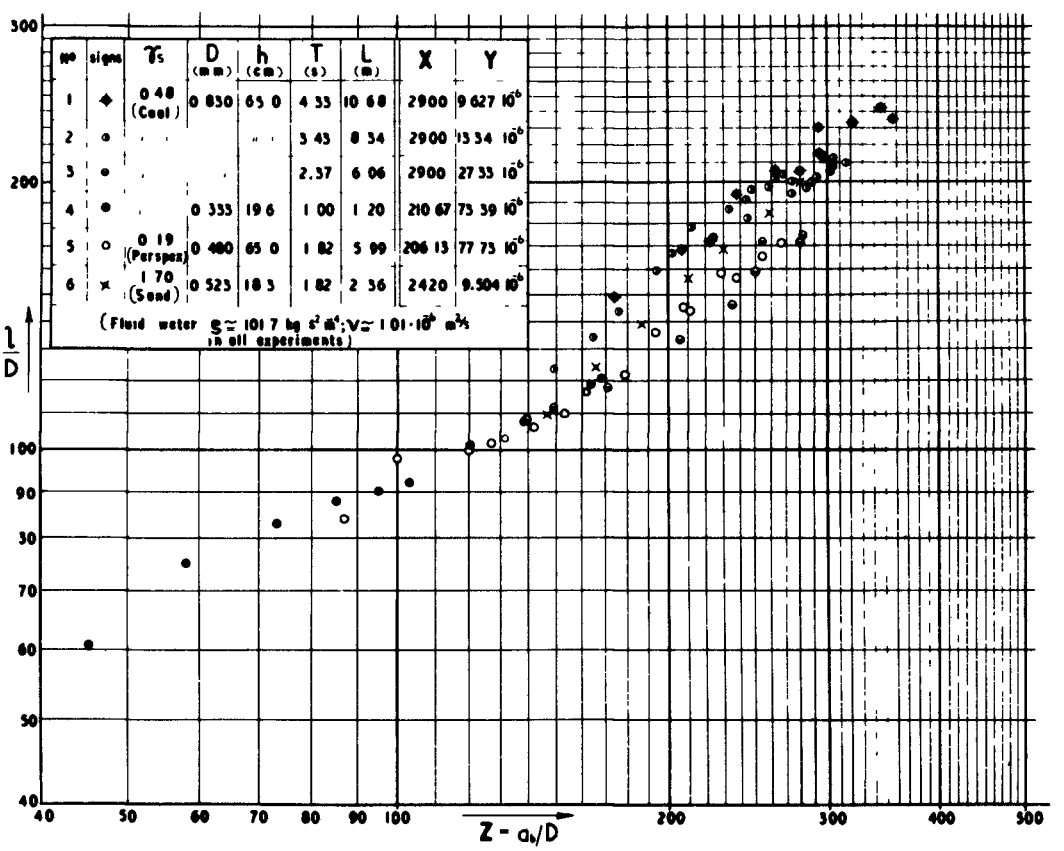

Fig. 3

2) DIMENSIONLESS EXPRESSION OF THE PHENOMENON

According to the theory of dimensions each dimensional relationship (2) can always be expressed in a dimensionless form as follows

$$\Pi_A = \varphi_A(X, Y, Z, W) \tag{3}$$

where the four variables X, Y, Z, W represent the following dimensionless combinations of 7 dimensional parameters (1)*);

$$X = \frac{\gamma_s D^3}{\rho \nu^2} \; ; \; Y = \frac{\rho \cdot D}{\gamma_s T^2} \; ; \; Z = \frac{a_b}{D} \; ; \; W = \frac{w_b T}{D} \tag{4}$$

while the function Π_A is the dimensionless power product

$$\Pi_A = A \cdot D^x \gamma_s^y T^z \tag{5}$$

e.g. if A = 1 ripple length $\Pi_1 = 1 \cdot D^{-1} = \varphi_1(X, Y, Z, W)$ (6)

A = Δ ripple height $\Pi_\Delta = \Delta D^{-1} = \varphi_\Delta(X, Y, Z, W)$ (7)

---

*) Selecting ρ, T, a_b as basic quantities we obtain from the "Π-Theorem"

$$\overline{X} = \frac{2 a_b D}{T \cdot \nu} \; ; \; \overline{Y} = \frac{\rho \cdot a_b}{\gamma_s T^2} \; ; \; \overline{Z} = \frac{a_b}{D} \; ; \; \overline{W} = \frac{w_b T}{a_b}$$

Considering that $2 \cdot a_b/T = U$ (mean orbital velocity) and $w_b T$ is the distance of translation of the orbit during the period T, it is realized that $\overline{X}$ is a "grain-size Reynolds number", $\overline{Y}$ characterizes the "ratio of the drag force to the weight of the bed material", $\overline{Z}$ is "initial relative roughness (or smoothness) of the bed" and $\overline{W}$ is the "relative translation of the orbit due to drift". However, these distinctly interpretable basic combinations are inappropriate for experimental purposes (e.g. variation in the orbit length a_b, the easiest case experimentally, lead to variations in each of the dimensionless variables, $\overline{X}$, $\overline{Y}$ $\overline{Z}$, $\overline{W}$. Since according to the theory of dimensions any set of dimensionless variables can be replaced by any independent combinations of them, the variables (4) have been chosen as the following independent combinations of $\overline{X}$, $\overline{Y}$, $\overline{Z}$, $\overline{W}$.

$$X = \overline{X}^2 \overline{Y}^{-1} \overline{Z}^{\frac{1}{4}}, \quad Y = \overline{Y} \cdot \overline{Z}^{-1}, \quad Z = \overline{Z} \; ; \; W = \overline{W} \overline{Z}$$

(See for "basic quantities", "Π-Theorem", "independent combinations" etc. in Ref. [1])

$$A = G \text{ the weight of the transported bed material (during a certain time t)}$$
$$\Pi_G = G\, D^3 \gamma_s^{-1} = \varphi_G(X, Y, Z, W) \text{ etc.} \qquad (8)$$

If the wave-height is "small" in comparison to the wave-length ("Waves with small amplitude") then the influence of the variable W is negligible, and thus the general form (3) can be assumed to be a function of 3 variables only:

$$\Pi_A = \varphi_A(X, Y, Z) \qquad (9)$$

For example, in this case the expression of ripple length (6) becomes

$$\Pi_1 = \frac{l}{D} = \varphi_1(X, Y, Z) \qquad (10)$$

which is the "family of the surfaces", or the "family of the family of curves". Putting X = const we obtain from (10) the following function of 2 variables only

$$\frac{l}{D} = \varphi_1(\text{const}, Y, Z) = \overline{\varphi}_1(Y, Z) \qquad (11)$$

which can be represented by a "family of curves". If in addition, Y = const, then l/D is a function of one variable only; and consequently can be represented by a "single curve":

$$\frac{l}{D} = \varphi_1(\text{const}, \text{const}, Z) = \overline{\overline{\varphi}}_1(Z) \qquad (12)$$

(This explains why, in plotting l versus a_b (which, in dimensionless plotting, implies (12)), the experimental points are so scattered (see for example ref. [2])*). This is not only because the two lengths l and a_b have not been measured properly, but also because it was attempted to represent a function of more than one variable by a single curve. Indeed, if fluid and bed material are kept constant then X is the only constant. In this case according to (11) the variation of l/D

*) R. A. Bagnold (ref. [3]) did not obtain such a scatter. He based his classification of experimental points on values of D and γ_s. In an exact "dimensional classification" the value of T should also be considered, since, if the fluid used is water, (ρ = const, ν = const) and w_b = 0, as in Bagnold's case, then, according to (2), A = l must be $l = f_1(D, \gamma_s, T, a_b)$ and thus in plotting l versus a_b we have D, γ_s, T as parameters. However in Bagnold's case the variation in T was not large and its omission did not therefore result in much scatter.

depends on both Y and Z, and thus a representation of 1 as a function of a_b only without taking into consideration the period T (i.e. Y) is theoretically impossible).

The results of the measurements of ripple-lengths carried out in the wave channel at H.R.S., Wallingford are shown on Fig. 3. It can be seen that the experimental points corresponding to the same constant values of X and Y form their own individual curves which represent the relationship $1/D = \overline{\Phi}_1(Z)$. Note that the points having the same value of X, but different values of Y, form different curves, a fact which confirms experimentally that $1/D = \overline{\Phi}_1(Y, Z)$ if X = const. Hence 1/D is in fact a function of the three variables X, Y, Z, as derived theoretically above.

3) CONDITIONS FOR DYNAMICAL SIMILARITY

Let α be any quantity;

α' the prototype value of α

α'' the model value of α

and $\lambda_\alpha = \frac{\alpha''}{\alpha'}$ the scale of α

The existence of dynamical similarity between the model and prototype implies

$\lambda_\alpha \equiv 1$ if α is a dimensionless quantity

$\lambda_\alpha = \text{const}$ if α is a dimensional quantity

If geometrical similarity exists, (i.e. the properties (i), (ii), (iii) are identical in model and prototype), then dynamical similarity of the two-phase phenomenon under consideration is provided by the identity of the model and prototype values of all dimensionless combinations defining the phenomenon. Thus the conditions of dynamical similarity for the two-phase phenomenon are

$$\lambda_X \equiv 1 \quad ; \quad \lambda_Y \equiv 1 \quad ; \quad \lambda_Z \equiv 1 \quad ; \quad \lambda_W \equiv 1 \qquad (13)$$

or considering (4) in terms of the scales of characteristic parameters:

$$\left(\begin{array}{r} \lambda_{\gamma_s} \cdot \lambda_D^3 \cdot \lambda_\rho^{-1} \cdot \lambda_\nu^{-2} \equiv 1 \\ \lambda_\rho \cdot \lambda_D \cdot \lambda_{\gamma_s}^{-1} \cdot \lambda_T^{-2} \equiv 1 \\ \lambda_{a_b} \cdot \lambda_D^{-1} \equiv 1 \\ \lambda_{w_b} \cdot \lambda_T \cdot \lambda_D^{-1} \equiv 1 \end{array} \right) \qquad (14)$$

There are 4 independent equations involving 7 independent scales. From a random choice of 3 scales the remaining 4 are obtained by solving (14). Thus theoretically it is always possible to obtain dynamical similarity of the two-phase phenomenon in the vicinity of the bed. However if in model and prototype the same fluid (water) is used then $\lambda_\rho = \lambda_\nu = 1$ and the system (14) reduces into

$$\left(\begin{array}{r} \lambda_{\gamma_s} \cdot \lambda_D^3 \equiv 1 \\ \lambda_D \cdot \lambda_{\gamma_s}^{-1} \cdot \lambda_T^{-2} \equiv 1 \\ \lambda_{a_b} \lambda_D^{-1} \equiv 1 \\ \lambda_{w_b} \lambda_T \cdot \lambda_D^{-1} \equiv 1 \end{array}\right) \qquad (15)$$

In this case there are 4 equations involving 5 independent scales. Thus only one of them can be chosen at random.

In practice system (15) is inconvenient to use since it involves the drift velocity, w_b, which must itself be estimated as a function of the properties of the wave motion. Therefore it would be more appropriate to modify (15) so that w_b is replaced by these properties.

According to M. S. Longuet-Higgins (ref. [4]) w_b can be obtained as follows

$$w_b = \overline{\text{const}}\ \frac{U^2}{C} \qquad (16)$$

where

$$U = 2\,\frac{a_b}{T} \qquad (17)$$

and

$$C = \frac{L}{T} \qquad (18)$$

Thus

$$w_b = \text{const}\ \frac{a_b^2}{T\,L} \qquad (19)$$

and therefore

$$\lambda_{w_b} = \lambda_{a_b}^2\ \lambda_T^{-1}\ \lambda_L^{-1} \qquad (20)$$

Consider that T, L and h are connected by the C-formula in following form

$$\frac{C^2}{gL} = \frac{L}{gT^2} = \Psi\left(\frac{h}{L}\right) \qquad (21)$$

where:

$$\Psi\left(\frac{h}{L}\right) = \frac{1}{2\pi} \tanh 2\pi \frac{h}{L} \tag{22}$$

This is an exact expression for the theory of "waves with small amplitude" and represents the first order of approximation for the "waves with finite amplitude" (Stokes). Assuming $\lambda_g = 1$, we obtain from (21)

$$\lambda_L = \lambda_\Psi \lambda_T^2 \tag{23}$$

Considering (20) and (23), the system (15) can be expressed as follows:

$$\left(\begin{array}{rcl} \lambda_{\gamma_s} \lambda_D^3 & \equiv & 1 \\ \lambda_D \lambda_{\gamma_s}^{-1} \lambda_T^2 & \equiv & 1 \\ \lambda_{a_b} \cdot \lambda_D^{-1} & \equiv & 1 \\ \lambda_{a_b}^2 \lambda_D^{-1} \cdot \lambda_L^{-1} & \equiv & 1 \\ \lambda_L \cdot \lambda_T^{-2} & \equiv & \lambda_\Psi \end{array}\right) \tag{24}$$

with

$$\lambda_\Psi = \frac{\tanh 2\pi h''/L''}{\tanh 2\pi h'/L'} = \frac{\tanh [2\pi h'/L'(\lambda_h/\lambda_L)]}{\tanh 2\pi h'/L'} \tag{25}$$

or for small prototype values h'/L' simply:

$$\lambda_\Psi \approx \frac{\lambda_h}{\lambda_L} \tag{26}$$

Thus the value λ_Ψ depends on the prototype value, h'/L', and the distortion, $\lambda h/\lambda L$. The system (24) consists of 5 equations involving 6 independent scales. Hence only one of them can be chosen at random.

DISCUSSION

a) UNDISTORTED MODEL: ($\lambda_h = \lambda_L$, i.e. $\lambda_\Psi = 1$)

Substituting $\lambda_\Psi = 1$ the system (24) gives unity for all scales. Thus by using the same fluid in model and prototype dynamical similarity of the two-phase phenomenon on an undistorted model is impossible.

If the influence of drift (the condition $\lambda_w \equiv 1$) can be neglected, i.e. if the fourth equation in (24) is rejected, then the solution of (24) gives

$$\left.\begin{array}{c} \lambda_D = \lambda_{a_b} \\ \lambda_{\gamma_s} = \lambda_{a_b}^{-3} \\ \lambda_T = \lambda_{a_b}^{2} \\ \lambda_h = \lambda_L = \lambda_{a_b}^{4} \end{array}\right\} \qquad (27)$$

This is a Froudian model ($\lambda_T = \sqrt{\lambda_L}$), where the bed material is heavier but finer than in prototype. The velocity scales in this case are:

$$\lambda_{w_b} = \lambda_{a_b}^{-4} \quad ; \quad \lambda_U = \lambda_{a_b}^{-1} \quad ; \quad \lambda_C = \lambda_{a_b}^{2} \qquad (28)$$

b) DISTORTED MODEL (DRIFT CONDITION IS SATISFIED) ($\lambda_\psi \neq 1$)

Preserving the fourth equation and assuming $\lambda_\psi \neq 1$ the solution of (24) gives

$$\left.\begin{array}{c} \lambda_D = \lambda_{a_b} \\ \lambda_{\gamma_s} = \lambda_{a_b}^{-3} \\ \lambda_T = \lambda_{a_b}^{2} \\ \lambda_L = \lambda_{a_b} \\ \lambda_\psi = \lambda_{a_b}^{-3} \end{array}\right\} \qquad (29)$$

Selecting $\lambda_L = \lambda_{a_b}$ we can obtain all the other scales including $\lambda_\psi = \lambda_{a_b}^{-3}$ i.e.

$$\frac{\tanh\left[2\pi h'/L'(\lambda_h/\lambda_L)\right]}{\tanh 2\pi h'/L'} = \lambda_L^{-3} \qquad (30)$$

Hence, knowing λ_L and the prototype value h'/L', λ_h is obtained as the solution of the transcendent equation above. The model is not Froudian ($\lambda_T = \lambda_L^2$) and the bed material consists of larger but lighter grains than in the prototype. Indeed if $\lambda_h < 1$ then (30) gives $\lambda_L > 1$, and thus $\lambda_{a_b} > 1$ and consequently $\lambda_D > 1$ and $\lambda_{\gamma_s} < 1$. Obviously this non-Froudian model in which $\lambda_L > 1$ and $\lambda_T > 1$ is not as convenient for practical purposes as the undistorted model discussed in (a): it therefore represents only a theoretical solution of the problem.

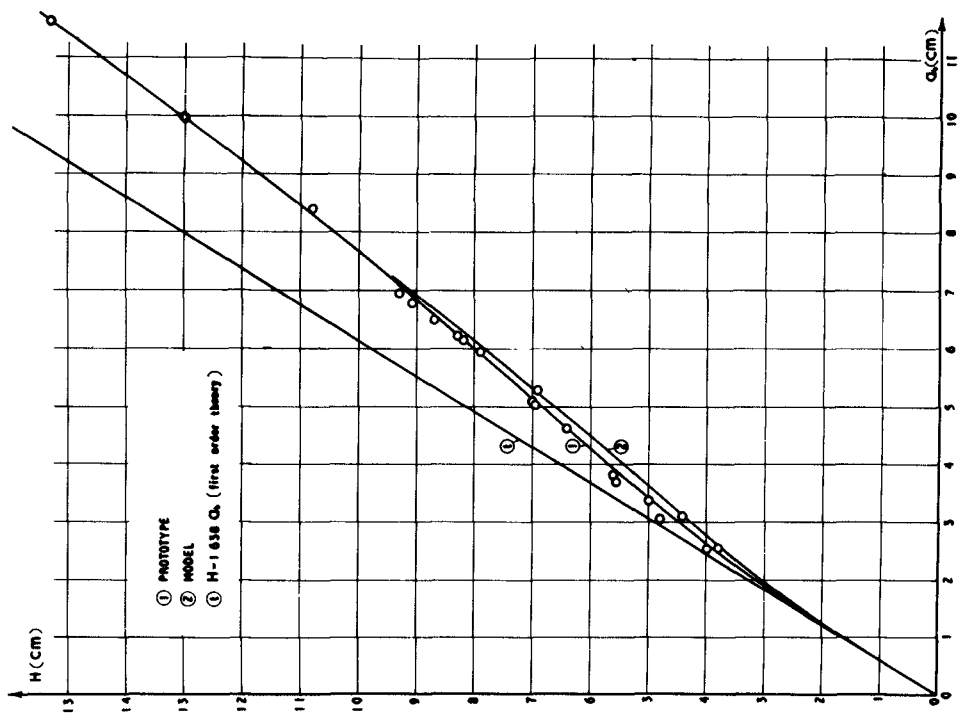
H(cm)
① PROTOTYPE
② MODEL
③ H-1 638 Q₀ (first order theory)
Q₀(cm)

Fig. 5

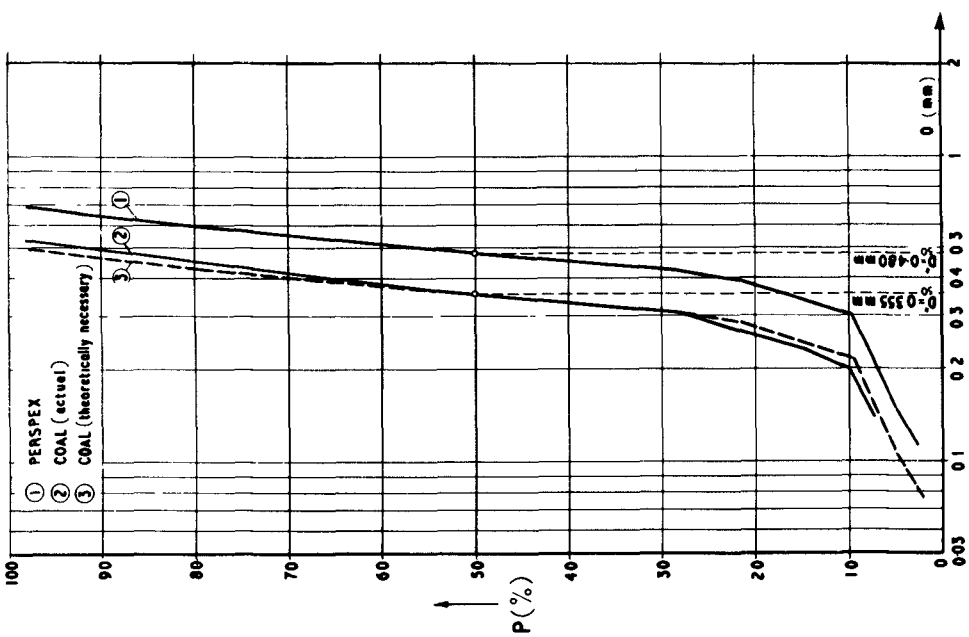
① PERSPEX
② COAL (actual)
③ COAL (theoretically necessary)
P(%)
D (mm)
D=0.480 mm
D=0.355 mm

Fig. 4

4) THE EXPERIMENTAL RESULTS

In order to confirm the theoretical considerations stated above, experiments were carried out in the 75 cm-wide wave channel at H.R.S., Wallingford. The measurements were made on a Froudian model (as described in 3(a)). It has to be proved that in such a model the conditions for dynamical similarity at the bed are

$$\lambda_X \equiv 1 \quad ; \quad \lambda_Y \equiv 1 \quad ; \quad \lambda_Z \equiv 1$$

(assuming of course that (i), (ii) and (iii) are specified). If, in fact X, Y, Z represent the "complete set" of dimensionless variables, then the conditions

$$X' \equiv X''$$

$$Y' \equiv Y''$$

$$Z' \equiv Z''$$

must make all corresponding dimensionless functions, φ_A' and φ_A'', identical

$$\varphi_A' = \varphi_A(X', Y', Z') = \varphi_A(X'', Y'', Z'') = \varphi_A'' \qquad (31)$$

with the scale of A

$$\lambda_A = \lambda_D^{-x} \cdot \lambda_{\gamma_s}^{-y} \cdot \lambda_T^{-z} \qquad (32)$$

Perspex ($\gamma_s' = 0.19$) was chosen as bed material for the prototype, and coal ($\gamma_s'' = 0.48$) for the model. Thus

$$\lambda_{\gamma_s} = \frac{\gamma_s''}{\gamma_s'} = 2.528 \qquad (33)$$

According to the first and second equations of (27)

$$\lambda_D = \frac{1}{\sqrt[3]{\lambda_{\gamma_s}}} = 0.735 \qquad (34)$$

Fig. 4 shows the particle-size distribution curves of the perspex and coal used in the experiments. In order to satisfy the geometrical condition, (ii), the coal was prepared so as to have a particle-size distribution curve similar to that for the perspex. As shown in Fig. 4 the actual ratio λ_D was

$$\lambda_D \cong \lambda_{D_{50}} = \frac{0.355}{0.48} = 0.74 \qquad (35)$$

correspondingly the system (27) yields:

$$\left.\begin{aligned} \lambda_{a_b} &= \lambda_D = 0.74 = 1/1.35 \\ \lambda_T &= 0.74^2 = 0.548 = 1/1.82 \\ \lambda_h &= \lambda_L = 0.74^4 = 0.301 \end{aligned}\right\} \quad (36$$

Selecting the prototype values

$$\left.\begin{aligned} T' &= 1.82 \text{ s} = \text{const} \\ h' &= 65.0 \text{ cm} = \text{const} \\ \text{and consequently } L' &= 399 \text{ cm} = \text{const} \end{aligned}\right\} \quad (37$$

the corresponding model values were

$$\left.\begin{aligned} T'' &= 1.00 \text{ s} = \text{const} \\ h'' &= 19.6 \text{ s} = \text{const} \\ L'' &= 120 \text{ cm} = \text{const} \end{aligned}\right\} \quad (38$$

Therefore:

$$X' = 206,13 = \text{const} \; ; \; Y' = 77,75.10^{-6} \quad (39)$$

and

$$X'' = 210,67 = \text{const} \; ; \; Y'' = 75,39.10^{-6} \quad (40)$$

Since $\frac{X'}{X''} = 97,84\%$ and $\frac{Y''}{Y'} = 96,65\%$ it can be assumed that the conditions $X' = X''$ and $Y' = Y''$ are satisfied from the point c view of the accuracy of measurement. Since a_b (i.e. Z) was the only variable, the experimental points for both model anc prototype must lie on the same curve ($\Pi_A = \overline{\varphi}_A(Z)$) in the dimensionless system of coordinates for any related mechanics quantity A. This statement was proved experimentally for 3 independent aspects of the phenomenon A_1, A_2, A_3 (which, according to the theory of dimensions is sufficient in order to prove the existence of dynamical similarity).

A_1 = l ripple length

A_2 = Δ ripple height

A_3 = G the total weight of the bed material transported during the certain time t from a tray inserted in the bed.

Π-values of these quantities are respectively

$$\Pi_1 = \frac{l}{D} \qquad \Pi_\Delta = \frac{\Delta}{D} \qquad \Pi_G = \frac{G}{\gamma_s D^3}$$

The measurement of the orbit lengths a_b was made by means of a pendulum which consisted of a disc which was weightless in water, moving on a spanned steel string parallel to a ruler. For the constant prototype values h = 65 cm and T = 1,82 s this instrument gave the relationship between a_b and H as shown in Fig. 5 by curve (1). As seen from Fig. 5, as H increases this experimental curve systematically deviates from the theoretical curve (T) ((T) representing the linear relation between a_b and H for waves of small amplitude). It was assumed that the ratio a_b/H given by the curve (1) is valid for all waves of the same L/h. Therefore the orbit lengths in the model were obtained from curve (2) (drawn homologous to curve (1) to the scale $\lambda a_b = 0.74$) by measuring the wave heights H.

For the measurements l and Δ the bed of the flume (8.00 x 0.75 m^2) was covered with material to a depth of not less than 3 cm. The values l and Δ were obtained as mean values of a "ripple train" (consisting of at least 20 ripples) which was traced from the central observation window on the side of the flume.

The total weight G leaving the tray (Fig. 6) during the time intervals t' = 15 min and t" = 8.25 min in prototype and model respectively was measured as

$$G = G_l + G_r$$

The results of measurements of ripple length in model and prototype are shown in Figs. 7 and 8. The dimensional plotting in Fig. 7 shows that the experimental points of prototype and model form two homologous curves to the scale $\lambda a_b = 0.74$; whereas both prototype and model points form the same curve $l/D = \overline{\Phi}_l(Z)$ in the dimensionless plotting in Fig. 8.

In Fig. 11 the dimensionless ripple heights Δ/D are plotted. Once again there is a tendency for both model and prototype experimental points to lie on the same curve $\Delta/D = \overline{\Phi}_\Delta(Z)$. (Note that l/D is always an increasing function of Z whereas Δ/D tends to zero at a certain value of Z.) Thus the ripples disappear because their height, and not their length, tends to zero.

Figs. 10 and 11 show the results of measurements of the total weight of bed material transported from geometrically similar trays during equivalent periods of time. In this case also, the experimental points form homologous curves (parallel

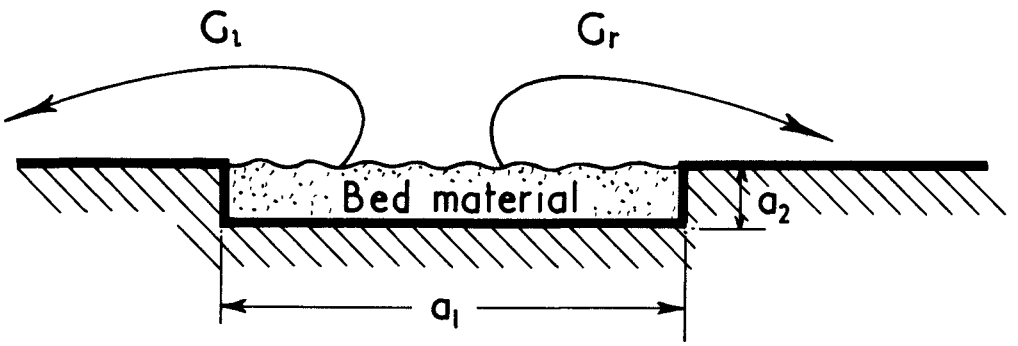

a_1'-1.50m; a_2'-3cm (Prototype)

a_1''-1.11 m, a_2''-2.2 cm (Model)

Fig. 6

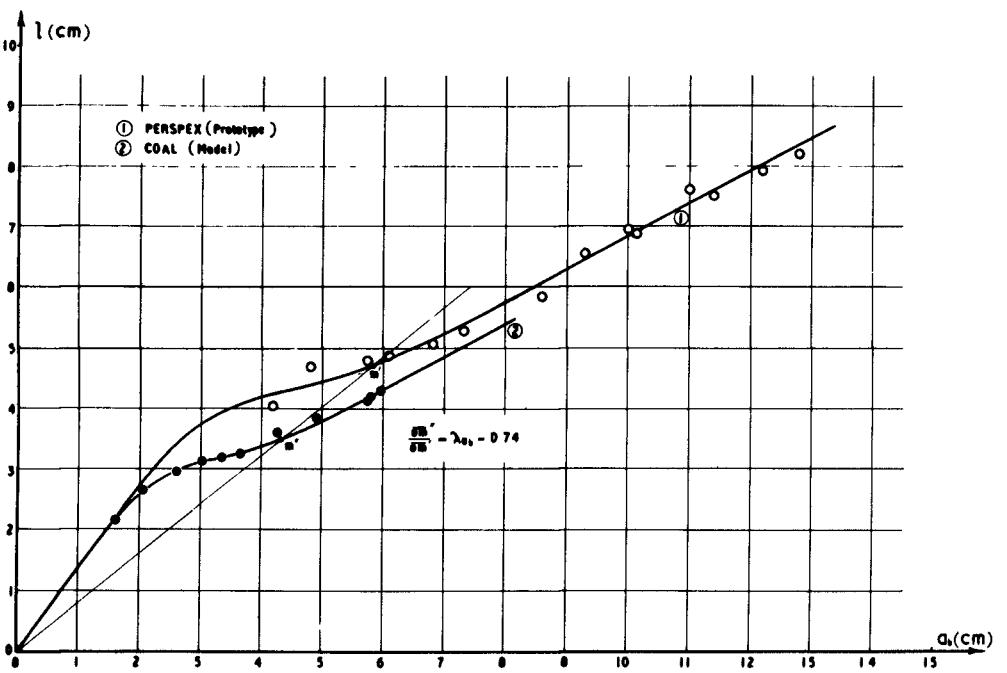

Fig. 7

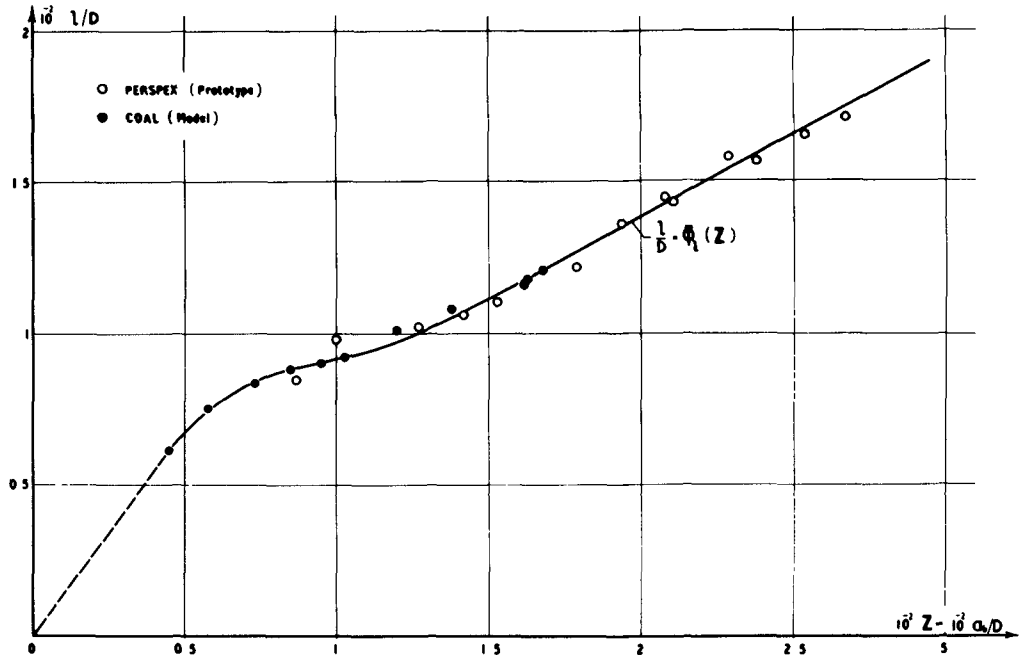
10^2 l/D
PERSPEX (Prototype)
COAL (Model)
$\frac{l}{D} \cdot \Phi_1(Z)$
10^2 Z - 10^2 a_b/D

Fig. 8

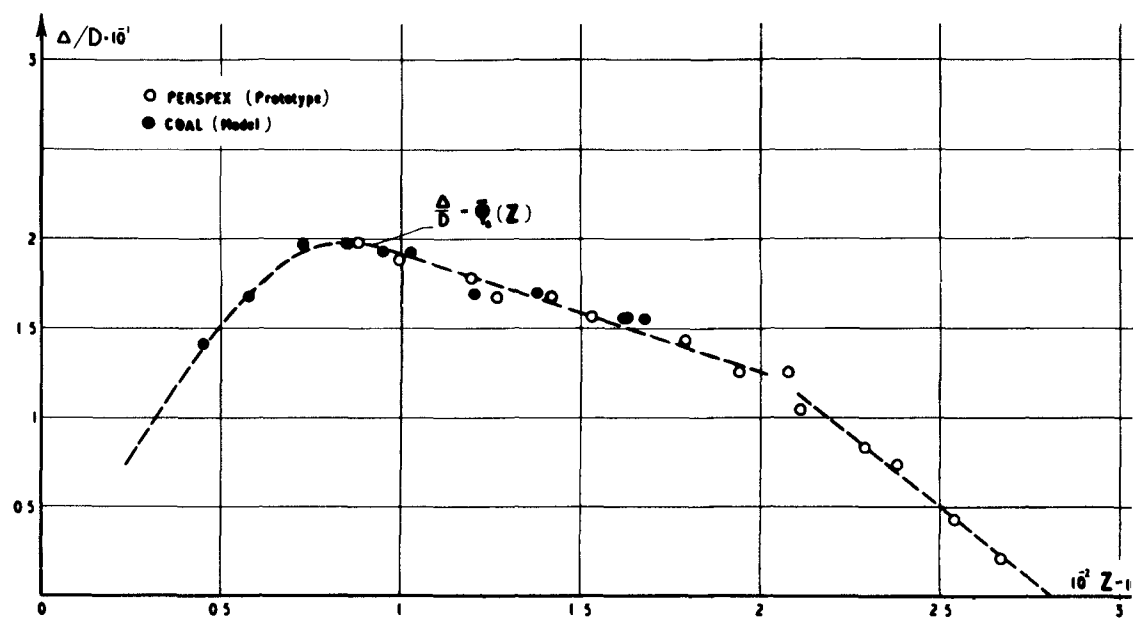
$\Delta/D \cdot 10^1$
PERSPEX (Prototype)
COAL (Model)
$\frac{\Delta}{D} \cdot \Phi_2(Z)$
10^2 Z-

Fig. 9

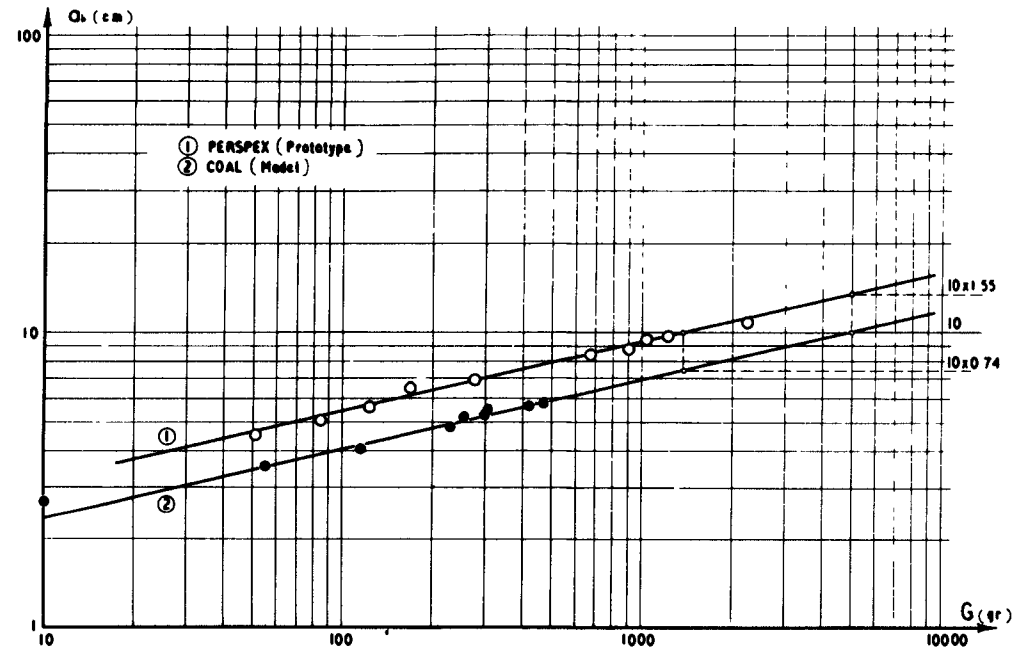
Qh (cm)
100
10
1
① PERSPEX (Prototype)
② COAL (Model)
10±1 55
10
10±0 74
10
100
1000
10000
G (gr)

Fig. 10

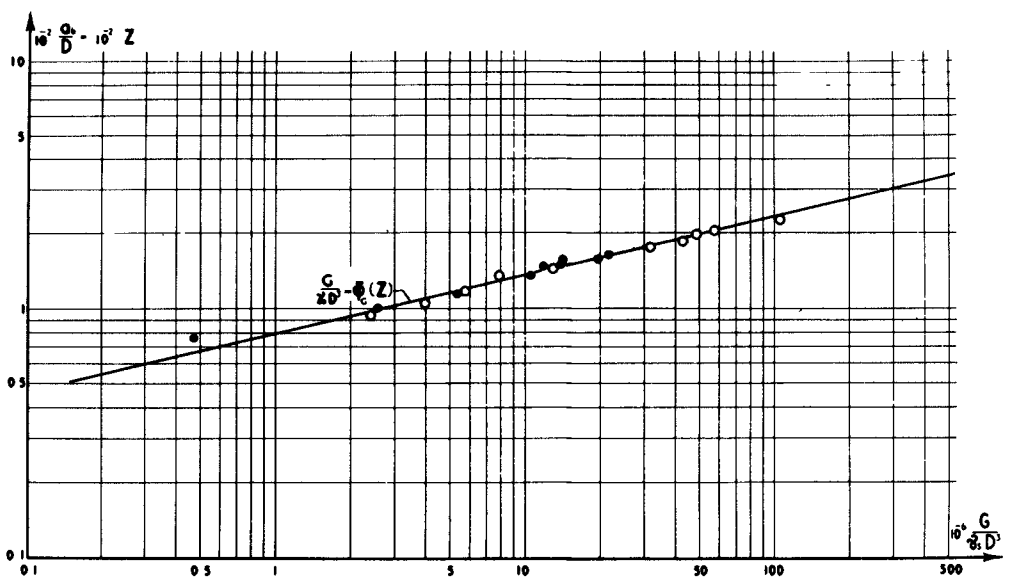
10² Qh/D - 10² Z
10
5
1
0 5
0 1
0 1
0 5
1
5
10
50
100
500
G/ΣD³ - Φc(Z)

Fig. 11

straight lines with log-log coordinates) to the scale $\lambda_{a_b} = 0.74$ in the dimensional plotting in Fig. 10; and a single curve (straight line) with logarithmic coordinates in the dimensionless representation in Fig. 11.

This study was carried out as part of the research programme of the Hydraulics Research Board of the Department of Scientific and Industrial Research, and is published with the permission of the Director of Hydraulics Research.

REFERENCES

Sedov, L. I. (1959). "Similarity and Dimensional Methods in Mechanics" London: Infosearch Ltd.,

Inman, D. (1957). "Wave-generated ripples in nearshore sand" T.M. 100, U.S. Beach Erosion Board.

Bagnold, R. A. (1946). "Motion of waves in shallow water, Interaction between waves and sand bottoms". Proceedings of the Royal Society, A, vol 187.

Longuet-Higgins, M. S. (1957). "The mechanics of the boundary-layer near the bottom in a progressive wave", Proceedings of sixth conference on Coastal Engineering, Chapter 10 - Appendix.

Manohar, M. (1955). "Mechanics of bottom sediment movement due to wave action", T.M. 75, U.S. Beach Erosion Board.

CHAPTER 13

SUSPENDED SEDIMENT DUE TO WAVE ACTION

Masashi Hom-ma and Kiyoshi Horikawa
Department of Civil Engineering, University of Tokyo
Tokyo, Japan

INTRODUCTION

The sediment movement in the littoral zone occurs in the form of bed load (material rolled and pushed along the bottom by shear stress) and suspended load (material maintained in suspension by action of waves and currents). The present paper is concerned with studies through both the field and laboratory investigations intended to determine the concentration patterns of suspended sediment due to action of surface waves. The distribution patterns of suspended sediment sampled at an open coast were highly interesting in relation to functional and structural design of the cooling water intake system for the atomic power plant now being under construction at the Pacific Ocean coast of Tokai, Ibaragi Prefecture, Japan.

As far as the authors are concerned, the clear relationship between hydraulic conditions, such as height and period of waves, water depth, water temperature, etc., and sediment characteristics has not yet been established, although a number of researches have been conducted in the laboratory and in the field. Main of them are as follows:

In Japan:
(1) Field observations at Tomakomai coast conducted by the staff of Hokkaido University (Refs. 1, 2, 3, 4, 5, 6 and 7),
(2) Experimental study at Kyushu University (Refs. 8 and 9),
(3) Field observations at Katase and Kamakura beaches, Kanagawa Prefecture (Refs. 10, 11 and 12), and at Tokai coast, Ibaragi Prefecture (Refs. 13, 14 and 15), both conducted by the staff of the Coastal Engineering Laboratory, University of Tokyo, and
(4) Field observations at Niigata coast, Niigata Prefecture (Refs. 16 and 17).

In the United States: Field observations (Ref. 18) and laboratory investigations (Refs. 19 and 20) at the Beach Erosion Board, Corps of Engineers, U. S. Army.

The present investigation consists of the field studies at Tokai and Niigata coasts and the laboratory studies at the Coastal Engineering Laboratory, University of Tokyo. In the field, two types of sampling device have been used, one consisting of instantaneous sampling of sediment suspended in water and the other of cumulative sampling by use of a bamboo staff which is held upright in various depths of water for a period of several days. The latter type was originally developed by the researchers at Hokkaido University. In the laboratory studies both syphon tubes and bamboo models were used in a two dimensional wave flume. In parallel to these empirical procedures, a theoretical consideration has been performed on the basis of several assumptions in order to analyze the results of field and laboratory investigations.

THEORETICAL CONSIDERATION

According to visual observations through the glassed wall of the wave flume, sand particles spread over the bottom are moved back and forth by the oscillatory motion of water and gradually form sand ripples having a particular dimension corresponding to the types of waves. The turbulence of the fluid is originally restricted to a very thin layer in the vicinity of the flat bottom, but is greatly magnified with formation of sand ripples. The vortices developed in the troughs of sand ripples travel upward, imparting a strong turbulence to almost the entire depth from bottom to surface and carrying with them concentration of bottom sediment. It is therefore realized that sand ripples may have an important effect on the mechanics of suspended sediment subjected to wave action.

We will now assume a two-dimensional turbulent fluid, and proceed to formulate a theoretical distribution pattern of suspended sediment. Taking the horizontal coordinate, x, in the direction of wave propagation and the vertical coordinate, z, upward from the still water level, the equation of sediment concentration is given by the well-known expression:

$$w_o \frac{\partial m}{\partial z} + \frac{\partial}{\partial z}\left(\varepsilon \frac{\partial m}{\partial z}\right) = 0 , \quad (1)$$

where w_o is the fall velocity of a sand particle, m the concentration of suspended sediment, and ε a coefficient of eddy viscosity. In analogy to the classical theory of turbulence, we will assume the following relationship for the value of ε ,

$$\varepsilon = \beta b^2 \left| \frac{\partial u}{\partial z} \right| , \quad (2)$$

in which b and u are the minor radius of an orbit and the horizontal velocity component of water particle, respectively, in the presence of oscillatory motion by waves; and β is considered to be practically constant. As a first approximation, η , vertical displacement of water surface above still water level, b and u may be expressed as:

$$\eta = \frac{H}{2} \sin\left(kx - \frac{2\pi}{T}t\right), \quad (3)$$

$$b = \frac{H}{2} \frac{\sinh k(z+d)}{\sinh kd} , \quad (4)$$

$$u = \frac{\pi H}{T} \frac{\cosh k(z+d)}{\sinh kd} \sin\left(kx - \frac{2\pi}{T}t\right), \quad (5)$$

$$k = \frac{2\pi}{L} , \quad (6)$$

where H. L and T are wave height, wave length and wave period, respectively, at the water depth d. Now, we will further assume the following expression for m:

$$m = \bar{m}(z) \cdot \left\{ 1 + \tfrac{1}{3} \sin 2\left(kx - \frac{2\pi}{T}t\right) \right\} . \quad (7)$$

Introducing Eqs. (2), (4), (5) and (7) into Eq. (1) and taking a time average over a cycle of wave period T, we have the differential equation:

$$w_o \frac{d\bar{m}}{dz} + \frac{d}{dz}\left[\frac{\beta H^3 k}{3T} \frac{\sinh^3 k(z+d)}{\sinh^3 kd} \frac{d\bar{m}}{dz} \right] = 0, \tag{8}$$

Integration of Eq. (8) by considering the boundary condition at the surface and the relationship $\bar{m} = \bar{m}_a$ at $z = -a$, reduces to

$$\frac{\bar{m}}{\bar{m}_a} = \exp\left[-\frac{3 w_o T}{\beta H^3 k} \sinh^3 kd \int_{-a}^{z} \frac{dz}{\sinh^3 k(z+d)} \right]. \tag{9}$$

Rewriting Eq. (9), we arrive at the final expression:

$$\left.\begin{aligned} &\frac{\bar{m}}{\bar{m}_a} = \exp\left[-\alpha \frac{w_o}{C} \left(\frac{L}{H}\right)^3 \left(\frac{d}{L}\right) \sinh^3 kd \cdot f(n, k) \right], \\ &f(n,k) = \int_{n_a}^{n} (\sinh knd)^{-3} dn = \frac{1}{2dk} \left[\left\{ \frac{\cosh k n_a d}{\sinh^2 k n_a d} \right. \right. \\ &\qquad \left. \left. - \frac{\cosh knd}{\sinh^2 knd} \right\} + \log \left| \frac{\tanh \frac{k n_a d}{2}}{\tanh \frac{knd}{2}} \right| \right], \\ &\alpha = \frac{3}{\beta}, \quad C = \frac{L}{T}, \quad n = \frac{d+z}{d}, \quad n_a = \frac{d-a}{d}. \end{aligned}\right\} \tag{10}$$

If the values of α and $\bar{m}_a$ at n_a are determined experimentally, the concentration of suspended sediment at an arbitrary level can be calculated by using Eq. (10) for variable conditions of H, L, T, d and w_o. The term w_o is closely related to sediment characteristics, namely grain diameter, and also the temperature of fluid.

FIELD OBSERVATIONS

In the field observations conducted at the beaches of Katase, Kamakura and Tokai, it was impossible to derive a generalized pattern of suspended sediment in terms of absolute quantity. It was due mainly to failure of adequate measurement of waves during the period of observation, although abundant data on the amount of suspended sediment were made available by bamboo samplers. However, the later phase of investi-

gation included the wave measurement done with special care simultaneously with the sediment sampling operation. A pressure-type self-contained wave gauge was installed on the sea bottom at the depth of about 10 m below the mean sea level, about 500 m offshore, in the field observation at the Tokai coast.

A horizontal-type instantaneous sampler, capacity being 1.5 ℓ, was devised for direct measurement of vertical distribution of sediment concentration, but it proved unfeasible due mainly to the difficulty of operation under rough sea conditions.

A cumulative bamboo sampler enables to determine a cumulative load of suspended sediment, but there exist several uncertainties as to the function of this type of sampler. They are: (1) What is the relationship between the cumulative amount of sediment collected by this sampler and the actual concentration of sediment? (2) What governs the effectiveness of sediment trapping mechanism by this sampler? In spite of such difficulties the authors have found so far this sampling device most preferable for use in the field observations. In order to clarify the said uncertainties of a bamboo sampler, a comparison test was necessary by using model samplers in a laboratory flume.

LABORATORY INVESTIGATIONS

The wave flume used for the comparison test is two-dimensional, 24 m long, 0.8 m deep and 1.0 m wide. Two types of sand, 175 μ and 100 μ in medium diameter, Md, were used. The suspended sediment was sampled, instantaneously, with a simple device of syphon tube, 6 mm I.D., which was equipped with a T-shaped suction mouth, and, cumulatively, with a plastic cylinder, 2.5 cm I.D. and 9 cm high, with a pair of openings of 1 cm diameter on the opposite sides. (Figs. 1, 2 and 3)

The temperature of water was carefully measured, since it may affect fluid viscosity and hence the suspended concentration, as suggested by Fairchild (Ref. 20), although the temperature effect seemed insignificant in the range of our experiment. The bottom level was difficult to define because of the presence of sand ripples. For the sake of convenience, we have used the original smooth bottom as the reference level for each run of experiment.

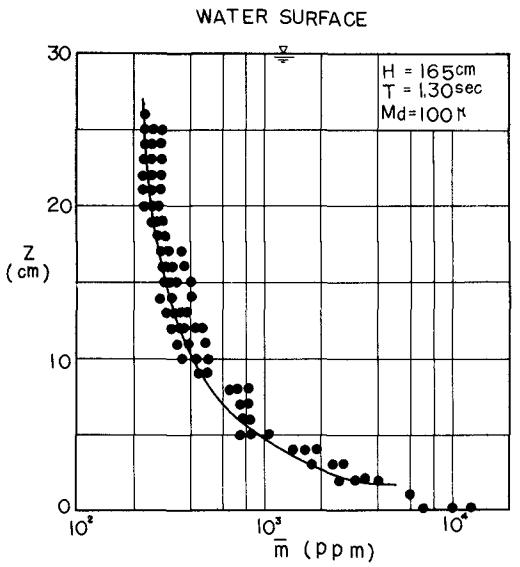

Figure 1. Vertical distribution curve of suspended sediment concentration (Coastal Engineering Laboratory, University of Tokyo).

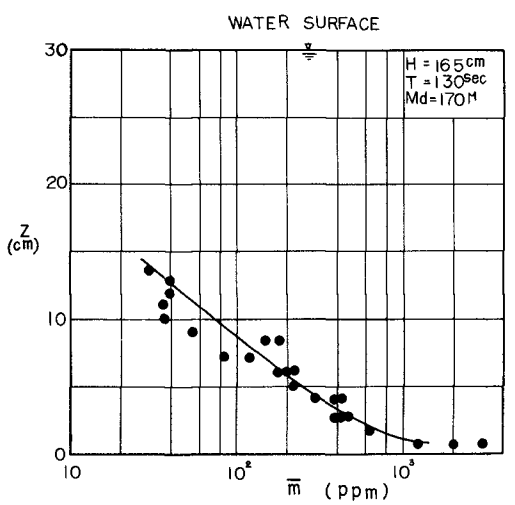

Figure 2. Vertical distribution curve of suspended sediment concentration (Coastal Engineering Laboratory, University of Tokyo).

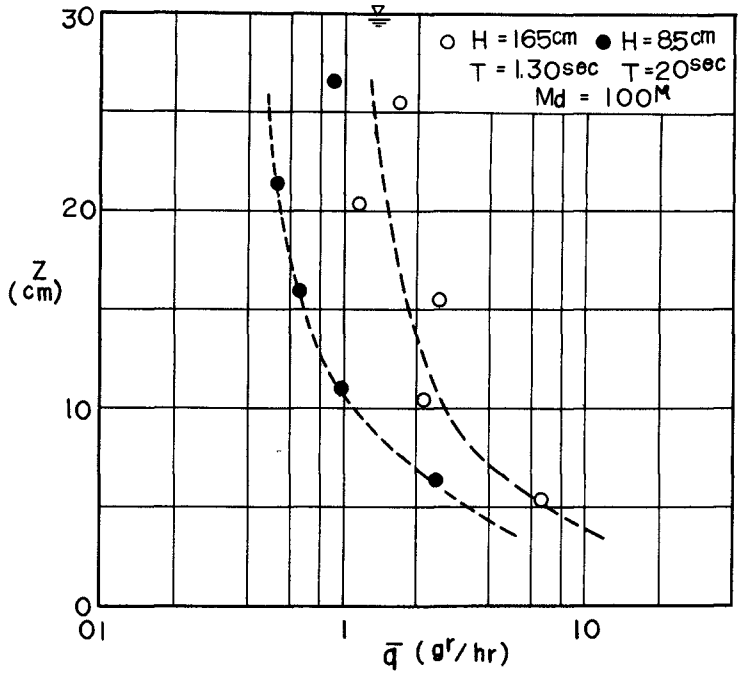

Figure 3. Vertical distribution curve of suspended sediment, cumulative amount by a bamboo model.

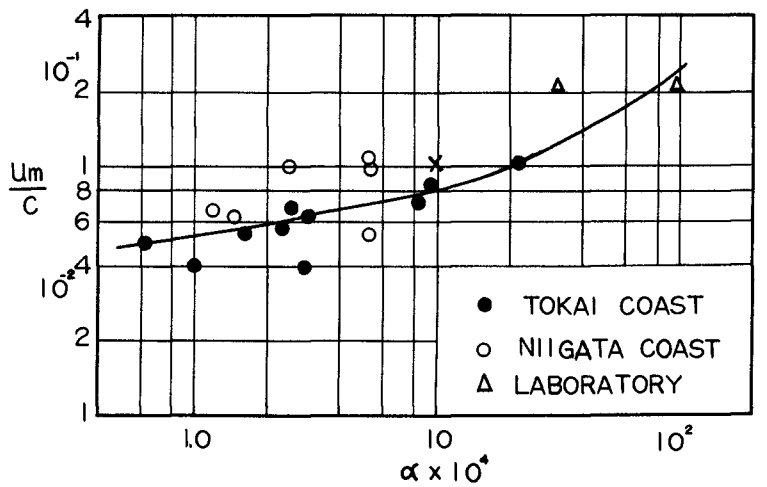

Figure 4. Relationship between $\bar{\alpha}$ and u_m/c.

Table 1. Calculated values of α.

(1) Laboratory (syphon tube, instantaneous)

Wave Height H(cm)	Wave Period T(sec)	Water Depth d(dm)	n	α	$\bar{\alpha}$	M_d (μ)
16.5	1.30	30	0.2	1.9×10^{-3}	3.2×10^{-3}	170
			0.3	2.8×10^{-3}		
			0.4	4.9×10^{-3}		
16.5	1.30	30	0.2	7.6×10^{-3}	9.5×10^{-3}	100
			0.3	9.2×10^{-3}		
			0.5	11.1×10^{-3}		
			1.0	10.3×10^{-3}		

(2) Field (bamboo sampler, cumulative, Tokai)

Wave Height $\bar{H}_{1/3}$ (m)	Wave Period $\bar{T}_{1/3}$ (sec)	Water Depth d (m)	n	α	$\bar{\alpha}$
1.09	6.2	4.8	0.21	1.3×10^{-3}	1.6×10^{-3}
			0.28	1.5×10^{-3}	
			0.30	1.6×10^{-3}	
			0.43	1.7×10^{-3}	
			0.58	1.7×10^{-3}	
			0.73	1.9×10^{-3}	
1.06	6.2	7.8	0.22	2.1×10^{-4}	2.3×10^{-4}
			0.31	2.1×10^{-4}	
			0.41	2.2×10^{-4}	
			0.52	2.6×10^{-4}	

ANALYSIS OF DATA

The concentration of suspended sediment tends to increase distinctly from water surface to bottom. The increase is especially pronounced near the bottom, producing a distribution curve with the shape of " \ ", as previously pointed out by Fukushima et al (Ref. 1). One of the most realistic explanation of this fact may be that the sand particles are picked up and maintained in suspension by the vortices formed in the ripple troughs and separated upward following the propagation of surface waves. The detailed mechamism of the above processes being still unknown, the existence of a fully developed turbulence has been assumed in the theoretical treatment as mentioned in the previous section. The vertical distribution curve of sediment amount trapped by a bamboo sampler is completely similar to that of the actual sediment concentration. In the following analysis the value at $n = 0.1$ will be consistently taken as the reference in view of the fact that almost all the data include the measured values of $\bar{m}$ or $\bar{q}$ at the elevation of 10 % of the total water depth above the bottom.

CALCULATED VALUE OF α

The value of α for each level is calculated, as listed in part in Table 1, by using the theoretical relationship. Reviewing the above result, it is recognized that α seems to vary slightly with the value of n depending upon hydraulic and sedimentary conditions. For the sake of simplicity, we will use the mean value, $\bar{\alpha}$, in the following discussions.

Figure 4 shows the variation of $\bar{\alpha}$ in relation to the variation of nondimensional term of $\frac{u_m}{c}$, where u_m is a maximum orbital velocity in the vicinity of the bottom and c the celerity of waves. The data obtained both in the field (Tokai and Niigata coasts) and in the laboratory have a consistent tendency in the graph in spite of scattering of data.

$\bar{m}_a$ AND $\bar{q}_a$

In order to determine quantitatively the concentration pattern of suspended sediments, we must know the value of $\bar{m}_a$. Fig. 5 shows that $\bar{m}_a$ is closely related with the value of u_m. But the field data (Tokai coast) deviate from and run parallel to the laboratory data which include that of Fairchild of the Beach Erosion Board. A possible reason for this pronounced discrepancy can be found in the difference of

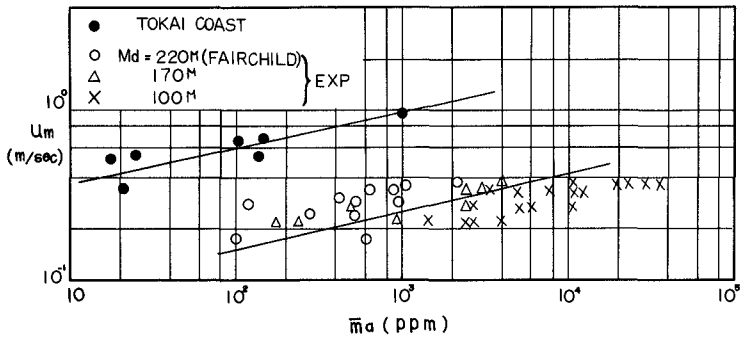

Figure 5. Relationship between $\bar{m}_a$ and u_m.

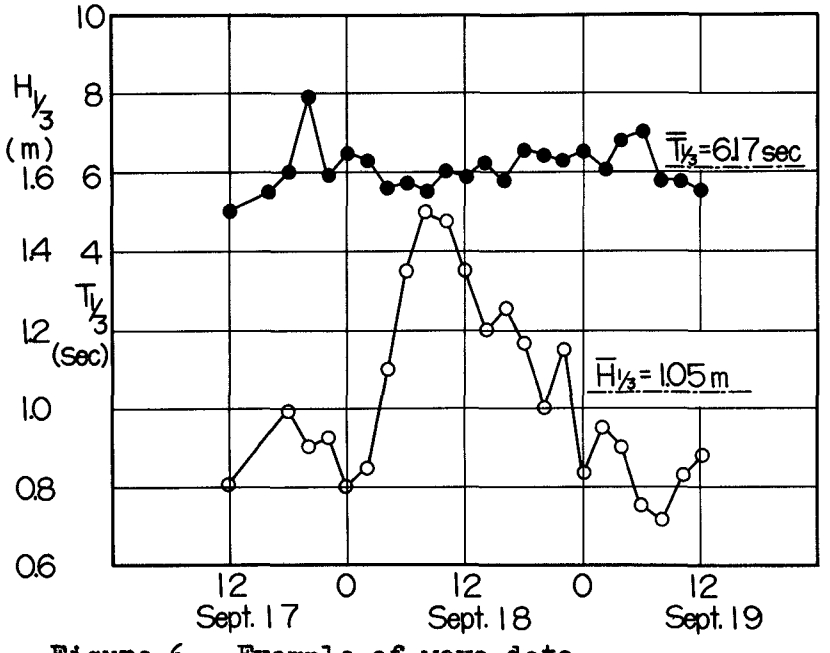

Figure 6. Example of wave data.

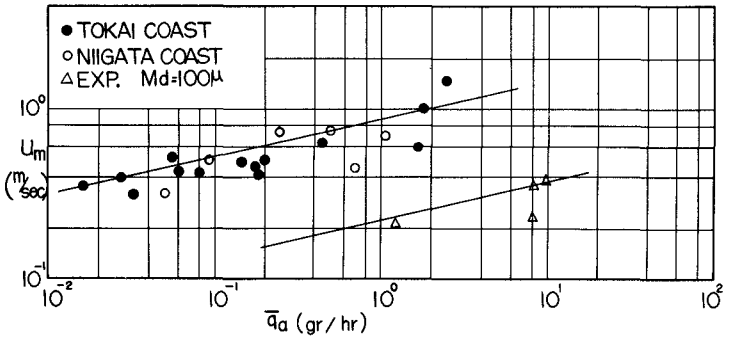

Figure 7. Relationship between $\bar{q}_a$ and u_m.

data processing. Since the wave in the field would tend to fluctuate as shown in Fig. 6, we have used the mean values of significant wave height and period, $\overline{H}_{1/3}$ and $\overline{T}_{1/3}$, respectively. On the other hand, the laboratory waves are very simple and their heights and periods are uniquely determined. The solid lines drawn in the figure may be applied to the present problem of fine sediment, although the grain size seems to have some effect on the relationship between u_m and $\overline{m}_a$.

In the same manner, the relationship between $\overline{q}_a$ and u_m is given in Fig. 7. The plotting of these data is completely similar to that in Fig. 5. From these figures the value of $\overline{q}_a$ is correlated with the value of $\overline{m}_a$ by using the intermediate parameter u_m, as shown in Fig. 8. The agreement of the two curves, one from the field and the other from laboratory measurements, is rather surprisingly well. Practically, it is extremely difficult to conduct an instantaneous sampling of suspended sediment under rough sea conditions, while the cumulative sampling with a bamboo sampler is less affected by sea conditions. From such a point of view, the authors believe that the correlation curve presented here may have a practical value in interpreting the data obtained by a bamboo sampler in terms of the equivalent sediment concentration.

COMPARISON OF DATA WITH ANALYTICAL VALUES

As a result of the analysis which has been described above, a concentration patter of suspended sediment can be determined after some numerical computation for given conditions of H, T, d, M_d and temperature of water. Several examples of comparison between measured data and analytical values are given in Figs. 9 and 10. Generally speaking, the agreement is satisfactory for engineering purposes.

The discussions so far presented have proved useful in determining the adequate height of the mouth of an intake pipe for the cooling water system of the atomic power plant at Tokai, Japan. Analyzing a long-term recording of wave height and period at the Tokai coast, the authors could estimate the moderate combination of significant wave characteristics in the rough sea conditions in the water of 8 m depth where the intake unit will be placed. The wave conditions are as follows. (Table 2)

The median diameter of bottom sediment has been assumed to be 250 μ. The value of $\overline{\alpha}$ for such a large value of u_m/c, as shown in Table 2, cannot be determined accurately from Fig. 4. Hence, the authors

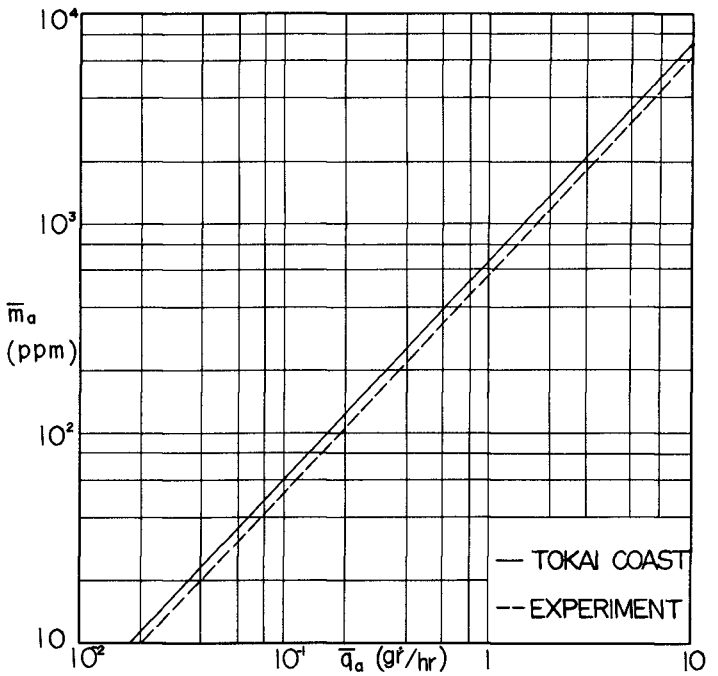

Figure 8. Relationship between $\bar{m}_a$ and $\bar{q}_a$.

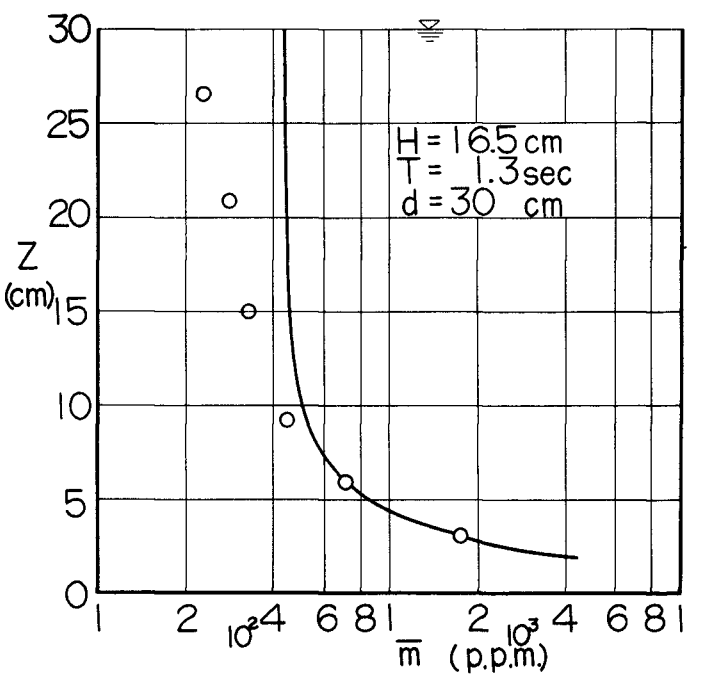

Figure 9. Comparison between analytical curve and measured data (laboratory).

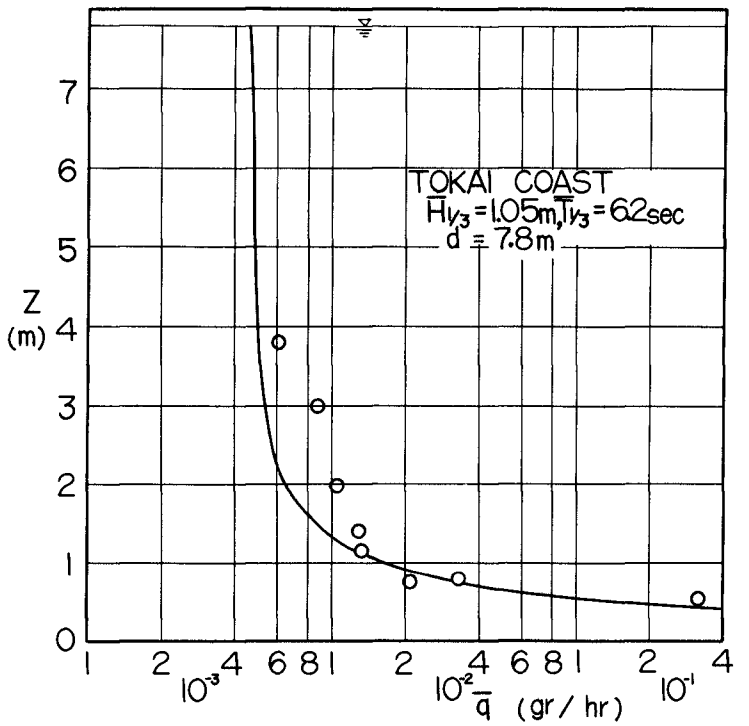

Figure 10. Comparison between analytical curve and measured data (field).

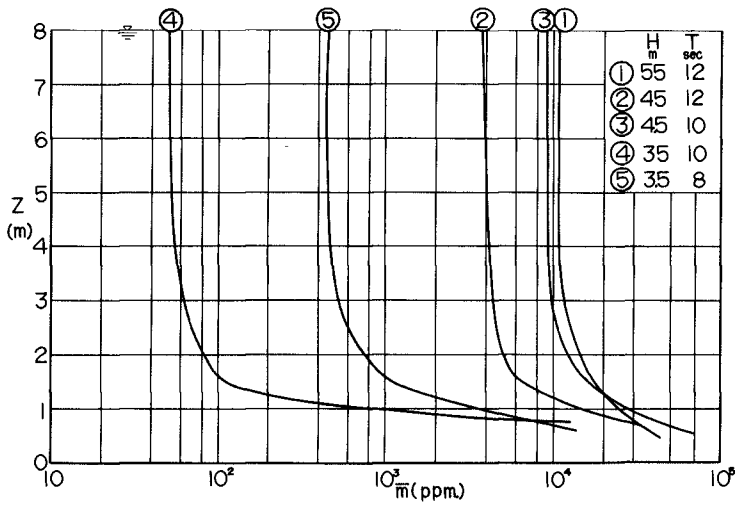

Figure 11. Analytical vertical distribution curves of suspended sediment concentration for variable wave conditions.

have chosen a unique value of 0.01 for α for all conditions considered. The results of computation are shown in Fig. 11, from which the following observation may be drawn.
(1) Up to about 2 m above the bottom the concentration of suspended sediment is considerably high.
(2) Above this level the concentration is rather uniform, and may reach 10^2 to 10^4 p.p.m. depending upon the conditions of waves.

Therefore, it was recommended to set the mouth of the intake pipe beyond 2 m above the bottom.

Table 2

Wave Height in m	Wave Period in sec	u_m/c
5.5	12.0	0.263
4.5	12.0	0.252
4.5	10.0	0.265
3.5	10.0	0.206
3.5	8.0	0.200

SOME RELATED CONSIDERATIONS

In the foregoing sections the phenomena of suspended sediment due to oscillatory wave motion have been treated in a very simplified form. However, the authors realize that the actual phenomena are so complicated that further analysis is necessary in order to complete the treatment. In fact, we have neglected the presence of sand ripples in the analytical procedure, since it is almost impossible at the present moment to treat the problem of a sand ripple in an analytical manner.

SAND RIPPLES

The authors have conducted a separate study on the behaviors of a sand ripple which will be described briefly in the accounts to follow. It has been repeatedly stressed in the previous sections that the sand ripples have an important role on the occurrence of suspended concentration. It is from recognition of this fact that the authors are interested in the formation and stabilized configuration of sand ripples which appear on the bottom of sediment materials.

Bagnold conducted his original study on this subject by using an oscillating plate in still water with variable size and specific gravity of sediment materials. (Ref. 21) Manohar did his extensive studies with a similar device at the University of California, introducing valuable conclusions on the behaviors of sand ripples, especially on formation, development and disappearance. (Ref. 22) On the other hand, Scott presented laboratory data on the characteristics of sand ripples, which were formed on the sloping bed due to a surface wave (Ref. 23). While these studies were accomplished in the laboratories, Inman carried out a unique field observation. (Ref.24)

Three questions may be raised as to the significant aspects of a sand ripple.

(1) What conditions may give rise to sand ripples?
(2) What are the stabilized configuration of sand ripples?
(3) What conditions may cause sand ripples to disappear?

The authors will confine themselves mainly to the second question. It is well known that the shape of sand ripples formed by an oscillatory wave motion is almost symmetrical, different from the asymmetrical ripples formed by a uni-directional current. Therefore, the shape of the oscillatory sand ripple may well be expressed simply by its rise, η , and pitch, λ .

We will consider some elementary factors which may affect the shape of sand ripples, namely:

u_m : horizontal component of maximum orbital velocity in the vicinity of bed,
d_o : horizontal displacement of water particle in the vicinity of bed,
M_d : medium diameter of bed material,
w_o : fall velocity of sediment,
ν : kinematic viscosity of fluid, and
θ : temperature of fluid.

As $f(w_o, M_d, \theta) = 0$, the following relationship may be introduced by dimensional analysis,

$$\varphi\left(\frac{\eta}{\lambda}, \frac{\lambda}{d_o}, \frac{\eta}{d_o}, \frac{u_m d_o}{\nu}, \frac{w_o M_d}{\nu}\right) = 0 \quad (11)$$

in which $\frac{\lambda}{d_o}$ and $\frac{\eta}{d_o}$ are the relative pitch and relative rise of a sand ripple, respectively, with respect to the horizontal displacement of particle in the vicinity of bed, and $\frac{\eta}{\lambda}$ is the steepness of ripple. Other terms are $\frac{u_m d}{\nu}$ and $\frac{w_o M d}{\nu}$, the Reynolds numbers related to the oscillatory motion and the sediment material, respectively.

Prior to an analysis of available data, extensive references have been made to the existing knowledge on the characteristics of wake which is developed behind a circular cylinder in order to utilize an analogy between the wake and formation of a vortex in the ripple trough. (Refs. 25, 26 and 27) In the wake phenomenon the periodical formation and separation of vortices has been noticed and studied experimentally by many authors. The shedding frequency of the wake is usually expressed in terms of the dimensionaless Strouhal number $S = n\,d/U_o$, where n is the shedding frequency (from one side of the cylinder), d the cylinder diameter and U_o the free-stream velocity. As a result of experiments, it is known that the Strouhal number is a function of the Reynolds number $\frac{U_o d}{\nu}$, which may approach a constant in the range of large Reynolds number.

Assuming $n = \frac{2\pi}{T}$, $d = 2\eta$ and $U_o = u_m$, the Strouhal number in our case may be expressed as follows:

$$S = \frac{2\pi \times 2\eta}{T u_m} = 4\eta \frac{\pi}{T u_m} = 4 \frac{\eta}{d_o}.$$

On the other hand, the Reynolds number may be expressed:

$$R_e = \frac{2 u_m \eta}{\nu}$$

The existence of some definite relationship between $\frac{\eta}{d_o}$ and $\frac{u_m \eta}{\nu}$ is suggested by the above discussions. On the other hand, it may be possible to consider that the space between the successive ripple crests is occupied by a single vortex formed behind a ripple crest. The size of the vortex must be a function of Reynolds number $\frac{u_m \eta}{\nu}$, similarly to the vortex size of a wake behind a bluff body. Hence, the authors expected the existence of a relationship between $\frac{\eta}{d_o}$ and $\frac{\eta}{\lambda}$, and attempted to verify this assumption by using the data of Inman (field), and Scott (laboratory) and the authors (laboratory) as shown in Fig. 12. The result is consistent to a surprising degree, and further intimates that the maximum steepness of a sand ripple seems to be about 0.23 which is approximately equal to 1/2 tan ϕ, where ϕ being the angle of repose of fine sand in water.

In the next step, a relationship among three other terms in Eq. (11), i.e. $\frac{d_o}{\lambda}$, $\frac{u_m d_o}{\nu}$ and $\frac{w_o M_d}{\nu}$, was investigated by using the same data as shown in Fig. 13. From this figure, it may be recognized that the parameter of $\frac{w_o M_d}{\nu}$ or M_d can be introduced in the relationship between $\frac{d_o}{\lambda}$ and $\frac{u_m d_o}{\nu}$ if more data for relatively coarse sand could be plotted in the same figure. The lower limit of $\frac{d_o}{\lambda}$ must be 1.0 as previously pointed out by Inman.

According to the above results, the ripple dimensions, λ and μ, of fine sand ($300\ \mu > M_d > 100\ \mu$) can be definitely determined for various combinations of wave characteristics, water depth and water temperature in the limited range of the plotted data.

In the above treatment the values of u_m and d_o were calculated through a first approximation of the oscillatory wave theory, and the value of ν was estimated to be 1.00×10^{-2} cm^2/sec.

In the previous sections which have dealt with suspended sediment, both the field and laboratory data were used on the same basis neglecting the scale effect. However, the scale effect must be expected to some extent in view of the following considerations. As pointed out previously, the sand ripples have an important role on the suspended sediment, but the similarity between prototype and model of ripple dimensions is not realized in Figs. 12 and 13, i.e. the sand ripples are relatively exaggerated in the model.

The authors are inclined to assume that the data by Bagnold and Manohar result from an experimental procedure which may not fully represent the oscillating motion by surface waves. Therefore, they have not been used in our analysis on the characteristic discussion of oscillatory sand ripples. The data of Manohar plotted on the graphs in a similar way to Figs. 12 and 13 show a fairly large scatter although they too agree with the upper limits of $\frac{\eta}{\lambda}$ or $\frac{d_o}{\lambda}$ versus $\frac{\eta}{d_o}$ or the Reynolds number, respectively. At the present moment, the authors feel to share the view of Vincent (Ref. 28) who admits a distinct discrepancy between the motions near the bed produced by an oscillating bed and by progressive surface wave.

Another point which must be mentioned is the fact that the measured pitch of sand ripples produced by a single train of waves is not unique but varies over a wide range as shown in Fig. 14. Despite scatter, the curve may be considered to represent a normal distribution, hence it may be allowed to take an arithmetic

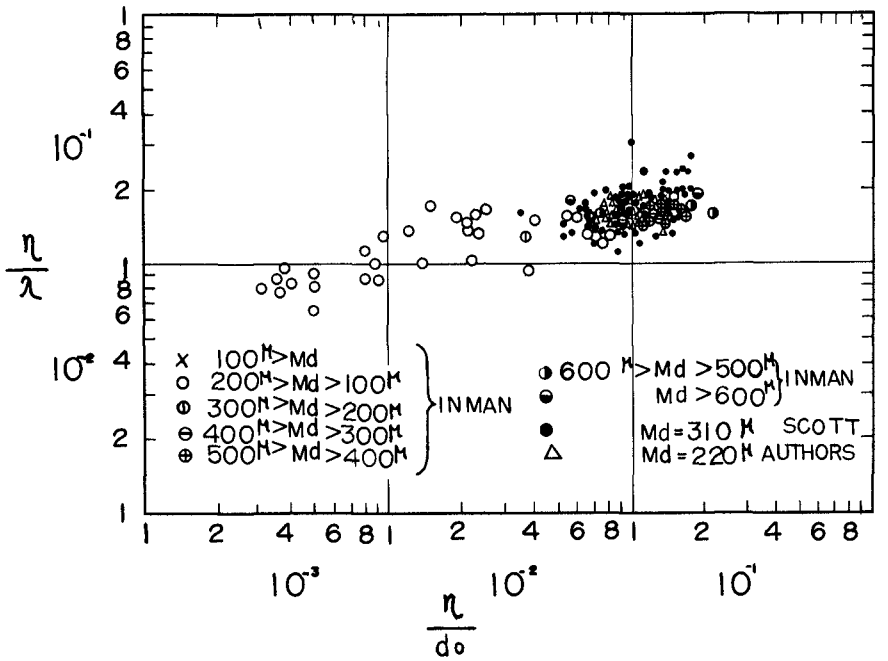

Figure 12. Relationship between η/λ and η/d_0 (oscillatory sand ripples).

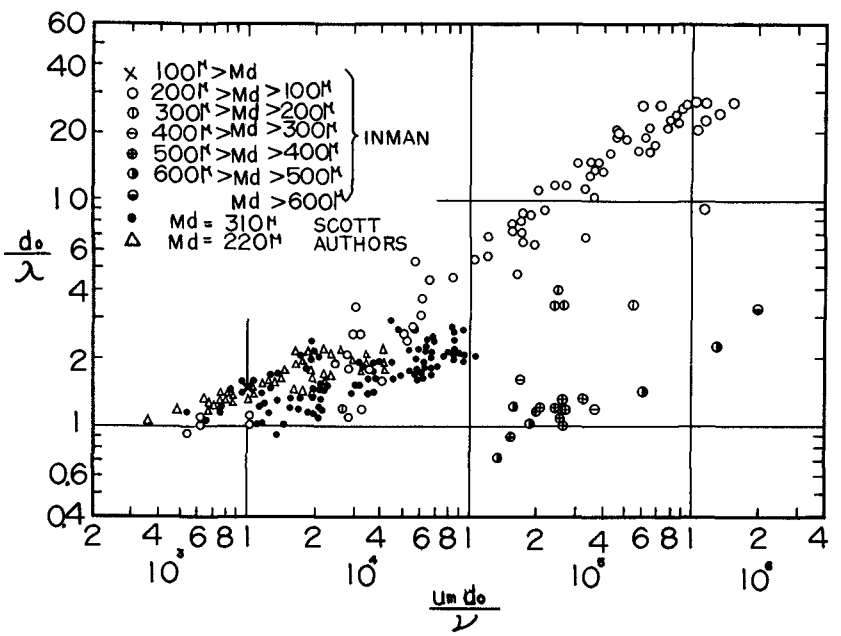

Figure 13. Relationship between d_0/λ and $U_m d_0/\nu$ (oscillatory sand ripples).

mean as a representative pitch of the measured samples. The rise also fluctuates to almost the same degree.

VERTICAL DISTRIBUTION OF GRAIN SIZE OF SUSPENDED SEDIMENT

In the foregoing treatment the grain size of suspended particles has been assumed for the sake of approximation to be uniform from water surface to bottom. However, as would be expected quite naturally, the grain size tends to decrease gradually upwards owing to the sorting action of turbulence in water. This tendency is clearly shown in Fig. 15, which is based on the data obtained at the Tokai coast. Beyond a certain level above the bottom the grain size is practically uniform. The data from the Niigata coast, which give a similar trend, also show that the grain size of suspended sediment at rough sea conditions is larger than that found at calm, even though the bottom sediment is the same. (Fig. 16) Our assumption of a uniform grain diameter for suspended sediment seems therefore substantially realistic, although it is not correct to assume that the grain diameter of suspended sediment is equal to that of the bottom sediment.

ADDITIONAL REMARK

Fig. 17 shows three examples of cumulative plotting of suspended concentration, each representing a different positions of sampling with regard to distance from shoreline and level from the bottom. These data were obtained with an instantaneous horizontal sampler (Fujiki type) at Ojoin, Niigata (Ref. 17) during December, 1957 to March, 1958. The highest concentration occurs invariably at a bar crest.

The authors have been carrying out a long-term project on the dispersion processes of a free vortex separated from the ripple trough. A minute baffle shaped either triangular or inverted-T is placed on the bottom of a two-dimensional wave flume and the effect of the baffle rise on the dispersion process is studied by visual observation or photograph. Fig. 18 shows an example in which the upper limit δ of vortex dispersion was compared with that normally observed with natural sand ripples. Observation was facilitated by using aluminium powder or potassium permanganate particles. The relationship between $\frac{\delta}{\ell}$ and $\frac{u_m \ell}{\nu}$, the Reynolds number with respect to the ripple rise, is fairly consistent and shows that the limiting range of vortex dispersion approaches the water surface as the wave size increases. This suggests that a layer of characteristic turbulence occurs near the bed which is

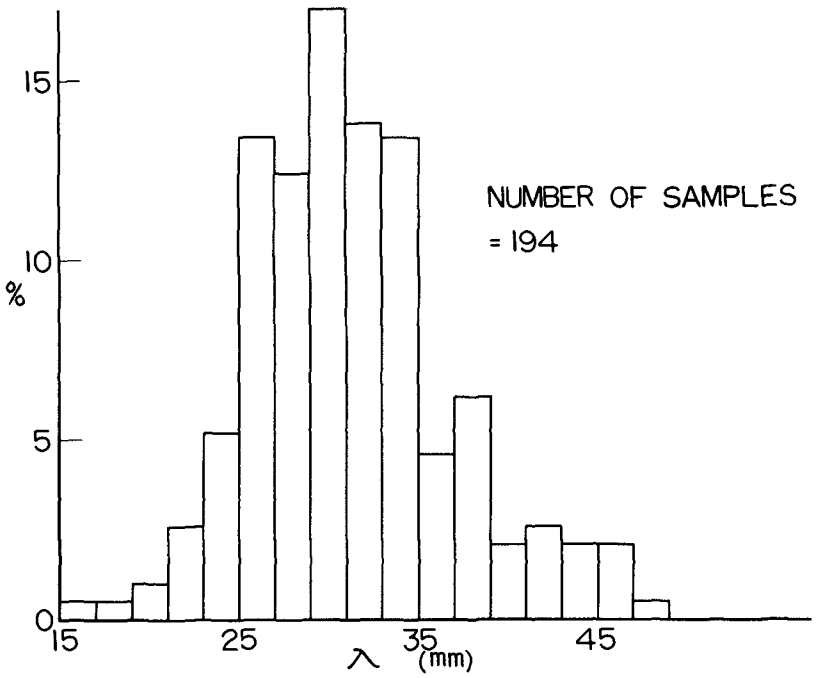

Figure 14. Scatter of ripple pitches found by a single train of waves.

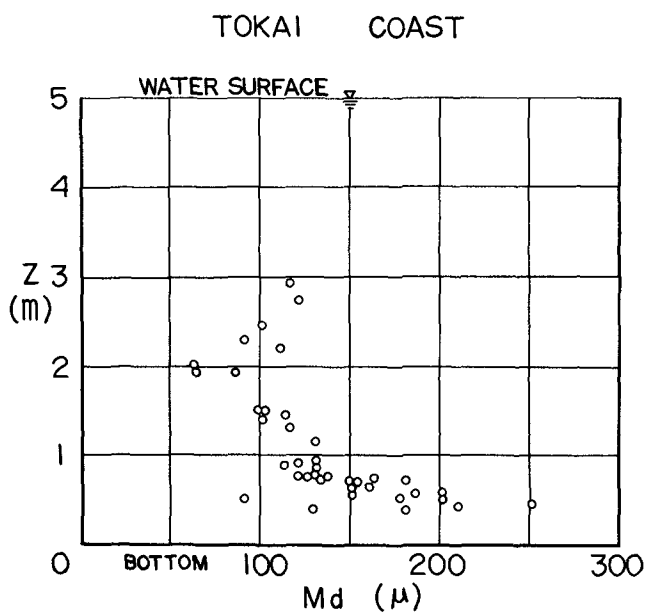

Figure 15. Vertical distribution of medium diameter of suspended sediment (Tokai coast, Japan).

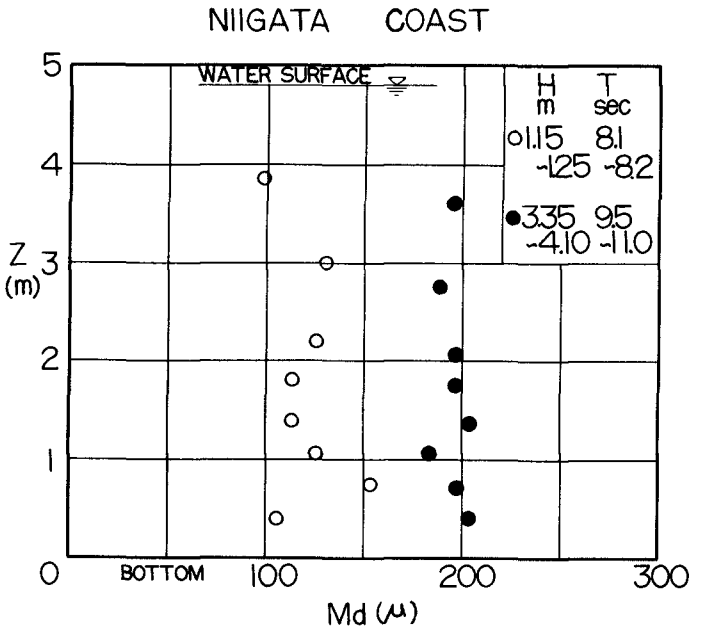

Figure 16. Vertical distribution of medium diameter of suspended sediment (Niigata coast, Japan).

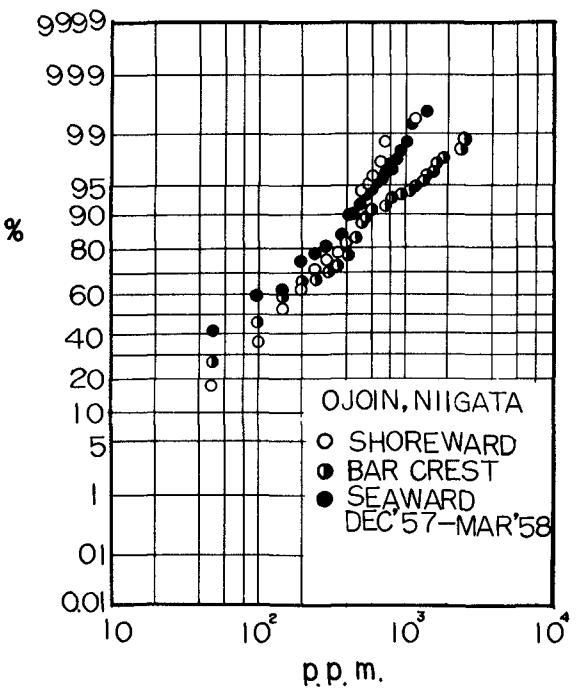

Figure 17. Cumulative occurrence curves of suspended sediment concentration at three different positions (Niigata coast, Japan).

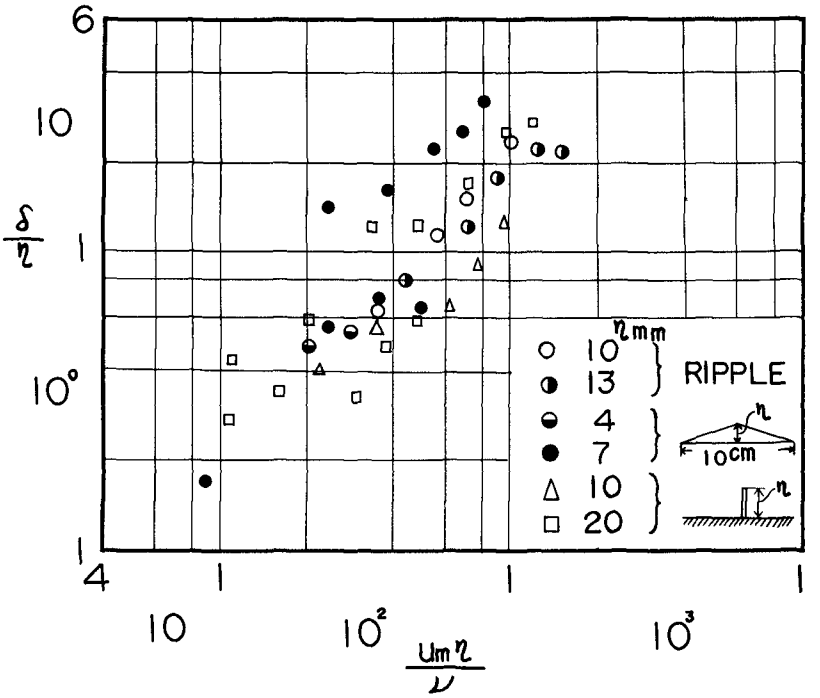

Figure 18. Relationship between δ/η and $U_m\eta/L$.

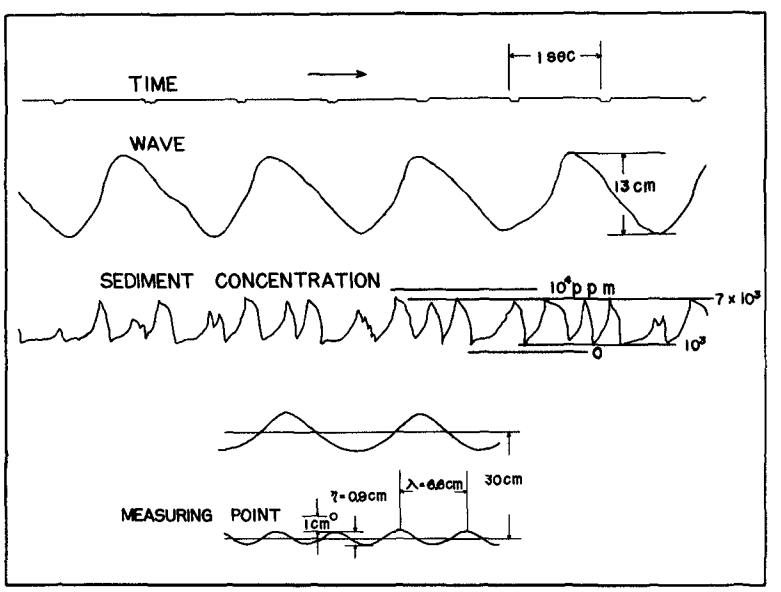

Figure 19. Sample record of suspended sediment concentration varying in time with passing phases of progressive wave (Coastal Engineering Laboratory, University of Tokyo).

acted upon by a relatively small wave, while it grows toward the surface as the wave size increases. Therefore, the assumption of a fully developed turbulence in the body of water which was made in our theoretical treatment should be interpreted to represent rough sea conditions.

Most difficulties in our subject seem to arise from inadequacy of available means of instrumentation. The authors have attempted to develop a device which may enable a continuous recording of suspended concentration which in fact fluctuates following the passage of a wave. Fig. 19 gives one of the preliminary data obtained by using the newly developed model, which works on photoelectric principle with a pick-up unit equipped with a phototransistor element. This instrument is still not fully satisfactory, and must be improved further. According to our measurement, the variation of concentration is much more complicated than has been expected in our theoretical treatment. At any rate the success of recording the actual variation of suspended sediment concentration encourages the authors to advance further with the present study.

CONCLUSIONS

In this paper the authors summarized the main results of their studies concerning the suspended sediment due to wave action. The data in the field and laboratories were utilized to determine the characteristics of several unknown factors, such as α, $\bar{m}_a$ and $\bar{q}_a$, which appear in the theory presented here. The agreement between the analytical and measured curves of vertical distribution of suspended sediment concentration is quite satisfactory for the engineering purposes.

In addition to the above, some other data were presented in order to clarify the actual phenomena and to discuss a similarity between prototype and model. In particular, the relationships, $\varphi\left(\frac{\eta}{\lambda}, \frac{\lambda}{d_0}, \frac{\eta}{d_0}, \frac{U_m d_0}{\nu}, \frac{w_0 M_d}{\nu}\right) = 0$, as proposed in Figs. 12 and 13, are of practical value to compare the results of field and laboratory studies concerning the bottom sediment movement due to oscillatory wave action. Finally, a continuous recording of the variation of concentration due to progressive wave was shown in Fig. 19, which was made possible by our latest model developed at the Coastal Engineering Laboratory, University of Tokyo.

ACKNOWLEDGEMENTS

The authors have made extensive reference to a number of existing works concerning the suspended sediment phenomena and the characteristics of sand ripples formed by oscillatory wave action. They should like to express their sincere gratitude and respect to those who have accomplished those initiative studies.

The authors' profound appreciation is due to Dr. Choule Sonu, Coastal Engineering Laboratory, University of Tokyo, who contributed to the operation of field and laboratory works and reviewing the manuscript, and also to the personnel of the same laboratory who assisted in the preparation of figures.

REFERENCES

1. Fukushima, H. and Y. Mizoguchi, Drift Sand and Its Measurement, Proc. of 2nd Conf. on Coastal Engineering in Japan, Nov. 1955. (in Japanese)

2. Fukushima, H., Y. Mizoguchi and M. Kashiwamura, Drift Sand and Its Measurement (2nd Report), Proc. of 4th Conf. on Coastal Engineering, in Japan, Nov. 1957. (In Japanese)

3. Fukushima, H. and M. Kashiwamura, Drift Sand and Its Measurement (3rd Report), Proc. of 5th Conf. on Coastal Engineering in Japan, Nov. 1958 (In Japanese)

4. Fukushima, H. and M. Kashiwamura, Drift Sand and Its Measurement (4th Report), Proc. of 6th Conf. on Coastal Engineering in Japan, Nov. 1959.(In Japanese)

5. Fukushima, H. and Y. Mizoguchi, Field Investigation of Suspended Littoral Drift, Coastal Engineering in Japan, Vol. 1, 1958.

6. Fukushima, H. and M. Kashiwamura, Field Investigation on Suspended Sediment by the Use of Bamboo Samplers, Coastal Engineering in Japan, Vol. 2, 1959.

7. Fukushima, H. and M. Kashiwamura, Some Experiments on Bamboo Samplers, Coastal Engineering in Japan, Vol. 4, 1961.

8. Kurihara, M., K. Shinohara, T. Tsubaki and M. Yoshioka, Beach Sand Movement due to Waves, Proc.

of 3rd Conf. on Coastal Engineering in Japan, Nov. 1956. (In Japanese)

9. Shinohara, K., T. Tsubaki, M. Yoshotaka and Ch. Agemori, Sand Transport along a Model Sandy Beach by Wave Action, Coastal Engineering in Japan, Vol. 1, 1958.

10. Hom-ma, M., K. Horikawa and C. Sonu, A Study on Beach Sediment at Enoshima and Kamakura, Proc. of 4th Conf. on Coastal Engineering in Japan, Nov. 1957.

11. Hom-ma, M., K. Horikawa and C. Sonu, A Study on Beach Erosion at the Sheltered Beaches of Katase and Kamakura, Coastal Engineering in Japan, Vol. 3, 1960.

12. Hom-ma, M. and K. Horikawa, Longshore Current and Sand Drift at Katase East Beach and Kamakura Beach, Investigation Report of Beach Erosion at Katase and Kamakura beaches, Kanagawa Prefecture, Aug. 1958. (In Japanese)

13. Hom-ma, M. (editor), Report of Field Investigations at Tokai-mura (1st Report), Japan Atomic Generation Company, Aug. 1959. (In Japanese)

14. Horikawa, K. and C. Sonu, Suspended Sediment due to Wave Action, Annual Convention of Japan Society of Civil Engineers, 1960. (In Japanese)

15. Hom-ma, M. and K. Horikawa, Concentration of Suspended Sediment due to Wave Action, Report of Field Investigation at Tokai-mura (2nd Report), Japan Atomic Generation Co., May, 1960. (In Japanese)

16. Niigata Prefecture, Suspended Sediment at Niigata West Beach, Shin-shi (Collected Data at the Shinano River Construction Office), No. 29, Feb. 1958. (In Japanese)

17. Niigata Prefecture, Observation Data on Suspended Sediment, Shin-shi (Collected Data at the Shinano River Construction Office), No. 33-3, 1959. (In Japanese)

18. Watts, G. M., Development and Field Tests of a Sampler for Suspended Sediment in Wave Action, Beach Erosion Board, Tech. Memo. No. 34, March, 1953.

19. Fairchild, J. C., Development of Suspended Sediment Samplers for Laboratory Use under Wave Action, Beach Erosion Board, Bulletin, Vol. 10, No. 1, July, 1956.

20. Fairchild, J. C., Suspended Sediment Sampling in Laboratory Wave Action, Beach Erosion Board, Tech. Memo. No. 115, June, 1959.

21. Bagnold, R. A., Motion of Waves in Shallow Water, Interaction between Waves and Sand Bottoms, Proc. of Royal Society, London, Vol. 187, A, October, 1946.

22. Manohar, M., Mechanics of Bottom Sediment Movement due to Wave Action, Beach Erosion Board, Tech. Memo. No. 75, June, 1955.

23. Scott, T., Sand Movement by Waves, Beach Erosion Board, Tech. Memo. No. 48, Aug. 1954.

24. Inman, D. L., Wave Generated Ripples in Nearshore Sands, Beach Erosion Board, Tech. Memo. No. 100, October, 1957.

25. Goldstein, S., Modern Developments in Fluid Dynamics, Vol. II, 1938.

26. Relf, E. F. and L. F. G. Simmons, The Frequency of the Eddies Generated by the Motion of Circular Cylinders through a Fluid, R. & M. No. 917, June, 1924, Tech. Rep. of Aeronautical Research Committee, Vol. 2, 1924 - 5.

27. Roshko, A., On the Development of Turbulent Wakes from Vortex Streets, National Advisory Committee for Aeronautics, Report 1191, 1955.

28. Vincent, G. E., Contribution to the Study of Sediment Transport on a Horizontal Bed due to Wave Action, Proc. of 6th Conf. on Coastal Engineering, 1958.

CHAPTER 14

LABORATORY STUDY OF SCALE EFFECTS IN TWO-DIMENSIONAL BEACH PROCESSES

Yuichi Iwagaki
Professor of Hydraulics
Disaster Prevention Research Institute
Kyoto University, Kyoto, Japan

and

Hideaki Noda
Assistant Professor of Hydraulics
Training Institute for Engineering Teachers
Kyoto University, Uji City, Kyoto, Japan

In order to disclose the essential relationship between the beach processes and wave characteristics, two dimensional model tests are often performed for beach profile changes due to incident breaking waves normal to the beach. In applying the results of such experiments to the prototype of beaches, the scale effects of waves and sediments on the beach processes with equilibrium beach profiles should necessarily be considered.

In this paper, as an approach to solve this problem in two dimensional beach studies, the effects of wave height and sediment size on the shore line movement and equilibrium beach profiles are discussed based on the results of experiments made by the authors and other experiments with smaller and larger scales by some researchers. It has been found that the ratio of wave height to sediment diameter is a very significant factor in this problem. In addition, the changes in a character of breaking waves during the time period of wave action from the beach having an initial constant slope to that with an equilibrium profile are presented.

INTRODUCTION

In order to understand correctly the problem of beach erosions, it is necessary to disclose the complicated phenomena of beach processes mainly by the wave action. In treating beach erosion phenomena, a study should be made generally dividing sediment transport into the following two modes:

1. Sand movement normal to the shore line by the direct action of waves; and
2. sand movement along the shore by currents due to breaking waves.

The sand movement in the first mode causes the beach process of a short period of time and it is well known that the characters of incident waves influence greatly this phenomenon. On the other hand, the sand movement in the second mode governs the beach process of a relatively long period of time which depends on an alongshore distribution of the littoral transport rate. From this point of view, many researches have been made at Kyoto University. Especially much effort has been made in establishing the mechanics of the beach process not only by laboratory experiments but also by field observations, on the beach profile changes with the problem of equilibrium beach profiles for the first mode of sand movement (Hayami, Ishihara and Iwagaki, 1953; Iwagaki and Sawaragi, 1955, 1956, 1958; Iwagaki and Noda,

1961a, 1961b) and on the estimation of the littoral transport rate as an approach to disclose the beach erosion mechanism for the second mode of sand movement (Sawaragi and Murakami, 1957; Iwagaki and Sawaragi, 1960). However, the method to analyze the beach process by observing under natural circumstances at actual beaches for the purpose of disclosing the beach erosion mechanism is generally not hopeful except under certain limited conditions because it is difficult to separate clearly the effects of main factors which influence this complicated phenomenon. Therefore, model experiments are often made considering hydraulic similarity to some extent, and then various phenomena which occur at actual beaches are explained or predicted, so that a counter-measure is established. Accordingly the most importance in such experiments is the problem of the similarity between models and prototypes. The purpose of this paper is to discuss how the relative sizes of deep-water waves and sediments in addition to the deep-water wave steepness influence the two dimensional beach process due to the sand movement normal to the shore line and the equilibrium beach profile, based on the results of experiments by the authors and other researchers.

A laboratory study for equilibrium profiles of beaches by Johnson (1949) indicated that the profile of a beach is changed with the value of the deep-water wave steepness H_0/L_0, and especially it is called the "normal" beach when the steepness is small and, on the other hand, the "storm" beach characterized by the appearance of longshore bars when the steepness is large, in which the critical wave steepness in deep-water for both is 0.025 to 0.030. Iwagaki and Sawaragi (1955, 1956, 1958) made experiments of equilibrium beach profiles and the sand movement due to breaking waves by using the sands of three different sizes. Kurihara and others (1956) and Shinohara and others (1958) compared the results of experiments by the pulverized coal having small specific gravity with those by the sand. In the United States of America, many experiments were made by Scott at the University of California (1954), and Rector (1954), Watts (1954) and Saville (1957) at the Beach Erosion Board. These experiments showed that the storm beach is developed even when the deep-water wave steepnesses are 0.019 and 0.0064 according to the results by Scott and Saville respectively. Especially it should be noted that the results by Saville who made experiments with as large waves as at actual beaches are remarkably different from those with small waves. Accordingly it is presumed that such phenomena involving the sand movement have much scale effect, and this is a reason why the authors began such an investigation.

Since the scale effect on the beach process is also expected as well as on the equilibrium beach profile, the distance of shoreline movement when the beach having an initial constant slope is changed into the state of equilibrium is treated as an example, and the experiments are made in an effort to disclose the effects of the relative size of waves and sediments on the two dimensional beach process with considerations for the equilibrium beach profile. In addition, the changes in a character of breaking waves in the beach process from a uniform slope to an equilibrium state are reported.

EQUIPMENTS AND PROCEDURES FOR EXPERIMENTS

Laboratory experiments of beach processes have been made using a concrete wave tank 70 m long, 1.0 m wide and 1.5 m deep (Fig. 1a) and a steel wave tank 70 m long, 0.5 m wide and 0.6 m deep (Fig. 1b) at the Ujigawa Hy-

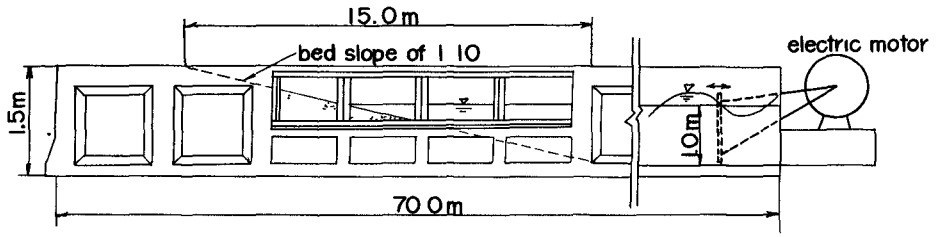

Fig. 1a. Schematic drawing of concrete wave tank.

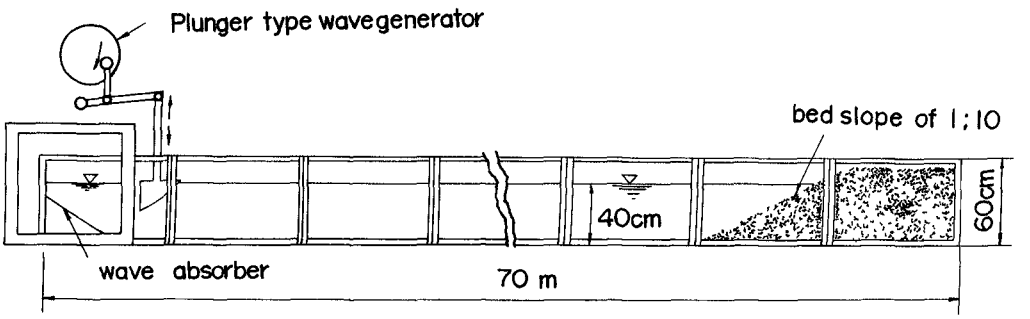

Fig. 1b. Schematic drawing of steel wave tank.

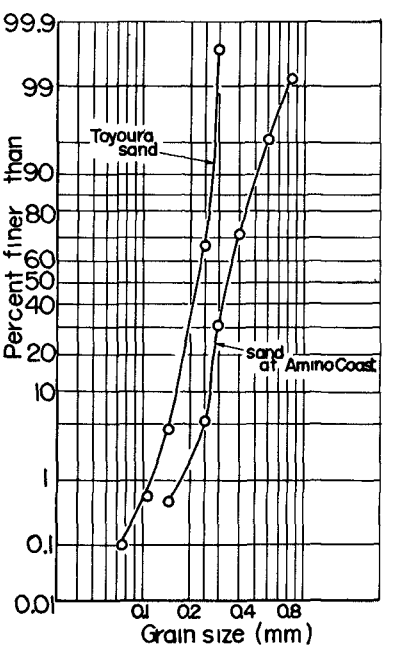

Fig. 2. Sieve analysis of sands used in the tests.

draulic Laboratory, Disaster Prevention Research Institute, Kyoto University. Some of the data were taken by dividing the beach in the concrete wave tank longitudinally into two parts and putting the sands of two different sizes to find the effect of sand sizes on beach processes.

In the concrete wave tank waves are generated by a multi-purpose flatter type generator with a 10 HP electric motor or by a pneumatic type wave generator with a 7.5 HP blower. In the steel wave tank a plunger type wave generator with a 2 HP electric motor is installed.

Incident wave heights were measured by an electric point gage or an electric resistance type wave gage with an inkwriting-oscillograph. Water depths tested were 1.0 m in the concrete wave tank and 0.4 m in the steel wave tank.

Two kinds of sands used in the experiments were the well-sorted sand at Amino Coast and the standard sand by JIS, which is called Toyoura sand, with median diameters of 0.34 mm and 0.22 mm and specific gravities of 2.62 and 2.59 respectively (Fig. 2). The initial slope of the beaches constituted by these sands was 1 on 10 every time. Table 1 shows the characters of waves and sands used, the duration times of the experiments and the data obtained.

The profiles of beaches were measured by a point gage 15 min, 30 min, 1 hr, 2 hrs, ... after the beginning of the experiment, and the measurements were continued until it appeared that the equilibrium state was reached. In the later experiments the measurements of the beach profiles in the course of beach processes were omitted because the duration time of 20 hours was considered to be almost enough to obtain the equilibrium state.

In order to investigate, furthermore, the changes in the character of breaking waves were filmed through the side glass wall of the concrete wave tank every one or two hours by a 16 mm cinecamera. A small wave tank 14 m long, 0.3 m wide and 0.4 m deep, was used to find the relationship between the beach slope and the characters of breaking waves on the fixed bed with the beach slopes of 1° to 5° and the deep-water wave steepnesses of 0.02 and 0.04. The profiles of breaking waves on the fixed slopes of beaches were photographed by a camera in the same manner as for those on the movable bed in the concrete wave tank. In this case a plunger type wave generator was used, by which the wave periods are varied from 0.5 sec to 3.5 sec and the wave heights from 1.5 cm to 4.0 cm continuously.

RESULTS OF EXPERIMENTS AND CONSIDERATIONS

PROGRESSION AND RECESSION OF SHORELINE

The beach profile having a uniform slope of 1 on 10 before testing was deformed with the lapse of time due to wave action and finally reached the equilibrium state after about 15 to 20 hours as shown in Fig. 3. During that time, the change in the beach profile near the shore line was very rapid for a few hours after the beginning of the test and then became gradual asymptotically or in some cases periodically. In this paragraph, the distance of progression or recession of the shore line until the beach having an initial uniform slope reaches the equilibrium state is treated and

Table 1

Characters of waves and sands used and data obtained.

Run No.	Wave period T (sec)	Desp-water wave height (H_o cm)	Deep-water wave steepness H_o/L_o	Median dia. d_{50} (mm)	H_o/d_{50}	Distance of shore-line mov. X_{SL}(m)	X_{SL}/L_o	Duration time(hrs)	Investi-gators
1	1.29	2.40	0.009	0.48	5.00×10^{1}	0	0	6	Iwagaki-Sawaragi
2	1.21	2.13	0.009	0.28	7.64 "	+0.060	$+3.0\times10^{-2}$	9	
3	1.29	2.41	0.009	0.93	2.59 "	+0.096	+ 3.7 "	5	"
4	3.58	20.3	0.010	0.34	5.97×10^{2}	+0.54	+ 2.6 "	12	Iwagaki-Noda
5	2.54	9.00	0.009	"	2.64 "	+0.43	+ 4.3 "	18	
6	2.69	11.6	0.010	"	3.40 "	+0.25	+ 2.2 "	15	"
7	3.58	19.8	0.010	"	5.81 "	+0.72	+ 3.6 "	18	"
8	2.93	20.4	0.015	"	6.00 "	+0.58	+ 4.0 "	20	"
9	2.07	9.9	0.015	"	2.90 "	+0.08	+ 1.3 "	13	"
10	2.52	14.9	0.015	"	4.38 "	+0.29	+ 2.9 "	15	"
11	3.26	24.5	0.015	"	7.20 "	-1.15	- 6.9 "	17	"
12	3.58	28.2	0.014	"	8.28 "	-0.58	- 2.9 "	18	"
13	0.96	3.34	0.023	0.48	6.95×10^{1}	-0.03	- 2.0 "	7	Iwagaki-Sawaragi
14	0.98	2.66	0.019	0.28	9.53 "	-0.084	- 6.0 "	6	
15	0.97	3.67	0.025	0.93	3.95 "	+0.055	+ 3.7 "	5	"
16	2.52	21.1	0.021	0.34	6.20×10^{2}	-1.48	-15.0 "	20	Iwagaki-Noda
17	2.19	17.6	0.023	"	5.17 "	-0.32	- 4.2 "	17	"
18	3.10	30.0	0.020	"	8.81 "	-0.57	- 3.8 "	20	"
19	2.84	25.0	0.020	"	7.34 "	-1.45	-11.4 "	20	"
20	3.00	20.2	0.020	"	5.93 "	-1.54	-14.8 "	20	"
21	3.00	29.1	0.021	0.22	1.32 "	-1.60	-11.4 "	20	"
22	2.50	19.0	0.020	"	8.64 "	-0.93	- 9.50 "	20	"
23	2.20	15.9	0.021	"	7.23 "	-0.70	- 9.3 "	20	"
24	1.86	11.3	0.021	"	5.14 "	-1.10	-20.3 "	20	"
25	1.56	8.0	0.021	"	3.64 "	-0.24	- 6.3 "	16	"
26	3.00	29.1	0.021	0.34	8.55 "	-0.35	- 2.5 "	20	"
27	2.50	19.0	0.020	"	5.59 "	-0.95	- 9.7 "	20	"
28	2.20	15.9	0.021	"	4.67 "	-0.64	- 8.5 "	20	"
29	1.86	11.3	0.021	"	3.32 "	-0.51	- 9.6 "	20	"
30	1.56	8.00	0.021	"	2.35 "	+0.08	+ 2.1 "	16	"
31	1.45	6.39	0.020	"	1.88 "	+0.21	+ 6.4 "	11	"
32	1.25	4.87	0/020	"	1.43 "	+0.02	+ 0.6 "	11	"
33	1.00	3.80	0.024	"	1.12 "	-0.12	- 0.8 "	11	"
34	0.98	6.90	0.046	0.48	1.26 "	-0.16	-10.0 "	12	"
35	2.00	23.8	0.038	0.34	6.99 "	-1.90	-30.5 "	20	Iwagaki-Noda
36	2.40	34.9	0.039	"	1.02×10^{3}	-1.75	-19.6 "	20	
37	2.20	30.0	0.040	"	8.81×10^{2}	-1.74	-23.0 "	20	"
38	2.40	35.4	0.039	0.22	1.61×10^{3}	-2.57	-28.6 "	20	"
39	1.90	22.0	0.039	"	1.00 "	-1.25	-22.2 "	20	"
40	1.65	17.3	0.041	"	7.86×10^{2}	-1.31	-30.8 "	20	"
41	1.20	9.7	0.043	"	4.41 "	-0.51	-22.6 "	15	"
42	2.40	35.4	0.039	0.34	1.04×10^{3}	-1.73	-19.2 "	20	"
43	1.90	22.0	0.039	"	6.50×10^{2}	-1.21	-21.4 "	20	"
44	1.65	17.3	0.041	"	5.10 "	-0.55	-12.9 "	20	"
45	1.20	9.7	0.043	"	2.85 "	-0.46	-20.4 "	15	"

the effects of the wave height and the sediment size on that distance are discussed. Although, of course, it may be dangerous to derive a general conclusion on the two dimensional beach process only from such shoreline movements, it would be significant to adopt the distance of the shoreline movement as a representative dimension of beach processes in investigating the effects of wave heights and sediment sizes.

The distance X_{SL} of shoreline progression (in this case, positive value) or recession (negative value) from the initial location is a function of the deep-water wave height H_o, the wave period T, the still water depth on the horizontal bed in a wave tank h, the initial slope of the beach i_o, the median diameter of sand d_{50}, the specific gravity of sand in water S, the duration time of wave action t and the gravity acceleration g. Since the deep-water wave length L_o is equal to $gT^2/2\pi$, the following dimensionless expression is derived by the method of dimensional analysis:

$$X_{SL}/L_o = f_1(h/L_o,\ H_o/L_o,\ H_o/d_{50},\ t/T,\ i_o,\ S), \tag{1}$$

in which the effect of fluid viscosity was neglected because it appears that the viscosity effect is much less than those of other factors by the presumption from sediment transport in alluvial channels except the attenuation of waves due to bottom friction. The effect of h/L_o is considered to be neglected as far as the zone of sand movement is limited on the beach slope and t/T can be dropped in the discussion for the equilibrium state. In addition, the specific gravity of sand in water S is also dropped if constant. Therefore, Eq. (1) is written

$$X_{SL}/L_o = f_2(H_o/L_o,\ H_o/d_{50},\ i_o). \tag{2}$$

If the fall velocity w_o is taken instead of the median diameter d_{50} and the specific gravity in water S of sand as a character of sand because of significance of the suspension phenomenon in beach processes, Eq. (2) is replaced as

$$X_{SL}/L_o = f_3(H_o/L_o,\ \sqrt{gH_o}/w_o,\ i_o). \tag{3}$$

Since, furthermore, the fall velocity of a spherical sand particle with a diameter d_{50} is expressed

$$w_o = \left\{(4/3)Sgd_{50}/C_D\right\}^{1/2}, \tag{4}$$

Eq. (3) is written as follows:

$$X_{SL}/L_o = f_4(H_o/L_o,\ H_oC_D/Sd_{50},\ i_o), \tag{5}$$

in which C_D is the drag coefficient of a sand particle. It is noted that Kurihara and others (1956) used a factor of H_o/Sd_{50} in analyzing their data of equilibrium beach profiles and beach material movements.

Figs. 4a, 4b, 4c and 4d show the relationships between X_{SL}/L_o and H_o/d_{50} with a parameter H_o/L_o obtained by the plots of data for the initial beach slope of 1 on 10 based on Eq. (2). The data include the results of experiments by Iwagaki and Sawaragi (1955, 1956) and Kurihara and others (1956) in addition to those by the authors. The similar plots of data by

Saville (1957) for a 1 on 15 initial beach slope and Rector (1954) for a 1 on 30 slope are shown in Fig. 5. The Rector's data consist of the results for four different sand sizes of 0.22, 0.47, 0.90 and 3.44 mm in median diameter and the wave heights of about 9 to 11 cm. The experimental results by Saville are for a median diameter of 0.22 mm and the wave heights of about 45 to 170 cm.

The same data as in Figs. 4a - 4d are plotted based on Eq. (5) in which H_0C_D/Sd_{50} is introduced instead of H_0/d_{50} as shown in Fig. 6.

The conclusions derived from these figures are as follows:

1. The progression and recession of a shoreline depend not only on the deep-water wave steepness but also on the ratio of the deep-water wave height to the median diameter of sand H_0/d_{50} or H_0C_D/Sd_{50}.

2. It is found that in the case of a 1 on 10 initial beach slope, the recession of a shoreline will take place whenever the values of H_0/d_{50} and H_0C_D/Sd_{50} are larger than approximately 650 and 1100 for a deep-water wave steepness H_0/L_0 of 0.015, 250 and 370 for H_0/L_0 of 0.02, and 60 and 40 for H_0/L_0 of 0.04 respectively. In the case $H_0/L_0 = 0.009$, the critical values of H_0/d_{50} and H_0C_D/Sd_{50} can not be determined from the figure because of no enough data for large values of H_0/d_{50} and H_0C_D/Sd_{50}.

3. The effect of H_0/d_{50} or H_0C_D/Sd_{50} on the shoreline movement is very complicated, but it is evident that the sand size affects the beach process with the scale of waves. The variations in the values of X_{SL}/L_0 become remarkable with increase in the values of H_0/d_{50} or H_0C_D/Sd_{50}.

4. In the case of a 1 on 30 initial beach slope, the variations in the values of X_{SL}/L_0 with H_0/d_{50} are much more systematic than in the case of a 1 on 10 beach slope. In this case, also, there exist the critical values of H_0/d_{50} for the change from progression into recession of a shoreline, which depend on the deep-water wave steepness. It appears that the sand size hardly affects the beach process when the values of H_0/L_0 and H_0/d_{50} are smaller than approximately 0.01 and 250 respectively. This tendency is also seen in Fig. 4a for the wave steepness of 0.009 and a 1 on 10 initial beach slope though the upper value of H_0/d_{50} is different.

5. Although there are no sufficient data to discuss for a 1 on 15 initial beach slope by Saville, it should be noted that they include the data for as large value of H_0/d_{50} as approximately 10^4. It is found from these data that even when the deep-water wave steepness is as small as 0.0023, the recession of a shoreline takes place if H_0/d_{50} is larger than a certain critical value, and that even if the order of magnitude of H_0/d_{50} is changed from 10^3 into 10^4 in the case $H_0/L_0 = 0.035$, the absolute value of X_{SL}/L_0 does not become large extremely. However, it is said that more data are needed to derive the correct conclusion.

Generally speaking, it is concluded that the effect of sand size on the beach process is remarkable at least within a certain range of H_0/d_{50} or H_0C_D/Sd_{50} including certain critical values of these factors for each value of H_0/L_0. It is presumed that this reason is because the mode of sand transport by breaking waves is changed from that of bed-load transport

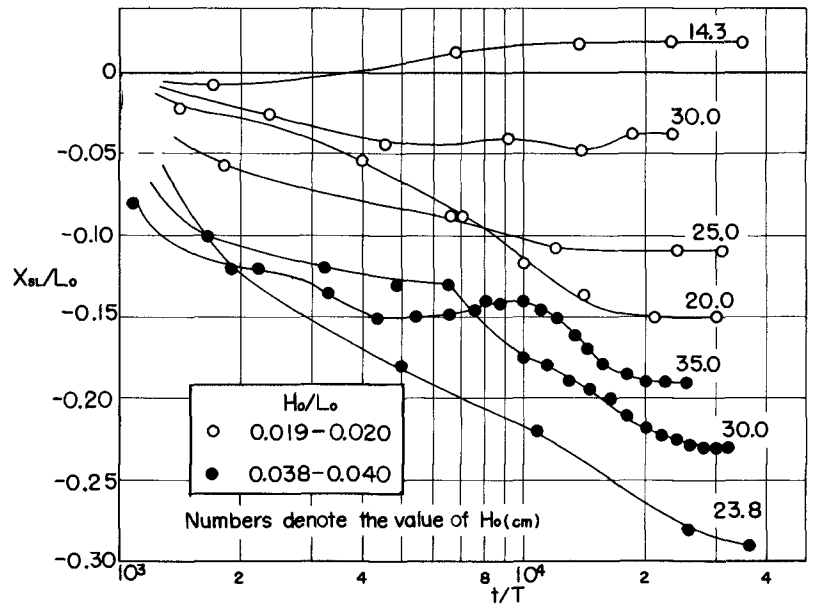

Fig. 3. Dimensionless plots of shoreline movement with time from an initial beach slope of 1 on 10.

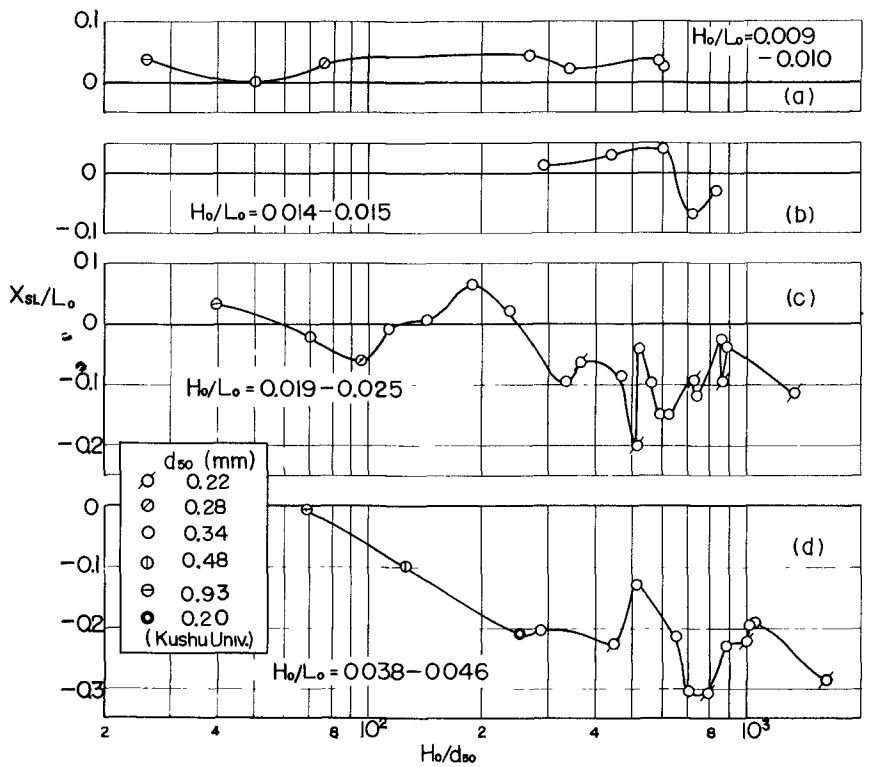

Fig. 4. Dimensionless plots of shoreline movement from an initial beach slope of 1 on 10 to the equilibrium state against the ratio of wave height to sand size.

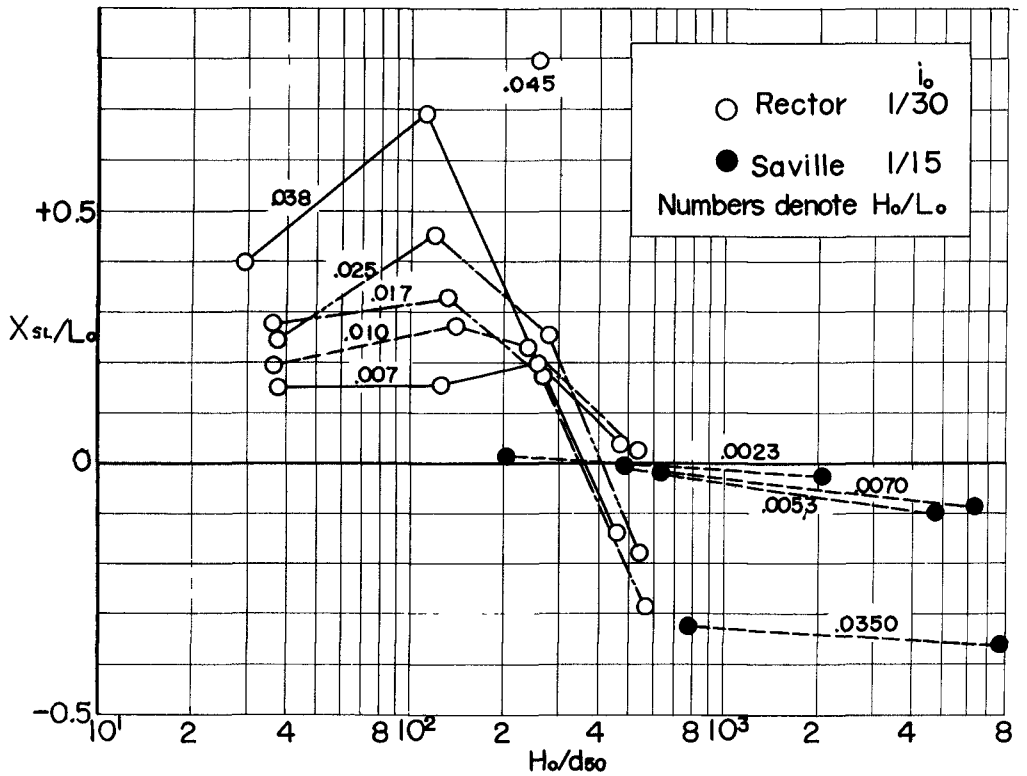

Fig. 5. Dimensionless plots of shoreline movement from initial beach slopes of 1 on 15 and 1 on 30 to the equilibrium state.

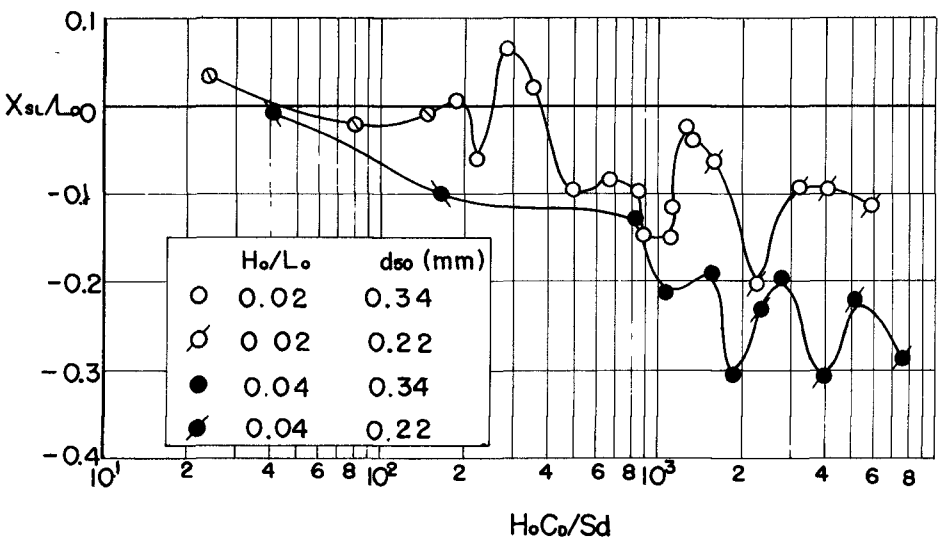

Fig. 6. Dimensionless plots of shoreline movement from an initial beach slope of 1 on 10 to the equilibrium state against H_0CD/Sd_{50}.

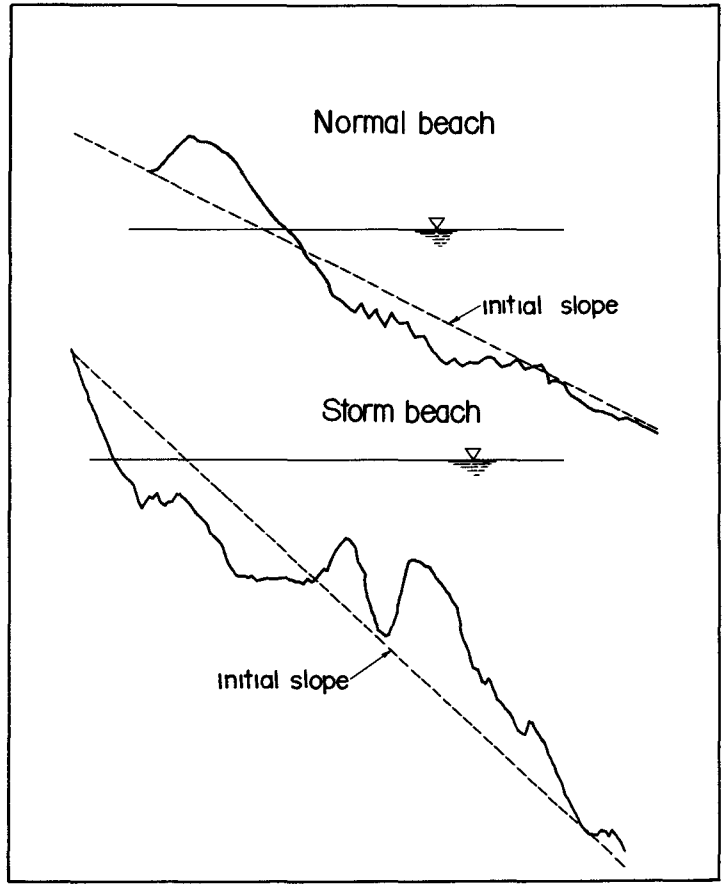

Fig. 7. Profiles of the normal beach and the storm beach.

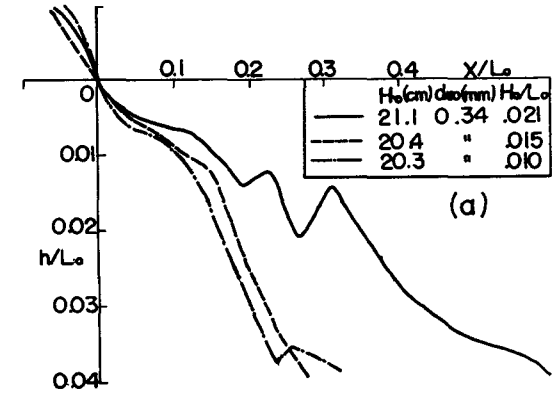

Fig. 8a

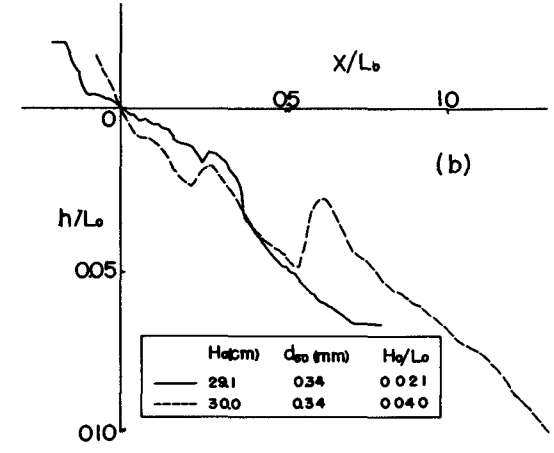

Fig. 8b
Dimensionless plots of equilibrium beach profiles for approximately same wave height and sand size, and different wave steepnesses.

for small values of H_0/d_{50} or H_0C_D/Sd_{50} into that of suspended-load transport for large values of H_0/d_{50} or H_0C_D/Sd_{50}.

EQUILIBRIUM BEACH PROFILES

A laboratory study by Johnson (1949) indicated that equilibrium beach profiles are classified those of the "normal" or "ordinary" beach, where there are no longshore bars, and of the "storm" beach, which is characterized by the development of longshore bars, as shown in Fig. 7. Rector (1954) made an effort to express the dimensionless equilibrium beach profile using the deep-water wave length L_0 as a function of H_0/L_0 and d_{50}/L_0. Watts (1954) made experiments to investigate the effect of varing wave periods on equilibrium beach profiles with an initial beach slope of 1 on 20. However, all of these experiments were of very small scales including the tests in Japan, compared with actual beaches. The results of the large scale experiments made by Saville (1957) showed the fact that even when the deep-water wave steepness is very small, storm beaches having longshore bars appear in the equilibrium state, which are not seen in the common experiments of small scale. From this reason, the scale effect on the equilibrium beach profile is considered by dividing the experimental results into three following cases:

Case when wave heights and sand sizes are same and wave steepnesses are different - Figs. 8a and 8b show the dimensionless plots of the equilibrium beach profiles, which are expressed by the ratios of a distance from the shoreline X and the water depth h to the wave length L_0, for the wave heights of approximately 21 cm and 30 cm, a sand size of 0.34 mm in median diameter and the different wave steepnesses. It is found from these figures that the wave steepness affects the equilibrium beach profile remarkably when H_0/d_{50} is constant. Furthermore, it should be noted that the beach profiles in the case $H_0/L_0 = 0.021$ are of the storm beach though this value of the wave steepness is smaller than the critical value 0.025 - 0.03 determined by Johnson.

Case when wave steepnesses and sediment sizes are same and wave heights are different - Fig. 9 shows comparisons of the equilibrium beach profiles for approximately constant wave steepnesses 0.021 - 0.024, a sand size of 0.34 mm in median diameter and various wave height. It is disclosed from the figure that the equilibrium beach profile depends not only on the wave steepness and sediment size but also on the wave heights. In the cases H_0 = 21.1 cm and 29.1 cm, the storm beaches were formed, and in the case H_0 = 3.8 cm the normal beach was developed though the wave steepness were almost same, and also the sediment size was constant. In the case H_0 = 11.3 cm it is undecided whether or not. Such differences in the equilibrium beach profile were already indicated by Saville (1957).

Case when wave steepnesses and wave heights are same and sand sizes are different - The equilibrium beach profiles are shown in Figs. 10a, 10b and 10c for two different sand sizes (d_{50} = 0.34 mm and 0.22 mm), same wave heights of 29.1 cm, 15.9 cm and 11.3 cm and same wave steepness of 0.021. As shown in Fig. 10a, the longshore bars of approximately same scale are formed and the profiles are very similar except in the vicinity of the beachface in spite of different sand sizes in the case of a large wave height of 29.0 cm. With decrease in the wave height as shown in Fig. 10b, longshore

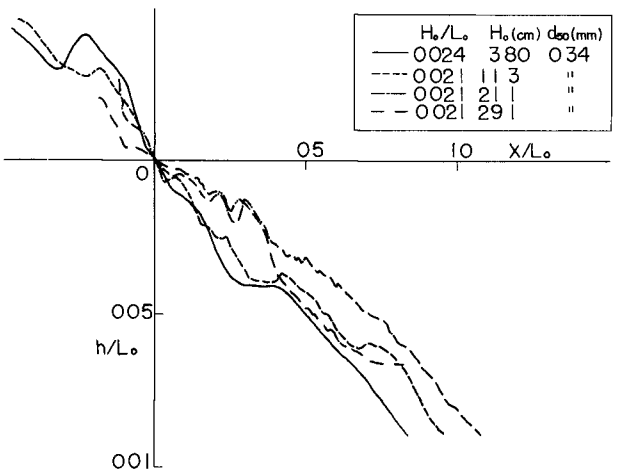

Fig. 9. Dimensionless plots of equilibrium beach profiles for approximately same wave steepness and sand size, and different wave heights.

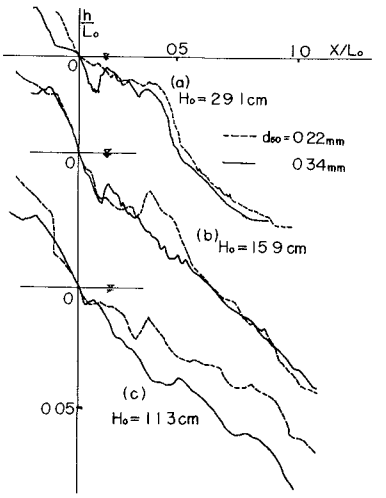

Fig. 10. Dimensionless plots of equilibrium beach profiles for same wave heights and constant wave steepness of 0.021, and different sand sizes.

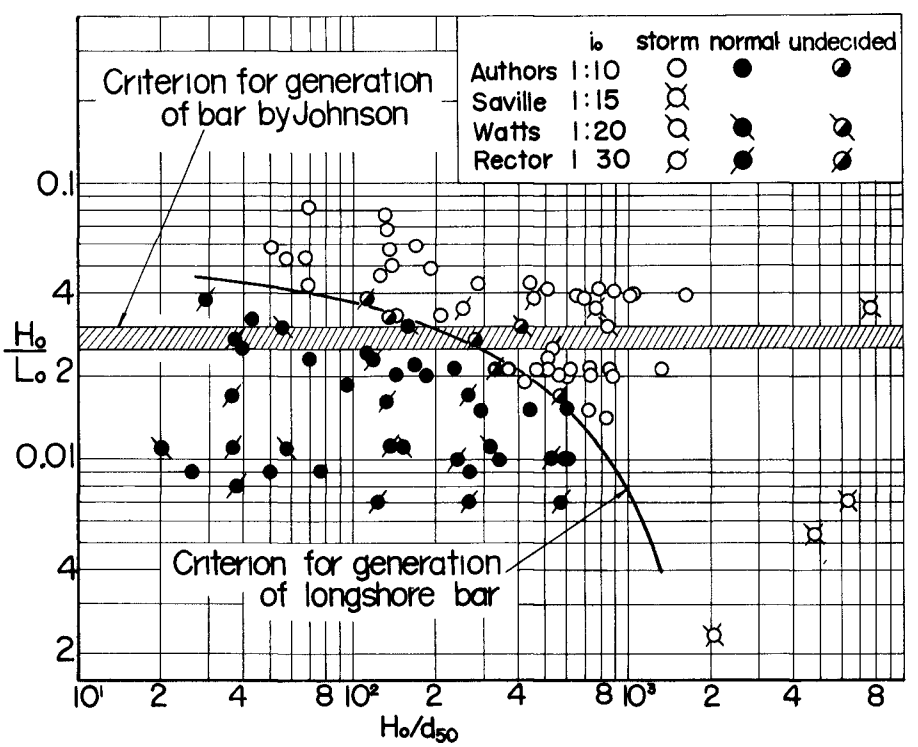

Fig. 11. Criterion for generation of longshore bars.

bars in the coarser sand (d_{50} = 0.34 mm) are reduced, thus the profiles are different in the inshore zone. Further decrease in the wave height produces the completely different profiles for the difference of sand size as shown in Fig. 10c. A longshore bar is still formed in the finer sand, and on the other hand, in the coarser sand it almost disappears. These facts can also be found in the results of experiments four different sand sizes and same waves by Watts (1954).

CRITERION FOR GENERATION OF LONGSHORE BARS

In the foregoing section, it has been found that the equilibrium beach profile depends not only on the deep-water wave steepness but also on the wave height and the sand size. From this fact it is presumed that a limitation between the storm beach and the normal beach, which is a criterion for generation of longshore bars, can also be expressed by the deep-water wave steepness H_0/L_0 and the ratio H_0/d_{50} or H_0C_D/Sd_{50}. Fig. 11 shows the log-log plots of experimental data by the authors and other investigators with the ordinate of H_0/L_0 and the abscissa of H_0/d_{50}, in which the data are distinguished between the normal beach and the storm beach, and plotted for each initial beach slope. In the figure the boundaries between the normal beach and the storm beach have been drawn, the one is by Johnson and the other is that proposed by the authors under the assumption that the initial beach slopes are independent of equilibrium beach profiles, especially the generation of longshore bars.

It is evident from this figure that when the value of H_0/d_{50} is smaller than a certain value, the critical value of H_0/L_0 proposed by Johnson is approximately valid; however, with increase in the value of H_0/d_{50} the critical wave steepness becomes small rapidly. This fact indicates that at the beach being constituted by fine sand and where large waves attack, the storm beach is formed and longshore bars appear even when the deep-water wave steepness is considerably small. It is very significant that the limitation between the storm beach and the normal beach is expressed by H_0/d_{50} and H_0/L_0.

CHANGES IN CHARACTERISTICS OF BREAKING WAVES DURING BEACH PROCESSES

It is well known that there are generally two types of breaking waves, which are called spilling breakers and plunging breakers. Laboratory studies by Iversen (1952) and Hayami (1955, 1958) indicated that the limitation between both types of breakers can be expressed by the deep-water wave steepness and the beach slope (Fig. 12). The critical wave steepness theory is based on the idea that the types of breakers are much related with the beach process; that is, beach erosion will occur with spilling breakers and beach accretion will take place with plunging breakers.

Since, however, the experimental results shown in Fig. 12 are for the fixed beds of uniform slopes, the question arises whether the same results can be applied to the beach of a movable bed or not. In Fig. 12, furthermore, the limitation is not clear when the bed slope is very small. For example, according to this figure plunging breakers appear whenever the deep-water wave steepness is 0.02, and thus beach accretion is to take place in this case. However, it is seen in Fig. 4c that beach erosion occurs even when H_0/L_0 is approximately 0.02. It is very difficult, therefore, to

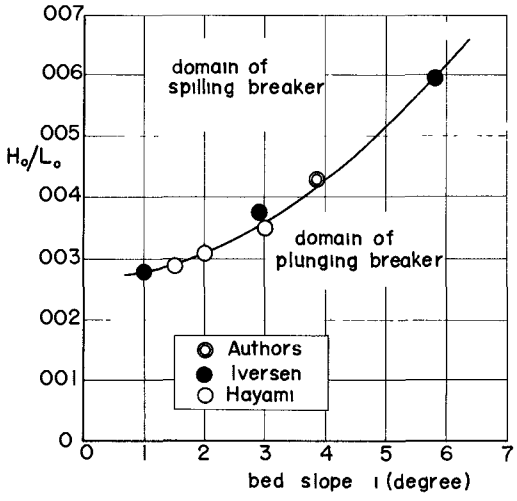

Fig. 12. Limitation between spilling breakers and plunging breakers.

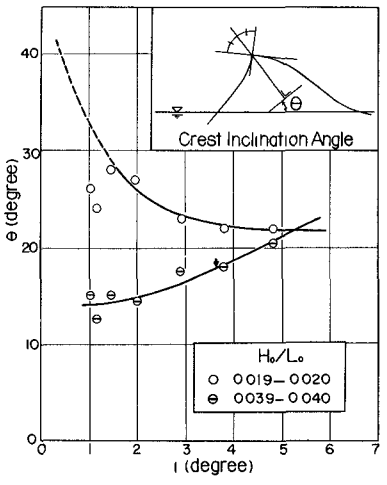

Fig. 13. Relationships between crest inclination angle of breakers and bed slope for fixed bed.

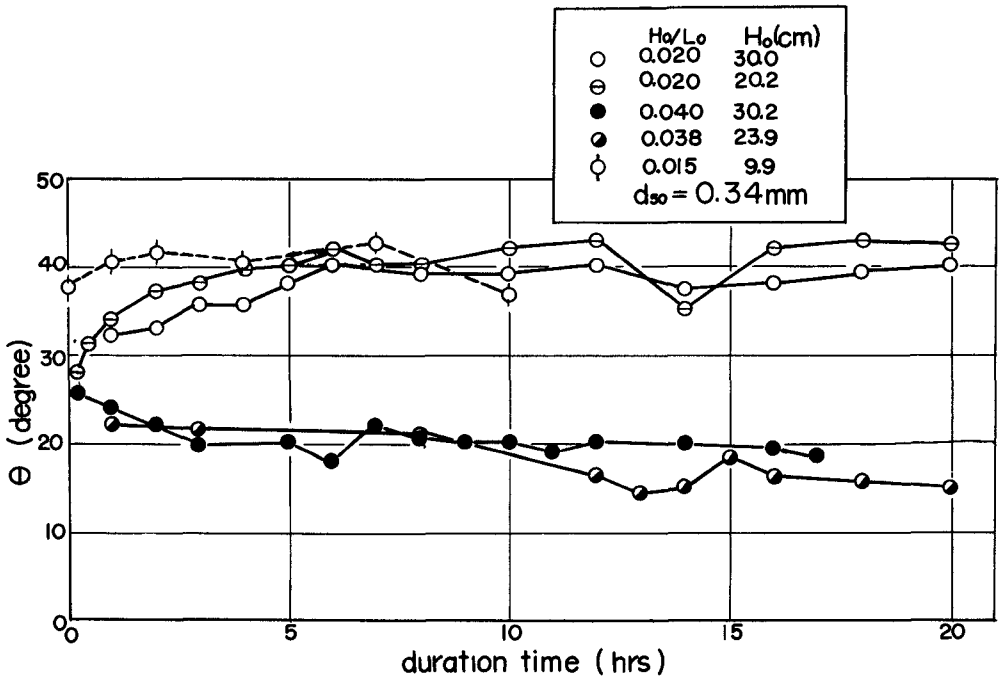

Fig. 14. Progressive changes in crest inclination angle of breakers with time for various wave steepnesses.

connect directly the critical wave steepness theory with the characters of breaking waves on the movable bed. From this reason, an effort is made in investigating the relationship between profiles of breakers and beach processes in this section.

As a quantitative expression for the profile of a breaking wave, the angle θ is treated, which is an angle between a bisector of the crest angle of a breaking wave and a perpendicular line as shown in Fig. 13. This crest inclination angle θ is very convenient to discuss asymmetricity of a breaking wave; that is, $\theta = 0^{\circ}$ if waves at breaking are symmetric completely, and $\theta = 45^{\circ}$ if they are extremely asymmetric. It is considered that the crest inclination angle becomes close to 45° in plunging breakers and to 0° in spilling breakers.

First, in order to disclose the relationships between the crest inclination angle θ and the bed slope i, an experiment was made by using a small wave tank with a fixed tilting beach slope. Fig. 13 shows the relationship in the cases $H_0/L_0 = 0.02$ and 0.04. From this figure the followings are made clear:

1. The angle θ is changed with the slope i even if the deep-water wave steepness H_0/L_0 is constant.

2. An arrow in Fig. 13 corresponds to the critical beach slope for the wave steepness of 0.04 decided by Iversen and Hayami. Therefore, the regions where the beach slopes are smaller and larger than the critical belong to those of spilling breakers and plunging breakers respectively.

3. In the case $H_0/L_0 = 0.02$, the angle θ increases with decrease in the slope i. However, the experimental results show the opposite tendency when the slope is smaller than 1.5°. It is considered that this opposite tendency may be caused by the capillary effect because of small waves. It was observed that breaking waves in this case were of the plunging type independently of the slope.

Next, the progressive changes in the crest inclination angle θ with time during beach processes are shown in Fig. 14. It is found from this figure that tha angle θ seems to reach a constant value for each wave steepness finally independently of an initial angle corresponding to an initial beach slope of 1 on 10. The duration time for the angle θ to become constant is much shorter than that for the beach to reach the equilibrium state.

In the case $H_0/L_0 = 0.04$, as shown in Fig. 14, the angle θ, which was approximately 27° on the initial beach slope of 1 on 10 ($i = 5^{\circ}43'$) after beginning of the experiment, became 19°- 20° at the equilibrium state. This final crest inclination angle agrees fairly with that at the beach slope i = 4°- 4.5° in Fig. 13 which corresponds approximately to the critical wave steepness theory of Iversen and Hayami. In the case $H_0/L_0 = 0.02$, the final crest inclination angle was approximately 40° as shown in Fig. 14, but the beach slope i corresponding to $\theta = 40^{\circ}$ can not be obtained precisely from Fig. 13 and it is impossible to compare that value with that by the critical wave steepness theory because there are no data for the beach slope less than 1° in Fig. 12.

LABORATORY STUDY OF SCALE EFFECTS IN TWO-DIMENSIONAL BEACH PROCESSES

CONCLUSIONS

It is concluded from the results of laboratory tests on the two dimensional beach process that:

1. Two dimensional beach processes are influenced not only by the deep-water wave steepness but also by the scale of waves and the sand sizes.

2. The influence of sand sizes on the beach process is not remarkable when the deep-water wave steepness is smaller than approximately 0.01 and, in addition, the ratio of the wave height to the sand size is smaller than a certain value for each wave steepness.

3. Equilibrium beach profiles are also influenced not only by the deep-water wave steepness but by the wave height and the sand size.

4. The limitation between the normal beach and the storm beach, which is a criterion for generation of longshore bars, can be expressed by the deep-water wave steepness and the ratio of the wave height and the sand size.

5. The crest inclination angle of breaking waves approaches a certain value for each deep-water wave steepness with the formation of the equilibrium beach profile independently of an initial beach slope. This value of the angle agrees fairly with that of breaking waves on the fixed bed of the critical beach slope based on the limitation between spilling breakers and plunging breakers when the deep-water wave steepness is 0.04.

ACKNOWLEDGEMENTS

The authors wish to express their great appreciations to Prof. T. Ishihara for his encouragement to perform this study and to Assist. Prof. Y. Tsuchiya, Messrs. Y. Kawasaki, T. Ibo, J. Sakai and M. Kuge for assisting the experiments and preparing this paper.

REFERENCES

Hayami, S., Ishihara, T. and Iwagaki, Y. (1953). Some studies on beach erosions: Disaster Prevention Research Institute, Kyoto University, Bulletin No. 5, 29 pp.

Hayami, S. (1955). Mechanism of breakers (II), Proc. of 2nd Conference of Coastal Engineering in Japan, pp. 13-15 (in Japanese).

Hayami, S. (1958). Types of breakers, wave steepness and beach slope, Coastal Engineering in Japan, Vol. 1, pp. 21-24.

Iversen, H. W. (1952). Waves and breakers in shoaling water, Proc. of 3rd Conference on Coastal Engineering, pp. 1-12.

Iwagaki, Y. and Sawaragi, T. (1955). Experiments on equilibrium slopes of beaches and sand movement due to breakers, Proc. of 2nd Conference of Coastal Engineering in Japan, pp. 99-105 (in Japanese).

Iwagaki, Y. and Sawaragi, T. (1956). Some problems on the equilibrium slopes

of beaches, Disaster Prevention Research Institute, Kyoto University, Bulletin, Memorial Issue of 5th Anniversary, pp. 233-240 (in Japanese).

Iwagaki, Y. and Sawaragi, T. (1958). Experimental study on the equilibrium slopes of beaches and sand movement by breaker, Coastal Engineering in Japan, Vol. 1, pp. 75-84.

Iwagaki, Y. and Sawaragi, T. (1960). A new method for estimation of the rate of littoral sand drift, Proc. of 7th Conference of Coastal Engineering in Japan, pp. 59-67 (in Japanese).

Iwagaki, Y. and Noda, H. (1961a). Scale effects in hydraulic models for beach process, Disaster Prevention Research Institute, Kyoto University, Annuals No. 4, pp. 210-220 (in Japanese).

Iwagaki, Y. and Noda, H. (1961b). A study of scale effects in experiments for beach processes, Proc. of 8th Conference of Coastal Engineering in Japan, pp. 139-143 (in Japanese).

Johnson, J. W. (1949). Scale effects in hydraulic models involving wave motion, Trans. Amer. Geophys. Union, Vol. 30, pp. 517-525.

Kurihara, M., Shinohara, K., Tsubaki, T. and Yoshihara, M. (1956). Sand movement on beaches by waves, Proc. of 3rd Conference of Coastal Engineering in Japan, pp. 151-159 (in Japanese).

Rector, R. L. (1954). Laboratory study of equilibrium profiles of beaches, Beach Erosion Board, Tech. Memo., No. 41, 38 pp.

Saville, T. Jr. (1957). Scale effects in two dimensional beach studies, Proc. of 7th General Meeting, I. A. H. R., Vol. I, pp. A3.1-A3.10.

Sawaragi, T. and Murakami, T. (1957). On the estimation of the rate of littoral sand drift, Proc. of 4th Conference of Coastal Engineering in Japan, pp. 41-49 (in Japanese).

Scott, T. (1954). Sand movement by waves, Beach Erosion Board, Tech. Memo., No. 48, 37 pp.

Shinohara, K., Tsubaki, T., Yoshitake, M. and Agenori, Ch. (1958). Sand transport along a model sandy beach by wave action, Coastal Engineering in Japan, Vol. 1, pp. 111-130.

Watts, G. M. (1954). Laboratory study of effect of varying wave periods on beach profiles, Beach Erosion Board, Tech. Memo., No. 53, 19 pp.

CHAPTER 15

LONGSHORE CURRENTS IN ONE AND MULTI-BAR PROFILES RELATION TO LITTORAL DRIFT

Per Bruun
Head, Coastal Engineering Laboratory
University of Florida, Gainesville

Abstract. This paper deals with longshore current theories. Introductorily it gives a brief review of wave theories for breaking waves including theoretical, laboratory as well as field results. Next the longshore current theory based on the momentum inflow over a uniformly sloping beach and bottom (Putnam, Munk and Traylor, 1949) is discussed with special reference to its friction factor. The following chapters deal with two new longshore current theories - both based on the continuity principle. One of them called the rip current approach assumes that all water thrown in by wave breaking runs out in rip currents and will probably be valid for profiles with well developed bars and waves approaching the shore almost perpendicularly. The other theory considers the fact that water from a wave breaking under an angle with the bar flows in with a certain phase difference in time longshore and this will create a longshore slope of the average water table, therefore also a longshore current. The water may return to sea uniformly as undertow or in rip currents or by a combination of both. This theory is particularly valid for waves breaking under a certain, not too small, angle with the bar. In both cases the momentum in the breaking waves is ignored because field observations show that in a well developed bar profile most of the momentum has disappeared inside the bar after wave breaking.

Examples of computation of current velocities for one bar as well as multi-bar profiles are given. Next the possible relation between longshore currents and littoral drift is discussed.

1. WAVE THEORIES AT WAVE BREAKING

Before entering in any discussion on currents caused by wave breaking it is desirable briefly to review the application of existing wave theories to the shallow water area just outside and in the breaker zone.

The assumption underlying the linear Airy wave theory, namely that the wave height is small compared to the water depth, is not fulfilled in the area of the breaker zone.

Mathematical arguments show that Stokes finite wave height theory is used when the depth to wave length ratio d/L is greater than about 1/8 to 1/10 (Keulegan, 1950).

In this connection it should be noted that Bretschneider's (1961) recently developed theory for waves of finite height represents an exact theory to any order to which it is extended. An approximation by expansion of the exact equations is identical to Stokes' theory extended to the same order.

The theory of cnoidal waves (initiated in 1895 by Korteweg and de Vries) accounts for a general class of long waves of permanent type and finite amplitude; one limiting case of the theory gives the solitary wave, while another limiting case gives the sinusoidal wave as accounted for by linearized wave theory. Cnoidal wave theory as described by Wiegel (1960) is appropriate to periodic waves progressing in water whose depth is less than about one-tenth the wave length.

Laitone (1961) showed how the higher-order terms describing the vertical velocity variation, or the reversal of the pressure gradient, can predict a limiting height for cnoidal as well as solitary waves. The maximum amplitude is 8/11 of the free water depth for the solitary wave. In addition it was found that the cnoidal waves are theoretically limited to the longer wave lengths corresponding to nearly critical, or supercritical speeds. It was also found that even for the higher approximations solitary waves can only occur at supercritical speeds.

When waves travel into water of depth less than a few times the wave height, wave crests narrow and become separated by long flat troughs. The character of these isolated crests scarcely depends upon the distance L between the crests. Meanwhile, in Stokes' theory the wave length is contained in the two fundamental parameters: the depth/wave length and the height/length of the wave. Because of the apparent inadequateness of Stokes' theory, the solitary wave theory was suggested for application to surf problems (see e.g. Munk, 1949). Its advantages were soon confirmed by an obvious resemblance between the theoretically derived wave profile and the observed profile in the region just outside the breaker zone. The theory of the solitary wave, first developed by Boussinesq in 1871, was improved by McCowan in 1891, but received little attention, until Keulegan and Patterson published their theories (1940).

LONGSHORE CURRENTS IN ONE AND MULTI-BAR PROFILES RELATION TO LITTORAL DRIFT

As described by Munk (1949), Boussinesq obtained a solution to the equations of motion for irrotational, non-divergent flow which is based on the expansion of the velocity potential in a power series.

$$\phi = \sum_{n=0}^{\infty} \phi_n \mathfrak{z}^n$$

Retaining only the first two terms in the power series, Boussinesq obtained for the wave profile, $\mu = r\,\mathrm{sech}^2(\sqrt{3r/4}\,x)$ and for the wave celerity $C = \sqrt{g(h+H)} = \sqrt{gh(1+r)}$ where g = acceleration of gravity, h = water depth, H = wave height, and $r = H/h$. The total volume of water per unit crest length above the still water level Q is given by (see e.g. Le Mehaute, 1960).

$$Q = 4h^2\sqrt{\frac{r}{3}}$$

For the breaking wave, McCowan found the crest to be formed by two branches equally inclined to the bottom and cutting an angle of 120°. The corresponding ratio of wave height/water depth was 0.78.

The energy flow at the breaking point is $C_b \frac{E_b}{L_b}$ where E_b/L_b is the mean energy per unit surface area which by comparison with the energy flow in deep water gives: $H_b = \gamma H_o / \sqrt[3]{3.3\,\gamma H_o/L_o}$ where H_b is breaker wave height and H_o = deep water wave height.

The momentum flow at the breaking point is $C_b \cdot Q_b$ where C_b is the wave celerity at breaking and Q_b the total volume of water per unit crest length above the still water level of the breaking wave.

Experiments on orbital velocities associated with wave action near the breaker zone carried out by the Scripps Institution of Oceanography from the Scripps pier at La Jolla, California as described by Inman and Nasu (1956) showed that the maximum horizontal orbital velocities as observed in general compare more favorably with velocities predicted from solitary wave equations than the equations of Airy and Stokes particularly when the ratio of the wave height to water depth is greater than about 0.4 (just outside the breaking point). In breaking theories the point of incipient breaking is where the maximum internal velocity at the crest is the same as the celerity of the wave form. The results of limiting amplitude-to-depth ratio obtained on this basis by various investigators are, according to Ippen and Kulin (1955): Boussinesq, 0.73;

McCowan, 0.78; Davies, 0.83; Packham, 1.03; and Gwyther, 0.83; (all for waves breaking perpendicular to the shoreline). Ippen and Kulin found by laboratory experiments that the amplitude-to-depth ratios at breaking are considerably higher than the theoretical McCowan value of 0.78 for solitary waves in water of constant depth. On a 2.3 per cent slope, which is comparable to many prototype conditions, the observed ratio was found to be constant at 1.2 for all initial waves. For the steeper slopes this ratio was found to be higher, and it increased sharply with decreasing wave height. Generally it could also be stated that all waves broke in water shallower than predicted by theory and the observed amplitude increase during shoaling was considerably smaller than the theoretical increase called for by constant energy consideration.

Iversen (1952) found, by laboratory experiments, that the beach slope has a marked effect in that, for a given wave train, the breaker is approximately 40 per cent higher on a 1:10 slope than on a 1:50 slope. In nature most bars on the open seacoast will have a comparatively gentle slope e.g. 1:30 on the front side and a rather steep slope e.g. 1:10 on the back side.

These findings refer to long-crested waves which have equal characteristics whether they occur in a wide basin or in a narrow channel.

Fuchs (1951) investigated the mechanics of the short-crested oscillatory waves which have no continuous crest because the turbulence of the wind is random not only in the direction of propagation but also at right angles to it. This helps to explain the absence of long-crested waves in deep water; in shallow water energy flux takes place, accounting for a more evenly distributed wave height. Long-crested waves, therefore, peak up more rapidly than the short-crested waves in shallow water. Energy flow along the wave crest is therefore also largest for high (steep) waves in shallow water and will increase rapidly as the waves approach breaking.

2. LONGSHORE CURRENTS OUTSIDE THE BREAKING ZONE

During the passage of a wave train over the offshore bottom, waves approaching the shoreline obliquely will turn by refraction. It is to be expected that this turning will cause a current along the wave crest. Meanwhile, wave characteristics change simultaneously and in the area $0.1 < d/L_o$

< 0.3 (d = water depth, L_o = wave length in deep water) the wave height will be smaller than the deep water wave height with the waves travelling perpendicular to shore and this will also be true with waves approaching shore obliquely with modifications due to refraction. By energy and mass transport considerations it may then be seen that the longshore current caused by the turning of waves by refraction must be very small and about zero apart from the area just before wave breaking when mass transport increases rapidly and the wave crest starts "sliding" a little sideways in down drift direction.

But longshore current of any magnitude first comes into existence when waves break causing water masses to move in one direction with great velocities.

3. LONGSHORE CURRENT THEORY BASED ON MOMENTUM THEORY

Using the solitary wave theory Putnam, Munk, and Traylor (1949) developed a longshore current theory based on momentum inflow under breaker angle with the shoreline of the water masses contained in the breaking wave (Figure 1) which is adequately described by the solitary wave theory. The momentum inflow's longshore component is $Q\cos\alpha_b \cdot C\sin\alpha_b$ (Q = water mass per unit length of wave crest, C = wave celerity (water velocity) at breaking, α_b = breaker angle). The loss of momentum by return flow of water to the area outside the breaker zone is $Q\cos\alpha_b \times V$, where V is the longshore current velocity. Balancing bottom shear stresses against momentum gives the expression for v:

$$V^2 = \frac{Q\cos\alpha_b}{akT}\,(C\sin\alpha_b - V)$$

where a is the distance between the breaking point of the waves and the shoreline, T is the wave period, and k is a friction parameter.

In above expression a uniformly sloping beach and offshore bottom are considered. Furthermore an immediate and direct return of water from the breaking waves to the offshore area is assumed. This may be correct for shores having steep bottom profiles and, therefore, little or no bar formation. With less steep shores and shores with one or more offshore bars the mechanism of the longshore current is different. Water masses thrown in by wave breaking do not return as a comparatively equally distributed "undertow" but will tend to flow a certain distance along the shore and

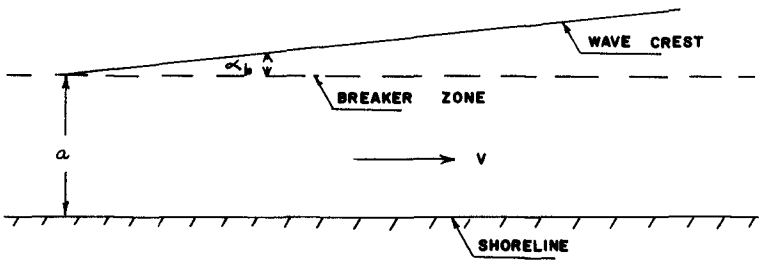

Fig. 1. Momentum approach.

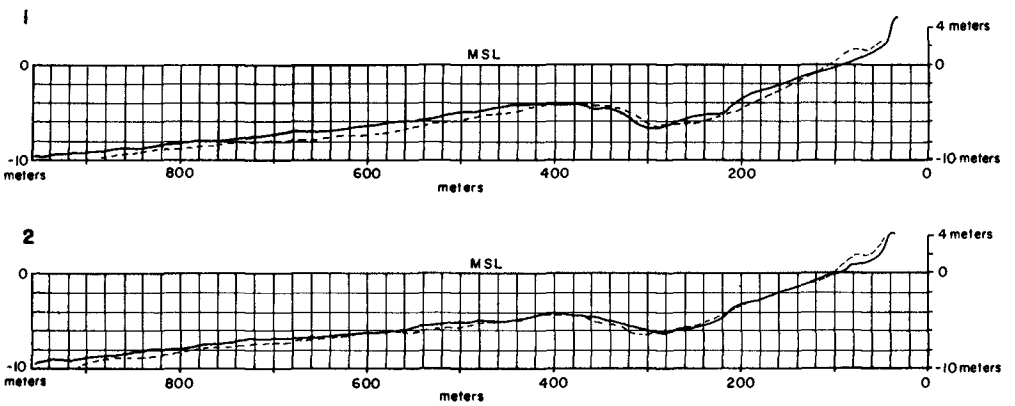

Fig. 2. Profiles at Bovbjaerg, Danish North Sea Coast.
---------- summer, ———————— winter.

return in rip currents, which are currents running out perpendicularly to the shoreline. With respect to the k-value, it should be borne in mind that k depends on the hydraulic roughness of the beach rather than on the absolute roughness of the beach surface. Certain laboratory and field data are available as described by Putnam, Munk, and Traylor, (1949).

Inman and Quinn (1952) describe current experiments at Torrey Pines Beach, north of La Jolla in Southern California. Surface and bottom currents in the surf zone (inside the breaking point) were measured at 15 equally spaced points along two straight beaches having approximately parallel bottom contours. The results were subject to a statistical evaluation which demonstrated that the variability of the longshore current component as measured by its standard deviation is equal to or larger than the mean longshore velocity. It was found that the momentum approach by Putnam et al leads to useful forecasts, provided the friction coefficient k is permitted to vary with the longshore velocity as indicated by the relation $k \sim V^{-3/2}$. For field data $k = 0.020 \times V^{-1.51}$ (dimensionless); for laboratory data $k = 0.029 \times V^{-1.54}$. In this respect it is interesting to note a certain similarity to unidirectional flow where the friction coefficient decreases with increasing mean velocity when the transition area from ripples to dunes causing a heavy increase in friction has been passed. The transition from rippled to duned bottom occurs at mean velocities from about 0.3 m/sec to 0.4 m/sec. Meanwhile this fact should not be misinterpreted because, as stated by Inman and Quinn (1952) the k-values found for longshore currents refer to bottom material ranging from ¼ inch pea gravel through sand to smooth concrete; the type of bottom apparently is not as important as the velocity is for the value of k. In other words the hydrodynamic elements involved in k may have the predominant influence on the actual k value.

Table 1 gives field data for k and C_f for various velocities in feet as well as in the metric system.

TABLE 1. k anc C_f friction values

V ft/sec	1	2	3	4	5
V m/sec	0.3	0.6	0.9	1.2	1.5
k	0.020	0.0071	0.0038	0.0025	0.0018
C_f ft$^{\frac{1}{2}}$/sec	40	67	91	112	134
C_f m$^{\frac{1}{2}}$/sec	22	39	50	62	74

For the velocity range 2 to about 4 ft. these values are comparable with those found by Bruun and Gerritsen (1960) for tidal inlets, although the flow conditions are different. Meanwhile, for troughs behind bars, it is probably better to use C_f values derived from the experience formula $C_f = 30 + 5\log A$, where A is the cross-sectional trough area in m^2 and C_f is in $m^{\frac{1}{2}}/sec$. The corresponding value for C_f in feet is $C_f = 45 + \log A$ where A is ft^2 and C_f's dimension is $ft^{\frac{1}{2}}/sec$. Values of k for $V > 5$ ft/sec are very small and can hardly be compared to C_f values from normal water courses. The velocities recorded by Inman and Quinn were of the order from 0.15m (½ ft) up to 1.25m (4 ft) per sec. with a predominance around 0.75m (2.5 ft) per sec.

4. LONGSHORE CURRENT THEORIES BASED ON THE CONTINUITY PRINCIPLE

GENERAL

Handling of the current problem by means of the "continuity principle" seems beforehand to be a somewhat more realistic approach because while there is no doubt that the mass of water involved in wave breaking is preserved (apart from a little spray and foam) it is certain that considerable amount of momentum is lost by the wave breaking in eddy momentum, shocks and pressures, transfer of momentum by shear stresses to the bottom material and finally heat. Only a part of the momentum actually involved in a breaking is regenerated in momentum behind the breaking point whether this is in current or wave momentum.

Wave breaking in the prototype is influenced by a number of factors, including the depth, the wind field, and the longshore and rip currents.

The water particles in a wave just before breaking are moving with high velocities, e.g. 3 to 10 meters (10 to 30 ft) per second, and it is therefore difficult to define any particular breaking depth. In fact waves at breaking may pass over the crest of the bar so fast that they do not succeed in a breaking. The depth over the crest of the bar is not equal to the breaker depth for the breaking wave. It indicates the minimum cross section through which the water masses held in the breaking wave flow with a velocity which will normally be less than the water particle velocity at the breaking point, unless waves break at the crest of the bar causing a maximum inflow of momentum at the minimum cross section. Inasmuch as no surveys of bottom topography can be made during stormy

weather it is not possible to give an exact figure for the actual breaker depth during storms, but it is increased by the tide (above normal) which usually occurs simultaneously and perhaps also by a minor figure indicating a certain erosion of the upper bottom layer during storms. It therefore depends upon local conditions, and tides and onshore winds will both increase the breaker depth. The laboratory ratio of 1.2 by Ippen and Kulin (1955), referring to experiments on solitary waves, can hardly be expected to be directly applicable in the prototype. Kressner (1928) states, on the basis of laboratory experiments, that waves will break on a slope when wave height equals water depth and that this is in agreement with field observations.

Technical Report No. 3 by the Beach Erosion Board (1948) describes a considerable number of bottom profiles obtained by long-term laboratory experiments and also gives some data on profiles from the German Baltic coast as well as from Lake Michigan. From these data it appears that the depth over the bar is 20 to 40 per cent smaller than the height of the breaking wave. This seems to be in agreement with Kressner's findings.

During calm weather periods between storms there will be certain movements of the bar as demonstrated by Figure 2 from the Danish North Sea Coast at Bovbjaerg. Full lines indicate winter (storm) and dotted lines summer (swell) profiles. It will be seen that there is only a minor difference between the two profiles and inasmuch as most summer swells do not break over the bar it must mean that the (vertical) dimensions of the bar are mainly governed by the storm (winter) waves with the accompanying high velocities of the water masses flowing over the bar.

To arrive at the velocity of the longshore current, detailed knowledge on wave data is necessary and particularly it is important to know which wave in the statistical picture is responsible for the development of the bar and the corresponding trough. Inasmuch as the current in the trough integrates the effect of all incoming waves it is a reasonable assumption that the trough is related to a current which depends upon the characteristics of the highest breaking waves. With respect to the bar, sand is pushed up on the bar by shear stresses by the incoming waves but the crest itself is shaved off by the breaking waves and its dimensions are most likely governed by the highest waves also. This means that the bar crest probably is located deeper than corresponding to the

height of the average wave. On the basis of present knowledge it is, as already mentioned, not possible to evaluate closely which wave height the crest will tend to follow, and rip currents and a possible return flow (undertow) over the crest may play a role.

From field observations it appears that probably a maximum of one-third of the (highest) waves make a complete breaking and that although breaking may start on the seaward slope of the bar it may actually take place on or close to the crest of the bar. Most waves seem to slip over the bar unbroken or without completing a breaking although their height is close to the depth on the crest of the bar. During the peak of the storm wave activity the number of breaking waves may be 50%.

For the computations mentioned below it is assumed that waves with actual height of H 1/3 (the average of the highest one-third of all waves) and up determined the elevation of the bar crest. This situation may be said to correspond to the swell situation after the peak of the wave action during the storm has been passed. Such situation will last considerably longer than the peak period. The "H 1/3 wave" is in the following named H (1/3) to distinguish it from the significant wave height H 1/3.

Based on the above mentioned results from laboratory and field experiments the breaker depth h_b is assumed to be equal to H_b and Dcr (depth over crest of bar) = 0.8 H_b (1/3). This assumption seems reasonable but remains to be checked more closely. To find the inflow of water from wave breaking and to relate that to known bar data, the actual breaking depth h_b for individual waves must be put in relation to Dcr. Reflection, usually of the order 5 to 10 per cent, as it may be seen during storms must be taken into consideration too.

One has: $h_b = H_b\ (1/3)$, $h_{bp} = H_{bp} = 1.25\ Dcr \frac{H_{bp}}{H_b\ (1/3)}$

Assuming 10 per cent reflection of wave height the breaker depth h_{bp} to be used for computation of Q_{bp} (the volume of water per unit length of wave crest) is $0.9 \times 1.25 \times Dcr \frac{H_{bp}}{H_b\ (1/3)} = 1.12\ Dcr \frac{H_{bp}}{H_b\ (1/3)}$.

Using the solitary wave theory on breaking waves (Munk, 1949) and considering Q_B as the inflow over a time period corresponding to H (1/3) actual height one has:

$$Q_B = \int_{H_b(1/3)}^{H_b(1/\infty)} Q_{bp}\, p(H_{bp})\, dH_{bp} = \int_{H_b(1/3)}^{H_b(1/\infty)} 4(1.12)^2 D_{cr}^2 \left(\frac{H_{bp}}{H_{b(1/3)}}\right)^2 \sqrt{\frac{\gamma}{3}}\, p(H_{bp})\, dH_{bp}$$

$\gamma = \frac{Hbp}{hbp}$ is considered to be constant and equal to one. This will be almost true, and smaller deviations are unimportant because of the square root.

One has: $$Q_B = \int_{H_{b(1/3)}}^{H_b(1/\infty)} 1.69\sqrt{3}\, D_{cr}^2 \left(\frac{H_{bp}}{H_{b(1/3)}}\right)^2 p(H_{bp})\, dH_{bp}$$

The statistical distribution of wave heights at breaking is so far little explored, but for the steep storm waves the distribution cannot be too different from the deep water spectrum. A comprehensive research program on this subject from towers placed in the ocean is being undertaken in Holland. For the computations below it is assumed that Longuet-Higgins' (1952) results for deep water waves are valid. With p indicating probability density one has: $p(H)\, dH = e^{-\frac{H^2}{a^2}} \frac{2H}{a^2}$ dH or $\frac{p(H)}{a} = e^{-\frac{H^2}{a^2}} \frac{2H}{a}$ where p (H) dH = probability that any wave height H will occur between H and H + dH and $\bar{a}^2 = \frac{1}{N}(H_1^2 + H_2^2 + \text{----} + H_N^2)$ or the mean of the squares of all occurring wave heights.

By taking

$$\frac{H_{b(1/3)}}{\bar{a}} = 1.416 \quad \text{or} \quad H_{b(1/3)} = 1.416\,\bar{a} \quad \text{then}$$

$$Q_B = \frac{1.69\sqrt{3}}{(1.416)^2} D_{cr}^2 \int_{H_{b(1/3)}}^{H_b(1/\infty)} \left(\frac{H_{bp}}{\bar{a}}\right)^2 e^{-\left(\frac{H_{bp}}{\bar{a}}\right)^2} \frac{2H_{bp}}{\bar{a}}\, d\left(\frac{H_{bp}}{\bar{a}}\right)$$

Noting $\frac{H_{b(1/3)}}{\bar{a}} = 1.416$, $\frac{H_{b(1/\infty)}}{\bar{a}} \to \infty$ the expression of Q_B is readily to be written into

$$Q_B = 1.46 \cdot 2 D_{cr}^2 \int_{1.416}^{\infty} \left(\frac{H_b}{\bar{a}}\right)^2 e^{-\left(\frac{H_b}{\bar{a}}\right)^2} \frac{H_b}{\bar{a}} d\left(\frac{H_b}{\bar{a}}\right)$$

$$= 2.92 D_{cr}^2 \int_{1.416}^{\infty} \left(\frac{H_b}{\bar{a}}\right)^3 e^{-\left(\frac{H_b}{\bar{a}}\right)^2} d\left(\frac{H_b}{\bar{a}}\right)$$

Let $\frac{H_b}{\bar{a}} = x$ and change to numerical integration, then

$$Q_B = 2.92 D_{cr}^2 \sum_{1.416}^{\infty} x^3 e^{-x^2} \Delta x$$

Example: From Fig. 2

$$D_{cr} = 4.4\ m, \quad H_{b(1/3)} = 1.25 D_{cr} = 5.5\ m, \quad \bar{a} = \frac{5.5\ m}{1.416} = 3.89\ m$$

Taking $\Delta \frac{H_b}{\bar{a}} = \Delta x = 0.05$

then

$$Q_B = 2.92 D_{cr}^2 \cdot 0.05 \sum_{1.416}^{\infty} x^3 e^{-x^2}$$

The numerical gives Q_B = 12.1 m^3 per meter crest. The actual amount of water thrown in by the wave breaking is 12.1 $m^3 \cdot \cos \alpha_b$ per meter of the shore.

LONGSHORE CURRENTS IN ONE AND MULTI-BAR PROFILES RELATION TO LITTORAL DRIFT

Comprehensive investigations by Hartnack (1926) on the coast of Pommern in the Baltic revealed the existence of up to six longshore bar systems although these systems were not continuous over a considerable length of shore. Along the Danish North Sea coast the number of bars increases in the direction of littoral drift from no bar at the very steep shore at Thyboroen located at the Lime Inlet to three to four bars at Skagen on the northernmost tip of Denmark, a distance of about 100 miles (Bruun, 1954). A similar phenomenon associated with decreasing steepness of the offshore bottom profile occurs when moving 70 miles south on the North Sea coast towards Blaavands Huk.

Each trough between the single bar systems carries its own longshore current and each bar system probably develops its own rip currents although because of the inertia included in a rip current it seems likely that one particular rip current may shoot directly through more than one (row of) bar(s), an assumption which seem to be confirmed to some extent by field observations.

When a wave breaks the water masses which it holds have a longshore velocity beforehand which may contribute to the longshore velocity inside the bar but the water included in the wave-breaking is derived from an area which does not carry strong longshore currents. When the water runs out again in a rip current longshore momentum is lost from the trough inside the bar and probably little longshore momentum is gained by the area or trough outside the bar because the rip current is nearly perpendicular to the shoreline. It receives water from both sides of the trough at its root.

APPROACH BASED ON REGULARLY SPACED RIP CURRENTS

Assumption for the approach described below, is that bars in a bar profile were built up by wave action with wave height characteristics as indicated by the water depth over the bars. It must be assumed that the individual parts of the bottom profile including bars, troughs, and the corresponding slopes, are in some kind of mutual interior balance with each other and with the wave and current forces which shaped them. Inasmuch as the depth surveys of such profiles are carried out not during, but after the storm it is not permissible uncritically to identify the calm weather (swell) profile with the stormy weather (steep-wave) profile. Certain adjustments of the storm profile took place at the end and after the storm. We do not know much about the quantitative extent of

these changes, but the qualitative trend undoubtedly goes in the direction of less depth over the bar during swell periods (Figure 2). The bar itself also moves a little closer to shore, thereby tending to decrease the cross-sectional area of the trough. A long calm-weather period may materially influence the configuration of the trough close to shore but may have comparatively little influence on troughs (and bars) farther offshore. The Coastal Engineering Laboratory of the University of Florida has initiated a field research program on this topic combined with littoral drift tracing with luminescent material.

Consider now a shore length of e.g. 1000 to 2000 ft., having transport of water perpendicular to the shore in the breaking zone and longshore transport of water in the trough between bar and shoreline. It is known that the longshore trough currents are irregular in velocity and in direction and it is observed that they flow toward the root of the rip current from both sides. Even if the general direction of the longshore current is indicated by the direction of wave approach and the breaker angle there is a local reversal of flow at every root of a rip current.

Rip currents occur at intervals determined by wave and offshore bottom characteristics. Larras (1957) lists 500 meters as an average space. They can usually be seen from the beach and are easily recognized from an airplane. They occur together with a lowering in the bar profile which moves slowly in downdrift direction (or it may jump a greater distance during storm periods). The flow characteristics (velocity and distribution of flow) in the longshore trough will gradually vary. Maximum cross-sectional area of the trough corresponds to maximum flow, but minor flow quantities do not necessarily cause the cross-sectional area (immediately) to adjust itself accordingly. This takes time. At the root of the rip current the shoreline will usually conform with the local flow conditions, and it may develop an S-shape or slight tombolo-like formation caused by the rip currents opposing the wave action. This may increase the loss of energy by wave breaking and change the wave characteristics, causing less erosive action.

In the theory mentioned below it is assumed that water derived from the breaking waves over a certain length parallel to shore flows out where hydraulically speaking it is easiest and because the inflow over the bar has caused a buildup of

head-difference between the (average) water table on the seaward and the shoreward side of the bar. It can still be discussed whether the more or less regularly spaced lowerings in the offshore bar system are caused by rip currents or whether the currents seek these incidental openings for discharge but this problem does not affect the theory discussed below. Also it must be assumed that part of the water may flow back over the bar outside the lowerings in a magnitude, depending upon how well the bar and trough are developed.

With reference to Figure 3:

$\frac{Q_B \cos \alpha_b}{T}$ = inflow per unit length of shore per sec from a breaking wave of known wave characteristics.

1 = average distance between rip currents, 1' is the effective distance of unidirectional longshore flow or a reduced 1, the reduction caused by a local reversal of flow at the root of the rip current.

A = the trough cross sectional area which carries a quantity of flow corresponding to the distance 1'.

The general expression for current velocity V_x at distance x from the point where the longshore current velocity is zero is:

$$V_x = \frac{Q_{Bx} \cos \alpha_b \cdot x}{A_x \cdot T}$$

With $x = 0$, $V_x = 0$ and A_x could in fact be zero too inasmuch as it does not carry any flow. Figure 4 is an aerial photo from the south shore of Long Island at East Hampton and shows a rip current and a bar/trough system where x and A_x seems to have such "ideal" linear relationship. This will normally not be the case and longshore current velocity will increase from $x = 0$ until $x = 1'$ and attain a maximum velocity:

$$V = \frac{Q_B \cos \alpha_b \, 1'}{A \, T}$$

In this expression only the preservation of water mass is considered. Writing $V_m = C_f \sqrt{\tau_s / \rho g}$ where V_m = the mean velocity of trough current, C_f = Chezy's friction coefficient,

τ_s = "the determining shear stress for bottom stability" (Bruun and Gerritsen, 1960), g = the acceleration of gravity and ρ = the density of water, one has:

$$\frac{l' Q_B \cos\alpha_b}{A T} = C_f \sqrt{\tau_s/\rho g} \quad , \quad A = \frac{(Q_B l' \cos\alpha_b)}{C_f \sqrt{\tau_s/\rho g}}$$

Table 2 has τ_s and the corresponding v-values, computed on the basis of Figure 2's average values of A ($1030 m^2$) and with breaker angle α_b = 25 degrees which with steep waves occurs with α_o = about 45° to 50°, T(1/3) = 8 and 10 sec all in agreement with observations and C_f values are 35 and 45 (metric) in accordance with results from tidal inlets. The above mentioned formula $C_f = 30 + 5 \log A$ gives $C_f = 45$ $m^{\frac{1}{2}}/sec$. Currents are computed for values of l' of 300 to 600 meters from actual observations and the Q_B value is based on breaking waves from probability p = 0.135 to p = $1/\infty$ corresponding to Figure 2 as mentioned in paragraph 3 when a Q_B value of $12.1 m^3$ per meter of the breaking wave crest was found.

Table 2. Continuity Rip Current Approach for Prototype Characteristics Corresponding to Figure 2.

α_b degrees	L_b meters	T(1/3) sec ave.	H_b(1/3) meters	l' meters	τ_s (C_f = 35 $m^{\frac{1}{2}}$/sec) kg/m^2	τ_s (C_f = 45 $m^{\frac{1}{2}}$/sec) kg/m^2	V_m meter/sec
25	55.0	8	5.5	300	0.130	0.078	0.40
				400	0.230	0.140	0.53
				500	0.360	0.218	0.67
				600	0.518	0.314	0.80
25	72.0	10	5.5	300	0.083	0.050	0.32
				400	0.148	0.089	0.43
				500	0.230	0.139	0.53
				600	0.332	0.201	0.64

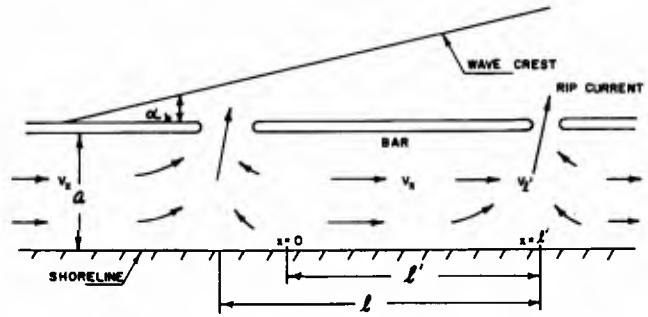

Fig. 3. Rip current approach.

Fig. 4. Bar, trough, beach and rip current at East Hampton, L. I.

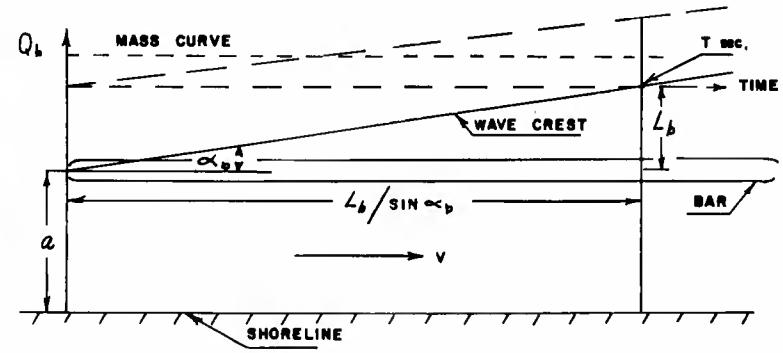

Fig. 5. Inflow under an angle with the shoreline approach.

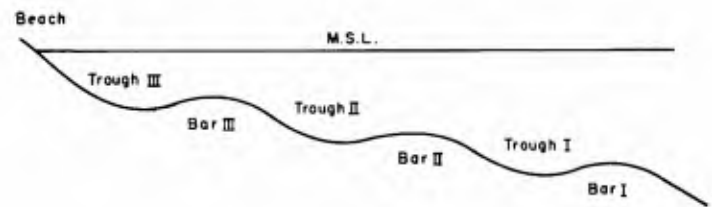

Fig. 6. Multi-bar profile, schematic.

With a 500-meter space between the rip current's average values of approximately 0.3 kg/m^2 for shear stresses and approximately 0.6 m/sec for velocities are obtained considering normal storm waves of $T(1/3) = 8$ sec. and $C_f = 35 m^{\frac{1}{2}}/sec$ (Table 1). When compared to the corresponding values for tidal inlets these figures are low. One explanation for this may be that the A value is counted higher than it actually is. Currents fill only part of the wave trough indicated in Figure 2. A reduction of A to 2/3 of its value or 700 m^2 gives values for τ_s and V which are close to the results from tidal inlets where τ_s for currents heavily loaded with sediments is approximately 0.50 kg/m^2 with velocities of about 0.9 - 1m/sec. Another and perhaps more correct explanation is mentioned in section 5 dealing with longshore currents in a multi-bar profile. The relatively low value of τ_s may be caused by the wave action.

APPROACH BASED ON INFLOW OF WATER UNDER AN ANGLE WITH THE SHORELINE

Consider a wave approaching the shore (Figure 5). Its wave length when breaking is L_b, breaker angle α_b and content of water mass per unit length Q_B. The inflow of water over a length of shore of unit length is $Q_B \cos \alpha_b$ in T sec. Water from a length of wave crest corresponding to one wave length L_b passes in over a length of shore of $L_b/\sin \alpha_b$. Total inflow of water in T sec over $L_b/\sin \alpha_b$ length of shore is $Q_B L_b \operatorname{cotg} \alpha_b$. A unit width of shore gets $\frac{Q_B \cos \alpha_b}{T}$ per sec. The inflow over a unit width takes place in $\frac{T \sin \alpha_b}{L_b}$ seconds. Assuming that the water table behind the breaking point is comparatively even and horizontal, the water level theoretically raises $\frac{Q_B \cos \alpha_b \sin \alpha_b}{1 \cdot a \cdot L_b}$ where a is distance from inside bar to the shoreline. One unit length downstream the water table is still undisturbed by the breaking wave, for which reason the slope of the water surface $I = \frac{Q_B \cos \alpha_b \sin \alpha_b}{1 \cdot a \cdot L_b} = \frac{Q_B \sin 2\alpha_b}{2 a L_b}$. Using Chezy's formula one has: $V_m = C_f \sqrt{R I}$ where R is hydraulic radius of trough.

It is here assumed that the water flows out again uniformly across the crest of the bar. This will normally not be the case because of the existence of rip currents but with rip currents spaced a considerable distance apart it will be true for a certain distance longshore. Close to the rips velocity may increase because of increase of slope caused by the discharge.

Table 3 has V-values computed on the basis of Figure 2's average values of A and the corresponding value of a and with the same A, T, and C_f values as determined in the preceding paragraph.

Table 3. Longshore Current Velocities Based on Inflow of Water under an Angle with the Shoreline for Prototype Characteristics Corresponding to Figure 2.

α_b degrees	L_b meters	T(1/3) sec ave	H_b(1/3) meters	Vm meter/sec ($C_f = 35m^{\frac{1}{2}}/sec$)	Vm meter/sec ($C_f = 45m^{\frac{1}{2}}/sec$)
25	55.0	8	5.5	1.20	1.55
25	72.0	10		1.12	1.45

With $T_{(1/3)} = 8$ sec and $T_{(1/3)} = 10$ sec and $C_f = 35m^{\frac{1}{2}}/sec$ these velocities are directly comparable to those found for tidal inlets. With $C_f = 45m^{\frac{1}{2}}/sec$ corresponding to the logarithmic formula they are somewhat high. This could be expected because of the idealized conditions. Moreover it should be remembered that Chezy's formula is valid for uniform flow, and a longshore wave current can hardly be classified as such.

COMPARISON WITH PUTNAM, MUNK, AND TRAYLOR'S MOMENTUM APPROACH

In order to make a comparison with this approach, current velocities were computed for the same profile and wave characteristics as used in earlier approaches. The velocity of the water particles at wave breaking is equal to the wave celerity $C = \frac{L_b}{T}$. Results are given in Table 4, which shows very high velocities that are not in agreement with field experience.

Table 4. Longshore Current Velocities Based on the Momentum Approach by Putnam, Munk, and Traylor, (bar-profile Figure 2 characteristics).

α_b degrees	L_b meters	$T_{(1/3)}$ sec ave	$H_b = H_{(1/3)}$ meters = 1.25 Dcr	Vm meters/sec
25	55.0	8	5.5	2.6
25	72.0	10	5.5	2.6

In this respect it should be remembered that waves are regenerated behind the bar after breaking, by which process momentum is transferred as wave and not current momentum. This will cause current velocities to be high by 10 to 30 per cent if computed without a proper reduction for regeneration of waves (Mashima, 1958).

Furthermore the longshore current was computed for the part of the profile located inside the 4.4m (equal to Dcr) depth contour in the profile (Figure 2) using Hm = Dcr and integrating from p = 0.5 to p = ∞

Results are given in Table 5, and it may be seen that current velocities are even higher than in Table 4. The k value according to Inman and Quinn (1952) is approximately 0.0007, corresponding to a very high and unrealistic C_f value (Table 1). Conditions on a sloping beach are neither comparable to trough nor tidal inlet conditions. Velocities of the order indicated in Table 5 may occur instantly but hardly averagely.

Table 5. Longshore Current Velocities Based on the Momentum Approach by Putnam, Munk, and Traylor (no-bar profile, Figure 2 slope characteristics).

α_b degrees	L_b meters	$T_{(1/3)}$ sec ave	H_b = Hm = Dcr meters	Vm meters/sec
25	55.0	8	4.4	> 3.0
25	72.0	10	4.4	< 3.0

5. LONGSHORE CURRENTS IN MULTI-BAR SYSTEM

Reference is made to the schematic Figure 6 depicting a multi-bar profile.

When waves have passed over the outermost bar no. I they continue travelling across the trough between the bars until breaking takes place on bar no. II. The wave height which determines the depth over the crest of bar no. II is assumed to have the same ratio to this depth as valid for bar no. I or:

$$\frac{H\ (1/3\ b1)}{H\ (1/x\ b2)} = \frac{D(cr1)}{D(cr2)} = k(1.2)$$

In the one-bar profile H(1/3 b1) = 1.25 (Dcr1) and can be computed from known Dcr data. H(1/x b2) in the above equation is H(1/3 b1)/k(1.2) where k(1.2) is determined from known Dcr data. Using Longuet-Higgins distribution of wave heights and frequencies the probability (p) value corresponding to H(1/3 b1)/k(1.2) can be found.

The corresponding Q_{B2}' value for the amount of inflow of water by breaking of waves the height of which lie between the boundaries mentioned above is:

$$Q_{B2}' = \int_{H(\frac{1}{x}b2)}^{H(\frac{1}{3}b1)} A(1/2)^2 (D_{cr})^2 \left(\frac{H_{bp}}{H(\frac{1}{x}b2)}\right)^2 \sqrt{\frac{r}{3}}\, p(H_{bp})\, d(H_{bp})$$

This quantity flows in during a period corresponding to the waves represented by the integration limits.

To this quantity has to be added the contribution by the waves which broke on bar no. I. A broken wave may not be regenerated as a single wave but as two or three waves with the result that the (apparent) wave period after wave breaking is smaller than the period before wave breaking. In the reasonings made below it is assumed that only one wave is regenerated. The height of this wave depends upon the loss of wave energy by the breaking process.

It is observed in the field that more waves break on bar no. II than on bar no. I and that more waves break on bar no. III than on bar no. II. The average height after first wave breaking therefore probably lies between H(1/3 b1) and D(cr2).

It is assumed that it is D(cr1)although there is no direct field experimental proof of this postulate. The Q_B quantity derived from these waves is:

$$Q_{B2}'' = 4\left[0.9\ D(cr1)\right]^2 \cdot \sqrt{\frac{r}{3}} \cdot p$$

(p = probability of occurrence)

This quantity of flow passes in during a period of time corresponding to T(1/3) from the breaking on bar no. I. T(1/3) is to be understood as the average value of periods in the spectrum from $T_{1/3}$ actual period and up.

Passing on to bar no. III the same approach may be used. One has:

$$\frac{H(1/3\ b2)}{H(1/x\ b3)} = \frac{D(cr2)}{D(cr3)} \text{ which gives } H(1/x\ b3)$$

The inflow of water over bar no. III, Q_{B3} is composed of the same two quantities as mentioned above:

$$Q_{B3}' = \int_{H(1/x\,b3)}^{H(1/x\,b2)} A(1/2)^2 \cdot D_{(cr3)}^2 \cdot \left(\frac{H_{bp}}{H(1/x\,b3)}\right)^2 \sqrt{\frac{r}{3}}\ p(H_{bp})\,d(H_{bp})$$

This water flows in during a period of time corresponding to an average value of the integration limits. To this must be added:

$$Q_{B3}' = 4\left[0.9 \cdot D(cr2)\right]^2 \cdot \sqrt{\frac{r}{3}} \cdot p$$

(p = probability of occurrence)

This quantity of flow passes in during a period of time corresponding to the integration limits for the inflow from breaking waves over bar no. II.

For computation of the longshore current the slope approach should be used because the rip current approach assumes knowledge about the outflow of water through a multi-bar system and such knowledge will hardly ever be available $r = 1$ as in preceding chapters of this article.

For the longshore current in trough no. I/II (between bars no. I and II) the Q_B-value to be used should be:

$$Q_{B1}' - (Q_{B2}' + Q_{B2}'')$$

with the corresponding A and α_b-values.

For the longshore current in trough no. II/III (between bars no. II and III) the Q_B-value to be used should be:

$$(Q_{B2}' + Q_{B2}'') - (Q_{B3}' + Q_{B3}'')$$

with the corresponding A and α_b-values.

Examination of a multi-bar profile including four bars surveyed repeatedly at the Old Skaw at the northernmost tip of the Danish North Sea coast (Figure 7) has given the average values for Dcr listed in Table 6 below. Table 7 indicates average values of trough areas between the bars measured between verticals placed at the top of the crest of the respective bars.

Table 6. Depth in Meters on Crest of Bar, Average of 5 Profiles Spaced Approximately 100 Meters Apart

Bar no.	I	II	III	IV
Depth, m	4.4	3.0	1.5	0.5

Table 7. Average Area in Square Meters of Trough Between Bars of 5 Profiles Spaced Approximately 100 Meters Apart

Trough no.	I/II	II/III	III/IV
Area, m^2	$15{,}8 \cdot 10^2$	$8.2 \cdot 10^2$	$2.6 \cdot 10^2$

With respect to the interrelation between depth on bar and area of trough in the multi-bar profile it should be remembered that the overall profile as we find it by surveys (in the summer time) does not necessarily correspond to one particular storm which created wave breaking on all bars. Most storms will hardly interfere with the outermost bar. Comparing conditions in the summer and winter seasons it is obvious that the nearshore bars will be most affected by the

wave activity in the summer season while the offshore bars are mainly related to winter storms. The bars may migrate a little closer to shore in the summer season and this may change the elevation of the crest slightly and also the configuration of the trough. Based on experience with one-bar as well as multi-bar profiles changes may not be very important (see Figure 2) and similar experience is available for the situation depicted in Figure 7.

Assuming a storm causing wave action with an average period of 8 sec by waves from $T_{1/3}$ and up and heights $\geq H_{1/3}$ actual height at breaking on bar no. I, the Q_B-values over four bars are computed as listed in Table 8.

Table 8. Q_B-Values in Cubic Meters Per Meter of Wave Crest for Multi-Bar System.

Bar no. I		Bar no. II		Bar no. III		Bar no. IV	
Q_{B1}'	Q_{B1}''	Q_{B2}'	Q_{B2}''	Q_{B3}'	Q_{B3}''	Q_{B4}'	Q_{B4}''
12.1	0	5.14	3.48	0.78	3.12	0.09	1.20
$\Sigma Q_{B1} = 12.1$ m^3/m of crest		$\Sigma Q_{B2} = 8.6$ m^3/m of crest		$\Sigma Q_{B3} = 3.9$ m^3/m of crest		$\Sigma Q_{B4} = 1.3$ m^3/m of crest	

The corresponding T-values are listed in Table 9.

Table 9. T-Values in Seconds Corresponding to Table 8's Q_B-Values

Bar no. I		Bar no. II		Bar no. III		Bar no. IV	
Q_{B1}'	Q_{B1}''	Q_{B2}'	Q_{B2}''	Q_{B3}'	Q_{B3}''	Q_{B4}'	Q_{B4}''
T = 8 sec		T = 6.6 sec	T = 8 sec	T = 5.7 sec	T = 6.6 sec	T = 4.9 sec	T = 5.7 sec

With $\alpha_{b1} = 25^\circ$, $\alpha_{b2} = 21^\circ$ and $\alpha_{b3} = 15^\circ$ the current velocities listed in Table 10 are obtained.

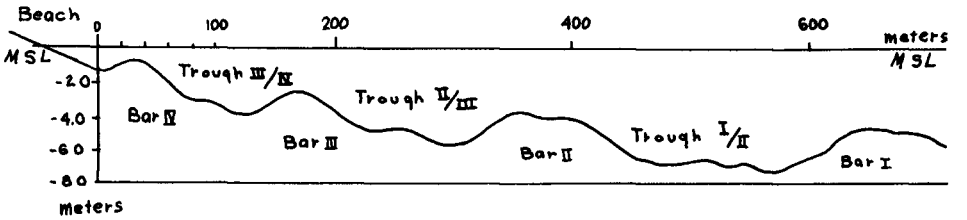

Fig. 7. Multi-bar profile at The Old Skaw, Denmark.

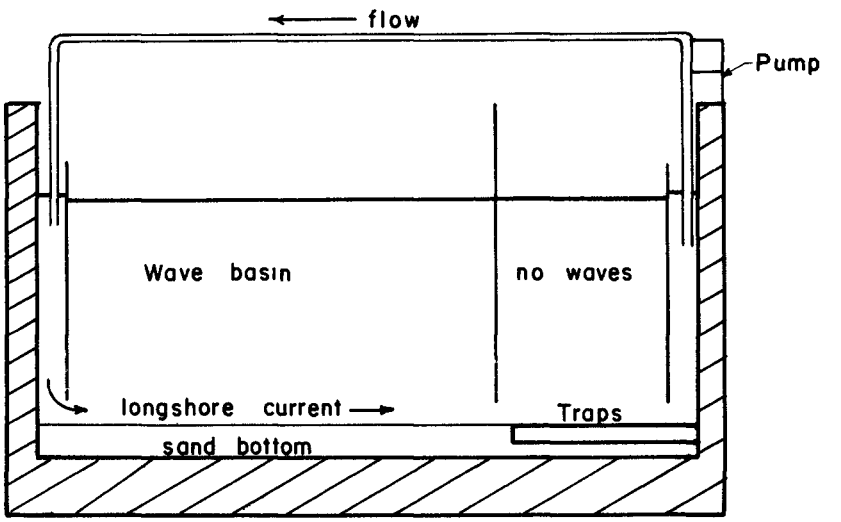

Fig. 8. Wave tank experiment on bed transport.

Table 10. Current Velocities in Meters Per Sec. in Troughs nos. I/II, II/III and III/IV C_f = 35 or 45 $m^{\frac{1}{2}}$ sec^{-1}

C_f $m^{\frac{1}{2}}/sec$	Trough no. I/II Q = 3.48 m^3/m	Trough no. II/III Q = 4.72 m^3/m	Trough no. III/IV Q = 3.90 m^3/m
35	0.4 m/sec	0.7 m/sec	0.5 m/sec
45	0.5 m/sec	0.9 m/sec	0.7 m/sec

These velocities seem to be realistic and are in good agreement with velocities derived from tidal hydraulics computations for inlets with alluvial bottom (Bruun and Gerritsen, 1960, referring to its Table 5's (p. 67) figures for τ_s under moderate to heavy wave action which corresponds to velocities of 0.5 to 0.8 m/sec as we have found here).

It is natural that currents in the multi-bar profile are slower than in the one-bar profile (Table 3) where the breaking wave delivers all of its water in one breaking while in a multi-bar profile water from each trough is passed on by breaking into the next following trough.

With respect to transfer of momentum from one trough to the other such transfer, needless to say, does take place but it is not accounted for in the above considerations. It should not be forgotten, however, that the transfer of water takes place from an area just outside the bar where longshore trough velocities are smallest. A certain momentum should still be added but at the same time another momentum derived from the loss of a similar quantity of water by outflow from the trough inside the bar in question to the trough outside the bar in question reduces the momentum of water flow inside the bar. If velocities are equal on both sides of the bar the final result may be close to zero. During storm conditions which are determining for pertinent dimensions of bars and troughs, velocities may not differ too much but local increases and decreases may occur in the area where water flows out more concentrated as e.g. in rip currents instead of in an equally distributed "undertow". Currents will then be accelerated on the updrift side of the rip and decelerated or even reversed on the downdrift side. Such situation is most predominant when waves propagate in a direction which is not far from being perpendicular to the shoreline. With waves coming in under a great angle of incidence (as they do at the Old Skaw) rips still come into existence but they may be turned downstream.

6. DISCUSSION

Comparing the results indicated in Tables 2 to 5, it may be seen that the continuity approach whether in the "rip current" or the "inflow under an angle" or "slope" approach gives realistic values for velocities and/or shear stresses for the above mentioned one-bar profile depicted in Figure 2. The momentum approach seems to give values which are too high for this profile and undoubtedly also too high for the longshore current inside the final breaking point on the beach, although such velocities may occur instantly in a narrow belt close to the breaker line at steep beaches.

It is encouraging to see that the continuity approach in the inflow under an angle version seems to be very suitable for use in a multi-bar profile as demonstrated by the velocities in Table 10. As in case of the one-bar profile, velocities are realistic and compare well with velocities found for tidal inlets in alluvial material although the velocity distribution and pattern must differ somewhat in the two cases.

Generally it may be said that the continuity approach, whether in the "rip current" or in the "longshore slope" approach, has an advantage over the momentum approach, because when used in a one or multi-bar bottom profile no reduction of momentum caused by the formation of waves inside the breaking point has to be considered. After breaking on the bar waves will travel shoreward and finally break on the beach slope, giving rise to up and down rush and a corresponding longshore zig-zag current superimposed on the current derived from earlier breakings. The momentum available inside the first breaking point is the difference between the momentum in the breaking wave and the momentum used for the formation of waves behind the bar after breaking. By not taking the formation of new waves into consideration the current based on the momentum approach will be too high, as mentioned above. The momentum approach for bar profiles is also less applicable because one is not only faced with the normal problem of selecting the waves which actually break over the bar, but also with the problem of a proper momentum reduction because of regeneration of waves behind the bar. The continuity approach also includes the problem of selection of waves which break, but the mass transport in the relatively smaller waves in the spectrum is less important. Reflection of wave energy occurs in both cases but is of minor importance.

The continuity approach compared to the momentum approach has one very definite advantage because it does not include an uncertain determination of the velocity of the water particles in the breaking wave. It seems, therefore, to be a reasonable conclusion that the continuity approach has several advantages in one or multi-bar profiles. On the other hand the longshore current occurring in connection with the final wave breaking and up and down rush on the beach itself may be computed by the momentum approach which was developed mainly for this particular case. The continuity approach ignores the momentum which does occur during wave breaking, but it is a fact that not too much is felt of that momentum at a certain distance inside the bar(s). Most of it disappears because of high turbulence and therefore rapid decrease in velocities just inside the bar.

On the other hand it is clear that this longshore current problem is of such a nature that it discourages a pure "desk-approach." It is necessary to go out in the field and make observations in order to furnish the data necessary for a reliable evaluation and computation. It may therefore be said that the continuity approach, particularly when based on a rip current distribution, requires prior information on the result one is seeking, but in this respect it should be remembered that after a certain number of observations a file of data may be built up allowing a reduction of field observations and permitting a higher degree of pre-determination by straight computation.

The field information needed is, first of all, detailed knowledge about the bottom topography and its fluctuations. Next, knowledge about the wave spectrum and the approach angle of wave crests is needed. An evaluation of the bottom friction must be based on experience, inasmuch as a pure estimation of relative roughness using results from fluid mechanics technology would not furnish us with any useful figure. Laboratory experiments of the nature depicted in Figure 8 and mentioned in the following section may be able to furnish valuable information useful in the prototype.

7. LITTORAL DRIFT AND LONGSHORE CURRENTS

The longshore littoral transport of material is caused by a combination of shear stresses by wave action which "breaks loose" the material and shear stresses by longshore currents which transport the material parallel to shore.

LONGSHORE CURRENTS IN ONE AND MULTI-BAR PROFILES RELATION TO LITTORAL DRIFT

The main direct contribution to the material movements by the waves is almost perpendicular to the shoreline and the maximum velocities of the oscillating water movement will normally exceed the longshore current velocities considerably. But the longshore material movement is still caused by the longshore current. If it were not there no longshore movement would take place.

In a uniform flow, shear stress between flow and bottom $\tau = \rho V_x^2$. The work transferred to the bottom is, therefore, proportional to $\tau \cdot f(V_x) \sim V_x^3 \sim \tau^{3/2}$ (Bagnold 1956). This work is used for bed-load movement and for stirring up material by lift forces which are also proportional to τ. The actual magnitude of bed-drift may depend upon $(\tau^{3/2})^n$ where n varies according to different authors from 1 to 2 with some modifications in power relationship mainly due to the introduction of τ_c which is the shear stress by which movement of bed material starts.

Considering the situation on sea shores and combining the material moving forces perpendicular to as well as parallel to shores it may be assumed that the magnitude of drift per unit area of the bottom is a function of W_* (in oscillating wave motion) times a function of V_* (in the longshore current) or $f(W_*) \cdot f(V_*)$.

Certain experiments of recent date seem to reveal that the erosion of a sand bottom in turbulent flow is proportional to the square of the standard deviation of velocity fluctuations σ^2 which in turn is proportional to $V_*^2 \sim \tau$. The work to be done to move the material perpendicular to shore is $\tau_{W_*} \sim W_*^3 \sim \tau^{3/2}$.

Bretting's (1960) expression for bed-load transport $q_s = 0.0617 \left(\frac{\tau}{\tau_c} - 1\right)^2 d_m^{3/2} \left(\frac{m^3}{m\ sec}\right)$ includes the factor $(\tau/\tau_c - 1)^2$ which for high values of $\tau/\tau_c \sim \tau^2$. DuBoys' and Shields' bed load formulas of earlier date have similar relationships.

With waves and longshore currents combined the total water current along the bottom includes as described above an oscillating wave part which is almost perpendicular to shore and an alongshore component by the longshore current. The first component will usually have the main responsibility for breaking loose the material from the bottom (by τ trans-

versal-shear stresses) while the longshore current carries the material sideways (by τ longshore-shear stresses). There seems, therefore, to be some reason to make the littoral transport per unit area proportional to $\tau_{trans} \times \tau_{longs}$ rather than $(\tau_{trans})^2$ or $(\tau_{longs})^2$. One has $\tau_{trans} \sim \frac{H^2}{T^2}$ for Stokes finite height waves and $\tau_{longs} \sim \frac{H^2}{T^2} \sin 2\alpha_b$ using the longshore slope theory described in section 4. Assuming that hydraulic radius of the longshore trough is proportional to the breadth "a" of the bottom affected by wave action one has $a \sim H$. This gives $\tau_{trans} \cdot \tau_{longs} \cdot H \sim \frac{H^5}{T^4} \sin 2\alpha_b \sim H^2 L \sin 2\alpha_b$ in as much as $H \sim T^2 L$ for storm waves. Similar reasonings may be made with Solitary and Cnoidal waves where the horizontal orbital velocity is $\sim\sqrt{g(H + d)}$. That the expression above is similar to the so-called "Los Angeles formula" according to which the littoral drift is proportional to the longshore wave energy should only be understood as "a possible indication of similarity." It is in this respect interesting to note that the results of laboratory experiments by Krumbein as explained by Bruun (1951) may be arranged on a second order parabola, or: $QT/L_o^2 H_o = k(\frac{H_o}{L_o})^2$ which gives $Q = k\, E_f \cdot \frac{H_o}{L_o}$ valid up to $\frac{H_o}{L_o} = 0.035$. (Q = quantity of drift).

The "Los Angeles formula" might to some extent have been confirmed by field experience. See Caldwell (1956) and Lillevang (1960). It points in the direction of maximum drift for breaker angles of 30°-40° which in turn corresponds to a α_o of 45° to 70°, all depending upon wave and depth characteristics.

Laboratory experiments showed maximum at 30° to 40° (see Johnson, 1951, 1952, and Savage, 1962), but this result should not be transferred uncritically to field conditions. Larras (1957) lists, with reference to Sauvage and Vincent, 53° (1954) based on laboratory experiments, Zenkovitch found 35°-40° on shingle beaches (1962) and Bruun (1954) approximately 50°-55° from field experiments of coastal morphology nature on prototype enminiature sand beaches. It is not likely that any "maximum angle" exists. It must vary with wave, bottom and bottom material characteristics.

Based on data from Florida (South Lake Worth Inlet) and Anaheim (California) Caldwell (1956) found the relationship:

$$M = 210\ E_f^{\ 0.8}$$

where M is the alongshore drift in cu. yd. per day and E_f is alongshore energy in millions of ft-lbs per day per foot of beach. This formula only deviates from the "Los Angeles formula" by its power for E_f which is 0.8 instead of 1.0. It is interesting to note this reduced power relationship which may be interpreted in the way that waves with high energy effect as e.g. storm waves are not utilized for littoral transport to the same extent as waves with less effect, a phenomena which may be explained by the loss of energy by plunging wave breaking including formation of heat and foam. Reference is made to the above mentioned experiments by Krumbein which also indicate that with high H_o/L_o ratios wave energy is not as effective for littoral transport as with waves with lower steepness ratios.

Considerations of such nature are, needless to say, of a "superficial" nature but they may give a preliminary idea of the "possible importance" of some of the pertinent factors involved.

Going back to the more theoretical aspects of the problem the situation today is that the "breaking loose" forces are not well known and the longshore currents under a variety of boundary conditions are not known either. In order to obtain any rational results both must be investigated carefully, first separately and then combined.

Inasmuch as we still do not have a full understanding on bed-load transport phenomena in unidirectional flow there may still be a long road left before we obtain a more thorough understanding on the details of the movement under oscillating water movement. It would be a great step forward if some of the laws governing the migration of material under the influence of oscillating water motion could be revealed without going down to the very details. The movement of sand on a plane bottom has been investigated by a few authors as e.g. Ippen and Verma (1953) and Eagleson et al (1961), but so far few results have been obtained to correlate this movement with the actual water motion referring to the boundary layer just above the bottom where the irregular fluctuation of velocities mainly takes place for which reason lift and shear forces necessary for material transport are produced. Hydraulic tests on the bottom roughness and friction problem (disclosing material transport) with varying depth and wave characteristics

may give some valuable information of primary interest for later detailed research on actual friction and transport characteristics including travel velocity, thickness of sheet layer and quantity of sand movement.

By the establishment of a longshore current of well known characteristics in a basin under wave action (see the schematic Figure 8) knowledge about the drift under conditions which have a great similarity to natural conditions may be obtained. A circulation system for water as well as sand is needed to imitate nature as closely as possible. Primary two-dimensional experiments on the roughness factors alone should be made. It would be a further advantage if introductorily tests could be made with a fixed bottom allowing observation of the bottom turbulence independent of disturbances by jumping sand grains from the bottom which may make independent recording of water turbulence very difficult.

In the field, research should probably concentrate on separate evaluation of two important problems, namely:

(1) An evaluation of the concentration of material in movement in suspension as well as in the bed-load sheet layer under various conditions of wave action at various depths and with various material. The individual parts of the bottom cross-section including the bar, the trough and the uprush zone should be investigated separately.

(2) An evaluation of the longshore current in the same sections of the profile at various depths and with various wave (and tide) characteristics.

Re. (1) With respect to evaluation of the quantity of material available for longshore drift as suspended-load and as bed-load modern tracing technique may be very helpful. Samples may be secured to give a complete picture of the concentration of material in the entire profile under known wave conditions to be described by a wave height and period spectrum and/or by a power spectrum.

The thickness of the moving sheet layer may be determined in the field by luminescent or other tracers allowing an estimation of quantity of drift in a certain area as function of time. The results should be compared with laboratory experiments as mentioned above. Such tests are at this time (1962) in progress at the Coastal Engineering Laboratory of the University of Florida.

Re. (2) Various ingredients are included in the longshore currents and they all make their contribution to the longshore drift. It will, therefore, be necessary to know these currents under a variety of circumstances also including conditions with no wave but possibly tide action. This will require a very detailed and comprehensive current measurement program.

The difficulty in determination of longshore current characteristics lies in the confused current pattern and the corresponding recording difficulties. In case the water is not greatly loaded with material recording of the current pattern may be made using dyes, but because of diffusion dyes will usually only be able to give an idea about the order of magnitude of the velocity. For recording of actual velocities staffs with vanes at different depths, jelly bottles and rugged current meters operated from fixed installations as e.g. piers are needed. Corresponding recording of the travel velocities of tracer grains may make it possible to interrelate observed longshore current velocities with the velocities of the migrating sand grains and thereby allow an estimation of drift quantities based on a combination of wave and longshore current velocity data. Even though a detailed understanding may not be secured, thereby much important and useful information may be obtained.

8. SUMMARY AND CONCLUSION

(1) This paper gives information on the preliminary results on longshore current theories based on a continuity approach.

(2) The earlier proposed momentum approach for computation of longshore currents (Putnam, Munk, and Traylor, 1949) may be valid under simplified conditions of bottom topography, but it seems to be less applicable for more involved conditions of coastal morphological and hydraulic nature as e.g. occurring at bar profiles, because knowledge is assumed about mass transport as well as water particle velocities involved in a wave breaking.

(3) The continuity approach is related to prototype conditions in a more simple way. Momentum inflow is omitted because it does not seem to be of much importance with a well developed bar profile. The continuity approach is to be preferred for use in one and multi-bar profiles.

(4) For computation of longshore currents, occurring in troughs between bars, detailed knowledge about the wave spectrum and its development or time history from deep water to the breaking point(s) is needed. Future research should, therefore include detailed studies of wave mechanics nature in the field.

A very comprehensive research program on transformation of waves from deep water to the shore is being undertaken by the Dutch "Deltadienst," using several towers loaded with instruments and placed on a line perpendicular to shore on the North Sea coast.

(5) Laboratory and field experiments seem to have furnished some information on the relationships between littoral drift characteristics and wave characteristics with special reference to longshore wave energy but not much understanding of the basic principles involved in the transport.

Further progress may be obtained by:

a. Basic laboratory research including investigations of the nature of bed-load transport related to flow, material and bottom friction characteristics. An approach based on shear stress analysis to be extended from uniform flow into oscillating flow conditions seems preferable. It requires knowledge on friction characteristics and velocity distribution.

b. Laboratory and field research of basic nature concentrating on evaluations of macroscopic problems as the characteristics of the migrating sheet bed-load layer and its relations to wave and current characteristics, the characteristics of the suspended-load motion, its distribution in the profile and relation to wave and current characteristics and the magnitude of the material migrating along the shore in sand humps and waves.

c. Newly developed tracing techniques which may prove of great value in securing reliable data from the field, particularly data on transport rate in short periods of time with well known wave and current data. Such field experiments are in progress at the Coastal Engineering Laboratory of the University of Florida.

d. Based on the knowledge obtained it may be possible to calibrate future models with movable beds on basic principles for material transport rather than on "time history."

REFERENCES

Bagnold, R. A., 1956, The flow of cohesionless grains in fluids: Royal Soc. London Trans., Sec. A., V. 249, p. 235-297.

Beach Erosion Board, Corps of Engineers, An experimental study of submarine bars, Technical Report No. 3, 1948, 40 pages.

Bowden, A. J., 1962, The investigation of the transport of sediment in uniform systems by observations of tracer distribution, Hydraulic Research Station, Dept. of Scientific and Industrial Research, Report no. IN 25, (England).

Bretschneider, C. L., A theory for waves of finite height, Coastal Engineering No. 7, Proceedings of the 7th International Conference on Coastal Engineering in The Hague, Netherlands, Council on Wave Research, Berkeley, 1961, pp. 146-183.

Bretting, A. E., 1960, Hydraulik: Copenhagen Danish Technical Press, 518 p.

Bruun, P., Coast Stability, Danish Technical Press, 1954, 400 pages.

Bruun, P., and Gerritsen, F., "Stability of Coastal Inlets", North Holland Publishing Company, Amsterdam, 1960, 123 pp.

Caldwell, J. M., 1956, Wave Action and sand movement near Anahein Bay, California Tech. Memo. No. 68, Beach Erosion Bd, Corps of Engineers, U. S. Dept. of the Army.

Chang, Y. L., 1939, Laboratory investigation of flume traction and transportation, Trans. Am. Soc. of Civil Engineers, Vol. 104, pp. 1246-1289.

Eagleson, P. S., Glenne, B., and Dracup, J. A., 1961, Equilibrium characteristics of sand beaches in the offshore zone, M.I.T., Hydrodynamics Laboratory, Technical Report, No. 41.

Fuchs, A., On the theory of short-crested oscillatory waves, Inst. of Eng. Research, Univ. of Calif., Berkeley, Series No. 3, Issue No. 326, 1951, 10 pages.

Hartnack, W., Die Küste Hinterpommerns, Greifswald 1926.

Inman, D. L., and Nasu, N., Orbital velocity associated with wave action near the breaker zone, Corps of Engineers, Beach Erosion Board, Tech. Memo. No. 79, 1956, 43 pages.

Inman, D. L., and Quinn, W. H., Currents in the Surf Zone, Proceedings of the 2nd Conference on Coastal Engineering, Houston, Council on Wave Research, Univ. of Calif., Berkeley, 1952, pp. 24-36.

Ippen, A. T., and Kulin, G., Shoaling and breaking characteristics of the solitary wave, Massachusetts Institute of Technology, Hydrodynamics Laboratory, Technical Report No. 15, 1955, 56 pages.

Ippen, A. T., and Verma, R. P., 1953, The motion of discrete particles along the bed of a turbulent stream: Minn. Internat. Hydraulic Convention (Minneapolis) Proc., p. 7-20.

Iversen, H. W., Discussion of results from studies of wave transformation in shoaling water, including breaking, Inst. of Eng. Research, Univ. of Calif., Berkeley, Series No. 3, Issue No. 331, 1952, 16 pages.

Johnson, J. W., and Shay, E. A., 1951, Model studies on the movement of sand transported by wave action along a straight beach, Inst. of Engineering Research, University of California, Berkeley, Issue 7, Series 14, (unpublished).

Johnson, J. W., 1952, Sand transport by littoral currents, Proc. Fifth Hydraulic Converence, State University of Iowa, Studies of Engineering, Bulletin 34.

Keulegan, G. H., and Patterson, G. W., Mathematical theory of irrational translation waves, U. S. Dept. of Commerce, National Bureau of Standards, Vol. 24, 1940, 100 pages.

Keulegan, G. H., Wave Motion, Engineering Hydraulics, Proc. Fourth Hydraulic Conf., ch. 11, pp. 711-68. Ed. by Hunter Rouse, Wiley, New York, 1950.

Kressner, B., Modellversuche über die Wirkungen der Brandungswellen und des Küstenstromes auf einen sandigen Meeresstrand und die zweckmässige Anlage von Strandbuhnen, Der Technischen Hochschule der Freien Stadt Danzig, 1928, 16 pages.

Laitone, E. V., Higher approximation to non-linear water waves and the limiting heights of Cnoidal, Solitary and Stokes' Waves, Hydraulic Engineering Laboratory, Wave Research Projects, Tech. Rept. 89-6, 1961, (Berkeley).

Larras, J., Plages et Cotes du Sable, Collection Du Laboratoire National D'Hydraulique, Eyrolles, Paris, 1957, 117 pages.

Le Méhauté, B., A theoretical study of waves breaking at an angle with a shore, Civil Engineering Department, Queen's University at Kingston, Ontario, Report No. 10, 1960, 8 pages.

Lillevang, O. J., 1960, Mean direction of waves and of wave energy, Proc. Jour. Waterways and Harbors Division, V. 86, No. WW1, pp. 123-143.

Longuet-Higgins, M. S., On the statistical distribution of the heights of sea waves, Journal Marine Research, Vol. 11, No. 13, Dec. 1952, pp. 245-266.

Mashima, Y., Study of the Typhoen Characteristics in Respect to Wave Development and the Distribution of Longshore Current, Coastal Engineering in Japan, Vol. 1, 1958, pp. 1-20.

Munk, W. H., The Solitary wave theory and its application to surf problems, Annals of the New York Academy of Sciences, Vol. 51, Art. 3, pp. 376-424, 1949.

Putnam, J. A., Munk, W. H., and Traylor, M. A., The prediction of longshore currents, Trans. Amer. Geophys. Un. Vol. 30, pp. 337-345, 1949.

Sauvage, M. G., and Vincent, M. G., 1954, Transport littoral formation de fleches et de tombolos, Proc. Fifth Conference on Coastal Engineering, Grenoble, France, (Council on Wave Research, Berkeley).

Savage, R. P., 1962, Laboratory determination of littoral transport rates, Am. Soc. of Civil Engineers, Proc. Jour. Waterways and Harbors Division, V. 88, No. WW2, pp. 69-92.

Wiegel, R. L., A presentation of cnoidal wave theory for practical application, Journal of Fluid Mechanics, Vol. 7, part 2, pp. 273-286, 1960.

Wiegel, R. L., Wind Waves and Swell, Coastal Engineering No. 7, Proceedings of the 7th Conference on Coastal Engineering, Den Haag, Holland. Council on Wave Research, Univ. of Calif., Berkeley, 1961, pp. 1-40.

CHAPTER 16

RHYTHMIC PATTERN OF LONGSHORE BARS RELATED TO SEDIMENT CHARACTERISTICS

Masashi Hom-ma and Choule Sonu
Department of Civil Engineering, University of Tokyo
Tokyo, Japan

INTRODUCTION

Despite a number of valuable contributions by many predecessors, namely F. P. Shepard (Ref. 1) and G. H. Keulegan (Ref. 2), our knowledge regarding the effect of a longshore bar on the sedimentary process of a coast has long remained a plausible, qualitative understanding that a longshore bar constitutes a zone of active migration of bottom deposit due to agitation of breakers and currents. This was probably due mainly to the difficulty of performing an accurate hydrographic survey near the breaker zone. On the other hand, the geometrical characteristics along a single bar profile, which was sounded off either from a stable pier (Ref. 1) or a suspended cable (Ref. 3) resulted in a hopeless scatter.

An aerial photograph, if taken under favorable conditions, may show an interesting picture of submerged topographies in a distinct contrast made by the bright tone of a shallow bar crest or a shoal, against the dark background of a deep trough or a rock bottom. By comparing such photographic records with convenient soundings derived from some of the Japanese coasts, an interesting topographical feature of a longshore bar has been disclosed. A longshore bar may attain a rhythmic pattern consisting of echelons of arcuate (or lunate) bar unit, which in entire appearance strongly resembles that of a honeycomb.

It has also been discovered that a rhythmic bar pattern is correlated with other important factors either dynamic or static, which participate in the general processes of a coast, namely the shoreline configuration, the shoreface slope and deposit, the topographies on the offshore bottom, transformation of incident waves, the longshore currents and the littoral drifts. The authors have further attempted to develop a hypothetical concept on the origin of littoral rhythms as well as the behaviors of alongshore movement of sediment, and to consider their engineering impli-

cations on the basis of such findings.

Although our success which has been achieved so far is yet incomplete due to lack of available data, it is believed that the approach and concept as proposed in the present paper may suggest an encouraging line of research toward formulating a unified macroscopic view on the mechanics of the littoral process.

LONGSHORE BAR PATTERNS

RHYTHMIC BAR PATTERNS

Figs. 1 - 5 show reproduction from aerial photographs which were taken over the Japanese coasts. An outstanding feature which is common to these pictures is that the crests constitute an assembly of arcuate units which are arranged in successive echelons of different spacings depending upon the distance from the shoreline. These places, equally located very close to a river mouth, are known for predominant action of littoral drift along the shoreline. It is recognized that the farther offshore, the longer the spacing of an arcuate unit tends to become. The bar echelons are not completely separated from each other. The feet of the outer units join those of the inner ones producing a wide shoal there due to broadening out of the bar crests. This shoal extends toward inshore, frequently at oblique angles, as far as the shoreline, where again the feet of the innermost bars join the interior topography, the shoreline. We notice a remarkable feature that where the bar group of the innermost echelon is merged with the shoreline there exists a slight outward projection of the beach.

Thus, a beach which is confronted with a rhythmic bar system is usually marked by a series of an orderly indentation having the inter-apex spacing essentially similar to that of the offshore bars and apparently greater than that ordinarily found with a beach cusp.

Such a striking combination between longshore bars and shoreline configuration will be seen, in the chapters to follow, to represent the basic rhythms which govern in effect the overall characteristics of other factors either conspicuous or so minute that they may otherwise evade our attention as mere irregularities.

OCCURRENCE OF BAR RHYTHMS

A scrutiny of extensive phtographic evidences derived from nearly entire stretch of the Japanese

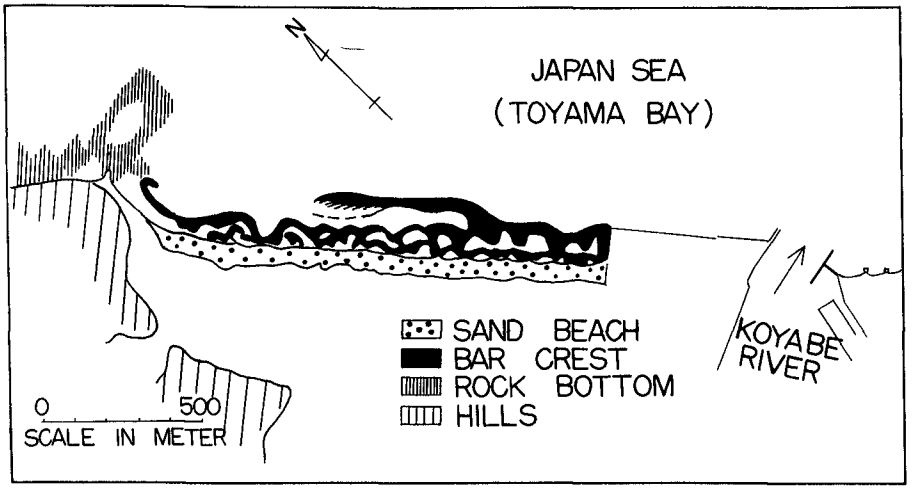

Figure 1. Rhythmic bar pattern, near Fushiki, 1961. (by courtesy of Japan Geogr. Inst.)

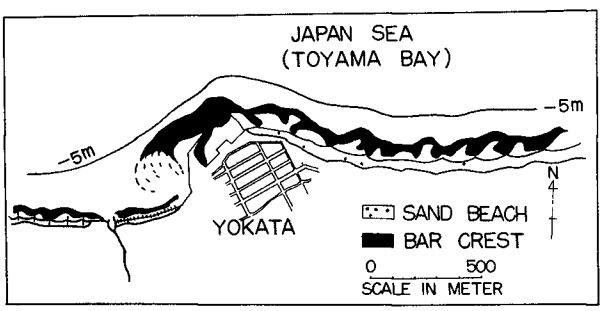

Figure 2. Rhythmic bar pattern, Yokata, 1961. (by courtesy of Japan Geogr. Inst.)

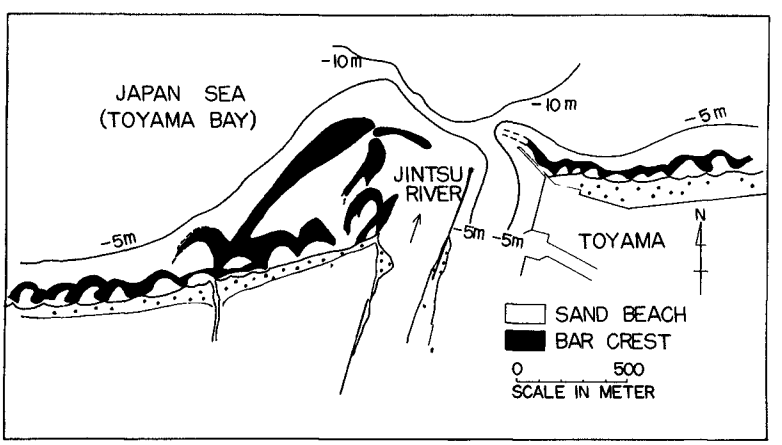

Figure 3. Rhythmic bar pattern, Jintsu, 1961. (by courtesy of Jap. Geogr. Inst.)

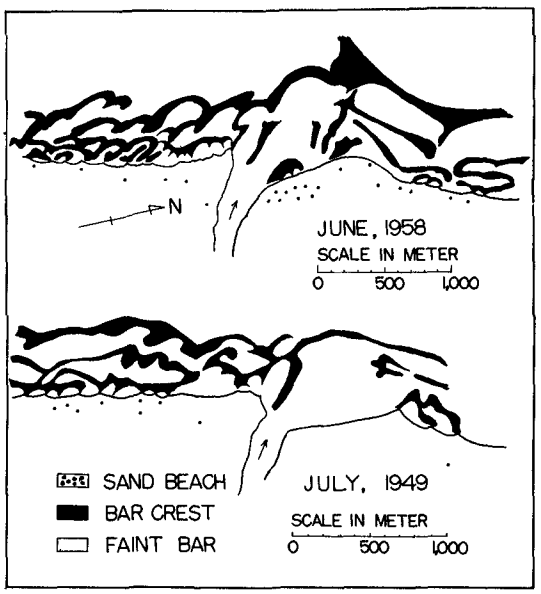

Figure 4. Rhythmic bar patterns of 1958 vs. 1949, Shin-shinano. (by courtesy of Jap. Geogr. Inst. and Niigata Prefecture)

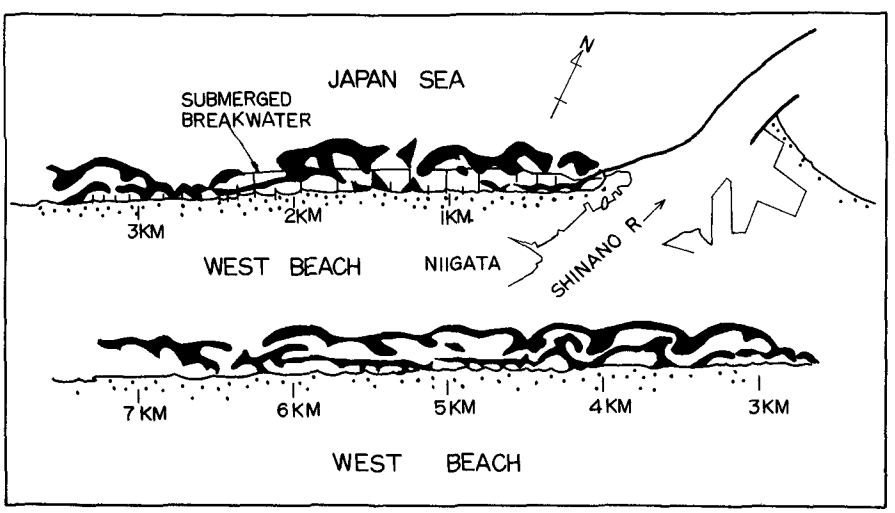

Figure 5. Rhythmic bar pattern, Niigata west beach, 1958. (by courtesy of Niigata Prefecture)

coasts shows that a rhythmic bar system may occur at localities where some fundamental requirements are satisfied. Primarily, a beach must be close to a rich source of supply. Secondly, the bottom must be sufficiently gentle in the shallow water zone. The local wave conditions merely affect the magnitude of predominant rhythms. The nature of bottom deposit is likewise ruled out as insignificant; the rhythmic bar pattern has been discovered not only on a sandy beach but also on a gravel beach. Therefore, the beaches lying close to a river mouth are frequently marked with bar rhythms. On the other hand, a beach skirting a sharply descending alluvial fan is often devoid of either a rhythmic bar or, on some occations, even a sign of a straight bar, although a shoreline indentation may still exist. Consequently, a delta beach adjacent to an estuary is the most likely place for occurrence of bar rhythms.

Fig. 6 demonstrates such an example. Along the eastern half of the Toyama Bay coast which is found at the rim of a group of alluvial fans of the Kurobe and other rivers, the bottom slope is as great as 4 % down to the depth of -10 m and 20 - 15 % down to -100 m, while along the delta beach westward from the mouth of the Joganji river the bottom slope becomes gentler, falling to 2 - 0.8 % down to -10 m and 3 - 2 % down to -100 m. The photographic evidences show that it is only at the western half of the Toyama Bay coast that a rhythmic bar pattern is found to exist, while the eastern half of the same coast totally lacks in a bar of any noticeable size. The experiences of the authors on the Japanese coasts show that a bottom slope of about 2 % down to -10 m is approximately the limit for occurrence of a rhythmic bar pattern.

In fact, the two requirements mentioned above may be summed up in one definitive condition that occurrence of a rhythmic bar pattern depends essentially on the extent to which the unconsolidated sediment on the nearshore bottom is subjected to significant agitation by waves. It is probably due to this reason that a rhythmic bar pattern is also found at a place which is located relatively far from a source of supply yet provided with a gentle bottom slope. Therefore, a source of supply must not always be a river. It may be an eroding beach where the sand supply is derived immediately from the regressing beach, or a tidal inlet where the alongshore component of sediment drift is intercepted over a shallow bottom near the shoreline by a transversal flush of tidal currents in and out of the inlet.

RHYTHMIC BAR VERSUS STRAIGHT BAR

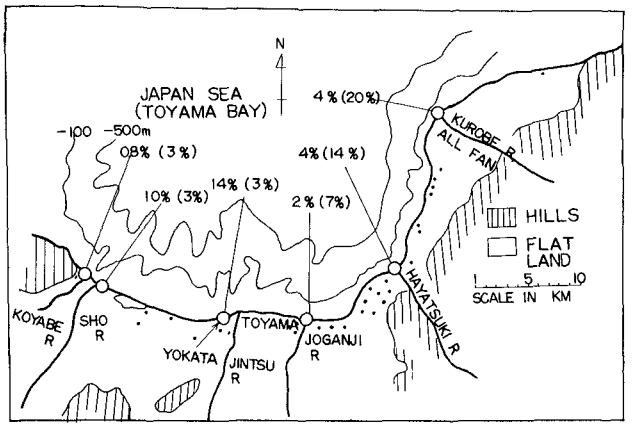

Figure 6. Bottom slopes along Toyama Bay coast. Attached figures out of and in parentheses indicate slopes down to -10m & -100m each.

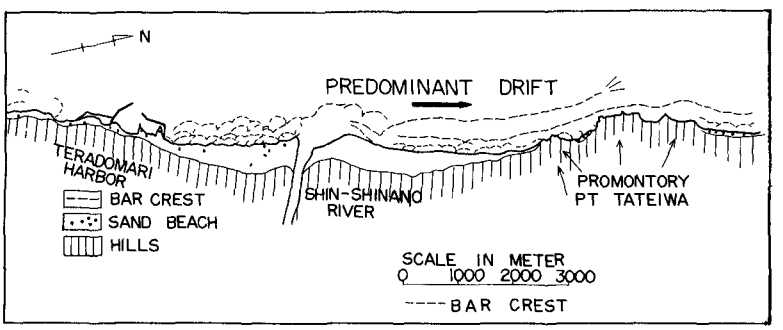

Figure 7. Comparison of rhythmic and straight bars at outlet of Shin-shinano, 1958.

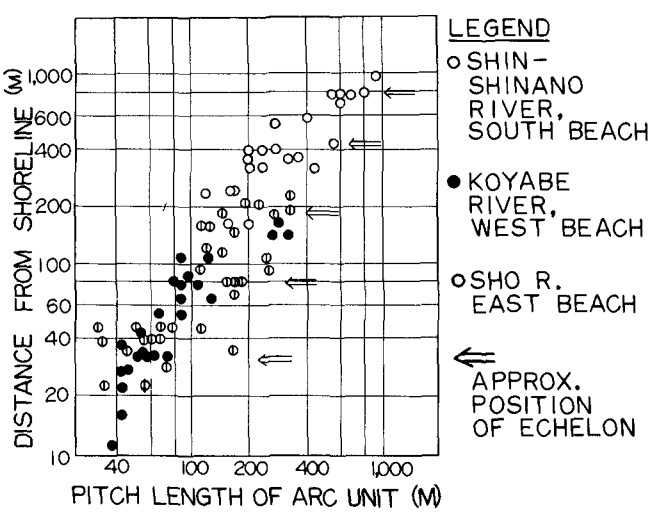

Figure 8. Size of arcuate bar with distance from shore.

A straight bar is encountered almost on any type of sandy beach, unless the bottom slope is too steep, say below about 2 % down to the depth of -10 m.

What are the physical properties which distinguish these two types of bars? On the beaches cited in Figs. 1 - 5, we find the rhythmic bars more pronounced on the updrift side of the source of supply than on the downdrift side. According to Fig. 7, along the beach of the Shin-shinano river the bars are largely straight on the downdrift side. It is interesting to recognize here that the middle echelon, a straight bar, continues to extend on the rocky bottom around the promontories and into a sandy bottom lying further north, while the innermost echelon which consists of rhythmic bars is absorbed into the sandy beach just short of Pt. Tateiwa, the first of the three promontories in this area. On the updrift side the rhythmic bars also fail to detour the rock bottom in front of the Teradomari harbor.

Summing up these evidences, we are inclined to presume that a straight bar may indicate the presence of a strong uni-directional drift of bottom deposit, which is so active that it may transport sediment even beyond promontories through a well-defined zone on the rock bottom without undergoing appreciable diffusion midway; while the rhythmic bar may rather imply a stagnating pattern of alongshore drift in which the bottom deposit is preserved more or less in a self-contained system of equilibrium. In fact, such an assumption seems largely allowable, for, as we will see later in the discussions on the movement of littoral rhythms, the rhythmic pattern of coastal topographies would not move an appreciable distance along the shoreline. However, in view of its heavy implications on the fundamental problems of coastal sediment, this point must not be emphasized without further evidences.

TOPOGRAPHICAL PROPERTIES OF RHYTHMIC BAR

TYPES OF BAR RHYTHMS

Fig. 8 gives a general relationship between the unit size of bar rhythms and the position of echelons, each expressed in terms of spacing between both feet of each arcuate unit and the distance of the arc center from the shoreline, respectively. Data have been read off from the aerial photographs on the west coast along the Toyama Bay and the south beach at the Shin-shinano river, where the bottom slope down to a depth of -10 m is approximately 1 %.

The unit size of a bar rhythm is almost uniform

within the same echelon, but varies to an appreciable degree by echelon and also by locality. The average unit size for each echelon, shown in the ordinate of Fig. 8, seems to increase by the doubling process, say $S \times 2^0$, $S \times 2^1$, $S \times 2^2$, ..., and $S \times 2^6$ in the order toward offshore, in which the most appropriate value for the basic multiplicand S will be 40 - 50 m on the beaches treated here. The value of S may vary by locality, mainly in accordance with the regional predominance of wave conditions.

The shape of an arcuate unit is not necessarily symmetrical. It is skewed toward the predominant drift direction on all the beaches cited here. The skew may be attributed to the predominant wave incidence or direction of longshore currents. According to Shepard (Ref. 1), rip channels will be formed on the bottom of the surf zone. However, this is obviously unable to affect the overall bar system for a durable period of time, because it is a passing topography with a life span of merely a few weeks. On the other hand, coastal structures may affect the shape of an arcuate rhythm of a bar to an appreciable extent, depending upon the magnitude of a structure as well as the nature of a bar. For instance, on the Niigata west beach (Fig. 5) where part of the shoreline is protected with a submerged breakwater and a series of groins in order to prevent erosion, the bar rhythms are disfigured considerably, particularly near the protected shoreline.

PROFILES ACROSS A RHYTHMIC BAR

Fig. 9 shows a bottom topography of the Niigata west beach which was obtained by a sounding, together with a rhythmic bar pattern traced from an aerial photograph. There is a lag of one month between these data; however, it may not impair the usefulness of this comparison since no significant wave action took place in the mean time.

According to Figs. 9 and 10, a correlation between the rhythmic patterns of a bar and the perpendicular bottom profiles is well defined, and our previous observation is confirmed that the foot of an arcuate unit corresponds to a shoal, while the center of the arc to a deep trough and a steep bottom slope in the surf zone. This fundamental relationship has also been recognized on the beach of Tokai, Japan, which is exposed to the sea and swell of the Pacific Ocean and frequently subjected to extremely violent waves due to a typhoon. The shoal may become so shallow that on some occasions it is wadable. The authors have encountered such an example at the gravel beach of the Ishikawa

Prefecture, where the bathing children walked over this shoal to play on the crest of an offshore bar. Here the crest of the bar rose to a depth of about 1.5 m, while the trough was about 3 m deep.

BAR RHYTHMS VERSUS NEARSHORE TOPOGRPHIES

TYPES OF SHORELINE RHYTHMS

Bibliographies are replete on the subject of beach cusp since the days of D. W. Johnson (Ref. 4). However, it has been only in recent years that the rhythmic undulation having a greater inter-apex spacing than that of an ordinary beach cusp has been given a serious attention.

Per Bruun (Ref. 5) recognized from investigation of the nearshore topographies along the Danish North Sea coast that these "shoreline waves" migrated alongshore as if they were a mass of land at a variable rate between 0 and 1,000 m per year. According to his measurement the spacing ranged between 300 and 2,000 m, while the amplitude between 60 and 80 m. Discussing on the origin of such a shoreline rhythm, he describes: "there may be some connection between the migrating undulations and breaches in the longshore bar, possibly due to erosion by rip currents because the wave trough is often formed behind a breach and the crest just ahead." He further pointed out that the rhythms ("humps") were also present on the offshore bottom along the same coast.

On the other hand, O. F. Evans (Ref. 6) made studies on the beach cusps, including a large undulation, on the southern beaches of the Lake Michigan. According to him, the beach cusp may be classified into five different categories, of which the significant types of natural origin are:

(1) "very large capelike cusps (or undulations) formed during storms along the beaches that are susceptible to considerable erosion and deposition."
(2) "large cusps (undulations) which have their apexes continuing out into the lake as a ridge of sand on the lake bottom."
(3) "ideal cusps which usually occur in series and come nearest of all to being evenly spaced."

According to his measurement, the "very large capelike cusps", which apparently are equivalent to Bruun's shoreline wave of the order of 10^3 m, are spaced within the range from 96 to 1,050 feet, the average being 296 feet allowing for an appreciable scatter. The "large cusps", the second largest of his classification

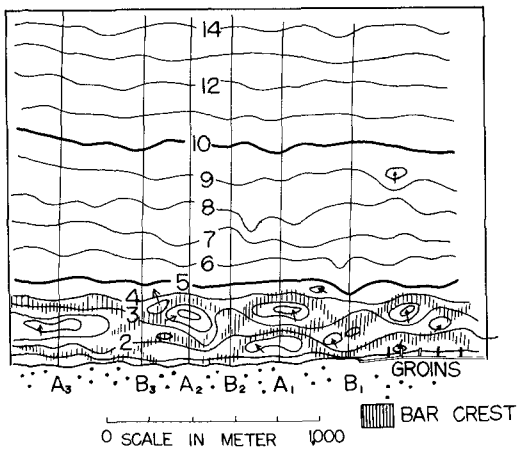

Figure 9. Nearshore topography shown with bar positions, Niigata west beach, 1958.

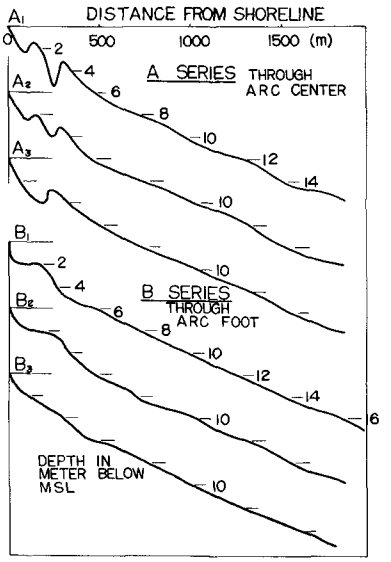

Figure 10. Perpendicular bottom profiles across bar crests and shoals, Niigata west beach. (Cf. Fig. 9)

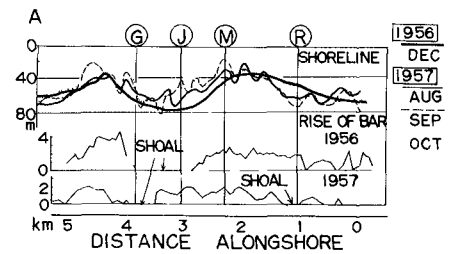

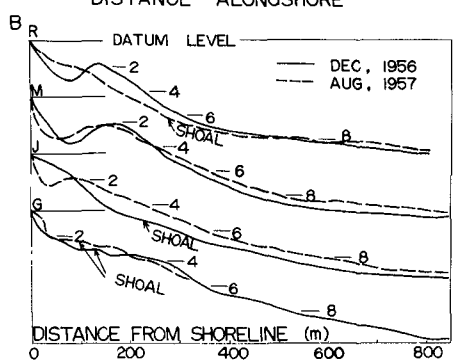

B. Perpendicular bottom profiles across bar crests and shoals, Tokai beach, Japan.

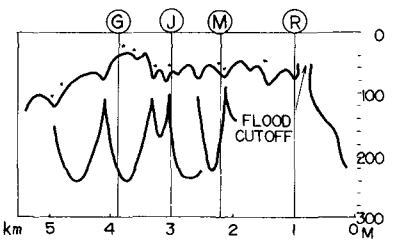

Figure 12. Bar rhythms reproduced from aerial photograph, 1961. (by courtesy of Jap. Atomic Gener. Co.)

Figure 11. Shoreline A. Shoreline rhythms compared with bars. (reproduced from Mogi, Ref. 8)

equivalent to Bruun's wave of the order of 10^2 m, have also uneven spacings ranging from 33 to 102 feet with the average being 69 feet. However, the scatter of spacing is improved to a considerable degree with this cusp as compared with the capelike cusp. Finally, the "ideal cusps" are the best graded in the inter-apex spacing of the three categories, ranging from 0.9 to 34.5 feet.

He also described the nature of the foreshore bottom which was found to occur in particular connection with these different shoreline rhythms. As for the large capelike cusp, "the underwater terrace slopes gently and has on it an excess of sand down to a depth of several feet." The capelike cuspate projection results from alternate accretion and erosion of such an accidental deposition on the shallow bottom due to changing conditions of waves and currents. On the other hand, the large cusps are always accompanied by their ridges called "ball and low." He admited further that "where the ends of the ridges join the shore, ... the increase in the supply of sand at the shoreline results in the formation of (this type of) cusp." Apparently, this transversal ridge is identical to the nearshore shoal which, as we have already recognized from the aerial photographs (Figs. 1 - 5), bridges the feet of a bar rhythm and the corresponding outward projection of a shoreline. As for the ideal cusps, however, he does not seem to have recognized any conspicuous topography on the corresponding foreshore bottom, except that their occurrence appeared to depend on the breaching of a (longshore) ridge. The relationship between the ideal cusp and the foreshore bottom has been somewhat better described by Ph. H. Kuenen (Ref. 7), who remarks that in front of the embayments the foreshore is sometimes built out under water in a delta shape.

In Japan, A. Mogi of the Japan Hydrographic Office was probably the first to demonstrate the presence of regular rhythms on the shoreline configuration. Fig. 11-A shows a partial reproduction from his result based on the shoreline investigation at the northern half of the Tokai beach, Japan. According to his measurement, the shoreline undulations found here consist of three different types of rhythms as tabulated below:

TABLE I. Dimensions of Shoreline Rhythms, Tokai, Japan.

class	largest	medium	smallest
spacing	2,000	300	30 - 60 m
amplitude	40 - 50	20 - 30	10^0 order m

In nature, these three types of rhythms are superposed on one another, each slightly skewed toward the predominant direction of littoral drift. He also recognized that the largest rhythms are associated with the geometrical properties of the longshore bar, i.e. that the apex and embayment are found behind the breaching and the center of a longshore bar, respectively. This finding seems just the contrary of what Dr. Bruun has previously discovered on the Danish North Sea coast, if we should interpret the term "breach" as used by him to mean a shoal which lies in the gap of a continuous bar.

The present authors have also recognized regular rhythms on the undulating configuration of a shoreline from aerial photographs as well as sounding data in Japan. Figs. 12 and 13 show such examples. Fig. 12 shows reproduction of an aerial photograph of the Tokai beach, which was taken in July, 1961, roughly three years after the beach investigation of Dr. Mogi, where the perpendicular scale has been exaggerated to help visualization. By comparing Fig. 12 with the preceding Fig. 11-A, we note a striking coincidence between the rhythmic phases of 1957 and 1961, each measured three years apart, although in 1961 a medium-sized rhythm of about 800 m in spacing occurred individually on the southern end of the beach.

Fig. 13 has been derived from the Niigata west beach. Here also, we recognize several types of shoreline rhythms, as classified in the table below:

TABLE II. Dimensions of Shoreline Rhythms, Niigata.

Class	I	II	III	IV
Spacing	7,000 or greater	3,000	200 - 300	10^1 order
Amplitude	40	30	20	10^0 order

unit: meter

The rhythms of the order of 300 m, measured at one-year interval, fit surprisingly well to each other, although those of greater orders show some appreciable amount of perpendicular displacements due possibly to active beach erosion which has long been in progress here. (See Fig. 13-B) Since our range of survey is limited only to 7 km along the shoreline, there is no way of asserting whether or not the greatest rhythm, Class I, having a spacing as great as or greater than 7,000 m, could be actually present in nature as a repeating phenomenon. In fact, this might have been brought about by scour at the foot of a long river jetty where the converging waves produced a large embayment. (See also Fig. 5)

It is often very difficult to recognize a shoreline rhythm beyond the order of 10^3 m in spacing either from an aerial photograph or by inspection in the field, since it may merely represent the general trend of a group of lesser rhythms of the order of 10^2 m and less. Only by convenient exaggeration of an accurate sounding data becomes such a long-range undulation sufficiently noticeable. On the other hand, the best defined of these various rhythms on the Niigata west beach is that belonging to Class III, which has the average spacing of 325 m, apparently a counterpart to the medium rhythm found at the Tokai beach. This average was taken from 60 such rhythms which were observed by three successive surveys conducted approximately at one-year interval. The type of sample distribution is roughly Poissonian, having the mode value exactly at 300 m and a negligible scatter by year.

SHORELINE RHYTHMS ASSOCIATED WITH BAR RHYTHMS

The predecessors in the subject of a shoreline rhythm as cited so far have equally pointed out a possibility, though to a varying degree, that the shoreline rhythms may be connected with longshore bars. Dr. Mogi (Ref. 8) compared the phases of the shoreline rhythms with the alongshore distribution of the rise of a bar, i.e. the height of a bar crest above trough, on the Tokai beach, Japan. (Fig. 11-A) The apex of the greatest spacing of the order of 2,000 m was found to lie behind the breaching of a bar, while the embayment behind the center of each bar unit where the rise seemed most pronounced. It is surprising to note that this bar-shoreline relationship is very strict, hardly variable even if the entire system of rhythms are displaced along the shoreline. We see this feature by examining the bottom profiles across the bar and shoreline. (Fig. 11-B) The survey lines R and J were both once close to an apex and once to an embayment, and on the bottom profiles were found once a shoal and once a bar, correspondingly. Along the survey line M, which was always closer to an embayment, we find a bar at all times. On the other hand, the survey line G remained closer to an apex, and a shoal was always there.

The similar relationship between the shoreline and the bar holds with respect to smaller rhythms of the order of about 300 m. Figs. 14 and 15 give an example derived from the precision survey along a portion of the beach stretch of Fig. 11. We recognize that it is the inshore bar that corresponds to the shoreline rhythm of about 300 m in spacing, while the bar of the outer echelon corresponds to the shoreline rhythms of the order of about 2,000 m. Unfortunately, due to limitation of accuracy in the surf-zone sounding as well as smoothing

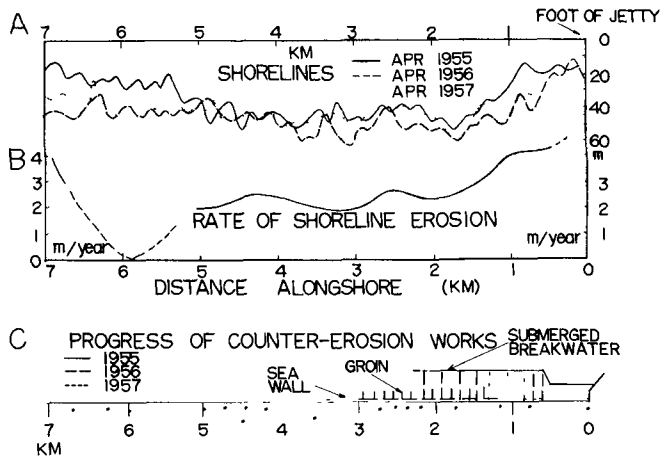

Figure 13. A. Shoreline rhythms, Niigata west beach.
B. Rate of erosion averaged over past 10 - 20 years shows a rhythmic trend.
C. Progress of recent counter-erosion works.

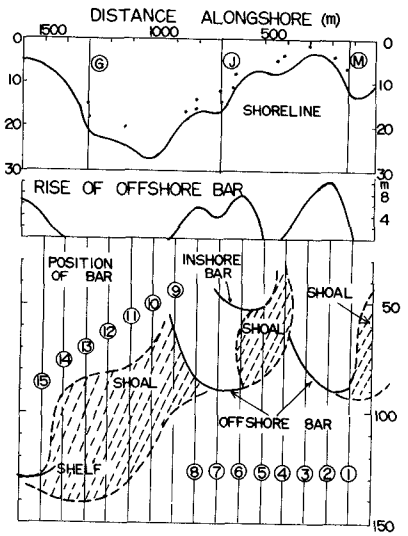

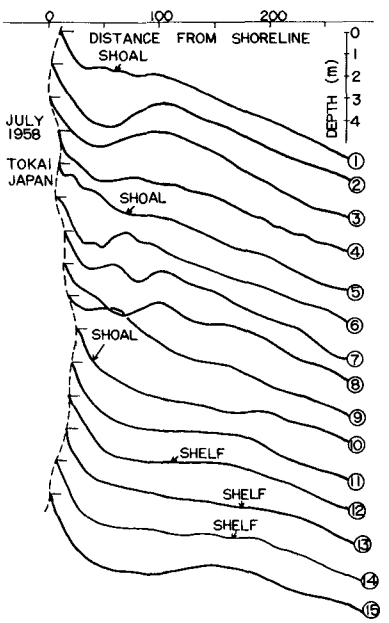

Figure 14. Shoreline and bar rhythms reproduced from sounding & air photo.

Figure 15. Bottom profiles along survey lines shown in Fig. 14, Tokai beach, Japan.

of the bottom features by summer swells, it is impossible to visualize the inshore bars from the sounding map except as a broad shoal. Figs. 14 and 15 further confirm the result of our previous observation that the feet of an offshore shoal is continued toward inshore and in effect join the apexes of the shoreline rhythms as well as those of an inshore echelon. Where such a double merging occurs, there is an apex of a large undulation, while at an isolated foot of the inshore bar we find a less conspicuous apex of a smaller rhythm. Likewise, according to Fig. 16, which has been reproduced from the result of Dr. Mogi (Ref. 8), the beach cusps, expressed in terms of inter-apex spacing, seem to correspond to their positions within the phase of a medium rhythm of the order of about 300 m, although an appreciable scatter is also recognized. The limitation of sounding accuracy prevents us from tracing a minute feature on the foreshore bottom in relation to a beach cusp.

The similar relationship has been checked by utilizing the sounding data on the Niigata west beach. Fig. 17 compares the shoreline undulations, the positions of bar crests, the rise of bar, and the refraction coefficients based on the wave period of 10 seconds and arriving at right angles to the mean shoreline. From here is also derived roughly the same conclusion as that already obtained on the Tokai beach, although the correspondence between the rhythms on the shoreline and the bar seems to have been largely obscured due probably to gradual extension of counter-erosion structures in the vicinity of the jetty. (See Fig. 13-C) Fig. 18 further compares the same factors on the basis of recent soundings. Agreement between the shoreline and bar rhythms seems largely satisfactory except for the portion between 1 - 2 km which is protected by counter-erosion structures.

The evidences so far presented as well as our experiences with aerial photographs emphasize that there exists a significant relationship between the rhythms of the longshore bars and of the shoreline configurations. However, as we will see later, this is not a cause-and-effect relationship; they are both a continuation of other rhythms which are found to lie on the offshore bottom.

RHYTHMS ON THE OFFSHORE BOTTOM

Per Bruun has discovered an undulating rhythm on the offshore bottom along the Danish North Sea coast which is spaced by about 1.5 - 3 km and distinguished in every respect from a mere irregularity. No other published study is available for reference on this subject, except for extensive bibliographies regarding the

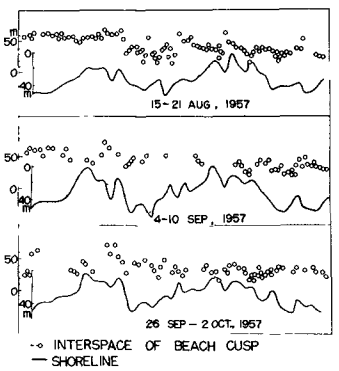

Figure 16. Alongshore distribution of inter-apex size of beach cusp, reproduced from Mogi, Ref. 8.

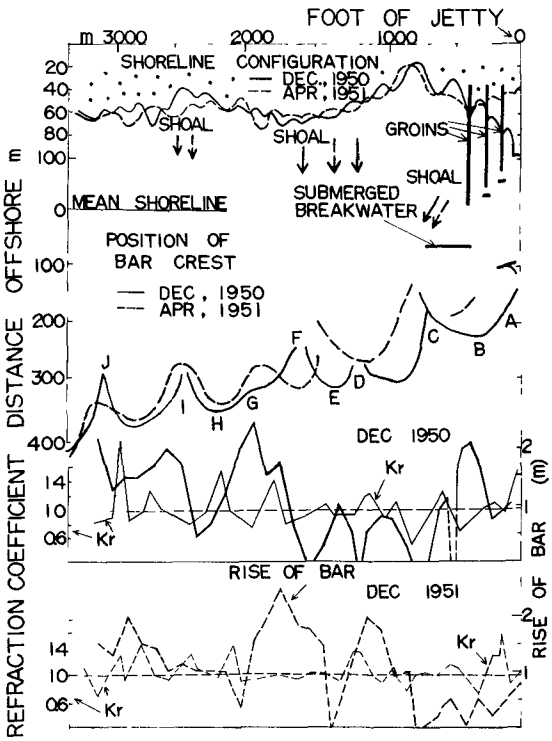

Figure 17. Shoreline rhythms, bar rhythms and refraction coefficients compared for two consecutive years, Niigata west beach. (Cf. Fig. 19)

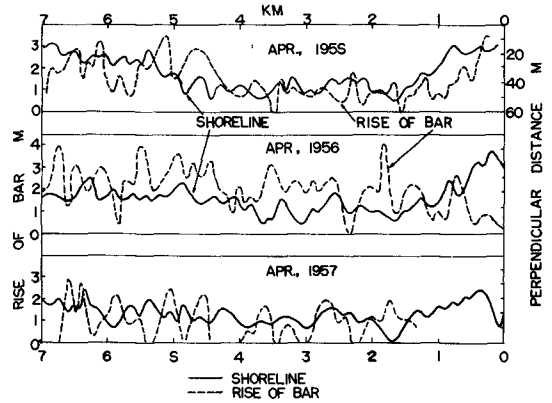

Figure 18. Shoreline and bar rhythms compared for three consecutive years over longer stretch of Niigata west beach, Japan.

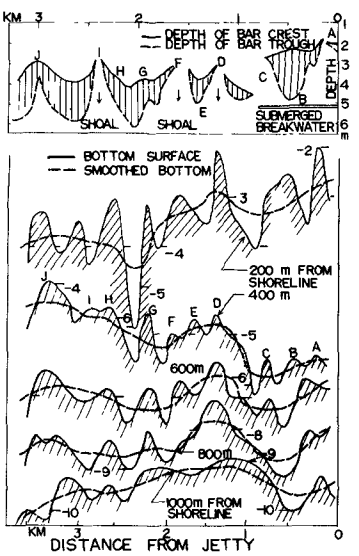

Figure 19. Rhythmic undulations on offshore bottom compared with bar topographies, shown in elevated view, Niigata. (Cf. Fig. 17)

submarine valleys which seem, however, to lie far beyond the scope of a shore process. Encouraged by his study, the present authors examined the nature of such a giant rhythm found on the offshore bottom in relation to other rhythms which have been already confirmed to exist on the inshore bottom. The result has been as yet too inconclusive to publish in a generalized form. However, some interesting features have been recognized.

Fig. 19 shows the elevated view of the bottom topographies of the Niigata west beach sounded in December, 1950. At about 1 km from the shoreline where the depth is about 10m we notice a gentle undulation on the bottom spaced by about 1.5 - 2 km between adjacent ridges, which is overlapped by a smaller inconspicuous rhythm of the order of about 300 m. As these rhythms approach the shore, there is a general increase of the rise of the rhythms not only in the mean trend (shown by dotted curves) but also in the minute pattern due to occurrence of dendritic ridges and valleys. Thus, at the distance of 400 m from the shoreline, i.e. immediately offshore of the bar crest, the entire bottom is covered with slender ridges spaced by about 300 m on average.

We recognize a remarkable feature by comparing the positions of these ridges with the elevated view of the longshore bars that each of the ridges is impressed on the bar topography. The ridge corresponds to a shallow crest and a shallow trough, and where this ridge or valley is pronounced - as it is always so at the crest or trough of the mean bottom (dotted curves), respectively - there is a breaching of a bar, i.e. a shoal. We further notice an important fact by comparing Fig. 19 with the shoreline configuration as shown in our previous Fig. 17, that these offshore undulations are virtually impressed on the shoreline, i.e. that there is an embayment behind a trough or valley and an apex behind a crest or ridge. (Compare alphabetical symbols attached in Figs. 17 and 19.) This pattern has been illustrated by an ideal sketch in Fig. 20.

Now, we realize that the role of a longshore bar is limited merely to smoothing the undulating curve on the shoreline and unable to extinguish completely the original rhythms which start at the offshore bottom. This also explains why a shoreline rhythm occurs where there is no bar at all. In fact, the present authors have observed a number of such examples from studies of aerial photographs on the Japanese coasts; a beach having a very steep bottom slope, exceeding 3 - 4 % sometimes, is marked with shoreline rhythms where no bar is visible.

Questions remain, however, as to the origin of

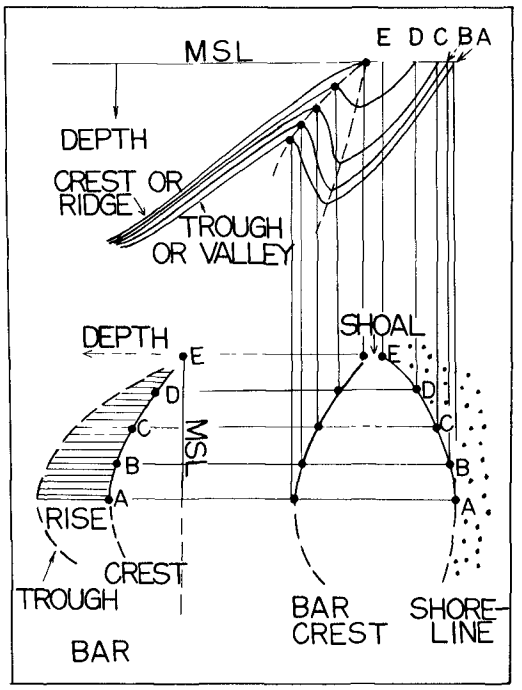

Figure 20. Ideal correlation between undulating rhythms on offshore bottom, size and position of longshore bars, and shoreline rhythms.

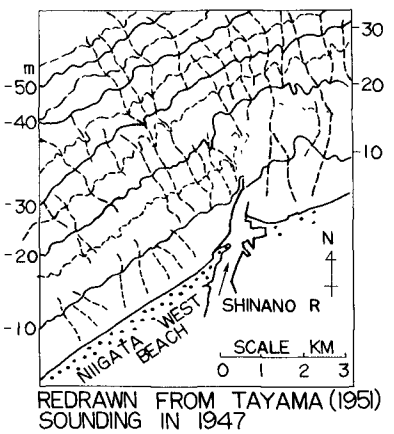

REDRAWN FROM TAYAMA (1951)
SOUNDING IN 1947

Figure 21. Submarine topography near Shinano river outlet, reproduced from T. Tayama et al (1951). Dotted curves indicate courses of submarine valleys.

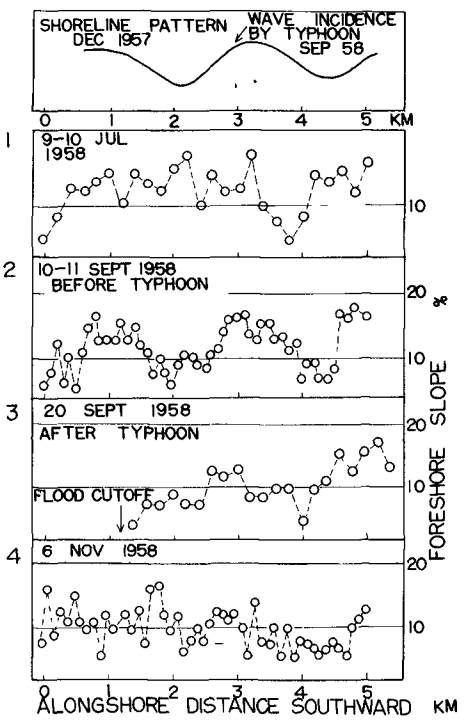

Figure 22. Shoreface slopes of Tokai beach, shown to retain basic rhythms.

such an offshore undulation and also of its dendritic breaking pattern on the nearshore bottom. The present authors have not been successful in providing any recommendable answer to these questions. However, a tentative explanation has been attempted as follows. It is recalled that in an early section of this paper we have noticed a frequent occurrence of rhythmic bar patterns in the vicinity of a large river mouth. Usually, submarine valleys are found to occur in an appreciable number on the foreset slope of the submerged delta of a large river. According to our Fig. 21, these valleys are spaced by about 1 km or so on the foreset bed off the mouth of the Shinano river, Niigata. Some of them are traced a long way to the nearshore bottom, attaining a depth of about 10 m. If all the large undulations which have been found on the offshore bottom could be a topography originating from the valleys of the foreset slope, it will follow that they are more or less a stationary feature. However, the accuracy of the available data prevents us from tracing every undulation found at a depth of 10 m as far away as the foreset bed where the depth is approximately 25 - 30 m. We must not go too far with an array of hypothesis which touches upon a field of the submarine geologists.

MOVEMENT OF RHYTHMS

Both Dr. Bruun (Ref. 5) and Dr. Mogi (Ref. 8) seem to believe that the shoreline rhythms migrate along the general direction of littoral drift. Interestingly enough, the rate of migration estimated by both authors are roughly congruous; 700 m/year in one instance and 0 - 1,000 m/year in general by Bruun, and 500 - 1,000 m/year by Mogi.

However, if we compare the shoreline configurations of the Tokai beach, Japan, measured by Mogi in 1956 and 57 (Fig. 11-A), with that read off by the present authors from an aerial photograph of 1961 (Fig. 12), it is realized that no substantial change has taken place on the shoreline rhythms over a period of 3 - 4 years, for the fundamental phase patterns of these two data agree with each other surprisingly well, even though the latter involves errors due to wave swashes and tide levels which might have obscured the shoreline position appreciably. In fact, as Dr. Mogi points out, the shoreline rhythms migrated slightly between winter, 1956 and summer, 1957, but they resumed their original positions in summer, 1961, roughly three years later. This leads us to assume that the shoreline rhythms may undergo a slight shifting and/or skewing movement under changing conditions of waves and currents, but not keep on migrating indefinitely at the rate suggested by these authors.

RHYTHMIC PATTERN OF LONGSHORE BARS RELATED TO SEDIMENT CHARACTERISTICS

The present authors have once interviewed an aggregate manufacturer in the Ishikawa Prefecture, Japan, who was engaged in exploiting beach gravels at an apex of a long shoreline rhythm which was spaced by about 1,000 m. He claimed that the site had been there with the same stationary apex since he started this business several years ago. According to him, the apex had not moved to any marked degree in either direction alongshore, although an appreciable change was noticed in the perpendicular direction due to erosion or deposition by seasonal conditions of waves and currents. There is another evidence which seems to support the view of the present authors. In our previous Fig. 13-B a long-term trend of shoreline regression is compared with the rhythmic undulation of the shoreline on the Niigata west beach. The former has been averaged from the results of continuous surveys conducted for the past 10 - 20 years during which the trend of regression has been almost consistent in time though variable in position. We notice an excellent fit between the rate of regression and the general rhythms of shoreline, i.e. that the regression has always been intensive at the embayment but relatively slow at the apex of each rhythm which has a spacing of about 2,000 m on average. This seems to enable us to assume that the general trend of the large shoreline rhythms will remain virtually unchanged for at least a period of a decade or two.

On the other hand, we have not made any particular attempt to check the validity of the concept of "migrating sand humps" on the offshore bottom as proposed by Dr. Bruun, owing partly to limitation of the accuracy of data on a deep bottom, and partly to the general interruption of bottom topographies caused by the subsidence of the Niigata area in recent years.

OTHER MINUTE RHYTHMS

Shoreface slope

We are familiar with the general topography of a small beach cusp where the shoreface is steep at the apex and gentle at the embayment. However, it is very hard to recognize this feature consistently with a medium rhythm of the order of 10^2 m. Frequently, the shoreface slope on both opposite sides of an apex may show a different trend. This scatter will be partly accounted for by the presence of a series of small beach cusps and partly by the behavior of the beach at the time of measurement, i.e. whether it is progressing or retreating.

With the large rhythm of the order of 10^3 m, however, it seems that the analogy of a beach cusp holds in general. According to our measurements at the Tokai

beach (Figs. 22-1 - 22-4), the shoreface slope was steep near the apex and gentle near the embayment, although there is a scatter due probably to a skewing pattern of the shoreline rhythms or to difference of exposure of each shoreline stretch. The most striking feature in Figs. 22 is that this basic trend does not undergo a material change even if the beach is subjected to formidable action of typhoon waves which attain a height of 5 - 7 m at breaking. (Compare Fig. 22-2 and 22-3.)

Beach deposit

We have compared the measured shoreface slope with the median size of deposit sampled at various foreshore levels between the step and the upper berm on the Tokai beach. The results show a hopeless scatter except for one case in which the grain size of the step deposit has been used from the samples of September, 1958 (before typhoon). (Fig. 23) Our data have been smoothed (shown in dotted curves in Fig. 23) and replotted against the result of Bascom (Ref. 9) in Fig. 24. It is recognized that the slope - grain size relationship is best defined where both factors best fit the shoreline rhythms of the order of 2,000 m. Also considering the fact that of all the levels on the foreshore the shoreline step is the place where the wave impact is most strongly displayed, we are inclined to presume that the shoreface slope is as subtly dependent on the wave impact as on the nature of deposit.

DYNAMICAL FACTORS ASSOCIATED WITH BAR RHYTHMS

WAVES

Over the nearshore bottom which undulates at regular rhythms, there will be a zonal convergence and divergence of incident waves due to refraction. In a three dimensional laboratory flume we often observe that a train of uniform waves are refracted and regrouped into separate fluxes having a finite crest length near the shallow water. This phenomenon seems to occur also in nature. We often encounter aerial photographs which show separate groups of wave trains progressing in the nearshore water almost at right angles to the shoreline. Judging from the crest patterns as observed on such photographs, this phenomenon is not always attributed to interference between two different trains of waves arriving from different generation areas.

We have constructed a refraction diagram by utilizing a wave of 10 seconds arriving at right angles to the shoreline, and compared the refraction coefficients Kr at the depth of 5 m with the shoreline configuration

and the longshore bars. (Fig. 17) The result is not fully convincing, mainly because the depth contours beyond -10 m was not available in our data. However, if we take into consideration a relatively slight change of the value of K_r at the positions F, G, H and I, it is recognized that there is a good correlation between wave transformation and undulating bottom topographies. The waves converge at the undulating ridge or shoal where the crest of a bar sways toward inshore and becomes shallower, while it diverges at the undulating valley or the position of the pronounced rise of a bar where the bar crest sways toward offshore and becomes deeper. We may neglect the portion A - E, since it is affected by artificial structures.

This relationship leads us to another interesting conclusion that a deep bar trough may not always be a result of high waves, for where such a deep trough, and hence a conspicuous bar having a large amount of rise, is found, the bar crest is also deep and the wave is diverged. A small wave breaking over a deep barrier may not be able to create a plunging action of sufficient violence which could account for such a deep trough as found in the center of a bar rhythm. It must be rather attributed to the influence of the offshore bottom topographies which are impressed continuously through the bar zone and into the shoreline. Then, a question arises as to why we find only a small rise near the shoal area where a greater effect of wave impact is expected to occur by our conclusion. One of the most likely causes will be that the converging waves advancing along this profile lose much of its energy by partial breaking over the undulating ridge on the offshore bottom, to such an extent that by the time they reach the final breaking position near the bar zone the height is reduced much lower than predicted by the theoretical refraction value. Another possible cause is ascribed to a surging action near the shoal which will result in smoothing of the bottom topography there. Whichever case it may be, it seems that a discrepancy of the local intensities of incident wave energies is obscured by the presence of an arcuate bar before they reach the shoreline.

Now a question arises as to how the littoral rhythms can remain stationary against rapidly changing conditions of waves. Is it possible that a particular type of littoral rhythms may represent a state of equilibrium where the wax and wane of the nearshore topography is delicately balanced against a particular type of waves? The present authors find it impossible to provide any promising clue to answer this extremely difficult yet vitally important question for the time being. However, as a helpful suggestion, an analogi-

cal example is drawn from our observation of the formation of a beach cusp which seems to correlate the stability conditions with the spectral properties of incident waves. The actual process of cusp formation is illustrated in Fig. 25; the wave was a gentle swell of 0.5 m in height and 8 seconds in period, arriving perpendicularly to the shoreline.

Stage 1. Backwash due to the preceding wave retards breaking of the following wave at the embayment, and breaking occurs prematuredly at the apexes.

Stage 2. Uprush at the apexes makes a two-thronged advance and a moment later a delayed breaking occurs at the embayment.

Stage 3. All the uprush begins to meet at the embayment. Impeded by flanking uprush from the apexes, that of the embayment is halted midway. Thus, a scarce amount of material is pushed upward from this part, while a relatively great amount of coarse material is carried up toward the summit of the apex.

Stage 4. All the uprushes clash at the center of the embayment causing a strong turbulence. Backwash starts toward offshore immediately thereafter, eroding the embayment and carrying fine material with them. Backwash gains in strength attaining a maximum momentum at the shoreline just where the following wave is about to break. And the same process is resumed.

It is doubted whether a group of waves each possessing a distinguished wave period could produce the same effect, for the backwash may be either too early or too late to create the breaking pattern of Stage 1, and consequently the succeeding stages will be largely interrupted. It seems necessary that the waves must have a relatively narrow optimum band of spectral frequencies in order to form a beach cusp. The shoreface slope will also count, since the time needed for the uprush and backwash to conclude a cycle should coincide with the wave period.

It is questionable if this observation with a small beach cusp could be extended to a greater rhythm of the order of 10^2 or 10^3 m. However, on the other hand, we realize that there exists a large-scale and long-period return of energy from the surf zone toward offshore in a manner of surf beat (having a time scale of 10^2 seconds) and rip currents, which represent a sporadic recompensation of the potential energies of the surf zone fed by the mass transport of the incident waves. Accordingly, our hypothesis is that there may

Figure 23. Shoreface slope and grain size at shoreline step shown to follow similar trend.(Cf. Fig. 22, upper insert, -2 and -3)

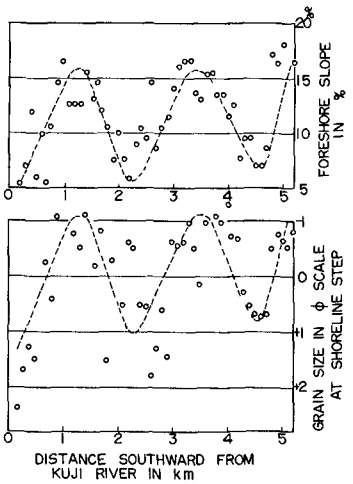

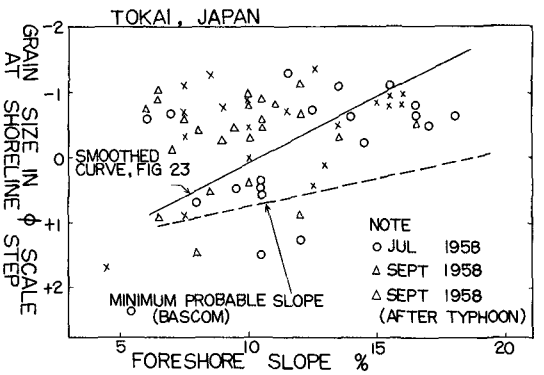

Figure 24. Grain size-shoreface slope relationship compared with result of Bascom. (Cf. Fig. 23)

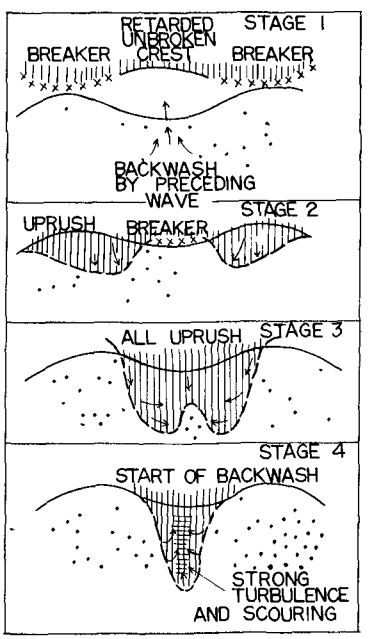

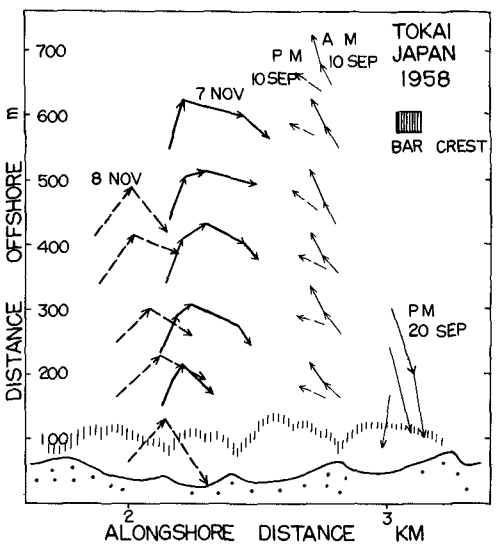

Figure 26. winding current path off Tokai beach.

Figure 25. Process of swash action at beach cusp, sketched on the basis of field observation.

be a particular long-term set of wave spells having a well graded ensemble property of spectra which is compatible with the particular stability equilibrium of a coast. However, there remain yet a number of other important questions which must be tackled before proceeding to answer ours.

LONGSHORE CURRENTS

According to our field investigation of longshore currents at the Tokai beach, the path of floats assumed a winding motion in space and time as they drifted along the shoreline. Fig. 26 shows some of such measurements, which were obtained by using a current vane placed at 1 m below the sea surface. An interesting feature of these simultaneous paths of the floats is that they follow roughly a similar curve over the entire zone of measurement ranging from the shoreline to an offshore distance of about 600 m (about 8 - 9 m deep). The current velocities were very low at all times, mostly around 30 cm/sec.

On the other hand, we measured the alongshore components of current velocities by using the same type of float. (Fig. 27 A-F) Despite that each run was carried out at different time and under different wave conditions, we recognize a feature which is largely common to all the measurements, that at an alongshore position of about 2.5 km, the approximate position of a large shoreline embayment (See Fig. 11-A.), there is always a sharp change of current velocities and occasionally a complete reversal of direction, while near the positions of about 1 km and 3 km, approximately the shoreline apex, the reverse currents seem to predominate.

An immediate conclusion which could be derived from the results of these measurements is that there seems to exist a rhythmic unit of current system which coincides with each position of embayment of the order of 10^2 and 10^3 m. This assumption has been illustrated in an ideal picture in Fig. 28. According to this assumption, there exists an independent whirling current in the embayment of the shoreline, while there is a continuous current in the offshore water which winds gently in accordance with the intervals of the whirling eddies. Therefore, in front of the embayment where the alongshore components of the whirling current come in phase with those of the offshore current, the measured values are higher than those in front of the apex where two currents are often opposed. It seems as if the longshore currents consisted of a nearshore circulating system of winding currents and eddies which is more or less independent from the neighbors and con-

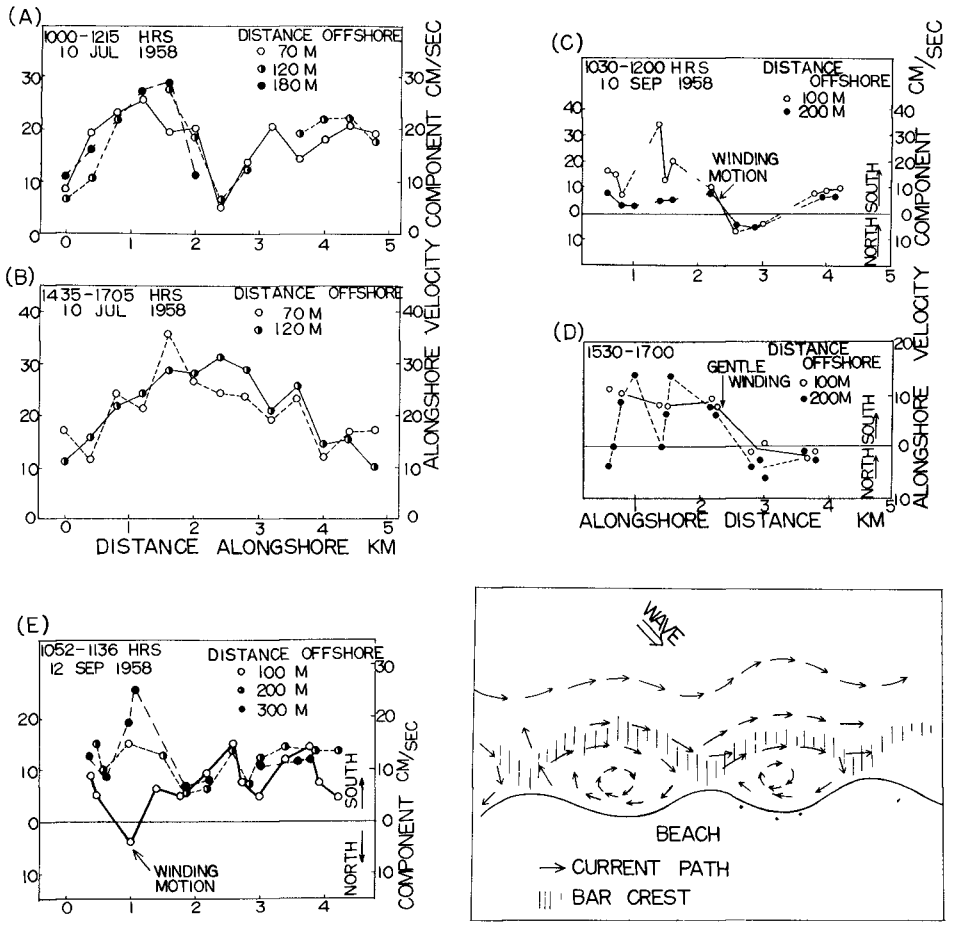

Figure 27. Distribution of alongshore velocity components, Tokai beach, Japan.

Figure 28. Ideal pattern of rhythmic circulation system shown to coincide with shoreline rhythm.

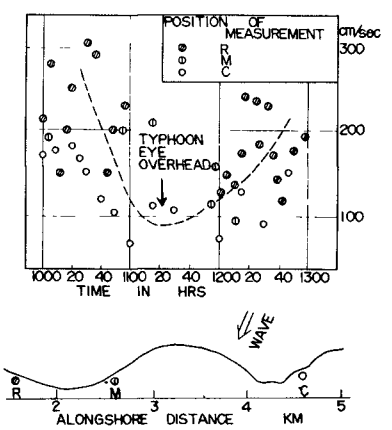

Figure 29. Alongshore components of swash currents by typhoon waves measured at different positions of shoreline rhythm, Sept. 1958, Tokai beach.

fined in an embayment of the rhythmic undulation of the shoreline.

This ideal pattern of currents will undergo a change if the current velocities are intensified. Fig. 29 shows an extreme case in which the alongshore components of swash currents were observed at the shoreline during the peak of typhoon waves. We still recognize the effect of the rhythmic configuration of shoreline on the current pattern, i.e. the currents are speedier at the place which is exposed to wave incidence (R), while they are relatively low at the sheltered side of the shoreline apex (M and C).

LONGSHORE DRIFT

Significant drift of longshore sediment occurs mainly along the shoreline and the bar crest where the bottom deposit are easily set in suspension by agitating action of breakers. According to the observation of the authors, these two types of longshore drift seem to occur in a step-and-rest manner following the rhythms on the shoreline and the bar.

In order to study the behavior of beach drift, the authors dumped brick fragments of about 16 mm in median diameter in front of a beach cusp on the Tokai beach. The breaker height was about 1 - 2 m, and the current velocities ranged from 5 to 30 cm/sec. The drifting fragments were washed away to the shoreline step and none was found to return to the shoreface, whereas it is usually believed that beach drift along the shoreline occurs in a continual zig-zagging action on the shoreface slope. Interestingly enough, they were discovered at the updrift step of the downstream apex in an appreciable quantity. Our explanation of this field experiment is that where there exists a conspicuous indentation of a beach cusp the beach drift will move in a stepping flight from one apex to another in the direction of the longshore current rather than dragged on the shoreface where exchange of swash between the neighboring embayments is hindered by a steep rise of the intermediate apex. In connection with this, it is recalled that the famous Einstein hypothesis on the movement of bottom deposit in a two-dimensional flow emphasizes on the rest time between flights of an individual grain. In the same analogy, it may be said in our case that the rate of beach drift along the shoreline will to some extent depend on the rest time of the bottom sediment on the updrift side of a beach cusp. However, we must think of a possibility that this ideal pattern will undergo a change, as has been the case with longshore currents, if wave conditions become more rigorous. Under such conditions,

a relatively stronger erosion will take place on the updrift side, producing a skew of the shoreline rhythm toward the downdrift direction.

In considering the littoral drift along the bar crest, it must be recalled that the longshore current takes a winding path roughly conforming the curvature of a longshore bar. There is no reason why the bottom sediment on the bar crest should not be affected by this winding behavior of current and carried along the same curvature from shoal to shoal. This path is a lengthy detour involving an appreciable process of diffusion midway, but it may still be relatively short as compared to the rest time during which the drifting sediment remain deposited at the shoal. Here again we are faced with the possibility of a rhythmic flight of littoral drift.

According to our hypothesis which has been discussed so far, we realize that it will be very difficult for the bottom sediment to travel perpendicularly across the surf zone between the shoreline and the longshore bar. In fact, as we have already seen, the embayment is a position which is most susceptible to erosion, or, in other words, a position where the drifting sediment will find it most difficult to arrive and settle. According to the observation of Dr. Mogi on the Tokai beach, when the beach was advancing the beach cusp occurred, but when it was retreating the beach cusp disappeared. It seems that only with appearance of a beach cusp the embayment can arrest a sufficient amount of beach drift.

Our hypothesis regarding the rhythmic behavior of littoral sediment will further lead us to propose a detailed process on the perpendicular movement of the surf-zone sediment. The conventional notion is that a steep wave erodes the beach by carrying an appreciable amount of beach material toward the offshore bottom, which is, however, carried back to the beach by a subsequent swell of a low steepness. Our explanation is that if a swell predominates there will be a strong onshore drag of bottom deposit at the shoal due to violent surging of refracted waves, thus giving rise to an increase in the portion of the beach drift as compared to the portion on the bar crest. On the other hand, if a strong wind wave predominates, there will be a reinforced component of offshoreward recompensation of incident energies in the form of a rip current or undertow, thus resulting in the increased portion of littoral drift along the bar crest and in the relative decrease in the beach drift. In the latter case, the result will often be an erosion at the shoreline.

SOME ENGINEERING IMPLICATIONS OF LITTORAL RHYTHMS

Dr. Bruun states in effect that a sudden silting may occur at a coastal inlet due probably to migration of a shoreline hump or wave. This statement seems an adequate warning, and in the light of our theory it must be afforded more emphasis since such an accident might recur due to the same wave which would not migrate away at a noticeable rate. The authors are aware of a case where a sudden advance of a shoreline at a portion of the eroding beach was attributed to some mysterious action of a newly built sea wall. Although the authors have not had an opportunity to investigate the sounding data on the beach in question, it is highly probable from our theory that it is due to the shifting action of a shoreline rhythm. No positive action of a sea wall could have been involved in this case.

The authors have been impressed, in reviewing a number of instances from aerial photographs, by an inadequately short length of coastal groins as compared to the distance of a longshore bar from the shoreline. However, in order to provide a workable design criterion on the functional specifications of groins or jetties, we will have to proceed further with a continuing effort to verify the hypothetical processes as tentatively proposed in the present paper with quantitative evidences.

The rhythmic distribution of wave impacts along the shoreline is also something to take into consideration in designing a coastal structure. This point commands a particular weight when a structure, such as a submerged breakwater, is to be placed on the offshore bottom where waves will act without undergoing a smoothing action by a bar. Further, by considering the stationary nature of the littoral rhythms and hence of the alongshore distribution of wave impacts, we may specify the local strength of a sea wall or a unit weight of armor elements for each position within the rhythm phase. In fact, on the Niigata west beach, the submerged breakwater was scoured by violent breakers and slumped from position to position. There is a sign that this failure pattern follows the undulation rhythms on the offshore bottom, although we have not yet completed numerical checking on the details of this process.

However, the most immediate and valuable gain from recognizing the presence of stationary littoral rhythms is a possibility that we can shed light on the seemingly intractible process of a coast by introducing an orderly procedure of approach. We are in a position to treat the undulating topographies on the coastal feature as

important "factors", which in the past have been understood as mere irregularities.

Finally, the present theory will provide helpful suggestions in planning a coastal investigation project, namely in determining the factors and areal extent to cover and emphasize as well as the reasonable procedures of measurement and the adequate period of investigation.

CONCLUDING REMARKS

1. A careful investigation of nearshore topographies by aerial photographs as well as sounding data has shown that a rhythmic bar system is tied in closely with various rhythms found along the littoral zone.

2. These rhythms are classified roughly into three different types of the order ranging from 10^0 to 10^3 m.

3. These rhythms, represented in various factors such as longshore bars, shoreline configurations, deposit and slope of shoreface, waves and currents, have been found to originate at the undulations inherent to the offshore bottom.

4. The origin of such a large-scale rhythm on the offshore bottom as well as dendritic ridges or valleys on the inshore bottom, has been left for a future problem.

5. Several hypotheses have been presented as to the rhythmic transformation of incident waves, rhythmic behaviors of littoral currents and drifts.

6. Recognition of the presence of stationary rhythms on a coast yields useful suggestions regarding the engineering purposes.

ACKNOWLEDGEMENTS

The authors have taken liberty of making extensive references to the existing contributions to the problems of coastal topography as well as the aerial photographs and sounding data by various agencies in Japan. A grateful appreciation is due to these authors.

Assistant Professor K. Horikawa, University of Tokyo, has provided the authors with generous suggestions and cooperation during the course of preparing this paper. Misses I. Nurino and R. Toyaku have been extremely helpful in preparing the figures of this paper. A profound gratitude of the authors is also

due to these people.

The authors remain profoundly grateful to Dr. M. Hosoi, Chief of Coastal Engineering Laboratory, Public Works Research Institute, Public Works Ministry, who has generously sponsored part of this project.

REFERENCES

1. Shepard, F. P. (1950). Longshore bars and longshore troughs, Beach Erosion Board, Tech. Memo. No. 15.

Shepard, F. P., K. O. Emery, and E. C. La Fond (1941). Rip currents; a process of geological importance, Journ. Geol., vol. 49.

2. Keulegan, G. H. (1948). An experimental study of submarine sand bars, Beach Erosion Board Tech. Rep. No. 3.

3. Fujiki, N. (1957). Instrumentation and accomplishments of the coastal investigation facilities for the winter stormy season at Niigata, Proc. of 4th Conference of Coastal Engineering, Japan, (in Japanese).

4. Johnson, D. W. (1919). Shore processes and shoreline development.

5. Per Bruun (1954). Migrating sand waves and sand humps, with special reference to investigations carried out on the Danish North Sea coast, Proc. of 5th Conference on Coastal Engineering.

6. Evans, O. F. (1938). The classification and origin of beach cusps, Journ. Geol., vol. 46.

Evans, O. F. (1945). Further observations on the origin of beach cusps, J. Sed. Petr., vol. 53.

7. Kuenen, Ph. H. (1948). The formation of beach cusps, Journ. Geol., vol. 56.

8. Mogi, A. (1960). On the topographical change of the beach of Tokaimura on the coast of Kanto district, Japan, Geographical Review of Japan.

9. Bascom, W. H. (1951). The relationship between sand size and beach-face slope, Trans. A. G. U., vol. 32, No. 6.

CHAPTER 17

LABORATORY APPLICATIONS OF RADIOISOTOPIC TRACERS TO FOLLOW BEACH SEDIMENTS

Norman E. Taney
Chief, Geology Branch, Beach Erosion Board
Department of the Army, Washington, D. C.

For many years coastal scientists and engineers have attempted to label sedimentary particles in order that their movement paths might be determined. Several attempts have been made at the Beach Erosion Board, none of which met with any measure of success. Furthermore, inherent in this system is an extensive sampling program and arduous identification of the labelled particles. Recently, however, the labelling of natural sediments or simulated sediments with radioisotopes as tracers has proved successful and a long sought goal has been achieved.

The utilization of radioactive material as sediment tracers has increased during the approximately 10 years since its inception. Since the initial test in the Thames River[1] in England, the utilization of this technique has spread until it is practically worldwide.[2-8] In the main, the objectives of these tests have been qualitative, the determination of movement path and of sedimentation areas of the tracer material, and thus of the sediments, which are being followed. Labelling techniques have varied widely and involve plating or precipitating a thin film of radioactive material on the natural sediments, the utilization of glass containing a radioactive tracer to simulate the natural sediments, the incorporation of radioactive material within the natural sediments or within simulated sediments, and ion exchange between the natural sediments and tracer material. The means of detection have also varied broadly: Geiger-Mueller systems with one or several GM tubes in gangs, scintillation systems making use of pulse-height spectrometry, and autoradiographic techniques have all been used. The monitoring has varied also as sediment and tracer materials have been monitored in situ or samples have been taken and the monitoring accomplished in the laboratory.

The staff of the Beach Erosion Board has been interested in this new application of radioisotopes since 1955. A literature survey was initiated at that time and is continuing at present. A feasibility study was completed in 1958 which indicated that radioisotopic tracers presented a new technique with which to study sediment transport. The report strongly recommended that studies be planned and executed utilizing this technique. In the Annual Bulletin of the Beach Erosion Board, 1960,[9] several test objectives and procedures were outlined.

EQUIPMENT

About the same time, May 1960, the equipment necessary for such types of tests was acquired. The equipment includes a commercial power supply, a linear amplifier, scaler, and electric timing device, and a single-channel pulse-height analyzer. A 2 x 2 inch sodium-iodide, thallium-activated crystal coupled to a photomultiplier tube form the

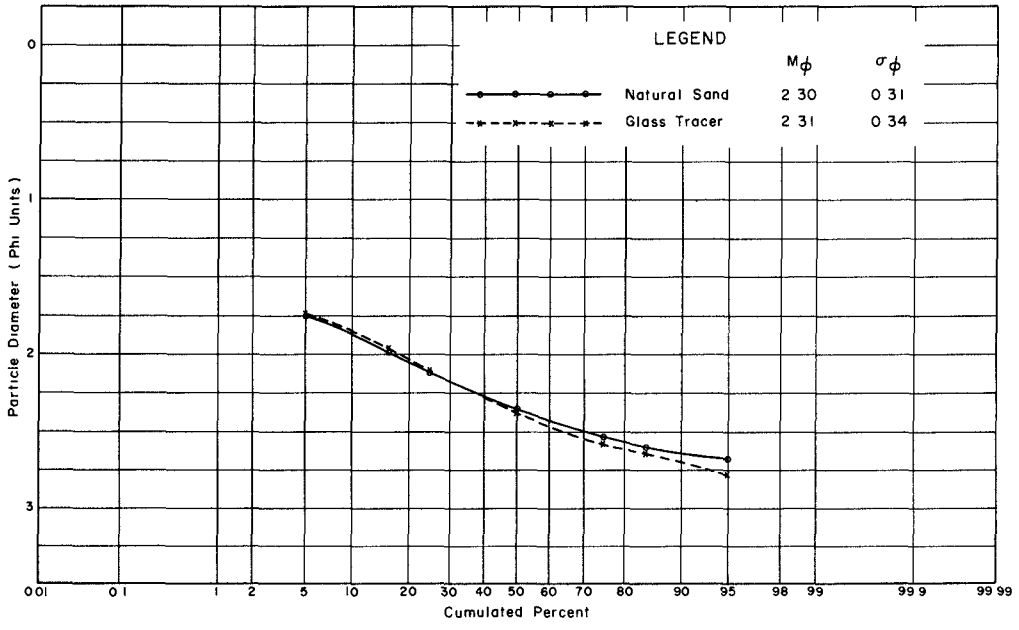

Fig. 1. Cumulated Particle Size Distribution of Natural Sand and Glass Tracer.

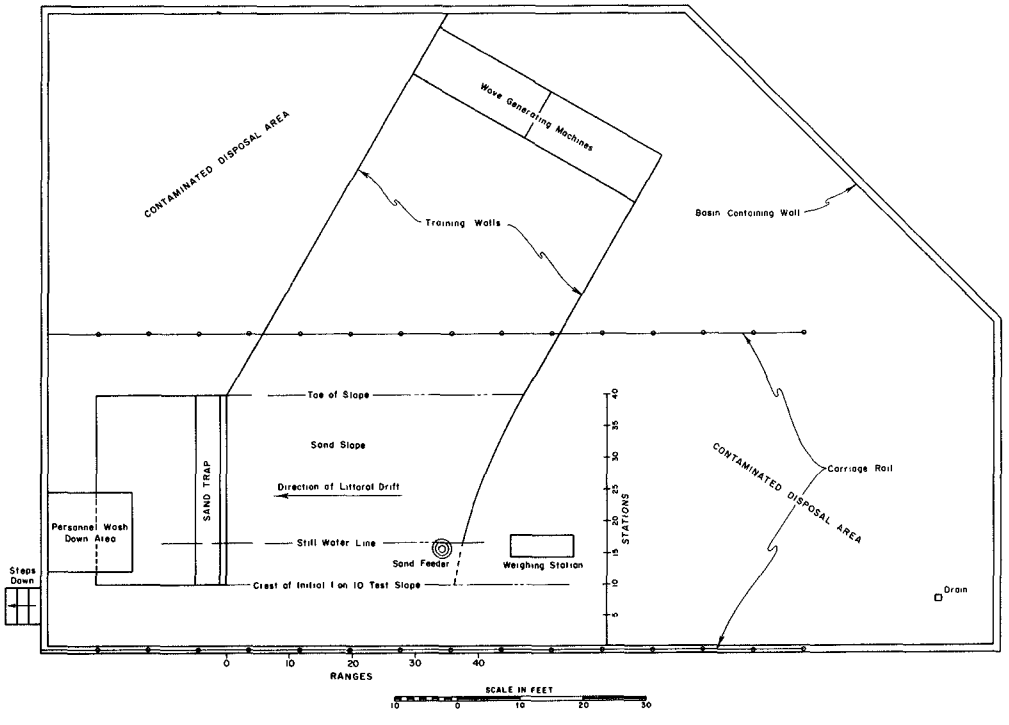

Fig. 2. North Sector Shore Processes Test Basin, Beach Erosion Board.

heart of the detection system. The crystal, photomultiplier and preamplifier are all enclosed within a waterproof aluminum can.

Glass

The the spring of 1962, three special glasses were prepared at the United States National Bureau of Standards. The first glass and one utilized in the test which is the subject of this paper contained aproximately 1.5 percent sodium as the tracer isotope. The density of the sodium glass is 2.656 grams per cubic centimeter. The glass was ground, separated into its size components by sieving, and recombined to make up a cumulated size distribution which is the same as that of the natural sand in the test sector. The glass size distribution was determined hydraulically and compared with the size distribution of the natural sand. Figure 1 shows the final distributions.

Shore Processes Test Basin

The laboratory facility in which the test took place is the north sector of the Shore Processes Test Basin at the Beach Erosion Board. Figure 2 is an illustration of this section of the basin. The test beach is approximately 30 feet long bound on one side by a sand trap and on the other side by an area called the feeder beach on which the sand feeder[10] is placed. The sand feeder is a device which supplie sand to the beach as it is required. Immediately to the right is the weighing station in which the sediments which have been removed from the trap are weighed to determine how much material has been moved in the alongshore direction. Contaminated disposal areas for the sand containing radioactive glass and all other contaminated materials were on eithe side of the test beach. The original slope in the test beach area was 1 on 10, with the toe of the slope at station 40. Still water elevation is 2.33 feet above tank bottom at station 17.6 and the uniform slope continues up to station 10 at elevation 3.0 feet above tank bottom Thence the beach is level to station 0 at the confining wall of this sector of the basin.

TEST CONDITIONS

Wave parameters remained constant during the entire test. The wave amplitude at the generator blade was 0.15 foot and the period was 1.5 seconds. The wave height at the plunge zone was approximately 0.2 foot. Prior to injection of irradiated glass, waves had been generated and had affected the test beach for 9 hours. The surface elevation of the beach had been measured after 1, 2 and 5 hours of wave action, Figure 3 shows the elevation of the beach and nearshore bottom as it was after 5 hours of wave action.

Background activity as determined with the detection system always proved very minor. Background in water decreased from approximately 250 counts per minute on the day of injection to 90 counts per minute during the last day of the test while the background counts in air were 90 and 60 counts per minute from the first to the last day respectively. Background as determined by autoradiographic means proved

nonexistent. Because of the low background it was decided arbitrarily to accept as statistically significant all values which were at least twice that of background.

TEST OPERATIONS

INJECTION OF TRACER

Approximately 56 grams of the sodium glass was sent to the United States Oak Ridge National Laboratory for irradiation. After a week of irradiation the glass was received by air freight on Tuesday August 21, 1962 in four shipping containers which contained of the order of 50 millicuries of sodium-24 activity. At the Beach Erosion Board three of the containers holding approximately 50 grams of irradiated glass were opened immediately. Some difficulty was encountered decapping the aluminum irradiation cans because, through an oversight, the proper instrument had not been sent from Oak Ridge. After tops were removed the quartz ampoules containing the glass were placed in a pipe with long-handled tongs, see Figure 4. The ampoules were crushed with a long-handled rammer and the pipe was emptied onto a screening device, placed in the concrete mixer, which permitted the glass particles to pass but retained the larger ampoule particles. Thirty-five pounds of sand and five fluorescent tracers were in the mixer.

After the three ampoules had been emptied into the concrete mixer the screen was shakened to be sure that all of the irradiated glass fell onto the sand. Then the screen, the long-handled rammer, the pipe and the pipe stand were removed to the contaminated disposal area and weighted to remain beneath the water surface in this area.

While the contaminated equipment was being removed brown wrapping paper was being fastened over the mouth of the concrete mixer to prevent loss of radioactive material during the 10 minute mixing period. Ten minutes were required to insure complete dispersal of the irradiated glass grains throughout the 35 pound mass of natural sediment. At the completion of the mixing period the brown wrapping paper was removed to the contaminated disposal area and the sand containing irradiated glass and fluorescent tracers was dumped into an ordinary garden fertilizer spreader mounted on tracks which were fastened to the carriage, see Figure 5. The spreader distributed sand over a 16-inch-wide path centered on range 28. The travel path was limited to 12 feet by two clamps, one being 2 feet landward from still water level at station 15.6 and the other being 10 feet seaward from still water level at station 27.6. Two sheet metal pans, one at each end of the spreader traverse, were placed to prevent an excessive accumulation of radioactive tracer material at each end of the injection area. The spreader gate was opened and the sand, irradiated glass and fluorescent tracers were injected in some eighteen passes over the injection area. When all of the sand had been dispersed including that which had been caught in the sheet metal pans the tracks were swept clean. A fluid to reduce surface tension was sprayed on the water surface to cause those particles which still floated to sink to the bottom in the injection area; however, a very small amount of material did not sink to the bottom but

LABORATORY APPLICATIONS OF RADIOISOTOPIC TRACERS TO FOLLOW BEACH SEDIMENTS

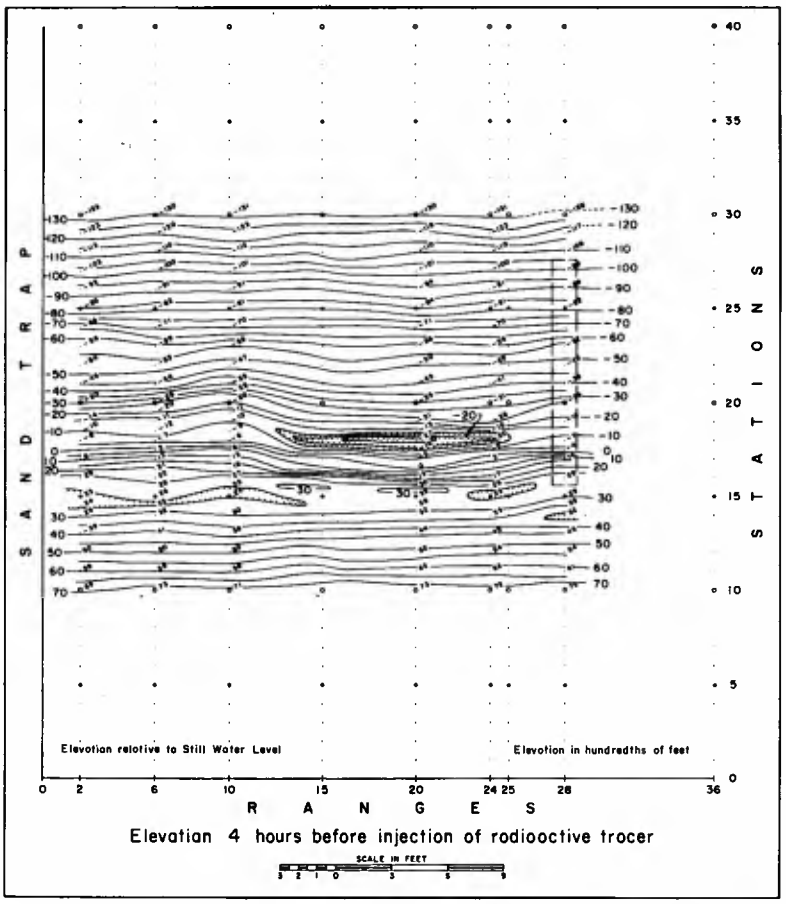

Fig. 3. Elevation 4 Hours Before Injection of Radioactive Tracer.

Fig. 4. Tracer Injection Equipment and Technique.

floated away. At this time the carriage was moved to a hazard-free area. The concrete mixer was removed from the track and placed in the water, the spreaker and all other contaminated gear were removed to the contaminated disposal area.

A thorough check was made at this time to be sure that no contamination remained in any area except the injection area in order to preclude any possible hazard. The carriage was now reestablished over range 28, the center of the injection area, and a radioactive survey was made by monitoring stations at 1 foot intervals. The detection device and monitoring equipment are shown in Figure 6. Three traverses normal to range 28 were also surveyed to define the extent and character of the injection area. Figure 7 shows the activity distribution in and around the injection zone.

OPERATIONS

The carriage was again moved to a hazard-free area and wave action was initiated and continued for 5 minutes. Because the incident waves approached the beach at an angle, sand and tracer materials were moved in the alongshore direction and deposited in the trap at the end of the test beach. During this time as the sediment was deposited in the trap it was removed from the trap through the eductor system and pumped to the weighing station. At the end of the 5-minute period of wave action, the wave generating machines were turned off and the area was surveyed. Ranges 2, 6, 10, 15, 20 and 25 and the injection range 28 were monitored at 1-foot intervals for 30-second counts at each station. This survey was extended sufficiently above and below still water level to stations where activity was not above background. Figure 8 is an isoactivity map corrected to time zero which shows the dispersion of activity as it occurred after 5 minutes of wave action. The decay correction will be discussed later. It is most interesting to note that after 5 minutes of wave action the activity had already reached the trap in very significant amounts. At the completion of the radiological survey, which took approximately 2 hours, samples were taken along ranges 2, 6, 10, 15, 20 and 24 at 1-foot intervals. A thin film of petroleum jelly was smeared on a card over a 1-square inch area. The card was then pressed onto the surface of the beach to secure a surface sample of sediment approximately 1 or 2 grains thick. These samples are for future study to determine the dispersion of the fluorescent tracer materials.

A second 5-minute period of wave action was initiated and upon its completion the same radioactive survey and sampling procedures were executed. At this time one core was secured. The core is approximately 1 3/4 inches in diameter and 6 inches long. It is essentially an undisturbed sample of the sediment with depth. In the laboratory the sediment core was extruded from the plastic coring tube and a sample essentially 1 or 2 grains thick was taken. Samples were secured from the surface and for every 0.01 foot increment to a depth of 0.1 foot. Then samples were secured for each 0.05-foot increment to a depth of 0.4 foot. The samples were dried and placed on standard X-ray film to determine the depth of penetration of irradiated glass particles by autoradiographic means. The exposure time for this technique was determined from

Fig. 5. Tracer Injection Equipment and Technique.

Fig. 6. Tracer Detector and Survey Equipment.

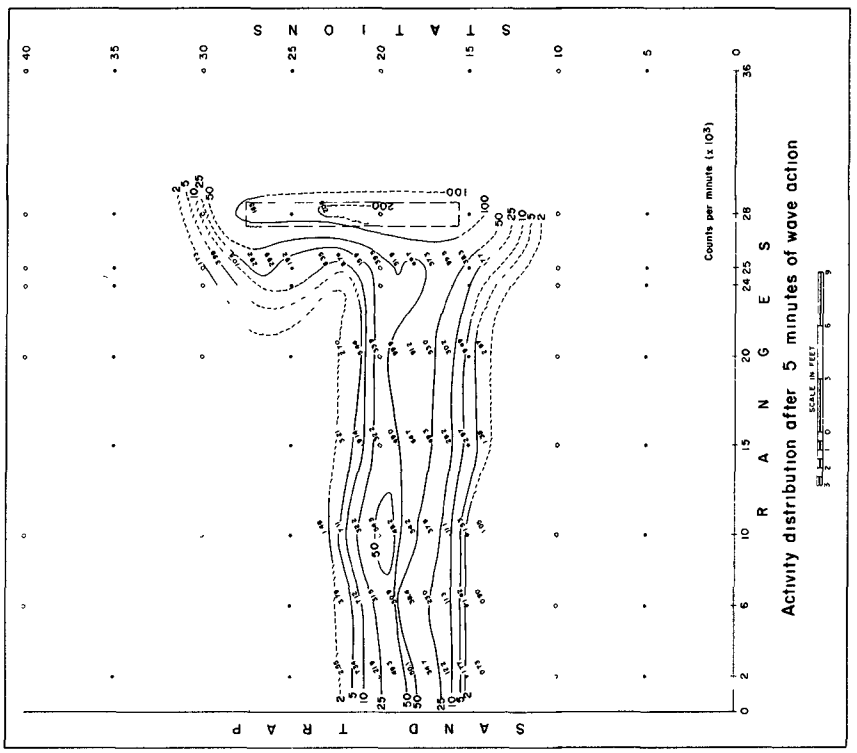

Fig. 8. Activity Distribution After 5 Minutes of Wave Action.

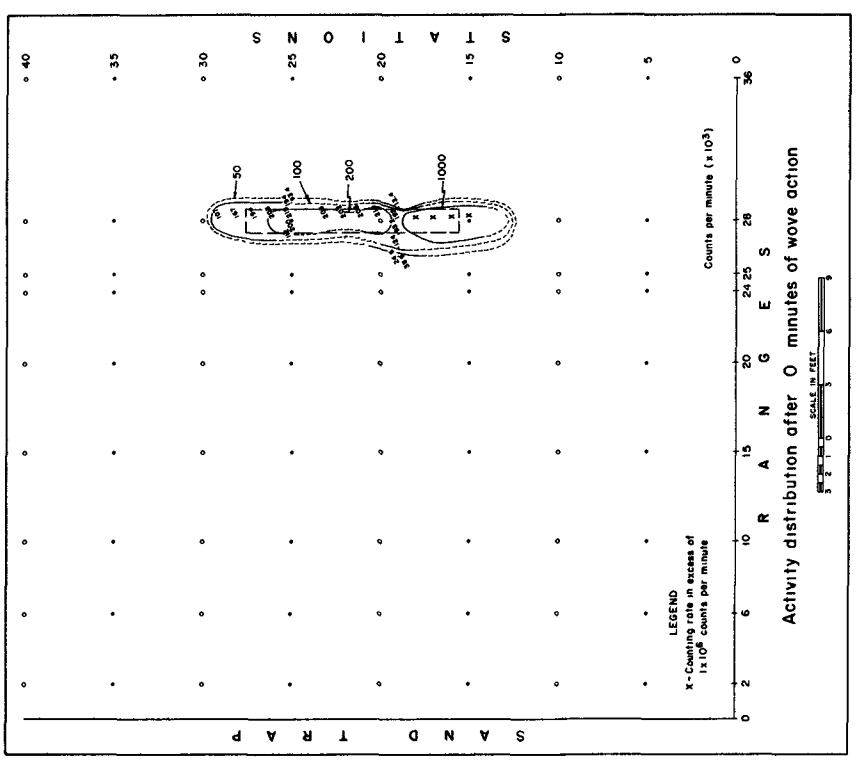

Fig. 7. Activity Distribution After 0 Minute of Wave Action.

a half-life study of the sodium glass and from a small pilot study utilizing sodium glass unmixed with sand.

Time reference

You will recall that 9 hours of wave action (H+9) had been completed prior to the injection of the tracer materials, the time of injection of the tracer materials is denoted as I+0. During the course of the radioactive tracer portion of the test the following wave action periods were executed; 5 minutes, 5 minutes, 5 minutes, 15 minutes, 30 minutes, and 60 minutes or a total of 2 hours of wave action. By Friday afternoon, the termination of the radioactive tracer portion of the test, the study was at H+11 hours or I+2 hours. After each period of wave action the activity was monitored and surface samples were taken. During the second 5 minutes of wave action it was realized that changes in surface elevation of the test beach might reflect the activity distribution; therefore elevation surveys were made after each period of wave action subsequent to I+5 minutes. Core samples were taken at I+10 minutes, I+15 minutes and I+60 minutes.

RESULTS

The results of the radioactive surveys are presented in Figures 7 through 13 as isoactivity maps. These maps portray the dispersion of the radioactive glass through space and time. All of these maps have been corrected to time zero, I+0. This correction is based upon the half life of the radioactive material which was determined to be approximately 17 hours. Inasmuch as sodium has a 15-hour half life, the longer half life indicated that some material other than sodium was present. Because of this correction each map may be compared directly with any of the others without considering the decrease in activity caused by radioactive decay. Figures 14 through 18 illustrate the elevation changes which occurred to the test beach after each period of wave action.

ACTIVITY DISTRIBUTIONS AND ELEVATIONS

At I+0 minute

Inspection of Figure 7 reveals that the activity distribution immediately after injection was fairly uniform over the portion of the injection area between stations 20 and 27 and that the average activity was determined to be between 200 and 210 thousand counts per minute. From station 18 shoreward to station 15, the shoreward limit of the injection area, the counts were in excess of 1,000,000 counts per minute, but could not be determined accurately because of mechanical limitation of the instruments. Water shielding probably caused the lower counting rates below water level.

At I+5 minutes

The activity distribution after 5 minutes of wave action is shown on Figure 8. By this time, the major dispersal patterns which were to be developed more fully with further wave action were already in

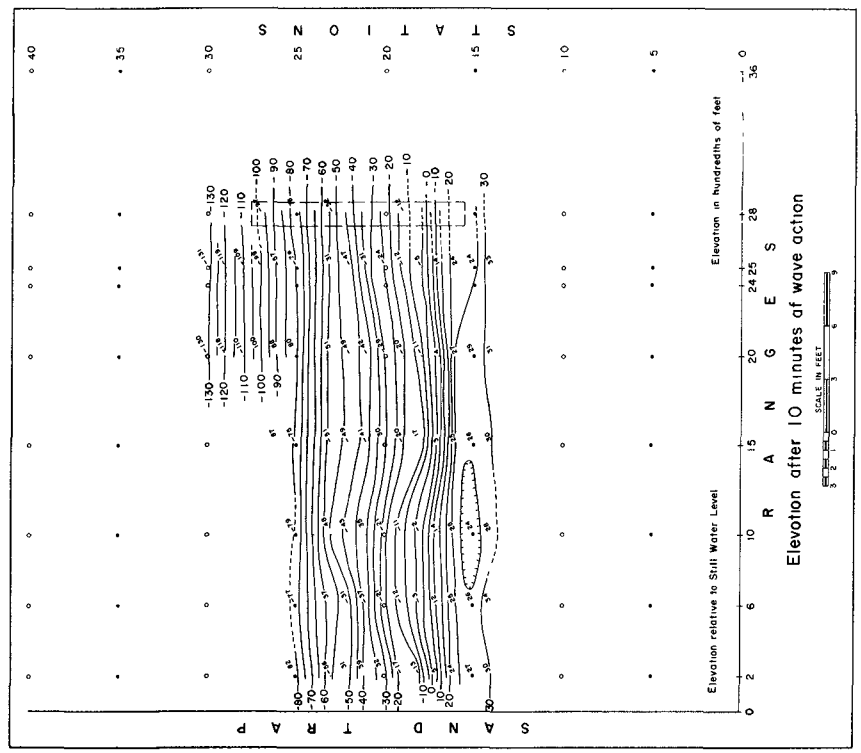

Fig. 14. Elevation After 10 Minutes of Wave Action.

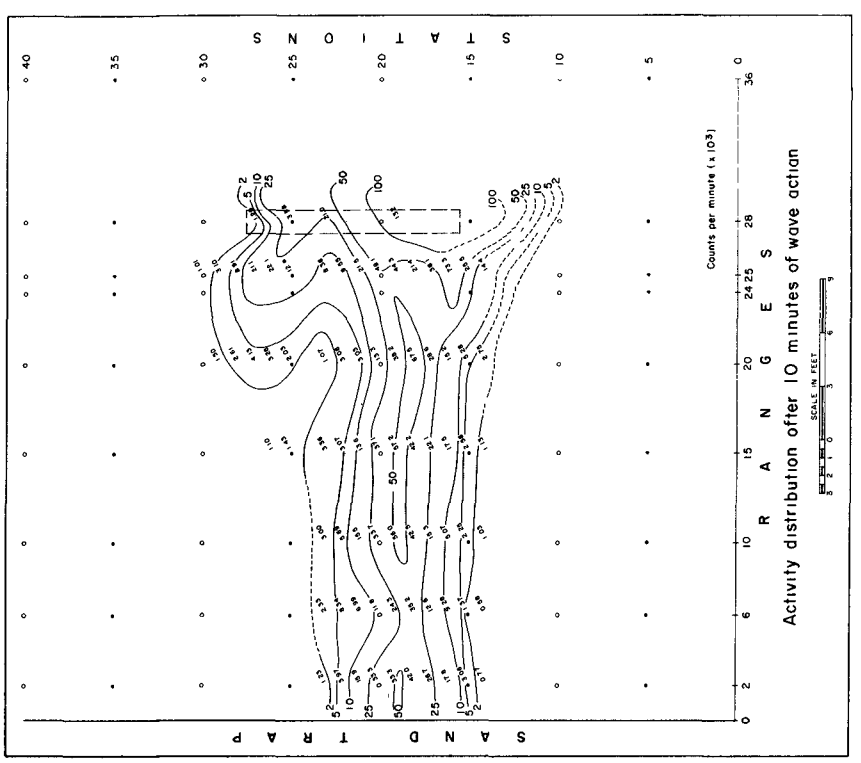

Fig. 9. Activity Distribution After 10 Minutes of Wave Action.

evidence. The major mode of alongshore transport is below or seaward from the still water level and appears to be in the vicinity of the plunge zone. Along range 25 a significant contribution to this major mode appears to come from above or landward from still water level, but by the time the material has reached range 20 much of the transport takes place below still water level. From range 20 to the trap the major alongshore transport mode is in the vicinity of stations 18 and 19. A most interesting mode of transport is shown at range 25 between stations 26 and 27, which appears to indicate a deep alongshore transport region. The counting rates are significantly high at these two stations which are separated from the major transport area by a low at station 22 of the order of one-fourth the counting rate at station 26. It may be coincidental but the deep alongshore transport zone is a little less than one wave length seaward from the plunge zone.

It is most interesting to note that during the first 5-minute period of wave action, significant quantities of activity had already reached the trap. This distance traversed was approximately 28 feet. This indicates that the alongshore transport rate in the vicinity of the plunge zone is in excess of 5 feet per minute. It should be pointed out that time required for the wave-generated littoral current to travel from the injection area to the trap (as determined by fluorescein dye tests) is of the order of 35 seconds.

At I+10 minutes

Figure 9 shows the activity distribution after 10 minutes of wave action. By this time the three zones of alongshore transport were well developed and were (from landward to seaward in direction) at approximately 2 feet above still water level, at the plunge zone, and some 9 or 10 feet seaward from the still water line. The magnitude of activity in these three zones, as determined by counting rates, appears to indicate that the transport above still water is approximately the same as at the plunge zone and that in the deep zone is of the order of one-half to one-third the intensity in the other two. Several most interesting phenomena are illustrated in Figure 9. The zone of alongshore transport above still water levels seem centered at about station 16 (range 25). This area is subject to wave uprush and alongshore transport is expected because of the angle of wave incidence. However by the time the movement reaches range 20, significant indications of a separate and distinct alongshore transport above still water level have disappeared. From range 20 to the trap the isoactivity contours are approximately parallel with still water line. Alongshore transport in the plunge zone is quite interesting in that for the first time this movement appears to be pulsating. A high activity area extends from about range 24 to beyond range 10, is interrupted by narrow neck of lower activity at range 6, and then increases again to the same order of activity magnitude at range 2. Finally, the zone of deep transport is now defined from range 28 to range 20 and appears centered about stations 26 and 27. It is most interesting to note that activities in the injection area are much reduced. There will be further discussion of this point later. Figure 14, the elevation map at this same time, shows a fairly regular surface with several small disturbances similar to the

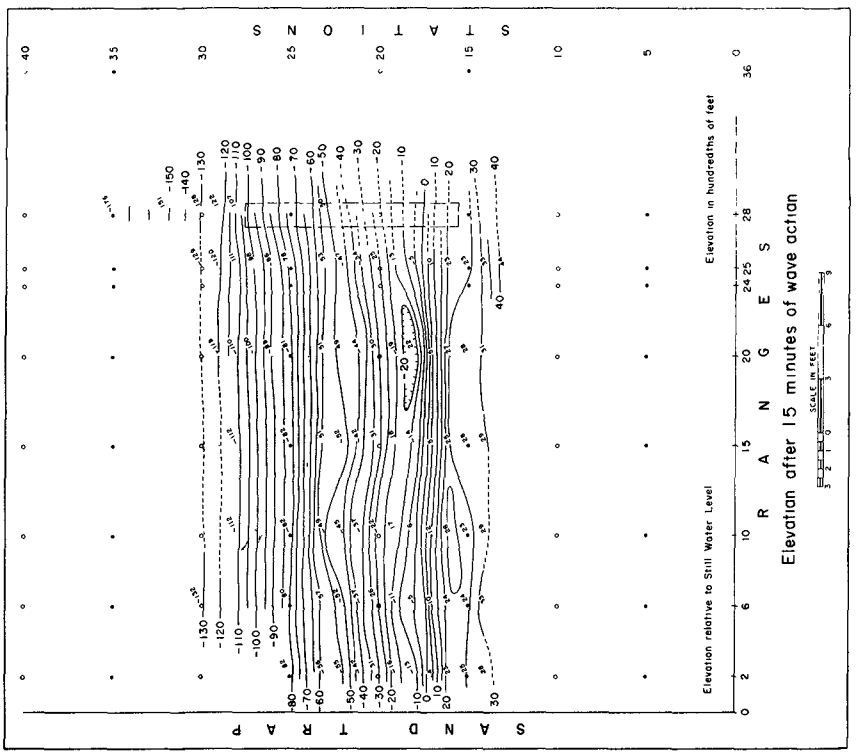

Fig. 15. Elevation After 15 Minutes of Wave Action.

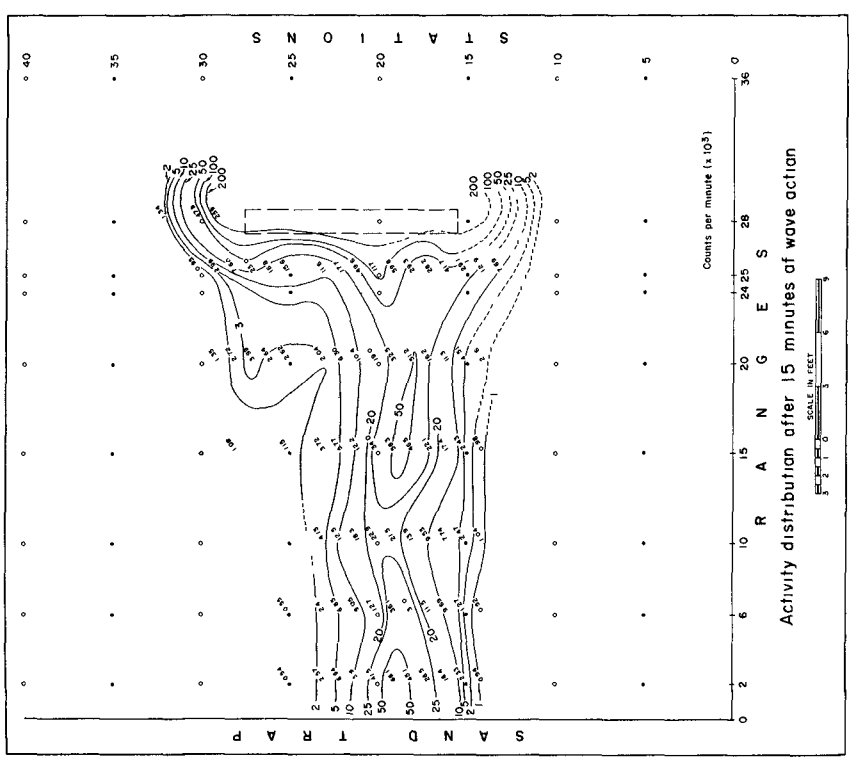

Fig. 10. Activity Distribution After 15 Minutes of Wave Action.

isoactivity map. These disturbances may be noticed at range 25 station 15, an area of high activity above still water level, and at ranges 10 to 6 at stations 23 and 22 respectively where the contour curvature approximates that of the isoactivity line. It is also interesting to note that no indication of the bulb-like protuberance shown on Figure 9 appears on Figure 14.

At I+15 minutes

Figures 10 and 15 portray activity distribution and elevation respectively after 15 minutes of wave action. Once again the alongshore transport is clearly defined in the vicinity of the plunge zone. The pulsating character of this movement is unmistakable and the narrow low-activity neck between the two pulses has been displaced from range 6 (at 10 minutes) to range 10. Also, the lateral extent of the pulse is much smaller. The 20,000-counts-per-minute isoactivity lines have been included to more clearly portray the changes which have occurred. The other two zones of the alongshore transport have been subdued and are not nearly as evident as they were in the previous slide; however in the deep zone of transport the 3,000-counts-per-minutes isoactivity line definitely indicates movement of a lower order of magnitude. It is interesting to note on Figure 15 that a scour area centered about range 20 station 18 corresponds with a high activity pulse in Figure 10. No similar condition is shown along ranges 2 or 6 to indicate the high activity adjacent to the trap.

At I+30 minutes

Figures 11 and 16 portray activity distribution and elevations after 30 minutes of wave action. In Figure 11 the three zones of alongshore movement are again clearly defined. The order of magnitude of each zone is approximately the same as it was earlier as well as are the positions of the three zones. The pulsating character of the movement in the plunge zone is again shown by the presence of a low counting rate area at range 6 station 19. The 15 and 20,000-counts-per-minute isoactivity lines further illustrate this event. A rather interesting deep zone appears for the first time on range 2 station 25 where high activity is approximately opposite the zone of deep alongshore transport which has been recognized as early as I+5 minutes and which is quite clearly defined on this figure at ranges 15, 20 and 25. It is most enlightening to note that there has been enrichment of the activity seaward from station 20 in the injection area and, for instance, at station 23 range 28 this enrichment amounts to of the order of ten times the activity that was present upon injection. Figure 16 is quite regular and gives very little indication of transport as is shown by the isoactivity map.

At I+60 minutes

Figures 12 and 17 and represents conditions at I+60 minutes. Starting at range 28 (Figure 12), the injection area, several interesting points are to be noted. In the transport zone above still water level the counting rate is now at least an order of magnitude below its former value at I+10. At still water level and for some 2 or 3 feet

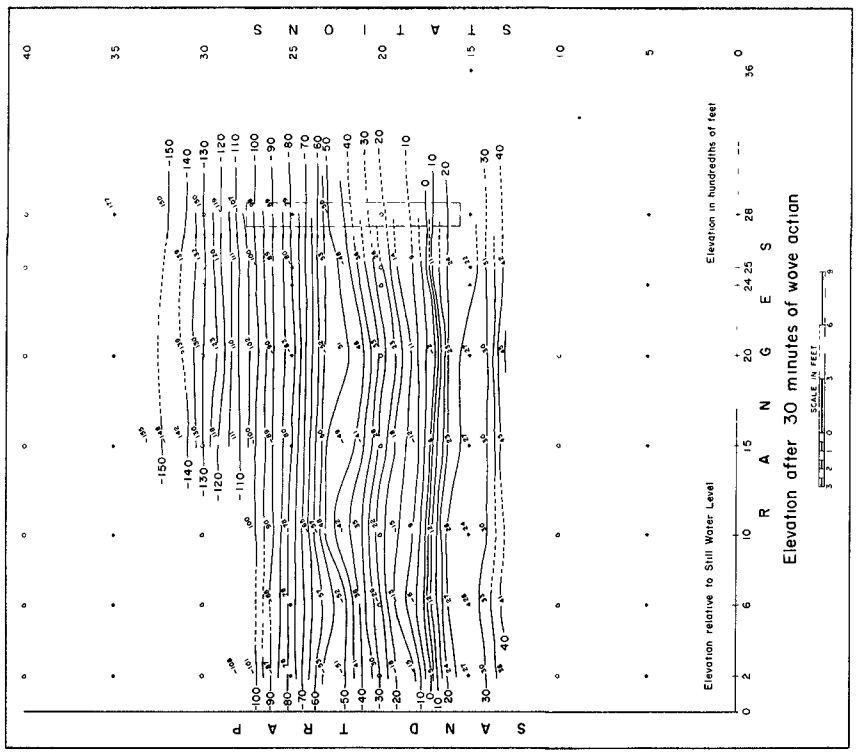

Fig. 16. Elevation After 30 Minutes of Wave Action.

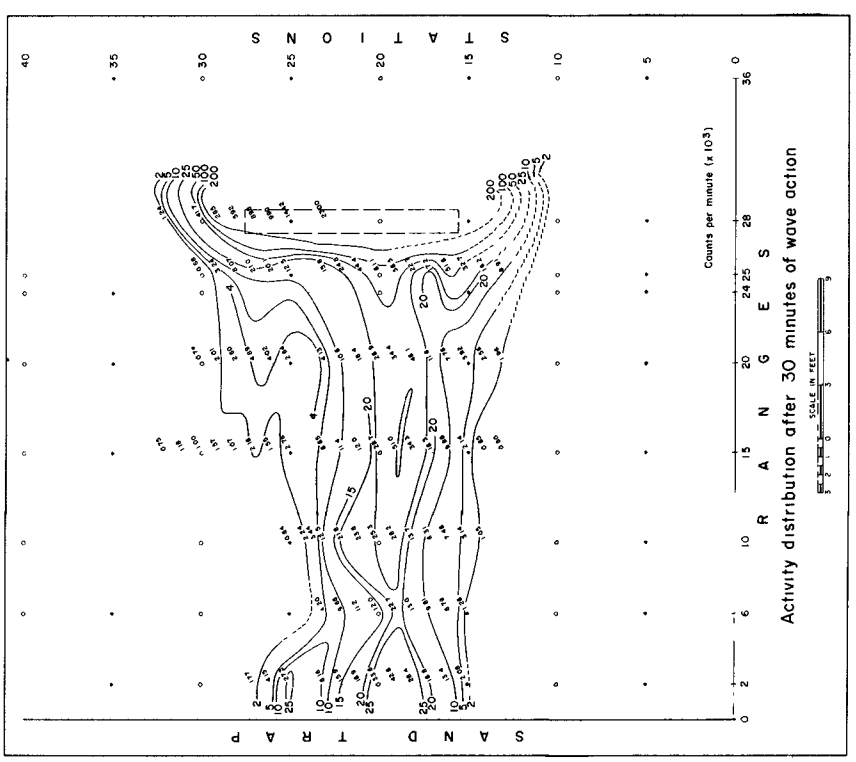

Fig. 17. Activity Distribution After 30 Minutes of Wave Action.

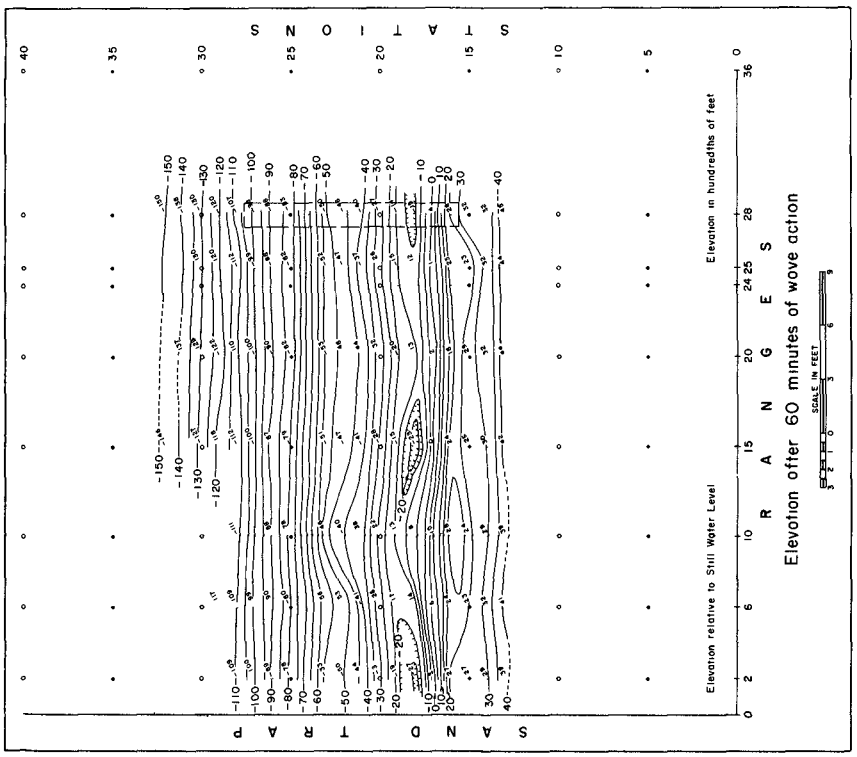

Fig. 17. Elevation After 60 Minutes of Wave Action.

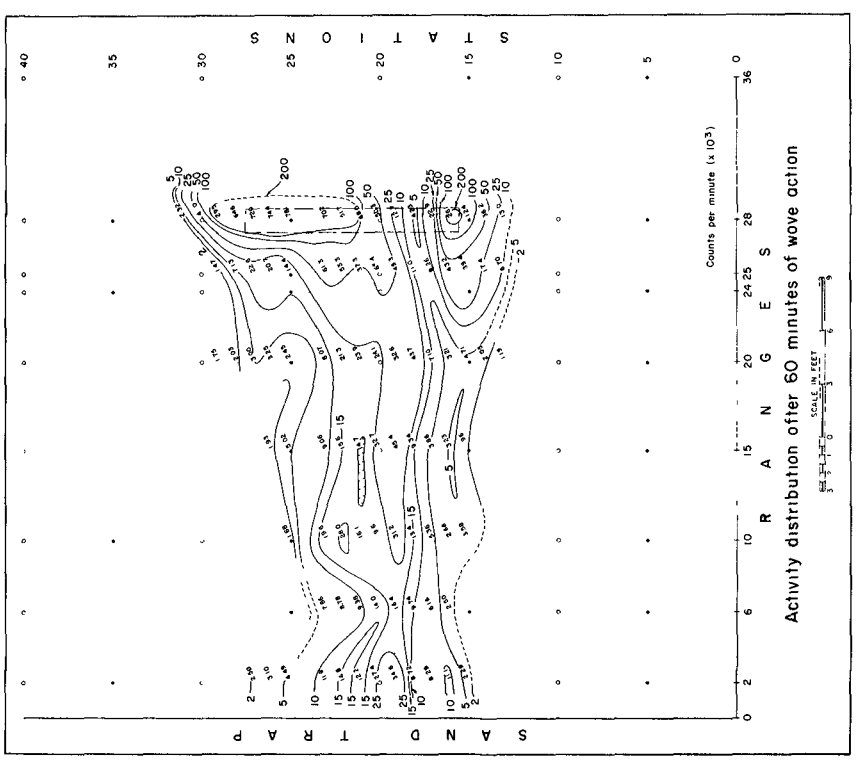

Fig. 12. Activity Distribution After 60 Minutes of Wave Action.

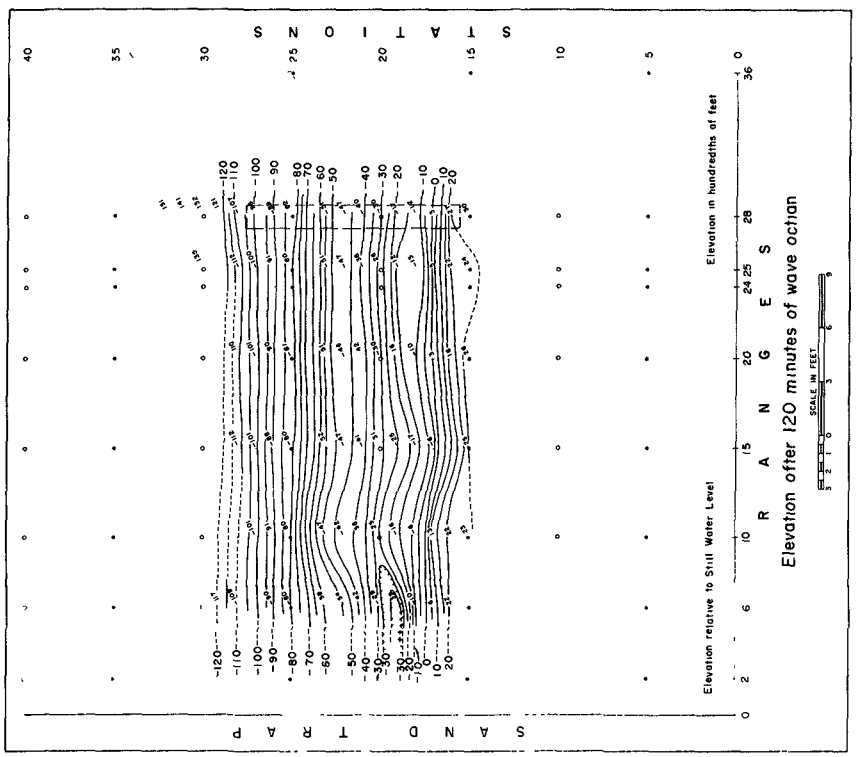

Fig. 18. Elevation After 120 Minutes of Wave Action.

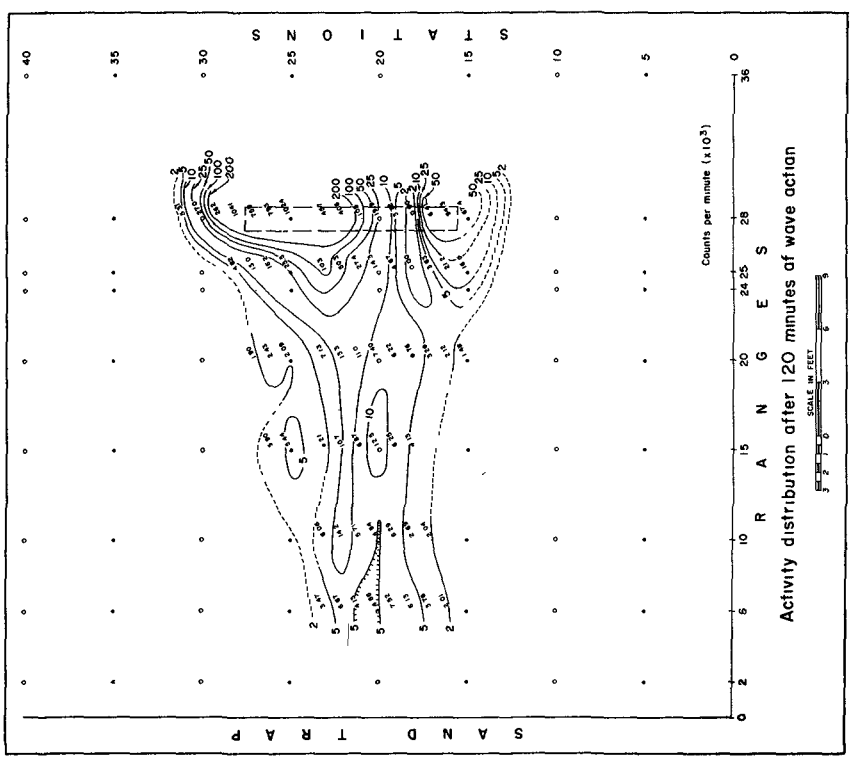

Fig. 13. Activity Distribution After 120 Minutes of Wave Action.

seaward, the counting rate is much lower than it was at injection time. Farther seaward it is some three to four times greater than it was at injection time. At range 25, there is definite indication of an above still water alongshore transport and a broad zone from station 19 to 23 indicates below still water level transport. The deep zone of transport is not as clearly defined along this range although there is a definite high at station 27. At ranges 15 and 20 the three zones of alongshore transport are very evident. Range 6 is once again the region which portrays the pulsating nature of sediment transport in the plunge zone. An erosion area in the injection zone on Figure 17 corresponds with a very low counting rate on Figure 12, and a similar erosion depression on range 2 station 18 corresponds to a low counting rate at that point. There is, however, no indication on Figure 17 of the high counting rate centered between stations 19 and 20 on range 2. Also, there is again no indication of the deep transport area on any of the ranges of Figure 17.

At I+120 minutes

Figures 13 and 18 portray conditions after 2 hours of wave action. There was, unfortunately, insufficient time to complete the surveys and when time was available the activity had completely disappeared. Two most interesting points to be noted on Figure 13 are that in the injection area from station 18 (1-foot seaward from still water line) to station 19 the activity has been completely removed and background counting rates exist. On either side of this zone much greater activities show movement away from still water line. The second point of interest is that the magnitude of the counting rates had diminished greatly by the time 2 hours of wave action had been completed. The elevation map does not reflect the dispersion patterns.

Cores

As was stated earlier, one core was taken after I+10 minutes, five after I+15 minutes and ten after I+60 minutes. All cores were sectioned, as described earlier, and all of the I+10 and I+15-minute samples were exposed to X-ray film. Only one core from the I+60-minute group was sectioned and exposed because of lack of time. Table 1 presents the results of the autoradiographic test. Only a short core was recovered at range 20 station 16 due to the difficulty of coring dry unconsolidated sediments.

ANALYSIS OF DATA

The next series of figures show changes which have occurred between periods of wave action. These figures have been derived as the difference in activity at a given geographic point between two successive survey periods. When the activity at the later time is greater than at the earlier time the value on the change figure is positive and the reverse holds true when the activity at the later time is less than the activity at the earlier time. Only changes in activity distribution are shown as the changes in elevation do not follow any systematic pattern.

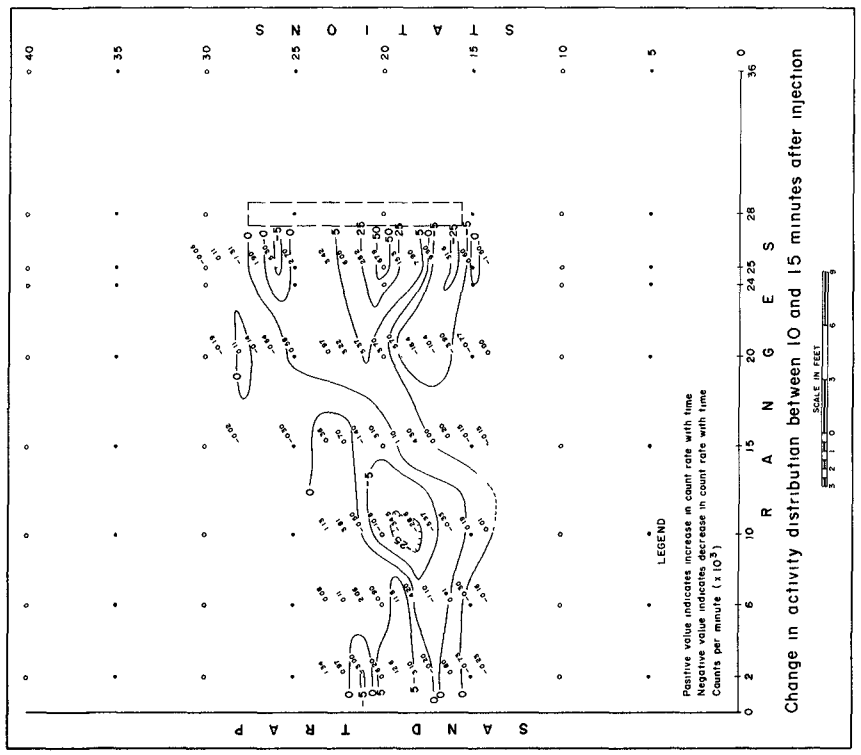

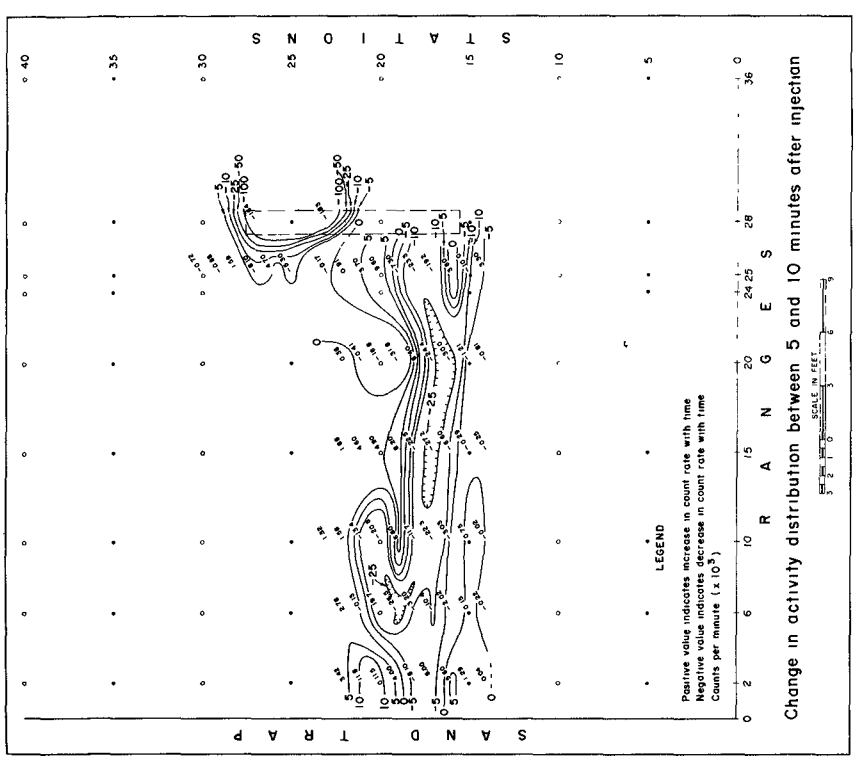

Fig. 19. Change in Activity Distribution Between 5 and 10 Minutes After Injection.

Fig. 20. Change in Activity Distribution Between 10 and 15 Minutes After Injection.

Table 1 - Depth of Penetration of Irradiated Glass Particles

Time (minutes)	I+10	I+15					I+60	
Range and Station	10-19	20-16	20-18	20-20	20-24.5	20-29	28-25	
Depth Below Surface(1)	Number of Radioactive Particles							Remarks
0	2	1	4	2	0	0	~ 70	
1		0	1	1	0	0	~ 50	
2	0	1	2	0	0	0	11	
3		0	3	0	0	0	4	
4	2	0	1	0	0	0	3	
5		0	3	0	0	0	1	
6	4		1	0	0	0	0	
7			2	0	1*	0	0	*Identifi-
8	2		3	0	0	0	0	cation
9			4	0	0	0	1	question-
10	0		2	0	0	0	0	able
15	0		0	0	0	0	0	
20	0		0	0	0	0	0	
25	0		0	0	0		0	
30	0		0	0	0		0	
35			0	0	0			
40				0	0			

(1) Depth measured in hundredths of a foot

CHANGES IN ACTIVITY DISTRIBUTION

Figure 19 portrays the change in activity between I+5 and I+10 minutes. The first point of importance lies within the injection area seaward from still water line. After 10 minutes of wave action the activity seemed to disappear in that the counting rate had decreased by an order of magnitude, 200,000 compared to 20,000. This decrease in activity could have been caused by the removal of the activity from the area or the covering of the activity by a movement of uncontaminated sand from some other area.

The negative lobe extending from the injection area in the vicinity of stations 25 and 26 clearly correlates with the deep zone of alongshore transport shown earlier in Figures 8 and 9. Above still water level in the vicinity of range 25 station 16, a small positive area indicates an above still water movement of activity from the injection area toward the trap. This small area continues to about midway between ranges 20 and 25. The zone of greatest movement, which is at the same location as the plunge zone, is indicated by a long narrow positive stringer stretching from the injection area to midway between ranges 6 and 10. Extending from range 6 toward range 10 is a small negative, Y-shaped area which points to the pulsating nature of the transport. Movement of activity into the trap is indicated at range 2 stations 17 and 18 while a build up of activity is indicated at stations

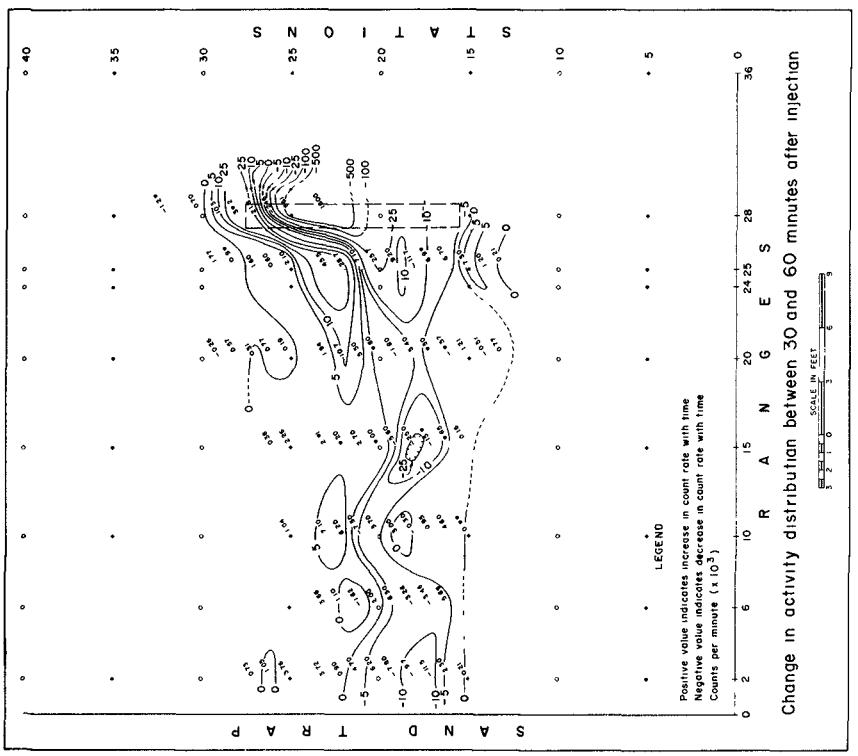

Change in activity distribution between 30 and 60 minutes after injection

Fig. 22. Change in Activity Distribution Between 30 and 60 Minutes After Injection.

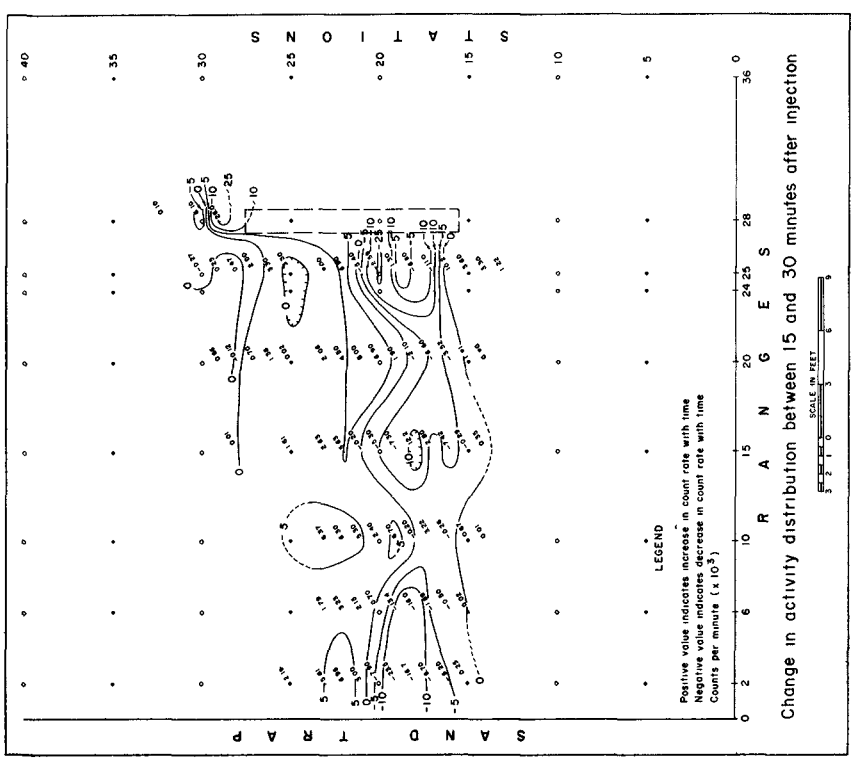

Change in activity distribution between 15 and 30 minutes after injection

Fig. 21. Change in Activity Distribution Between 15 and 30 Minutes After Injection.

20 and 21. The large negative area shown along ranges 15 and 20 appears to indicate movement not only in the alongshore direction but also toward the offshore where it joins with the transport along the plunge zone.

Figure 20 is quite different in character from Figure 19. The alongshore sediment transport zone above still water level and the deep trend are both negative indicating movement away from the injection area. In the wave plunge zone the formation of a new pulse of sediment moving from the injection area is denoted by a positive area in the vicinity of station 20 range 25. The negative values near station 30 range 25 indicate that the irradiated particles have either been removed from the area or that they have been covered by uncontaminated sediments. The negative area in the vicinity of stations 19 and 18 range 10 appears to be a break between the pulse which is just starting from the injection area and the pulse which is leaving the test area and being deposited in the trap.

Figure 21 portrays the changes in activity which occurred between 15 and 30 minutes after injection. Except in the vicinity of ranges 10, 20 and 25 all values above still water level are negative. Along range 20 at station 15, and range 25 at stations 16 through 14 the positive values appear to be the beginning of a movement of a new pulse or slug of material from the injection area. The very small positive value at station 15 range 10 indicates the placement by wave uprush of a small amount of activity near the berm. The negative values along range 25 from station 17 through station 21 reflect the removal of activity from this zone as a slug of material moves away from the injection area toward the trap. Further movement along the wave plunge zone is not clearly defined except in the vicinity of station 19 range 10 where a small positive area indicates the movement of a pulse of material. Between ranges 2 and 6 at stations 18 and 19 the negative values portray the removal of material. The general increase in activity in the offshore direction confirms offshore transport and deposition in deeper water.

It is important to understand that this Figure 21 and the two which follow do not clearly show the pulsating nature of the sediment transport. The reason is that the time between measurements for this and the two figures which follow is probably in excess of that required for a slug to form and be moved. As a consequence, only indications of pulses may be defined by the differences in activity illustrated by these figures.

Figure 22 shows the changes in activity distribution between 30 and 60 minutes of wave action after injection. The values below still water level in the injection area are highly negative, probably due to the interposition of uncontaminated sediment between the tracer particles and the detector. This fact is borne out in Figure 12 which shows counting rates of the order of three or four times in excess of those which were found immediately after injection. The positive tongue shown at station 15 range 25 probably correlates with the tongue of material moving above the still water level on Figure 12. The positive boot-shaped area extending from station 28 in the injection area to

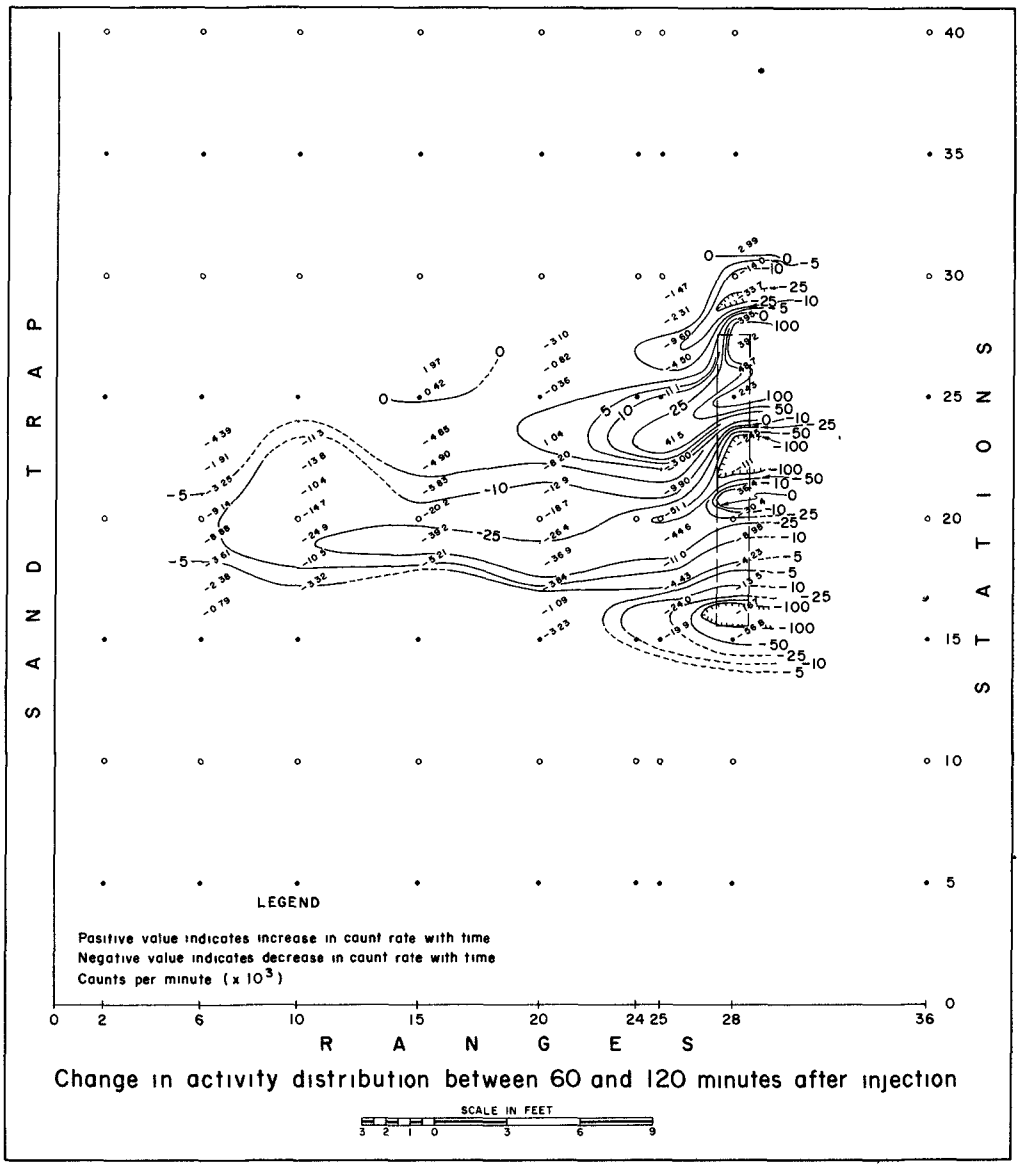

Fig. 23. Change in Activity Distribution Between 60 and 120 Minutes After Injection.

station 22 on range 20 indicates alongshore drift with a separate pulse probably indicated at a positive area in the vicinity of stations 22 and 23 on range 10. The negative areas at station 18 range 15 and stations 17 and 18 range 2 suggest pulsating transport of sediments with the center of the slug at station 19 range 10.

Figure 23 shows a general decrease in activity in practically all areas except the deep zone of the injection area. In this deep zone, stations 25 through 28 and 31, seaward or offshore movement of sediments is strongly indicated. The long narrow negative tongue which extends from range 10 to the injection area correlates with the removal of activity from in the vicinity of still water level to the plunge zone.

Seaward movement of activity is shown by all of the change in activity figures. Activities in excess of ten times background are found as deep as $1\frac{1}{2}$ feet below still water level at stations 32 and 33, some 5 or 6 feet seaward from the limit of injection. This offshore movement has clearly been defined from range 28 to range 15.

The data developed by autoradiographic means and presented in Table 1 were to be used to describe the thickness of the sediment zone disturbed by wave action. However the paucity of data makes the analysis inconclusive. The deepest irradiated particle was found 0.1 foot beneath the surface at range 20 station 18, the greatest depth in the trough in front of the bar crest present at station 19. This depth was corroborated in two other cores. It is interesting to note that the activity distribution with depth is random. The thickness at the landward limit (station 16) of the zone is 0.02 foot and at the seaward limit (station 24.5) is 0.01-foot. The 0.09-foot depth at station 25 range 28 is attributed to gradual deposition caused by seaward movement of the sediments.

Unfortunately the period of initial wave action was too long, so that significant quantities of activity had traversed the 28 feet between the injection area and the trap during the 5 minutes of initial wave action. For this reason it is impossible to make a definitive statement concerning the velocity of particle movement; however, the negative aspect of these data also furnishes information that the sedimentary particles are moving at velocities in excess of 5 feet per minute. The wave induced littoral current moves at a velocity which is approximately 45 to 50 feet per minute and the sedimentary particle at some slower velocity but greater than 5 feet per minute.

The results shown in Figures 7 through 23 seem to indicate several mechanisms which had not formerly been detected. The first of these is a changing movement in the onshore-offshore direction. An example of this movement is given by the increase in activity in the injection area in the vicinity of station 25 and deeper. While there has been an enrichment of the activity by a seaward movement of sediment and tracer material, there are also periods of low activity or low counting rate (an example is after 10 minutes of wave action). Seaward moving uncontaminated sediments could cover the activity and lower the count rate. However, the uncovering of the isotopic tracer as

evidenced by the high rates (at for instance 15 minutes and 30 minutes after injection) negates such reasoning and points toward an oscillatory motion, onshore-offshore. Analysis of the elevation data fail to clarify this problem as the phenomenon is not recognized in those data. A second mechanism of somewhat similar nature has been discussed as the pulsating transport of sediments in the alongshore direction. It appears quite clear that slugs of activity move in the alongshore direction. These slugs are separated from each other by areas of low activity and appear to form and move independently from each other. Again, no indication of this type of movement is shown by the elevation maps. Finally the deep alongshore movement had not been determined before by elevation measurements although it was known to exist from earlier experimental work. It may be that this deep movement, in water depths of approximately 1 foot, is quite significant in that the magnitude of activity appears to be of the order of one-half that of the material moving in the zone of wave swash and one-fourth or less of that moving along the zone of wave plunge.

Future plans involve further analysis of the data which resulted from the test which has been discussed and from a second test which was completed approximately a month ago. As a result of this first test, it is recognized that the use of sodium with its very short half life (15 hours) presents severe limitations which could be overcome by using an isotope with a longer half life, such as lanthunum ($T\frac{1}{2}$=40 hours) which was used in the second test. Also, as a result of this test, it would appear that measurements might well be taken at much shorter time intervals than formerly. Units of time such as 5 minutes would not prove excessively long.

In the over all it is considered that this first radioactive tracer test was eminently successful. Procedural techniques for this type of testing were gained. Limitations of the use of isotopes such as sodium were realized and data heretofore unavailable were measured and became available for analysis.

ACKNOWLEDGMENTS

The test described and the resulting data herein, unless otherwise noted, were obtained from research conducted under the Civil Works Investigation Program of the United States Army Corps of Engineers by the Beach Erosion Board with assistance from the United States Atomic Energy Commission. The permission granted by the Chief of Engineers to publish this information is appreciated. The conclusions reached and the methods presented herein are those of the author and they do not necessarily reflect the policy or views of the Corps of Engineers or Chief of Engineers.

REFERENCES

1. Great Britain Hydraulics Research Station (1956). Radioactive Tracers in the Thames Estuary: HRS/PLA Paper 20, Howberry Park, Wallingford, Berks, England.

2. Inose, S. and others (1955). The Field Experiment of Littoral Drift Using Radioactive Glass Sand: A/Conf. 8/P/1053, International Conference on the Peaceful Uses of Atomic Energy, Japan.

3. Krone, R. B. (1957-1960). Silt Transport Studies Utilizing Radioactive Isotopes: Annual Reports Numbers 1, 2, and 3, Institute of Engineering Research, University of California at Berkeley, California, U.S.A.

4. Arlman, J. J., P. Santema and J. N. Svasek (1958). Movement of Bottom Sediments in Coastal Waters by Currents and Waves; Measurements with the Aid of Radioactive Tracers in the Netherlands: Tech. Memo. No. 105, U. S. Beach Erosion Board, Corps of Engineers, Washington, D. C., U. S. A.

5. Davidsson, J. (1958). Investigation of Sand Movement Using Radioactive Sand: Lund Studies in Geography, Ser. A, No. 12, The Royal University, Lund, Sweden.

6. Gibert, A (1959). Observations on Sand Movement Under Seawater with Radioactive Silver Ag 110: No. IV/C/17/1 Radioelements, Home et Industrie, Geneva, Switzerland.

7. Hours, R. and P. Jaffry (1959). The Application of Radioactive Isotopes to the Study of Motion of Silt and Pebbles in the Rivers and in the Sea: La Houille Blanche, 14 Annee, Nr. 3, pp 318-347.

8. Poona Central Water & Power Research Station (1959). Radioactive Tracer Study for Sediment Movement Near Bombay Harbour: Annual Research Memoirs, Poona, Government of India, Ministry of Irrigation and Power, pp 343-346.

9. Taney, N. E. (1960). Preliminary Considerations of the Use of Radioisotopes for Laboratory Tracer Techniques: The Annual Bulletin of the Beach Erosion Board, Vol. 14, pp 16-27.

10. Savage, R. P. (1961). A Sand Feeder Beach for Use in Laboratory Littoral Transport Studies: The Annual Bulletin of the Beach Erosion Board, Vol. 15, pp. 1-5.

CHAPTER 18

A STUDY OF CRITICAL DEPTH AND MODE OF SAND MOVEMENT USING RADIOACTIVE GLASS SAND

Shoji Sato, Takeshi Ijima and Norio Tanaka
Hydraulics Division, Harbor Technical Research Institute,
Ministry of Transportation, Yokosuka, Japan.

INTRODUCTION

In Japan, in order to get foundamental data for harbor construction planning, radioactive glass sand has been used on the coasts of Tomakomai Irako, Fukue, Isohama, Kashima and Niigata as shown in Figure 1. The authors have directed these field experiments excepting Tomakomai and been doing model experiments using radioactive glass sand.

The field observation of sand movement using radioactive tracers has been already performed in several contries of the world and many works have been published. Authors have aimed to make clear the direction of sand transport in several depths of water and the critical water depth of sand movement where harbors are to be constructed, in order to get basic data for the best arrengement of breakwaters on sandy beach. The activity of radioactive glass sand (Co-60 and Sc-46) used at one point was several millicuries in the inland coast and several tens millicuries in the open coast.

In this paper, the qualitative characteristics of sand movement in the offshore and the breaker zone and the relations of waves, depth and bottom materials are estimated from the field experiments. Moreover, in the model test, the glass sand containing Cr-51 was used in order to study the mode of sand movement due to waves, in particular, the direction of ripple movement and sand transport.

THE PROPERTIES OF SAND MOVEMENT FROM FIELD EXPERIMENTS

METHOD OF FIELD EXPERIMENT

Preperation of radioactive glass sand The radioactive glass sand has mainly been made by irradiating glass sand containing cobalt or scandium in the nuclear reactor of Japan Atomic Power Reseach Institute.

The weight ratio of materials for the glass sand containing cobalt used at Kashima Coast is shown as an example.

SiO_2	$CaCO_3$	Na_2CO_3	$NaNO_3$	Co_2O_3
56.5%	15.1%	18.8%	1.6%	7.9%

These materials are melted together in an electric furnance and glass of specific gravity 2.65 containing 6.8% Of cobalt in weight is obtained. Then, it is crushed and seived to the required size and irradiated to have 80 microcuries of cobalt-60 per gram of glass sand.

A STUDY OF CRITICAL DEPTH AND MODE OF SAND MOVEMENT USING RADIOACTIVE GLASS SAND

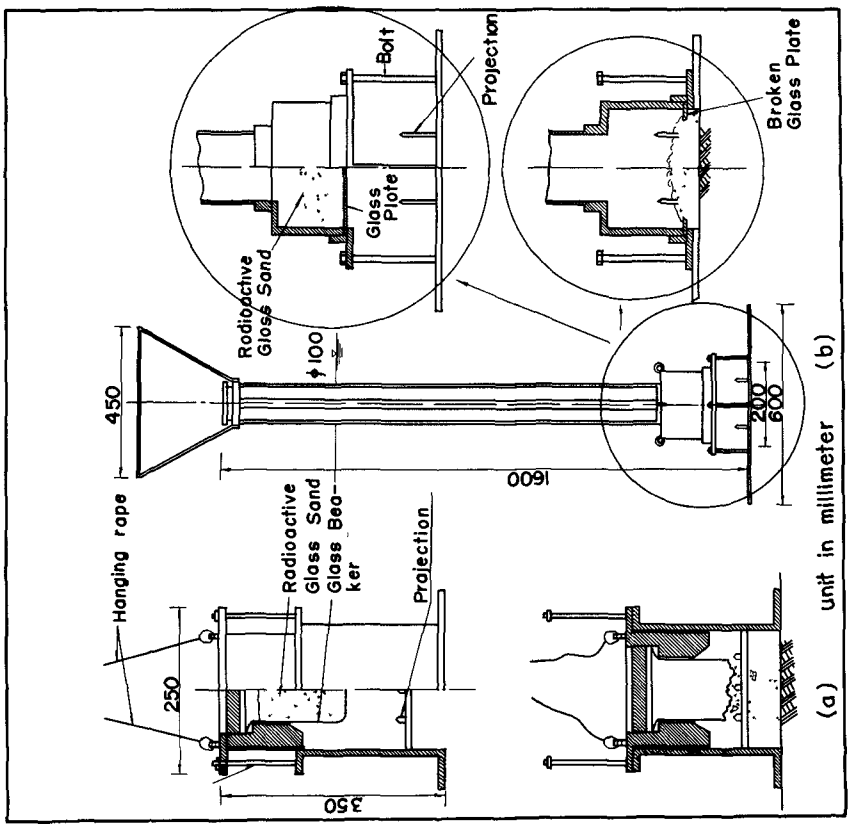

Fig.2. Injecton apparatus.

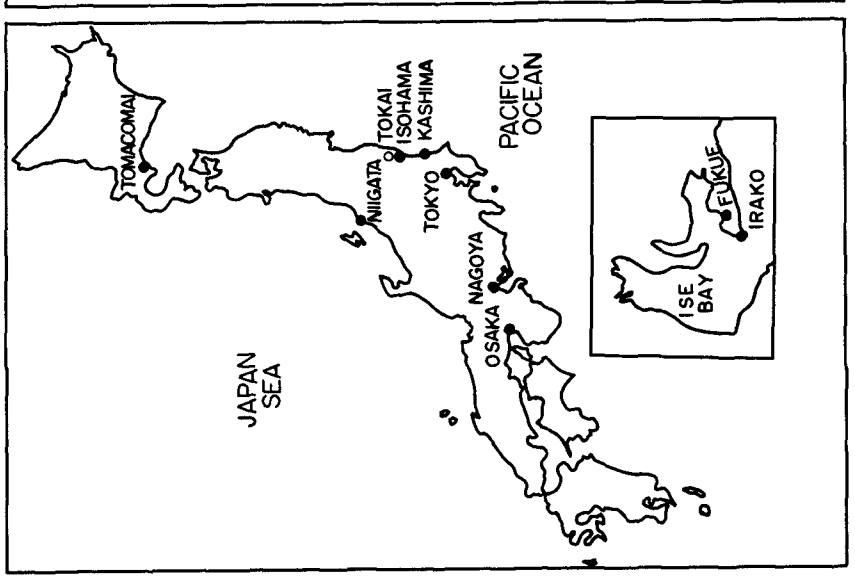

Fig. I. Map of the Japan Islands.

Specific gravity is adjusted by changing the mixing weight ratio of $CaCO_3$ and Na_2CO_3 or by addition of Pb_3O_4 and activity is adjusted by changing the containing ratio of cobalt. The glass sand of scandium-46 is also made in the same way. The specific gravity of glass sand of our field experiments was all 2.65.

Injection of glass sand Eliminating the short life activities in three weeks or more after irradiation, the radioactive glass sand in polyechiren bags sheilded with lead container is carried to the site. The injection apparatus for small amount of glass sand is shown in Figure 2 (a) and the one for large amount is in Figure 2 (b). The glass sand is poured into the injection apparatus through a funnel on the mouth of it by breaking the polyechiren bag of glass sand with a heated iron bar or a knife. Then, the injection apparatus is dropped down into sea with a rope. When it touchs the sea bed, its upper portion drops down by its own weight and the bottom of beaker or the glass plate is broken by projections of the base. Thus, the glass sand is injected on the sea bed.

Tracing of glass sand The distribution of the glass sand injected on the bottom is traced by means of a watertight detection unit connected to a ratemeter with a cable. The detection unit contains Geiger-Muller tube or scintillation tube. The survey boat is fixed nearly the injection point with ancker ropes and then the detector is placed down on the sea bed. The tracing points of the detection unit is measured by transits on the beach. The distance of successive measuring points is usually about two to five meters. The counts per second measured by the detection unit, substracting the natural count, are protted on paper and equi-count-lines are drawn. At the same time, waves and currents are measured during the period of field experiment.

THE SAND MOVEMENT IN THE OFFSHORE ZONE

As the example of the field experiment in the offshore zone, the distributions of glass sand injected in the depth of 10 meters at Irako, 4.5 meters at Isohama, 9 meters at Kashima and 6.9 meters at Niigata are shown in Figure 3, 4, 6, and 7 where the injection point, the distribution of equi-count lines and waves and currents are shown in that order. In these figures, depth counter lines are shown in meters below L.W.L . Waves are given at the depth of injection points and currents are those of one meter above sea bottom.

The experiment at Irako Irako Habor is situated at the entrance to Ise Bay, where the wind waves from NW-NNW prevail in winter. The tidal currents are so fast and the current velocity gets to about 60 centimeters per second in flood tide and the direction of tidal current is ESE during about twenty hours a day.

The results of this experiment are shown in Figure 3. The glass sand was moved toward ESE in accodance with the direction of tidal currents in flood tide, though the waves came from the direction of NW

A STUDY OF CRITICAL DEPTH AND MODE OF SAND MOVEMENT USING RADIOACTIVE GLASS SAND

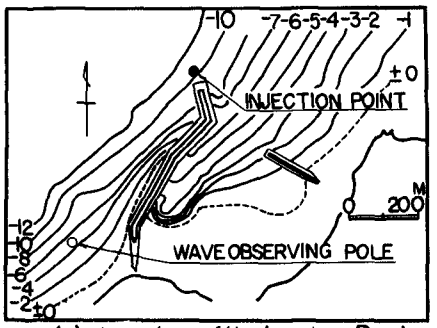

(a) Location of the Injection Point

Properties of GLASS SAND
- activity 2.3 milli curies
- Weight 150 g
- mean grain size 0.25 mm

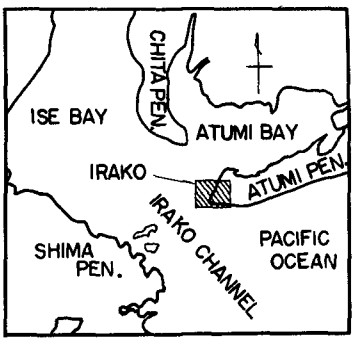

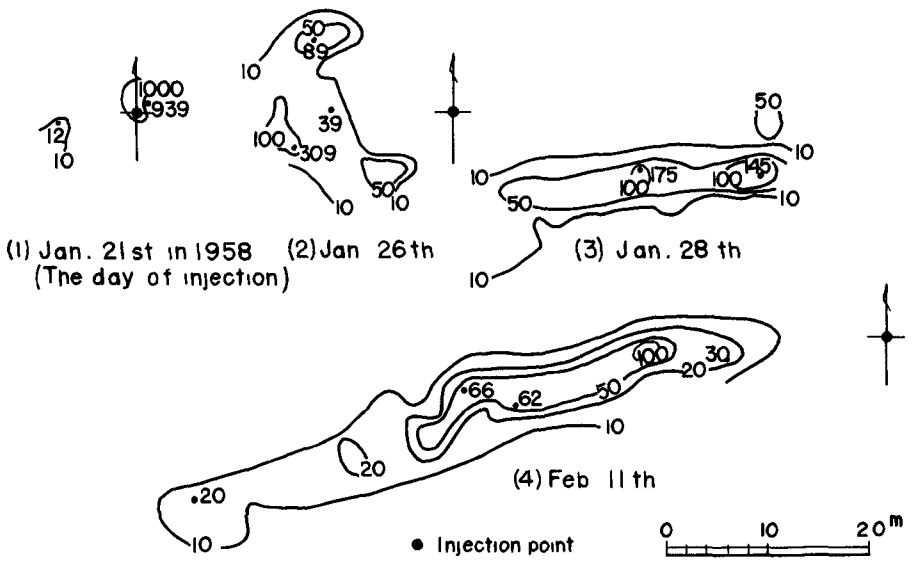

(1) Jan. 21st in 1958 (The day of injection) (2) Jan 26th (3) Jan. 28 th

(4) Feb 11 th

(b) Distribution of equi-count lines (unit cps)

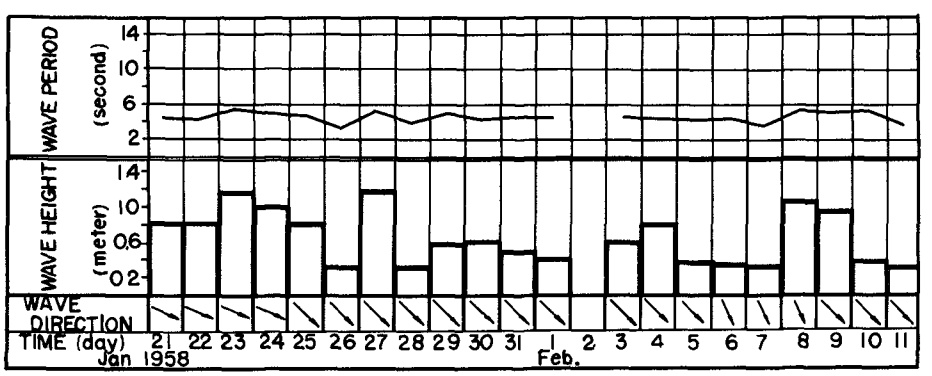

(c) Chracteristics of waves

Fig. 3. Experiment at 10 meters deep of Irako.

and NNW during this experiment and the maximum significant wave height was 1.2 meters.

The experiment at Isohama Coast Isohana Coast is on the Pacific Ocean, where the velocity of tidal current one meter above the sea bottom is about 3~5 centimeters per second on calm day. The result of experiment is shown in Figure 4. It is seen from the measurement of the injection day that a part of glass sand at first moved toward ESE in accordance with the current direction, and opposite to the wave direction. After that, glass sand was dispersed toward WNW due to the wave of Nov. 20th and that of from 23rd to 27th which were 1.4 and 2.3 meters in the maximum significant wave height, respectively. On the measurement after the waves on Dec. 6th of 2.6 meters in the maximum height and 12 second in period, the glass sand could not be detected anywhere except at the injection point. In the above distributions, equi-count lines distribute closer in its onshore side than in its offshore side. This may be considered to show that a part of glass sand suspended by waves was flowed in the offshore direction by underwater currents.

Then, on Jan 18th in 1960 the undisturbed bottom samples were taken by a diver with the cylinder of 6 centimeters in diameter and 30 centimeters long and the vertical distributions of glass sand were measured by scintillation counter. From the result shown in Figure 5, it is known that most of the glass sand distribute vertically from the bottom surface to only five centimeters deep.

The experiment at Kashimanada Coast Kashimanada Coast is also on the Pacific Ocean. An example of the experiment at 9 meters deep of this coast is shown in Figure 6. It is known from the measurement of the injection day that a part of glass sand was at first moved in the direction of currents. The result of measurement on March 3rd after the waves of 1.5 meters in height and 10 second in period shows that the glass sand dispersed in the same degree in the direction of both wave and current. Moreover, as seen from the measurement on March 27th, the glass sand was transported shoreward in accordance with the direction of the waves of March 21st and 22nd, of which the maximum significant wave was 2.5 meters in height and 10 second in period. The equi-count lines is closer in the north side than in the south side in these distributions of glass sand. This seems to show that the predominant direction of tidal currents was toward the south during this experiment.

The experiment at Niigata Coast Niigata Coast is on the Japan Sea, where it is calm in summer and stormy in winter. The results of tracing of glass sand injected in 7 meters deep is shown in Figure 7. A part of glass sand was transported in the direction of SW by tidal currents until July 18th. In the measurements on July 23rd after waves of 0.9 meters in height came from the NNW, the glass sand dispersed in the same degree both shoreward and seaward. Moreover, in the distribution of glass sand after the waves of 2.3 meters high, the point of the maximum counts was apart from the injection point

A STUDY OF CRITICAL DEPTH AND MODE OF SAND MOVEMENT USING RADIOACTIVE GLASS SAND

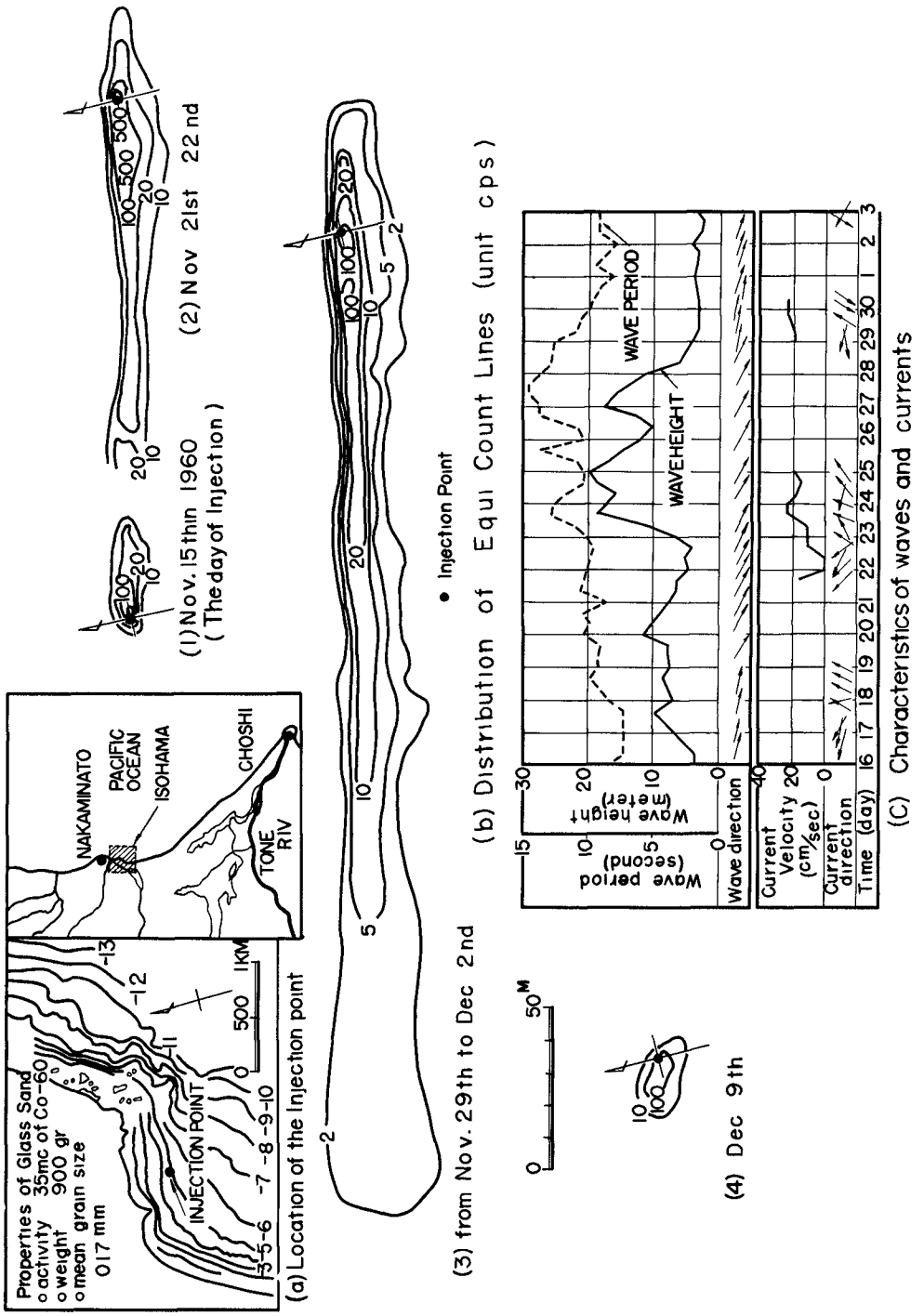

Fig. 4. Experiment at 4.5 meters deep of Isohama.

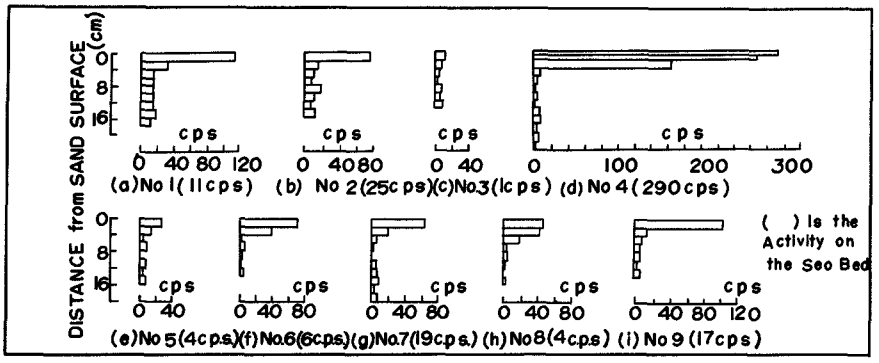

Fig. 5. Vertical Distribution of radioactive glass sand.

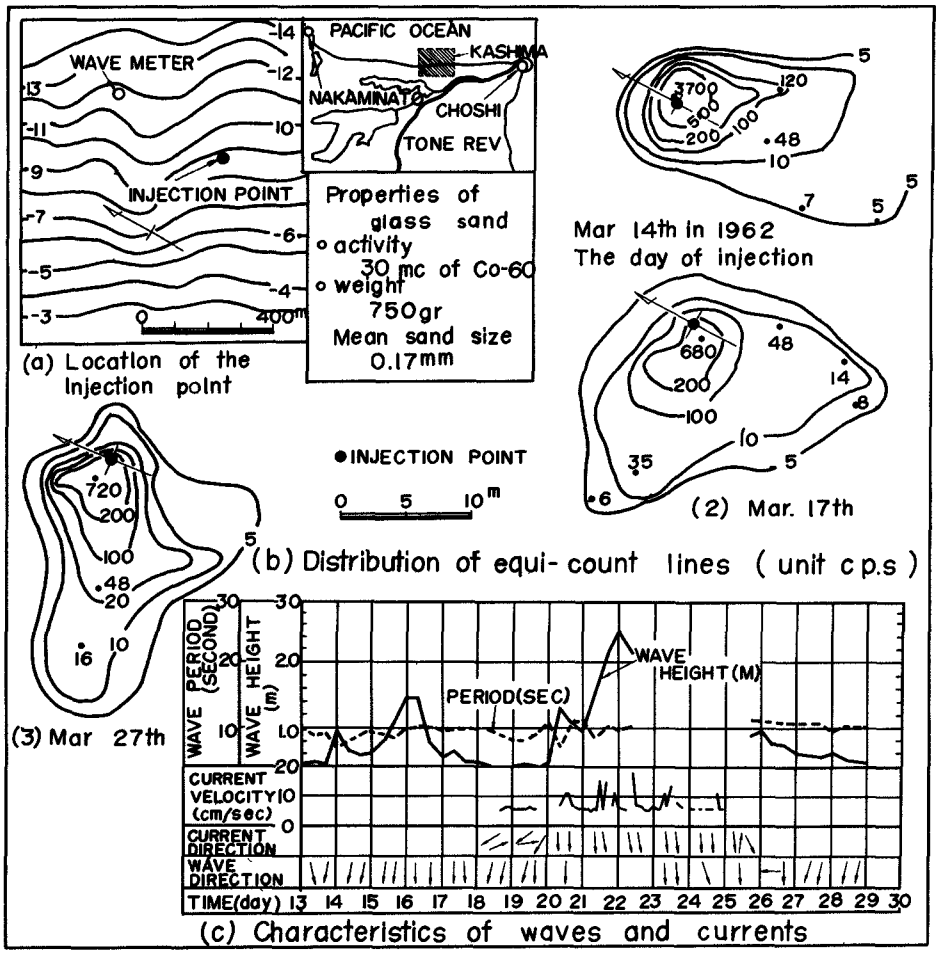

Fig. 6. Experiment at 9 meters deep of Kashima.

A STUDY OF CRITICAL DEPTH AND MODE OF SAND MOVEMENT USING RADIOACTIVE GLASS SAND

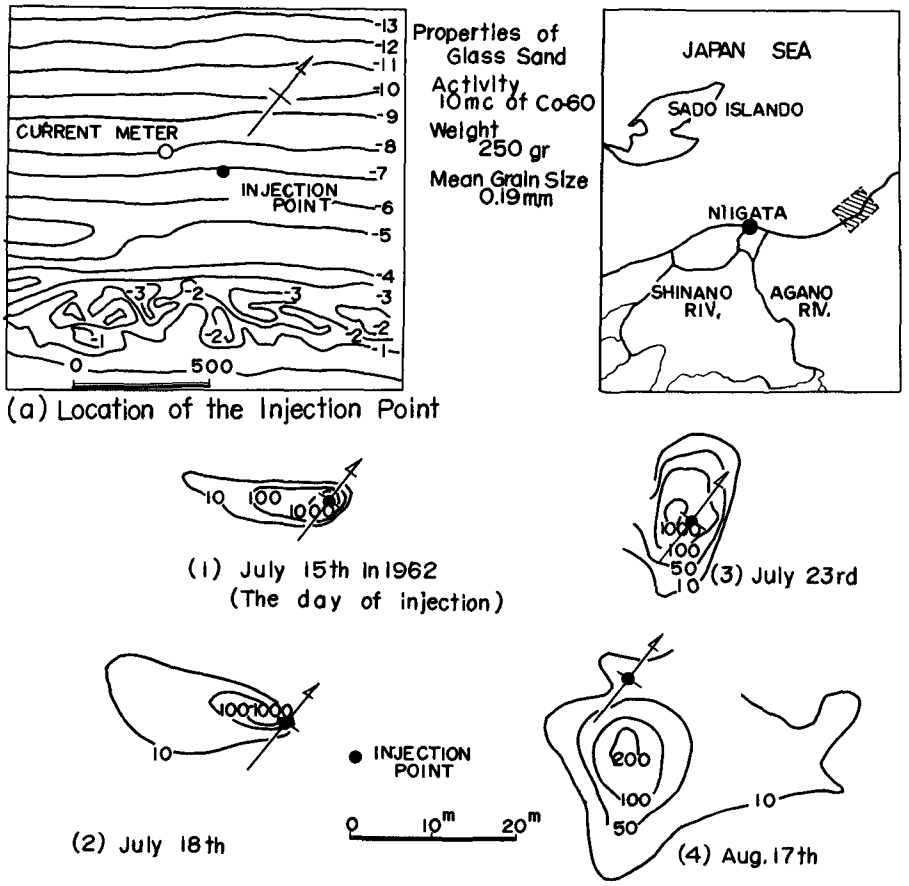

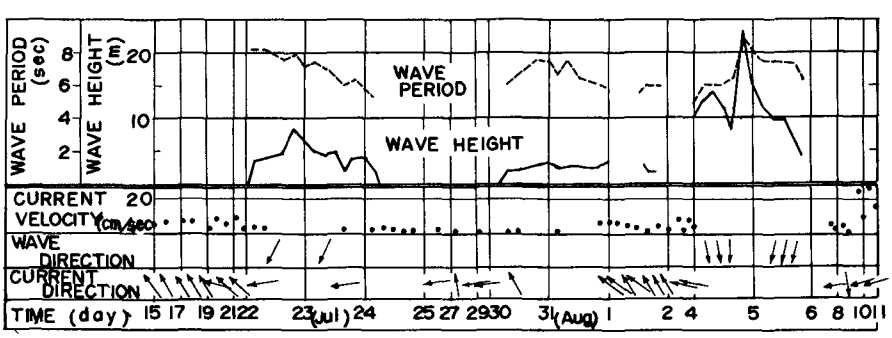

Fig. 7. Experiment at 7 meters deep of Niigate.

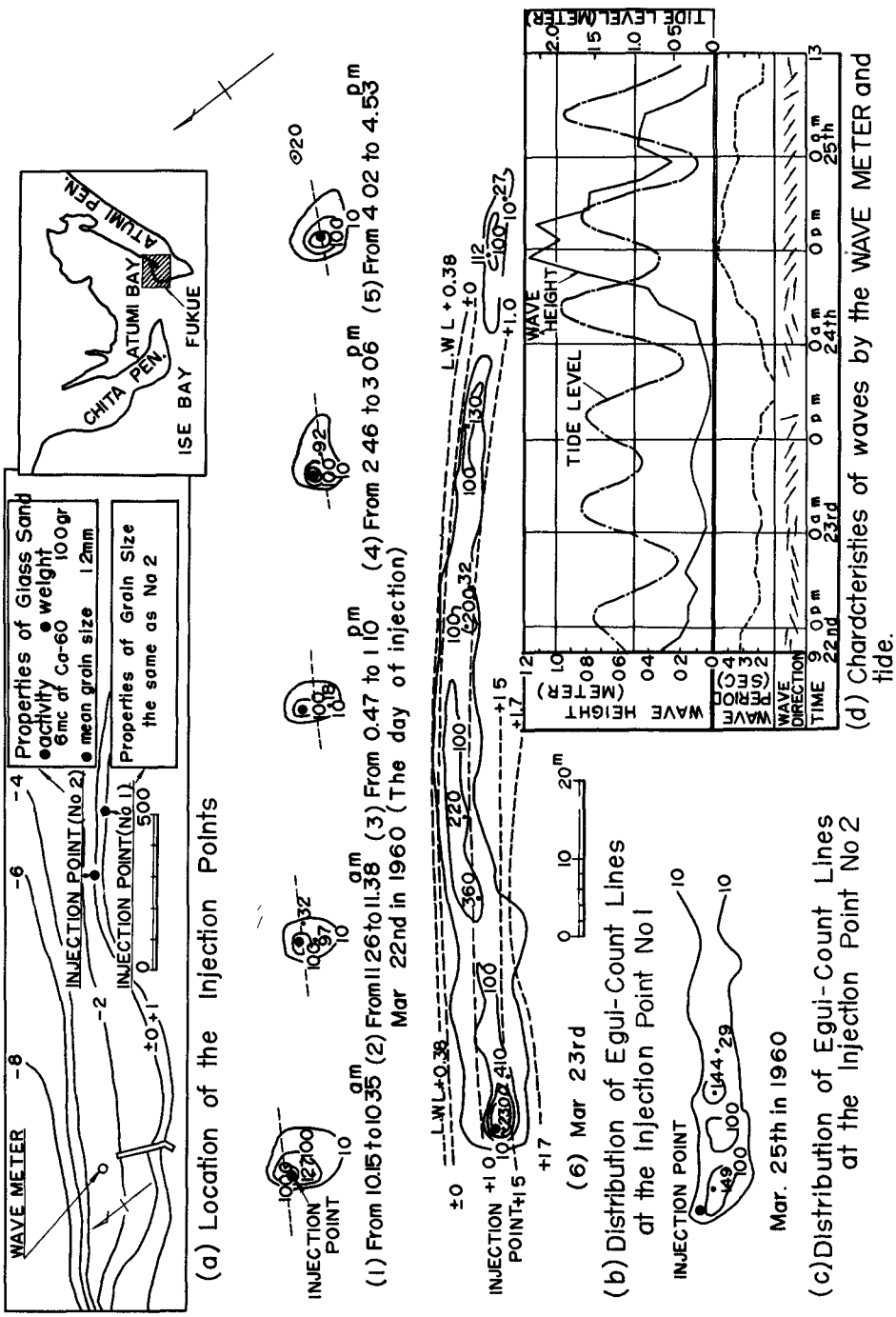

Fig. 8. Experiment at I.23 meters above and L.W.L. of Fukue.

and all equi-count lines streched shoreward.

The characteristics of the sand movement in the offshore zone
From the above-mentioned and authors' other experiments, it is considered as follows on the sand movement in offshore zone.

(1) On the coast of open sea, the direction of sand transport coincides with the wave direction in general, and where the tidal currents is beyond one or two knot in velocity it coincides with the direction of tidal currents.

(2) If the wave height is small on the coast of open sea, the bottom sand tends to move in the direction different from the wave, that is, a part of sand suspended by wave flows in the same direction as tidal currents. Therefore, in the point of about 10 meters deep, sand has a tendency to be transported in the direction of tidal currents as shown in Figure 6, and at the point of about 4 to 6 meters deep it tends to move in the opposit direction to the waves as shown in Figure 5 and 7.

(3) When most of sand has to be transported in the direction of wave, if there is a current of the direction different from the wave, a part of sand tends to be moved to the direction of current.

(4) Considering from the vertical distribution of glass sand at Isohama, it would be assumed that the layer thickness of sand movement is the same degree as the height of ripple on the sea bottom.

THE SAND MOVEMENT IN THE SURF ZONE

As the examples of the field experiment in the surf zone, results of Fukue and Kashimanada Coast are shown in Figure 7 and 8, respectively.

The experiment at 1.23 meters above L.W.L. of Fukue Coast
Fukue Coast is on the Atsumi Bay, where M.W.L. and H.W.L. are 1.90 and 2.20 meters above L.W.L. respectively, and the wave height in stormy season is only about one meter. The result of tracing at the point of 1.23 meters above L.W.L. is shown in Figure 8. On the injection day, the incident angle of breakers against the coast line was about 30°at 10 a.m. and became gradually larger to 60°at 2 p.m.; this seems to be related with the streching of 10 c.p.s. line. While, in the results of measurement of about 18 hours after the last measurement of the 22nd, most of glass sand distributed in long and narrow between L.W.L. of 8.35p.m. 22nd and H.W.L. of 3.30a.m. 23rd, while the wave height decreased gradually after the last measurement of the 23rd. This shows clearly that the influence of tidal level on sand movement in the forshore zone is remarkable, this is, the glass sand suspended by the breaking of waves was transported on the beach in the zig-zag form, because waves became to break near the injection point with the rising of tidal level from the night of the 22nd to the morning of the 23rd.

The experiment on the point of L.W.L. at Fukue Coast The glass

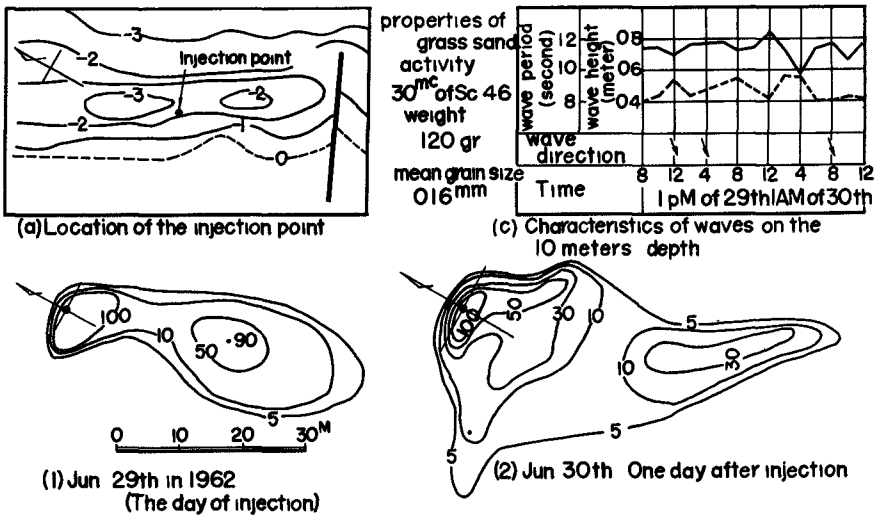

Fig. 9. Experiment at 2.3 meters deep of Kashima.

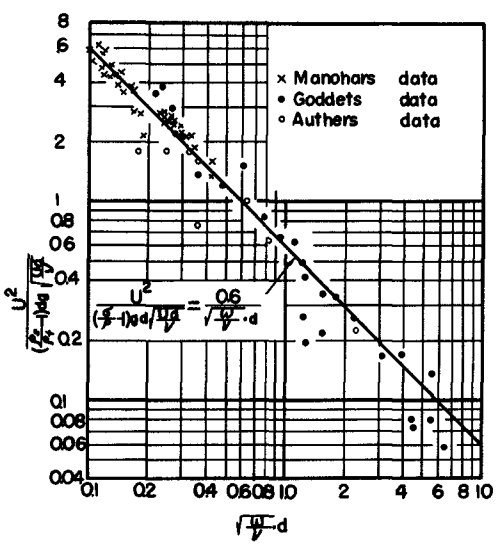

Fig. IO. The begining of general movement by laboratory test.

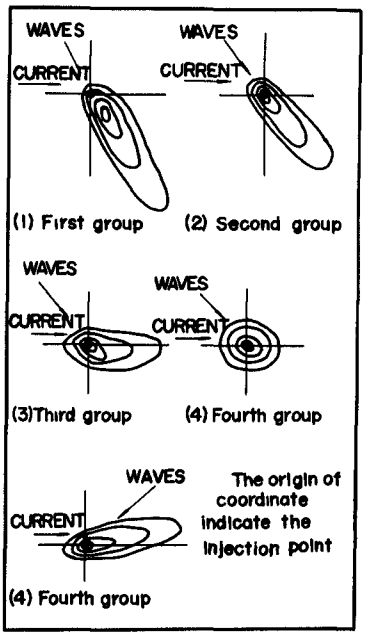

Fig. II. Classification of the distribution of radioactive glass sand.

sand was injected about 4 p.m. of March 23rd, when the sea was very calm and the glass sand could be seen to be dropped in a point. This point was below water level during this experiment, and acted by breaking wave. The result of measurement in two days after injection is shown in Figure 8-(c), where the higher equi-count lines strech in the direction of SSW and the lower equi-count lines strech to SE. This indicates that some portion of glass sand suspended by waves was transported by littotal current when glass sand was pushed in the direction of waves.

The experiment at Kashimanada Coast The glass sand was injected inside of the longshore bar when the wave height was comparatively small. The result of measurements is shown in Figure 9, where the glass sand distributed in the direction of both perpendicular and parallel to coastal line like the results of experiment at L.W.L. of Fukue Coast.

Tha characteristics of the sand movement in the surf zone As mentioned above, authors have only a few data of the experiment in the inshore zone and, also all of them are taken when the wave height is small. Therefore, authors can not present clearly the characteristics of sand movement, but the following properties would be estimated on the base of the above mentioned examples.

(1) In the inshore zone, the littoral currents and waves after breaking are main factors of the sand movement. The sand on the sea bottom is flushed by breaking waves in their direction, and at the same time, the sand disturbed by breaking waves transported along the coast in the direction of littoral currents.

(2) In the foreshore zone, the uprush and backwash of waves and the rising of tidal level mainly control the sand movement. The sand in the foreshore zone has a remarkable tendency to be transported in parallel to the coast line, even when the wave height is small.

THE CRITICAL DEPTH OF SAND TRANSPORT OBTAINED FROM THE FIELD EXPERIMENT USING RADIOACTIVE GLASS SAND

THE CRITICAL DEPTH OF SAND MOVEMENT DUE TO WAVES

It is known experimentally that the sand grains begin to move when the force of waves acting on the sea bottom become a certain value and is transported by waves through each steps of initial movement, general movement and initiation and disappearance of ripples with the increase of wave action. There are different experimental equations as to the initiation of above steps, but authors also derived the equation for the initiation of general Movement from laboratory experiments.

Sand grains start to move when the drag force of waves acting on sand grains overtakes the friction force due to gravity. At this moment the following equation is given.

$$\left\{\left(\frac{\sigma}{\rho}-1\right)gd^3\frac{\pi}{6}\tan\varphi\right\}=K\frac{\pi}{8}C_D U_b^2 d^2, \qquad (I)$$

where σ = specific gravity of sand grains, ρ = specific gravity of fluid, g = acceleration due to gravity, d = diameter of sand grain, φ = angle of repose, C_D = coefficient of drag, U_b = maximum horizontal particle velocity due to wave at the top of sand grain, and K = constant.

U_b is expressed as $U \cdot f\left(\sqrt{\frac{\omega}{\nu}}d\right)$ in the boundary layer, where U is the maximum velocity due to wave in the outside of boundary layer, ν the kinematic viscosity of fluid and ω angular velocity of water particle. Therefore, assuming that the coefficient of drag C_D is inversely proportional to the square root of the Reynolds Number Ud/ν, the above equation can be modified as

$$\frac{U^2}{\left(\frac{\sigma}{\rho}-1\right)gd\sqrt{Ud/\nu}} = K' \cdot f\left(\sqrt{\omega/\nu}\, d\right) .$$

In order to make clear the value of constant K' and the form of the function $f\left(\sqrt{\omega/\nu}\, d\right)$, the data of the experiments on the begining of general movement by authors' , Manohor's and Goddet's experiments are plotted in Figure 10 with $U^2/\left(\frac{\sigma}{\rho}-1\right)gd\sqrt{Ud/\nu}$ against $\sqrt{\omega/\nu}\, d$. From this figure, the following equation for the initiation of general movement is obtained.

$$\frac{U^2}{\left(\frac{\sigma}{\rho}-1\right)gd\sqrt{Ud/\nu}} = \frac{0.6}{\sqrt{\omega/\nu}\, d} \qquad (2)$$

Substituting the above equation with $U=\frac{\pi}{T}\frac{H}{\sinh\frac{2\pi h}{L}}$, $\omega=\frac{2\pi}{T}$, and $T^2=\frac{2\pi}{g}L_o$

$$\frac{H}{L_o}=\left\{0.4243\frac{2}{\pi}\left(\frac{\sigma}{\rho}-1\right)\right\}^{\frac{2}{3}}\left(d/L_o\right)^{\frac{1}{3}}\sinh\frac{2\pi h}{L}$$

Or from $H/L_o=(H_o/L_o)(H/H_o)$, $\sigma=2.65$ and $\rho=1.03$

$$H_o/L_o = 0.565\left(\frac{d}{L_o}\right)\sinh\frac{2h}{L}\cdot\frac{H_o}{H} \qquad (3)$$

and

$$H_o/L_o=\left(\sinh\frac{2\pi h}{L_o}\right)^{-1}\left(\frac{H_o}{H}\right)^{-1}=0.565\left(\frac{d}{L_o}\right)^{\frac{1}{3}} , \qquad (4)$$

where H and L are height and lenght of wave, and suffix o indicats the value of deep water wave.

In general, one of the most important problem in the construction of harbor on sandy coast is to extend breakwaters to the depth enough to prevent the entrance of harbor from shoaling. For this purpose, it is desirable to extend breakwaters to the depth obtained from equation (3), but it is unpractical . In the field experiment of the offshore zone mentioned previously, the glass sand of less than 0.3 millimeters in size was transported in the direction different from the wave when the height of waves was very small, and was mainly transported in the same direction as wave when it was little larger. Therefore, the depth at which sand starts to move remarkably in the same direction as that of waves would be thought to be one of criterion for the determination of depth to which breakwaters should be extended. Such a critical depth should be obtained from the results of field experiments.

THE CRITICAL DEPTH FOR SAND TO BEGIN TO MOVE IN THE DIRECTION OF WAVES

The distribution of radioactive glass sand in the offshore zone

measured by authors are classified into the following four groups, as shown in Figure 11.

(1) The first group This is the case that the point of the maximum counts moves in the same direction as waves, and all equi-count lines also extend in the same direction as waves. Such a distribution of glass sand indicates that the bottom material is completely transported by waves.

(2) The second group This is the case that the point of the maximum counts does not move, but all equi-count lines extend in the same direction as waves. In this case, the distribution of equi-count lines is not wider than that of the first group.

(3) The third group This is the case that the point of the maximum couts does not move and only a part of equi-count lines extends in the same direction as waves. This group also contains the case that the counts decrease remarkably as a whole, despite the distribution of equi-count lines scarecely changes.

(4) The fourth group This is the case that the distribution of equi-count lines remains unchanged and also the counts do not decrease so much. The case that the equi-count lines extend in the same direction as tidal currents and the direction opposite to waves is also contained in this group.

Then, classifing the glass sand distributions of our experiments into these four groups, $H_0/L_0 \cdot (\sinh \frac{2\pi h}{L})^{-1} (\frac{H_0}{H})^{-1}$ and d/L_0 in Equation (4) are calculated for each distribution of which the results are shown in Table-1. The wave period T and wave height H used in this calculation are those of the maximum significant waves on the injection point during the successive measurement of distribution and the depth h is the mean water depth of the injection point. H_0 and L_0 are those for the equivalent deep water wave of H and T. In Figure 12, the data of Table 1 are plotted with $H_0/L_0 (\sinh \frac{2\pi h}{L})^{-1} (H_0/H)^{-1}$ as ordinate and d/L_0 as abscissa. In this figure, the transition from the second group to the third group is shown by the following equation.

$$\frac{H_0}{L_0} = 1.35 \left(\frac{d}{L_0}\right)^{\frac{1}{3}} \sinh \frac{2\pi h}{L} \left(\frac{H_0}{H}\right), \qquad (5)$$

which expresses the relation of sand size, characteristics of wave and water depth when the bottom materials start to move in the same direction as waves. Equation (4) for the initiation of general movement by laboratory experiments is also shown in this figure. All the points of the third group and a few points of the fourth group are distributed between the curves of Equation (4) and (5) and the other points of the fourth below the curve of Equation (4). Therefore, it is considered that Equation (4) coincides with the results of the field experiment.

THE MODE OF SAND MOVEMENT BY MODEL EXPERIMENT

SAND MOVEMENT IN THE OFFSHORE ZONE

Table I. The value of $H_0/L_0 (\sinh \frac{2\pi h}{L})^{-1}(H_0/H)^{-1}$ and d/L_0 for each distribution of radioactive glass sand.

No.	Coast	Group	Date	d (mm)	h(m)	T (sec)	Ho(m)	$\frac{H_0}{L_0}$	$\frac{d}{L_0}\times10^{-3}$	$\frac{(H_0)}{(L_0)}\frac{(H_0)}{(H)}^{-1}(\sinh\frac{2\pi h}{L})^{-1}$	Remorks
1	Tomakomoi	1st Gr	629 to 71354	017	38	50	10	00256	436	00241	
2		2nd	714 to 72454	017	38	80	08	00087	195	00166	
3		3rd	724 to 81154	017	38	60	17	00362	303	00286	
4		4th	520 to 52155	012	70	80	04	00044	131	00509	
5		2nd	521 to 52755	012	70	60	16	00285	213	00216	
6		1st	527 to 60355	012	70	100	26	00162	0767	00298	
7		2nd	63 to 61355	012	70	50	18	00460	308	00245	
8		3rd	613 to 62355	012	70	70	12	00158	158	00157	
9		3rd	623 to 7755	012	70	50	14	00359	308	00191	
10		3rd	83 to 81355	012	100	60	13	00231	213	001265	
11		2nd	813 to 9855	012	100	150	26	00074	342	00185	
12		2nd	1111 to 111956	012	100	90	16	00125	075	00141	
13		3rd	1119 to 113056	012	100	100	13	00084	077	00113	
14		4th	1130 to122456	012	100	100	06	00039	077	00052	
15	Iroko	4th	121 to 12658	025	110	50	13	00334	641	00099	Fig. 3 (2)
16		4th	126 to 12858	025	110	50	13	00334	641	00099	(3)
17		4th	128 to 21158	025	110	50	12	00308	641	00091	(4)
18		2nd	126 to 12958	017	40	50	13	00334	436	00303	
19		1st	129 to 21058	017	40	50	12	00308	436	00299	
20		1st	210 to 22358	017	40	60	13	00231	303	00285	
21		1st	223 to 31158	017	40	60	16	00308	303	00380	
22		4th	916 to 92057	025	105	50	10	00254	641	00087	
23		4th	928 to1010 57	025	105	120	09	00039	112	00065	
24		4th	1010 to102557	025	105	40	09	00344	100	00047	
25	Fukue	4th		03	30	40	09	00348	120	00275	
26	Isohamo	1st	1116 to 112260	017	55	100	13	00084	108	00164	Fig. 4 (2)
27		1st	1122 to 112960	017	55	110	23	00120	090	00300	(3)
28		1st	1129 to12960	017	55	110	26	00156	090	00388	(4)
29		4th	120 to 12161	017	100	90	04	00030	135	00034	
30		2nd	121 to 2361	017	100	130	24	00090	0647	00189	
31		3rd	23 to 21061	017	100	80	15	00161	185	00139	
32		4th	210 to 22361	017	100	130	10	00037	0647	00074	
33		4th	120 to 12161	017	55	90	04	00033	135	00060	
34		1st	121 to 2261	017	55	130	27	00101	0647	00324	
35	Koshimo	3rd	17 to 1862	017	80	110	071	00038	0901	0007	
36		2nd	18 to 11262	017	80	100	14	00092	109	00148	
37		2nd	112 to 12662	017	80	120	15	00065	0759	00137	
38		2nd	314 to 31762	017	100	120	15	00065	0759	00134	Fig. 6 (2)
39		3rd	317 to 32762	017	100	100	26	00165	109	00224	(3)
40		4th	314 to 31762	28	100	100	15	00095	178	00127	
41		3rd	317 to 32762	28	100	100	26	00165	178	00187	
42		1st	429 to 43062	015	60	80	13	00142	163	00187	
43		1st	430 to 51062	015	60	80	17	00190	163	00251	
44		2nd	428 to 51062	015	120	80	17	00190	163	00137	
45	Nilgata	1st	718 to 81762	016	90	90	24	00190	128	00236	
46		3rd	718 to 72362	019	75	80	093	00093	194	00079	Fig. 7 (3)
47		1st	723 to 81762	019	75	90	24	00190	154	00267	(4)

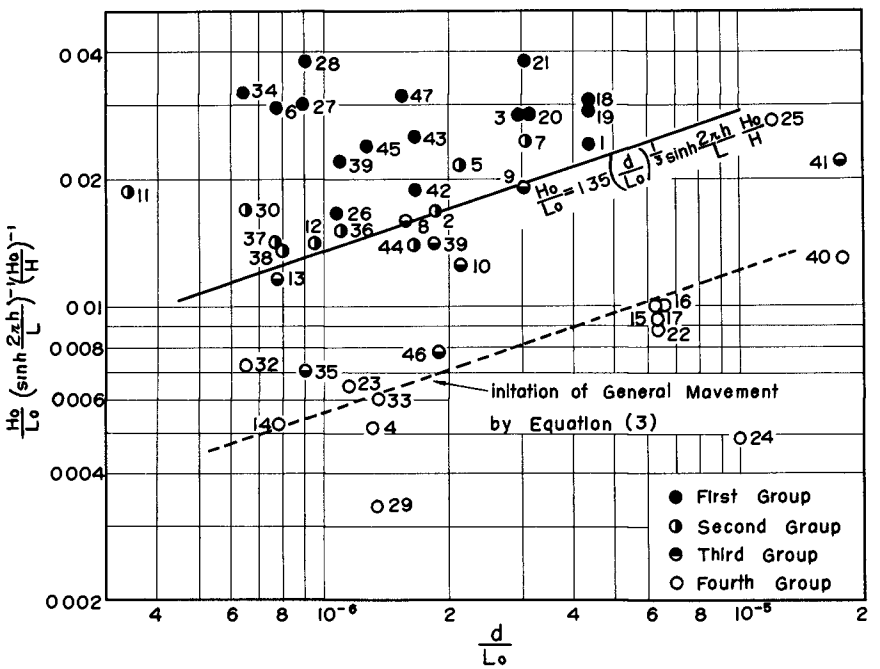

Fig. I2. Relation between $\frac{H_o}{L_o}\cdot\left(\sinh\frac{2\pi h}{L}\right)^{-1}\cdot\left(\frac{H_o}{H}\right)^{-1}$ and d/L_o for each distribution of radioactive glass sand.

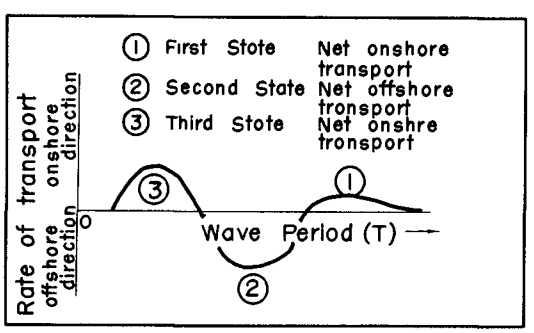

Fig. I3. Three states of sand transport.

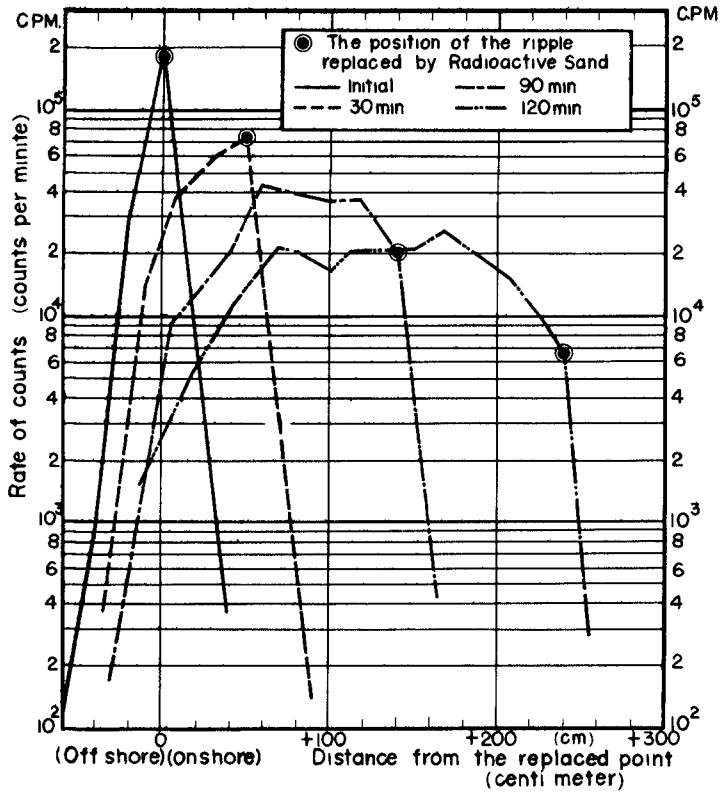

Fig. I4. Time change of radioactivity distribution in the first state.

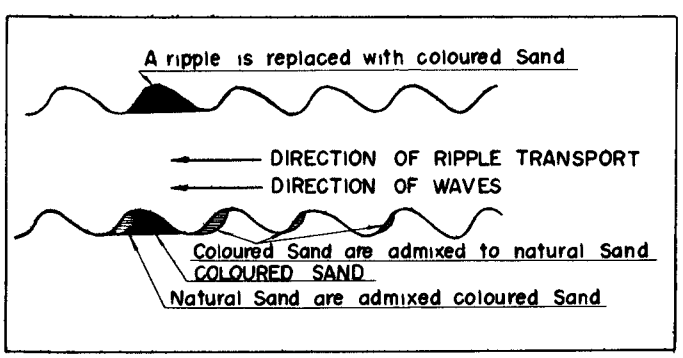

Fig. I5. Sketch of dyed sand movement.

A STUDY OF CRITICAL DEPTH AND MODE OF SAND MOVEMENT USING RADIOACTIVE GLASS SAND

In the channel experiment of horizontal bed with constant depth, as the wave period gradually decrease, bed sand is at first moved onshore (the first state), and then moved offshore (the second state). As the period further decrease, sand is again moved onshore (the third state) and finally stops moving. Such a state of movement is sketched in Figure 13.

When the grain size is large, there appears only the first state. When the grain size is small, all of these state apper. In order to find which state the movement of glass sand in our field experiment belongs to, authors performed some model test using glass sand containing Cr-51.

EXPERIMENTAL PROCEDURES

The experiment were conducted in a glass walled channel 50 centimeters wide, 80 centimeters deep and 40 meters long, with a flap wave generator at one end a seaward slope 1:10 at other end. Sand was placed in five centimeters thick on the horizontal bed between 8 and 17 meters from the wave plate. The water depth was 40 centimeters to the sand surface through all test runs.

In each run, after ripples were fully developed a ripple was replaced with the radioactive glass sand of Cr-51 or dyed sand, of which the movement due to waves was traced. Cr-51 has the half life of 27 days and emits only soft γ - ray of 0.3 MeV. Only a ripple was replaced because it was seen by preliminary tests that sand particles moved by waves were only portions forming ripples. The radioactive glass sand was traced with the watertight scintillation tube fixed on the carriage moving on the channel.. The lower end of the tube always kept 5 centimeters above the crest of each ripple.

PRESENTATION AND DISCUSSION OF RESULTS

An example of time change of distribution of radioactive glass sand in the first state is shown in Figure 14, where the distances from the original situation of ripple crest replaced by radioactive glass sand are shown in abscissa, taking positive in the direction of wave propagation and the measured counts per minute or second are shown in ordinate. And also, the situation of the crest of the replaced ripple in each measurement is shown with double circle in the same figure.

From Figure 14 it is clear that the glass sand particle are not transported beyond the replaced ripple and most of them is left behind it. This depends, as known by many other experiments, on the phenomena that when the crest of the wave passes over ripple, sand particles in surface layer move up on the offshore slope of it and at the same time a swirl of water is generated on the onshore slope of the ripple, and when the trough of the wave passes over it, sand particles picked up by the swirl move back to the offshore direction. This mode of sand movement is also clear by Figure 15 showing the distribution of dyed sand replaced for a ripple. The ripple replaced by dyed sand is gradually lightened from its onshore slope by sand transported from the

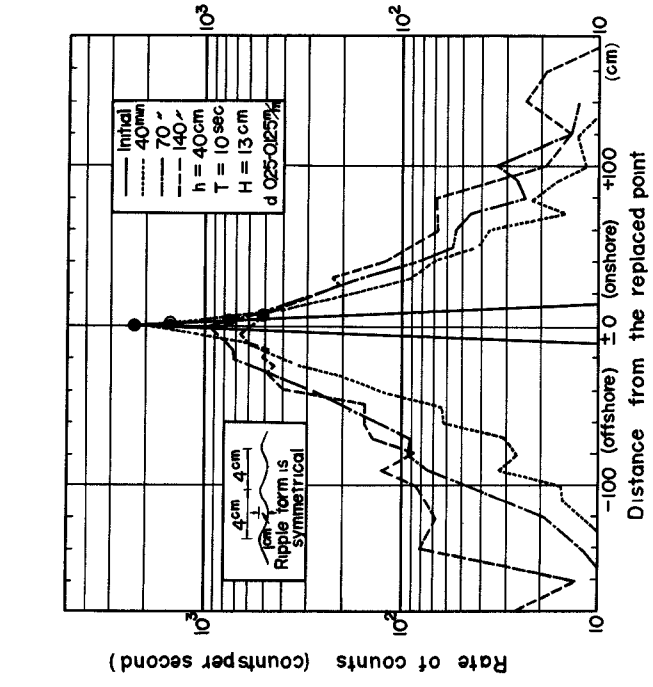

Fig.17. Time change of radioactivity distribution in the third state.

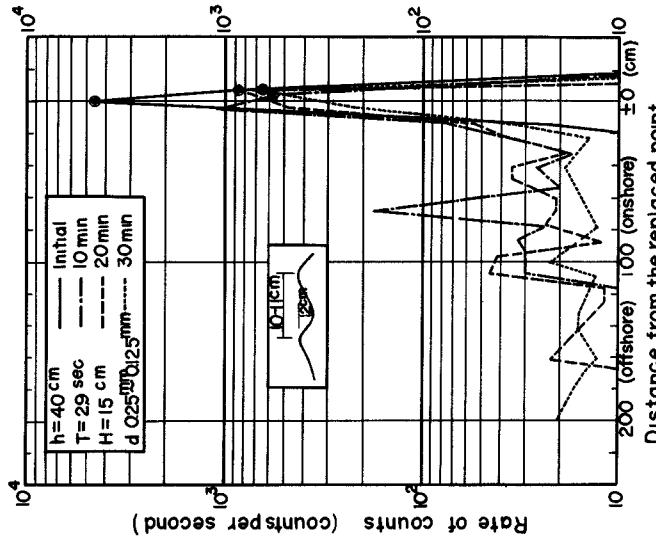

Fig.16. Time change of radioactivity distribution in the second state.

onshore side ripples and offshore side ripples are colored mainly from its onshore side by sand from the onshore slope of the replaced ripple. Accordingly, sand is not so much supplied to the offshore of ripples, so that ripple always move shoreward, but in the first state the volume of the suspending sand transported seaward is less than that transported shoreward along the offshore slope of ripples, so that the direction of net sand transport is shoreward.

On the contrary, in the second state, though ripples move slowly shoreward, the volume of sand suspended and transported seaward is more than that transported along the seaward slope of ripples, so that the direction of net sand transport is seaward. An example of the distribuion of glass sand in such a case is shown in Figure 16.

An example of the third state is shown in Figure 17. The remarkable characteristics of this state is for glass sand to be transported beyond the replaced ripple. In this case, the form of ripple is almost symetrical and swirls of water generate not only when the crest passes but also when the trough of the wave passes on the ripple, so that sand is suspended also shoreward beyond the ripple. In Figure 17, as the wave height is very small, net sand transport is almost zero, but if the wave height is large, the suspending sand transported shoreward would increase and in this result the net sand transport would become shoreward.

From the fact that the situation of the maximum counts in generally deviats seaward from the center of the distribution of equi-count lines in the field experiment, the mode of glass sand movement in offshore zone is possibly considered to be the same as that of the third state in this model test. Therefore, Equation (5) showing the begining of the onshore sand transportation may be also the equation presenting the transition from the second state to the third state in this model test. Accordingly in the field, the sand on the sea bed would be assumed to be transported in the mode of the second state when wave height is very small and in the mode of the third state when wave height becomes a little larger

The above-described properties of sand movement have been derived from a few kinds of field and model experiment, so that there may be some questionable points in them, and also many points remain not clear. Authors intend to complemented and make clear them by further many experiments.

REFERENCES

Madhav Manohar (1955). Mechanics of bottom sediment movement due to wave action; Tech. Memo. No.75, Beach Erosion Board, Corps of Engineers U. S. Army.

J. Goddet (1960). Etude du debut d'entrainement des materiaux mobiles sous l'action de la houle: La Houille Blanche, Vol.15 No. 2.

CHAPTER 19

TRACING COASTAL SEDIMENT MOVEMENT BY NATURALLY RADIOACTIVE MINERALS

A. M. Kamel and J. W. Johnson
College of Engineering
University of California
Berkeley

INTRODUCTION

The process by which sediments are moved along the shore is known as littoral drift and it includes beach drifting and longshore drift (Johnson, 1919). Coarse material is moved along a foreshore in zig-zag paths under the influence of swash and backwash of the waves. The process of longshore drift is due to longshore currents set up within the breaker zone by breaking waves approaching the shoreline at an angle. Although the waves tend to become parallel to the coast as a result of refraction, they usually break at a slight angle to the shore with the result that a littoral current is induced and is effective in moving a mass of water (and the sediment placed in suspension by the breaking waves) slowly along the coast. It is this current combined with the agitating action of the breaking waves, that is the primary factor in causing movement of sand along a coastline. It is believed that the largest percentage of the littoral transport occurs shoreward of the breaking point of the waves.

METHODS OF TRACING THE SOURCE AND DIRECTION OF LITTORAL DRIFT

Knowledge of sand sources and direction of littoral drift along a coast are of prime importance in beach erosion studies. These factors may be determined broadly by several distinct methods of approach, some of which are necessarily complementary to each other. These include:

(1) The use of standard hydrographic methods of mapping the sea bed and shoreline, aerial surveys, wave data, and refraction diagram analyses, current measurements, sampling of suspended load and bed load sediments, etc.

(2) The use of natural tracers such as heavy mineral fractions or shell inclusions in sediment samples, in relation to their source areas.

(3) The use of radioisotopes as tracers for labeling sediment

samples, either by incorporation of the activated material in artificial sediment, or by chemical or physical adhesion as a radioactive film on the particles of the real sediment, or by embedment within the particles (in the case of pebbles).

(4) The use of luminophors as tracers for labeling sediment samples, either by incorporation of the fluorescent material in artificial sediment or shingle, or by adhesion as a luminescent film on particles of natural sediment.

(5) The use of hydraulic models with movable beds of artificial materials to simulate prototype sediment processes.

In this study thorium (Th^{232}, 0.238 mev) was used as a natural tracer to determine the direction of littoral drift along the California coast. This radioactive thorium is added naturally at discrete places along the coast where rivers flowing through thorium rich granite outcrops reach the coast or where the thorium rich granite itself outcrops at the sea coast.

SOURCE OF RADIOACTIVITY

For a natural rock practically all the gamma radiation comes from three sources, namely: K^{40}, U^{238} series, and Th^{232} series (Adams, et al, 1958). Uranium is generally found with thorium in nature in a ratio of about 10 parts of thorium to one part of uranium. The gamma rays from U^{238} and Th^{232} themselves are of such a low energy value as to make direct measurements impractical. Where secular radioactive equilibrium prevails, the abundance of U^{238} or Th^{232} can be determined by measuring the activity of any daughter in the respective series. This follows from the constant ratios that exist between the concentrations of the various members of a series in an equilibrated sample.

The spectra of uranium and thorium series (Fig. 1) show that the peak caused by lead 212 in the thorium series occurred in a region of fairly constant response in the uranium series and might best fulfill the needs for discrimination of the two series. Furthermore, higher counting rates at this low-energy part of the spectrum make it desirable to work in this part of the spectrum. For a complete discussion on this method of radioactive assay the reader is referred to the work of Kamel, 1962.

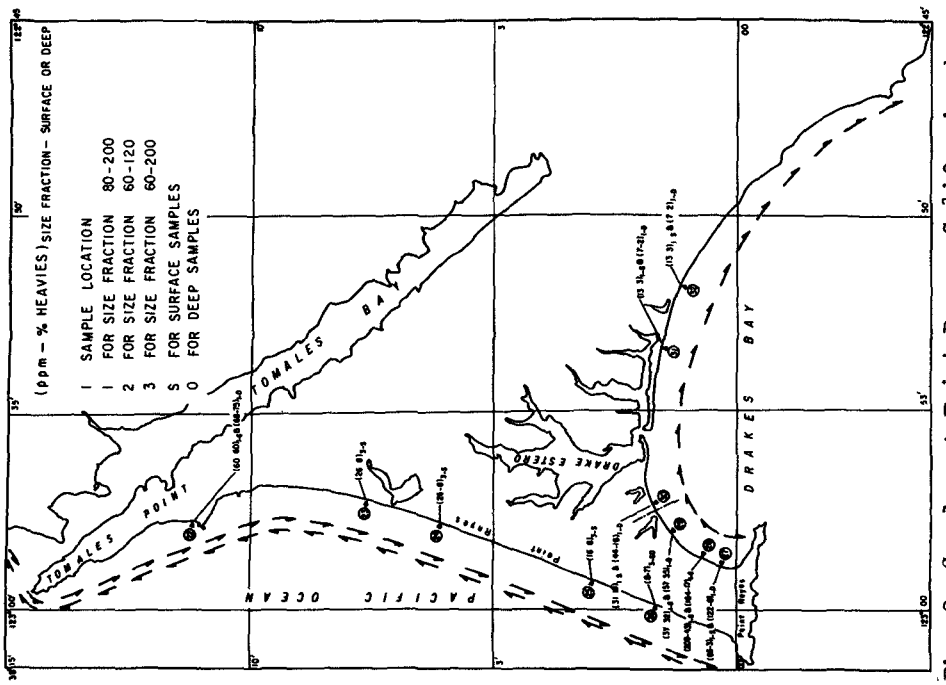

Fig. 2. Samples at Point Reyes, California showing the thorium and heavy minerals concentration.

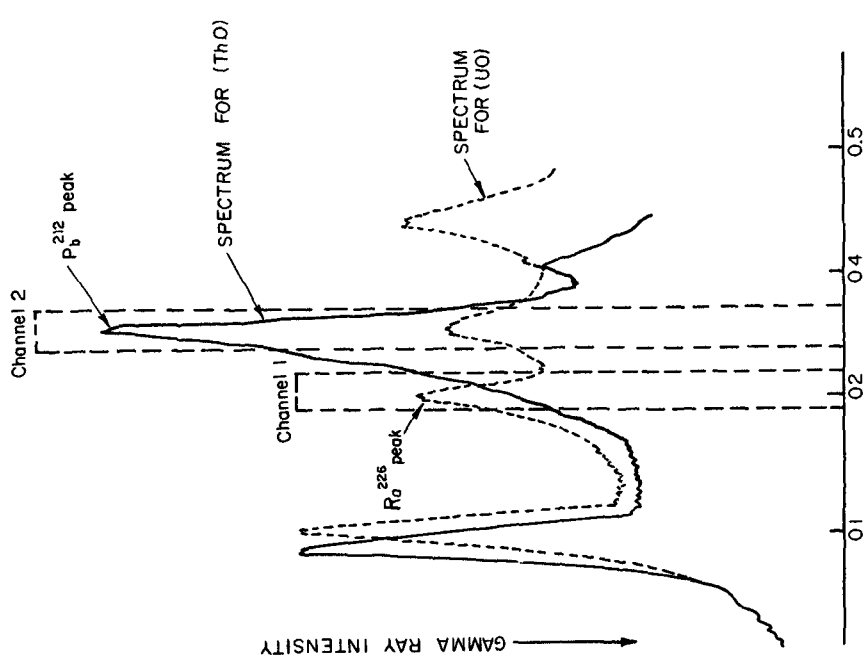

Fig. 1. Counting channels for thorium and uranium.

TRACING COASTAL SEDIMENT MOVEMENT BY NATURALLY RADIOACTIVE MINERALS

INVESTIGATIONAL APPROACH

It is well known that beach sands are among the best sorted of natural sediments. They are subject to a progressive sorting when transported by longshore currents and to a very effective local sorting by the oscillatory motion of the waves. The contention that sediment transported by longshore currents travels chiefly in suspension is supported by the textural characteristics of the beach sands. Silt and clay are absent, very fine sand is rare. Any effects of progressive sorting along the shore must, therefore, be explained on the basis of transportation in suspension. These effects may be due to sorting according to grain shape, size, and specific gravity. Progressive sorting according to size, shape, and specific gravity may be due to a progressive decrease in the competency with a lagging behind of the larger, spherical, and heavier particles which move only occasionally during periods of maximum competency. The competency of the longshore current would seem to depend on the ability of the waves to put sediment of a certain grain size in suspension, and then of the ability of the current to move the suspended load. In the present study the choice of the concentrations of both thorite and heavy minerals in parts per million and per cent, respectively, in sand samples collected at mid-tide from different places along the beach, are believed to be two good parameters for the study of the effect of progressive sorting and consequently the determination of the direction of littoral drift along the coast.

A decrease from a source area in the concentration of thorium in ppm and/or the concentration of the heavy minerals in per cent, should indicate a longshore drift in the direction of decreases of both parameters (Fig. 2).

Local sorting on the other hand, need not be a result of transport in suspension, and its effects must not be confused with those of progressive sorting. To eliminate the effect of local sorting on the sand samples, comparisons between the concentrations of thorium and heavy minerals present in these samples should be made only for a very limited size fraction and not for the whole sample, e.g. a size fraction from 74 to 177 microns.

Since thorium is generally found in the size fraction finer than 125 microns (Hutton, 1951), and since the concentration of heavy minerals is also higher in the fine fraction, it was found that the best size fraction suited for this study is that from 74 to 177 microns.

ANALYSIS OF RESULTS

Based on the distribution of beach samples and their thorium and heavy mineral concentrations and wave refraction diagrams (Fig. 3) it

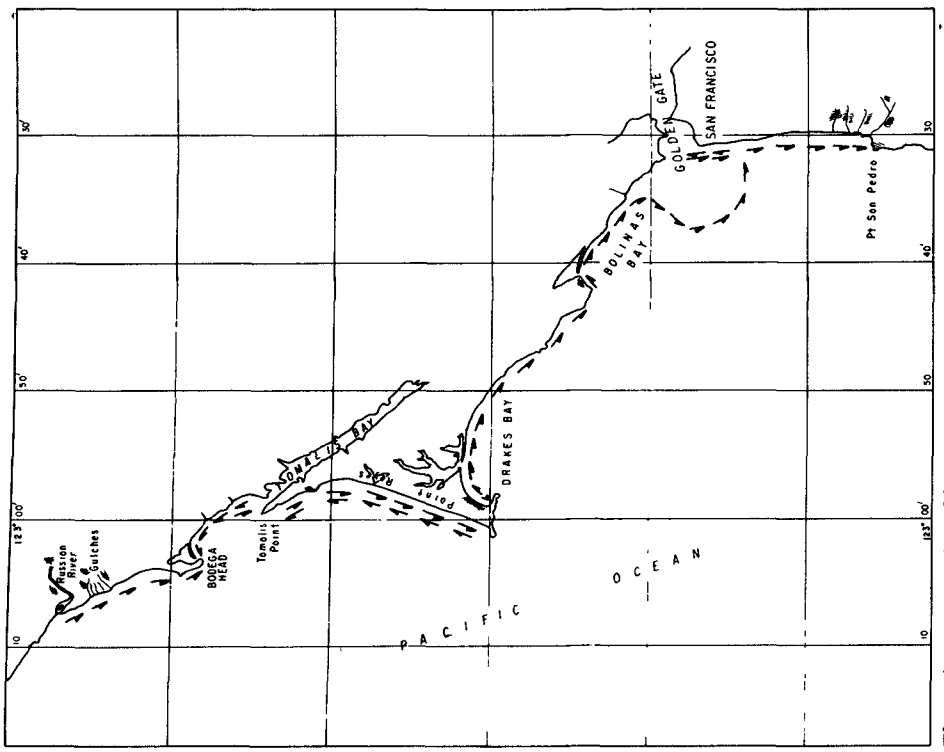

Fig. 4. Probable direction of littoral drift and the sources of thorium from streams and coastal outcrops.

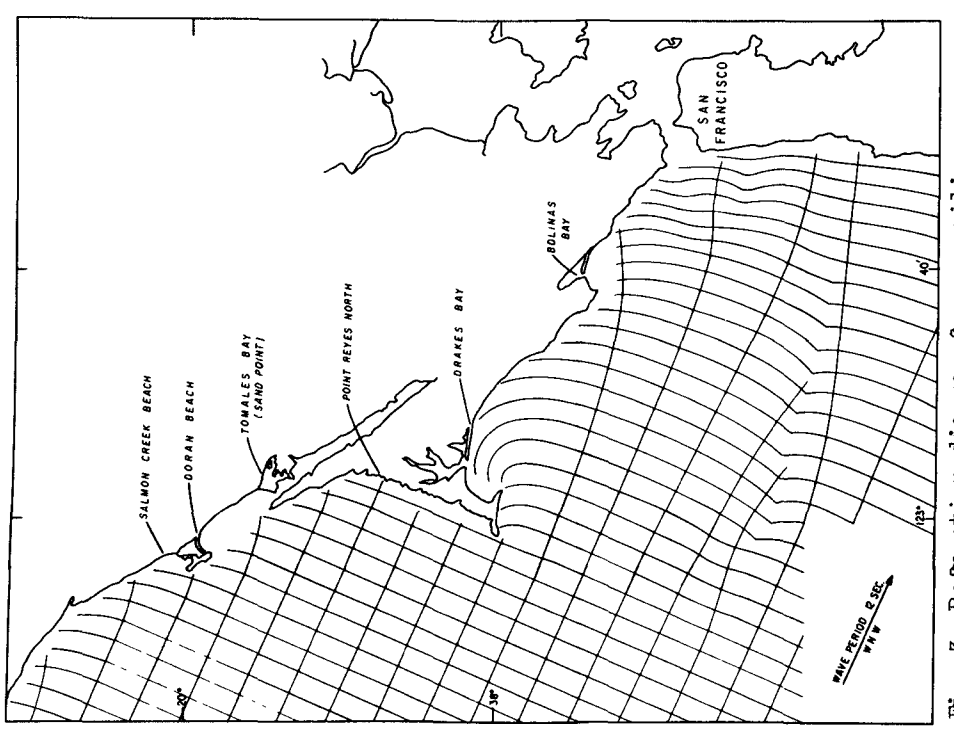

Fig. 3. Refraction diagram for prevailing wave condition in the region under study.

is believed that the pattern of sand movement along the California coast from the Russian River mouth to Point San Pedro takes the following form (Fig. 4).

For the part of the coast north of the Russian River mouth though the refraction diagrams indicate a southward drift, the concentrations of both thorium and heavy minerals do not show any consistent or significant decrease in any direction which suggests a possible reversal direction of littoral drift for this part.

South of the Russian River mouth the concentration of both thorium and heavy minerals decreases gradually and consistently in a southward direction. This indicates a southward direction of sand movement which is also confirmed by the wave refraction diagram pattern for this part of the coast.

For Bodega Bay, although a northward direction of drift is indicated by the northward decrease in concentration of both thorium and heavy minerals, the great preponderance of chert and greenstone among the pebbles on Point Reyes Beach indicates that most of the beach material comes from the mainland east of the Point Reyes Peninsula, because no rocks of this character are found on the Peninsula which shows a southward direction of drift. This is also confirmed by the wave refraction diagram pattern.

Wave refraction diagrams drawn for Point Reyes Beach for W.N.W. waves with a period of 12 seconds which represents the predominant wave condition in this part, (Fig. 3), show that the direction of wave approach is parallel to the shore. However, waves approaching the shore from the north or south of the W.N.W. direction will result in a southward or northward littoral drift respectively which indicates that sand movement along Point Reyes Beach is subject to reversals in direction.

For Drakes Bay the decrease in both thorium and heavy minerals concentration to the east, wave refraction diagram pattern and the presence of porphyry pebbles all indicate an eastward direction of littoral drift.

The eastward decrease in thorium and heavy minerals concentration wave refraction diagram pattern, and the presence of numerous pebbles of Miocene rocks along the sand spit at Bodega Bay, which can only come from the west, all indicate an eastward direction of sand movement along this beach.

The high concentration of both thorium and heavy minerals for the samples taken from the top of the San Francisco Bar and the respective northward and southward decrease of both these concentrations north and south the top of the bar in front of Fleishhacker Zoo at Ocean Beach, suggests very strongly the migration of material from the north to the south

along the top of the bar. This material then enters Ocean Beach in front of Fleishhacker Zoo and is diluted in both a northward and southward direction by wave action.

REFERENCES

1. Adams, J. A., et al, 1958, Determination of thorium and uranium in sedimentary rocks by two independent methods. Geochemica et Cosmochemica Acta. Vol. 13, p. 270-279, 1958.

2. Hutton, C. O., 1951, Uranium, thorite, and thorium monasite from black sand pay streaks, San Mateo County, Calif., Geol. Soc. Amer. Bull. Vol. 62, No. 12, 1518-1519, 1951.

3. Johnson, D. W., 1919, Shore processes and shoreline development, John Wiley & Sons, New York.

4. Kamel, A. M., 1962, Littoral studies near San Francisco using tracer techniques, B.E.B. Tech. Memo. No. 131, 1962.

CHAPTER 20

MODES OF SEDIMENT BEHAVIOR AND SELECTION OF HARBOR DESIGN AND MAINTENANCE TECHNIQUES FOR MINIMUM SHOALING IN ESTUARIES

R. B. Krone and H. A. Einstein
Sanitary Engineering Research Laboratory
and
Hydraulic Engineering Laboratory
University of California, Berkeley

INTRODUCTION

Recent field and laboratory studies on San Francisco Bay sediment have revealed modes of sediment transport and shoaling processes there. These studies have been partially described in reports (Krone et al., 1959, 1960) and articles (Einstein and Krone, 1961a, b) and sufficient information has now been accumulated to encourage qualitative recommendations for selecting harbor designs and maintenance programs causing minimum shoaling in this bay.

San Francisco Bay is a transitional region between the nearly steady uniform fresh-water flows in contiguous rivers and the marine environment. In this region unsteady quasiperiodic flows and water depths prevail, and salinities range from very low values in the rivers to that of sea water. Water density variations due to salinity differences complicate hydraulic conditions resulting from the transition from river to tide-induced flows, particularly in channels, to the extent that flows in opposite directions are found near the channel bottom and near the water surface. Large areas exist in the Bay with MLLW depths less than six feet. In these areas wind and tide-induced currents having low flow velocities, and wave action are the important hydraulic conditions.

The sediments transported into the Bay generally range from fine sand downward in size, and compose the "wash loads" of entering streams that have found conditions in the Bay favoring deposition. Sediments involved in shoaling problems are generally composed of more than half clay minerals. These minerals are a heterogeneous mixture but are predominately montmorillonite and illite. Organic matter content of deposits within the Bay are on the order of .02 by dry weight.

Similar estuarial conditions and clayey sediments to those in San Francisco Bay are believed to occur widely in other areas, with variations in detail of configuration, flows, salinities, wave action, and sediment composition and loads. Such details are more or less subject to modification, however, and are the principal interest of those concerned with harbor design. This paper first presents descriptions of the factors and physical processes important to sediment transport and shoaling in an estuarial environment as bases of later general recommendations for harbor design and maintenance. These descriptions are based on the San Francisco Bay studies, with supplementary information from other estuarial regions when known.

SEDIMENTS

The large clay mineral portion of San Francisco Bay sediment results from the enhanced deposition of such particles when they enter an estuarial

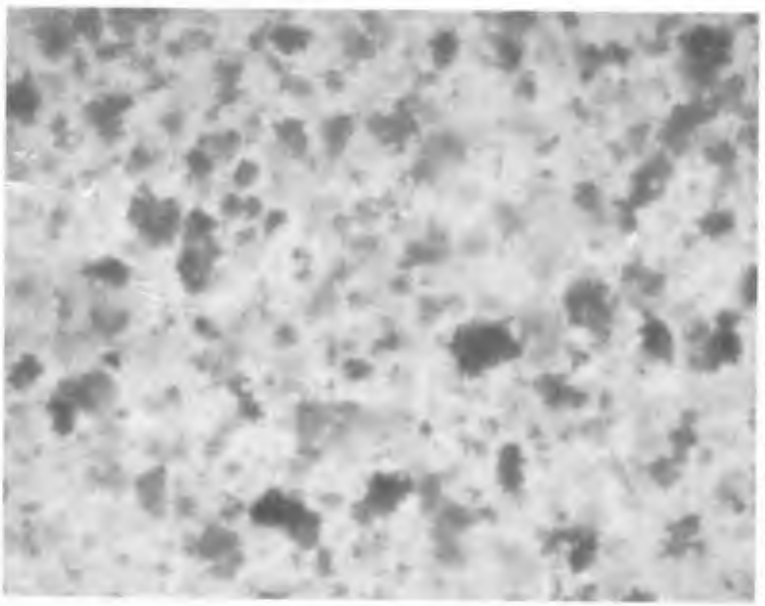

Fig. 2. Photograph of flocs developed in salt water by shear.

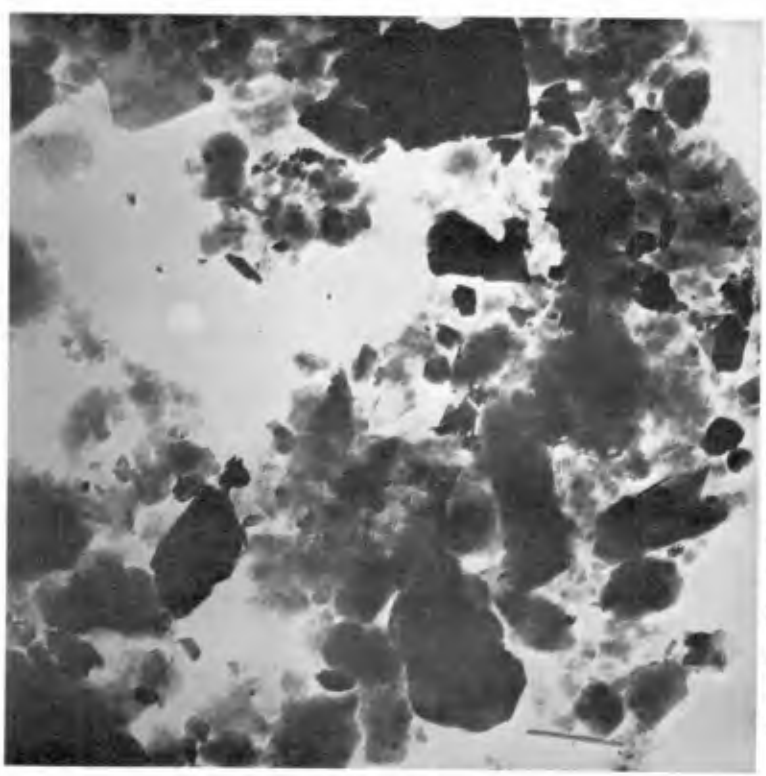

Fig. 1. Electron micrograph of Mare Island Strait sediment.

environment. An electron micrograph of sediment taken from a part of the San Francisco Bay system is shown in Figure 1. The particle sizes in Figure 1 can be estimated by comparison with the approximately one-micron long halloysite tube in the lower left-hand corner. The large flakes in the figure are illite particles, and the fine indistinct masses are believed to be montmorillonite. Figure 1 shows the variety of shapes and sizes of such minerals.

The mineral composition depends on the soils in the areas drained by entering streams. It is unlikely that an estuarial sediment contains only one mineral kind, although one can predominate. Mineral compositions determined by X-ray analyses of sediments supplied by the Corps of Engineers, U. S. Army, from estuaries in the United States are summarized in Table 1. The compositions given in Table 1 show similar minerals with different relative abundances for samples taken from widely separated estuaries. The large fractions of particles less than 2 μ give all of these samples a clayey character.

TABLE 1. Mineral Compositions of Estuarial Sediments

	Location	Fraction < 2	Minerals Present, in order of abundance
1.	Philadelphia	0.54	montmorillonite, vermiculite, kaolinite, illite, quartz
2.	Brunswick Harbor	0.76	kaolinite, illite, montmorillonite, vermiculite, quartz
3.	Gulfport Ship Channel	0.78	montmorillonite, kaolinite, quartz
4.	Potomac River	0.30	kaolinite, montmorillonite, illite, quartz
5.	Delaware River	0.47	illite, montmorillonite, kaolinite, quartz
6.	Mare Island Strait (San Francisco Bay)	0.60, 0.47	montmorillonite, illite, kaolinite, quartz

FLOCCULATION

Fine particles usually remain dispersed in river waters because coulombic repulsive forces predominate between colliding particles. The distribution of the energy of repulsion from a mineral particle surface depends on the valence and concentration gradient of ions in river waters attracted by the charges of the mineral surfaces. The charge density on a mineral is fixed by the mineral composition, so that as the concentration of

salt ions in the surrounding water increases, the gradient of ion concentr tion from the particle diminishes with a consequent lessening of repulsior

Short range attractive forces also exist between particles. These attractive forces are believed to be due to electro-magnetic interactions between atoms resulting from oscillations of the atomic nuclei within thei associated electron clouds. These forces are strong, short range, and add tive. Whether the repulsive or attractive forces predominate between coll ing particles depends on the salt and its concentration, for a given miner For San Francisco Bay sediment the attractive forces are completely effect at sea-salt concentrations of 1 g/l and higher (Einstein and Krone, 1961a) Since ocean water has a salt concentration of about 35 g/l, the salinity c most of the mixing zone is sufficient to allow colliding particles to stic together.

Flocculation, or aggregation, of particles in an estuary requires both that particles be brought together and that colliding particles stick Three mechanisms of bringing particles together have been described (Krone et al., 1962): thermal agitation of the suspension, the internal shearing that comprises the flow process, and differential settling velocities. Thermal agitation, or Brownian movement, results from thermal jostling of suspended particle by the erratic movements of neighboring water molecules The frequency of collisions on a particle or floc depends on the number of particles per cubic centimeter and the absolute temperature. Collisions b this mechanism are important among the large number of particles per cubic centimeter that sometimes occur near the bed.

The frequency of collisions on a particle due to internal shearing in the water depends on the number of particles per cubic centimeter, on t collision radius of the particles cubed, and on the shearing rate. The co lision radius is approximately the sum of the radii of the two colliding particles. Collisions are enhanced by a wide range of particle sizes (in cluding flocculent particles) which provide both large collision radii and large numbers per cubic centimeter. Internal shearing at rates up to 6 cm/sec per cm cause growth of flocs of suspended San Francisco Bay sedi- ment. At higher rates flocs are broken apart.

An enlarged photograph of sediment flocs developed in the laborat by shearing the suspension between concentric cylinders is shown in Figur The aggregation of smaller flocs into large ones can easily be seen in Fi, ure 2. The darker areas in Figure 2 are flocs.

Collisions by differential settling velocities depend on the numb of particles per cubic centimeter, the difference in radii of the colliding particle pair and the collision radius cubed. Collisions due to both internal shear and differential settling are enhanced by a range of floc si the large flocs tend to gather up the smaller ones, and to grow even larg Differential settling can continue growth of flocs initiated by shearing, and the two mechanisms enhance one another under conditions of gentle int nal shearing. These phenomena are utilized in water treatment to remove suspended particles.

Of the various factors that promote flocculation, two are subject modification by the designer. They are the suspended sediment concentrat and the rates of internal shearing in a waterway.

MODES OF SEDIMENT BEHAVIOR AND SELECTION OF HARBOR DESIGN AND MAINTENANCE TECHNIQUES FOR MINIMUM SHOALING IN ESTUARIES

SETTLING VELOCITIES

A significant consequence of flocculation is the alteration of settling velocities of suspended particles resulting from the increase in size of aggregates. The density of flocs depends on the salinity of the water, on the shapes and size distribution of the minerals, and on the composition of the individual sediment particles. The density of San Francisco Bay sediment flocs was found to be between 1.03 to 1.07 g/cm^3 for a water density of 1.013 g/cm^3. The difference in density between the water and the floc is less for the floc (0.02 to 0.05) than for an individual particle in fresh water (1.6), but the settling velocity is proportional to the radius squared, and the lower density is rapidly compensated by the increase in size. The settling velocity of a floc is greater than that of a 2-μ particle for floc sizes above 18 to 12 μ for the densities given. Large flocs have much higher settling velocities than do individual particles. When suspended sediment encounters conditions favoring rapid flocculation and the formation of large flocs, the increased settling velocities facilitate deposition.

A condition of "fluid mud" has been reported in estuaries. It has been observed in the laboratory that at suspended sediment concentrations above about 10 g/l the settling flocs hinder the upflow of displaced water, and during the period of "hindered settling" the mud has a well-defined surface, just as would a more dense fluid under water. This phase lasted from 100 to 200 minutes for the sediments tested, and was followed by a slow "consolidation" phase.

VISCOUS PROPERTIES

Viscometer measurements on sediments from San Francisco Bay, Philadelphia, and the Gulfport Channel show that these sediments have the properties of a Bingham fluid. Both a capillary viscometer and a rotating cylinder viscometer show linear shear as shearing rate relations with an extrapolated initial shear strength at zero shearing rate. The initial shear strength increases with increasing concentration from a minimum concentration that provides a connected structure.

The initial shear strength also increases with salinity up to a maximum at the salinity of 1 g/l for San Francisco Bay sediments, showing that maximum cohesion prevails at that and higher salinities.

The properties of the other sediments listed have not yet been studied with a viscometer. In view of their mineral compositions, however, they are expected to have similar rheological properties, but different strengths and differential viscosities.

SEDIMENT BED-FLOW INTERACTIONS

Deposition rates of flocculent particles in suspension from flowing water depends on the amount of material in suspension, the floc settling velocities, and the bed shear. The settling velocities depend on the concentration of suspended material and internal shearing as described above Flume studies (Einstein and Krone, 1961b) have shown that flocculent particles of San Francisco Bay sediments striking the bed can stick at bed shears

less than 0.6 to 0.8 dynes/cm^2. Such shears occur in a 30-ft deep channel at average uniform flow velocities of 0.93 ft/sec. At lower shears the probability of a floc sticking to the bed increases proportionately.

Suspension of deposited flocculent sediment at bed shears greater than 0.8 dynes/cm^2 appears to occur by two processes. Mass failure of the sediment deposit occurs when the bed shear exceeds the sediment shear strength--which can easily occur for freshly deposited sediment or suspensions in the "fluid mud" concentration range on an increasing tidal current. When the shear strength of the bed is greater than the shear applied by the flow, a relatively slow erosion of the bed occurs. The erosion rate is weakly dependent on the suspended sediment concentration.

TRANSPORT AND SHOALING PROCESSES

A description of modes of transport and of shoaling processes can be derived from the foregoing descriptions of cohesive sediment behavior in suspension and of flow-bed interactions. These are summarized briefly:

1. Sediment can be transported long distances in suspension by tidal flows when the floc sizes are small or when the bed shears exceed the maximum at which deposition occurs. Floc sizes would remain small under conditions of high internal shearing rates or low suspended sediment concentrations. At high shearing rates and when the concentration of suspended sediment is high, the growth of flocs combined with destruction of large flocs by internal shearing is believed to narrow the distribution of floc sizes. Limited field data support this.

2. When mud-laden water encounters flow conditions providing gentle internal shearing, such as those near sudden channel enlargements, docks and pilings in regions of low flow velocities, and near the interface of a saline wedge, very rapid growth of flocs occurs. The collision frequency on a flocculent particle under conditions of internal shearing depends on the collision radius cubed, making flocs grow at an increasing rate.

3. In areas and at times when the bed shear is sufficiently low, deposition of flocs can be rapid. Low bed shears and conditions of gentle internal shearing often occur together in docking areas constructed in channel enlargements.

4. Movement of "fluid mud" or high concentrations of flocculent sediment can occur as gravity flows wherever the bed slopes are sufficient to start and maintain such flows. Gravity flows can be an important mode of transport from zones of rapid deposition at the edge of a channel into the center part of the channel. Movement of a layer of fluid mud by shear of the water above alone is contradictory to the rheological characteristics of sediments studied and has not been found in radioactive tracer studies made to observe such movement in San Francisco Bay (Krone et al., 1959).

MODES OF SEDIMENT BEHAVIOR AND SELECTION OF HARBOR DESIGN AND MAINTENANCE TECHNIQUES FOR MINIMUM SHOALING IN ESTUARIES

PRINCIPLES OF DESIGN AND MAINTENANCE TECHNIQUES

Preparations for design of harbors or harbor modifications should include determination of sediment character, salinity distributions, and a description of the hydraulic regime. Procedures for making such determinations are outside the scope of this paper. Such information is necessary, however, for determining whether cohesive sediments and the regime described here is applicable, and for applying the principles suggested below. These principles are:

1. Minimize the suspended sediment concentration of water entering a probable shoaling area. Even occasional high concentrations can cause serious shoaling and should not be overlooked. Methods of minimizing the concentrations of suspended sediments include:

   a. Prevent suspension of sediments in source areas. Shallow areas were found to provide sediment to suspension in San Francisco Bay during daily periods of wave action. Such areas can sometimes economically be filled in.

   b. Prevent tidal movements of water from source areas to the shoaling area. Dikes are feasible for containing dredge spoil and for increasing currents in channels through shallow areas. Such dikes can often be designed to include all shallow source areas.

   c. Avoid contaminating an area of shoaling by dredge spoil from adjacent maintenance operations. Such difficulty is probable in a long, gradually widening estuary wherein dredging is in progress in some part of the estuary most of the time, and when dredge spoil is released into the waterway. Disposal in areas contained by dikes has been found to reduce shoaling by more than one-half from that which occurred during a period of spoiling to the waterway in the Delaware River (Simmons, 1962).

2. Minimize flow conditions combining enhanced internal shearing and low bed shears.

   a. Channel enlargement for docking facilities reduces bed shears. Shoaling can be minimized by avoiding or minimizing flow conditions that provide gentle internal shearing such as those near pilings, sudden enlargements, and in salinity gradients. Gradual channel transitions, particularly those of the bed, and smooth channel boundaries are suggested. Parallel docking, if feasible, with covered dock faces should provide minimum disturbance to flows.

   b. Both gentle internal shearing and low bed shears are provided by salinity intrusions, and shoaling is inevitable when clayey sediments are present. By combining flows or channel narrowing, the toe of a salinity intrusion can be moved and the shoaling area can be moved to a location where maintenance is more easily accomplished (Simmons, 1962).

3. Minimize the amount of sediment-laden water entering off-channel harbors. Since flow conditions that prevent deposition in such

areas cannot be provided, limitation of the amount of sediment-laden water entering a side channel or basin appears to be the best solution. Single narrow openings, providing essentially fill and draw water movement with a minimum of circulation, and entrance channels walled to water having low suspended sediment concentrations, are suggested.

4. Maintenance of bed shears greater than the maximum that allows deposition during most of a tidal cycle can be facilitated by dikes, which can be economical when used for multiple purposes as described in 1b.

These principles support many present practices developed over many years of experience in estuaries. While they are based on laboratory and field studies in one transition region and are supported by experience in a limited number of other regions, they are based on widely applicable phenomena, and should serve as aids to selection of measurements in the field, evaluation of designs, interpretation of model data, and planning of maintenance operations.

REFERENCES

Krone, R. B., Einstein, H. A., Kaufman, W. J., and Orlob, G. T. (1959). Silt transport studies utilizing radioisotopes: 2nd Annual Progress Report, Hydraulic Engineering Laboratory and Sanitary Engineering Research Laboratory, University of California, Berkeley.

_____ (1960). Silt transport studies utilizing radioisotopes: 3rd Annual Report, Hydraulic Engineering Laboratory and Sanitary Engineering Research Laboratory, University of California, Berkeley.

Krone, R. B. (1962). Flume studies of the transport of sediment in estuarial shoaling processes: Final Report, Hydraulic Engineering Laboratory and Sanitary Engineering Research Laboratory, University of California, Berkeley.

Einstein, H. A. and Krone, R. B. (1961a). Estuarial sediment transport patterns: Proc. ASCE, vol. 87(HY2), Pt. 1, pp. 51-59.

_____ (1961b). Experiments to determine the modes of cohesive sediment transport in salt water: J. Geophys. Res., vol. 67, pp. 1451-1461.

Simmons, H. B. (1962). Private communication.

CHAPTER 21

MEDICIONES DE ARENA EOLICA EXTRAIDA DE LA PLAYA DE SANTA ROSA POR DEFLACION

Jorge Broggi R.
Lima, Peru

Por cientos de kilómetros la asfaltovía Panamericana Roosevelt recorre nuestro litoral, sucesión alternada de acantilados rocallosos con otros areno-arcillosos o de grava compacta alternando con playas en su mayor parte o de grava suelta o sea guijarros.

El viento sur dominante, llamado Virazón por los marinos, es poco perceptible en las mañanas y particularmente intenso en las tardes, con ráfagas de velocidades que llegan a pasar 5 m/s. (metros por segundo), viéndose entonces que extrae la arena seca de las playas para llevarla tierra adentro hasta centenares de metros sobre el nivel del mar, invadiendo en su camino poblados y vías de comunicación con acumulaciones a veces masivas o sea de dunas eólicas, que dificultan y encarecen el transporte y la vida de los pobladores pues caminos, vías férreas y pueblos quedan parcialmente sepultados en forma tal que solo a fuerza de brazos se logra descubrirlos pues las dunas extienden su pesado manto de muerte y desolación desértica a grandes sectores de nuestra Costa o sea playas y aéreas inmediatas.

A la latitud de Lima no es menos visible este panorama que estudiamos en un deseo de encontrar soluciones generales que hagan la actividad humana menos azarosa y se facilite con ello el desarrollo de nuestras vitales industrias. Solucionar el problema de la migración eoloarenosa, es pues dar salida segura y barata a los principales productos de nuestro comercio y facilitar la vida de los transeuntes y poblados en general.

El valor de nuestras observaciones no deja de tener carácter universal, pues al margen de muchos mares y lagos del Orbe, se ofrecen fenómenos similares a los que ocurren en nuestra extensa Costa, siendo muchos los países que se interesan por eliminar las dificultades que causa el movimiento de las arenas por el viento, porque tal migración afecta donde quiera las actividades del hombre.

Es así, como observé fenómenos parecidos a los nuestros en la Bahía de Arcachón (Francia) (Golfo de Biscaya) donde quedamos sorprendidos al constatar que paralelamente a la playa se elevaban grandes dunas costeras, que se podían seguir con algunas soluciones de continuidad por donde la invasión arenosa ofrecía un ancho de 3 á 10 kilómetros. Allí el movimiento en masa de las dunas, o transporte masivo, se hace a veces con una velocidad hasta de 30 metros por año amenazando destruir los bosques artificiales de pinos adya-

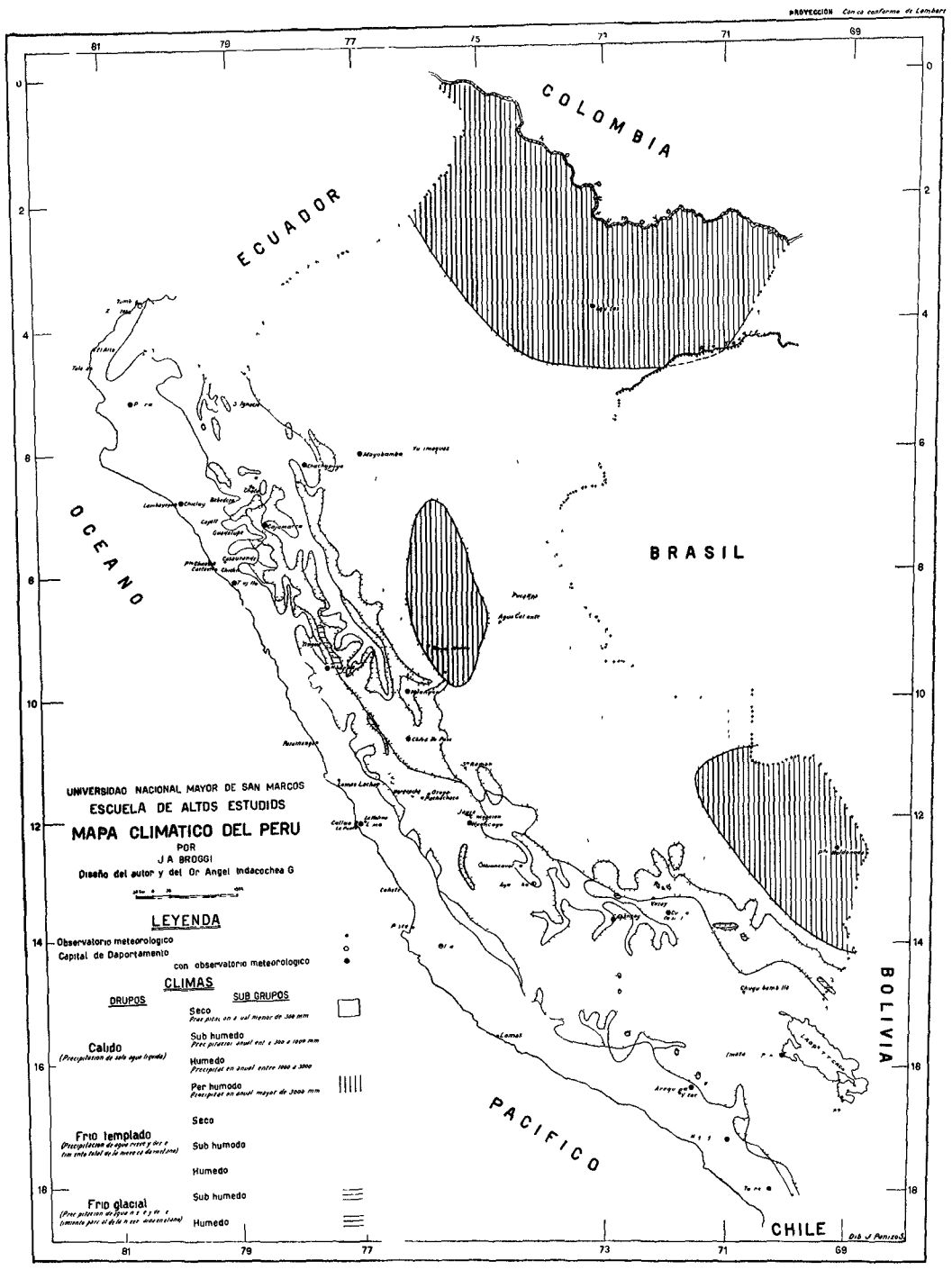

Mapa Climatico del Peru

centes a la playa y que se han sembrado para ponerle atajo en su avance desolador. (1)

Otra importante área localiza también a lo largo de la Costa Báltica Alemana, donde una pequeña villa fué sepultada por arenas el año 1839 y desenterrada solo en 1869.

No siempre, sin embargo, la migración eoloarenosa en el Continente es totalmente perjudicial, pués como puede verse a 24 kilómetros al sur de Lima (contados de la Plaza de Armas) una industria de ladrillos calcáreos, dá nueva vida a la construcción civil, utilizando como materia prima la arena eólica acumulada en la base del cerro Lomo de Corvina, en la playa de Conchán, entre el Morro Solar y Lurín. También las arenas tienen valor como componente principalmente mecánico de las tierras arables muy arcillosas, al volverlas porosas y airables como desde medio siglo atrás se usan de antideslizante para las locomotoras que trafican en zonas lluviosas andinas, así como material de construcción mezclado a cal y cemento; y por último para filtrar agua y también de abrasivo.

En suma, el estudio que hemos realizado, no solo tiene pues valor científico, didáctico, sino eminentemente económico y de aplicación inmediata a la actual cultura en sus diversos aspectos, pues descubre fenómenos antes desconocidos pero que han tenido influencia decisiva en nuestra civilización pretérita y aún la tienen en la actual.

CAPITULO I

GEOGRAFIA DE LA PLAYA SANTA ROSA

UBICACION E HISTORIA DE LA PLAYA SANTA ROSA

Esta playa arenosa que ubica al sur de Ancón, es la pequeña parte también meridional de la conocida Playa Grande, de ella separada por un pequeño morro al cual se llama C° Santa Rosa; ver en el plano al 20 000 publicado por el Instituto Geográfico Militar a base del relevado fotográficamente por el Servicio Aerofotográfico Nacional a solicitud y costo del Instituto Geológico del Perú (véase Anexo N° 1, Lám. 1)

La zona que hoy lleva el nombre del Balneario Santa

(1) Sobre este problema y otra de las costas véase:
Johnson, Douglas Wilson.- Shore processes and shoreline development, 1st Ed. pp. 584, 1919.

Rosa, ha sido ocupada por el hombre desde los tiempos preincaicos, pués la existencia de extensos y profundos conchales con restos de cocina y cerámica primitiva, lo acredita;pero hace tan solo 5 años que la empresa particular The Peruvian Trust Company hizo un camino con pavimento de concreto desde la Autovía Panamericana o Roosevelt Norte, tres piscinas, calles, campo de golf y todo un balneario deportivo.

ACCESIBILIDAD

Del km. 36 de la Plaza de Armas de Lima siguiendo la actual asfaltovía Roosevelt Norte, sale el ramal pavimentado de concreto de 1000 m. de longitud hasta la Playa de Santa Rosa, el que después de ascender 50 m.(verticales) hasta un pequeño portachuelo con arco ojival de concreto a mayor nivel del cual se han instalado tanques de agua potable bombeada desde la margen cultivada del valle de Chillón en Puente Piedra y baja por el nuevo bàlneario por cerca de 2 km. hasta el mismo Océano Pacífico.

CLIMATOLOGIA

Según la clasificación termohidrológica de J.A.Broggi (1947) la zona se halla en el ärea de Clima Seco (CS) con menos de 300mm. de precipitación anual de sólo agua líquida que califica normalmente toda nuestra costa desde la frontera con el Ecuador hasta la frontera con Chile.

Ofrecemos como Anexo Nº2 los cuadros de observaciones meteorológicas realizadas por los técnicos de la ya citada empresa urbanizadora de Santa Rosa y control de la Dirección de Meteorología del Ministerio de Aeronáutica y que dan idea de algunas particularidades climáticas principales del lugar.

VIENTOS, ARENAS Y DINAMISMO DEL MAR

La aridez del clima de Santa Rosa, los vientos de mar a tierra o virazones, cuyas velocidades al nivel del suelo exeden a veces 5 m/s y la existencia de una extensa playa arenosa, son condiciones que favorecen el eolismo o sea un régimen en que la acción mecánica del viento determina la morfología superficial con montículos de arena o dunas que ascendiendo las cumbres circundantes setentrionales descienden a la conocida Pampa de Ancón.

Dada la predominancia del viento marino, particularmen-

te fuerte en las tardes de Noviembre a Mayo, las formas dunáceas revelan en sus sombras y convexidades barcanoides la constancia de su dirección media S-N.

Como Santa Rosa es solo la parte meridional y algo abrigada de Playa Grande, separada de ella por el Morro de ese nombre, el oleaje de alta mar dominante (tumbos) no incide perpendicularmente sino a la parte de la playa situada al N del Morro lo que significa un oleaje generalmente más reducido en altitud y violencia en su rompiente de Santa Rosa. Esto no quiere decir que a veces bravezas de origen lejano puedan presentarse siendo particularmente las del NW (ocurrida por ejemplo hace 3 años y que destrozó el rompeolas de piedra cuya construcción se iniciaba en la parte sur de la ensenada de Santa Rosa) las que son más temibles porque no hay abrigo para ellas.

El carácter abierto de la bahía nos dá un régimen normal de mareas semejante al de casi toda nuestra Costa Central y cuyas características se conocen, pues se ha determinado su amplitud máxima de sicigias que ocurre dos veces cada 24 horas, y que es de 2.6 piés (1) en el Callao, lo que daría para Santa Rosa cerca de 2.5 piés ó sea 76.2 cm. de máxima y media anual de solo 57.9 cm.

En lo que respecta a oleaje normal, debemos anotar que el dominante de altamar tiene dirección SSW por lo que al quedar la Playa de Santa Rosa abrigada en parte por el macizo de Piedras Gordas, es sobre todo intenso en Playa Grande, que está más al N. donde las olas inciden con una rompiente inicial que frecuentemente pasa de un metro y que con la inclinación media de la playa arenosa de 3° de lugar a que simultáneamente avancen varias olas rotas y que el área de ella expuesta al viento tenga un promedio de 11 m. de ancho entre alta y baja mar con oleaje normal.

CAPITULO II

V I E N T O S

DE LOS VIENTOS EN GENERAL

A toda masa de aire en movimiento se le dá el nombre de viento y de acuerdo con los caracteres de su dinamisno local,

(1) Tablas de mareas.- Ministerio de Marina. República Peruana. Servicio Hidrográfico.- 1958 y 1959.

se clasifica en relación al medio terrestre sobre el cual discurre; pero también es de importancia conocer su temperatura, humedad y sobre todo su carácter pulsátil o rafagosidad en relación al transporte eólico porque es con las ráfagas que este tiene importancia.

DE LOS VIENTOS EN SANTA ROSA

Desde tiempo atrás en los observatorios meteorológicos se mide solo la dirección de la componente horizontal y velocidad del viento en el aerozocalo o parte inferior de la atmósfera (20 M. o verticales inferiores) en contacto con la litósfera o la hidrósfera; pero los anotados por la empresa Urbanizadora Santa Rosa (Anexo N° 2), omiten sensiblemente su dirección. Con el anemógrafo Lambreth, de que hemos dispuesto por préstamo bondadoso de la Dirección General de Meteorología, se han podido obtener con todo direcciones horizontales en algunos días correspondiente tanto a un punto medio entre la playa y el abra de entrada a la Urbanización, como en el mismo malecón de la playa en los puntos señalados en el plano con las letras M y P.

De una manera general podemos decir que se conoce poco de los vientos en el aerozócalo peruano y menos en altitud. La Capital de la Republica es el sitio donde se han investigado más; "pero aún falta mucho por conocer de su estructura mecánica detallada" aún de los dominantes en sus 3 M. (inferiores sobre el suelo) que para los efectos de nuestro estudio son los más importantes.

Habiéndose fijado nuestra atención en la estructura fina de este estrato basal, hemos podido observar que los vientos horizontales varían mucho de intensidad en cortos intervalos y que son precisamente los momentos en que su velocidad aumenta o de ráfagas, que el transporte de arena reviste mayor importancia. Es así como se vé con frecuencia en corta fracción de minuto que la arena es transportada en suspensión, o sea flotando en olas, entre las cuales hay períodos hasta de calma casi absoluta de duración mucho mayor.

A este respecto reproducimos el siguiente párrafo de la obra de K. Middleton y Spilhaus (3).

"Besides speed and direction, a third characte-

(3) W.E. Knowles Middleton and Athelstan F. Spilhaus: Meterological Instruments, 3rd. Ed. revised-University of Toronto Press, p. 136, 1953.

"ristic of the wind is of importance in meteoro-
"logy. The flow of air over the ground or over
"the sea is not smooth, but turbulent: and the
"degree of turbulence may be indicated by a quan-
"tity known as the gustiness. At least six defi-
"nitions have been suggested for this quantity;
"that used by English authors (2) is convenient
"for use with the records of many anemometers.
"It is

$$(6.1)\ldots G=\frac{V\ max-V\ min}{V\ mean}$$

"The value being taken over a period of 10 minu-
"tes.
"It is comparatively easy to build an instrument
"which will make some sort of record each time
"the wind speed changes by one unit (e.g., 1 mile
"per hour). Given such an instrument, a useful
"measure of gustiness would be the number of ti-
"mes per hour that this change takes place. In
"symbols

$$(6.2)\ldots G=\frac{\Delta V}{T}$$

"Note that the direction of the change does not
"matter.....

"(2) See for example, F.J. Scrase, Geophys Memo-
"irs N° 52 (London Meterological Office 1930)."

El malogrado Dr. Angel Indacochea G., que actuó como Secretario del Comité Geofísico del Año Geofísico Internacional 1957-58, acompañó como asistente a mi señor padre en el problema de medir y estudiar los vientos en nuestra costa con un anemógrafo Lambrecht (Göttingen) que, adaptado a una pequeña torre portátil de acero Dexion de 2 M., le dió registros del 17 de Marzo de 1958 al 5 de Abril en la parte central de la Urbanización Santa Rosa (punto P de Láminas del Anexo N° 1) y en el Malecón de la misma playa, del 9 al 24 del mismo abril (punto M). de los cuales obtenemos las siguientes conclusiones:

1) Los vientos dominantes en todo el sector de Santa Rosa vecino a la playa, son del S con desviación al SW durante las tardes en que su intensidad aumenta y al SE por las noches en que disminuye.

2) Las mayores velocidades, se han registrado después del medio día hasta el anochecer con ráfagas hasta de 25 m/s y por pocos segundos solamente.

3) Desde la media noche, las velocidades son generalmente mínimas y del SE, llegando hasta la calma absoluta a las 9 ó 10 de la mañana en que comienza a soplar el viento del SW.

4) Con la modificación del anemógrafo Lambreth a velocidades de giro del tambor registrador diez veces mayor que la de fábrica, se obtuvo, en períodos de más de tres minutos de duración total, promedios hasta de 10 m/s durante los cuales se anotaron picos de 25 m/s.

Las ráfagas diurnas fueron visiblemente acompañadas de fuerte migración arenosa en la playa y a no más de 25 cm. de altura, que tierra adentro excedía de un metro cuando la turbulencia crecía y se producían visibles remolinos.

Los registros de la playa (M=malecón), rara vez tuvieron picos de 10 m/s; pero en los sitios de mayor altitud, las ráfagas pasaron con frecuencia de esa velocidad.

5) Por fuerte transporte salino (por atomización del agua de mar), tuvo que eliminarse previamente por barbotaje en agua pues la sal marina en suspensión en aire que ingresaba al anemógrafo obstruía el instrumento.

De todo esto se deduce, que es de gran valor continuar las investigaciones de rafagosidad, estudios que deben extenderse a la superficie del mar y continente adentro, pues tan pronto como en los desiertos produce fuerte acarreo de arena origina en el mar corrientes superficiales y de fondo, que tienen gran importancia como transportadora de sedimentos. En Pisco estas virazones son llamadas paracas y causan hasta naufragios de pequeñas embarcaciones a vela y notable acarreo de polvo y arena por decenas de kilómetros.

Como no se ha observado estrecha relación entre las diferencias de temperaturas de mar y tierra con los vientos, como entre la dirección de estos y la línea de playa o sea su angularidad, creo que se impone un estudio más profundo de las virazones o vientos dominantes del mar (S y SW). Se ha podido constatar, con todo que las virazones son más intensas cuando desaparece el conocido "banco de nubes", lo que se explica porque estos estratos bajos son barridos por vientos originados en capas altas de la atmósfera.

MEDICIONES DE ARENA EOLICA EXTRAIDA DE LA PLAYA DE SANTA ROSA POR DEFLACION

CAPITULO III

ARENAS

Definición.- Entre los sedimentos acuosos o sea depósitos granulares con poca adherencia entre sus partículas, está la arena, cuya definición y diferenciación se hace por las dimensiones de sus granos que varían, según la mayor parte de los geólogos y petrólogos, entre diámetros de 2.5 mm. y 0.05 mm. (4)

Origen.- Por su constitución de fragmentos cristalinos se puede decir que derivan de la desintegración de rocas de tal carácter, pudiéndose afirmar que primariamente lo son de ígneas o metamórficas, pero que también pueden provenir de sedimentarias particularmente detríticas poco cementadas. Muchos autores creen que al hallarse en las playas fuertes acumulaciones, las arenas se forman en las rompientes como resultado del embate de sus aguas sobre las rocas o fragmentos rocosos de las orillas; pero tan solo se puede ver trituración cuando el oleaje desmenuza las conchas adheridas a peñascos. Por felicidad ya son pues pocos los geólogos que consideran esta acción mecánica como la causante principal de su formación.

Es evidente que las arenas se producen principalmente por la acción fisicoquímica primera del intemperismo atmosférico, que desintegra los elementos cristalinos de las rocas cuya resistencia es muy variable dando como resultado un sedimento granular incipiente. Las aguas de escorrentía transportan después sus granos, en un principio angulosos y más tarde de aristas redondeadas, hasta el mar en donde se verifica su transporte con selección dimensional simultánea por corrientes marinas de fondo para ser llevadas a las rompientes y formar playas arenosas o sea acrecencias continentales con terrazas playeras a nivel superior a las de las más altas mareas.

De las arenas playeras y eólicas en general.- Bastante diferente es el comportamiento fisicoquímico de un grano de arena bajo el agua que bajo el aire; pero cabe, a primera vista, distinguir el mecánico, pues al tener que yacer en un medio cuya densidad se aproxima a la propia, su resistencia al movimiento del flúido en que yace, tiene que ser menor que ba-

(4) Véase p. ej: F.H. Lahee: Field Geology p. 34 y siguientes. Ed. 1941 como W.C. Krumbein and Pettijohn: Manual of Sedimentary Petrography.

jo la atmósfera cuya densidad es relativamente pequeña.

Siendo la playa la parte de la litósfera que sufre la periódica invasión del agua de las rompientes, los granos de arena que a ella convergen del mar o del continente, tienen que estar sujetos a un cambio constante de medio y por lo tanto de adhesión a granos colindantes. Una arena húmeda bajo el agua es diferente que bajo el aire. En ambos casos el flúido se interpone entre sus granos, pero dá a la arena propiedades distintas. Complejo es el caso de que esta impregnación de agua de mar, por ejemplo, esté en proceso de desaparecer por evaporación en la atmósfera libre, pues entonces se produce la adherencia de sus granos no solo por el agua sino por los sólidos que tiene en solución. Estas arenas no son pues propiamente eólicas sino están secas, proceso que lento y varía con el viento, temperatura y humedad del ambiente subaéreo tan tornadizo.

Secas o casi tales, las arenas playeras están entonces constantemente expuestas a la deflación o sea al fenómeno geomorfológico de desgaste en masa por el viento que constantemente se lleva sus granos superficiales y en proceso dinámico ocupa áreas netamente continentales.

Las playas de Santa Rosa y vecinas, nos muestran estos fenómenos, que pueden y deben ser objeto de una investigación fisicoquímica más exhaustiva.

Las arenas eólicas, entendiéndose por tales las que aparentemente no poseen adherencia entre sus granos por tener sus poros ocupados solamente por aire, se extienden pues a casi la totalidad de nuestra Costa, excepción de su extremidad norte donde la precipitación atmosférica es considerable (Tumbes). Su coloración de tierra es general en grandes masas, siendo oscura cuando dominan los granos de magnetita y clara cuando lo hacen feldespatos o el cuarzo lechoso. En lo que respecta a dimensiones de granos diremos que son de grano grueso cuando están en áreas abiertas donde los vientos son fuertes; y fino, o sea casi loess, cuando los vientos son solo débiles como en las quebraditas abrigadas y en la parte de la zona climática de Lomas al llegar a las altitudes máximas de invasión de las virazones.

En Santa Rosa y Playa Grande las arenas cubren siempre las pendientes que miran al mar hasta transmontar las cumbres que no exceden 300 M y llegar continente adentro, a altitudes en donde domina el "Banco de stratus de la Costa" que cubre las"Lomas" en envierno y buena parte del otoño y primavera.

MEDICIONES DE ARENA EOLICA EXTRAIDA DE LA PLAYA DE SANTA ROSA POR DEFLACION

La humedad salina de las vecindades del mar, solo permite en la playa el crecimiento espontáneo de una que otra planta de hojas carnosas como de sesuvium y más lejos, de las resistentes tillandsias y musgos con cactáceas (5). Es esta la vegetación espontánea más visible. La irrigación con aguas dulces, al disolver el cloruro de sodio, favorece el crecimiento de vegetación netamente continental. Como las arenas son originadas mayormente por la desintegración de las rocas granodioríticas de las vertientes occidentales de los Andes (6) y llevadas al océano para migrar en buena parte hacía las playas por corrientes marinas de fondo y de allí, por las virazones, volver al continente en ciclo cerrado que tiene por teatro el litoral, no se diferencian mucho en su naturaleza mineralógica y solamente se nota cierta selección dimensional como resultado de la acción mecánica clasificadora de los flúidos que la transportan según su velocidad.

En apoyo de esta afirmación, podríamos transcribir la que expresa el destacado geólogo suizo Amstutz (7) profesor en Rolla, Missouri, en una última contribución sobre "Las arenas de las barcadas del Sur del Perú", en que ya menciona a mi señor padre (J.A. Broggi. 1952) en estudio anterior suyo sobre su origen en las rocas granodioríticas del Superbatolito Circumpacífico. Dice así:

> "The mineralogic composition is: quartz, some
> "felspar and some biotite, augite and hornblende.
> "The percentage of these minerals changes from
> "one barchan to the nex and also from one part of the
> "barchan to another part. Crests of secondary wa-
> "ves are often darker, containing a larger number
> "of dark minerals or (¡) exhibiting a horizontal
> "lineation of the dark platy or lathy minerals,
> "whereas the valleys are lighter, due to less ma-
> "fics or (¡) a vertical orientation of the mafics.
> "The sands most probably originated from granites
> "and dacitic volcanics outcropping at the southern
> "of the desert".

(5) Weberbauer, A.- El Mundo Vegetal de los Andes Peruanos, pp. 776, 1945.

(6) Broggi, J.A.- Migración de las Arenas a lo largo de la Costa Peruana, pp. 25, separata de Bol. Soc. Geol. del Perú. T. XXIV (Vol. Unico). 1952.

(7) Amstutz G.C. y Raimundo Chico.- Sand size fraction of South Peruvian barchans and a brief review of the genetic grain shape funtion; separata of Bull. Ver. Schweizer Petrol Geol. u Ing. Vol. 24,Nr 67, S 47-52, Fig. 28,February 1958.

Aunque la poca variabilidad de constitución mineralógica de las arenas, no ha estimulado su análisis mineralógico detallado, lo dicho por Amstutz es suficiente para reconocerla a grandes líneas.

El peso específico de las arenas varía además bastante, siendo mayor cuando está húmeda (8). La arena de las barcanas es superficialmente más húmeda con el rocío de las mañanas, desecándose a medida que el sol y el viento se intensifican. Cuando está húmeda es algo coherente, coherencia que se pierde con su desecación al viento y sol.

La constitución granular de dos muestras de arena eólica recogidas en un frasco de boca ancha, colocado en el suelo y contra el viento por mi señor padre en 1952, en la playa de Santa Rosa, y analizadas en el laboratorio del Cuerpo de Ingenieros de Minas, por el químico Walter A. Solis, fué la siguiente:

ANALISIS GRANULOMETRICO

Muestra		Nº 1		Nº 2	
Malla Nº	Lado de la malla en mm.	Peso Parcial %	Peso Acumulado %	Peso Parcial	Peso Acumulado
+ 48	0.295	17.1	17.1	0.1	0.1
+ 65	0.208	35.0	49.0	9.7	9.8
+ 100	0.147	20.4	69.4	38.2	48.0
+ 150	0.104	24.7	94.1	47.4	95.4
+ 200	0.074	4.7	98.8	4.1	99.5
- 200	0.074	1.2	100.0	0.5	100.0

(8) En experiencia de laboratorio con arena desecada de Santa Rosa, hemos observado un incremento de volúmen de solo 1.85 % por 25 % de peso cuando se satura de agua o sea un incremento de peso específico de más de una quinta parte.

MEDICIONES DE ARENA EOLICA EXTRAIDA DE LA PLAYA DE SANTA ROSA POR DEFLACION

Un promedio de la constitución química según análisis del mismo químico, fué:

Insoluble en H Cl	77.50%
$Fe_2 O_3$	5.68%
$Al_2 O_3$	2.50%
Ca O	2.36%
M_g O	1.05%
Cl Na	5.30%
	94.40%

CAPITULO IV

TRANSPORTE DE ARENAS POR EL VIENTO

Del transporte de arenas por flúidos en general.- El transporte por el viento no es sino un caso particular del transporte por los flúidos, sobre los cuales la bibliografía es muy nutrita, tanto en la parte teórica como experimental. Con todo el problema es tan complejo, que falta aún mucho por conocer.

Recomendamos por hoy las obras clásicas de Bagnold (9) sobre Neumodinámica y de Rubey (10) Hjulström (11) sobre Hidrodinámica. Ambas dejan ver las complicaciones del movimiento de flúidos en movimiento sobre sólidos fragmentados. "Bourdary Layer" "Bottom Layer" son vocablos aplicados a la zona limítrofe entrambos, en la cual tanto las partículas del flúido como del sólido tienen movimientos complicados como son los laminares y turbulentos en caso de líquidos y de arrastre, rodamiento, saltación y flotación de gases como el aire. Bagnold da énfasis a la saltación, la que a nuestro modo de ver se produce solo cuando hay turbulencia del flúido.

(9) Bagnold. R.A.- The physics of blown sand and desert dunes: 1941. Reprinted 1954.
(10) Rubey, William W.- The force required to move particles on a stream bed. U.S. Geological Survey. Professional Paper 189 - Ed. 1938.
(11) Hjulström o Hjulstroem, Filip; Bull. Geological Institution of University of Upsala. Vol. XXV, pp. 223-525,1934-35.

Hjulström dice: (op. Cit. p. 328)

"The current and other physical conditions prevailing "in the lowest zone of a river, are extremely compli- "cated, and have defied every effort to make a fairly "exact description. They are presumebly very variable.

Y mas adelante (p. 331-332), al tratar del transporte, dice:

"A factor that renders it more difficult to understand "the conditions in the bottomlayer and also the velo- "city distribution as well as the whole transportation "of solid material, is the imperfect knowledge of "transportations mechanics.- The writer has previously "made a difference between the transportation of bed- "load and suspended material, and in Chapter II transi- "tion stage, saltation, has been mentioned. The trans- "portation of the bed-load may, however, be effected "in still more way.
"GILBERT (1914) has further explained these ways in "his admirable book on transportation of debris by "running water. He at first makes a difference between "movement of individual particles and collective move- "ment. In the movement of individual particles "sliding" "is a negligible factor. The roughness of the bed cau- "ses particles that retain contact to roll - Rolling "is the mere prelude to saltation". (op. cit. p. 26). "Saltation or jumping was caused by the hydrodynamic "upthrust, but of course the vertical velocities of "the turbulence are also rather important at least in "the toplayer of the saltation zone where a transi- "tion to suspended matter exists.

" Individual particles in bed-load thus move in one "of the following ways:

1. sliding
2. rolling
3. saltation

" Transportation by rolling may casily be effected "without saltation, especially of mixed debris. On the "other hand saltation would not appear usual otherwise "than in connection with the transition state, rolling.
" There is perhaps more of a graduation difference "than a species diference between the transportation "states mentioned. And also when sliding and rolling "the grans are forced to lose contact with the bed for

"very short distances; these little jumps increa-
"sing in length, we get a transition to saltation".

Se deja pues comprender la falta de conocimiento fundamental sobre las energías puestas en juego para la traslación de cada grano de arena desde sus lugares de reposo.

Krumbein y Pettijohn (12) expresan además:

"One of the fundamental principles on which mecha-
"nical analysis is based, is that small particles
"will settle with a constant velocity in water or
"other fluids. It is universally true that small
"particles reach this constant velocity in a fluid
"medium as soon as the resistance of the fluid
"exactly equals the downward constant force (gravi-
"ty) which acts on the particles. In general the
"settling velocity of the particle depends on its
"radius, its shape, its density, its surface textu-
"re, and the density and viscosity of the fluid. A
"number of mathematical expressions have been deve-
"loped to show the relations among these factors
"some based on empirical grounds and others on theo-
"retical grounds. Several of these laws will be
"discused in varying detail, depending upon their
"applicability in mechanical analysis".

Pero tratándose de la traslación eólica de varias partículas de arena y no de una sola, cabe agregar otro factor no mencionado por los tratadistas, tal es el de incorporación en ellas de líquido que le dá adhesión o coherencia a sus granos. En el caso de las arenas y el agua, este penetra en sus poros y actua como de débil cemento, por lo que es bien visible el diferente comportamiento en masa, cuando húmedas o secas, pues la mayor o menor humedad que las impregna es factor decisivo en disminuir o aumentar su migración. Cuando saturadas, se comportan pues más como conglomerado granular que como sedimento detrítico o sea más como un arenisca que como simple arena suelta (eólica).

La forma como se acomodan los granos de arena al sedimentarse, tiene también influencia aparte de su forma individual. Experiencias realizadas er el laboratorio por mi señor padre, muestran que al dejar caer arena suelta dentro de una probeta, su volumen se reduce en un 10% al sacudirla suavemente

(12) Krumbein E Pettijohn - Mannual of Sedimentary Petrography, p. 95; 1938.

por algunos segundos debido al más estable acomodo de sus granos.

De otro lado, cuando el aire discurre sobre una superficie rugosa como es la de una masa de arena, en el lecho de base se produce una turbulencia microscópica ha sido poco o nada estudiada; pero por lo que se observa en la migración de masas de aire en los desiertos relativamente planos, el mismo incremento de velocidad del viento les dá poder ascencional de sólidos o líquidos sobre los que discurre. En menor escala tal cosa debe ocurrir también cuando el movimiento es aparentemente laminar.

De todo lo dicho, se infiere la complejidad del fenómeno físico de migración de las arenas por dinamismo de los flúidos que discurren sobre ellas, en mayor proporción cuando se trata del aire cuya movilidad molecular es tan grande en relación al agua.

CAPITULO V

MEDIDA DEL TRANSPORTE DE ARENAS POR EL VIENTO

Introducción.- Dada la complejidad del transporte eólico y las grandes dimensiones del ambiente geológico en que tiene lugar en los continentes,la medida integral de la cantidad de arena transportada por el viento es difícil de lograr con exactitud, pues o bien el lecho de fondo en la superficie del suelo se desliza por arrastre y rotación cuando el viento es muy suave, como puede ser llevado saltando y flotando en el aire. En ambos casos extremos escapa a la observación y mensura instrumental en buena proporción.

Sin embargo, como en nuestra costa es visible que nuestros vientos rara vez lleguen a velocidades mayores de 10 m/s. el transporte se hace normalmente flotando o saltando a alturas de no más de pocos centímetros sobre el suelo con simultáneo arrastre y rotación por el suelo. Como aparentemente casi la totalidad tiene lugar por baja saltación y flotación, en nuestro deseo de llegar a conclusiones numéricas de valor, siguiendo las indicaciones de mi Sr. Padre y su técnica para tal fín, acometimos en Santa Rosa la tarea de medir la cantidad de arena extraida por el viento en esa playa de egresión arenosa (13) más como un medio de evidenciar tal fenómeno que

(13) Broggi. J. A.- Op.cit., 1952

de llegar a obtener guarismos precisos de las masas transportadas puesto la escasez de recursos económicos de que dispusimos hizo incompletas nuestras investigaciones.

A lo largo de nuestra Costa, la egresión arenosa eólica de la gran mayoría de playas, es un fenómeno evidente. Extensas áreas arenosas, casi planas, frente al mar como las de Conchán. Playa Grande y Ventanilla en las proximidades de Lima y a un nivel de solo pocos centímetros sobre el de las más altas rompientes (salvo del oleaje de maremotos y muy grandes bravezas) no tienen otra explicación. En esas áreas, se originan lo que mi padre ha designado chiflones arenosos (14) o sea cadenas o cursos alargados de barcanas que por kilómetros ascienden y descienden las bajas estribaciones andinas obedeciendo al dominante viento Sur llamado virazón. Son pues el equiverso de los pótamos, que por gravedad van de arriba hacia abajo; y si bien es difícil estimar numéricamente el transporte integral de sedimentos acuosos por dificultad de conocer a fondo las modalidades de su transporte, cuando más no ha de ser el producido por un flúido tan liviano como el aire, cuyas corrientes llenas de turbulencia varían tanto horizontal como verticalmente a través del tiempo, llevando los sedimentos finos de abajo hacia arriba.

La apreciación geológica integral subjetiva, tan sugerente, llevó a mi Sr. Padre a obtener una apreciación cualitativa del eolismo en las costas desérticas arenosas de nuestro país; pero en esta tésis, usando su técnica e instrumental en Santa Rosa, hemos logrado los resultados cuantitativos que pasamos a exponer.

Arenómetros.- Por varios años y persiguiendo mi Padre la mensura de la cantidad de arena transportada por el viento, diseñó instrumentos sencillos que llamó arenómetros.

El principio físico en que se fundan, es el de provocar la sedimentación o caída por gravedad de los sólidos en suspensión o saltación en el aire, mediante la intercepción de un receptánculo sin escape que obligue al aire a estar en reposo. Esto lo obtuvo mediante vasijas con una sola abertura o boca, en cuyo interior era visible la deposición de la arena eólica en el colchón de aire de su fondo en condiciones de ser pesada. Después de varias experiencias, logró decidirse por los ordinarios tubos de prueba inclinados 45°, los que colocados boca al viento, no solo dejaban entrar la arena flotante sino la que saltaba. La que se arrastraba o rodaba era imposi-

(14) Broggi. J. A.- Op. cit. p. 10

ble medirla; pero es aparente que solo en débil porcentaje escapaba a la mensura pues llegaba a saltar y flotar con la acción continuada del viento.

Aunque en un principio mi padre usó un tubo de prueba, la necesidad de conocer la migración en altitud sobre el suelo con algún detalle, lo llevó al diseño de los arenómetros que denominó de Zócalo (BZ) y de Altitud (BH) que se muestran en el Anexo N° 3. Consistían ambos en una superposición de tubos de prueba en contacto en el BZ y separados a distancia no menor de 10 cm. en el BH. En la práctica se observó que solo cuando el nivel de la arena en el interior de cada tubo pasaba de 1 cm. de la boca, la turbulencia la extraía hacia afuera; de otro modo quedaba inmóvil en su interior.

Como cuando las velocidades del viento que exceden de 5 m/s. es visible la saltación y suspensión de los granos de arena y tal velocidad adquiere el viento cuando discurre más fácilmente sobre las pistas asfaltadas en donde la fricción de las capas del flúido con el piso disminuye, se ven entonces con claridad sobre el fondo negro del asfalto las trayectorias que siguen los granos que flotan y que nunca son líneas rectas horizontales o verticales, sino irregulares y más bien helicoidales con ángulo de tangencia de 5° a 10° solamente con sus ejes o sea hélices muy alargadas y de eje también curvilíneo irregular. Con estas trayectorias los granos de arena entran fácilmente a los tubos de los arenómetros cayento en su fondo. Como la base de todo arenómetro se coloca horizontalmente en la arena del suelo y los tubos orientados a sus rizaduras, se logra recoger en ellos la mayor parte de la arena visiblemente transportada por flotación y también entra la que salta.

Con el fin de que el arenómetro recoja al máximo la arena que salta, se ha procurado que la del suelo cubra su soporte-base hasta un nivel medio tangente inferior a la boca del tubo más bajo del arenómetro, lo que se logra excavando en el suelo arenoso algo ondulado la depresión consiguiente. El Anexo N° 3 exhibe fotos de dicho arenómetro en acción en Santa Rosa.

Como entre tangente y tangente inferior hay un desnivel de una boca de tubo hay un desnivel de 2.12 cm. en el arenómetro BZ (Broggi de Zocalo) el tubo N° 2 queda a esta altura sobre el suelo si el N° 1 es tangente a él.

Con el fin de obtener datos numéricos del transporte en altitud mayor, es que construyó mi padre el arenómetro de 2 m. que llamó BH o de Altitud, con huecos cada 10 cm. para colo-

car en ellos los tubos de prueba inclinados 45º como se ve en fotos del mismo Anexo 3.

Estimaciones.- Después de haber colocado los arenómetros el tiempo adecuado bocas libres al viento, se retiraron cubriendo los tubos con los mismos tapones de jebe provistos de las numeraciones necesarias para reconocerlos al ser pesados sus contenidos arenosos en el laboratorio.

Muy conveniente es conocer la proyección, en plano vertical, de la boca de cada tubo, puesto que consideramos en promedio horizontales las trayectorias de los granos de arena que saltan o flotan en el aire, constituye dicha proyección la superficie efectiva de captación o ingreso al tubo. Fácil es ver, en las ilustraciones del arenómetro BZ, que esta proyección es elíptica con el eje mayor igual al diámetro del tubo y área de 93.83mm^2 o sea de 1 cm^2 en cifras redondas. En el Anexo 6 se exhiben los cálculos sencillos que nos llevan a este resultado.

Mensura del transporte eoloarenoso en general.- Las experiencias con arenómetros BZ, las podemos agrupar en 3 tipos reveladores de las modalidades de la extracción (egresión) y transporte de arena por el viento en la playa de Santa Rosa que son:

1) Experimentos con un solo arenómetro BZ, expuestos en orden de fechas (Anexo 4)

2) Experimentos con 3 y 4 BZ en linea paralela a la rompiente en orden de fechas (Anexo 5)

Estos experimentos se pueden considerar como preliminares pero son los suficientemente precisos para arrojar evidencias indiscutibles que constituyen la escencia de esta tésis.

Los del primer grupo, 8 en total. (Anexo 4), son experimentos individuales: 2 en Enero, 2 en Febrero, 2 en Marzo y 2 en Abril de 1958. Como los Instrumentos destinados a medir el viento regional (X) se trasladaron en Febrero de un costado de la Piscina Grande de la Playa de Santa Rosa, al abra de entrada de la Urbanización, no hay datos de ese mes; pero en

(X) Instrumentos suministrados por la Dirección General de Meteorología correspondientes a estaciones de segunda categoría cuyo manejo dejó bastante que desear como se constata por las fallas de observación de Anexo 2.

los dos días de Enero los experimentos se realizaron cuando el viento regional, considerando ráfagas, era de 6 a 8 m/s (véase Anexo 2: Observaciones Meteorológicas en Santa Rosa). Las mediciones más precisas hechas con anemómetros Fuess a 1.6 m. sobre el suelo al lado de los arenómetros, revelaron que el viento fué más fuerte en el Experimento I que en el II, lo que es visible también en el mayor peso recogido de arena a casi iguales alturas en los tubos 2 y 3 ó 4 y 5 de los arenómetros de ambos experimentos.

En Febrero la mayor cantidad de arena recogida en el Experimento III con relación al IV fué también resultado de la mayor velocidad del viento, pero tambien de la mayor distancia del arenómetro a la línea mojada de playa (30 m. en vez de 10 m.), lo que permitió mayor área seca de extracción de arena por el viento y cuyo ancho podemos asimilarlo al fetch oceanográfico denominándolo fetch eoloarenoso.

De lo realizado en las 4 primeras experiencias individuales con BZ y confirmado por los 4 siguientes, se puede pues colegir:

a) que con vientos regionales fuertes, el acarreo de arena es mayor
b) que cuando es mayor la amplitud de arena seca en la playa o fetch eoloarenoso, es mayor la cantidad de ella extraída por el viento.
c) que cuando es mayor ese fetch eoloarenoso se forman rizaduras (ripple marks) y mayor es tambien el acarreo de arena en altitud.

Determinadas las causas de variación en un punto, nos dedicamos a medirla simultáneamente en otros puntos de la playa, en posición paralela a la rompiente, con los resultados que consignamos a continuación:

Variaciones horizontales del transporte eoloarenoso.- Con la finalidad de conocer las variaciones del transporte en frente horizontal y altura del zócalo eoloarenoso, usamos de observaciones simultáneas hasta con 4 arenómetros BZ, las que forman parte del Anexo Nº 5, que consigna primeramente los resultados del Experimento Nº I con 3 arenómetros expuestos casi simultáneamente durante el mismo lapso a 10 m. de la línea húmeda de playa o sea con + 10 m. de fetch nunca cubierto por el agua del mar durante el período de la experiencia a 30 m. uno de otro. Este experimento se hizo el 26 de febrero de 1958 y como se puede notar en el arenómetro Nº 2 o intermedio, la cantidad de arena recogida fué casi la mitad de las Nº 1 y 3.

Los tubos 7 - 12 no recogieron sino trazas. Esto revela tal vez que la velocidad promedio del viento también era variable en frente horizontal.

Las pequeñas diferencias de tiempo de pocos minutos en los INICIOS Y TERMINOS, se deben a que no hubo ayuda para cubrir y descubrir los tubos de los arenómetros con simultaneidad.

Con el fín de comprobar estas variaciones horizontales, el 28 de Marzo de 1958 colocamos otros tres arenómetros BZ a lo largo de la playa: el N° 1, donde realizamos el Experimento I del Anexo 4 o sea bajando la escalinata de la vereda que conduce a la playa (Anexo 3) inmediatamente a pocos metros al sur; el N° 2 100 m. más al S y el N° 3 a 150 m.más lejos ó sea el extremo meridional de la pequeña caleta de Santa Rosa, los 3 á 20 m. de la línea húmeda de playa. Los resultados se indican en los cuadros respectivos del Anexo N° 5. Como se trata de operaciones simultáneas, quedó demostrada la variabilidad tanto en línea horizontal como vertical del transporte eoaloarenoso en el aerozócalo, pues la observación duró cerca de 6 horas. En dicho anexo consignamos el anemograma obtenido con Anemógrafo Lambrecht en las horas de observación (x).

Otro Experimento realicé el 9 de Abril con 4 arenómetros BZ distantes 30 metros entre ellos y a 15 m. de la línea mojada de alta marea del día (Experimento III, Anexo N° 5). Entre los arenómetros 2 y 3 (siendo el 1 el más próximo a la escalinata de bajada a la playa), se midió la velocidad del viento a 15 cm. sobre el suelo con anemómetros de precisión, obteniéndose:

Hora	Velocidad en m/s
1522	4.0
1524	4.7
1526	3.9
1527	3.9
1528	5.0
1529	5.0
1530	4.7
1532	4.0
1533	4.5
1535	4.0

(x) Estos experimentos fueron realizados por el malogrado Dr. Angel Indacochea G., en el punto P del plano al 20 000 del Anexo N° 1.

1537	----------	4.5
1540	----------	4.2
1736	----------	3.9
1735	----------	6.3
1740	----------	6.6
1740	----------	6.?
	Promedio --	5.75 m/s

Con el Experimento IV, colocando 2 arenómetros a 50 m. uno de otro y a 10 m. de la línea mojada de alta marea, se obtuvieron los guarismos respectivos del Anexo 5. El Arenómetro Nº 2 estuvo colocado a solo 40 m. al S del término de la escalinata ya mencionada y ambos revelaron que al norte de la playa el viento y transporte arenoso era más intenso, lo que se podía comprobar por simple observación visual.

Dos arenómetros BZ fueron nuevamente colocados el 12 de abril en los mismos lugares de la playa, día que tuvo caracteres de insolación semejantes al 10 pero con el viento más fuerte, obteniéndose los dos últimos registros del Anexo Nº 5. Como un solo tubo de prueba y hasta solo 1.3 cm. de la boca se pudo recibir 33 gm. de arena, en los registros respectivos el tubo 1 cuya boca estaba al nivel medio del suelo resultó pues casi lleno de arena.

Medida la inclinación media de la playa Santa Rosa entre la baja y alta marea, resultó ser en promedio de 3º.

Variaciones verticales del transporte eoloarenoso.- Hasta aquí las variaciones del transporte en altitud observables en los registros de los Experimentos (Anexo 4 y 5), no habían pasado del zócalo o sea la altura de los tubos de tal arenómetro (± 25 cm.) pudiéndose solo observar pequeñas anomalías consistentes en inversiones poco saltantes de la gradiente de decrecimiento de los pesos de arena en altitud; pero deseosos de conocer estas más arriba, hicimos uso del arenómetro BH de 2 m. con tubos separados 10 cm. de otro, con la misma inclinación de 45º (Anexo 6). Un BH fué colocado fijo a uno de los postes chicos de la parte más meridional de la antena radial existente en el Minitrack de la Pampa de Ancón y dejado por 33 días, desde el 8 de marzo hasta el 10 de abril de 1958, dió desde el tubo inferior con boca a 5 cm. sobre el suelo, los siguientes pesos de arena depositada en tubos distanciados verticalmente 20 cm. los más bajos y solo 10 cm. los 3 más altos o sea los 10, 11 y 12.

MEDICIONES DE ARENA EOLICA EXTRAIDA DE LA PLAYA DE SANTA ROSA POR DEFLACION

Tubo N°	Peso de arena mg	Altura sobre el suelo de la tangente inferior a la boca del tubo
1	12.0	5.
2	10.0	25.
3	11.0	45.
4	9.	65.
5	8.4	85.
6	9.3	105.
7	8.7	125.
8	5.3	145.
9	4.6	165.
10	4.1	185.
11	3.3	195.
12	3.4	205.
	89.1	

cifras que revelan que la menor densidad arenosa del viento no es también uniforme en altitud pues los pesos de los tubos 3, 6 y 12 son poco mayores que los de sus inmediatos inferiores. De todos modos, estos guarismos expresan que el transporte en altitud sobre el zócalo es muy pequeño dado el largo tiempo de duración del experimento. Como en el caso de los esperimentos con BZ, las anomalías de gradientes de deposición posiblemente se deben a la misma causa o sea mayor densidad de los granos de mineral o a desigual distribución de ellos en el viento, siendo esto lo más probable.

En otro experimento con BH, 50 m. sur de la cresta intersección de la trocha de carros de Santa Rosa a Playa Grande con tubos 20 cm. de diferencia de nivel, se obtuvo del 28 de febrero al 8 de marzo de 1958:

Tubos de abajo hacia arriba N°	BH Meridional Peso de arena mg	Altura sobre el suelo de la tangente inferior a la boca del tubo cm	BH Setentrional o sea con mayor fetch Peso de arena mg
1	167.0	20.	363.
2	106.3	40.	60.9
3	77.6	60.	48.
4	78.4	80.	71.
5	67.	100.	45.5
6	54.6	120.	34.6
7	40.5	140.	26.6
8	45.2	160.	26.2

9	----------	32.3	---------- 180.	--------	23.3
10	----------	29.4	---------- 200.	--------	22.5
		698.3			722.6

Las primeras experiencias con BH, habían sido hechas por mi padre el 11 de febrero de 1958 con tres BH (también llamados palos entubados) y con solo 3 tubos a 10, 20 y 30 cm. de alturas de boca sobre el suelo arenoso de la playa Santa Rosa en tres puntos distantes 25 m. uno de otro y 10 m. de la línea mojada por la rompiente, quien obtuvo de las h. 1720 a las h. 1820 los siguientes pesos:

Altura del tubo sobre el suelo al bajar la escalinata a la playa	BH N° 1 Peso arena	BH N° 2 25 m al S del N° 1 Peso arena	BH N° 3 25 m al S del N° 2 Peso arena
10 cm	132.6 mg	1171. mg	350. mg
20 "	4.	39.	7
30 "	1.	3.8	nada
	137.6	1243.8	357.

Estimación en peso del transporte eoloarenoso.- La irregularidad de las trayectorias de los granos de arena dentro del viento y la turbulencia de éste, son incógnitas que dificultan una estimación precisa del transporte arenoso con los arenómetros. Solo se pueden hacer estimaciones aproximadas a base de posibilidades, como serían las de considerar que en promedio las trayectorias de los granos de arena sean rectas horizontales y la turbulencia sea mínima o sea que el viento sea laminar y horizontal con densidad arenosa proporcionalmente decreciente en altitud. El área efectiva de captación de cada tubo BZ en este caso, sería la normal a las corrientes horizontales o sea la proyección vertical de los círculos inclinados de sus bocas de 1.3 de diámetro interior. El espesor de las paredes de los tubos es de ± 1 mm.

En la Fig. 2 del Anexo 6 se exhiben proyecciones verticales que viene a ser elipses con área de 93.83 mm² o sea de 1 cm² en cifras redondas, considerando los granos que al rebotar en los bordes del tubo caen dentro de él.

Como entre una y otra elipse de las 12 de captación de un BZ, cabe considerar otras 11 de igual área virtual (véase Fig. 2 Anexo 6 y fotos de Anexo 3). puede estimarse la arena

acarreada hacia las virtuales, por interpolación entre los pesos de arena del tubo inmediato inferior y el superior; o sea, por ejemplo, que en el Experimento I del Anexo 5 con el primer arenómetro, en vez de las pesadas registradas en los tubos 1 a 12, se puede constituir el cuadro siguiente que comprende la sucesión vertical contínua de 23 elipses de captación con área de 1 cm^2 cada una: 12 reales y 11 virtuales:

Tubo	Arena Virtual	Cantidad de arena real mg
1	.....	6463.8
	.... 1_V.....	4480.2
2	.....	2496.6
	.... 2_V	1989.1
3	.....	481.5
	.... 3_V	361.3
4	.....	241.0
	.... 4_V	160.5
5	.....	80.0
	.... 5_V	51.8
6	.....	23.6
	.... 6_V	16.6
7	.....	9.6
	.... 7_V	6.6
8	.....	3.5
	.... 8_V	2.3
9	.....	1.0
	.... 9_V	0.7
10	.....	0.4
	....10_V	0.4
11	.....	0.4
	....11_V	trazas
12	.....	trazas
		16870.9 mg

o sea que la columna contínua vertical de elipses reales y virtuales de bocas a 45°, habría captado 16 870.9 mg en vez de los 9 801.4 mg pesados realmente pesados.

En un estudio inédito de mi padre, sobre Agrupamientos Equicirculares, se demuestra que el poro máximo de un espacio intercircular de un tetracírculo equicircular o tetraequicírculo, es igual en área a un solo equicírculo; y como se puede probar que igual cosa ocurre con las elipses, a cada columna BZ de 12 tubos de prueba le corresponde 12 medias elipses de captación a cada lado por concepto de espacio poral entre columna y columna tangente, con lo que el área restangular circunscrita a las elipses sería el doble de la calculada por

los pesos reales y virtuales. Esto se podría expresar llamando A_r al área elíptica de captación real y A_v la virtual, por la fórmula:

$$A_c = 2 \ (A_r + A_v)$$

Para los efectos de una estimación más precisa, hemos calculado que el diámetro medio interior de cada tubo de prueba es de 13 mm. y el exterior de 15 mm. y como los granos que inciden sobre la pared redondeada de la boca de cada tubo rebotan en promedio con ángulo de reflexión igual al de la incidencia hacia el interior o exterior de cada tubo, se puede considerar solo 1 mm. como espesor efectivo adicional al área elíptica de captación o sea que tal columna rectangular de captación tendría 15 mm. de ancho horizontal y que en cada metro horizontal habría:

$\frac{1000 \text{ mm}}{15 \text{ mm}}$ = 66.66 columnas de captación contínua de 9.19 mm x 12 x 12 = 220.56 mm de altura más 24 mm por espesor del vidrio desde el nivel de la tangente inferior a la boca del tubo más bajo hasta el de la superior al tubo más alto o sea lo que prácticamente es la altura del Zócalo Eoloarenoso o sea 250 mm.

La estimación a base del promedio de las tres mediciones del Anexo 5 Experimento I, nos daría así el peso de 37 835.4 mg por hora de viento normal en las condiciones especificadas en los cuadros respectivos, que duplicándolo arrojaría 75 670 mg ó sea la media de 25 225 mg por columna y por centímetro y medio de frente perpendicular al viento, que daría 252'250.000 mg de arena por cada 150 m. de playa en una hora con una superficie seca anterior o fetch eoloarenoso seco de 10 m. o sea 253 ks. o en cifras redondas 1/4 de tonelada métrica. Esto equivale a 168 148 850 mg. por 100 m. de playa o sea casi 170 ks. en una hora.

Con el fin de saber los límites de los cuales varía el transporte arenoso de acuerdo con las mediciones efectuadas por los arenómetros BZ desde el nivel del suelo hasta $\pm$ 0.25 m. que es lo que se considera el zócalo para lo cual nos valemos de unidades de extracción arenosa o sea extracción por unidad de tiempo, encontramos que el máximo registrado corresponde al Experimento VIII del Anexo 4 o sea Experiencia con un solo arenómetro. El mínimo se halló en el V del mismo Anexo 4. En el primero se observó, el 17 de Abril, 39 180 mg. en 30 minutos con solo 6 tubos (1 al 6) o sea en medio zócalo y el 5 de marzo solo 1.7 mg en 362 minutos.

MEDICIONES DE ARENA EOLICA EXTRAIDA DE LA PLAYA DE SANTA ROSA POR DEFLACION

Formulando las columnas y los cálculos respectivos, obtenemos para estos dos casos extremos un transporte de 7 gramos por hora por cada 100 m. de playa con velocidad de viento de 3 m/s a la altura de BZ por un máximo de 1746 ks. con viento en ráfagas que exedieron de 20 m/s y promedio de 8.5 m/s. Este viento fuerte del SW se inició antes de las 10 a.m. y duró hasta las 4 p.m. en que continuó fuerte pero con menos intensidad.

En esta misma tarde se colocó un BH sobre la duna de sombra del Morro de Santa Rosa en la parte más alta o cresta, desde h.1230 hasta h.1800 registrándose en tubos a desnivel de 10 cm. entre si.

TUBO Nº	ARENA mg
1	442
2	137
3	69
4	43
5	32
6	26
7	21
8	18
9	16
10	14
11	12.4
12	12
13	10.5
14	9.1
15	8.7
16	8.1
17	6.9
18	6.
19	5.2

NOTA.- El tubo nº 1 estubo a 5 cm. sobre el suelo de la cresta de la duna de sombra del Morro Santa Rosa.

CONCLUSIONES

1.- Una playa arenosa en clima árido seco, con viento predominante de mar a tierra (S.SSW) de velocidad no menor a los 5 m/s caracterizado por ráfagas (golpes de viento), que incida sobre una franja de playa de arena de superficie suficientemente desecada, proporciona las condiciones principales que favorecen al transporte eoloarenoso. Determinando así un proceso geomorfológico típico de las áreas arenosas, en donde la deflación por el viento en

la playa arenosa y la deposición sobre ella de arena acarreada por el mar, pasa desapercibido en un medio ambiente donde la litósfera, la hidrósfera y la atmósfera juegan cada una de ellas un rol importante en la realización de este fenómeno eólico clásico.

2.- Las playas tendidas de más o menos 3º de inclinación,ofreciendo mayor área de exposición al viento y de deposición de arenas aportadas por corrientes de fondo (submarinas), son las de más fuerte y voluminosa extracción eólica,siempre y cuando se cumplan las condiciones expuestas en el acápite Nº 1 y se sumen: una favorable amplitud de mareas y oleajes,baja humedad atmosférica, e insolación;elavorando así, los factores imprescindibles para la deflación playera

3.- El mayor porcentaje de arena acarreada por el viento por deflación tiene lugar a muy baja altura, siendo mayormente por arrastre, rotación y saltación,en el aerozócalo(25cm).

BIBLIOGRAFIA

AMSTUTZ.g.c. Raimundo Chico.Sand size fraction of South Peruvian barchans and a brief review of the genetic grain shape funtion.Separata of Bull.Ver Schweizer Petrol.Geol.u ing. Vol 24 February 1958.

BROGGI.J.A.Migración de arenas a lo largo de la Costa Peruana. Bol.Soc.Geol.del Perú.T. XXIV (Vol.Unico).1952.

HJLSTRON o HJULSTROEM.FILIP.Bull. Geological Institution of University of Upsala,Vol.XXV.

KRUMBEIN.W.X. and Pettijohn. Manual of Sedimentary Petrography.

KNOWLES MIDDLETON.W.E., and Spilhaus F.,Athelstan. Meteorological Instruments, 3rd. id revised University of Toronto Press p.136. 1953.

LAHEE F.H.Field Geology.p. 34,Ed. 1941

MINISTERIO DE MARINA República Peruana.Tablas de mareas.Servicio Hidrológico 1958 y 1959

RUBEY,William W. The force required to move particles on a stream bed.U.S. Geological Survey,Professional Paper, 189-Ed.1938.

WEBERBAUER,A. El Mundo Vegetal de los Andes Peruanos p.776, 1945.

MEDICIONES DE ARENA EOLICA EXTRAIDA DE LA PLAYA DE SANTA ROSA POR DEFLACION

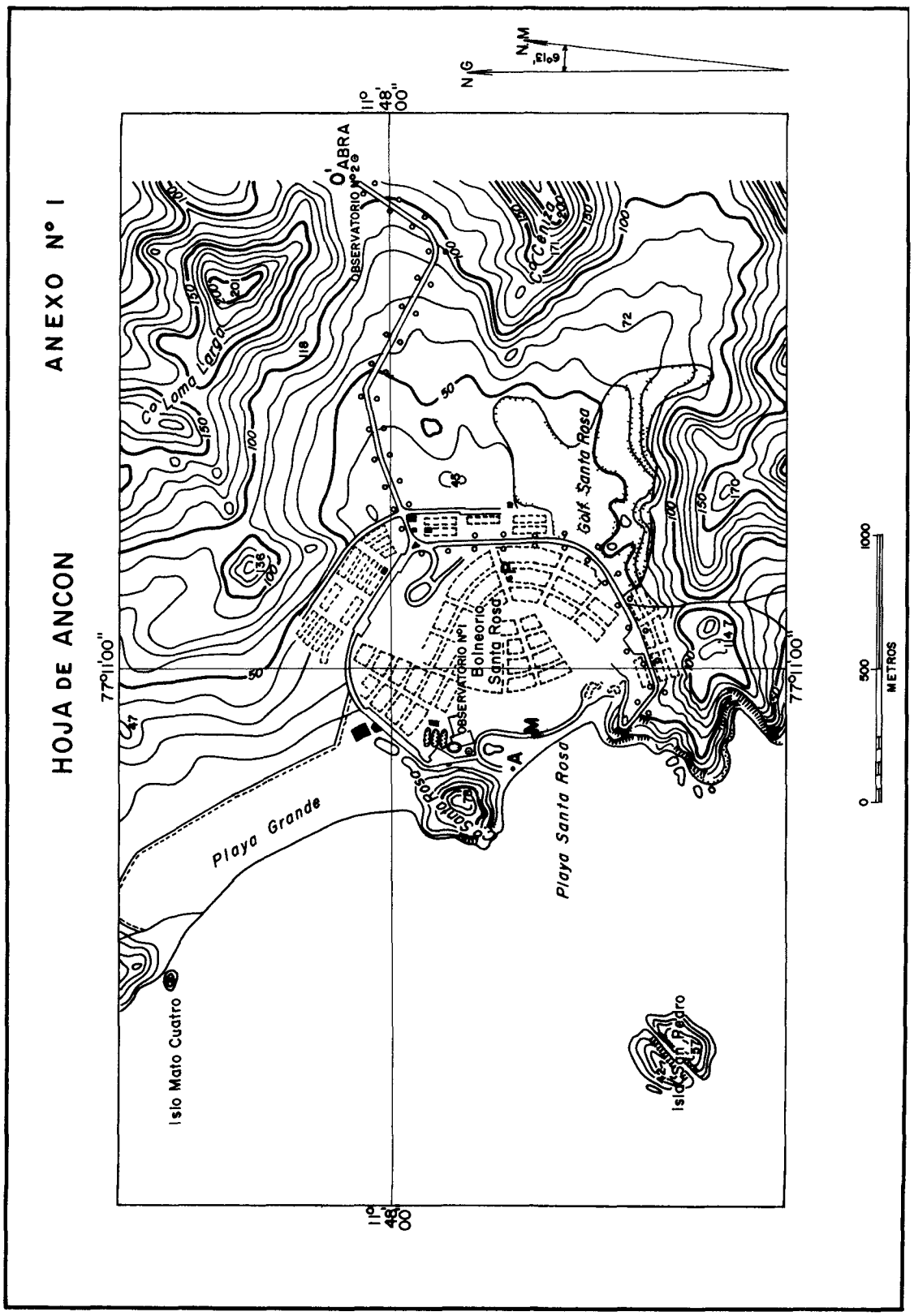

ANEXO. NO. 2

OBSERVACIONES METEOROLOGICAS EN LA URBANIZACION SANTA ROSA

(Observatorio No. 1)

Observatorio No. 1 — **Julio 1957**

Día	°C TEMPERATURA			% HUMEDAD RELATIVA			m/seg VELOCIDAD DEL VIENTO		
	Horas día			Horas día			Horas día		
	7	13	18	7	13	18	7	13	18
7	20	21	22	70	60	65	0	6	8
8	19	21	22	59	60	63	2	4	6
9	19	20	22	60	60	60	2	6	8
10	19	20	21	68	63	60	2	6	8
11	18	20	21	77	70	75	2	4	6
12	18	20	21	73	70	73	2	4	8
13	19	20	21	75	70	72	2	4	4
14	-	-	-	-	-	-	-	-	-
15	-	-	-	-	-	-	-	-	-
16	18	20	21	71	70	72	0	2	4
17	19	20	21	71	68	72	0	0	2
18	19	20	21	76	75	73	0	2	4
19	18	19	20	85	83	85	2	4	6
20	19	19	20	90	85	85	0	4	4
21	21	20	21	85	80	83	2	4	6
22	20	20	21	73	65	70	2	4	6
23	-	-	-	-	-	-	-	-	-
24	19	20	21	72	65	70	2	4	4
25	19	21	20	73	68	71	2	2	2
26	19	19	20	75	65	70	2	6	10
27	19	18	20	72	65	70	2	8	10
28	19	18	21	75	68	70	2	6	10
29	19	18	20	75	68	71	2	8	14
30	19	18	21	73	65	70	2	2	4
31	19	18	20	73	71	71	4	6	14
Medias del	13	14	15	52	49	50	2	4	7
Máxima	21	21	22	90	85	85	4	8	14
Mínima	18	18	20	59	60	60	0	0	2

Observatorio No. 1 — **Agosto 1957**

Día	°C TEMPERATURA			% HUMEDAD RELATIVA			m/seg VELOCIDAD DEL VIENTO		
	Horas día			Horas día			Horas día		
	7	13	18	7	13	18	7	13	18
1	20	19	21	80	78	75	2	4	6
2	21	19	20	78	75	73	0	4	4
3	20	19	20	78	80	83	0	4	6
4	20	18	19	80	80	85	0	4	4
5	20	19	20	75	78	80	0	0	4
6	20	19	20	78	70	75	0	8	14
7	18	19	19	80	78	78	2	8	10
8	19	17	18	83	75	80	0	2	2
9	19	17	18	85	78	80	2	4	8
10	16	17	18	80	78	80	0	4	8
11	19	19	21	76	80	79	2	2	2
12	22	19	21	75	80	79	2	4	8
13	19	18	20	80	78	79	0	2	4
14	18	19	21	80	78	79	0	4	8
15	17	19	18	80	70	75	0	4	6
16	18	19	18	80	70	75	0	4	4
17	18	19	18	80	70	75	0	8	6
18	20	21	21	76	73	80	0	4	2
19	19	20	21	80	73	75	0	4	6
20	19	20	21	80	73	75	0	4	4
21	19	20	19	80	67	68	2	0	0
22	19	20	19	75	65	70	2	0	0
23	19	20	19	80	75	80	4	0	0
24	19	20	19	91	75	78	0	0	0
25	22	21	21	69	83	76	2	6	4
26	20	19	20	90	94	95	0	6	6
27	19	19	20	85	80	75	0	4	0
28	19	18	19	75	70	73	0	6	8
29	19	18	19	83	75	78	0	4	4
30	17	19	18	96	83	85	0	4	4
31	19	-	-	85	-	-	0	-	-
Medias del	19	19	20	80	76	78	1	4	5
Máxima	22	21	21	96	94	95	4	8	14
Mínima	16	17	18	69	65	68	0	0	0

Observatorio No. 1 — **Setiembre 1957**

Día	°C TEMPERATURA			% HUMEDAD RELATIVA			m/seg VELOCIDAD DEL VIENTO		
	Horas día			Horas día			Horas día		
	7	13	18	7	13	18	7	13	18
1	19	20	19	81	76	78	4	6	8
2	20	19	19	90	80	83	2	4	4
3	18	19	19	80	73	80	2	4	4
4	16	19	18	80	73	75	2	4	6
5	16	18	19	80	73	75	4	6	4
6	17	18	19	80	80	83	4	6	6
7	16	17	19	85	80	83	4	4	6
8	17	18	17	85	73	72	0	0	4
9	18	19	18	85	75	78	0	2	4
10	18	19	18	85	73	76	0	2	4
11	18	19	18	85	75	78	2	6	4
12	19	19	18	85	80	85	2	4	4
13	18	19	19	85	75	80	2	4	6
14	19	18	19	85	73	80	2	4	4
15	19	17	19	85	80	83	2	4	4
16	17	19	19	85	75	83	2	4	4
17	19	18	19	73	70	75	0	4	4
18	19	18	20	75	70	75	0	4	6
19	17	19	19	75	70	78	2	4	4
20	16	18	17	80	73	80	2	4	4
21	17	19	18	80	75	80	0	2	4
22	17	19	18	85	75	78	2	2	2
23	18	19	18	85	78	80	0	0	0
24	19	18	19	80	78	80	2	2	0
25	16	18	19	85	70	80	2	4	4
26	17	18	19	85	73	78	2	4	4
27	17	18	19	80	73	78	0	4	6
28	17	18	19	83	73	78	0	6	8
29	18	19	19	85	78	80	0	6	8
30	17	19	19	83	72	80	4	6	8
Medias del	18	19	19	83	73	79	2	4	5
Máxima	20	20	20	90	80	85	4	6	8
Mínima	16	17	17	75	70	72	0	0	0

Observatorio No. 1 — **Octubre 1957**

Día	°C TEMPERATURA			% HUMEDAD RELATIVA			m/seg VELOCIDAD DEL VIENTO		
	Horas día			Horas día			Horas día		
	7	13	18	7	13	18	7	13	18
1	16	18	17	83	72	78	0	2	4
2	16	18	17	80	70	73	0	6	8
3	16	19	17	80	75	78	4	4	2
4	17	18	17	83	70	73	2	4	6
5	17	18	17	85	70	73	0	4	4
6	18	19	17	75	70	78	0	4	6
7	17	18	17	83	81	83	2	4	6
8	18	18	17	83	80	81	0	4	6
9	18	18	17	81	80	81	0	4	6
10	18	19	17	80	73	80	0	4	4
11	18	17	18	83	75	80	0	4	6
12	18	17	19	85	75	78	0	4	4
13	19	18	18	75	70	74	0	2	4
14	19	18	19	78	70	75	0	2	4
15	19	21	20	78	75	76	0	2	6
16	20	19	19	80	75	80	0	2	4
17	21	19	19	85	80	93	0	4	2
18	20	18	19	83	75	80	0	8	10
19	20	19	19	85	75	80	0	4	6
20	20	19	20	75	70	70	2	0	2
21	21	19	20	78	70	75	0	2	2
22	21	19	20	75	70	73	2	4	6
23	20	19	21	75	70	75	2	4	6
24	21	19	20	80	75	78	2	4	6
25	20	19	21	75	70	72	2	4	8
26	21	19	20	78	70	73	0	2	4
27	21	19	20	78	65	70	4	6	4
28	20	19	21	78	68	75	2	6	8
29	21	18	20	78	65	80	0	4	6
30	20	19	21	80	65	75	4	4	6
31	20	19	21	80	65	75	4	0	4
Medias del	19	19	19	80	72	77	2	4	5
Máxima	21	21	21	85	81	81	4	6	10
Mínima	16	17	17	75	68	70	0	0	2

MEDICIONES DE ARENA EOLICA EXTRAIDA DE LA PLAYA DE SANTA ROSA POR DEFLACION

ANEXO NO. 2

Observatorio No. 1 — **Noviembre 1957**

Día	Cº TEMPERATURA Horas día 7	13	18	% HUMEDAD RELATIVA Horas día 7	13	18	m/seg VELOCIDAD DEL VIENTO Horas día 7	13	18
1	21	19	19	85	68	78	-	2	4
2	20	19	21	83	63	78	-	2	4
3	21	18	20	85	65	75	-	4	6
4	21	19	20	83	73	75	-	5	4
5	21	19	21	85	75	80	-	-	4
6	20	18	20	83	78	80	-	4	6
7	21	19	20	80	75	80	-	4	6
8	21	14	19	85	70	83	-	6	8
9	21	16	19	83	75	83	-	4	6
10	21	19	20	80	75	78	-	-	4
11	21	19	21	85	78	80	-	4	6
12	20	19	21	80	75	80	2	6	8
13	20	19	21	80	75	83	-	4	6
14	19	17	21	83	63	70	2	6	8
15	19	18	19	83	73	80	-	4	6
16	20	19	21	80	75	70	2	4	6
17	22	20	21	65	63	65	8	10	10
18	21	19	20	70	65	70	6	8	10
19	20	19	21	75	63	70	6	10	4
20	19	14	19	83	70	83	2	6	10
21	19	14	19	83	73	65	-	6	8
22	18	14	19	82	65	80	2	4	8
23	19	15	19	80	63	80	0	6	6
24	19	15	20	82	65	80	2	4	4
25	19	14	19	82	65	80	4	6	4
26	19	15	19	83	64	85	4	8	10
27	19	14	18	85	65	84	4	6	8
28	19	15	19	83	65	80	4	6	8
29	19	14	19	83	67	83	4	6	10
30	19	15	18	83	63	85	2	4	6
31	-	-	-	-	-	-	-	-	-
Medias del mes	20	17	20	81	69	78	3	5	7
Máxima	22	20	21	85	78	85	8	10	10
Mínima	18	14	18	65	63	65	0	2	4

Observatorio No. 1 — **Diciembre 1957**

Día	Cº TEMPERATURA Horas día 7	13	18	% HUMEDAD RELATIVA Horas día 7	13	18	m/seg VELOCIDAD DEL VIENTO Horas día 7	13	18
1	23	19	14	80	75	78	2	4	4
2	20	15	19	75	67	78	2	4	6
3	23	14	19	76	70	75	0	0	2
4	23	14	20	60	56	60	0	2	4
5	24	17	21	60	56	65	0	4	4
6	21	18	20	65	56	60	0	4	2
7	22	19	20	65	62	65	0	4	8
8	22	22	21	65	62	63	4	6	8
9	22	16	22	65	62	64	4	8	8
10	21	15	19	70	62	65	0	4	6
11	22	15	19	67	64	67	0	4	8
12	22	15	21	68	63	65	2	4	8
13	22	15	18	75	65	65	0	2	6
14	22	15	19	75	65	70	2	4	6
15	20	15	19	80	65	75	4	6	8
16	21	16	19	80	67	75	0	0	2
17	20	15	19	80	67	75	0	0	2
18	20	14	19	83	70	76	4	6	8
19	20	15	19	80	70	80	2	2	6
20	20	18	19	80	70	80	2	2	6
21	20	17	19	83	73	80	2	4	6
22	20	19	20	80	62	70	4	6	0
23	20	19	20	83	73	70	4	6	8
24	22	17	19	83	73	76	4	6	6
25	25	22	23	81	73	78	4	6	8
26	28	25	28	83	73	80	1	6	8
27	28	25	28	81	73	80	4	6	8
28	27	21	27	80	70	80	0	4	6
29	27	21	27	83	73	80	2	4	4
30	28	21	27	80	70	80	4	6	8
31	27	19	21	80	70	80	0	0	4
Medias del mes	23	18	21	75	67	73	2	4	6
Máxima	28	25	28	83	75	80	4	6	8
Mínima	20	14	14	60	56	60	0	0	0

ANEXO NO. 2

OBSERVACIONES METEOROLOGICAS EN LA URBANIZACION SANTA ROSA
(Observatorio No. 2)

Observatorio No. 2 — **Enero 1958**

DIA	C° TEMPERATURA Horas día 7	13	18	% HUMEDAD RELATIVA Horas día 7	13	18	m/seg VELOCIDAD DEL VIENTO Horas día 7	13	18	HORAS DE SOL
1	30	28	30	80	65	55	4	4	4	-
2	30	27	30	80	65	75	0	4	4	-
3	30	25	30	80	70	80	2	4	6	8
4	30	26	28	80	70	80	-	-	-	7
5	28	22	26	80	60	80	4	6	8	11
6	28	22	26	80	60	80	4	6	8	10
7	29	26	28	80	60	75	2	4	6	10
8	28	22	28	80	60	75	4	6	8	11
9	30	22	28	80	60	75	-	4	6	11
10	30	22	28	80	55	75	4	6	8	11
11	27	25	28	65	55	70	2	6	8	12
12	30	30	28	75	55	60	0	0	2	10
13	28	30	28	75	68	70	0	4	8	11
14	28	30	28	85	65	70	0	4	8	12
15	28	30	28	85	65	70	2	4	8	10
16	27	28	28	80	65	70	0	4	8	5
17	26	28	29	80	65	75	0	4	6	10
18	24	28	28	80	65	75	0	4	8	8
19	26	28	26	90	65	70	2	6	8	12
20	26	28	26	90	65	70	2	6	8	10
21	26	30	26	85	60	70	2	4	6	10
22	26	28	27	85	60	65	2	4	8	10
23	26	27	27	85	65	70	0	4	6	10
24	25	28	27	85	70	75	2	4	6	12
25	25	28	27	85	70	75	0	4	8	12
26	26	29	27	85	60	75	-	-	-	12
27	26	28	26	80	65	75	4	6	8	10
28	25	28	26	85	60	75	2	2	4	12
29	26	28	27	80	60	70	4	4	6	12
30	26	29	27	80	65	75	4	6	8	10
31	25	28	26	85	60	70	4	6	6	12
Medias del me	28	27	28	82	63	73	2	5	7	10
Máxima	30	30	30	90	70	80	4	6	8	12
Mínima	24	22	26	65	55	55	0	0	2	5

Observatorio No. 2 — **Febrero 1958 (**

DIA	C° TEMPERATURA Horas día 7	13	18	% HUMEDAD RELATIVA Horas día 7	13	18	m/seg VELOCIDAD DEL VIENTO Horas día 7	13	18	HORAS DE SOL
1	29	30	27	80	60	65		-		10
2	27	29	27	85	55	65		-		12
3	27	28	27	80	60	65		-		12
4	28	29	27	85	65	60		-		10
5	28	28	29	80	60	65		-		10
6	28	29	27	80	60	65		-		10
7	28	29	27	80	65	63		-		10
8	29	25		80	65					10
9	29	26		80	65					10
10	30	25		80	60					9
11	29	26		80	65					10
12	29	26		85	60					10
13	29	26		85	65					10
14	29	26		80	60					10
15	30	26		85	60					9
16	29	27		80	65					8
17	29	26		80	60					9
18	29	26		80	60					10
19	30	26		80	55					10
20	29	25		80	55					10
21	29	26		85	60					9
22	29	26		85	60					10
23	28	25		85	65					10
24	29	25		85	60					10
25	29	27		85	60					10
26	29	27		85	60					10
27	28	26		80	55					10
28	29	27		80	55					10
Medias del me	29	27	27	82	60	63				9
Máxima	30	30	28	85	65	65				12
Mínima	27	25	27	80	55	60				8

(x) En este mes se trasladaron los instrumentos al sitio, (Observatorio No. siendo de este sitio los datos consignados aquí.

Observatorio No. 2 — **Marzo 1958**

DIA	C° TEMPERATURA Horas día 7	13	18	% HUMEDAD RELATIVA Horas día 7	13	18	m/seg VELOCIDAD DEL VIENTO Horas día 7	13	18	HORAS DE SOL
1	27	29	28	80	75	78	4	4	6	10
2	25	28	26	83	73	78	-	2	4	10
3	26	29	27	80	75	73	-	-	2	9
4	27	30	27	80	75	73	4	6	8	9
5	27	29	26	80	75	76	2	6	8	10
6	26	29	28	78	70	78	4	8	10	8
7	23	28	26	78	73	75	-	-	-	9
8	24	28	27	85	70	80	2	6	8	8
9	23	27	26	83	75	78	2	2	4	9
10	23	29	25	85	73	80	-	-	-	7
11	22	28	27	84	73	78	-	4	4	9
12	23	28	27	85	70	73	-	-	4	8
13	24	27	26	83	70	73	-	-	-	-
14	23	28	25	80	70	73	-	-	-	-
15	24	27	26	83	71	73	2	2	2	-
16	23	28	26	85	73	74	4	2	6	8
17	24	28	26	85	70	73	-	4	6	9
18	24	28	26	83	70	73	-	4	6	9
19	23	28	26	80	70	73	-	-	-	9
20	24	29	25	80	70	71	4	6	6	9
21	24	29	25	78	60	70	2	4	6	9
22	20	28	23	78	60	70	-	4	8	10
23	21	27	24	78	63	65	2	4	6	10
24	23	28	25	80	58	60	-	4	4	10
25	21	28	25	80	58	65	-	4	4	10
26	21	27	24	80	60	65	2	4	4	10
27	20	27	24	85	65	68	-	-	2	10
28	20	26	24	85	58	69	-	4	6	10
29	21	26	24	83	68	69	-	4	6	10
30	21	26	24	80	70	68	-	4	6	10
31	21	25	24	80	75	69	4	4	6	10
Medias del mes	24	28	26	84	70	73	3	4	6	8
Máxima	27	30	28	85	75	80	4	8	10	10
Mínima	20	25	23	78	60	60	2	2	2	7

Observatorio No. 2 — **Abril 1958**

DIA	C° TEMPERATURA Horas día 7	13	18	% HUMEDAD RELATIVA Horas día 7	13	18	m/seg VELOCIDAD DEL VIENTO Horas día 7	13	18	HORAS DE SOL
1	23	26	24	80	70	74	-	-	-	10
2	23	27	24	80	60	63	2	4	6	10
3	21	27	23	80	63	65	2	4	4	10
4	21	27	23	80	63	65	2	4	6	10
5	21	26	23	83	60	65	-	4	8	10
6	21	27	24	83	60	60	4	8	10	10
7	23	27	24	80	61	57	4	8	10	10
8	23	27	23	80	61	57	4	8	10	10
9	23	27	24	80	65	60	2	4	8	9
10										
11	24	26	23	83	68	65	2	4	4	9
12	23	28	24	85	65	63	2	6	8	8
13	24	26	24	83	63	60	4	6	10	9
14	24	27	24	83	65	60	4	6	6	9
15	23	27	23	80	65	60	4	6	6	8
16	23	26	24	80	65	63	2	4	6	9
17	23	26	24	83	68	63	2	4	8	9
18	23	27	24	80	65	62	2	6	10	9
19	23	26	24	81	65	62	4	6	8	9
20	23	26	24	81	60	62	4	4	6	8
21	22	26	23	80	63	62	2	4	8	8
22	22	26	23	80	63	61	-	4	8	8
23	22	27	23	83	64	60	2	-	-	8
24	23	27	22	85	65	61	2	-	4	8
25	21	27	22	85	65	70	-	-	-	8
26	23	26	23	85	60	71	-	-	-	8
27	23	27	22	83	63	70	2	4	6	8
28	23	26	23	83	63	70	2	4	6	8
29	22	27	22	85	65	71	2	2	4	8
30	23	26	22	83	63	70	2	4	8	6
Medias del mes	22	26	23	79	61	62	3	5	7	9
Máxima	24	28	24	85	70	74	4	8	10	10
Mínima	21	26	22	80	60	57	2	2	4	6

MEDICIONES DE ARENA EOLICA EXTRAIDA DE LA PLAYA DE SANTA ROSA POR DEFLACION

ANEXO NO. 2

Observatorio No. 2 — **Mayo 1958**

DIA	cº TEMPERATURA Horas día 7	13	18	% HUMEDAD RELATIVA Horas día 7	13	18	m/seg VELOCIDAD DEL VIENTO Horas día 7	13	18	HORAS DE SOL
1	20	26	23	85	65	80	–	2	4	10
2	20	26	22	85	65	80	–	2	4	8
3	20	26	22	85	65	80	–	4	6	6
4	19	25	21	85	80	80	–	4	6	5
5	19	25	21	88	60	80	–	4	4	5
6	19	23	21	87	60	80	–	2	4	–
7	19	24	21	85	63	70	–	4	6	10
8	19	25	21	80	60	70	–	4	4	10
9	18	23	19	82	63	90	2	4	4	10
10	18	23	19	85	65	85	–	4	6	8
11	19	23	19	85	65	84	2	2	4	6
12	18	20	21	92	80	72	–	4	2	6
13	18	20	21	90	80	75	–	4	6	6
14	18	20	21	87	80	75	–	–	–	2
15	18	21	20	85	65	75	–	2	4	4
16	17	20	21	90	67	75	2	2	4	6
17	18	21	20	90	70	80	–	–	–	8
18	17	21	20	90	70	80	–	–	–	4
19	17	21	20	92	70	80	–	–	–	4
20	17	21	20	90	70	80	–	–	–	6
21	18	21	20	90	70	80	–	–	–	4
22	17	21	18	90	70	88	–	–	–	–
23	17	21	18	90	70	85	–	–	–	–
24	17	20	19	90	72	80	–	–	–	–
25	17	20	19	91	70	80	2	–	–	–
26	17	20	19	90	70	82	–	–	–	–
27	18	20	19	90	70	82	–	–	–	4
28	17	21	19	85	70	82	–	–	–	4
29	17	21	19	83	70	82	–	–	–	6
30	17	21	19	83	70	82	–	–	–	8
31	17	20	18	85	73	80	–	–	–	8
Medias del mes	18	22	20	88	69	80	2	3	5	5
Máxima	20	26	23	92	80	90	2	4	6	10
Mínima	17	20	18	80	60	70	–	2	2	2

Observatorio No. 2 — **Junio 1958**

DIA	cº TEMPERATURA Horas día 7	13	18	% HUMEDAD RELATIVA Horas día 7	13	18	m/seg VELOCIDAD DEL VIENTO Horas día 7	13	18	HORAS DE SOL
1	16	19	17	90	70	80	–	–	–	6
2	16	19	18	90	70	85	–	–	–	5
3	16	19	18	91	70	85	–	–	–	4
4	17	19	18	90	72	80	–	–	–	4
5	16	18	17	90	75	80	–	–	–	5
6	16	19	18	90	71	85	–	–	–	–
7	16	19	18	91	72	82	–	–	–	6
8	17	19	18	90	70	80	2	–	–	–
9	16	19	18	91	71	82	–	–	–	–
10	17	19	18	90	71	80	–	–	–	6
11	16	19	18	90	71	80	–	–	–	–
12	16	19	17	91	70	81	–	–	–	6
13	16	18	17	91	70	80	–	–	–	6
14	16	19	17	91	70	80	–	–	–	5
15	16	19	17	90	70	80	–	–	–	4
16	16	19	16	90	70	80	2	2	–	–
17	17	18	16	90	70	82	–	–	–	–
18	16	18	17	91	71	81	–	–	–	6
19	16	18	17	92	74	83	–	–	–	–
20	16	18	17	90	71	80	–	–	–	6
21	16	18	17	90	72	80	–	–	–	–
22	16	18	17	89	70	78	–	–	–	–
23	16	18	17	85	70	78	–	–	–	–
24	16	22	19	80	55	70	–	–	–	–
25	18	22	19	80	55	70	–	–	–	–
26	17	21	18	80	58	70	4	4	6	–
27	16	21	18	80	55	70	2	–	–	–
28	17	21	18	80	55	70	–	–	–	–
29	17	21	18	80	55	70	–	–	–	4
30	16	21	17	80	55	70	–	–	–	–
Medias del mes	17	16	17	85	65	76	3	3	6	3
Máxima	18	22	19	92	75	85	4	4	6	6
Mínima	16	18	16	80	55	70	2	2	6	4

Observatorio No. 2 — **Julio 1958**

DIA	cº TEMPERATURA Horas día 7	13	18	% HUMEDAD RELATIVA Horas día 7	13	18	m/seg VELOCIDAD DEL VIENTO Horas día 7	13	18	HORAS DE SOL
1	17	19	17	80	60	80	–	–	–	5
2	16	19	17	82	60	80	–	2	4	5
3	16	19	17	80	55	80	2	4	6	3
4	17	19	17	80	55	80	2	–	–	3
5	16	19	17	80	58	80	–	2	4	5
6	16	19	17	80	55	80	2	4	6	5
7	16	19	17	80	55	80	–	4	4	5
8	17	19	17	80	58	80	–	4	4	5
9	17	19	17	80	55	80	–	4	4	5
10	17	19	17	80	55	80	–	2	4	5
11	16	18	17	80	60	80	2	2	4	5
12	17	18	17	80	60	80	6	2	4	6
13	17	18	17	80	60	80	2	2	2	–
14	16	18	17	80	60	80	–	2	4	–
15	16	18	17	80	55	80	–	2	2	4
16	16	18	17	80	55	80	–	4	6	6
17	16	18	17	80	55	80	2	4	4	5
18	16	18	17	80	55	80	–	4	8	5
19	17	18	17	80	55	80	–	–	–	–
20	17	18	17	79	58	80	–	–	2	4
21	17	18	17	78	55	80	–	–	–	–
22	16	18	17	80	60	80	–	–	2	3
23	16	18	16	80	60	85	–	–	2	–
24	16	18	16	83	60	85	–	–	–	–
25	16	18	16	83	60	85	–	–	–	–
26	16	18	16	84	60	80	–	2	–	–
27	17	18	16	83	55	80	–	4	4	4
28	17	18	16	80	57	80	–	4	4	2
29	16	18	16	83	57	80	–	4	4	–
30	16	18	16	85	60	80	–	4	4	–
31	16	18	16	85	57	80	2	2	6	–
Medias del mes	23	19	17	80	58	80	3	3	4	3
Máxima	17	19	17	85	60	85	6	4	8	6
Mínima	16	18	16	78	55	80	2	2	2	2

Observatorio No. 2 — **Agosto 1958**

DIA	cº TEMPERATURA Horas día 7	13	18	% HUMEDAD RELATIVA Horas día 7	13	18	m/seg VELOCIDAD DEL VIENTO Horas día 7	13	18	HORAS DE SOL
1	16	18	17	83	55	80	–	–	–	–
2	16	18	17	83	58	82	–	6	2	–
3	17	19	17	83	60	80	–	2	2	–
4	17	18	17	84	55	80	–	–	–	–
5	16	18	17	83	57	80	–	–	–	–
6	16	18	17	83	55	80	–	–	–	–
7	16	18	17	83	60	82	–	–	2	3
8	16	18	17	80	58	82	–	2	4	–
9	16	18	17	80	55	80	–	–	4	–
10	17	18	17	84	60	83	2	–	2	6
11	17	18	17	84	60	83	2	–	–	–
12	17	18	17	80	55	83	2	2	4	8
13	16	18	17	80	58	80	–	–	–	6
14	16	18	17	82	60	80	–	–	–	8
15	16	18	17	82	60	80	–	–	–	9
16	16	18	17	80	55	80	2	2	4	6
17	16	18	18	80	56	82	–	–	–	5
18	16	18	16	83	58	80	–	–	–	–
19	16	18	17	83	58	80	–	–	–	–
20	16	18	17	83	58	80	–	–	–	–
21	17	19	18	83	56	80	2	2	2	4
22	17	18	17	80	56	80	–	–	–	6
23	17	18	17	82	55	82	–	2	4	4
24	16	18	17	82	56	82	–	–	–	2
25	17	18	17	83	54	80	–	4	6	–
26	17	18	17	84	60	83	–	2	2	3
27	17	18	17	82	57	82	–	–	–	–
28	17	18	17	82	57	82	–	–	–	6
29	17	18	17	80	57	80	–	–	–	6
30	17	18	17	80	57	80	–	–	–	6
31	17	18	17	80	57	78	–	–	–	6
Medias del mes	17	18	17	82	57	84	2	3	3	3
Máxima	16	19	18	84	60	83	2	6	6	9
Mínima	17	18	17	80	54	78	2	2	2	2

ANEXO NO. 2

Observatorio No. 2 — Setiembre 1958

DIA	C° TEMPERATURA Horas día 7	13	18	% HUMEDAD RELATIVA Horas día 7	13	18	m/seg VELOCIDAD DEL VIENTO Horas día 7	13	18	HORAS DE SOL
1	15	23	17	83	53	80	2	4	6	6
2	16	23	17	83	53	80	2	4	6	-
3	16	23	17	82	55	75	2	4	6	5
4	16	25	17	82	55	75	2	2	2	-
5	16	25	17	83	55	75	-	2	2	6
6	16	25	17	80	55	75	-	2	2	6
7	16	25	16	80	57	78	-	-	-	-
8	16	26	16	83	56	78	-	-	-	6
9	16	25	17	83	53	80	-	2	2	6
10	16	24	16	83	53	80	-	2	2	-
11	16	23	17	83	55	80	-	-	-	-
12	16	23	17	80	55	80	-	-	-	4
13	16	23	16	80	55	80	-	-	-	4
14	15	25	17	83	56	78	-	-	-	6
15	16	25	18	83	57	78	-	2	2	6
16	16	25	17	85	57	78	-	-	-	6
17	16	25	16	80	57	78	-	-	-	7
18	16	24	17	80	53	75	-	-	-	7
19	16	24	16	83	60	78	-	2	2	7
20	16	24	16	80	60	78	-	-	-	-
21	15	23	16	81	60	78	-	2	2	6
22	15	23	16	80	60	78	2	-	-	6
23	15	21	16	81	60	75	-	-	-	4
24	16	21	16	80	60	74	-	-	-	6
25	16	20	16	80	60	74	-	-	-	6
26	16	20	17	80	60	75	-	-	-	6
27	15	21	17	82	60	75	-	-	-	4
28	16	21	17	83	60	75	-	-	-	6
29	16	21	17	80	57	75	2	2	4	6
30	16	21	17	80	57	74	2	4	4	-
Medias del mes	15	23	16	79	55	75	2	2	3	4
Máxima	15	26	18	85	60	80	2	4	6	7
Mínima	16	20	16	80	53	74	2	2	2	4

Observatorio No. 2 — Octubre 1958

DIA	C° TEMPERATURA Horas día 7	13	18	% HUMEDAD RELATIVA Horas día 7	13	18	m/seg VELOCIDAD DEL VIENTO Horas día 7	13	18	HORAS DE SOL
1	16	17	16	80	57	70	-	2	4	6
2	16	17	16	82	58	70	-	2	4	6
3	16	17	16	80	60	70	-	4	6	7
4	16	18	16	80	60	70	-	-	-	6
5	16	18	16	80	60	70	-	-	-	7
6	16	18	16	80	60	80	-	-	-	8
7	15	18	16	83	60	80	-	-	-	8
8	15	18	16	83	60	70	-	2	2	7
9	16	17	16	81	70	73	-	2	2	7
10	15	17	17	80	65	70	-	2	2	7
11	16	17	18	80	65	73	-	2	4	7
12	16	17	18	80	57	73	-	2	4	7
13	16	17	17	80	57	73	-	4	6	-
14	15	17	17	80	57	73	-	-	-	6
15	16	17	16	80	57	73	-	-	-	7
16	17	16	16	83	57	73	-	-	-	6
17	16	17	16	82	65	73	-	2	2	6
18	15	16	16	82	65	73	-	2	4	6
19	16	17	16	82	63	80	-	-	-	6
20	16	17	16	80	60	80	-	2	2	6
21	16	17	16	80	60	80	-	-	-	6
22	15	17	16	81	60	70	-	2	4	6
23	15	17	16	80	60	70	-	2	2	7
24	16	17	16	80	60	70	-	2	2	6
25	16	17	16	80	60	70	-	2	4	6
26	16	17	16	80	60	70	-	-	-	6
27	16	18	16	80	60	70	-	2	2	6
28	16	18	16	80	60	70	-	-	-	6
29	16	18	17	81	61	72	-	2	2	6
30	16	18	17	82	60	70	-	-	-	6
31	15	17	16	80	60	70	2	2	4	7
Medias del mes	16	17	16	81	61	73	2	2	3	6
Máxima	17	18	18	83	70	80	2	4	6	8
Mínima	15	16	16	80	57	70	2	2	2	6

Observatorio No. 2 — Noviembre 1958

DIA	C° TEMPERATURA Horas día 7	13	18	% HUMEDAD RELATIVA Horas día 7	13	18	m/seg VELOCIDAD DEL VIENTO Horas día 7	13	18	HORAS DE SOL
1	16	24	18	80	50	70	-	2	4	6
2	18	23	18	76	52	70	-	2	4	7
3	18	24	18	78	50	70	-	4	8	6
4	18	21	18	75	55	70	-	-	6	7
5	17	21	18	76	55	70	-	2	4	7
6	17	21	18	76	55	70	-	2	4	8
7	17	21	18	76	54	70	-	2	4	8
8	16	21	18	76	54	70	2	2	4	8
9	16	21	18	76	55	70	2	4	8	6
10	16	22	18	75	54	70	2	4	8	6
11	16	21	18	75	58	70	-	2	4	6
12	16	21	18	75	54	80	2	4	4	7
13	16	21	18	74	54	80	2	2	4	7
14	16	21	18	75	54	70	-	2	2	8
15	16	21	18	75	54	70	-	2	2	7
16	16	20	18	74	68	70	-	2	2	7
17	17	20	18	75	68	74	-	2	2	8
18	17	21	18	83	55	70	-	2	2	8
19	17	21	20	83	55	70	-	2	2	8
20	17	21	20	84	55	70	-	-	-	8
21	17	20	18	84	55	75	-	-	-	8
22	16	21	18	84	55	75	-	2	4	8
23	16	24	20	80	55	82	-	4	4	8
24	16	21	20	80	55	82	-	-	-	8
25	16	21	20	80	55	82	-	-	-	8
26	16	24	20	82	50	72	-	2	4	9
27	16	23	20	80	50	74	-	-	-	9
28	16	24	20	80	50	74	-	2	4	9
29	16	24	20	80	50	74	-	2	2	9
30	16	24	20	80	50	73	2	2	4	9
Medias del mes	16	22	19	78	54	73	2	2	4	8
Máxima	18	24	20	84	68	82	2	4	8	9
Mínima	16	21	18	74	50	70	2	2	2	6

Observatorio No. 2 — Diciembre 195

DIA	C° TEMPERATURA Horas día 7	13	18	% HUMEDAD RELATIVA Horas día 7	13	18	m/seg VELOCIDAD DEL VIENTO Horas día 7	13	18	HORAS DE SOL
1	19	21	22	85	72	70	-	-	-	10
2	19	21	22	85	72	80	-	2	2	10
3	19	21	22	85	72	70	2	2	4	10
4	19	20	21	85	72	70	-	2	4	12
5	19	20	21	85	73	70	-	4	6	9
6	19	20	22	80	73	70	-	4	6	10
7	18	20	21	80	73	70	-	-	-	12
8	19	24	20	80	53	58	-	2	-	10
9	18	24	20	80	53	58	-	2	2	10
10	18	24	20	80	52	76	-	2	4	12
11	19	24	20	75	52	76	-	-	-	12
12	19	24	20	71	53	76	-	-	-	10
13	19	22	23	75	53	65	-	-	-	8
14	19	21	23	75	53	65	-	2	4	8
15	19	21	23	75	53	65	-	2	4	8
16	19	21	23	75	52	65	-	-	-	6
17	18	22	20	80	63	72	-	-	-	4
18	18	22	20	80	63	72	-	4	8	10
19	18	20	19	80	70	72	2	4	8	10
20	18	22	20	75	52	72	-	-	-	12
21	18	22	20	75	52	71	-	-	-	10
22	18	21	19	75	53	71	-	-	-	10
23	18	20	19	75	53	70	-	-	-	10
24	18	22	20	77	54	70	-	-	-	10
25	18	21	20	70	54	70	2	4	6	12
26	18	21	20	70	54	70	2	4	8	9
27	19	21	20	70	54	70	-	2	4	9
28	19	20	21	76	55	70	6	2	4	9
29	18	20	21	75	54	70	-	2	4	9
30	18	20	21	75	54	70	-	2	4	10
31	18	20	21	75	54	70	-	-	-	9
Medias del mes	19	21	21	77	59	69	2	2	3	10
Máxima	19	24	23	85	73	76	6	4	8	12
Mínima	18	20	19	70	52	58	2	2	2	2

MEDICIONES DE ARENA EOLICA EXTRAIDA DE LA PLAYA DE SANTA ROSA POR DEFLACION

ANEXO NO. 3

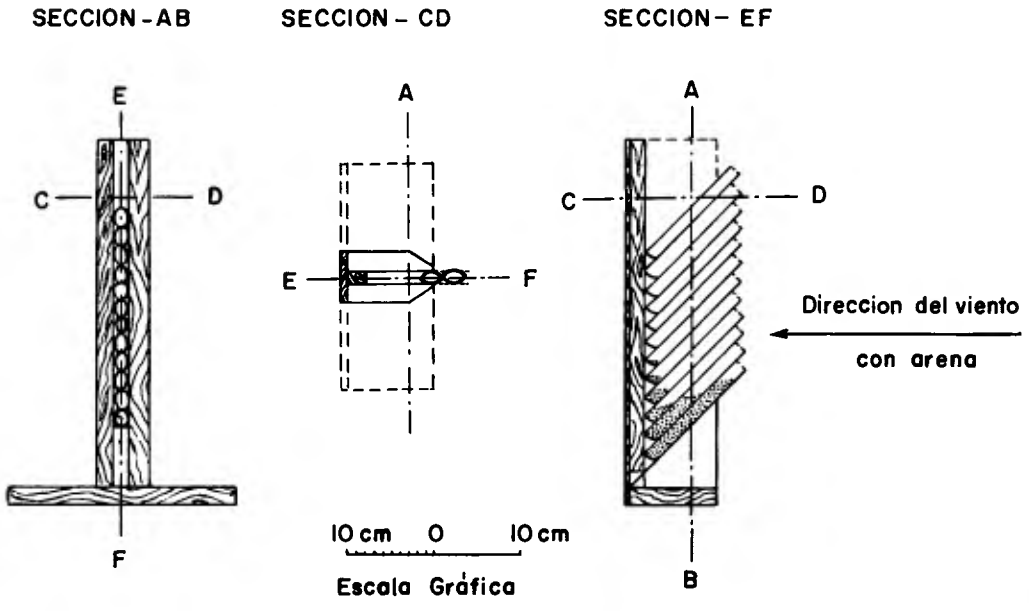

Fig. 1

Foto No. 1. Arenómetro BZ o de Zocalo puesto en estacion. En la Playa de Santa Rosa.

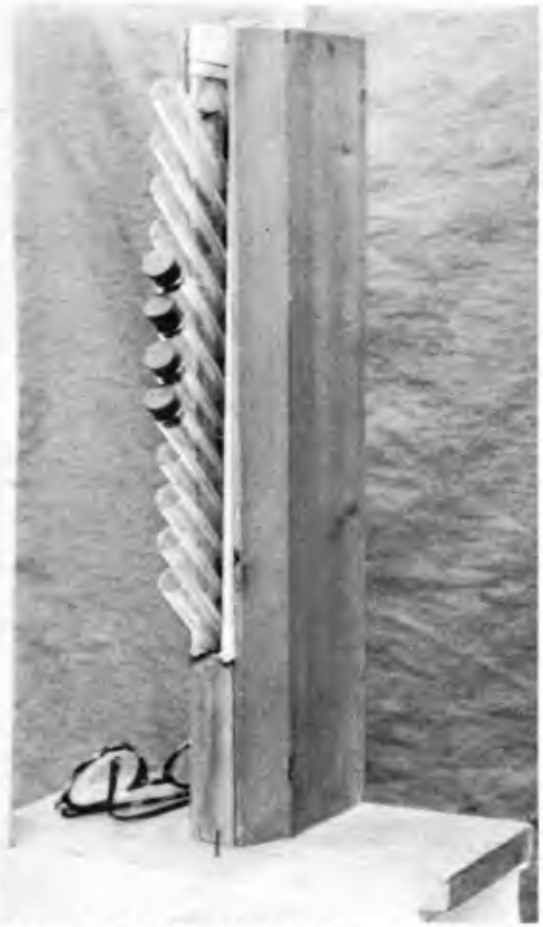

Foto No. 2. Arenómetro BZ o de Zócalo para experiencia.

Foto No. 3. Arenómetro BH o de altura en estación.

MEDICIONES DE ARENA EOLICA EXTRAIDA DE LA PLAYA DE SANTA ROSA POR DEFLACION

ANEXO NO. 4

Mensuras individuals con arenometros "BZ" O Broggi de Zocalo

EXPERIMENTO I

a - LUGAR: Playa de Sante Rose, punto A del plano al 20.000 de Anexo No. 1

b.- FECHA: (14 1.58) Catorce de Enero de 1958

c - DATOS DE MAREAS EN CALLAO (1)

Pleamar		Bajamar	
Hora	Alt. pié	Hora	Alt. pié
0012	2 4	0711	0.5
1413	2.9	2013	1 5

d - DISTANCIA DEL ARENOMETRO A LA LINEA MOJADA DE ALTA MAREA U OLEAJE (2) DEL DIA EN LA PLAYA: 10 m.

e - VELOCIDAD PROMEDIO DEL VIENTO REGIONAL MEDIDA CON ANEMOMETRO A 1 6 M (vertical) SOBRE EL SUELO: 4 7 m/e (metroe por segundo)

f - MEDIDAS DE ARENA CON EL ARENOMETRO:

TUBO No	HORA Inicio	EXPOSICION Término	ARENA DEPOSITADA EN CADA TUBO POR EL VIENTO mg	PORCENTAJE DEL PESO TOTAL %	ALTURA SOBRE EL SUELO DE LA TANGENTE INFERIOR A LA BOCA DEL TUBO (3)
1	1724	1754	404	64 53	4.00
2	"	"	140	22.37	6 12
3	"	"	50		8.24
4	"	"	18		10,36
5	"	"	7		12.48
6	"	"	2		14 61
7	"	"	1		16.73
8	"	"	1		18 85
9	"	"	1		20.97
10	"	"	1		23 09
11	"	"	-		25 21
12	"	"	1	13.10	27 33
			626	100 00	

PESO TOTAL DE ARENA RECOGIDA EN MILIGRAMOS: 626 mg

TIEMPO TOTAL DE OBSERVACION: 30 minutos

(1) - Table de mareas 1958, Servicio Hidrográfico del Ministerio de Marina, p 92

(2) - El nivel a que llegan las lenguas de agua en las playas, depende más de la amplitud del oleaje que de las mareas.

(3) - Diámetro interior de cada tubo de prueba: 13 mm, y exterior: 15 mm, longitud: 148 mm.

EXPERIMENTO II

a - LUGAR: Playa de Santa Rosa, punto A del plano el 20.000 de Anexo No.1

b.- FECHA: (20-1-58) Veinte de Enero de 1958

c - DATOS DE MAREAS EN CALLAO (1)

Pleamar		Bajamar	
Hora	Alt.pié	Hora	Alt.pié
0554	2 2	0046	1,0
1849	3 4	1155	0,3

d.- DISTANCIA DEL ARENOMETRO A LA LINEA MOJADA DE ALTA MAREA U OLEAJE DEL DIA EN LA PLAYA: 10 m.

e - VELOCIDAD PROMEDIO DEL VIENTO REGIONAL MEDIDA CON EL ANEMOMETRO A 1,6 M (Vertical) SOBRE EL SUELO 4 m/s (metros por segundo)

f - MEDIDAS DE ARENA CON EL ARENOMETRO:

TUBO No.	HORA Inicio	EXPOSICION Término	ARENA DEPOSITADA EN CADA TUBO POR EL VIENTO mg	PORCENTAJE DEL PESO TOTAL	ALTURA SOBRE EL SUELO DE LA TANGENTE INFERIOR A LA BOCA DEL TUBO (2)
1	1758	1818	35	61,40	6,00
2	"	"	15	26,32	8,12
3	"	"	5		10,24
4	"	"	1		12 36
5	"	"	1	12,28	14,48
			57	100,00	

PESO TOTAL DE ARENA RECOGIDA EN MILIGRAMOS 57

TIEMPO TOTAL DE OBSERVACION: 20 minutos

(1) - Tomados de la Tabla de Mareas - p. 92 correspondiente al Callao, del Servicio Hidrográfico del Ministerio de Marina del Perú.

(2).- Diámetro interior de cada tubo de prueba 13 mm. y exterior 15 mm; longitud 148 mm.

EXPERIMENTO: III

a - LUGAR: Playa de Santa Rosa, punto A del plano el 20.000 de Anexo No 1

b - FECHA (20-2-58) Veinte de Febrero de 1958

c.- DATOS DE MAREAS EN CALLAO

Pleamar		Bajamar	
Hora	Alt pié	Hora	Alt.pié
0654	2 5	0115	0 9
1920	3,0	1251	0 8

d.- DISTANCIA DEL ARENOMETRO A LA LINEA MOJADA DE ALTA MAREA U OLEAJE DEL DIA EN LA PLAYA 30 M.

e.- VELOCIDAD PROMEDIO DEL VIENTO REGIONAL MEDIDA CON EL ANEMOMETRO A 1 6 M (Vertical SOBRE EL SUELO 5 m/seg (metros por segundo).

f.- MEDIDAS DE ARENA CON EL ARENOMETRO

TUBO No	HORA Inicio	EXPOSICION Término	ARENA DEPOSITADA EN CADA TUBO POR EL VIENTO mg	PORCENTAJE DEL PESO TOTAL %	ALTURA SOBRE SUELO DE LA TANGENTE INFERIOR A LA BOCA DEL TUBO
1	1420	1615	32 384.	63 07	0 00
2	"	"	12 970.	25 26	2 12
3	"	"	3 761		4 24
4	"	"	1 621.		6 36
5	"	"	394		8 48
6	"	"	124		10 61
7	"	"	61.		12,73
8	"	"	19.		14 85
9	"	"	6		16 97
10	"	"	3		19 09
11	"	"	2.	11,67	21 21
			51 345.	100,00	

PESO TOTAL DE ARENA RECOGIDA EN MILIGRAMOS 51 345

TIEMPO TOTAL DE OBSERVACION 115 minutos

Nota: En este mismo día, de 1630 a 1700 hubo un viento de 4,7 m/s a 0 5 M (de altitud) Se introdujo verticalmente en la arena al lado del instrumento BZ un tubo de prueba aislado cuya boca sobresalía sólo un 1 cm del nivel del suelo y en media hora se recogió 21 285 6 mg. cifra superior a la obtenida del tubo No. 1 en relación al tiempo que ambos estuvieron expuestos lo que expresa que éste tubo recogió la arena arrastrada y rotante Esto se pudo comprobar porque el poco tiempo de estar expuesto, la arece del suelo se acumulaba y subía de nivel hasta caer directamente al llegar por arrastre y rotación.

EXPERIMENTO: IV

a - LUGAR Playa de Santa Rosa, punto A del plano el 20.000 No 1

b - FECHA (21-2-58) Veintiuno de Febrero de 1958

c - DATOS DE MAREAS EN CALLAO (1)

Pleamar		Bajamar	
Hora	Alt pié	Hora	Alt pié
0727	2 4	0143	0 9
1943	2 8	1323	0 9

d - DISTANCIA DEL ARENOMETRO A LA LINEA MOJADA DE ALTA MAREA U OLEAJE DEL DIA EN LA PLAYA 10 m

e - VELOCIDAD PROMEDIO DEL VIENTO (no se midió) (2)

f - MEDIDAS DE ARENA CON EL ARENOMETRO

TUBO No.	HORA Inicio	EXPOSICION Término	ARENA DEPOSITADA EN CADA TUBO POR EL VIENTO mg	PORCENTAJE DEL PESO TOTAL %	ALTURA SOBRE EL SUELO DE LA TANGENTE INFERIOR A LA BOCA DEL TUBO
1	1420	1820	7,923	70,54	0 00
2	"	"	1,663	14 81	2,12
3	"	'	987		4 24
4	"	"	182.		6,36
5	'	"	115		8 48
6	"	"	77		10 61
7	'	"	74.		12 73
8	"	"	44		14 85
9	"		49		16 97
10	"	'	36		19 09
11	"	"	33		21 21
12	'	"	30		23 33
13	"	"	19.	14,65	25 45
			11 232	100,00	

PESO TOTAL DE ARENA RECOCIDA EN MILIGRAMOS 11 232

TIEMPO TOTAL DE OBSERVA CION 240 minutos

(1) Por la marea y el oleaje las lenguas de agua en la playa llegaron a las 1420 hasta 3 m de la gradería o escala de concreto que baja a la playa

(2) Había viento poco intenso pero con ráfagas fuertes

ANEXO NO. 4

EXPERIMENTO V

a - LUGAR Playa de Santa Rosa

b - FECHA (5-3-58) Cinco de Marzo de 1958

c.- DATOS DE MAREA EN CALLAO

Pleamar Hora	Alt.pies	Bajamar Hora	Alt.pies
0506	2 8	1111	0 3
1740	3.5	0000	0 0

d - DISTANCIA DEL ARENOMETRO A LA LINEA MOJADA DE ALTA MAREAU F'L LA PLAYA EN EL DIA 10 m

e - VELOCIDAD PROMEDIO DEL VIENTO A 18 cm SOBRE EL SUELO 3 m/s

f - MEDIDAS CON EL ARENOMETRO

TUBO No.	HORA Inicio	EXPOSICION Término	ARENA DEPOSITADA EN CADA TUBO POR EL VIENTO mg	PORCENTAJE DEL PESO TOTAL %	ALTURA SOBRE EL SUELO DE LA TANGENTE INFERIOR A LA BOCA DEL TUBO
1	1048	1650	1.0	59	0.00
2	"	"	0.4	24.	2.12
3	"	"	0 2		4 24
4	"	"	0 1	17.	6 36
5	"	"	Trazas		
6	"	"	"		
7	"	"	"		
8	"	"	"		
9	"	"	"		
10	"	"	nada		
11	"	"	"		
12	"	"	"		
			1 7	100 00	

PESO TOTAL DE ARENA RECOGIDA EN MILIGRAMOS 1 7

TIEMPO TOTAL DE CONSERVACION 0602

EXPERIMENTO VI

a - LUGAR: Playa de Santa Rosa, punto A del plano al 20.000 de Anexo 1

b.- FECHA: (17.3 58) Diecisiete de Marzo de 1958

c - DATOS DE MAREAS EN CALLAO

Pleamar Hora	Alt.pies	Bajamar Hora	Alt. pies
0421	2 4	1016	0.8
1046	3 1	2312	0 9

d - DISTANCIA DEL ARENOMETRO A LA LINEA MOJADA DE ALTA MAREA U OLEAJE DEL DIA EN LA PLAYA 10 m.

e - VELOCIDAD PROMEDIO DEL VIENTO REGIONAL MEDIDA CON ANEMOMETRO A 1 6 m. (Vertical) SOBRE EL SUELO: SUAVE Y UNIFORME (sin ráfagas)

f.- MEDIDAS CON EL ARENOMETRO

TUBO No,	HORA Inicio	EXPOSICION Término	ARENA DEPOSITADA EN CADA TUBO POR EL VIENTO mg	PORCENTAJE DEL PESO TOTAL %	ALTURA SOBRE EL SUELO DE LA TANGENTE INFERIOR A LA BOCA DEL TUBO
1	1725	1810	276.	67.15	0.00
2	"	"	96	23 36	2 12
3	"	"	28.		4 24
4	"	"	8.		6 36
5	"	"	2		8.48
6	"	"	1	9.49	10 61
			411	100.00	

PESO TOTAL DE ARENA RECOGIDA EN MILIGRAMOS 411

TIEMPO TOTAL DE OBSERVACION: 45 minutos

OBSERVACIONES - Fuerte humedad y formación de costra salina dura sobre la superficie de la arena, que la cementa e impide su migración.

EXPERIMENTO: VII

a - LUGAR: Playa de Santa Rosa, punto A del plano al 20 000 de Anexo No. 1

b.- FECHA: (5-4-58) C nco de Abril de 1958

c.- DATOS DE MAREAS EN CALLAO

Pleamar Hora	Alt.pies	Bajamar Hora	Alt pies
0632	3.5	0009	0.2
1835	3.1	1244	0.6

d.- DISTANCIA DEL ARENOMETRO A LA LINEA MOJADA U OLEAJE DEL DIA EN LA PLAYA: 20 m

e.- VELOCIDAD PROMRDIO DEL VIENTO REGIONAL MEDIDA CON EL ANEMOMETRO A 1,6 M (vertical) SOBRE EL SUELO 6 27 m/s

f.- MEDIDAS CON EL ARENOMETRO

TUBO No.	HORA Inicio	EXPOSICION Término	ARENA DEPOSITADA EN CADA TUBO POR EL VIENTO mg	PORCENTAJE DEL PESO TOTAL %	ALTURA SOBRE EL SUELO DE LA TANGENTE INFERIOR A LA BOCA DEL TUBO
1	1230	1830	18.632.	50.73	4 00
2	"	"	8.640.	23 54	6.12
3	"	"	3.960		8.24
4	"	"	2.080		10.36
5	"	"	1.117.		12 48
6	"	"	663		14.61
7	"	"	440.		16.73
8	"	"	345.		18.85
9	"	"	278		20 97
10	"	"	227		23 09
11	"	"	188.		25.21
12	"	"	145.	25.73	27 33
			36 731	100.00	

PESO TOTAL DE ARENA RECOGIDA EN MILIGRAMOS 36.731

TIEMPO TOTAL DE OBSERVACION 360 minutos

EXPERIMENTO VIII

a - LUGAR: Playa de Santa Rosa, punto A del plano al 20.000 de Anexo No. 1

b.- FECHA: (17-4-58) Diecisiete de Abril de 1958

c - DATOS DE MAREAS EN CALLAO

Pleamar Hora	Alt.pies	Bajamar Hora	Alt pies
0511	2 8	1112	1 1
1701	2.7	2320	0.7

d - DISTANCIA DEL ARENOMETRO A LA LINEA MOJADA DE ALTA MAREA U OLEAJE DEL DIA EN LA PLAYA 10 m

e.- VELOCIDAD PROMEDIO DEL VIENTO REGIONAL MEDIDA CON EL ANEMOMETRO A 1 6 M (Vertical) SOBRE EL SUELO no se tomó

f.- MEDIDAS CON EL ARENOMETRO

TUBO No.	HORA Inicio	EXPOSICION Término	ARENA DEPOSITADA EN CADA TUBO POR EL VIENTO mg	PORCENTAJE DEL PESO TOTAL %	ALTURA SOBRE EL SUELO DE LA TANGENTE INFERIOR A LA BOCA DEL TUBO
1	1104	1134	25.303	64.58	0 00
2	"	"	9.530.	24 32	2 12
3	"	"	2.931		4 24
4	"	"	989		6 36
5	"	"	316.		8.48
6	"	"	111. 39.180	10.10 100.00	10.61
7	"	"	911	56 05	12 73
8	"	"	430.	24.32	14 85
9	"	"	192		16 97
10	"	"	87		19.09
11	"	"	45		21.21
12	"	"	23. 1.768	19.67 100 00	
			40.948		

PESO TOTAL DE ARENA RECOGIDA EN MILIGRAMOS 40.948

TIEMPO TOTAL DE OBSERVACION

a - del tubo No. 1 al No 6 30 minutos

b - " " " " 7 " " 12 431 minutos

Nota - Se taparon los tubos 1 al 6 a los 30 minutos porque habían recibido mucha arena y se temía que las ráfagas extrajesen la depositada

MEDICIONES DE ARENA EOLICA EXTRAIDA DE LA PLAYA DE SANTA ROSA POR DEFLACION

ANEXO NO. 5

Mensuras con 2, 3, y 4 Arenómetros BZ

Experimento I

EXPERIENCIAS CON TRES ARENOMETROS DE ZOCALO O BZ EN FRENTE PARALELO A LA PLAYA Y DISTANCIADOS 30. m UNO DE OTRO

a.- LUGAR: Playa de Santa Rosa, punto A-N del plano di 20.000

b.- FECHA: (26-2-58) Veintiseis de Febrero de 1958

c.- DATOS DE MAREAS EN CALLAO

Pleamar		Bajamar	
Hora	Alt.pies	Hora	Alt.pies
1128	2,5	0409	1.1
2151	2,0	1727	1.6

d.- DISTANCIA DEL ARENOMETRO A LA LINEA MOJADA DE ALTA MAREA EN EL DIA EN LA PLAYA: 10 m.

e.- VELOCIDAD PROMEDIO DEL VIENTO A 1.6 M: 4 m/s

ARENOMETRO No. 1

TUBO No.	HORA Inicio	EXPOSICION Término	ARENA DEPOSITADA EN CADA TUBO POR EL VIENTO mg	PORCENTAJE DEL PESO TOTAL %	ALTURA SOBRE EL SUELO DE LA TANGENTE INFERIOR A LA BOCA DEL TUBO
1	1730	1850	6.465.8	65.95	0.00
2	"	"	2.496.6	25.47	2.12
3	"	"	481.3		4.24
4	"	"	241.0		6.36
5	"	"	80.0		8.48
6	"	"	29.6		10.61
7	"	"	9.6		12.73
8	"	"	5.5		14.85
9	"	"	1.0		16.97
10	"	"	0.4		19.09
11	"	"	0.4		21.21
12	"	"	Trazas	8.58	
			9.801.4	100.00	

PESO TOTAL DE ARENA RECOGIDA EN MILIGRAMOS: 9.801.4

TIEMPO TOTAL DE OBSERVACION: 60 minutos

ARENOMETRO No. 2

TUBO No.	HORA Inicio	EXPOSICION Término	ARENA DEPOSITADA EN CADA TUBO POR EL VIENTO mg	PORCENTAJE DEL PESO TOTAL %	ALTURA SOBRE EL SUELO DE LA TANGENTE INFERIOR A LA BOCA DEL TUBO
1	1734	1854	3.215.6	70.94	0.00
2	"	"	925.8	25.79	2.12
3	"	"	269.0		4.24
4	"	"	88.5		6.36
5	"	"	28.5		8.48
6	"	"	9.6		10.61
7	"	"	tr.		
8	1734	1854	tr.		
9	"	"	"		
10	"	"	"		
11	"	"	"		
12	"	"	"	5.27	
			4.533.0	100.00	

PESO TOTAL DE ARENA EN MILIGRAMOS: 4.533.0

TIEMPO DE OBSERVACION: 60 minutos

ARENOMETRO No. 3

TUBO No.	HORA Inicio	EXPOSICION Término	ARENA DEPOSITADA EN CADA TUBO POR EL VIENTO mg	PORCENTAJE DEL PESO TOTAL %	ALTURA SOBRE EL SUELO DE LA TANGENTE INFERIOR A LA BOCA DEL TUBO
1	1734	1850	5.651.3	69.06	0.00
2	"	"	1.803.1	22.20	2.12
3	"	"	400.0		4.24
4	"	"	197.6		6.36
5	"	"	72.5		8.48
6	"	"	26 1		10.61
7	"	"	10.7		12.73
8	"	"	4.5		14.85
9	"	"	1.5		16.97
10	"	"	0.9		19.09
11	"	"	Trazas		21.21
12	"	"		8.74	
			8.168.0	100.00	

PESO TOTAL DE ARENA RECOGIDA EN MILIGRAMOS: 8.168.0

TIEMPO TOTAL DE OBSERVACION: 60 minutos

OBSERVACIONES.- Durante el tiempo que duré la experiencia notamos la existencia de varias ráfagas veloces que transportan la arena flotante en dirección paralela a la playa o sea de dirección SE en vez de la SW que era la dominante horas antes. Esta arena avanzada en forma de grandes blancos fáciles de distinguir y las ráfagas que la transportaban variaban de intensidad y duración. Por la posición del muro de concreto que delimita el malecón en algunos sitios, la arena lo transmontaba y en la escalinata de acceso a la playa se observó marcada acumulación provocada por ser allá al paso mas bajo en su migración continental hacia al N. Como las ráfagas duraban algunos segundos, durante ellas la arena en suspensión se extendía en toda la longitud de la playa pareciendo venir en masas que rebotaban sobre el suelo para su turbulencia extraer de él la arena ya seca y levantar hasta algunos metros. Pasadas las ráfagas ocurría en irregularias parcelas al suelo para unirse a la que saltaba obligándola a realizar saltos más largos.

Experimento II

EXPERIENCIA CON TRES ARENOMETROS BZ EN 250,m PARALELOS A LA PLAYA

a.- LUGAR: Playa de Santa Rosa

b.- FECHA: (28-3-58) Veintiocho de Marzo de 1958

c - DATOS DE MAREAS

Pleamar		Bajamar	
Hora	Alt.pies	Hora	Alt.pies
1152	2.6	0406	1.1
2304	1.8	1908	1.6

d - DISTANCIA DEL ARENOMETRO A LA LINEA HUMEDA DE OLEAJE O DE ALTA MAREA AL INICIO: 20 m.

e.- VELOCIDAD PROMEDIO DEL VIENTO A 1.6 m.: de 5 m/s a las 1730 CON RAFAGAS

ARENOMETRO No. 1

Colocado 100 m al Norte del No. 2 y coincidiendo con Punto A de Lam. 1 Anexo 1

TUBO No.	HORA Inicio	EXPOSICION Término	ARENA DEPOSITADA EN CADA TUBO POR EL VIENTO mg	PORCENTAJE DEL PESO TOTAL %	ALTURA SOBRE EL SUELO DE LA TANGENTE INFERIOR A LA BOCA DEL TUBO
1	1230	1851	24,306	51.68	0.00
2	"	"	14,409	30.64	2,12
3	"	"	5,329		4.24
4	"	"	1,948.		6,36
5	"	"	676.		8.48
6	"	"	246.		10,61
7	"	"	77.		12 73
8	"	"	25.		14.85
9	"	"	8.		16.97
10	"	"	3.	17.68	
	Peso total en mg.		47.027	100.00	

ARENOMETRO No. 2

Colocado(100,m al Sur) del No. 1

TUBO No.	HORA Inicio	EXPOSICION Término	ARENA DEPOSITADA EN CADA TUBO POR EL VIENTO mg	PORCENTAJE DEL PESO TOTAL %	ALTURA SOBRE EL SUELO DE LA TANGENTE INFERIOR A LA BOCA DEL TUBO cm
1	1215	1815	6,487.	64.03	0,00
2	"	"	2,268.	22.39	2.12
3	"	"	794.		4.14
4	"	"	511.		6,36
5	"	"	126.		8,48
6	"	"	73.		10,61
7	1215	1815	32.		12.73
8	"	"	28.		14.85
9	"	"	9.		16.97
10	"	"	3.	15.58	19.09
Peso Total	en mg.		10.131	100.00	

ARENOMETRO No. 3

Colocado al sur de la playa y cerca del cerro.

TUBO No.	HORA Inicio	EXPOSICION Término	ARENA DEPOSITADA EN CADA TUBO POR EL VIENTO mg	PORCENTAJE DEL PESO TOTAL %	ALTURA SOBRE EL SUELO DE LA TANGENTE INFERIOR A LA BOCA DEL TUBO cm
1	1205	1825	8,609.	65.70	0.00
2	"	"	2.815.	21.28	2,12
3	"	"	997.		4.24
4	"	"	327.		6.36
5	"	"	127.		8,48
6	"	"	127.		10,61
7	"	"	92.		12.73
8	"	"	62.		14.85
9	"	"	51.		16.97
10	"	"	32.		19.09
11	"	"	71.	13.02	21.21
	Peso total en mg.		13.226.	100.00	

EXPERIMENTO II

ARENOMETRO	PESO TOTAL DE ARENA RECOGIDA EN MILIGRAMOS	TIEMPO TOTAL DE OBSERVACION
I	47.027 mg	361'
II	10.131 "	358'
III	13.226 "	378'

ANEXO NO. 5

Experimento No. III

EXPERIENCIA CON CUATRO BZ PARALELOS A LA PLAYA Y A PARTIR DE LA ESCALINATA AL SUR, DISTANCIADOS 30.m UNO DE OTRO

a.- LUGAR: Playa de Santa Rosa

b.- FECHA. (9-4-58) Nueve de Abril de 1958

c.- DATOS DE MAREAS EN CALLAO

Pleamar		Bajamar	
Hora	Alt.pié	Hora	Alt.pié
1022	3.1	0316	0 7
2214	2.0	1713	1.3

d.- DISTA NCIA DE LOS ARENOMETROS A LA LINEA HUMEDA DE OLEAJE O DF ALTA MAREA AL INICIO: 15 m.

e.- VELOCIDAD PROMEDIO DEL VIENTO A 0.15 m: 4.54 m/seg. a las 1525

ARENOMETRO No. 1

TUBO No.	HORA Inicio	EXPOSICION Término	ARENA DEPOSITADA EN CADA TUBO POR EL VIENTO mg	PORCENTAJE DEL PESO TOTAL %	ALTURA SOBRE EL SUELO DE LA TANGENTE INFERIOR A LA BOCA DEL TUBO
1	1455	1809	2.236.	72.11	0.00
2	"	"	588.	18.96	2.12
3	"	"	188.		4.24
4	"	"	60.		6.36
5	"	"	20.		8.48
6	"	"	71		10.61
7	"	"	2.	8.93	
	Peso total en mg.		3.101.	100.00	

ARENOMETRO No. 2

TUBO No.	HORA Inicio	EXPOSICION Término	ARENA DEPOSITADA EN CADA TUBO POR EL VIENTO mg	PORCENTAJE DEL PESO TOTAL %	ALTURA SOBRE EL SUELO DE LA TANGENTE INFERIOR A LA BOCA DEL TUBO
1	1500	1807	5.433.	65.18	0.00
2	"	"	1.908.	22.89	2.12
3	"	"	669.		4.24
4	"	"	195.		6.36
5	"	"	56.		8.48
6	"	"	16.		10.61
7	"	"	6.		12.73
8	"	"	2.	11.93	14.85
	Peso total en mg		8.335.	100.00	

ARENOMETRO No. 3

TUBO No.	HORA Inicio	EXPOSICION Término	ARENA DEPOSITADA EN CADA TUBO POR EL VIENTO mg	PORCENTAJE DEL PESO TOTAL %	ALTURA SOBRE EL SUELO DE LA TANGENTE INFERIOR A LA BOCA DEL TUBO
1	1505	1805	2.217.	72.14	0.00
2	"	"	609.	19.82	2.12
3	"	"	176.		4.24
4	"	"	52.		6.36
5	"	"	14.		8.48
6	"	"	4.		10.61
7	"	"	1.	8.04	12.73
	Peso total en mg.		3.073.	100.00	

ARENOMETRO No. 4

TUBO No.	HORA Inicio	EXPOSICION Término	ARENA DEPOSITADA EN CADA TUBO POR EL VIENTO mg	PORCENTAJE DEL PESO TOTAL %	ALTURA SOBRE EL SUELO DF LA TANGENTE INFERIOR A LA BOCA DEL TUBO.
1	1510	1800	3.686	64.88	0.00
2	"	"	1.262.	22 22	2.12
3	"	"	472.		4.24
4	"	"	176.		6.36
5	"	"	58.		8.48
6	"	"	19.		10.61
7	"	"	6.		12.73
8	"	"	2.	12.90	14.85
	Peso total en mg.		5.681.	100.00	

MEDICIONES DE ARENA EOLICA EXTRAIDA DE LA PLAYA DE SANTA ROSA POR DEFLACION

ANEXO NO. 5

Experimento I V

EXPERIENCIA CON DOS BZ A 20 y 70.m DEL EXTREMO SUR DE LA ESCALINATA

e – LUGAR Playa Santa Rosa

b – FECHA (10-4-58) Diez de Abril de 1958

c – DATOS DE MAREAS EN CALLAO

Pleamar Hora	Pleamar Alt piés	Bajamar Hora	Bajamar Alt piés
1136	3 0	0419	0 9
2347	1 9	1846	1 3

d – DISTANCIA DE LOS ARENOMETROS A LA LINEA HUMEDA DEL OLEAJE O DE ALTA MAREA AL INICIO 10 m

e – VELOCIDAD PROMEDIO DEL VIENTO e 1 6 m

ARENOMETRO No. 1
A 20 m al S de la escalinata

TUBO No	HORA Inicio	EXPOSICION Término	ARENA DEPOSITADA EN CADA TUBO POR VIENTO mg	PORCENTAJE DEL PESO TOTAL %	ALTURA SOBRE EL SUELO DE LA TANGENTE INFERIOR A LA BOCA DEL TUBO
1	1530	1800	332	66,00	0.00
2	"	"	120.	23 86	2 12
3	"	"	42		4 24
4	"	"	-		6 36
5	"	"	5		8 48
6	"	"	2		10 61
7	"	"	1		12 73
8	"	"	-		14 85
9	"	"	1.	10 14	16 97
Peso total en mg			503.	100 00	

Tiempo total de exposición 150 minutos

ARENOMETRO No. 2

TUBO No	HORA Inicio	EXPOSICION Término	ARENA DEPOSITADA EN CADA TUBO POR VIENTO mg	PORCENTAJE DEL PESO TOTAL %	ALTURA SOBRE EL SUELO DE LA TANGENTE INFERIOR A LA BOCA DEL TUBO
1	1530	1800	2 917	58 74	0 00
2	"	"	1 288	25 94	2 12
3	"	"	497		4 24
4	"	"	172		6 36
5	"	"	61		8 48
6	"	"	19		10 61
7	"	"	7		12 73
8	"	"	3		14 85
9	"	"	1		16 97
10	"	"	1.	15,32	19,09
Peso Total en mg			4 966	100,00	

Tiempo total de exposición 150 minutos

Experimento V

EXPERIENCIA CON DOS BZ UNO A 20.m AL N.DE LA ESCALINATA Y OTRO 80.m AL SUR DE ELLA

a – LUGAR: Playa de Santa Rosa b – FECHA (12-4-58)Doce de Abril de 1958

c – DATOS DE MAREAS EN

Pleamar Hora	Pleamar Alt.piés	Bajamar Hora	Bajamar Alt.piés
0125	2 0	0701	1,2
1356	2.9	2056	1.1

d.– DISTANCIA DE LOS ARENOMETROS A LA LINEA HUMEDA DE OLEAJE O DE ALTA MAREA AL INICIO: 10 m

e – VELOCIDAD PROMEDIO DEL VIENTO A 1,6 m: 4 66 m/s con ráfagas fuertes

ARENOMETRO No. 1 Colocado 20,m al S. de la escalinata.

TUBO No	HORA Inicio	EXPOSICION Término	ARENA DEPOSITADA EN CADA TUBO POR VIENTO mg	PORCENTAJE DEL PESO TOTAL %	ALTURA SOBRE EL SUELO DE LA TANGENTE INFERIOR A LA BOCA DEL TUBO
1	1535	1805	33.862.	55.64	0,00
2	"	"	17.281.	28.40	2,12
3	"	"	5.923		4.24
4	"	"	2 906		6 36
5	"	"	598.		8,48
6	"	"	188.		10 61
7	"	"	61.		12 73
8	"	"	22.		14.85
9	"	"	8.		16 97
10	"	"	4.		19,09
11	"	"	2.		21.21
12	"	"	2.	15,96	23 33
Peso total en mg.			60,857.	100.00	

ARENOMETRO No. 2 Colocado 20. m al N.

TUBO No.	HORA Inicio	EXPOSICION Término	ARENA DEPOSITADA EN CADA TUBO POR VIENTO mg	PORCENTAJE DEL PESO TOTAL %	ALTURA SOBRE EL SUELO DE LA TANGENTE INFERIOR A LA BOCA DEL TUBO
1	1530	1800	32,135	47,90	0,00
2	"	"	20.923.	31.18	2,12
3	"	"	8 626.		4,24
4	"	"	3 300.		6,36
5	"	"	1.255.		8,48
6	"	"	511.		10,61
7	"	"	194.		12 73
8	"	"	76.		14,85
9	"	"	37.		16,97
10	"	"	20.		19,09
11	"	"	10.		21,21
12	"	"	6.	20,92	
Peso total en milig.			67.095.	100 00	

ANEXO NO. 6

Planos mostrando las áreas de captación

AD = Diámetro interior del tubo de prueba = 13mm

AB = A'B' = Proyección vertical del eje menor de la elipse de captación

real = AD x sen 45° = 13mm x 0 7071 = 9 19 mm

Area elipse de captación = $\frac{\pi}{4}$ x eje mayor x eje menor = 0 7854x13 x 9 19

Area elipse de captación = 93 83mm^2 = ± 1cm^2

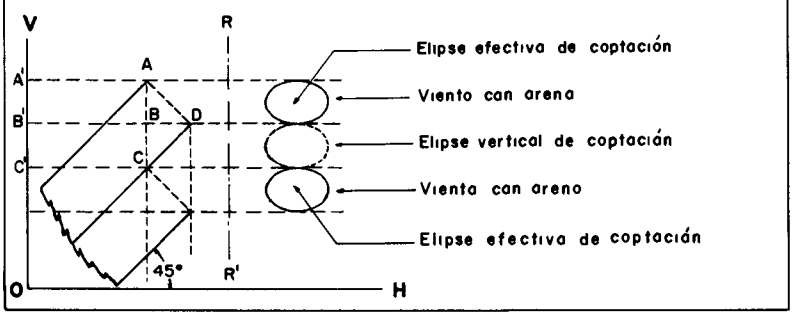

CHAPTER 22

EXPERIMENTAL STUDY OF DUNE BUILDING WITH SAND FENCES

Rudolph P. Savage
Hydraulic Engineer, Beach Erosion Board
Department of the Army, Washington D. C.

ABSTRACT

In 1957 the State of North Carolina, in cooperation with the Beach Erosion Board and the Wilmington District of the Corps of Engineers undertook an experimental dune building study on the Outer Banks of North Carolina. The experimental study consists of the construction of various types and arrangements of sand fences to determine the fence type and arrangement most effective in building a dune by trapping windblown sand. Four miles of experimental fencing were constructed in 1960. During the following year, four sets of profiles were made to determine the sand accumulation of the fences and a rather intermittent wind record was made in the area. The performance of the various fence types and arrangements has been compared and some conclusions have been reached concerning the best fence type and arrangement.

INTRODUCTION

The Outer Banks of North Carolina is a series of sand barrier islands which lie between the Atlantic Ocean and the mainland. The islands are separated from the mainland by a series of shallow sounds varying in width from 1 to 20 miles and are broken by several inlets, some as much as 1 mile wide. The Outer Banks form a protective barrier between the Atlantic Ocean and the mainland and serve as the basis for some recreational and commercial activities based on the hunting and fishing potentialities of the area.

Core Banks is that part of the Outer Banks that lies between Portsmouth Island and Cape Lookout (Figure 1). The islands composing Core Banks presently range from 1/4 to 1/2 mile in width. While in historic times they may have been high and covered with lush vegetation, the disappearance of the dune formations now allows waves to wash completely across the barrier during storms. This frequently results in the opening of temporary inlets that serve to increase the rate of erosion of the islands.

In 1957, after the rash of hurricanes which swept the North Carolina coast in the early and mid 1950's, officials of the State became quite concerned about the condition of North Carolina's barrier islands, especially those in the Core Banks area. It was felt that if the islands were permitted to deteriorate any further, they might no longer provide protection for the mainland from the waves and surges of hurricanes and other storms.

EXPERIMENTAL STUDY OF DUNE BUILDING WITH SAND FENCES

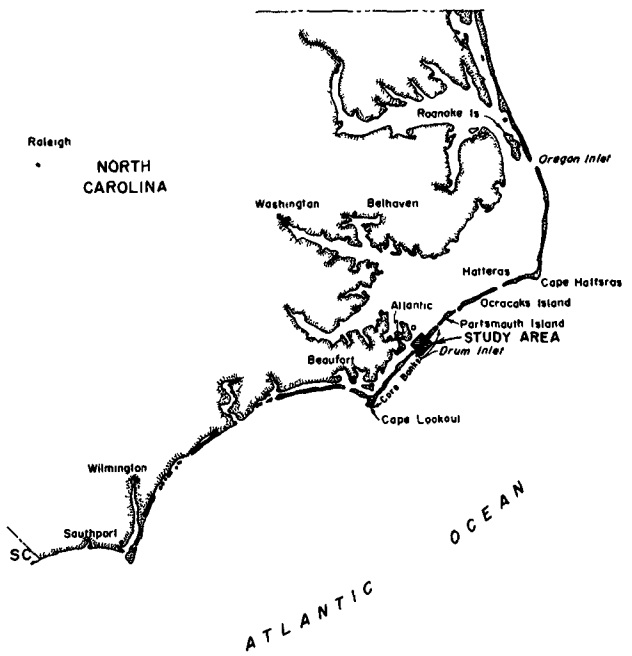

Fig. 1. Location Map.

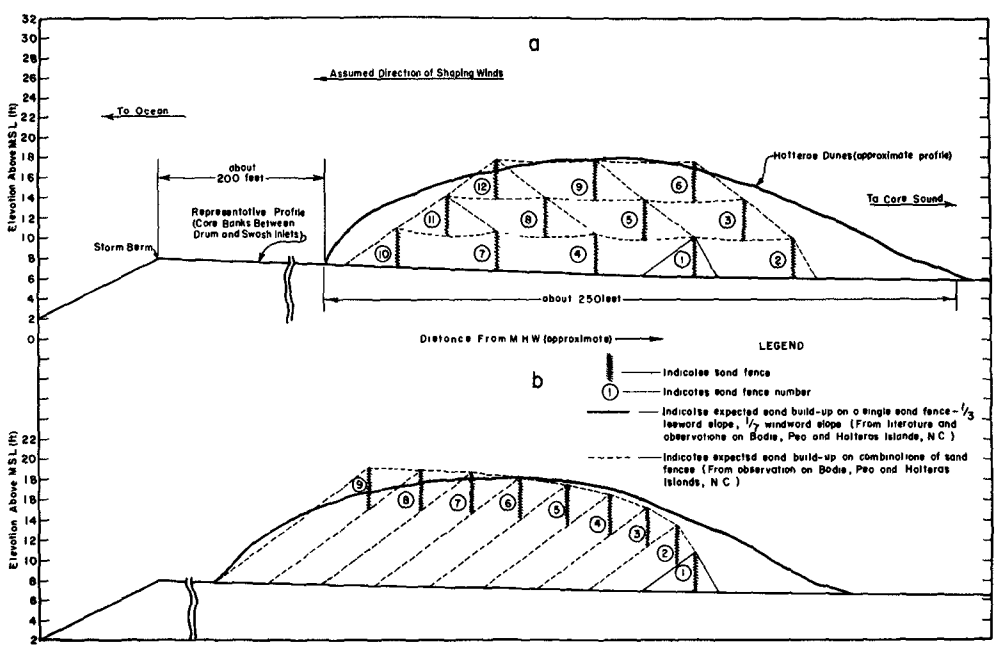

Fig. 2. Proposed Programs for Building a Barrier Dune on Core Banks.

As a result, the State in 1957 asked the Beach Erosion Board staff to enter into a cooperative research study aimed at developing a method for restoring the dunes along Core Banks. The Beach Erosion Board staff indicated that sand fencing might be used to restore the dunes and agreed to enter into a cooperative research study to determine by experimental field installations the comparable effectiveness of various types of sand fences and sand fence arrangements in restoring the dunes. The final cooperative arrangement provided that the State would provide fencing and install it in the study area. The Beach Erosion Board staff would provide consultative advice in setting up and conducting the program of study and furnish the instrumentation required for the study. Since the study area was a part of an area which was to be the subject of a cooperative beach erosion control study by the Corps of Engineers, the District Engineer in Wilmington was interested in the study and came into the cooperative arrangement to provide personnel for making field measurements.

PROPOSED STUDY PROGRAM

In October, 1957, the Beach Erosion Board submitted a proposed study program to the State which covered the setting up of the study and the measurements to be taken during the first year. The study program visualized as its objective the construction of a barrier dune about 500 feet from the sea to a height of +20 feet MSL with a base width of about 300 feet. Two possible methods of constructing the dune with sand fencing were presented (see Figure 2). Using method (a) of this Figure, fences 1 and 2 would be installed and allowed to fill by installing either fence first and installing the other after the first had filled, or by installing them both at the same time and allowing them to fill together. Fence 3 would then be installed atop the accumulation of fences 1 and 2. Fence 4 would be installed concurrently with fence 3 or after fence 3 had filled. Fence 5 would be installed after fence 4 had filled and then fences 6 and 7 would be added. This process would be followed, using the fences in numerical order, to achieve the desired dune profile. Using method (b), fence 1 would be installed and allowed to fill. Fence 2 would be constructed 2/3 of the distance up the front slope of the accumulation of fence 1 and allowed to fill. Fence 3 would then be constructed 2/3 of the distance up the front of the accumulation of fences 1 and 2 and allowed to fill. This process would be continued until the desired dune profile had been created.

In order to obtain the information needed to use the sand fences efficiently and economically, the study program proposed initial experimentation with 21 sections of fencing, each about 1,000 feet in length, along Core Banks just north of Drum Inlet. It was proposed that two types of fencing be used - brush fencing and snow fencing. Each of these fence types would be constructed in three arrangements (see Figure 3). Each fence type and arrangement would be tested as a single fence and as a double fence (two fences side-by-side) to establish their relative

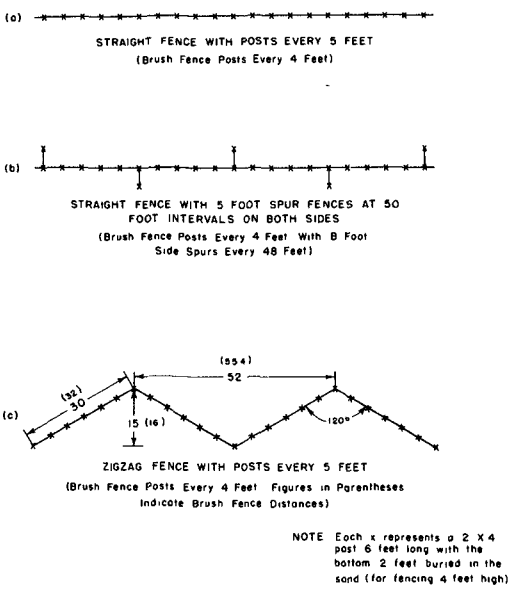

Fig. 3. Proposed Sand Fence Arrangements.

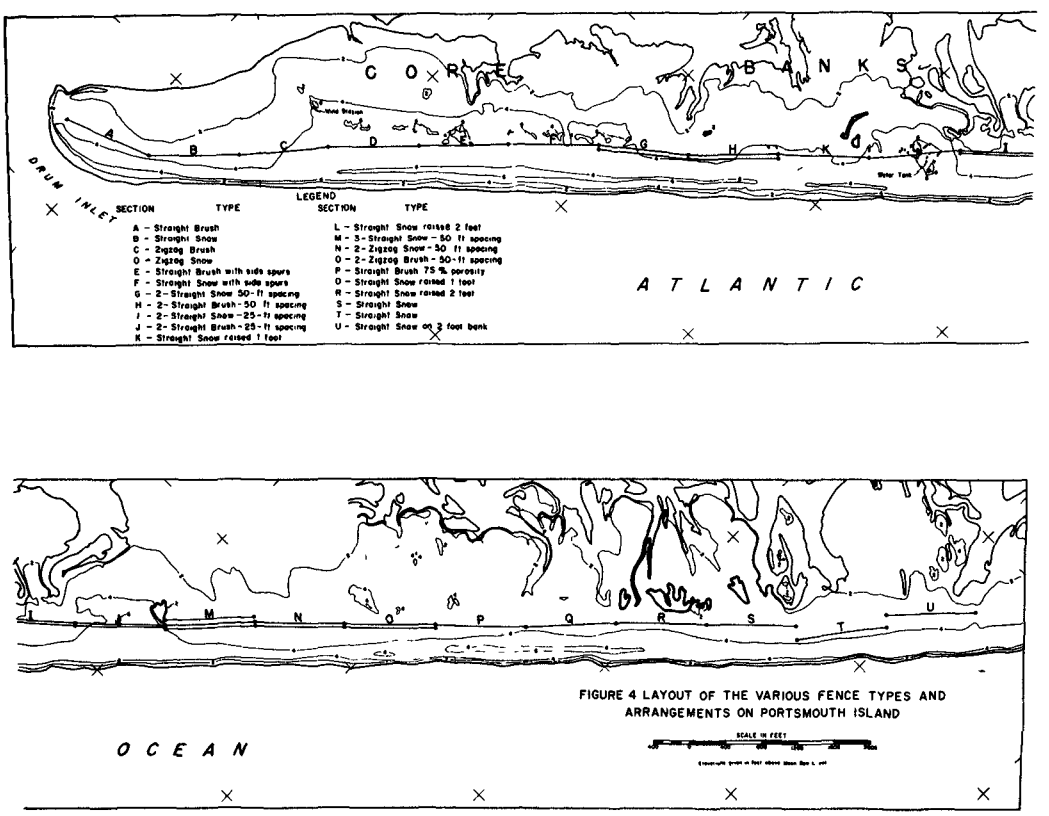

Fig. 4. Layout of the Various Fence Types and Arrangements on Core Banks.

sand trapping efficiencies and to determine the best spacing between multiple fences. To determine the best spacing between multiple fence sections, fence spacings of 25 and 50 feet were recommended for initial testing. In addition, it was proposed that two sections of the straight snow fencing be constructed with the bottom of the fencing one foot off the ground and that two sections be constructed with the bottom of the fencing two feet off the ground. This arrangement was proposed to determine whether or not the effective height of the fencing could be increased by constructing it initially in this higher position. The construction of one section of brush fencing atop a 2-foot bulldozed dune was also proposed to evaluate starting the fencing on an artificial dune.

It was proposed that the sand accumulation of the fences be measured by periodic surveys across three ranges for each fence section - one in the middle of the fence section and one 250 feet on either side of the middle range. The proposed surveys covered enough distance landward and seaward of the fences to include all of the area in which there would be any sand accumulation.

Measurements of the winds, existing sand characteristics, and other natural conditions in the study area were considered desirable in the hope that some data might be obtained on the relationship between the winds and the rate of sand movement.

CONDUCT OF THE STUDY

The Beach Erosion Board's recommendations were accepted by the State of North Carolina and the fences were installed on Core Banks in late 1960 and early 1961. The layout of the various fence types and arrangements is shown on Figure 4. The contours show the island condition before the fences were installed.

Cross-section surveys of the sand accumulations during the year were made by the Wilmington District personnel in December 1960, April 1961, and July 1961, and October 1961.

A wind station was installed in the study area (see Figure 4) in April 1961. The station was installed in a steel tower with the anemometer and wind direction indicator devices approximately 30 feet above ground level. Since no electrical power was available locally, the recording mechanism was spring wound.

RESULTS OF THE FIRST YEAR OF THE STUDY

Considerable difficulty developed with the recording mechanism of the wind station and the records from it were somewhat intermittent,

however, records were obtained during most of the period from April to December 1961. This data is shown on Figure 5. Wind data available from the U. S. Weather Bureau station at Hatteras, North Carolina, about 45 miles northwest of the temporary station on Core Banks, are shown in Figure 6. In the Figures, it has been assumed that the sand transporting capacity of the winds is proportional to the third power of the wind velocity and the relative transporting capacities of the sand-moving winds from various directions are shown. The Figures show that the onshore transporting capacity is relatively small, especially the eastern and southeastern components. Also, the transporting capacity of the winds parallel to the fences is relatively large. Since most of the sand available for movement is on the seaward side of the fences, the fences in the study area operated at a considerable disadvantage. However, the sand fences were effective in trapping windblown sand. Even fences which were installed in or near areas of ponded water on the island completely filled in the first year after their installation.

Some of the fencing was destroyed by waves which overtopped the front of the island, and since the island then slopes gently toward the sound, washed across the island and into the sound. Too, the fences were subjected to some flooding by high tides from the sound, but this is thought to have been much less likely to have caused damage than the waves overtopping the ocean side of the island. It is estimated that approximately 50 percent of the fencing had been damaged by October 1961. The area was affected by Hurricane Esther in September 1961, which may have caused a considerable portion of the damage.

Volumes of sand collected by the fences are given in Table 1. Table 2 contains summaries of data for all single-fence sections, all double-fence sections, and the one triple-fence section. The values given in these tables are the volume of sand collected by each test fence section in cubic yards per foot of beach. These figures show that, on the average, the fence sections caught about 2.5 cubic yards of sand per foot of beach during the first 8 or 9 months after installation.

It should be noted that these values are given in volume per foot of beach and not per foot of fence. However, volume per foot of beach becomes volume per foot of fence where single-fence sections were used. Too, in arriving at these values, fence sections which were damaged or lost were not considered. This was done by ignoring the cross-sections at points where the fence was lost and averaging the remaining cross-sections available for the experimental section under consideration.

Tables 3 and 4 have been prepared from the data given in Table 1. Table 3 is a comparison of the volume of sand trapped by various brush

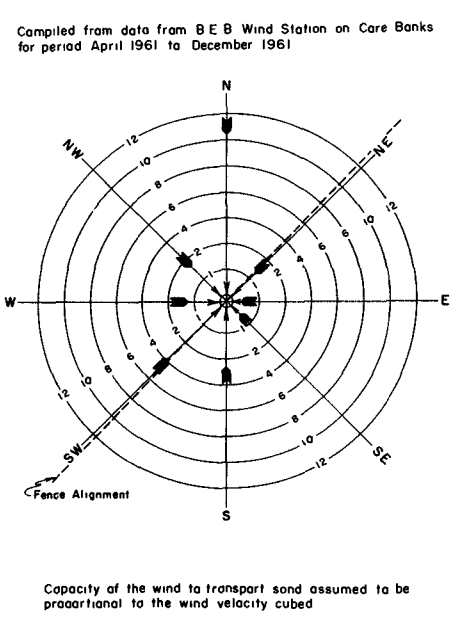

Fig. 5. Relative Transporting Capacity of the Sand-Moving Winds in the Study Area (B.E.B. Data.

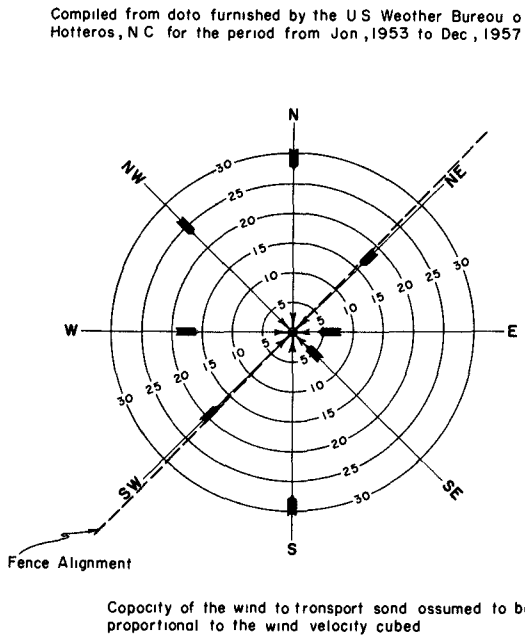

Fig. 6. Relative Transporting Capacit of the Sand-Moving Winds in the Stud Area (U. S. Weather Bureau Data).

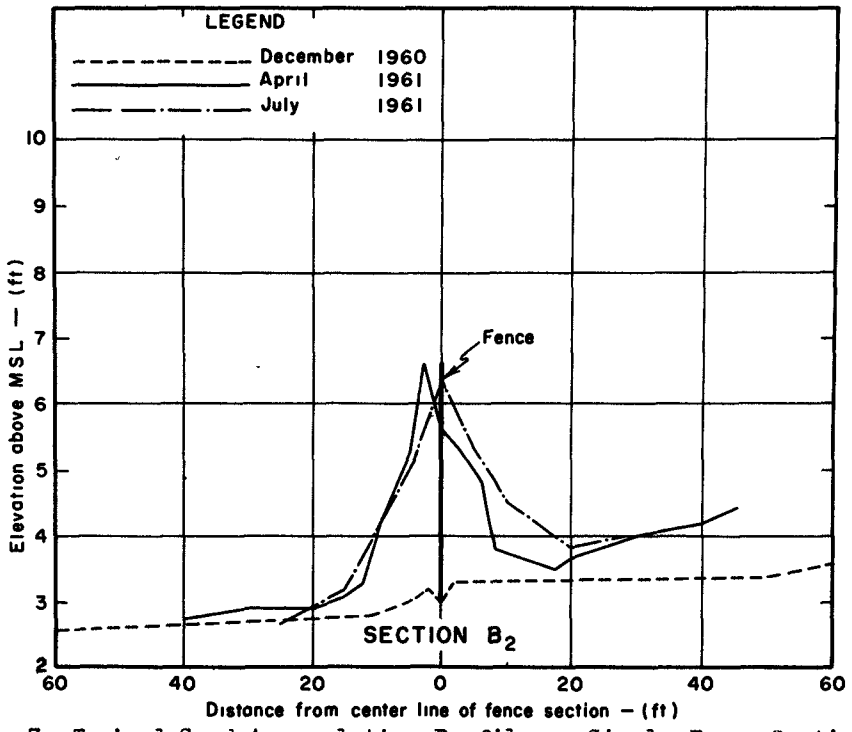

Fig. 7. Typical Sand Accumulation Profiles - Single Fence Section.

EXPERIMENTAL STUDY OF DUNE BUILDING WITH SAND FENCES

TABLE 1

VOLUME OF SAND COLLECTED BY SAND FENCES ON CORE BANKS
Cubic Yards Per Foot of Beach

Section	Type	Installation* to December 1960	December 1960 to April 1961	April 1961 to July 1961	Installation to July 1961
A.	St. Brush	0	0.96	1.04	2.00
B.	St. Snow	0	2.27	0.35	2.62
C.	Zigzag Brush	0.89	1.39	0.24	2.52
D.	Zigzag Snow	0.59	1.20	0.59	2.38
E.	St. Brush with side spurs	0.51	0.87	0.51	1.89
F.	St. Snow with side spurs	0.44	0.96	0.37	1.77
G.	2-St. Snow 50-ft. spacing	0.37	1.98	0.51	2.86
H.	2-St. Brush 50-ft. spacing	0.51	1.58	0.87	2.96
I.	2-St. Snow 25-ft. spacing	0.56	1.64	0.23	2.43
J.	2-St. Brush 25-ft. spacing	0.15	1.17	0.91	2.23
K.	St. Snow raised 1 ft.	0.37	0.77	1.14	2.28
L.	St. Snow raised 2 ft.	0	0	0	0
M.	3-St. Snow 50-ft. spacing	0.56	1.82	0.42	2.80
N.	2-Zigzag snow 50-ft. spacing	0.33	2.31	0.48	3.12
O.	2-Zigzag Brush 50-ft. spacing	1.09	1.36	0.80	3.25
P.	St. Brush 25% Porosity	1.17	1.06	0.74	2.97
Q.	St. Snow raised 1 ft.	0	1.82	0.84	2.66
R.	St. Snow raised 2 ft.	0	0	0	0
S.	St. Snow	0.60	1.75	0.18	2.53
T.	St. Snow	0.80	1.57	0.17	2.54
U.	St. Snow on 2-ft. bank	0	0.86	0.34	1.20
	Average all fences**	0.47	1.44	0.57	2.47

*Installation of Sections A-T made in October-November 1960

* Installation of Section U made in January 1961

** Does not include Sections L&R

TABLE 2

VOLUMES OF SAND COLLECTED BY SAND FENCES ON CORE BANKS FROM INSTALLATION TO JULY 1961

Section	Type	Cubic Yards per foot of beach
	Single-Fence Sections	
A.	Straight Brush	2.00
B.	Straight Snow	2.62
C.	Zigzag Brush	2.52
D.	Zigzag Snow	2.38
E.	Straight Brush with Spurs	1.89
F.	Straight Snow with Spurs	1.77
K.	Straight Snow raised 1 ft.	2.28
L.	Straight Snow raised 2 ft.	2.22
P.	Brush fence 75% Porosity	2.97
Q.	Straight Snow raised 1 ft.	2.66
R.	Straight Snow raised 2 ft.	--
S.	Straight Snow	2.53
T.	Straight Snow	2.54
U.	Straight Brush on 2 ft. Bank	1.20
	Average of all single fence sections	2.28
	Double-Fence Sections	
H.	Straight Brush 50-ft. spacing	2.96
I.	Straignt Snow 25-ft. spacing	2.43
G.	Straight Snow 50-ft. spacing	2.86
J.	Straight Brush 25-ft. spacing	2.23
O.	Zigzag Brush 50-ft. spacing	3.25
N.	Zigzag Snow 50-ft. spacing	3.12
	Average of all double fence sections	2.81
	Triple-Fence Sections	
M.	Straight Snow 50-ft. spacing	2.80

TABLE 3

COMPARISON OF THE VOLUME* OF SAND TRAPPED BY VARIOUS BRUSH FENCE SECTIONS WITH THE VOLUME TRAPPED BY COMPARABLE SNOW FENCE SECTIONS

Section	Type	Volume-Installation To July 1961	Ratio Brush/Snow
C.	Brush	2.52	1.06
D.	Snow	2.38	
E.	Brush	1.89	1.07
F.	Snow	1.77	
H.	Brush	2.96	1.04
G.	Snow	2.86	
J.	Brush	2.23	0.92
I.	Snow	2.43	
O.	Brush	3.25	1.04
N.	Snow	3.12	

*Volume given in cubic yards trapped per foot of beach.

TABLE 4

COMPARISON OF THE VOLUME* OF SAND TRAPPED BY STRAIGHT FENCING WITH THE VOLUME TRAPPED BY ZIGZAG AND SIDE SPUR FENCING

Section	Type	Volume-Installation to July 1961
B.	Straight	2.62
S.	Straight	2.53
T.	Straight	2.54
	Average	2.56
C.	Zigzag Brush	2.52
D.	Zigzag Snow	2.38
E.	St. Brush with Side Spurs	1.89
F.	St. Snow with Side Spurs	1.77

*Volume given in cubic yards of sand trapped per foot of beach.

Fig. 8. Filled Single Fence Section.

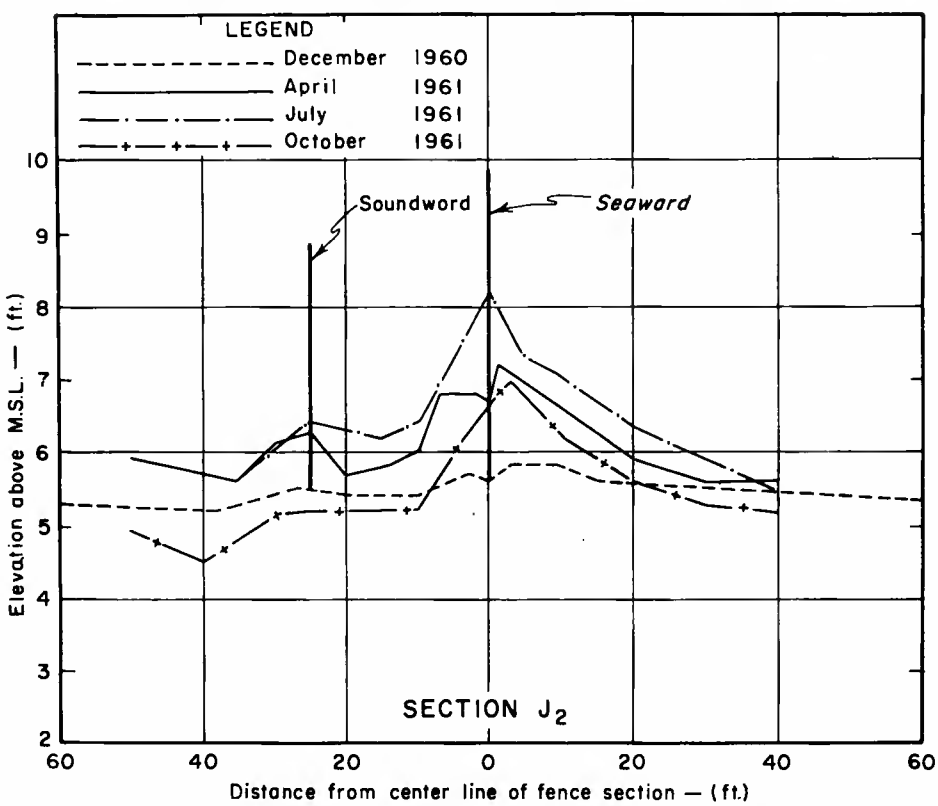

Fig. 9. Typical Sand Accumulation Profiles, Double Fence Section, 25-foot Spacing.

fence sections compared with the volume of sand trapped by comparable snow fence sections. Since the brush-to-snow ratio averages about 1.05, with one unexplained exception of 0.92, it appears that generally brush fencing traps about 5 percent more sand than comparable snow fencing. However, in this study, installed brush fencing cost about twice as much as installed snow fencing. Therefore, the use of brush fencing would appear to be economically unjustified.

In Table 4, the average volume of sand trapped by three different straight fence sections (Figure 3a) is compared with the volume of sand trapped by single zigzag fences (Figure 3b) and single fence with side spurs (Figure 3c). From this comparison it appears that the straight fences trap and hold more sand than the other configurations, at least in the study area over this period of measurement. Typical sand accumulation profiles for a single fence section are shown in Figure 7, and a filled fence section is shown in Figure 8.

The performance of the multiple-fence sections (double fence rows) which were included in the study to determine if a barrier dune could be built using the method shown in Figure 2a were generally disappointing, in that the center area between the fences did not fill significantly (see Figures 9, 10, and 11). If the area between the fences will not fill, little progress can be made toward heightening the dune by placing new fences on the accumulation between the existing fences. However, some caution should be exercised before this plan is completely abandoned, for the following reason. Comparison of the sand trapped by the single-fence sections and the multiple-fence sections shows that the single-fence sections trapped almost as much sand as the multiple fence sections (about 2.3 compared to 2.8 cubic yards of sand per lineal foot of beach) even though at the end of the year most of the multiple-fence sections had ample sand trapping capacity remaining. A possible and logical explanation for this is that the fences trapped essentially all the sand which was moving during the year, and thus the multiple fence sections had not yet been filled to capacity. If this is true, the multiple-fence sections have not been amply tested in the first year of the study and any conclusions which may be drawn about their total effectiveness would be premature. The first year of the study does indicate, however, that if multiple-fence sections are to be used, the 50-foot spacing between fences is too large. The 25-foot spacing between fences also appears to be too large, but enough doubt about this remains to justify continuing this phase of the tests for another year.

The concept of installing the fences initially on a 2-foot bank appears to have both advantages and disadvantages. One advantage is that under conditions such as those existing on Core Banks, the initial 2-foot bank protects the fence and makes it more difficult for the water to destroy the fencing. However, as a disadvantage, the fencing

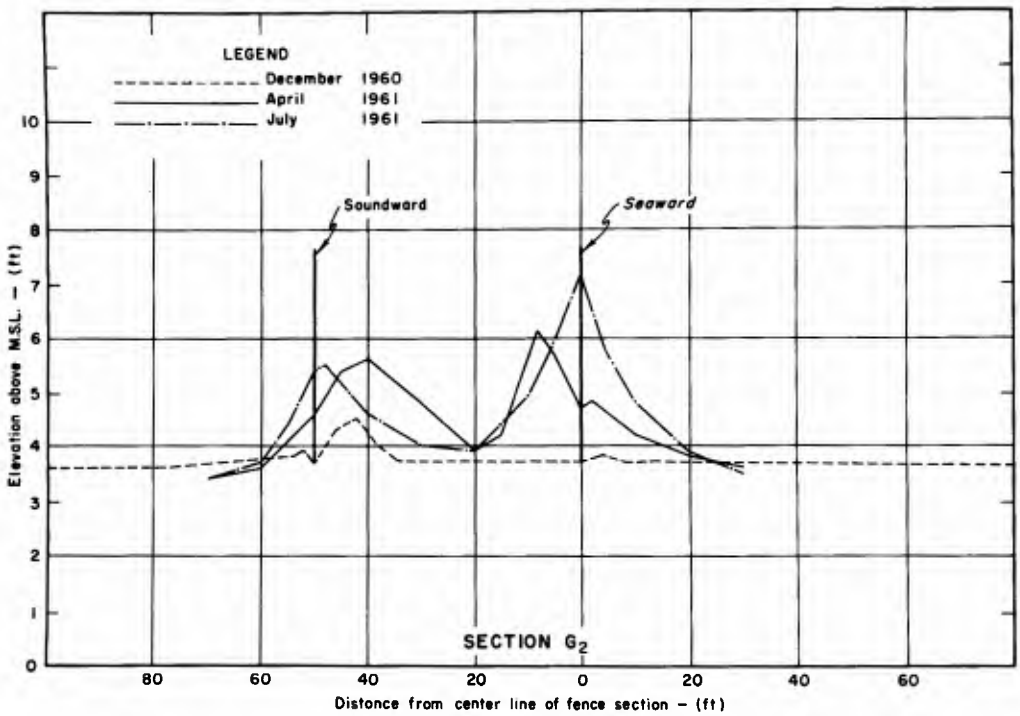

Fig. 10. Typical Sand Accumulation Profiles, Double Fence Section, 50-Foot Spacing.

Fig. 11. Partially Filled Double Fence Section, 50-foot Spacing.

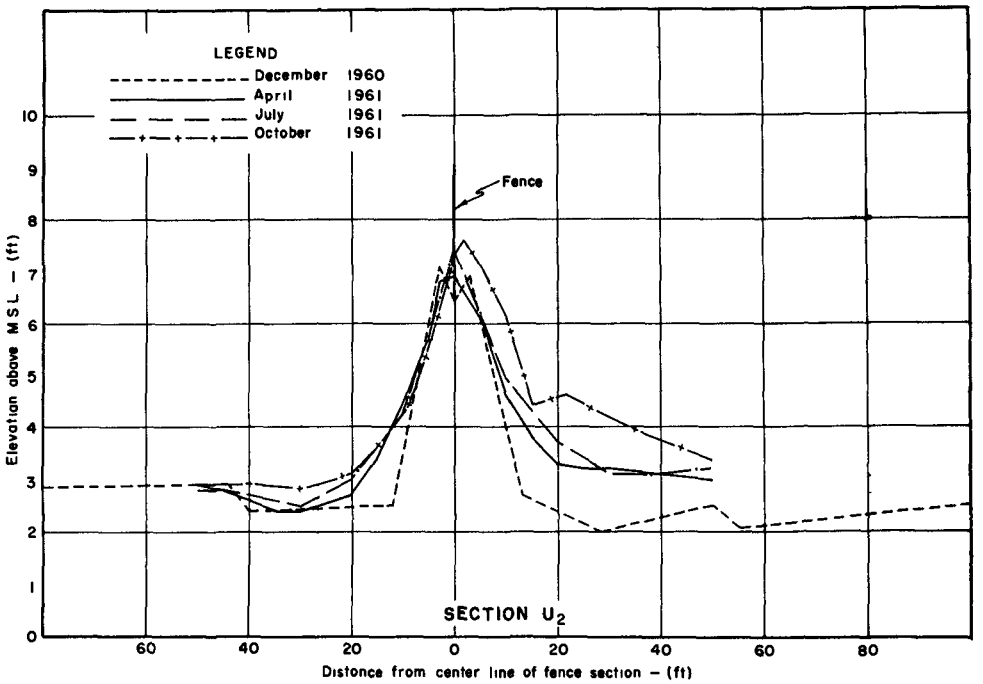

Fig. 12. Sand Accumulation Profiles, Fence on Bulldozed Dune.

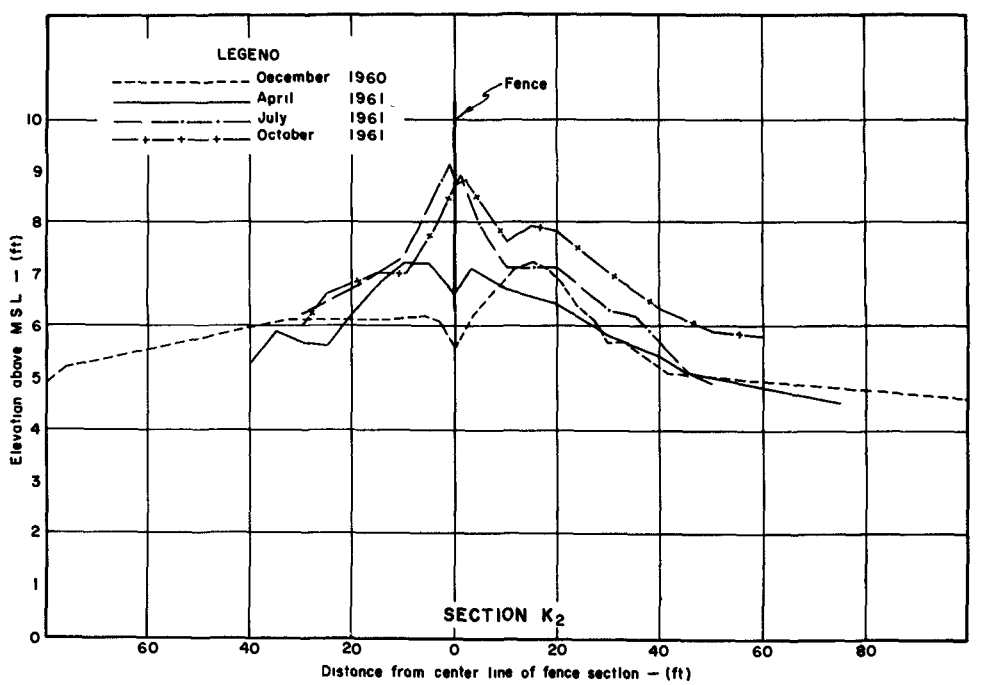

Fig. 13. Sand Accumulation Profiles Single Snow Fencing with Bottom One Foot off the Ground.

which was installed on the 2-foot bank was among the slowest of the fences in filling and, at the end of the year, was the fence, other than the fences which were completely lost, which had trapped the least of any of the test fence sections. (See Figure 12). The other fences in the immediate vicinity of this fence section had trapped quantities of sand which compare very favorably with those of the other fence sections along the test area. Therefore, it can be concluded that fences which are set at the general ground level fill more quickly than fences which are placed on an initial 2-foot bank.

The one section of straight brush fencing of 25 percent porosity (Section P) trapped more sand than either comparable brush or snow fence sections having a porosity of 50 percent. The fencing of Section P trapped 2.97 cubic yards per foot of beach while the average volume trapped for other comparable test snow-fence sections, all with a porosity of 50 percent, was 2.56 cubic yards per foot of beach (see Tables 1 and 4).

From the performance of Section K, it appears that it is possible to increase the effective height of sand fences one foot by leaving a one-foot space between the bottom of the fence and the sand when the fence is installed (see Figure 13). However, this procedure appears to have certain disadvantages, particularly in this study area, in that the fencing does not fill as quickly as fencing which is initially set on the ground and would be susceptible to loss by water damage for a longer time.

Apparently, increasing the height of the fences by 2 feet is impractical in that the posts must be set much deeper in the sand than the posts of fencing set at ground level. Thus, the advantage gained by having the fence taller may not justify the extra effort involved in setting the posts in the sand well enough to hold the heightened fence section. However, this conclusion must be tentative because the higher fences which were tested did not remain upright long enough to trap sand and, therefore, their efficiency in trapping sand is still not known.

PLANNED CONTINUATION OF THE STUDY

It is planned that this will be a continuing study and preparations are now being made for the installation of new fencing in the study area in November 1962.

The objectives of the program for the coming year will be:

(a) To establish new fences on top of the existing sand fence accumulations to determine if the desired dune section can be created using the method shown in Figure 2b.

(b) To establish a dune at least one fence (4 feet) in height along the entire experimental area. Since the indications from the first year of study are that the straight slat-type snow fencing traps essentially as much sand as either the zigzag configuration or the spur-type fencing it has been recommended that only straight snow fencing be used.

(c) To determine to a higher degree of accuracy the conditions which are necessary for significant sand movement. This is believed to be desirable since the people who frequently visit the island report that for perhaps weeks and months the sand accumulation of the fences remains constant. However, over a few hours or days during favorable conditions, large quantities of sand are trapped by the fences.

(d) To test some of the new plastic materials becoming available for use as sand fences.

It appears from the results of the first year of observations that some type of continuous observation and maintenance program will be required to successfully build a barrier dune on Core Banks. Under such a program, any fencing which is lost would be replaced as soon as possible. Thus every favorable sand-moving condition would be utilized to fill in the weak spots in the dune and deterioration of the remaining dune would be minimized.

CONCLUSIONS

From the results of the first year of the experimental study, the following conclusions appear to be justified:

1. Single fencing which is initially 4 feet high appears to hold about 3 cubic yards of sand per lineal foot of fencing. However, during the first 7 months of this study, the average volume of sand trapped by all of the fence sections, single and double, was about 2.5 cubic yards per lineal foot of beach.

2. Brush fencing apparently traps about 5 percent more sand than comparable snow fencing. However, brush fencing installed costs approximately twice as much as snow fencing installed. Therefore, the use of brush fencing is not economically justified.

3. Straight fencing appears to trap and hold more sand than either straight fencing with side spurs or zigzag fencing.

4. A 50-foot spacing between two fences installed simultaneously is too large if it is desired that the area between the fences fill significantly. A 25-foot spacing appears to be somewhat too

large; however, this spacing needs to be subjected to further study.

5. The effective height of sand fencing can be increased by installing it with the bottom one foot off the ground. However, fencing installed in this manner fills slower immediately after installation than fencing set at ground level.

6. The rate of filling and final trapping capacity of fencing with a porosity of approximately 25 percent appears to be larger than that of fencing with a porosity of approximately 50 percent.

ACKNOWLEDGEMENTS

The test described and the resulting data herein, unless otherwise noted, were obtained from research conducted under the Civil Works Investigation Program of the United States Army Corps of Engineers by the Beach Erosion Board. The permission granted by the Chief of Engineers to publish this information is appreciated. The conclusions reached and the methods presented herein are those of the author and they do not necessarily reflect the policy or views of the Corps of Engineers or Chief of Engineers. The cooperation of the State of North Carolina and the Wilmington District Office of the Corps of Engineers is appreciated.

SALINA CRUZ

PART 3
COASTAL STRUCTURES AND RELATED PROBLEMS

ENSENADA

CHAPTER 23

RECENT ADVANCES IN COASTAL STRUCTURE DESIGN

Charles E. Lee
Office, Chief of Engineers
U. S. Army Corps of Engineers
Washington, D. C.

INTRODUCTION

The type and scope of work accomplished and responsibility and authority of the office to which he is attached is indicative of the interests of an author and of the information available to him. It is therefore pertinent to cover in this general section a summary of the responsibility and the delegated authority of the Corps of Engineers as regards Coastal Engineering.

The subject of recent advances in coastal structures is quite broad and complex and modern design practice incorporates old and new findings. This paper discusses various aspects of proper modern design of breakwaters and jetties with special attention to newer findings, their proper application and the means by which the findings were made.

The Corps has the responsibility for the planning, investigation, design and construction of Federal civil works navigation projects. This consists generally of harbor and channel works. Their responsibility extends to the control of all works, private or governmental, to assure that navigation will not be adversely affected. They are also charged with the responsibility of planning, investigation, design and construction of Federal civil works projects involving shore protection from wave and currents, protection from effects of hurricane, tsunamis and tidal flooding, and of beach erosion control. The accomplishment of such a mission therefore includes research of an applied nature to permit advancement in knowledge and technique. Most of this research is based on small scale model studies accomplished at the U. S. Army Engineer Waterways Experiment Station at Vicksburg, Mississippi, and at the laboratory of the Corps of Engineers Beach Erosion Board in Washington, D. C. In addition a limited number of prototype studies are being initiated in the charge of the staffs of various District Engineers.

RESEARCH

WATERWAYS EXPERIMENT STATION

Research accomplished at the Waterways Experiment Station is of two general types, Civil Works Investigations (CWI), which are applied research of a general nature, and Project Studies, which are investigations for a specific project. The combined results of these investigations and the analysis have been the subject of many reports from WES and are the basis of much advancement in the design of coastal structures, especially those

constructed of stone. Studies concerned with coastal structures include wave force on breakwaters, stability of rubble-mound breakwaters, orientation of harbor structures, effects of scale on harbor models, scale effect tests of rubble breakwaters and design of rubble wave absorbers. Project studies are many and varied. Especially for the more complex conditions, model studies are made for alignment, evaluation of effect, and stability of structures. Surge problems are also a popular subject for project model studies. These results for specific conditions are, of course, integrated into general test data for the purpose of developing design criteria. The findings of CWI and Project Studies are published as Technical Reports and Miscellaneous Papers, which are distributed throughout the Corps of Engineers and may be purchased at nominal cost by others.

BEACH EROSION BOARD LABORATORY

A wide variety of applied research generally pertaining to shore protection and beach erosion control is accomplished by the Beach Erosion Board staff. The research is of two types, Civil Works Investigation Studies, administered through the staff of Office, Chief of Engineers, and Beach Erosion Development Studies, administered by the Beach Erosion Board These studies are more or less overlapping in subject and include the following subjects, methods of by-passing sand, criteria for artificial beaches, design of shore protection structures, wave refraction and diffraction, uses of radio-active tracers in shoaling studies, and others. The results of the studies are published as Technical Memoranda and are integrated into Technical Report No. 4 at each time of its revision.

PROTOTYPE TESTS

To obtain data generally unobtainable in other ways, substantiate model data, and to give direction to future model programs, a number of prototype tests have been initiated. The locations selected for the presently proposed tests are the harbors at Umpqua River, Oregon; Morro Bay, California; Santa Cruz, California; and Nawiliwili, Maui, Hawaii. These studies have been recently undertaken and no results have yet been obtained. These studies consist generally of the following:

a. An as-built survey of the new or reconstructed structure. This includes marking of individual armor units for comparison with future surveys.

b. The installation of pressure type wave gages generally located in the deeper water to obtain a measurement of the impinging wave before it is significantly altered by structures or on-shore topography. In some cases the gage will be located on concrete blocks setting on the ocean floor and others, located in deeper water, will be placed on steel piles to eliminate loss of gage accuracy due to excessive depth.

c. Visual inspection will be made after each storm of significant amplitude. Where damages are noted in the structure, instrument type survey will be made to determine the quantity of loss of material.

d. An annual summary report will be made to record the results of the tests. It is assumed that these observations will continue over a period of 3-5 years and a completion report will be prepared upon termination of the studies. It is also probable that technical papers, based on these results, will be published in technical society publications.

CONFERENCES

Model tests and theoretical analysis are invaluable to the advancement of design techniques but equally important is the translation of the data into usable construction techniques. For instance, an almost indestructible structure can be constructed of fitted units keyed together or with units of extremely high area of contact. The fitting can be easily accomplished above the water line, but how can such complex work be accomplished beneath the water surface? Design criteria are prescribed by the Office, Chief of Engineers, based generally on past experience. As these new criteria are formulated and methods prescribed, what particular difficulties are the field offices encountering in applying these criteria and methods? To answer such questions as these and to obtain a consensus of opinion throughout the Corps of Engineers, a series of harbor design conferences were held. First, a general conference was held in Washington wherein the broad aspect was considered, and later a series of regional conferences were held to discuss specific problems of the various regions. The present criteria for the design of harbor structures have, in general, been formulated through the consideration of past experience, research accomplished at the Waterways Experiment Station and the Beach Erosion Board and through the opinions expressed in these conferences. In recent years the Corps of Engineers has placed great emphasis on the design of stone structures, both for new work and rehabilitation of existing structures. Therefore, the design portion of this paper is principally concerned with the advancements in technique of design of stone structures.

DESIGN NOTES

STRUCTURE TYPES

Rigid and Semi-rigid Structures - The principal structures of this classification are walls, revetments, breakwaters and jetties constructed of steel, concrete, timber or combinations. The principal coastal engineering features of these designs are the determination of topography, hydrography, still water elevation and wave characteristics with a final result of the specification of the forces to which the structure will be subjected. Then, with the possible exception of toe protection, the design procedures are structural in character.

Determination of still water level is made by statistical study of tides or lake levels and the selection of a frequency to be used in design. The design still water level will contain additional elevation due to hurricane surge or wind and wave set-up during storms. This feature has been covered in previous publications or is to be covered by others of this conference.

Determination of design significant wave height has been covered by others and is presented in Beach Erosion Board Technical Report No. 4. However, about 13 percent of the waves in a train are higher than the significant wave and some may severely damage or even cause complete failure of a rigid or semi-rigid structure. Therefore, it is necessary to use a wave of height within the train occurring less frequently than the significant wave. For a rigid structure it is recommended that the 1% train frequency (that is, the maximum height that occurs once in a typical 100 wave train) be used for design wave (significant height x 1.6) For semi-rigid structures a value ranging between the 10% and the 1% train frequency, based on the effect of failure on the project, is generally used. General concensus is that the 10% train frequency (significant wave x 1.1) should be used for steel sheet pile cell design, as such a structure can absorb considerable racking. If the depth of water at the structure is less than required to support the wave that is based on generation potential, depth criteria should be used to determine the height of the design wave.

Upon determination of design still water level and design wave height forces are computed based on the character os the wave upon reaching the structure.

a. For breaking waves the theory of Minikin is best for computing wave force. Studies have indicated that force is maximum when the wave approach is normal to the centerline of the structure. The effect on force of waves approaching a structure at an angle has not been adequately investigated, but investigation of this aspect is planned for the near future. Meanwhile, it is general practice to reduce computed pressures according to $\sin^2 B$, where B is the angle between the approach direction of the wave and the normal to the structure alignment. This is an unverified method and should be used with caution.

b. For unbroken waves the theory of Sainflou is best for use. For waves approaching at an angle to the structure, pressure is often reduced by straight line extrapolation between full clapotis and the design wave height, depending on the angle of approach.

c. With present knowledge, computing pressure due to broken waves may be more complex than for the other two wave types. If a wave breaks near enough to a structure some of the energy is transmitted to it. This pressure would be related to the incident velocity and the run-up on the structure. In most cases the maximum force would be that caused by the wave that would break at the depth in which the structure is located rather than a larger wave breaking seaward.

Flexible Structures - Flexible structures are those composed of stone or concrete components. Design of flexible coastal structures are based on empirical data as it is impossible to determine accurately by analytical methods the effect of the interplay of forces on the individual units. Upon wave attack a large area of the cover layer can be displaced down the slope en masse or individual units may be lifted and rolled up the

slope or rolled down the slope. Short period wind waves impinging upon a rubble-mound structure may break completely, projecting a jet of water approximately perpendicular to the slope, or they may break partially with a poorly defined jet, or they may establish an oscillatory motion of water particles along the structure front similar to the motion of a clapotis at a vertical wall. Because of the empirical nature of the basis of design, and the amount of investigation made in recent years, the discussion of rubble-mound structures is made in a separate section.

DESIGN OF RUBBLE-MOUND

Still Water Level and Design Wave - The determination of elevation of still water level and height of the design wave is computed as previously described. The equation used in the design of rubble-mound structures has been devised and evaluated on the basis of using a design wave equal to the significant wave height. There has been many discussions on the desirability of using a statistical value higher than significant wave height for use in the Hudson equation. However, due to the flexibility of the structure and to the fact that design methods are empirical in nature, the affect of using a rarer frequency is not known. Since the significant wave height is an average of the highest one-third of the waves in the train, about 13% of the waves in the train should be higher than the signif icant wave. It is assumed that the rare occurrence of these higher waves will not by themselves extricate components from the structure, that many of the units that will be slightly moved will be reinterlocked by the pounding of the smaller waves and that it is more economical to repair slight damage than to design the structure for absolute stability. The using of a slightly higher wave results in a much higher stone size requirement since wave height is cubed in the numerator of the equation.

Height and Crest Width - The height of the structure depends primarily upon the degree of protection that must be furnished, that is, the amount of overtopping that might be tolerated. The amount of overtopping is a function of the wave run-up and the width of crest. The structure crest width depends on the size of stones in the cover layer and should be wide enough to provide the necessary roadway if the structure is to be initially constructed or to be maintained from the top. In cases of relatively sever wave action, and especially if overtopping is to occur, the structure crest width should be wide enough to allow for three stones.

Cover Layer Stability - The Hudson or WES equation is generally used throughout the United States for determining the size of units and the corresponding slopes required for stability when subjected to waves. This equation is:

$$W_r = \frac{\gamma_r H^3}{K_\Delta (S_r - 1)^3 \cot \alpha} \qquad (1$$

where,

W_r = weight of the individual units in pounds.

γ_r = the specific weight of the component material.

K_Δ = experimentally determined coefficient.

S_r = specific gravity of the stone or cover unit material relative to the fluid in which it is immersed.

α = the angle of structure face.

Most coastal engineers are familiar with the application of this equation. Therefore, these remarks will be in reference to the evaluation of K_Δ and indications from recent model studies.

Based principally upon model studies using nonbreaking waves but with some amount of data from project studies using breaking waves, the K_Δ values shown in Table 1 are recommended for use as averaged values. These values should be modified depending upon the shape and roughness of the stones, the method of placement, the frequency of occurrence of the design wave, and the economics of frequent repair. The cover layers composed of units of the weight determined by this equation should be arranged as follows: (a) On structures located in relatively deep water and of sufficient height to eliminate overtopping, the cover stone should extend across the crest and down the seaward slope to a point one wave height below lowest still water. Below this elevation the stone may be reduced to one-half the size. The stone on the inside slope should be based on the size waves that can be generated within the harbor. (b) For structures in shallow water and no overtopping, the cover stone should extend across the crest and down the seaward slope to the bottom. (c) When overtopping is to occur, the large cover stone should extend as before on the seaward side as well as to at least still water elevation on the harbor side.

There are many who believe that for most conditions graded riprap provides the most economical and effective covering for a flexible structur While this method may be most economical for small structures, as the entir quarry production could probably be used, it is not effective for protectio from larger waves. Studies made for the design of riprap cover layers for railroad relocation fills at Ice Harbor and John Day Lock and Dam projects indicated riprap cover layers were not economical for wave heights greater than about 6 feet.

This conclusion was based on the following equation developed by Hudson for riprap sizes.

$$W_{50} = \frac{\gamma_r \, H_D^3}{K_{RR} \, (S_r - 1)^3 \, \text{Cot} \, \alpha} \qquad (2)$$

and,

$$W_{max} = 3.6\ (W_{50}) \qquad (3$$

and,

$$W_{min} = 0.2\ (W_{50}) \qquad (4$$

where,

W_{50} = 50 percent size by weight of cover material, in pounds,

H_D = Design wave height for selected damage criterion, in feet.

K_{RR} = Experimental coefficient for riprap.

W_{max} = Weight of maximum size of riprap in the gradation, in pounds.

W_{min} = Weight of minimum size of riprap in the gradation, in pounds.

The average K_{RR} values determined in the model was 1.3 for a water depth of 20 feet and 1.7 for a water depth of 40 feet.

Table 1

AVERAGE K_Δ VALUES

ARMOR	CONDITION*			
	1	2	3	4
Rounded Stone, 2 layers pell mell	2.6	2.5	2.4	2.0
Rough Stone, 2 layers pell mell	3.5	3.0	2.9	2.5
Rough Stone, 2 layers placed**	5.5	5.0	4.5	3.5
Tribars, 2 layers pell mell	10.	8.5	7.5	5.0
Tribars, 1 layer uniform***	15	12	9.5	7.5
Tetrapods, 2 layers, pell mell	8.5	7.5	6.5	4.5
Quadripods, 2 layers pell mell	8.5	7.5	6.5	4.5

* Condition
1. Trunk, nonbreaking waves
2. Trunk, breaking waves
3. Conical head, non-breaking waves
4. Conical head, breaking waves

** Good placement with centerline of long diameter of stone placed normal to structure face.

*** For special conditions.

One of the major problems in the construction of structures subjected to wave action is the actual lifting and placing of the larger units. This problem became critical at Kahului, Hawaii since the nearness of the channe to the structures prevented flattening of the slope. With a 34-foot design

wave, concrete units weighing 35 tons were stable on a 1 on 3 slope except along the portion of the head where the jet action occurred. Available equipment would handle a maximum of 35 tons with a reasonable reach. The largest equipment available for limited length of time could be rigged and counterweighted so that 50 tons could be lifted with a maximum reach of about 50 feet. To compensate for these limiting conditions, units weighing 50 tons are to be placed in the area where damage occurs and 35-ton units along the remainder. Beneath a point one wave height below design still water level 18-ton units will be used.

A similar remedy was contemplated for use at the Oregon Harbor of Siuslaw, Umpqua and Coos Bay. Suitable stone was available for use in these harbors and a reasonable percentage could be expected to break in pieces in which the longest dimension would be about three times the smaller dimension. For these cases, the stone is to be placed in the critical areas with the long dimension perpendicular to the structure face. This additional friction and keying action will provide the desired stability. It must be recognized that such special placement can be accomplished only above the water surface, therefore, flatter slopes or larger units are required below mean still water level.

Both of these special placement procedures were tested in wave flumes at the Waterways Experiment Station. These tests indicated that such special placement is desirable especially in cases where the range in direction of wave approach is limited.

Tests using non-breaking waves have shown a more or less constant pattern of energy effect vertically along a structure. Breaking waves have shown greater variability in this effect. The shape of the wave at a breaking point apparently has a large affect on the pressure exerted and upon the distribution of this pressure. The non-breaking waves and earlier tests using breaking waves showed significant pressure ranging to about one wave height below still water level. Later project tests have indicated variability in this pattern. Some of the tests of the project model studies of Tsoying Harbor on Taiwan and Kahuluai Harbor, Hawaii, have indicated that breaking waves of some shapes exert pressures only a very short distance below still water level. Additional tests and analyses will be made to determine the governing factors in this variance in pressure distribution. However, until this effect is further investigat primary cover layers should extend at least one wave height below lowest still water level.

Head Stability - The design of the head of the breakwater and jetty is very critical since this portion of the structure is more frequently dan than any other. This is due principally because of the rounded shape which allows waves from all directions to break directly upon it. In this breaki a jet is formed across the slope which tends to roll out the units. Model studies have emphasized the fact that this damage generally occurs on a rear quadrant from the direction of wave approach. Several thoughts have been proposed to overcome this effect. One method is to flatten the slope in the direction of wave approach and steepen the slope of the rear quadrar

so that the wave will be forced to break earlier and that the water may fall free after breaking. Special attention must be given to head design as greater forces are acting on the head than on the trunk section. It may be noted in Table 1 that separate K_Δ values are given for the head and the trunk.

Concrete Components - Because of the need of heavier individual units and also to the dwindling supplies of stone near out coasts, significant attention has been given to the use of concrete components. In the United States principal investigation has been on tetrapods, tribars and quadripod Other shapes have been proposed, but at the present time sufficient information is not available to the author to comment on these various shapes.

The first of the armor units, of significant value, was the tetrapod, developed and patented in 1950 by the Neyrpic Laboratories of Grenoble, France. The tetrapod is an unreinforced concrete shape with four truncated conical legs projecting radially from a center point. The tetrapod was discussed by Mr. Pierre Danel in the Proceedings of the Fourth Conference on Coastal Engineering.

A more recent concrete shape is the tribar, developed and internationally patented by Mr. R. Q. Palmer of the Corps of Engineers, Honolulu District. The tribar is an unreinforced concrete shape consisting of three ba tied together by three radial arms. The use of tribars was discussed in a paper by Mr. Palmer entitled "Breakwaters in the Hawaiian Islands", publish in the Journal of the Waterways and Harbor Division, A.S.C.E., June 1960. The quadripod was developed by the Corps of Engineers, and is a concrete shape of four truncated legs with three of them in the same plane and projecting from a center point. The fourth pod projects from the same center with its centerline making an angle of 90° with the plane of the other pods. In the United States tetrapods have been used at Crescent City Harbor, California, Kahului Harbor, Hawaii and on Rincon Island, California Tribars were used at Nawiliwili Harbor, Hawaii. Quadripods will be used on the east breakwater of Santa Cruz Harbor, California, which is now under construction.

The design of cover layers using concrete components is similar to that for quarry stone structure. The Hudson equation may be used with the applicable value of K_Δ. The principal point to consider in the design of these structures is to contain them on the slope so that rolling movement will not occur. Experience has indicated that principal damage to the unit is the shearing of legs caused by rolling. To obtain this containing featu it is generally necessary to provide a concrete cap with the possible addition of spaced concrete posts along the side of the cap to further reduce the possibility of the units being rolled to the crest of the structure. Casting, curing and placing techniques are discussed by Blume and Keith in their article entitled "Rincon Offshore Island and Open Causeway", A.S.C.E. Proceedings Paper No. 2170, published in September 1960, and by Deignan in his paper entitled "Breakwater at Crescent City, California", published

in A.S.C.E. Proceedings Paper No. 2174 of September 1959. It is evident that greater porosity is obtained by these concrete units and back pressures, which are often a problem in stone construction, are reduced. The feature in which more information is needed is on the actual durability of the units in a prototype structure. Limited experience to date indicates that their structural durability is adequate except in cases where rolling on the slope occurs.

One of the major advantages of concrete components is the amount of porosity obtained which permits dissipation of the energy of the attacking wave. The amount of porosity in percent voids, determined from model units for various cover units follows in Table 2.

Table 2

POROSITY OF VARIOUS ARMOR UNITS

ARMOR UNIT	NO. OF LAYERS	POROSITY IN %
Riprap	graded	37
Quarrystone	2	38
Quarrystone	3	40
Tetrapod	2	50
Quadripod	2	50
Tribar	2	54
Tribar*	1	47

* Uniform placement.

CONCLUSIONS

Design of coastal structures cannot, because of the variability of forces and the nature of the phenomena, become a handbook process. Ingenui and judgment will always be a major requirement of a designer. However, greater understanding of the phenomena and the development of the empirical data is needed for development of methods for designing more economical anc efficient structures. To obtain this need there must be even greater cooperation between the designer and the researcher and the governments, the universities and the individuals must place greater and greater emphasis on oceanographic research.

This paper has attempted to point out some of the laboratory findings that have been applied to practical design methods and the manner in which it was applied. It is hoped that areas of needed research have also been inferred.

ACKNOWLEDGMENT

The opinions expressed herein are those of the author but are based on investigations made by the Corps of Engineers. The permission granted by the Chief of Engineers to publish this paper is appreciated.

REFERENCES

Beach Erosion Board (1961). Shore Protection, Planning and Design: Tech. Report No. 4, Corps of Engineers, Washington, D. C.

Bretschneider, C. W. (1959). Wave Variability and Wave Spectra for Wind Generated Gravity Waves: Beach Erosion Board Tech. Memorandum No. 118, Corps of Engineers, Washington, D. C.

Minikin, R. C. R. (1950). Wind, Waves and Maritime Structures: Griffin, London.

Sainflou, M. (1928). Essay on Vertical Breakwaters: Annales des Ponts et Chaussees, 1928-IV (Translated from the French by C. R. Hatch for the Corps of Engineers).

Hudson, R. Y. (1959). Laboratory Investigation of Rubble-Mound Breakwaters Paper No. 2171, Journal of the Waterways and Harbors Division, A.S.C.E. September 1959 and discussions thereon.

Hudson, R. Y. (1961). Wave Forces on Rubble-Mound Breakwaters and Jetties: Waterways Experiment Station Miscellaneous Paper No. 2-453, Corps of Engineers, Vicksburg, Mississippi.

Hudson, R. Y. and Jackson, R. A. (1962). Design of Riprap Cover Layers for Railroad Relocation Fills, Ice Harbor and John Day Lock and Dam Projects: Waterways Experiment Station Miscellaneous Paper No. 2-465, Corps of Engineers, Vicksburg, Mississippi.

Danel, Pierre (1954). Tetrapods: Proceedings, Fourth Conference on Coastal Engineering.

Palmer, R. Q. (1960). Breakwaters in the Hawaiian Islands: A.S.C.E. Proceedings Paper No. 2507, June 1960 and discussions thereon.

Jackson, R. A. (1960). Design of Quadripod Cover Layers for Rubble-Mound Breakwaters: Waterways Experiment Station Miscellaneous Paper No. 2-372, Corps of Engineers, Vicksburg, Mississippi.

Blume, J. A. and Keith, J. M. (1960). Rincon Offshore Island and Open Causeway: A.S.C.E. Proceedings Paper No. 2170, September 1960.

Deignan, J. E. (1959). Breakwater at Crescent City, California: A.S.C.E. Proceedings Paper No. 2174, September 1959.

CHAPTER 24

LABORATORY STUDY OF RUBBLE FOUNDATIONS FOR VERTICAL BREAKWATERS

A. Brebner
Chairman, Department of Civil Engineering
Queen's University at Kingston, Ontario
and
P. Donnelly
Engineer, Harbour and Rivers Branch
Department of Public Works, Canada

ABSTRACT

Laboratory tests have been conducted to determine the stability characteristics of pell-mell placed rubble of sensibly uniform shape and size used as a foundation or as toe protection for the vertical superstructure of a composite breakwater. Data are presented for the design of such breakwater foundations.

INTRODUCTION

An investigation is being conducted in the Hydraulic Laboratories at Queen's University at Kingston, on the behaviour under wave attack of the rubble portion of a composite breakwater consisting of a vertical breakwater atop a rubble-mound.

This study is part of a general program on harbour problems on the Great Lakes of Canada and is a preliminary effort to provide a rational basis for the design of such rubble sections to withstand the erosive action of waves.

The forces exerted by wind-generated waves on breakwaters and allied structures have, for many years, being the subject of theoretical, laboratory and field study. Most of this effort has been directed towards evaluating the effects of waves on rubble-mound breakwaters, Iribarren (1951), Beaudevin (1955) and Hudson (1959), and the forces exerted on the face-walls of vertical breakwaters, Minikin (1950) and Nagai (1960).

Apparently no systematic study of the well recognized problem of erosion of the foundations (usually rubble-mound) of composite breakwaters has been made.

Figure 1 illustrates the three main types of breakwater, 1(c) being the type under investigation. This latter type might well be selected instead of the purely vertical structure for the following cases:

a) where the sea-bed has insufficient strength to bear the concentrated loads associated with vertical gravity walls;

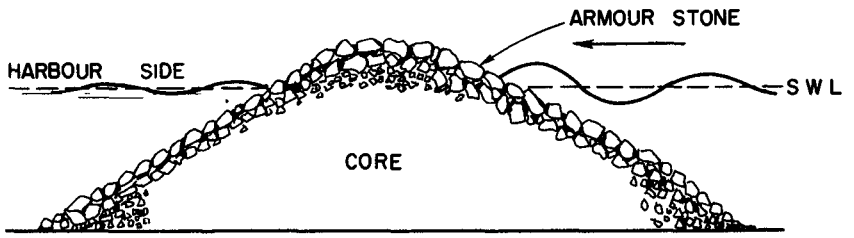

(a) TYPICAL RUBBLE MOUND BREAKWATER

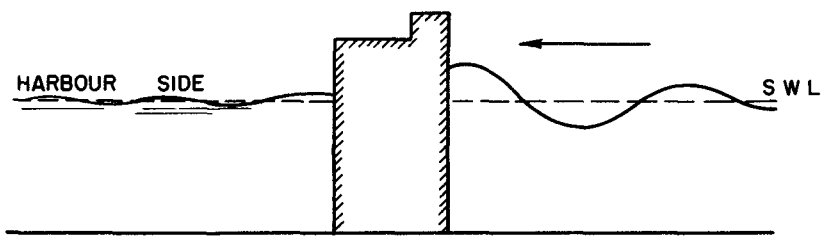

(b) TYPICAL VERTICAL WALL BREAKWATER

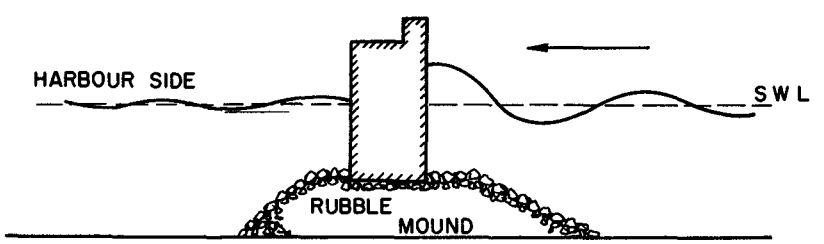

(c) TYPICAL COMPOSITE BREAKWATER

Fig. 1. Breakwater cross-sections.

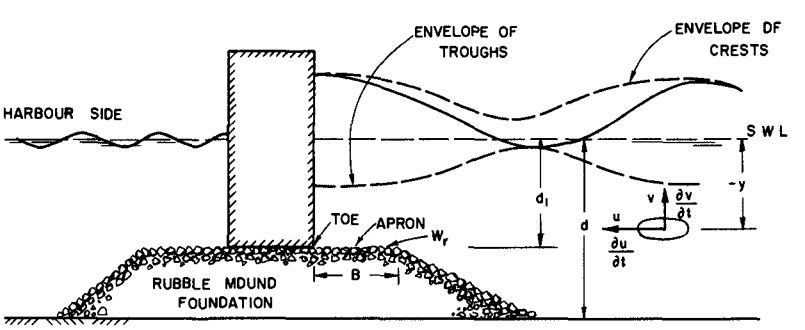

Fig. 2. Composite breakwater under wave attack (Definitions of nomenclature).

b) where scour of the bed material is a problem;

c) where great depths make it uneconomical to build a rubble-mound breakwater - a 33% increase in height requires a 50% increase in volume of stone for the same side-slopes and top width of rubble-mound.

From a practical viewpoint the design of the superstructure of the composite breakwater may follow established procedures, B.E.B. (1961), whereas the necessary size and weight of stone for the foundation portion is, at present, a matter of engineering judgement.

In what follows an attempt is made to make the selection of stone size a rational one based on extrapolated laboratory tests.

STABILITY ANALYSIS

The forces on an individual unit of a rubble mound foundation of a vertical wall situated at a depth d_1 below the S.W.L. will be considered. The conditions are illustrated in Figure 2. The disturbing force is taken to consist of inertia and drag components. The inertia force on a body submerged in an oscillating fluid is proportional to the product of the volume of the body, the mass of the fluid and the local acceleration of the fluid; thus

$$\text{Inertia Force} = F_I = C_M D^3 (\gamma_f/g) \frac{\partial v}{\partial t} \qquad (1)$$

where C_M is an inertia coefficient. (Notation is defined in the appendix.)

The drag force on a body in an oscillating fluid is proportional to the product of the cross-sectional area of the body, the mass of the fluid, and the square of the velocity of the oscillating fluid; thus

$$\text{Drag Force} = F_D = \frac{1}{2} C_D D^2 (\gamma_f/g)\, v|v| \qquad (2)$$

where C_D is a drag coefficient.

In the case of the rubble unit of the foundation under study, the velocities and accelerations in the vicinity of the rubble unit are not known since the presence of the mound modified the orbital velocities and accelerations which would exist in the clapotis arising from a vertical wall with no mound in front of it. However, it will be assumed that the velocities and accelerations actually existing around the rubble units are directly proportional to those which would exist at the corresponding depth in a total clapotis. A rubble unit will be subjected to disturbing forces with horizontal and vertical components. The restoring force will be the buoyant weight. Considering incipient horizontal displacement of the unit, the condition of limiting equilibrium is:

$$\sum F_H = \mu \sum F_V \qquad (3)$$

where $\sum F_H$ = sum of horizontal forces

$\sum F_V$ = sum of vertical forces

μ = friction coefficient

$\sum F_H$ = Horizontal Inertia Force + Horizontal Drag Force

$$= F_{HI} + F_{HD} \qquad (4a)$$

$\sum F_V$ = Buoyant Weight + |Vertical Inertia Force| + |Vertical Drag Force|

$$= \text{Buoyant Weight} + F_{VI} + F_{VD} \qquad (4b)$$

According to first order gravity wave theory, the horizontal and vertical components of orbital velocity and acceleration, in a total clapotis at a depth d_1 below the S.W.L. where the water depth is d, are:

$$U = Hk \frac{\cosh md\,(1 - d_1/d)}{\sinh md} \sin mx \sin kt$$

$$= U_{max} \sin kt \qquad (5a)$$

where U_{max} denotes the maximum horizontal component of orbital velocity at a point. Similarly,

$$v = -Hk \frac{\sinh md\,(1 - d_1/d)}{\sinh md} \cos mx \sin kt$$

$$= -v_{max} \sin kt \qquad (5b)$$

$$\frac{\partial u}{\partial t} = Hk^2 \frac{\cosh md\,(1 - d_1/d)}{\sinh md} \sin mx \cos kt$$

$$= \left[\frac{\partial u}{\partial t}\right]_{max} \cos kt \qquad (5c)$$

$$\frac{\partial v}{\partial t} = -Hk^2 \frac{\sinh md\,(1 - d_1/d)}{\sinh md} \sin mx \cos kt$$

$$= -\left[\frac{\partial v}{\partial t}\right]_{max} \cos kt \qquad (5d)$$

Recalling equations (1) and (2), the horizontal and vertical force components are written:

Horizontal Inertia Force (F_{HI})

$$F_{H1} = C_{MH} D^3 (\gamma_f/g) \left[\frac{\partial u}{\partial t}\right]_{max} \cos kt \qquad (6a)$$

Horizontal Drag Force (F_{HD})

$$F_{HD} = \frac{1}{2} C_{DH} D^2 (\gamma_f/g)\, u_{max}^2 \sin kt\, |\sin kt| \qquad (6b)$$

Vertical Inertia Force (F_{VI})

$$F_{VI} = - C_{MV} D^3 (\gamma_f/g) \left[\frac{\partial v}{\partial t}\right]_{max} \cos kt \qquad (6c)$$

Vertical Drag Force (F_{VD})

$$F_{VD} = \frac{1}{2} C_{DV} D^2 (\gamma_f/g) \cdot v_{max}^2 \sin kt\, |\sin kt| \qquad (6d)$$

The coefficients C_{MH}, C_{DH}, C_{MV}, and C_{DV} are the appropriate horizontal and vertical inertia and drag coefficients whose values take care of the discrepancy between actual and assumed velocities and accelerations.

$$\text{Buoyant Weight} = \beta D^3 (\gamma_r - \gamma_f) \qquad (6e)$$

where the coefficient β depends on the shape of the unit.

It is evident that the maximum values of the above periodic forces do not occur at the same time. However, movement of the stone in question is initiated by action of vertical wave forces, which reduce the effective buoyant weight of the stone, simultaneous with, or closely followed by, a horizontal wave force which tends to displace the "lightened" stone. It will further be assumed that the "lightening" action is effected by the combined efforts of the maximum vertical inertia and drag forces, and that the disturbing force is given by the combined efforts of the maximum horizontal inertia and drag forces. Since here we are dealing with proportionalities rather than real, actual forces, this simplification is justified. Therefore, dropping the periodic terms of equation (6) which define the magnitude and direction of each component force at the particular point, the equation of limiting equilibrium is written:

$$C_{MH} D^3 (\gamma_f/g) \left[\frac{\partial u}{\partial t}\right]_{max} + \frac{1}{2} C_{DH} D^2 (\gamma_f/g) \cdot u_{max}^2$$

$$= \mu \left\{ \beta D^3 (\gamma_r - \gamma_f) - C_{MV} D^3 (\gamma_f/g) \left[\frac{\partial v}{\partial t}\right]_{max} - \frac{1}{2} C_{DV} D^2 (\gamma_f/g) \cdot v_{max}^2 \right\}$$

Since the weight of the rubble unit = $W_r = \beta D^3 \gamma_r$ we have

$$\frac{W_r}{\gamma_r} = \frac{\beta}{8} \left[\frac{C_{DH} u_{max}^2 + C_{DV} v_{max}^2}{\mu \beta g (S_r - 1) - \left\{ C_{MH} \left[\frac{\partial u}{\partial t}\right]_{max} + \mu C_{MV} \left[\frac{\partial v}{\partial t}\right]_{max} \right\}} \right]^3$$

where $S_r = \frac{\gamma_r}{\gamma_f}$

Now recalling from equation (5) the values of u_{max}, v_{max}, $\left[\frac{\partial u}{\partial t}\right]_{max}$ and $\left[\frac{\partial v}{\partial t}\right]_{max}$, substituting these values in the above equation, and then multiplying both sides of the resulting equation by $\left[\frac{S_r - 1}{H}\right]^3$ gives:

$$\frac{W_r (S_r - 1)^3}{H^3 \gamma_r} = \frac{\beta}{8} \left[\frac{C_{DH} \frac{\cosh^2 md(1 - d_1/d)}{\sinh^2 md} + C_{DV} \frac{\sinh^2 md(1 - d_1/d)}{\sinh^2 md}}{\frac{\mu \beta g}{Hk^2} - \frac{1}{S_r - 1} \left\{ C_{MH} \frac{\cosh md(1 - d_1/d)}{\sinh md} + \mu C_{MV} \frac{\sinh md(1 - d_1/d)}{\sinh md} \right\}} \right]$$

Now, if we put $C_{DV} = \sigma_1 C_{DH}$, $C_{MV} = \sigma_2 C_{MH}$ and $\mu = 1$, recall that:

$$k = 2\pi/T$$

$$L = (gT^2/2\pi) \tanh md$$

and adopt the notation of Hudson (1959) by writing the above equation in terms of the Stability Number, N_s, such that

$$N_s = \frac{\gamma_r^{1/3} H}{W_r^{1/3} (S_r - 1)}$$

the result is:

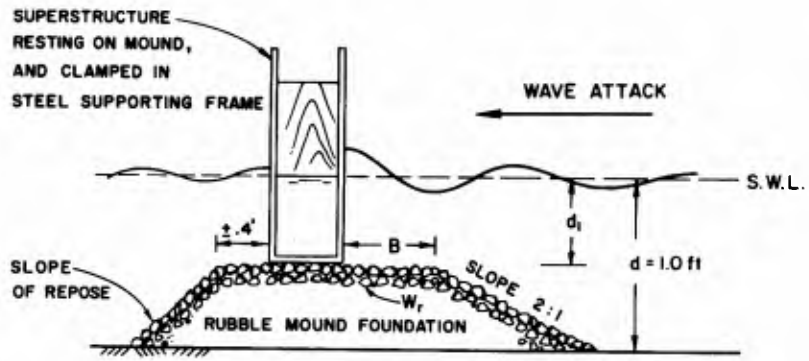

(a) RUBBLE MOUND AS FOUNDATION ONLY

NOTES: (1) WIDTH OF TEST CHANNEL WAS 20 INCHES

(2) AVERAGE DISTANCE OF MODEL FROM WAVE GENERATOR WAS 40 FT.

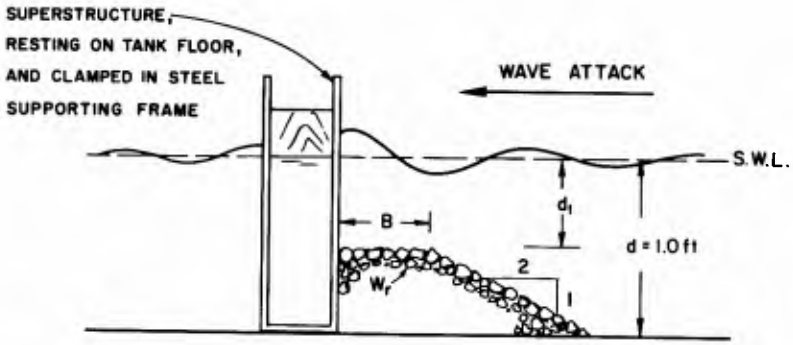

(b) RUBBLE MOUND USED AS TOE PROTECTION

Fig. 3. Model test conditions.

Fig. 4a

Fig. 4b

Fig. 4. Model test conditions for rubble mound as a foundation.

$$N_s = \frac{2}{\beta^{1/3}} \frac{\left[\frac{\beta}{2\pi \tanh md} \cdot \frac{1}{C_{MH}} \cdot \frac{L}{H}\right] - \frac{1}{S_r - 1} \cdot \frac{\cosh md\,(1 - d_1/d)}{\sinh md} \left\{1 + \sigma_2 \tanh md\,(1 - d_1/d)\right\}}{\frac{C_{DH}}{C_{MH}} \cdot \frac{\cosh^2 md\,(1 - d_1/d)}{\sinh^2 md} \left\{1 + \sigma_1 \tanh^2 md\,(1 - d_1/d)\right\}} \qquad 7(a)$$

Although equation 7(a) is based on very simplified assumptions and contains a number of unkown coefficients, it does serve the useful purpose of identifying the principal parameters involved in the problem. These may be listed as follows:

1) the term β , i.e. related to the shape of the rubble units, Δ,

2) the term C_{DH}/C_{MH} , i.e. elated to the ratio of inertia and drag coefficients, C_D / C_M .

3) the term $\frac{1}{C_{MH}} \frac{L}{H}$, i.e. related to the product of wave steepness and inertia coefficient, $C_M H/L$.

4) the specific gravity of the rubble units, S_r .

5) the term md , i.e. related to the relative depth, d/L .

6) the relative depth of the foundation with reference to the S.W.L., d_1/d .

Therefore the Stability Number may be written:

$$N_s = f(\Delta, C_D/C_M, C_M H/L, S_r, d/L, \text{and } d_1/d) \qquad 7(b$$

where f reads "a function of".

EXPERIMENTAL WORK

A series of experiments was carried out to investigate the influence of the various parameters as noted in equation (7) on the Stability Number.

Figure 3 illustrates the experimental conditions and Figure 4 shows photographs of the installation under test.

Range of Test Conditions:- The following tabulation gives the ranges of wave characteristics and breakwater dimensions used in the tests:

Characteristics and Dimensions	Range of Test Conditions
Water depth (d)	1.00 ft.
Wave height (H)	0.04 to .445 ft.
Wave period (T)	1.00 to 2.00 secs.
Wave length (L)	4.51 to 10.76 ft.
Relative depth (d/L)	0.0930 to 0.2215
Wave steepness (H_{crit}/L)(at limiting equilibrium)	.0074 to .0576
Specific weight of stone (γ_r)	165.4 lbs./ cu.ft.
Average weight of individual rubble units (W_r)	0.00183 to 0.0190 lbs.
Specific weight of water (γ_f)	62.4 lbs./ cu.ft.
Relative depth of top surface of foundation mound below S.W.L. (d_1/d)	0.00 to 0.75
Top width of foundation mound on seaward side (B)	0.15 d to 0.75 d
(Note: Main body of tests conducted at B = 0.4 d)	
Slope of foundation mound on seaward side	1 on 2
Crown elevation of vertical superstructure	No overtopping
Test sections	See Figure 3

Most of the tests were conducted with a top width of the foundation mound on the seaward side, B , of four-tenths the water depth (i.e. B = 0.4 d), and zero penetration of the vertical superstructure into the rubble mound foundation. Additional tests, in which the top width, B , and the penetration of the superstructure into the foundation mound were varied, are discussed in the section headed SUPPLEMENTARY TESTS.

In the experiments, the shape, Δ, of the rubble units was kept sensibly constant, sub-rounded to sub-angular beach gravel of specific gravity 2.65 being used throughout. Four different stone sizes were used to correlate the parameters, 3/ 4"-5/ 8", 5/ 8"-1/ 2", 1/ 2"-3/ 8", 3/ 8"-1/ 4". The grading curves within each size range showed that the distribution of sizes was very similar in all cases; that is, similitude of size variation was being closely followed.

Since neither the drag nor the inertia coefficient of the stone was determined experimentally the data of Keulegan and Carpenter (1958) was used to provide an indication of the likely variations in the magnitude of these coefficients in the range of laboratory conditions encountered. These data indicated that the variation in numerical value was small over a wide range of wave steepnesses and stone sizes.

Thus the effective functional equation guiding the experimental work was reduced to the form

$$N_s = \frac{\gamma_r^{1/3} H}{W^{1/3}(S_r - 1)} = f(d/L, d_1/d, \text{and } H/L) \qquad (8)$$

and each of these dimensionless terms was investigated as outlined in the following.

For given fixed values of d_1/d and T, i.e. a fixed value of wavelength, a foundation of one size of stone was tested with increasing values of wave-height, H. At small values of H no movement of the stone was discernable whereas at high values of H the rubble either rocked violently or was washed out from under the superstructure. It was consistently found that a relationship of the form shown in Figure 5 existed between H and the number of stones rocking at the base of the vertical superstructure. The point of critical stability normally occurred when about four pieces per lineal foot were rocking; but, as might be expected, this critical condition was not always exactly definable. However by plotting the test results as definitely stable (sensibly no movement) or unstable (wash out of at least two pieces) it was possible, as is seen in a typical test result, Figure 6, to arrive at a reasonably accurate relationship between stone size and wave height at the point of limiting equilibrium between stable and unstable conditions.

Using the curve defining the conditions of limiting equilibrium for a given stone weight (under the fixed values of d_1/d and L) the ratio $\frac{\gamma_r^{1/3} H_{crit}}{W_r^{1/3}(S_r - 1)}$, that is the critical stability number, N_s' was calculated and plotted against the wave steepness $\frac{H_{crit}}{L}$. Such a plot is shown on Figure 7 and gives evidence of little effect of $\frac{H_{crit}}{L}$ on N_s'.

From the whole series of tests treated in this manner with varying values of d_1/d and varying values of T (and hence L and d/L) it was found that the critical stability number N_s' could, as a first approximation, be regarded as independent of the wave steepness H_{crit}/L. In view of this, the mean value of N_s' as determined from the tests on the four sizes of stone was calculated and this mean value used to determine subsequent relationship between N_s and d/L or d_1/d.

Figure 8 shows the variation of the critical stability number with d/L using d_1/d as a parameter.

Again it appears from Figure 8 that relative depth d/L is of secondary importance except where the depth of the foundation below S.W.L. is great. However, since it is possible to achieve a range of values of d/L in a wave system in nature, the value of N_s' for the worst case of d/L (i.e. the lowest point on each N_s' versus d/L curve) is selected and plotted against d_1/d.

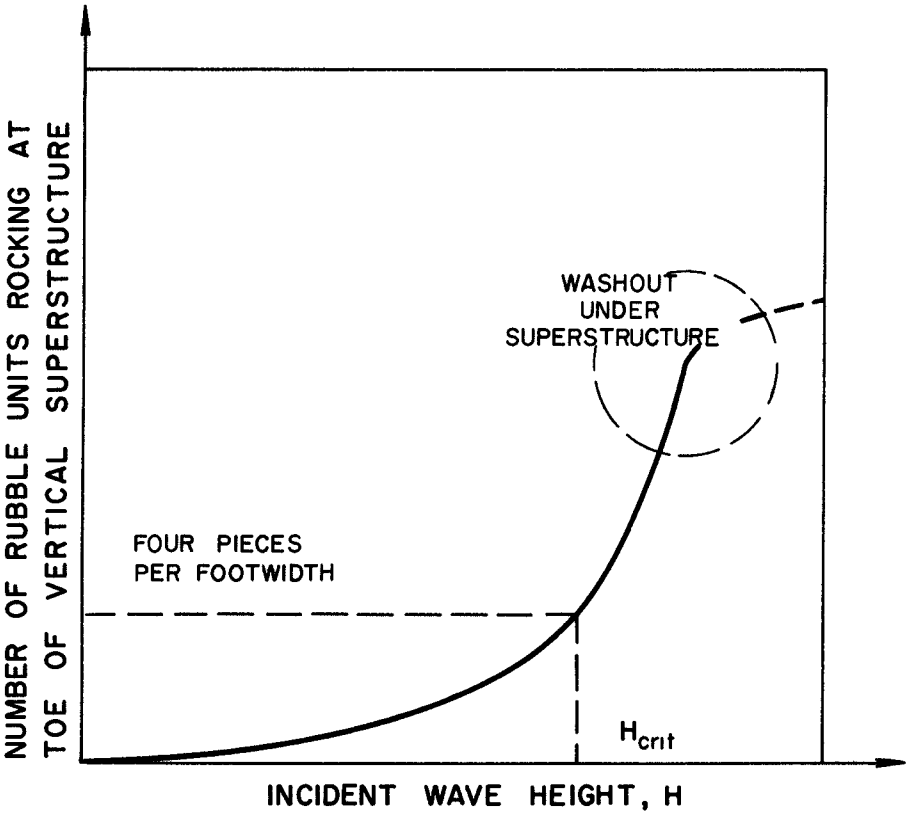
NUMBER OF RUBBLE UNITS ROCKING AT TOE OF VERTICAL SUPERSTRUCTURE
WASHOUT UNDER SUPERSTRUCTURE
FOUR PIECES PER FOOTWIDTH
H_{crit}
INCIDENT WAVE HEIGHT, H

Fig. 5

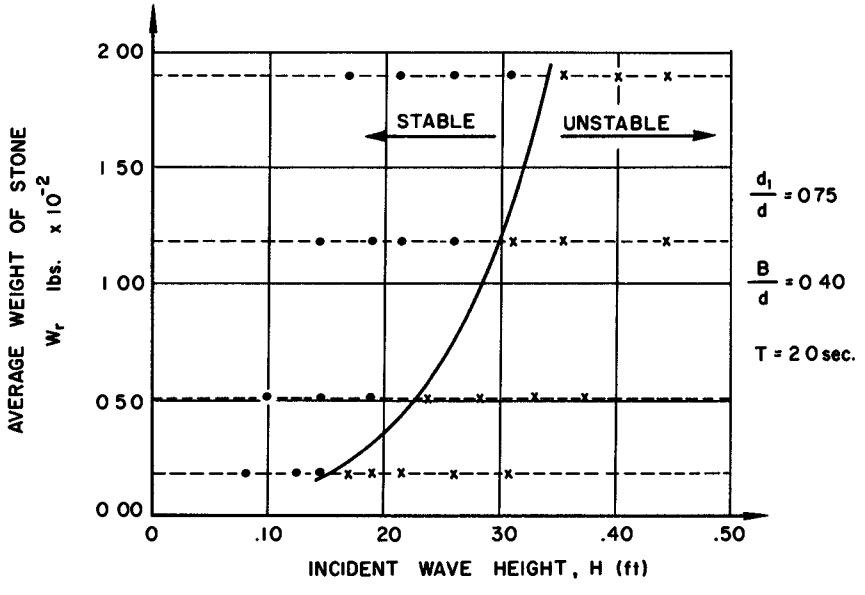
AVERAGE WEIGHT OF STONE W_r lbs. x 10^{-2}
2 00
1 50
1 00
0 50
0 00
STABLE
UNSTABLE
$\frac{d_1}{d}$ = 075
$\frac{B}{d}$ = 0 40
T = 2 0 sec.
0
.10
20
30
.40
.50
INCIDENT WAVE HEIGHT, H (ft)

Fig. 6

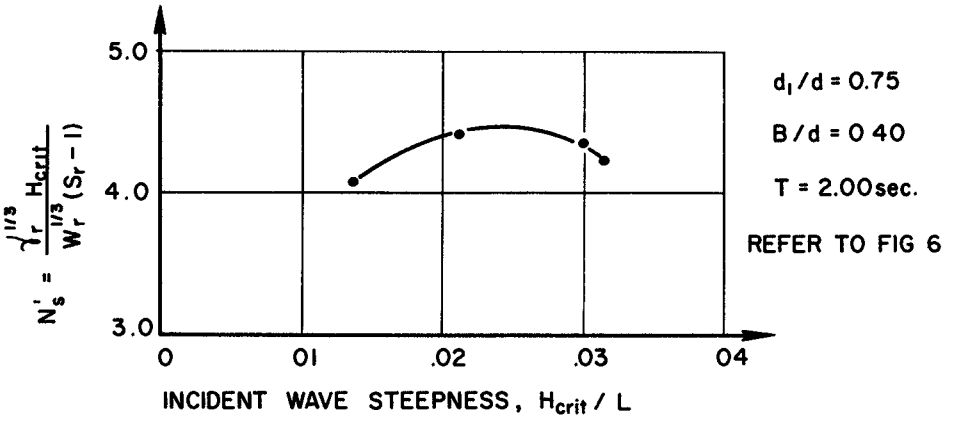

Fig. 7

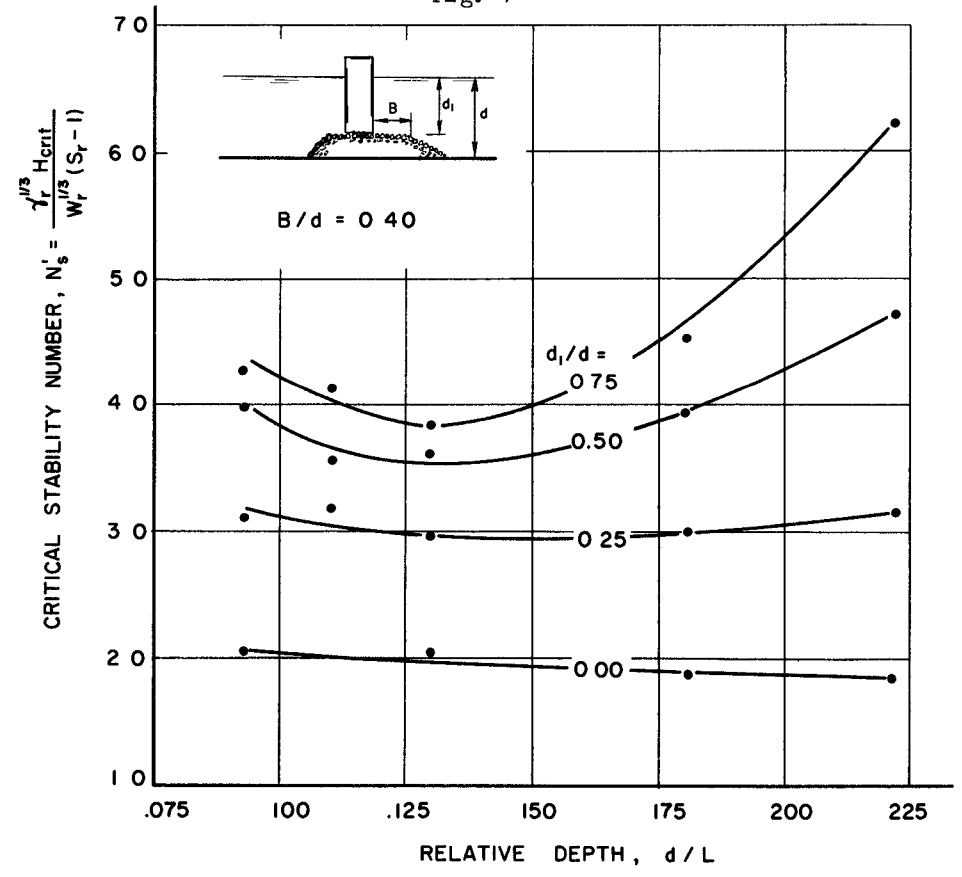

Fig. 8. Rubble mound as a foundation. Critical stability number, N_s', as a function of relative depth, d/L.

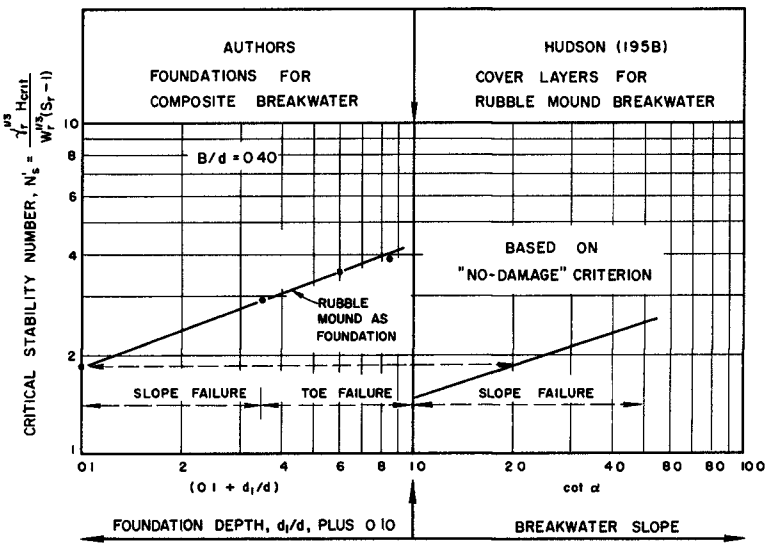

Fig. 9. Comparison of test results for composite breakwaters with results of Hudson (1958) for rubble mound breakwaters.

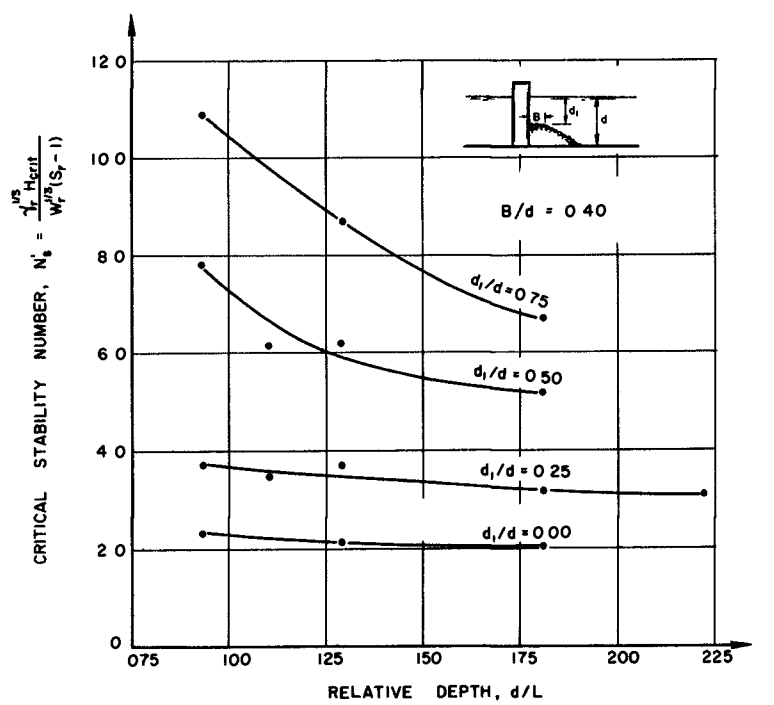

Fig. 10. Rubble mound as toe protection; critical stability number, N'_s, as a function of relative depth, d/L.

Such a plot derived from Figure 8 is shown in Figure 9 along with Hudson's test results. (The comparison with the latter's results is permissible since Hudson used somewhat the same criterion of damage/no damage or stable/unstable conditions.)

SUPPLEMENTARY TESTS

Top Width of Mound:

In this series of tests the top width of the foundation mound, B, on the seaward side was varied. (Reference may be made to Figure 3.) The additional widths tested were $B = 0.15\,d$ and $B = 0.75\,d$. These tests were conducted only for the foundation depth $d_1/d = 0.50$ and $d_1/d = 0.75$.

It was found that variation in the top widths within the range stated above, did not result in significantly different Critical Stability Numbers from those already presented in Figure 8 for a foundation top width, $B = 0.4\,d$.

Penetration of Superstructure in Mound:

To obtain an estimate of the effect of increasing the penetration of the superstructure into the mound foundation, the conditions illustrated in Figure 3(b) were tested. Here the superstructure extended to the floor of the wave tank and the rubble mound was piled in front to act as a toe protection. The results of these tests are depicted in Figure 10 where the variation of the Critical Stability Number, N_S', with d/L and d_1/d is shown.

PRACTICAL APPLICATION OF RESULTS TO PROTOTYPE STRUCTURES

Test results have, so far, been presented in terms of a Critical Stability Number, N_S', on the assumption that the structure was at the point of limiting equilibrium and that its ultimate safety was in some doubt. In the design of a structure, a definite margin of safety is required, and to arrive at a Design Stability Number, N_S, the Critical Stability Number, N_S', must be reduced. The reduction of the Critical Stability Number was achieved by re-examining the model test results and noting the wave height which caused no damage to the foundation. This wave height was denoted $H_{D=0}$ "No damage" was defined as follows:

a) When instability resulted from wash-out of the rubble from under the toe of the vertical superstructure (i.e. when $d_1/d > 0.25$ and with little or no penetration of the superstructure into the rubble mound), "no damage" was taken as the condition where not more than two pieces per foot rocked slightly at the toe of the vertical superstructure.

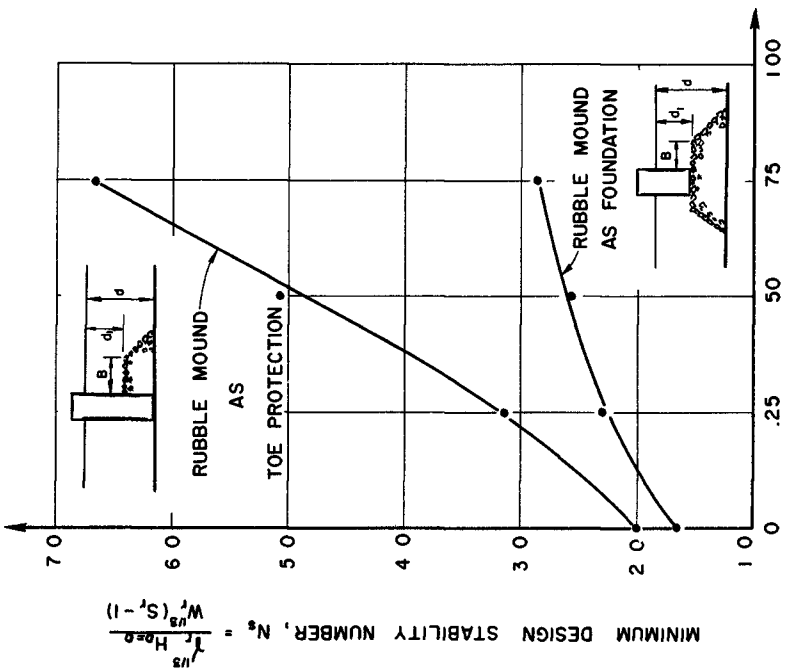

Fig. 12. Minimum design stability number, N_s, as a function of foundation depth, d_1/d.

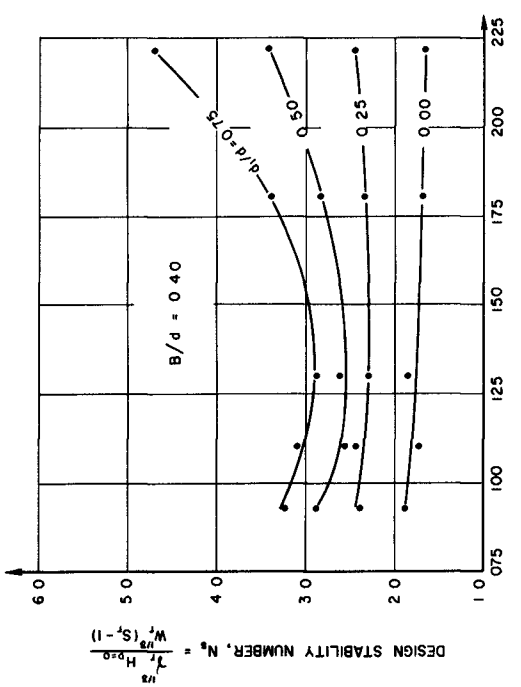

Fig. 11. Rubble mound as a foundation. Design stability number, N_s, as a function of relative depth, d/L. (Modification of Fig. 8 for design purposes.)

b) When instability resulted from erosion of the seaward slope of the rubble mound (i.e. (i) when $d_1/d < 0.25$ and with little or no penetration of the superstructure into the rubble mound, and (ii) for all values of d_1/d when the superstructure extended through the mound to the floor.) "No damage" was taken as the condition where not more than 1 per cent of the rubble units was displaced from the slope.

It must be emphasized that in effect there are two different stability criteria in use.

When $H_{D=0}$ was determined for all cases, the Critical Stability Number N_s', was reduced by multiplying it by the ratio $\frac{H_{D=0}}{H_{crit}}$.

$$\text{Thus, Design} \quad N_s = N_s' \frac{H_{D=0}}{H_{crit}} \tag{9}$$

In the test results for the case where the rubble mound was used primarily as a toe protection (Figure 10) it was not considered necessary to reduce the Stability Numbers for design purposes. (H_{crit} for this case was taken as the height causing 1% of the outer layer of rubble units to be displaced - a permissible amount of damage in the field.)

Figure 11 shows the variation of the Design Stability Number, N_s, with d/L and d_1/d, for zero penetration of the superstructure into the rubble mound.

Figure 12 is obtained from Figures 10 and 11 by noting the minimum values of N_s for each value of d_1/d and plotting this minimum N_s as a function of d_1/d. Figure 12, then, presents the curves which are, at present, recommended for use in the design of rubble mound foundations and rubble mound toe protections for vertical breakwaters and seawalls.

Figure 12 has been used to calculate the curves shown in Figure 13 where the weight of rubble stone units required for given values of incident wave height, and selected values of specific weights of rock and water, may be obtained.

Design Wave Heights:

The proposed design curves of Figure 12 represent the relationship:

$$\text{Design} \quad N_s = \frac{\gamma_r^{1/3} H_{D=0}}{W_r^{1/3} (S_r - 1)} = f(d_1/d) \tag{10}$$

The wave height in question is that which exists at the site of the structure and in the absence of the structure.

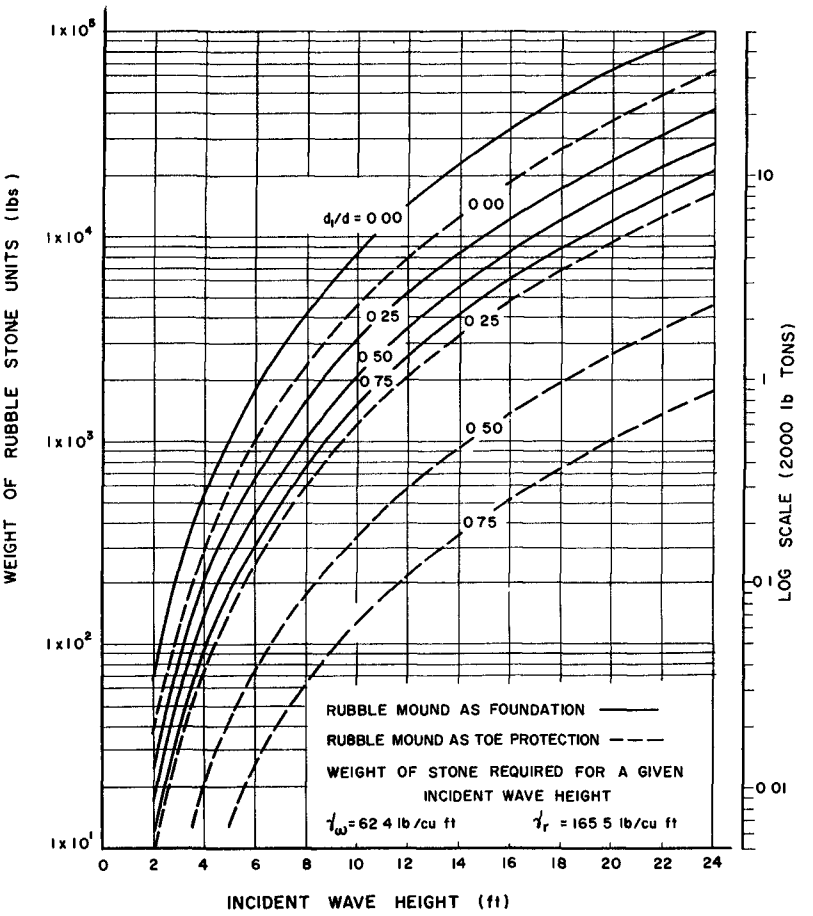

Fig. 13

Most modern methods of wave forecasting give what has been termed the "significant wave", whose height is often denoted $H_{1/3}$. (The significant wave height, $H_{1/3}$, is defined as the average height of the highest one-third of waves.) Analysis of the statistical distribution of wave heights by Longuet-Higgins (1952) and Saville (1955) has shown that one wave in every hundred is likely to be 1.6 times the height of the significant wave, and that in a prolonged storm the maximum wave could be twice the height of the significant wave.

In the case of a composite breakwater with the superstructure resting directly on a rubble mound foundation, the safety of the whole structure and perhaps a whole harbour and the shipping in it, may depend on the ability of the foundation to resist the erosive effects of the highest waves.

Therefore, for use of the test results given herein, in the design of such structures, it is at present suggested that the design wave height, $H_{D=0}$, should be either

1. the maximum wave height measured at the vicinity of the site of the structure, if the duration of measurement is judged to be sufficiently long and accurate.

OR

2a. for important structures at very exposed sites where failure would be disastrous, and in the absence of factual records, the design wave height, $H_{D=0}$, should be twice the value of the expected wave height at the structure based on $H_{1/3}$ in deep water corrected for refraction and shoaling. (Breaking might preclude a wave of such magnitude and in such a case the greatest non-breaking wave should be taken for the design value of $H_{D=0}$.)

2b. for less important structures where some risk of exceeding design conditions is acceptable, one and a half times the expected wave height.

DISCUSSION OF RESULTS

In the present series of tests the rubble mound was composed entirely of stones of approximately uniform size. In practice, a rubble mound foundation would be constructed with a core of dumped blast-run rock or quarry waste. The superstructure might consist of concrete or timber cribs which would be founded on the core of blast-run rock. An alternative method of constructing the superstructure would be to drive a pair of parallel tied-together walls of steel sheet piling into the rubble core. Finally, the apron and side-slopes of the core would be protected from erosion, by a cover layer of heavier, more uniformly sized, rock.

It is to the design of this cover layer that the tests described herein are intended to apply.

The practical prototype foundation is unlikely to correspond exactly to the conditions used in the present series of experiments. A situation where a superstructure, composed of steel sheet pile walls, is driven into the rubble core, corresponds most closely to the condition depicted in Figure 12 as "Rubble mound as toe protection". Other practical methods of construction are likely to fall somewhere between the two extreme conditions shown in Figure 12.

The outstanding points of uncertainty are, therefore, the effects of varying degrees of impermeability in the layers composing a prototype foundation, and the effects of varying amounts of penetration of the vertical superstructure into the rubble mound. Increased penetration of the superstructure certainly increases the overall stability and safety, and a relatively impermeable core is anticipated to produce similar results.

In addition, the conditions at the pierhead, or seaward extremity of the structure, have not been investigated.

An analysis of prototype successes and failures in relation to the model test results would be invaluable in assessing the validity of the design curves proposed herein, and, if necessary, in their modification. Publication of data concerning such successes and failures would make this possible.

CONCLUSIONS

It is concluded from the results of model tests on the behaviour under wave action of a rubble mound foundation of a composite breakwater composed of rock of nearly uniform shape and size that:

a) the Stability Number, $N_s = \frac{\gamma_r^{1/3} H}{W_r^{1/3}(S_r - 1)}$ is a useful and logical parameter for use in the study of the stability of rubble mounds under wave attack.

b) the Stability Number is primarily affected by the depth of the rubble mound foundation below the S.W.L. and by the relative depth (d/L) at the breakwater site.

c) since waves in nature have widely differing wave-lengths it is advisable to design the foundation on the basis of the minimum value of design Stability Number appropriate to the particular foundation depth (d_1/d).

d) increase in penetration of the superstructure into the rubble mound greatly increases the overall stability.

e) variation of the top width of the foundation mound on the seaward side, does not, for normal values of top width, appear to substantially affect the hydraulic aspects of the structure. In this respect, construction requirements and the dictates of Soil Mechanics will govern.

f) in the case of natural wave trains, the selection of the design wave height requires a decision on the part of the designer as to the acceptable risk of exceeding design conditions.

ACKNOWLEDGEMENT

The authors wish to acknowledge the contribution of the National Research Council of Canada and the Department of Public Works of Canada who made funds available for this study.

REFERENCES

Beach Erosion Board, "Shore Protection, Planning and Design", Tech. Report No. 4, 1961.

Beaudevin, C., "Stabilite des diques a talus a carapace en vrac", La Houille Blanche - Mai-Juin, (1955).

Hudson, R.Y., "Laboratory Investigation of Rubble-mound Breakwaters", Proc. A.S.C.E., Waterways and Harbours Division, Vol. 85, No. WWS, Sept. 1959.

Iribarren, R., and Nogales, C., "Generalization of the Formula for Calculation of Rock-fill Dikes and Verification of its Coefficients", Translation No. 51-4, Vickburg, Missippi, 1951.

Keulegan, G.H., and Carpenter, L.H., "Forces on Cylinders and Plates in an Oscillating Fluid", Journal of Research of Nat. Bur. of Standards, Vol. 60, No. 5, May 1958.

Minikin, R.R., "Winds, Waves, and Maritime Structures", Griffin and Company Ltd., London, 1950.

Nagai, S., "Shock Pressures Exerted by Breaking Waves on Breakwaters", Proc. A.S.C.E., Waterways and Harbours Division, Vol. 86, June 1960.

Saville, T. Jr., "Wave Forecasting", Proc. of 1st Conf. on Ships and Waves, Council on Wave Research, Richmond, Calif., 1955.

Longuet-Higgins, M.S., "On the Statistical Distribution of Heights of Sea-waves", Sears Foundation, J. Mar. Res., Vol. 11, 1952.

APPENDIX - NOTATION

LIST OF SYMBOLS AS USED IN THIS PAPER

Symbol		Definition	Units
B	:	Top width, on seaward side, of foundation mound.	ft.
C_D	:	A drag coefficient.	
C_M	:	An inertia coefficient.	
d	:	Depth of Still Water measured from the bottom normal to that Still Water surface; also, the depth of water in the vicinity of a structure.	ft.

d_l : Depth of top of foundation mound below the Still Water Level. ft.

d/L : Relative Depth: ratio of still water depth of wave length.

D : A characteristic linear dimension of a rubble unit; the diameter of a sphere having an equal volume. ft.

$-_D$: A subscript referring to a drag force.

f : "a function of"

g : Gravitational acceleration (= 32.2 ft/sec^2). ft/sec^2

H : Wave height; amplitude; height of incident wave. ft.

$H_{D=0}$: Incident wave height causing "no-damage" to structure. ft.

H_{crit} : Critical wave height: Incident wave height at condition of limiting equilibrium of structure. ft.

$-_H$: A subscript referring to the horizontal direction.

H/L : Wave steepness: ratio of wave height to wave length.

$-_I$: A subscript referring to inertia force.

k : $= 2\pi/T$

L : Wave length. ft.

m : $= 2\pi/L$

$-_{max}$: A subscript referring to the maximum value.

N_s : A Stability Number for rubble mounds.

$$N_s = \frac{\gamma_r^{1/3} H}{W_r^{1/3} (S_r - 1)}$$

N_s' : Critical Stability Number: Stability number at condition of limiting equilibrium -

$$N_s' = \frac{\gamma_r^{1/3} H_{crit}}{W_r^{1/3} (S_r - 1)}$$

S_r	: Specific Gravity of rubble or armour stone. ($S_r = \gamma_r / \gamma_f$)	
S.W.L	: Still Water Level.	
t	: A time.	secs.
T	: Wave period.	secs.
u	: Horizontal component of orbital velocity.	ft/sec
v	: Vertical component of orbital velocity.	ft/sec
V	: A velocity.	ft/sec
$-_v$	: A subscript referring to the vertical direction.	
W_r	: Weight of individual unit of rubble mound foundation (actually the mean weight of a unit in a "nearly one-size" rubble mound.)	lbs.
x	: A horizontal distance from the origin of co-ordinates.	ft.
y	: Depth below Still Water Level. (negative downwards)	ft.
α	: Angle of a rubble mound (or breakwater) slope measured from the horizontal.	degrees
β	: A coefficient stating the proportionality of the weight of a rubble unit to its volume.	
γ_f	: Unit weight of the water in which the structure is located. γ_r = 62.4 lbs/ cu.ft. for fresh water γ_f = 64.0 lbs/ cu.ft. for salt water.	lbs/ cu.ft.
γ_r	: Unit weight of rock (rubble).	lbs/cu.ft.
Δ	: Denotes the shape of the rubble or armour units.	
μ	: A friction coefficient.	
σ_1, σ_2	: Constants.	

CHAPTER 25

AKMON ARMOUR UNIT FOR COVER LAYERS OF RUBBLE MOUND BREAKWATERS

A. Paape and A.W. Walther
Hydraulics Laboratory Delft
Netherlands

A new specially shaped concrete block, the "Akmon", to be used as armour unit for protective cover layers of rubble mound breakwaters is presented.

The characteristics as have been derived from laboratory tests are compared with those of various other types of blocks.

Some considerations are given on the design procedure for cover layers, as it appears that this procedure has an influence on the block-type and -weight to be chosen.

If armour units have to be placed at random, which is in many cases an imperative necessity, the akmon appears to be one of the most suitable blocks developed up till now.

For two different breakwaters, the results are given of model investigations concerning the stability under the attack of waves generated by a wave board and wind.

INTRODUCTION

One of the designs of "Rijkswaterstaat" for the new harbour mole at IJmuiden was a rubble mound breakwater with a protective layer of concrete blocks. For this design the laboratory investigated different types of blocks with regard to stability against wave attack. First a series of comparative tests was conducted in a wave flume with regular paddle-generated waves. In these tests quarry stone was compared with cubes and other types of artificial blocks, some of which are given in figure 1.

Because of the restricted time only the three most promising blocks cubes, tetrapods and akmons were used for the second series of comparative tests which was conducted in a wind flume. Especially the akmon (Greek for anvil, see figure 2) appeared to have excellent qualities with regard to stability and porosity of the cover layer. Meanwhil however, important progress was made in the handling of stone-asphalt mixtures below the water level and the rubble mound breakwater appeared to be in this case no longer competitive. Then the investigations were stopped in an advanced stage.

The results were used for the design of other breakwaters invest gated by the laboratory and some data of the investigations are also given below. Moreover some general considerations are given with regard to the design procedure and especially the comparison of different type of blocks from an economical point of vue.

AKMON ARMOUR UNIT FOR COVER LAYERS OF RUBBLE MOUND BREAKWATERS

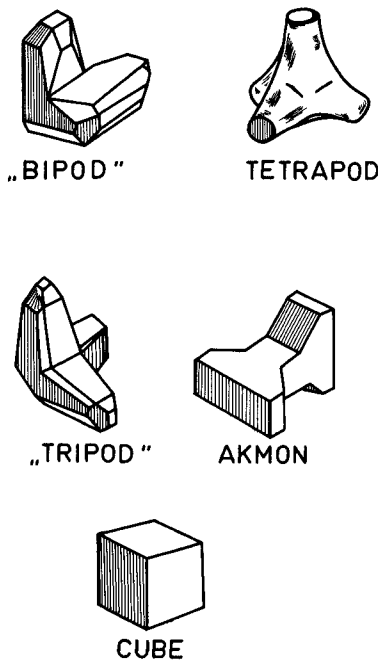

Fig. 1. Complete armour units.

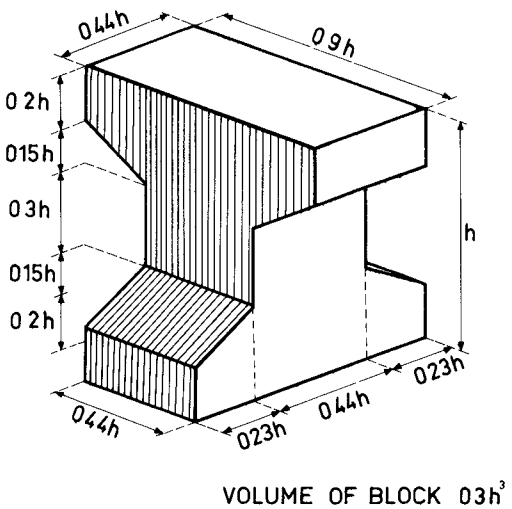

Fig. 2. Akmon armour unit.

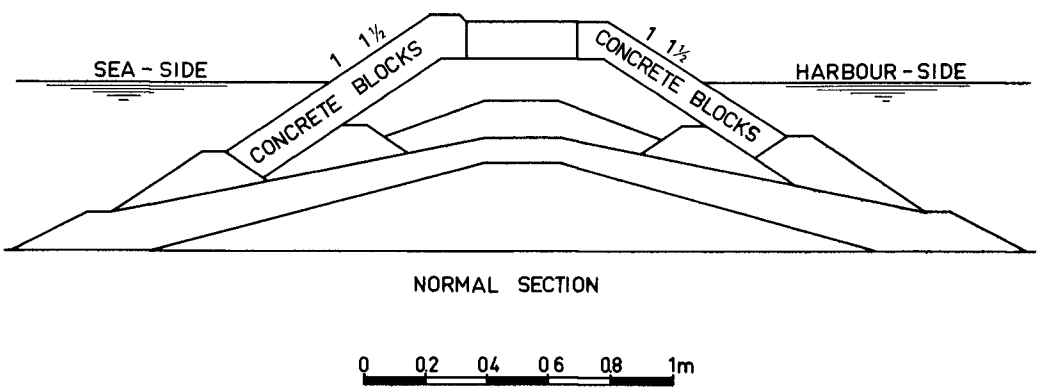

Fig. 3. Model of IJmuiden breakwater as used for comparative tests.

CHARACTERISTICS OF THE ARMOUR UNITS

The comparative tests started with six different armour units: quarrystone, cubes, tetrapods, "tripods", "bipods" and akmons.

The volumes and specific weights of the different types were the same. Sketches of the artificial blocks are given in figure 1. As the akmon (the Greek word for anvil) was found to be the most promising of the new types that were investigated, a detailed sketch of this block is given in figure 2.

The number of blocks required for covering a certain area with a double layer, placed pell-mell, can be expressed as:

$N = C.A.V.^{-2/3}$, in which:

N is the number of blocks in a double layer on a surface A.
V is the volume of one block.
C is a coefficient, depending on the shape of the blocks.

A similar formula is given by the Waterways Experiment Station (W.E.S.) (see reference 2, page 11) and values of C for various shapes of blocks can be derived from the data presented in the report mentioned above. The results obtained by W.E.S. and the authors are as follows:

Armour Unit	$C_{W.E.S.}$	$C_{HYDR.LAB.}$
Quarrystone	1,24	1,22
Modified cube	1,16	-
Tetrapod	1,0	1,03
Quadripod	1,0	-
Hexapod	1,22	-
Tribar	0,92	-
Akmon	-	0,90
Cube	-	1,18
"Tripod"	-	1,05
"Bipod"	-	1,08

The results obtained for tetrapods are in accordance with those given by SOGREAH (3).

Needless to say that the amount of stone or concrete required to construct a cover layer is, for the same blockweight, proportional to the value of C.

A quick, but somewhat rough impression about the porosity of a number of stone layers was obtained by filling a box with blocks, placed at random. The dimensions of the box were about 5 x 6 x 6 times the "diameter" of a block.

For the different types of blocks tested, the results are as follows:

	Akmon	Cube	Tetrapod	"Tripod"	"Bipod"	Quarrystone
Porosity (%)	60	47	53	53	51	45

For akmons the porosity of a double layer was determined by measuring the thickness of the layer by means of a sounding rod, equipped with a ball and socket foot, in order to obtain a result comparable with the W.E.S. (2).

The foot was circular with a diameter of one-half times the diameter of the blocks. In this way the porosity was found to be 55%.

AKMON ARMOUR UNIT FOR COVER LAYERS OF RUBBLE MOUND BREAKWATERS

COMPARATIVE TESTS

REGULAR WAVES

Models - The first series of comparative tests for the design of IJmuiden breakwater were carried out in a wave tank, 2,5 m wide and 29 m long and equipped with a wave board, generating regular waves. In front of the wave machine a filter was provided in order to reduce the waves reflected by the models. In this flume five sections (fig. 3), each 0.5 m wide and covered with different types of armour units were tested simultaneously by gradually increasing the wave height.

These wave heights were measured at different places in front of the breakwater by a parallel wire resistance gauge and recorded by a pen recorder. From the records the incident wave height was determined. The wave period was kept at 1.4 sec.

The slope was 1 : 1.33, 1 : 1.5 and 1 : 1.6 (only for the first slope enough results are available). The waterdepth was as indicated in fig. 3, namely 0.27 mat the toe of the breakwater but in front of the breakwater there was a slope of 1 : 5 till a depth of 0.42 m.The blocks had a mean density of 2200 kg/m^3 and a volume of 38.10^{-6} m^3.

In order to be able to make a comparison the results were plotted as a function of the wave height as defined by Hudson (1) (2) viz. the average height of the highest one third of the waves in the wave trains. Then the highest waves which occur when starting and stopping the wave machine are approximately 12% higher. This, however, does not mean that the tests may be considered as being identical to Hudson's.

Results - The results of the stability tests are plotted in fig. 4 with K_D as a function of the damage. K_D is the damage coefficient:

$$K_D = \frac{H^3}{V \Delta^3 \operatorname{cotg} \alpha}$$

with H = wave height, causing a certain damage.
V = volume of the block.

$$\Delta = \frac{\rho_s - \rho_w}{\rho_w} .$$

ρ_s = density of the stone.
ρ_w = density of the water.
α = angle of inclination of the slope.

For some blocks also results with cotg α = 1.6 were obtained. Then K_D generally is greater, but the small number of tests does not lead to a definite conclusion whether the function of α in the Hudson formula (1) is somewhat optimistic for the steeper slopes.

WIND WAVES

Models - For the second series of tests for the design of IJmuiden breakwater a wind flume was used, 4 m wide and 100 m long equipped with a wave board and an electrically driven fan blowing wind over the entire length of the flume. The fan is provided with adjustable vanes by means of which the air current can be regulated up to a wind velocity of 20 m/sec. Here the same method of measuring wave heights was used

and the wave attack is characterized by H_{15} being the wave height exceeded by 15% of a series of waves.

Although it is possible to raise in the windflume by wind only a spectrum of wave heights as will occur in nature, the wave period is limited. When the scale of the model requires a period exceeding this limit, the waves are generated by wind combined with the wave board. This means that somewhat less higher waves occur. The more the period exceeds the limit, the greater this deviation can be, but generally it is still acceptable. Especially for the investigation of IJmuiden breakwater this meant no draw-back, because in the limited depth present the highest waves were broken before reaching the structure, but for general application the results are not suitable.

The waterdepth in these tests was 0.27, 0.30, 0.33 and 0.36 m. The density of the blocks was 2600 kg/m^3 and the volume of the blocks was 50.10^{-6} m^3.

Results - Damage coefficients were obtained for three types of blocks on a slope of 1 : 1.5 in a waterdepth of 0.27 m with a wave period of 1.1, 1.4 and 1.8 sec of which 1.4 sec was the most dangerous period.

K_D		Akmons	Cubes	Tetrapods
Damage	0%	4.8	3.5	4.7
	1%	11	7	9
	2%	12	8	11
	5%	± 17	± 14	± 15

REMARK

Because doubt was expressed whether the stability of the akmon might be mainly due to its sharp edges comparative tests were performed with normal akmons, tetrapods and akmons of which the sharp edges were rounded off. In these tests, with oblique and normal wave attack, the "rounded off akmons" showed no significant difference with the normal akmons, although the blocks were rounded off much more than is found to happen with concrete blocks in prototype breakwaters. So it may be concluded that the stability characteristics of the akmon are due to its principal form and not to its sharp edges.

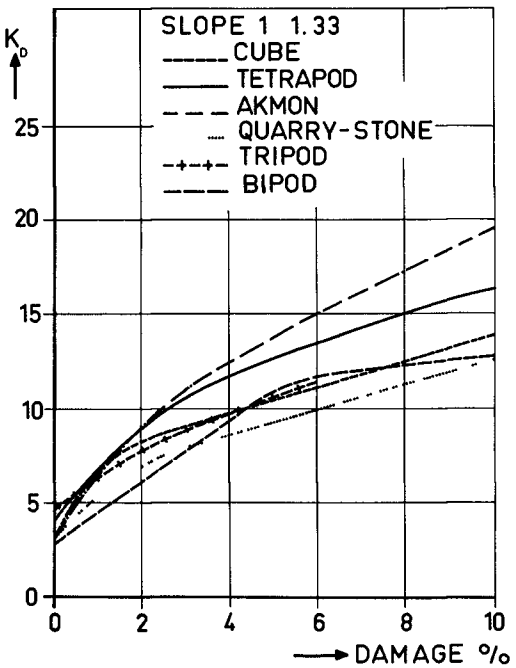

Fig. 4. Test results with regular waves.

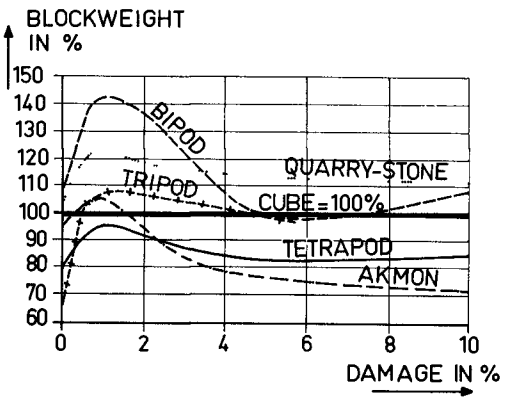

Fig. 5. Required block weight compared with cubes.

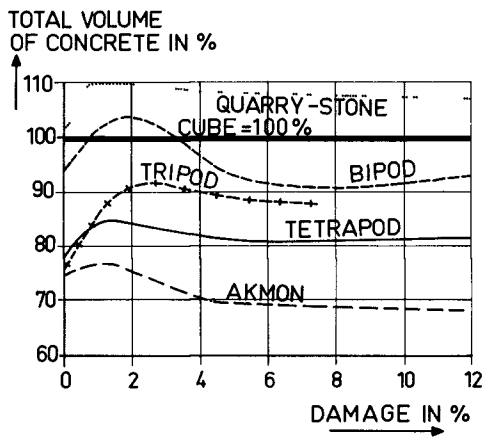

Fig. 6. Required volume of concrete compared with cubes.

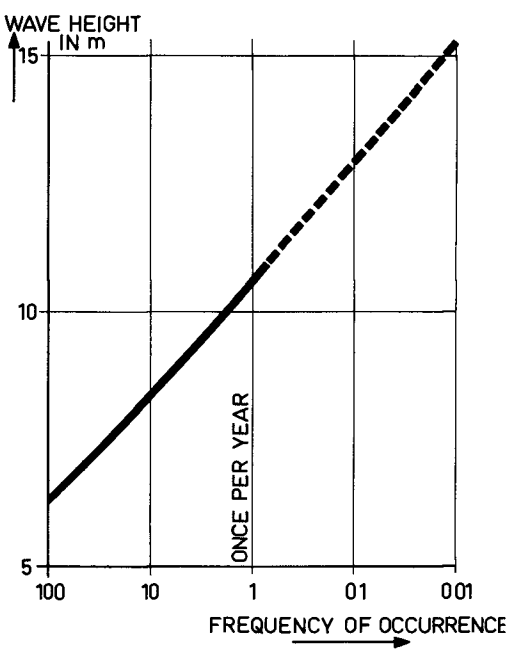

Fig. 8. Frequency of occurrence of individual wave heights near the Dutch coast.

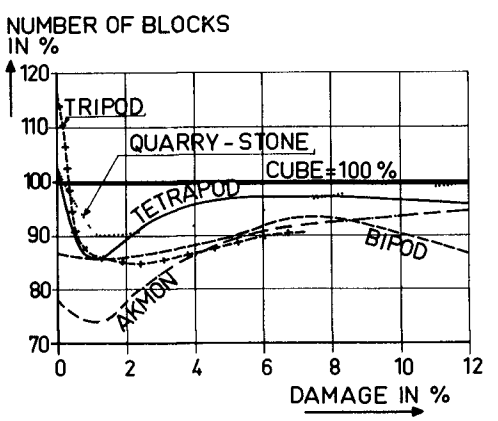

Fig. 7. Number of blocks required in comparison with cubes.

DESIGN PROCEDURE FOR COVER LAYERS

GENERAL CONSIDERATIONS

Some considerations are given below on the design prooedure for cover layers, as it appears that this procedure has an influence on the block-type and -weight to be chosen.

One of the most important requirements for the design of a breakwater is of course that the investment and costs of maintenance are minimum.

In case that natural stones are applied, the possibilities given by the quarry are often determinative. When designing a oover layer of concrete blocks, the specific conditions for the breakwater concerned can be taken into account next to the general requirements. As such can be mentioned a.o.:

1. The blocks must allow the application of steep slopes, in order to reduce the material in the core. A praotical limit is 1 : 1.5 to 1 : 1.3 depending on the oore material and the wave motion during excecution.

2. Manufacturing of the blocks shall be relatively easy.

3. It is often necessary to place the blocks at random, in case of building in a rough sea and in order to reduce the time for placing.

4. The covering of special points, such as bends and the head, must be possible without extreme difficulties.

The costs of realising a cover layer, as far as dependent on the shape of the blocks, are determined by:

1. The total amount of concrete which is required.

2. The weight of the individual blocks (in view of the equipment that is available).

3. The costs of manufacturing.

4. The number of blocks to be placed (number of moulds and manipulations).

The data required to evaluate the various types of blocks in the light of these factors, as far as can be derived from model tests are given below.

BASIC DATA FOR DIFFERENT TYPES OF ARMOUR UNITS

Slope - From the tests it appeared that the application of a slope of 1 : 1.33 is, in principle, possible for all types of blocks.

Method of placing - Although it is very difficult to reproduce in the model exactly the method of placing in nature (see (2)), a comparison can be made between the different types of blocks, based on model tests in whioh the blocks are placed at random.

Block weight - An estimate of the block weight which is required can be made based on the coefficients K_D given in the foregoing chapter The block weight is inversely proportional to the value of K_D. For comparison the results are given compared to the values for cubes, which have been set to 100%.

For armour unit X and cubes, the ratio of the block weights is $\frac{W_X}{W_C} = \frac{K_{DC}}{K_{DX}}$. In figure 5 this ratio is plotted as a function of the damage.

Total volume of material - The total volume of material in the cover layer of a certain area is: $Q = N.V$, in which N is the number of blocks at area A and V the volume of one block. It was derived that $N = C.A.V^{-2/3}$, hence:

$$Q = C.A.V^{1/3}$$

Compared to the values for cubes: $\frac{Q_X}{Q_C} = \frac{C_X}{C_C} \cdot \left(\frac{K_{DX}}{K_{DC}}\right)^{1/3}$.

This ratio is given in figure 6.

Number of blocks - From the formula $N = C.A.V^{-2/3}$ it appears that the number of blocks which is required can be expressed as:

$$\frac{N_X}{N_C} = \frac{C_X}{C_C} \cdot \left(\frac{K_{DX}}{K_{DC}}\right)^{2/3}.$$

The results are shown in figure 7.

From the results it appears that besides K_D the coefficient C has a great influence on the evaluation of the various types of blocks. A relationship between C and K_D is not yet established.

A difficulty in praotice is that the influence of the block weight on the costs depends on the equipment available, which is normally not known until an advanced stage of the design.

The remarkable path of the curves between 0 and 2% damage is due to the relative great increase in the value of the coefficient K_D for oubes which was found between 0 and 1% damage. The influenoe of accidental conditions, however, increases for very small damage, so the reliability of the results beoomes less.

Restriction - It must be noticed that the results whioh are presented here are based on tests with regular waves, and for a slope of 1 : 1.33 only. Data for general application for wind generated waves and other slopes are not yet available.

DESIGN CONDITIONS

Within the scope of this paper, a restriction is made to wave conditions under direct influence of the wind. Swell is not dealt with.

In case of deep water relative to the wave heights the wave conditions to be expected at the breakwater location have to be related to the frequenoy of occurrance. Consequently the damage criterion has to be expressed in terms of probability. Once the probability with which a certain damage is accepted has been chosen, the accumulative wave attack corresponding with this probability must be determined.

The accumulated wave attack can be defined as the sum of all wave conditions up to and including those generated by a storm which has the frequency of occurrence equal to the probability with which damage is accepted. This definition implies that the probability on damage is a time dependent factor due to the accumulative effect. Moreover it is known that consolidation occurs under moderate wave conditions.

For the design, by calculation of modeltests, the disposal of a representative criterion for the wave conditions including the accumulative effect is essential. Experiments have shown that the total damage, caused by wave conditions generated by successive storms, cannot be derived from the sum of the contributions of the individual wave heights since the damage is not determined by one individual wave, however, depends on the composition of the series of waves.

For instance: the highest waves in a series with a significant height H_s = 4 m and a duration of 10 hours, can be the same as in a series with H_s = 5 m during 1 or 2 hours. The damage, however, is found to be different and in general greater in the latter case. Further researoh on this point is necessary.

At present the normal testing procedure in the windflumes is, that based on the distribution curve for significant wave heights in prototype a series of tests is carried out. In each series with a selected significant wave height, the wave height distribution from nature is reproduced as good as possible. Taking into account the duration of the storms it is tried to approach the phenomena in nature. A diffioult point in this procedure remains the reproduction of the effects of high waves in the very frequently occurring series, with smaller significant wave heights, i.e. long duration of tests.

It may be noted that a decision on the probability with which damage to the structure is accepted, cannot be made without oonsidering the rate of damage, as both the investment and the costs of maintenanoe are determinative.

Moreover, when a cover layer is built up of blocks placed at random, the blocks that had an unfavourable position will be removed first, after which the struoture is stable again for the same conditions. So a slight damage may be acceptable without repairing.

The foregoing considerations will be illustrated by an example.

EXAMPLE

For the moment we assume for simplicity that the damage can be related to the individual wave height.

Considering the conditions along the Dutoh coast the frequency of occurrance of individual wave heights can be represented approximately as shown in figure 8. When the design is based on 1% damage with a probability of on the average once in 15 years the oorresponding wave height is 13.7 m. The wave height corresponding with a frequency of occurrance on the average once in 100 years is 15.6 m, so 1.18 times higher.

The various quantities, in which the values for cubes are set to 100 for once in 15 years, are as follows:

Armour units	Block weight	Total amount of material	Number of blocks	Damage with a probability of 1% per year
Cube	100	100	100	5½ %
Quarry-stone	123	110	90	4½ %
Tetrapod	95	85	86	4 %
Akmon	105	77	75	2½ %

The last column gives an idea about the maintenance that is required.

Based on the criterion that 2% damage is accepted (without repairing) with a probability of once in 15 years, the following results are obtained:

Armour units	Block weight	Total amount of material	Number of blocks	Damage with a probability of 1% per year
Cube	100	100	100	9 %
Quarry-stone	118	109	92	8 %
Tetrapod	91	84	92	7½ %
Akmon	92	74	81	5½ %

Needless to say that the probabilities given above are arbitrary.

BREAKWATERS WITH AKMONS

The results of the comparative tests led to the designs of some breakwaters investigated by the laboratory. At the time of these investigations the above described design procedure was not developed so far that application in details was possible. As a criterion the significant wave height with a probability of 5% per year (prototype) was chosen to effect a damage of about 1%.

For the first design this resulted in a significant wave height between 0.102 and 0.108 m with an average duration of the storm of 1.3 hours (values on model scale). In the tests the breakwater was exposed to wave attack with a gradually increasing significant wave height up to 0.108 m and more. In view of the damage criterion of 0-1% the damage was sensitive to small variations. For this reason the duration of some storms was exaggerated. The wave heights greater than 0.108 m were applied in order to get an idea about the damage during storms with a probability less than 5% per year (prototype).

In the tests the waterdepth was 0.20 m. With a slope of 1 : 1.75 and a density of the concrete of 2400 kg/m^3 the volume of the block, based on a rather safe value of K_D had to be 40.10^{-6} m^3. The wave period was 1.4 seconds.

Four series of tests were performed on a normal section and the head as given in figure 9 and 10. For illustration a review of the tests is given below:

Test 1. Normal section (figure 9).

H_{15}	duration in model	results
0.06 m	1 hour	no damage
0.078 m	1.5 hrs	no damage
0.088 m	2 hrs	no damage
0.098 m	2 hrs	1% damage to akmon layer on sea-side slope
0.104 m	2 hrs	1% damage to akmon layer on harbour-side slope due to over-topping
0.108 m	0.7 hrs	no further damage
0.112 m	2.5 hrs	damage to harbour-side slope increased to 2% of the akmon layer
0.116 m	2 hrs	damage to harbour-side slope increased to 3% of the akmon layer

During wave attacks with $H_s > 0.11$ m, the highest waves were breaking before they reached the structure.

Test 2. Normal section.

0.06 m	1 hour	no damage
0.072 m	2 hrs	no damage
0.10 m	6 hrs	no damage
0.11 m	4 hrs	no damage

Test 3. Normal section.

0.06 m	1 hour	no damage
0.078 m	1 hour	no damage
0.098 m	2 hrs	no damage
0.104 m	4 hrs	no damage
0.11 m	1.7 hrs	damage to harbour-side slope of the akmon layer due to over-topping 2-3%

The same procedure of gradually increasing the wave height was followed by testing the head and the results can be summarized as follows: Up to 0.10 m no damage occurred. With H_{15} = 0.11 m generally no damage occurred but in one test four blocks had rolled down. With H_{15} = 0.12 m four to six blocks had rolled down and with H_{15} = 0.13 m the damage increased to about fifteen blocks. From these tests and the probability of occurrance of different wave heights, the probability that a certain damage will be caused can be estimated.

For a second design the block weight was limited because of the available equipment. On model scale the maximum block weight was 0.16 kg. The waterdepth was 0.22 m and the design wave height was given by the highest wave possible in this waterdepth as waves higher than the maximum possible wave height in this waterdepth had to be expected with a probability greater than 5% per year (prototype). So for this design the normal design procedure could not be followed and the breakwater had to be stable for the maximum wave in the waterdepth present. The wave period was 1.4 sec.

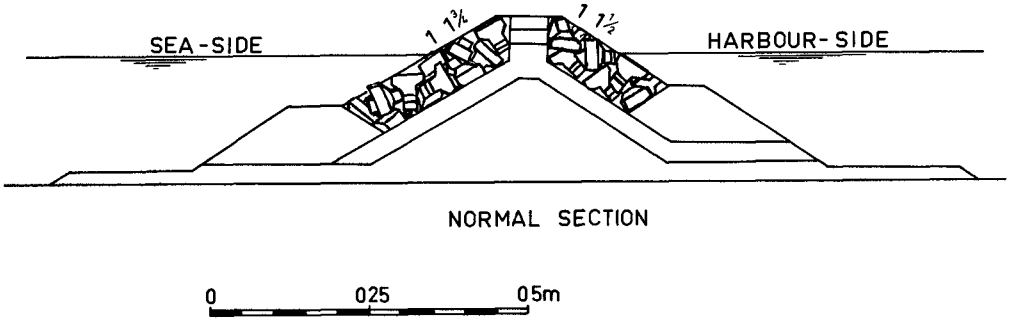

Fig. 9. Design of breakwater with akmons.

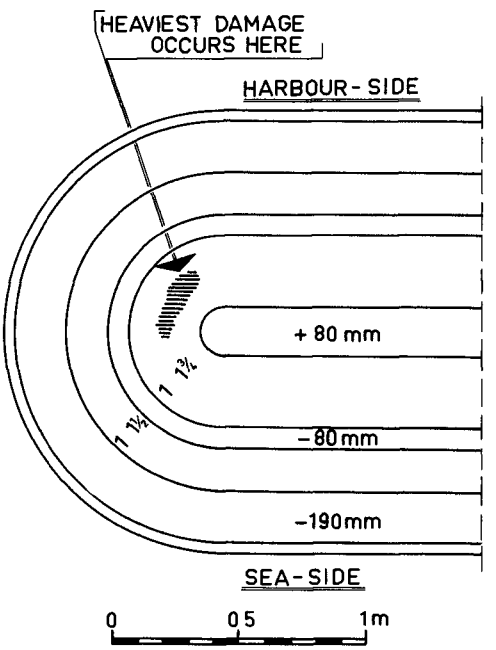

Fig. 10. Head of breakwater.

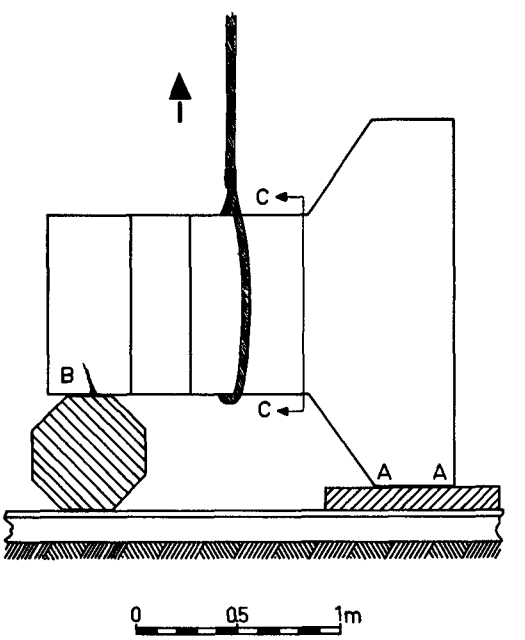

Fig. 11. Disposition of 6 ton akmon for test on mechanical strength.

With the given block weight and a density of 2450 kg/m^3 at first a slope of 1 : 1.5 was tried. Then until a significant wave height of 0.13 m no damage occurred but with 0.16 m wave height (measured in sufficient deep water at some distance from the breakwater toe) the damage was considered too much. A slope of 1 : 2 with a crest on + 0.16 m could meet the design criteria and in two tests only small acceptable damage of 0 to 2% occurred to the sea-side cover layer. Due to the limited waterdepth this damage will not be exceeded.

MECHANICAL STRENGTH OF THE AKMON

In order to get an idea about the mechanical strength of the akmons, which is important with regard to handling and placing of the blocks and with respect to oscillation or displacement under wave attack, tests were made on a block with a weight of 6 tons (see ref. 4).

The block was made of non-reinforced concrete with 325 kg Portland cement per cubic metre and had a density of 2500 kg/m^3. After 24 hours the compressive strength of a test cube was 1.88 kg/mm^2.

After 5 days the strength of the block was tested by dropping it from increasing heights on a floor constructed as follows: On a bottom of sandy clay, I beams with a height of 0.15 m were placed close together. On this beams at one end a steel armour-plate, 0.10 m thick, and at the other end a reinforced concrete block, 0.5 m high, were placed, supporting the akmon (see figure 11). The block was lifted by means of a sling around the centre part and fixed to the hook of a crane which could be released suddenly, thus dropping the akmon on the armour-plate and concrete block. The damage caused to the akmon was thoroughly investigated. The results that were obtained can be summarized as follows:

Height of fall	Remarks
0.5 m	None
1 m	Slight damage to sharp angles (see A on figure 11)
1.5 m	Small crack visible at one side (see B)
2 m	Akmon broken in cross section C-C

Assuming for the moment that this single test may be considered as representative for the strength of the akmon, it may be expected that this block can withstand the forces excerted during handling and those caused by oscillation or displacement under wave attack.

CONCLUSIONS

- When designing a breakwater, the damage criterion has to be expressed in terms of probability. This criterion has to include initial damage and the damage that may possibly be of interest for maintenance.
- Once the probability with which a certain damage is accepted has been chosen, the accumulative wave attack corresponding

with this probability must be determined.

- Starting from the chosen damage criteria a comparison between the different block types can be made, based on economical and practical considerations.
- As a result it will appear that the akmon is one of the most suitable blocks developed up till now.
- From a test on the mechanical strength it appeared that the akmon is sufficiently strong for practical application.

ACKNOWLEDGEMENTS

The akmon was developed starting from a suggestion of Mr. J.G.H.R. Diephuis, Chief Engineer of the laboratory.

The authors wish to express their gratitude to Mr. C. Stigter who carried out part of the tests and to Mr. J.E. Prins, Chief Engineer of the laboratory for his help in compiling the report.

REFERENCES

(1) R.Y. Hudson. Laboratory Investigation of Rubble-Mound Breakwaters. Vicksburg 1959.
(2) R.Y. Hudson. Wave Forces on Rubble-Mound Breakwaters and Jetties. Vicksburg 1961.
(3) Sogreah. Pose et Manutention des Tetrapodes. Grenoble 1958.
(4) P. Danel, E. Chapus and R. Dhaille. Tetrapods and other Precast Blocks for Breakwaters. Proceedings ASCE 86 1960 No. WW3.

PATENT

International patent applied for by the commissioners of the research, viz. "Rijkswaterstaat", The Hague and Royal Netherlands Harbour Works Co. Ltd., Amsterdam.

CHAPTER 26

A SIMPLE MATHEMATICAL MODEL OF WAVE MOTION ON A RUBBLE MOUND BREAKWATER SLOPE

Anton Brandtzaeg, Dr.techn.
Professor of Construction and Harbour Engineering
Technical University of Norway
Trondheim, Norway

A. INTRODUCTION

In the improvement of design criteria for the layer of cover blocks on rubble mound breakwaters important advance has been made in recent years (1), (2), (3). Still, some points seem to require further study, among them the effect o the spesific weights of block material and fluid on the stabi lity of the cover. In this respect the magnitude of the flui accelerations involved, of which little information is availab may be of some importance. For evaluation of the acceleratic as well as for other purposes, a roughly approximate mathemat description of the motion of the water rushing up and down th breakwater front may be of some use.

This motion certainly is neither steady nor uniform. Visual and photographic observation through the glass panel c a wave channel seems to indicate, however, that unsteadiness the more important characteristic of the motion during the up and downrush proper. It seems reasonable, therefore, to atte a first approximation to a description of the motion by negle ing, to a certain extent, its non-uniformity. Necessarily, a the same time also the requirement of continuity must be part disregarded.

In the following a mathematical model based on this point of view is presented for consideration. It is believec that by means of this model values of displacements, velociti and accelerations can be calculated, which may reasonably be considered as useful, although quite rough, approximations tc the actual values. For a few particular cases, experimental evidence is reported.

The model has reference only to the up- and downrush proper, that is, to the motion of the water above some limit level, at or somewhat below the Still Water Line (referred t hereafter as the SWL). The motion below this level, where tl downrush meets the oncoming next wave, could hardly be conce of as being uniform.

The velocities indicated in Figures 5 and 6 indicate that the limiting level, below which the model is not applicable, may be placed considerably lower than the SWL, perhaps even one wave height lower. In the absence of sufficient data the SWL has for the time being been chosen as the limit.

Because during uprush an unknown but not negligible quantity of water will disappear into the breakwater, and also for other reasons, useful numerical results are obtainable only for the case of downrush. Nevertheless the case of uprush has been briefly included, to show that also for that case does the model give a picture of the motion fully compatible with observation.

While the present study aims only at contributing somewhat towards a description of the fluid motion involved, and not at the development of design formulae, still such a description would be pointless if it did not cover that region of the breakwater slope, which in the cases considered, is the critical one with regard to failure by dislocation of cover blocks. This point, therefore, requires some consideration.

Sigurdsson (4), in a very illuminating treatise, recently found that the maximum normal (lifting) force on the cover blocks mostly occurred at the approximate level of lowes wave retreat. With regard to failure in this region, mainly caused by normal forces, the model will be of scant interest. Probably this type of failure is predominant with most breakwaters whose cover layers consist of blocks of regular shape closely stacked with only narrow slots open between them.

However, with regard to cover layers of natural stones placed pell-mell on the breakwater slope, numerous observation among them the very careful ones made by Hedar (2), indicate t region about or even above the SWL as the critical one. *) Observations during a great number of tests at the River and Harbour Research Laboratory of the Technical University of Nor (referred to hereafter as the RHRL) fully confirmed this resul It seems, therefore, that our model should not be irrelevant to the study of the conditions of failure of rubble mound breakwaters covered by broken rock, placed pell-mell, by far the most common type in Norwegian and apparently also in U.S.A. practice.

As the model can yield numerical results only in the case of downrush, it can be of use only in the study of cases where failure occurs during downrush. This, according to Heda (2), holds true for slopes steeper than about 1:2,5. Only a sl of 1:1,5 has been treated here. It is the slope most common i Norwegian practice, and seems to be fairly commonly used also the U.S.A.

*) Out of records from 29 test runs, only 2 included stones be moved from a level slightly more than one wave height below while all records included stones being moved from levels a considerably above, the SWL. ((2),Table 65.1 and 65.2).

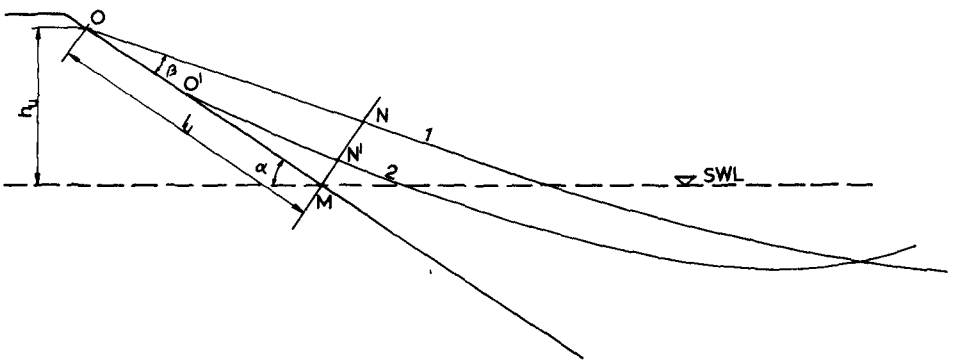

Fig. 1

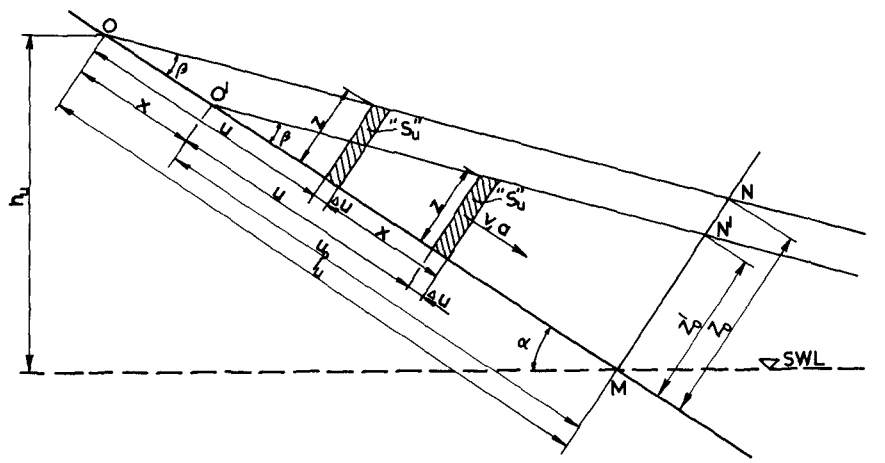

Fig. 2

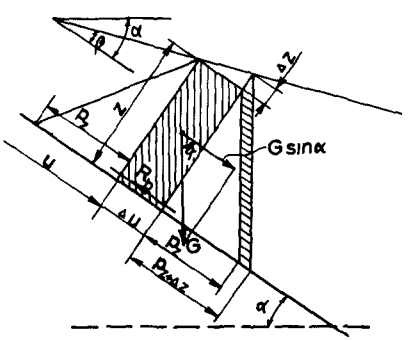

Fig. 3

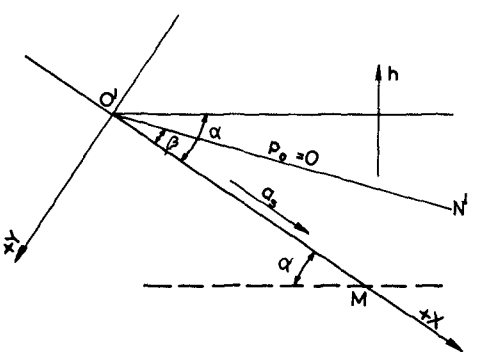

Fig. 4

A SIMPLE MATHEMATICAL MODEL OF WAVE MOTION ON A RUBBLE MOUND BREAKWATER SLOPE

B. THE MODEL

Let the sketch in Fig. 1 represent the breakwater slop and two successive profiles of the downrushing wave, profile 1 taken at the start of downrush and profile 2 at some later moment. The height of uprush is h_u, corresponding to a distan l_u, along the slope, from the starting point of downrush, O, t the SWL. Only the body of water above the line MN, will be considered, it being assumed that during downrush the motion above MN will not be significantly influenced by what happens below that line.

The following assumptions will define the model with regard to downrush (Fig. 2).

1. At the start of downrush, the surface profile, ON, is a straight line, forming the angle, β, with the breakwater front, OM. Any individual slice, "S_u", of the triangular body of water, MON, is defined by its original distance, u, from the top of the triangle, O, measured along OM. The height of the slice is $z = u \tan \beta$, its width being Δu.

2. Within each slice the motion of the fluid will be uniform, each slice will move parallel to the slope as a unit, without change of shape.

3. The several slices will move independently of each other, without regard to continuity of the fluid.

4. The displacement, x, of any slice, "S_u", from its top position, the velocity of the slice, v, and the acceleration, a, at the time, t, from the start of the motion down the slope can be calculated from the components parallel to the slope of the forces acting on the slice. These forces are: the weight of the slice, the pressure difference between the two sides of the slice due to the difference in slope between the breakwater front and the surface of the fluid, and the forces acting on the slice from the rough cover layer, equal of magnitude and opposite of direction to the parallel forces acting on the cover blocks from the fluid. It is assumed that the pressure forces will be practically the same as if the fluid were an ideal one, with no boundary influence, while the force from the cover layer can be approximately calculated independently of the other two, and can, without too much error in the fi result, be considered as acting at the center of gravity of th slice.

By calculation of the displacement, x, of neighbouring slices, the extent of discontinuity involved in the model may be evaluated. This point will be considered in Section F.

C. FORCES ACTING ON THE SLICE "S_u"

On the assumptions stated in Section B, the componer parallel to the slope of the forces acting on any slice, pe unit of depth, normal to the paper, can be calculated as follows, (Fig. 3):

1. The weight of the slice, G. Ignoring the small upp triangle $\Delta u \Delta z$, we obtain the parallel component per unit of depth:

$$G \sin\alpha = z \Delta u \gamma_f \sin\alpha \qquad ($$

2. The pressures on the upper and lower sides of the slice.

Assuming the fluid to be ideal, and taking no accoun of boundary effects, we may derive the pressure distribution in the down-rushing body of fluid from the well known Euler equation, according to which the acceleration in any directi s, is:

$$a_s = -\frac{1}{\rho} \frac{\delta}{\delta s}(p + \gamma_f h) \qquad ($$

where p is the pressure at any point and h is the vertical elevation of that point, positive upwards. Using the axes o co-ordinates shown in Fig. 4, we obtain for the direction no to the slope:

$$a_y = 0 = -\frac{1}{\rho} \frac{\delta p}{\delta y} + g \cos\alpha$$

Taking the pressure at the surface O'N' to be zero, find that under the assumptions stated, the pressure at any x, y, in the fluid, will be:

$$p = \gamma_f (x \tan\beta + y) \cos\alpha \qquad ($$

The total resultant pressure upwards along the slope per unit of depth of the slice, perpendicular to the paper, will be (Fig. 4):

$$F_p = \gamma_f z \cdot \Delta u \tan\beta \cos\alpha \qquad ($$

3. The boundary resistance along the breakwater front, I

This resistance obviously is related as well to the velocity as to the acceleration of the fluid. There seems tc a difference of opinion as to whether or not the two effects

be considered independently of each other. Discussion of evidence in favour of either view would exceed the scope of the present study. On the strength, among other data, of the investigation of wave forces on piles by Bretschneider (7) and Wilson (8) it is here assumed that the two types of resistance to the motion of the fluid, the one due to drag forc on the cover blocks and the other due to inertial forces, may with sufficient approximation, be estimated separately.

a) Assuming, like Hedar (2), that the well known equations relating to "sand roughness" in pipes may be applied to the very rough surface of a rubble mound breakwater, the resistance, per unit of depth, derived from the velocity of the fluid at any moment, as if the motion were steady, may be written:

$$R_{bv} = \tau \, \Delta u = \gamma_f \, z \, h_f = \frac{\gamma_f^2 \, v^2 \Delta u}{32 g (\log_{10} \frac{14,8 \cdot z}{k})^2}$$

where h_f is the loss of head over the distance Δu and k is the equivalent "sand roughness", taken to be equal to some me diameter of the cover blocks. (References: (5), Equations (3 and (10) of III, § 11, and (6), Equations (28) and (33) of Chapter VI). Here the depth of water measured normal to the slope, z, has been substituted for the hydraulic radius of th pipe.

Certainly, Eq. (5) can not be expected to apply with too much accuracy to the case considered here. Reinius (9) ir a recent investigation found that in wide channels with actua sand roughness of 0,5 to 4,0 mm, the factor 14,8 in the denon nator of Eq. (5) should be replaced by the factor 12,4. However, the degree of roughness in that case was very differen from that of a rubble mound breakwater slope. A few tests ma at the RHRL in June-July 1962 with a channel bottom practical identical with the cover layer on the breakwater model, refe to in Section E, indicated that within the range of velociti and depths of water relevant in this case (v = about 30 cm/s to about 90 cm/sec and z = 3,3 cm to 9,7 cm), Eq. (5) gave a fair representation of the resistance to a steady current.

Nevertheless, it is of course possible that in our case the Prandtl equation, (5), should be replaced by some other relationship. There has, however, been no possibility of further study of this problem, aside from the few tests, ferred to above. In view of the confirmatory indications ap from them, it was felt that for the present purpose Eq. (5) tentatively be applied. Certainly, however, the problem of turbulent shear in cases where k and z are of the same order of magnitude needs clearing up.

b) The boundary resistance related to the acceleration must be equal to the inertial forces on the cover blocks. Assuming an inertial coefficient C_{Mp} for the force parallel to the slope, and taking the volume of a block to be $C_V k^3$ and the area of the slope occupied by the block to be $C_A k^2$, we can state this part of the boundary resistance on our slice, "S_u", per unit of depth normal to the paper, to be

$$R_{ba} = \frac{\gamma_f}{g} \frac{C_V}{C_A} k C_{Mp} \cdot a \, \Delta u \qquad (6)$$

Very few facts on which to base an estimate of the proper magnitude of the coefficient of mass, C_{Mp}, to be appli in the present case, are known to the writer. For a large diameter cylinder, where the theoretical value would be 2,0, Wilson (8) indicates figures around 1,5 for confused sea conditions. For a sphere the theoretical value would be 1,5. In the model experiments discussed in Section E, natural stor were used, whose average largest linear dimension was about twice the average smallest linear dimension, - something between a cylinder, a disc and a sphere. This might suggest a rather large value of C_{Mp}, perhaps somewhere between 1,o and 1,5, rather closer to the latter value.

On the other hand, only the upper parts of the cover blocks will be fully exposed to the forces from the moving fluid. This shows up in the fact that the value of the drag coefficient, C_D, derivable from Eq. (5), is very small, only somewhere around 0,1 to 0,15. Alltogether it has been decide to apply in the present study the value $C_{Mp} = 0,4$.

Further values chosen for use in the following are: $k = 6$ cm, $C_V = 0,5$ and $C_A = 1,o$, which are believed to correspond reasonably well to the dimensions and the shape of the stones actually used in the experiments discussed in Section

D. CALCULATION OF MOVEMENT OF THE SLICE "S_u"

For the Case of Downrush

The total downward force parallel to the slope, actin on the slice, "S_u", per unit of depth, is:

$$F = G \sin\alpha - F_p - R_{bv} - R_{ba}$$

By entering Eq. (1), (4), (5) and (6) and dividing by the mass of the slice, $\frac{\gamma_f}{g} z \, \Delta u$, we get the acceleration of tl slice, directed downward, parallel to the slope.

$$a = \frac{F \cdot g}{\gamma_f z \Delta u} = g \sin\alpha - g \tan\beta \cos\alpha$$

$$- \frac{v^2}{32 z \left(\log_{10} \frac{14,8 z}{L}\right)^2} - \frac{C_V}{C_A} \frac{k}{z} C_{Mp} \cdot a \qquad (1$$

By entering Eq. (3) in Eq. (2) it may be seen that the two first members on the right hand side of Eq. (7) represent a_o, the acceleration which we would have with no boundar resistance.

Eq. (7) can be written:

$$\frac{dv}{dt} = A^2 - \frac{v^2}{B^2}$$

where

$$A^2 = \frac{g(\sin\alpha - \tan\beta \cos\alpha)}{1 + \frac{C_V}{C_A}\frac{k}{z} C_{MP}}$$

$$B^2 = \left(1 + \frac{C_V}{C_A}\frac{k}{z} C_{MP}\right) 32\, z \left(\log_{10} \frac{14{,}8\, z}{k}\right)^2$$

It is seen that A^2 and B^2 contain no term variable with the motion of the particular slice "S_u", although $z = u\,t$ varies from one slice to another. Therefore A^2 and B^2 are invariant with respect to t, and Eq. (8) has the solution:

$$v = AB \tanh\left(\frac{A}{B} \cdot t\right) + C$$

Taking t = 0 at the moment of start of downrush, when v = 0, we obtain the downward velocity at any moment, t,

$$v = AB \tanh\left(\frac{A}{B} \cdot t\right)$$

and the distance, x, travelled from the highest position of the slice:

$$x = B^2 \ln\left(\cosh\left(\frac{A}{B} \cdot t\right)\right)$$

while the acceleration at any moment is:

$$a = \frac{A^2}{\cosh^2\left(\frac{A}{B}\, t\right)}$$

For the Case of Uprush

If the slice "S_u" moves up the slope, instead of down which of course presupposes an initial upward velocity, v_o, the only change in the basic equation (7) will be that the si of the third member on the right hand side changes from - to

(Note that F, a, v and x all are still considered as positiv when directed downward). Instead of Eq. (8) we get:

$$\frac{dv}{dt} = A^2 + \frac{v^2}{B^2}$$

where A and B are given in Eq. (9) and (10). The solution for v now is:

$$v = AB \tan\left(\frac{A}{B}t\right) + C$$

If we assume that at t = 0 our slice "S_u" just passe the line M N, Fig. 2, going up with a velocity

$$v_o = -\sqrt{C_w g H}$$

where H is the wave height in front of the breakwater and C_w is a coefficient, we find that at a later moment, t,

$$v = -\sqrt{C_w g H} + AB \tan\left(\frac{A}{B}t\right)$$

Our particular slice "S_u" reaches its top position, where v = 0, when t is equal to

$$t_o = \frac{B}{A} \operatorname{arc}\left(\tan = \frac{\sqrt{C_w g H}}{AB}\right)$$

We further get:

$$x = -\sqrt{C_w g H}\, t - B^2 \ln \cos\left(\frac{A}{B}t\right)$$

and

$$a = \frac{A^2}{\cos^2\left(\frac{A}{B}t\right)}$$

In this case the zero point for x, at t = 0, will be at the line M N, Fig. 2, instead of at the top, O. And since different slices pass this line at different times, the zero moment, t = 0, will vary from slice to slice.

Let the common datum of reference for the time apply to all slices be the moment when a certain slice, "S_u", passe the line M N, let the total time elapsed from that moment be designated as σ, and let the time when slices "$S_{n+\Delta u}$", "S_{n+2}, "$S_{n+3\Delta u}$" ..... pass M N be designated as σ_1, σ_2, σ_3, ... respectively. Let it further be assumed that all slices pass

M N with the velocity $v = v_o$ (Eq. (15)) and with no gap between them. The moment, σ_p, when the slice "$S_{n+p\Delta u}$" passes M N is then given by:

$$\sigma_p = \frac{p\Delta u}{v_o} \qquad (2$$

The position of the slice "$S_{n+p\Delta u}$" at any subsequent moment σ, provided $\sigma_p < \sigma < (\sigma_p + t_o)$ can now be calculated from Eq. (18) by entering

$$t = \sigma - \sigma_p \qquad (2$$

E. COMPARISON WITH EXPERIMENTS

Extensive studies will be required to establish rang of applicability of the model and what values of l_u and β, should be used under different conditions. Such elaboration has not hitherto been possible.

To obtain at least a preliminary indication of the degree of compatibility of the model with real motion, a comparison has been made of the results of calculation by means of the model, with detail studies of the actual motion in three specific cases.

The downrush motion of three different test waves, with wave heights and periods: H = 15,5 cm, T = 1,6 sec, H = 15,5 cm, T = 2,1 sec, and H = 21,3 cm, T = 2,1 sec respe tively were studied. In all three cases the wave was run against a 1:1,5 slope of a breakwater model in the 60 cm wid wave channel of the RHRL. The depth of water from SWL was 7 and the distance from the breakwater slope at SWL to the wav paddle was 23,2 m.

In Fig. 5, a) to d), are shown four photographs from a series taken by a motion picture camera during one wave sy of Test Run 1. *)

The white dots and lines seen in the water are due t confetti introduced to indicate velocities. Although the dis of confetti could show up in the pictures only when turning flat side more or less directly against the camera, still a of them should be expected to be visible during most of the posure, and thus indicate velocities close to the real ones.

*) The photographs were taken as part of an investigation carried out by Mr Alf Tørum, Laboratory Engineer at the RH

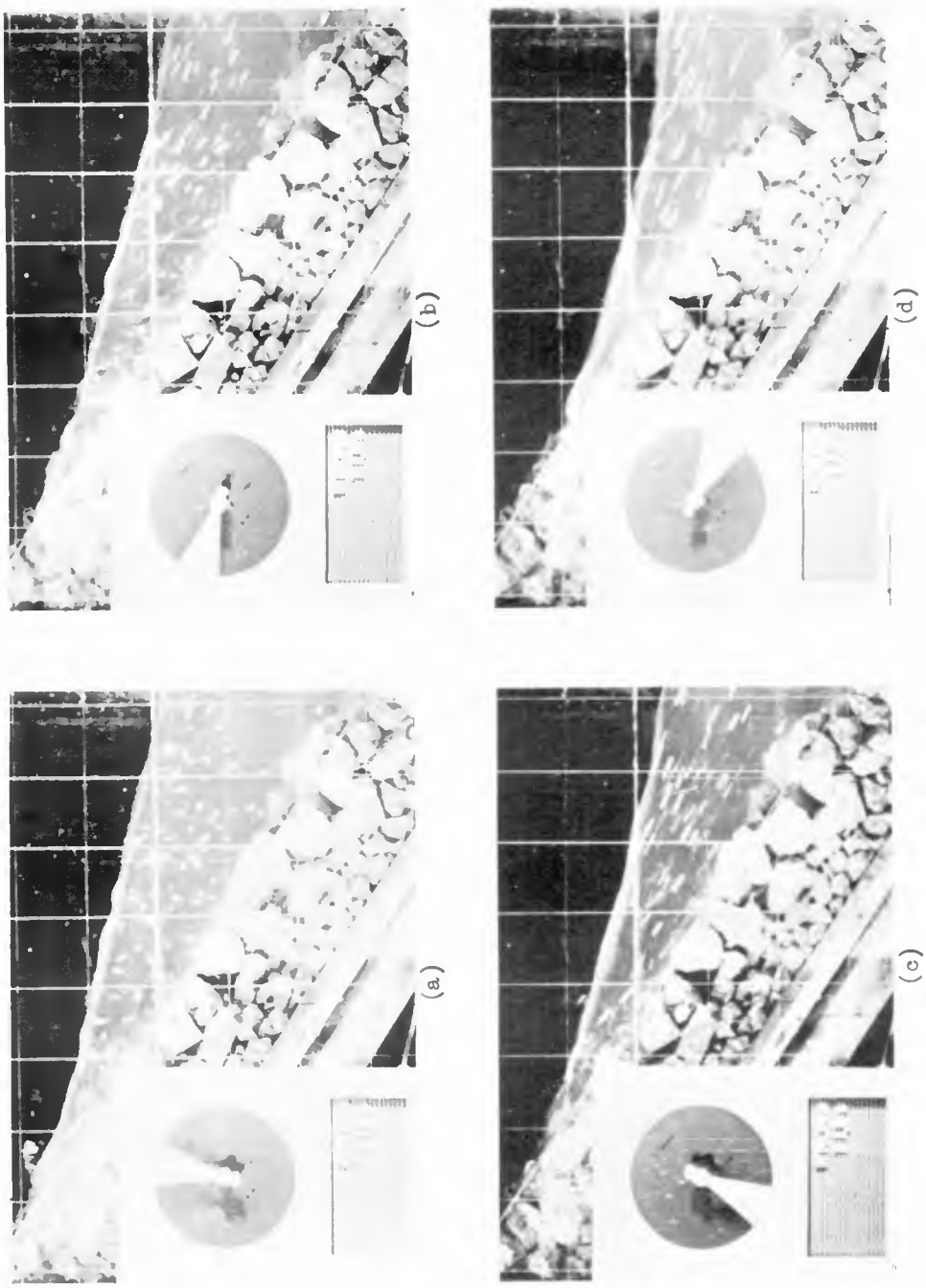

Fig. 5. Photographs of downrushing wave at four different moments.

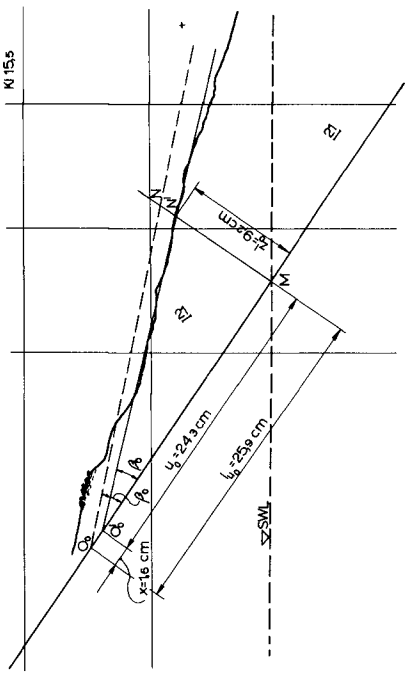

Fig. 6b. Surface profile from Fig. 5b.

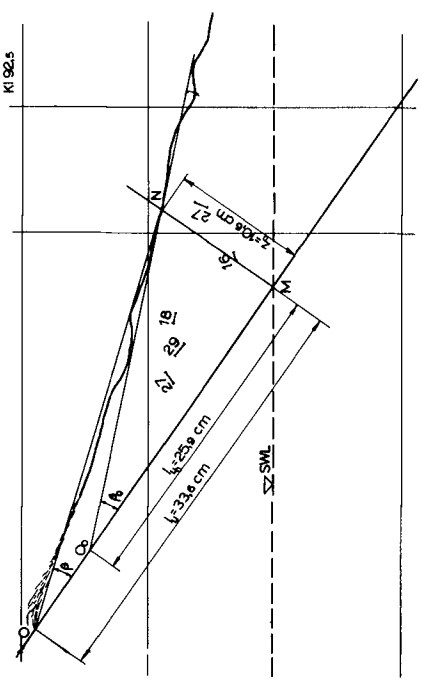

Fig. 6a. Surface profile from Fig. 5a.

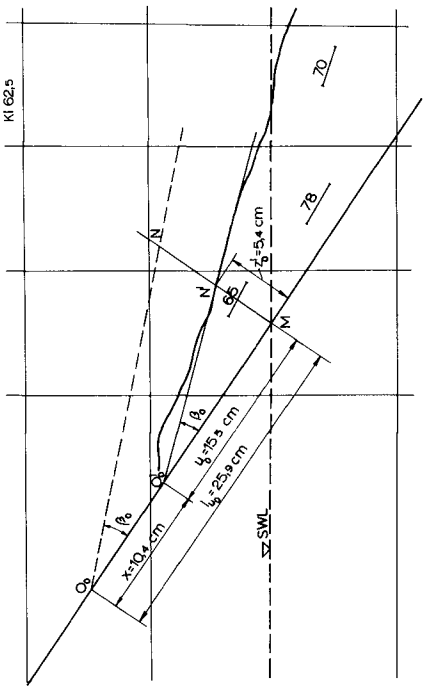

Fig. 6d. Surface profile from Fig. 5d.

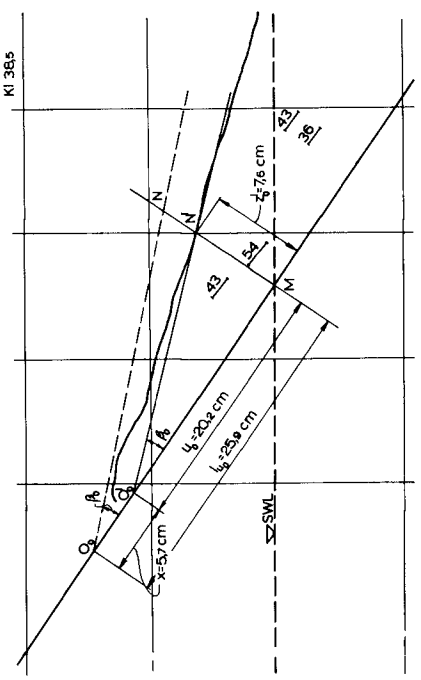

Fig. 6c. Surface profile from Fig. 5c.

Picture a) obviously was taken very nearly at the start of downrush, *) and picture d) shortly before the entire body of water had passed the SWL. The lengths of time between each start of exposure are indicated by the rear edge of the shadow left by the hand of the clock on the pictures and the duration of exposures by the width of this shadow, less the width of the hand itself. The hand moved anti-clockwise one full revolusion in 1/2 second.

In the pictures are seen the white lines drawn on the glass panel of the wave channel, indicating the theoretical front line of the cover layer, the SWL and a grid of horisontal and vertical lines 10 cm apart.

Projections of the picture, to about one-half of natural size, were made on sheets of paper on which were traced off, besides the lines on the glass panel, the upper edge of the water at the panel, indicating the surface profile at the start of exposure. (Fig. 6, a) to d)). A few of the longer lines traced by the confetti in each picture also were marked off, and the corresponding velocities, in cm/sec, noted on the sheets. The number at the upper right hand corner of each sheet shows the reading of the clock at the start of exposure, the unit being 1/200 of one second.

In the drawing, Fig. 6 a), the highest point of uprush was estimated to be at 0, and the length of uprush (see Fig. 2) to be l_u = 33,6 cm, while at SWL the depth, M N, of water normal to the slope was z_o = 10,6 cm, and, determined in this way, tan β = 0,316.

However, due to some spray around the upper tip of the downrushing water, definition of the point 0 in Fig. 6 a) and of the points corresponding to 0' (Fig. 2) in the subsequent pictures was rather difficult.

Moreover, as previously explained, our predominant concern is with the situation at SWL, in the region of expecte failure. In particular the value of the angle β to be applied should correspond to the actual slope of the water surface at SWL, rather than to the line 0 N.

Therefore, in Fig. 6 a) to d), tangents 0_0N, respectively $0_0'N'$, were drawn to the surface profile at SWL, and the triangles 0_0M N, respectively $0_0'$ M N', with their top angles β were taken as representative of the slice just passing the SWL at the moment indicated in each figure. The distances 0_o - $0_o'$ l_{uo} - u_o in Fig. 6, b) to d), accordingly represent the distance, x, travelled by that particular slice until the moment stated.

*) In this picture the confetti shows the whole of the visible body of water to be nearly at rest or in only slight and ver confused motion.

For comparison, the values of x corresponding to the three different values of t at the moments of Fig. 5 and 6, b). c) and d) have been calculated as outlined in Sections C and D. as well as the velocities and accelerations. In this calculation the particular values of u_o and β_o found from each of the three pictures were used.

It should be especially noted that the calculations concern in all cases the particular slice "S_u", which is just passing the SWL at the moment considered.

The results are stated in Table I. It is seen that there is a fair agreement between the measured values of x and those calculated as described above. It seems therefore probable that also the velocities and accelerations calculated on the same basis should not be too far off from the actual value

While such application of the model in the interpretation of one particular set of test data is not without interes since approximate figures for accelerations and velocities are obtained, a wider applicability of the model depends on the possibility of basing the calculation on a simpler and more general set of parameters, not to be determined separately for each moment considered.

The total length of uprush along the slope, l_u, Fig.2 and Fig. 6 a), the variation of which with wave and breakwater characteristics has already been widely studied, is proposed as one such parameter. The other parameter must be some angle β, selected on the basis of test data.

For reasons already stated, β should be selected with regard to the situation at the SWL, rather than at the top of uprush. In the present case tan β was chosen as the average o the measured values stated in the table, ommitting, however, the figure corresponding to the moment, t = 0, when there was as yet no motion.

Using the value of tan β thus selected, together with the measured value of l_u (Fig. 6 a)), a set of x-, v- and a-values have been calculated and included in Table I.

It is seen that these figures do not deviate materiall from those found by the previous calculation.

The two subsequent test runs, No 2 and No 3, were made and interpreted in the same manner as run No 1, except that nc confetti was used. Only the results are reproduced here, in Ta II and III.

Table I
MEASURED AND CALCULATED QUANTITIES COMPARED
Test Run 1
H = 15,5 cm, T = 1,6 sec (Fig. 5, a) to d) and Fig. 6,a))

Measured Quantities				Quantities calculated with					
				l_{uo} or u_o and β_o as measured			l_u = 33,6 cm tanβ = 0,367		
Clock Readings 1/200 sec	t sec	x cm	$\tan\beta_o$	x cm	v cm/sec	a cm/sec^2	x cm	v cm/sec	a cm/sec^2
92,5	0	0	0,409	0	0	186	0	0	224
15,5	0,115	1,6	0,378	1,4	24	208	1,5	26	222
38,5	0,230	5,7	0,376	6,1	47	200	5,8	50	217
62,5	0,350	10,4	0,348	12,9	72	194	12,8	73	206

Table II
MEASURED AND CALCULATED QUANTITIES COMPARED
Test Run 2
H = 15,5 cm, T = 2,1 sec.

Measured Quantities				Quantities calculated with					
				l_{uo} or u_o and β_o as measured			l_u = 38,1 cm tanβ = 0,329		
Clock Readings 1/200 sec	t sec	x cm	$\tan\beta_o$	x cm	v cm/sec	a cm/sec^2	x cm	v cm/sec	a cm/sec^2
08	0	0	0,407	0	0	202	0	0	276
32	0,120	0,8	0,362	1,7	27	227	2,0	30	250
55	0,235	5,8	0,329	6,7	57	241	6,8	58	243
81	0,365	13,7	0,320	16,0	86	224	15,6	85	221
04	0,480	23,5	0,306	24,5	97	161	24,3	96	173

Table III
MEASURED AND CALCULATED QUANTITIES COMPARED
Test Run 3
H = 21,3 cm, T = 2,1 sec.

Measured Quantities				Quantities calculated with					
Clock Readings 1/200 sec	t sec	x cm	$\tan\beta_o$	l_{uo} or u_o and β_o as measured			l_u = 53,0 cm $\tan\beta$ = 0,257		
				x cm	v cm/sec	a cm/sec^2	x cm	v cm/sec	a cm/sec^2
22,5	0	0	0,321	0		263	0	0	306
46,5	0,120	2,6	0,289	2,0	34	283	2,2	37	305
70,5	0,240	9,4	0,278	8,2	68	281	8,7	72	297
96,0	0,368	18,4	0,244	19,9	107	274	19,7	106	273
19,6	0,483	30,2	0,217	31,2	124	204	30,8	123	219

Table IV
CALCULATED VALUES OF THE ACCELERATION AT SWL AT THE MOMENT OF MAXIMUM BOUNDARY RESISTANCE AT SWL
$\tan\beta = 0,367$

H cm	l_u cm	At $R_{b\,max} = (R_{bv} + R_{ba})_{max}$				
		t cm	u_o cm	x cm	a cm/sec^2	$R_{b\,max}/\Delta u$ g/cm^2
15,50	33,6	0,56	8,1	25,4	105,0	0,423
19,38	42,0	0,63	9,2	32,8	106,5	0,476
23,25	50,4	0,68	10,6	39,8	112,8	0,523
27,13	58,8	0,73	11,8	47,0	116,1	0,568

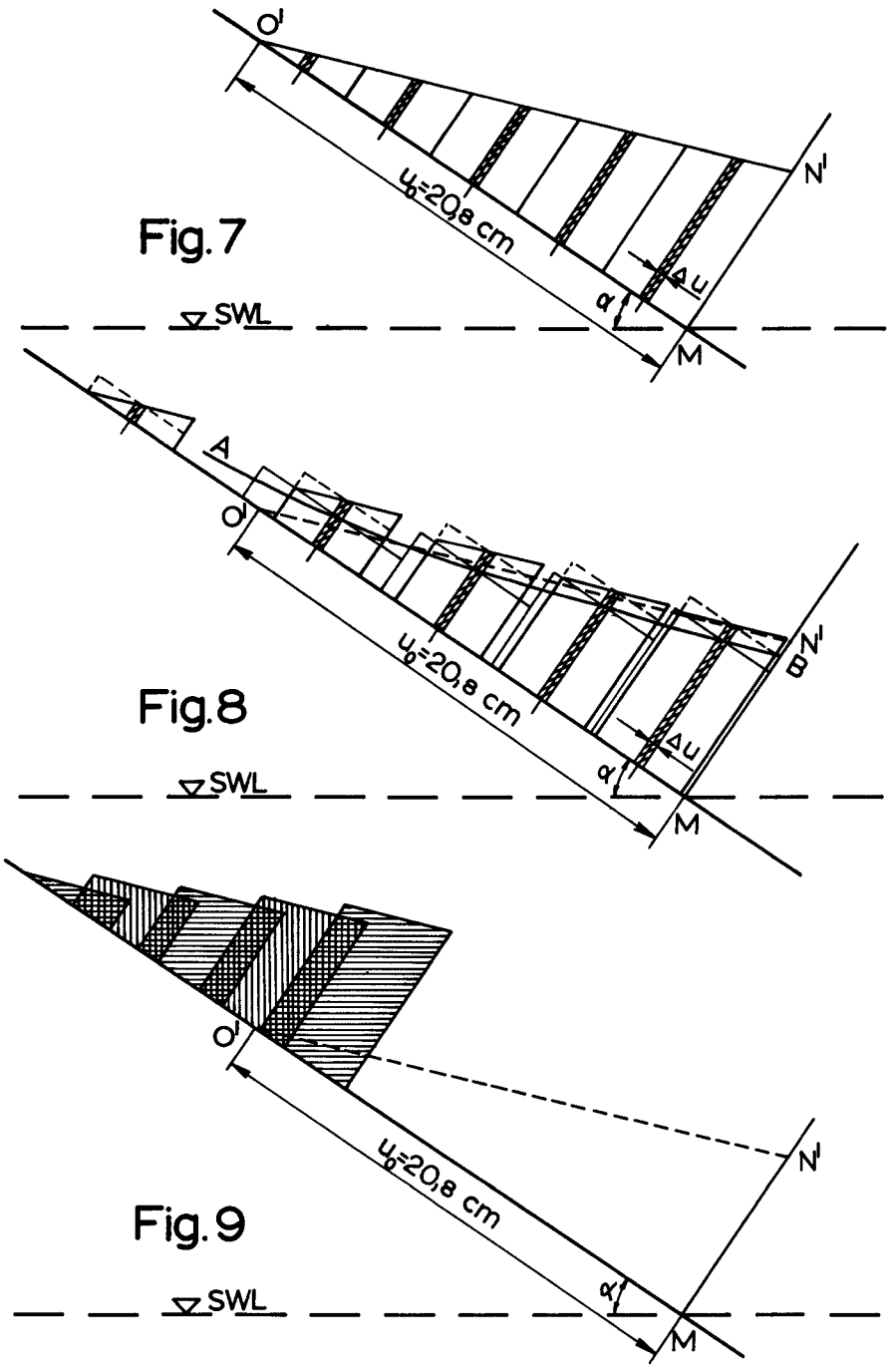

Fig. 7. Subdivision of triangle.
Fig. 8. Discontinuity in downrush.
Fig. 9. Discontinuity in uprush.

It is seen from the tables that also in these cases there is fair agreement *) between measured and calculated values of x, as well as betwen x-, v- and a-values calculated from direct measurement of individual values of l_{uo}, u_o and β_o, and those calculated from the actual maximum length of uprush in the test, l_u, with tan β equal to the average of all but the first one of the individual values.

F. DISCONTINUITY OF THE MODEL

In the Case of Downrush

As stated in paragraph 3 of Section B, the slices into which the body of water on the breakwater slope is thought to be subdivided, are assumed to be moving independently of each other, without regard to continuity. Since this assumption cannot possibly be correct, it is important to get some indication as to what is the actual extent of the discontinuity inherent in the model, and how this should be expected to affect its applicability.

For this purpose a study was made of one particular case: that presented in the last three columns of Table I, at the time t = 0,35 sec, with x = 12,8 cm. Since l_u = 33,6 cm, the value of u_o for the particular slice just then passing the SWL is 20,8 cm. (For notation, see Fig.2).

The study was made as follows: By dividing O'M (Fig. 2) into five equal pieces and raising normals to the slope in the dividing points, the triangle O'M N' was divided into five parts (Fig. 7). Next, the movement, x, from their top position, of slices located at the middle of the base of each of these five parts was calculated for the time t = 0,35 sec.

The result is shown in Fig. 8. The five slices have moved differently. Assuming that each of the five parts will move as the middle of its base, without change of shape, ther will at t = 0,35 sec be the gaps between the parts shown in the figure. Near the SWL the gaps are rather insignificant, they increase, however, very much close to the top, which is natural, since the resistance must there be great, due to the low values of z.

*) The difference seen in Table II between measured and calculated values of x for t = 0,120 sec may be due to the first exposure in the series starting, not at t = 0, but slightly later.

Continuity might be restored, if, in the process of motion, the several parts were made to decrease in height and increase in width without change of area, until they touched. We should then have a surface at t = 0,35 somewhat like the curve A-B in Fig. 8.

Of course this transformation of the surface would not compensate for the discrepancies in our model, inherent in the assumption that z is invariant with respect to t. But it seems plausible to assume that the surface profile A-B in Fig. 8 gives an indication of what the real surface would be like. The profile A-B agrees quite well with what is generally seen in tests.

In Fig. 7 the surface line O'N' of the original triangle has been drawn as a dotted line. It seems reasonab to conclude from the figure that calculation based on the su face O'N' may be expected to conform fairly well to actual motion, as far as regions not too close to the top of the triangle are concerned.

It also seems reasonable to consider Fig. 8 as a confirmation of the expediency of basing the calculations of Section E on the surface slope at SWL, rather than at points nearer the top.

In the Case of Uprush

As already stated, useful numerical treatment of the uprushing wave by means of our model can hardly be possible. Nevertheless a calculation has been made, by means of the fo mulae of Section D, and using the same method of dividing the same triangle O'M N' into five parts and calculating the motion, as used for Fig. 8. In Fig. 9 is shown the position of the five parts at the moment, t_o (Eq. 17), when the middl slice of the top triangle stops. The initial velocity, v_o, has been taken to be $v_o = \sqrt{1,3\ g\ H} = 141$ m/sec when H = 15,!

As seen from the figure, the five parts would, accor ing to this calculation, overlap. In actual motion the wate towards the end of uprush would pile up higher, with a great z_o and a greater angle β, than the model would indicate. Pen tration of some water into the body of the breakwater probab would partly counteract this development. It is submitted t there is a fair qualitative agreement between the model and actual experience also in the case of uprush.

G. BOUNDARY RESISTANCE

A point of particular interest is the magnitude of the boundary resistance to the motion of the fluid due to dra

and inertial forces. (Eq. (5) and (6)). In Fig. 10 the drag and inertial boundary resistance per unit of area of the slice just passing the SWL, and their total, $R_b/\Delta u$, have been plotted against the time, t, from start of downrush and also against u_o, the remaining length of the triangle belonging to the slice just passing the SWL ($u_o = l_u - x$), at the time, t.

It is seen that at the start of downrush the inertial forces are dominating, but as velocity increases the drag forces become more important, and towards the end, dominating. The total, $R_b/\Delta u$, at SWL, reaches a maximum fairly late in the process of downrush.

The curves in Fig. 10 were calculated with l_u = 33,6 c and tan β = 0,367, for the case H = 15,5 cm and T = 1,6 sec. This is the same case as treated in the last three columns of Table I, although the calculation has been carried on to higher values of t and x than covered by the table. Similar curves have been drawn for the cases H = 19,4 cm, 23,3 cm and 27,1 cm, assuming l_u to vary in direct proportion to H and tan β = 0,367 in all cases.

The curves all show a maximum value of R_b at fairly high values of t and x, rather far out on the doubtful side of Fig. 8. Still the maximum values of $R_b/\Delta u$ in the four cases have been listed in Table IV, together with the corresponding values of t, x, u_o and a.

Interesting is that at $R_{b\ max}$ the calculated acceleration is nearly the same in all cases, on an average around 110 cm/sec^2. It seems probable that due to the shortcomings of the model, the maximum may actually occur somewhat earlier at lower values of x and higher values of a, than indicated by the model. From consideration of both Table I and Table I it seems to be indicated that at the point of maximum boundar resistance at SWL the acceleration will be somewhere between 100 and 200 cm/sec^2, probably closer to the former, and will not vary very much with the wave height.

Another point to be noted is the surprisingly low values of the total resistance, R_b, indicated by the model. Actually it is a matter of only a couple of hundred kg pr sq of the slope surface, translated to full scale conditions.

Directly this result is due to the assumptions made in Section C, 3, with regard to resistance relations and the coefficients to be applied to them. The apparent agreement between the model and actual motion found in the three cases discussed previously, might possibly indicate that the assump tions made are not too far from reality, but of course the

Table V

Calculation of x, v and a with Particular Values of tan β, or with tan β = 0.3.

Reference Table	l_u cm	tan β	t sec	Calculated with average tan β in each case, as shown			Calculated with approximate grand average of tan β tan β = 0,3			Measured x cm
				x cm	v cm/sec	a cm/sec^2	x cm	v cm/sec	a cm/sec^2	
I	33,6	0,367	0,115	1,5	26	222	1,8	31	265	1,6
	"	"	0,230	5,8	50	217	6,9	54	253	5,7
	"	"	0,350	12,8	73	206	14,9	84	223	10,4
	"	"	0,450	19,6	85	169	21,6	91	164	-
II	38,1	0,329	0,120	2,0	30	250	1,9	32	268	0,8 x)
	"	"	0,235	6,8	58	243	7,3	62	258	5,8
	"	"	0,365	15,6	85	221	16,6	90	230	13,7
	"	"	0,480	24,3	96	173	25,1	99	168	23,5
III	53,0	0,257	0,120	2,2	37	305	2,0	33	277	2,6
	"	"	0,240	8,7	72	297	7,6	64	272	9,4
	"	"	0,368	19,7	106	273	17,7	96	254	18,4
	"	"	0,483	30,8	123	219	29,0	118	224	30,2

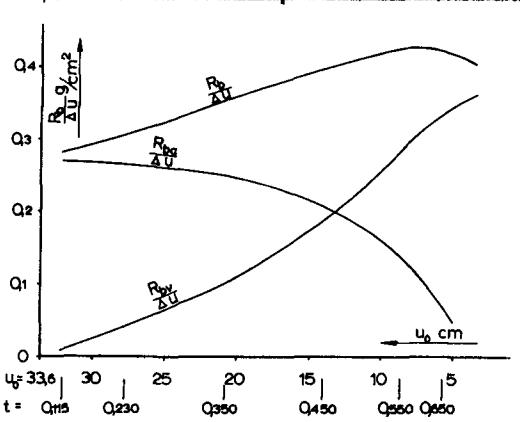

Fig. 10. Boundary forces plotted against u_o (remaining length of triangle above SWL), and against t, time since start of downrush.

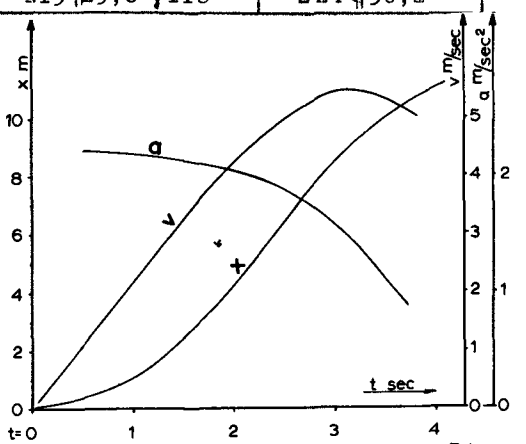

Fig. 11. Full scale application. Displacements, velocities and accelerations for H = 40 · 15.5 = 620 cm.

evidence is entirely insufficient as a basis of any such conclusion. In the present context the main interest lies with the indication that the model may actually prove helpful in the study of these boundary forces.

H. FULL SCALE APPLICATION

In Fig. 11 has been shown how the model works out when applied to full scale dimensions. Curves for the variation of x, v and a with t have been computed for a case with lineal dimensions 40 times those of the first test run, Table using tan β = 0,367, as in the last three columns of Table I. Comparison with Table I shows that the relations between the x-, v- and a-values for the two scales follow closely Froude's law.

Curves similar to those of Fig. 10, showing the variation in boundary resistance during downrush, have been prepare but are not included here. They are quite analogous to those of Fig. 10. The maximum total resistance at SWL is found at about t = 3,5 seconds, corresponding to about x = 10,2 m. Since l_u has been taken to be 40 times 0,336 m = 13,4 m, u_o for the slice just passing the SWL at the time of maximum resistance is $u_o = l_u - x$ = 3,2 m. Again the maximum resistar at SWL is found to be very small, only about 170 kg/m^2 .

As mentioned before, it may possibly be proper to consider, not the SWL, but a section even as much as one whole wave height lower, as the critical one. In that case l_u becor 13,4 m + 40·0,155/ sin α = 24,6 m.

Calculation on this basis gives a maximum total resistance at the lower critical point of 233 kg/m^2, found at t = 4,8 sec with x = 20,o m and u_o = 4,6 m. The corresponding velocity is 7,7 m/sec and the acceleration 1,1 m/sec.

I. POSSIBILITY OF APPLYING MORE GENERAL PARAMETERS

To apply the model one needs to know what values of the parameters l_u and tan β to use in each case.

The value of l_u, the actual length of uprush along th slope, can be calculated from the height of uprush, h_u, the relation of which to wave and breakwater characteristics have already been, and are still being, widely studied in many lab ratories.

About the proper value of tan β, on the other hand, no such information is available at present. However, it seems that quite wide variations in the value of tan β does not very much affect the results of calculations based on the model. An indication of this is given in Table V, where a comparison has been made between the x-, v- and a-values calculated by using the average values of tan β found for each individual test run, and a general value of tan $\beta = 0,3$. (The average of the values for the three test runs is tan β = 0,318). It is seen that in order of magnitude there is no essential difference between the results.

It is believed that for the type of breakwater considered here, with a front slope of 1 : 1,5 and for waves of ordinary steepness, a general value of tan β = 0,3 may tentatively be used, where the object is merely to get a general picture of the motion.

CONCLUSIONS

1. The model presented, crude as it is, seems promis because:

a) in three different cases where the kinematics of the downrushing wave has been studied in some detail, calculations based on the model yields results well compatibl with actual motion,

b) the discontinuity inherent in the model does n seem to affect too much the general picture of the motion, at least not in the region around the SWL,

c) applied to the case of uprush, the model yield results qualitatively in fair accordance with observed motion

d) when applied to the same case in two different scales (1 to 1 and 1 to 40) it yielded results in close agree ment with Froude's law,

e) it seems to provide a useful means of studying wave forces on the cover blocks parallel to the slope.

2. The acceleration of the water down along the slop seems generally to be of magnitude between 200 cm/sec^2 and 300 cm/sec^2 during the first part of the downrushing motion, and to diminish to somewhere between 100 and 200 cm/sec^2 at t moment when the sum of drag and inertial forces passes its maximum.

3. Only breakwater fronts with a slope of 1 : 1,5 and waves of steepness between 0,03 and 0,05 have been considered in this paper. For such cases it seems that the value of tan β = 0,3 may be used in approximate calculations.

ACKNOWLEDGEMENT

First of all the writer is deeply indebted to Mr. E. Palm, Ph.D., Professor of Fluid Mechanics at the Norwegian Technical University, for very needful criticism and correction, and for valuable suggestions. Helpful suggestions from Mr. S.I.O. Selberg, Ph.D., Professor of Mathematics at the same university, are also gratefully acknowledged. The writer further expresses particular gratitude to Mr. Alf Tørum, Laboratory Engineer at the Institute of Construction and Harbour Engineering at this university, for making his technique for measuring wave motion on slopes available for this investigation, and for carrying out the tests described. Grateful acknowledgement is also extended to the writer's assistants, Mr. H.P. Sundh, Civil Engineer, and Mr. E. Ellingsen, Civil Engineer, who made the calculations and contributed valuable suggestions.

REFERENCES

(1) Robert Y. Hudson: "Laboratory Investigations of Rubble Mound Breakwaters", Trans.A.S.C.E.,Vol.126,1961,Part IV, p.491.

(2) P.A. Hedar: "Stability of Rock-Fill Breakwaters", Akademiförlaget - Gumperts, Göteborg, 1960.

(3) Roald Svee: "Formulas for Design of Rubble Mound Breakwaters". Proc.A.S.C.E.,Vol.88, WW2, May 1962, Part I, pp.11-21.

(4) Gunnar Sigurdsson: "Wave Forces on Breakwaters". Dissertation, University of California, Berkeley, Ca. October 1961.

(5) Ludwig Prandtl: "Führer durch die Strömungslehre", Fifth Edition, Friedrich Vieweg und Sohn, Braunschweig 1

(6) Hunter Rouse: "Engineering Hydraulics", Chapman and Hall Ltd., London 1950.

(7) Charles L. Bretschneider: "Evaluation of Drag and Inertial Coefficients from Maximum Range of Total Wave Force", Technical Report No. 55-5, The A and M College of Texas, May 1957. Department of Oceanography and Meteorology.

(8) Basil W. Wilson: "Results of Analysis of Wave Force Dat Confused Sea Conditions round a 30-Inch Diameter Test Pi Gulf of Mexico". Final Technical Report No. 55-7, July The A and M College of Texas, Department of Oceanography and Meteorology.

(9) Erling Reinius: "Steady Uniform Flow in Open Channels", Bulletin No. 60 of the Division of Hydraulics at the Royal Institute of Technology, Stockholm, Sweden 1961.

CHAPTER 27

THE "TETRAPOD"

by P.DANEL
"Président d'Honneur" of SOGREAH
and L. GRESLOU
Head of the Maritime Research
and Design Department at SOGREAH

The Tetrapod was invented twelve years ago and the first breakwater with a Tetrapod protection was built eleven years ago.

It is felt that a review of the results since obtained with these artificial blocks may be of some interest, preferably in the form of an objective practical examination of the behaviour of Tetrapod-protected structures during the past few years, and of the way in which they have stood up to bad wheather during the period. First, however, a brief description will be given of the development of the Tetrapod and the Tetrapod technique.

Most breakwaters are of the rubble-mound type, because of the very good hydraulic properties of this type of design ; the seaward slope, roughness and "porosity" of their facings are generally such as to ensure the gradual destruction of wave energy, reduce wave overtopping and reflection and minimize toe erosion risks.

Unfortunately, however, rubble mound breakwater designs vary considerably, and some of them do not successfully combine all these essential features. Following an examination of a large number of designs of this type, therefore, it was decided to try, by systematic research, to determine ways and means of improving the properties of rubble mound breakwaters, especially in respect of the following :

a) Hydraulic properties : (i) Stability of armour components.
(ii) Strength of the structure as a whole.
(iii) Reduced overtopping by waves.

(iv) Reduced wave reflection.

b) Structural make-up : (i) Limitation of individual material weights.

(ii) Convenient artificial block fabrication.

(iii) Simpler block positioning

(iv) Reduction of use of waterborne equipment to a minimum.

c) Financial aspects : Cutting of costs to a minimum.

I - THE INVENTION OF THE TETRAPOD AND THE DEVELOPMENT OF "TETRAPOD" TECHNIQUES

The direct outcome of this research was the Tetrapod, an artificial facing block with novel outlines which is particularly suitable for the construction of very stable facings or armour. A further result was the development of a new breakwater profile design and constructional technique.

The shape of the Tetrapod is the result of research in the following subjects :

I - HYDRAULICS (first and foremost) :

With its special shape, the Tetrapod lends itself to the construction of very rough facings which, being very "porous" (50% voids), are unaffected by upward pressures (up-thrust), and, where laid to a very steep slope (3/4, and even 1/1), are capable of standing up to waves of a very considerable height. In addition, a Tetrapod designed to stand up to given waves under given conditions is much lighter than a lump of rock fulfilling the same purpose.

Several different-shaped blocks had been selected to begin with, all of which had fairly similar hydraulic properties to those of the final design. The fact that the latter turned out to be the only one giving a satisfactory performance from every point of view shows that its design could not be based on hydraulic considerations alone ; strength of materials and work-site problems also had to be investigated by the appropriate specialists before a final shape could be adopted.

II - STRENGTH OF MATERIALS :

The Tetrapod has a relatively compact shape, with generously-proportioned transition sections between the legs and the central "body" of the block, which give it considerable strength ; both experimental breaking tests and work site experience have shown steel reinforcement to be unnecessary, which is a great advantage for any constructional material intended for maritime work.

The Tetrapod is very easily handled, even if its concrete is still comparatively fresh. Simple special equipment has been developed, whereby the block is lifted with its concrete entirely in compression, instead of being under tension as it would be if it merely had an ordinary steel lifting eye at the end of one of its legs for instance.

III - WORK SITE OPERATIONS :

Thanks to the symmetrical geometrical properties of the Tetrapod, it was possible to develop casting moulds (or forms) consisting of four identical interchangeable shell sections, which are simplicity itself to fit and remove.

The shape of the Tetrapod lends itself well to the concrete pouring and vibrating operations and is easy to handle with very simple equipment.

Tetrapods are very easily positioned on the structure by means of a sling. The blocks forming the first layer of the facing automatically assume the required "three legs down" position, and the second-layer Tetrapods then key into them "one leg down".

IV - AN EXAMINATION OF SEVERAL HUNDRED ORIGINAL TETRAPOD PROFILES AND "TETRAPOD"ALTERNATIVES TO CONVENTIONAL LAYOUTS

showed that the special properties of Tetrapods enabled structures to be designed along novel lines resulting both in lower costs and more convenient building operations. The main features of these new methods are as follows :

(i) They require fewer rock fill categories.

(ii) The embankment slopes are similar to the natural slope of the heaped rock fill, so that the proportions of the structure are reduced to a minimum and a very precise adjustment of its various rock fill embankments or berms becomes unnecessary.

(iii) The Tetrapod-positioning equipment need only have a comparatively limited working range.

(iv) The crest of the structure can be set at a lower level and the toe mound built up to a higher level, thanks to the considerable energy-dissipating capacity of the Tetrapod armour.

(v) The structural profile can easily be matched to the quarry output, which often cannot be determined accurately until after

the construction work has started.

(vi) The structure can be built progressively from the shore outwards thus reducing the amount of equipment required (i.e.cranes etc.) and work stoppages due to bad weather to a minimum.

(vii) Where either weather, the state of sea, or financial considerations make it imperative to suspend operations, temporary breakwater heads can be built in very little time, which not only stand up very well to wave attack, but the expensive parts of which (e.g. artificial concrete blocks) can easily be recovered afterwards and re-used elsewhere.

II - RESULTS OBTAINED

The first Tetrapod patent was registered in 1950, i.e. about twelve years ago . After a certain period of cautious reserve, Project Authorities, Contractors and Consulting Engineers soon came to realize the qualities it was possible to give a breakwater by protecting it with Tetrapods, and these artificial blocks very soon came into widespread use throughout the world. This trend is still continuing at the present day.

It would of course be quite out of the question to discuss each and every one of the fifty-five structures which have either been completed or are now under construction* in such a very general review of the subject. Instead, it seems both more appropriate and interesting to analyse the behaviour of just a few representative structures ; five breakwaters which have all withstood very violent gales (in fact, probably the very worst that were liable to occur) since their completion five, six, eight, and even ten years ago will, therefore, be discussed in detail. One of the reasons for selecting these particular examples is that comprehensive objective observations by the Project Authorities concerned in respect of wave characteristics and Tetrapod behaviour are available for each and every one of them.

In order to ensure an objective assessment, two structures which have suffered slight damage since their completion will be examined, for the information they provide should be of particular interest to designers of new projects.

* At the time of writing (September 1962), ten more Tetrapod projects have been given the final "go-ahead" including the breakwater at Bayonne, which is the first new breakwater to have been built on the French Atlantic coast for very many years.

THE "TETRAPOD"

I - PROTECTION OF THE COOLING WATER INTAKES FOR A THERMAL POWER STATION AT CASABLANCA, MOROCCO (fig.1)

This project, which was carried out during the winter of 1950/51, involved the protection of the ends of the two parallel piers forming the power station sea water intake with Tetrapods. This was the first time Tetrapods had ever been used on a real-life structure.

The sea bed on which the pier heads stand is at a level of -2.5m (-8') and the spring tide high water level is at about + 4.0 m. (+13'). Maximum wave heights at sea are liable to reach 8 metres (26') and more, with periods of up to 16 seconds. At the water intake pier heads, the local depth of water limits wave amplitudes to 5-6 metres (16-20').

It was found during the design studies that 50 metric ton rectangular blocks laid to a slope of 2:3 would not provide a stable form of protection. Absolute stability under local conditions (i.e. long breaking waves, the very tight radius of pier head curvature, and the need to lay the Tetrapods to a slope of 1:1 owing to the limited capacity of the work site equipment) would have required 10 cubic metre (13cu.yds) Tetrapods. Scale model tests showed, however, that 6.3 cu.m (8 cu.yds) Tetrapods weighing about 15 metric tons were able to stand up to these conditions quite satisfactorily ; it was found that only about 6 per cent of these blocks were lost on the model under the worst possible simulated gale conditions for the pier heads. This was the solution to be finally adopted, therefore, as a result of which 256 - 6.3 cu.m (8 cu.yds) Tetrapods were positioned on the structure.

Because the crane used to position the Tetrapods only had a working range of about 4 metres (13'), quite a lot of Tetrapods tipped over when being laid and, consequently, did not "key" in properly with the others. In spite of this, however, and even though the contractors had been unable to remove the small quantities of rock from the bed as recommended in order to increase its roughness, and though the rock pile providing a backing for the Tetrapod facing was not built to begin with, less damage occurred during the initial 1951 gales than had been feared. The Tetrapod facing has remained steady ever since, and has been providing an efficient protection for the pier heads during the past eleven years, a fact which is, incidentally, confirmed in a letter dated the 3rd January 1962 from Mr. A.Desgigot the Director of the Equipment Branch of "Energie Electrique du Maroc". This is a particularly interesting result, for it is quite definite that, winter after winter, the structure has been undergoing repeated batterings by the strongest waves that can possibly occur in the shallow water in which it stands.

II - PROTECTION OF A NEW "POLDER" AT SOUSSE, TUNISIA (fig.2)

This was the second Tetrapod project to be built. The "polder" is over 800 metres (2,600 feet) long and lies to the south of Sousse harbour.

Built on the sea bed at a level of -4.5m (-15'), the Tetrapod structure is subject to attack by up to 3-3.5m (10-12')waves; as it is protecting

Fig 1

ROCHES NOIRES _ Thermal power station

CASABLANCA _ MOROCCO _

Protection of the ends of two jetties forming the side walls of a sea water intake

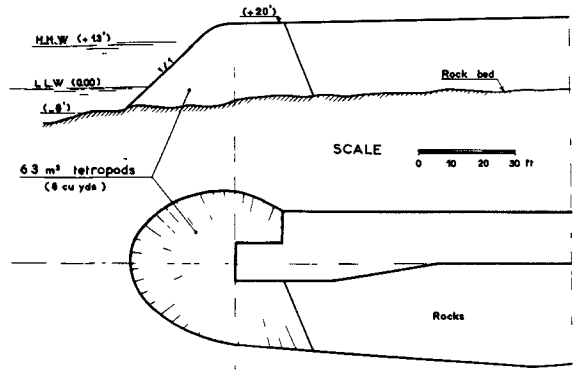

Fig 2

SOUSSE _ TUNISIA

Protection of a harbour area reclaimed from the sea

Typical section

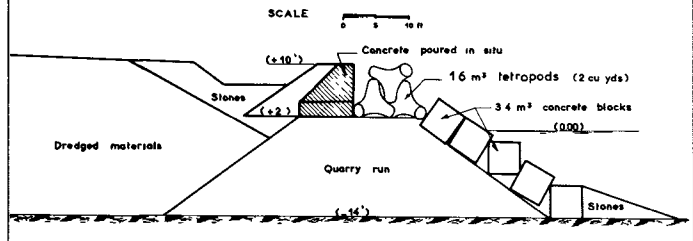

Fig 3

SAFI _ (Morocco)

Extension of the main breakwater

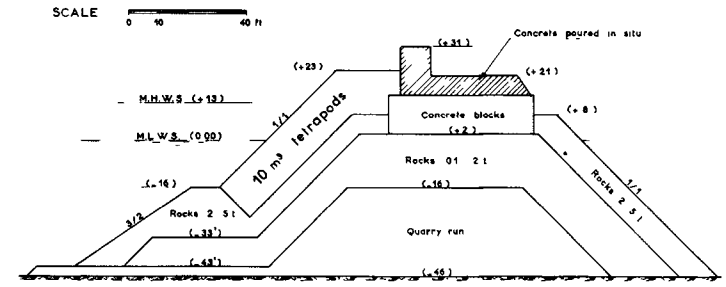

Fig 4

CRESCENT CITY _ (California _ USA)

Extension of the outer breakwater

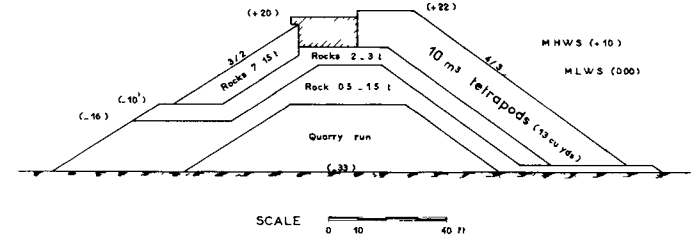

a "polder", no overtopping can be allowed.

The initial scheme provided for a facing of 8 and 10 metric ton cubic blocks, the upper part of which, however, suffered storm damage in January 1951 while work was still in progress. Subsequent investigation showed that 4 metric ton Tetrapods (1.6 cu.m or 2 cu.yds)in the upper part of the facing would both provide a very stable structure and effectively prevent overtopping.

The structure was completed in the spring of 1953, involving the use of 1550 - 1.6 cu.m (2 cu.yds) Tetrapods.

On the 12th January 1956, Mr. Raiton, the Engineer-in-charge of the Tunisian Public Works Maritime Branch confirmed that the 4 metric ton Tetrapods had provided a satisfactory replacement for the original 8 - 10metric ton cubic blocks which had proved unstable under wave action. He added that the structure had behaved satisfactorily in heavy weather, and that the Tetrapods in the facing appeared to have remained firmly in position.

III - EXTENSION OF THE MAIN HARBOUR BREAKWATER AT SAFI, MOROCCO (fig.3)

This was the fourth Tetrapod project to be carried out. It involved protecting a new 200 metre (660 feet) extension to the main harbour breakwater standing on the sea bed at a level of about -14.0 m (-46'). Spring tide high water level is at +4.0 m (+13'), and maximum wave heights vary from 7 to 9 metres, (23 to 30') with periods between 8 and 16 seconds.

The facing on the existing breakwater extended from -5.0 m to +7.0m (-16' to +23') and consisted of 45 metric ton rectangular blocks laid to form a slope of 1:2. Investigations showed that 10 cu.m (13 cu.yds) Tetrapods weighing about 24 metric tons each, laid to a slope of nearly 1/1, were not only capable of standing up to the severest wave action, but that they would also enable a substantial reduction in costs to be achieved, as they would require 5 per cent less rock fill and 70 per cent less facing concrete.

1450 - 10 cu.m (13 cu.yds) Tetrapods were used on the running section of the extension and the new breakwater head. Work was completed in 1955.

This structure gave full satisfaction during an exceptional three-day storm in December 1957, during which 9-metre (30') wave heights were recorded. This gale damaged the tip of the transverse breakwater in the harbour, which was not protected with Tetrapods at the time, but was reinforced later on.

In August 1959, Mr. Clos, the Engineer-in-charge of the Southern Area of the Moroccan Ministry of Public Works reported that observations made after the storm had shown that the Tetrapod facing had provided a perfect form of protection for the structure, and that, except for some slight local settling down, no damage to the facing (e.g. broken, displaced, or scattered Tetrapods) had been observed, even on the most exposed parts of the breakwater head.

IV - CONSTRUCTION OF A BREAKWATER AT RONGOTAI, NEAR WELLINGTON, NEW ZEALAND

This was the fith Tetrapod project to be carried out. It involved the protection of an extension to Wellington airport.

The structure stands on the sea bed at -7.0m (-23'). High water levels are +1.2m (+4'), and +1.8m (+6') at highest tide conditions. Waves breaking on the structure are up to 5 or 6 metres (16 to 20') high, with periods ranging from 7 secs. to 15 secs.

The initial project provided for a facing of 30 metric ton rectangular blocks forming a slope of 2/3. Experimental investigations showed, however, that a facing of 6.3 cu. (8cu.yds) Tetrapods (15 metric tons) laid to form a slope of 1/1 would be perfectly stable under local conditions.

The latter solution was the more economical of the two, and was finally adopted. 619 - 6.3 cu.m (8 cu.yds) Tetrapods were used, and work was completed in 1955.

The facing was seen to settle down slightly in April 1955, during the first two major gales after its construction. The amount of sag was about 1m, and occurred in places where pockets of sand occurred on the rock bed. This particular facing had been built straight on to the bed, as opposed to the generally recommended practice of providing a stone blanket between the bed and the foot of the facing. No further settling has since been observed and the structure has afforded satisfactory protection without requiring any repairs or reinforcement.

V - CRESCENT CITY BREAKWATER EXTENSION, CALIFORNIA, U.S. (fig.4)

Although, unlike the four examples described above, this was not one of the very early Tetrapod projects, the behaviour of this breakwater is particularly interesting, as it has had to stand up to five very violent storms since its completion, the last of them quite exceptional.

The design study for the breakwater extension was carried out at Vicksburg (U.S.A.). Observed data and wave-hindcasting methods were used to determine the maximum wave heights the structure would have to be able to withstand without damage ; this was finally taken as 7 metres (23 feet with periods of up to 14 seconds. Spring tide high water levels are at +2.1m (+7'), and exceptionally + 3.0m (+10'). Sea bed levels at the structure range between -9.0m (-30') and -11.0m (-36').

Several schemes with rock-fill armour were investigated, but in all of them, the rock sizes available from the quarry or suitable for the handling capacity of the work site equipment turned out to be unable to provide the required degree of structural stability. The final scheme provided for a facing of 10 cu.m (13 cu.yds) Tetrapods forming a slope of 3/4. Work was completed in October 1957, with 1836 Tetrapods on the final 170 metre (560 feet) section of the breakwater and the breakwater head.

The characteristics of the five very severe storms the structure has since withstood have been reconstructed by the application of wave hind-casting methods to a point some 40 miles north-west of Crescent City, with the following results :

February 1958	Significant height	20 feet
	" period	10 seconds
	Approach direction	south
April 1958	Significant height	20 feet
	" period	13 seconds
	Approach direction	west, west-north-west
November 1958	Significant height	21 feet
	" period	13 seconds
	Approach direction	north-west
February 1959	Significant height	20 feet
	" period	13 seconds
	Approach direction	south
February 1960	Significant height	32 feet
	" period	13 seconds
	Approach direction	west

From these calculations and refraction diagrams, it appears likely that maximum wave heights of 10.5 m (35') may have affected the structure during the February 1960 gale. Photographs taken during the afternoon of the 9th February 1960 show evidence of waves breaking over depths of 12 metres (40'), and it can be estimated that at least 9-metre (30') waves were breaking on the structure at the time.

The structure and its Tetrapod facing stood up to these gale conditions very well, and subsequent inspection merely showed that a few Tetrapods had moved out of position on the seaward side of the breakwater head, which was affected by tangential wave attack, and that the whole structure had settled slightly as the Tetrapods tended to "key" together more firmly.

The need for reinforced facings on the seaward ends of such structures is made fairly plain by this example. This point will be discussed more fully later on.

VI - ANALYSIS OF TWO STRUCTURES HAVING SUFFERED SLIGHT DAMAGE

An exact analysis of possible damage is particularly important, for though the Tetrapod technique has certainly been thoroughly tested, it is nevertheless still comparatively recent. The following examination of two representative cases will provide a few useful indications in respect of breakwater design and construction.

a) Reinforcement of the South Breakwater at Wick, Scotland (fig. 5)

This was originally a vertical jetty standing on a rubble mound provided with a thick concrete facing. With the local spring tide range of 3 metres,(10') this structure had the properties of a composite breakwater on which 4.5 metre (15') 10 second period waves broke owing to the shallow depth of water in which it stood.

Wave flume tests showed that 3.2 cu.m (4 cu.yds) Tetrapods weighing about 7.5 metric tons each would provide the structure with the requisite amount of reinforcement ; unfortunately, however, the funds available for the repair scheme limited the number of Tetrapods to be used to 625, which was not enough for a facing extending all the way out to the breakwater head. The breakwater consists of two straight sections with a change of heading of about 15° from one to the other.

The reinforcement could only be taken as far as the point of junction of the two straight alignments, which happened to be a particularly vulnerable point, being affected by reinforced wave activity due to the layout of the structure.

Soon after the reinforcement work had been completed, storms in Novem ber and December 1956 damaged the end of the facing, affecting about 10 pe cent of the Tetrapods on the structure. The 3.2 cu.m (4 cu.yds)Tetrapods were displaced by the violent wave impacts occurring against the vertical wall of the breakwater beyond the end of the facing. This damage was subsequently reproduced in three-dimensional model tests, as a result of whic it was concluded that heavier Tetrapods should have been used at the end c the facing along the vertical wall.

b) Reinforcement of breakwater heads at Kahului, Maui Island, Hawaii (fig.6)

These structures, which were originally provided with a heavy rock fill armour, had repeatedly suffered storm damage, especially in 1947, 1952 and 1954.

If it is considered that waves breaking at a distance of roughly 0.4l in front of the structure are the most dangerous (L being the wave length at that point), it can be assumed that the breakwater heads are liable to be affected by waves over 10 metres in height (34'). Wave periods observed in 1947 and 1954 were 17 secs. and 18 secs.

Fig 5

WICK HARBOUR

South breakwater

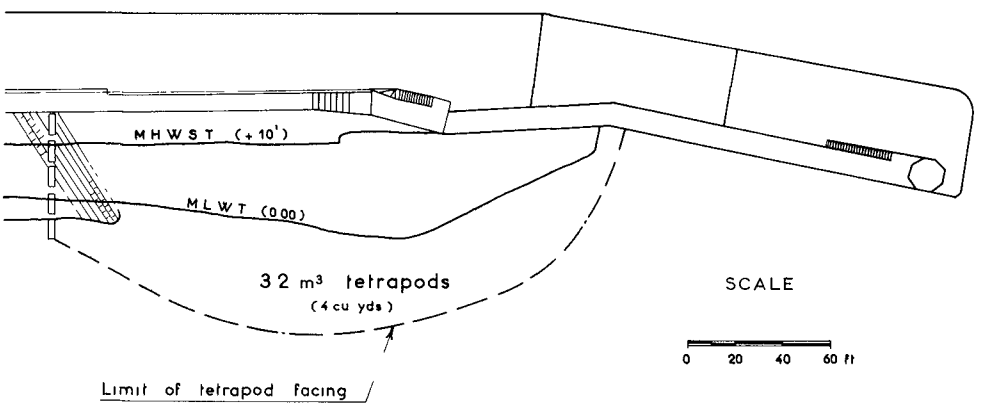

Fig 6

KAHULUI HARBOUR

Reinforcement of the breakwater heads

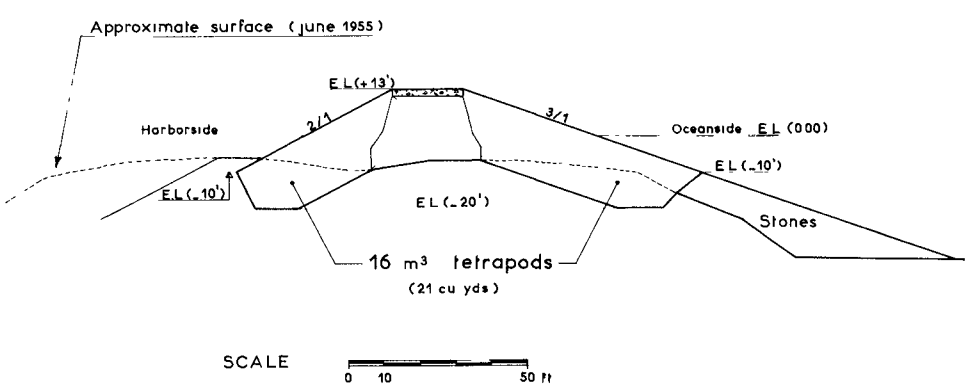

Before any contracts were awarded for the work, the attention of the Project Authority was drawn to the need to use Tetrapods of at least 16 cu.m (21cu.yds), and, if possible, to build the facing down to the 9.0m (-30') level. However, partly due to a shortage of funds, and partly because of the limited capacity of the available work site equipment, these recommendations could not be followed, and the Project Authority accepted the risk of damage occurring on the structure under exceptionally severe storm conditions.

Work was completed in March 1957, involving the use of 603-12 cu.m (16 cu.yds) Tetrapods (29 metric tons), with the facing only extending down to about - 3.0 m (-10'). It successfully withstood two storms in 1957, but suffered slight damage in November 1958, due to the breaking of waves of an estimated height of 7.6 metres (25'). Most of this damage occurred on an unreinforced part of the East Breakwater, in which a 20m (70') breach formed at the end of the Tetrapod facing, which provided clear evidence of the effectiveness of these artificial blocks. Six Tetrapods, which the breach had deprived of their footing, were swept away through it, and some of the Tetrapods on the breakwater head were dislodged. About thirty Tetrapods were dislodged on the West Breakwater. Altogether, about 6 per cent of the Tetrapods on the whole structure were displaced, which can reasonably be qualified as the kind of "slight damage" the Project Authority had been prepared to accept, especially if compared with the damage the structure had been suffering before it was given its Tetrapod armour.

The conclusion to be drawn from the behaviour of these last two structures is as follows :

> The breakwater head facing should definitely be made stronger than that on the running section, especially in the case of structure like the one at Wick where the facing is in front of a vertical wall and does not extend right up to the end of the structure. Experimental work has repeatedly shown that the Tetrapods used on the breakwater head should be 1.6 times to twice as heavy as those on the running section, and that it is also important that the breakwater head should be given an adequate radius of curvature.

III - THE USE OF TETRAPODS ON COASTAL PROTECTION STRUCTURES

Tetrapods have frequently been used on coastal protection works. The following are a few examples of this type of application :

I - MARINE DRIVE, BOMBAY, INDIA

Here ,7000 - 1.6 cu.m (2cu.yds) Tetrapods were used to protect a 1200 metre (4,000 feet) length of the promenade along the sea front. Their purpose was to dissipate the energy of 2 - 3 m (6-9') waves breaking against the sea wall, and to prevent waves from overtopping it on to the Drive

The protection work was completed in 1959 and has since proved to be both stable and effective.

II - SALIN-DE-GIRAUD, CAMARGUE COAST, FRANCE

The purpose of the Tetrapods in this project was to protect both the sea water intake and concentration tanks of the "Compagnie Salinière de la Camargue" plant on the sea shore. 1000 - 0.8 cu.m (1cu.yds) and 0.2cu.m (7 cu.feet) have been positioned so far, providing a form of protection which has been both more effective and less expensive than one built of natural stones, as the quarries from which these would have had to be obtained are a long way from the site.

III - ISLAND OF SYLT, GERMANY

In 1960, the sea wall in the town of Westerland was provided with a facing structure of 570-2.5 cu.m (3 cu.yds) Tetrapods, which is now being extended to the north of the town in order to prevent erosion of the dunes which protect the hinterland from flooding. It is expected that some 2000 Tetrapods will have been positioned by the end of 1962. The final structure is to be about 10 metres broad, consisting of five rows of Tetrapods in the initial layer, and four rows in the second layer, the whole standing on a fascine mattress protected with a suitable asphalt product. This structure has been erected on the part of the beach above mean sea level, in order to absorb the energy of waves occurring at exceptionally high water level conditions.

CONCLUSION

The Tetrapod is a recent invention. Though its first application only dates back to some twelve years ago, its early success was instrumental in rapidly changing the attitude of Project Authorities, Consulting Engineers and Contractors from one of prudent reserve to a realisation of its advantages. Now accepted as a useful alternative to conventional methods, Tetrapod schemes are included in tender specifications as a matter of course, frequently as the only solution to be put forward. Thus, the Tetrapod technique can be said to have entered the field of standard practice.

A careful analysis of all the local conditions involved in a project is nevertheless still most important before deciding on a given layout, as well as comprehensive experimental investigations, which generally provide the only means of ensuring that the structure concerned will be able to offer the reliability its size requires.

CHAPTER 28

DYNAMIC ANALYSIS OF OFFSHORE STRUCTURES

by

Donald R. F. Harleman
Associate Professor, Department of Civil Engineering
Massachusetts Institute of Technology

William C. Nolan
Lt. (U.S.C.G.)

and

Vernon C. Honsinger
Lt. (U.S.N.)

ABSTRACT

Analytical procedures are presented for calculation of the dynamic displacements of fixed offshore structures in oscillatory waves. The structure considered has four legs in a square configuration with waves impinging normal to one side; however, the procedures are general and may be applied to other configurations and wave directions.

The horizontal displacement of the deck is determined as a function of time by application of vibration theory for a damped, spring-mass system subject to a harmonic force. The instantaneous wave force on each leg is composed of a hydrodynamic drag component and an inertial component as in the usual "statical" wave force analysis. The wave force expression is approximated by a Fourier series which permits calculation of the platform displacement by superposition of solutions of the equation of motion for the platform.

Depending on the ratio of the wave frequency to the natural frequency of the platform, the structural stresses may be considerably higher than those found by methods which neglect the elastic behavior of the structure.

The highest wave to be expected in a given locality is not necessarily the critical design wave. Maximum displacements and structural stresses may occur for smaller waves having periods producing a resonant response of the platform.

Displacement measurements in a wave tank using a platform constructed of plastic are presented to show the validity of the analytical method. Both small and finite amplitude waves are used over a wide range of frequency ratios. A digital computer program (7090 FORTRAN) is used for the displacement calculation.

DYNAMIC ANALYSIS OF OFFSHORE STRUCTURES

INTRODUCTION

The usual method of design of a fixed offshore structure (i. e., a deck located above the limit of wave motion and supported by three or more legs driven into the ocean bottom) is by means of a "statical" wave force analysis. In this approach the procedure has generally been to select a "design wave" which is the largest wave to be expected in the locality. Using applicable wave theory (for particle velocities and accelerations) and appropriate wave force coefficients, the maximum forces and moments are computed assuming the structure is in static equilibrium.

Recent field experience, including the tragic failure of a major structure off the East coast (U. S. Senate, 1961) have indicated that the maximum or "design wave" may not be the wave which causes the greatest stresses in the structure. In other words, a smaller wave whose fundamental period approaches the natural period of vibration of the structure may be critical for design in view of the large amplification of deflections and stresses near resonance.

A method of analysis which considers the elastic nature of the structure and its dynamic response to wave forces is presented for use in the design of future offshore platforms.

ANALYTICAL DEVELOPMENT

DYNAMIC ANALYSIS OF PLATFORM

Equation of Motion

Analytical procedures are developed for the dynamic analysis of an offshore platform supported by four cylindrical legs and acted upon by a train of oscillatory surface waves. The horizontal displacement of the platform is represented by X measured with respect to the neutral position of the center of gravity of the deck as shown in Fig. 1. The equation of motion for a single degree of freedom, equivalent spring-mass system, with linear damping and restoring force subjected to a sinusoidal exciting force as shown in Fig. 2 is given by eq. (1),

$$m\frac{d^2X}{dt'^2} + C\frac{dX}{dt'} + KX = P(t') = P_m \sin \sigma t' \qquad (1)$$

where:

m = effective mass of system
C = damping coefficient of structure
K = spring constant of structure
Pm = amplitude of harmonic exciting force
σ = frequency of harmonic exciting force = $\frac{2\pi}{T}$
t' = time in the equivalent system

The solution of equation (1) (Housner and Hudson) is,

$$X(t') = \frac{P_m}{K\sqrt{\left[1-\left(\frac{\sigma}{\sigma_n}\right)^2\right]^2 + \left[2\frac{C}{C_c}\frac{\sigma}{\sigma_n}\right]^2}} \cdot \sin(\sigma t' - \phi) \qquad (2)$$

where,

$X(t')$ = horizontal displacement due to $P(t')$

$\sigma_n = \sqrt{\frac{K}{m}}$, undamped natural frequency of spring-mass system (3)

$C_c = 2\sqrt{mK}$, critical damping coefficient (4)

$$\phi = \tan^{-1}\left[\frac{2\frac{C}{C_c}\cdot\frac{\sigma}{\sigma_n}}{1-\left(\frac{\sigma}{\sigma_n}\right)^2}\right] \quad (5)$$

The crux of the proposed method of analysis may be seen by comparing Figs. 1 and 2. The equation of motion (1) is considered to apply to the equivalent spring-mass system shown in Fig. 2. The effective mass of the equivalent system is concentrated at the deck and the legs are considered to act as cantilever springs of zero mass.

The harmonic exciting force $P(t')$ acts in the plane of the deck which undergoes a pure translatory motion since it is assumed to have a stiffness which is large compared to the legs and is therefore not subject to deflection due to bending. The actual exciting force for the platform is $F(t)$ which is the resultant of the time dependent wave force distribution acting at variable distance $\bar{s}$ above the bottom. (Fig. 1) The problems involved in relating the actual platform motion to the vibration of the equivalent spring-mass system (Fig. 2) are described in the following section.

Platform Characteristics

1. The actual exciting force $F(t)$ must be related to the exciting force $P(t')$ in the equivalent system. Since $F(t)$ is composed of both hydrodynamic drag and inertial contributions, it cannot be represented by a single term of the form $F \sin \sigma t$. However, by means of a Fourier series approximation, $F(t)$ can be represented by a series of sine terms to any desired degree of accuracy. Each F term in the series can be related to a P term through the method of influence fractions. Since the equation of motion (1) is linear, the component displacements due to the individual exciting force terms ($P_m \sin \sigma t'$) in the Fourier series can be summed to determine the total platform displacement as a function of time. Hence,

$$X_{tot.}(t) = \sum_{m=0}^{m} X_m(t) \quad (6)$$

The usual procedures of structural analysis may then be used to relate displacements (strains) to stresses.

The static deflection of the platform is obtained from cantilever beam theory. The equation for the maximum deflection of the deck (X_{max}

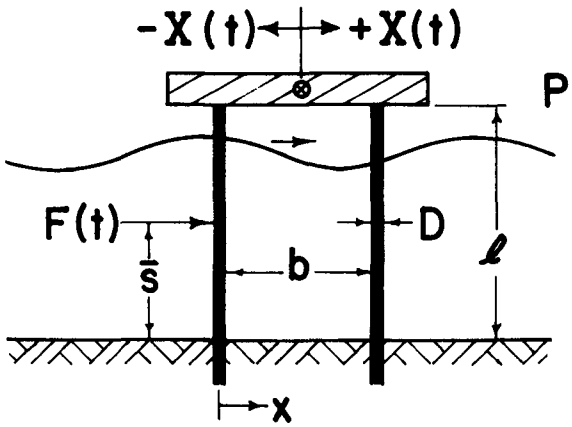

Fig. 1 Unbraced Platform Four Cylindrical Legs

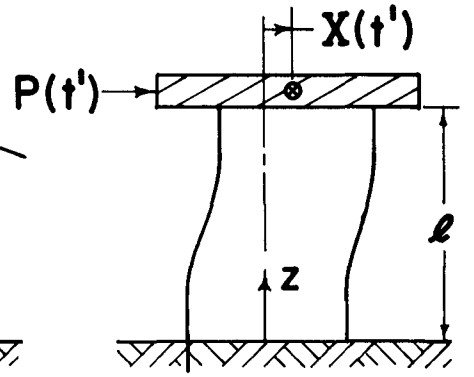

Fig. 2 Equivalent Spring-Mass System

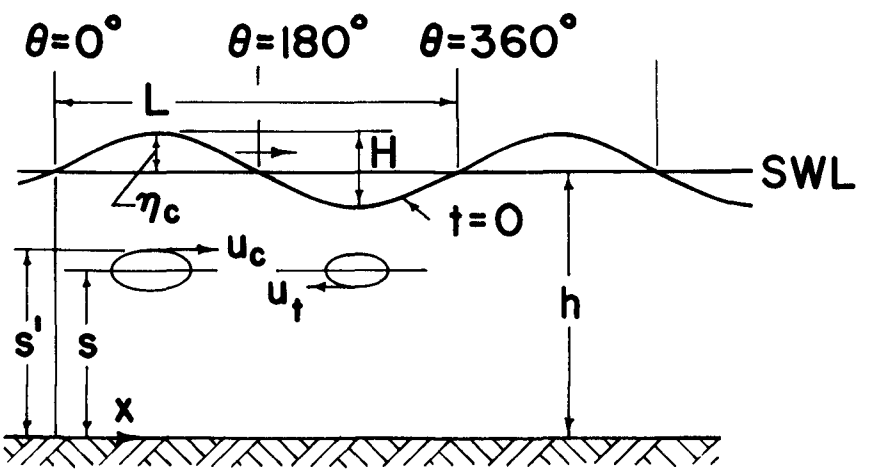

Fig. 3 Definition Sketch for Wave Motion

for a force F applied at an elevation $\bar{s}$ (see Fig. 1) is

$$[X_{max}]_{act.} = \frac{F\bar{s}^2}{NEI}\left(\frac{\ell}{4} - \frac{\bar{s}}{6}\right) \tag{7}$$

In the equivalent system, with a force P applied at the elevation of the deck (see Fig. 2), the deflection is found from eq. (7) by letting $\bar{s} = \ell$, hence,

$$[X_{max}]_{equiv.} = \frac{P\ell^3}{12NEI} \tag{8}$$

In the above equations,

E = elastic modulus of actual platform leg
I = moment of inertia of actual platform leg
N = number of legs = 4
ℓ = vertical length of legs

The influence fraction which relates F and P is determined from the requirement that the static deflection of the equivalent system under a force P must equal the static deflection of the actual platform under a force F. Hence, by equating eqs. (7) and (8) the ratio, P/F = f, becomes

$$\frac{P}{F} = f = 3\left(\frac{\bar{s}}{\ell}\right)^2 - 2\left(\frac{\bar{s}}{\ell}\right)^3 \tag{9}$$

2. The spring constant of the equivalent system is by definition

$$K = \frac{P}{[X_{max.}]_{equiv.}} \tag{10}$$

Therefore from eq. (8), with N = 4,

$$K = \frac{48\,EI}{\ell^3} \tag{11}$$

3. The natural frequency of the equivalent system is equal to the natural frequency of the actual platform. Rayleigh's Energy Method (Thomson, 1953) can be applied to determine the natural frequency of the equivalent system using the static deflection curve to calculate kinetic and potential energies. In the equivalent system the deflection X(z) of the legs at any section z in terms of $X_{max.}$ can be found from simple beam theory to

$$\frac{X(z)}{X_{max.}} = 3\left(\frac{z}{\ell}\right)^2 - 2\left(\frac{z}{\ell}\right)^3 \tag{12}$$

The maximum kinetic energy is given by,

$$[K.E.]_{max.} = \frac{W}{g} \frac{\sigma_n^2 X_{max}^2}{2} + N \int_0^{\ell} \frac{w}{g} \frac{\sigma_n^2 X(z)}{2} dz$$

Substituting for X(z) from eq. (12),

$$[K.E.]_{max.} = \frac{\sigma_n^2 X_{max.}^2}{2g} (W + \frac{13}{35} Nw\ell) \tag{13}$$

where,

W = weight of deck
w = weight per foot of leg

The maximum potential energy is given by,

$$[P.E.]_{max.} = \frac{KX_{max}^2}{2} \tag{14}$$

Upon equating the kinetic and potential energy eq. (13) and (14), the natural frequency is,

$$\sigma_n = \sqrt{\frac{K}{\frac{1}{g}(W+\frac{13}{35} Nw\ell)}} \tag{15}$$

4. By comparing eqs. (3) and (15), the effective mass of the equivalent system is,

$$m = \frac{1}{g}(W + \frac{13}{35} Nw\ell) \tag{16}$$

In a simple vibrating spring-mass system, the effect of the mass of the spring can be accounted for by increasing the rigid mass by one-third of the mass of the spring. The factor 13/35 obtained above is close to this value and represents the proportion of the mass of the legs to be added to the weight of the deck in the actual structure. If the legs had been considered to be pinned to the deck the fraction would be 33/140. The added mass due to vibration in water has been found to be negligible compared to the mass of the platform. The effect of bracing between legs can be accounted for by modifications in the above procedures. (Nolan and Honsinger, 1962).

5. The critical damping coefficient, C_c, is a function of m and K and can be calculated from eq. (4).

6. The damping coefficient, C, of the equivalent system is equal to the damping coefficient of the actual platform. A convenient way to determine the magnitude of the structural damping coefficient is to measure the decay of the amplitude of oscillation under the action of a single impulsive force (Thomson, 1953) either in the actual structure or in a model. Thus, if X_1 and X_2 are two successive positive displacement amplitudes, the ratio of C/C_c is proportional to the logarithmic decrement

$$\frac{C}{C_c} = \frac{1}{2\pi} \left(\ln \frac{X_1}{X_2}\right) \tag{17}$$

The magnitude of viscous damping due to vibration in water has been found to be small compared to the structural damping.

7. The frequency of the harmonic exciting force is equal to the wave frequency

$$\sigma = \frac{2\pi}{T}$$

where T is the period of the wave motion.

8. The phase angle ϕ can be calculated from eq. (5) since it is a function of C, C_c, σ, and σ_n.

The above series of equations provide the necessary information for the determination of all of the coefficients in the equation of motion of the equivalent system (eq. 1) in terms of known quantities for the actual platform.

Wave Force Theory

The wave force on a single vertical cylinder follows the method of Harleman and Shapiro (1955) which is a modification of the development by Morison, et al (1953). The method has been shown to be well adapted to finite amplitude waves as used in the laboratory experiments. However the dynamic platform analysis is essentially independent of the particular wave force theory and any procedure which can be approximated by a Fourier series can be employed.

The following functions are used for the total wave force F on a single vertical cylinder, following the notation shown in Fig. 3:

$$F = F_c \sin^2 \theta + F_I \cos \theta \qquad 0° \leq \theta \leq 180° \tag{18}$$

$$F = F_T \sin^2 \theta + F_I \cos \theta \qquad 180° \leq \theta \leq 360° \tag{19}$$

where,

F_c = hydrodynamic drag force at crest ($\theta = 90°$)
F_T = hydrodynamic drag force at trough ($\theta = 270°$)
F_I = inertial force at $\theta = 0°$ and 180°
θ = phase angle = ($\sigma t - kx$)
k = wave number = $2\pi/L$
L = wave length

1. The hydrodynamic drag forces F_c and F_T are expressed in terms of a drag coefficient C_D:

$$F_c = \int_0^{h+\eta_c} C_{D_c} \rho \frac{u_c^2}{2} D\, ds' = C_{D_c} \frac{\gamma D h^2}{2} \cdot A \qquad (20)$$

$$F_T = \int_0^{h+\eta_c - H} C_{D_T} \rho \frac{u_T^2}{2} D\, ds' = C_{D_T} \frac{\gamma D h^2}{2} \cdot B \qquad (21)$$

where,

u_c = particle velocity under the wave crest
u_T = particle velocity under the wave trough
ρ = density of water
γ = specific weight of water
C_D = drag coefficient for cylinder
s' = instantaneous elevation of particle
D = cylinder diameter
η_c = wave amplitude at crest
h = depth to s.w.l.

and

$$A = \int_0^{1+\eta_c/h} \frac{u_c^2}{gh}\, d(s'/h) \qquad (22)$$

$$B = \int_0^{1+\frac{\eta_c - H}{h}} \frac{u_T^2}{gh}\, d(s'/h) \qquad (23)$$

The equations for u_c and u_T used to evaluate the A and B integrals are those of the Stokes third approximation for large amplitude waves in water of finite depth. The wave equations and numerical tables of the wave properties are available (Skjelbreia, 1959) and will not be reproduced here. The integrals can be evaluated graphically or, as was done in this study, programmed for a digital computer.* The drag coefficients in the crest and trough region are determined from a standard steady state plot of C_D versus Reynolds number. The Reynolds numbers are defined as follows:

$$R_c = \frac{\sqrt{\overline{u_c^2}\, D}}{\nu} = \frac{D}{\nu}\sqrt{ghA} \tag{24}$$

and

$$R_T = \frac{D}{\nu}\sqrt{ghB} \tag{25}$$

The line of action of the hydrodynamic drag force passes through the centroid of the curve of u^2 versus s'. For the crest, the distance from the bottom to the line of action of F_c is designated by $\overline{s}_c$, hence, by taking the first moment,

$$\frac{\overline{s}_c}{h} = \frac{1}{A}\int_0^{1+\eta_c/h} \frac{u_c^2}{gh} \cdot \frac{s'}{h} \cdot d(s'/h) \tag{26}$$

In a similar manner, for the trough,

$$\frac{\overline{s}_T}{h} = \frac{1}{B}\int_0^{1+\frac{\eta_c - H}{h}} \frac{u_T^2}{gh} \cdot \frac{s'}{h} \cdot d(s'/h) \tag{27}$$

Harleman and Shapiro (1955) have shown that $\overline{s}_c$ can be assumed constant for $0° \leq \theta \leq 180°$, and $\overline{s}_T$ can be assumed constant for $180° \leq \theta \leq 360°$.

2. The inertial force due to particle accelerations is evaluated from the Newtonian equation of motion for an object in an accelerating flow field,

* For the waves used in the experimental study, relatively little error is introduced if the Airy equations for particle velocity are used.

$$F_I = C_M \rho \frac{\pi D^2}{4} \int_o^h a_{x_o} \, ds \tag{28}$$

where,

C_M = added mass coefficient

a_{x_o} = horizontal acceleration at $\theta = 0°$

The acceleration integral may be evaluated from the Stokes third order tables (Skjelbreia, 1959). For the range of waves in the experimental study it is sufficient to use the Airy equations with $C_M = 2.0$ and eq. (28) then becomes,

$$F_I = \frac{\gamma \pi D^2 H}{4} \tanh kh \tag{29}$$

The line of action of the inertial force is,

$$\frac{\bar{s}_I}{h} = \frac{1 + kh \sinh kh - \cosh kh}{kh \sinh kh} \tag{30}$$

which is assumed constant for all values of θ.

It should be emphasized that this paper is not primarily concerned with the particular wave force computational procedure for a single vertical cylinder or with the various arguments in regard to the numerical values for C_D and C_M. The values chosen agree with the laboratory experiments. Under field conditions other values in accordance with the experience of the designer may be used.

The wave force functions, eqs. (18) and (19), may now be approximated by a Fourier series in the following manner:

let F, the resultant wave force on one of the vertical legs, be given by,

$$F = a_o + \sum_{n=1}^{\infty} (a_n \cos n\theta + b_n \sin n\theta) = F_c \sin^2\theta + F_I \cos\theta \quad (0° \leq \theta \leq 180$$

$$= -F_T \sin^2\theta + F_I \cos\theta \quad (180° \leq \theta \leq 3$$

(3

where,

$$a_o = \frac{1}{2\pi} \int_o^{2\pi} F \, d\theta$$

$$a_n = \frac{1}{\pi} \int_o^{2\pi} F \, (\cos n\theta) \, d\theta$$

$$b_n = \frac{1}{\pi} \int_0^{2\pi} F \, (\sin n\theta) \, d\theta$$

whence,

$$a_o = \frac{F_c - F_T}{4}$$

$$a_1 = F_I \qquad b_1 = \frac{4}{3\pi} (F_c + F_T)$$

$$a_2 = -\left(\frac{F_c - F_T}{4}\right) \qquad b_2 = 0$$

$$a_3 = 0 \qquad b_3 = -\frac{4}{15\pi} (F_c + F_T)$$

Therefore,

$$F = \frac{F_c - F_T}{4} + F_I \cos\theta + \frac{4}{3\pi} (F_c + F_T) \sin\theta$$

$$- \left(\frac{F_c - F_T}{4}\right) \cos 2\theta - \frac{4}{15\pi} (F_c + F_T) \sin 3\theta + \text{---} \qquad (32)$$

The last two terms tend to cancel and contribute little to the total force, hence only the initial three terms of the series are used, in addition, since $\cos\theta = \sin(\theta + 90°)$:

$$F = \frac{F_c - F_T}{4} + F_I \sin(\theta + 90°) + \frac{4}{3\pi} (F_c + F_T) \sin\theta \qquad (33)$$

This series of sine terms is valid for $0° \leq \theta \leq 360°$.

Before using the series expression for wave force, eq. (33), in the dynamic analysis of the platform it is of interest to see how it compa with experimental measurements on a single vertical cylinder. The com parison with earlier experimental measurements (Harleman and Shapiro, 1955) is shown in Fig. 4. The agreement, considering that only three te are used in the Fourier series, is considered reasonable. In addition, b $C_D \cong 1.2$ and $C_M = 2.0$ were chosen "a priori", and a better fit could be tained, if desired, by adjusting these coefficients.

Platform Displacement

From eq. (9) the following influence fractions may be defined,

$$f_c = \frac{P_c}{F_c} = 3\left(\frac{\bar{s}_c}{\ell}\right)^2 - 2\left(\frac{\bar{s}_c}{\ell}\right)^3 \qquad (34a)$$

$$f_T = \frac{P_T}{F_T} = 3\left(\frac{\bar{s}_T}{\ell}\right)^2 - 2\left(\frac{\bar{s}_T}{\ell}\right)^3 \tag{34b}$$

$$f_I = \frac{P_I}{F_I} = 3\left(\frac{\bar{s}_I}{\ell}\right)^2 - 2\left(\frac{\bar{s}_I}{\ell}\right)^3 \tag{34c}$$

where eqs. (26, 27, **30**) are to be used to calculate the appropriate values of $\bar{s}/\ell$.

The Fourier series for the forcing function P at the elevation of the deck in the equivalent system is obtained from the wave force equation (33), hence,

$$P = \frac{F_c f_c - F_T f_T}{4} + \frac{4}{3\pi}(F_c f_c + F_T f_T)\sin\theta + F_I f_I \sin(\theta + 90°) \tag{35}$$

To simplify the notation, let,

$$P_1 = \frac{F_c f_c - F_T f_T}{4}$$

$$P_2 = \frac{4}{3\pi}(F_c f_c + F_T f_T)$$

$$P_3 = F_I f_I$$

Therefore, since $\theta = (\sigma t - kx)$, eq. (35) becomes,

$$P = P_1 + P_2 \sin\sigma\left(t - \frac{kx}{\sigma}\right) + P_3 \sin\sigma\left(t - \frac{kx}{\sigma} + \frac{90}{\sigma}\right) \tag{36}$$

or

$$P = P_1 + P_2 \sin\sigma t' + P_3 \sin\sigma t'' \tag{37}$$

where $t' = t - \frac{kx}{\sigma}$

and $t'' = t - \frac{kx}{\sigma} + \frac{90°}{\sigma}$

Each of the P terms in eq. (37) gives rise to a displacement X given by eq. (2). The P_1 term is independent of both x and t, hence,

$$X_1 = \frac{4P_1}{K} \tag{38}$$

The factor 4 appears in eq. (38) since the P terms represent the force on the equivalent system due to the wave force on a single leg of the structure. As shown in Fig. 1, x = 0 is taken to coincide with the two forward legs of the platform. To simplify the notation, let the denominator of eq. (2) be given by,

$$G = \sqrt{\left[1 - \left(\frac{\sigma}{\sigma_n}\right)^2\right]^2 + \left[2\frac{C}{C_c}\frac{\sigma}{\sigma_n}\right]^2} \tag{38}$$

For the forward legs, x = 0,

$$t' = t$$
$$t'' = t + \frac{90°}{\sigma}$$

For the rear legs, x = b, $\frac{kx}{\sigma} = \frac{2\pi b}{\sigma L} = \frac{360°b}{\sigma L}$,

$$t' = t - \frac{360°b}{\sigma L}$$

$$t'' = t - \frac{360°b}{\sigma L} + \frac{90°}{\sigma}$$

Therefore, from eq. (2), the sum of the instantaneous displacements for the two forward and two rear legs due to the forcing term P_2 in eq. (37) is given by,

$$X_2(t) = \frac{2P_2}{KG}\left[\sin(\sigma t - \phi) + \sin\left(\sigma t - \frac{360°b}{L} - \phi\right)\right] \tag{39}$$

In a similar fashion, the instantaneous displacement due to the forcing term P_3, becomes

$$X_3(t) = \frac{2P_3}{KG}\left[\sin(\sigma t + 90° - \phi) + \sin\left(\sigma t - \frac{360°b}{L} + 90° - \phi\right)\right.$$

(40)

In accordance with eq. (6) the total displacement of the platform deck at any instant of time is given by,

$$X_{tot.}(t) = X_1 + X_2(t) + X_3(t) \tag{41}$$

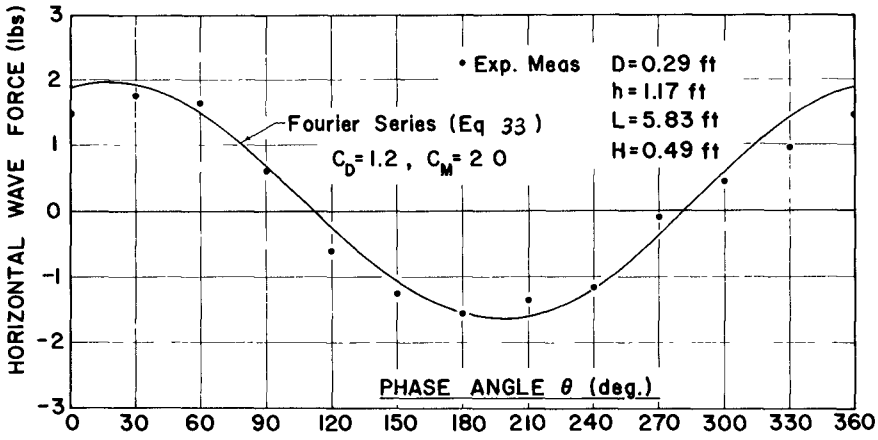

Fig. 4 Comparison of Fourier Series with Experimental Wave Force on a Single Vertical Cylinder

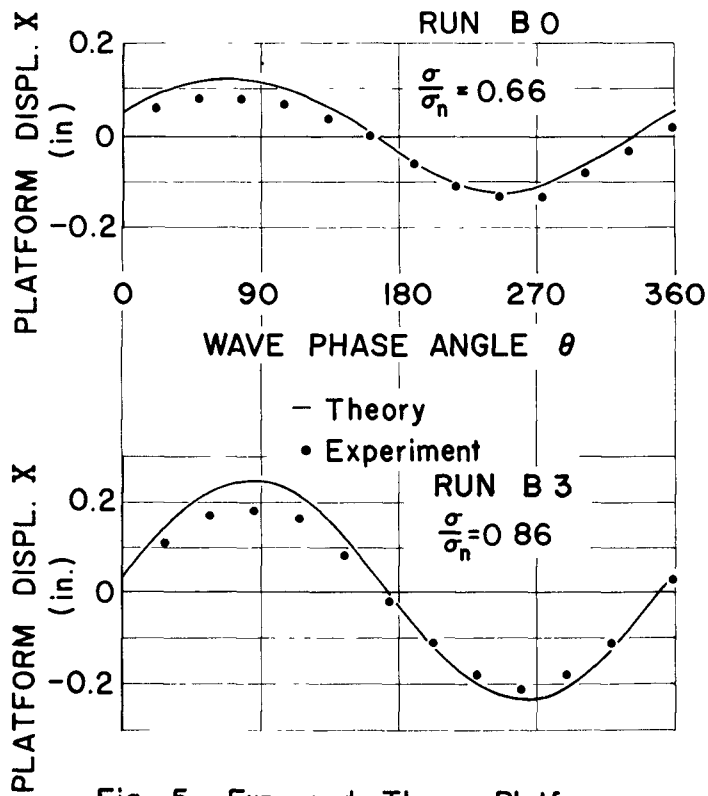

Fig. 5 Exp. and Theor. Platform Displacement. Wave B

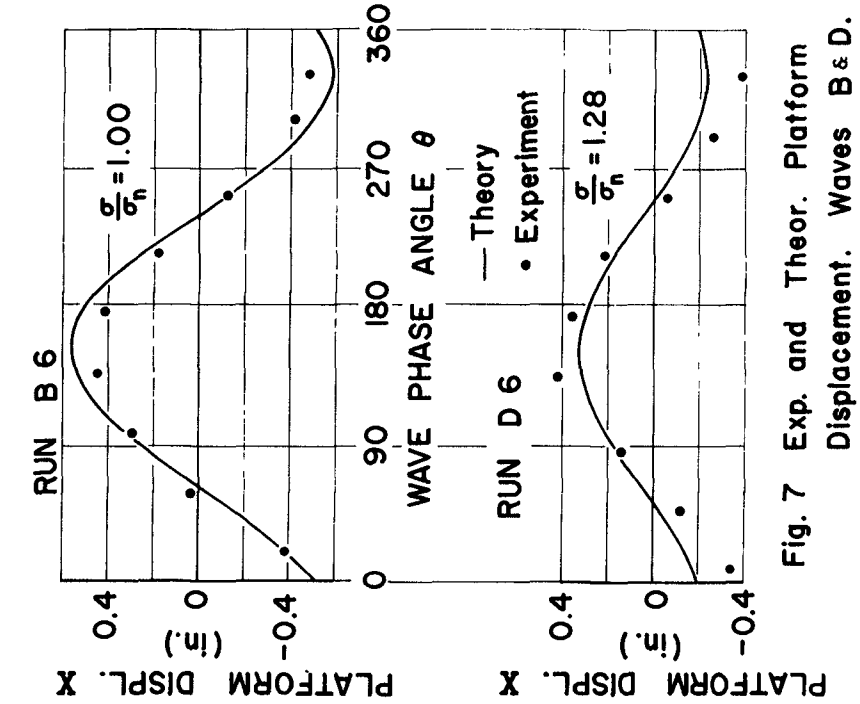

Fig. 7 Exp. and Theor. Platform Displacement. Waves B & D.

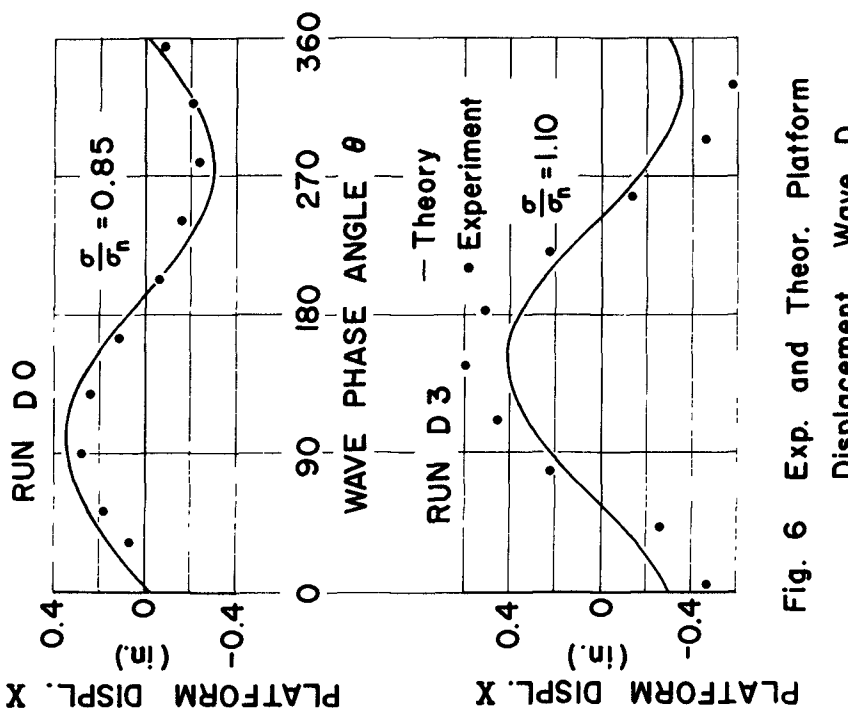

Fig. 6 Exp. and Theor. Platform Displacement. Wave D

EXPERIMENTAL RESULTS

The experimental measurements were made in the 90-foot wave channel in the M.I.T. Hydrodynamics Laboratory. Waves were generated by a variable speed and amplitude piston type generator located at one end of the channel. Wave reflections from the beach at the far end of the channel were avoided by starting each run from rest and recording the data during the passage of the eighth wave.

The platform was located 40 feet from the wave generator and was constructed of plastic. The four legs are 1/2 inch diameter, 42 inches lon and are located on 16-inch centers in a square pattern. The platform deck is 5/8" x 18" x 18" and contained a bolt in the center for observing platforn displacements and for holding weights to change the natural frequency of th structure. The legs were rigidly fixed to the bottom of the wave tank. The platform displacements were recorded by means of a 16 mm movie camera A two channel oscillograph was used to record wave profiles by means of parallel wire resistance wave gages. The two gages were adjusted until th two wave profiles were in phase on the recorder paper at which point the measured distance between the gages is equal to the wave length. The wav period was determined by comparing the measured wave length on the recorder paper with the known speed of the paper. The wave characteristics for the tests reported are given in table I.

TABLE I

Wave Characteristics

Wave	H (ft)	L (ft)	h (ft)	h/L	H/L	$\sigma=2\pi/T$ (1/sec)
B	0.31	10.86	2.25	0.21	0.029	4.00
D	0.40	7.33	2.25	0.31	0.055	5.13

The parameters used in the wave force theory are given in table II

TABLE II

Wave Force Parameters

Wave	A (22)*	B (23)*	C_{D_c}	C_{D_T}	F_c (20)* (lb)	$\bar{s}_c$ (26)* (ft)	F_T (21)* (lb)	$\bar{s}_T$ (27)* (ft)	F_I (29)* (lb)
B	0.0042	0.0028	0.92	0.88	0.027	1.54	0.017	1.26	0.023
D	0.0067	0.0034	0.96	0.92	0.042	1.81	0.022	1.41	0.033

The spring constant of the platform was determined to be K = 7.5 The natural frequency of the platform was varied by adding weights to the d The damping ratio C/C_c was determined experimentally by a measuremen the logarithmic decrement as given in eq. (17). The platform characterist are summarized in table III.

* equation number

TABLE III

Platform Characteristics

Added wt. (lb)	σ_n (1/sec)	C/C_c
0	6.01	0.050
3	4.67	0.055
6	4.00	0.061

The experimental runs are designated by a letter indicating the wave characteristics and a number indicating the amount of added weight. Thus, run D3 used wave D and 3 pounds were added to the deck of the plat form.

The experimental results for six runs are shown in Figs. 5, 6, and in which the horizontal platform displacement is plotted as a function of wave phase angle. The theoretical displacement as calculated from eq. (is also shown for comparison. The runs were chosen to illustrate the agr ment between theory and experiment for ratios of wave frequency to natur frequency (σ/σ_n) ranging from 0.66 to 1.28. In general, the agreement is good, considering that all wave force parameters were determined analyt cally. The most serious disagreement occurs, as would be expected, for run D3 ($\sigma/\sigma_n = 1.10$) which corresponds to the damped resonant condition maximum displacement.

A digital computer program (Fortran) was developed for the theoret displacement calculations. The calculations were done at the M.I.T. Cor putation Center on an I.B.M. 7090 computer.

CONCLUSIONS

The analytical procedure using the equivalent spring-mass system f the dynamic analysis of offshore structures has been verified by laborato tests. The magnitude of the dynamic displacement of the platform deck m be of interest in itself. More generally, the dynamic displacement is use in the stress analysis of the entire structure. The usual practice has bee to design statically on the basis of the largest wave to be encountered. It may well be true that for the "design" wave the statical analysis is correc since, in general, the period of the highest wave may be large compared t the natural period of vibration of the platform. However, smaller waves lesser period may approach resonance with the platform. It is not difficu to foresee cases in which stresses under near resonant conditions could e ceed the stresses of the statical design wave. For example, the steepnes of wave D is almost twice as high as wave B; however, the displacement (hence, the stresses) for wave B at $\sigma/\sigma_n = 1.00$ is twice as high as for wa D at $\sigma/\sigma_n = 1.28$. Another comparison may be made on the basis of the ra of displacements calculated both statically and dynamically. For test B6, the measured dynamic displacement is six times the calculated static dis- placement. Consequently, stresses will be greater by the same ratio.

Field tests on Texas Tower No. 4 (Ref. 8) off the eastern coast of the U.S. indicate that platform displacements (about 3 inches) were greater for 10 foot waves than for 30 foot waves. This would appear to be further evidence of the necessity of considering dynamic behavior in the design of offshore structures.

- - -

This paper is based upon a thesis submitted by Lieutenants Nolan and Honsinger for the degree of Naval Engineer under the supervision of the senior author.

- - -

REFERENCES

1. Harleman, D. R. F. and Shapiro, W. C. Experimental and Analytical Studies of Wave Forces on Offshore Structures: Part 1, Results for Vertical Cylinders: Tech. Report No. 19, M.I.T. Hydrodynamics Laboratory, May 1955.

2. Housner, G. W. and Hudson, D. E. Applied Mechanics Dynamics: Van Nostrand Co., N. Y., 2nd Ed., 1959.

3. Morison, J. R., Johnson, J. W. and O'Brien, M. P. Experimental Studies of Forces on Piles: Proc. 4th Conf. on Coastal Eng., p. 340, 1953.

4. Nolan, W. C. and Honsinger, V. C. Wave Induced Vibrations in Fixed Offshore Structures: Naval Eng. Thesis, M.I.T., May 1962.

5. Skjelbreia, L. Gravity Waves, Stokes Third Order Approximation. Tables of Functions: Council on Wave Research, 1959, Calif. Research Corp.

6. Thomson, W. T., Mechanical Vibrations: Prentice-Hall, Inc., Englewood Cliffs, N. J., 2nd Ed., 1953.

7. United States Senate. The Collapse of Texas Tower No. 4: Report by Preparedness Investigating Subcommittee of the Committee on Armed Services, U. S. Senate. 87th Congress, 1st Session. Government Printing Office, Washington, D. C., 1961.

8. Report 173, Texas Tower No. 4, Platform Motion Study: Brewer Engineering Laboratories, Inc., Marion, Mass., June 10, 1959.

CHAPTER 29

ATTENUATION OF WIND WAVES BY A HYDRAULIC BREAKWATER

John A. Williams, Grad. Res. Engineer
and
R. L. Wiegel, Assoc. Prof. of Civil Engineering

University of California, Berkeley

ABSTRACT

Waves generated in a tank by air blowing over the water surface were subjected to a horizontal current of water created by horizontal water jets issuing from a manifold at the water surface (hydraulic breakwater). The energy spectra of the waves were computed for conditions before and after the hydraulic breakwater was turned on. It was found that the shorter, steeper wave components were attenuated to a much greater extent than were the longer wave components. Thus, although a large portion of the wave energy could get past such a breakwater, the waves in the lee of the breakwater looked considerably lower to the observer.

INTRODUCTION

The literature* on harbor protection contains a number of articles on an "air breakwater" or a "pneumatic breakwater." This type of breakwater consists of a pipe on the ocean bottom, supplied with compressed air which issues from the pipe through a series of ports. In some manner this results in a decrease in wave height in the lee of the breakwater. Th mechanism, or mechanisms, by which the waves are attenuated is in dispute, with apparent discrepancies between results of model and prototype studies. The most likely mechanism is the one suggested by Schijf (1940) and studied theoretically by Taylor (1955). The air bubbles formed when the air discharges through the ports mix with the water, and as the mixture is less dense than the surrounding water, it rises. The air bubbles escape to the atmosphere at the surface while the water turns through ninety degrees forming horizontal currents. The thickness of the current was found to be proportional to the one-third power of the volume rate of flow of air per foot of pipe. The claim that the bubbles themselves some how attenuate the waves has been shown to be incorrect both theoretically (Schiff, 1948a, 1948b) and experimentally (Carr, 1950) in studies of the effect of a bubble-water field one-half a wave length thick.

*See, for example, Green (1961) which contains an extensive list of references on the subject, and a discussion of this paper by Schijf (1961).

ATTENUATION OF WIND WAVES BY A HYDRAULIC BREAKWATER

Because it seemed that the surface current produced by the pneumatic breakwater had the main effect on waves, tests were made using a series of horizontal jets to generate a surface current, this device being called a hydraulic breakwater (Dilley, 1958; Horikawa, 1958; Snyder, 1959; Williams, 1960). It was found that a manifold placed at the mean water level, discharging water jets horizontally into the waves, generated a surface current similar to the current created by the pneumatic breakwater, and that this current had the same effect on the waves as in the case of a pneumatic breakwater.

Why should there be a discrepancy between the observations in various model studies and claims made for the prototype pneumatic breakwater? Many of these claims stem from early stories of experiments at a pier at El Segundo, California. However, it was concluded from these studies that the apparatus was of no utility or benefit and therefore abandoned (U.S. District Court, 1923), but these conclusions apparently were never published. Thus, part of the claims are not valid. It is believed that the reasons for the claims are in part real, and in part psychological. Waves that are still in the generating area are steep, many of them breaking due to their steepness, and many of them nearly breaking. Because of this, an opposing current, which will cause the waves to steepen, will force many of them to break and dissipate wave energy. In addition, waves in the ocean are irregular and for many purposes can be described by an energy spectrum. On the other hand most laboratory tests are performed with periodic waves of uniform height. For many purposes the laboratory waves can be, and have been, associated with the portion of the energy spectrum in the vicinity of the peak energy density which in turn is closely related to the significant wave (Wiegel, 1960). Now, suppose we can generate a surface current by a pneumatic breakwater, or some other means, that is neither thick enough nor fast enough to stop the longer component waves in the spectrum associated with the maximum energy density, but which can stop the shortest wave components and cause those wave components somewhat longer than the shortest waves to steepen and break. Most of the wave power will be transmitted into the lee of the breakwater, but it will look much smoother than the original wave system as the short steep wave components will have either been reflected by the current or greatly attenuated. This is the psychological part--the wave system no longer looks as high as it did before.

If irregular wave systems can be treated to a certain extent as a superposition of linear wave trains, then a current might be able to affect the wave components in the selective manner described above. The data obtained by Kurihara (1958) in his field tests suggested to the authors that this might be possible. In order to test this possibility laboratory experiments were performed using a hydraulic breakwater to generate the surface current, and blowing wind over the water surface to create the waves.

STATISTICAL ANALYSIS OF WIND-GENERATED WAVES

It has been recognized from analyses of wind-wave records that the ordinate-time history of the water surface may be represented for many practical purposes as a "stationary Gaussian process." This statistical model in turn implies a distribution of energy over a range of frequencies which is independent of time and a distribution of probability over a range of ordinates (i.e. ordinates of the time-surface elevation record) (Putz, 1954, Pierson, 1954, Bretschneider, 1959).

The most direct method of analyzing any given wind-wave record is to extract from it the apparent wave heights and periods--that is, to consider the individual "bumps" of the record to be waves themselves. The problem remains then to show that such "wave heights" and "wave periods" are statistically congruous with the stationary Gaussian process This has been done by Putz (1954). In regard to the probability distribution curve containing two parameters σ_0 , the root-mean-square ordinate, and ρ_0 , the ratio of the number of zero crossings of the ordinate to the number of zero crossings of the first derivative of the ordinate (the number of wave maxima and minima). Zero crossing means the crossing of the time axis, this axis being through the mean of the ordinates. When $\rho_0 = 1$, this distribution function coincides with the Rayleigh distribution function. A comparison of this derived probability distribution with "wave heights" as extracted from a record of 20-minute length shows that the actual distribution coincides with a theoretical distribution curve where $\rho_0 = .92$. Thus, the actual distribution curve is approximately the Rayleigh distribution curve. This result is in agreement with the work of several others, namely, Bretschneider (1959), Longuet-Higgins (1959), and Miche (1952).

In regard to the energy distribution with respect to frequency, Putz employed the fact that the Fourier spectrum of the covariance of the stationary Gaussian process is the energy spectrum of the wave record. Further, the covariance is shown to depend on the zero crossings of the record. Consequently the apparent periods of the waves are related to the energy spectrum. These results apply to wave records of length no greater than about twenty minutes, as records of longer duration do not satisfy the time stationary requirement.

In view of the above it may be concluded that the "wave heights" and "wave periods" of the individual "bumps," as extracted from the wave record, are compatible with the stationary Gaussian process and may therefore serve as indications of the energy distribution with respect to frequency and of the probability distribution of the ordinates.

ATTENUATION OF WIND WAVES BY A HYDRAULIC BREAKWATER

EXPERIMENTAL APPARATUS AND PROCEDURE

The experiments were carried out in two different wind-wave tanks. The larger tank was 106' long by 3' deep by 1' wide, while the smaller tank was 60' long by 1/28' deep by 1' wide. The larger tank was located on the U. C. campus and will be referred to as the UCB tank, and all data taken from it will be noted as UCB data. The smaller tank was located at the University's Richmond Field Station and will be referred to as the RFS tank, and the data taken from it noted as the RFS data. The wind in the RFS tank was generated by a blower, while the wind in the UCB tank was generated by an exhaust fan. Wind speeds in both tanks were measured with a pitot tube and a draft gage.

The wind waves were recorded by parallel wire resistance probes connected to a Brush oscillograph. The flow through the breakwater for the UCB tank tests was measured by an orifice plate inserted in the breakwater supply line, and a water manometer. The breakwater flow rate in the RFS tank was measured volumetrically by noting the change in water level in the tank during a given run together with the run time. As the run times were short, the increase in water levels in the tank was not sufficient to affect the performance of the breakwater during the run.

The hydraulic breakwater used to generate the horizontal current is shown in Fig. 1. The designation $\lambda = 8$ on the drawing is to tie it in with the results of several other scale breakwaters used in model tests on the scale effect of hydraulic breakwaters (Williams, 1960). A performance curve for the breakwater is shown in Fig. 2. It shows the length of the longest wave that can be attenuated to only 5% of its original height for a given breakwater discharge. This curve pertains essentially to nearly deep water waves since the points which define the curve resulted from data where $1.77 \leq L/d \leq 4.92$. Figures 3 and 4 show the arrangement of the resistance probes, breakwater, pitot tube, etc., for the UCB and RFS tanks, respectively. The experimental procedure was similar in both tanks, except for measuring the breakwater discharge. First, the waves were recorded for a given wind speed without the breakwater in the tank; next, the waves were recorded after the breakwater was installed but before it was turned on, and, finally, the waves were recorded for several breakwater discharges while holding the wind speed constant. This procedure was repeated in the UCB tank for two water depths, 6 inches and 27 inches, using one wind speed at each depth, and in the RFS tank using one depth, 6 inches, and two wind speeds. In the UCB experiments only two resistance gages were used, one in front of and one behind the breakwater. In the RFS experiments three gages were

used, two behind and one in front of the breakwater. The exact positions of these gages with respect to the breakwater are shown in Figs. 3 and 4.

ANALYSIS OF DATA

Two problems presented themselves: first, the method of taking the sample and second, the size of the sample. In view of the excessive amount of work required in extracting the "wave heights" and "wave periods" from a wave record, an attempt was made to determine the minimum length of record that would give a realistic account of the physical situation involved. A record from the UCB tank was analyzed using samples of 100 consecutive waves and 50 consecutives waves, and the cumulative distribution curves were plotted of the "heights" and the "periods" (see Figures 5a and 5b). Since there was no appreciable difference in these two curves, it was decided that about 50 waves could be selected as an adequate sample size.

There are several methods available for picking the "wave heights" and "wave periods" from the record. Two of these methods are the zero-upcrossing method and the crest-to-trough or trough-to-crest method. In the zero-upcrossing method the periods are taken as the distance between the successive upcrossings of the wave record, f(t), with the axis through the mean of the ordinates. This quantity is denoted as $\tilde{T}$. The wave height, H, corresponding to a given $\tilde{T}$ is taken as the vertical distance from the crest to the trough found on the interval $\tilde{T}$. The crest-to-trough method defines the "period" as the distance between successive dominant crests. This period is indicated by T. The height is taken as the vertical distance from the first crest of T to that point which is lowest between the two crests. The trough-to-crest method defines T as the distance between successive troughs, and the height, H, as the distance between the first trough and the highest point on the record between the two troughs. From these definitions it is clear that $\bar{T} \geq \tilde{\bar{T}}$ where the bars indicate averages of a number (N) of waves. The equality sign holds in the limit as $N \to \infty$, provided there are only a finite number of small ripples which intersect the time axis in the unlimited record. These ripples are considered as "waves" in the zero-upcrossing method, but are neglected in the crest-to-trough method (see Pierson, 1954).

To illustrate the differences between these two methods a section of wave record was analyzed both ways, and the resulting cumulative distribution curves plotted in Figs. 5a and 5b. Figure 5a illustrates the difference between the two methods for a 100 wave-period sample, and the difference between a 50 wave-period sample and a 100 wave-period sample for the zero-upcrossing method. Figure 5b shows the difference

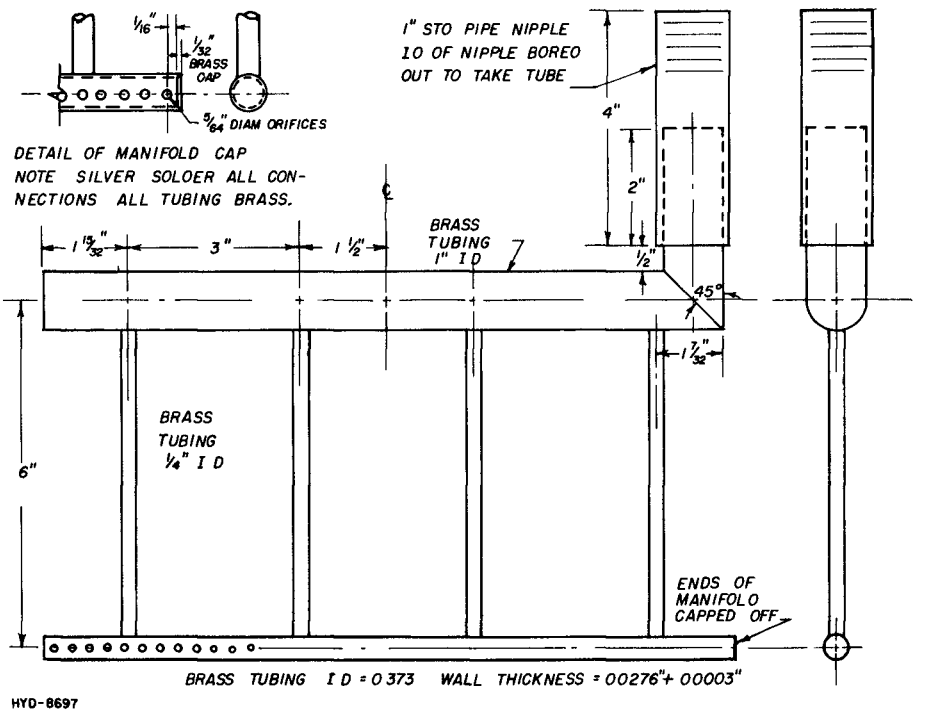

Fig. 1 - Model manifold hydraulic breakwater, $\lambda = 8$

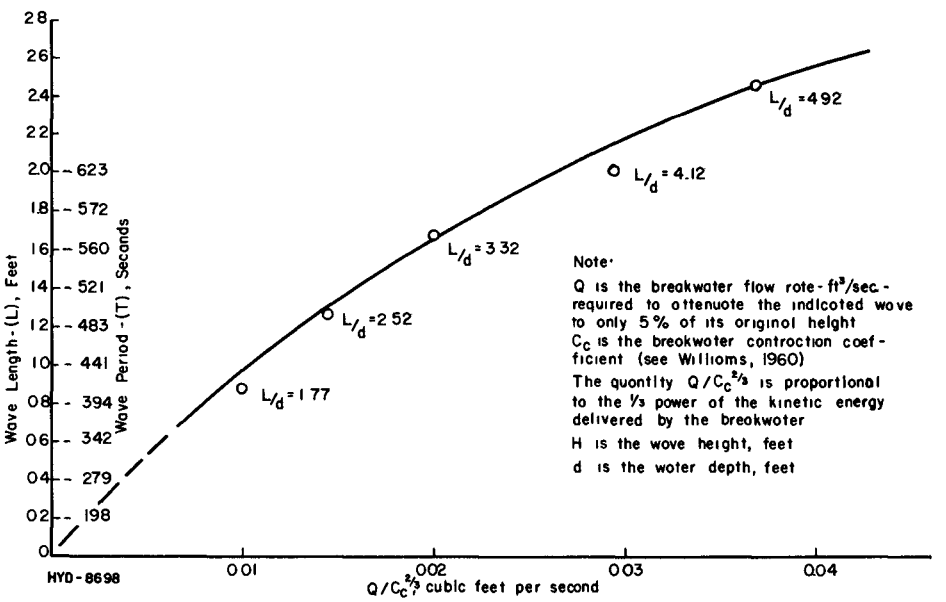

Fig. 2 - Wave length (period) vs $Q/C^{2/3}$ for $\lambda = 8$ model breakwater, wave steepness - $H/L = .038$

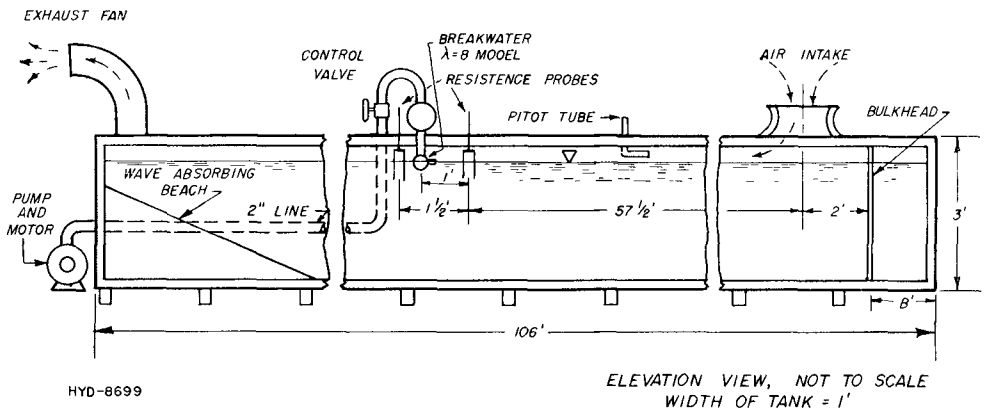

Fig. 3 - UCB wind-wave tank

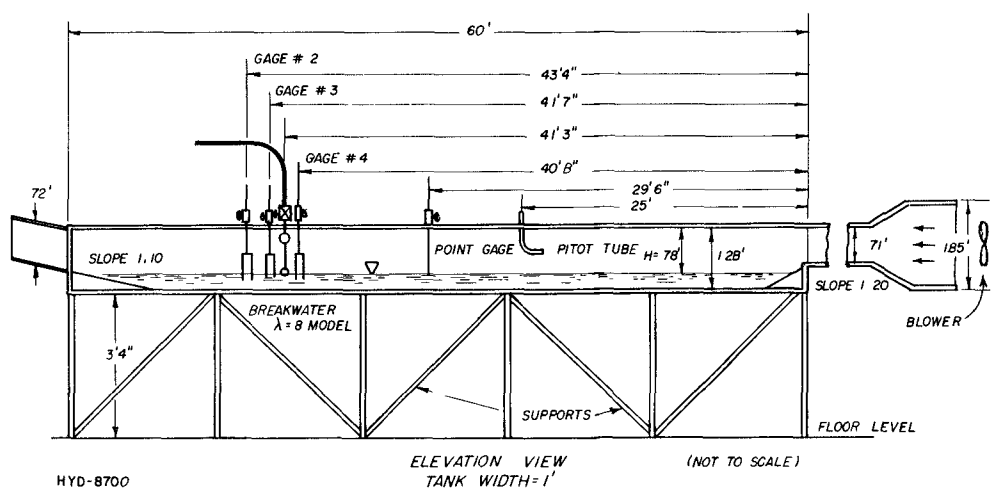

Fig. 4 - Richmond Field Station wind-wave tank

between a 50 wave-height sample and a 100 wave-height sample for the zero-upcrossing method. It is to be noted that the wave heights taken from the record by both of these methods will be identical provided there are no small ripples intersecting the time axis between two larger waves. In view of this fact and the results indicated in Fig. 5a, it was decided that the selection of the method could be based solely on its utility for the purpose at hand, and subsequently the zero-upcrossing method for the sample size of 50 plus waves was chosen. In these and subsequent figures the term "maximum wind speed" refers to maximum speed obtained from a velocity traverse from near the water surface to the top of the tank (see Fig. 6).

It should be emphasized that the sample size of 50, plus, waves pertained only to the wave record obtained without the breakwater in the tank. These 50 plus waves represented a time interval on the wave record of 25 to 35 seconds. It was this time interval that was kept constant throughout a set of breakwater discharges at a given wind speed, and consequently determined the sample sizes for each breakwater discharge. This was done so that the total energies of the wave spectrum could be compared realistically with one another before and during breakwater operation. Also, an effort was made to select as closely as possible the same set of "waves" at each gage location for a given run. An example of the records before and after the hydraulic breakwater was turned on is given in Fig. 7.

After the wave heights and periods were measured on records from the several wave gages for a given breakwater discharge and wind speed, the following quantities were calculated: $\overline{H}$, $\overline{T}$, σ_H, $\sigma_{\tilde{T}}$, $\overline{H^2}$, $\overline{H/\tilde{T}^2}$, $H_{1/3}$ and $H_{1/3}/\overline{H}$. Here the bars denote arithmetic averages, σ_H and $\sigma_{\tilde{T}}$ are the usual standard deviations of H and $\tilde{T}$ respectively, $\overline{H/T^2}$ is taken as being representative of the wave steepness, and $\overline{H^2}$ is representative of the wave energy per unit surface area. These quantities were calculated for the conditions of no breakwater in the tank, breakwater in tank with zero discharge, and at least two discharges. For the RFS tank two such sets of quantities were calculated, one for each wind speed used. These results are presented in Table 1. Similarly two sets of such quantities were calculated from the UCB tank records, one for each water depth used. These results are presented in Table 2.

Finally, joint frequency plots for H^2 and T, and frequency histograms for H/T^2 were plotted. These data appear in Figs. 8 through 11 for the RFS tests and in Figs. 12 through 15 for the UCB tests.

TABLE 1. SUMMARY OF RESULTS, RFS DATA

Gage No.	Number of Waves	$\bar{H}$, ft.	$\bar{T}$, sec.	σ_H, ft.	σ_T, sec.	$\overline{H^2}$, ft^2	$\overline{H/T^2}$	$H_{1/3}$, ft.	$H_{1/3}/\bar{H}$
Maximum wind speed = 29.5 ft/sec, water depth 0.5 ft.									
	No breakwater in tunnel								
2	54	.081	.475	.0271	.0621	.0072	.358	.111	1.37
3	54	.079	.472	.0228	.0615	.0068	.361	.106	1.34
4	54	.081	.465	.0282	.0638	.0073	.387	.110	1.36
	Breakwater in tunnel, no discharge								
2	55	.091	.480	.0253	.0719	.0090	.408	.119	1.31
3	55	.079	.480	.0257	.0748	.0069	.352	.109	1.38
4	55	.083	.478	.0230	.0731	.0075	.381	.108	1.30
	Breakwater in tunnel, Q = .00775 cfs., C_c = 815*								
2	52	.077	.511	.0228	.0651	.0065	.305	.102	1.33
3	53	.059	.492	.0221	.0737	.0039	.253	.083	1.41
4	55	.092	.471	.0345	.0782	.0097	.417	.129	1.40
	Breakwater in tunnel, Q = .0104 cfs. C_c = .700								
2	52	.064	.516	.0260	.0832	.0047	.244	.091	1.42
3	50	.057	.535	.0242	.0764	.0039	.205	.084	1.47
4	53	.111	.500	.0393	.0605	.0139	.437	.151	1.36
Maximum wind speed = 41.4 ft/sec., water depth = 0.5 ft.									
	No breakwater in tunnel								
2	55	.129	.636	.0323	.0983	.0178	.335	.163	1.26
3	56	.134	.622	.0329	.112	.0190	.372	.167	1.24
4	56	.138	.627	.0396	.122	.0200	.369	.178	1.29
Maximum wind speed = 41.4 ft/sec., water depth = 0.5 ft.									
	Breakwater in tunnel, no discharge								
2	55	.129	.635	.0300	.132	.0178	.347	.159	1.23
3	55	.137	.624	.0288	.128	.0197	.383	.169	1.23
4	55	.127	.630	.0291	.113	.0170	.343	.159	1.24
	Breakwater in tunnel, Q = .0155 cfs., C_c = .640								
2	53	.112	.662	.0309	.104	.0134	.260	.144	1.30
3	51	.116	.677	.0329	.0908	.0152	.277	.156	1.34
4	53	.188	.654	.0427	.0868	.0371	.455	.232	1.23
	Breakwater in tunnel, Q = .0190 cfs., C_c = .625								
2	52	.095	.671	.0316	.136	.0101	.223	.129	1.36
3	49	.112	.699	.0355	.123	.0128	.230	.149	1.33
4	54	.168	.645	.0536	.106	.0300	.423	.226	1.35

*C_c is the discharge coefficient of the orifice as determined experimentally.

TABLE 2. SUMMARY OF RESULTS, UCB DATA

Gage No.	Number of Waves	$\bar{H}$, ft.	$\bar{T}$, sec.	σ_H, ft.	σ_T, sec.	$\overline{H^2}$, ft^2	$\overline{H/T^2}$	$H_{1/3}$, ft.	$H_{1/3}/\bar{H}$
Maximum wind speed = 21.3 ft/sec, water depth = 0.5 ft.									
No breakwater in tunnel									
2	54	.064	.478	.0203	.0394	.0044	.287	.0861	1.35
3	54	.065	.475	.0185	.0336	.0045	.289	.0823	1.27
Breakwater in tunnel, no discharge									
2	53	.0614	.481	.0203	.0471	.0042	.273	.0844	1.37
3	53	.062	.477	.0193	.0405	.0042	.277	.0835	1.35
Breakwater in tunnel, Q = .0059 cfs, C_c = .970									
2	53	.0607	.494	.0178	.0565	.0040	.251	.0793	1.31
3	53	.0800	.494	.0255	.0519	.0071	.338	.110	1.38
Breakwater in tunnel, Q = .0071 cfs, C_c = .860									
2	52	.043	.510	.0157	.0466	.0021	.164	.0611	1.42
3	53	.086	.500	.0245	.0537	.0080	.351	.111	1.29
Breakwater in tunnel, Q = .0079 cfs, C_c = .805									
2	49	.034	.544	.0122	.0502	.0014	.118	.0474	1.39
3	53	.094	.500	.0341	.0590	.0098	.390	.133	1.41
Breakwater in tunnel, Q = .0089 cfs, C_c = .757									
2	48	.019	.550	.0081	.0788	.00041	.0645	.0271	1.43
3	53	.098	.500	.0276	.0602	.0104	.402	.127	1.30
Maximum wind speed = 31.9 ft/sec, water depth = 2.25 ft.									
No breakwater in tunnel*									
2	52	.170	.532	.0395	.0758	.0305	.622	.212	1.25
3	54	.164	.506	.0387	.0810	.0283	.641	.200	1.22
Maximum wind speed = 31.9 ft/sec, water depth = 2.25 ft.									
Breakwater in tunnel, no discharge									
2	55	.131	.486	.0360	.0647	.0186	.559	.171	1.31
3	55	.110	.489	.0323	.0582	.0132	.465	.144	1.31
Breakwater in tunnel, Q = .0102 cfs, C_c = .713									
2	50	.095	.535	.0323	.0554	.0100	.330	.131	1.38
3	54	.123	.489	.0369	.0763	.0167	.520	.159	1.29
Breakwater in tunnel, Q = .0120 cfa, C_c = .666									
2	51	.071	.530	.0285	.1120	.00590	.264	.104	1.46
3	51	.122	.536	.0456	.0808	.0170	.434	.173	1.42

*Note The reaults recorded for the condition "no breakwater in tunnel" were reduced from data which was not taken at the same time aa the rest of the data for the above wind speed and water depth.

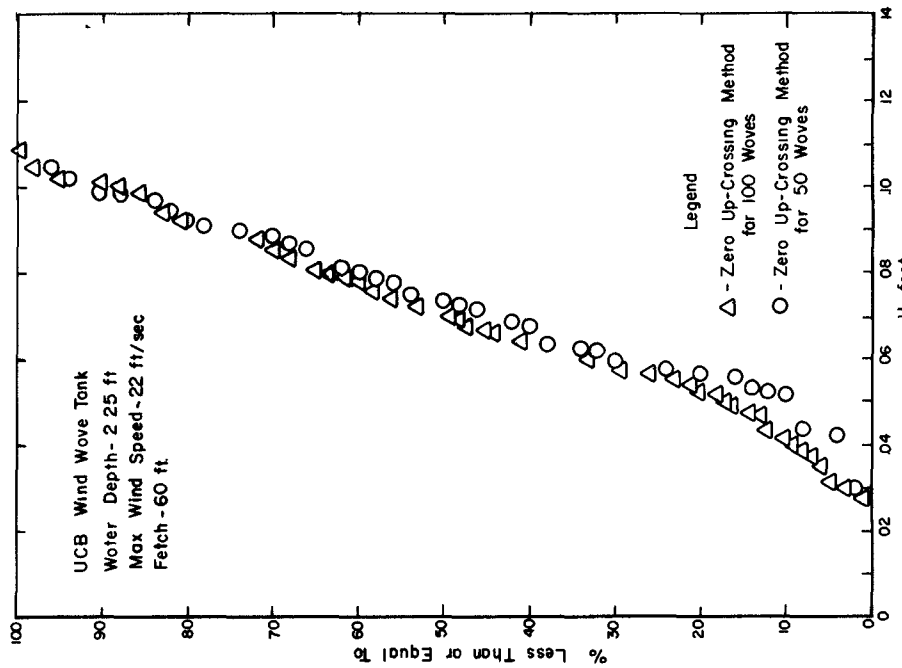

FIGURE 5b - COMPARISON OF CUMULATIVE FREQUENCY DISTRIBUTION CURVES OF WAVE HEIGHT FOR 50 AND 100 CONSECUTIVE WAVES

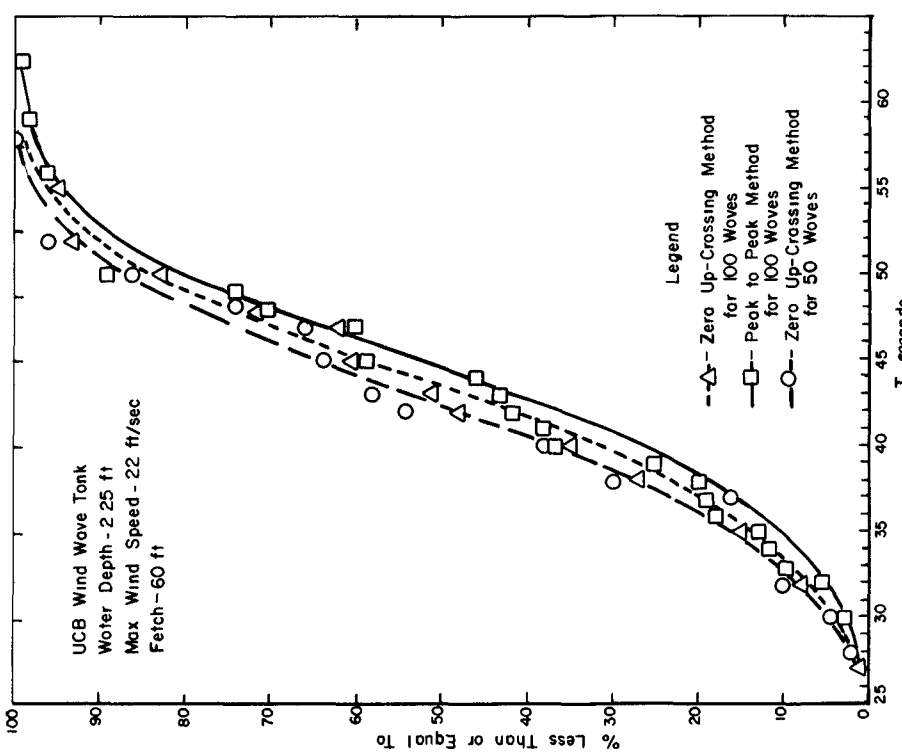

FIGURE 5a - COMPARISON OF CUMULATIVE FREQUENCY DISTRIBUTION CURVES OF WAVE PERIOD FOR 50 AND 100 CONSECUTIVE WAVES.

HYD-8701

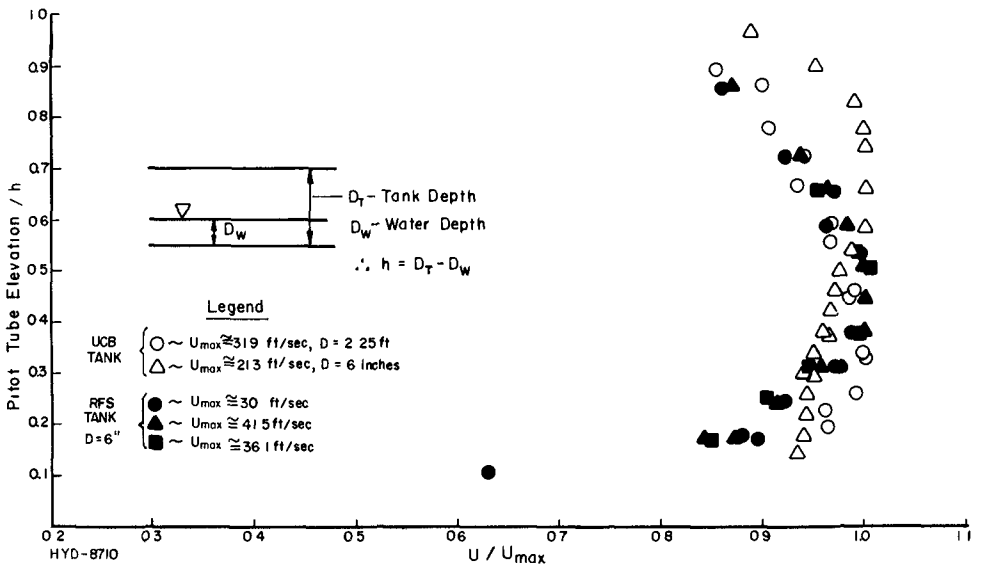

Fig. 6 - Wind speed profiles

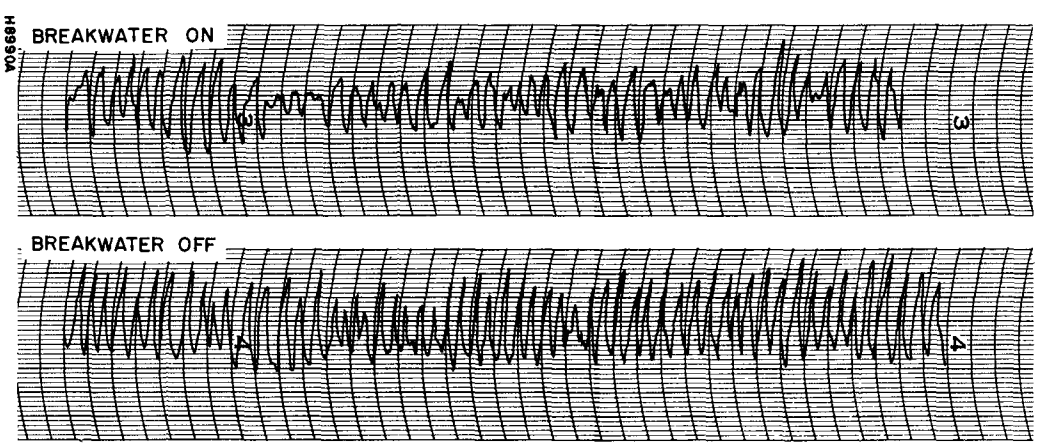

Fig. 7 - Sample wave record

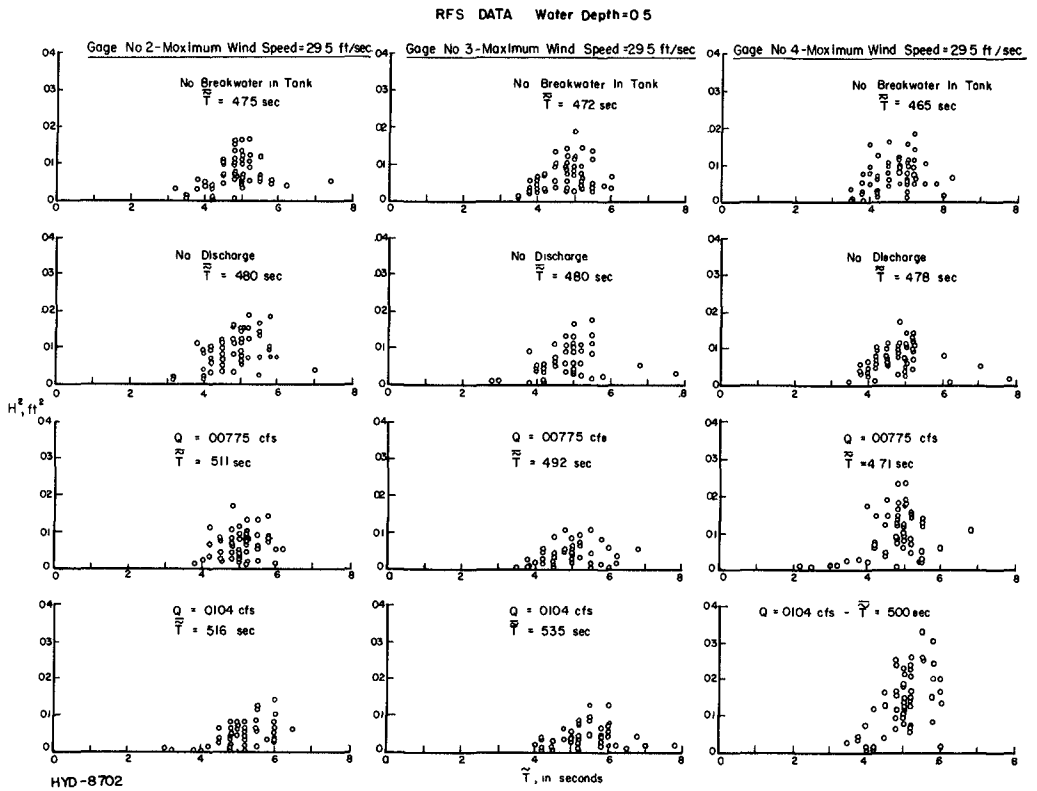

Fig. 8 - Joint frequency distribution

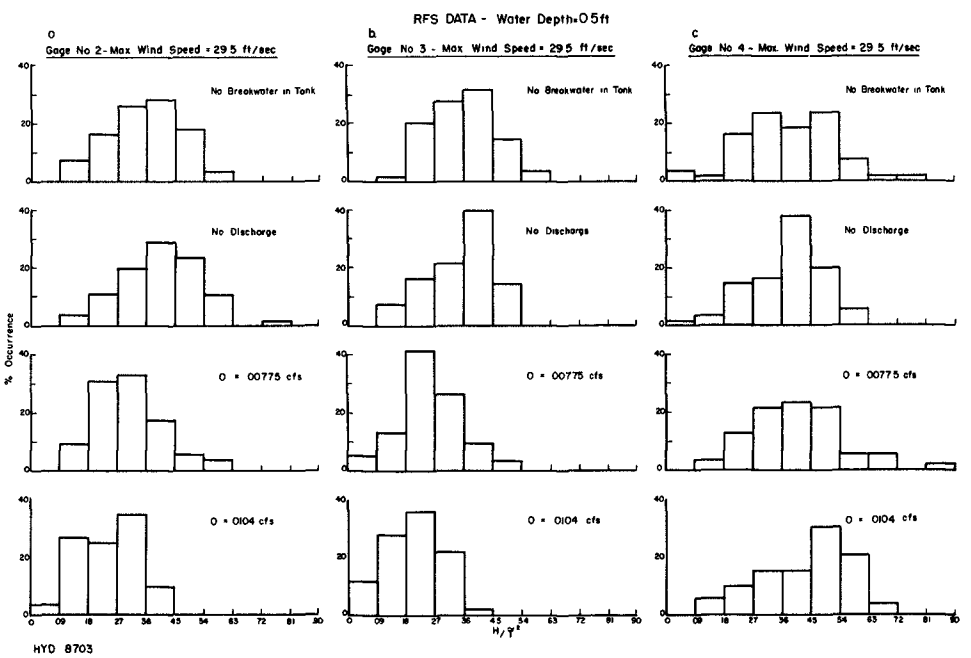

Fig. 9 - Frequency distribution

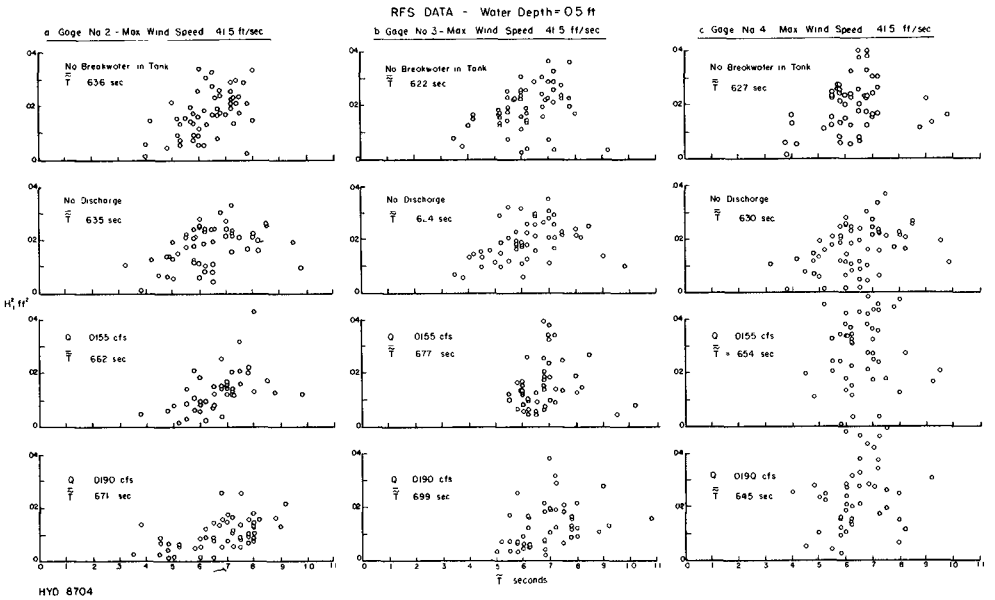

Fig. 10 - Joint frequency distribution

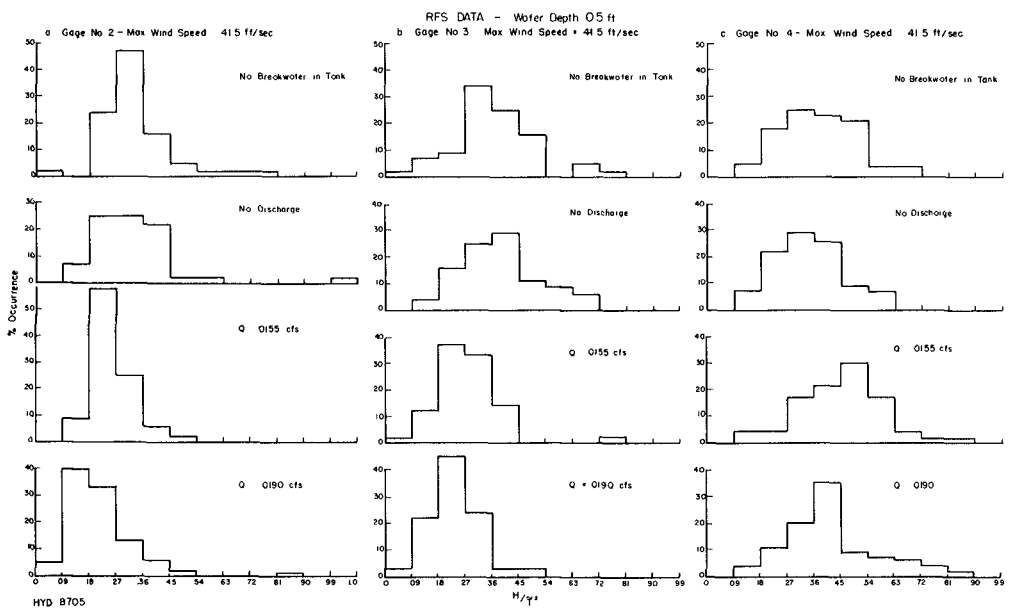

Fig. 11 - Joint frequency distribution, $H/\tilde{T}^2$

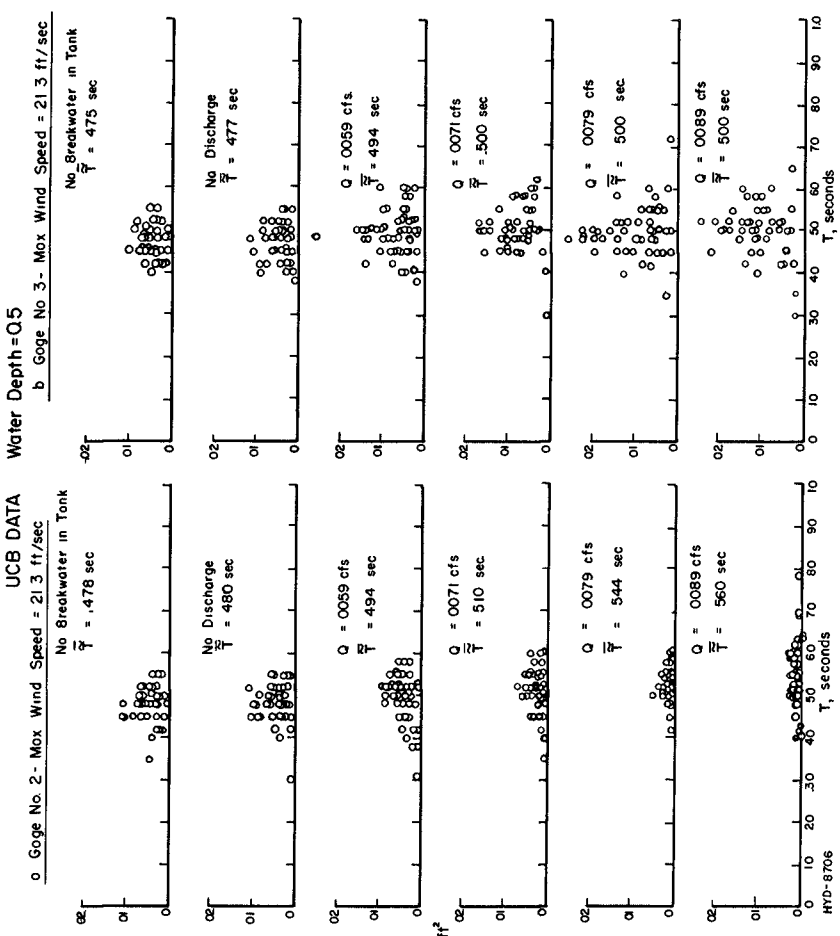

Fig. 12 - Joint frequency distribution

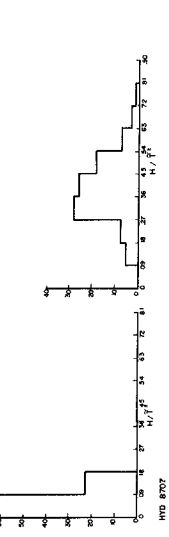

Fig. 13 - Joint frequency distribution, $H/\tilde{T}^2$

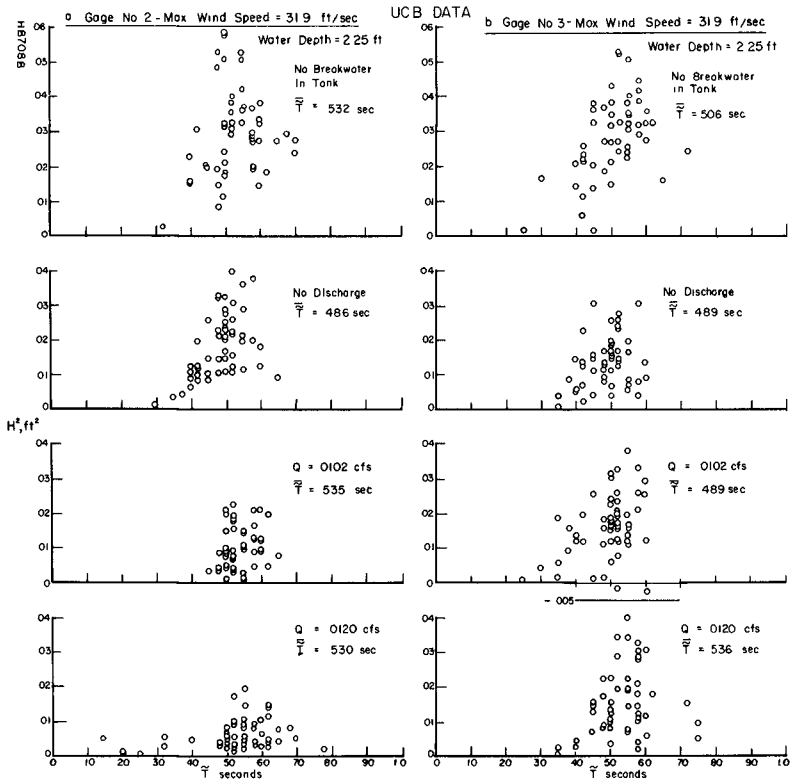

Fig. 14 - Joint frequency distribution

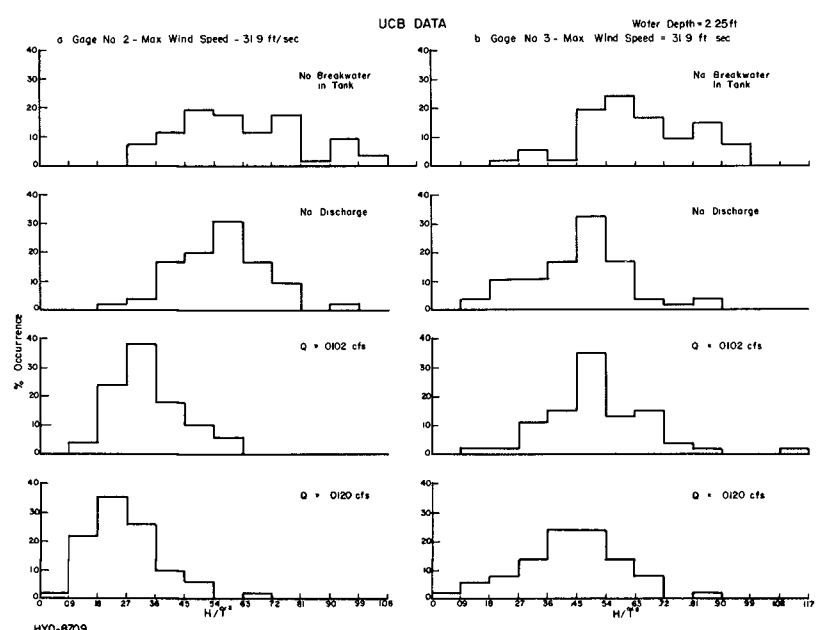

Fig. 15 - Frequency distribution, $H/\tilde{T}^2$

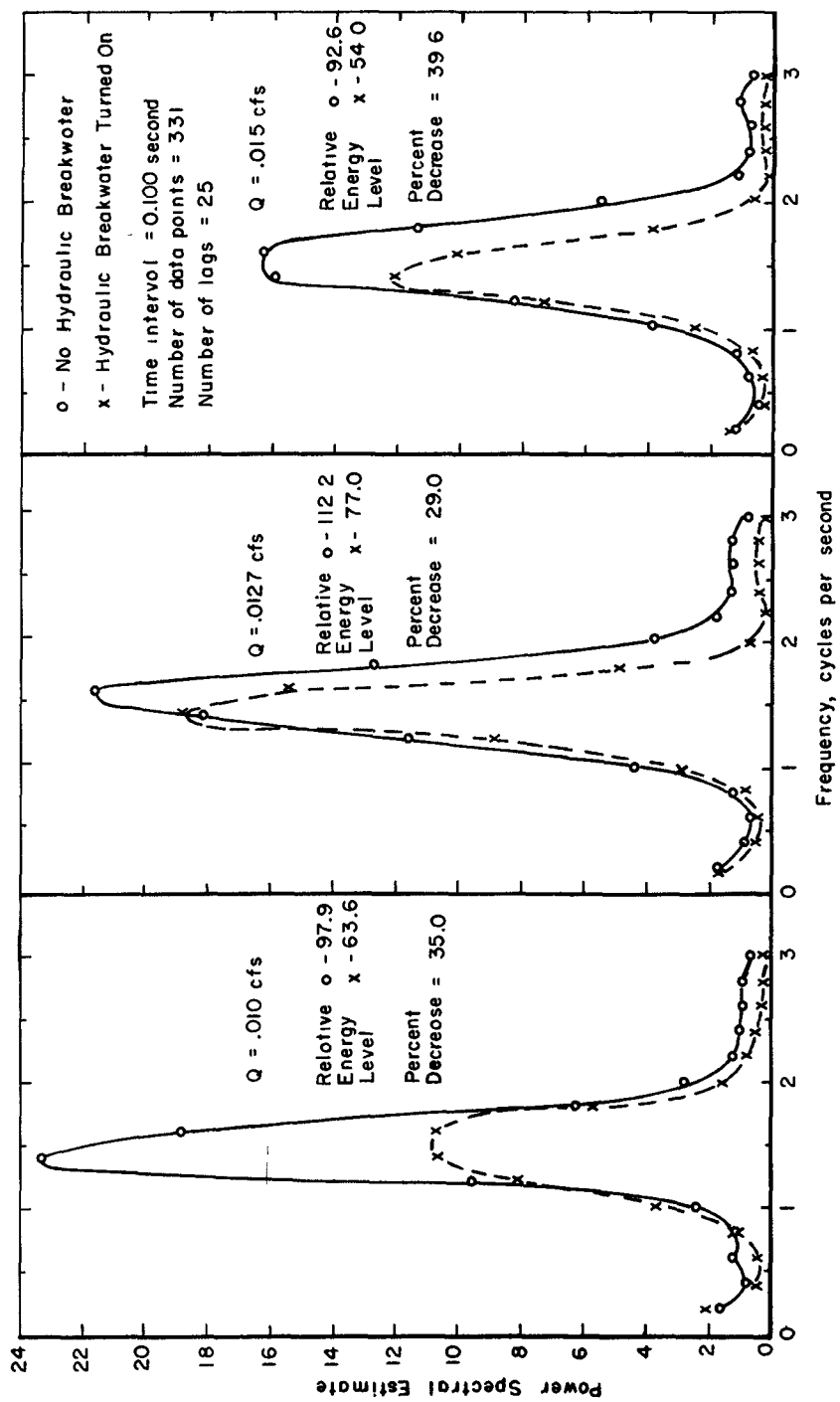

FIGURE 16 - SPECTRAL ANALYSIS OF WAVE RECORDS BEFORE AND AFTER HYDRAULIC BREAKWATER TURNED ON
RICHMOND FIELD STATION DATA -- ADDITIONAL RUNS
WIND SPEED 41 FT/SEC, FETCH - 41.5 FT

Several of the records were analyzed to obtain power spectra, using the IBM 7090 computer at the Computer Center, University of California, Berkeley, Calif., using the share sub-routine #574 "CS TUKS". The results are shown in Fig. 16.

EXPERIMENTAL RESULTS AND CONCLUSIONS

The joint distribution plots of H^2 and $\tilde{T}$ reveal two facts: (1) the highest waves occur at a period approximately equal to the average period, $\bar{\tilde{T}}$, both behind and ahead of the breakwater, and (2) the average period $\bar{\tilde{T}}$ increases consistently with increasing breakwater discharge for waves in the lee of the breakwater. Since the sample time interval for a given set of runs was constant, fact number two implies that the shorter period waves were eliminated from the given portion of the record. From fact number one it is clear that the steepest waves are those which in general have periods such that

$$\tilde{T} \leq \bar{\tilde{T}}$$

hence it is concluded that the steepest wave components are filtered out of the spectrum by the current and those longer than the average pass through the current. The frequency distribution plots of percent occurrence of $H/\tilde{T}^2$ also leads to this conclusion. That is, the range of $H/\tilde{T}^2$ narrows and $H/\tilde{T}^2$ decreases behind the breakwater for increasing breakwater discharge. In viewing these data it should be kept in mind that the wind was still blowing over the water surface so that some new relatively high frequency waves were formed in the lee of the breakwater by this wind. In front of the breakwater just the opposite occurs, the range widens and the average value increases for an increasing breakwater discharge. This filtering action was recently verified in experiments carried out for a two-frequency system of waves that were combined linearly with the higher frequency component (twice the frequency of the lower frequency component) completely filtered out and the lower frequency component getting through undistorted (Williams, 1961). However, this test was a simplification of the actual case, as the steep wind waves have higher harmonics which, in a spectral analysis, would show up as high frequency components as the spectral analyses presumes linear superposition. Thus, some of the higher frequency components shown in Fig. 16 are in reality higher harmonics of lower frequency components.

The fact that a surface current will filter out the shortest (which are th steepest in a wind-wave system, being at a limit of stability) waves while permitting the longer waves to pass may well explain the discrepancy in the reported success of breakwaters utilizing the action of such a current. That is, if the reported degree of effectiveness of the breakwater was

based on visual observation (as it was in several instances, see Laurie, 1955) then the observer would likely be misled by the filtering action of the current, since long waves are not as easily detected by visual observation as the shorter and steeper waves. Hence, in spite of the apparent attenuation of the sea surface, considerable energy may still be transmitted by the longer waves, and it is this energy which may be damped out only at the expense of a disproportionate increase in the energy input to the breakwater. Thus, the difference between the power requirements as based on controlled laboratory experiments and those as observed in prototype action in the fields, as well as the disagreement between the different prototype operations themselves, may be due to inadequate field measurements. It is interesting to note that in the two prototype tests involving the visual observation (Laurie, 1955; Kurihara, 1958) the efficiency of the breakwater was reported as higher than predicted or observed elsewhere (Evans, 1955a, b). In one of the cases (Evans, 1952(b); Laurie, 1955) later measurements using a wave recorder rather than visual observations indicated little effect due to a pneumatic breakwater.

A reason which might account for an actual increase in effectiveness of the prototype breakwater has been suggested by R. C. H. Russell (personal communication, 1962). Because actual spectra of wind waves are two dimensional, some component waves are advancing at angles to the direction of mean wave advance, so that the component wave speed heading into the current is lower for these component waves which would permit a lower current to attenuate them. It is difficult to access this effect as the current would tend to cause the wave components to refract at the same time.

ACKNOWLEDGMENTS

The authors wish to thank Mr. Walter Louscutoff for his help in taking and reducing the data. The work was performed under Contract Nonr-222(46) with the Office of Naval Research.

REFERENCES

Bretschneider, C. L., Wave variability and wave spectra for wind generated gravity waves, U. S. Army, Corps of Engineers, Beach Erosion Board, Tech. Memo. No. 118, 192 pp., August 1959.

Carr, John H., Mobile breakwater studies, Calif. Inst. of Tech., Hydro. Lab., Report No. N-64. 2, 54 pp., Dec. 1950 (unpublished).

Dilley, R. A., Shipboard hydraulic breakwater, Jour. Waterways and Harbors Div., Proc. ASCE, Vol. 84, No. WW2, Paper No. 1569, 21 pp., March 1958.

Evans, J. T., Pneumatic and similar breakwaters, Proc. Roy. Soc., London Series A, Vol. 231, No. 1187, pp. 457-466, 1955(a).

Evans, J. T., Pneumatic and similar breakwaters, The Dock and Harbor Authority, Vol. 36, No. 422, pp. 251-256, Dec. 1955(b).

Green, James L., Pneumatic breakwaters to protect dredges, Jour. Wate ways and Harbors Div., Proc. ASCE, Vol. 87, No. WW2, pp. 67-87, May 1961.

Horikawa, K., Three-dimensional model studies of hydraulic breakwaters Univ. of Calif., IER, Tech. Rept., No. 104-8, 43 pp., Oct. 1958 (unpublished).

Kurihara, M., Pneumatic breakwater III, field tests at Ha-Jima, Proc. Third Conf. on Coastal Eng. in Japan, Nov. 1956, translation by K. Horikawa, Univ. of Calif., IER, Tech. Rept. 104-6, 23 pp., Nov. 1958.

Laurie, A. H., Pneumatic and other breakwaters, A correspondence, The Dock and Harbor Authority, Vol. 36, No. 422, p. 265, Dec. 1955.

Longuet-Higgins, M. S., On the statistical distribution of the heights of sea waves, Jour. Mar. Res., Vol. 11, No. 13, pp. 245-266, Dec. 1952.

Miche, R., Principal statistical criteria characterizing real irregular sea waves and the methods of reproducing these waves in the laborator Revue Générale de l''Hydraulique, No. 69, pp. 115-133, May-June 195

Pierson, W. J., Jr., An interpretation of the observable properties of 'sea' waves in terms of the energy spectrum of the Gaussian record, Trans. Amer. Geophys. Union, Vol. 35, No. 5, pp. 747-757, Oct. 1954.

Putz, R. R., Measurement and analysis of ocean waves, Proc. of the First Conf. on Ships and Waves, Council on Wave Research, The Engineering Foundation, Berkeley, Calif., pp. 63-72, 1954.

Schiff, Leonard I., Air bubble breakwater, Calif. Inst. of Tech., Hydro. Lab., Rept. No. N-64. 1, 8 pp., June 1949 (unpublished).

Schiff, Leonard I., Gravitational waves in a shallow compressible liquid, Calif. Inst. of Tech., Hydro. Lab., Rept. No. N-64, 5 pp., May 1949 (unpublished).

Schijf, J. B., Het vernietigen van golven door bet inspuiten van lucht (pneumatische golfbrekers), De Ingenieur, Vol. 55, pp. 121-125, 1940.

Schijf, J. B., Discussion of pneumatic breakwaters to protect dredgers, Jour. Waterways and Harbors Div., Proc. ASCE, Vol. 87, No. WW4, pp. 127-136, Nov. 1961.

Snyder, C. M., Model study of a hydraulic breakwater over a reef, Jour. Waterways and Harbors Div., Proc. ASCE, Vol. 85, No. WW1, Paper No. 1979, pp. 41-68, March 1959.

Taylor, Sir Geoffrey, The action of a surface current used as a breakwater, Proc. Roy. Soc. (London), Ser. A, Vol. 231, No. 1187, pp. 466-478, Sept. 1955.

U. S. District Court, Northern District of California, Case at Law No. 16879, 16 April 1923.

Wiegel, R. L., Wind waves and swell, Proc. Seventh Conf. on Coastal Eng., Council on Wave Research, The Engineering Foundation, Berkel Calif., pp. 1-40, 1961.

Williams, John A., Small amplitude water waves and their superposition, Report for C. E. 299, Univ. of Calif., Berkeley, Calif., Dept. of Civil Engineering, 1961 (unpublished).

Williams, J. A., Verification for the Froude modeling law for hydraulic breakwater, Univ. of Calif., IER, Tech. Rept. 104-11, 43 pp., Aug. 1960 (unpublished).

CHAPTER 30

WINTER REGIME OF A TIDAL INLET IN THE ARCTIC AND THE USE OF AIR BUBBLES FOR THE PROTECTION OF WHARF STRUCTURES

Simon Ince

Hydraulics Laboratory, National Research Council
Canada

INTRODUCTION

Shipping in the Canadian Arctic is limited to about 2½ months in summer. During this short period all communities have to be supplied with sufficient provisions and fuel to last the long winters. The Department of Public Works of Canada has built wharves and docking facilities in various Arctic centres to speed up the unloading operations. Many of the conventional pile structures have been destroyed by the 6 ft. thick ice laye which grips the piles and moves them up and down in response tc the tide. To prevent this, an air bubbler system was installed three years ago at Tuktoyaktuk, N.W.T. to inhibit the formation of ice around the wharf. This unit has been operating successfully since that time and no further damage has been reported. This first success inspired the installation of a second unit at Cambridge Bay, N.W.T. where similar difficulties were being encountered. The air bubbler system at Cambridge Bay did not fulfill its promise and the wharf was damaged. This had been predicted, but the success at Tuktoyaktuk - despite the suspected influence of the Mackenzie River - was a mystery. In April 1961 the author investigated the bubbler system and its oceanographic environment at Cambridge Bay, and in April 1962 those in Tuktoyaktuk. The results of these surveys are reporte in the following paragraphs.

AIR BUBBLER SYSTEMS

Air bubblers have been extensively used in lakes - in most cases successfully - to prevent the formation of ice or melt the existing ice cover. There is a voluminous literature on the subject; the essential hydrodynamic and thermodynamic features have been summed up by Baines (1961), Bulson (1961) and Williams (1961). Pounder (1961) has analysed the thermodynamic aspects in sea water.

According to Baines, when an air jet is discharged from an orifice under water a heterogeneous mixture of bubbles rises at rates varying with size in a cone with a total include angle of 12 degrees. Viscosity and lateral turbulent fluctuations induce a vertical water current with maximum velocity ove the air source and decreasing along an s-curve outward. Upon reaching the water surface, the momentum of the water jet is

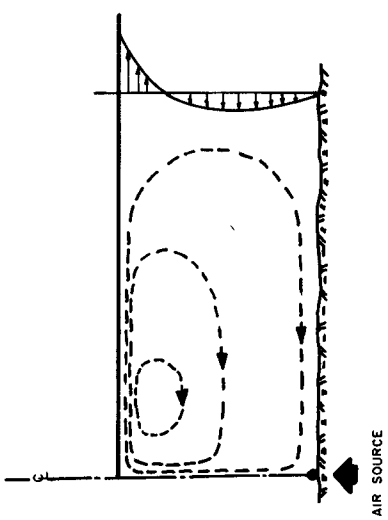

Fig. 1. Circulation pattern and velocity profile (after Baines).

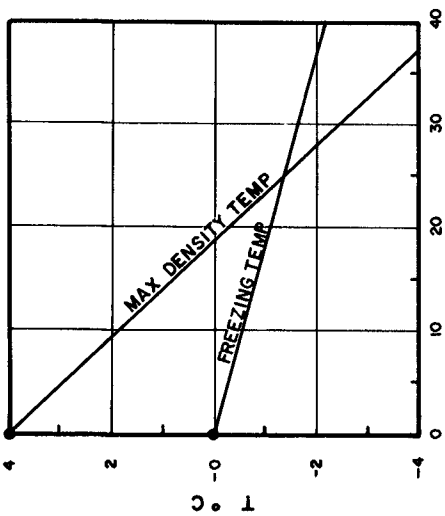

Fig. 3. Maximum density and freezing temperatures as a function of salinity.

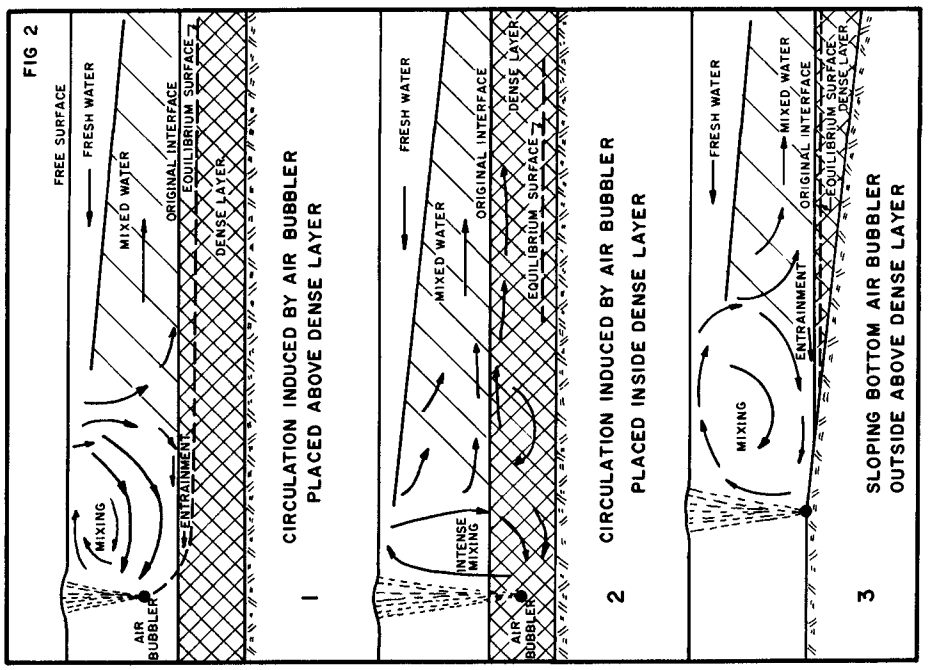

Fig. 2. Circulation in stratified liquids.

converted into a horizontal surface jet. This jet has the characteristics of free turbulence; kinetic energy is obtained entirely from the vertical jet and hence decreases in the direction of flow. The vertical and surface jets consist entirely of water which has entered the jet from the side as entrainment. The large scale circulation induced by the air bubbles is a ring vortex (Fig. 1).

The circulation pattern shown by Baines applies to homogeneous fluids. In stratified fluids the initial stages of the circulation are quite different. Fig. 2 shows the results of experiments made in a narrow flume at the Hydraulics Laboratory of the National Research Council. Although the investigation was of an exploratory nature, it showed clearly the mechanism by which the denser liquid was mixed with the overlying lighter water. The most noteworthy fact was the relatively rapid establishment of a near equilibrium interface, after which entrainment progressed at a very slow rate.

Whether Fig. 1 or Fig. 2 is taken as the starting point, it is clear that if the water has some thermal reserve within the range of action of the bubbler, heat will be brought to the open surface or transferred to the ice sheet. If the water is well mixed and the temperature uniform and close to the freezing point - a case frequently encountered in fast flowing rivers - no heat will be available on the surface.

Instances are reported, however, where an air bubbler has kept an ice-free surface despite the lack of any thermal reserve in the water. This is entirely possible if the air bubbler has been installed before freeze-up. The agitation on the surface prevents the formation of a solid ice cover; instead, tiny discs of frazil ice are formed which are carried away by the induced current to be deposited at the underside of the surrounding ice sheet. Each gram of water releases upon freezing its latent heat which compensates for the losses to the atmosphere.

FREEZING CHARACTERISTICS OF SEA WATER

In Fig. 3 are shown the freezing and maximum density temperatures of water as a function of salinity. With increasing salinity the temperature of maximum density decreases more rapidly than that of the freezing. At a salinity of 24.70 p.p.t. both temperatures are -1.33°C. From these characteristics it is seen that up to a salinity of 24.70 p.p.t. a layer of sea water of uniform salinity has the freezing characteristics of a lake. Cooling will increase the density of the surface water, and a vertical convection will develop until the whole layer reaches the temperature of maximum density. From this point on only the surface will be cooled until ice begins to form. There will then be a positive temperature gradient between the surface and bott

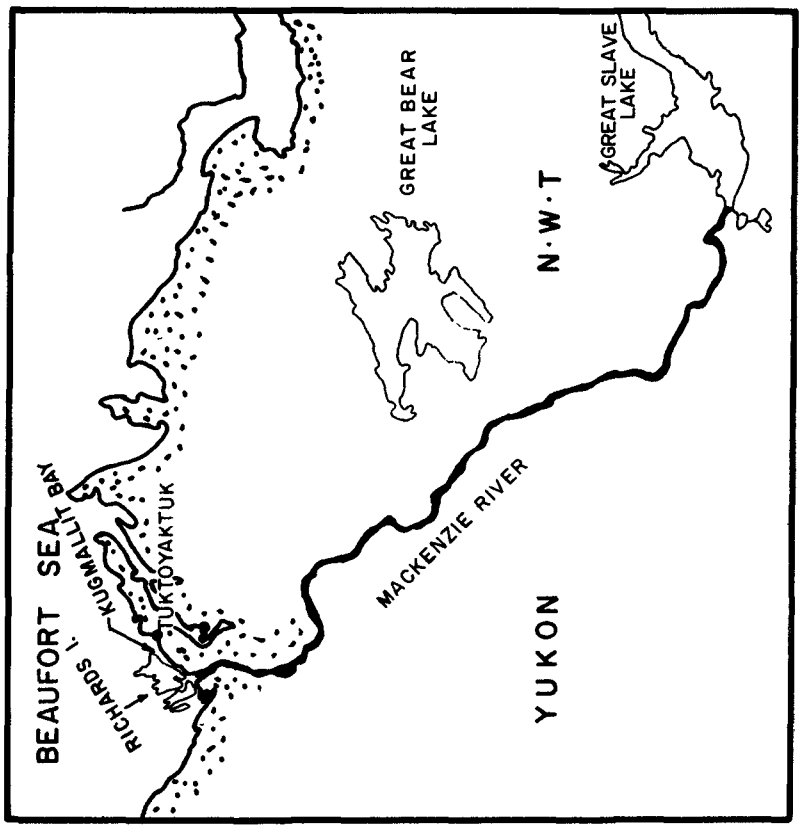

Fig. 5. Mackenzie River and Tuktoyaktuk.

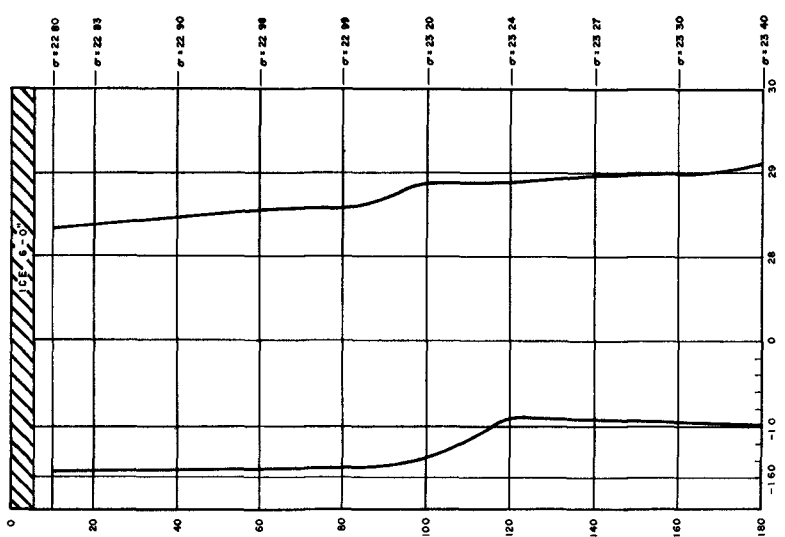

Fig. 4. Temperature and salinity structure at Cambridge Bay.

of the layer. Here the analogy to a lake structure ends. Durir the freezing of sea water, the salt is expelled from the ice cry tals and collects in small pockets of brine. This process continues until the brine becomes more and more concentrated and leaches out. Thus the water below the ice surface increases in salinity, and hence density, and the convection continues until all the salt is leached out. If the salinity is greater than 24.70 p.p.t. the freezing point is reached before the temperatu of maximum density and the layer is isothermal at the freezing temperature corresponding to the salinity.

Thus, depending upon the oceanographic conditions, a layer of warmer water may or may not be present. The success o the air bubbler will depend on the size of the heat reservoir a its efficient utilization. In sea water, in addition to the temperature, the influence of the salinity must be taken into account. In a stratified system, mixing will increase the sali of the upper layers and make available more energy.

INVESTIGATION OF FIELD INSTALLATIONS

It is evident that the success of any air bubbler unit depends upon the oceanographic conditions existing not only in immediate vicinity of the installation, but in the system of co necting waters. To evaluate properly and quantitatively the op tion of air bubblers systematic and detailed measurements of currents, salinity, temperature, ice growth, and meteorological factors is necessary. The surveys made at Cambridge Bay and Tuktoyaktuk were of an exploratory nature; nevertheless, they were extremely useful in confirming in broad lines the prognostications based on theory.

CAMBRIDGE BAY

Not much is known about the general oceanographic features at Cambridge Bay. Fig. 4 shows the temperature and salinity structure found in the bay. This is representative fo the region within a 2 mile radius of the air bubbler. It is on necessary to cut the curves at the appropriate depth to get the structure of the water at any point of lesser depth than shown the figure. The air bubblers were installed in 20 ft. of water on a shelf very gradually increasing in depth to 45 ft. and the dropping abruptly. It is obvious from the figure that within t zone of influence of the bubbler the temperature is nearly constant at the freezing temperature $T = -1.52°C$ of water at $S = 28.4$ p.p.t. Hence it is not surprising that the installati was not effective in maintaining an open water belt around the wharf.

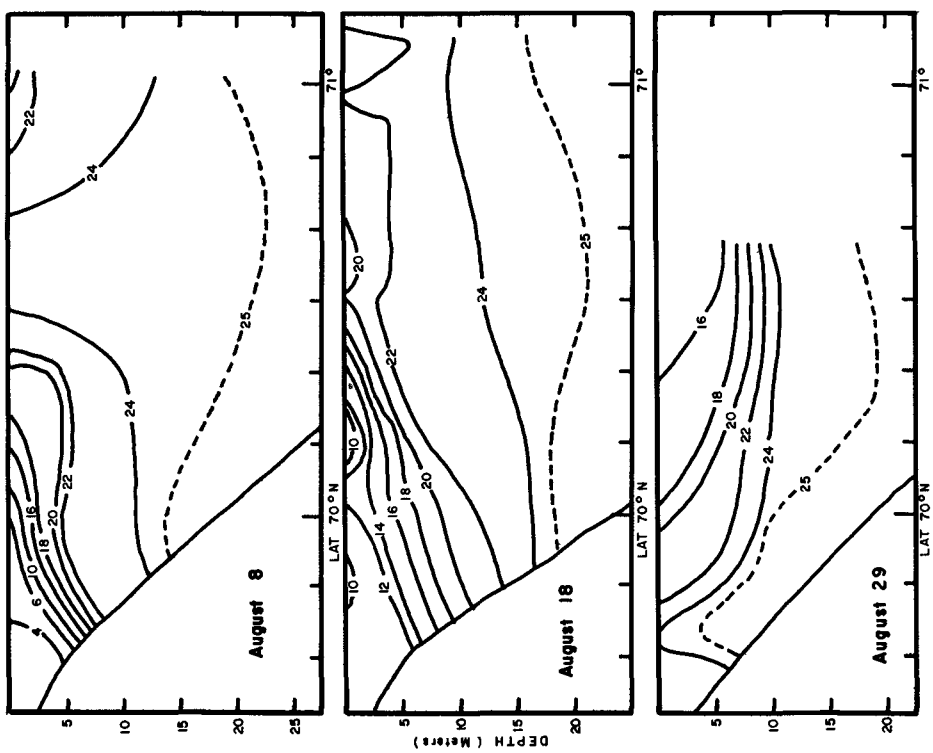

Fig. 8. σ_t sections northward from Kugmallit Bay illustrating extensive upwelling with easterly

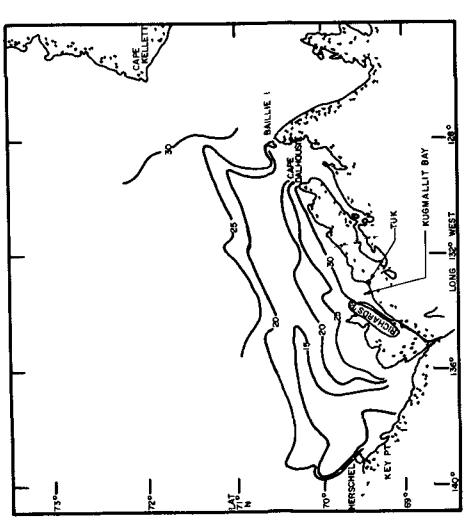

Fig. 6. Surface salinity (p.p.t.). Beaufort Sea, 1952 under conditions of easterly winds. (I.O.U.B.C. Report)

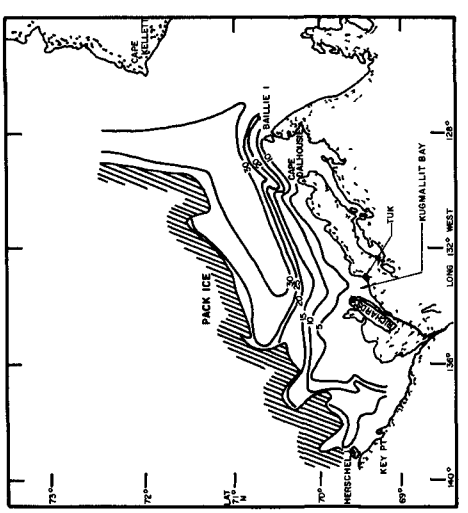

Fig. 7. Surface salinity (p.p.t.). Beaufort Sea. 1952 under conditions of west-

WINTER REGIME OF A TIDAL INLET IN THE ARCTIC AND THE USE OF AIR BUBBLES FOR THE PROTECTION OF WHARF STRUCTURES

TUKTOYAKTUK

In the summer of 1952 the Institute of Oceanography of the University of British Columbia made hydrographic and oceanographic observations in the Beaufort Sea and in Kugmallit Bay, which shed a great deal of light on the estuarine dynamics of this area (Fig. 5). The following observations are taken from the report of Dr. W.M. Cameron, senior scientist on this expedi

"The principal oceanographic features of the south-eastern Beaufort Sea are established by the interaction of rive discharge and wind.

In the absence of wind the river water reacts to the influence of the Coriolis force and hugs the right-hand mainlan boundary, moving eastward along the coast. Salt water is contr buted by a southeasterly flow past Herschel Island. Mixing is relatively slow because of the high stability of the water colu and the absence of strong tidal currents. A significant propor tion of the river water moves into Amundsen Gulf mixing with oceanic water and flowing westward past Cape Kellett. Westerly winds accentuate the magnitude of the circulation.

Easterly winds of force 5 or more are sufficient to reverse the circulation. The river water moves offshore to the north and west. A compensating shoreward movement of saline wa is set up in the deeper levels and a westward circulation is established along the mainland coast.

Local vertical density gradients are altered drastical by wind. The study in the Beaufort Sea indicates that reductio in the stability of a vertical column is not due primarily to vertical mixing, but rather to horizontal advection of water layers of different density. The direction of the wind is an important feature in coastal waters of this type. The areas of Herschel Island and northeast of Richards Island increase or decrease in vertical stability not in reaction to the speed of the wind but instead to its direction."

The situations described by Cameron are graphically demonstrated in Fig. 6, 7, 8 which are reproduced from the same report. The U.B.C. expedition did not investigate conditions i Tuktoyaktuk harbour (Fig. 9). but it is obvious that it will react to situations in Kugmallit Bay. This was confirmed by th local residents, Eskimo and Caucasian; and in particular, by Father Lemeur who has widely travelled in this region. Kugmall Bay opens up in July, but ice floes still exist on the Beaufort Sea (Fig. 7). During calm periods, Mackenzie River water can b seen, due to its muddy colour, as far out as Baillie Point and Herschel Island. Due to mixing by wind and waves this surface water is brackish. With easterly winds the water in the inlet becomes more saline, cold, and clear, indicating inflow from th Beaufort Sea. With westerly winds, the water in Tuktoyaktuk

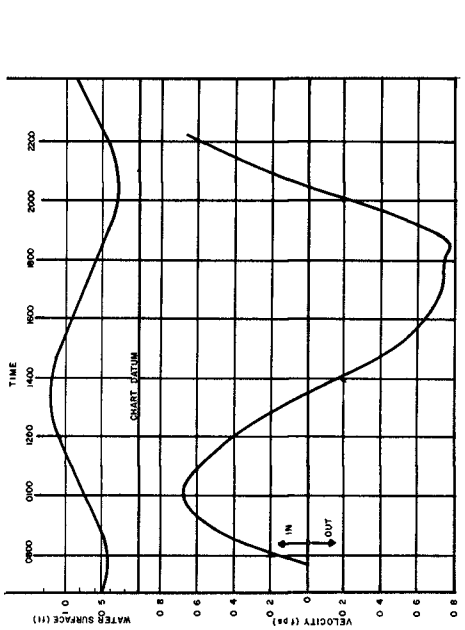

Fig. 10. Typical tide curve in Tuktoyaktuk Harbour and mean velocities at East Entrance (April 30, 1962).

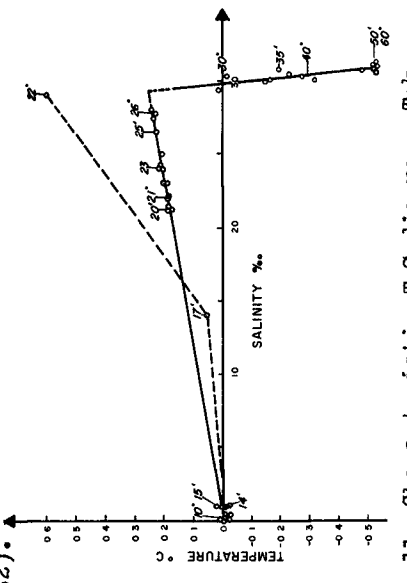

Fig. 11. Characteristic T-S diagram, Tuktoyaktuk.

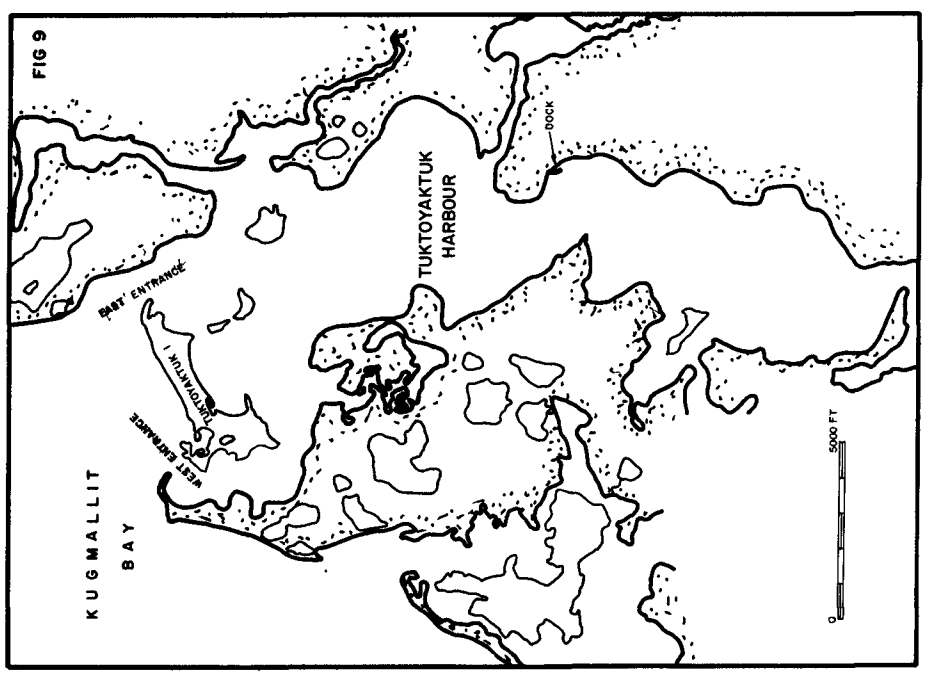

Fig. 9. Tuktoyaktuk Harbour.

Harbour is brownish, brackish and warm, indicating inflow of Mackenzie River water. Perhaps the most characteristic feature of the area - confirmed by the Canadian Hydrographic Service - is the high set-up produced by North-westerly winds, raising the water in the harbour as much as 4 ft. above mean sea level. With south-easterly winds the water level falls as low as 3 ft. below mean sea level. The higher tide range is about 1.5 ft., while the average tide range is 1.1 ft. The flow of the Mackenzie River has not been accurately gauged, but Water Resources Branch of Canada estimate that the flood discharge may be in the order of 400,000 c.f.s.

Once the ice cover has formed the wind ceases to have a predominant effect on the dynamics of the inlet. The water in Kugmallit Bay, where the depth does not exceed 18 ft., is practically fresh Mackenzie water.

Winter Regime of Tuktoyaktuk Harbour - It is clear that the winter regime of the inlet will be dominated by the oceanographic conditions prevalent during freeze-up, modified gradually by the tide.

Tuktoyaktuk Harbour is connected to Kugmallit Bay by the East and the West Entrances. The West Entrance is very narrow and shallow and the tidal flow through it is only 12% of the total. The main tidal flow is through the East Entrance, which is the navigation channel. A typical tide curve for the harbour and mean velocity curve through the East Entrance are shown in Fig. 10. The characteristic T-S diagram for the inlet and temperature and salinity profiles are shown in Fig. 11 and 12 in solid line. Although the depth within the harbour varies, it is only necessary to cut Fig. 12 at the desired depth to get the salinity and temperature structure at any point. This remarkable stratification extends practically unaltered 15 miles into Kugmallit Bay. Since this bay is very shallow (15-18 ft.) the water here has very low salinity (0.3-0.5 p.p.t.). The ice cover protects this structure from the mixing effect of the wind. Temperature and salinity measurements at the East Entrance over a tide cycle indicated that the tidal flow consists only of this top layer of fresh Mackenzie River water, except for entrainment at the interface.

The wharf and air bubbler installation are shown in Fig. 13. A cross-section of the inlet opposite the wharf is shown in Fig. 14. This is remarkably similar to the stylized scheme 3 of Fig. 2. Although no quantitative statements can be made at this time, it is clear that the air bubbler line on the side facing the harbour will entrain more saline and warmer water and be effective in preventing the formation of ice or in melting the existing ice. In April the open water was 3 ft. wide. The airline facing the shore was not nearly as effective.

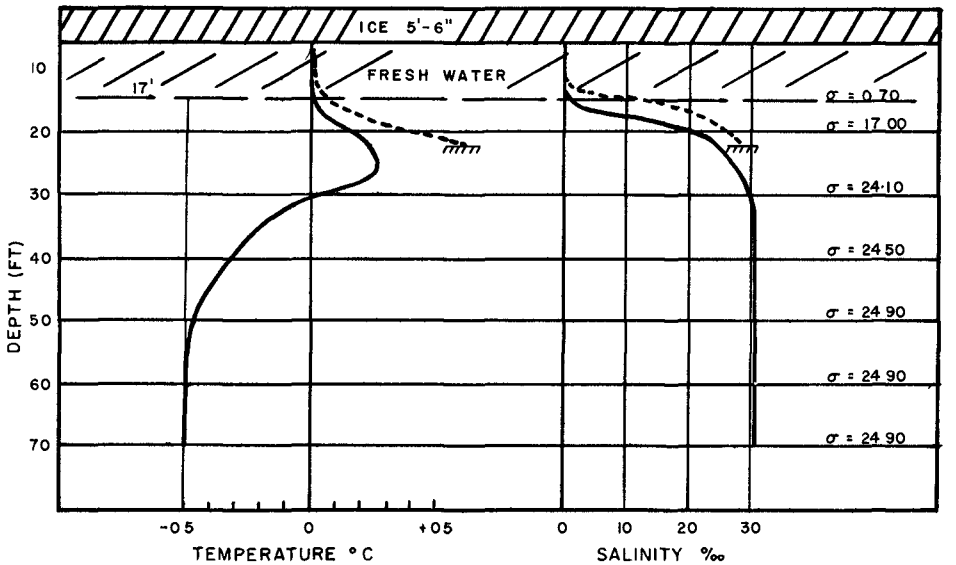

Fig. 12. Characteristic temperature and salinity structure at Tuktoyaktuk.

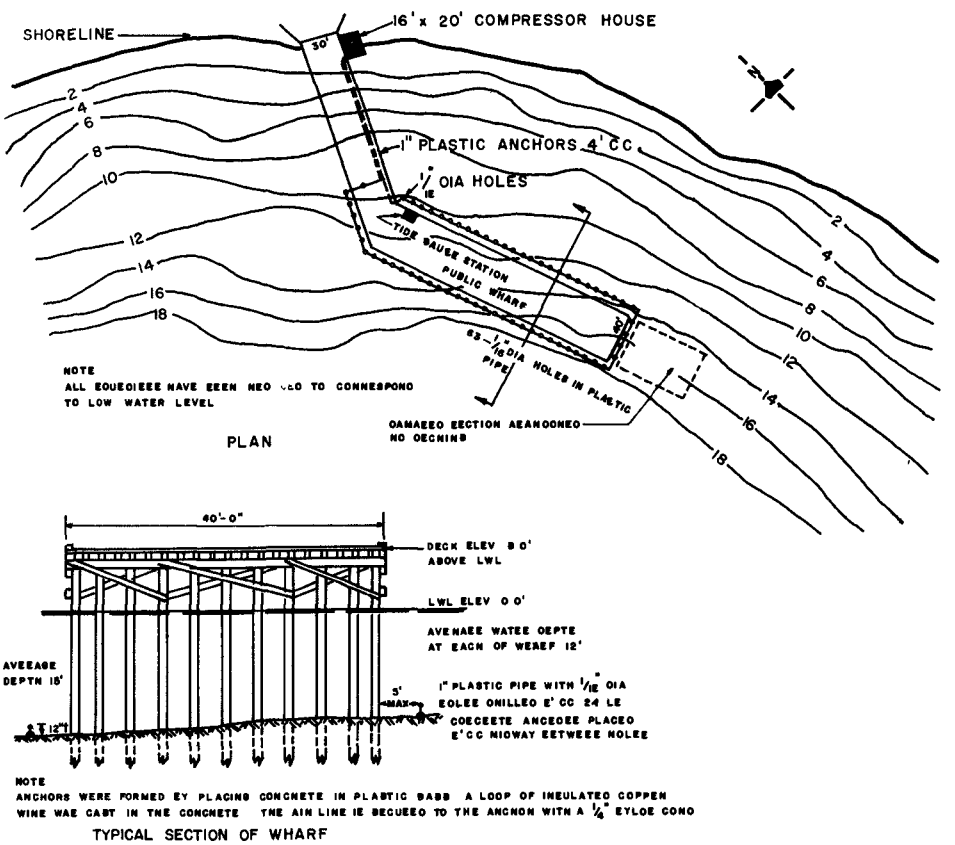

Fig. 13. Wharf and air bubbler system.

The advection of saline and warmer water could not be unequivocally measured. Under conditions observed in April, there appears to be a delicate balance between heat losses and energy supply. It is hard to imagine that during the severe Arctic winter, when temperatures fall to 40 below zero, there is sufficient heat supplied to keep the water open. The operation of the air bubbler under these conditions may consist partly of the mechanical action of preventing the formation of an ice cover, and supplying additional heat by producing frazil ice. In fact, a rough cross-section of the ice cover near the bubbler (Fig. 14) indicates frazil ice deposition. On the othe hand, the technician in charge reported that several times duri the winter, the compressors had been deliberately or accidental shot down and each time a 6-12" layer of ice had been formed ov the air bubbler. When the compressors were turned on again, th ice disappeared within a short time, indicating supply of heat appreciable quantities. This could happen if the original inte face between fresh and salt water had been higher so that the a bubbler was submerged along its entire length in the dense laye and the operation was similar to scheme 2 of Fig. 2. In Fig. 1 and 12 are plotted the salinity and temperature at an isolated depression with a sill of 17 ft. inside the inlet. Below 17 ft the water is warmer and more saline. This may have been the structure in the harbour at freeze-up time and may have changed gradually to the conditions observed in April.

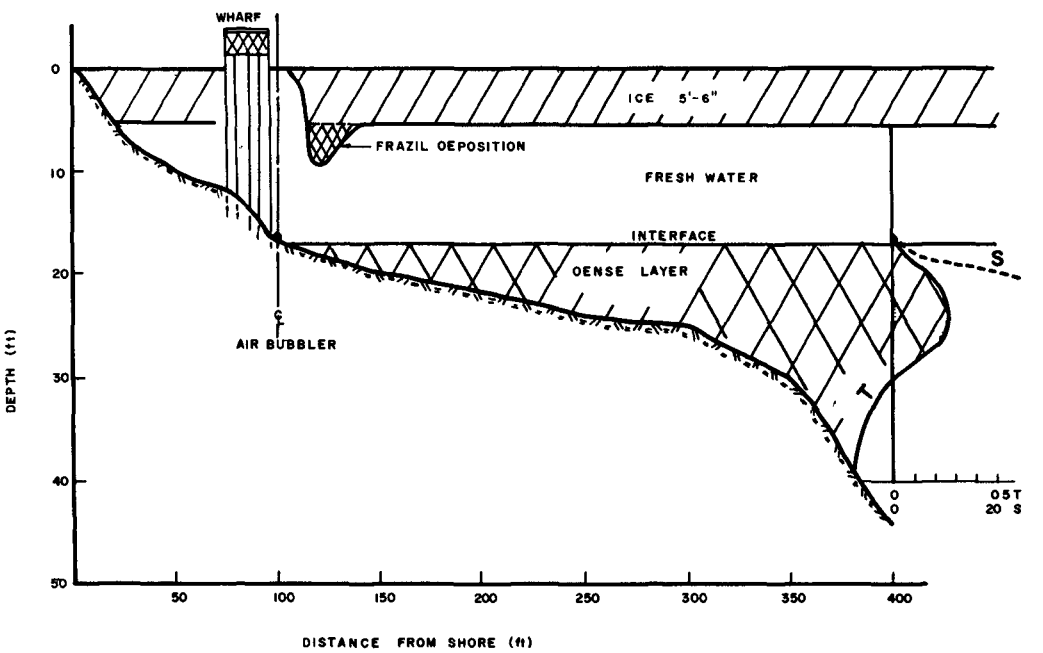

Fig. 14. Cross-section of inlet near wharf.

CONCLUSIONS

More questions have been raised than answered. This was intentional; the author himself does not know the answers. It is planned to study the estuarine dynamics and the energy budget of the Tuktoyaktuk area in greater detail.

REFERENCES

Baines, W.D. (1961). The principles of operation of bubbling systems: Proceedings of the Symposium on Air Bubbling, National Research Council, Canada, pp. 12-22.

Bulson, P.S. (1961). Currents produced by an air curtain in deep water: The Dock and Harbour Authority, May 1961, pp.

Williams, G.P. (1961). Thermal regime of lakes and rivers wit reference to air bubbling systems: Proceedings of the Symp on Air Bubbling, National Research Council, Canada, pp. 1-

Pounder, E.R. (1961). Thermodynamic considerations on the use air bubbling systems in salt water: Proceedings of the Sym posium on Air Bubbling, National Research Council, Canada, pp. 41-46.

ACKNOWLEDGEMENTS

The Department of Northern Affairs and National Resources has arranged and facilitated the stay in Tuktoyaktuk and Cambridge Bay. The Department of Public Works has supplie equipment, plans of the installations and facilitated the inspection. The Marine Sciences Branch of the Department of Min and Technical Surveys has supplied oceanographic equipment and processed the salinity samples. The author is particularly indebted to Mr. F. Barber of the Oceanographic Research Group for his constant advice and assistance.

GUAYMAS

PART 4
COASTAL ENGINEERING PROBLEMS

VERA CRUZ

CHAPTER 31

DEEP WATER WAVES GENERATED BY HURRICANE "AUDREY" OF 1957

Basil W. Wilson

Senior Staff, National Engineering Science Company
Pasadena, California

ABSTRACT

A post-mortem analysis of Hurricane Audrey of June 24-27, 1957, in the Gulf of Mexico, is described using all available ship reports and weather data from USA and Mexican sources. A detailed meteorological analysis defines the changing surface pressure and wind systems at 3-hour intervals, from which the space-time wind-fields have been derived for selected paths of wave generation bearing on the Louisiana coastline. A numerical technique of moving-fetch wave-prediction has been used to determine the characteristics of the waves in deep water that would have been prevalent in various parts of the Gulf of Mexico during passage of the hurricane. For two deep water locations in particular the effects of multi-directional wave generation are considered.

1. INTRODUCTION

Hurricane "Audrey" of June 24-27, 1957, will long be remembered as a vicious killer-storm which brought stark tragedy and destruction to the Louisiana-Texas coast and to the town of Cameron, Louisiana, in particular. Coming hard on the heels of the disastrous series of hurricanes of 1954, 1955 and 1956, which devastated the eastern seaboard of the United States, it spurred the research then already beginning through the organization of the National Hurricane Research Project in 1956. On this account the features and effects of hurricane Audrey were particularly well documented [Weather Bureau, 1958] and made this storm a natural choice early in 1959 for a wave study designed to examine what was then still a relatively new and unproved procedure in wave forecasting [Wilson, 1955(i), (ii), (iii)].

The essence of this procedure is that it removes completely any subjectivity in the definition of fetch and duration over which waves are under wind domination; it caters for the moving storm and for variable winds within the storm, and though its limitation in the first instance is uni-directional, it may be shown that it is capable of yielding the multi-directional effects of wave generation and, ultimately, precise information on the spectral composition of the sea at any point in space and time [Wilson, 1962].

The original graphical technique [Wilson, 1955] has been adapted to a numerical process [Wilson, 1961] permitting extremely rapid calculation of large amounts of input wind data by means of high speed computers. What is described herein are essentially the results of deep water wave predictions made in respect of hurricane Audrey on a modern No. 709 IBM (International Business Machines) electronic computer. As the technique itself has been fully described already [Wilson, 1961], no attempt will be made here to retrace the arguments upon which it is based; suffice it to say that the method depends on empirical relationships governing the observed properties of waves generated by uniform winds blowing steadily, without cessation, over finite fetches of deep water.

2. THE WEATHER STRUCTURE OF HURRICANE AUDREY

To secure the greatest amount of available data for determining the surface wind structure of hurricane Audrey during its lifetime over water, recourse was had to the assembled data of the National Weather Records Center [Weather Bureau, 1958], together with data kindly supplied by the Instituto de Meteorologia Nautica [Servicio Meteorologico Mexico 1959]. Valuable data were also secured from A. H. Glenn [1959] in the form of weather maps, pressure and wind information and a report to the offshore oil industry [Lindblom, 1957], which was essentially a rapid analysis of the storm and its effects in coastal waters. A partial analysis was also available in an unpublished report of the Weather Bureau [Hudson, 1957] and other useful information was found in descriptions of the hurricane given in the Monthly Weather Review [Ross and Blum, 1957; Moore, et al, 1957], and elsewhere [Sartrain, 1957; Corps of Engineers, 1957; Visser, 1957; Cross, 1957; Zumwalt, 1958; Harris, 1958; Skjelbreia, 1958]. In addition, a limited amount of actual wind data in the form of visual readings and automatic traces of anemometers at coastal stations and offshore drilling digs was obtained from offshore oil and mining industry sources [Freeport Sulphur Co., 1959; Kerr-McGee Oil Industries, Inc., 1959].

All these data were carefully screened and integrated into the series of synoptic maps of surface pressure (Figs. 1 to 5) and surface wind velocity (Figs. 7 to 11) over the Gulf of Mexico. These maps, however, are almost entirely complete re-analyses of the weather situation, elaborated rather painstakingly from ship and land station reports and

adjusted for consistency by close attention to trends of change at the 3-hour intervals for which, in the main, they are compiled.

An early difficulty was non-agreement of the locations of the eye of the hurricane at the different times, as given by the Weather Bureau [Hudson, 1957], by A. H. Glenn [Lindblom, 1957], by Visser [1957] and by Skjelbreia [1958]. The Weather Bureau track was ultimately judged to be the most accurate and fitted best with the pressure patterns evolved from ship reports. This essentially is the track shown in Figs. 1 to 5; 7 to 11, though it bears slightly more to the east at its coastal crossing than that of the Weather Bureau.

Inspection of Fig. 1(a) shows that hurricane Audrey had formed with a weak pressure center in the Gulf of Campeche at 0300 CST on June 24, 1957. An easterly storm front is there revealed crossing the west end of the Yucatan peninsula. By 1200 CST of the same day (Fig. 1b) the low pressure centers had apparently coalesced like two amoebae and the pressure pattern distorted by the impending dissipation of the front. The gain in strength of the hurricane, moving slowly at first, can be noticed by the expanding diameter of the 1010 mb. contour and by the successive expansions of the 1005 and 1000 mb. rings in Figs. 1 to 5.

As far as can be judged the hurricane moved erratically along its path at speeds of progression which fluctuated considerably, as shown in Fig. 6. These speeds were evaluated from a distance-time plot of the storm's forward advance and are probably reasonably accurate. The mean forward speed was about 13 knots.

Figs. 1 to 5 do not attempt to record central pressures at 1 mb intervals below about 1000 mb because of the density of the concentric isobars near the storm center. As the hurricane approached the Louisiana Coast (Fig. 5), pressures near the center were somewhat better defined by the increasing number of observations, permitting reasonable identification of pressure levels to as low as 980 mb, (Fig. 5d). For purposes of computing surface wind velocities near the hurricane center during transit over water it was necessary, however, to determine the probable central pressures p_o and radii R to zones of maximum wind velocity. Values of central pressure over the ocean shown in Fig. 6(a) are based largely on Weather Bureau (Naval) aerial reconnaissance advisories as issued by Glenn [Lindstrom, 1957] and on the fortunate fact that at least two ships were caught in the eye of the hurricane and recorded central conditions. The trend of fall of pressure, shown in Fig. 5(a), from about 1008 mb to the 971 mb level at the time of the hurricane's crossing of the Louisiana coastline was established also from extrapolations of the pressure profile of the synoptic maps of Figs. 1, 2 and 5. There is some descrepancy between the lowest pressure of 971 mb found collectively in this way and the much lower pressures of 958 mb and 967 mb apparently recorded respectively at Hackberry, La. (2 miles from the storm track) and at Port Ar-

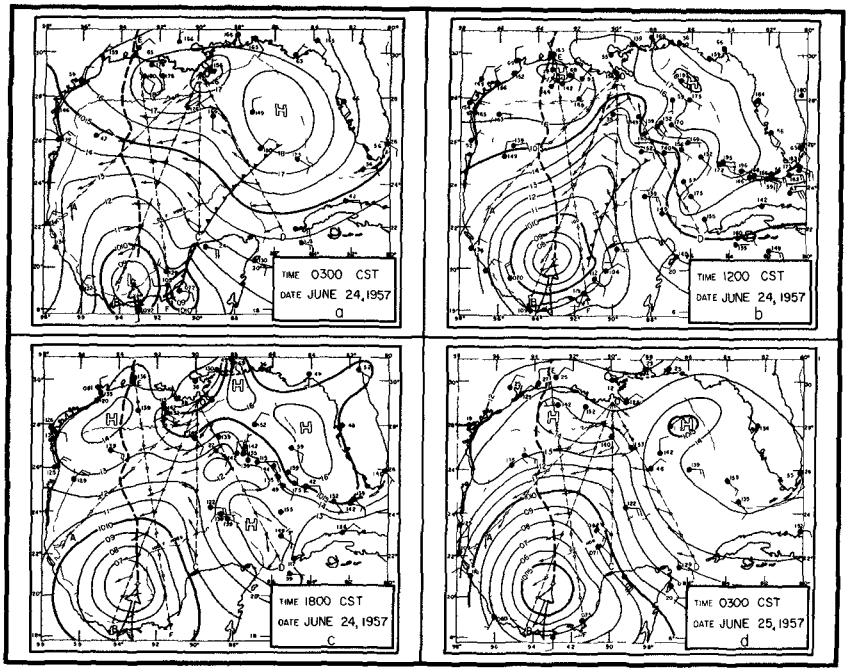

Fig. 1. Synoptic surface pressure patterns (mbs) for the Gulf of Mexico, 0300 CST, June 24, to 0300 CST, June 25, 1957.

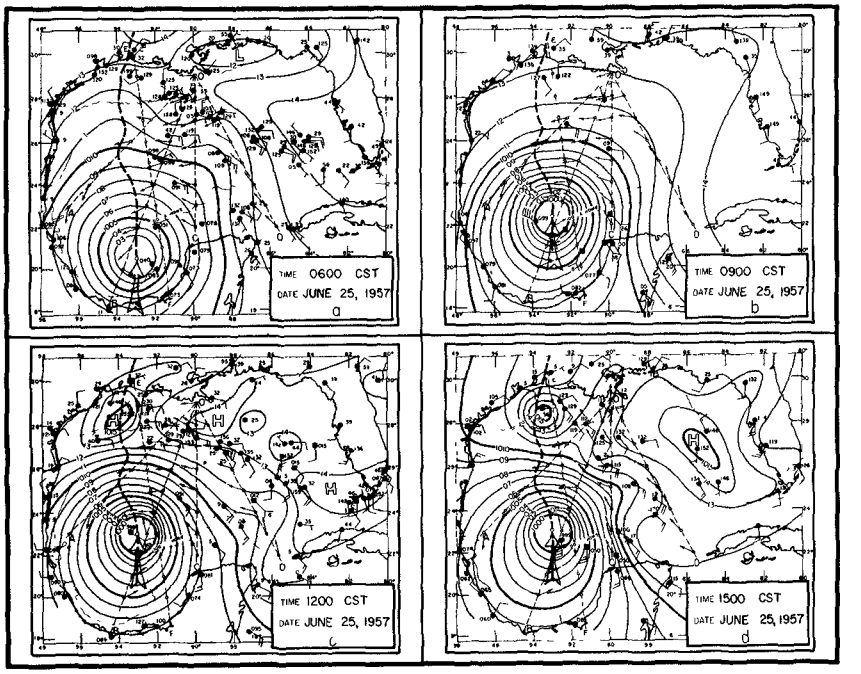

Fig. 2. Synoptic surface pressure patterns (mbs) for the Gulf of Mexico, 0600 - 1500 CST, June 25, 1957.

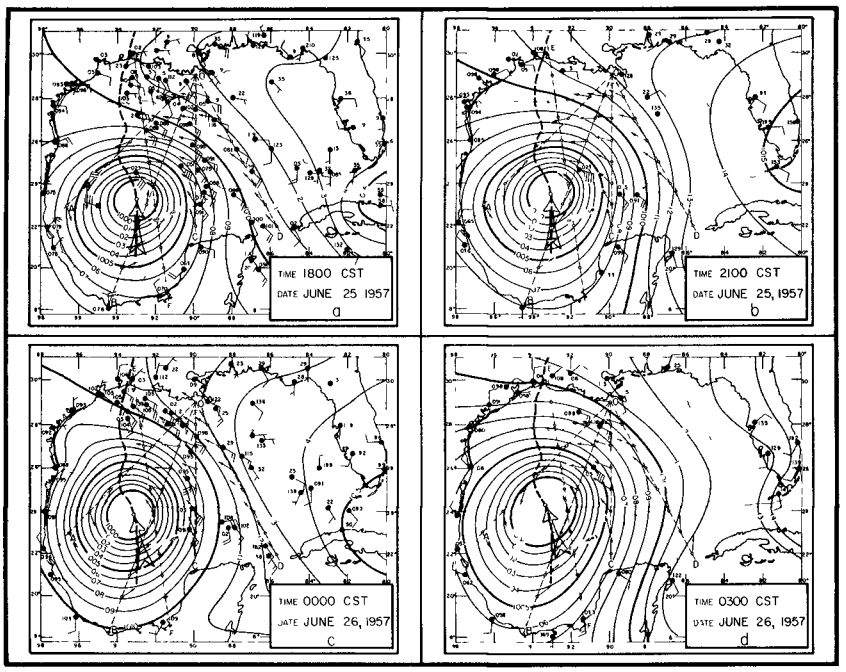

Fig. 3. Synoptic surface pressure patterns (mbs) for the Gulf of Mexico, 1800 CST, June 25, to 0300 CST, June 26, 1957.

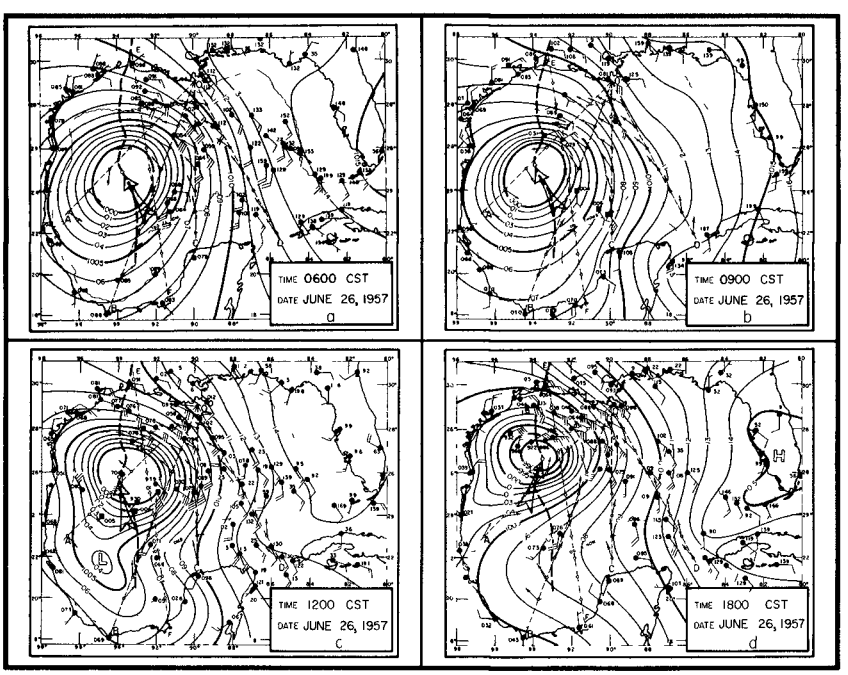

Fig. 4. Synoptic surface pressure patterns (mbs) for the Gulf of Mexico, 0600 - 1800 CST, June 26, 1957.

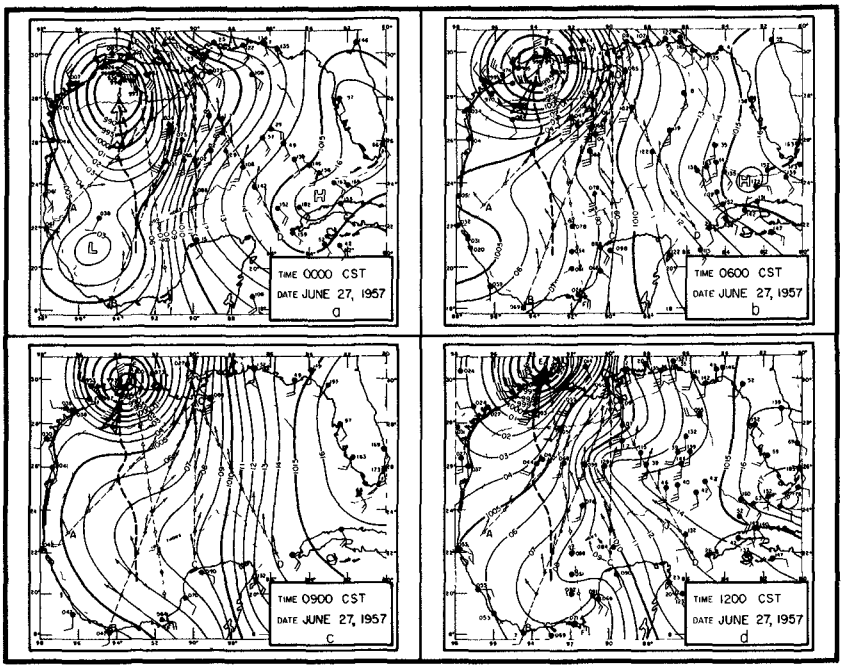

Fig. 5. Synoptic surface pressure patterns (mbs) for the Gulf of Mexico, 0000 - 1200 CST, June 27, 1957.

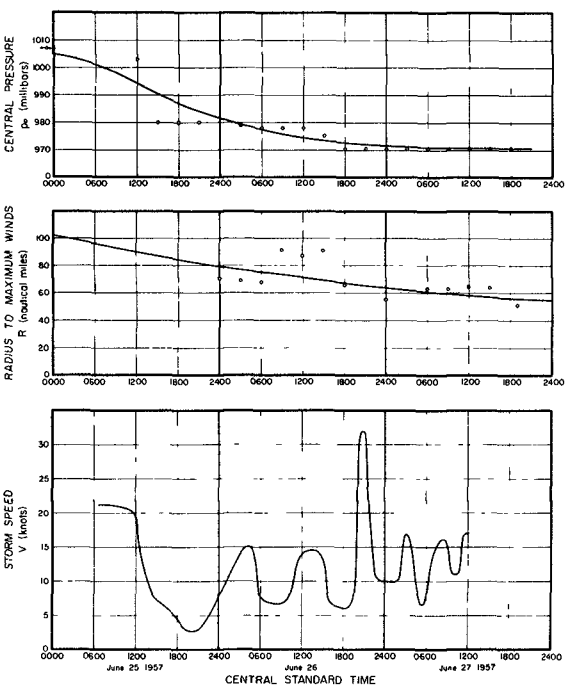

Fig. 6. Intensity, size and speed characteristics of hurricane Audrey (a) central pressure, p_o; (b) radius to maximum winds, R, (c) speed of advance.

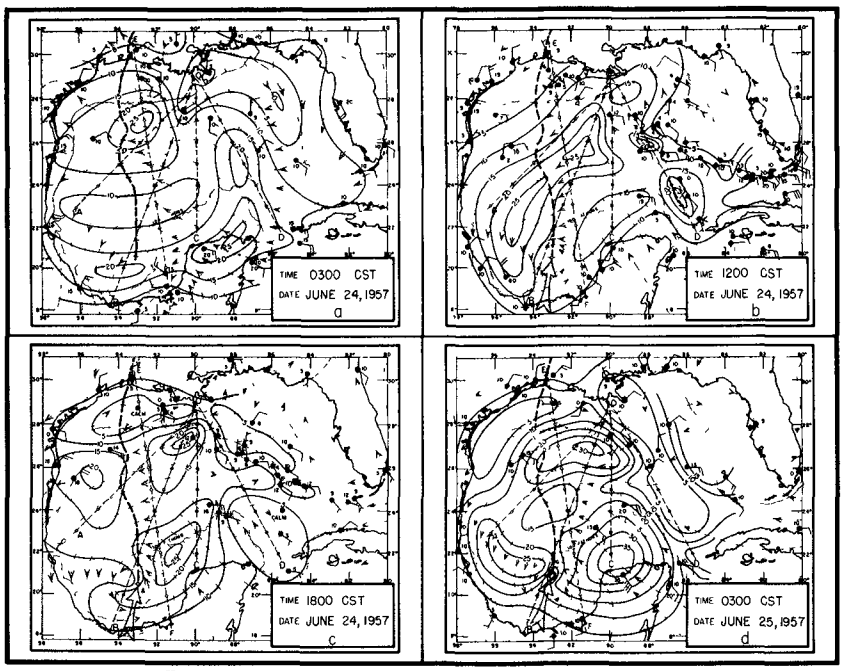

Fig. 7. Synoptic surface wind velocity (knots) and circulation patterns for the Gulf of Mexico, 0300 CST, June 24, to 0300 CST, June 25, 1957.

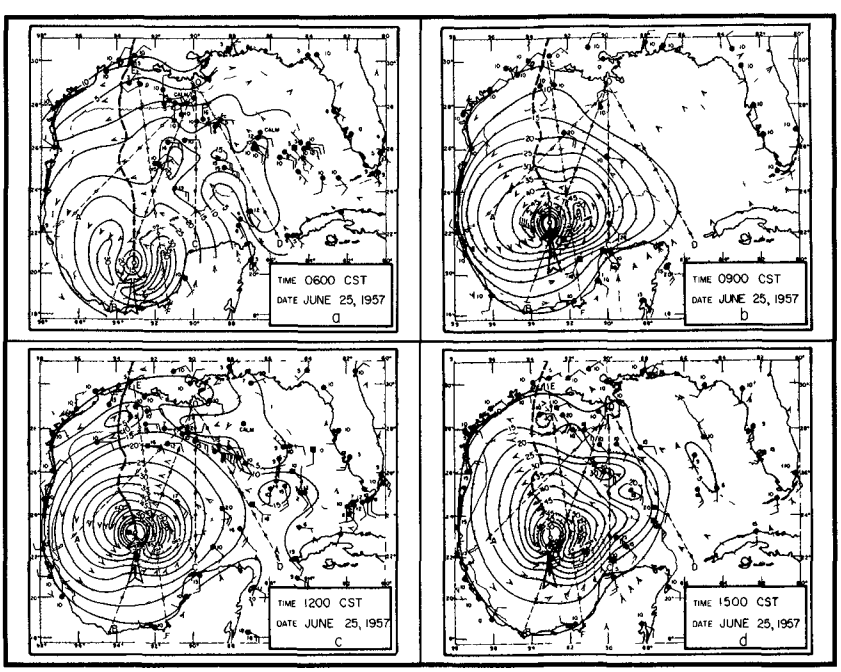

Fig. 8. Synoptic surface wind velocity (knots) and circulation patterns for the Gulf of Mexico, 0600 - 1500 CST, June 25, 1957.

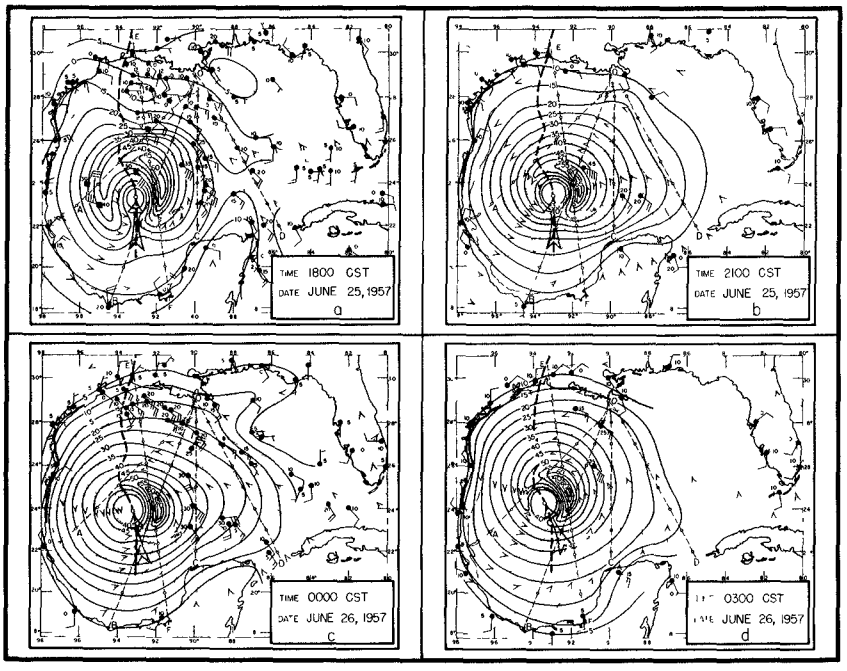

Fig. 9. Synoptic surface wind velocity (knots) and circulation patterns for the Gulf of Mexico, 1800 CST, June 25, to 0300 CST, June 26, 1957.

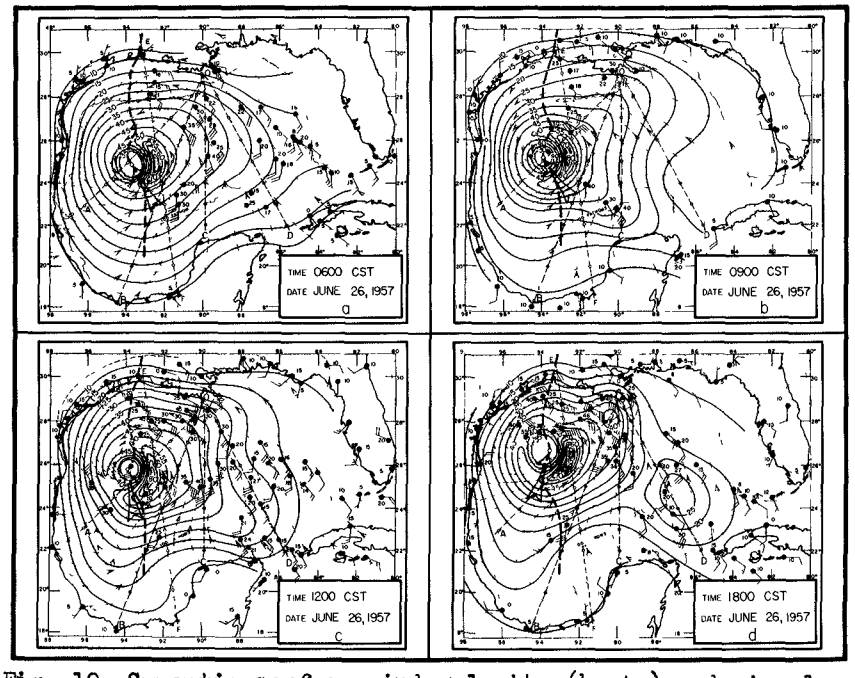

Fig. 10. Synoptic surface wind velocity (knots) and circulation patterns for the Gulf of Mexico, 0600 - 1800 CST, June 26, 1957.

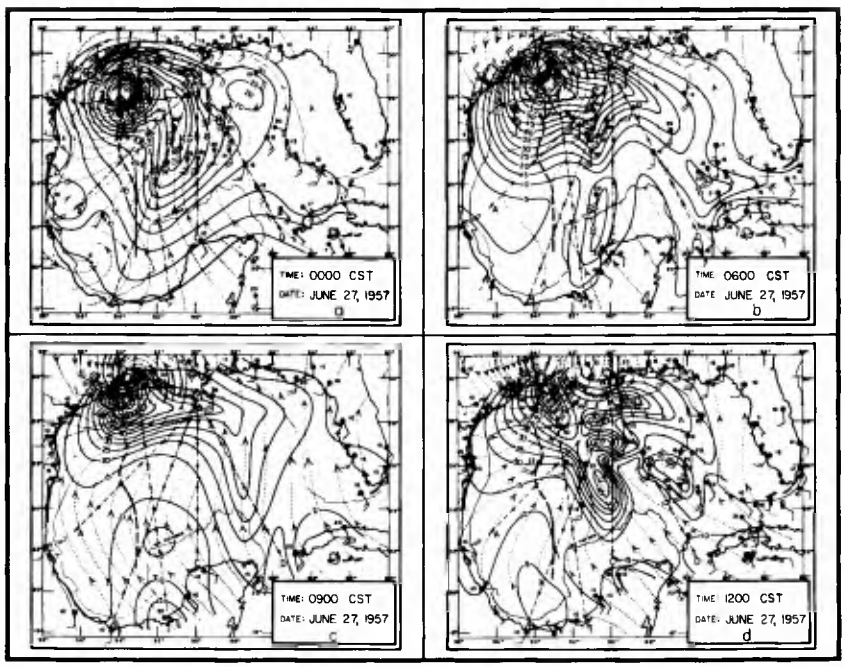

Fig. 11. Synoptic surface wind velocity (knots) and circulation patterns for the Gulf of Mexico, 0000 - 1200 CST, June 27, 1957.

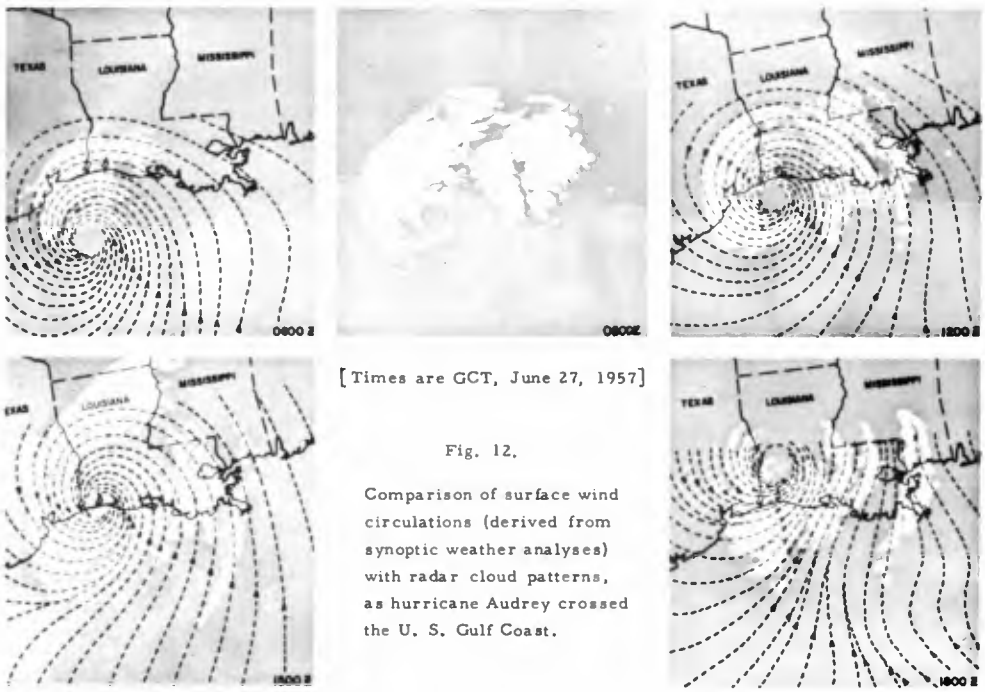

[Times are GCT, June 27, 1957]

Fig. 12.

Comparison of surface wind circulations (derived from synoptic weather analyses) with radar cloud patterns, as hurricane Audrey crossed the U. S. Gulf Coast.

Fig. 12

thur, Texas (25 n. miles from the storm track), as reported by Graham & Hudson [1960]. At Lake Charles, La., only 3 n. miles from the storm track, the lowest pressure recorded was only 971 mb, however, while the calibrated barometer reading of the American tanker "Tillamook", about 10 n. miles from the pressure center, was 973 mb, when the storm was almost at the coast. The total available evidence does not favor the existence of a lower pressure than 971 mb while the hurricane was still over water and the low values at Hackberry and Port Arthur must be ascribed to transient pressure fluctuations induced perhaps by the coastal crossing or to other unknown effects.

Graham and Hudson [1960] have concluded that hurricane Audrey crossed the coast with a probable lowest pressure $p_o = 946$ mb and a radius to maximum winds $R = 19$ n. miles. Such a deep intense storm is again not supported by the available evidence over water. Thus, if the history of lowest pressure p_o is accepted as that of Fig. 6(a), it is found that the corresponding best-fit values of R obtained by the spiral-diagram method [Wilson, 1957(i)(ii)] are those shown in Fig. 6(b). This method incorporates the same exponential pressure formula, given originally by Myers [1954], which was used by Graham and Hudson in arriving at their values of p_o and R. Contrary to their interpretation, it suggests that Audrey crossed the coast at 0840 CST on June 27, 1957, with a radius to maximum winds $R \simeq 55$ n. miles, already shrunk by almost a half from its value when the hurricane first formed in the Bay of Campeche.

Use of the mean line curves (Figs. 6 a and b) for p_o and R permitted spot calculations being made of wind velocities, at different times, in areas not covered by ship reports. These calculations followed procedures already used previously, [Wilson, 1957(i), (ii)]. The combined information on wind velocities and directions available from ship and land observations and from calculation were finally used in deriving the contours of wind velocity and directional stream-lines shown in the wind patterns of Figs. 7 to 11. These had to withstand the overriding test for consistency that they show sequential trends of change at the 3-hour intervals for which the maps were constructed, and that they accommodate withal the scattered data of spot observations. It seems possible to claim for these analyses that they meet these requirements in the main, while being consistent with the radii to maximum winds, R, given in Fig. 6(b).

The wind patterns of Fig. 11, as the hurricane crossed the coast, are rather markedly different from those derived by Graham and Hudson [1960], but are quite akin to the wind pattern found by Glenn [Lindstrom, 1957], being distinguished by the channels of high wind which spiral or radiate out over the Gulf from the storm center. Figs. 7 to 11 show the gradual formation of the characteristic horse-shoe type wind-pattern of the hurricane with highest winds concentrating on the right-hand side of its track. Maximum winds are seen to increase

from about 40 knots at 0600 CST, June 25, to about 88 knots (101 mph) at the time that the storm crossed the coast near 0900 CST, June 27, 1957. All velocities shown are mean values and may be considered to fluctuate about the mean in gusts by approximately $\pm$ 45%. One satisfactory feature of the wind analysis is the degree of concurrence between the wind streamlines of Fig. 11 and the composite radar cloud patterns obtained from several shore-based radar stations. These cloud patterns are shown in Fig. 12 along with the surface wind streamlines, reproduced from Fig.11. Fig. 12 confirms that the center of the eye of the hurricane passed directly over Calcasieu Lake just west of Cameron, La., in agreement with the hurricane track adopted.

3. WIND FIELDS FOR SELECTED DIRECTIONS

For purposes of wave prediction, two areas of principal interest were indicated at the outset of this study. One was the point O in Figs. 1 to 5, 7 to 11, identified as the site of the California Company's offshore oil platform in Bay Marchand, Louisiana, and the other point E, on the Louisiana coastline, just east of Cameron, which received the full brunt of the storm. Reliable wave data had been collected at the California Company platform [Skjelbreia, 1958], and point O was therefore an obvious checkpoint for the wave predictions. Somewhat less accurate wave data were available for the Cameron area and the Louisiana coastline in general from the various sources already referred to in Section 2.

It was decided to investigate wave conditions along five approach directions to the coast, four bearing on O and one on E. The wave paths AO, BO, CO and DO conform closely to the SW, SSW, S and SE directions, respectively, converging on O ; the wave path FE , on the other hand, was somewhat arbitrarily selected to parallel the track of the hurricane at a distance such that waves would be dominated by the highest possible winds for the longest period of time.

The wind-fields for these five wave paths are shown in Figs. 13 and 14. These show space-time plots of the components of wind velocity directed along each wave path. Contours define the velocity values in knots and shaded areas of the wind-field represent zones for which the wind components are headed toward the coast; white areas are zones of wind headed away from the coast. Limitations of cost made it necessary to restrict the areas of wind-field which could be investigated by the numerical prediction technique. Accordingly only the darker shaded zones of Figs. 13 and 14 were specifically investigated as likely to yield maximum wave conditions in the hindcast study. For these areas values of wind velocity were tabulated for each interval of 10 n. miles and 1 hour to provide the input (space-time lattice) data for the machine prediction of the waves [cf. Wilson, 1961].

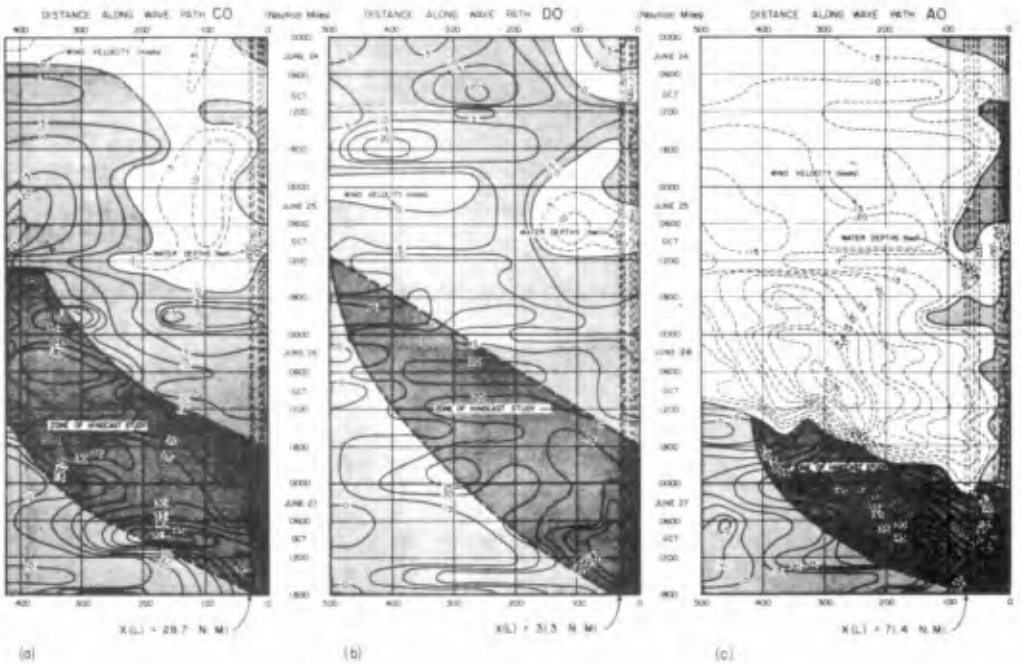

Fig. 13, Space-time wind-fields for hurricane Audrey along wave paths CO, DO and AO in the Gulf of Mexico.

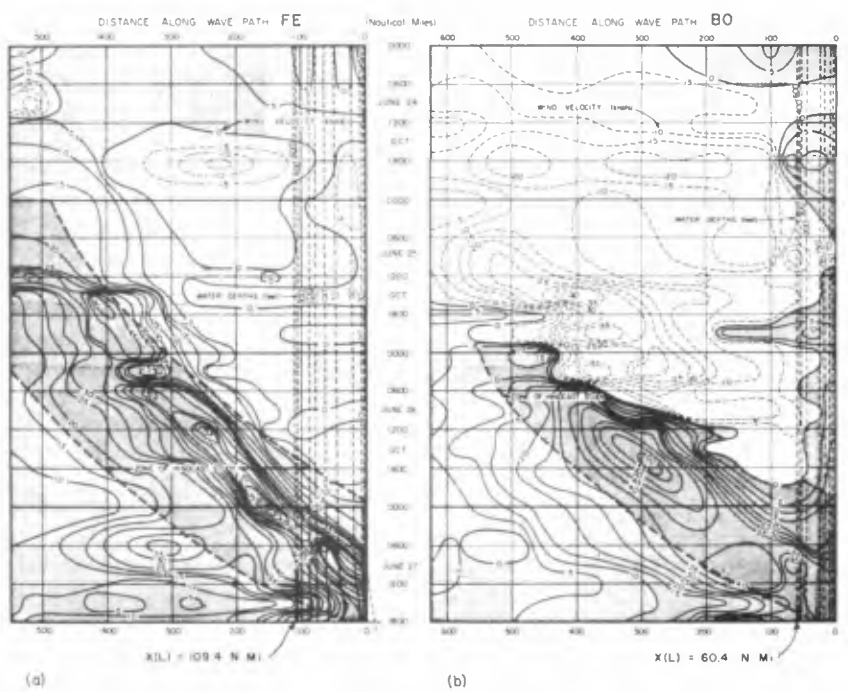

Fig. 14. Space-time wind-fields for hurricane Audrey along wave paths FE and BO in the Gulf of Mexico.

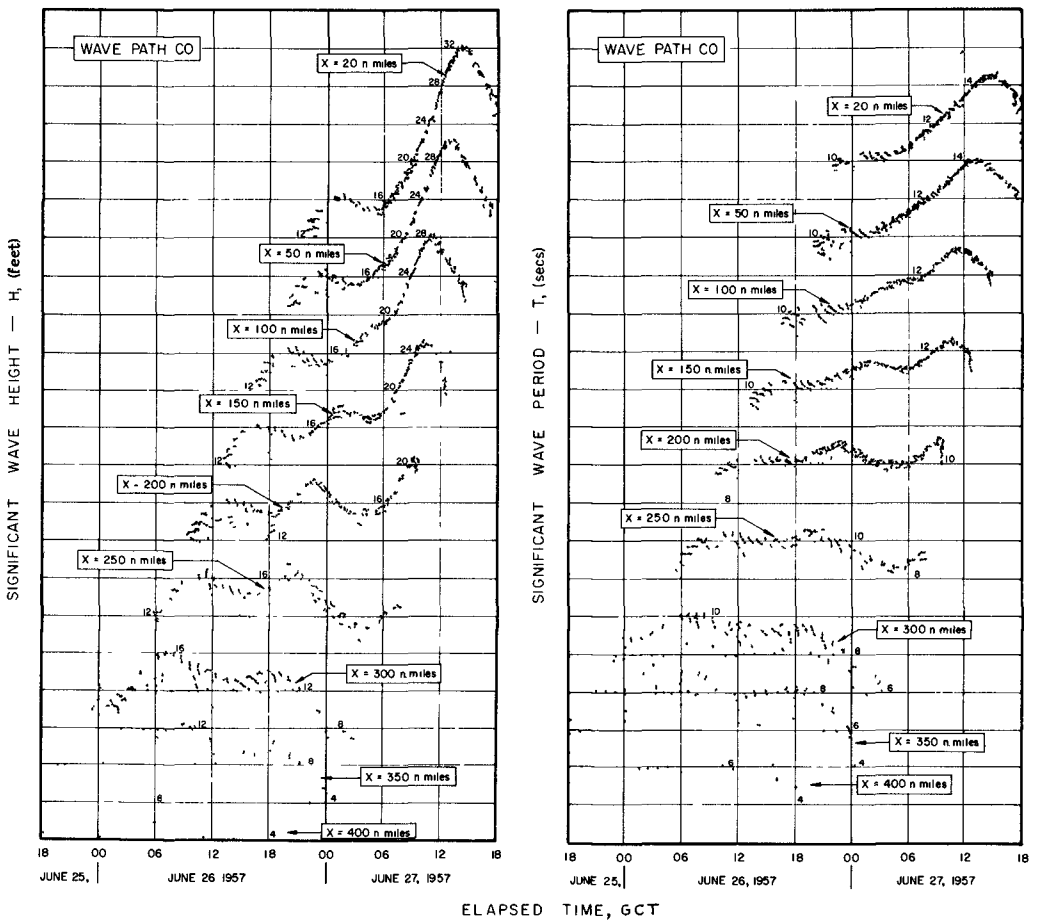

Fig. 15. Numerical computations of significant wave height and period at different distances from O along wave path CO.

It is immediately apparent from Fig. 14 that the wave paths FE and BO provide zones of highest wind velocity directed respectively towards E and O and that the highest waves may be expected to occur in these directions. Next to BO, wave path AO (Fig. 13) concentrates the highest winds bearing on station O.

4. DEEP WATER WAVE PREDICTIONS

In the hindcast procedure [Wilson, 1961] each space-time lattice point of wind input-data provides the starting point for an independent wave height and period computation along a particular wave path. Since the computation can be made to yield the significant wave height and period at any point along the wave path, it is possible to extract as output data all the possible heights and periods, with times of occurance, predicted for selected points along the wave path, such as every 50 n. miles from the coastal station. Fig. 15 is an example of these results as applicable to the wave path CO. Each plotted point of these figures represents the significant wave height (or period) occuring at the indicated time after starting from some reticulation point of the wind field in Fig. 13(a). In general the plotted points fall in a scatter with a well-defined upper-bound, to which an envelope curve is easily fitted. In the uppermost diagrams of Fig. 15, the scatters of points below the boundaries have been largely omitted for obvious reasons. Only the envelope itself is held to have significance as the time history of significant wave height (or period) at the indicated distance along the wave path.

When the envelope curves themselves are superimposed on each other the results appear in the form of Fig. 16. Along a southerly approach to station O in Bay Marchand, La., it is seen that at the distance of 400 n. miles (off Yucatan), significant wave heights at no time exceeded about 5 ft, nor the periods about 6.5 secs. Heights and periods increase as the distance lessens towards O and, as might be expected, the peak waves occur at increasingly later times. The final prediction for the wave path CO is at the distance of 20 n. miles, which defines the edge of the continental shelf off Louisiana. Between this point and the station O the waves would have to transgress shallow water and the computation technique would have to be rather radically altered to allow for this fact. It is unfortunately not possible within the limits of the present paper to enter into the complications of the continuing shallow water generation of the waves.

The corresponding sets of envelope curves of wave paths AO, BO, DO and FE are portrayed in Figs. 17 to 20. As expected, wave paths BO and FE yield the largest waves with significant wave heights, H, and periods T, of H = 40 ft, T = 16 secs for BO and H = 46 ft, T = 17 secs for FE.

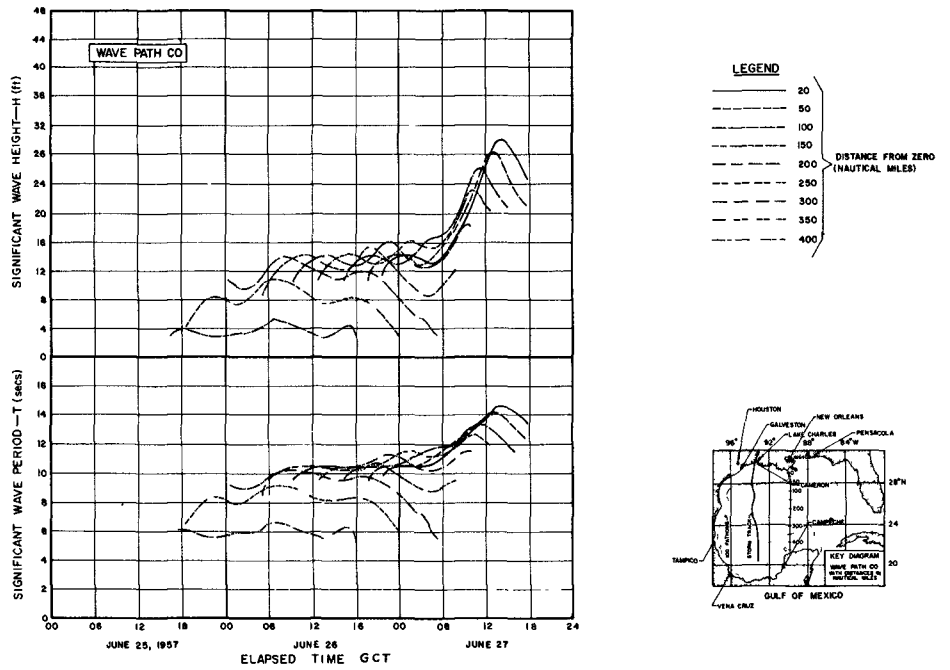

Fig. 16. Envelopes from Fig. 15 superimposed to record time-histories of significant wave height and period at different distances along wave path CO.

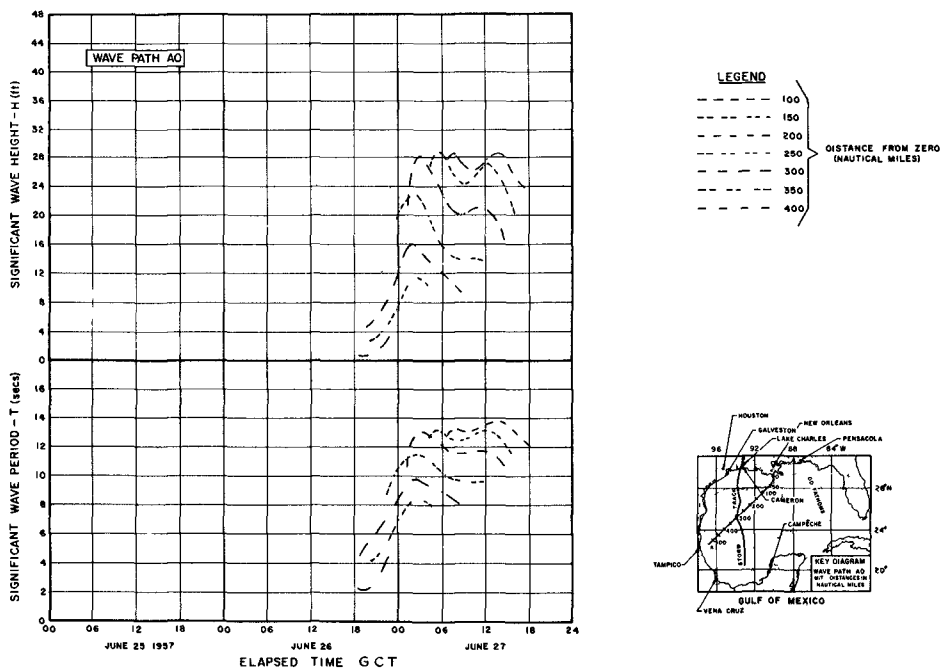

Fig. 17. Envelope histories of significant wave height and period at different distances along wave path AO.

At the distance of 300 n. miles along the wave path FE (Fig. 20) an interesting double peak is indicated by the trend of the envelope curves. Reference to the wind field in Fig. 14(a) suggests that this is the result of the two separated zones of high wind velocity falling to the left of the 300 n. mile distance mark.

5. MULTI-DIRECTIONAL WAVE EFFECTS

The uni-directional concept in deep-water wave prediction techniques has hitherto left unanswered what the interference effects may be of waves generated along a multiplicity of directions, all of which converge to a point. The present study offers some insight into this aspect, for it is conveniently found that the intersection point G between wave paths FE and AO (Fig. 21) is located 150 n. miles from E and 200 n. miles from O. On superimposing the independent predictions for the points G and H on these wave paths, extracted from Figs. 17, 18 and 20, the envelope curves (shown in Fig. 21 by actual scatter points) are found to be staggered in time.

Considering location G first, it is evident that at the time the waves from the south (along FE) attained their peak, the waves from the south-west (along AO) were quite insignificant. On the otherhand, when the waves along AO reached their peak of H = 28 ft at about 0300 GCT, June 27, waves along FE had dropped off in height to about H = 13 ft. Since these are significant waves - a statistical concept - the significant wave height of the interfering wave trains may simply be taken as the higher of the two values, on essentially the same premise that it is valid in the uni-directional case to accept the envelope curve as the criterion of the significant wave [Wilson, 1961]. In justification of this it is possible to conceive of another approach direction to G differing by only a very small angle from that of AO, and yielding substantially the same scatter-envelope of H-values. Obviously the interference of such two-directional waves would not summarily double the height of the significant waves by an additive process. Making the angular difference as small as we please, we reach the conclusion that the highest significant waves found for any particular direction at a particular time must define the significant wave height of the interference waves from all directions. On this basis then it is possible to hypothesize that the multi-directional (confused sea) significant wave heights at station G in the northwestern area of the Gulf probably accorded with the dash-line envelope (upper diagram, Fig. 21) that could be expected to form the upper-bound to all possible sets of scatter-envelopes (such as those of FE and AO) from a multiplicity of directions. The same reasoning applies in establishing the dash-line curve for location H in Fig. 21, in the southwestern area of the Gulf.

It has been shown [Wilson, 1962] that it is possible to proceed from the output data of the machine wave-prediction process to the calculation of the wave energy spectrum at any point in space and time

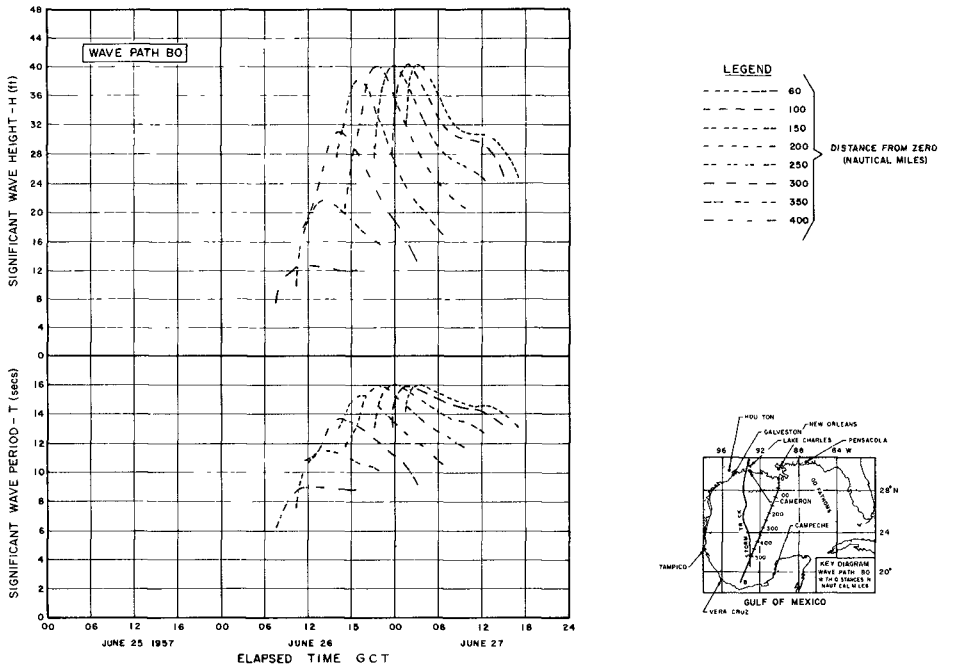

Fig. 18. Envelope histories of significant wave height and period at different distances along wave path BO.

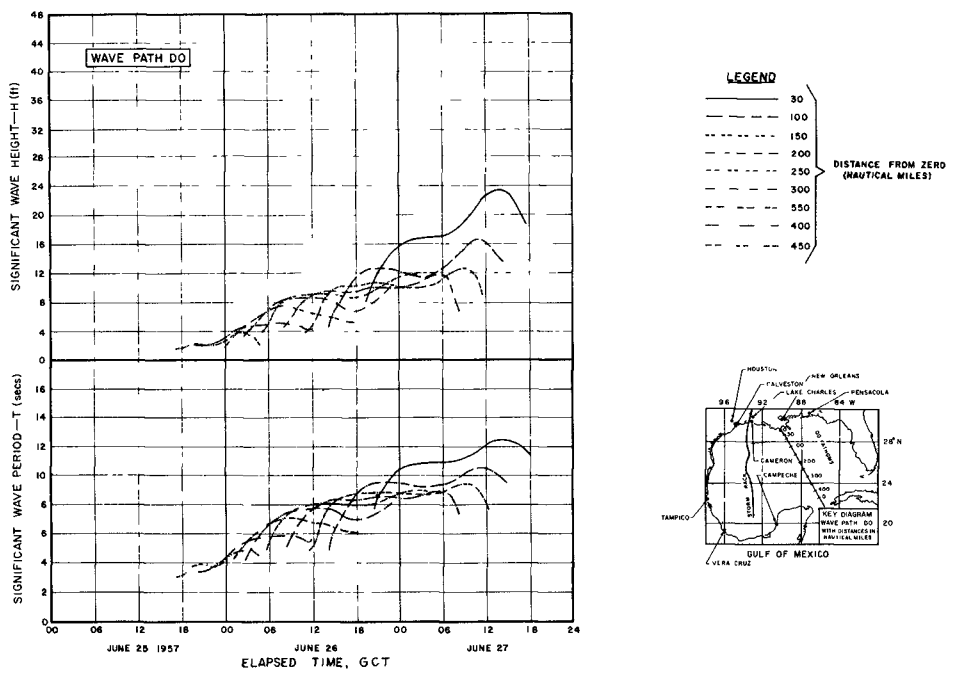

Fig. 19. Envelope histories of significant wave height and periods at different distances along wave path DO.

for a given wave path. This has not been done in respect of hurricane Audrey, although quite feasible. It appears possible in the light of the present paper that this development could readily be extended to arrive at the directional wave energy spectrum.

6. CONCLUSIONS

According to the calculations of this study hurricane Audrey was likely to have generated significant waves of a peak height of 46 ft. and period 17 secs. at the edge of the continental shelf, 100 miles from the Louisiana coast, in a direction bearing from almost due south. In terms of available hurricane wave statistics for the Gulf of Mexico [Wilson, 1957(i)(ii)], the storm frequency likely to produce such a result at Gilchrist, Texas (which may be considered roughly equivalent to the selected landfall station E) would be 1 in 80 years. For a hurricane of just such a frequency Reid's [1955] wave energy index would be about 68, this being the product of the radius to maximum winds R in n. miles and the pressure anomaly Δp ($= p_n - p_o$; p_n = normal pressure measured in ins of mercury. A fair value of p_n would be 1013 mb and for the values of p_o = 971 mb and R = 55 n. miles, found in this study, we obtain the interesting result that storm wave energy index E ($= R \Delta p$) = 68.8, providing very good confirmation that hurricane Audrey is probably to be classed for severity, statistically, as a storm likely to occur about once in 80 years.

Although the original objective of this study - direct confirmation of the wave prediction technique - still requires the extension of the latter into shallow water, interesting light is believed shed on the magnitudes of the deep water waves generated in the open sea during the lifetime of a hurricane. In particular some insight is obtained in the prediction of multi-directional wave effects, so evident in hurricanes.

The long and laborious task required to assess the wind structure of hurricane Audrey and its subtle changes with time would seem to preclude the possibility that the necessary input data for a numerical machine-process wave-prediction could ever be evolved in sufficient time to make accurate forecasts of waves during the lifetime of a hurricane. However, the methods here described could be developed into a successful forecasting tool by pre-calculating the waves that would be generated by a number of typical (design) hurricanes of various sizes and intensities, moving along given paths at appropriate speeds. The rapid forecasting procedure would then lie in matching the real hurricane for intensity, size, direction and speed with one of the design hurricanes and extracting the appropriate pre-calculated wave data for any desired direction of wave attack.

DEEP WATER WAVES GENERATED BY HURRICANE "AUDREY" OF 1957

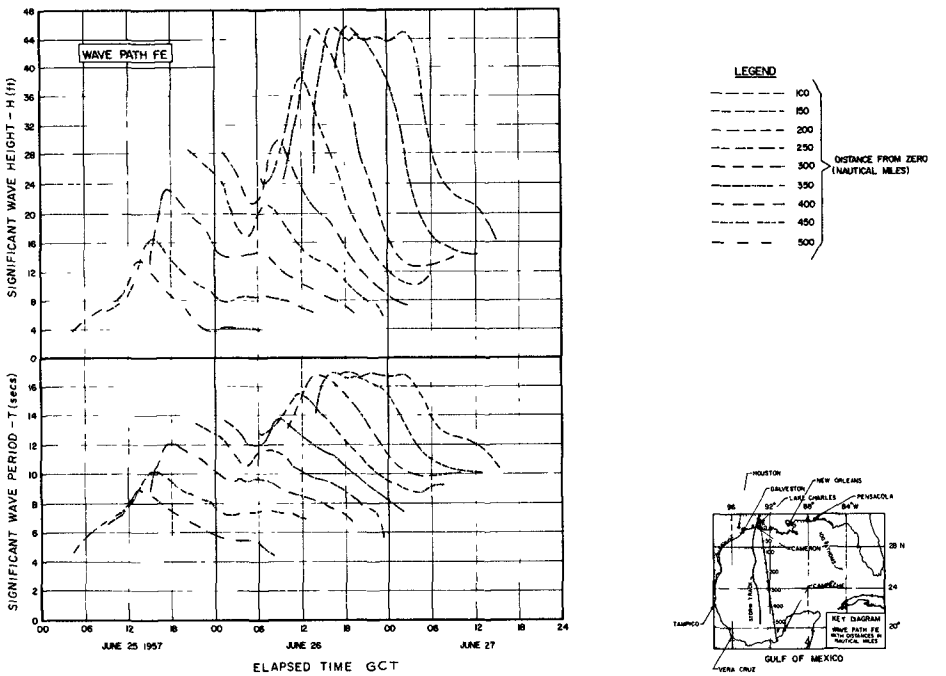

Fig. 20. Envelope histories of significant wave height and period at different distances along wave path FE.

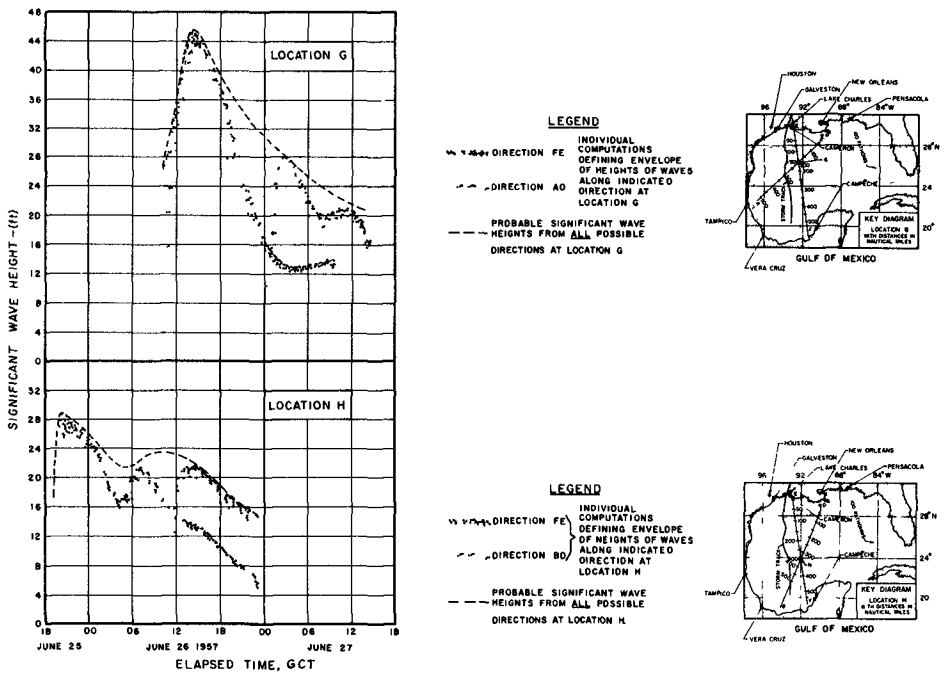

Fig. 21. Numerical computations of significant wave heights occurring at location G, along wave paths FE and AO, and at location H, along wave paths FE and BO, and expected heights of significant waves from all directions at the two locations.

7. ACKNOWLEDGEMENT

The writer wishes to acknowledge with appreciation the joint support of the Engineering Foundation of New York, the Magnolia Oil Company of Texas, the Humble Oil and Refining Company of Houston and the Office of Naval Research (Contract No. N7 ONR 48702), which made possible the major part of the work reported in this paper. To the National Engineering Science Company, however, belongs the credit for independently supporting the final preparation and presentation of this work. The ready co-operation of Mr. A. H. Glenn in furnishing valuable data to the project is worthy of special mention, although to all who likewise contributed information the writer would record his sincere thanks. The writer is particularly grateful to Mr. R. E. Kilmer who programmed and conducted the numerical calculations on the No. 704 and 709 IBM electronic computers at the Data Processing Center, A & M College of Texas.

REFERENCES

Corps of Engineers, U. S. Army [1957]; Hurricane Audrey, 1957; Report to 4th Meeting Hurricane Survey Co-ordinating Committee, New York, N. Y., Oct 22-23, 1957, 4 pp.

Cross, R. V. [1957]; Hurricane Audrey, June 26-28, 1957; Report to the California Co., 1957 (unpublished).

Freeport Sulphur Co. [1959]; Miscellaneous data for Port Sulphur, Grand Ecaille, Bay St. Elaine, Cocodrie and Garden Island Bay; Freeport Sulphur Co., New Orleans, La., 1957 (unpublished).

Glenn, A. H. [1959]; Supplied weather maps, wind records, report (see Lindblom), and sundry other data, A. H. Glenn & Associates, New Orleans, La.

Graham, H. E. and Hudson, G. N. [1960]; Surface winds near the center of hurricanes (and other cyclones); Report No. 39, National Hurricane Research Project, Weather Bureau, Washington, D. C. Sept. 1960; pp. 112-123.

Harris, D. L. [1958]; Hurricane Audrey storm tide; Report No. 23, Nat. Hurricane Research Project, Weather Bureau, Washington, D. C., Oct. 1958; 19 pp.

Hudson, G. [1957]; Pressure, wind speeds and direction in Hurricane Audrey, June 27, 1957, Report, Hydrometeorolog. Sect., Weather Bureau, U. S. Dept. Commerce, Dec. 1957, 17 pp. (unpublished).

Kerr-McGee [1959], Supplied anemometer tapes for Rig 47, Block 139, Ship Shoal and Rig 48, Block 120, Vermillion, June 24-27, 1957; Kerr-McGee Oil Industries, Inc., Morgan City, La.

Lindblom, D. E. [1957]; Meteorological-oceanographic conditions over the Louisiana-North Texas coastal and offshore area during the hurricane of June 25-28, 1957, Report of A. H. Glenn & Associates, Nov. 1957 (unpublished).

Moore, P. L. et al [1957]; The hurricane season of 1957; Monthly Weather Rev., Dec. 1957, pp. 401-408.

Myers, V. A. [1954]; Characteristics of United States hurricanes pertinent to levee design for Lake Okeechobee, Florida, Hydrometeorolog. Report No. 32, Weather Bureau, U. S. Dept. of Commerce, Washington, D. C., Mar. 1954, 106 pp.

Reid, R. O. [1955]; On the classification of hurricanes by storm tide and wave energy indices, Meteorological Monographs (Am. Met. Soc.), v. 2(10); June 1957, pp. 58-66.

Ross, R. B. and Blum, M. D. [1957]; Hurricane Audrey, 1957; Monthly Weather Rev., June 1957, pp. 221-223.

Sartain, R. R. [1957], Offshore damage - hurricane "Audrey", Preliminary Report, Gulf Oil Corporation, July 16, 1957, 11 pp. (unpublished).

Servicio Meteorologico Mexico [1959], Observaciones simultaneas, Junio 23-28, 1957; Centro de Prevision del Golfo de Mexico, Instituto de Meteorologia Nautica, Veracruz, Ver., Mexico; 1957 (unpublished).

Skjelbreia, L. [1958]; Storm data obtained in the Gulf of Mexico during the hurricane season, 1957; Proc. 1st Tech. Conf. on Hurricanes, (Miami, Fla., Nov. 1958), Am. Met. Soc., 1959.

Visser, R. C. [1957]; Hurricane Audrey; Report to the Shell Oil Company, 1957 (unpublished)

Weather Bureau [1958]; Index of assembled meteorological data related to hurricane "AUDREY", 2330 EST, June 24 through 0500 EST, June 28, 1957; National Weather Records Center, Ashville, North Carolina; 1958.

Wilson, B. W. [1955]; Graphical approach to the forecasting of waves in moving fetches; Tech Memo No. 73, Beach Erosion Board, Corps of Engineers, U. S. Army, April 1955, 31 pp.

Wilson, B. W. [1957(i)]; Hurricane wave statistics for the Gulf of Mexico; Tech Memo No. 98, Beach Erosion Board, Corps of Engineers, U. S. Army, June, 1957, 95 pp.

Wilson, B. W. [1957(ii)]; Hurricane wave statistics for the Gulf of Mexico; Proc. 6th Coast. Eng. Conf. (Gainsville, Fla., Dec. 1957), Council Wave Research, Berkeley, 1958.

Wilson, B. W. [1957(iii)]; Incipient wind-generation of ocean waves by a norther; Bulln. Am. Met. Soc. v. 38(7), Sept. 1957, pp. 399-404.

Wilson, B. W. [1961]; Deep water wave generation by moving wind systems; Proc. ASCE, v. 87(WW2), May 1961, pp. 113-141.

Wilson, B. W. [1962]; Deep water wave generation by moving wind systems; Proc. ASCE, v. 88(WW3), Aug. 1962, pp. 175-185.

Zumwalt, T. H. [1958]; Louisiana and Texas Hurricanes; Paper presented to joint meeting Louisiana and Texas sections ASCE, Beaumont, Texas, May 1958, 24 pp. (unpublished).

CHAPTER 32

THE MARCH 1962 STORM ON THE ATLANTIC COAST OF THE UNITED STATES

M. P. O'Brien and J. W. Johnson
College of Engineering
University of California
Berkeley

Introduction

As far back as 1635, records show that the East Coast of the United States has repeatedly suffered from severe storm damage (McAleer, 1962). Most of these storms appear to have been of the hurricane type. Such storms generally form in the Atlantic to the east of the Bahama Islands and move eastward and then turn northward to sweep along the Atlantic Coast line (Fig. 1). Along the southern part of the Atlantic Coast the hurricanes move relatively slowly; damage results principally from flooding caused by direct wind action. North of Cape Hatteras the hurricanes move more rapidly (speeds of 40 to 50 miles per hour) and damage is largely due to sudden flooding from a rapidly moving storm surge (Simpson, 1962). The combination of storm surge, wind-driven water, and storm waves inundating large areas along the coast has on numerous occasions caused great damage and loss of life.

The great Atlantic Coast storm of March 1962, however, differed in character from the usual hurricane. It proved to be the most disastrous winter coastal storm on record, causing damage from southern New England to Florida. This storm, of relatively large diameter and having gale force winds, remained nearly stationary off the Coast for almost 36 hours. The size and location of the storm, as further discussed below, was such that persistent strong northeasterly winds blowing over a relatively long fetch raised the spring tides (maximum range) to near-record levels. The tidal flooding which attended this storm was in many ways more disastrous than that which accompanies hurricanes (Cooperman and Rosendal, 1962). The storm surge in tropical cyclones generally recedes rapidly after one or two high tides, but the surge accompanying this storm occurred in many locations on four and five successive high tides! The great destruction was caused by high waves and breakers superimposed on these high tides.

In many ways the March 1962 storm was similar to the unusual and disastrous storm of February 1, 1953 in the Netherlands. This latter storm was different meteorologically than the usual North Sea gales that occur in this area. It had an extremely long duration and the

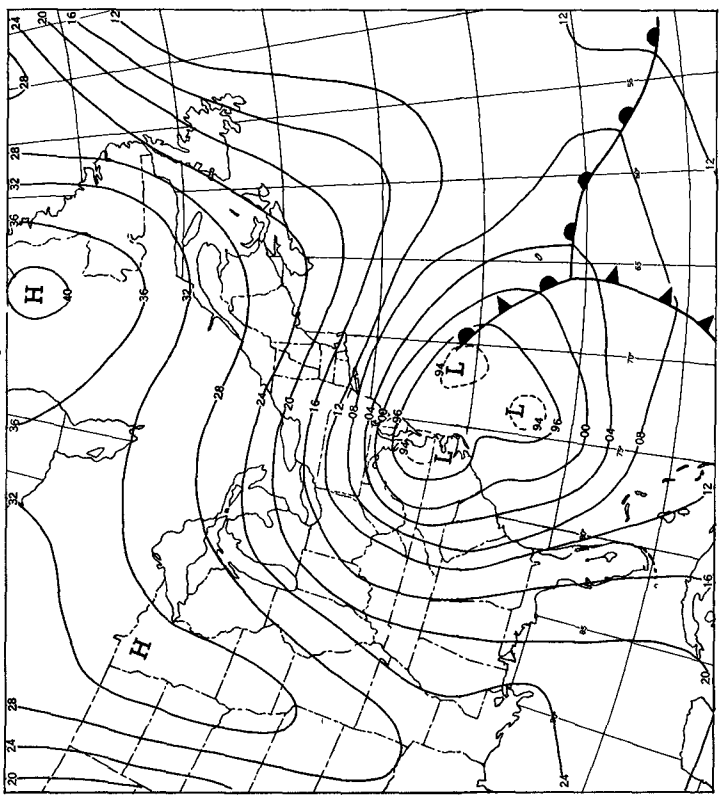

Fig. 2. Sea level pressure chart (mb) at 1200 GMT, March 6, 1962.

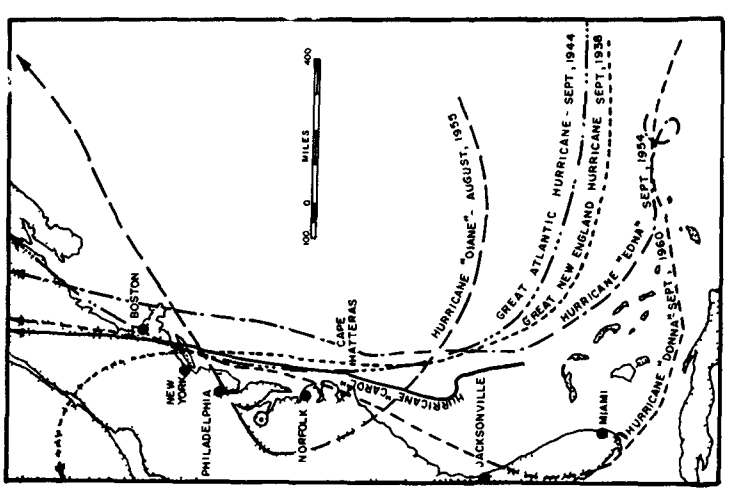

Fig. 1. Typical East Coast hurricane paths, 1938-1960.

track of the storm was very favorable for the generation of a high storm tide and high waves at critical locations along the Netherlands Coast (Wemelsfelder, 1953).

A broad factual summary of the principal features and results of the March 1962 storm follows.

Meteorological Conditions

On March 4, a weak circulation along a cold front started in the Atlantic east of Florida. Almost simultaneously a widespread but weak storm area was moving slowly eastward through the Mississippi Valley. On the following day these two storms deepened and partially merged (Cooperman and Rosendal, 1962; Anonymous, 1962). The offshore storm center continued to intensify on March 5 and 6 and slowly moved northward. On March 6, the main center of the large storm, which actually consisted of a series of lows, stopped moving and became nearly stationary (Fig. 2). During this time the storm became elongated and, on March 7, appeared to have two centers (Fig. 3). The storm slowly moved eastward out into the Atlantic on the 7th and 8th. During this time, a gradually increasing fetch developed to the north between the center and New England (Fig. 3). Strong winds blowing over this fetch for a long time were responsible for raising the water level of the shore and generating waves of increasing heights. These large waves, breaking at a large angle to the shoreline of Long Island (Fig. 4), were particularly effective in removing large quantities of sand from the shore front and exposing the buildings and other improved property to a terrific battering over several high tides. Great swells from the extraordinary fetch occurring during the storm reached the South Atlantic States and caused substantial shore damage as far south as Miami Beach.

Of interest is a comparison between the March 6-8 storm and the usual hurricane. Although the March 1962 storm was not as intense as a hurricane, it had a lesser degree of symmetry, covered a much broader area, and was longer in duration, That is, the storm was roughly 1,500 miles in diameter compared to 600-700 miles for a hurricane.

Wave Conditions

Very little information on recorded wave data is available from this storm, since the only wave gage in the area (Atlantic City pier) was carried away early on the first day of the storm after recording waves approximately 12 feet in height. A summary of ship observations of wave conditions, however, was made by the U. S. Navy Fleet Weather Central and is shown in Figure 5. It is noted in this figure that on

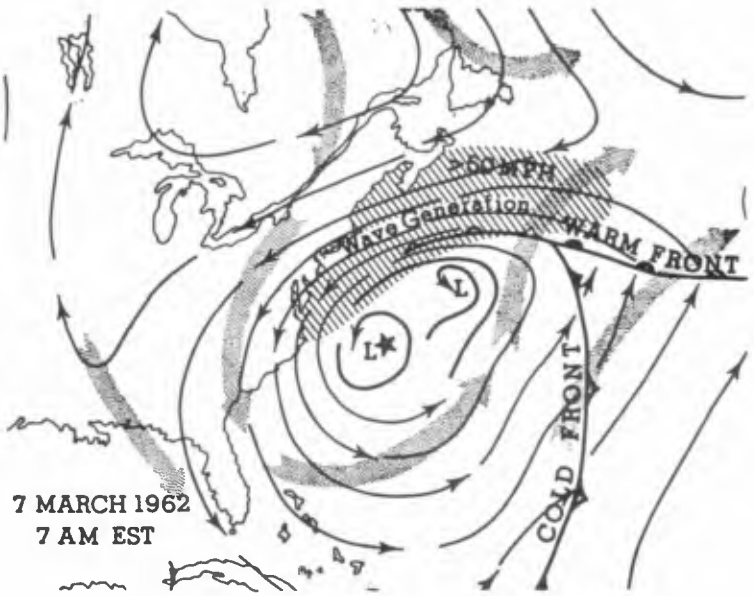

Fig. 3. Chart showing flow of surface winds (narrow arrows) acting over long fetch on March 7. Broad arrows show flow of upper air.

Fig. 4. Aerial view of Fire Island, N. Y. showing offshore bars and large angle of wave attack (Long Island State Park Commission).

March 8 the waves in the long fetch along the Northeastern States were 40 feet in height in deep water.

Extreme Water Levels

Although the extreme water levels at various localities along the Atlantic coast during the period of March 6-9 did not exceed the highest tide ever recorded, a near approach to the maximum did occur at many stations. Table 1, for example, lists for several stations the date and stage of the highest tide on record, the date, hour, and stage of tide in the March storm, and the feet that the stage in the March storm exceeded the predicted tide for the corresponding time.

TABLE 1

Summary of Extreme Water Levels Along the Atlantic Coast
(From U. S. Coast and Geodetic Survey)

Location	Highest Tide on Record		Extreme Water Levels March 6-9, 1962			
	Date	Feet Above MLW	Day	Hour (75°W)	Feet Above MLW	Feet Above Predictions
New Rochelle, N.Y.			6	11:00	12.0	3.3
Montauk, N. Y.			7	9:36	5.7	3.1
Eatons Neck, N.Y.			6	23:36	11.6	3.4
Port Jefferson, N.Y.			6	23:30	10.9	3.3
Willets Point, N.Y.			6	11:18	12.1	3.6
New York (Battery), N.Y.	9/12/60	10.4	6	20:54	9.3	4.1
Sandy Hook, N.J.	9/12/60	10.6	6	20:24	9.9	4.5
Atlantic City, N.J.	9/14/44	9.5	6	7:06	9.1	3.9
Fort Miles, Del.			6	21:00	9.7	4.9
Reedy Point, Del.			8	00:06	9.4	3.3
Philadelphia, Pa.	11/25/50	10.6	8	3:12	9.5	3.2
Washington, D.C.	10/17/42	11.5	8	8:54	6.4	3.1
Sewells Pt., Va.			7	10:00	8.0	5.0
Portsmouth, Va.			7	10:24	8.6	5.3
Wilmington, N.C.			8	23:54	6.2	2.2
Myrtle Beach, S.C.			8	21:24	8.2	2.2
Charleston, S.C.	8/11/40	10.7	8	22:00	8.2	2.2
Ft. Pulaski, Ga.	10/15/47	11.4	8	22:06	9.8	1.7
Fernandina, Fla.	10/2/98	13.9	8	23:18	8.4	1.6
Jacksonville, Fla.			9	00:24	3.2	0.9
Mayport, Fla.			8	22:30	6.5	1.3
Miami, Fla.	10/18/50	6.4	8	22:00	4.3	1.4

Fig. 6. Aerial view of Maryland coast showing damage both by wave attack and inland flooding (U. S. Navy photograph).

Fig. 5. Wave heights in Western Atlantic Ocean on March 8 (U. S. Navy Fleet Weather Central).

THE MARCH 1962 STORM ON THE ATLANTIC COAST OF THE UNITED STATES

In the New York area the tide stage almost equaled the highest on record which occurred during Hurricane "Donna" in September 1960; however, the damage during the March 6-9 storm was much more severe because of the long duration. That is, during Donna the high water occurred at only one high tide, after which the waters receded rapidly (Anonymous, 1962), but in the March storm damaging high waters occurred on five successive high tides over a period of 48 hours! Added to this were waves reported to be 20 to 30 feet high. Their momentum carried the water inland, and it reached houses and buildings which would ordinarily be beyond the reach of relatively high tides. Respite between successive high waters was only about 6 hours since flooding stages were maintained 2-3 hours before and after high tide.

Along the New Jersey coast the tides were approximately equal to those in the September 1944 hurricane, but the recent storm lasted much longer.

In the Hampton Roads, Virginia, area the storm caused greater wave and flooding damage than any coastal storm of recent record, and in the outer banks of North Carolina the storm was as destructive as a major hurricane.

General Character of Damage

The March storm occurring at the peak of the spring tides and extending over five tides (generally 3 to 5 feet above normal--Table 1) with waves up to 30 feet high caused tremendous damage (Fig. 6) as a result of the protective sand beaches being destroyed (Cassidy, 1962). The effect of the heavy wave action was to remove sand from the beach face and deposit it as offshore underwater bars (Fig. 4). The waves then were able to overtop the berm or dune line, with water and sand sweeping across the barrier islands. Shoreline buildings thus were exposed to the full impact of wave and current action resulting in their total destruction in most instances (Fig. 6).

Strong tidal currents combined with the storm waves opened new inlets and eroded the sides of many existing inlets and moved sand through the inlets into the bays. The new inlets occurred at points where the barrier island was low and unprotected by a suitable dune or seawall. Because of the long duration of the storm, damage by flooding at inland localities not exposed to direct wave or current attack was considerable (Fig. 6). As a result of the many breaks in the line of dunes, large areas are now open to attack by storms of substantially less intensity than that of early March and immediate restoration of beaches and dunes in threatened areas is a necessity. It is of course also necessary to insure that once such shore protection is re-established it is not destroyed by leveling dunes at street ends or for the construction of homes

and business enterprises as has been done in the past (Anonymous, 1962). To summarize the damage problem the following statement by Cassidy (1962) is of importance:

"The physical damage was closely related not only to the general elevation of the shore but also to the adequacy of the dune, sea wall, and beach fronting the shore. In some areas wide beaches afforded good protection, and in others high dunes gave almost complete protection. Where there was insufficient beach and dune protection, severe damage resulted. In areas with the least protection beaches were completely eroded and shifted."

REFERENCES

1. Anonymous, East Coast Atlantic Storm, Preliminary Reports, Shore and Beach, Vol. 30, No. 1, April 1962, pp. 4-9.

2. Cassidy, W. F., Recovery operations after Atlantic Coast Storm, The Military Engineer, Vol. 54, No. 360, July-August 1962, pp. 246-248.

3. Cooperman, A. I. and Rosendal, H. E., Great Atlantic Storm, 1962, Mariners Weather Log, U. S. Dept. of Commerce, Vol. 6, No. 3, May 1962, pp. 79-85.

4. McAleer, J. B., Hurricane protection of Narragansett Bay, The Military Engineer, Vol. 54, No. 358, March-April 1962, pp. 112-115.

5. Simpson, R. H., Improvement of storm forecasting procedures, Hearings before Subcommittee on Oceanography of the Committee on Merchant Marine and Fisheries, House of Representatives, 87th Cong., 2nd Sess., 1952, p. 20.

6. Wemelsfelder, P. J., The disaster in the Netherlands caused by the storm flood of February 1, 1953, Proc. Fourth Conference on Coastal Engin., 1954, pp 258-271.

CHAPTER 33

DESIGN OF HURRICANE FLOOD PROTECTION WORKS ON THE UPPER TEXAS COAST

Albert B. Davis, Jr.
Chief, Planning and Reports Branch
U. S. Army Engineer District, Galveston, Galveston, Texas

INTRODUCTION

One of the recurring natural phenomena that causes enormous damages in the destruction of property and loss of lives on the upper Texas Gulf coast is the tropical hurricane. The terrific wind velocities, overflowing tide surges and tremendous waves that accompany these disturbances are overwhelming in their devastating effects on man made structures. In 1955, the Congress of the United States directed that a comprehensive study be made of hurricanes on the Gulf and Atlantic coasts and of means for protecting coastal areas from their destructive effects. Under this authorization, the Corps of Engineers has made extensive studies of hurricane behavior and frequency and of means of preventing loss of human lives and damages to property. The Weather Bureau cooperated fully in the studies of hurricane characteristics and phenomena. This paper concerns the studies and the design of protective structures at Texas City on the upper Texas coast. The location of Texas City with respect to the Gulf of Mexico is shown on figure 1.

Texas City is located on the mainland shore of Galveston Bay, one of the large coastal lagoons that border Texas. Galveston Bay, as shown on figure 2, is separated from the Gulf of Mexico by the offshore bars of Galveston Island and Bolivar Peninsula and is connected with the Gulf by two natural passes: San Luis Pass, at the southwest end of Galveston Island; and Galveston entrance, at the northeast end of Galveston Island between the island and Bolivar Peninsula. The barrier islands are generally 1 to 3 miles in width with maximum elevations on old beach ridges of 8 to 10 feet above mean sea level. A massive sea wall(1) consisting of a concrete gravity section backed by sand fill extends along about nine and one-half miles of the Gulf shore and protects the northeastern portion of Galveston Island, which is occupied by the city of Galveston. The seawall lies about 9 miles southeast of Texas City.

Galveston Bay, including its smaller connecting bays has a maximum length of about 30 miles in a north-northeast and south-southwest direction and extends about 17 miles in an east and west direction. Natural oyster shell reefs extend across the bay in two locations dividing it into separate parts. Depths of 6 to 8 feet at mean sea level are available over most of the bay areas. Two small bays on the north side of Texas City have a combined surface area in excess of 2,000 acres and average depths of 2 to 3 feet below mean sea level.

Texas City has a frontage of about 12 miles on Galveston Bay. The ground surface in the city slopes generally from maximum elevations of 20 to 25 feet along the west city limits to elevations of less than 5 feet above mean sea level along the east shore line. A ridge extends in

an east to west direction through the central part of the city, from 15 feet above mean sea level on the west to about 5 feet on the east. The principal industrial development and business area is on this ridge, while the residential areas extend down the slope to lower elevations. The adjoining city of LaMarque is developed to elevations of 8 to 9 feet in its southerly portion. As shown on figure 2 a storm surge of 15 feet above mean sea level would inundate most of the developed areas of Texas City and LaMarque.

DESIGN HURRICANE

The initial studies were to determine the design hurricane and the storm surge on the Texas coast that would be caused by the design hurricane. The U. S. Weather Bureau undertook intensive studies of the phenomena of all hurricanes on which it had records and the determination of frequencies of occurrence of given characteristics of hurricanes. In this study, as reported by Graham and Nunn(2), the coastal areas were divided into regions and a determination made of the characteristics of a hurricane with a recurrence interval of 100 years in each of these regions. The principal features of this storm are selected as representative of a standard project hurricane. The results of this study are presented in a series of publications of the U. S. Weather Bureau of which the pamphlet referring to the region of the upper coast of Texas is entitled, "HUR 7-45"(3). The characteristics of the standard project hurricane in the Gulf region off Galveston are as follows:

Maximum wind velocity (30 feet above water surface)- 101 miles an hour
Radius from center to region of maximum winds - 14 nautical miles
Forward speed of storm - 11 knots
Central barometric pressure - 27.52 inches of mercury
Asymptotic barometric pressure - 29.92 inches of mercury

These storm characteristics are identified by the atmospheric pressure in the center of the storm which is referred to as the central pressure index (CPI). It was found by the Weather Bureau that the central pressure of a given hurricane is an index to its general magnitude of severity. However, the other characteristics, particularly the radius of the storm, are essential in the evaluation of the magnitude of the storm and of the accompanying wind velocities, tide surge elevations and wave heights.

The frequency of recurrence of the standard project hurricane is estimated by the Weather Bureau as once in one hundred years in the regior off the upper Texas Gulf coast; however, its occurrence on a path to give maximum surge in the Texas City area would be less frequent. The authorized project provides for hurricane tide protection at Texas City against a tide with a recurrence frequency of once in 100 years. A study of frequencies based on tide records at Galveston and frequencies based on computed storm surges in the Gulf indicated that a hurricane surge elevation of 15 feet above mean sea level has a recurrence interval of once in 100 years. Accordingly, the characteristics of the standard project hurricane in the Gulf of Mexico at Galveston were modified to represent a design hurricane that would generate a storm surge of 15 feet at Galveston. The

DESIGN OF HURRICANE FLOOD PROTECTION WORKS ON THE UPPER TEXAS COAST

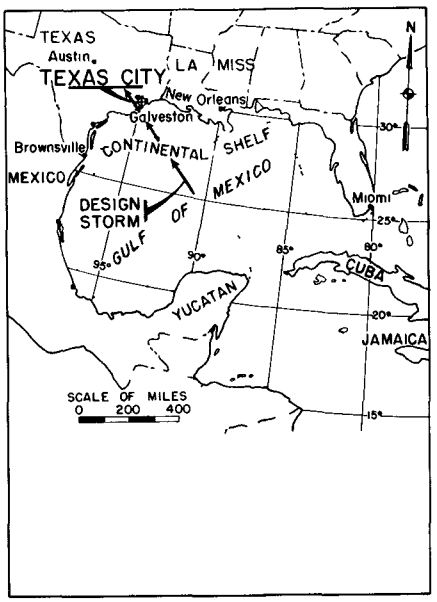

Fig. 1. Location Map, showing location of Texas City on the Gulf of Mexico.

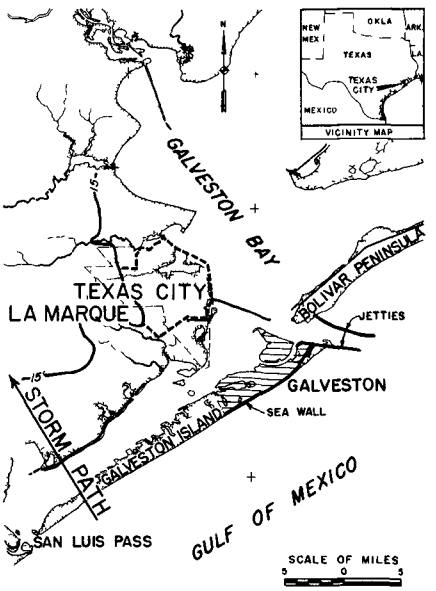

Fig. 2. Vicinity of Texas City.

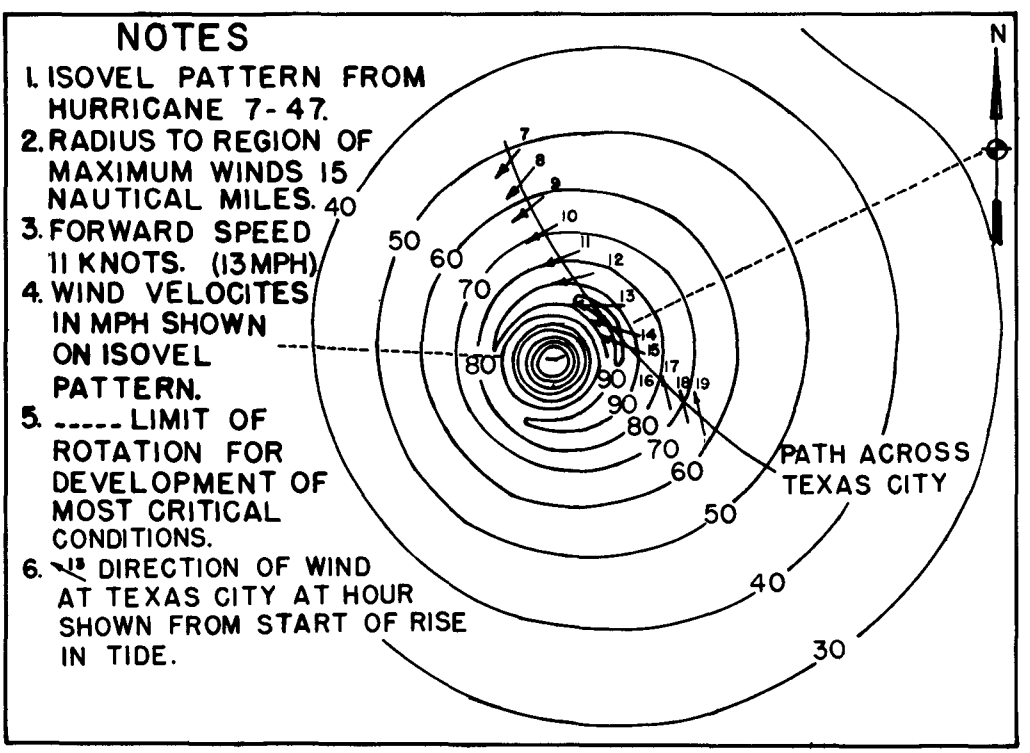

Fig. 3. Wind pattern of design storm.

characteristics of the design hurricane are as follows: Maximum onshore component of wind velocity, 30 feet above the water, 99 miles an hour; central pressure, 27.54 inches of mercury; asymptotic barometric pressure at periphery of the storm 29.92 inches of mercury; radius to region of maximum wind speed, 15 nautical miles; forward speed of the storm mass, 11 knots. The path of the design storm to result in the most severe tide surge elevation and wave heights in the vicinity of Texas City would be alined normal to the coast and lie 15 miles southwest of Texas City, as shown on figure 1. The wind pattern of the design hurricane is given in Weather Bureau Memorandum HUR 7-47(4) and is shown on figure 3.

DESIGN STORM SURGE

On the Gulf shore the total hurricane storm surge consists of a rise in water level caused by the wind stress and an increase in elevation from the reduction in atmospheric pressure in the storm center, all superimposed on the local astronomical tide.

The formula for dynamic storm tide on a constant sloping continental shelf, exclusive of the component caused by atmospheric pressure reduction, developed by Reid(5) was used in the studies at Texas City. This formula is as follows:

$$N_m = K \frac{T}{\overline{C}_1} \left(\frac{d_1}{d_o} \right)^{0.25} W_m^2 S$$

where N_m = maximum rise in water level caused by wind stress (in feet).

d_1 = mean water depth at seaward edge of the continental shelf just landward of the sharp increase in slope on the continental slope (in feet).

d_o = mean water depth at shoreward edge of continental shelf just seaward of the sharp increase in slope in the near-shore zone (in feet).

$K = 3.0 \times 10^{-6}$, wind stress parameter

$C_o = \sqrt{gd_o}$ speed of free wave at d_o (in feet per second)

$C_1 = \sqrt{gd_1}$ speed of free wave at d_1 (in feet per second)

$\overline{C} = 1/2 (C_o + C_1)$ average speed of free wave (in feet per second)

B = breadth of continental shelf between the location of d_1 and d_o (in feet)

$T = \frac{B}{\overline{C}}$, period of travel of free wave over continental shelf (in seconds)

W_m = maximum sustained wind speed in feet per second, 30 feet above the water surface

S = Response factor depending on the ratio of fetch length to breadth of continental shelf and the ratio of the forward speed of the hurricane to the propagational speed of the free wave $\overline{C}$

The profile of the continental shelf off Galveston, parallel to the design storm path is shown on figure 4. The characteristics of the profile used in computing the storm surge at Galveston are as follows:

d_o = 36 feet; d_1 = 180 feet; $\left(\frac{d_1}{d_o}\right)^{0.25} = 1.495$

$C_1 = \sqrt{g \times 180} = 76$ ft/sec = 51.7 miles/hr

$\overline{C} = \frac{1}{2}\left(\sqrt{gd_o} + \sqrt{gd_1}\right)$

$= \frac{1}{2}(34 + 76) = 55$ ft/sec = 37.5 miles/hr

B = 110 nautical miles = 127 miles

T = 3.39 hours

Substitution of these characteristics of the shelf with factors for conversion to the proper units, in the general formula gives for the Galveston area

$N_m = 1.55 \times 10^{-3} W_m^2 S$, where W_m is in miles per hour

The response factor S for a hurricane is obtained from figure 13 "Response Diagram: Isolines of S versus F/B and V/ $\overline{C}$" by Reid(5).

Data on characteristics of two hurricanes of 1900 and 1915 that crossed the coast near Galveston are given in additional U. S. Weather Bureau memoranda. Records of the storm surge caused by these storms are known and the constant in the formula was adjusted to reproduce the actual storm surges. The adjusted formula is:

$N_m = 1.69 \times 10^{-3} W_m^2 S$

The adjusted formula was then used with the characteristics of the design storm to compute the maximum rise in water level that would be caused by the design storm wind stress. Using a maximum wind speed, W_m, of 99 miles an hour and a value of the response factor S of 0.82 from figure 13 of reference 5 for the characteristics of the design storm, the maximum wind setup is computed to be 13.5 feet.

The rise in water surface level from the reduced atmospheric pressure in the zone of maximum winds was computed from the following formula from Beach Erosion Board Technical Report No. 4(6).

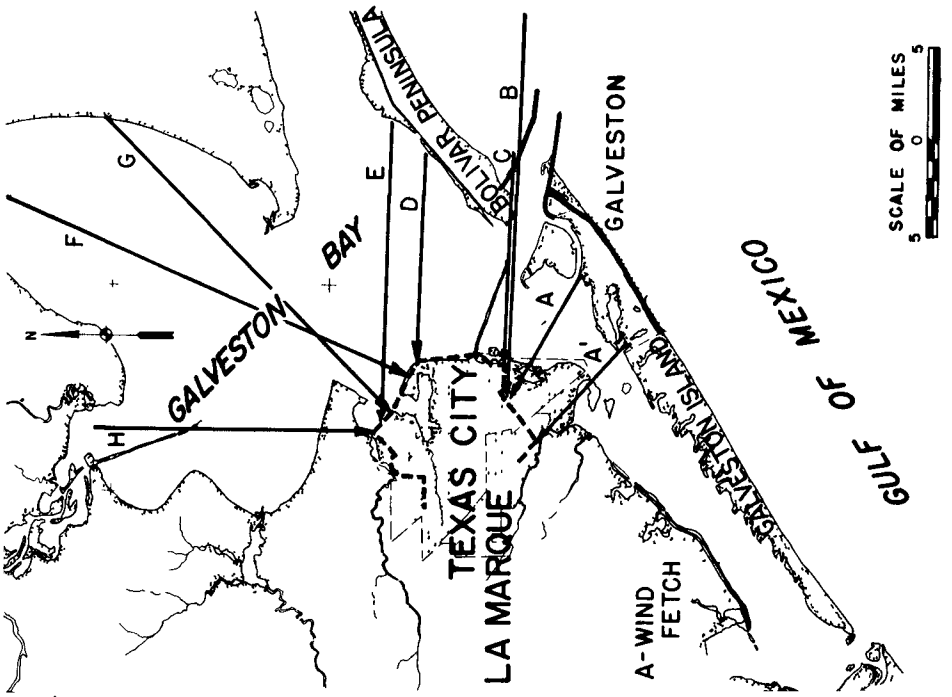

Fig. 6. Direction and fetch of wave attack by reaches of protective structure at Texas City.

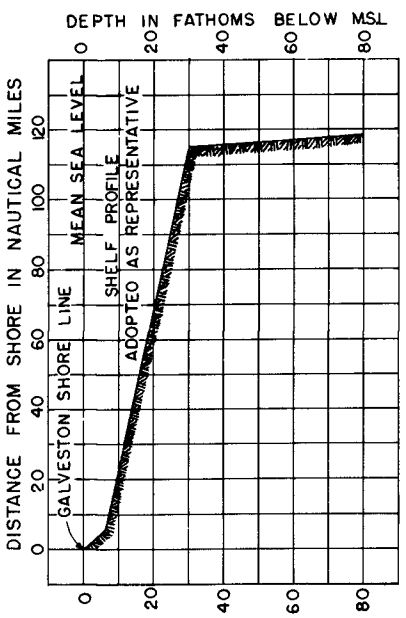

Fig. 4. Profile of continental shelf along storm path through Galveston.

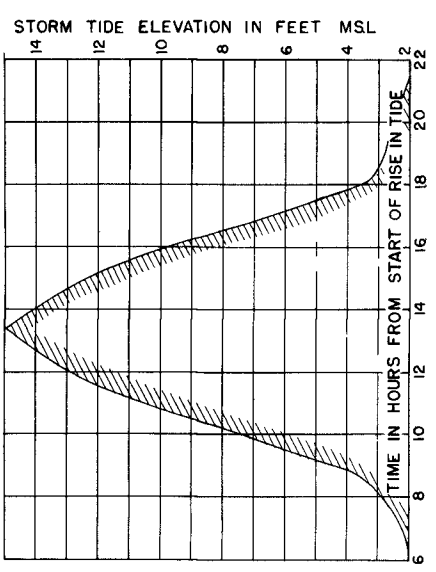

Fig. 5. Design storm hydrograph.

$$N_p = 1.14 \Delta P \times 0.63$$

where N_p is rise in water surface level in feet

1.14 factor to convert inches of mercury to feet of water
ΔP - difference between atmospheric pressure at center of storm and the asymptotic pressure
0.63 - factor to reduce pressure difference to difference at zone of maximum wind

The difference in atmospheric pressure of the design storm is 29.92 - 27.54 = 2.38. Substitution of the ΔP in the formula gives a rise in water surface level of 1.7 feet. The astronomical tide at Galveston has a range of only about 1.5 feet and is not included in the total design storm surge which is estimated at 15.2 feet above mean water level for a recurrence frequency of once in 100 years.

The propagation of the storm surge through the Galveston Harbor entrance and San Luis Pass and, as the tide rises above 6 feet, across the low areas of Galveston Island and Bolivar Peninsula into Galveston Bay is a most complex problem in tidal hydraulics, and one that cannot be accurately computed. The time sequence of the rising storm tide, the variation in storm winds, the irregular topography and the length of beach on the Gulf front add materially to the complexity of this problem. Undoubtedly there is a reduction in stage as the waters pour across barrier islands and the harbor entrance. However, the bay surface is also subject to the wind forces and further setup occurs against the bayshores. In the Galveston area, use was made of the records of the 1900 and 1915 storm surges. Based on these data, it has been estimated that the design storm surge at Texas City would be at the same height as the storm surge in front of Galveston or 15 feet. There would be a slight time lag in occurrence of the peak tide at Texas City, but it would be short.

The design storm hydrograph at Texas City, shown on figure 5 was developed from consideration of actual hydrographs of storms of record. The peak of 15 feet m.s.l. for the design storm compares with 14.5 feet for the 1900 storm and 12.7 feet for the 1915 storm. The 1961 storm which crossed the Texas coast at Matagorda Bay 110 miles from Galveston, generated crest elevations of 9.0 feet in the Gulf at Galveston; 9.7 feet in Galveston Bay in front of Texas City and 11.7 feet in Texas City. The hurricane of September 11, 1961 was particularly severe because of the long duration of the extreme high tides. At Freeport a tide in excess of 10 feet was experienced for approximately 14 hours. This duration is much greater than that shown by the design storm hydrograph. The available records of hurricane tides on the Texas coast show no other instance of duration of maximum or near maximum storm tide that even approached the 14 hours of the September 1961 storm. The recurrence interval of this phenomenum is believed to be greater than 100 years.

WAVE CHARACTERISTICS

As shown on figure 2, the proposed protective structures will enclos the city of Texas City and part of the city of LaMarque. There are nine reaches of the structure that have distinct differences in orientation an that are affected by waves from different directions and across different fetch lengths. Galveston Island and Bolivar Peninsula afford considerabl protection to Texas City from large waves from the Gulf of Mexico and it is considered that the critical waves for design of the structures would be those generated in Galveston Bay during a design storm. The size and direction of approach of the waves at Texas City depend upon the time position of the storm, the depth of water including natural depths and storm surge, the windspeed and the duration and direction of approach of the storm.

For analysis of wind speed and water level conditions at Texas City the design hurricane wind field was moved in from the Gulf of Mexico on a path normal to the coast about 15 nautical miles southwest of Galveston. A time history of the wind and tide data was computed for the Texas City area. The results are shown in table 1.

TABLE 1

TIME HISTORY - DESIGN HURRICANE
AT TEXAS CITY

Time in hours(1)	Distance storm center from shore	Computed storm surge in feet	Average storm surge in feet	Wind direction and speed mph(2)	Average wind direction and speed mph (2)
9.0	56	4.3		39 NE	
			5.8		42 NE
10.0	44	7.2		45 NE	
			8.8		55 NE
11.0	31	10.5		65 NE	
			11.7		66 NE
12.0	18	12.9		67 ENE	
			13.6		76 E
12.9	6	14.4		85 E	
			14.7		90 ESE
13.4	0	15.0		95 ESE	
			14.7		97 ESE
13.9	6 (3)	14.4		99 ESE	
			13.6		90 SE
15.0	20 (3)	12.8		80 S	
			11.4		75 S
16.0	33 (3)	10.0		70 S	
			8.3		
17.0	46 (3)	6.6			

(1) Zero on time scale is start of water surface rise at shore in response to storm.
(2) Estimated maximum wind speeds at Texas City.
(3) Distance is inland from shore.

The data shown in table 1 are for a given storm moving on a given path. However, many variations can occur in the hurricane isovel pattern and in the path of the hurricane. The storm wind pattern was therefore rotated within the 150 degree limits shown in Weather Bureau Memorandum HUR 7-45A; that is 100 degrees counter-clockwise and 50 degrees clockwise. The rotations were made to obtain the most severe wind and tide conditions for each of the nine reaches of the protective structures. The isovel pattern of the design storm shown on figure 3 was used in this study.

Trial computations of wave heights along the several reaches of the protective levees at Texas City resulted in the conclusion that the maximum wave that could be generated in Galveston Bay during a severe hurricane would be limited by the water depth and that the fetch length would not be critical. The following criteria were used for wave computations:

a. The depth used was the average depth over a five-mile reach extending out from the structure.

b. The storm tide elevation was the average elevation during a period from 30 minutes before the peak tide to 30 minutes after the peak.

c. The wind speeds of the design storm were averaged along the fetch line for each reach and adjusted for the angle with the fetch line to determine the component normal to the structure.

The wave characteristics along each fetch line for the critical location of the storm tide and wind pattern were computed in accordance with the procedures set forth in Technical Report No. 4 of the Beach Erosion Board(6). The wave characteristics for fetch line A were determined as follows:

Wind velocity, U = 82 miles an hour or 120.5 feet per second

Average depth, d = 18 feet

Wind fetch length, f = 7 miles

H_s, T_s, and L_s are the height, period and length of the shallow water significant wave

H_o, T_o, and L_o are the height, period and length of the equivalent deep water wave

$$\frac{gd}{U^2} = \frac{32.2 \times 18.0}{(120.5)^2} = 0.04$$

$$\frac{gf}{U^2} = \frac{32.2 \times 7.0 \times 5280}{(120.5)^2} = 82.0$$

With these two arguments, the graph on figure 15C of Technical Memorandum No. 4 (6) gives $\frac{gH_s}{U^2} = 1.48 \times 10^{-2}$

or

H_s, the significant wave height = $\frac{1.48 \times 10^{-2} \times 120.5^2}{32.2}$ = 6.7 feet

T_s, the significant wave period = $2.12 \sqrt{6.7}$ = 5.5 seconds

L_o, significant wave length = $5.12 \times (5.5)^2$ = 155 feet

$d/L_o = \frac{18.0}{155} = 0.1160$

With the argument d/L_o the following relations are taken from table D-1 in Technical Report No. 4 (6).

$H_s/H_o = 0.9223$

$d/L_s = 0.1547$

$H_o = H_s/0.9223 = \frac{6.7}{0.9223}$ = 7.3 feet

$L_s = d/0.1547 = \frac{18}{0.1547}$ = 116 feet

H_{max}, maximum wave height = 1.87 H_o = 13.7 feet

In similar manner the characteristics of waves generated by the hurricane rotated to critical positions on each fetch line, were computed. These data are given in table 2.

TABLE 2

WAVE CHARACTERISTICS

Fetch line on plate 1	Average effective wind vel. (mph)	Wind fetch length (miles)	Average depth of water (feet)	Significant waves in shallow water				Equivalent deepwater wave values				
				H_s (feet)	L_s (feet)	Ratio H_s/L_s	T_s (secs.)	H/H_o (feet)	H_o (feet)	Ratio L/L_o	L_o (feet)	Ratio H_o/L_o
(1)	(2)	(3)	(4)	(5)	(6)	(7)	(8)	(9)	(10)	(11)	(12)	(13)
A	82	7.0	18.0	6.7	116	0.058	5.5	0.92	7.3	0.750	155	0.047
A[1]	82	8.0	12.0	5.0	83	0.060	4.7	0.93	5.4	0.722	115	0.047
B	92	20.0	16.2	6.6	110	0.060	5.4	0.93	7.1	0.727	151	0.047
C	93	10.5	21.5	8.0	138	0.058	6.0	0.92	8.7	0.750	184	0.047
D	92	10.5	21.5	8.0	138	0.058	6.0	0.92	8.7	0.730	184	0.047
E	92	15.0	21.6	8.0	138	0.058	6.0	0.92	8.7	0.750	184	0.047
F	67	20.0	20.6	6.4	118	0.054	5.4	0.91	7.1	0.803	147	0.048
G	83	20.0	19.4	7.0	122	0.057	5.6	0.92	7.6	0.760	161	0.047
H	53	3.0	10.0	3.3	60	0.055	3.9	0.92	3.6	0.789	76	0.047

DESIGN OF HURRICANE FLOOD PROTECTION WORKS ON THE UPPER TEXAS COAST

Protection against the design storm surge and waves would be provided by earth levees and concrete sea walls. Determination of the levee grades and side slopes was based on considerations that the levee should be safe against destruction by design storm waves attacking its exposed face and that it should be of sufficient height to prevent excessive overtopping by storm waves that would endanger the inside slope and cause excessive interior drainage problems. Because of the low probability of occurrence of the design storm, it was considered that in the interest of economy in construction, appreciable damage to the levees during design storm occurrences could be accepted and repaired provided that the integrity of the structure was not endangered. To determine the combination of levee height and side slope that would best meet these conditions, estimates were made of the wave runup and wave overtopping of levees of various side slopes and crest elevations. Each reach of protective structure affected by different wave attack was analyzed individually.

Runup factors developed by Saville, McClendon and Cochran(12) were used to determine wave runup on the levees. Figure 9 in reference (12) is a graph of the runup factor (R/H_o) plotted against wave steepness (H_o/L_o) for embankment slopes varying from 1 on $1\frac{1}{2}$ to 1 on 30. Factors are given for smooth earth embankments and for riprap slopes. The factors are based on model tests made at the Waterways Experiment Station and at the Beach Erosion Board. Examples of the runup factors and runup are shown in the following table 3 which gives the runup of the significant wave for each fetch line under design storm conditions on a smooth embankment with 1 on 6 slope.

TABLE 3

WAVE RUNUP
BY SIGNIFICANT WAVE

Wave characteristics			Runup on smooth 1 on 6 slope		
Fetch line (1)	H_o (feet) (1)	Ratio H_o/L_o (1)	Runup factor R/H_o(2)	Runup R (feet)	Maximum elevation (feet msl)(3)
A	7.3	0.047	0.87	6.4	21.4
A^1	5.4	0.047	0.87	4.7	19.7
B	7.1	0.047	0.87	6.2	21.2
C	8.7	0.047	0.87	7.6	22.6
D	8.7	0.047	0.87	7.6	22.6
E	8.7	0.047	0.87	7.6	22.6
F	7.1	0.048	0.87	6.2	21.2
G	7.6	0.047	0.87	6.6	21.6
H	3.6	0.047	0.87	3.1	18.1

(1) Wave data from table 2.
(2) From figure 9 of reference (12).
(3) 15-foot storm tide surge plus wave runup.

The rates and volume of overtopping of levees that would occur during a design hurricane were estimated using diagrams and graphs developed by A. L. Cochran for use in the design of storm protection at Texas City. The diagrams by Cochran are based on model tests of wave overtopping by Saville and reports of the Beach Erosion Board on model tests. The procedures used by Cochran are presented in an unpublished memorandum dated 15 January 1962. The rates and volumes of overtopping of levees of various slopes and grades for the design hurricane surge and waves at Texas City are shown in the following table 4.

TABLE 4

SUMMARY OF WAVE-OVERTOPPING VOLUMES
DURING ENTIRE DESIGN HURRICANE

Levee slope (water side)	Volumes corresponding to various levee grades (crests), elev. above MSL			
	Grade 24.6	Grade 22.6	Grade 20.6	Grade 19.6
Part (a) volumes in cubic feet per foot levee length				
Vertical wall	3,640	6,800	14,300	20,900
Smooth 1:3	8,570	15,700	27,700	35,100
Smooth 1:4	1,440	4,932	12,900	18,720
Smooth 1:6	0	540	1,980	5,480
Smooth 1:8	0	0	72	504
Part (b) volumes in acre feet per mile levee length				
Vertical wall	441	824	1,730	2,530
Smooth 1:3	1,040	1,900	3,370	4,250
Smooth 1:4	174	597	1,560	2,270
Smooth 1:6	0	65	240	664
Smooth 1:8	0	0	9	61

Examination of the results of Cochran's study, shown in table 4, and the data on wave runup, shown in table 3, show that levee grades sufficiently high to prevent overtopping by the significant wave would prevent all but a comparatively small volume of all overtopping. Since about 14 percent of waves in a wave spectrum exceed the significant wave in height, some overtopping of the levee would occur during the design hurricane. For example, table 3 shows that along fetch line D at the peak of the storm surge and wind, the significant wave would run up a 1 on 6 slope to an elevation of 22.6 feet above mean sea level. As shown in table 4, waves greater than the significant wave during the passage of the design hurricane would produce about 540 cubic feet of overtopping per foot of length of levee, or 65 acre-feet per mile on a levee to 22.6 feet grade with smooth 1 on 6 slope. The overtopping estimated by Cochran would occur over a period of about three hours and the peak rate at the height of the storm would be about 1 cubic foot per second, per foot of levee. This rate and duration of overtopping would not endanger the interior levee slope, and would not cause excessive interior ponding.

Accordingly, levee grades and slopes were selected on the basis that the levees would not be overtopped by the significant wave. A comparison was made of the cost of levees of various side slopes to grades that would prevent overtopping by the significant wave. Estimates were made for levees with side slopes ranging from 1 on 3 to 1 on 10 with both smooth surfaces and riprap protected surfaces. From this analysis, it was found that a levee with a slope of 1 on 6 on the waterside, 1 on 3 on the land side with a turfed face and 24-foot crown would be the most economical levee section. The grades of the different reaches, as shown in table 3, vary from 18.1 feet to 22.6 feet above mean sea level. The levee on higher ground elevations and not exposed to wave attack would have grades of 15 feet above mean sea level.

Divergence from the minimum section determined in the manner discussed above was found necessary in the reach along the bay side of Texas City and in the reach across the entrance to Moses Lake where the foundation conditions dictate a greater base width. The foundation conditions require a levee with a berm width of 50 feet at an elevation of 15 feet above mean sea level. Where reaches of the levee extend in open water of Galveston Bay, the toe of the levee would be protected by riprap to an elevation of 5 feet above mean sea level to prevent erosion under normal tide and wave conditions. The wave runup on the composite section was computed and it was found that the runup from the significant wave would be somewhat less than on the uniform slope section and that the crest elevation could be reduced. In two short reaches through the developed sections of Texas City it will be necessary to construct vertical concrete walls.

INTERIOR DRAINAGE

The high tides accompanying a hurricane will block all gravity drainage from the area behind the protective structures. Measures must be provided to prevent undue damage from the ponding of the runoff from rainfall behind the protective structures and from the wave overtopping of the levees that would occur during the storm. The criteria tentatively considered as basis for design of the interior drainage system would provide the following drainage facilities:

a. Gravity drainage outlets adequate to discharge runoff from interior rainfall of 14 inches in 24 hours under normal tide conditions without ponding to damaging stages. This rainfall has an estimated all season frequency of occurrence of once in about 50 years.

b. Pumping capacity adequate to remove the runoff from a rainfall of 9 inches in 24 hours plus the wave overtopping with all gravity outlets blocked by the storm tide. This rainfall has an estimated frequency of occurrence under all conditions of once in about 7 years, and a frequency coincident with tides of 2 feet or more, that would block gravity drainage, of once in 30 years.

The combined discharge capacity of gravity outlets and pumps would remove runoff from a rainfall of 23 inches in 24 hours under normal tide conditions, which is equal to the rainfall of a standard project storm.

The area enclosed by the protection system drains to three separate outlets through the levee. Two small areas on the south side of the city, with contributing drainage areas of 4.52 and 4.64 square miles, drain southward into Galveston Bay; while all of the north portion of the city, with a contributing drainage area of 32.30 square miles, drains northward into Moses Lake. In the two smaller areas, pumping capacity of about 700,000 gallons a minute was found necessary in order to limit ponding to non-damaging stages from the runoff from rainfall of 9 inches in 24 hours plus wave overtopping, when high tide blocks gravity drainage.

In the Moses Lake ponding area, it was found that the interior runoff and wave overtopping could be ponded at low-damage levels and pumps would not be required. If the outlets were closed when the rising exterior tide reached 2 feet and opened as soon as the exterior tide fell below the interior water level, the runoff from a rainfall of 14 inches would pond to an elevation of 5.46 feet and the wave overtopping of about 500 acre feet would increase the ponding about one-fourth foot, to 5.71 feet above mean sea level. With the gravity outlets open, the runoff from a rainfall of 17 inches would pond to an elevation of 3.67 feet with an external tide of 0.0 mean sea level, and to 5.02 feet with an external tide of 2.0 feet mean sea level. Ponding to these elevations would not cause excessive damages and would be permissible in the Moses Lake area.

ACKNOWLEDGMENT

The studies described in this paper and the resulting data presented herein, were obtained from studies conducted under the public works program of the United States Army Corps of Engineers. The permission granted by the Chief of Engineers to publish this information is appreciated.

REFERENCES

1. Davis, A. B. History of the Galveston Seawall; Proceedings Second Coastal Engineering Conference (1952).

2. Graham, H. E. and Nunn,Dwight E. Meteorological Considerations Pertinent to Standard Project Hurricane, Atlantic and Gulf Coasts of the United States; National Hurricane Research Project, Report No. 33 (1959).

3. U. S. Weather Bureau Memorandum HUR 7-45.

4. U. S. Weather Bureau Memorandum HUR 7-47.

5. Reid, R. O. Approximate Response of Water Level on a Sloping Shelf to a Wind Fetch Which Moves Directly Towards Shore; Technical Memorandum No. 83; Beach Erosion Board, Corps of Engineers (1956)

6. Beach Erosion Board Shore Protection Planning and Design; Technical Report No. 4.

7. Bretschneider, C. L. Engineering Aspects of Hurricane Surge; Proceedings of Technical Conference on Hurricane sponsored by American Meteorological Society (1958).

8. Bretschneider, C. L. Hurricane Surge Predictions for Delaware Bay and River; Miscellaneous Paper 4-59, Beach Erosion Board, Corps of Engineers (1959).

9. Beach Erosion Board, Technical Memorandum No. 80; Model Study of Overtopping of Wind-Generated Waves on Levees with Slopes of 1:3 and 1:6, (1956).

10. Waterways Experiment Station, Report N2-449; Wave Run-Up and Overtopping of Levee Sections, Lake Okeechobee (1957).

11. Beach Erosion Board, Technical Memorandum No. 108; Laboratory Data on Wave Run-Up on Roughened and Permeable Slopes (1959).

12. Saville, Thorndike, Jr.; McClendon, E.W. and Cochran, A. L. Freeboard Allowance for Waves in Inland Reservoirs, Proceedings of the American Society of Civil Engineers (1962).

CHAPTER 34

DESIGN OF DEEP DRAFT NAVIGATION CHANNEL FROM GULF OF MEXICO INTO MATAGORDA BAY, TEXAS

E. A. Weiser
Chief, Advance Planning Section
Planning and Reports Branch
Engineering Division
Galveston District

Jack Armstrong
Project Engineer
Matagorda Ship Channel Project
Advance Planning Section
Engineering Division
Galveston District

INTRODUCTION

It was in July 1956 when the senior writer of this paper was requested to prepare a program for investigations and studies required in connection with the proposed deep-draft channel from the Gulf of Mexico to Point Comfort.

During 1938 to 1940, the senior writer had attempted to analyze the available field and model study data which were then available on Galveston Bay in the hope of thus being able to reduce the shoaling in the various deep draft channels in Galveston Bay.

In 1940, the senior writer had been in charge of two field parties one of which measured the flow of water in the Colorado River and the Gulf Intracoastal Waterway near their crossing near Matagorda, Texas. A peak discharge of about 80,000 cubic feet per second was measured in the Colorado River at the Palacios Road bridge, about 15 miles upstream from its mouth during this period. At that time there were no locks nor gates in the Intracoastal Waterway adjacent to the Colorado River. It was found then that about one third of this peak river discharge flowed southwest through the Intracoastal Waterway.

On the basis of the above experience and the information obtained from a review of the Matagorda Ship Channel, Texas, project report (1) and other literature, then, available (2) thru (5) a program was formulated in June 1958 and submitted to the Division Engineer in Dallas with the request that the Office of the Chief of Engineers, the Southwestern Division Engineer Office, the Beach Erosion Board and the Committee on Tidal Hydraulics review the program.

The program was later placed on the agenda of the Committee on Tidal Hydraulics, which submitted a final report in December 1958, recommending a model study and listing the following more important matters to be resolved:

a. The best location of the entrance channel.

b. The distance between jetties.

c. The best route for the channel from the north boundary of the barrier beach to Point Comfort.

d. Whether the channel across the bays should be diked on one side or both sides.

e. The effects of the proposed project on the salinity and temperature regimens of the bay system.

Lack of funds in fiscal year 1959 prevented the Galveston District from actively starting the necessary gathering of basic field data; however, local interests began collecting prototype data, as outlined by the Committee on Tidal Hydraulics, in January 1959. These data included tide records at selected stations and long term current and salinity observations.

In October 1959 the Waterways Experiment Station, after reviewing the prototype measurements made by the local interests, recommended certain modifications of the prototype data collecting program which had been recommended by the Committee on Tidal Hydraulics.

In the meantime, the River and Harbor Act of 3 July 1958 authorized the Matagorda Ship Channel as described in House Document 131, 84th Congress, 1st session, and in (1). The latter document describes the studies made of various plans for a dependable deep draft navigation channel from the Gulf of Mexico to Point Comfort, Texas, via Pass Cavallo, Greens Bayou, mouth of the Colorado River, and an artificial inlet through Matagorda Peninsula.

Interest in a navigable channel from the Gulf of Mexico to Matagorda Bay goes back more than a hundred years. The first Corps of Engineers report on this area was submitted in 1853 (6). There have been more than fifteen reports submitted by the Corps of Engineers on this area. Those pertaining to the authorized project work are listed in the annual report of the Chief of Engineers under "Matagorda Ship Channel, Texas."

DESCRIPTION

PROBLEM AREA

Matagorda Bay is located near the center of the Texas coast. (see figure 1). Under normal conditions, it is connected with the Gulf of Mexico by Pass Cavallo, which is located at the southwest corner of the bay and about 51 miles northeast of Aransas Pass, Texas, and 79 miles southwest of Freeport, Texas. During periods of high tide, water interchange between the Gulf of Mexico and Matagorda Bay also occurs across the many low areas of Matagorda Peninsula. The largest of these, Greens Bayou, is located about 15 miles northeast of Pass Cavallo. The

fresh water runoff and the sediment transported thereby from about 40,000 square miles of area can enter Matagorda Bay.

MATAGORDA BAY

Matagorda Bay is one of the larger bays located along the Texas coast. Including its many arms, it has an area of about 400 square miles (see figure 2). It is separated from the Gulf of Mexico during normal periods by a nearly continuous strip of land about one mile wide known as Matagorda Peninsula, which extends in a northeast to southwest direction a total distance of about 51 miles. Its many arms, which include Lavaca Bay, connect the main area of the bay with the many small fresh water streams which drain into Matagorda Bay.

The main area of Matagorda Bay which is immediately north of Pass Cavallo has a depth of water of about 12 feet over an area about 14 miles long and 13 miles wide. The depth of water in the remainder of the bay, including the arms, drops off rapidly to about 6 feet and then diminishes gradually. Prior to about 1930, the Colorado River emptied into an arm of Matagorda Bay which extended about 37 miles northeast of the 12-foot depth area of the bay. At present, the Colorado River empties into the gulf and the northeast 17 miles of this arm is practically isolated during normal conditions.

PASS CAVALLO

Deep water in Pass Cavallo extends in a general north to south direction for about 6 miles from the 12-foot depth area in Matagorda Bay across the outer bar into the Gulf of Mexico (see figure 3). Depths of 20 to 40 feet extend across a width of about 2,000 feet. The cross-sectional area of the pass is about 100,000 square feet. Records indicate that this deep water channel has been at its present location for at least 200 years. At its junction with the 12-foot depth area in the bay a long narrow bar about 2 miles long separates the main channel into two branch channels, the smaller of the two branch channels continues in a north to south direction and the larger of the branch channels extends in a northeast to southwest direction. The depth of water over the inner bar is only about 3 to 4 feet. The south end of the deep water in Pass Cavallo is separated from deep water in the gulf by a bar over which the water is only about 8 feet deep. The southwest end of Matagorda Peninsula, known as Decros Point, is about 3 miles northeast of the northeast end of Matagorda Island; and a small island known as Pelican Island, is located about midway between Matagorda Island and Matagorda Peninsula. A small channel extends from the deep water channel in a northwest to southeast direction towards the Gulf of Mexico.

MATAGORDA PENINSULA

Matagorda Peninsula (see figure 2), which separates Matagorda Bay from the Gulf of Mexico during normal conditions, varies in elevation

DESIGN OF DEEP DRAFT NAVIGATION CHANNEL FROM GULF OF MEXICO INTO MATAGORDA BAY, TEXAS

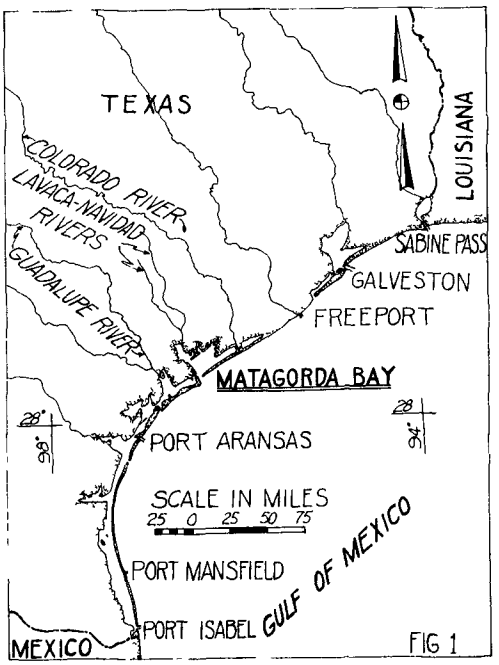

Fig. 1. Texas coast showing Matagorda Bay.

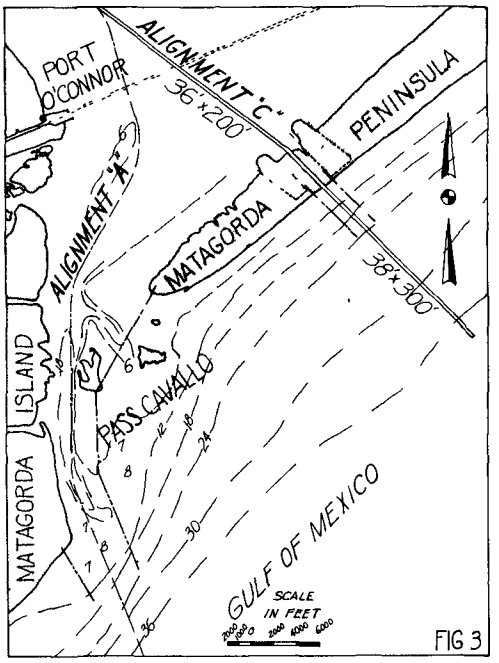

Fig. 3. Pass Cavallo and vicinity showing proposed channel alignment "A" and "C".

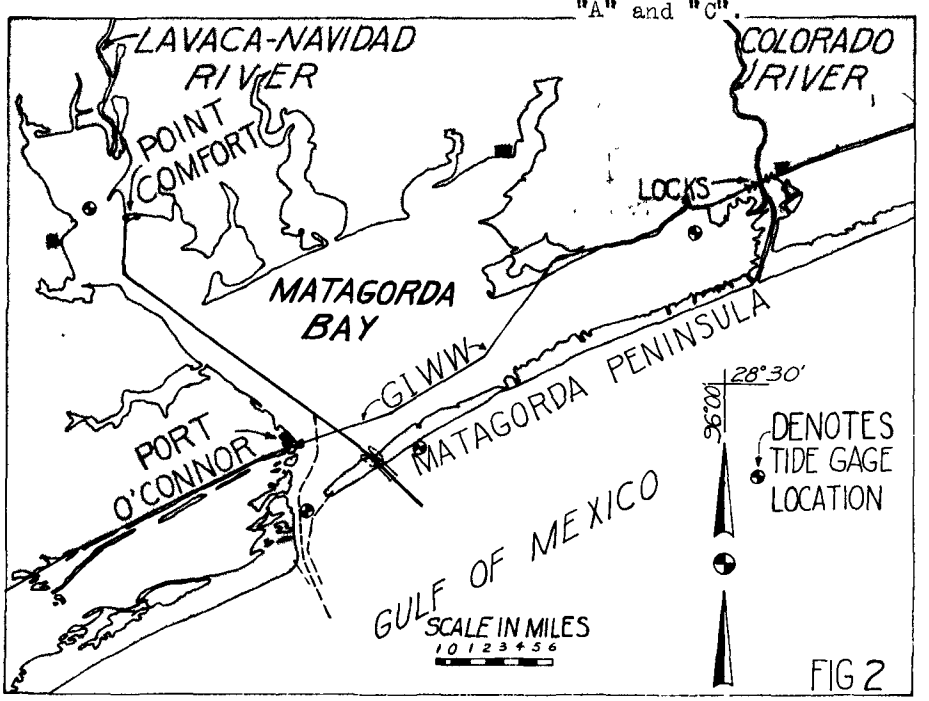

Fig. 2. Matagorda Bay showing the Matagorda deep draft ship channel and the original project plan providing for a channel through the existing pass.

from about 20 feet above mean sea level at the sand dunes to about a foot or two above mean sea level or lower at the various low areas (where high tides pass across the paninsula). During hurricane "Carla" which occurred in September 1961, water from the gulf passed across these low areas and eroded about six channels which persisted for some time after this hurricane. The largest of these channels, known as Greens Bayou, has had sufficient water in it at times to permit navigation by small vessels.

BED MATERIALS

Soil samples were obtained in 6 to 12 feet depth of water in Matagorda Bay along the channel alignment immediately northwest of Matagorda Peninsula, and in 6 to 18 feet depth of water in the Gulf of Mexico on ranges one, two and three miles west of Pass Cavallo. The grain size distribution of some of these samples is shown in the following tabulation:

Bed sample location	Depth	Percent finer than			
		90%	50%	30%	10%
		(Grain size in mm)			
Bay 2000' from shore	6'	0.23	0.074	.008	
Bay 5000' from shore	10	0.14	0.080	0.033	
Bay 8000' from shore	10	0.14	0.059	0.01	
Bay 11,000' from shore	12	0.15	0.080	0.03	
Bay 14,000' from shore	11	0.18	0.074	0.03	
BP 1W Gulf*	6	0.15	0.092		0.05
BP 2W Gulf	6	0.16	0.12		0.055
3W Gulf	6	0.18	0.12		0.09
1W Gulf	12	0.10	0.074		0.054
2W Gulf	12	0.11	0.072		0.044
3W Gulf	12	0.10	0.088		0.028
1W Gulf	18	0.14	0.09		0.05
2W Gulf	18	0.2	0.09		0.05
3W Gulf	18	0.11	0.088		0.048

*BP 1W - denotes bed sample taken in the gulf on beach profile located one mile west of Pass Cavallo.

SLOPE OF SHORE

The available soundings immediately adjacent to the 12-foot depth portion of Matagorda Bay indicate a slope of about 1 on 240 between mean sea level and the 6-foot depth and about 1 on 100 between the 6 and 12-foot depths. Available soundings along the gulf shore indicate a slope of about 1 on 140 between mean sea level and the 12-foot depth, about 1 on 200 between 12 and 18-foot depths, and about 1 on 350 beyond the 18-foot depth. The slopes near Pass Cavallo differ from the above.

TEMPERATURE

The average temperature in the Matagorda Bay area is about 70 degrees, varying from a maximum of about 102 degrees to a minimum of

about 11 degrees. The temperature ranges from an average of 56 degrees in January to 83 degrees in July.

RAINFALL

The average annual rainfall in the Matagorda Bay area is about 41 inches varying from a maximum of about 67 inches, to a minimum of about 13 inches.

WIND

The average wind in the area has a velocity of about 12 miles per hour. During hurricane "Carla" on 11 September 1961, a wind velocity of 153 miles per hour was recorded, and gust velocities up to about 170 miles per hour were estimated (7). Figure 4 shows the percent of time and the direction from which hourly winds of various strength blew at Corpus Christi during 1905 to 1944.

FRESH WATER INFLOW

The principal streams which emptied directly into the Matagorda Bay system prior to about 1930 were the Colorado and Lavaca-Navidad Rivers. Water from the Guadalupe River can enter Matagorda Bay (see figure 1)

Colorado River - The Colorado River drains an area of about 42,000 square miles of which about 30,000 square miles contribute surface runoff. The average annual runoff rate of the Colorado River is about 2,100,000 acre-feet and varies from a maximum of about 6,000,000 acre-feet annually to a minimum of about 770,000 acre-feet annually. From its headwaters to the mouth, the Colorado River is about 900 miles in length over which distance it drops about 3,000 feet. It is estimated that the Colorado River watershed has an annual rate of sediment production of 9,300 acre-feet. Prior to 1929, the Colorado River emptied directly into Matagorda Bay. Between 1925 and 1929 clearing of a log jam in the lower reaches of the river caused an enormous amount of drift and silt to be brought downstream, which deposited in Matagorda Bay and rapidly built a delta across the bay, dividing this arm of the bay into two separate bodies of water. The delta formation caused flooding of the lowlands near the mouth of the river. To relieve this condition a channel was dredged from the original mouth of the river across Matagorda Bay and through Matagorda Peninsula to the Gulf of Mexico. The spoils placed in Matagorda Bay along both sides of the river prevent most of the normal river flows from entering Matagorda Bay directly. During periods of high water in the Colorado River, fresh water can flow across the low areas of ground into Matagorda Bay.

Lavaca River - The Lavaca River is now the only river emptying directly into the Matagorda Bay system. It actually empties into Lavaca Bay, an arm of Matagorda Bay, at a point about 15 miles northwest of the 12-foot depth area of the bay. The Lavaca River, including its major tributary, the Navidad River, drains an area of about 2,500 square miles. The average annual runoff rate of the Lavaca River is about 525,000 acre-feet and varies from a maximum of about 1,770,000 acre-feet annually to a minimum of about 23,400 acre-feet annually. From

its headwaters to its mouth, the Lavaca River is about 112 miles in length over which distance it drops about 350 feet. It is estimated that the Lavaca-Navidad Rivers watersheds have an annual rate of sediment production of 625 acrefeet.

Other drainage - It is estimated that the average annual fresh water inflow into Matagorda Bay from the many small creeks emptying into the bay which drain a total of about 1,700 square miles of area is about 450,000 acre-feet.

Total drainage - The average total annual fresh water inflow into Matagorda Bay, exclusive of the flow from the Colorado River, is about 1,850,000 acre-feet, which includes about 875,000 acre-feet of rainfall on the bay system.

SEDIMENT TRANSPORTATION BY FRESH WATER

Sediment deposition rates as measured at various reservoirs were found to vary with the type of land resource and the size of the drainage area (8). The major land resource area of the Colorado River watershed is the Edwards Plateau which covers 13,500 square miles. The High Plains and the Rolling Plains resource areas cover 9,800 and 8,200 square miles respectively (8). The annual sediment production rates are low in the Edwards Plateau and in the High Plains areas. Annual sediment production rates are moderate in the Rolling Plains area. There are 1,300 square miles of Blackland Prairies and 1,250 square miles of West Cross Timbers, in the Colorado River watershed, in which the sediment production rates are high. Sediment from the West Cross Timbers consists of sand which usually is deposited close to its origin. The Blackland Prairies contributes from 1.5 to 2.5 acre-feet of sediment per square mile of area, part of which finds its way to the gulf. The present annual sediment production rate of the Colorado River watershed above Austin, which has a contributing drainage area of about 26,000 square miles is only 0.02 acre-foot per square mile. At Columbus, above which the contributing drainage area is about 29,100 square miles which include Blackland Prairies, the annual sediment production rate is 0.31 acre-foot per square mile.

A survey made in 1941 of Lake Buchanan, above which the watershed drainage area is about 21,000 square miles, indicated an annual rate of sediment production of 0.21 acre-foot per square mile.

There are three types of land resource areas in the Lavaca River watershed. There are 916 square miles of Blackland Prairies, 866 square miles of Coast Prairie, and 693 square miles of East Texas Timberlands. The estimated annual sediment production rate at the mouth of the Lavaca River is 0.25 acre-foot per square mile.

It is possible for sediment from the Guadalupe River to enter Matagorda Bay through the Gulf Intracoastal Waterway. The northeast edge of San Antonio Bay, into which the Guadalupe River empties, is only about 20 miles by the GIWW from Pass Cavallo. The Guadalupe River watershed has a total area of about 6,000 square miles, of which about 2,200 square miles are Edwards Plateau, about 1,700 square miles are

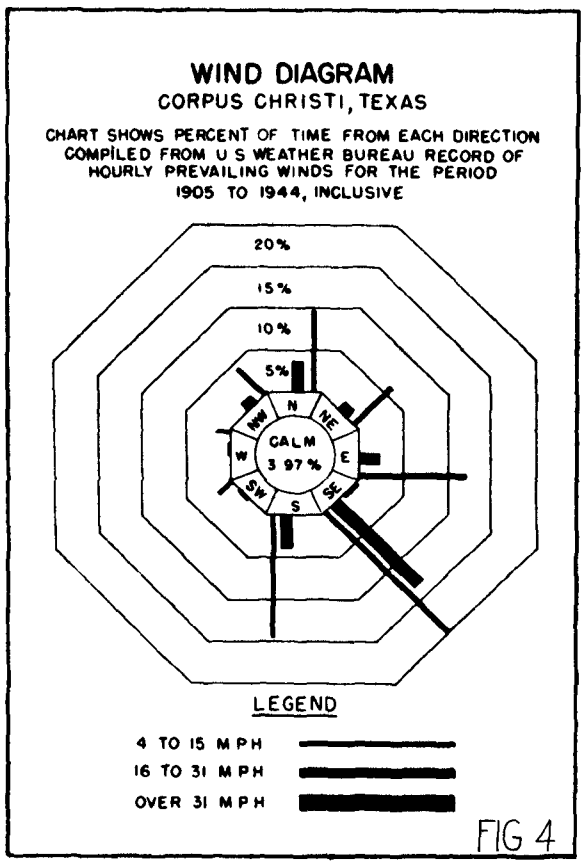

Fig. 4. Wind diagram based on hourly prevailing winds at Corpus Christi, Texas, for the period 1905 to 1944, inclusive.

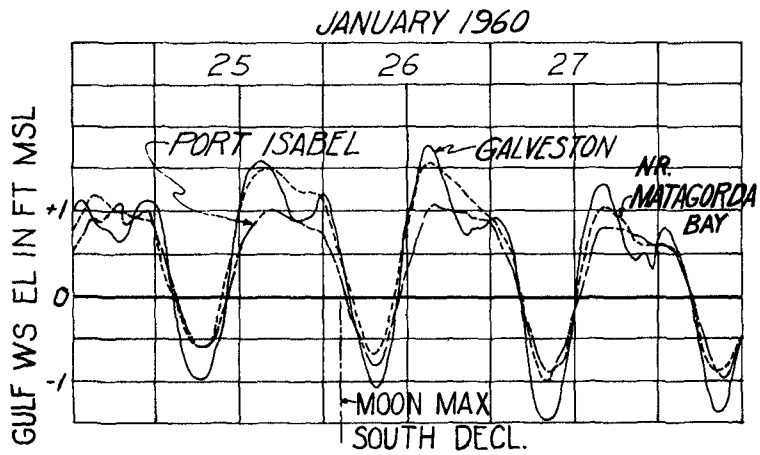

Fig. 5. Variations in the water surface elevation of the Gulf of Mexico at Port Isabel, near Matagorda Bay and at Galveston during 25 through 27 January 1960, when moon was at maximum south declination.

Blackland Prairies, about 1,100 square miles are East Texas Timberlands, about 700 square miles are Rio Grande Plain, and about 300 square miles are Coast Prairie. The Guadalupe River watershed above Victoria, which has an area of about 5,300 square miles, has an estimated annual rate of sediment production of 0.11 acre-foot per square mile.

The annual sediment production rate of the area drained by the small creeks is about 0.23 acre-foot per square mile (9).

TIDES

The movement of the earth in relation to the moon, sun and planets causes the water in the Gulf of Mexico to move, producing a variation in the water surface elevation in the gulf and thus causing an exchange of water between the gulf and Matagorda Bay. The position of the moon in relation to the earth appears to be the major influence on the gulf water.

Observations made along the gulf shore near Pass Cavallo, using a pressure type gage, indicated a 24.84-hour variation in water surface elevation of about 2 feet during the period 25 to 27 January 1960, when the moon was near its maximum south declination. The 12.42-hour variation in water surface of the gulf during 3 to 5 September 1959, when the moon was over the earth's equator, was about 0.7 foot.

The above water surface variations were slightly less than those observed at Galveston where the diurnal tide variation was about 2.5 feet and the semidiurnal tide variation was about one foot. Figures 5 and 6 show the diurnal and semidiurnal water surface variations as observed in the gulf outside of Matagorda Bay, at Glaveston, and at Port Isabel. The tide gage at Port Isabel is located about 5 miles from the gulf in the Port Isabel Turning Basin.

Tide gages were installed at various points in Matagorda Bay to determine the variation in water surface elevation in the bay at these points. The locations of some of these gages are shown on figure 2. Figures 7 and 8 show the actual observed water surface variation at these locations during a period when the moon was near its maximum declination and a period when the moon was near the earth's equator. Note that the variation in the water surface elevation in the bay generally diminishes with the distance of the area from Pass Cavallo. The area in the vicinity of Port O'Connor appears to be an exception to this rule.

TIDAL CURRENTS

Current measurements made on a range across Pass Cavallo on 15 April 1959 indicated flow from the gulf into Matagorda Bay for a period of about 12 hours. During this period a total of about 200,000 acre feet of water entered Matagorda Bay through Pass Cavallo. Figure 9 shows a

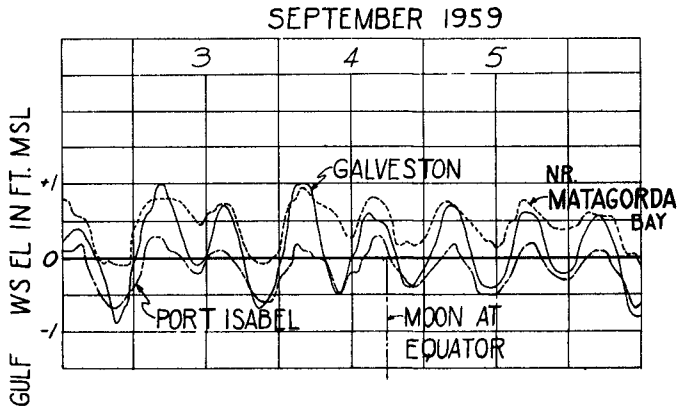

Fig. 6. Variations in the water surface elevation of the Gulf of Mexico at Port Isabel, near Matagorda Bay, and at Galveston during 3 through 5 September 1959, when moon was over earth' equator.

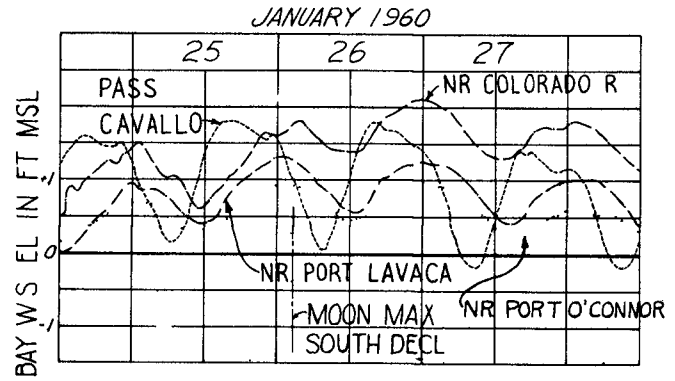

Fig. 7. Variations in the water surface elevation of Matagorda Bay during 25 through 27 January 1960, when moon was at maximum south declination.

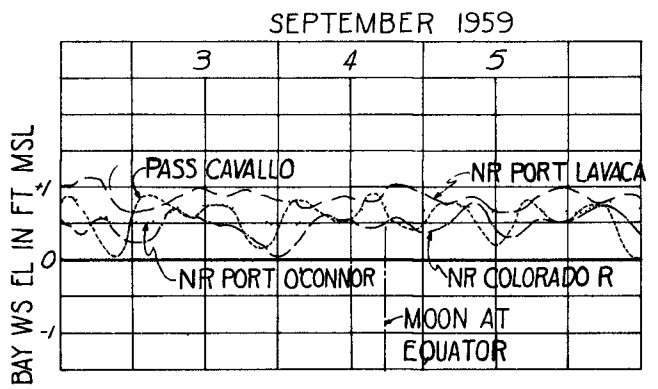

Fig. 8. Variations in the water surface elevation of Matagorda Bay during 3 through 5 September 1959, when moon was over earth's equator.

cross section of Pass Cavallo at this range and the velocities observed at one of the six points where current measurements were made.

SEDIMENT TRANSPORTATION NEAR COAST

The movement of the gulf water, particularly along the shore where the depth of water is less than about 6 feet causes the bed materials to move. Also, there is normally some sediment suspended in the gulf water near the shore. Samples of water taken from the gulf on 29 June and 17 August 1960 contained 50 and 60 parts per million by weight of suspended materials respectively. Bed samples taken near the water's edge and at 6, 12, and 18-foot depths along three ranges immediately west of Pass Cavallo in July 1960 consisted of grains varying in median diameter from about 0.135 millimeter to 0.072 millimeter. The amount of movement of sediment along the gulf coast in the vicinity of Matagorda Bay is not known, however, the information obtained by the New Orleans District of the Corps of Engineers by use of test pits in the vicinity of Chandeleur Sound (9) is probably indicative of the size of this movement.

Test pits near coast - Five test pits were dug, three in 8 to 15 feet of water in Chandeleur Sound and two in 13 and 16 feet of water in the gulf northeast of the mouth of the Mississippi River. Each pit was about 100 feet wide by 500 feet long with bottom at 50 feet below mean low gulf. Soundings were obtained at various intervals of time to determine the rate of sediment deposition in these pits. Soundings taken from 31 to 60 days after completion of the pits indicated a rate of shoaling varying from a maximum of about 292 cubic yards per foot of length of pit per year to a minimum of about 34 cubic yards per foot of length of pit per year. The following tabulation shows the location, depth of water and the median size of initially deposited materials in each of the five pits; and also shows the top width, the original capacity in cubic yards of the center 300 feet of pit, and the initial shoaling rate per annum per foot of length of pit based on the first two sets of soundings obtained after completion of the pits. The number of days between soundings at each pit are indicated.

TEST PIT SHOALING

Pit(1)	Location	Natural depth of water (ft)	Median size of deposited mtl. (mm)	Width top (ft.)	Initial capacity of central 300 ft. of pit(cy)	Initial rate shoaling (cu.yds/ lin.ft/yr)	Interval (days)
A	Gulf	13	0.150	250	32,150	292	31
B	Gulf	16	0.080	230	27,040	286	40
C	Sound	11	0.035	205	38,500	34	59
D	Sound	8	0.030	214	47,060	52	60
E	Sound	15	0.009	180	29,360	34	57

(1) Pit dimensions: approximately 30' x 100' x 500', with 1 on 3 side slopes.

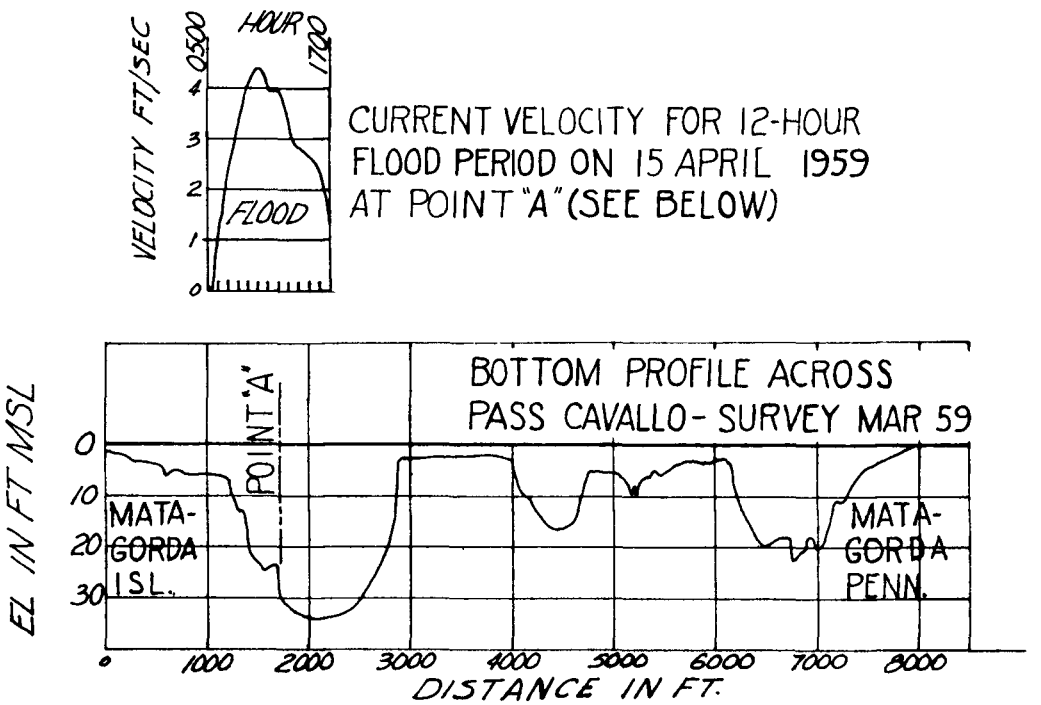

Fig. 9. Variation in velocity of water flowing through Pass Cavallo during 12-hour flood period of 15 April 1959; and cross section of Pass Cavallo showing location of current observation.

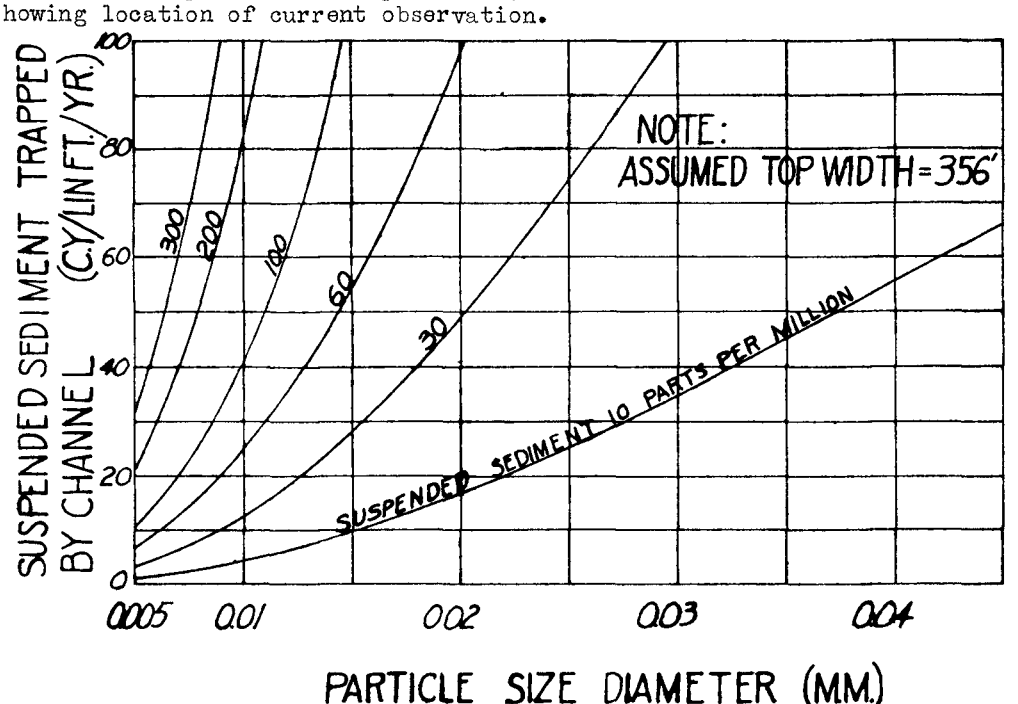

Fig. 10. Volume of suspended sediment which can be trapped by a pit or channel with top width of 356 feet.

Suspended load captured by pits - It is possible to estimate roughly that part of the deposition observed in the test pits which resulted from capture of suspended sediment. The rates at which particles of various size and specific gravity fall in water of a given temperature have been determined (10). These falling velocities of particles are based on ideal laboratory conditions, which exclude convection currents, turbulence and wind action on the surface of the water. Based on purely ideal conditions the rate at which various particles will be trapped during the crossing of the test pits is found to vary directly with (1) the concentration of suspended sediment in the water; (2) the rate of falling of the suspended material in water at a given temperature; and (3) the top width of the channel across which the suspended sediment is being transported. Based on the above, the volume of suspended sediment in cubic yards which can be trapped annually per foot length of pit (or channel) is equal to $2.262\ CV_f\ W$, where C equals the concentration of suspended sediment in parts per million by weight, V_f equals the falling velocity of the suspended particles in feet per second and W equals the top width of the pit or channel in feet. This equation is based on a weight of water equal to 64 pounds per cubic foot and a weight of trapped sediment of 33 pounds per cubic foot. Figure 10 illustrates graphically the above equation for a top width of test pit or channel of 356 feet.

The observed concentration of suspended materials in the vicinity of the test pits was about 50 parts per million by weight. The estimated rate of shoaling due to capture of suspended sediment, based on a grain size of 0.01 millimeter which has a falling velocity through water of 50° F of 0.154 millimeter, or 5.05×10^{-4} feet, per second, varies with the top width of the pit from about 10 to 14 cubic yards per foot of length of pit per year. These rates represent the maximum possible under ideal conditions based on a grain size of 0.01 millimeter. Any turbulence would tend to reduce these rates; and a larger grain size would increase these rates.

Bed movement near coast - Based on the above it was possible to estimate the rate of bed movement into the test pits, which was assumed to be equal to the total rate of sediment capture minus the rate of deposition from suspension. To permit comparison of the rates of bed movement at the different test pits it was assumed that the bed movement takes place in the form of a ribbon having a thickness equal to the diameter of the median bed particle. It is thus possible to represent the rate of bed movement by the velocity at which a ribbon of bed particles, as described above, must advance to obtain the determined volume of bed movement. The following tabulation shows the estimated velocity of the bed movement at the five test pits.

ESTIMATED VELOCITY OF BED MOVEMENT

Pit	Initial rate of shoaling (cu.yds./ lin.ft./ year)	Top width of pit (ft.)	Est. rate of suspended sediment capture (cu.yds./ lin.ft./ year)	Rate of bed movement trapped (cu.yds./ lin.ft./ year)	Median size of deposited material (mm)	Est. velocity* of bed movement (ft/sec.)
A	292	250	14	278	0.150	0.48
B	286	230	13	273	0.080	0.89
C	34	205	12	22	0.035	0.16
D	52	214	12	40	0.030	0.35
E	34	180	10	24	0.009	0.70

* Current velocities observed in Chandeleur Sound at 13-foot depth varied from 0.34 ft/sec during 72 percent of the time to 1.02 ft/sec during 0.28 percent of the time. Velocities at 9-foot depth varied from 0.34 ft/sec during 72 percent of the time to 1.19 ft/sec during 0.39 percent of the time.

Sediment capture by jetties - There have been no test pits excavated in the Galveston District; however, there have been completed recently two jetties near Raymondville. These jetties are about 35 miles north of Port Isabel (see figure 1). Hydrographic surveys made in November 1960 and in August 1961 south of the south jetty indicate a deposition behind the south jetty between the 2-foot contour and the -4.5-foot contour of the November 1960 survey of about 48,500 cubic yards of sediment, which is equivalent to about 432 cubic yards per foot per year.

Inasmuch as sediment can be brought into the test pits from both sides, whereas sediment was brought into the area behind the jetties from only one side, it would be expected that the rate of sediment capture by the jetties should be less than by test pits if other conditions were the same. The large rate of deposition behind the south jetty near Raymondville may be due to the shallow depth of water in which the deposition was observed and the large component of the prevailing wind parallel to the gulf shore near Raymondville during the period of observation.

ECONOMIC DEVELOPMENT

The towns of Port O'Connor, Port Lavaca, Point Comfort, Palacios, and Matagorda are located along Matagorda Bay. All of Matagorda, Jackson, and Calhoun Counties; and adjacent parts of Wharton, Victoria, and Refugio Counties would receive the most benefit from a deep draft channel from the Gulf of Mexico to Point Comfort. The total area of the above counties and partial counties is about 4,000 square miles. This area has a population in excess of 100,000, of which about 80,000 is urban. The city of Victoria in Victoria County is the largest in the area; and has a population of about 33,000.

The 4,000-square mile area is largely an agricultural region producing principally cotton, corn, grain, sorghums, rice, hay and vegetables. Several producing gas wells are located in Matagorda Bay and there are numerous active oil and gas wells throughout the area. Because of the availability of natural gas at seaside, the Aluminum Company of America constructed a giant plant at Point Comfort. There is a Union Carbide plant located at Seadrift, which is about 18 miles west of Port O'Connor; and Du Pont plant located at Bloomington, which is about 18 miles west of Port Lavaca. There are oyster beds, shrimp, and fish in Matagorda Bay. According to the Bureau of Commercial Fisheries, the acceptable ranges of salinity are: 10 to 20 parts per thousand for oysters; 10 to 17 parts per thousand for shrimp; and 10 to 25 parts per thousand for 13 of the most important finfishes inhabiting local estuaries. The salinity of Matagorda Bay varies from nearly zero near the mouths of the existing streams to 25 to 32 parts per thousand near Pass Cavallo.

PROBLEM

It is possible on the basis of a thorough knowledge of the forces of nature involved and the best means for controlling these forces (11) to determine which of several or many possible plans would produce the results desired at the least annual costs, in other words, the plan which would provide the greatest benefits at the least cost, including first cost and cost of annual maintenance and operation.

Various public hearings were held in 1949 and 1954 to determine the desires of the local interests. These developed the fact that all of the communities along Matagorda Bay were interested in obtaining a navigable channel from the Gulf of Mexico to their area. Originally, the local interests desired a shallow draft channel. In 1955, the Calhoun County Navigation District requested Federal assistance in the construction of a pass and main channel, 36 feet deep and 200 feet wide, extending from the Gulf of Mexico through Matagorda and Lavaca Bays to a proposed turning basin 36 feet deep and 1,000 feet square at Point Comfort, Texas, with jetties extending into the gulf to protect the pass from shoaling by littoral drift and to afford a reliable outlet to the gulf. In support of this latter request local interests stated that the Aluminum Company of America proposed to construct in Calhoun County adjacent to its existing smelting plant a refining plant for the production of 3,000,000 pounds of aluminum daily, which would require using 3,000 tons of bauxite daily. The bauxite would be imported from the Dominican Republic and Surinam, South America and would be carried by carriers of the Alcoa Steamship Company. Two units of the refining plant were completed in 1959. Bauxite is being shipped to Port Aransas where it is transferred to shallow draft vessels and brought to Point Comfort via an existing shallow draft channel.

Various plans which would provide a navigation channel from the Gulf of Mexico to Point Comfort were investigated. The problem was to determine which of these plans for a deep-draft channel to Point Comfort was the most feasible at the present time.

DESIGN OF DEEP DRAFT NAVIGATION CHANNEL FROM GULF OF MEXICO INTO MATAGORDA BAY, TEXAS

DISCUSSION

The Aluminum Company of America plant at Point Comfort is located about 26 airline miles northwest of the 40-foot depth of water in the Gulf of Mexico. Considering only the aluminum plant, a channel with a nearly straight northwest to southeast alignment extending from deep water in the gulf to the plant would have certain advantages, particularly from the standpoint of time of travel and ease of navigation.

The interchange of water between the gulf and Matagorda Bay takes place through Pass Cavallo. Considering the desirability for a channel to coincide as nearly as practicable with the direction of the predominant water currents, the channel alignment should follow the existing deep water at Pass Cavallo.

A landlocked channel would have certain advantages. There would be no cross currents in a landlocked channel.

It is not too difficult to determine the first cost of a deep draft channel, including the auxiliary works considered necessary to control the velocities and directions of flow in the channel and thereby control the movement of waterborne materials which would otherwise shoal the channel; and the work required to prevent the entrance of wind blown materials. To determine the shoaling which would occur with the various plans of improvement is much more difficult with our present knowledge of the science of tidal hydraulics.

On the basis of the high first cost and the possible adverse effect to existing oyster beds, the plan for a landlocked channel was dropped.

On the basis of first cost, it was evident that the existing shallow draft channel between a point near Port O'Connor and Point Comfort should be utilized as part of the deep-draft channel project. The total length of the existing channel between near Port O'Connor and the proposed turning basin near Point Comfort is about 17 miles, which is less than 0.5 mile longer than the straight line distance. The existing channel is about 12 feet deep and the water depths along the straight line alignment are less than 12 feet.

There remained only to determine the best alignment for the deep-draft channel from opposite Port O'Connor to deep water in the gulf. The distance from opposite Port O'Connor via a straight alignment to deep water in the gulf is about 8.5 miles; and via Pass Cavallo - about 11.0 miles. Based on the latest available data it was estimated that the alignment through Pass Cavallo, which is about 2.5 miles longer than the straight alignment, would require about 2.5 million cubic yards of dredging more than for the straight alignment (about 16.5 vs about 14 million).

It was thought at first that jetties along the alignment through Pass Cavallo could be built at nearly the same cost as those along the straight alignment. This thinking was based on the data which were available in 1955, which showed a maximum depth of water of about 10 feet between the end of Matagorda Peninsula and Pelican Island. It was reasoned that timber sheet piles only 15 feet long could be used

along 17,400 feet of the necessary training works along the east side of Pass Cavallo immediately south of the end of Matagorda Peninsula. It was thought that the littoral drift material being transported along the gulf coast in this area would soon cover these timber piles. The latest thinking is that rubble mound jetties are best suited for the Texas gulf coast, providing sufficient crown width to permit construction and maintenance with vehicles.

In 1959 while making flow measurements near the end of Matagorda Peninsula, it was discovered that the water depth between the peninsula and Pelican Island had increased to about 20 feet.

Near the end of 1959 it was decided to make a model study of the Matagorda Ship Channel problem. A fixed-bed model was built by the Waterways Experiment Station at Vicksburg, Mississippi. It was not considered practicable to build a movable bed model of the entire problem area. Model tests were started on three different alignments. Alignment A as shown on figure 3 is that through Pass Cavallo, which was considered to be the most feasible at first. Alignments B and C are variations of a straight alignment. Alignment B extends in a direction nearly normal to the gulf shore; and alignment C extends along the extension of the existin shallow draft channel between Port O'Connor and Port Lavaca Bay.

The first model tests made showed very little difference in current patterns produced by alignments B and C. It was, therefore, decided to eliminate alignment B and make further model tests only on alignments A and C. Alignment C was preferred to B, because it placed the artificial opening from the bay into the gulf farther from Pass Cavallo and the cross currents.

Tests were made of alignments A and C using the model to try to determine which of these would produce the greater amount of shoaling. Sediment was introduced into the model at both the bay and gulf ends of the entrance channels. It was found, when the sediment was introduced in the bay, that more shoaling occurred in the channel following alignment C than alignment A. When the sediment was introduced in the gulf, the greater amount of shoaling occurred in the channel following alignment A.

The movement of sediment along the gulf shore is probably many times that in the bay areas because air and water movement are generally greater along the gulf shore. Observations made using test pits in Chandeleur Sound and in the gulf immediately outside the sound indicated that much more sediment moves along the gulf shore than in the sound. The actual transport of sediment along various reaches of the gulf shore can be expected to vary with the type of bed materials present, the velocity and direction of the wind in relation to the shore, and the depth of water in the area. An area with little offshore slope and thus with a larger area of shoal water is more conducive to sediment movement than one with a steep offshore slope.

Both plans for the Matagorda Ship Channel, A and C, include jetties to protect the gulf entrance. The sediment moving along the gulf shore would be trapped by the jetties at either location; therefore,

sediment movement along the gulf shore was not a prime consideration in choosing the more feasible of these two plans.

The sediment movement in Matagorda Bay depends on the velocity and direction of tidal and wind produced currents, the depth of water in the bay, and the type of bed material. In a bay it can be expected that suspended sediment brought into it by fresh water streams may play a large role. The amount of sediment moving from the outer bar at Pass Cavallo to the inner bar at this pass may become the important factor.

Under existing conditions, the inner bar at Pass Cavallo has not grown, indicating that a sort of equilibrium exists - as much sediment moves away from the inner bar as moves towards it. As long as existing conditions in the vicinity of Pass Cavallo are not disturbed, it would be reasonable to assume that this near equilibrium would continue. Excavation of a deep draft channel along alignment C may disturb this near equilibrium and cause a movement of sediment into the deep draft channel. If this amount of sediment is found to be very large, say more than about one million cubic yards per year, consideration would need to be given to providing training works along alignment C to reduce the movement of sediment into the channel.

At the same time that model tests were being made, the Galveston District prepared estimates of costs of various plans for a deep draft channel from the gulf to Point Comfort and found that the plan which would provide for alignment C would cost approximately $7,000,000 less than the plan which would provide for alignment A through Pass Cavallo ($25,000,000 vs $32,000,000). Reduced to annual charges on the basis of a 100-year life, the first cost for alignment C is about $205,000 per year less than for alignment A. There are other advantages that alignment C would have over alignment A such as fewer navigation aids and thus a lesser amount required for maintenance and replacement of navigation aids. Also alignment C is about 2.5 miles shorter and straighter - thus would reduce cost of transportation.

It is obvious from the above that alignment C is preferable to alignment A in all respects except possibly cost of annual maintenance.

CONCLUSIONS

The obvious conclusion from the above is that our knowledge, particularly of sediment movement, is not complete enough to enable a determination of the amount of shoaling which will occur under the proposed plan of improvement. Also, it is questionable whether a model study, even using a movable bed model would answer this question on the amount of shoaling.

This points up the fact that the amount of shoaling which can be expected in connection with any navigation improvement in tidal waters is the factor about which our present knowledge is most incomplete.

Test pits, which are one way to obtain more information on this subject, can provide only partial answers to the amount of shoaling which

will actually occur in a channel where currents will be present which can move some of the sediment.

Studies of the tractive forces required to move sediment of various shapes, sizes, and specific gravity would provide more basic information. It is known for instance, that water would at times during the tidal cycle move through the jetty channel of alignment C at velocities of nearly 6 feet per second. Such velocities would produce sufficient tractive forces along the bed of the channel to move a large part if not all of the sediment carried into the channel by cross currents. Beyond the confined reach of entrance channel these velocities become small and would not be capable of moving sediment brought into the channel by cross currents.

A detailed study of the velocities of the water in and adjacent to the proposed improvement, particularly the velocities near the bed, and knowledge of the bed materials and the forces required to move them could perhaps lead to an answer of the question on the amount of shoaling which will occur.

Acknowledgments

The tests described and the resulting data presented herein, unless otherwise noted, were obtained from research conducted by or under the United States Army Corps of Engineers. The permission granted by the Chief of Engineers to publish this information is appreciated.

References

(1) House Document No. 388, 84th Congress, 2d Session, on "Matagorda Ship Channel, Texas". This document does not contain certain appendices and illustrations made in connection with the report of the Galveston District Engineer.

(2) U. S. Corps of Engineers, U. S. Army, Committee on Tidal Hydraulics, Report No. 1, "Evaluation of Present State of Knowledge of Factors Affecting Tidal Hydraulics and Related Phenomena", February 1950.

(3) U. S. Department of Commerce, U. S. C. & G. S., "Manual of Current Observations", Special Publication No. 215, revised 1950.

(4) U. S. Department of Commerce, U S. C. & G. S., "Manual of Tide Observations", Special Publication No. 196, revised 1941.

(5) Caldwell, Joseph M., U. S. Corps of Engineers, Beach Erosion Board, "Research Activities of the Beach Erosion Board", Second Conference on Coastal Engineering, Houston, Texas, November 1951.

(6) Executive document, volume 2, 1853-54, page 561; and page 1256 of the Annual Report of the Chief of Engineers for fiscal year 1880.

(7) U. S. Corps of Engineers, U. S. Army Engineer District, Galveston, Texas. "Report on Hurricane Carla", January 1962.

(8) Texas Board of Water Engineers, "Inventory and Use of Sedimentation Data in Texas", Bulletin No. 5912, January 1959.

(9) U. S. Corps of Engineers, U. S. Army Engineer District, New Orleans, La., "Mississippi River - Gulf Outlet Louisiana", Design Memorandum No. 2, General Design, June 1959.

(10) Steel, Earnest W., "Water Supply and Sewerage", Third Edition, McGraw Hill Book Company, Inc., 1953.

(11) U. S. Corps of Engineers, "Preliminary Engineering Manual Civil Works Construction - Hydraulic Design - Tidal Hydraulics", Part CXVI, Chapter 7, January 1953.

CHAPTER 35

CONTRIBUTION OF MATAGORDA BAY MODEL TO DESIGN OF MATAGORDA BAY DEEP DRAFT NAVIGATION PROJECT

H. J. Rhodes and R. A. Boland

Waterways Experiment Station
Corps of Engineers, Department of the Army
Vicksburg, Mississippi

INTRODUCTION

DESCRIPTION OF PROTOTYPE

The area under discussion in this paper is located on the central Texas coast in the Matagorda Bay area (see Fig 1). Matagorda Bay is one of the larger coastal bays on the Texas coast and is separated from the Gulf of Mexico by a long, narrow barrier beach known as Matagorda Peninsula. The long northeast arm of the bay is divided into two separate bodies of water by the delta of the Colorado River. Natural depths of 11 to 12 feet are available over a large portion of Matagorda Bay. Lavaca and Tres Palacios Bays, arms of Matagorda Bay, have natural depths of 6 to 7 feet.

The Lavaca and Navidad Rivers, which are the two major fresh-water streams emptying into Matagorda Bay, drain a total of 2,500 square miles. They discharge an average of about 525,000 acre feet of water annually into the bay, with a maximum annual discharge of four times the average. Observations of suspended sediment concentrations indicate that these rivers bring an average of about 700,000 cu yds of silt into Matagorda Bay annually. The lower six and one-half miles of the Colorado River, from its crossing of the Gulf Intracoastal Waterway to the Gulf of Mexico, is located across a low delta area in Matagorda Bay. This delta is subject to inundation by floods on the Colorado River, so that a large volume of fresh water may enter Matagorda Bay from this source during flood stages on the Colorado River. The Colorado River is also connected to Matagorda Bay by Tiger Island Cut; however, the fresh water contributed to Matagorda Bay by the Colorado River from this source is unknown.

Matagorda Peninsula is about 50 miles long and has an average width of about 1 mile. The normal erosional process is one of erosion and regression landward of the bay shore. The general elevation of the peninsula is about 4 to 5 feet above mean low tide. Off the west tip of Matagorda Peninsula lies Pass Cavallo. Pass Cavallo is a natural pass between Matagorda Bay and the Gulf of Mexico that has been in its approximate present position for over 200 years. The pass is approximately 1.8 miles wide. The gorge channel, about 2,000 feet wide with depths of 20 to 42 feet between the submerged bars on the gulf and bay side of the pass, lies approximately in a north-south direction

against the northeast end of Matagorda Island. The deepest water over the outer bar is a narrow tortuous channel on the downdrift end of the bar with a controlling depth of about 7 feet. Controlling depths in the channels adjacent to the inner bar are 10 to 11 feet. Navigation through Pass Cavallo has long been considered hazardous because of the shifting channel of shallow depth across the outer bar. In 1948 a controlling depth of about 9 feet was available, but the bar shoaled considerably during the summer of 1949 and navigation was limited to boats drawing less than 6 feet. A channel with controlling depth of 17 feet, width of 135 feet, and length of 3,000 feet was dredged in 1949 across the outer bar as an emergency measure to relieve the restricted navigation conditions. The channel was completed on 9 September 1949, but shoaled to a controlling depth of 10 feet by 2 November 1949, and to a controlling depth of 8 feet in March 1952. Existing information indicates a large littoral drift of sand towards the southwest along the gulf shore of Matagorda Peninsula. The origin of some of the beach material appears to extend at least as far northward as the Brazos River. Under normal conditions, the materials are moved to Pass Cavallo where an expansive shoal area has formed southward from Decros Point at the southwest tip of Matagorda Peninsula. Tide action moves these materials into and out of lower Matagorda Bay.

Congress recently authorized construction of a deep-draft navigation channel from the Gulf of Mexico through Pass Cavallo, or other suitable location, to a turning basin at Point Comfort; consisting of an outer bar and jetty channel, 38 feet deep, 300 feet wide, and about 6 miles long, from the Gulf of Mexico through Pass Cavallo; an inner channel, 36 feet deep, 200 feet wide, and about 22 miles long across Matagorda and Lavaca Bays; a turning basin, 36 feet deep and 1,000 feet square; and dual jetties at the entrance, the southwest jetty extending to the 16-foot depth in the gulf and the northeast jetty extending to the 24-foot depth. It was recommended by the Committee on Tidal Hydraulics that a hydraulic model study be conducted by the Waterways Experiment Station at Vicksburg, Mississippi, to determine the following important features of the project: (a) the best location for the entrance channel, together with such appurtenant structures as may be required in the interests of navigation and maintenance of the entrance; (b) the best route for the channel from the north boundary of the barrier beach to Point Comfort; (c) whether the channel across the bays should be diked on one or both sides; (d) the effects of the deep-draft navigation project on the salinity and hydraulic regimens of the bay system. The model was constructed at the Waterways Experiment Station in June 1960.

This paper covers in a general way the use of a hydraulic model as an aid to design engineers in the design of a deep-draft navigable channel from the Gulf of Mexico across Matagorda and Lavaca Bays. It covers problems subject to model analysis, the type of model used, field data requirements, adjustment and verification of the model, testing of proposed improvement plans, the analysis of test results, and the limitations of the model.

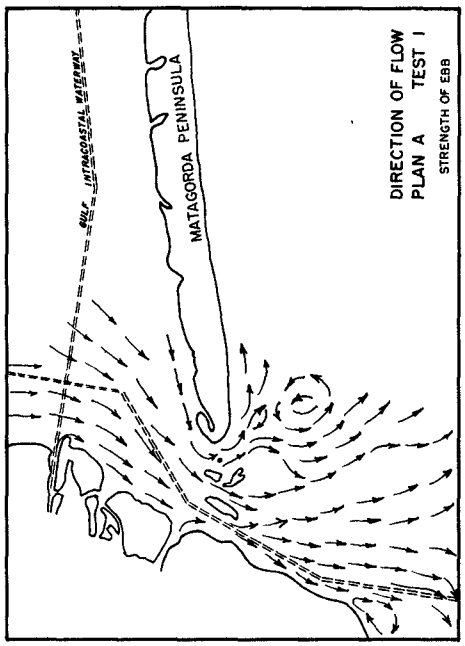

Fig. 2

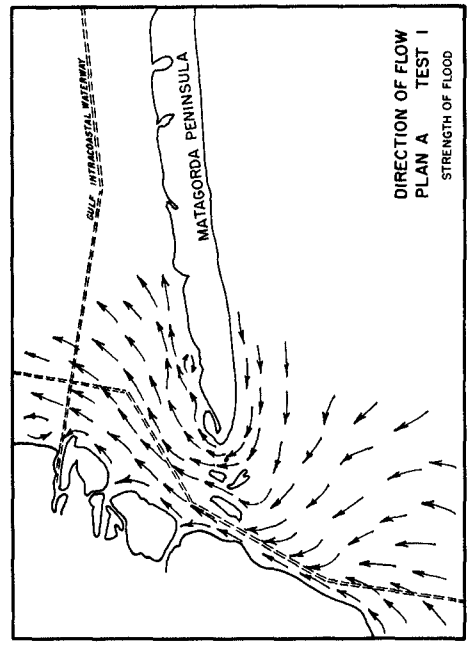

Fig. 3

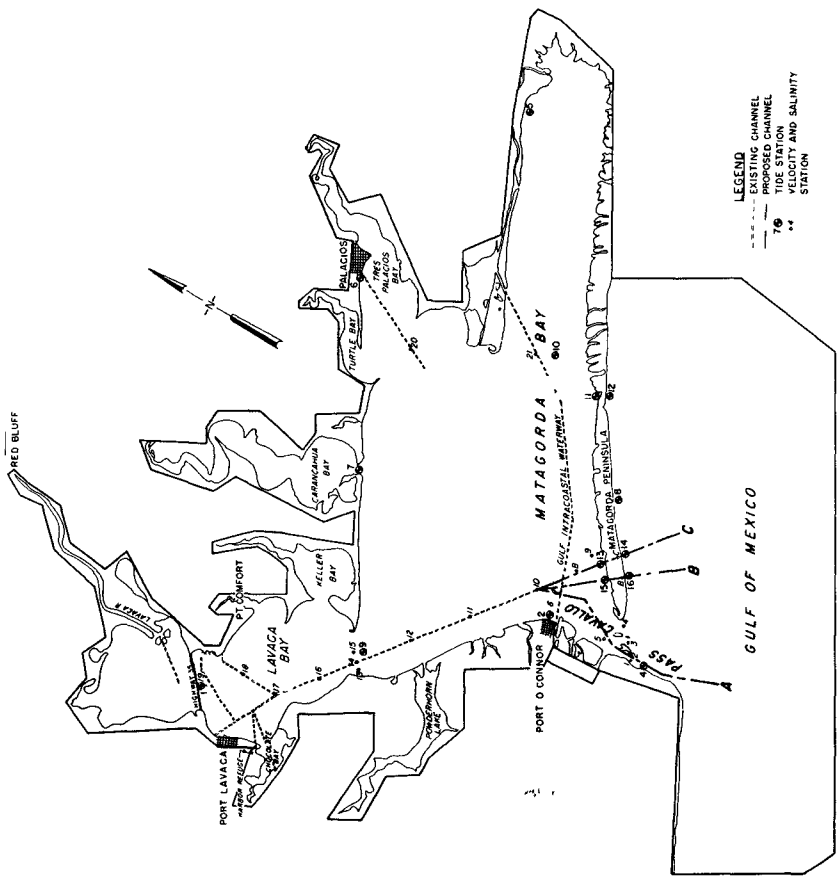

Fig. 1

CONTRIBUTION OF MATAGORDA BAY MODEL TO DESIGN OF MATAGORDA BAY DEEP DRAFT NAVIGATION PROJECT

THE MODEL

DESCRIPTION AND SCALES

The Matagorda Ship Channel model reproduces approximately 800 square miles of prototype area, including all of Matagorda Bay and connecting bay systems from the Colorado River on the east to Espiritu Santo Bay on the west and Lavaca Bay and River to Red Bluff, at the head of the authorized project. A portion of the Gulf of Mexico adjacent to Pass Cavallo is included in the model; this area extends 19 miles to the east and 11 miles to the west of the pass and offshore to about the 70-foot contour of depth in the gulf. The limits of the area reproduced are shown in Fig 1.

The entire bed of the model is molded of concrete to conform to the prototype conditions that existed in 1960. All areas affected by alignments of the proposed ship channel were molded in removable blocks so that desired alterations could be readily made.

The model was equipped with the necessary appurtenances to reproduce and measure all pertinent phenomena such as tidal elevations, salt water concentrations, current velocities, and fresh-water inflow. Apparatus used in connection with the reproduction and measurement of these phenomena included a primary tide generator and recorder, secondary tide generator, fresh-water inflow devices, skimming and measuring weirs, chemical titration equipment, current velocity meters, photographic equipment, and tide gages.

The reproduction of tidal action in the model gulf area was accomplished by means of a primary tide generator located in the model gulf and a secondary tide generator located in Espiritu Santo Bay. The primary tide generator maintained a differential between a pumped inflow of salt water to the model and a gravity outflow of salt water from the model as required to reproduce all characteristics of the prototype tides at the model control stations. The primary tide generator was equipped with a continuous tide recorder so that the accuracy of the model tide reproduction could be checked visually at any time. The secondary tide generator reproduced, in phase, the proper flow conditions in and out of Espiritu Santo Bay.

Constant-head tanks were located at the fresh-water inflows of tributaries emptying into the bay system. Calibrated valves were used on the tanks to obtain precise measurements of the fresh-water inflow values obtained from prototype data.

The mixed salt and fresh water that accumulated in the model gulf had to be removed in order to maintain a constant source salinity. This was accomplished by means of a skimming weir which removed a quantity of mixed water from the surface layer and returned it to the sump where provisions

were made to constantly maintain salinities and levels of salt water. There were provisions in the return line from the model to add additional salt to keep the gulf salinity at the correct level.

Salinity concentrations were determined by chemical titrations with silver nitrate in all cases involving a large number of simultaneous measurements or requiring a high degree of accuracy. Water samples were taken from selected locations in the model by hand, or with a special sampler which would simultaneously draw samples at various desired depths. The samples were then titrated with equipment consisting of a graduated burette for measuring silver nitrate, a selected group of pipettes for measuring the volume of the salinity samples, sample jars, and potassium chromate for use as an end-point indicator in the titration process.

Current-velocity measurements were made in the model with miniature Price-type current meters. The meter cups were about 0.04 ft in diameter, representing 4.0 ft in the prototype. The center of the cups were 0.05 ft from the bottom of the frame, representing 5.0 ft prototype. The meters were calibrated frequently to insure their accuracy and were capable of measuring current velocities as low as about 0.05 ft per sec (0.5 ft per sec prototype).

Permanently mounted point gages were installed on the model at the locations used for collection of field tide data. The model gages were graduated in 0.001 ft (0.1 ft prototype) and were used to measure tidal elevations throughout the model. When necessary, portable gages were used to obtain more detailed tidal data at specific locations.

The model was constructed to linear scale ratios, model to prototype, of 1:1000 horizontally and 1:100 vertically. From these basic ratios, the following scale relations were computed: slope, 10:1; velocity, 1:10; time, 1:100; discharge, 1:1,000,000; volume, 1:100,000,00(The salinity scale ratio required for an investigation of this type is 1:1.

One prototype tidal cycle of 24 hr and 50 min is reproduced in the model in 14.9 min. The model is approximately 200 ft long and 225 ft wide at the widest point, and covers an area of about 24,500 sq ft. It is completely inclosed in a shelter to protect it from the weather and to permit uninterrupted operation.

PROTOTYPE DATA REQUIREMENTS

The accuracy of results from any model study depend to a large extent upon the accuracy and completeness of data obtained from comprehensive prototype investigations. The completeness and accuracy of such prototype studies are most essential, since the model study would unquestionably produce erroneous results if its adjustment and

verification were based upon inaccurate or incomplete field data. It is also essential that adequate field data be available for a proper analysis of the problem before the selection of model scales and design of the model and appurtenances are undertaken.

A field data collection program was set up to insure that all field measurements needed for construction, verification, and operation of the Matagorda Bay Ship Channel model were adequate. Tide gages were located throughout the model limits. Their locations were as follows:

1. Southwest of Colorado River
2. Near mouth of Tres Palacios Bay
3. Near Alcoa Plant site
4. Near Port O'Connor
5. Near northwest end of Espiritu Santo Bay
6. Near Pelican Island
7. Gulf of Mexico

The above recording tide gages were operated for the duration of all other measurements carried out under the program. Other gages in the model area were put in use when the need arose.

Other prototype data needed for the model study were:

1. Current observations at particular ranges and points.
2. Salinity and temperature observations.
3. Fresh water and solids entering Matagorda Bay.
4. Topographic and hydrographic surveys.

VERIFICATION OF MODEL

HYDRAULIC VERIFICATION

The accurate reproduction of hydraulic and salinity phenomena in an estuary model is an important phase in the preparation of the model for its ultimate use in evaluating the effects of proposed improvement works.

It should be emphasized that the worth of any model study is wholly dependent upon the proven ability of the model to produce with a reasonable degree of accuracy the results which can be expected to occur in the prototype under given conditions. It is essential, therefore, before there are undertaken any model tests of proposed plans of improvement with a view to predetermining their effects in the prototype, that the required similitude first be established between the model and prototype and that all scale relationships between the two be determined.

The hydraulic verification was preceded by a series of hydraulic adjustment tests to obtain a proper reproduction of prototype tidal phenomena throughout the bay system. Prototype tidal data from nine recording tide gages, the locations of which are shown on Fig 1, were available to verify the accuracy of the model adjustment. These prototype gages operated continuously in 1959 and 1960 during the periods in which prototype observations of current velocities and salinity were being observed.

The tide selected for reproduction in the model gulf area was of the typical one-a-day type of spring tide having a range of about 1.8 ft. This type of tide is known as a "great declination" tide, since such tide occurs when the moon reaches its greatest north or south declination. The reason for selecting a tide of maximum range was to obtain the greatest possible tidal influence in the bay area and thereby produce maximum current velocities in Pass Cavallo and in the entrance to the bay.

Adjustment of the model tidal elevations and times was accomplished by reproducing in the model gulf a tide of about 1.8 ft in range, then adjusting the roughness (strips) in Pass Cavallo until the tidal elevations throughout the bay were reproduced as correctly as possible. Further refinements were made in the model roughness during the adjustments of current velocities, until a satisfactory model verification of tidal heights and phases had been obtained. The maximum discrepancy between model and prototype was of the order of 0.1 ft prototype, or 0.001 ft in the model, while the times of high and low tides were identical for the model and prototype at all tide gage locations. Ratio of ranges of tides reproduced in the model indicate very close agreement with ranges that occurred in prototype.

The next step in the model adjustment was to obtain an accurate reproduction of the vertical and lateral distribution of prototype currents in Pass Cavallo and throughout the bay system. Prototype current velocity data was available for 21 stations (see Fig 1). The procedure followed for adjustment of currents was to reproduce a spring tide of 1.8 ft in the model gulf and adjust the model roughness until the distributions of velocities were similar to prototype velocities for each velocity station.

Based on the accuracy with which the model reproduced tidal elevations and phases and current velocities and directions observed in the prototype during the field data collecting program, it was the consensus that the hydraulic verification of the model was entirely satisfactory.

CONTRIBUTION OF MATAGORDA BAY MODEL TO DESIGN OF MATAGORDA BAY DEEP DRAFT NAVIGATION PROJECT

SALINITY VERIFICATION

The model salinity verification involved reproducing the inflow hydrographs of all tributaries to the bay system, in accordance with inflow data furnished by the Galveston District, for the prototype period January 1959 through June 1960. Salinity measurements were made in the model at locations, depths, and times of tidal events corresponding to the prototype measurements, and direct comparisons were made to determine the accuracy with which the model reproduced prototype salinities. The results of the test indicated excellent agreement between model and prototype for all portions of the model except in Lavaca Bay. Beginning at about Sand Point (the south end of Lavaca Bay), model salinities were slightly higher than those of the prototype, and the difference between the two increased with distance upstream so that, in the northerly portion of the bay, model salinities were substantially greater than those of the prototype. It was the consensus that excessive salinities in the Lavaca Bay portion of the model could be attributed to a deficiency in runoff from the Lavaca-Navidad watersheds. A detailed review of the runoff data was made by the Galveston District and the results indicated that the runoff from the Lavaca-Navidad watersheds was the equivalent of about 8 inches per year rather than the 4 inches per year that was used in the salinity verification test. The average runoff of 8 inches per year was used for both base and plan tests for sustained flow conditions.

GENERAL INVESTIGATIONS IN MODEL

SELECTION OF OPTIMUM ENTRANCE CHANNEL

The three entrance routes for the navigation channel that were chosen to be tested in the model, designated Routes A, B, and C, are shown on Fig 1. Route A was essentially the same as the deep-draft navigation channel authorized for construction. The dimensions and alignment of this route were covered in the description of the prototype. Routes B and C consisted of a 300-ft-wide channel 38 feet deep, running from deep water in the Gulf of Mexico to the gulf shore of Matagorda Peninsula; thence a decrease depth from 38 feet to 36 feet in first 500 feet of land cut from gulf shore, width remaining at 300 feet, to the bay shore of Matagorda Peninsula; thence a decrease in width to 200 feet, depth remaining at 36 feet, in the first 500 feet of the Bay starting at the bay shore of Matagorda Peninsula; thence 200 feet wide and 36 feet deep to Point Comfort. Each route was tested separately, in conjunction with a common channel route from the vicinity of Port O'Connor to Point Comfort, as a basis for selection of the optimum route from deep water in the Gulf of Mexico into Matagorda Bay. These tests were made with and without jetties extending into the Gulf of Mexico.

In the model test of the three alternate entrance routes, special attention was given the following: (a) the effects of each channel route on the tidal prism of the bay system; (b) the effects of each channel route on current velocities at critical locations throughout the bay; (c) the maximum velocities in each entrance channel; (d) the effects of Routes B and C on current velocities in the existing Pass Cavallo; (d) the directions and strengths of surface and subsurface currents along the navigation channel; and (f) the effects of each entrance channel route on salinities for conditions of sustained fresh-water inflow. In addition, some very qualitative shoaling tests were made as an indication of relative shoaling characteristics of the Routes A and C entrances.

Each proposed channel route was tested first without jetties to aid in the design of a jetty system for each route. The initial model tests without jetties showed that the Route A entrance would have no measurable effects on the tidal prism of the bay or on current velocities throughout the bay. Salinities within the new channel, below the plane of the existing bottom, were appreciably higher than now occur at comparable locations; however, there were no appreciable changes in salinity outside the limits of the new channel, or within the limits of the new channel above the plane of the existing bottom. Maximum current velocities in the Pass Cavallo portion of the Route A entrance were of the order of 5.3 ft per sec during ebb, with velocities of this magnitude extending over approximately a 0.5 mile length of the entrance channel. The directions of tidal currents were in fairly good agreement with the channel alignment during both flood and ebb, except in the outer portion of the entrance channel (see Figs 2 and 3).

The addition of jetties at the Route A entrance caused an appreciable reduction in the tidal prism of the bay, accompanied by reductions in current velocities throughout the bay. Velocities throughout most of the length of the jettied portions of the entrance channel were increased, the maximum velocities being of the order of 5.0 ft per sec during flood and 5.8 ft per sec during ebb. Maximum velocities in excess of about 5.0 ft per sec were observed over essentially the full length of the jettied channel, or a length of about 5 miles. The alignment of the tidal currents was in good agreement with the channel alignment, except at the outer ends of the jetties where some eddy action was noted.

Tests of the Route B entrance without jetties indicated that the tidal prism of the bay would be increased slightly, accompanied by slight increases in tidal current velocities throughout the bay.

Velocities in Pass Cavallo were not changed, thus indicating that hydraulic conditions in the existing channel would not be affected by the Route B entrance. Maximum current velocities in the Route B entrance were about 5.0 ft per sec during flood and 5.5 ft per sec during ebb. Cross-current action in that portion of the entrance channel between the bay shore of Matagorda Peninsula and Port O'Connor was rather severe because of the normal flow patterns into and out of Pass Cavallo during both flood and ebb currents (see Figs 4 and 5). As was the case with the Route A entrance, salinities in the new channel below the plane of the present bottom were substantially greater than occur at present at comparable locations; however, salinities outside the channel, especially in Lavaca Bay and the east portion of Matagorda Bay were also increased by as much as 2 parts per thousand.

The addition of jetties extending into the Gulf of Mexico had no measurable effects on hydraulic or salinity conditions observed during tests of the Route B entrance without jetties. The spacing between the jetties was 2400 feet, so the jetties did not change the tidal discharge through the Route B entrance.

The effects of the Route C entrance without jetties on the tidal prism of the bay, on current velocities throughout the bay and in Pass Cavallo, and on salinities throughout the bay system were essentially the same as for the Route B entrance. However, since the Route C entrance was farther from Pass Cavallo than the Route B entrance, the effects of tidal currents in Pass Cavallo in producing cross-current action in the Route C entrance were appreciably less severe than for Route B. Detailed measurements of current directions and velocities in the Route C channel showed that cross currents extended only down to about the plane of the present bottom, or to about -10 ft MSL, while currents below this plane were in almost perfect alignment with the navigation channel during both flood and ebb. Surface flow patterns for Route C are shown in Figs 6 and 7. The addition of jetties extending into the Gulf of Mexico at the Route C entrance, spaced 2400 ft apart, indicated no measurable effects on hydraulic or salinity conditions observed during tests without jetties.

Based on the results of the hydraulic tests described above, it was agreed by all concerned that Route C was superior to Route B in all respects, and Route B was therefore excluded from further consideration. As a basis for selection of either Route A or Route C, it was felt that some information was needed on the relative tendencies toward shoaling of these two routes downstream from about Port O'Connor.

Three different model operating techniques were employed for qualitative shoaling tests. In the first technique, equal quantities of synthetic sediment, representing suspended sediments of the prototype, were injected into the model on one range running from Port O'Connor to the bay shore of Matagorda Peninsula east of the Route C entrance, and a second range running across Pass Cavallo just north of Decros Point. Material at the Port O'Connor range was injected during the ebb current phase only, while that at the Pass Cavallo range was injected during flood only. Identical tests were made with the Route A entrance installed in the model and with the Route C entrance installed. The second technique involved injection of all the material on the Port O'Connor range during the ebb current phase, while the third involved injecting all of the material on the Pass Cavallo range during the flood current phase.

The three techniques described above were employed because it was not possible to determine the primary source of sediment to the channel, and this procedure permitted a rough evaluation of the shoaling characteristics of the two entrance routes under all possible combinations of primary source. For example, the first technique assumed an upstream source and a downstream source of equal magnitude, the second assumed a primary upstream source, and the third assumed a primary downstream source. Since there is no basis for estimating rates of shoaling in the area involved, either under present conditions or following construction of one or the other of the deep channel routes, these tests were designed to determine only if one channel route showed a marked tendency to shoal more rapidly than the other, and the conditions of direction of source material under which such tendency was most marked.

The results of the qualitative shoaling tests indicated the following: (a) the Route C entrance would shoal at a slightly greater rate than the Route A entrance if the source of shoaling material is equally divided between upstream and downstream; (b) the Route C entrance would shoal at an appreciably greater rate than the Route A entrance if the primary source of sediment is upstream; and (c) the Route A entrance would shoal at an appreciably greater rate than the Route C entrance if the primary source of sediment is downstream. The meager information on shoaling of the area under consideration for existing conditions indicates that active shoaling takes place at the Intracoastal Waterway entrance into Matagorda Bay, just south of Port O'Connor, and that the sediments responsible for such shoaling come from Pass Cavallo. On the other hand, that portion of the Intracoastal Waterway to the east of the deep draft channel route, which lies below the plane of the natural bay bottom, shows little if any tendency to shoal. This provides some evidence, therefore, that Matagorda Bay is probably not a primary source of sediment, but that Pass Cavallo is a primary

CONTRIBUTION OF MATAGORDA BAY MODEL TO DESIGN OF MATAGORDA BAY DEEP DRAFT NAVIGATION PROJECT

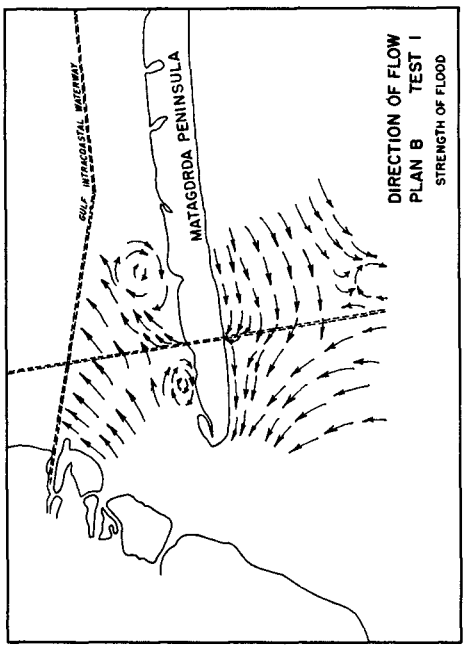

Fig. 5

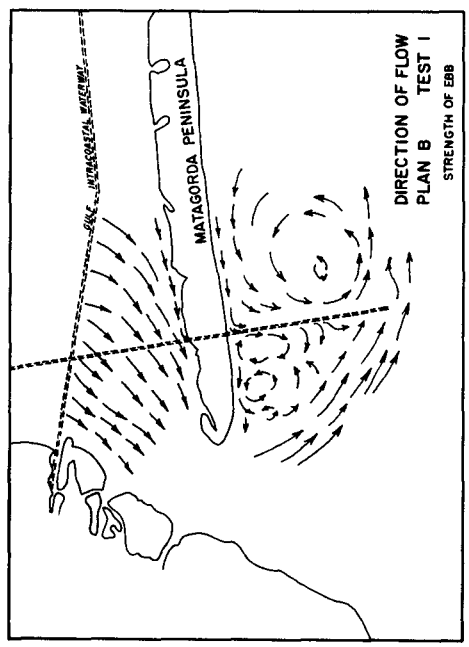

Fig. 4

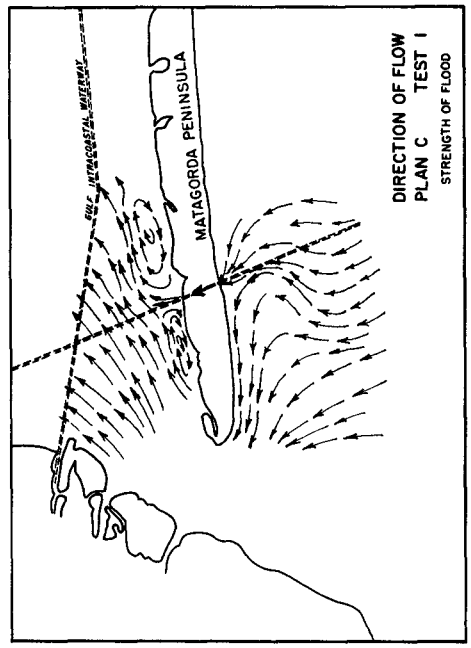

Fig. 7

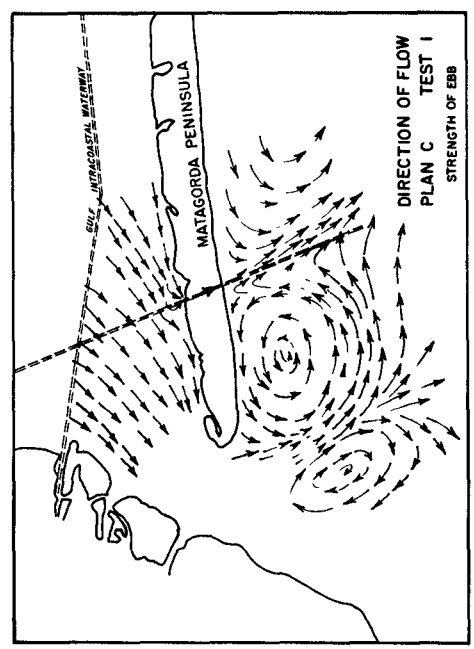

Fig. 6

source of sediment, and under such conditions the qualitative shoaling tests indicate that shoaling of the Route C entrance would probably be less than that of the Route A entrance.

Based on the results of hydraulic and shoaling tests made in the model, it appears that the Route C entrance is superior to the Route A entrance for the following principal reasons: (a) the Route C entrance provides the shortest and straightest route to deep water in the Gulf of Mexico; (b) the initial cost of dredging the Route C entrance would be significantly less than for Route A; (c) the jetties required for Route C are much less extensive than would be required for Route A, and thus the cost of construction and maintenance of jetties would be appreciably less; (d) if the principal source of potential shoaling material is from downstream, as appears to be the case, maintenance dredging of Route C would be less than for Route A; and (e) ships navigating the Route C entrance would be exposed to fairly high velocity currents (in excess of about 4.0 ft per sec) only in the short land cut across Matagorda Peninsula, while for Route A currents of this magnitude would be encountered over essentially the full length of the jetty channel, or for a distance of about 5 miles.

The only apparent advantage of Route A over Route C is that cross-current action in that portion of the channel downstream from Port O'Connor would be less for Route A. However, detailed observations of the directions and velocities of cross currents in this portion of the Route C channel indicate that such currents are confined to the upper 10 ft or less of the depth, with currents below this plane being in good alignment with the navigation channel. Furthermore, the results of observations made in the Galveston Harbor model have shown that cross currents in the approach to the Texas City Channel are equal to or greater than those which would be encountered in the Route C entrance, and since no complaints have been registered that cross-current effects are detrimental to navigation in the Texas City Channel, it appears that currents of equal or lesser magnitude would cause no serious problem in the Route C entrance.

Following the conclusion that the Route C entrance was the optimum route, a series of tests was made to determine the effects of parallel jetties varying in length from 2,950 ft to 15,500 ft (from the 15-ft contour in the Gulf to the 36-ft contour of depth) on flow patterns and velocities in the Gulf portion of the entrance and in the land cut across Matagorda Peninsula. The results of these tests showed that jetty length, with a spacing of 2400 ft between jetties, would have little if any effect on flow patterns and velocities in the entrance channel. While the model tests indicated some minor cross-current action just off the ends of the jetties, the locations of which would be shifted gulfward as the lengths of jetties were increased, the magnitudes of such currents did not appear to be sufficient for any jetty length to cause problems to navigation.

CONTRIBUTION OF MATAGORDA BAY MODEL TO DESIGN OF MATAGORDA BAY DEEP DRAFT NAVIGATION PROJECT

For the various jetty lengths mentioned in the previous paragraph, assumed beach accretions were placed in the model east of the east jetty and west of the west jetty to determine if such accretions would appreciably change flow patterns or velocities in the entrance. The most drastic assumed beach accretions extended essentially out to the Gulf ends of the jetties, and even under such conditions there were no indications that flow patterns and velocities in the entrance would be adversely affected.

Tests were also made of dikes, spaced 2400 ft apart, on both sides of the channel extending into Matagorda Bay from the bay side of Matagorda Peninsula. The purpose of these tests was to determine how cross-current action in the channel between Matagorda Peninsula and Port O'Connor would be affected by such dikes. The conditions tested consisted of 1,000-ft-long dikes on both sides of the channel, extension of the west dike to 3000 ft, and further extension of the west dike to 5000 ft. The results of the dike tests indicated that 1,000-ft-long dikes on both sides of the channel would appreciably improve cross-current action in the channel. Extensions to the west dike would decrease the length of channel exposed to cross currents, but the velocities of the cross currents just off the end of the dike would be increased progressively as the length of the west dike is increased. It was concluded that the effects of the 1,000-ft-long dikes on both sides of the channel are entirely beneficial, but that extensions to the west dike should be made only if navigation interests have a definite preference to a lesser length of channel exposed to higher cross-current velocities, as opposed to a greater length of channel exposed to cross currents of moderate velocities.

A one-year salinity test was made in the model to determine the effects of the Route C navigation channel on salinities throughout the bay system. In addition to the deep-draft channel, the plan installed in the model included jetties 2400 feet apart extending into the Gulf of Mexico to the -24 ft contour of depth; 1000-ft-long spoil dikes, also 2400 ft apart, extending into Matagorda Bay from Matagorda Peninsula; and the spoil bank arrangement in Matagorda and Lavaca Bays arrived at in the following discussion of spoil bank location and alignment.

Two tests of approximately one-year's duration were made, one for existing conditions (base test) and the other with the Route C channel and appurtenant works installed in the model. In both tests, the fresh-water discharges of all tributaries to the bay system were controlled in accordance with prototype hydrographs for the

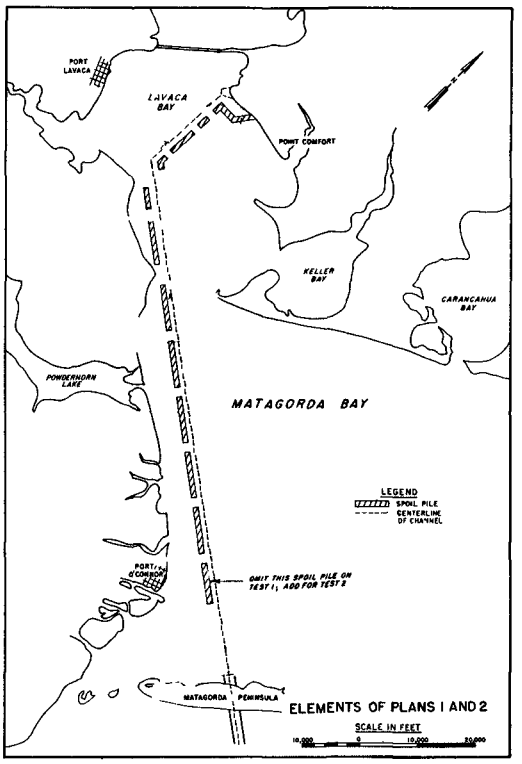

Fig. 8

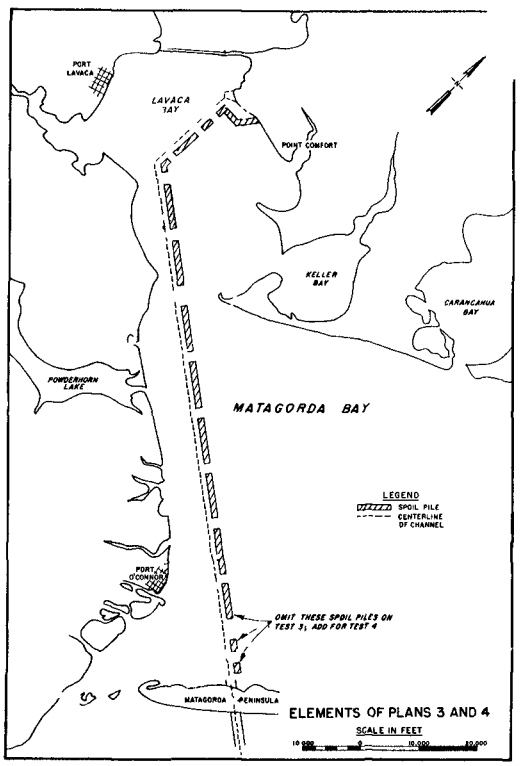

Fig. 9

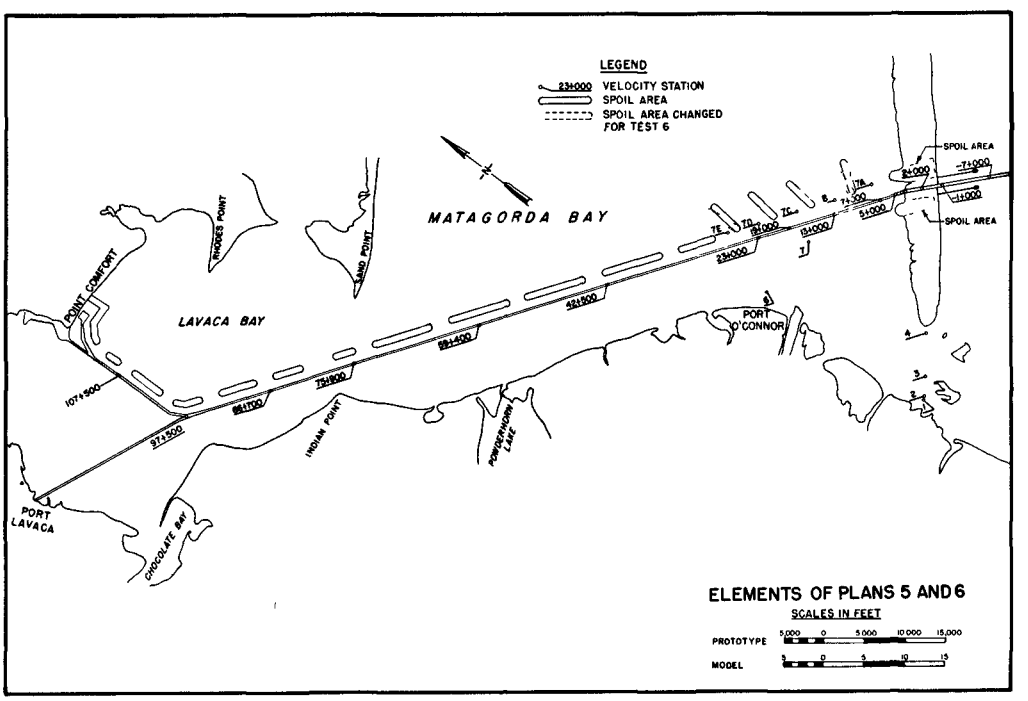

Fig. 10

period 27 May 1959 through 2 June 1960. Samples for salinity determination were obtained at intervals of about one week at all stations and depths at which samples were obtained in the prototype for model verification purposes.

In general, it appeared that the Route C channel would not effect a major change in the salinity regimen of the bay system. Considering annual average salinities in the major subdivisions of the bay system, the maximum increases (2.0 to 3.8 parts per thousand) occurred in Lavaca Bay system and the east portion of Matagorda Bay. Maximum salinities throughout the test year were increased by the plan at most stations and depths, but in general the increases amounted to one or two parts per thousand; however, minimum salinities at some locations in Lavaca Bay were increased by as much as 8.7 parts per thousand.

SPOIL BANK LOCATION AND ALIGNMENT

To aid in formulating a spoil disposal plan for disposal of spoil dredged during construction of the deep-draft channel, surface current pattern photographs were taken in the model along the channel alignment from Matagorda Peninsula to Point Comfort. From the above photographs the Galveston District proposed four tentative plans for disposal of the spoil to be tested in the model. Two plans (plans 1 and 2) involved placement of most of the spoil on the west side of the channel, in series of fills parallel to the channel with gaps between fills (see Fig 8), while the other two plans (plans 3 and 4) involved placement of most of the spoil on the east side of the channel in a similar manner (see Fig 3). The two plans involving placement of most of the spoil on the west side of the channel had no measurable effects on tidal prism or mass flow patterns in the bay system. However, it was noted that some cross-current action developed opposite essentially every gap between spoil banks. While the intensities of such current were probably insufficient to affect navigation, it seemed likely that shoaling would be accelerated in the channel opposite each gap.

Plans 1 and 2 were discarded from any further tests when it was learned that there are two oyster reefs on the southwest side of the channel, in the vicinity of Indian Point in Lavaca Bay and Powder Horn Lake in Matagorda Bay. It was agreed that placement of the spoil piles on the west side of the channel would be detrimental to these oyster reefs. It was also agreed that by the placement of the spoils on the east side of the channel they would afford more protection to navigation.

In plan 3 the spoil piles were placed on the east side of the channel in a manner similar to that employed in plan 1. The first spoil pile was located east of Port O'Connor approximately four miles from the bay shore of the Peninsula. This plan was subjected to model tests, and the results showed that it had no detrimental effect on conditions in the channel. For plan 4, three additional spoil piles (Fig 9) were added between Matagorda Peninsula and the first spoil pile for plan 3. The addition of the three spoil piles increased cross current velocities in the openings of the added spoil piles. The first cost of dredging the deep-draft channel through lower Matagorda Bay would be greatly reduced by permitting deposition of spoil in the 4-mile reach between Matagorda Peninsula and station 28+000. Plan 5, (Fig 4) which consisted of 4 spoil areas 5,000 ft apart in the 4-mile reach, was then tested in the model. Each spoil pile had bottom dimensions of 900 by 4600 feet, top dimensions of 100 by 3800 feet, and side slopes of about 1 on 20. Observations of surface and subsurface velocities and current directions at the entrance of the ship channel into Matagorda Bay for Plan 5 indicated that the arrangement of spoil banks in this area could be improved. Several trial alignments were installed in the model and tested. It was found that by rotating the first and fourth spoil banks (nearest the entrance) 20 degrees and 10 degrees, respectively, from the plan 5 alignment, closer conformity of the banks with the current patterns could be achieved (plan 6, Fig 10). The intensity of cross-current action for plans 5 and 6 was probably insufficient to affect navigation, except at station 7+000 where current directions departed from normal with the channel alignment by about 90 degrees on flood and about 60 degrees on ebb, with corresponding current velocities of about 2.0 ft per sec. This variance decreased progressively from station 7+000 to station 23+000 where the departure was about 50 degrees on flood and about 30 degrees on ebb, with maximum velocities of 1.8 ft per sec and 1.2 ft per sec, respectively.

CONCLUSIONS

The project that has been selected for construction in the field is essentially the same as plan C with some minor alterations. The project consists of a 300-ft-wide by 38-ft-deep entrance channel, with 1 on 3 side slopes from deep water in the Gulf of Mexico to the end of the jetties; thence 1 on 5 side slopes from the end of the jetties in the Gulf to about 1000 ft north of the bay shore of Matagorda Peninsula; and thence a 200-ft-wide by 36-ft-deep channel with 1 on 3 side slopes from a point 1000 ft north of the bay shore of Matagorda Peninsula to Point Comfort. The 300-ft-wide channel through Matagorda Peninsula is aligned eight degrees south from the alignment of the 200 ft channel and has twin jetties 2000 ft apart, extending from the Gulf shoreline of Matagorda Peninsula to the 24-ft contour of depth in the Gulf; and twin protective spoil embankments, 25 ft in height at mlw across Matagorda Peninsula, extending about 1000 ft into Matagorda Bay.

CONTRIBUTION OF MATAGORDA BAY MODEL TO DESIGN OF MATAGORDA BAY DEEP DRAFT NAVIGATION PROJECT

SUMMARY

In resume, the authors have attempted to emphasize the importance of the Matagorda Bay model as an aid to the design engineers in selection of the optimum route for the deep-draft channel route from the Gulf of Mexico through Matagorda and Lavaca Bays to Point Comfort. With the aid of information provided by the model, the route selected for construction (Route C) will result in substantial savings over the route proposed originally (Route A), because of its shorter length, the lesser requirements for length of entrance jetties, and the fewer number of navigation aids which will be required because of its straighter alignment.

The model also provided a wealth of valuable information as to the optimum arrangement of spoil disposal areas to be used during construction and subsequent maintenance of the channel. The arrangement of spoil disposal areas selected will not cause cross currents in the channel which would be hazardous to navigation, and they will have a minimum effect on tidal circulation and salinity distribution in the bay system so as to preserve existing conditions to the extent possible in the interest of the fish and wildlife resources of the area.

It is further emphasized that the hydraulic model is not capable of providing in a quantitative sense all of the information that design engineers need in selecting the significant features of a major navigation project such as the Matagorda Bay project. However, in the hands of experienced hydraulic laboratory personnel who are thoroughly familiar with the capabilities and limitations of hydraulic models, the cost and effort invested in a model is usually returned with dividends in terms of lower cost of construction in the field as well as in terms of more effioient performance of the final project.

CHAPTER 36

ACRECENTAMIENTOS Y EROSIONES COMO CONSECUENCIA DE OBRAS MARITIMAS CONSTRUIDAS EN EL LITORAL CENTRAL DEL DISTRITO FEDERAL DE VENEZUELA

Bernardo A. Nouel
Ingeniero Jefe de la Oficina
de Ingeniería "Proyectos y Construcciones Marítimos S.A."
Venezuela

- - -

SINOPSIS

En la costa Norte y Central de Venezuela, en el sector del Distrito Federal, se han construído obras marítimas, habiéndose registrado deposiciones de sedimentos, erosiones y cambios interesantes en la línea de costa, siendo el objeto del presente trabajo, recopilar la información, analizar los fenómenos y establecer conclusiones en aquellos casos - en que el material informativo disponible y el análisis de los mismos, permitieron llegar a ellas. Se pudieron determinar volúmenes de rellenos y erosiones en lapsos definidos - como consecuencia de las obras construídas. Así mismo se pudo establecer una inter-relación entre las características del oleaje en un sitio definido, su profundidad y la velocidad de decantación del sedimento, caracterizada por la de - su diámetro medio, en un intento de verificar en la naturaleza, los estudios de Ippen y Eagleson sobre distribución - de sedimentos por efecto de las olas (7). Por el contrario, no se pudo establecer relaciones definidas entre el coeficiente de uniformidad del sedimento y la profundidad (8).

INTRODUCCION

El Litoral Central de Venezuela, con una longitud de 125 millas, se extiende desde Cabo Codera por el Este, hasta la desembocadura del río Morón, Estado Carabobo por el - Oeste, con un rumbo general S. 88° O. en su mitad oriental hasta Punta Calera y S. 82° O. en su mitad occidental entre dicha Punta y el río Morón (Figs. 1 y 2). El Litoral Central del Distrito Federal a que se refiere el presente estudio, queda comprendido dentro del antes citado sector de costa y con una longitud de 35 millas, se extiende desde el Centro Recreacional de Los Caracas por el Este, hasta Arrecifes - por el Oeste, con rumbo general S. 88° O. como antes se expresó (Fig. 2).

ACRECENTAMIENTOS Y EROSIONES COMO CONSECUENCIA DE OBRAS MARITIMAS CONSTRUIDAS EN EL LITORAL CENTRAL DEL DISTRITO FEDERAL DE VENEZUELA

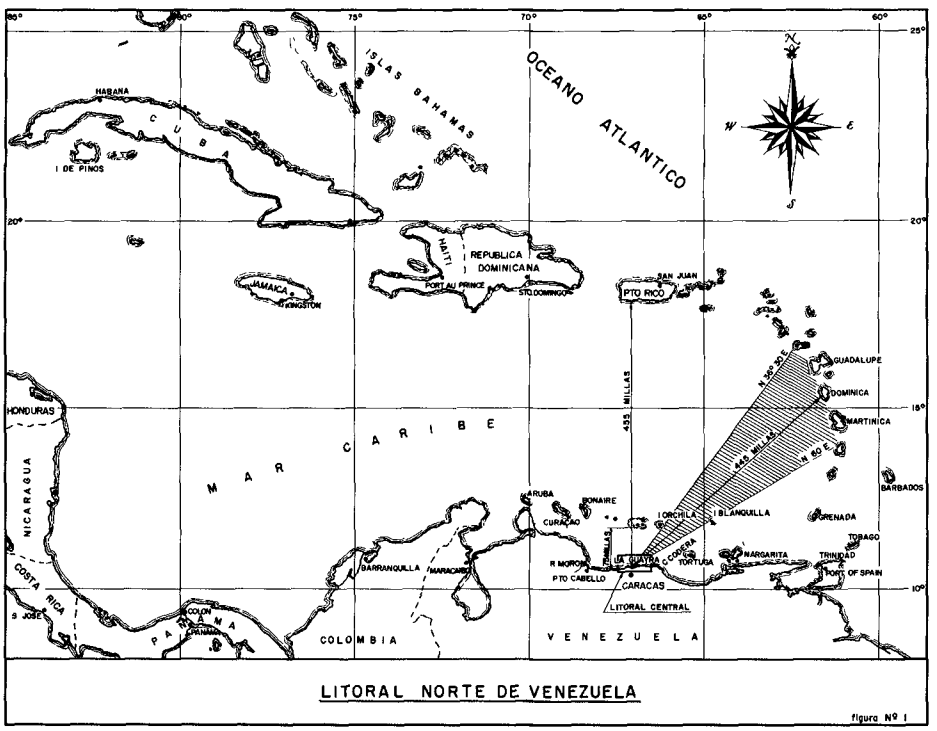

LITORAL NORTE DE VENEZUELA

figura Nº 1

Fig. 1

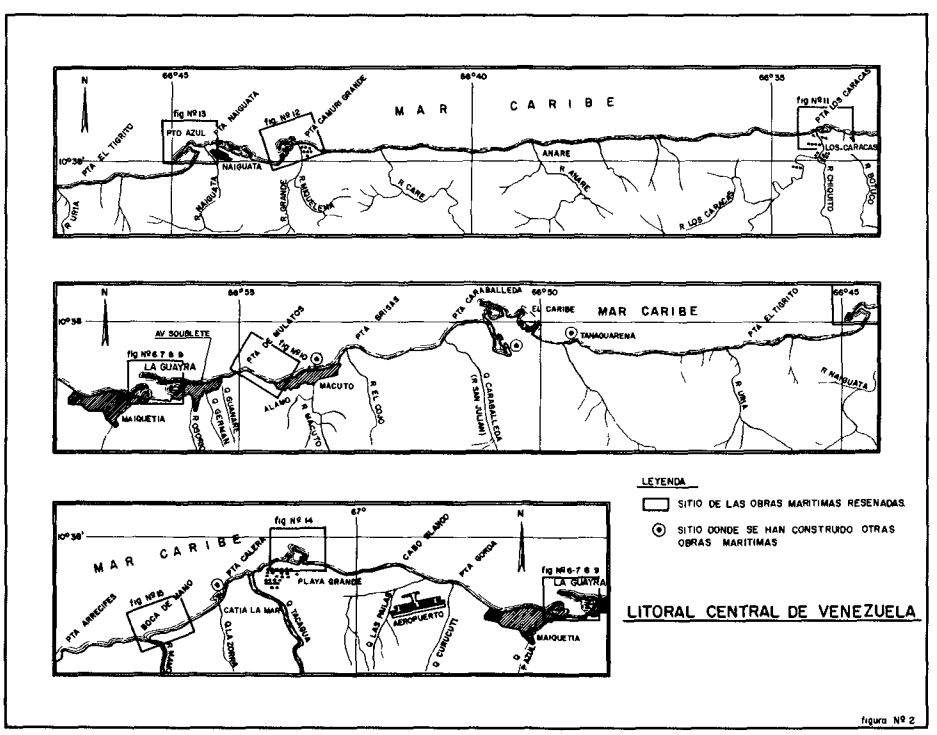

LITORAL CENTRAL DE VENEZUELA

figura Nº 2

Fig. 2

Este sector de ribera corre paralelo a la Cordillera de la Costa, la cual se levanta abruptamente al Sur del litoral, quedando caracterizada por el corto espacio que dista entre la cresta de la cordillera y la orilla del mar. En efecto, podemos encontrar los picos de Izcaragua, Naverán, Naiguatá, Pico Oriental, Pico Occidental, El Avila y Alto de No León, con elevaciones respectivas sobre el nivel del mar de 2.320 m.; 2.300 m.; 2.765 m.; 2.640 m.; 2.480 m.; 2.159 m. y 2.106 m., a distancias correspondientes de apenas 8.8 kms.; 8.5 kms.; 7.7 kms.; 8.5 kms.; 7.1 kms.; 7.6 kms. y 13.5 kms. al Sur de la ribera.

El aspecto fisiográfico del Litoral Central en referencia, es el de una sucesión de conos aluviales de deyección, bajos y de cierta anchura, separados entre sí por sectores rectos de costa desprovistos de playa o con playas muy reducidas, elevándose los cerros en algunos de estos sectores como verdaderos acantilados. En general se extiende una franja de terreno entre el mar y la cordillera relativamente angosta, con poca elevación, la cual está constituida por detritus de playa y materiales aluvionales, para continuar hacia el Sur con un cambio brusco en las elevaciones según una serie de cerros que van a culminar en el macizo de montañas de la cordillera.

La ciudad de Caracas está situada al Sur de la Cordillera de la Costa y en el Litoral Central, utilizando los conos aluvionales de deyección, se han desarrollado las varias poblaciones de La Guayra, Maiquetía, Naiguatá y las Urbanizaciones y Centros Vacacionales y Recreacionales.

La Cordillera de la Costa, en el sector en consideración, está formada por rocas metamórficas. Una primera franja angosta que colinda por el Norte con el aluvión, está compuesta por esquistos calcáreos micáceos, con capas delgadas de calizas negras intercaladas, encontrándose atravesada por numerosas vetas de cuarzo (Formación Las Mercedes). Inmediatamente al Sur de esta formación está, en contacto de falla con ella, una formación compuesta principalmente de gneisses (Formacion Peña de Mora). Esta falla que se extiende en dirección Este-Oeste y con buzamiento 60° Norte, es prominente y forma un escarpado en la topografía (1), (11).

La referida cordillera tiene innumerables torrentes o ríos torrenciales, con poco o ningún caudal en la época de sequía y con gastos hidráulicos que pueden alcanzar en épocas de lluvias excepcionales, en algunos de estos ríos, hasta 1.000 m3/seg., como sucede en los ríos Mamo y Los Caracas (2), (4). Los cauces de estos torrentes están caracterizados por una zona baja, correspondiente al cono de deyección, con pendientes suaves y por una cuenca superior con pendientes abruptas que se elevan hasta la cresta de la cor

dillera.

La precipitación de las lluvias en la cuenca superior de estos torrentes, ocurre casi todo el año con valores muy reducidos en el verano y con alturas medias de 921 mm/año, según promedio de un lustro y con valor promedio máximo durante el mismo lapso, de 1.844 mm/año y en su cuenca inferior un máximo promedio de 1.605 mm/año (9). En tormentas excepcionales, la precipitación en su epicentro ha alcanzado hasta 500 mm/día, tormentas éstas que acontecen en época de invierno en el hemisferio boreal y posiblemente debido al avance pronunciado hacia el Sur de frentes fríos. Estas lluvias excepcionales no coinciden en general con oleajes de tormenta, mares de fondo o mares de leva.

Una de las primeras lluvias excepcionales de que se tiene noticia, acaeció en el año 1780. Entre los años de 1912 a 1954, se registraron diez lluvias excepcionales que azotaron la zona del Litoral Central (2). La tormenta acaecida entre el 15 y 19 de febrero de 1951 fué desastrosa, produciendo arrastres de grandes masas de lodo y detritus desde las montañas y depositando el aluvión en las zonas bajas, con espesores de varios metros en algunos sitios, cambiando bruscamente los cauces normales de los ríos y quebradas y arrojando al mar importantes volúmenes de sedimentos y rocas.

Fenómenos similares a éste sucedieron en épocas pretéritas y debido al tamaño relativamente grande de los materiales acarreados, los conos de deyección existentes en el litoral, avanzan como verdaderos cabos y han persistido como tales, siendo característico de ellos, que la desembocadura de las quebradas o de los ríos, viene a quedar en la zona central y saliente del cono aluvional.

Los sedimentos finos acarreados por los ríos y quebradas, sometidos a la acción de las olas, son arrastrados, clasificados y distribuídos por el mar a lo largo de la costa. El oleaje juega papel principal en la distribución, clasificación y arrastre de los materiales granulares, siendo típica la disposición de un cabo aluvional, en el cual se establece playa, más o menos estable, en su lado oriental y en donde el ángulo de incidencia del oleaje con la línea de costa es relativamente pequeño y por tanto, la capacidad de arrastre de la corriente litoral producida por el oleaje es pequeña; por el contrario, el lado occidental del cabo está formado por bloques de roca, cantos rodados y peñones, coincidiendo con un ángulo de incidencia del oleaje grande y por tanto, de una mayor capacidad de arrastre de sedimentos (Fig. 3). Es notable la similitud de la inclinación de la orilla oriental de los cabos en los varios conos de deyección existentes en el litoral (Fig. 4); por el contrario, el flanco occidental de dichos cabos presentan direcciones

varias que parecen indicar ser más bien consecuencia de la forma como fueron depositados los materiales en los momentos de grandes crecientes fluviales, que a la acción del oleaje (5). El proceso de arrastre de los mayores bloques de roca y cantos rodados, de este lado occidental de los cabos, es más bien un proceso lento, en donde además del efecto de la corriente litoral del oleaje, intervienen las contracorrientes generales originadas en las ensenadas (3).

Es interesante la existencia de lomas submarinas como continuación de los conos de deyección y la de valles profundos entre conos inmediatos, como el existente en frente de la población de Macuto entre los conos de deyección de los ríos El Cojo y Macuto y un pequeño valle sumergido situado entre las dos lomas submarinas en frente a la desembocadura de la quebrada Mapurite y el río Piedra Azul, al Oeste del puerto de La Guayra.

Los perfiles submarinos típicos del litoral, se muestran en la figura N° 5, en donde se puede ver que la zona entre La Guayra y río San Julián, frente a márgenes aluvionales, tienen pendientes del 4.5 al 6% y en cambio la zona comprendida entre Cabo Blanco y Catia de La Mar, precisamente en frente de la formación geológica de areniscas y conglomerados y en donde existe a lo largo de la ribera, capas de rocas coralíferas, la pendiente es suave, alcanzando apenas el 1% aproximadamente. La zona entre Catia de La Mar y Mamo, similar a la primera nombrada, vuelve a tener pendientes del orden del 3.5%.

La corriente general en el mar Caribe en frente a la costa del Litoral Central, es hacia el Oeste, alcanzando velocidades moderadas del orden de 3/4 a 1½ nudos, produciendo contracorrientes en dirección opuesta al Oeste de algunos cabos prominentes. Corrientes al Este de débil intensidad se registran en algunas épocas del año.

La oscilación de la marea en esta costa, según registros promediados en el lapso 1949-1960, alcanza los siguientes valores: Altura de pleamar máxima sobre el nivel medio del mar 1.75'; pleamar media superior 0.53'; pleamares medias 0.29'; bajamar máxima -1.45'; bajamares medias inferiores 0.45' y bajamares medias 0.35'. La amplitud media es de 0.64' y la amplitud máxima 3.2'. Como se ve, el mar Caribe en la zona del Litoral Central, se puede clasificar como un mar sin mareas (6).

En la costa en consideración, no existen registros sistemáticos del oleaje y solamente disponemos de observaciones practicadas en la oficina del autor, durante lapsos cortos y correspondientes a observaciones de reglas flotantes graduadas o a la interpretación de las oscilaciones registradas por un ecosondeador . Del análisis de estas infor

ACRECENTAMIENTOS Y EROSIONES COMO CONSECUENCIA DE OBRAS MARITIMAS CONSTRUIDAS EN EL LITORAL CENTRAL DEL DISTRITO FEDERAL DE VENEZUELA

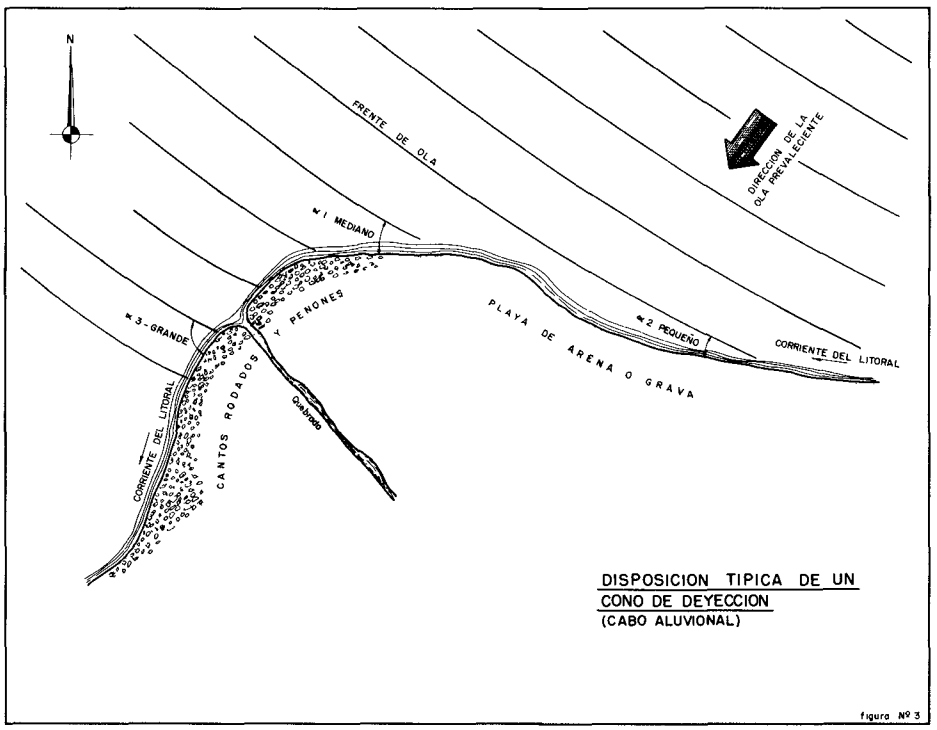

Fig. 3

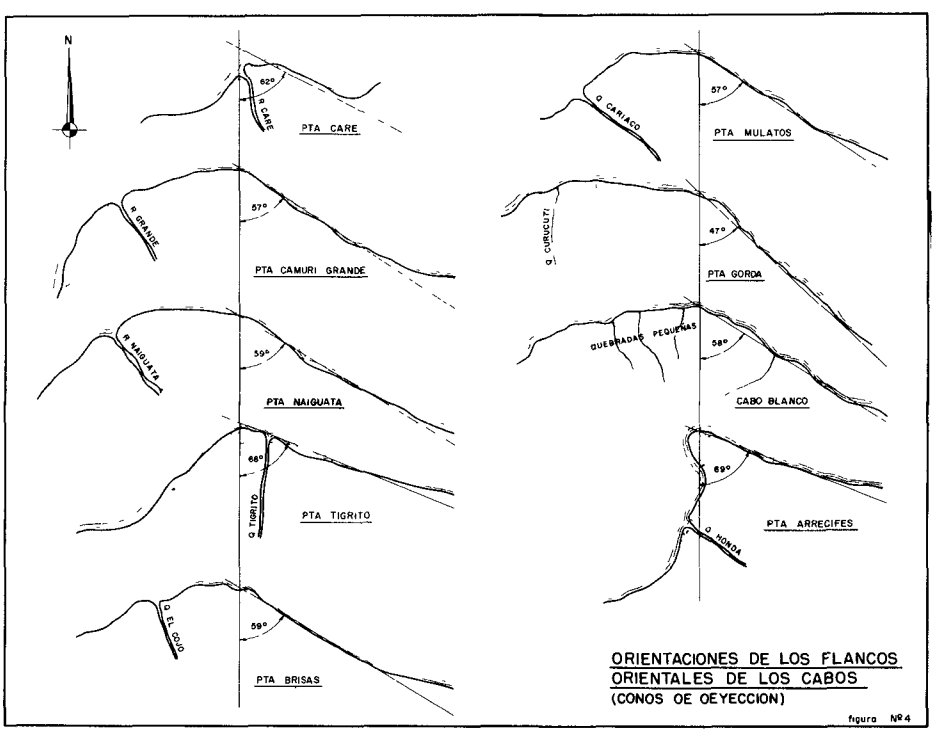

Fig. 4

maciones, se han establecido como valores tentativos, una ola significativa con dirección Noreste, con amplitud de 0.95 metros y período de 8 segundos. La amplitud máxima del oleaje normal es de 1.65 metros y su valor promedio de 0.60 metros. En realidad se pueden distinguir dos espectros superpuestos de olas, el uno con período de 8 segundos y el otro con período de 5½ segundos aproximadamente.

El oleaje de tormenta se ha determinado por observación directa de la amplitud alcanzada en el muelle de la toma de agua de la Planta Eléctrica situada al Este del puerto de La Guayra y transportada a mar profundo por planos de refracción del oleaje, habiéndose establecido tentativamente en H_o = 4.6 metros de altura en mar profundo, período T = 10 a 12 segundos y dirección N.NNE. La amplitud del oleaje de tormenta ha sido materia discutida entre los ingenieros ocupados de estos estudios en Venezuela, siendo opinión de algunos, que esta amplitud no debería considerarse superior a los 3.5 metros en mar profundo. Durante la construcción del primer puerto de La Guayra del 3 al 4 de diciembre de 1887, los constructores de las obras acusaron un mar de fondo capaz de mover masas de concreto pesando 40 toneladas, las cuales vueron levantadas hasta el nivel del muelle y luego movidas de 20 a 30 pies (10); de lo cual se establece que la amplitud del oleaje y su período fueron excepcionales, aunque no podemos inferir sobre sus valores. Durante la construcción de la ampliación del puerto de La Guayra en 1949-1951 y en el lapso de construcción de los varios puertos deportivos vecinos (1954-1956), en opinión del autor, los mares de fondos acaecidos, fueron moderados y de características similares al de 4.6 metros de amplitud. En algunas oportunidades se han observado oleajes con período de 20 segundos, pero este fenómeno parece ser debido a interferencia de olas de períodos del orden antes anotado de 10 a 12 segundos. (3).

Los vientos locales son moderados y alcanzan según promedio de un lustro, las siguientes frecuencias y velocidades medias: N. 4%, 9 kms/hora; N.NE. 1%, 6 kms/hora; N.E. 9%, 10 kms/hora; E.NE. 8%, 13 kms/hora; E. 31%, 14 kms/hora; y 22% de calmas. Los vientos máximos registrados en forma de rachas del Este, alcanzaron el día 4 de febrero de 1950, 74.2 kms/hora; el 2 de febrero de 1951, 92.8 kms/hora; el 18 de octubre de 1952, 74.1 kms/hora (9).

Los fetchs posibles de generación de oleaje para el litoral en consideración, se establecen en el mar Caribe dentro de la cadena de islas de las Antillas Mayores a las Antillas Menores entre Aruba por el Oeste y La Blanquilla por el Este, según las zonas entre altas y bajas presiones barométricas, con distancia de decaimiento hasta la costa misma. Corresponden a estos fetchs, los oleajes de mayor amplitud y período. Debe considerarse además, el fetch local

ACRECENTAMIENTOS Y EROSIONES COMO CONSECUENCIA DE OBRAS MARITIMAS CONSTRUIDAS EN EL LITORAL CENTRAL DEL DISTRITO FEDERAL DE VENEZUELA

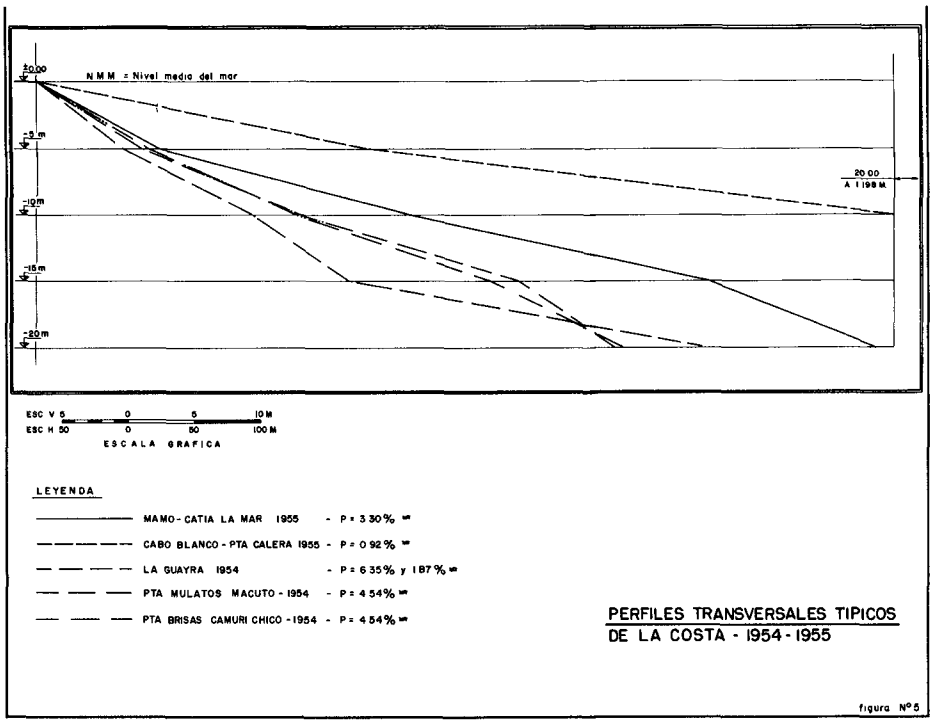

Fig. 5

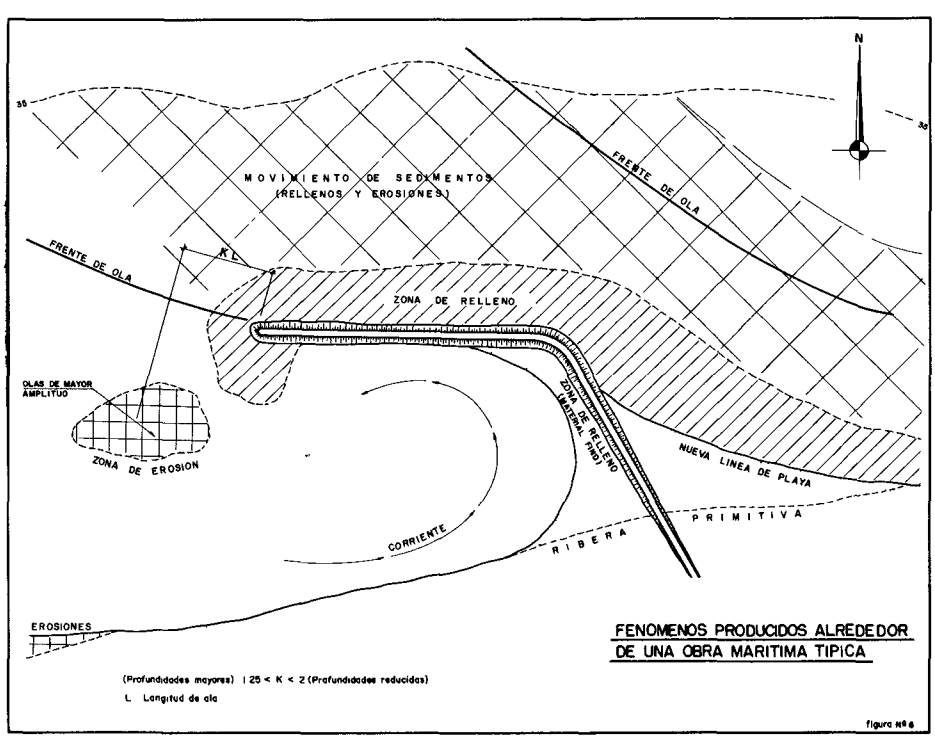

Fig. 6

correspondiente a la zona inmediata al litoral sometido a los vientos locales, en donde se generan las olas de poca amplitud y corto período. Debe observarse, por otra parte, que el sector entre N. 36° 30' E. a N. 60° E., es abierto desde el litoral venezolano hasta la cadena de islas exteriores de las Antillas y con distancia de 445 millas náuticas (Fig. 1). La distancia entre la Guaira y las Antillas Mayores en dirección Norte-Sur es de 455 millas, pero queda interceptada a una distancia de 75 millas al Norte de La Guayra por la cadena de islas Menores entre Aruba y La Orchila.

SEDIMENTACIONES Y EROSIONES COMO CONSECUENCIA DE LAS OBRAS MARITIMAS

La observación de los fenómenos producidos en la vecindad de las varias obras marítimas construídas en el litoral bajo estudio, permite establecer los siguientes hechos, como se evidenciará de la reseña, que de varias de dichas obras, se anota más adelante.

Cuando se construye un rompeolas emergente, normal a la línea de costa, o con rumbo franco al Norte o ligeramente inclinado hacia el Oeste, la ribera en su lado oriental, avanza hacia el mar sin alcanzar el extremo de la obra y quedando a una distancia de éste, aproximadamente igual a una longitud de la onda en el sitio considerado; por tanto, se produce relleno en los fondos a barlovento. A medida que la dirección del rompeolas es más inclinada al Oeste, menos definido es el avance de la orilla y cuando tiene dirección Oeste franco, como en el caso del rompeolas principal del puerto de La Guayra, no se registra cambio en la orilla en el lado de barlovento, pero sí relleno de los fondos y movimientos de sedimentos hasta profundidades importantes.

Despues de cierto lapso de construídos rompeolas con direcciones entre Noroeste y Oeste, se inicia la formación de flechas o conos de sedimentación en su extremo y tendiendo al Oeste o al Sur-Oeste (Fig. 6).

Al Sur-Oeste del extremo occidental de los rompeolas principales, existe una zona definida de erosión, correspondiendo a las mayores alturas de ola en la vecindad de la obra y por tanto, a una mayor sobreelevación del nivel medio del mar, siendo aparentemente ésta, combinada con la turbulencia en la vecindad del extremo de la obra, una de las causas principales de tal fenómeno. En ensayos sobre modelo reducido, se han comprobado estas mayores amplitudes del oleaje en dicha zona (12).

En la zona abrigada por el rompeolas, se produce una

corriente en sentido contrario al de las agujas del reloj - (Fig. 6), principalmente debido al gradiente producido por diferencia de sobreelevación del nivel medio del mar entre la zona agitada y la zona tranquila protegida, y al efecto de expansión lateral de la onda. Como consecuencia se produce sedimentación del lodo, limo y arena fina hacia el extremo Noreste de la dársena protegida.

Puerto de La Guayra, 1885-1891.- Esta obra marítima, la primera construída en el Litoral Central, consistió en - un rompeolas de 625 metros de longitud con dirección Oeste franco, como continuación en tal dirección del cabo correspondiente al cono de deyección del río Osorio y abrigando - hacia el flanco occidental de dicho cabo, un área de alrededor de 35 hectáreas, con una profundidad promedio de 9 metros (30') (Fig. 7).

Como consecuencia de esta obra, se produjo relleno - en el lado Norte de la obra, relleno éste que se prolongó - en el extremo occidental del rompeolas, según una flecha hacia el Suroeste. En la zona inmediatamente al Oeste de esta flecha se registraron erosiones que aún en el año 1937 alcanzaban valores de 1 metro por debajo del nivel de 1888. - Esta erosión se presenta hacia el Suroeste del extremo occidental del rompeolas y a una distancia aproximada, medida - en la dirección de la cresta de las olas en dicho extremo, de 1.75 L, (L = longitud de la ola).

Se observan movimientos de sedimentos en profundidades de 15 a 20 metros hacia el Noroeste del extremo occidental del rompeolas y a una distancia de 4 L aproximadamente. Se observa igualmente cierta zona exterior de erosión.

En el extremo Nororiental de la rada protegida y en la zona de los muelles, se produjo sedimentación de material fino que necesitó periódico y sistemático dragado para permitir el acceso de las embarcaciones. Erosiones al Oeste - del puerto y a lo largo de la línea de costa posiblemente - existirían, pero como dicha zona para aquel entonces estaba despoblada y sin interés inmediato, no hay información de - cambios que pudieran haber ocurrido. En la figura N° 7 se - muestran las modificaciones habidas entre 1888 y 1937, así como los volúmenes de relleno y erosiones correspondientes a dicho lapso, volúmenes éstos que no sirven para la determinación de una rata media anual, por cuanto para fechas anteriores al año de 1937, ya los sedimentos evidentemente, - pasando al Oeste del extremo occidental del rompeolas, seguían su curso aguas abajo.

Ampliación del puerto de La Guayra, 1949-1951.- Las obras consistieron en la construcción de un rompeolas según la prolongación del tajamar construído en 1891, con dos

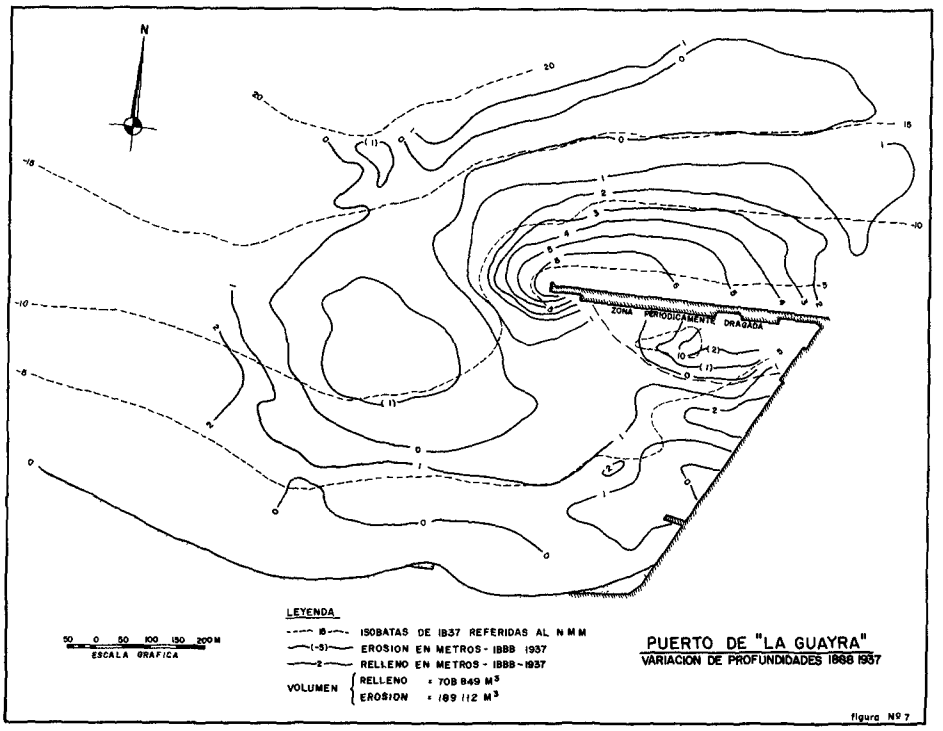
N
ZONA PERIODICAMENTE DRAGADA
LEYENDA
ISOBATAS DE 1837 REFERIDAS AL N M M
EROSION EN METROS - 1888 1937
RELLENO EN METROS - 1888-1937
VOLUMEN
RELLENO = 708 849 M3
EROSION = 189 112 M3
50 0 50 100 150 200 M
ESCALA GRAFICA
PUERTO DE "LA GUAYRA"
VARIACION DE PROFUNDIDADES 1888 1937
figura Nº 7

Fig. 7

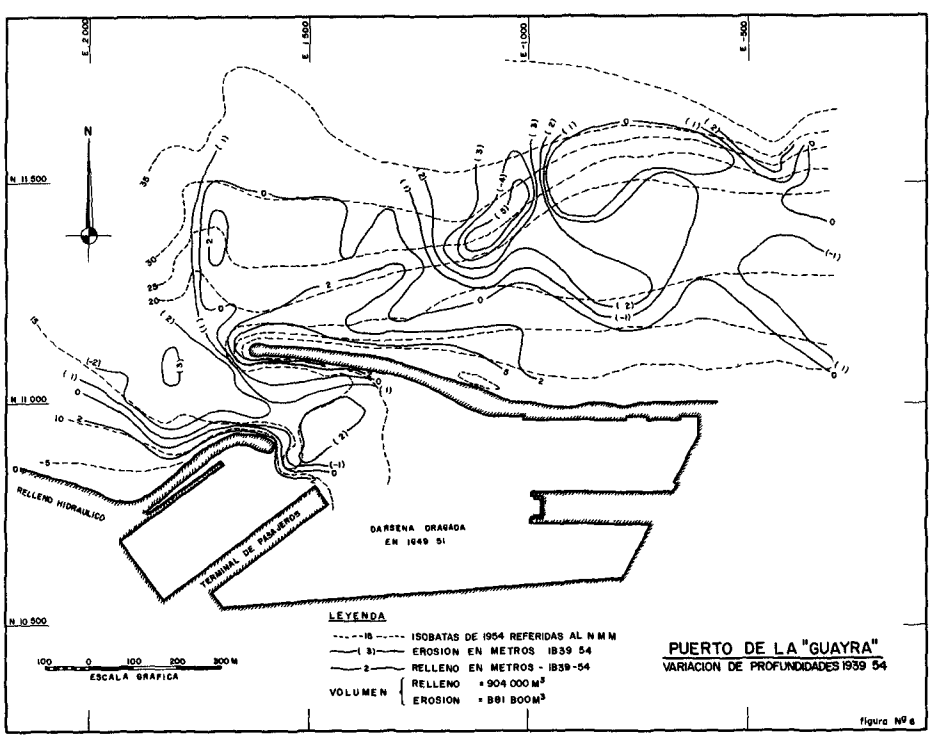
E 2.000
E 1.500
E 1.000
E 500
N 11.500
N 11.000
N 10.500
N
RELLENO HIDRAULICO
TERMINAL DE PASAJEROS
DARSENA DRAGADA
EN 1949 51
LEYENDA
ISOBATAS DE 1954 REFERIDAS AL N M M
EROSION EN METROS 1839 54
RELLENO EN METROS - 1839-54
VOLUMEN
RELLENO = 904 000 M3
EROSION = 881 800M3
100 0 100 200 300 M
ESCALA GRAFICA
PUERTO DE LA "GUAYRA"
VARIACION DE PROFUNDIDADES 1939 54
figura Nº 8

Fig. 8

ramas, la primera de 290 metros de longitud con rumbo N. - 66° 30' O. y la segunda de 300 metros con rumbo N. 82° O., enlazadas entre sí con una curva. Igualmente se construyó - un rompeolas occidental de 400 metros de longitud, con su - sector principal en dirección N. 52° 30' E., con su extremo curvado hacia el interior de la rada. Entre ambos rompeolas queda un canal de acceso de 170 metros aproximadamente, para las embarcaciones (Fig. 8). Con estas obras se dá protección a una rada de 50 hectáreas; rada ésta que fué dragada durante la construcción de las citadas obras marítimas a - 10.5 metros de profundidad (34'), utilizando el material obtenido del dragado para relleno y depositando un importante volúmen de él, en el lado occidental del puerto, relleno éste que fué luego protegido por un enrocado en todo su frente Norte. Como consecuencia de las obras citadas, se han - producido rellenos en el lado Norte del rompeolas principal con algunas zonas de erosión en esta parte y otra erosión - pronunciada hacia el Suroeste del rompeolas principal y al exterior del canal, (Fig. 8). Esta erosión para el año 1954 alcanzaba a 3 metros por debajo del nivel de 1939. Para - 1959 el relleno en el lado Norte del rompeolas principal aumentó en forma importante y el sedimento, pasando al Oeste - del citado rompeolas, comienza a llenar la zona erosionada antes referida, pero todavía acusando 1 metro por debajo - del nivel de 1939 (Figs. 9 y 10).

A profundidades del orden de los 20 a 30 metros, se registran algunas zonas de erosión que alcanza en algunos - sitios valores importantes y que arroja un valor máximo para la fecha del sondeo de 1954, el cual en la zona mas cercana al rompeolas, se ha reducido apreciablemente para 1959.

Los rellenos son como dunas sumergidas, no coinci- - diendo las lomas y depresiones en los planos batimétricos - preparados para las varias fechas citadas, notándose una migración hacia el Oeste a medida que disminuyen los fondos, (que aumenta la sedimentación). El movimiento de sedimento es evidente hasta profundidades de 35 metros y a distancias de 600 metros al Norte del rompeolas principal.

Las erosiones dentro de la rada, que aparecen en la figura N° 8, parecen tener su causa en el efecto de las hélices de las embarcaciones que en dicha zona practican la ciaboga para atracar en el lado occidental del terminal de pasajeros.

Los volúmenes de rellenos y de erosiones obtenidos - en los lapsos de 1939 a 1954, 1939 a 1959 y 1954 a 1959, lamentablemente no pueden servir de base para una estimación fidedigna del volúmen anual promedio de arrastres de sedimentos granulares a lo largo del Litoral Central, debido a las siguientes circunstancias.

Entre las desembocaduras de los ríos El Cojo y Macu-

to y en frente de la población de este mismo nombre, existe un valle submarino profundo, entre los conos de deyección - de los citados ríos; este valle tiene profundidades importantes a distancia relativamente corta de la costa. En los años 1950-1951, fueron construídos en este sector de costa unas escolleras casi perpendiculares a la ribera, que se extendieron hasta profundidades de 7 metros. Como consecuencia de estas obras, parte de los sedimentos arrastrados a - lo largo del litoral, muy probablemente fueron atrapados en este cañón submarino, con la consecuente disminución de la alimentación hacia el Oeste.

En el sector comprendido entre Punta de Mulatos y Macuto, zona ésta situada inmediatamente aguas abajo de di- - chas obras, se registraron en el lapso 1950-1954, importantes movimientos de fondos con preponderancia de erosión - (Fig. 11). Esta zona es intermedia entre Macuto y el puerto de La Guayra. Dada la magnitud de las erosiones registradas en esta zona, deberá tomarse con cautela dicha información, hasta tanto no se realicen sondeos periódicos para verificar las variaciones de fondos. El sector Punta de Mulatos-Macuto, por otra parte, a lo largo de su línea de playa ha presentado problemas de erosiones en años anteriores a la - construcción de las citadas obras, como se desprende de los frecuentes trabajos de reparación que se necesitaba practicar a lo largo de una vía férrea que corría entre las poblaciones de La Guayra y Macuto, hasta el año de 1948 aproximadamente.

En 1954 fué construída la Avenida Soublette entre La Guayra y Punta de Mulatos, para lo cual se requirió hacer - rellenos hacia el mar, de cierta importancia, los cuales - fueron protegidos del oleaje por escolleras de rocas paralelas a la costa, en unos sectores, y por espigones en forma de L, perpendiculares a la misma. Durante el lapso de construcción estima el autor, que importantes volúmenes de sedimentos fueron arrastrados por la corriente litoral.

Por otra parte, desde 1955 a 1956 en la costa situada al Oeste de Macuto y en el extremo occidental de la Urbanización Alamo, se practicó un relleno hacia el mar de bastante extensión, con materiales provenientes de banqueos y movimientos de tierras de otras obras; tal relleno no fué - protegido del oleaje por ninguna obra especial, de tal manera que éste lavó los agregados finos hasta que peñones y - cantos rodados de mayores dimensiones quedaron expuestos en la ribera, siendo capaces de establecer la nueva línea de - costa al resistir el oleaje. Estos rellenos aportaron volúmenes importantes de sedimentos a la corriente de arrastres litorales.

Por las razones antes dichas, los volúmenes relativos a los lapsos 1939-1954, 1939-1959 o 1954-1959, no pue-

ACRECENTAMIENTOS Y EROSIONES COMO CONSECUENCIA DE OBRAS MARITIMAS CONSTRUIDAS EN EL LITORAL CENTRAL DEL DISTRITO FEDERAL DE VENEZUELA

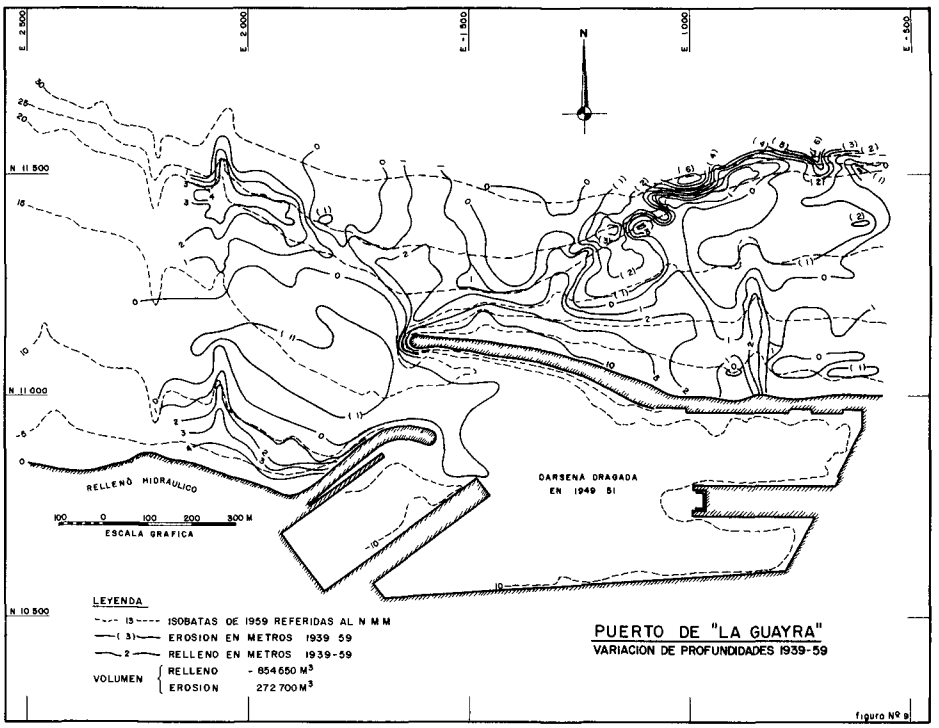

Fig. 9

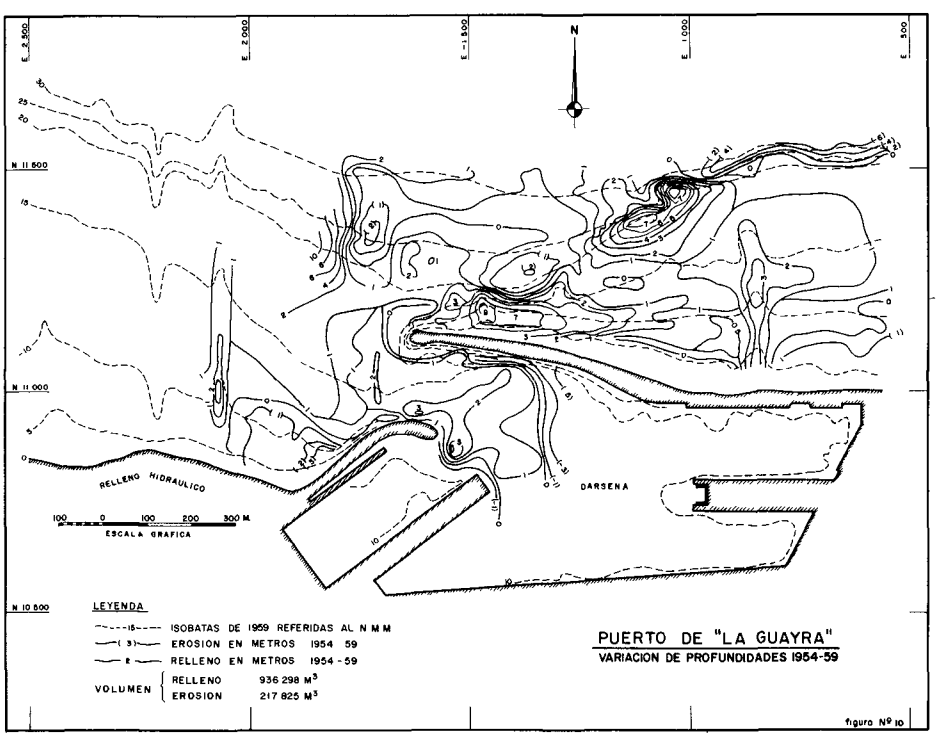

Fig. 10

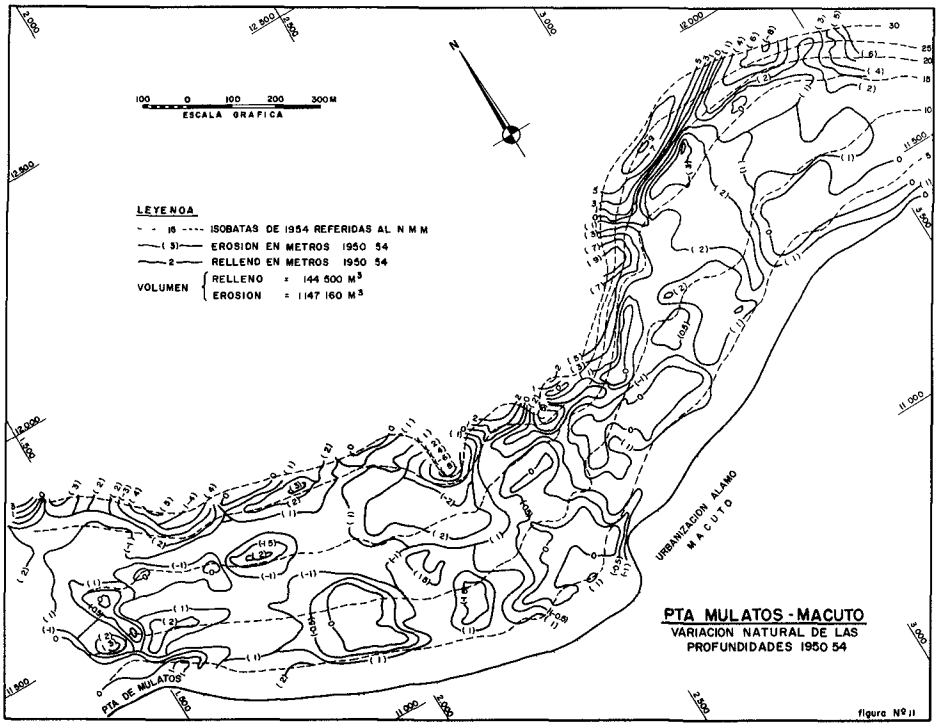
ESCALA GRAFICA
LEYENOA
ISOBATAS DE 1954 REFERIDAS AL N M M
EROSION EN METROS 1950 54
RELLENO EN METROS 1950 54
VOLUMEN
RELLENO = 144 600 M3
EROSION = 1147 160 M3
URBANIZACION ALAMO
MACUTO
PTA MULATOS - MACUTO
VARIACION NATURAL DE LAS
PROFUNDIDADES 1950 54
PTA DE MULATOS
figura Nº 11

Fig. 11

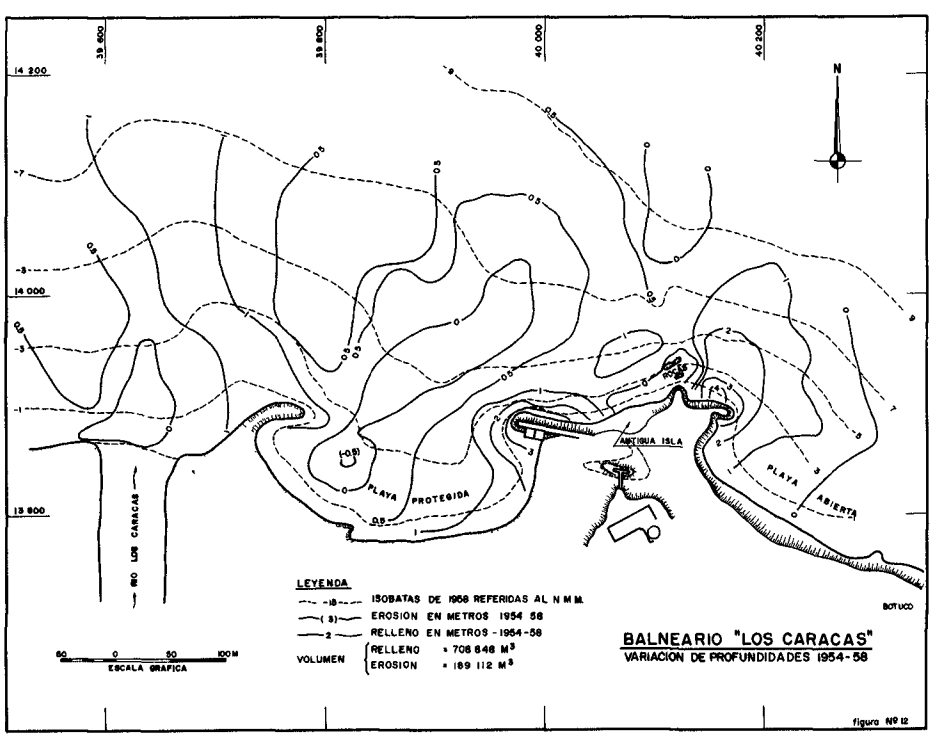
ESCALA GRAFICA
LEYENDA
ISOBATAS DE 1956 REFERIDAS AL N M M.
EROSION EN METROS 1954 56
RELLENO EN METROS - 1954-56
VOLUMEN
RELLENO = 706 646 M3
EROSION = 189 112 M3
RIO LOS CARACAS
PLAYA PROTEGIDA
ARRIBUA ISLA
PLAYA ABIERTA
BALNEARIO "LOS CARACAS"
VARIACION DE PROFUNDIDADES 1954-56
figura Nº 12

Fig. 12

den servir, como antes se expresó, de base para la estimación de volúmenes promedios anuales de arrastres.

Del análisis de las figuras Nos. 8, 9 y 10, se desprende que despues de 1954 la acumulación de sedimentos en el lado Norte del rompeolas principal ha aumentado y que hacia el Oeste del extremo occidental de este rompeolas, están pasando sedimentos según la dirección general del flujo de materiales sólidos y que las lomas y depresiones submarinas correspondientes a las zonas de rellenos y de erosiones muestran una marcada migración al Oeste. El movimiento de sedimentos en profundidades hasta de 35 metros, es evidente. En el canal de acceso al puerto y dentro de la rada, se inicia una importante sedimentación no registrada en 1954.

Balneario Los Caracas.- En este Centro Vacacional, situado al extremo oriental del Litoral Central del Distrito Federal y entre las desembocaduras de los ríos Los Caracas y El Botuco, se construyeron en el año de 1954, rompeolas y escolleras para la formación de playas. Básicamente las obras consistieron en la prolongación, hacia el Este y hacia el Oeste, de una pequeña isla que quedaba a corta distancia del cerro que abruptamente caía en la distancia media entre ambos ríos, la cual fué unida a tierra. La rama occidental de esta obra, con 65 metros de longitud y rumbo N. 80° O. y la rama oriental con 70 metros aproximadamente y con dirección general N. 83° E. y la citada isla, constituyen la principal obra de protección. Al Oeste de ésta y en la margen derecha de la desembocadura del río Los Caracas, se construyó otro rompeolas con 100 metros aproximados de longitud y rumbo N. 50° E., seguido de un pequeño espigón de modelado de playa (Fig. 12). Entre el río El Botuco y la isla central, se construyeron pequeños espigones de modelado de playa.

El resultado final de estas obras, según comparación de planos batimétricos de 1954 y 1958, fué el de un amplio relleno, ya sea en el lado oriental correspondiente a la playa abierta del río El Botuco, o bien en la playa principal semiprotegida inmediata al Este del río Los Caracas. Las variaciones de los fondos con preponderancia de rellenos, son moderadas. Esta obra, estando al extremo oriental de las obras del Litoral Central y por lo tanto, sin ningún disturbio aguas arriba, hacia el Este, en lo que respecta a alimentación de sedimentos, puede fijar un orden de los volúmenes anuales promedios de arrastres sólidos a lo largo del litoral, con la salvedad de la fuerte alimentación de sedimentos que localmente puede aportar el río Los Caracas y en menor proporción el río El Botuco. El volúmen medio de transporte en esta zona, alcanzaría así un valor de 111.400 m3/año.

Nótese en la figura N° 12, la zona de erosión hacia

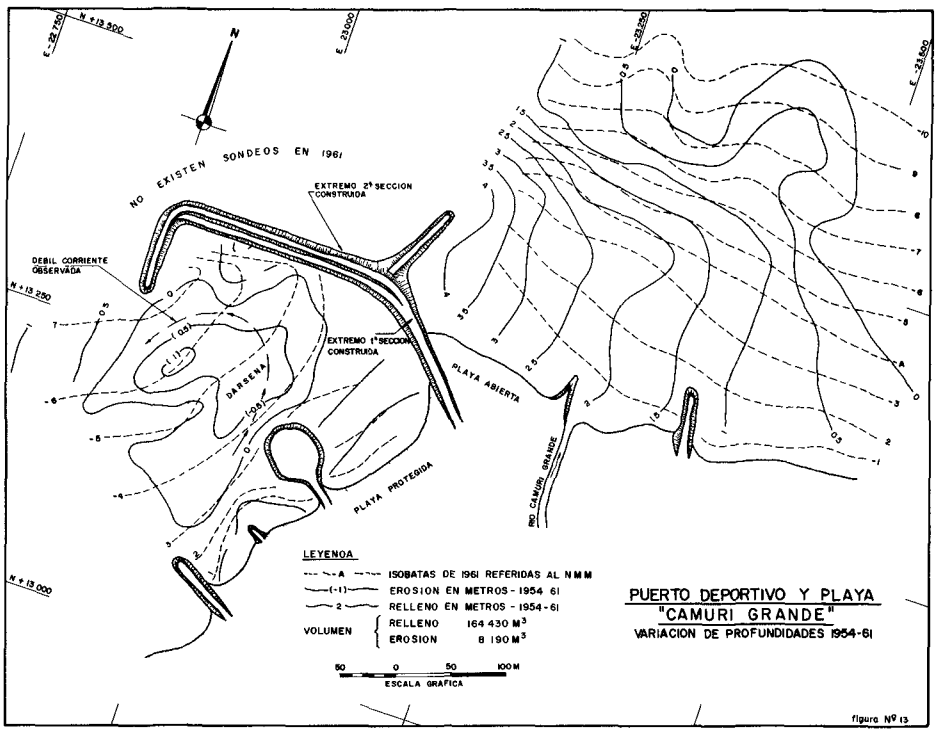
N
E - 22 750
N + 13 500
E - 23000
E - 23 250
E - 23 500
NO EXISTEN SONDEOS EN 1961
EXTREMO 2ª SECCION CONSTRUIDA
DEBIL CORRIENTE OBSERVADA
N + 13 250
EXTREMO 1ª SECCION CONSTRUIDA
DARSENA
PLAYA ABIERTA
PLAYA PROTEGIDA
RIO CAMURI GRANDE
N + 13 000
LEYENDA
ISOBATAS DE 1961 REFERIDAS AL N M M
EROSION EN METROS - 1954 61
RELLENO EN METROS - 1954-61
VOLUMEN
RELLENO 164 430 M3
EROSION 8 190 M3
50 0 50 100 M
ESCALA GRAFICA
PUERTO DEPORTIVO Y PLAYA
"CAMURI GRANDE"
VARIACION DE PROFUNDIDADES 1954-61
figura Nº 13

Fig. 13

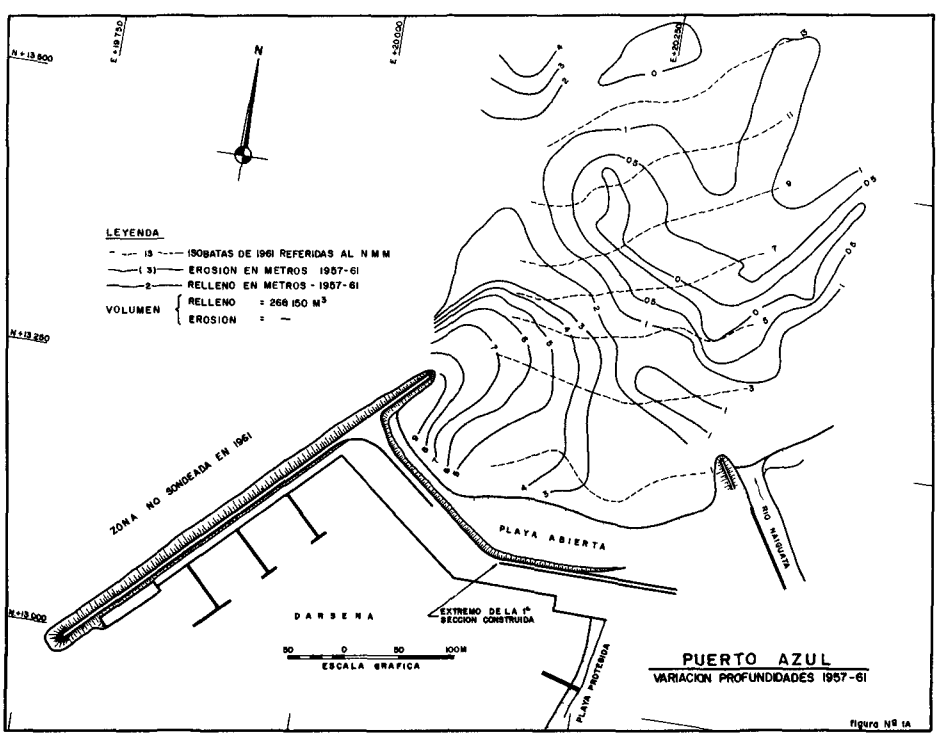
N
E 19 750
E 20 000
E 20 250
N + 13 500
N + 13 250
N + 13 000
LEYENDA
ISOBATAS DE 1961 REFERIDAS AL N M M
EROSION EN METROS 1957-61
RELLENO EN METROS - 1957-61
VOLUMEN
RELLENO = 266 150 M3
EROSION = —
ZONA NO SONDEADA EN 1961
PLAYA ABIERTA
RIO MATAGUA
DARSENA
EXTREMO DE LA 1ª SECCION CONSTRUIDA
PLAYA PROTEGIDA
50 0 50 100 M
ESCALA GRAFICA
PUERTO AZUL
VARIACION PROFUNDIDADES 1957-61
figura Nº 14A

Fig. 14

el Suroeste del extremo occidental del rompeolas principal, frente a la playa protegida y donde normalmente el oleaje es de mayor amplitud que en las zonas vecinas, fenómeno similar al registrado en el puerto de La Guayra.

Puerto Deportivo y Playa Camurí Grande.- Las obras marítimas de este Centro Recreacional, consistieron en un rompeolas principal de tres ramas, la primera de 155 metros con rumbo N. 45° O.; la siguiente de 210 metros y dirección Este-Oeste y la tercera de 100 metros de longitud con dirección Norte-Sur. Este rompeolas principal abriga una dársena deportiva (marina) de 3 hectáreas y sirve de abrigo a una playa protegida hacia el Sur de dicha obra (Fig. 13).

En la intersección de la primera y segunda rama del rompeolas principal, arranca un espigón con rumbo N. 22° 30' E. y con longitud aproximada de 100 metros, que interceptando los arrastres de sedimentos, ha formado playa en su lado oriental, la cual queda modelada con espigones complementarios de escolleras de roca, aproximadamente perpendiculares a la costa. Esta playa es abierta, de suaves pendientes y de material arenoso mediano.

En la costa protegida por el rompeolas principal y previamente a la construcción de éste, se construyeron espigones de modelado de playa que permitieron formar una playa que posteriormente fué abrigada por la obra principal.

La consecuencia de estas obras, según comparación de planos batimétricos de 1954 (fecha de construcción de las obras) y de 1961, fué la acumulación de sedimentos en el lado oriental y Norte del rompeolas principal; la acumulación de sedimentos hacia el extremo Nororiental de la dársena protegida y la erosión al Sureste del extremo del rompeolas principal, de cierta extensión hasta 1 metro por debajo del nivel de 1954.

Dentro de la dársena protegida, se observan corrientes en el sentido contrario al de las agujas del reloj, aparentemente debido a las mismas causas citadas anteriormente.

Debe observarse aquí, que la primera rama del rompeolas principal, fué construída simultáneamente con los espigones de modelado de playa del flanco occidental del cabo (actual playa protegida); que la segunda rama de este rompeolas se construyó sólo parcialmente, interrumpiéndose las obras por un lapso del orden de 1 año; y que el espigón exterior con rumbo N. 22° 30' E., sólo fué construído al final de las obras de protección de la dársena; y por tanto la erosión que se observa en la figura N° 13, dentro de la dársena actual, correspondió a zona abierta al Suroeste del extremo del rompeolas, para aquel entonces, mostrándose así una situación similar a las registradas en el puerto de La Guayra y en el Balneario de Los Caracas.

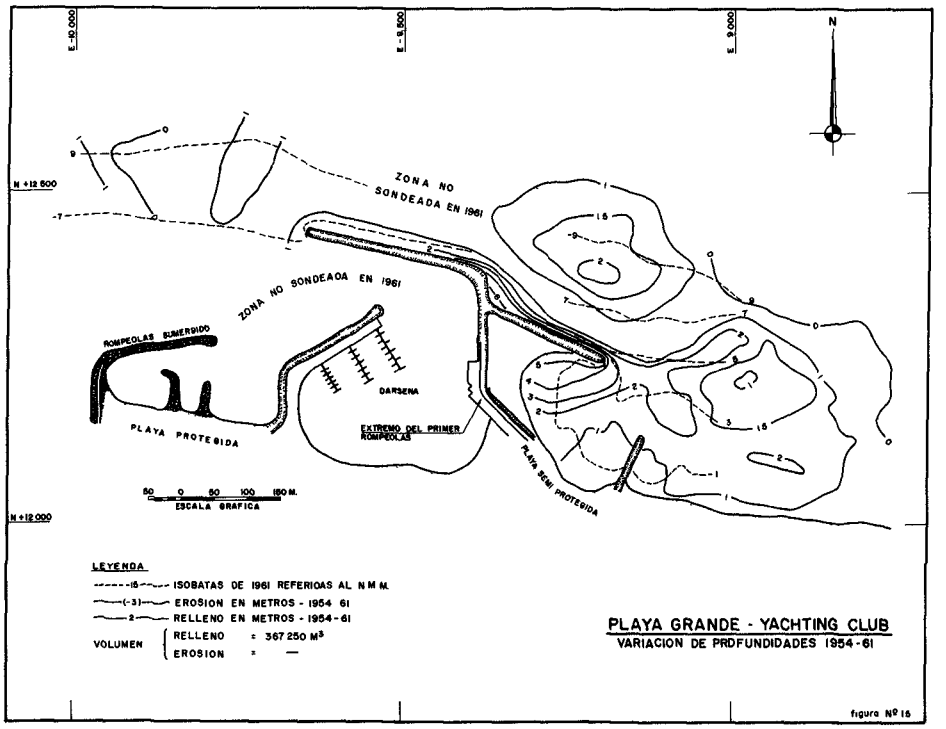
E - 10.000
E - 9.500
E - 9.000
N
N +12 500
N +12 000
ZONA NO SONDEADA EN 1961
ZONA NO SONDEADA EN 1961
ROMPEOLAS SUMERGIDO
DARSENA
PLAYA PROTEGIDA
EXTREMO DEL PRIMER ROMPEOLAS
PLAYA SEMI PROTEGIDA
50 0 50 100 150 M.
ESCALA GRAFICA
LEYENDA
-15- ISOBATAS DE 1961 REFERIDAS AL N M M.
(-3) EROSION EN METROS - 1954 61
2 RELLENO EN METROS - 1954-61
VOLUMEN RELLENO = 367 250 M3
EROSION = —
PLAYA GRANDE - YACHTING CLUB
VARIACION DE PROFUNDIDADES 1954-61
figura Nº 15

Fig. 15

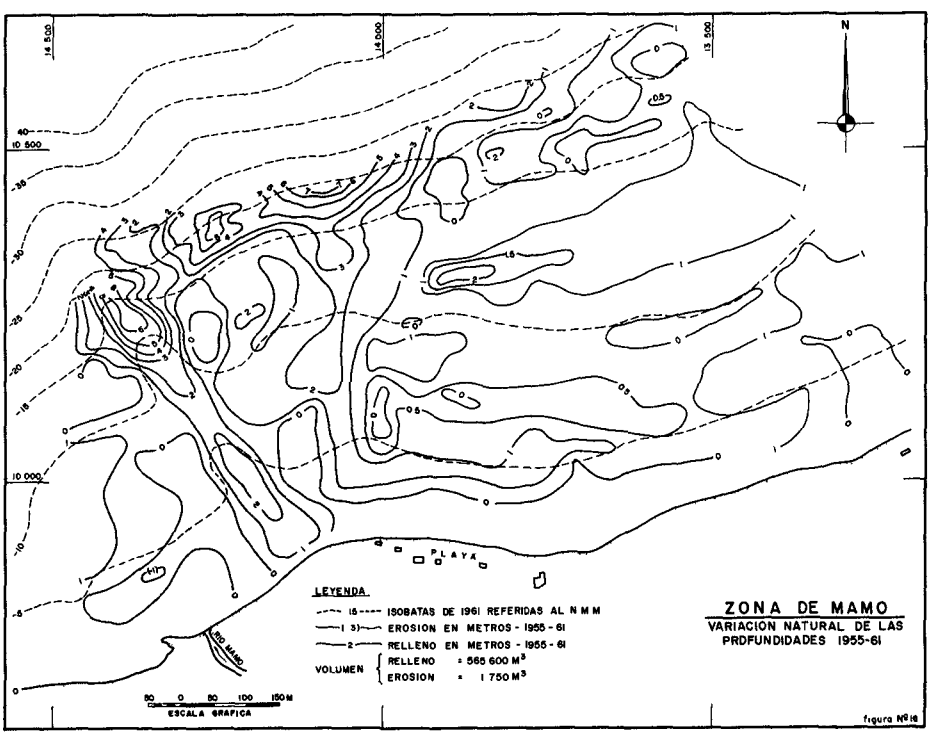
14.500
14.000
13.500
N
10 500
10 000
PLAYA
LEYENDA
-15- ISOBATAS DE 1961 REFERIDAS AL N M M
(-3) EROSION EN METROS - 1955 - 61
2 RELLENO EN METROS - 1955 - 61
VOLUMEN RELLENO = 565 600 M3
EROSION = 1 750 M3
80 0 80 100 150 M
ESCALA GRAFICA
ZONA DE MAMO
VARIACION NATURAL DE LAS PROFUNDIDADES 1955-61
figura Nº 16

Fig. 16

ACRECENTAMIENTOS Y EROSIONES COMO CONSECUENCIA DE OBRAS MARITIMAS CONSTRUIDAS EN EL LITORAL CENTRAL DEL DISTRITO FEDERAL DE VENEZUELA

Los volúmenes de relleno y de erosión anotados en la figura N° 13, correspondiente al lapso 1954-1961, son incompletos, por cuanto la zona exterior al Norte y Noroeste del rompeolas principal, no fué sondeada en 1961.

Puerto Azul.- En el flanco occidental del cono de deyección del río Naiguatá, se desarrolló un Centro Vacacional en donde se construyeron obras marítimas interesantes. Un rompeolas principal compuesto de tres ramas: la primera con dirección Oeste franco, de 120 metros; la siguiente de 200 metros y rumbo N. 52° 30' O. y la tercera con rumbo S. 45° O., de 345 metros aproximadamente. Complementan dicha obra, espigones de modelado de playa exteriores en la playa abierta (oceánica) y en la playa protegida al Sureste de la dársena. La primera rama del rompeolas principal fué construída conjuntamente con los espigones de modelado de playa del flanco occidental del cabo (actual playa protegida). La dársena (marina) es de 6 hectáreas.

Lamentablemente los sondeos practicados en el año 1961, sólo se extendieron a la zona nororiental en frente de la playa abierta (oceánica), de tal manera que la información disponible es incompleta en cuanto a los volúmenes de rellenos o erosiones producidos como consecuencia de las obras.

Dentro de la dársena se observa una débil corriente en el sentido contrario a las agujas del reloj.

Playa Grande Yachting Club.- Este Club Naútico situado al Oeste de Cabo Blanco, se construyó en la ribera situada frente a la formación geológica de rocas sedimentarias, areniscas y conglomerados (11), en cuya playa afloraban capas de coral cimentado. Poco antes del año 1950 se construyó un pequeño rompeolas de dos ramas; la primera con dirección Norte franco y 100 metros de longitud y la segunda de 115 metros con rumbo N. 45° O. La consecuencia inmediata de esta obra fué la formación de playas en ambos lados de la misma, siendo la protegida situada en su lado occidental y constituída por arena fina. Se registraron dentro de esta zona protegida, corrientes en el sentido contrario a las agujas del reloj, algunas veces de fuerte intensidad (Fig. 15).

En 1955 se construyeron las obras marítimas para el Puerto Deportivo y para playa, consistiendo estas obras en un rompeolas principal, que arrancando del extremo Norocciental del anterior, avanza 100 metros en dirección Norte franco en su primera rama, para luego cruzar con rumbo N. 65° O. con 115 metros de longitud. Esta es la obra principal de abrigo de la dársena portuaria y de la playa protegida. La dársena portuaria queda cerrada hacia el Oeste con

otro rompeolas de dos ramas; la primera en dirección Norte franco, con 130 metros y la segunda con rumbo N. 64° E. de 160 metros. La dársena portuaria tiene una amplitud de 6 - hectáreas y el canal de acceso para las embarcaciones es de 80 metros de ancho.

Arrancando del rompeolas principal del puerto y hacia el Sureste, se construyó un espigón de modelado de playa que conjuntamente con otro espigón que arranca desde la orilla, encierran la playa semiprotegida (Fig. 15). Al Oeste de la dársena portuaria se construyó una playa protegida por el rompeolas principal del puerto y por un rompeolas sumergido, situado a 120 metros de la orilla.

Como consecuencia de estas obras marítimas, se produjo una fuerte acumulación de sedimentos en el lado oriental del rompeolas principal, formándose una playa estable (playa semiprotegida). Las variaciones de fondo al Oeste del - rompeolas principal y en las inmediaciones de la playa protegida, no se pudieron constatar por no haber sido sondeada dicha zona en 1961. Es importante observar el fuerte relleno producido en la zona oriental. El volúmen de relleno anotado en la figura N° 15, sólo se refiere a la zona común a los planos batimétricos de 1954 y 1961 y por tanto, no representa el volúmen total de rellenos, para dicho lapso.

Al Oeste de Playa Grande, no se han registrado erosiones importantes a lo largo de la línea de costa, debiéndose observar que toda la zona hasta la desembocadura del - río Tacagua, corresponde a la formación geológica antes referida (11) y que a lo largo de la ribera hay formaciones - coralíferas cimentadas. La quebrada Tacagua, la quebrada La Zorra y el río Mamo, aguas abajo (al Oeste) de este Puerto Deportivo, aportan importantes cantidades de sedimentos.

En la figura N° 16, se muestran la variación de profundidades, por comparación entre planos batimétricos de - 1955 a 1961, en la zona de Mamo y en ella podrá observarse que las variaciones naturales del fondo no dejan de ser importantes, aún cuando la loma submarina que aparece inmediatamente al Este de la desembocadura del río Mamo, posiblemente ya existía en 1955, pero como los perfiles transversales tomados para los sondeos en dicha fecha eran distanciados, precisamente dicha loma quedó entre dos de ellos, por lo cual no fué registrada, de tal manera que los rellenos - anotados en dicha figura para esta zona, posiblemente exceden a la realidad. Esto hace resaltar la necesidad de establecer los perfiles transversales para los levantamientos - batimétricos, bastante cercanos y perfiles paralelos a la - costa, como comprobación de los transversales usualmente utilizados.

Otras obras marítimas construídas en el litoral.- A-

demás de las obras marítimas antes reseñadas, en el Litoral Central en consideración, se han construído rompeolas para formación de la playa del Club Tanaguarena; rompeolas emergentes y sumergidos para la playa y Puerto Deportivo del Hotel Sheraton-Macuto; las obras de protección de la Avenida Soublette al Este del puerto de La Guayra; espigones de modelado de playa para el Balneario de Catia de La Mar; rompeolas y espigones de modelado de playa para la formación del Balneario público de Naiguatá, al Este de la desembocadura del río del mismo nombre; y otras obras menores. Lamentablemente no existe información sobre la batimetría en dichos sitios para fechas posteriores a su construcción, por lo cual no se puede establecer para ellos, ningún análisis sobre los fenómenos de sedimentación y erosión. Sin embargo, es importante observar que al Oeste de las obras del Puerto Deportivo del Hotel Sheraton-Macuto, situado en la Urbanización Caribe, especialmente en el sector comprendido entre los ríos San Julián y El Cojo, se ha registrado una retrogradación de la línea de costa, del orden de 18 metros con relación a la línea primitiva correspondiente al año de 1956, en que fueron construídas dichas obras (véase fotografía). En este sector de costa la alimentación de sedimentos quedó cortada por las obras citadas, además de que en el Club Tanaguarena, en donde se construyó una playa con el auxilio de rompeolas parcialmente terminados, se practican dragados sistemáticos de las arenas acumuladas, las cuales son utilizadas para trabajos en tierra.

DISTRIBUCION SELECTIVA DE LOS SEDIMENTOS

En los varios estudios marítimos practicados por la oficina del autor en el litoral en referencia, en los años de 1954 a 1955 y en los meses de mayo a octubre, fueron tomadas muestras de sedimentos en varias zonas y practicados análisis granulométricos de los mismos.

En una forma general se constató un aumento del grano medio en la zona de rompiente y a partir de allí hacia el mar y hasta profundidades del orden de 12 metros, una disminución progresiva de dicho diámetro medio; a profundidades entre 12 y 30 metros, la granulometría no registró una tendencia definida, notándose sin embargo, en general, un aumento del diámetro medio en ciertas zonas; pero de una manera general no se pudo establecer una correlación definida entre la profundidad y el diámetro medio del sedimento.

En un intento para verificar en la naturaleza, los estudios hechos en modelo por Ippen y Eagleson sobre la distribución de los sedimentos por efecto del oleaje (7), se seleccionaron aquellas muestras comprendidas entre profundidades del orden de 3 a 12 metros, es decir, desde una pro-

Fotografia No. 1. Retrogradación de la línea de costa. Camuri Chico - Sector Rio San Julián - Punta Brisas.

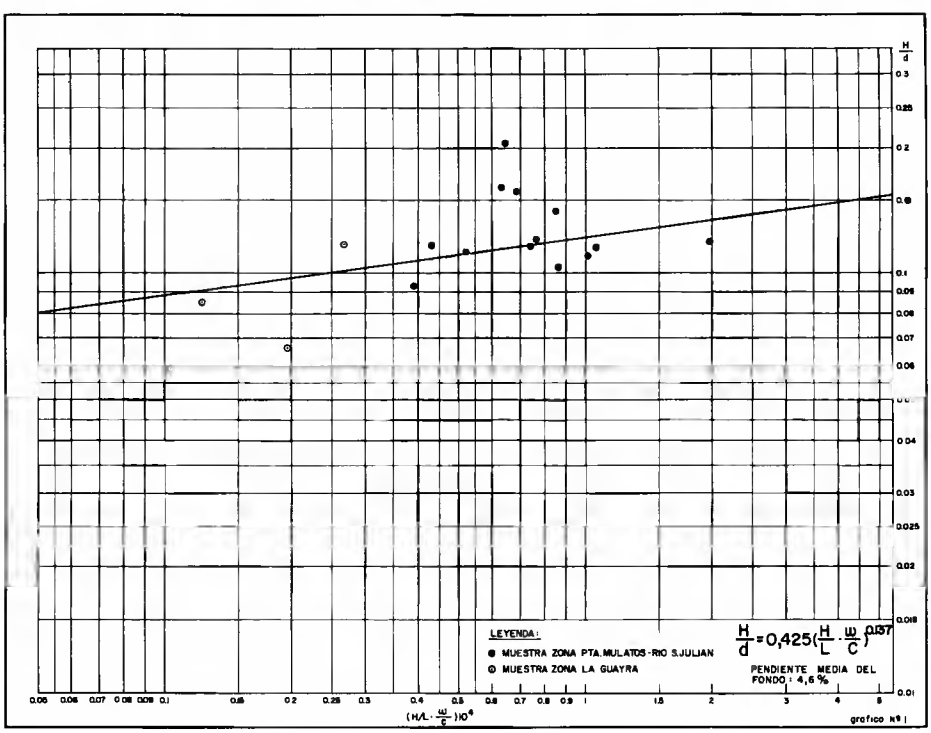

Grafico No. 1

ACRECENTAMIENTOS Y EROSIONES COMO CONSECUENCIA DE OBRAS MARITIMAS CONSTRUIDAS EN EL LITORAL CENTRAL DEL DISTRITO FEDERAL DE VENEZUELA

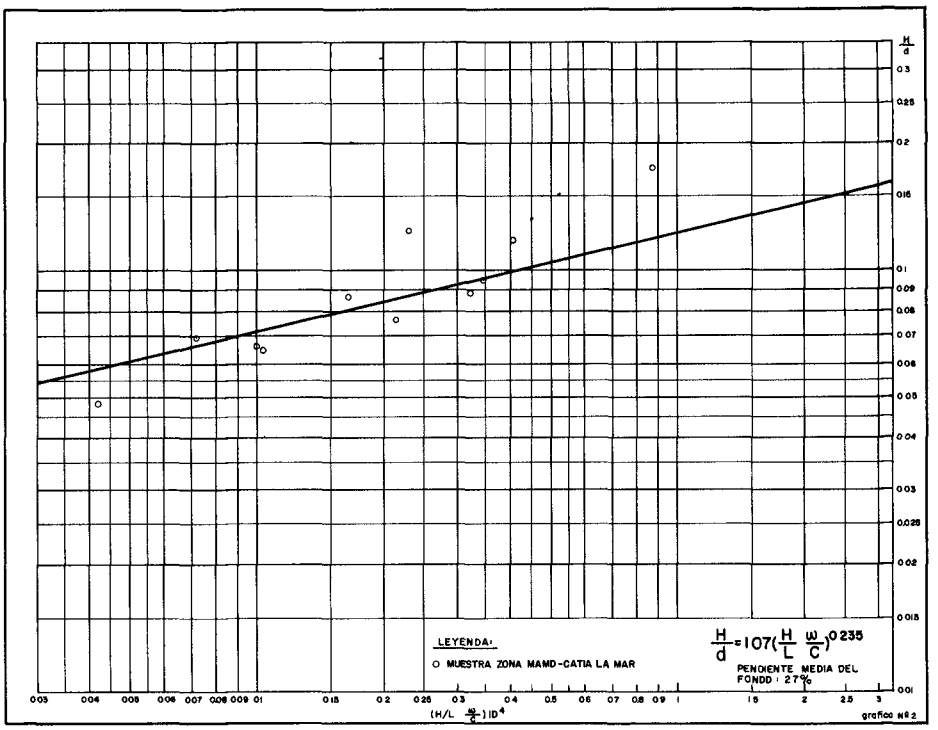

Grafico No. 2

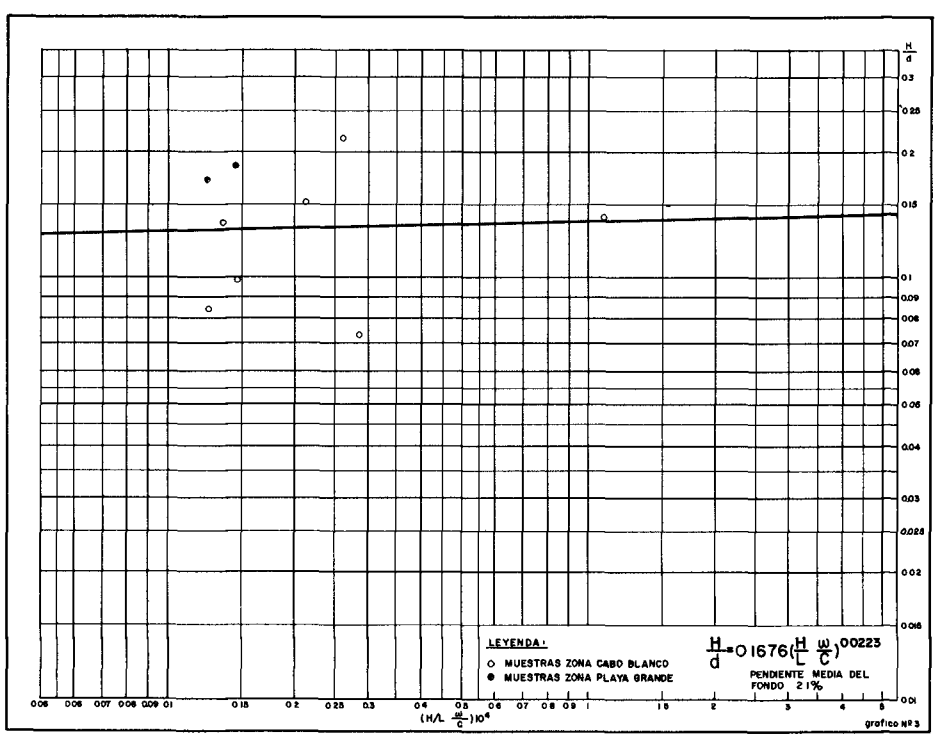

Grafico No. 3

fundidad no influenciada por las rompientes, hasta la profundidad en que era aparente en forma general, la disminución del diámetro medio. Las muestras fueron tomadas en una extensión de 12 millas naúticas, desde la desembocadura del río San Julián, por el Este, hasta la desembocadura del río Mamo, por el Oeste.

La densidad del grano de las arenas, se estableció en 2.65 y la velocidad de sedimentación de la muestra, se caracterizó por la de su grano medio.

Las muestras fueron separadas en tres grupos, a saber: a) las correspondientes a la zona comprendida entre el puerto de La Guayra y el río San Julián, cuya pendiente general del fondo es uniforme (4.5 a 6% aproximadamente); en donde la pendiente local en los sitios de toma de muestras tenía valores bastante cercanos (4.6% promedio); y situados frente a una costa aluvional; b) las correspondientes a la zona entre Cabo Blanco y Catia de La Mar, con suave pendiente general (0.92% aproximadamente); con pendientes locales en los sitios de toma de muestras similares (2.1%); y situada frente a la costa de arenisca y conglomerados de la formación geológica Cabo Blanco; y c) las correspondientes a la zona entre Catia de La Mar y Mamo, con pendiente general de 3.3% y local de 2.7% y situada frente a una costa aluvional.

Las muestras tomadas en lugares de poca profundidad y muy cerca de la desembocadura de los ríos y quebradas, fueron eliminadas por considerar que no eran representativas para el estudio, por no haber sido aún convenientemente clasificados y distribuídos los sedimentos por la acción del oleaje.

Luego fueron relacionadas las características del oleaje en el sitio de toma de cada muestra, su profundidad y la velocidad de sedimentación del grano medio, según una expresión teórica adimensional correspondiente a la condición de equilibrio (7).

La inter-relación entre dichos parámetros se pudo establecer, para el litoral en consideración, en el lapso considerado y para las pendientes medias del fondo del mar antes establecidas, según las funciones siguientes:

$$[1] \quad \frac{H}{d} = 0.425 \left(\frac{H}{L} \cdot \frac{w}{C}\right)^{0.137} \qquad P = 4{,}6\%$$

$$[2] \quad \frac{H}{d} = 1.07 \left(\frac{H}{L} \cdot \frac{w}{C}\right)^{0.236} \qquad P = 2{,}7\%$$

$$[3] \quad \frac{H}{d} = 0.1676 \left(\frac{H}{L} \cdot \frac{w}{C}\right)^{0.0223} \qquad P = 2{,}1\%$$

en donde H es la altura de la ola en el sitio considerado; L su longitud; d la profundidad; C la celeridad de la ola; ω la velocidad de sedimentación del grano medio para una densidad de 2.65 y p la pendiente del fondo del mar en el sitio de la toma de muestra, como valor promedio en una extensión de 50 metros aproximadamente alrededor de dicho sitio.

Las características de la ola significativa, como se expresó en el capítulo de Introducción son: H_o = 0.95 metros L_o = 100 metros, T = 8 segundos, con dirección en mar profundo del Noreste, siendo H_o L_o y T respectivamente, la altura de la ola, su longitud en mar profundo y su período.

En los gráficos se hace la representación en escalas logarítmicas, de las expresadas funciones.

Se intentó obtener una correlación similar con olas de 5.5 segundos de período y de igual amplitud, correspondiente a la ola corta observada normalmente en el litoral, como se expresó en la primera parte de este estudio, pero la dispersión de puntos en el gráfico fué muy amplia, no pudiendo establecerse función definida entre las variables.

Se intentó establecer una inter-relación entre el coeficiente de uniformidad del sedimento: $\frac{S_{80} - S_{20}}{S_{50}}$ y la profundidad del sitio de la toma de muestras (8), no pudiéndose obtener una relación o tendencias definidas. (S_{80}, S_{50} y S_{20}, son diámetros correspondientes al 80%, 50% y 20% de pesos retenidos en el análisis granulométrico).

CONCLUSIONES

De las consideraciones anteriores podemos establecer las siguientes conclusiones válidas para el Litoral Central del Distrito Federal:

1). La ola significativa se puede establecer tentativamente con H_o = 0.95 metros, T = 8 segundos y dirección en mar profundo del Noreste; en donde H_o y T son respectivamente la altura en mar profundo y el período.

2). La ola de tormenta para el cálculo de la estabilidad de las obras marítimas, puede tentativamente establecerse con H_o = 4.6 metros, T = 10 segundos.

3). La corriente litoral del oleaje y consecuentemente la dirección general de los arrastres de sedimento, a lo largo de la costa, es hacia el Oeste.

4). Los movimientos de sedimentos en el litoral son notorios hasta profundidades de 35 metros.

5). Como valores promedios en las zonas y lapsos considerados, las ecuaciones [1], [2] y [3] pueden ser buena guía en el estudio de la distribución selectiva de los sedimentos bajo la acción de la ola significativa.

6). Se impone la necesidad de establecer y operar por lapsos importantes, oleógrafos y correntógrafos en sitios adecuados del litoral y practicar la medición simultánea, periódica y sistemática de la dirección del oleaje.

7). Es deseable que todo trabajo marítimo a efectuarse en el futuro, incluya la toma de muestras de los sedimentos, desde el límite superior correspondiente al roción de la ola hasta profundidades del orden de los 35 metros, con el objeto de continuar las investigaciones tendientes a complementar con datos de la naturaleza, los estudios antes referidos de Ippen, Eagleson y asociados (7), (8).

8). Como valor tentativo de los volúmenes medios anuales de sedimentos a lo largo del litoral y como valor para diseño, se puede aceptar 111.400 m3.

Como conclusiones de carácter general, podemos anotar lo siguiente:

1). Los levantamientos batimétricos deben efectuarse con la mayor profusión de perfiles transversales que sea posible y con la inclusión de perfiles complementarios paralelos a la línea de costa, lo cual permitirá una mayor precisión en la determinación de los estimados de volúmenes de relleno y erosiones, cuando se comparen batimetrías de fechas distintas.

2). Las sedimentaciones y erosiones alrededor de una obra marítima de protección, siguen en forma general el esquema mostrado en la figura N° 6.

3). Las erosiones registradas a cierta distancia al Oeste del extremo del rompeolas de protección, corresponde a las mayores elevaciones del oleaje que se produce en esa zona por el efecto mismo de las obras.

4). Es deseable, en un futuro, que se practiquen estudios adicionales tendientes a correlacionar la amplitud de la erosión antes referida, con el espectro de oleaje, por los efectos combinados de refracción y de difracción de las obras marítimas, las amplitudes del oleaje y la sobreelevación relativa del nivel -

medio del mar.

5). Es deseable, que especialistas en Ingeniería de Costa, continúen estudios tendientes a correlacionar las características del oleaje y del sedimento, la batimetría y los volúmenes de arrastres, como parámetros principales medidos en la naturaleza, con los estudios teóricos y de modelos reducidos.

RECONOCIMIENTO

Especial reconocimiento quiero hacer a los Ingenieros Nicolás Nouel H. y Raúl Luis Larghi, por su cooperación en el ordenamiento de la información y en la revisión del estudio.

REFERENCIAS

AUTOR	TITULO
(1). PEREZ MENA, RAMON L.	Las corrientes marinas como factor importante en la deposición de sedimentos. Dirección Técnica de Geología Ministerio de Minas e Hidrocarburos.
(2). SARDI SOCORRO, VICTOR.	Gasto máximo de los ríos y las quebradas del Litoral Central. Revista N° 275 del Colegio de Ingenieros de Venezuela.
(3). NOUEL, BERNARDO A.	Desarrollo del Litoral Central. Revista N° 246 del Colegio de Ingenieros de Venezuela.
(4). FIORINI, GAETANO.	Planta de tratamiento del río Mamo. Estudio de la Defensa contra las crecientes del río. Revista del I.N.O.S. N° 8.
(5). JOHNSON, J. W.	Informe privado. Oficina Técnica Bernardo Nouel Ingenieros S.A., sobre Shoreline development along the Venezuelan coast east of La Guayra harbor, (inédito).

(6). DIRECCION DE CARTOGRAFIA NACIONAL. MINISTERIO DE OBRAS PUBLICAS. VENEZUELA. Registros de mareas del Puerto de La Guayra.

(7). IPPEN AND P. S. EAGLESON. A study of sediment sorting by waves shoaling on a plane beach. Technical Memorandum N° 63. Beach Erosion Board.

(8). P. S. EAGLESON, B. GLENNE AND J. A. DRACUP. Equilibrium characteristics of sand beachs in the offshore zone. Beach Erosion Board. Techn. Mem. N° 126.

(9). SERVICIO DE METEOROLOGIA Y COMUNICACIONES. MINISTERIO DE LA DEFENSA. VENEZUELA. Anuarios meteorológicos de Venezuela. Años 1950 a 1954.

(10). W. C. PUNCHARD AND J. LENNOX HOUSTON. La Guayra Harbour Works. Minutes of Proceedings of the Institution of Civil Engineers. Vol. CXV. 1893-1894.

(11). DIRECCION DE GEOLOGIA. MINISTERIO DE MINAS E HIDROCARBUROS. VENEZUELA. Mapa geológico de la región de Caracas.

(12). PROYECTOS Y CONSTRUCCIONES MARITIMOS S.A. (PROCONMAR). Estudio y proyecto de las obras de acondicionamiento de la playa del Centro Recreacional de Catia de La Mar y puerto para la Escuela Naval. Informe sobre el modelo reducido, 1962. (Comunicación privada e inédita).

CHAPTER 37

"DRAGADO DE AGITACION CON BRAZO" EN EL CANAL DE MARACAIBO — VENEZUELA

Instituto Nacional de Canalizaciones

CAPITULO I

INTRODUCCION

La cuenca hidrográfica del Lago de Maracaibo situada en la parte Norte de la América del Sur, principalmente en Venezuela, está limitada al Oeste por la Sierra Perijá, al Sur y Sur-Este por el ramal venezolano de la Cordillera de Los Andes, al Este por la línea divisoria entre las aguas que corren al Lago y las que corren al mar Caribe, y por el Norte el Golfo de Venezuela. Su extensión total es de 89 756 kilómetros cuadrados de los cuales 73 658 están en territorio venezolano y 16 098 kilómetros en territorio colombiano; la parte venezolana a su vez se divide en 60 555 kilómetros cuadrados de tierra firme y 13 103 cubiertos por agua, incluyendo las islas. El aporte de agua dulce de la cuenca es de $50,57 \times 10^9$ metros cúbicos anuales aproximadamente, provenientes de numerosos ríos y riachuelos, especialmente abundantes en la región suroeste.

En el curso de su célebre exploración de la costa Norte de Sur América, Alonso de Ojeda descubrió, el 24 de agosto de 1499 el Lago de Maracaibo, llamado Coquivacoa por los naturales, y al cual dió el nombre de San Bartolomé. Alonso Pacheco fundó a Ciudad Rodrigo el 20 de enero de 1571, junto al estrecho o Brazo que conecta El Tablazo con el Lago. Esta ciudad fue reconstruída en 1574 por Pedro Maldonado quien le cambió el nombre a Nueva Zamora, pero mas tarde se la conoció como Maracaibo y con este último nombre ha llegado hasta nuestros días. Hoy es la población mas grande de la región, es la capital del Estado Zulia, y tiene 457 000 habitantes.

Geográficamente podemos dividir al Lago de Maracaibo y sus aguas colindantes en cuatro partes: el Lago propiamente dicho, el Brazo de Maracaibo, la Bahía de El Tablazo y el Golfo de Venezuela. (Ver Dibujos Nos. 1 y 2). De las tres primeras, la de mayor superficie, es el Lago de Maracaibo el cual tiene 12 013 kms. cuadrados, con una profundidad media de 25.9 metros (cerca de 85 pies) llegando en algunos sitios hasta los 33.50 metros (110 pies). El 87% del área del Lago (10 500 kms.2) tiene 10 o más metros (32.8 pies) de profundidad.

El Brazo de Maracaibo que conecta al Lago con El Tablazo, tiene una longitud de 40 kms., un ancho de 6 kms. en su extremo Norte y un máximo de 17 kms. en su extremo Sur, con un área total de 480 kms. 2,

aproximadamente. A todo lo largo del Brazo corre un canal natural, cuya anchura media es de 1 000 mts. aproximadamente, con 11.6 mts. (38 pies)de profundidad mínima y 17.7 mts. (58 pies)de profundidad máxima.

La Bahía o estuario de El Tablazo tiene forma trapezoidal y en general es de poca profundidad; limita al Sur con el Brazo de Maracaibo y se comunica con el Golfo de Venezuela por el Canal de la Barra de Maracaibo y las bocas llamadas de Cañonera y Cañonerita. Tiene en el sentido Norte-Sur una longitud de cerca de 24 kms., en el Este-Oeste un promedio de 27, y una superficie de 610 kms. 2. Es en El Tablazo donde se mezclan las aguas más o menos dulces que vienen del Lago por el Sur, teniendo lugar el movimiento principal de las corrientes a lo largo de un canal que, en su forma natural, serpenteaba por la parte central del estuario y tenía profundidades mínimas de 15 pies.

La costa Sur del Golfo de Venezuela está en constante variación, especialmente en la parte correspondiente a las bocas de San Carlos (principal) y Cañonera y Cañonerita (secundarias), debido al encuentro allí del movimiento litoral de arenas cuya dirección general es hacia el Oeste, con las corrientes originadas por la salida de aguas del Lago y las mareas, de rumbo hacia el Norte o Sur. El canal natural de El Tablazo pasaba frente a San Carlos para conectarse con el Golfo después de cruzar la Barra Exterior.

Las zonas de El Tablazo y de la Barra Exterior o Barra de Maracaibo han constituído tradicionalmente el problema básico para la navegación entre el Lago y el mar libre; solo que la de El Tablazo era algo difícil pero no peligrosa, mientras que la de la Barra Exterior era tan difícil como peligrosa. El canal natural que cruzaba ambas zonas tenía en El Tablazo una forma sinuosa relativamente estable en cuanto a posición y profundidad, pero en el cruce de la Barra Exterior, tanto la posición como la profundidad del canal de navegación eran muy variables. El sitio de cruce de la Barra Exterior variaba entre un punto extremo situado a varios kms. al Oeste del Castillo de San Carlos y otro entre San Carlos y Zapara; el canal se deslizaba entre islotes de arena y bancos muy movibles de igual material, que influenciaban tanto su posición como su profundidad y atrapaban los barcos que perdían la ruta. Otros factores de inestabilidad lo constituyen la sedimentación de materias en suspensión, las corrientes de densidad, y la floculación en las zonas de contacto del agua dulce con la salada. Esto último tiene lugar solamente en El Tablazo, especialmente en la zona deltaica alcanzada por las aguas turbias del río Limón, pues las del Lago mismo son perfectamente claras ya que éste último actúa como decantador de sus afluentes.

Las dificultades naturales del acceso al Lago de Maracaibo que acabamos de describir no tenían mayor esperanza de solución mientras el comercio de la cuenca estuviera limitado a una exportación relativamen

"DRAGADO DE AGITACION CON BRAZO" EN EL CANAL DE MARACAIBO — VENEZUELA

Dibujo No. 2

Dibujo No. 1

te pequeña de productos agrícolas y pecuarios, y a la importación de valores similares de bienes de consumo. El descubrimiento del petróleo al requerir el transporte de grandes cantidades de ese producto por la vía marítima, transformó completamente la situación y presentó la justificación económica necesaria para la construcción de obras adecuadas de canalización.

CAPITULO II

CONSTRUCCION DEL CANAL

El proyecto original preparado por el Coronel Robinson del Cuerpo de Ingenieros del Ejército Americano (abreviado U.S.A.C.E.) en 1940 y reformado en 1947, sirvió de base para los trabajos. Dicho proyecto consistía en la construcción de un canal rectilíneo con profundidad de 35 pies referida a la marea media baja (M.M.B.), cuyo rumbo quedó fijado en S. 8° 48' 40" O., tanto para el cruce de la Barra Exterior como para el eje de El Tablazo, con excepción de un pequeño sector al final de este último al cual se le dió un rumbo de S. 29° 11' 20" E., a fin de empatar con el canal natural frente a Punta de Palmas. Este canal quedaba naturalmente dividido en una parte Interior con 182.88 mts. (600 pies)de ancho y 22.560 kilómetros de longitud contados hacia el Sur, a partir del punto Cero situado en Zapara, y una parte Exterior con 304.80 mts. (1 000 pies) de ancho y 12.450 kms. de largo a partir del mismo punto Cero, hacia el Norte. Para la protección de la parte exterior del canal cercana a la costa, se recomendaba la construcción de dos malecones, uno al Este y otro al Oeste, partiendo respectivamente, de las islas de Zapara y San Carlos.

La construcción del Canal Interior se contrató a partir de 0 kms. 600 S. hasta 22 kms. 560 S., se comenzó el 28 de abril de 1953 y la obra fue inaugurada el 7 de diciembre de 1954. En total se extrajeron 30 655 170 metros cúbicos de material en 588 días, con las dragas de tubería Caribbean y Jamaica Bay. En general se puede decir que este dragado, no ofreció mayores problemas.

El día 28 de noviembre de 1954 se iniciaron los trabajos en el Canal Exterior contratados a partir del mismo punto 0 kms. 600 S. hasta 12 kms. 450 N., y el 8 de diciembre de 1956 fue inaugurado. En este trabajo tomaron parte en distintas oportunidades tres dragas de tubería, cinco de tolvas y una de brazo, aunque nunca hubo más de tres dragas de tolvas trabajando al mismo tiempo. El volumen removido en los dos años y diez días de trabajo, fue de 20 015 617 metros cúbicos. El dragado del Canal Exterior fue particularmente difícil debido al tipo de material encontrado cerca de la costa, especialmente entre los Kms. 3 y 6 N. y también por lo agitado del mar, usualmente en los meses de diciembre a marzo. Por este último motivo las dragas de tolvas se vie-

ron frecuentemente obligadas a refugiarse en el Canal Interior durante los días de mal tiempo y a fin de realizar trabajo útil dragaban en dicho sector.

Las dragas de tolvas sumaron un total de 46 656 horas, 39 minutos de presencia en su trabajo de construcción del Canal Exterior, distribuído de la manera siguiente: el 61,5% se dedicó al dragado efectivo, es decir, al bombeo de material, el 9,7% a mantenimiento, (reparaciones, abastecimiento y otros servicios), el 18,7% se perdió debido al mal tiempo y el 10,1% permanecieron inactivas por circunstancias varias.

El Malecón del Este se comenzó a construir el día 19 de febrero de 1954 y se terminó al 14 de junio de 1956. Dicha estructura tiene una longitud de 3 250 mts. contados desde su punto de arranque en la Costa Norte de la Isla Zapara hasta la línea de 24 pies de profundidad en el Golfo de Venezuela. Su plataforma de coronamiento tiene 7,20 metros de ancho con taludes de 1:2 del lado Este y de 1:1,5 por el Oeste. La construcción de piedra suelta, se efectuó con caliza de la isla de Toas, y se emplearon en ella 1 100 000 toneladas. La construcción del Malecón del Oeste fue aplazada por existir dudas acerca de su conveniencia o necesidad inmediata.

CAPITULO III

MANTENIMIENTO Y MEJORAS SIN LA DRAGA ZULIA

El 8 de diciembre de 1956, fecha de conclusión de los trabajos contratados para el Canal Exterior, marca el término oficial del período de construcción; sin embargo, por haberse dragado primero la mitad oriental del canal, se permitió el tráfico de salida para tanqueros tipo T2 de 18 000 toneladas (114 000 barriles), con seis meses de anterioridad, es decir desde junio de 1956. Pero la experiencia adquirida durante el último año de construcción y las tendencias mundiales en cuanto al tamaño de tanqueros, indicaban ya la conveniencia de una serie de mejoras a las cuales se dió comienzo inmediatamente después de la inauguración.

En primer lugar se decidió cambiar el nivel de referencia de la mara media baja (M. M. B.) que veníamos usando, y con respecto a la cual teníamos 35 pies de profundidad, por el nivel medio de las mareas mínimas mensuales (M. M. M.) que nos daba solamente $33\frac{1}{2}$ pies, efectuado este cambio, debíamos profundizar el canal $1\frac{1}{2}$ pies para mantener los 35 pies proyectados originalmente. En segundo lugar se resolvió que el Canal Interior no era suficientemente seguro con sólo 600 pies de anchura en el fondo, por lo cual convenía elevar esta cifra a 800 pies y finalmente, se llegó a la conclusión de que era necesario aumentar la profundidad de 35 a 45 pies (M. M. M.) debido al incremento en las dimensiones

de los tanqueros. En este capítulo se presentan los resultados de los esfuerzos del Instituto para llevar a cabo el anterior programa con los equipos disponibles, sin la ayuda de la draga Zulia.

La nueva profundidad de 45 pies (M. M. M.) significó una extensión del dragado hacia el Norte, de 11 342 metros hacia el Sur de 14 140 metros, además de tres tramos entre el Brazo y la entrada del Lago, con un total de 19 950 metros. El trecho de canal contínuo sometido a mantenimiento tiene ahora, por lo tanto, una longitud total de 60 582 metros, y además hay un trecho discontínuo de 40 300 metros lo cual arroja un total por supervisar superior a los cien kilómetros (100 882 metros).

El ensanche y gran parte de la profundización del Canal Interior se efectuaron empleando la draga de tubería Jamaica Bay, la cual había quedado inactiva en la zona a la terminación de los trabajos de construcción. El volumen extraído alcanzó la cantidad de 16 293 155 de metros cúbicos, y el trabajo se realizó en el período del 21 de junio de 1957 al 21 de febrero de 1960, en que dicha draga fue retirada por haber comenzado sus actividades la Zulia tres días antes.

En el mantenimiento y profundización del Canal Exterior, estuvieron trabajando cinco dragas de tolvas (sin incluir la Zulia) la última de las cuales fue retirada el 6 de agosto de 1960. En ningún momento trabajaron más de tres de ellas a la vez y cuando el mal tiempo interrumpia su trabajo pasaban a colaborar en el Canal Interior. El volumen dragado por estasen el período del 5 de diciembre de 1956 al 6 de agosto de 1960, fue de 11 464 335 metros cúbicos para el Canal Exterior y de 7 263 862 metros cúbicos para el Canal Interior.

El dragado en la parte Exterior hizo crisis en 1957 pues con las dos dragas de tolvas que tenía bajo contrato, no solamente estaba el Instituto incapacitado de efectuar la profundización sino que sus esfuerzos por alcanzar y mantener los 35 pies (M. M. M.), no tenían éxito, y en algunos sitios se estaba perdiendo profundidad. En esta emergencia el U. S. A. C. E. arrendo al Instituto, por pocos meses, la draga Chester Harding con ayuda de la cual logró recuperar algo de la profundidad perdida.

Basándose en los resultados obtenidos con la draga HAM-302, el Instituto decidió arrendar la nueva draga HAM-303 de iguales características, la cual comenzó a operar el 30 de octubre de 1958. La crisis del equipo de dragado para el mantenimiento del Canal Exterior quedó así aparentemente resuelta empleando las tres dragas de tolvas: HAM-302, Sandpiper y HAM-303, pero el ritmo del progreso era tan lento que hubiera sido imposible con ellassolas alcanzar dentro de un tiempo, ni remotamente razonable la profundidad de 45 pies. Por otra parte siendo los costos unitarios obtenidos con el empleo de varias dragas

pequeñas, naturalmente superiores a los que se obtendrían con una de gran capacidad, el costo final de la profundización a 45 pies M.M.M. hubiera sido mucho mayor.

Durante el período crítico de 1957, habiamos podido observar el excelente trabajo que estaba realizando en el dragado de Boca Grande, en el Delta del Orinoco, la draga experimental Sealane funcionando con el nuevo sistema de dragado de "agitación" con brazo, que con tan buenos resultados ya habíamos ensayado por tres (3) semanas en el Canal Exterior de Maracaibo en Noviembre de 1956. Este nuevo tipo de draga, descrito con más detalles en el Capítulo que sigue, parecía ofrecer la única solución satisfactoria de los problemas tanto técnicos como económicos que presentaban el mantenimiento y mejoras del Canal de Maracaibo y por ello el Instituto resolvió continuar y llevar a feliz término, las negociaciones iniciadas con la National Bulk Carriers (casa matriz de la Seadredge Company, Inc.), para la construcción y arrendamiento de una gran draga de este tipo, la actual Zulia.

CAPITULO IV

DRAGADO POR AGITACION

EL DRAGADO POR AGITACION CON DRAGAS DE TOLVAS

El "Dragado por agitación", efectuado hasta hace poco únicamente con dragas de tolvas, es un método por medio del cual se hace desbordar sobre la superficie del agua toda la mezcla de líquido y sólidos extraídos del fondo, sin buscar o esperar su concentración en las tolvas, a fin de que una parte importante de dicho material sea transportado por las corrientes litorales, fluviales o de mareas que actúen en la zona de trabajo, hasta alcanzar un área de deposición fuera de los límites del Canal. En el libro "The Hopper Dredge" publicado por U.S.A.C.E. en 1954, se detallan el origen y aplicaciones de este método.

El Dibujo No. 3 ha sido preparado por el I.N.C., siguiendo el presentado en la página 308 del libro citado, igualmente basado en la Ley de Stokes para las siguientes condiciones:

Gravedad específica de la partícula:	2.65
" " del agua:	1.oo
Aceleración de la gravedad:	981 cm/seg.2
Temperatura del agua:	20°, 25° y 30° C

Para el uso de este gráfico es necesario determinar el tiempo (T), en minutos, que tarda en caer, en un metro de profundidad, la partícula de mayor tamaño que llega al área de depósito. A este fin se parte de la fórmula siguiente:

$$T = 0.0167 \times \frac{D}{p \times v} \text{ (minutos)}$$

donde: D = Distancia entre el punto de caída del material agitado y el sitio de depósito; expresada en metros.
p = Profundidad del sitio de depósito, en metros.
v = Velocidad de la corriente, en mts./seg.

Por medio de dicho gráfico se puede estimar el porcentaje del material agitado que sale definitivamente fuera de la zona dragada. Para su empleo se deberán efectuar previamente análisis granulométricos del material, a fin de determinar las proporciones en que se encuentran los tamaños de los granos que lo forman; se necesitará además, estudiar la velocidad y dirección de las corrientes principales, la topografía del fondo y las distancias de las probables trayectorias del material agitado.

Una vez analizada la posibilidad teórica de realizar el dragado por el método de agitación deberán efectuarse exhaustivos ensayos prácticos con la draga destinada al trabajo proyectado, en las condiciones más variadas que se espera encontrar en el sitio. Partiendo de estos ensayos y de los volúmenes efectivos a dragar, obtenidos por medio de sondeos, se podrá tomar la decisión acerca del método más adecuado, escogiendo entre el dragado con tolvas, es decir, cargando y transportando lejos al material excavado, y el método de dragado por agitación en el cual la naturaleza se hace cargo del transporte.

En síntesis, el dragado por agitación con dragas de tolvas, es especialmente ventajoso cuando la mayor parte del material extraído del fondo se deposita naturalmente en sitios de donde no puede regresar a su lugar de origen, en un tiempo razonable. Este método no puede emplearse por lo tanto, cuando se opere en aguas tranquilas, o cuando las corrientes predominantes puedan hacer regresar cantidades apreciables de material dragado al Canal o puerto en construcción, o causar su deposición en algún sitio donde exista la posibilidad de dragados futuros.

EL DRAGADO POR AGITACION CON BRAZO

Casi medio siglo después de iniciado el dragado por agitación se introdujo la variante de lanzar el material extraído lo más lejos posible de la draga, bombeándolo por un conducto o brazo (boom). En esta forma el dragado por agitación se hace aplicable en aguas tranquilas y de mejor rendimiento cuando existen corrientes que arrastren la mayor parte del material dragado fuera de la zona de trabajo. Todos estos aspectos eran de mucho interés en relación con los canales de Maracaibo y del Orinoco.

El estudio del régimen de corrientes, comprendiendo no sólo las del

"DRAGADO DE AGITACION CON BRAZO" EN EL CANAL DE MARACAIBO — VENEZUELA

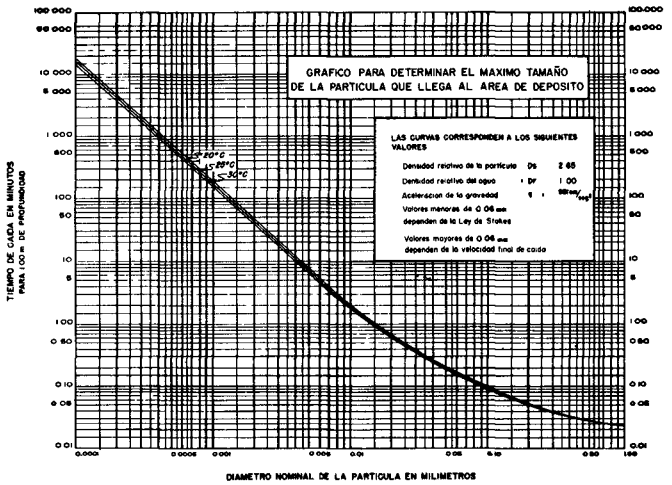

Dibujo No. 3

CANAL DE MARACAIBO

OPERACION DE LA DRAGA "SEALANE" DURANTE EL MES DE NOVIEMBRE DE 1956

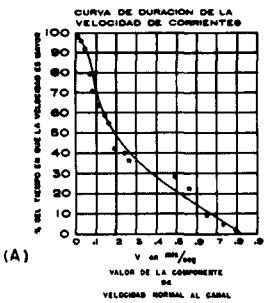

(A)

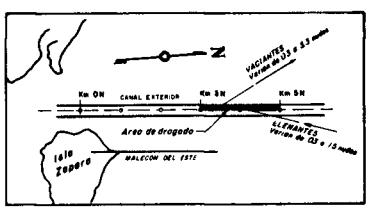

(B) ESQUEMA DE CORRIENTES EN EL AREA DE DRAGADO

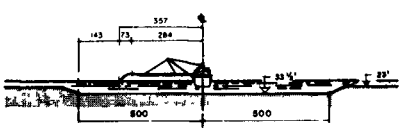

(C) DRAGA "SEALANE EN EL CANAL EXTERIOR

CURVA GRANULOMETRICA TIPICA
ENTRE LAS PROGRESIVAS KM 3 N Y KM 5 N

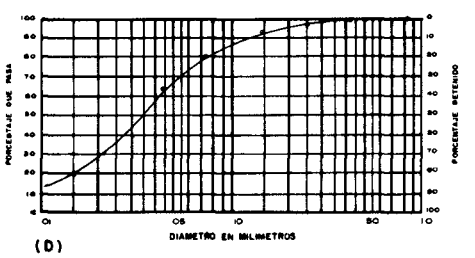

(D)

Dibujo No. 4

río Orinoco sino las originadas de las mareas, y el de la granulometría del material del lecho, basado en numerosas muestras obtenidas por la Orinoco Mining Company, indicaron condiciones favorables al empleo del dragado de agitación con brazo. Como resultado de todas las circunstancias anteriores, dicha compañía contrató el uso de la draga experimental Sealane.

La Sealane fue construída tomando un tanquero del Tipo T-2 e instalándole una rastra a cada lado con los correspondientes equipos de bombeo y arreglando la descarga en forma que todo el material fuera expulsado por un brazo formado por dos tubos de 25 pulgadas de diámetro y 76,20 metros de largo medidos a partir del costado del buque. El brazo de descarga sostenido por una trípode, era naturalmente rígido y no ofrecía las ventajas que tendría la draga definitiva cuyo brazo estaría montado en una plataforma giratoria.

El Instituto Nacional de Canalizaciones en conocimiento de las tramitaciones anteriormente mencionadas y con vista a las dificultades que se tenían para terminar la construcción del Canal Exterior (ver Capítulo II) de la Barra de Maracaibo, obtuvo de la Orinoco Mining Company, permiso para que la Sealane hiciera su primer ensayo en dicho canal antes de pasar al Orinoco.

La Sealane inició sus trabajos el 7 de noviembre de 1956 y, a fin de utilizar al máximo las corrientes predominantes de la zona las cuales tienen una componente normal al eje del canal, se ordenó limitar el dragado con brazo a la mitad occidental del Canal Exterior, entre las progresivas 3 Kms. 000 N y 5 Kms. 000 N bombeando hacia el Oeste únicamente. De esta manera se buscaba garantizar un mayor volumen de dragado efectivo evitando las contingencias que podían presentarse a consecuencia del bombeo de material hacia el Este, contra la corriente usual, dentro de un canal de 1 000 pies de ancho. En la estimación teórica de la eficiencia de esta operación de dragado que presentaremos más adelante, se podrá apreciar que, efectivamente, esta disposición garantizaba la salida de todo el material bombeado fuera del área del canal.

Por ser éste el primer trabajo de una draga de brazo, creemos interesante presentar un análisis de las condiciones y características del trabajo realizado por la Sealane en el canal de la Barra de Maracaibo.

La distribución del tiempo de trabajo entre las 16:00 horas del 7 de noviembre, cuando comenzó, y las 12:00 del 1º de diciembre cuando terminó, es como sigue:

"DRAGADO DE AGITACION CON BRAZO" EN EL CANAL DE MARACAIBO — VENEZUELA

Horas de bombeo (dragando):	316:55
" en viaje de regreso: (sin dragar)	68:18
Total horas de operación	385:13
Demoras por accidentes, reparaciones, etc.:	186:47
Total de horas empleadas	572:00

La producción total estimada a base de las curvas de operación de las bombas fue de 384 670 m3, y de élla se calcularon los siguientes rendimientos:

Producción por hora de bombeo:	1 214 m3/hora
" " " " operación:	999 "
" " " " presencia:	672 "

Las estimaciones teóricas de que la totalidad del material bombeado por el brazo saldría fuera del canal quedaron confirmadas por sondeos posteriores al dragado. Dichas estimaciones se efectuaron con base a los tres elementos que se describen a continuación:

1) Un estudio aproximado de corrientes en la zona, el cual nos indicó que tanto las originadas por la marea llenante como por la vaciante, mantenían uncomponente hacia el oeste, normal al eje del canal según se puede apreciar del Dibujo No. 4-B. Los valores y duración promedio de esta componente transversal al canal se presentan en forma gráfica mediante la curva de duración, del Dibujo No. 4-A, de la misma página.

2) Las diversas posiciones del punto de agitación. En el croquis del Dibujo No. 4-C se indica la ubicación del punto de agitación es decir, el punto de caída del chorro de material en la superficie del agua, cuando la draga está en su posición extrema del área de dragado. Este punto varió entre la distancia máxima indicada en el croquis, 44 mts. (143'), al Este del borde Occidental del Canal, y 109 mts. (357') al Oeste del mismo borde. Para la profundidad media del banco se usó 7 mts. (23').

3) La curva granulométrica típica del material dragado por la Sealane, el cual se podría clasificar como un limo fino conteniendo arena muy fina. Esta curva se presenta en el Dibujo No. 4-D.

De la curva de duración de la componente Oeste de la velocidad de corriente, obtenemos 0.10 mts/seg. como el valor sobre el cual estará la velocidad durante el 80% del tiempo de dragado; dicho valor será usado para obtener las estimaciones de asentamiento del material agitado.

En el cuadro que sigue se calculan los porcentajes de material que salen del canal para varias distancias del punto de agitación a su borde-occidental mediante la aplicación del gráfico No. 1 mencionado en la primera sección de este Capítulo, y del uso de la curva granulométrica del material dragado.

Distancia al borde (mts.)	Velocidad corriente mts/seg.	T (minutos)	d m.m.	% que sale del canal
44	0.10	1.136	0.14	93
24	0.10	0.572	0.22	96
12	0.10	0.286	0.35	98

De los valores obtenidos en el cuadro anterior para los porcentajes de material que salen del canal se establecía que, aún en las condiciones más desfavorables de posición de la draga, más del 93% del material - bombeado debía considerarse como efectivamente dragado durante más del 80% del tiempo de operación.

Una vez terminado con éxito este dragado de ensayo en la Barra de Maracaibo, la draga Sealane siguió a la desembocadura del Orinoco para iniciar la construcción del canal de la Barra de Boca Grande. La Sealane comenzó el dragado a las 10:00 horas del 10 de diciembre de 1956 y para el 15 de noviembre de 1958 había terminado la construcción de un canal de 48 150 metros (26 millas) de longitud, 122 mts. (440 pies) de ancho y profundidad mínima de 10.40 mts. (34 pies), además de haber realizado otros dragados de menor magnitud aguas arriba del Orinoco.

El trabajo de la Sealane demostró ampliamente la efectividad y economía del dragado de agitación por brazo. Con el empleo de este método que alteraba a fondo algunos conceptos sostenidos hasta entonces en materia de dragados, se abrían nuevas perspectivas para dragar y mantener canales como el de Maracaibo y el de la Boca Grande del río Orinoco, cuyos problemas eran antes considerados de muy difícil si no de imposible solución.

"DRAGADO DE AGITACION CON BRAZO" EN EL CANAL DE MARACAIBO — VENEZUELA

CAPITULO V

DESCRIPCION DE LA DRAGA ZULIA

La urgente necesidad de acelerar la profundización del canal de Maracaibo y de asegurar adecuadamente su mantenimiento, unidas a la imposibilidad de obtener equipos adicionales de dragado, llevaron al Instituto Nacional de Canalizaciones, como se dijo antes, a la conclusión de que era necesario emplear el nuevo sistema de dragado por agitación con brazo.

Como resultado de esta decisión se contrató con la Seadredge Co. el diseño, construcción y arrendamiento de una draga que pudiera a voluntad, trabajar con brazo o cambiar a tolvas. A esta draga se le dió el nombre "Zulia", en honor del Estado venezolano en el cual se encuentra el Lago de Maracaibo.

La draga Zulia por la ubicación de sus tolvas en el medio del buque, está clasificada como una draga de tolvas tipo tanquero. En su construcción se tuvo en cuenta toda la experiencia adquirida en el funcionamiento de la draga Essayons del U.S.A.C.E., la cual hasta el momento de la botadura de la Zulia, era la más moderna y efectiva draga de tolvas del mundo. Como draga de tolvas, la draga Zulia desplazó a la Essayons del puesto número uno en el mundo y, como draga de brazo, fue la única en su tipo hasta que se construyó en el mismo astillero, para trabajar en el Canal del Orinoco, la draga ICOA que es muy similar a ella.

En el cuadro a continuación pueden compararse las características de la draga Zulia con las de la Essayons:

	Draga Zulia	Draga Essayons
Entrada en servicio	Diciembre 1959	---
Año de construcción	1958	1949
Eslora	548' 6"	525' 0"
Manga	95'	72'
Puntal	40' 0"	40' 5"
Largo del brazo (boom):		
A partir del eje del barco	114.5 mts. (375'6")	No tiene
" " " costado	100.0 " (378')	" "
Diám. Int. del brazo	1.45 " (57')	" "
Capacidad de tolvas	6 580 m3	6 116 m3
Calado máximo cargada	26' 6"	28' 0"
" en lastre	16'	---

Profundidad máxima de dragado	60'	60'
Número y diámetro de tubos de succión	2 laterales de 36" 2 en fosas de 36"	2 laterales de 36" No tiene
No. y tipo de rastras	4 - California	2 - California
No. y tipo de muñoneras	2 deslizantes 2 fijas	2 deslizantes No tiene
Bombas de dragado:		
Número y diámetro	4 de 32"	2 de 32"
Impulsión de las bombas	2 turbinas de vapor de 6 000 HP c/u	2 motores eléctricos de 1 850 HP c/u
Propulsión:		
Hélices	2 de paso fijo	2 de paso fijo
Maquinaria	2 turbinas de vapor con engranaje de reducción de 6 000 HP c/u	2 turbinas eléctricas de 4 000 HP c/u
Velocidad máx. cargada	13 nudos	16.55 nudos

NOTA: La draga ICOA, diseñada especialmente para trabajar en el Orinoco, difiere de la Zulia principalmente en su capacidad de tolvas que es sólo de 2 982 metros cúbicos y en el uso de motores diessel en lugar de turbinas a vapor. -

El brazo de la Zulia está constituído por una estructura tubular que soporta, en forma de voladizo, por un lado la tubería aérea de descarga, y por el otro el contrapeso de 1 080 toneladas, necesario para balancear su propio peso y el de la tubería llena de la mezcla dragada.

Mediante un complejo sistema de conexiones, derivaciones, válvulas de paso y válvulas de retención, se combinan las tuberías de descarga de las cuatro bombas y se puede conducir el flujo del material dragado bien sea a las tolvas, bien al brazo. Dichas bombas tienen una capacidad nominal total de 43 150 metros cúbicos por hora para una mezcla con densidad de 1 050 gr/litro, lo cual equivale a una producción aproximada de 5 000 m3/hora de material dragado, considerando una densidad para el material en sitio, igual a 2 000 gr/litro.

La tubería de descarga de 32" de cada bomba empalma en la cubierta principal con una tubería de recolección de 57" y de ahí sube para conectar con la tubería del brazo aéreo de igual diámetro. Todo el sistema de la tubería de descarga, a partir de su empalme con las bombas está recubierta con goma para evitar la abrasión que produciría en la tubería de acero, la mezcla de agua y sólidos dragados, la cual sale, en forma de impresionante chorro, con velocidad aproximada -

de 25 pies por segundo, por la boca de la tubería, situada a 20 metros sobre el nivel del agua.

CAPITULO VI

ESTUDIOS TEORICOS PARA LA OPERACION DE LA DRAGA ZULIA

Mientras se construía la Zulia se comenzaron una serie de estudios con objeto de encontrar la manera mas eficiente de emplearla en el Canal de Maracaibo. Dichos estudios han continuado y se continuarán en el futuro, buscando obtener un rendimiento cada vez mayor y más económico.

Fundamentalmente los estudios consistieron en:

a) Establecer las condiciones que determinarían la selección del sistema de dragado que se debía usar para cada caso, es decir, si se dragaba con tolvas o se empleaba el dragado de agitación con brazo, y

b) En caso del dragado con brazo, determinar si se colocaba éste a babor o estribor, en relación con las corrientes predominantes y la granulometría del material dragado.

Para el análisis teórico de estos problemas, se ha preparado el siguiente conjunto de gráficos, en los cuales hacemos uso de las características de sedimentación del material agitado según la composición granulométrica:

1) Un gráfico (Dibujo No. 5) que, hecho a base de la fórmula establecida en el Capítulo IV, relaciona los siguientes elementos:

a) La componente normal al canal de la velocidad de corrientes;

b) El cociente que resulta de dividir la distancia (D) del punto de caída del material dragado y la línea de borde del canal, entre la profundidad (p) de dicho borde, y

c) El diámetro nominal (d) de la partícula de mayor tamaño que se deposita fuera del canal para una temperatura de 25° C y se presentan frente al respectivo valor de "T" en el eje de las abcisas.

2) Sobre un gráfico similar podrían llevarse las curvas granulométricas de los distintos suelos, las cuales nos determinarán los porcen

tajes de material que, para cada suelo, caen fuera del canal, según el tamaño que determinen la velocidad y la relación $\frac{D}{p}$; tal cosa, sin embargo, no sería práctica por la confusión que significaría el trazado de cien o más curvas en un mismo gráfico. Para evitarlo se han agrupado los suelos según la característica que hemos considerado de mayor importancia en su distribución granulométrica, y la cual se define como el diámetro nominal de una partícula tal, que el 80% del material sea más fino que élla. Esta característica, , a la cual representamos con el símbolo D80, ha sido seleccionada con el fin de determinar con mayor precisión las cualidades del suelo que se identifica, dentro del rango de valores comprendidos entre el 60% y el 100% de la curva granulométrica.

Al hacer el agrupamiento de los suelos según el tamaño fijado del 80% (D80), se notará que hay variación en la distribución granulométrica para suelos de igual valor de D80. Se observó que esta variación es de magnitud mayor a medida que aumentan los tamaños del D80 y también a medida que la curva se aleja de los valores de dicho D80, siendo esto último muy natural por lo explicado en el párrafo anterior. Sin embargo, si se toma en cuenta la precisión dentro de la cual trabajamos, no sólo en lo que se refiere a los métodos de laboratorio utilizados en los análisis de suelos, sino también en lo que se relaciona con lo representativo del muestreo, distribución y medición de la dirección y magnitud de velocidades de corrientes, estimación de distancias y velocidad real de caída de las diferentes partículas, podemos considerar que variaciones que se encuentren dentro del margen del 10% son aceptables para las estimaciones teóricas que pretendemos realizar.

Basados en este criterio, fueron llevados a un gráfico en escalas semilogarítmicas los porcentajes de material más finos que los diámetros nominales de 0.010; 0.015; 0.025; 0.05 y 0.10, correspondientes a las 72 muestras de suelos tomadas a lo largo del canal, y de acuerdo a sus respectivos valores D80. Para cada diámetro fueron trazadas las curvas promedio obteniéndose la familia de curvas que forman el Dibujo No. 6-A.

Este gráfico nos da, aproximadamente, un promedio de la distribución granulométrica de suelos según su D80, en forma de porcentajes más finos que las partículas de diámetro "d" que se indican en cada curva. De él sacamos los valores que utilizamos en el trazado de las curvas promedio granulométricas, correspondientes a los suelos con D80 igual a: 0,007; 0,010; 0,015; 0,020; 0,040; 0,070; 0,10 y 0,20, las cuales aparecen superpuestas al gráfico usado para la determinación del diámetro de la partícula de mayor tamaño que sale fuera del canal. (Dibujo No. 5, parte central).

Las curvas granulométricas de aquellos suelos que tengan características muy particulares y que se consideren importantes para el pro-

"DRAGADO DE AGITACION CON BRAZO" EN EL CANAL DE MARACAIBO — VENEZUELA

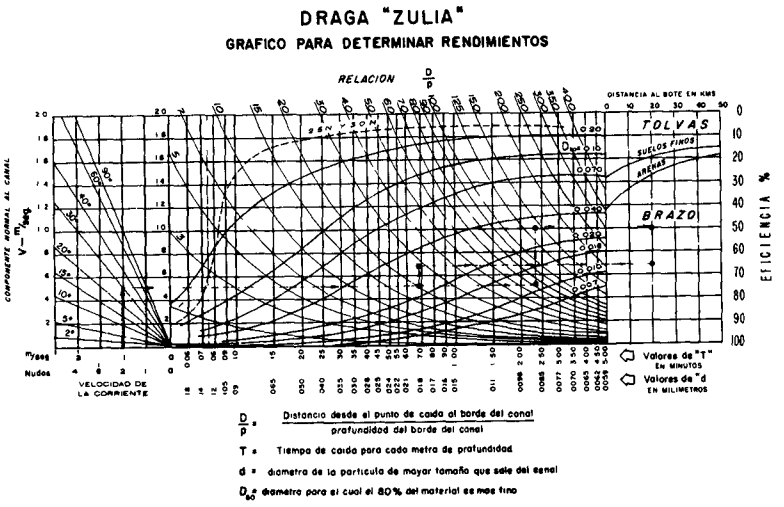

Dibujo No. 5

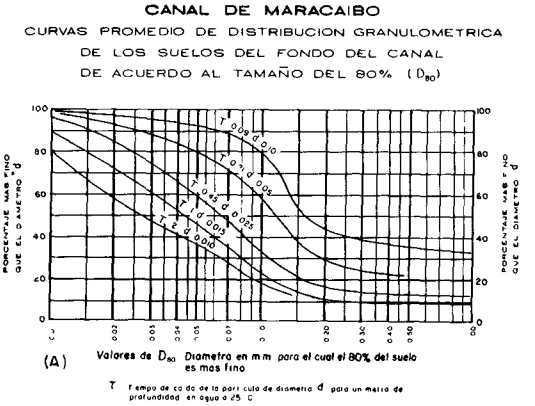

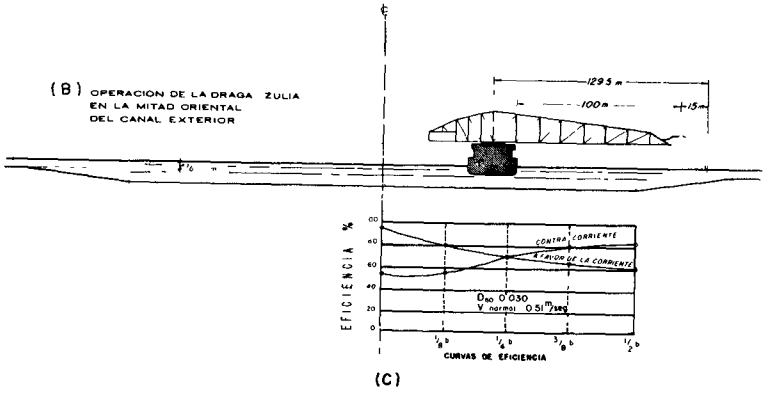

Dibujo No. 6

ceso de dragado, pueden incluirse especialmente, dentro del gráfico;tal como se ha hecho con la curva que corresponde al suelo entre las progresivas 2 kms. 500 y 3 kms. 000 Norte, debidamente identificada.

3) El Dibujo No. 5 (parte izquierda) nos da la componente normal al canal, de la velocidad de la corriente. Se ha dibujado adyacente al gráfico principal y en él se entra con la magnitud de la corriente en las abcisas, obteniendo el valor de la componente en las ordenadas, según el ángulo de la corriente con el eje del canal.

4) Curva comparativa entre rendimientos del dragado con brazo y del dragado con tolvas para el caso de la Zulia. El objeto de esta comparación es determinar si el volumen efectivo de dragado con brazo es igual o mayor que el dragado con tolvas para un tiempo igual de presencia, escogiéndose el método que resulte mayor.

La comparación se representa mediante la siguiente desigualdad:

$$Pb \times Tc \times E \geq V_{\dagger}$$

Donde Pb = Volumen promedio de material bombeado por el brazo en metros cúbicos por minuto.
Tc = Tiempo de ciclo de la operación con tolvas
E = Eficiencia del dragado con brazo
$V_{\dagger}$ = Volumen transportado en las tolvas en cada ciclo

Considerando a Pb y $V_{\dagger}$ constantes, tendremos como variables a Tc y E, las cuales se calculan en los dos números siguientes.

5) El tiempo total del ciclo de operación con tolvas está expresado por la ecuación:

$$Tc = tl + te + tv + td + tr$$

en la cual:

tl = tiempo de bombeo necesario para llenar las tolvas
te = tiempo de evoluciones
tv = tiempo de viaje al sitio de bote
td = tiempo de descarga de las tolvas
tr = tiempo de regreso al corte

El tiempo de ciclo se puede considerar constante para un sitio de corte y otro de bote determinados, y para un mismo tipo de suelo dragado.

Los factores que hacen variar el tiempo de ciclo del dragado con

tolvas son los siguientes:

a) El tiempo de bombeo necesario para llenar las tolvas (tl) el cual varía de acuerdo con la velocidad de asentamiento de las partículas que forman el suelo, es decir de su granulometría.

Para suelos de grano grueso, el tiempo de carga es menor que para los suelos finos. Esta característica es muy importante y siempre debe ser tomada en cuenta para la programación de los dragados. En el caso de la Zulia, hemos observado que el tiempo de carga varía entre 160 y 270 minutos según las características de asentamiento del material, pero no se ha tenido todavía la oportunidad de determinar las relaciones que deben existir entre las variaciones granulométricas y las del tiempo de carga. Para tener una idea de cómo nos influiría esto en el dragado, tomaremos las cifras dadas anteriormente para el tiempo de bombeo, como valores extremos entre suelos de grano grueso y suelos de grano fino, aptos para ser dragados con tolvas; esta última observación se debe a que hay suelos cuya granulometría es tan fina que descarta definitivamente el dragado con tolvas por su poco rendimiento.

b) El tiempo de evoluciones (te) es la suma de los tiempos que invierte la draga en suspender el bombeo de material para virar al fin de cada pase. Aunque varía según la longitud del corte y el tiempo de carga, puede considerarse constante ya que estas variaciones son muy pequeñas e influyen poco en el tiempo total del ciclo. Para este tiempo hemos tomado el valor de 32 minutos, que es un promedio obtenido de varias operaciones de la draga Zulia.

c) Los tiempos de viaje para descargar (tv) y de regreso al sitio de corte (tr) varían con la distancia entre este último y el sitio de bote seleccionado, siempre que se considere uniforme la velocidad de la draga. Por lo regular el sitio de bote permanece fijo, variando estos tiempos solamente según el lugar del corte en el canal. Para nuestro caso, los calcularemos a base de una velocidad de la draga igual a 12 nudos y para los sitios de botes ubicados cerca de las progresivas 11+000 Norte y 25+000 Sur del Canal de Maracaibo.

En la práctica los viajes de ida al sitio de bote y regreso al de corte se aprovechan dragando con brazo durante el trayecto recorrido en el canal, siendo por lo consiguiente los tiempos invertidos mayores que si se efectuara la operación tradicional con tolvas. Sin embargo, para los efectos comparativos que se persiguen, debemos considerar la operación normal es decir, que la draga navega libremente tanto en su viaje al lugar de bote como al regreso de él.

Los tiempos de viaje serán entonces:

$$tv = tr = \frac{L}{v}$$

Siendo v = 12 millas/hora = 0.20 millas/min. = 0.37 km/min. y estando L expresado en kilómetros tendremos de acuerdo con la fórmula anterior:

$$tv = tr = \frac{L}{0.37} \text{ (minutos)} = 2.70 \times L \text{ (minutos)}$$

d) El tiempo de descarga de las tolvas (td) es constante e igual a 7 minutos.

e) Sustituyendo los valores obtenidos anteriormente en la relación que nos da el tiempo de ciclo total en minutos, tenemos:

1º) Para suelos de grano grueso que llamaremos arenas

$$tc = 160 + 32 + 2 \times 2.70\ L + 7 = 199 + 5.40\ L$$

2º) Para suelos de grano fino

$$tc = 270 + 32 + 2 \times 2.70\ L + 7 = 309 + 5.40\ L$$

En ambos casos L será la distancia del sitio de dragado al sitio de bote, expresado en kilómetros.

6) Como valor de la producción del brazo (Pb) utilizaremos el valor garantizado por las especificaciones de construcción y el contrato de arrendamiento, el cual es de 5 070 m3/hora. A esta producción debemos afectarla de un coeficiente de reducción, debido al tiempo necesario para evoluciones, el cual se estima en 30 minutos cada 6 horas, o sea 5 minutos por hora. La producción efectiva será:

$$\frac{(60 - 5)}{60} \times 5\,070 = 4\,647 \text{ m3/hora} = 77.45 \text{ m3/minuto}$$

7) Volviendo ahora a la desigualdad mencionada en el No. 4 anterior para sustituir en ella los valores que acabamos de determinar para Tc y E y considerando que en la Zulia el volumen de tolvas (Ve) es igual a 6 500 m3 tendremos sustituyendo y despejando E en la desigualdad establecida:

$$77.45 \times Tc \times E \geq 6\,500 \text{ de donde } E \geq \frac{6\,500}{77.45 \times Tc}$$

Sustituyendo a Tc por sus respectivos valores y expresando la eficiencia en porcentajes obtendremos:

Para arenas: $E\% \geq \frac{6\,500 \times 100}{77.45\ (199 + 5.40\ L)} \geq \frac{8\,393}{199 + 5.40\ L}$

Para suelos finos: $E\% = \frac{6\,500 \times 100}{77.45\,(309 + 5.40\,L)} = \frac{8\,393}{309 + 5.40\,L}$

Esta desigualdad se representa en el Dibujo No. 5 (parte derecha), que nos relaciona los valores de E y L, presentado anexo al diagrama que nos da la eficiencia del dragado con brazo, para mayor facilidad.

En este gráfico puede observarse que el tiempo de carga y el de la distancia del sitio de bote, no son los que más influyen en la selección del sistema de dragado, siendo más importantes la relación D/p y la componente normal de velocidad.

De la relación establecida entre la eficiencia del dragado con tolvas y brazo, se deduce además que en todo caso, siempre será más económico dragar con brazo dos veces el mismo material (eficiencia = 50%) que realizar el dragado con tolvas, con la única condición que el material así dragado sea depositado en un sitio donde no pueda regresar al área de excavación.

Iguales consideraciones pueden establecerse para el caso de que sea necesario dragar tres veces el mismo material, (eficiencia: 33.33%) dependiendo esta vez de la distancia del bote y de la granulometría del material, es decir del tiempo de carga de las tolvas. Asi tenemos que, para suelos finos, será siempre más económico remover el material tres veces para cualquier distancia al sitio de bote. Para arenas, esto será cierto sólo en el caso de que el sitio de bote esté a una distancia mayor de 10 kilómetros del área de dragado.

A partir de lo establecido anteriormente y de las dimensiones del brazo de la draga Zulia, podemos concluir que no será necesario el uso de tolvas para el dragado del Canal de Maracaibo cuyo ancho, (1.000 pies), garantiza una eficiencia del dragado con brazo, superior al 50% del material bombeado para cualquier condición de corrientes, exceptuando solamente circunstancias especiales como la presencia de obstáculos (por ejemplo las cuatro torres de enfilación) en cuyo caso sería necesario usar las tolvas.

USO DE LOS GRAFICOS

Los gráficos que acompañan nos permiten fácilmente analizar para varias condiciones, los rendimientos del dragado con brazo y con tolvas. El siguiente ejemplo servirá para explicar el uso de ellos:

Supongamos que se desee dragar con la Zulia, un tramo de canal de 1.000 pies de ancho, según el croquis y condiciones que se presentan en el Dibujo No. 6-B.

Datos:

Velocidad de la corriente = 2 nudos = 3.70 kms/hora
Rumbo " " " = N 21° W
" del eje = N 9° E
Distancia media al sitio de bote = 20 Kms.

La granulometría del suelo señala un D80 = 0.030 mm.

Para estas condiciones de dragado ya hemos establecido anteriormente la mayor economía del dragado con brazo: queda entonces por determinar la posición que debe darse al brazo según el sitio de la draga en el canal.

Supongamos que la draga está trabajando en la mitad occidental del Canal o en el eje del mismo. En este caso es evidente que la posición del brazo debe ser a favor de la corriente es decir hacia el Oeste, aún cuando el chorro de material no caiga sobre el borde del Canal.

Pero supongamos ahora que la draga está trabajando en la mitad oriental del canal bajo las mismas condiciones de corrientes, etc., en cuyo caso el material podría descargarse sobre el banco oriental de donde viene la corriente, y consideremos la posición extrema, es decir, que la draga trabaja a lo largo del borde oriental del Canal. Necesitaremos determinar lo siguiente:

1) El material que sedimenta sobre banco oriental del canal

2) El material que sedimenta en el canal

3) El material que alcanza al banco occidental y se sedimenta allí.

Para el primer punto, partimos de los datos:

$$D = 129.5 \text{ m.} \qquad p = 20'\!=6 \text{ mts.} \qquad \frac{D}{p} = 21.5$$

Angulo de la dirección de la corriente con el eje del canal = 21° + 9° = 30°
Intensidad de la corriente = Vc = 2 nudos = 1.03 mts/seg.

Entramos en el Dibujo No. 5 con el valor Vc = 1.03 m/seg. y cortando la recta correspondiente a los 30°, se determina el valor de la componente normal al canal (v) igual a 0.51 m/seg.. Seguimos paralelamente a las abcisas hasta encontrar el punto correspondiente a D/p=21,! que nos determina la partícula de mayor tamaño que sale del banco oriental cuyo diámetro nominal es de 0.019 mm.. De aquí se localiza en sentido de las ordenadas el punto de corte con la curva granulomé-

trica correspondiente a un suelo con D80 = 0.030, el cual determina una eficiencia del 67%; es decir, que el 33% del material bombeado sedimenta sobre el banco oriental.

Pasando ahora al punto 3° partimos de los siguientes datos:

$$D = 433.5 \quad p = 20' = 6 \text{ mts.} \quad \frac{D}{p} = 72.2$$

Entramos en el gráfico con los mismosvalores de corriente y llegamos hasta D/p = 72.2, la partícula de mayor tamaño que sedimenta sobre el banco occidental tendrá diámetro nominal igual a 0.0088 m.m. y el punto correspondiente en la familia de curvas granulométricas nos determina una eficiencia del 50%, para lo cual, el gráfico comparativo de rendimientos entre las operaciones con brazo y con tolvas, nos indica la mayor ventaja del dragado con brazo, para la distancia media de bote establecida (20 kms.).

El punto 2º se deduce de los dos anteriores, es decir que en el Canal se deposita el 17% del material bombeado, porcentaje constituído por el material comprendido entre los díametros nominales de 0.0088 m.m. y 0.019 m.m..

En síntesis, el análisis teórico de la operación de la draga Zulia en estas condiciones nos da un rendimiento total del 83%. Este valor, comparado con el rendimiento del 60% que nos da la operación efectuada con el brazo colocado hacia el oeste, es decir en dirección de la corriente, para el cual $D/p = \frac{174.5}{6} = 29$, nos indica que es más efectiva la descarga contra corriente.

Si,mediante el mismo método, determinamos la eficiencia para las diferentes posiciones que pueda tener la draga en una mitad del canal, obtendremos las curvas que se presentan en el Dibujo No. 6-C las cuales representan los rendimientos comparativos del dragado con brazo a favor de la corriente y en contra de ella. Para este caso y para estas condiciones se observa que a partir del punto medio de la distancia entre el eje y el borde oriental del canal, es más efectivo el dragado contra corriente.

Refiriéndonos a las curvas de eficiencia del Dibujo 6-C, si llamamos "m" la distancia entre el punto de cambio de la orientación del brazo y el eje del canal, podemos establecer que "m" será función de la velocidad (v), de la granulometría del suelo (la cual expresaremos en función de su D80) y de la profundidad de los bancos que limitan el área de dragado (p), o sea:

$$m = f(v, D80, p)$$

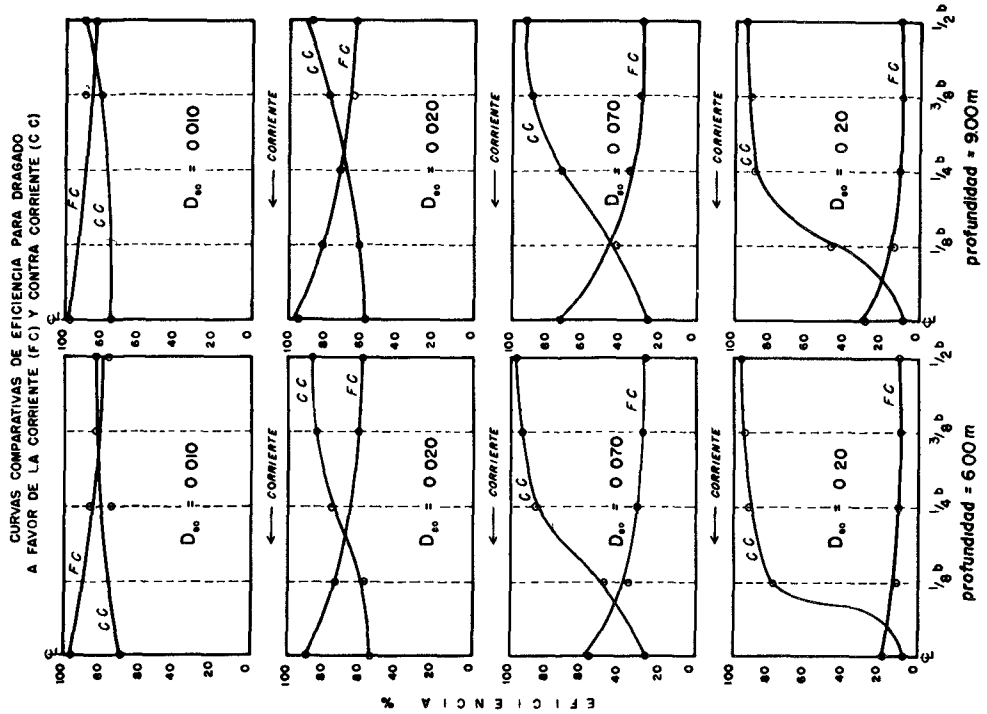

Dibujo No. 8

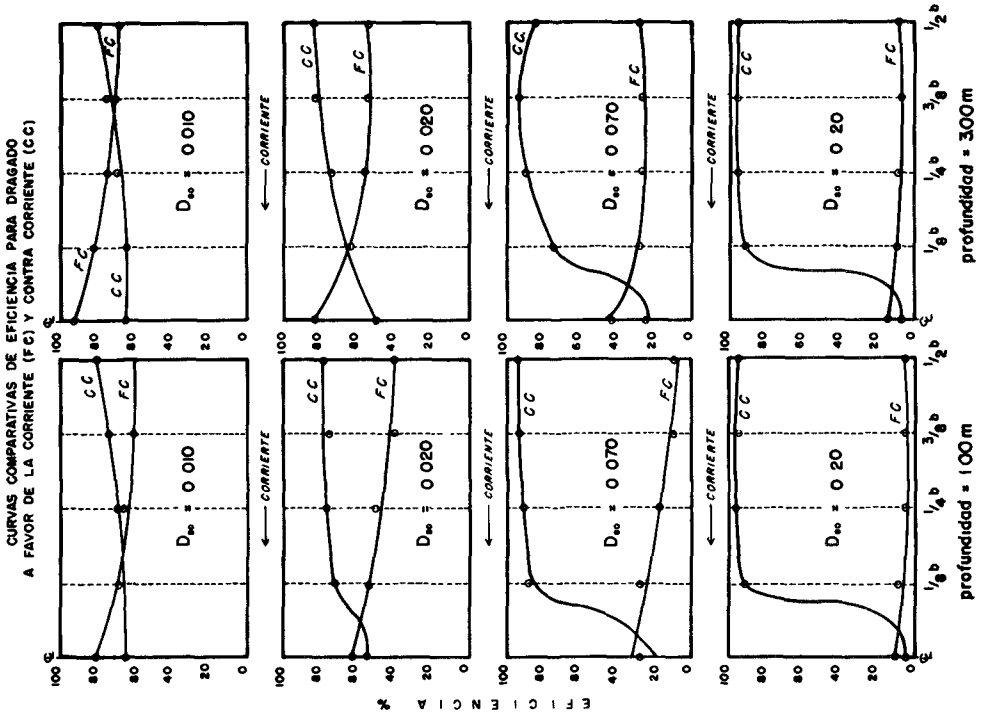

Dibujo No. 7

Si trazamos curvas de eficiencia similares para diferentes valores de los parámetros v, D80 y p observaremos, de manera general lo siguiente:

1) Para suelos finos tales como limos y arcillas, y para los valores más frecuentes de la velocidad de corriente, la variación de "m" es mayor que para arenas, sin embargo, la diferencia que existe entre la eficiencia para una y otra condición, no pasa del 15% durante la mayor parte del tiempo.

2) Para suelos arenosos con D80 mayor de 0.06 mm. la distancia "m" al punto de cambiar es menor que 1/8 del ancho del canal, y la eficiencia, dragando contra la corriente a partir de ese punto, es notablemente mayor que operando a favor de ella.

Esto se puede apreciar muy bien de las curvas de eficiencia obtenidas para diferentes profundidades y para suelos con D80 igual a 0.010; 0.020; 0.070 y 0.20 milímetros (ver Dibujos Nos. 7 y 8), para los cuales se usa el valor promedio de la componente normal al canal: 0.20 m/seg., obtenido durante los estudios de corriente del canal exterior de Maracaibo. (Veánse Capítulo IV y Dibujo No. 4-A).

De estos resultados se establece que, en caso de frecuente tráfico por el canal, podría ser ventajoso operar con el brazo hacia el banco más próximo a la draga, independientemente del sentido de la corriente, ya que aún en los casos en que teóricamente exista un ligero aumento de la eficiencia cuando se descarga en sentido contrario, la diferencia podría ser tan pequeña que no compensase el tiempo perdido en maniobras de giración del brazo cada vez que haya que dar paso a los buques que transitan por el canal, ni sea suficiente para justificar el riesgo, por pequeño que este sea, que dicha maniobra conlleva.

Es evidente que análisis teóricos de esta clase, sólo permiten establecer normas generales para la operación de la draga, que estarán más o menos ajustadas a la realidad según la precisión con la cual sean determinados los siguientes parámetros básicos: a) el régimen de corrientes y b) las características y distribución granulométrica del material por dragar.

Las dificultades prácticas existentes para una determinación precisa de estos parámetros a todo lo largo del canal y para cualquier tiempo de operación, obligan a una verificación constante de los rendimientos efectivos del dragado mediante análisis comparativos de operación de la draga, basados en frecuentes sondeos del canal; siendo estos análisis los que en definitiva nos permitirán establecer las mejores normas de trabajo.

CAPITULO VII

RESULTADOS OBTENIDOS CON LA DRAGA ZULIA

A continuación presentamos un resumen de los resultados de la operación de la Zulia en el Canal de Maracaibo desde el inicio de sus trabajos el 17 de febrero de 1960 hasta el 17 de julio de 1962.

Durante este período de dos años y cinco meses la draga Zulia trabajó a todo lo largo del Canal de Maracaibo desde su extremo norte hasta el extremo sur. La distribución de volúmenes extraídos se señala en los cuadros Nos. 9, 10, 11, 12, 13 y 14.

Puede notarse que en este tiempo la Zulia ha bombeado a través del brazo la cantidad de 104 663 000 m3 de material y dragado por medio de tolvas 2 801 000 m3 lo cual arroja un gran total de 107 464 000 m3. Por otra parte los volúmenes de profundización y de sedimentación, calculados mediante planos de sondeos, indican que el total de material extraído por la Zulia por el método de agitación con brazo, representa un volumer efectivo de dragado igual a 70 462 000 m3., lo cual nos da una eficiencia promedio para dicho método, abarcando todo el canal dentro del período considerado, igual al 67,32%.

Es necesario admitir sin embargo, que existen dificultades para determinar, con la exactitud deseable, los rendimientos efectivos obtenidos en cada kilómetro. Estas dificultades se pueden resumir de la siguiente manera:

1) La máxima precisión que puede obtenerse en el sondeo es de 0.30 mts. (un pie) lo cual representa una posibilidad de error en las estimaciones volumétricas, para un canal de 305 mts. de ancho (1 000'), que puede llegar a ser igual a 50 000 m3/por kilómetro. Este error puede disminuir y aún ser despreciable, en aquellos casos en que el espesor de la capa dragada sea relativamente grande (mayor de cinco pies); sin embargo para volúmenes de dragado relativamente pequeños la inevitable imprecisión instrumental de los sondeos influye en forma importante.

2) La rata de bombeo y el porcentaje de sólidos de la mezcla varían constantemente durante todo el proceso de dragado y los métodos usados para su determinación son relativamente imprecisos. Las cifras que se usan, por lo regular, son promedios estadísticos, válidos solamente para un gran número de valores.

3) La distribución del tiempo de operación por unidad de longitud de canal, sufre también de algunas imprecisiones, por causa de su distribución proporcional en el intervalo comprendido entre las progresivas

"DRAGADO DE AGITACION CON BRAZO" EN EL CANAL DE MARACAIBO — VENEZUELA

Cuadro No. 9

CARACTERISTICAS DEL DRAGADO DE LA ZULIA EN EL CANAL DE MARACAIBO

PROGRESIVA	GRANULOMETRIA D 80 mm	% QUE PASA EL CEDAZO N 1/4	4	10	60	270	0.06 mm	PROF MEDIA BORD. DEL CANAL (m)	DENSIDAD MEDIA EN EL BRAZO gr/lt	% DE SOLIDOS	BOMBEO CON BRAZO m³	VOLUMEN PROFUNDO m³	VOLUMEN SEDIMENTADO m³	VOLUMEN EFECTIVO DRAGADO m³	EFICIENCIA MEDIA DRAGADO CON BRAZO %	VOLUMEN DRAGADO CON TOLVAS m³
NORTE																
0 1	3	100	85	74	19	5	2	2 10	1925	14 0	2 079 000	533 000	802 000	1 268 000	61 0	67 000
1 2	1 5	100	98	84	40	8	6	2 40	1935	13 5	2 079 000	733 000	608 000	1 274 000	61 3	67 000
2 3	0 15	100	100	100	94	11	7	5 20	1950	11 0	3 180 000	997 000	1 192 000	2 189 000	68 8	
3 4	0 082	100	100	100	98	63	7	7 00	1945	11 0	4 911 000	1 007 000	2 460 000	3 467 000	70 5	
4 3	0 077	100	100	100	99	71	14	7 30	1940	13 5	5 403 000	882 000	2 912 000	3 794 000	70 2	
3 6	0 035	100	100	100	100	91	60	7 90	1925	15 5	6 069 000	949 000	3 311 000	4 260 000	70 2	
6 7	0 028	100	100	100	100	91	62	8 05	1900	17 0	5 866 000	1 012 000	2 787 000	3 799 000	65 0	
7 8	0 026	100	100	100	100	94	54	9 80	1850	19 0	4 202 000	970 000	1 931 000	2 921 000	69 3	
8 9	0 028	100	100	100	99	92	43	9 80	1820	22	3 131 000	814 000	1 399 000	2 213 000	70 7	
9 10	0 030	100	100	100	100	93	43	9 80	1773	24 5	1 983 000	812 000	696 000	1 508 000	76 0	
10 11	0 060	100	100	100	97	84	32	10 00	1750	26 5	1 903 000	1 121 000	288 000	1 409 000	74 0	
11 12	0 030	100	100	100	99	95	30	10 40	1733	28 0	1 531 000	1 001 000	58 000	1 059 000	69 2	
12 13	0 025	100	100	100	100	93	46	10 40	1725	28 5	1 531 000	1 003 000	51 000	1 034 000	68 8	
13 14								10 70	1725	29 0	1 531 000	1 123 000	60 000	1 183 000	77 3	
14 15								11 00	1723	19 0	1 531 000	1 056 000	61 000	1 117 000	73 0	
13 16								11 30	1725	31 0	1 331 000	984 000	95 000	1 079 000	10 3	
16 17								11 30	1723	33 0	1 222 000	893 000	10 000	903 000	73 9	
17 18								11 60	1710	34 3	1 038 000	751 000	20 000	771 000	74 3	

/mas

Cuadro No. 10

CARACTERISTICAS DEL DRAGADO DE LA ZULIA EN EL CANAL DE MARACAIBO

PROGRESIVA	GRANULOMETRIA D 80 mm	% QUE PASA EL CEDAZO N 1/4	4	10	60	270	0.06 mm	PROF MEDIA BORD. DEL CANAL (m)	DENSIDAD MEDIA EN EL BRAZO gr/lt	% DE SOLIDOS	BOMBEO CON BRAZO m³	VOLUMEN PROFUNDO m³	VOLUMEN SEDIMENTADO m³	VOLUMEN EFECTIVO DRAGADO m³	EFICIENCIA MEDIA DRAGADO CON BRAZO %	VOLUME DRAGADO CON TOLVAS m³
NORTE																
18 19								11 90	1680	33 5	933 000	670 000	21 000	691 000	72 4	
19 20								12 20	1663	36 0	933 000	671 000	11 000	682 000	71 4	
20 21								12 50	1650	36 5	933 000	549 000	55 000	604 000	63 2	
21 22								12 80	1643	36 0	955 000	530 000	67 000	397 000	62 3	
22 23								13 10	1645	36 0	436 000	330 000	47 000	377 000	39 3	
								TOTAL CANAL EXTERIOR			35 181 000	18 391 000	14 962 000	28 219 000		134 000

/mas

Cuadro No. 11

CARACTERISTICAS DEL DRAGADO DE LA ZULIA EN EL CANAL DE MARACAIBO

PROGRESIVA	GRANULOMETRIA D 80 mm	% QUE PASA EL CEDAZO N 1/4	4	10	60	270	0.06 mm	PROF MEDIA BORD. DEL CANAL (m)	DENSIDAD MEDIA EN EL BRAZO gr/lt	% DE SOLIDOS	BOMBEO CON BRAZO m³	VOLUMEN PROFUNDO m³	VOLUMEN SEDIMENTADO m³	VOLUMEN EFECTIVO DRAGADO m³	EFICIENCIA MEDIA DRAGADO CON BRAZO %	VOLUMEN DRAGADO CON TOLVAS m³
SUR																
0 1	0 60	100	100	100	77	27	13	4 85	1910	15 0	1 680 000	462 000	691 000	1 008 000	60 0	185 000
1 2	0 095	100	100	100	99	47	28	4 57	1870	17 0	1 376 000	635 000	633 000	825 000	60 0	443 000
2 3	0 11	100	100	100	98	37	17	1 50	1850	18 5	1 418 000	729 000	650 000	892 000	62 9	487 000
3 4	0 15	100	100	100	93	18	12	3 65	1840	21 5	1 401 000	725 000	621 000	859 000	61 3	487 000
4 5	0 18	100	100	100	98	12	6	3 65	1760	23 3	1 651 000	614 000	699 000	869 000	32 6	444 000
5-6	0 10	100	100	100	96	45	23	2.15	1770	26 0	1 719 000	631 000	691 000	1 088 000	63 2	234 000
6-7	0 20	100	100	100	95	19	8	1 40	1730	27 0	1 673 000	473 000	765 000	1 004 000	60 0	234 000
7-8	0 085	100	100	100	97	67	9	1 20	1760	27 3	1 289 000	668 000	308 000	937 000	67 3	39 000
8-9	0 10	100	100	100	99	56	36	1 80	1750	28 0	1 312 000	532 000	392 000	883 000	67 3	39 000
9 10	0 07	100	100	100	99	75	29	2 75	1730	28 5	1 187 000	540 000	300 000	801 000	67 3	39 000
10-11	0 08	300	100	100	98	64	29	3 00	1760	29 0	1 070 000	423 000	300 000	723 000	67 8	
11-12	0 09	300	300	100	97	60	24	3 63	1770	29 3	1 098 000	482 000	238 000	720 000	65 6	
12 13	0 09	100	100	100	98	56	20	3 95	1775	30 0	1 098 000	460 000	250 000	710 000	64 7	
13 14	0 03	100	100	100	97	90	24	4 57	1780	30 0	1 098 000	505 000	250 000	755 000	68 8	
14-13	0 035	100	100	100	97	89	25	3 20	1783	29 3	1 098 000	490 000	224 000	714 000	65 6	
15 16	0 10	100	100	100	93	57	13	3 65	1798	29 5	1 082 000	461 000	160 000	621 000	37 4	
16 17	0 15	100	100	100	87	38	10	3 93	1790	29 5	1 082 000	429 000	228 000	637 000	60 7	
17 18	0 10	100	100	100	99	30	25	4 85	1783	29 0	1 082 000	480 000	297 000	777 000	71 3	
18 19	0 09	100	100	100	96	56	22	4 57	1780	29 0	1 082 000	360 000	406 000	766 000	70 8	
19 20	0 07	100	100	100	96	78	26	6 00	1773	29 0	1 082 000	427 000	190 000	617 000	57 0	

Cuadro No. 12

CARACTERISTICAS DEL DRAGADO DE LA ZULIA EN EL CANAL DE MARACAIBO

PROGRESIVAS	GRANULOMETRIA: D 50 mm	% QUE PASA EL CEDAZO Nº 1/4	4	10	60	270	200 M.M.	PROF. MEDIA BORD. DEL CANAL (m)	DENSIDAD MEDIA EN SITIO gr/lt	% DE SOLIDOS	BOMBEO CON BRAZO m³	VOLUMEN PROFUNDO m³	VOLUMEN SEDIMENT m³	VOLUMEN EFECTIVO DRAGADO m³	EFICIENCIA MEDIA DRAGADO CON BRAZO %	VOLUMEN DRAGADO CON TOLVAS m³
SUR																
20 21	0 07	100	100	100	99	73	60	6 70	1775	28 5	1 082, 000	477 000	200 000	677 000	62, 6	
21 23	0 08	100	100	100	95	65	25	7 90	1770	28 0	1 082, 000	532, 000	227 000	759 000	70 1	
22-23	0 07	100	100	100	97	79	28	9 49	1765	27 0	2, 123 000	580 000	765 000	1 325 000	62, 3	
23 26								10 80	1760	25 0	1 682 000	552, 000	319 000	871 000	58, 7	
26 25								10 10	1755	23 5	1 726 000	992, 000	972, 000	1 324, 000	65 1	
25 26								11 50	1750	23 0	1 355 000	169 000	850 000	561 000	50 0	
26 27								10 10	1740	23 5	1 355 000	46 000	639 000	681 000	80 0	
27-28								11 30	1735	26 0	361 000	67 000	386 000	319 000	59 0	
28 29								11 30	1730	25 0	590 000	53 000	277 000	330 000	60 0	
29 30								12 50	1725	25 5	266 000	86 000	252 000	166 000	67 5	
30 31								14 00	1720	26 5	402, 000	133 000	335 000	368 000	61 7	
31 32								12 50	1715	27 0	266 000	47 000	319 000	166 000	67 5	
32 33								12 20	1705	27 5	266 000	132 000	34 000	166 000	67 5	
33 34								12 20	1700	26 0	266 000	100 000	66 000	166 000	67 9	
34 35								11 00	1700	28 5	270 000	70 000	96 000	166 000	61 5	
50 51								15 10	1720	28 5	134, 000	90 000		90 000	67 2	
51-52								12, 40	1780	29 5	160 000	94 000		94, 000	67 1	
52-53								12, 50	1750	30 0	328, 000	220 000		220 000	67 1	
53-54																
54 55								12, 50	1775	30 0						
54 55								13 10	1815	29 9	630 000	288, 000		288, 000	67 0	

Cuadro No. 13

CARACTERISTICAS DEL DRAGADO DE LA ZULIA EN EL CANAL DE MARACAIBO

PROGRESIVAS	GRANULOMETRIA: D 50 mm	% QUE PASA EL CEDAZO Nº 1/4	4	10	60	270	200 M.M.	PROF. MEDIA BORD. DEL CANAL (m)	DENSIDAD MEDIA EN SITIO gr/lt	% DE SOLIDOS	BOMBEO CON BRAZO m³	VOLUMEN PROFUNDO m³	VOLUMEN SEDIMENT m³	VOLUMEN EFECTIVO DRAGADO m³	EFICIENCIA MEDIA DRAGADO CON BRAZO %	VOLUMEN DRAGADO CON TOLVAS m³
SUR																
55 56								12 20	1835	27 5	292, 000	169 000		169 000	67 1	
56 57								12 50	1860	33 5						
57 58								14 00	1885	18 0						
58-59								13 10	1920	14, 5	95, 000	69 000		69 000	72, 6	
59-60								12, 80	1935	14 5	612, 000	443 000		443 000	72, 4	
60-61								12 28	1935	16 0	612, 000	443 000		443 000	72 4	
61-62								11 80	1950	18 0	622, 000	450 000		450 000	72, 3	
62 63								11 60	1915	21 0	598, 000	433 000		433 000	72, 6	
63 64								11 90	1885	23 0	455 000	329 000		329 000	72, 3	
64 65								12, 40			473 000	342, 000		342, 000	72, 3	
65 66								13 70			91 000	34 000		34 000	72, 9	
66 67								16 30								
67-68								14, 65								
68 69								13 30	1505	34, 0	604, 000	226 000	198 000	384, 000	63 6	* 38 000
69-70								11 90	1569	33 0	963 000	637 000	158 000	979 000	63 1	* 38 000
70 71								11 60	1543	32, 5	963 000	463 000	352, 000	623 000	54 9	
71 72								11 60	1570	31 0	963 000	532, 000	198, 000	690 000	73 2	
72-73								11 90	1575	28 9	984, 000	547 000	158 000	709 000	73 6	

* DRAGADO FUERA DEL CANAL

Cuadro No. 14

CARACTERISTICAS DEL DRAGADO DE LA ZULIA EN EL CANAL DE MARACAIBO

PROGRESIVAS	GRANULOMETRIA: D 50 mm	% QUE PASA EL CEDAZO Nº 1/4	4	10	60	270	200 M.M.	PROF. MEDIA BORD. DEL CANAL (m)	DENSIDAD MEDIA EN SITIO gr/lt	% DE SOLIDOS	BOMBEO CON BRAZO m³	VOLUMEN PROFUNDO m³	VOLUMEN SEDIMENT m³	VOLUMEN EFECTIVO DRAGADO m³	EFICIENCIA MEDIA DRAGADO CON BRAZO %	VOLUMEN DRAGADO CON TOLVAS m³
SUR																
73-76								12, 40			913 000	533 000		533 000	52, 6	
76 75								12 80			827 000	450 000		680 000	52, 0	
75-74								13 30			589 000	363 000		363 000	52, 2	
76 77								13 38			662, 000	381 000		381 000	57 6	
								TOTAL CANAL INTERIOR			8 482, 000	10 858 000	13 976 000	8, 363 000		2, 667, 000

NOTA

indicadas en las órdenes de dragado, lo cual no es rigurosamente cierto.

Sin embargo, las dificultades e imprecisiones anteriores desaparecen cuando se usan cifras globales y se obtienen a partir de ellas los valores promedios de rendimiento y sedimentación. Con estas salvedades, se presentan separadamente para el Canal Interior y Exterior, las cifras de los cuadros siguientes:

RELACION DE VOLUMENES DRAGADOS CON BRAZO
(Del 17-2-60 al 17-7-62)

Descripción	Unid.	Canal Interior	Canal Exterior	Total
Volumen de bombeo	m3	49 482 000	55 181 000	104 663 000
Volumen de profundización (incl. tolvas)	m3	20 858 000	19 391 000	40 249 000
Volumen de sedimentación (incl. tolvas)	m3	13 976 000	18 962 000	32 938 000
Volumen efectivo de dragado	m3	32 243 000	38 219 000	70 462 000
Eficiencia media del dragado		65.16%	69.26%	67.32%

RELACION DE TIEMPOS

TRABAJO EFECTIVO:	Horas	% tiempo de operación
Tolvas:		
Bombeo	1 380.77	7.04
Evoluciones	160.35	0.82
Ida y vuelta a descarga	232.20	1.18
Descarga	64.98	0.33
Total por Tolvas	1 838.30	9.37
Brazo:		
Bombeo hacia el Este	4 466.22	22.78
Bombeo hacia el Oeste	9 686.08	49.40
Evoluciones	613.32	3.13
Total por Brazo	14 765.62	75.31
TRABAJO NO EFECTIVO:		
Mantenimiento y reparaciones	2 738.23	13.97
Transferencias en el trabajo	9.28	0.05
Otras demoras	1.95	0.01
Mal tiempo	2.98	0.02
Tráfico	12.10	0.06
Cese	85.57	0.44
Accidentes	151.47	0.77
Total trabajo no efectivo	3 001.98	15.32
Tiempo total de operac.	19 605.90	100.00

A partir de las cifras dadas anteriormente, se obtienen los siguientes rendimientos medios:

a) Dragado con brazo:

Volumen bombeado por hora neta de bombeo	7 088 m3/hora
Volumen efectivo dragado por hora neta de bombeo	4 772 "

b) Dragado con tolvas:

Volumen dragado por hora de ciclo	1 524 "

REFERENCIAS

The Hopper Dredge - Corps of Engineering - U.S. Army Government Printing Office - Washington - 1954.

Fundamentals of Soils Mechanics -Donald W. Taylor-John Wiley & Sons New York - 1948.

Engineering Hydraulics -Hunter Rouse -John Wiley & Sons -New York- 1958.

Paper on Sidecast (Boom) Dredging-Foreign Experience and Local application at A.S.C.E. Fall Meeting by Henry G.A. Hayward-New York-1961.

CHAPTER 38

ANALISIS HIDRAULICO DEL COMPORTAMIENTO DE LA ONDA DE MAREA A TRAVES DE LA BAHIA DE TOPOLOBAMPO Y SUS EFECTOS EN LA BARRA

Hector Lopez Gutierrez y Jose Aguilar Alcerreca
Secretaria De Marina
Mexico

1.- INTRODUCCION.- El puerto de Topolobampo se encuentra localizado al Noroeste del estado de Sinaloa, sobre el -- Golfo de California. Su importancia como puerto tiende a incrementar notablemente por dos factores:

- El Ferrocarril Chihuahua-Pacífico que liga la costa Noroeste de la República Mexicana con la zona Norte de la - misma y varios estados del Sur de los Estados Unidos.
- El notable desarrollo agrícola de las tierras irrigadas

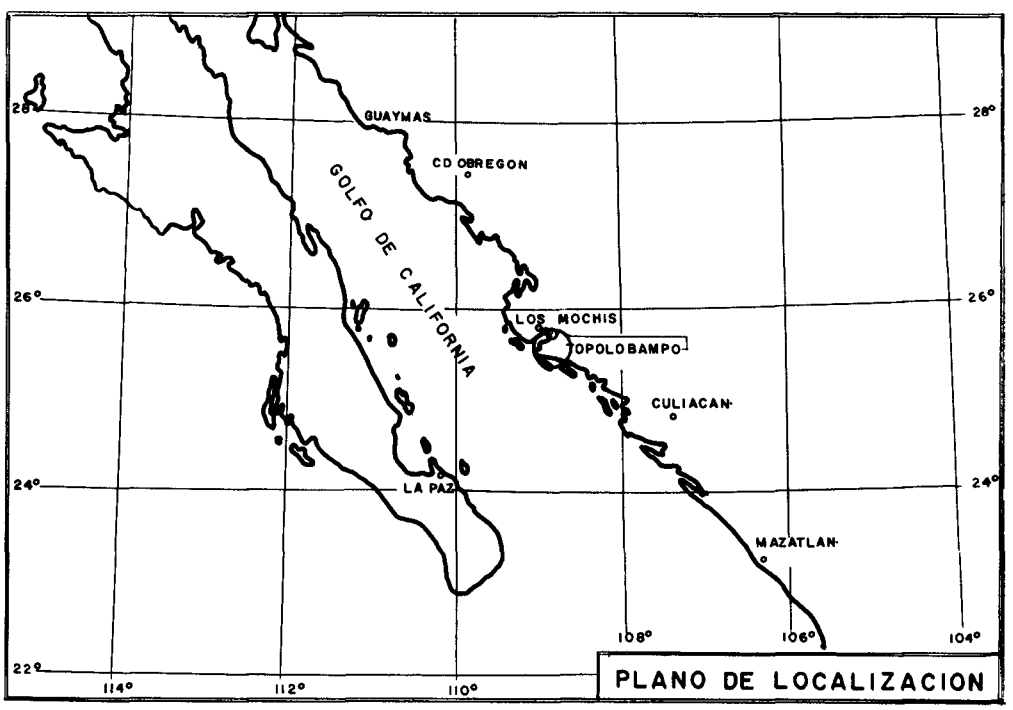

Fig. 1

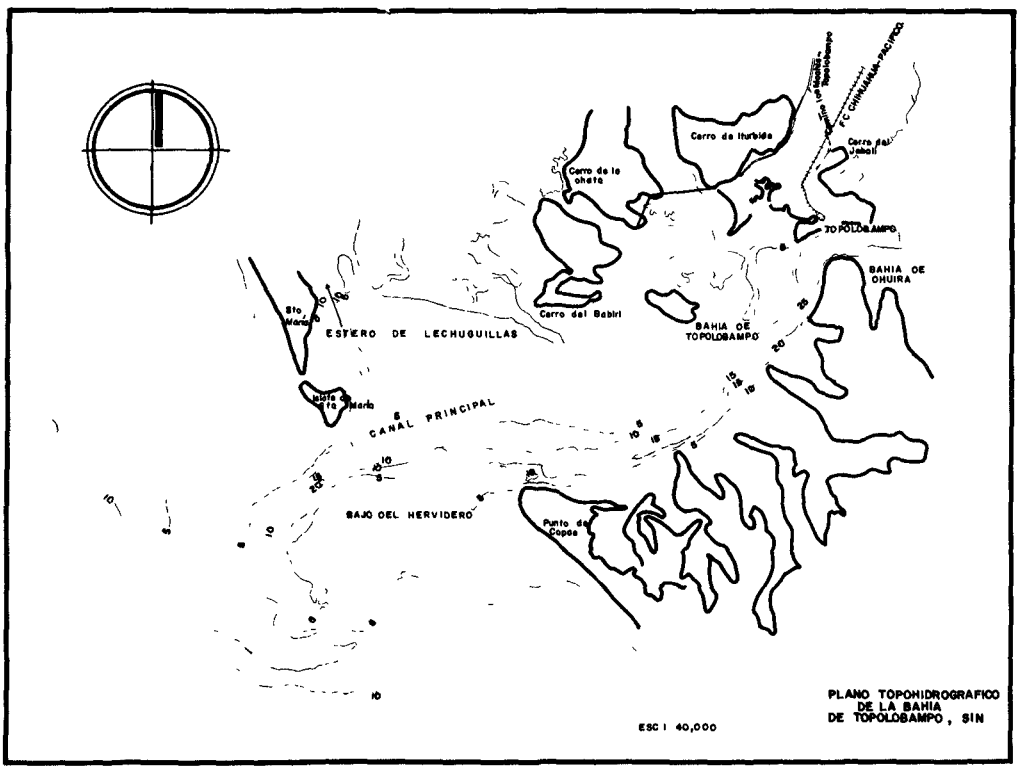

Fig. 2

por los ríos Fuerte y Mayo, cuya área se estima, en la - actualidad en 300 000 Ha.aproximadamente.

La Bahía de Topolobampo tiene un área aproximada de 48,254 Km^2, cuenta con numerosas zonas bajas y esteros secundarios, de los cuales, el más importante es el de Lechuguillas. Existen dos canales perfectamente definidos, el principal que corre a todo lo largo de la Bahía con una dirección NE-SW hasta el sitio denominado Punta Copas, donde cambia su dirección de E a W; en el Islote de Santa María se le une el 2o. canal proveniente del Estero de Lechuguillas, formándose un solo canal de salida con dirección SSW.

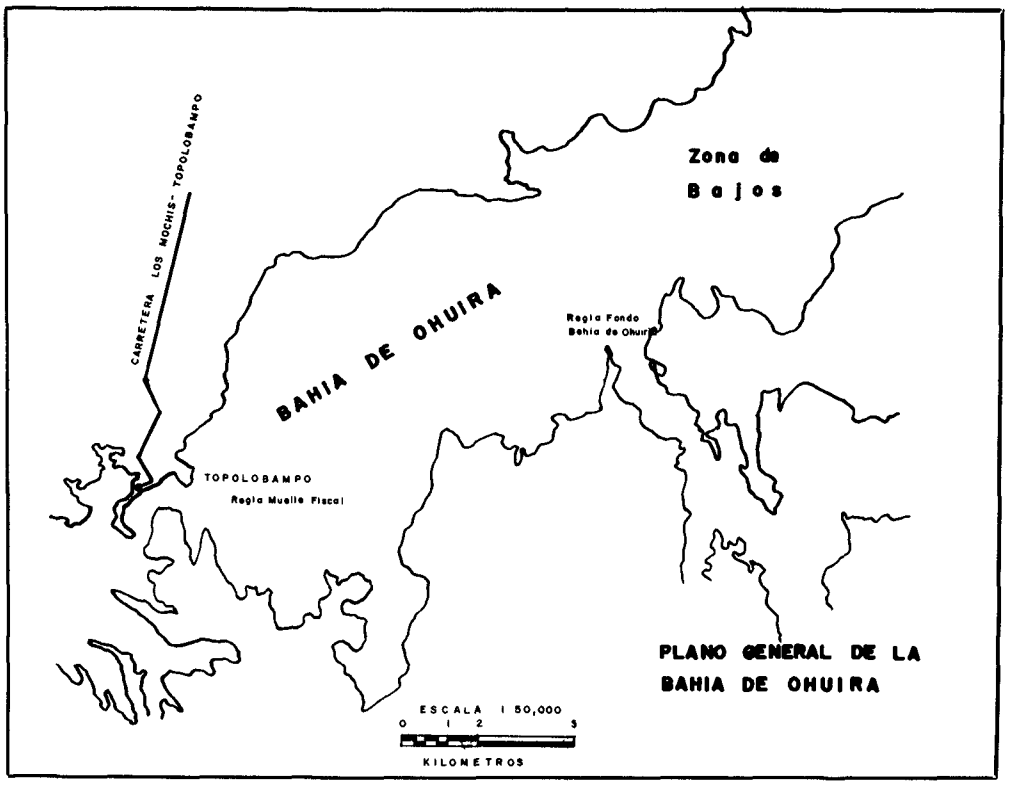

Fig. 3

Al fondo de la Bahía de Topolobampo se tiene un paso estrecho que comunica con la Bahía de Ohuira que tiene una área de 147.998 Km^2. Esta bahía es relativamente poco profunda, pero dada su extensión el prisma de marea movido en cada ciclo es de una importancia considerable.

El Puerto de Topolobampo presenta características inmejorables en cuanto a profundidad y protección, pero tiene el problema de acceso a él, ya que debido al efecto de las corrientes de marea y el acarreo litoral se forma una barra que disminuye en forma considerable la profundidad.

El objetivo de este trabajo es presentar una posible solución a este problema, señalando que, para proponerla, hubieron de hacerse varias suposiciones, debido, fundamentalmente, a la carencia de datos de campo. Esta observación se hace a fin de que en el juicio que se haga del presente comunicado se tome en cuenta este factor.

2.- DATOS.- Es conveniente mencionar los datos de que se disponían para atacar el problema.

a).- Aerofotografía de la Bahía de Ohuira a escala 1:20,000.

b).- Plano general batimétrico topográfico de la Bahía de Topolobampo excluyendo los esteros secundarios inclusive el de Lechuguillas.

c).- Observaciones de mareas en 4 puntos, durante los días 14 y 15 de marzo de 1961.

d).- Medición de vectores velocidad en puntos cercanos a los de observación de mareas en las mismas fechas.

e).- Mareogramas de 5 años (1955-1961) obtenidos del mareógrafo instalado en el Muelle Fiscal.

3.- ESTUDIO DE LA SOLUCION.

Para la aplicación de las observaciones de marea efectuadas el 14 y 15 de marzo de 1961 hubo necesidad de determinar primero el nivel medio del mar, a fin de poder referir a él los ceros de las reglas de marea, ya que dichas

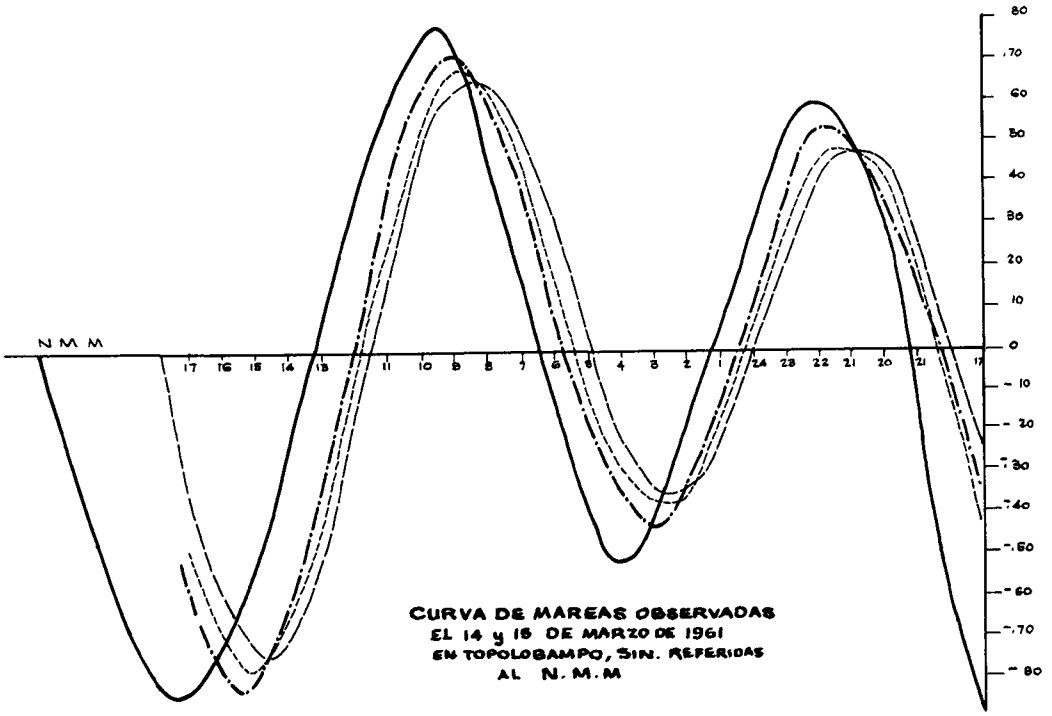
N M M
CURVA DE MAREAS OBSERVADAS
EL 14 y 15 DE MARZO DE 1961
EN TOPOLOBAMPO, SIN. REFERIDAS
AL N.M.M

Fig. 4

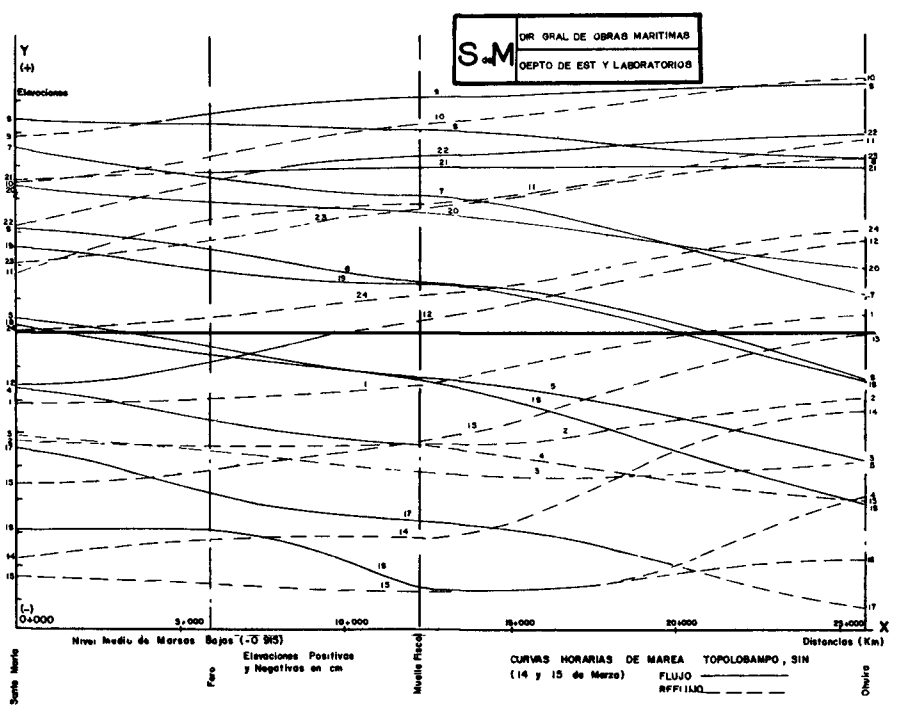
S.M
DIR GRAL DE OBRAS MARITIMAS
DEPTO DE EST Y LABORATORIOS
Elevaciones
Nivel Medio de Mareas Bajas (-0.915)
Elevaciones Positivas y Negativas en cm
CURVAS HORARIAS DE MAREA TOPOLOBAMPO, SIN
(14 y 15 de Marzo)
FLUJO
REFLUJO
Distancias (Km)

Fig. 5

reglas no estaban relacionadas entre sí. Definido este nivel de acuerdo con las observaciones hechas se trazaron las curvas que permitieron estudiar la forma de propagación de la onda de marea, desde la entrada hasta el fondo de la Bahía de Ohuira.

Conocido ya la forma de propagación de la onda de marea tanto dentro de la Bahía de Topolobampo como de la Bahía de Ohuira, se procedió a la valuación de los volúmenes de agua que se movían durante cada ciclo de marea, a fin de determinar sus efectos sobre el canal principal de acceso al puerto.

El método de cálculo usado fue el de cubicación por incrementos finitos, partiendo de la ecuación de continuidad.

En nuestro problema se tomaron 4 secciones de cubicación; en tres de ellas podrían comprobarse los cálculos con las mediciones hechas el 14 y 15 de marzo. Las cuatro secciones consideradas fueron:

1.- Sección al fondo de la Bahía de Ohuira.- Esta sección tenía por objeto poder cuantificar el volumen que se movía entre la regla de marea localizada al fondo de dicha bahí y el punto máximo alcanzado por la marea; la zona cubiert por la marea se definió de la observación de la aerofotografía.

2.- Sección del Muelle Fiscal.- Se encuentra localizada en una garganta formada entre la Isla Gallinas y el Cerro San Carlos; es el paso de la Bahía de Topolobampo a la de Ohuira.

3.- Sección Punta Copas.- El Babiri.- Presenta la característica de tener una amplitud extraordinaria compuesta de ur

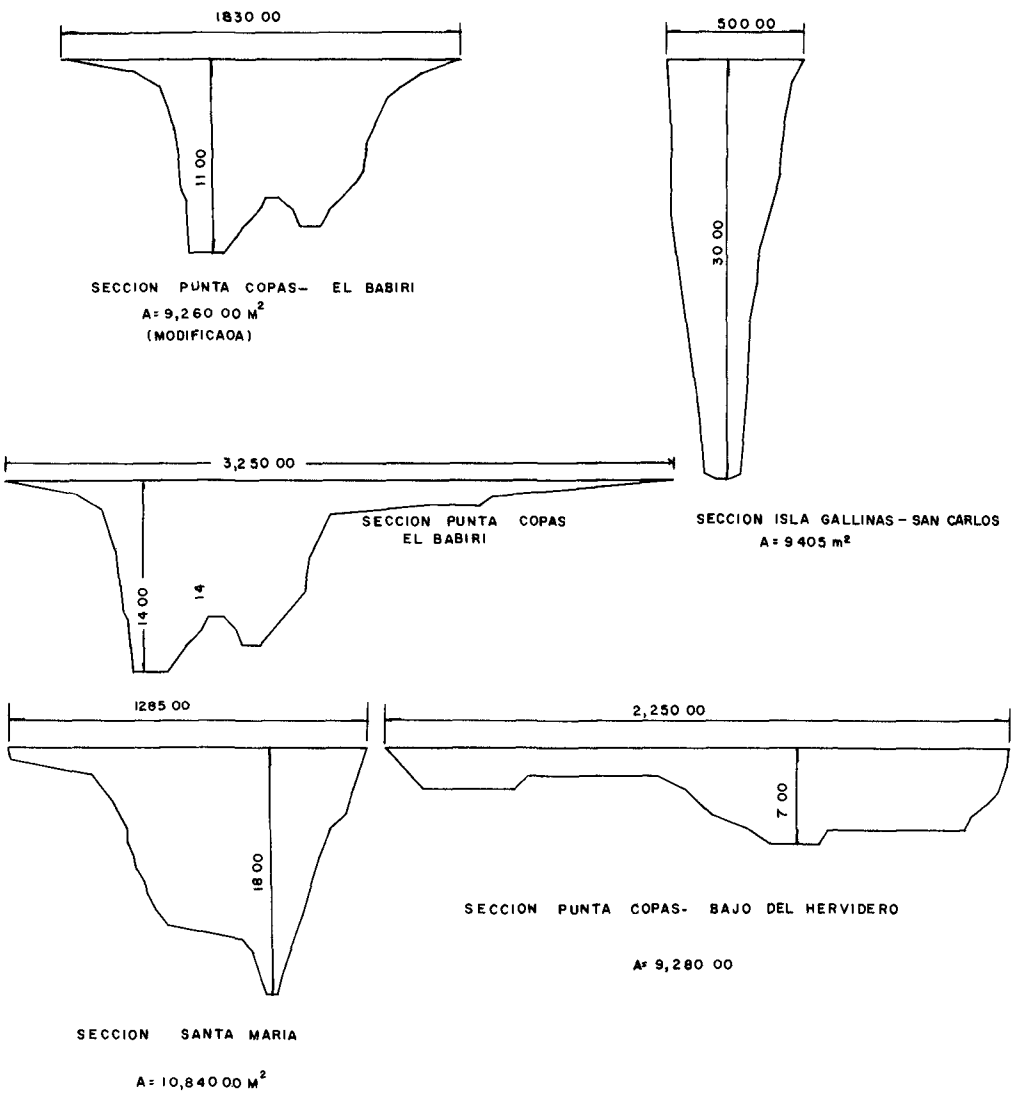
1830 00
11 00
SECCION PUNTA COPAS– EL BABIRI
A= 9,260 00 M2
(MODIFICAOA)
500 00
30 00
SECCION ISLA GALLINAS – SAN CARLOS
A= 9405 m2
3,250 00
14 00
14
SECCION PUNTA COPAS
EL BABIRI
1285 00
18 00
SECCION SANTA MARIA
A= 10,840 00 M2
2,250 00
7 00
SECCION PUNTA COPAS- BAJO DEL HERVIDERO
A= 9,280 00

Fig. 6

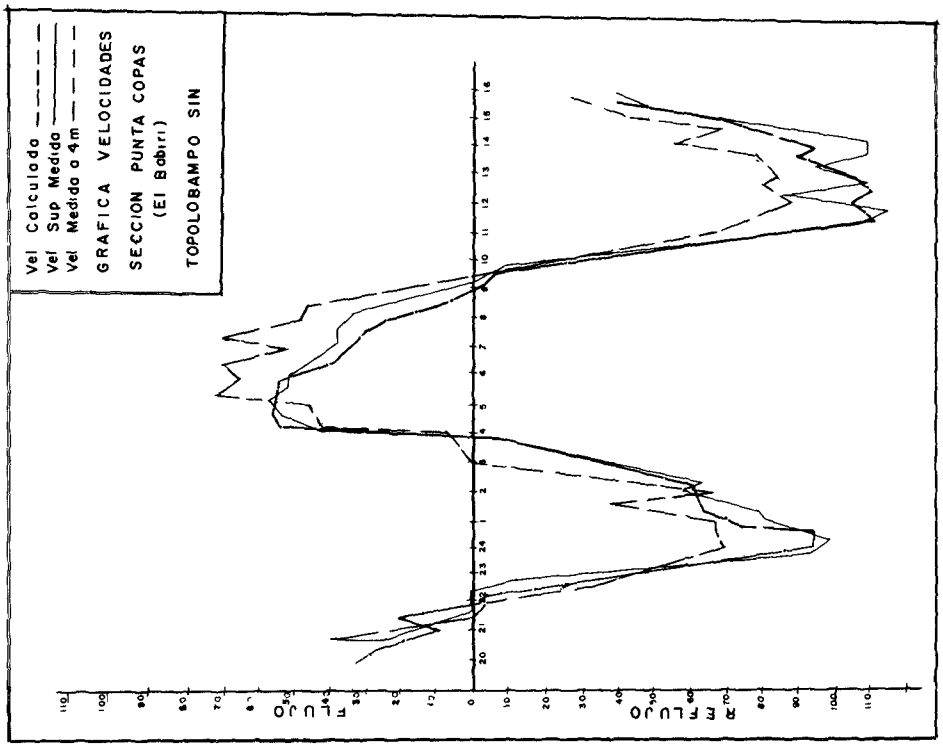
Vel Calculada
Vel Sup Medida
Vel Medida a 4m
GRAFICA VELOCIDADES
SECCION PUNTA COPAS
(El Bobiri)
TOPOLOBAMPO SIN
FLUJO
REFLUJO

Fig. 8

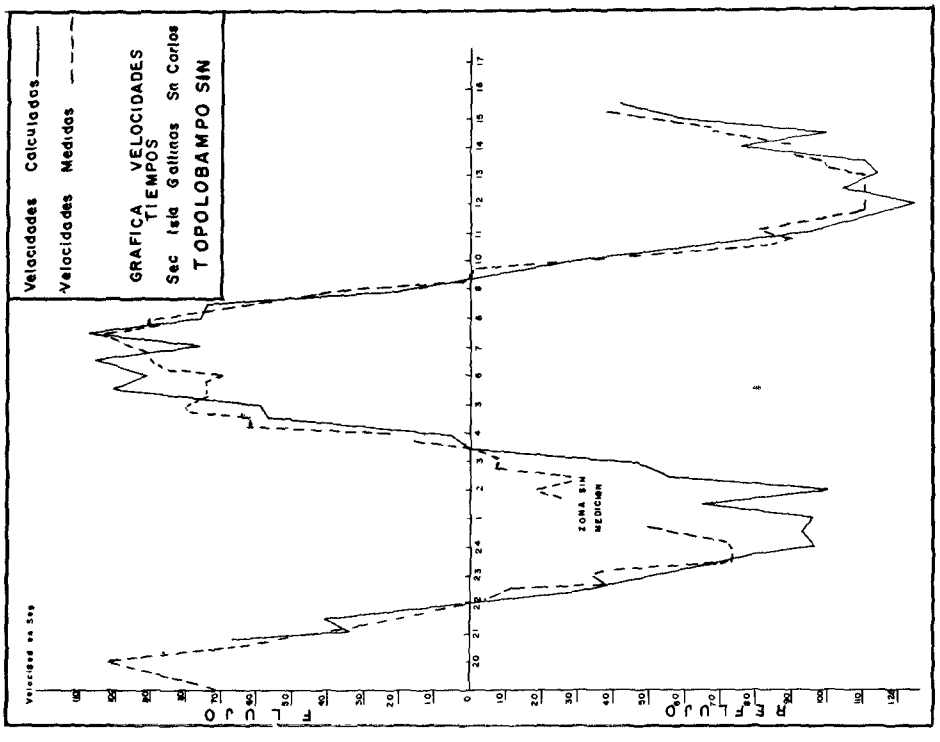
Velocidades Calculadas
Velocidades Medidas
GRAFICA VELOCIDADES
TIEMPOS
Sec Isla Gallinas Sn Carlos
TOPOLOBAMPO SIN
ZONA SIN MEDICION
FLUJO
REFLUJO

Fig. 7

extensa zona de poca profundidad y el canal principal de propagación de la onda. Dada esta geometría, se consideró como sección efectiva la constituida por el canal antes mencionado.

4.- Sección Santa María.- Esta es la sección de salida, en ella se unen los canales de lechuguillas y el proveniente de la bahía; Para fines de cálculo se tomó unicamente la sección definida por el canal de salida.

Posteriormente hubo que considerar una cuarta sección, la de Punta Copas - Islote del Hervidero, en la que no se hicieron mediciones.

La cubicación se hizo bajo las siguientes hipótesis:

a).- Sección de fondo de la Bahía de Ohuira.

- Se parte con condición de pleamar.
- A la zona cubierta por el ascenso de la marea se le dió una pendiente uniforme y se considera que las variaciones del nivel del agua son siempre según un plano horizontal.

b).- Sección Muelle Fiscal.

- Para el cálculo del aporte de la bahía de Ohuira el área del espejo libre considerada fue siempre la misma, salvo en los casos en que se presentaron puntos de marea nulos entre la regla del fondo y la salida de la bahía.

c).- Sección Punta Copas - El Babiri.- Como sección efectiva sólo se consideró la del canal principal. El aporte del estero de El Babiri se calculó con base en las mediciones de velocidad hechas a la salida de él y sólo para reflujo.

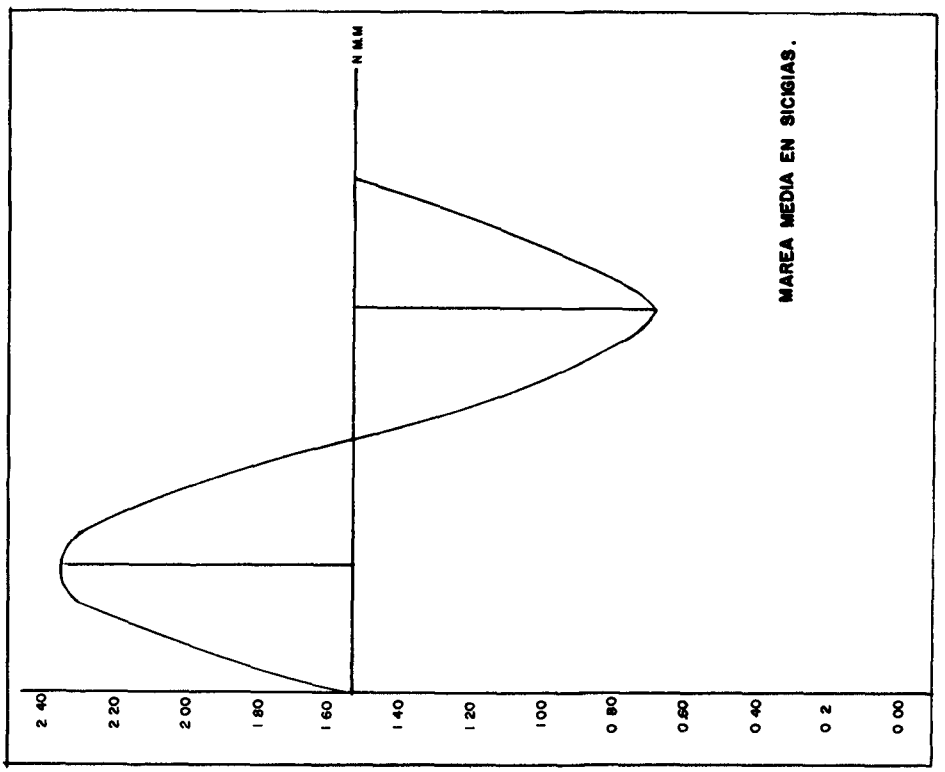
MAREA MEDIA EN SICIGIAS.
N.M.M
2.40
2.20
2.00
1.80
1.60
1.40
1.20
1.00
0.80
0.60
0.40
0.2
0.00

Fig. 10

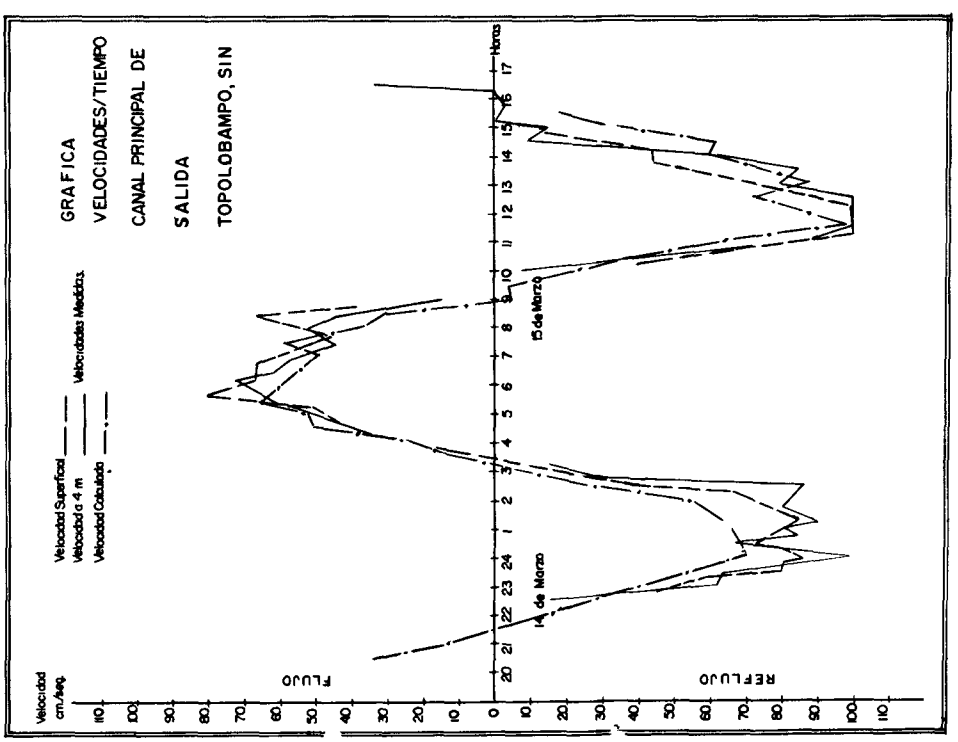
GRAFICA
VELOCIDADES/TIEMPO
CANAL PRINCIPAL DE
SALIDA
TOPOLOBAMPO, SIN
Velocidad Superficial
Velocidad a 4 m
Velocidad Calculada
Velocidades Medidas.
Velocidad cm/Seg
FLUJO
REFLUJO
14 de Marzo
15 de Marzo
Horas

Fig. 9

d).- Sección Santa María.- Para esta sección ya no fue posible aplicar este método, debido fundamentalmente a la diversificación de gastos a la salida de la Bahía de Topolobampo. Se usó entonces el concepto de niveles de energía aplicando la ecuación de Bernoulli, la fórmula de Chezy y además la consideración de división del gasto total en cuatro partes:

- Gasto del estero de Lechuguillas.- Calculado a partir de las mediciones hechas a la salida del estero.
- Gasto de la sección considerada.
- Gasto de la sección Punta Copas - Islote del Hervidero.
- Gasto de la seccion Punta Copas - El Babiri.

Hechas todas las consideraciones señaladas en los párrafos a, b, c y d se calcularon los volúmenes y consecuentemente las velocidades, quedando entonces en posibilidad de compararlas con las medidas superficialmente y a 4 m. de profundidad, corrigiendo por resistencia estas últimas.

Las mediciones de velocidades se hicieron cada 30 minutos, sin embargo hubo ocasiones que transcurrieron lapsos mayores entre dos medidas consecutivas además de que el método usado no da una gran precisión. Sin embargo la comparación entre las velocidades calculadas y las medidas da una aproximación aceptable.

CALCULO DE LA MAREA DOMINANTE.-

Se puede establecer una similitud entre el concepto de gasto dominante, sobre todo cuando el canal de propagación de la misma está también definido como en el caso de Topolobampo. Partiendo de lo anterior y basados en las mediciones de mareas que durante 5 años ha hecho el Instituto de Geofí-

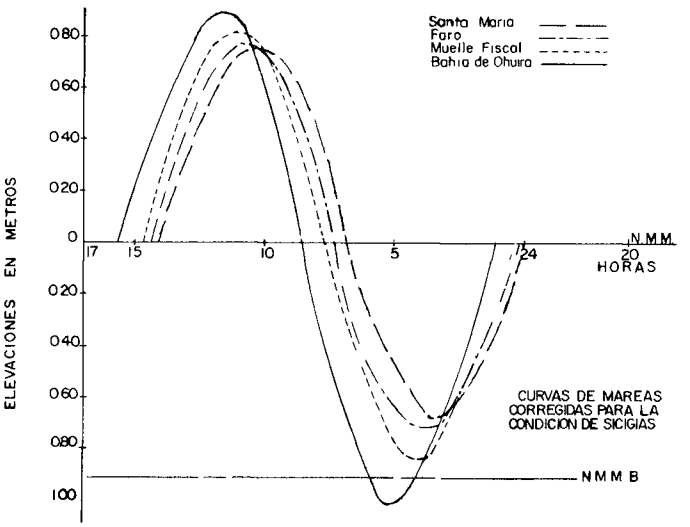

Fig. 11

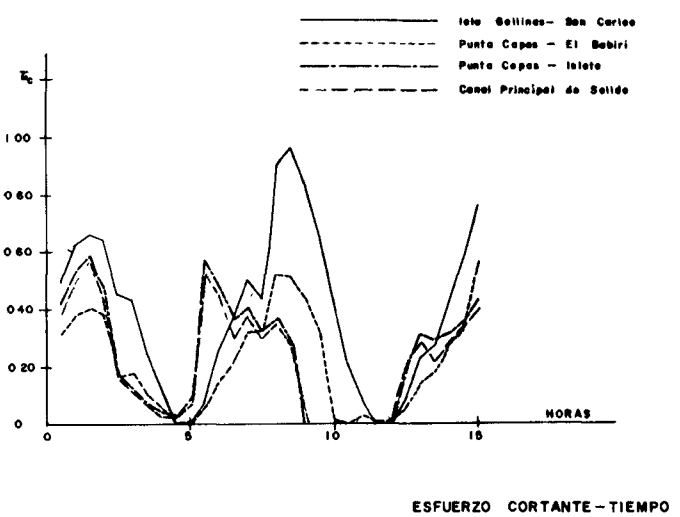

ESFUERZO CORTANTE – TIEMPO

Fig. 12

sica de la Universidad Nacional Autónoma de México y en el - concepto de gasto dominante se procedió a calcular la marea dominante.

La marea dominante se calculó tomando el promedio de las amplitudes mensuales máximas, con sus períodos correspondientes.

El resto de la curva se define tomando también los - promedios de las amplitudes intermedias correspondientes a - ciertos períodos de las mareas máximas de cada mes.

Determinada la curva de marea dominante en el Muelle Fiscal, el siguiente problema era la obtención de esta curva en los sitios en que no se tienen mas que las mediciones del 14 y 15 de marzo de 1961.

Inicialmente se pensó usar el método de Runge, corrigiendo los coeficientes, pero debido a la gran diferencia de las secciones transversales, las curvas obtenidas eran muy - diferentes entre sí. Hubo entonces necesidad de recurrir a la similitud geométrica entre las curvas medidas el 14 y 15 de marzo.en Santa María, Punta Copas y la Bahía de Ohuira -- con la del Muelle Fiscal para las mismas fechas. Definidas - las características geométricas, partiendo de la marea dominante en el Muelle Fiscal se obtuvieron las curvas correspondientes a los puntos restantes.

El defasamiento entre cada una de las curvas se obtuvo con la aplicación simple de las fórmulas de la celeridad.

Definidas todas las características de la marea dominante, (amplitud, período, defasamiento, etc.), se aplicó el método de cálculo usado para el 14 y 15 de marzo a fin de determinar las velocidades correspondientes a ella.

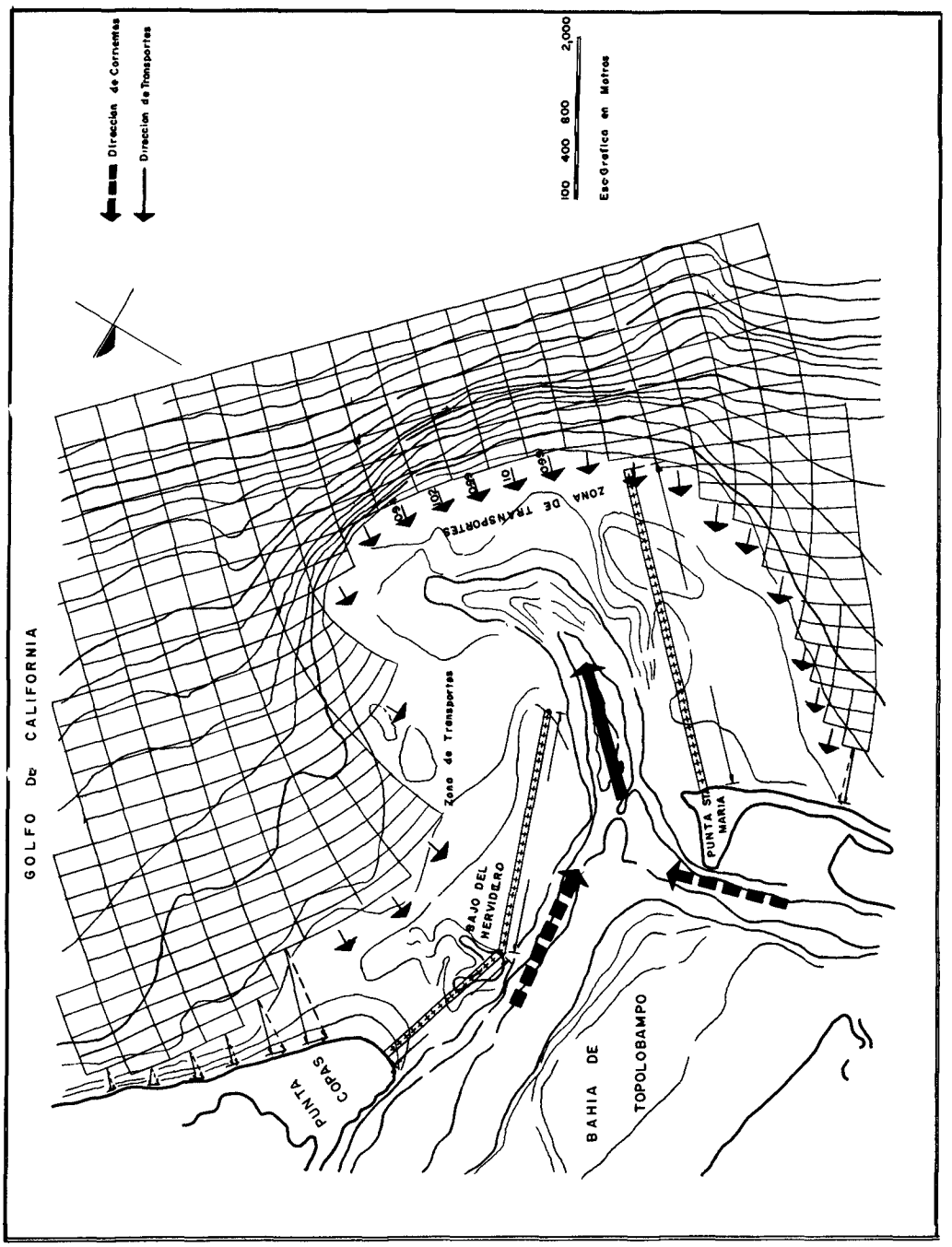
Direccion de Corrientes
Direccion de Transportes
100 400 800 2,000
Escala Grafica en Metros
GOLFO De CALIFORNIA
ZONA DE TRANSPORTES
Zona de Transportes
BAJO DEL MERVIDERO
PUNTA STA MARIA
PUNTA COPAS
BAHIA DE TOPOLOBAMPO

ESTABILIDAD DEL ACCESO.-

El estudio del comportamiento del canal propiamente - dicho, se hizo considerando que estaba en equilibrio dinámico. Esta consideración fue posible hacerla de la comparación y análisis de planos topohidrográficos de la Bahía de Topolobampo obtenidos de 1939 a 1961.

Al calcular los gastos sólidos para flujo y reflujo - en función del esfuerzo cortante de arrastre, usando una fórmula como la de DuBoys, por ejemplo; sí las velocidades calculadas fueran correctas, y dado que los esfuerzos cortantes estarían en función ellas, la diferencia de gastos sólidos -- debería ser aproximadamente nula.

Se hicieron los cálculos correspondientes para el canal de salida, y dd acuerdo con lo antes dicho la relación de los gastos sólidos debería ser unitaria para el estado de - - equilibrio. El resultado obtenido fue de 0.9. Considerando las hipótesis simplificatorias hechas y la influencia del --- acarreo litoral cuya presencia se tiene a corta distancia, el resultado se consideró correcto.

El problema que se presentó a continuación fue el de analizar el efecto de la marea dominante a la entrada del canal principal.

Debido al efecto del acarreo litoral cuya componente_ principal es del SW, el canal principal, cuya dirección de salida es NE-SW, se obstruye y se desvía hacia el SE perdiendo gradualmente profundidad hasta desaparecer en la parte media de la barra, que va de Punta Copas en dirección Oeste hasta - el Islote del Hervidero continuando hacia el Sur nasta la zona de acarreos más intensa recurvando para tomar dirección --

Norte y unirse con la Punta de Santa María.

Por la complejidad del problema de la salida del canal, agudizada por la carencia de datos, con objeto de no dar una respuesta aventurada y sin fundamento ni forma de comprobación, la Dirección General de Obras Marítimas ha ordenado el dragado de un canal de navegación con el doble fin de permitir la entrada al puerto de barcos de calado medio y a través de observaciones periódicas estudiar el comportamiento de dicho canal.

Como solución mediata se ha pensado en la construcción de 2 escolleras, una que salga de Punta Santa María en dirección S 45° W con 4 Km. de longitud y la segunda que vaya de Punta Copas hasta el bajo del hervidero y de allí seguir con dirección S 70° W a fin de dar una convergencia con la escollera norte.

Estas escolleras tendrían como objetivos el detener el acarreo litoral y encauzar las corrientes de marea con fines de profundidad.

Puede, entonces, hacerse el análisis, usando la teoría del esfuerzo cortante de arrastre, de los efectos que las mencionadas obras tendrían en el canal de salida. Este análisis se hizo a partir de los resultados obtenidos en el curso de este comunicado. Es decir, usando la marea dominante y sus gastos y bajo la consideración de que la totalidad del gasto saldría por la sección de las escolleras, se calcularon los esfuerzos cortantes, en función de las velocidades, en las secciones inicial y final de las escolleras; encontrándose que los esfuerzos serían de tal magnitud que inclusive pondrían en peligro la estabilidad de las escolle

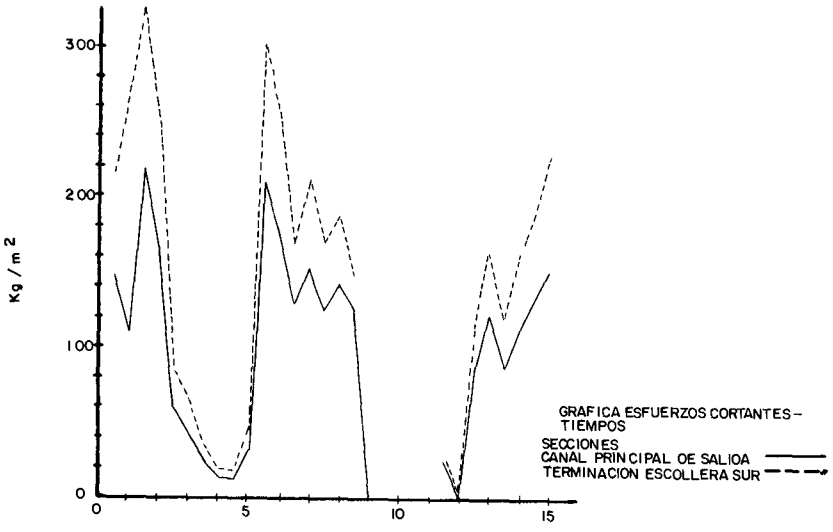
300
200
100
0
Kg / m²
0
5
10
15
GRAFICA ESFUERZOS CORTANTES – TIEMPOS
SECCIONES
CANAL PRINCIPAL DE SALIDA
TERMINACION ESCOLLERA SUR

Fig. 14

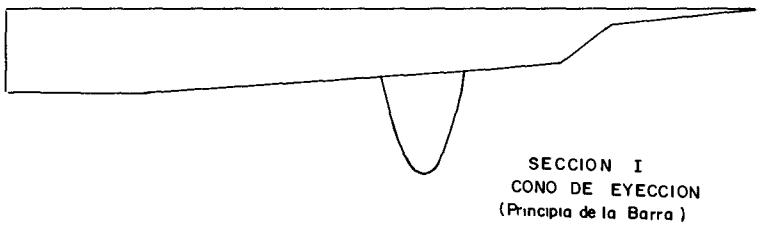
SECCION I
CONO DE EYECCION
(Principia de la Barra)

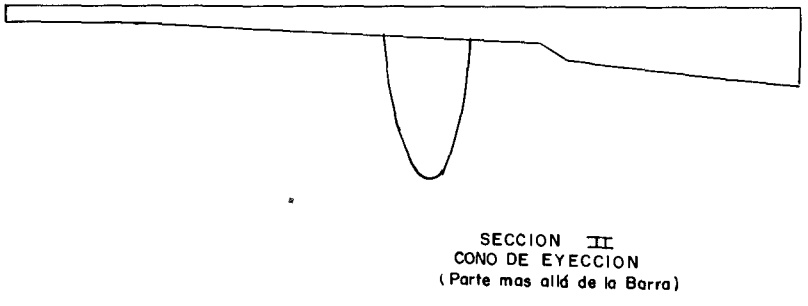
SECCION II
CONO DE EYECCION
(Parte mas allá de la Barra)

Fig. 15

ras. Esta conclusión está basada en observaciones hechas - en otros países en lo que a estabilidad de accesos de marea se refiere, ya que en dichas observaciones y para caracte-- rísticas de acarreo litoral y de sedimento semejantes a las de Topolobampo; el esfuerzo cortante de estabilidad es de - 0.5 Kg/m^2 en tanto que en nuestro caso se obtuvieron valo-- res de 2 Kg/m^2 en una sección media entre escolleras y 3 Kg/ m^2 a la salida de ellas.

Podría concluirse de los anteriores cálculos que el canal de acceso que se dragué inicialmente, no sólo se conservará sino se ampliará, sin embargo su conservación o -- azolve dependerá también de los límites del cono de deyec-- ción. Este aspecto creemos que sólo podría comprobarse en un modelo de fondo fijo.

Sin embargo y a fin de tener una idea, aunque fuera - aproximada, del comportamiento de las obras mencionadas, se supusieron el cono de deyección de Hinds y las secciones -- dragadas a una profundidad de 10 m., comprobándose nuevamente que el canal de navegación que se dragara se ampliaría - en forma considerable. Esto sería un índice de que cons--- truídas las escolleras no habría necesidad de efectuar ningún dragado previo.

Por lo que se refiere al aspecto constructivo de las escolleras los problemas fundamentales serán la calidad del material a usarse y su transporte hasta el sitio de cons--- trucción, posteriormente se tendría el problema de socava-- ción.

Presentada esta idea de solución, podemos obtener -- las siguientes

ANALISIS HIDRAULICO DEL COMPORTAMIENTO DE LA ONDA DE MAREA A TRAVES DE LA BAHIA DE TOPOLOBAMPO Y SUS EFECTOS EN LA BARRA

CONCLUSIONES.-

1.- Los resultados obtenidos son puramente teóricos y servirán sólo para fijar una base en el análisis definitivo del problema.

2.- Es necesario realizar una campaña de medidas que abarque un período de tiempo mayor y planeada adecuadamente.

3.- Basados en la campaña de medidas, construir un modelo de fondo fijo a fin de determinar posición y dirección más adecuadas para las escolleras y fijar los límites del cono de deyección.

4.- Efectuar con los datos obtenidos en los incisos 2 y 3, de nueva cuenta, los cálculos presentados en este trabajo a fin de poder definir si la onda de marea en la bahía de Topolobampo tiene sobre la barra, la influencia que se ha definido después de este estudio preliminar.

Sólo de esta manera creemos que la solución que se proponga para resolver el problema del acceso al Puerto de Topolobampo puede resultar adecuada y asegurar un funcionamiento eficiente del puerto.

CHAPTER 39

TOPOLOBAMPO
IDEAS PARA UN ANTEPROYECTO DE MEJORAMIENTO

Ing. Civ. Fernando Dublan
Presidente del Consejo Tecnico
Consultivo de la Direccion General
de Obras Maritimas de la Secretaria de Marina

RESUMEN

Situado en la costa del Estado de Sinaloa de la República Mexicana, es uno de los puertos del Golfo de California o Mar Bermejo. Sus coordenadas - geográficas son: 25° - 36' - 01" latitud norte y 109° - 02' - 52" longitud oeste.

Sus instalaciones portuarias interiores son escasas y deficientes, porque las limitaciones que la barra impone a la navegación de altura, no justifican hoy día obras de mayor magnitud a las actuales, sino hasta que resuelto convenientemente el acceso para barcos hasta de 11 m. de calad deba contarse con muelles e instalaciones apropiadas.

Está ampliamente comunicado con el centro, este y norte del país y con Estados Unidos de Norteamérica, tanto por ferrocarril como por carretera y por aire, además de que por agua sostiene comunicación marítima.

Su prometedor hinterland, el reciente ferrocarril Chihuahua-Pacífico y otros factores favorables, conducirán necesariamente a hacer de Topolobampo un puerto moderno, bien planeado y suficientemente capaz en sus servicios marítimos, realizaciones éstas que está reclamando un potenci futuro próximo.

Esperanzado en estos hechos, me uno a los buenos propósitos de los ingenieros portuarios mexicanos, para contribuir con mi ponencia, a fijar ideas respecto a la solución de Topolobampo como puerto de primer categoría.

CHAPTER 40

PHENOMENA AFFECTING IMPROVEMENT OF THE LOWER COLUMBIA ESTUARY AND ENTRANCE

John B. Lockett
Chief, Special Projects Investigation Section
U. S. Army Engineer Division, North Pacific
Portland, Oregon

This paper describes work undertaken to improve the lower Columbia Estuary and Entrance for navigation and discusses past concepts of phenomena controlling the regimen of this area as related to these improvements. Recent advances in technology have given birth to a new concept of tidal hydraulic phenomena which emphasizes the relation of salinity intrusion and littoral movement to the degree of shoaling experienced in estuarine areas. The findings of prototype measurements undertaken in 1959 along the lower Columbia, and other endeavors to expand the knowledge of controlling phenomena, including statistical wave studies, analyses of offshore changes, studies of attrition and accretion of adjacent shorelines, and comprehensive investigations of the distribution of Columbia River sediments are reviewed in the light of this new concept. Authorization, construction and verification of the comprehensive lower Columbia Estuary hydraulic model are discussed, as well as tests proposed for identification of controlling phenomena and for development of the most effective and economical plan of improvement. Finally, the paper summarizes the extent of present knowledge and outlines considerations for the future under conditions of controlled upland discharge resulting from contemplated headwater reservoir operation.

INTRODUCTION

THE RIVER

Physical Characteristics - Columbia River rises in Columbia Lake, British Columbia, Canada, and flows in a circuitous course for 462 miles to cross the International Boundary, from where it flows generally southward 435 miles across the State of Washington to the Washington-Oregon State line, thence generally westward for 310 miles through the Cascade and Coast Ranges to empty into the Pacific Ocean near Astoria, Oregon, as shown on Figure 1. The river and its tributaries drain an area of 259,000 square miles, consisting

of rugged mountain ranges separated by valley troughs, trenches, and plateaus, of which 39,500 square miles lie in Canada. Elevations in the basin range up to nearly 14,000 feet above sea level in the Rocky Mountain system on the east. The total fall of the Columbia River from its source to the Pacific Ocean is 2,652 feet.

Run-off - The normal annual run-off of the Columbia River is 180,100,000 acre-feet and the discharge pattern of the lower river is quite regular with low flows occurring from September through March and high flows from April through August. At The Dalles, Oregon, 192 miles above the entrance, the mean annual run-off is 133,700,000 acre-feet and extremes in mean daily discharge at this point have ranged from 36,000 cfs to 1,240,000 cfs.

Role in Economic Development - Water resource development has been of basic significance in the economic evolution of the Pacific Northwest which has in recent years emerged from an almost complete dependency on its basic resources of agriculture and timber to diversification and broadening of economic activities by production of more and more finished products. Water transportation by inland rivers, the Pacific Ocean, and the Puget Sound area has played a major role in the economic expansion of this great region. With suitable harbors that are strategically located, a flourishing trade has developed with Alaska, Canada, the Far East, California and the East Coast of the United States. The Columbia River, the most important inland waterway, provides a route for ocean-going traffic from its mouth to Vancouver, Washington, and, through the connecting Willamette River, to Portland, Oregon. Improvements are being undertaken to extend deep-water navigation with authorized channel depth of 27 feet to The Dalles. Barge traffic extends up the Columbia to Pasco, Washington, by a combination of open-river regulation and slackwater navigation provided by Bonneville, The Dalles, John Day, and McNary Dams. With completion of four authorized dams on the Lower Snake River, slackwater navigation for barge traffic will then extend to Lewiston, Idaho. Progressive improvement of the Columbia River has been accompanied by significant increases in ocean-going commerce as shown by traffic trends of major commodity groups in the following tabulation:

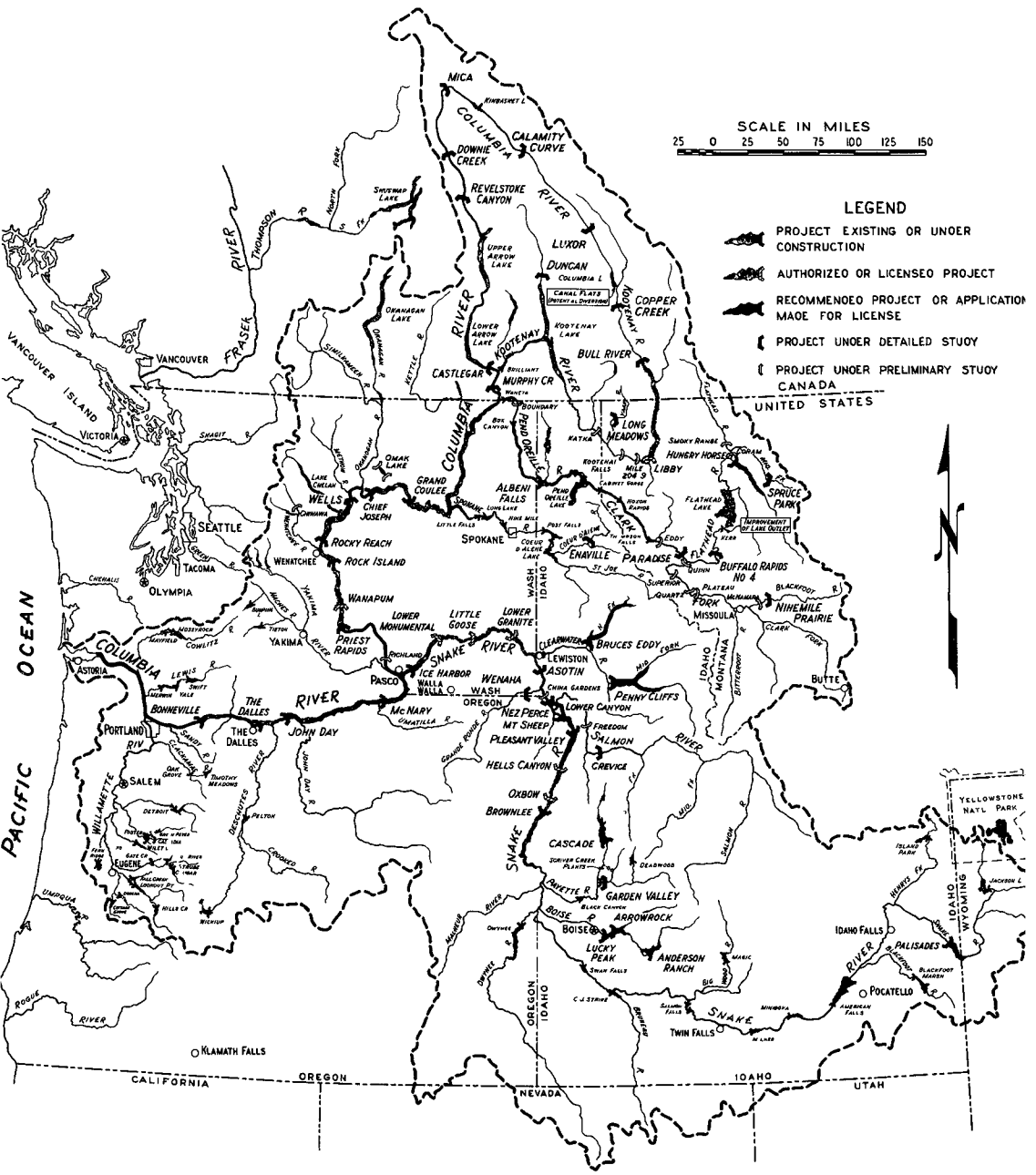

FIGURE 1. COLUMBIA RIVER BASIN

	OCEAN-BORNE COMMERCE (Thousands of Tons)				
	1925	1940	1950	1955	1960
Agricultural Products	733	812	695	1,153	4,417
Animal Products	41	49	61	20	69
Minerals	31	86	323	71	989
Forest Products	1,998	1,962	1,372	1,775	1,041
Petroleum Products	1,720	3,050	5,971	7,090	5,551
Miscellaneous	713	965	792	820	426
Total	5,236	6,924	9,214	10,929	12,493

THE LOWER ESTUARY

Extent - The Columbia Estuary proper, as affected by tidal variations, extends during periods of low river flows up to Bonneville Dam, on the Columbia River, 140 miles above the entrance, and to Willamette Falls at Oregon City, on the Willamette River. At higher river stages the sections of the river thus affected by tidal conditions progressively move downstream. The reach below Oak Point, Washington (River Mile 52), shown on Figure 2, forms the lower Columbia Estuary and tidal conditions in this section generally have more effect on stages than river flows. In this reach the main river channel traverses a meandering course between generally widening bank lines, past many low islands and shoals to eventually join the Pacific Ocean between the rugged headlands of Cape Disappointment on the north and the low-lying Point Adams on the south.

Tidal Influence - Normally reversals of current direction occur throughout the lower Columbia Estuary as the result of tidal fluctuations of the Pacific Ocean. At Fort Stevens, River Mile 8, the average daily tidal variation is about 8 feet. The lowest tide observed at this point was estimated to be 3.0 feet below mean lower low water and the highest stage, which resulted from a combination of storm activity and tidal action, was 11.6 feet above mean lower low water. The tidal prism of the Columbia Estuary has been estimated at 732 square-mile feet.

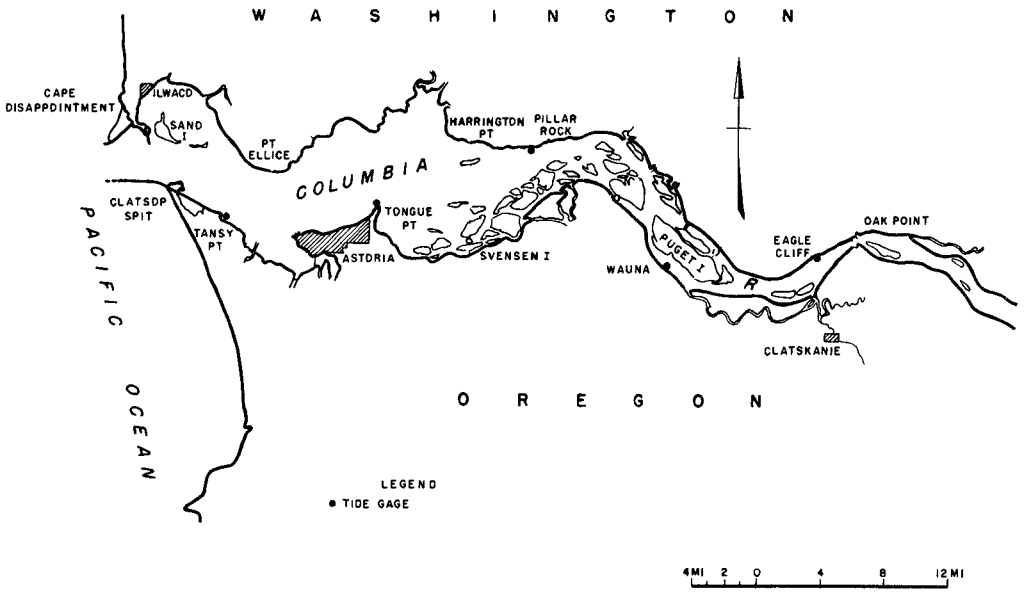

Fig. 2. Lower Columbia estuary.

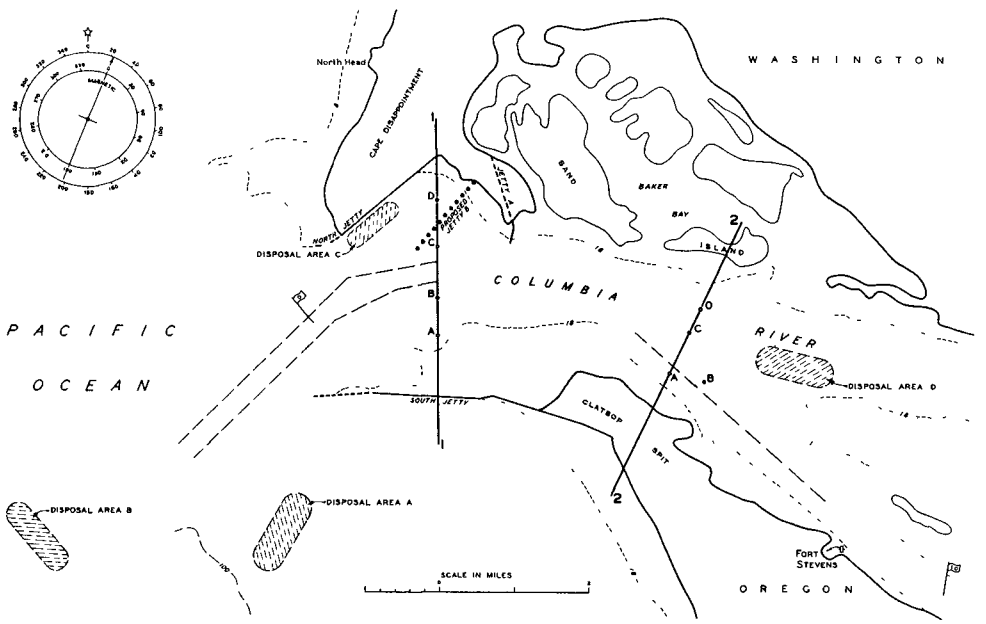

Fig. 3. Columbia entrance.

THE ENTRANCE

General - Perhaps the most consistent characteristic of the Columbia Entrance, Figure 3, is its continually changing regimen which strives to create a balance between the forces of the ocean and those of the river. This balance is quite delicate as any modification of the river forces in the entrance area, no matter how minor, is accompanied by a corresponding change in ocean forces and, as a consequence, throughout the period of man's endeavor to improve conditions for navigation the entrance has undergone many changes and has assumed many different complexions.

Tides - Tides at the Columbia River Entrance have the diurnal inequality typical of the Pacific Coast with a long run-out from higher high to lower low water. The mean range is 6.5 feet, the range from mean lower low water to mean higher high water is 8.5 feet, and extreme tides range from minus 2.6 feet to plus 11.6 feet, mean lower low water.

Winds and Storms - Two seasons having wide variance in wind and sea conditions generally occur each year at the entrance. The season of severe storms usually extends from October to April and storm winds, beginning generally in the south quadrant, gradually veer to the southwest and finally blow themselves out as they move around to the west or northwest. Storms are often continuous for several days and are accompanied by extremely heavy seas mostly from the southwest During the summer season, the conditions of wind and sea are much less severe than those of the winter season. From May through September, winds from the north or northeast begin in the morning, increase in force during the day, and diminish at night. Occasionally during the winter and spring there are several days when an easterly wind predominates and the weather is cold.

HISTORY

PRIOR TO IMPROVEMENT

A chart, Figure 4, made under direction of Admiral Vancouver clearly indicated the existence in 1792 of a single channel at the Columbia entrance with a depth of 4-1/2 fathoms between Cape Disappointment and Point Adams. In 1839 Sir Edward Belcher revealed the existence of two channels at the entrance separated by a large shoal area which forced the deeper channel northward against Cape

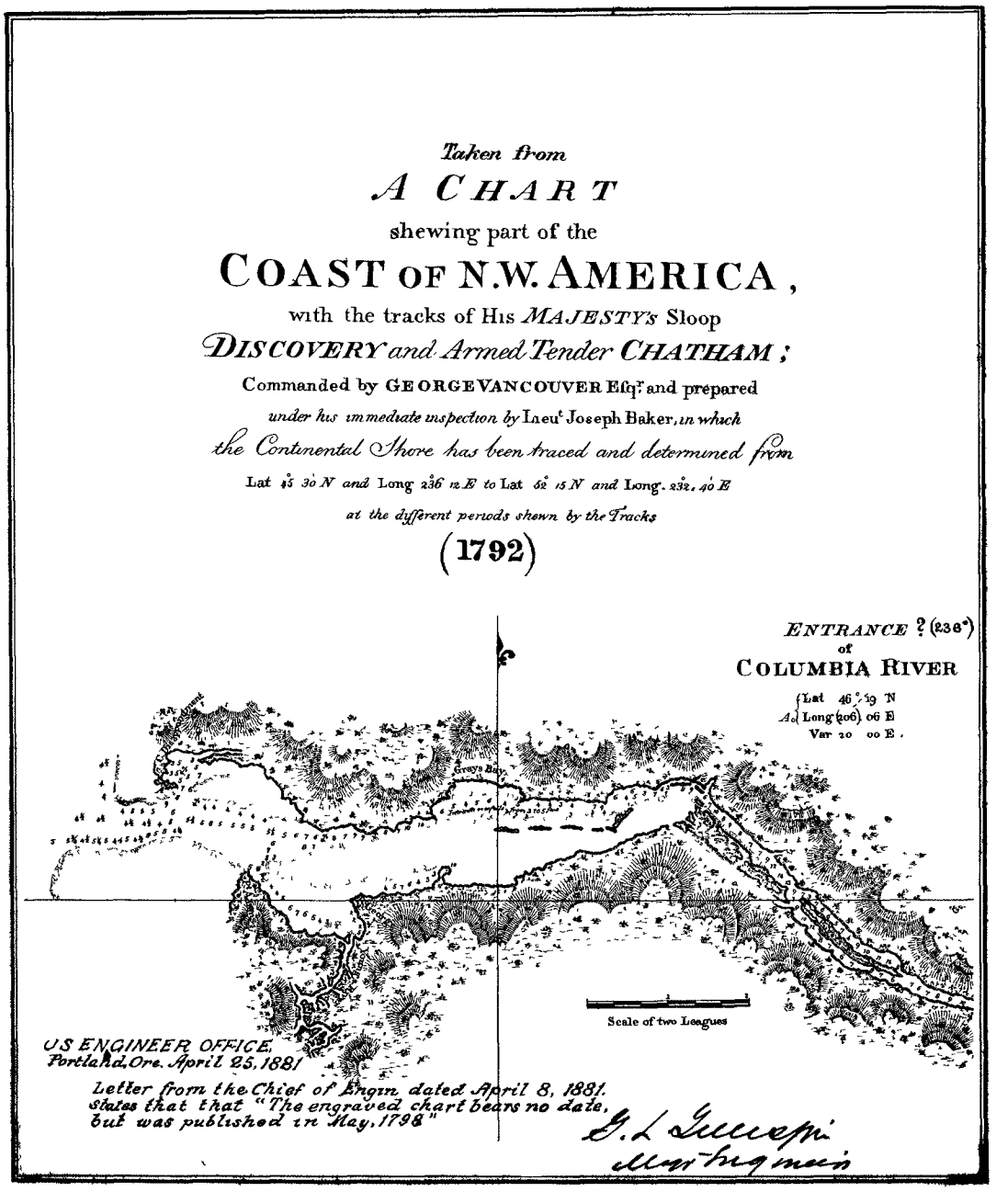

FIGURE 4. CHART BY ADMIRAL VANCOUVER

Disappointment to turn sharply southward and join a generally shallower channel along Point Adams, as shown in Figure 5. This shoal area, called the Middle Sands, grew in size until its 18-foot contour in 1874 embraced a very large area seaward and south of Cape Disappointment and covered almost all of the area now occupied by the present entrance. A portion of the Middle Sands formed an island inside the entrance which later separated from the main shoal area and, migrating to the north to form Sand Island, restored a single channel to the entrance in 1885. At that time the main portion of the Middle Sands had moved westward to create a westward extension of Cape Disappointment and minimum depths of 20 feet prevailed on the ocean bar as shown in Figure 6.

30-FOOT ENTRANCE PROJECT

Early attempts to improve the entrance, prior to the adoption by Congress in 1882 of the initial permanent navigation project, consisted of sporadic dredging in combination with the construction of temporary training structures. It was soon realized even in those early days that such limited work could not be effective in controlling, or even influencing to any appreciable degree, the outsized forces at work in the entrance and that improvement of more permanent character would be required. The first project was adopted on August 2, 1882, pursuant to the recommendations of the Board of Engineers for the Permanent Improvement of the Mouth of the Columbia River[1]. This project provided for the construction of a South Jetty, 4-1/2 miles in length, lying in a generally northwesterly direction from its base at Point Adams to secure a depth of 30 feet over the entrance bar. Construction of the rubble-mound structure was initiated in April 1885 and completed, with four groins along its northerly side, in October 1895. The crest of the completed jetty sloped from 12 feet above mean lower low water at its shore end to plus 10 feet at a point 1-1/8 miles from the shore, thence to plus 4 feet at its outer end. A total of 946,000 tons of stone were placed in the structure at a total cost of $1,969,000. Although shoals marking the beginning of Clatsop Spit began to form along the north side of the jetty during its construction, a general improvement of depths over the bar was soon evident. By 1895 depths of 31 feet were available on an alignment which, under the influence of the jetty, had migrated to the north about three miles. These favorable conditions were only temporary, however, as the continued northward migration of the channel by 1898 reduced depths to 29 feet and by 1901 caused further

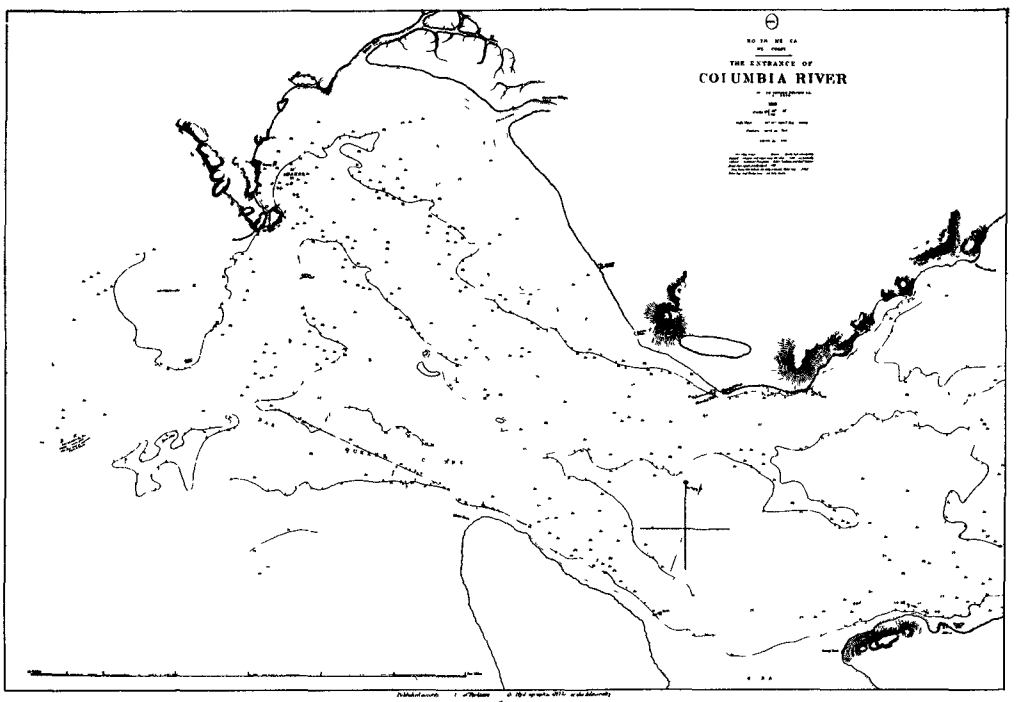

Fig. 5. Chart by Sir Edward Belcher.

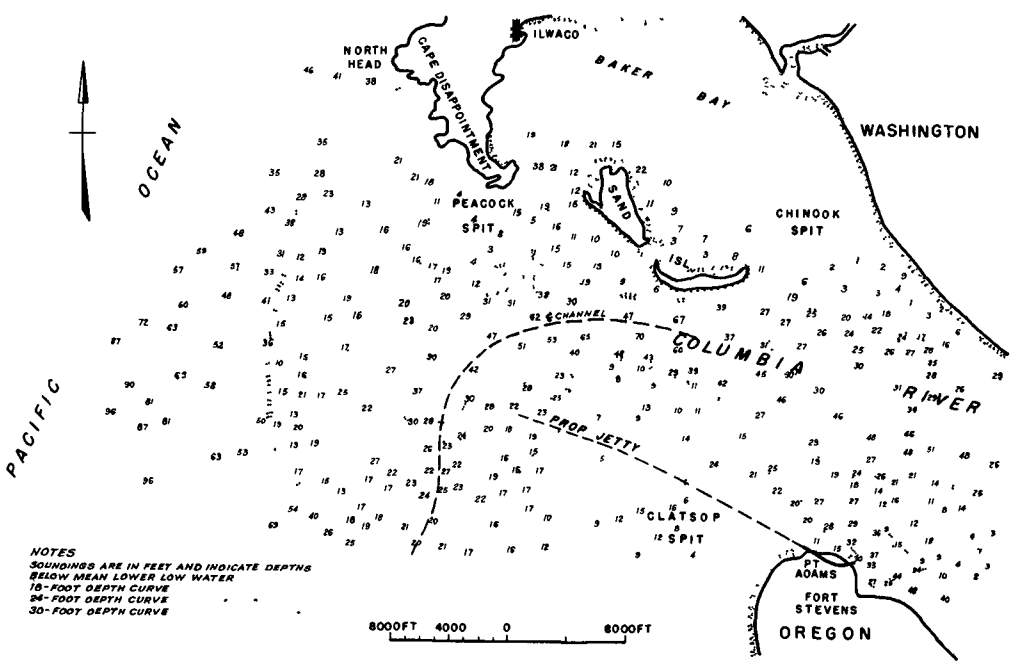

Fig. 6. Columbia entrance - 1885.

deterioriation of the entrance channel until in 1902, as shown in Figure 7, there existed three entrance channels, each only about 22 feet deep. In the meantime Clatsop Spit had grown to form a hook-shaped island through the South Jetty at its mid-length which later extended to create a solid land connection with Point Adams.

40-FOOT ENTRANCE PROJECT

Construction Phase - In view of these deteriorating conditions and the need for increased entrance depths to furnish a margin of safety to navigation Congress, in the River and Harbor Act of March 3, 1905, adopted the recommendations of the Board of Engineers on Project for Improvement of the Mouth of Columbia River[2] which provided for extension of the existing South Jetty, construction of a North Jetty and groins, in combination with dredging, to secure an entrance channel one-half mile wide and 40 feet deep. As the South Jetty was being extended seaward, a single entrance was restored and by 1911 a depth of 24 feet was again available across the ocean bar. As completed to a total length of 6.6 miles in August 1913, the South Jetty had an average top width of 25 feet and an elevation of plus 10 feet from the shore to the "knuckle" end of the original project, from whence the height was increased by stages to an elevation of plus 24 feet at the outer end. Construction of the North Jetty began in 1913 and by the next year, when only about 1 mile in length, entrance depths had increased to 30 feet. As constructed the North Jetty had a top width of 25 feet, sideslopes of 1 on 1-1/2, and crest elevation of 28 to 32 feet above mean lower low water. Completion of the jetty to its full length of 2.4 miles in August 1917 was accompanied by further improvement of entrance depths to 40 feet through a narrow bar channel. In addition to 410,000 tons of stone used for rebuilding the outer end of the original South Jetty, a total of 4,427,000 tons of stone was placed in the extension of the South Jetty, at a total cost of $5,657,000. Nearly 3 million tons of stone were used in the construction of the North Jetty at a cost of $4,319,000.

Adjustment Phase - Completion of the North Jetty, with its positive control on flows, marked the beginning of the achievement of the long-sought goal of securing dependable depths through the entrance for navigation. By 1920 the 40-foot depth contours had retreated considerably providing an entrance channel about one mile wide and, during the next five years, further deepening occurred to make a mini-

mum entrance depth of 45 feet available in 1925. By 1927 minimum depths of 47 feet were available over the bar as shown in Figure 8. It is interesting to note that for the first time depths in excess of 40 feet then prevailed along the channel side of the North Jetty. However, concurrently with improvement of navigation conditions, shoals developed immediately north of the North Jetty and formed a solid land mass extending almost to its full length. Clatsop Spit continued to grow until by 1931 its westward and northward extension had reduced entrance depths to about 43 feet.

Refinement Phase - Rehabilitation of the South Jetty was begun in 1931 and completed in 1936. Later in 1936 the outer 500 feet of the structure was impregnated with a hot asphaltic mix in an attempt to prevent disintegration at this point by heavy seas. This expedient did not prove successful and a solid concrete terminal was constructed at the outer end in 1941. Further growth of Clatsop Spit was accompanied by movement of the navigation channel closer to the North Jetty and by development of increased depths along the channel side of the outer end of that structure. In an effort to prevent the continued movement of the channel to the north, four permeable dikes were constructed along the south shore of Sand Island and Jetty "A", extending southward from Cape Disappointment, was completed in 1939. In spite of this, the continued westward movement of Clatsop Spit was accompanied by removal of more and more of the shoal area protecting the North Jetty and some damage was caused by undercutting along the channel face of the structure. In 1939 the North Jetty was rehabilitated and a concrete terminal block placed at its outer end. Continued advance of the Spit through 1951 coincided with definite movement of the 40-foot depth contour along the north side of the entrance channel to the east and south and in 1952, for the first time, an inner bar in extension of Clatsop Spit had formed between the jetties. Reconstruction of the South Jetty involved the placement of 4,288,000 tons of stone in the superstructure at a cost of $4,930,000. Rehabilitation of the North Jetty required the placement of 244,000 tons of stone and 234,000 tons of stone were used in the construction of Jetty "A", all at a total cost of $1,271,000.

Dredging - As ample depths prevailed over the ocean bar, dredging under the 40-foot entrance project was confined to the face of Clatsop Spit. Amounts dredged since 1939 under that project were as follows:

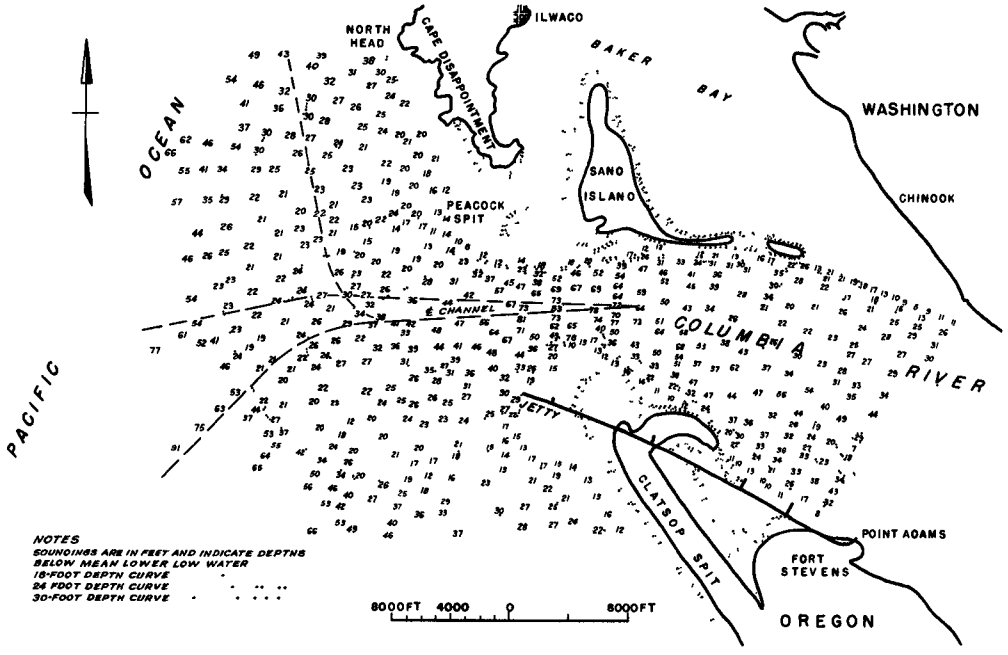

Fig. 7. Columbia entrance - 1902.

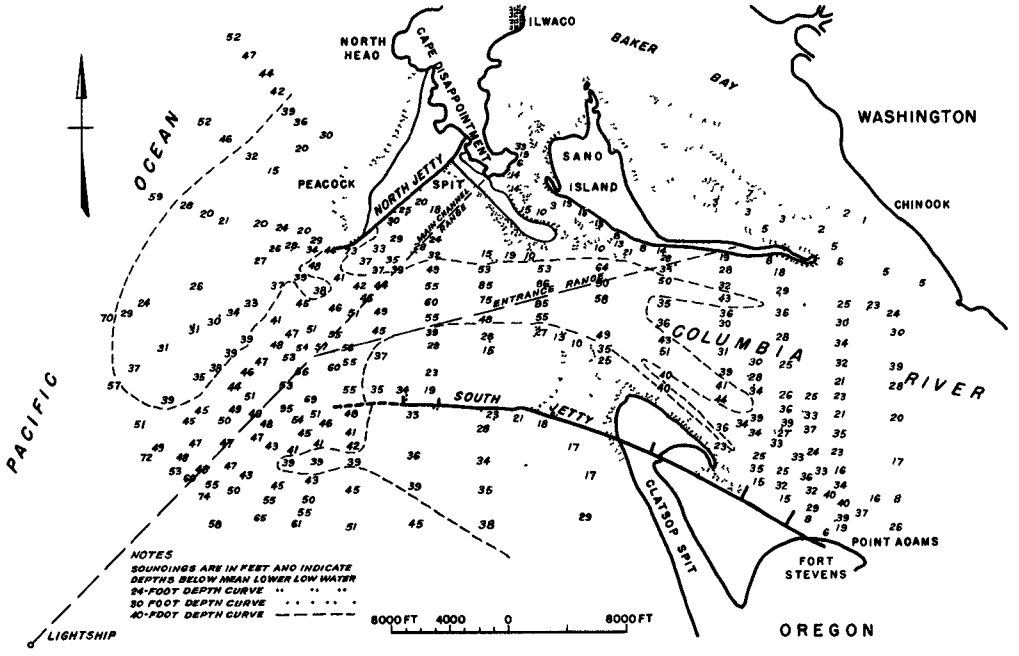

Fig. 8. Columbia entrance - 1927.

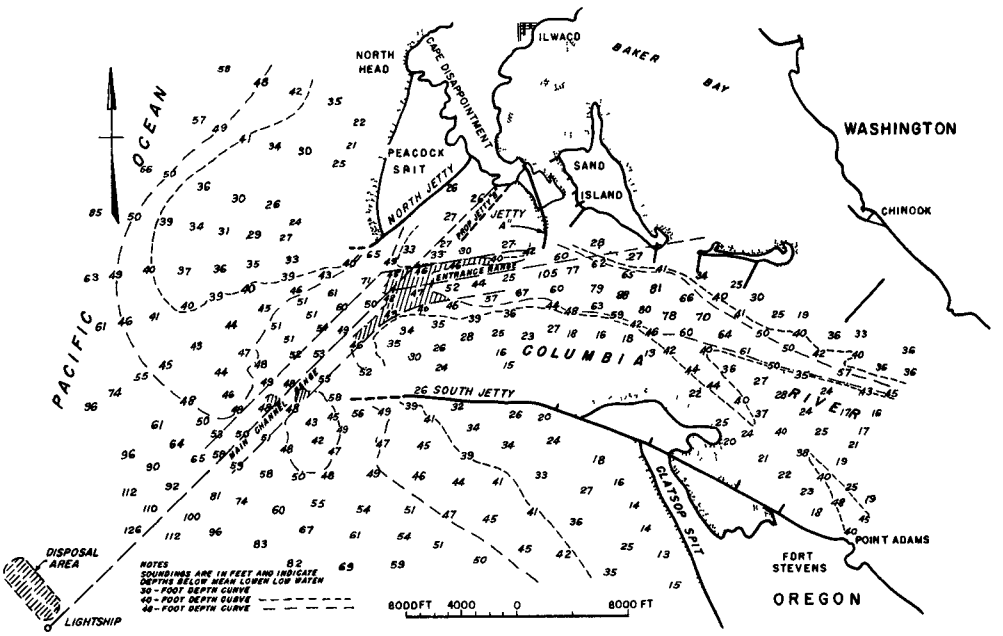

Fig. 9. Columbia entrance - 1962.

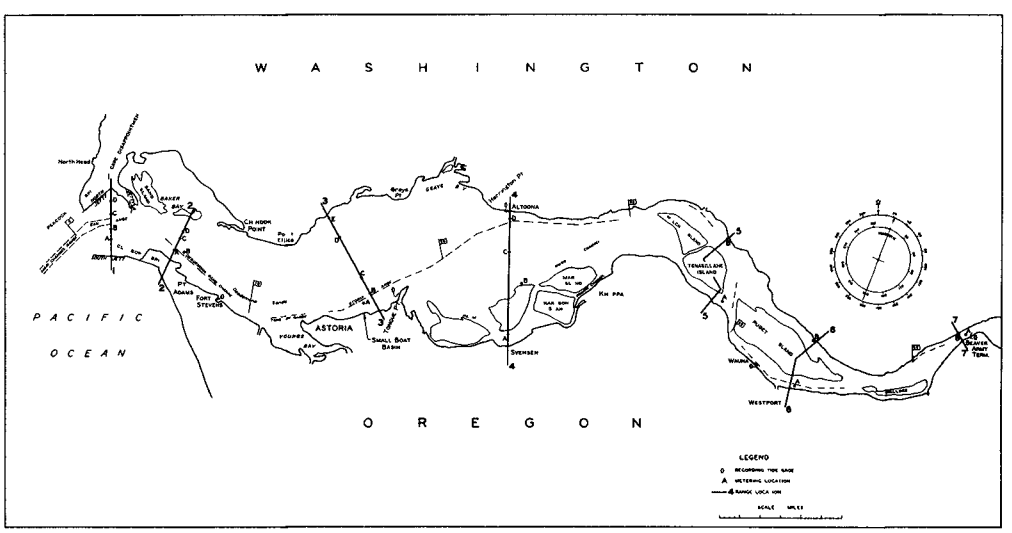

Fig. 10. Prototype measurement ranges and stations.

FISCAL YEAR	AMOUNT DREDGED CUBIC YARDS	FISCAL YEAR	AMOUNT DREDGED CUBIC YARDS
1939	501,300	1949	1,023,800
1940	1,319,800	1950	923,200
1941-44	None	1951	1,000,300
1945	393,100	1952	1,267,400
1946	186,900	1953	2,796,800
1947	483,000	1954	2,141,700
1948	1,030,200	1955	1,749,300

The full project width was obtained only during the last three fiscal years listed above.

48-FOOT ENTRANCE PROJECT

Project Progress - To meet the needs of modern ocean navigation Congress, in 1954, modified the entrance project to provide for minimum depths of 48 feet throughout the half-mile channel width to be secured initially by dredging and subsequently, if experience so warranted, by construction of spur Jetty "B" along the north shore, shown on Figure 9, which also shows conditions prevailing in 1962. Dredges were successful in 1956, the initial year of dredging on the modified project, in securing by the end of the season in October depths of 48 feet over the full channel width, in spite of heavy amounts of erratic shoaling and scouring which accompanied the dredging operations. Extremely heavy shoaling of the newly dredged channel during the following winter months, together with lack of sufficient dredging plant, resulted in the decision to concentrate the 1957 dredging effort to securing project depths throughout a channel of only 1,500-foot width. Dredging in 1957 was also accompanied by erratic shoaling and scouring over the 1,500-foot channel and was similarly followed by proportionately heavy shoaling during the ensuing winter season. Approximately 75% of the material dredged in 1956 and 1957 was disposed in an offshore area approximately one mile south of the extreme end of the South Jetty (Area A), as shown on Figure 3, with the balance disposed in deep water along the entrance range (Area B), adjacent to the inside of the North Jetty (Area C), and upriver in the vicinity of Chinook Point (Area D). Quantities dredged during these and subsequent years and the amounts of total apparent shoaling and scouring noted within the authorized channel width by frequent condition surveys are given in the following tabulation:

CALENDAR YEAR	QUANTITY DREDGED, 1,000 C.Y.	AMOUNT SHOALING 1,000 C.Y.	AMOUNT SCOURING 1,000 C.Y.	NET SHOAL 1,000 C.Y.	NET SCOUR 1,000 C.Y.
		1956 and 1957			
1956	14,436	8,492	6,263	2,229	---
1957	3,909	7,279	7,436	---	157
Total	18,345	15,771	13,699	2,229	157
		1958 through 1961			
1958	2,603	3,216	5,942	---	2,726
1959	2,289	6,146	3,361	2,785	---
1960	2,286	5,008	4,048	960	---
1961	2,054	3,559	3,007	552	---
Total	9,232	17,929	16,358	4,297	2,726

Modification of Spoil Disposal Areas - Tests of pilot equipment designed to measure subsurface current directions and velocities, conducted early in 1958 in preparation for the general prototype measurement program of the following year, revealed the fact that spoil disposed in Areas A and C returned to the dredged entrance channel. As a consequence, disposal practices were subsequently modified so as to concentrate disposal of dredged materials in deeper water offshore (Area B) and to eliminate as much as possible the disposal of these materials south of the South Jetty and near the North Jetty. Although since that date shoaling and scouring has generally followed the previously noted pattern, the magnitude of such occurrences has been reduced somewhat from that experienced in previous years as shown above.

Rehabilitation of Entrance Structures - Rehabilitation of Jetty "A" in 1961 involved the placement of about 214,000 tons of stone at a cost of about $814,000. In that same year, 213,460 tons of stone were used in rehabilitation of the upper portion of the South Jetty between the land connection with Point Adams and the "knuckle" at a cost of $2,328,000. Rehabilitation of the South Jetty seaward of the "knuckle" involving the placement of 268,000 tons of stone is scheduled for completion in 1963.

PAST CONCEPTS OF CONTROLLING PHENOMENA

APPROACH TO PAST CONCEPTS

Any discussion of past concepts of phenomena controlling the regimen of the lower Columbia Estuary and Entrance as related to the constructed improvements should, of course, recognize the state of knowledge prevailing at that time. Engineers had little but readily observable conditions and apparent reactions of surface currents to obstacles to guide their thinking, planning, and design, of improvements, since estuarine instrumentation as it is known today did not then exist. Hence it is small wonder that some works constructed under these circumstances failed to yield the desired results. The surprising thing is that many of these works did somehow accomplish their mission, perhaps not in the exact manner predicted, and have nevertheless survived to this day as monuments to the integrity and ingenuity of their planners. Accordingly, as we review these past accomplishments in the light of present knowledge, engineers of today should feel quite grateful and, indeed humble, for the advancement in technology which alone is responsible for their more enlightened position.

PAST EXPERIENCE

With little to guide their efforts other than the observed conditions in the natural estuary and entrance, it was apparent to engineers charged with planning the Columbia Entrance structures that in order to provide a dependable channel, the waters of the entrance area should be confined to an area smaller than then existed in nature. To effect such an accomplishment a South Jetty was constructed with its base at Point Adams which, while temporarily improving entrance conditions during the subsequent period of estuarine adjustment, did not fulfill the needs of then-existing navigation as depths over the ocean bar had not been permanently improved by this expedient. In view of this engineers then studied the bankline geography of the lower estuary and concluded that further confinement of entrance flows should be effected by opposing jetties spaced about two miles apart at their ends, roughly the minimum distance between banklines in the lower estuary[2]. Accordingly, the South Jetty was extended and a North Jetty constructed. Although some improvement was effected by the extension of the South Jetty, this betterment of conditions was relatively minor and of a tentative nature only. It was not until the North Jetty had

been constructed that a truly dependable channel was made available in the Columbia River entrance. Although ever-changing controlling depths over the entrance bar were achieved in different phases of estuarine adjustment following the completion of the North Jetty, these depths were much greater than those which previously existed. As a result, by confinement of entrance flows to a relatively smaller area, engineers achieved a "breakthrough" in their efforts to control depths over the entrance bar.

PAST CONCEPT AS DEVELOPED BY EXPERIENCE

Thus the success gained by confinement of entrance flows supported the conclusion that in order to achieve greater entrance depths it was only necessary to confine flows to the extent required. Although recognizing that there existed a number of observed phenomena such as formation of shoals in unexpected places, which somehow did not conform to this concept, these engineers were primarily concerned, and justifiably so, with net results as measured by past accomplishments. As a consequence, the theory of confinement of flow was accepted by these engineers as a basic principle in the planning, design and construction of estuarine improvements.

1932 Current Measurements - Notwithstanding the apparent validity of the theory of flow confinement there prevailed some question whether this theory properly integrated all factors and forces in estuarine areas. Consequently in 1932 the Corps of Engineers[3] undertook a program of prototype measurements at five stations across a range located some 5 miles above the ends of the jetties. Over 5,600 individual current meter observations were made at several depth levels at these stations during three different stages of upland discharge. Although no instruments were specifically employed for the purpose of determining sub-surface current directions, the measurements taken were interpreted to indicate that mean ebb tide velocities were greater than flood tide velocities for all stages of the upper river and, during freshet stages, were much stronger. Also at high river stages, ebb bottom velocities were much higher than flood bottom velocities for all percentages of time. At intermediate river stages bottom velocities were lower than at high stage with ebb bottom velocities predominating for about half the measurements. At low river stages flood bottom velocities were generally predominate. Considering the magnitude of ebb bottom velocities as compared to flood bottom velocities and their assumed greater transporting

power, it appeared evident at that time that the ebb flow was sufficient to maintain a channel between the jetties of at least 40 feet deep at mean lower low water and that no further contraction of the entrance appeared necessary for satisfactory channel maintenance. Thus, the results of the 1932 current measurement program were interpreted as confirming the theory of flow confinement as applied to improvements in the Columbia Estuary and Entrance.

Jetty "A" - Notwithstanding the indication revealed by the 1932 current measurements that further contraction works would not be necessary to secure project depths, Clatsop Spit continued to advance to the northwest, crowding the entrance channel against the North Jetty and reducing the available depths in a channel which was at that time assuming an undesirable alignment. To correct this condition Jetty "A" was constructed in 1938 and 1939 to further confine flows in the entrance area. Although Jetty "A" provides a degree of protection to vessels using the west Baker Bay channel against winter winds and waves, this structure, even in combination with the concurrently constructed Sand Island dikes, has had little beneficial influence on navigation depths or conditions through the lower Columbia Estuary or Entrance.

Jetty "B" - Although the failure of Jetty "A" to produce the desired channel control could not be explained at that time, the validity of the theory of flow confinement was still accepted, although to a somewhat lesser degree, by engineers as late as the early 1950's when planning for the 48-foot entrance channel was initiated. Accordingly, as part of the 48-foot project, Jetty "B", to be located between the North Jetty and Jetty "A", was recommended and authorized in 1954 as a structure to supplement and enhance the confining influence of Jetty "A", if initial operations to secure the 48-foot entrance channel proved impracticable. Subsequent events and almost explosive expansion of knowledge regarding estuarine phenomena have cast considerable doubt on the value of the proposed Jetty "B" as a regulating structure and, consequently, no further action has been undertaken by the Corps of Engineers leading toward its construction.

MODERN CONCEPTS OF CONTROLLING PHENOMENA

APPROACH TO MODERN CONCEPTS

Much credit should be given to the Corps of Engineers' Committee on Tidal Hydraulics and to the Waterways Experiment Station for their pioneering efforts and studies which have led to a broadening of engineering knowledge of character and

magnitude of forces controlling the regimens of estuaries and their entrances. Early hydraulic model studies at the Waterways Experiment Station included a model of the Savannah Estuary and Entrance (Georgia) and, as was the practice at that time, fresh water was employed throughout the model system. Considerable difficulty was initially experienced in attempting to verify current measurements made in the model with those observed in the prototype. All efforts to secure accurate verification of the model failed until someone suggested that salt be added to the ocean portion of the model in the amount necessary to simulate salinity conditions in the prototype ocean. When this was done, verification was a relatively easy task as the model, thus operated, completely and accurately reproduced observations of current direction and velocity noted in the prototype. This "breakthrough" in model techniques led to study and definition by many engineers and scientists of the important role that salinity intrusion plays in the development of forces controlling estuarine environment. These studies and companion investigations of related phenomena by others during the last 15 years have produced a new concept of estuarine phenomena which has given the waterways engineer a more complete and accurate understanding to the end that it is no longer necessary to resort to a trial and error approach to estuarine improvements. Although this new concept has completely revolutionized all past thinking and has given birth to the embryonic science of tidal hydraulics, investigations of all estuarine phenomena are being prosecuted at an ever-expanding rate under the favorable technological climate prevailing in the world today. Hence, new discoveries will be made and new techniques will be developed which will further assist the engineer of the future to solve estuarine problems more completely than is now possible.

SALINITY INTRUSION

Although of extreme importance in the development of the estuarine regimen, the role that salinity intrusion plays in this development has to date been only broadly defined. Schultz and Simmons[4] point out that engineers concerned with the solutions of problems in estuarine environments have become keenly aware in recent years that the amount of fresh water discharged into an estuary, and the degree to which it mixes therein with the salt water of the sea, are major factors in establishing the hydraulic and shoaling regimens of the estuary. The presence in estuaries of water of variable density causes marked differences in the magnitudes, distributions, and durations of the currents, as compared to those of

a single density system. As a result of the density difference between the heavier salt water at the seaward end of the estuary and the fresh water at the upstream end, each type of water tends to assume a rough wedge shape with the base of the wedge at the source. The interface of (or line of demarcation between) the salt and fresh water may vary from well defined to almost obscure, depending on the degree of mixing of the salt and fresh water in any given estuary. Where mixing is slight the transition from fresh to salt water is well defined and occurs within a small percentage of the channel depth. On the other hand, where the mixing is appreciable no definite interface of the salt and fresh water exists except in isolated instances. For convenience, the degree of mixing may be classed into three broad categories of highly stratified, partly mixed, and well mixed, with the transition from one type of mixing to another being gradual instead of well defined. The most significant effect of salinity intrusion, thus defined, is the creation of density currents in estuaries which cause the bottom flood currents to predominate over the bottom ebb currents by increasing the velocity and duration of the former and decreasing the velocity and duration of the latter. The resulting net upstream movement of bottom currents within the saline region of the estuary constitutes an effective trap for sediments on and near the bottom, preventing their movement to the sea and causing the bottom to be shoaled and unstable. From their studies Schultz and Simmons arrived at the following general conclusions:

a. The degree of mixing of salt and fresh water in estuaries plays an important role in the establishment of their hydraulic regimens. As the shoaling regimens of some estuaries are related directly to their hydraulic regimens, it follows that the degree of mixing also plays an important role in establishing their shoaling regimens.

b. Because of incomplete mixing of salt and fresh water in estuaries, the predominance of flow in the bottom strata is almost always upstream while that in the surface strata is downstream; the degree of such predominance is dependent on the degree of mixing, being most prominent in the highly stratified estuary and least prominent in the well-mixed type.

c. Changes in upland discharge, tidal prism, and physical configurations of estuaries will frequently change the degree of mixing of salt and fresh water therein and thus affect such important features as the vertical distribution

of current velocities, the direction and degree of flow predominance, the amount of shoaling, and the location of major shoal areas.

d. As lightweight sediments are supplied to estuaries principally through the medium of upland discharge, it follows that such discharge plays a dual role in estuarine sedimentation.

e. The magnitude of changes in upland discharge into estuaries usually far exceeds that of changes in tidal prism or physical configuration. For this reason, and because upland discharge is of primary importance, it follows that major changes in upland discharge should be accomplished only after consideration of all probable effects.

Continuing Research on Salinity Intrusion - An analytical investigation of salinity intrusion and related phenomena was initiated by the Committee on Tidal Hydraulics in January 1954. This general investigation was designed to determine for conditions of open channels subject to salt water intrusion and tidal oscillations from the sea the following four aspects of the phenomena: (a) The extent of salinity intrusion and the mean salinity distribution, (b) the vertical mixing of fresh and salt water and the resulting vertical salinity distribution, (c) the vertical distribution of current velocities as affected by salinity distribution, and (d) the movement and deposition of sediments as affected by density-current phenomena. On the basis of studies undertaken on phase (a) of this general investigation, Ippen and Harleman[5] indicate that it is possible to make quantitative predictions regarding salinity intrusions in partially or well-mixed estuaries of essentially uniform cross section without prior knowledge of any existing salinity conditions. Further, the factors which cause changes in salinity intrusions have, for the first time, been quantitatively evaluated. Thus by means of intrusion equations, the effect of changes in the fresh water discharge, channel depth, etc., can be predicted. Of even greater importance is the possibility that the diffusion and tidal parameters developed in this study will have important significance in understanding the intrusion mechanics of estuaries of non-uniform geometry. Analyses will be made of phases (b), (c), and (d) of this investigation in the light of findings of studies of phase (a) as may be applicable.

SHOALING PROCESSES

Much remains to be learned regarding the processes involved in the formation and stabilization of shoals in estuarine channels. In 1957 the Committee on Tidal Hydraulics launched a broad program of studies considered necessary to develop essential knowledge of these processes. The different phases of work contemplated under this program are summarized as follows:

Basic Laws for Movement and Deposition of Muddy Sediments - Since most estuarine shoals in the United States are composed of muds rather than sands a contract has been made with the University of California to study the rheological properties of consolidating sediments. Natural sediments from a number of estuaries are being furnished to the University as a basis for the studies.

Effects of Repetitive Scour and Deposition on Sedimentation - As it appears that successive scour and deposition of sediments may play an important role in shoaling processes, early flume tests to determine the significance of these factors are planned.

Techniques for Radioactive Tracing of Sediment Action - These techniques offer a great potential in the development of knowledge in shoaling processes, making it mandatory that their use be encouraged in connection with specific investigations and that consultation and advice be extended to those engaged in this work. Field tests planned by the District Engineers, Galveston and Norfolk, will be closely followed.

Development of In-Place Turbidity Meter - Because of the great areas embraced by most estuaries and the constantly changing conditions of tide and fresh-water inflow, it is apparent that complete and simultaneous coverage of such systems for measurements of suspended sediment concentrations, with only approximately accurate results, will yield much more valuable information than will long-term coverage and highly accurate results. Available evidence indicates that an instrument operating on the basis of light extinction as a measure of turbidity may fulfill these needs. Development of such an instrument is under way at Johns Hopkins University.

Flocculation - Flocculation of suspended and dissolved solids plays an important role in shoaling processes as sea water is an efficient flocculating agent, but little work of scientific value has yet been accomplished to evaluate its

significance. A comprehensive literature survey of this subject has been made and a report thereon completed. Recommendations for further work in this field are now under review and it is probable that further research will shortly be initiated.

Stabilization of Deposits - The physical and chemical changes which occur in sediments after deposition appear important to an over-all appraisal of the matter of shoaling processes. A literature survey of this subject has been completed and additional research is forthcoming.

Analysis and Correlation of Prototype Data - Proper analysis and correlation of existing prototype hydraulic, hydrographic, and other data will reveal certain relationships among estuaries which should lead to a better understanding of the over-all subject of shoaling processes. Data on important estuaries are now being assembled and analyzed and it is anticipated that direct comparisons and correlations should reveal definite characteristics.

Shoaling in Slips and Tributary Channels - It is anticipated that test facilities for general investigations of hydraulic and shoaling phenomena in slips and tributary channels will shortly be constructed as additions to existing hydraulic models at the Waterways Experiment Station and tests initiated to determine the factors involved.

Classification of Sediments - Proper classification of the sediments which contribute to shoaling of the different estuaries in the United States is of importance from the viewpoint of a comprehensive understanding of shoaling processes. This effort is being carried out concurrently with the analysis and correlation of prototype data previously described.

LITTORAL PROCESSES

Waves of all character and magnitude breaking on a coastline generate movements of beach materials in the alongshore component direction of the generating waves. These movements establish the littoral regime of the shoreline and the intensity of these movements determine the quantity of material or littoral drift moving past a point on the shoreline. As, during the course of an extended period of time, waves attack a shore generally from one predominant direction, so too will the littoral movements of material passing a point on that shore move in one predominant direction parallel to the coast.

Just as waves also attack this shore from other directions over an extended period of time, though less predominately from those directions, so too will there be littoral movements past the point which may be in a direction opposite that of the predominate littoral drift. Thus, from a point along a shoreline, such as the entrance to an estuary, the total quantity of littoral material in movement is the sum of all littoral movements in both the up-coast and down-coast directions. Both of these material movements contribute to shoaling in major estuarine entrances. They also affect the delicate balance between erosion and accretion of the shoreline. In instances where littoral drift is intercepted by coastal structures such as groins or jetties, the shore updrift of these structures will grow seaward to a point, fed by the cessation of the littoral movement, while the shore downdrift from the structures will recede, being starved by the intercepted littoral drift.

PROTOTYPE MEASUREMENT PROGRAM OF 1959

BACKGROUND

In view of difficulties experienced in maintenance of the 40-foot entrance project resulting from the continual encroachment of Clatsop Spit shoals on the adopted channel alignment, the problem at the Columbia River Entrance was reapproached in 1956 in the light of new concepts and expanding knowledge of tidal hydraulic phenomena concurrently with initiation of work on the newly authorized 48-foot entrance project. In making this new approach the advice and guidance of the Committee on Tidal Hydraulics formed the basis for an intensive investigation of several aspects of the problem. As the initial step in this investigation the Committee recommended that a program of prototype measurements of current velocity and direction, as well as salinity, be undertaken to broadly define the density current regime established by environmental river, ocean and hydrographic conditions prevailing in the lower estuary. With effects of density currents thus defined it was the view of the Committee that any additional structural measures designed to reduce shoaling in the entrance area, such as Jetty "B", could be properly analyzed and evaluated in a hydraulic model study.

GENERAL SCOPE OF PROGRAM

In order to achieve the above goal it was necessary that the program provide data sufficient to meet the design and

verification needs of a hydraulic model study. To this end the program required three cycles of measurements to obtain data for conditions of low, normal, and high river discharge, each cycle including observations of current direction and velocity for a continuous full tidal period of about 25 hours at 23 stations located along seven ranges across the lower 52 miles of the estuary, shown in Figure 10. At each station current velocity and direction measurements were taken at 30-minute intervals at the surface and near the bottom and at the intervening quarter-points of depth. Initially, simultaneous observations were made at one station on each range for a continuous period of about 25 hours to establish the relationship between the ranges. This was followed by simultaneous observations at all stations on each range until all observations had been obtained. Salinities and temperatures were also observed throughout the vertical at each station concurrently with the measurements of currents and directions. This program, due to its magnitude and the complexities involved in instrumentation, administration and operation, not to mention the trying conditions of weather and heavy seas, represented a monumental task. A total of approximately 26,000 observations were taken during the three cycles of measurements. However, in spite of the magnitude of work involved and the difficulties experienced, reliable measurements were secured.

PROGRAM INSTRUMENTATION

Velocity - Azimuth - Depth Assembly - Equipment being tested by the United State Geological Survey to measure tidal flow was used as a guide in the prototype measurement program for the development of an instrument designed to measure subsurface current velocity and direction, as well as depth of the instrument above the bottom. This instrument consisted of a transducer for a Raytheon Fathometer, mounted in the bottom of 140-pound streamline brass weight with fins, suspended on the bottom of a Price current meter hanger bar. Also mounted in the weight was a Magnesyn compass transmitter which monitored on a remote panel the direction in which the assembly was facing as deflected by the current. A seven-conductor, pancake swivel was mounted between the current meter hanger bar and the seven-conductor, 1/4" diameter, suspension cable. The assembly as finally developed and used in the program is shown in Figure 11.

Salinity - Temperature Assembly - Although consideration was given to the advisability of taking water samples at the five elevations of each station and determining salinity by

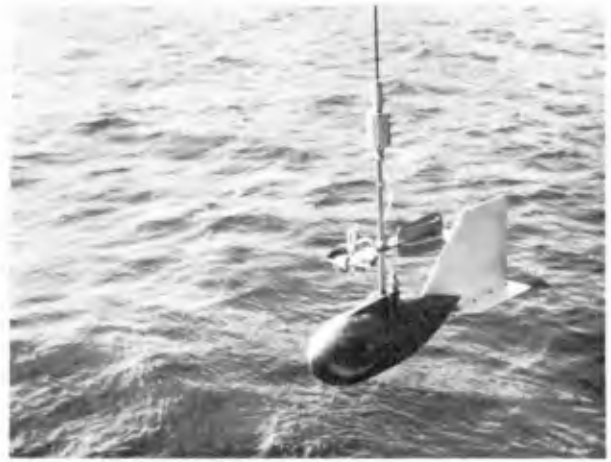

Fig. 11. Velocity - azimuth - depth assembly.

Fig. 12. Salinity - temperature assembly.

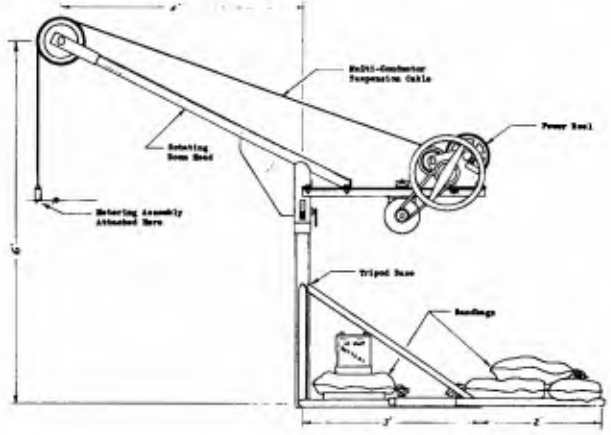

Fig. 13. Pillar crane.

laboratory tritration procedures, it was felt that, in the interest of reducing the workload, a less exact method of measuring salinity would suffice for the needs of the data collection and analysis program. It was also considered advisable to secure concurrent measurements of water temperature. To meet these requirements a conductivity cell with remote-reading resistance indicator was used to measure salinity and a temperature cell, together with wheatstone-balanced bridge, was used to obtain temperatures. The conductivity and temperature cells were mounted on a bracket above a 140-pound brass weight and short leads from the cells were connected to leads from the suspension cable inside a short stainless steel hanger that was clamped to the lower end of the suspension cable, as shown in Figure 12. The soldered connections were embedded in a hard, waterproof plastic filler. A seven-conductor suspension cable identical to that used for the velocity-azimuth-depth assembly was employed.

Pillar Crane - As the metering and salinity-temperature assemblies were to be used over the sides of small boats, a special crane was designed and fabricated to raise the bottom of the assembly weights 30 inches above the boat deck and far enough away from the side of the vessel so that the danger of striking the assembly instruments against the boat hull would be minimal. Pipe was used for the main structural members of the pillar crane shown in Figure 13.

Other Equipment - In addition to 12-volt batteries for each metering vessel, one complete set of current metering and salinity - temperature assemblies, and pillar crane were kept in readiness for use. Automatic tide gage recorders were maintained at strategic points in the lower estuary to record tidal stage variations during the data measurement periods.

PROGRAM ADMINISTRATION

General - Administrative tasks associated with the program included the procurement of necessary equipment, rental of vessels, training of equipment operators and coordination of program details with fishery and navigation interests.

Procurement of Equipment - Assemblies and pillar cranes previously described were obtained by contract with local manufacturers. Small items, including repair parts and flashing lights for buoys, as well as battery chargers, were

obtained by direct purchase. Storage batteries were rented for each of the measurement periods. All equipment was assembled at the Government Moorings in Portland prior to movement by truck to the small-boat basin at Astoria which served as the field headquarters for the program. Specifications were prepared to meet the particular requirements of the control boat, the master metering boat, and four metering boats. These vessels were hired through normal contractual procedures on an hourly rental basis.

Operator Training - Professional engineers and engineer technicians from the Engineering Division of Portland District were selected as equipment operators and indoctrinated by means of a special training program. Each operator was furnished a 20-page brochure describing the purpose of the prototype measurement program and related administrative and technical details, prior to a general orientation session to insure a thorough understanding by all of their specific duties. This was followed by a 4-hour session in which each operator was taught how to assemble, operate, and maintain each item of measuring equipment.

Coordination - Discussions were held with the United States Coast Guard to determine the type of buoy most desirable to mark the location of each measurement station in the lower estuary, and to insure the availability of such buoys and needed appurtenant equipment. At the request of the Columbia River Fisherman's Protective Association, arrangements were made to forego the use of buoys at Stations C and D on Range 2 to eliminate interference with fishermen's nets on established drifts and to remove and replace buoys at Stations D and E on Range 3 during and after the August fish runs. Some minor shifting of station locations in the back channels was made at the suggestions of tug and barge operators to avoid accidental removal of buoys by log tows. The Columbia River Bar Pilots Association was notified of proposed activities and the Coast Guard was furnished the latitude and longitude of each buoy for publishing in its notice to mariners well in advance of the placement of buoys.

PROGRAM OPERATION

Field operations, with the attendant requirement for extreme accuracy and timing of observations, occasionally in the face of adverse weather and wave conditions, represented the most difficult phase of the measurement program. Initial operations involved the placement of first class can buoys by the Coast Guard early in April 1959 to mark the location of the measurement stations.

Distribution of Vessels - Four equipment operators were assigned to each of the six vessels providing two 2-man operator crews for alternate 12-hour shifts throughout each 8-day measurement cycle. The control boat, the SUJAN, in addition to representing an immediate source of supply of spare equipment and the means for supervision and control of operations, was also used to ferry operator crews to and from shore bases established at Fort Stevens, Astoria, Svenson, Knappa, and Westport for the purpose of reducing the time required for changing shifts. Station A, Range 3, the master metering station, was occupied by the metering boat, CATANA, continuously throughout each 8-day measurement cycle. The four other metering boats, the MORNING STAR, ROSIE, MARY K, and MY BOAT, were phased among the remaining 22 stations to obtain combinations of 25-hour measurements at each station as shown in the following tabulation:

DISTRIBUTION OF METERING BOATS

25-HOUR METERING PERIOD	BOAT AND STATION OCCUPIED				
	CATANA	MORNING STAR	ROSIE	MY BOAT	MARY K
1	3-A	3-C	3-B	3-D	3-E
2	3-A	1-A	1-B	1-C	1-D
3	3-A	2-A	2-B	2-C	2-D
4	3-A	4-A	4-B	4-C	4-D
5	3-A	5-B	5-A	6-A	6-B
6	3-A	5-B	6-A	7-A	7-B
7	3-A	4-D	2-C	5-B	7-B

Observations - Measurements of current velocity and direction, salinity and temperature at five different levels were made every half hour at each station. These levels were located 3 feet below the water surface, 2 feet above the bottom, and at the intervening 1/4, 1/2, and 3/4 depth levels.

Cycles of Measurement - The initial cycle of measurement was undertaken from May 5 through May 13, 1959, a period of normal river flow, when the discharge ranged from 365,000 to 404,000 cfs in the lower estuary. The second cycle of measurement was accomplished between June 16 and June 24, 1959, a period of high river flow, when the discharge ranged between 532,000 and 577,000 cfs. The final cycle of measurement was made between September 15 and September 23, 1959, a period of low river flow, when the discharge ranged between 153,000 and 214,000 cfs.

ANALYSIS OF PROTOTYPE DATA

General - An office analysis of observed prototype data was undertaken by the District Engineer, Portland, and a record of all observations obtained and his analyses of these data are contained in a four-volume manuscript report [6] which provides the most complete source of observed data relating to the current, salinity and temperature regimes of the lower estuary and entrance. Due to weather and sea conditions, which precluded the undertaking of a program of measurements near the point where Clatsop Shoals encroach upon the entrance channel, all observations were made upstream from this problem area. While the measurement program did not reveal conditions prevailing in that area, it did show the vagaries of currents and other measured phenomena throughout other portions of the lower estuary and, thus, provided data for competent verification of a hydraulic model of the entrance and lower estuary. In such a model physical phenomena contributing to shoaling in the problem area are now in the process of being observed, understood, and analyzed to the extent feasible by tests of possible structural expedients.

Flow Predominance - In analyzing observations of current direction and velocity, plots similar to that shown in Figure 14 were prepared for each station. Changes in current

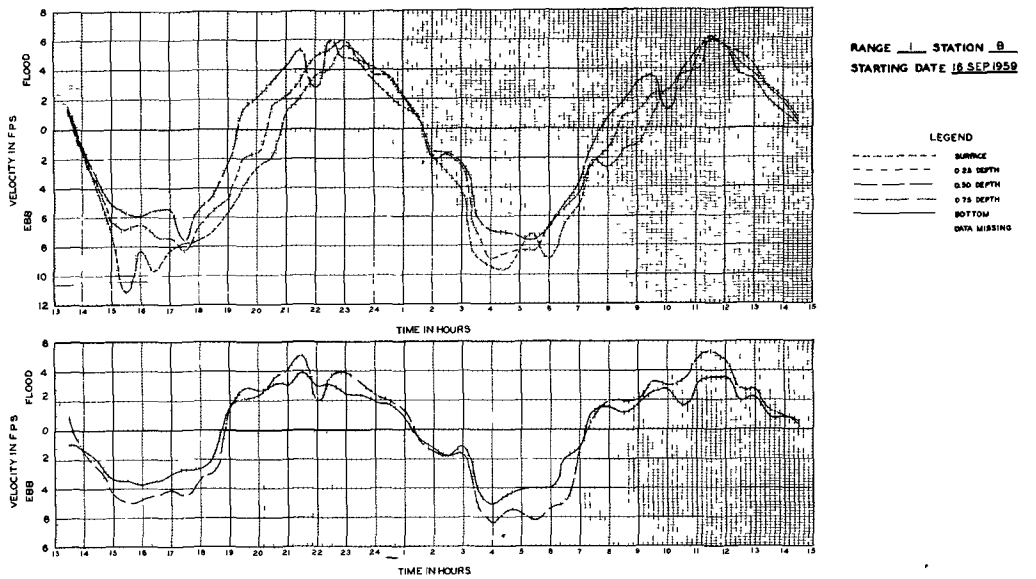

Fig. 14. Typical velocity - time - direction curve.

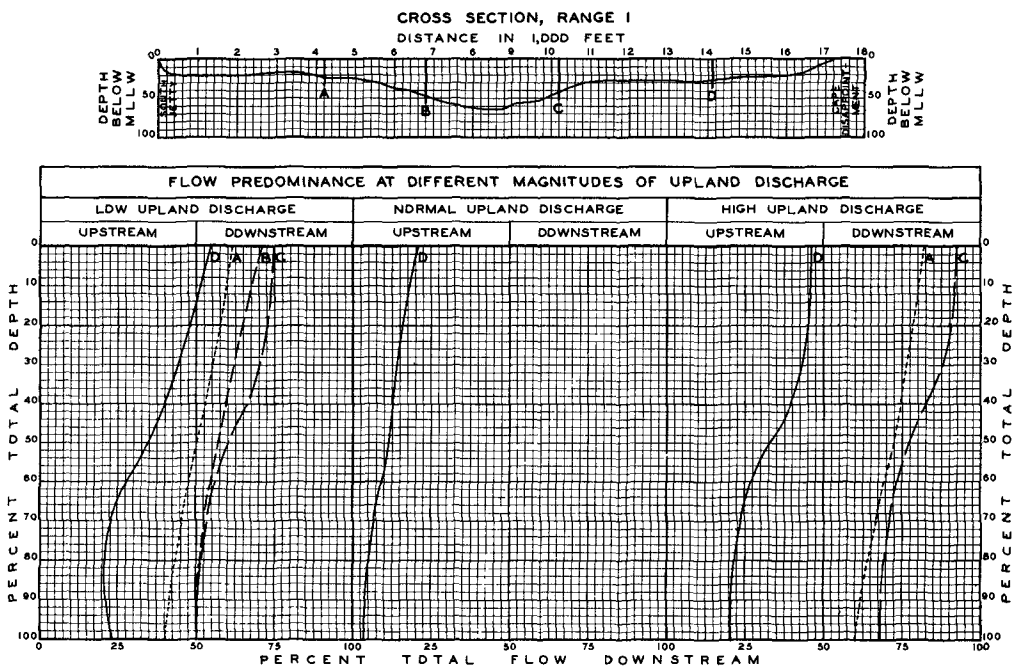

Fig. 15. Flow predominance - Range 1.

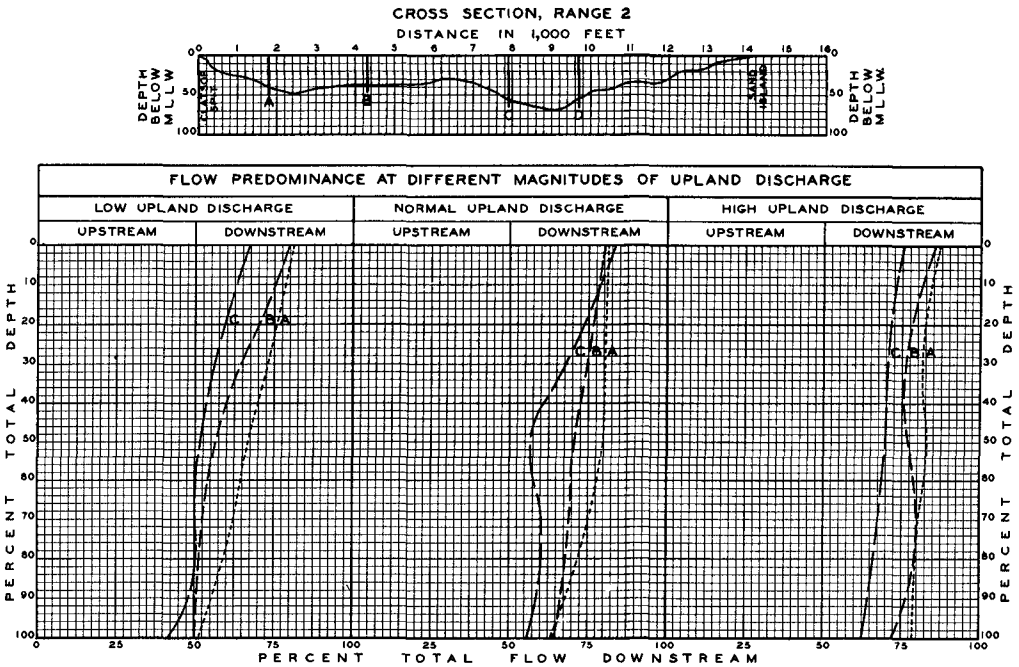

Fig. 16. Flow predominance - Range 2.

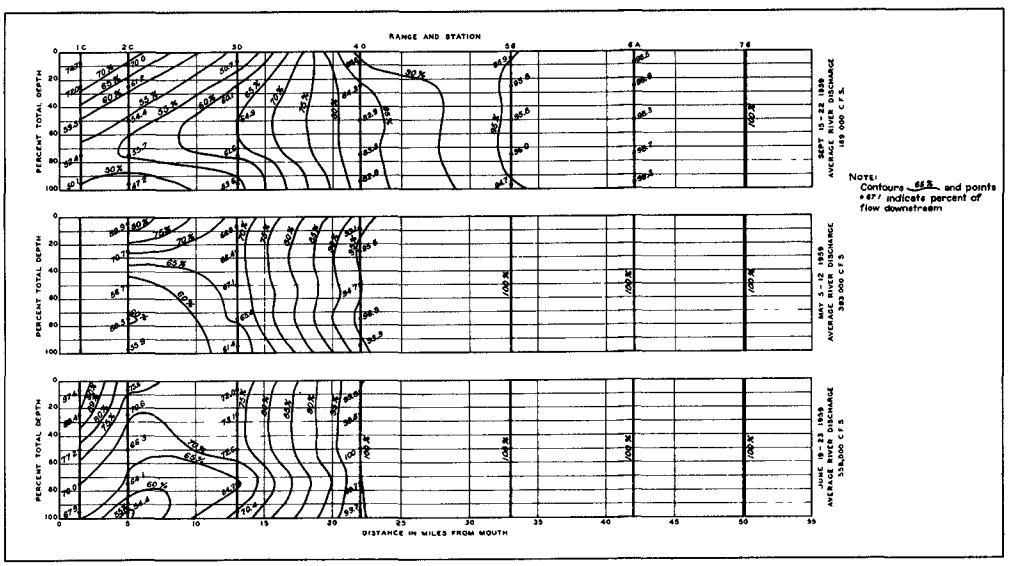

Fig. 17. Flow predominance profile - north channel.

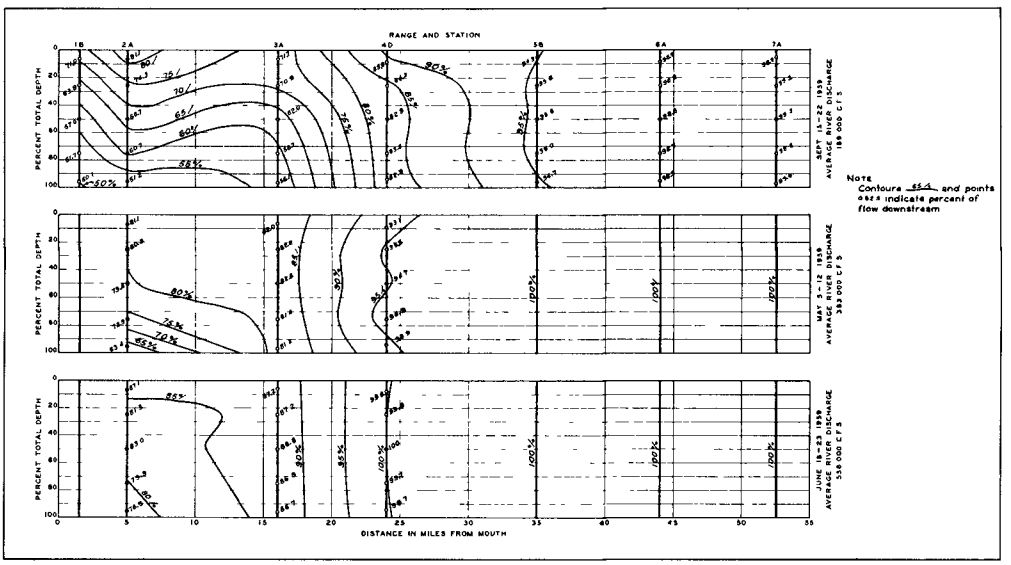

Fig. 18. Flow predominance profile - ship channel.

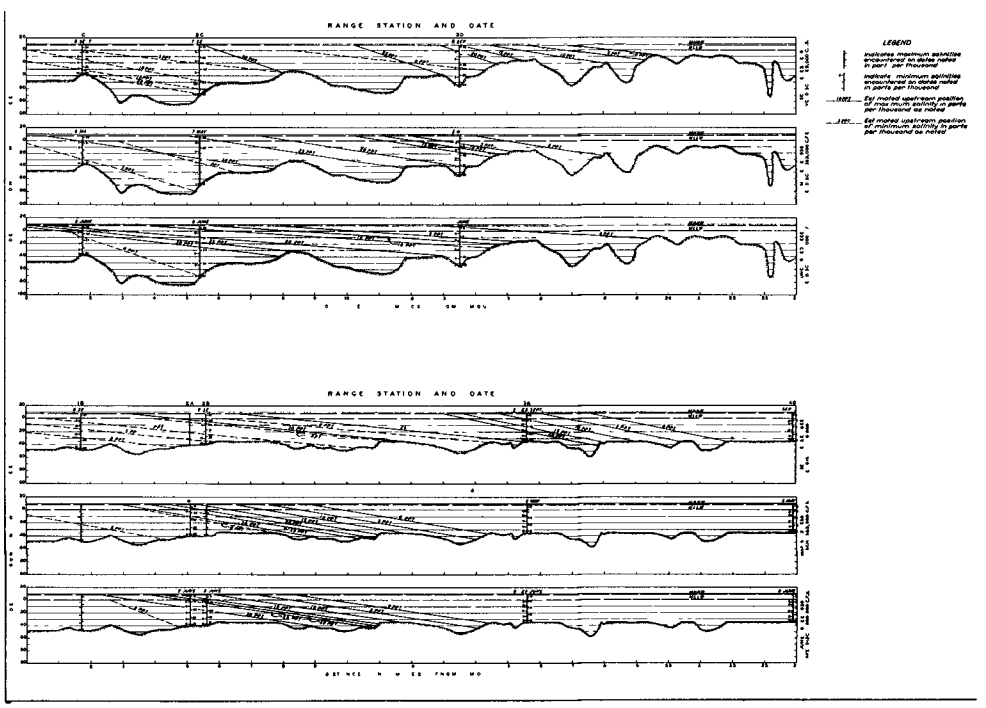

Fig. 19. Salinity profiles.

direction between flood and ebb and velocity were noted at each depth level throughout each observation cycle of approximately 25 hours' duration. From these plots it was possible, by computing the subtended areas above and below the zero velocity line, representing the volumes of flood and ebb flows, to determine the predominant direction of flow and the degree of predominance of such flows at those levels. Figure 15 shows changes in flow predominance noted at all stations and levels during each river discharge cycle of measurement on Range 1, and Figure 16 shows similar information obtained from observations taken on Range 2. From similar data developed along each measurement range it was possible to obtain flow predominance profiles along the northerly portion of the lower estuary, as shown in Figure 17, as well as along the adopted ship channel alignment shown in Figure 18.

Salinity Intrusion - Measurements of salinity, taken concurrently with those of velocity and direction, revealed significant intrusion by salinity within the lower 20 miles of the estuary, shown in Figure 19.

Temperature - Although a general trend of correlation between salinity and temperature was noted, this correlation was not conclusive due possibly to the time lag between the taking of the salinity and temperature observations.

FINDINGS OF THE PROGRAM

The prototype measurement program confirmed the view that the Columbia Estuary, like any other major estuary, is influenced by tidal forces to an extent governed by geography and the complex interaction of these forces with density, littoral, and perhaps other forces significant to the various problems experienced in the estuary. The program definitely identified the normal estuarine characteristic of upstream flow predominance along the bottom levels of the lower estuary in contrast to the downstream predominance noted in the upper levels. This revealed existence of a generally defined pattern of circulation within that region, which has governed the deposition of sediments forming the shoals obstructive to navigation. It has also given rise

to the view that the estuary now acts as a vast sediment trap, in which the phenomenon of density currents preclude, except during rare periods of extreme upland discharge, the movement of bottom sediments to the sea. In consideration of these findings, the Committee on Tidal Hydraulics concluded that while it would be possible to secure, by extensive and costly analytical analyses of observed data together with collection of additional data, an element of success in determining the cause or causes of the existing shoaling and other problems, such analyses could not accurately predict the effects of improvements works. Analyses of anticipated future problems would be even more difficult, if not impossible. Also, the effects of regulatory works that are completed, in progress, or planned for the Upper Columbia River and its tributaries, will be very significant in the estuarine section of the river. In the light of all these conditions, the Committee felt that more must be learned regarding the physical factors governing the behavior of the waterway and that a comprehensive hydraulic model of the lower estuary represented the most important and urgently needed tool to aid in the development of this knowledge. Accordingly, the Committee recommended that immediate steps be taken toward construction of a suitable hydraulic model of the Lower Columbia Estuary from Oak Point to the sea as the initial phase of a comprehensive model investigation.

OFFSHORE AND ESTUARINE SCOUR AND SHOAL

LONG-TERM TRENDS

Concurrently with the analysis of observed data, studies were made of the general shoaling patterns since 1945 reflected by condition surveys made of the immediate offshore area, the entrance area and two shoal areas upstream therefrom (Desdemona and Flavel shoals). These latter shoal areas are located in the vicinities of miles 8.8 and 10.7, respectively. In reviewing these particular studies it should be recognized that they show only the changes occurring within the limits of the authorized channel and, consequently, such studies are not capable of showing the character or magnitude of changes occurring elsewhere throughout the vast estuary and entrance area. Although these studies represent an analysis of known changes, they cannot, due to the limited area

covered, reveal more than an indication of the changes occurring in this vast area. A somewhat clearer indication of the changes occurring in the lower estuary is revealed by a preliminary study of long-term scour and shoal trends made in 1961 which compared bank-to-bank hydrographic surveys of 1868 and 1958 within an 11-mile reach between north and south lines passing through Upper Sand Island and Tongue Point. This study indicated that the total net shoaling occurring within this reach of the estuary, which did not include the tremendous Clatsop Shoals, amounted to 77,000,000 Cubic Yards of material over the 90-year period. Deposition of this amount of material represents an average shoaling of about 3 feet over the 40 square miles of area considered. This preliminary study tends to confirm the view that the Columbia Estuary, since the days of initial improvement, has been acting as a vast sediment trap. Of this amount of shoaling, 66,000,000 Cubic Yards, or approximately 90%, occurred in the lower 6-mile reach below Astoria which includes the Desdemona and Flavel Shoal areas.

OFFSHORE

A study of offshore conditions landward of the 16-fathom depth line from 6 miles south to an equal distance north of the Columbia Entrance shows that great changes have occurred in this area since 1877. During the 50-year period, 1877 to 1926, which corresponds roughly to the period of jetty construction, this study revealed that there occurred a net accretion of 183,000,000 Cubic Yards of material north of the entrance and a net erosion of 374,000,000 Cubic Yards of material south of the entrance, as shown on Figure 20. This change is attributed in large part to the interception by the North Jetty of the predominately south-bound littoral drift which resulted in the accumulation of material north of the entrance and starvation of the offshore area immediately to the south. During the following 32-year period, 1926 to 1958, in which the influence of the jetties was continued, the study revealed that the incremental net accretion to the north of the entrance amounted to about 134,000,000 Cubic Yards while incremental erosion to the south amounted to about 130,000,000 Cubic Yards as shown in Figure 21.

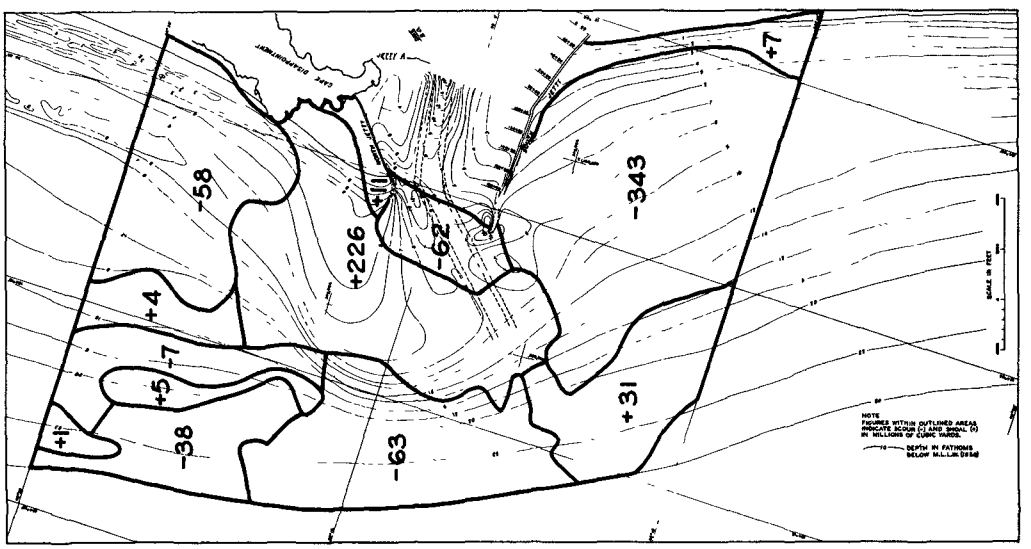

Fig. 20. Offshore scour and shoal volumes, 1877-1926.

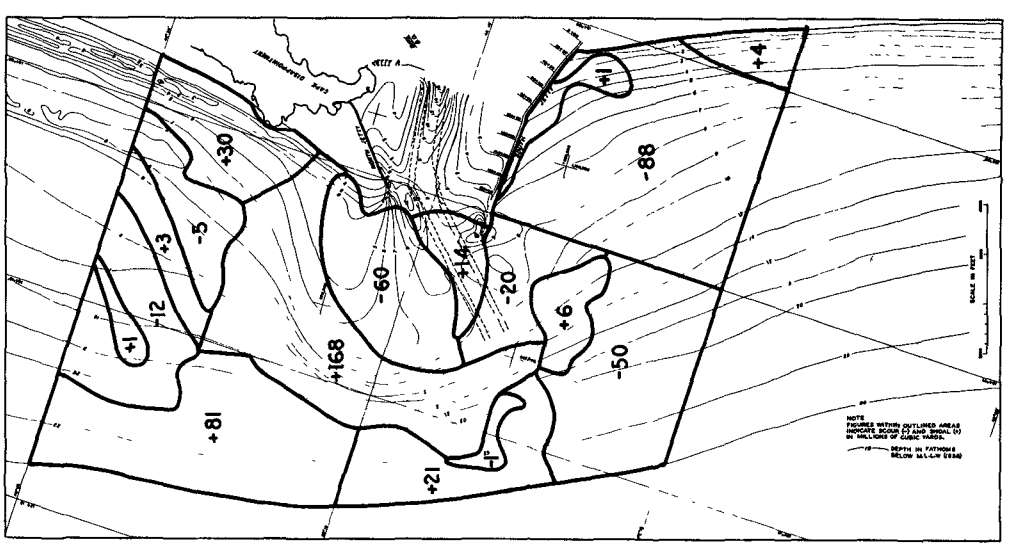

Fig. 21. Offshore scour and shoal volumes, 1926-1958.

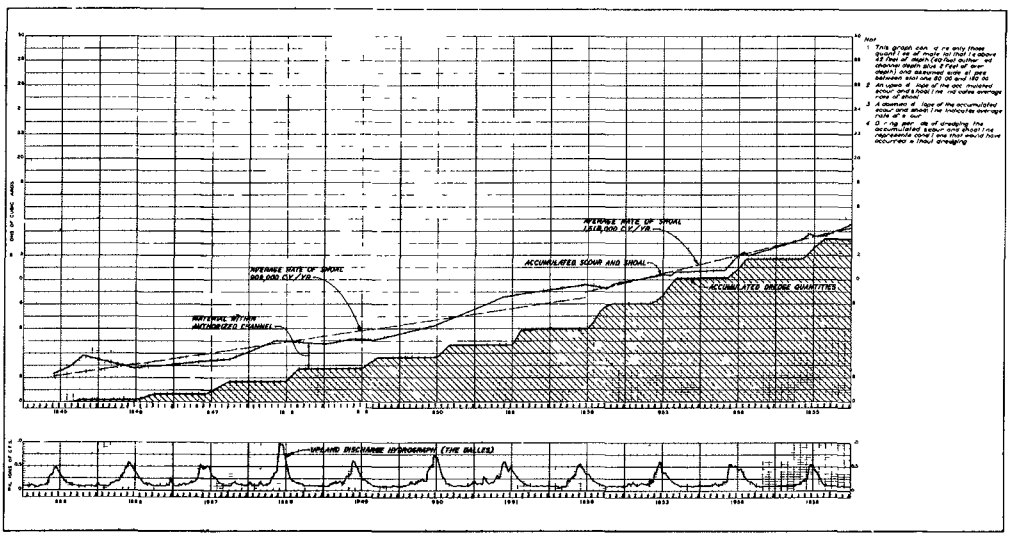

Fig. 22. Scour and shoal, 40-foot channel.

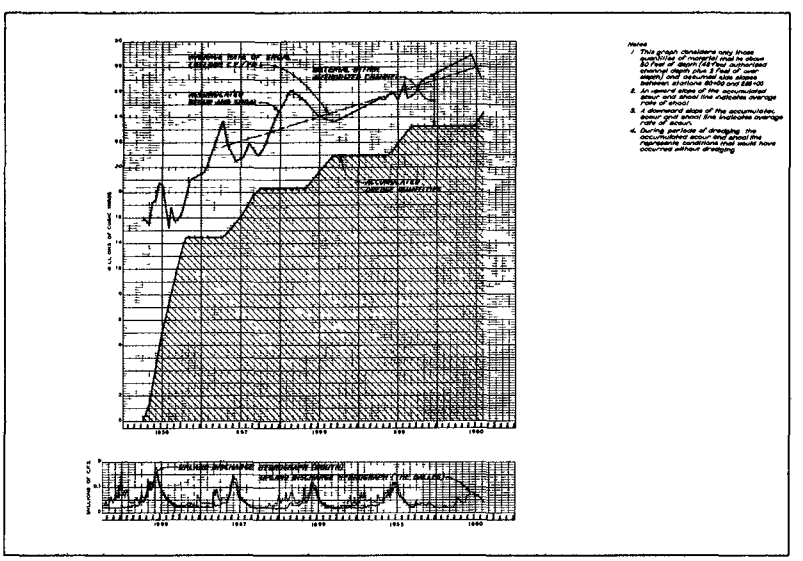

Fig. 23. Scour and shoal, 48-foot channel.

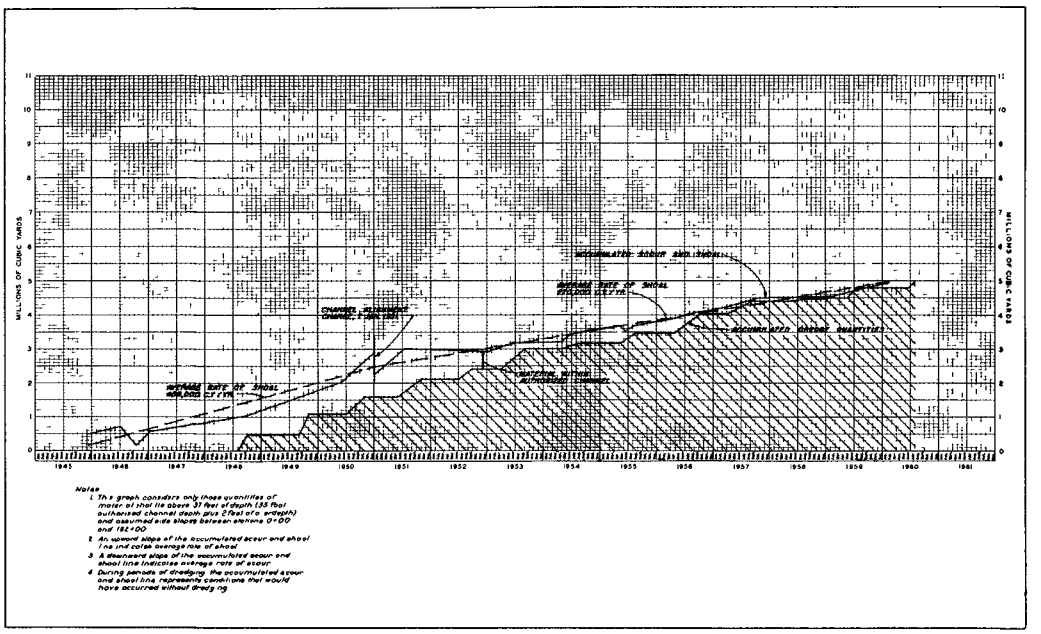

Fig. 24. Scour and shoal, Desdemona Shoal.

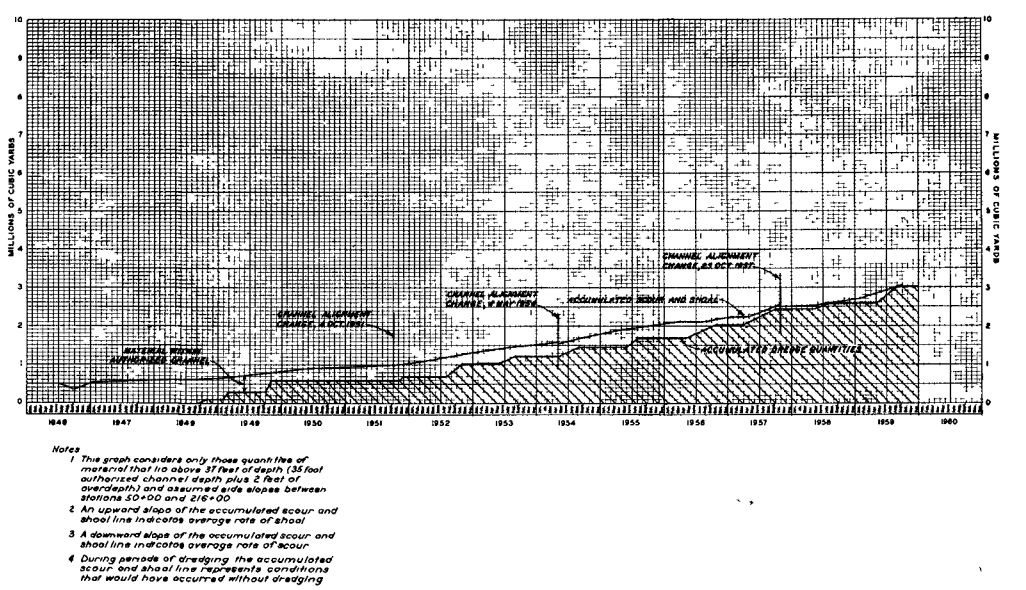

Fig. 25. Scour and shoal, Flavel Shoal.

ENTRANCE CHANNEL

Studies of changes occurring within the entrance channel since 1945 have revealed a trend for increased shoaling in this channel throughout this period notwithstanding the change in project depths from 40 to 48 feet effected in 1956, and the associated increased dredging made necessary thereby. Figure 22 shows in graphical form accumulated dredge quantities, material remaining in the authorized entrance channel above 42 feet of depth, accumulated scour and shoal, and average rates of shoaling from 1945 to 1955, during which time the 40-foot project was being maintained. Figure 23 shows similar information for the period from 1956 to 1960, during which the 48-foot project was being developed. The average rates of shoaling within the entrance channel during these periods as shown on these graphs are as follows:

PERIOD	AVERAGE RATE OF SHOALING, CY/YR
1945 - 1952	909,000
1953 - 1955	1,518,000
1956 - 1960	1,931,000

DESDEMONA SHOAL

The results of similar studies of changes occurring within the authorized navigation channel, 35 feet deep and 500 feet wide, through Desdemona Shoal during the period 1945 to 1960 are reflected on Figure 24. The average rate of shoaling prior to the change in channel alignment effected in January 1951 amounted to about 458,000 Cubic Yards a year. Since that time the shoaling rate has been reduced to an average of about 270,000 Cubic Yards a year.

FLAVEL SHOAL

Figure 25 shows the results of studies made of changes occurring within the authorized navigation channel through Flavel Shoal since 1946. The average shoaling rate in this area during this period has been about 270,000 Cubic Yards a year.

PHENOMENA AFFECTING IMPROVEMENT OF THE LOWER COLUMBIA ESTUARY AND ENTRANCE

ATTRITION SOUTH OF SOUTH JETTY

As previously mentioned, serious attrition has been taking place in adjacent offshore areas along the Oregon coastline immediately south of the South Jetty since the days of initial improvement. Perhaps the most startling visual evidence of this change is the gradual erosion during the last 25 years of the massive sand dunes which protected the arm of land connecting the mid-point of the South Jetty as completed in 1895 with Point Adams. These dunes have been breached along several hundred feet of shore immediately south of the structure and are quite thin for some distance farther south. The driftwood line indicates that the remaining beach berm has been overtopped during recent storms and it now appears that a complete breach to the lagoon in rear of the shore may occur at any time and is inevitable within a few years unless action is taken to prevent such a catastrophe. The low, permeable enrockment along the remains of the trestle at the root of the jetty separates the lagoon from the estuary proper, as shown in Figure 26, but the tide ebbs and flows freely through this structure. Because of the lag in tidal time between this part of the estuary and the open sea, about 40 minutes, a substantial head would develop along this light enrockment in the event of a breach between the sea and the lagoon. It is quite probable that failure of the structure by scour would be rapid in that eventuality and the breach would quickly develop into the primary course of the river outlet. A program of study and surveillance of offshore conditions in the vicinity of the South Jetty has been launched in an effort to determine the cause or causes of this problem with the view to undertaking appropriate corrective action. In the meantime, a temporary structural strengthening of the threatened area has been made to prevent a relocation of the entrance channel, pending completion of the study and surveillance program and analysis of the problem in the hydraulic model hereinafter described in detail.

STATISTICAL WAVE STUDIES

In continuation of Corps of Engineers' studies of characteristics of waves off the California coast, a

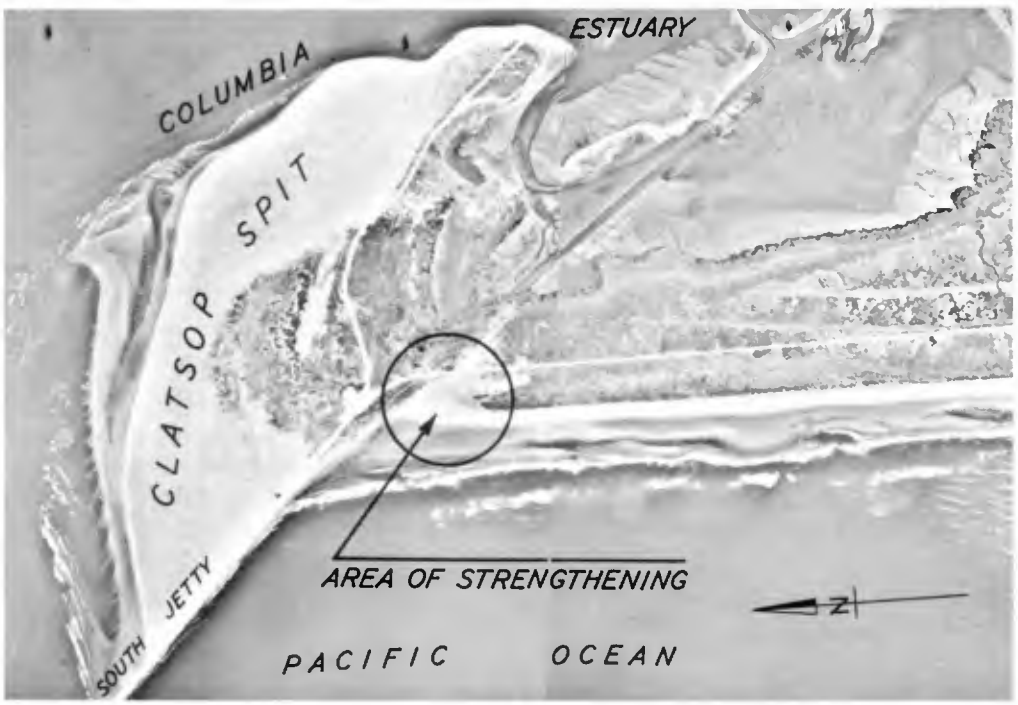

Fig. 26. Erosion south of south jetty.

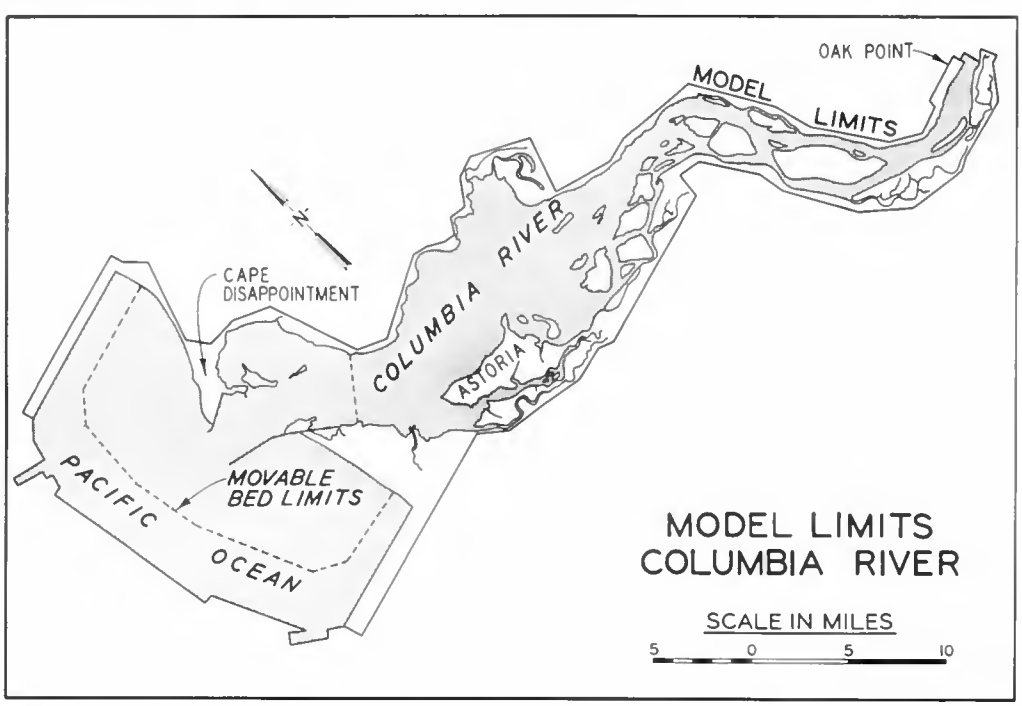

Fig. 27. General layout of Columbia hydraulic model.

contract was awarded in August 1960 to the National Marine Consultants, Inc., Santa Barbara, California, for accomplishment of studies leading to the development of characteristics of waves prevailing off the coasts of Oregon and Washington. These particular studies had as their objectives: (1) the development of wave statistics for three deep-water stations off the Oregon and Washington coasts based on conditions prevailing in 1956, 1957, and 1958; (2) statistics for 12 most severe storms at these selected stations during the period from 1950 to 1960; and (3) structural design wave analyses and wave modification analyses of conditions prevailing at and near the Columbia Entrance during the period 1940-1960. The results of these studies, discussed in the following paragraphs, are contained in manuscript reports[7] prepared by National Marine Consultants, Inc.

HINDCAST STUDIES, 1956, 1957, and 1958

The general area covered by these studies embraced the entire Pacific coast of Oregon and Washington as represented by three selected deep-water stations, one located off the entrance to Yaquina Bay, one off the Columbia Entrance, and one off the coast between Grays Harbor and the Strait of Juan De Fuca. On the basis of 6-hour U. S. Weather Bureau synoptic charts covering extratropical cyclones and the Pacific high cell, these studies routed the paths and decay of meteorological disturbances to develop the height, direction, and period of the resulting wave conditions at the deep-water stations. The extratropical cyclones considered in these studies included storms moving into the Gulf of Alaska, storms moving directly into the study area, storms moving onto the California coast, and western Pacific storms. In addition to development of the characteristics of waves resulting from these meteorological conditions termed "Swell", the studies also determined similar characteristics for waves caused by local wind conditions termed "Sea". This latter condition often constituted a separate source of swell at an adjacent station, inasmuch as a wave in the form of Sea at one station would show up as Swell at an adjacent station not under the influence of the same wind condition. It was frequently found during the course of the studies that as many as six separate wave trains would sometimes occur simultaneously

at the deep-water stations. As a consequence, in the annual summary shown in Table I, the time over which "Swell" conditions occur is greater than the elapsed time over the period covered. This tabulation and Table II show the significant wave height and direction frequency of waves caused by swell and sea, respectively, at the deep-water station off the Columbia Entrance, located at latitude 46° - 12' North and longitude 124° - 30' West:

TABLE I - SWELL

AVERAGE ANNUAL HEIGHT - DIRECTION[1] FREQUENCY DISTRIBUTION (PERCENT)[2]

AVERAGE TOTAL HOURS· 10,508.45

H_s (FEET)	NNW	NW	WNW	W	WSW	SW	SSW	S	Σ
1 to 2.9	0.68	8.20	12.67	13.69	6.67	2.31	2.85	1.90	48.97
3 to 4.9	0.04	2.16	12.36	13.61	4.67	1.83	1.88	0.81	37.36
5 to 6.9	0.04	1.18	6.14	5.51	1.37	0.98	1.07	0.39	16.68
7 to 8.9	0.04	0.45	2.50	2.67	0.54	0.74	0.55	0.23	7.72
9 to 10.9	0.05	0.20	1.11	1.43	0.47	0.36	0.30	0.16	4.08
11 to 12.9		0.09	0.66	0.63	0.30	0.09	0.11	0.13	2.01
13 to 14.9		0.02	0.28	0.61	0.21	0.06	0.12	0.04	1.34
15 to 16.9		0.02	0.13	0.21	0.09	0.04	0.13	0.10	0.72
17 to 18.9		0.07	0.06	0.20	0.06	0.02	0.02	0.02	0.45
19 to 20.9		0.04	0.04	0.07	0.02				0.17
21 to 22.9			0.02	0.09					0.11
23 to 24.9				0.04	0.07				0.11
25 to 26.9									
27+				0.04[3]					0.04
Σ	0.85	12.43	35.97	38.80	14.47	6.43	7.03	3.78	119.76

[1] Direction from which waves approach the deep-water station
[2] Based on 365-1/3 days
[3] 30 feet (March 1956)

TABLE II - SEA
AVERAGE ANNUAL HEIGHT - DIRECTION FREQUENCY DISTRIBUTION (PERCENT)

H_s (FEET)	N	NNW	NW	WNW	W	WSW	SW	SSW	S	OFF-SHORE 6.03	[1] CALM 28.67	Σ 34.70
1 to 2.9	2.06	2.25	7.32	1.44	2.77	1.00	2.49	1.57	3.07			23.97
3 to 4.9	0.84	1.76	5.25	1.45	1.51	1.21	1.61	1.40	2.43			17.46
5 to 6.9	0.42	0.62	1.71	0.54	0.79	0.73	1.11	1.44	1.85			9.21
7 to 8.9	0.16	0.28	1.22	0.53	0.60	0.46	1.14	1.04	1.06			6.49
9 to 10.9	0.02		0.37	0.21	0.16	0.14	0.23	0.63	0.80			2.56
11 to 12.9		0.04	0.43	0.13	0.09	0.11	0.35	0.45	0.95			2.55
13 to 14.9		0.07	0.05	0.09	0.09	0.10	0.23	0.45	0.45			1.53
15 to 16.9			0.05		0.09			0.12	0.25			0.51
17 to 18.9		0.02	0.07	0.02		0.02	0.05	0.19	0.35			0.72
19 to 22.9				0.02				0.12	0.06			0.20
23 - 27							0.04	0.02	0.04			0.10
Σ	3.50	5.04	16.47	4.43	6.10	3.77	7.25	7.43	11.31	6.03	28.67	100.00

[1] Includes waves of 0 to 0.9 feet.

PHENOMENA AFFECTING IMPROVEMENT OF THE LOWER COLUMBIA ESTUARY AND ENTRANCE

SEVERE STORM WAVE CHARACTERISTICS, 1950 - 1960

Generally, extratropical cyclones giving rise to severe wind and wave conditions along the Oregon-Washington coast originate near Japan and move eastward across the Pacific towards the Gulf of Alaska. The degree to which these disturbances affect conditions off the Columbia Entrance depends not only upon the intensity of the storm but also on the disposition of the Pacific high cell. During the summer months this cell is sufficiently removed to the north so that only a few storms approach the Oregon-Washington coast and those that do are relatively weak. During the period from October to May, however, with the southward shift of the Pacific cell, intense storms approach the coast. These storms develop in the form of rapidly moving intense frontal systems on low pressure centers and occur several times each winter. Although pre-frontal southerly winds often attain velocities of over 100 miles per hour in gusts along the coast, the winds associated with these storms seldom reach hurricane force over much of the area. However, the extent of storms in terms of duration and fetch can produce hurricane magnitude waves that last for relatively long periods of time. Principal wind fields associated with these storms produce south to southeasterly winds preceding a warm front, southwest to west southwest winds in the warm sector, and west southwest to northwest winds behind a cold front. Each of these wind regimes can develop high waves but offshore topography and coastal promontories dictate shallow water effects at coastal locations. Hindcast methods reveal the following characteristics of severe storm waves in deep water off the Columbia Entrance during the period 1950 to 1960:

DATE	SIGNIFICANT HEIGHT, FT.	SIGNIFICANT PERIOD, SEC.	DIRECTION FROM
27 October 1950	24	11	SW
21 January 1951	27	14	WSW
2 February 1951	25	13	WSW
18-19 December 1951	23	12	NW
6-7 December 1952	25	11	SW
5 December 1953	24	14	WSW
12-13 February 1954	30	13	SSW
19 November 1954	23	12	SW
15 January 1956	24	12	SW

DATE	SIGNIFICANT HEIGHT, FT.	SIGNIFICANT PERIOD, SEC.	DIRECTION FROM
3 March 1956	30	12	W
26 December 1957	23	13	W
23 January 1958	26	11	SSW
11 December 1959	25	13	SW

STRUCTURAL CRITERIA - COLUMBIA ENTRANCE

This study was composed of two parts, one part considered the characteristics of storm waves as applied to the design of structures at the Columbia Entrance and the other part related to refraction patterns assumed by waves from different directions and of different periods as they approach a 20-mile sector of the coast centered on the Columbia Entrance. The structural design wave analyses were based on hindcast studies of a number of severe storms which approached the entrance during the last 20 years. Considering the deep-water characteristics of waves generated by the previously-mentioned severe storms and the physical factors tending to modify these waves, such as exposure, refraction, shoaling, bottom friction and percolation, bottom slope and still-water depth at the entrance site, as well as the frequency distribution of wave heights, it was determined that structural criteria at the Columbia entrance should be based on the following general wave conditions:

Significant Wave Height	(H_s)	30.0^{+4}_{-2}	feet
Significant Wave Period	(T_s)	13.0^{+1}_{-1}	seconds
Direction of Approach	(θ)	235^{o+20}_{-15}	(from)

With a tide range of 8.5 feet, storm setup of 2.5 feet, and design depth of 51 feet, the most severe condition occurring within the period of study produced a wave with a significant height of 33.5 feet, significant period of 13 seconds, and an angle of approach of 234° as shown in the following tabulation:

DEEP WATER			MODIFICATION		DESIGN WAVE AT ENTRANCE		
			Refraction	Shoaling			
H_s	T_s	θ	Coefficient	Coefficient	H_s	T_s	θ
Feet	Sec.	Dir.	K_r	K_s	Feet	Sec.	Dir.
30	13	205°	0.94	0.996	28.0	13	206°
25	13	225°	1.11	0.996	27.5	13	218°
28	13	245°	1.20	0.996	33.5	13	234°
30	13	270°	0.97	0.996	29.0	13	254°
28	13	295°	0.71	0.996	20.0	13	263°
23	12	315°	1.24	0.996	27.5	13	278°

RADIOACTIVE ANALYSIS OF BOTTOM SAMPLES

In connection with the broad study being conducted by the Atomic Energy Commission of the distribution of Columbia River sediments as related to discharge of radioactive waste effluent from the Hanford complex, which is subsequently discussed, samples of bottom materials were obtained from five different points within the Columbia Entrance and from one location in the lower Estuary. In the Entrance area, one (Sample A) was obtained from the channel on Range 2, two (Samples B and C) were obtained from each side of the entrance channel on Range 1, one (Sample D) in the entrance channel between the ends of the jetties, and one (Sample E) in the channel about 1 mile outside the jetties. In the lower estuary one sample (Sample F) was obtained from the channel near Harrington Point. These samples were analyzed by the General Electric Company in Hanford to ascertain the relative ages of isotopes present in an endeavor to determine the source of materials forming the samples. In these samples, the radio-isotope concentrations were extremely low in comparison with the natural radioactive content of the material. However, it was possible to make age estimates based on the Zn^{65} (245 day half-life) and Cr^{51} (26 day half-life) concentrations. A high Cr^{51} concentration relative to the Zn^{65} concentration would represent a "new" material whereas a low Cr^{51} concentration relative to Zn^{65} would represent much "older" material. The observed Zn^{65} and Cr^{51} concentrations in the above samples and their calculated ratio and relative ages were determined to be as follows:

Sample	Concentration D/M/Gram Zn^{65}	Concentration D/M/Gram Cr^{51}	Ratio $\frac{Cr^{51}}{Zn^{65}}$	Relative Age
A	17.1	11	0.64	New
B	3.9	1	0.3	Old
C	5.8	5	0.85	New
D	3.2	1	0.3	Old
E	6.3	5	0.79	New
F	7.6	30	3.95	Very New

The newer sediments suggest the likelihood that the material has been recently formed of particles moved into the estuary from upland areas while the older sediments very likely have moved into the entrance area from the ocean.

DISTRIBUTION OF COLUMBIA RIVER SEDIMENTS

The Atomic Energy Commission has launched a broad program of study and investigation aimed to (1) explore Columbia River sediments as they bear on the fate of radioisotopes released from the Hanford production complex and to (2) determine the interactions taking place in the Columbia Estuary related to the ultimate distribution of sediments as measured by the concentration of radioactivity on these sediments. In this study, it is proposed to collect and analyze samples of bottom and suspended sediment to determine the principal chemical and physical exchange reactions involved, the sedimentation rates and accumulations, and the character of transport downstream of the sediments of sorbed or precipitated isotopes with the view to depicting in a quantitative manner the radioactive material balance in regard to its interactions with the sediments. In the estuarine section of the river the study is directed toward measurement of the physical forces of tides and currents and to sample the estuarine waters, biota, and sediments to determine:

a. The dispersion patterns and rates of interchange of the dissolved radioactivity in the fresh waters with those of the saline, brackish waters;

b. The removal of radioactivity from solution by means of chemical exchange with suspended and bottom sediments in the estuary; and

c. The rate and degree of removal of radioactivity from solution into the biological food web.

STATUS OF INVESTIGATION

It is not difficult to visualize that a study of this broad scope and complexity, considering its pioneering nature, will require several years to complete. Nevertheless, considerable progress has already been made along several broad phases of the investigation. Pursuant to contracts made with the Atomic Energy Commission, the Department of Oceanography, University of Washington, has conducted field investigations to determine the characteristics of movement of Columbia River waters in the Pacific Ocean and has traced the freshwater plume of flow for many miles seaward. Other field investigations by that Department are directed at measurements of ocean salinity, chemical composition, transparency, temperature, density, plankton, and analysis of bottom sediments along the coast, across the continental shelf and into the abyssal plain of the ocean. In addition, studies by the Laboratory of Radiation Biology of that University of the radioactivity in biological organisms are under way. Through another contract, the U. S. Geological Survey has activated a program to study fluvial sediment transport in the river as may be related to the sorption of radio-nucleides associated with such movement. Although this program will initially investigate sediment phenomena at a number of ranges across the Columbia River above Portland, it is possible that this program will be later extended to cover reaches of the river below that point. It is anticipated that the comprehensive hydraulic model of the lower Columbia Estuary and Entrance, subsequently described, will eventually be of much value in revealing the distribution of sediments in these regions.

RELATED STUDIES

The Department of Oceanography, Oregon State University, for a number of years has been engaged in the study of coastal and ocean phenomena prevailing along the coast of Oregon. In addition to its investigation of the nature of sediments in estuarine waters along this coast, the Department is engaged in preparing bathymetric charts of the offshore areas and plans shortly to map and study the physical features of the Astoria Canyon lying off the Columbia Entrance. Its study of the distribution of Columbia River water has revealed the seasonal offshore movements of ocean currents to the south during the summer and to the north during the winter. Offshore cruises have revealed large lenses of traceable river water upwards to 50 miles in diameter and 100 feet thick located hundreds of miles at sea. These lenses of water are somewhat warmer than the river water flowing from the Columbia Entrance.

COMPREHENSIVE HYDRAULIC MODEL INVESTIGATION

AUTHORIZATION

Pursuant to the previously-mentioned recommendations of the Committee on Tidal Hydraulics, which received the concurrence of the District Engineer, Portland, and Division Engineer, North Pacific Division, Portland, Oregon, the Chief of Engineers in March 1961 authorized the undertaking of a comprehensive hydraulic model investigation of the lower Columbia Estuary and Entrance. As the result, the U. S. Army Engineer Waterways Experiment Station in Vicksburg, Mississippi, has constructed and will shortly place into operation a hydraulic model which will reproduce the lower 52 miles of the Columbia Estuary and a portion of the Pacific Ocean extending about eight miles north and south of the river entrance and offshore to the 20-fathom contour.

DESIGN FEATURES

The hydraulic model has been constructed to linear scale ratios, model to prototype, of 1:500 horizontally and 1:100 vertically. Tides and tidal currents are being reproduced by a primary tide generator located in the ocean portion of the model and a secondary tide generator located

at the upstream limit of the model at Oak Point, Washington. The model ocean is equipped with wave generators to reproduce ocean wave effects on the movement and deposition of sediments, as well as a circulating system to reproduce the effects of alongshore littoral currents on sedimentation phenomena. The model will be operated with salt water, salinity scale 1:1, in the model ocean, and with fresh water supplied by the Columbia River and its significant tributaries, so that density effects on hydraulic and shoaling phenomena will be reproduced. The model will be of a combination fixed-bed and movable-bed type, so that critical portions of the model estuary and entrance can be converted from one type to another, thus employing the advantages of each type in conducting studies of the various problems involved. Figure 27 shows the general layout of the model as well as the limits of the fixed-bed and movable-bed portions.

MODEL VERIFICATION

Hydraulic and salinity verifications of the model were based on prototype measurements of tides, current velocities, current directions, and salinities observed during the 1959 prototype measurement program. The observation stations manned during that program, as well as the range of conditions covered, were specifically planned to provide the data needed for these phases of model verification. As the model is adjusted to reproduce simultaneously all pertinent phenomena observed at the prototype stations during the 1959 measurement program, pertinent phenomena at intermediate points in the prototype are also being reproduced to scale. Verification of bed movement in the movable-bed portion of the model involves an empirical process of adjusting the forces involved, the nature of the bed material, and the duration of model operation until the model will reproduce within sufficient accuracy the significant changes in bed conditions which have occurred in the prototype during known periods of time. These significant changes include the formation of shoals in the navigation channel, accretion and/or erosion in areas outside the navigation channel, and accretion or erosion attributable to structures constructed in the prototype during the period of time used for model verification purposes. Once the model has demonstrated its

ability to reproduce all significant changes in bed conditions of the prototype, the actual model operation time required to effect such changes is used as a measure of the time scale for bed movement. Thus, if the model consistently shows that changes which occurred in the prototype between hydrographic surveys made at intervals of one year are being reproduced in the model during 20 hours of operation, then the time scale for bed movement would be 20 hours model to one year prototype, or about one to 438. Although the time scale for bed movement in the Columbia model will not be known until the movable-bed verification is accomplished, the time scale for reproduction of hydraulic and salinity phenomena, derived mathematically from model linear scales, will be about one to 50. Thus the model, within the time scales thus determined, will reproduce tidal elevations and phases, current velocities from bank to bank and from surface to bottom, salinity concentrations and distribution throughout the saline portion of the estuary, and movements of sediments within the movable-bed portion of the model. In addition to reproducing these phenomena, the model will automatically reproduce the dilution, dispersion, and flushing patterns of any contaminants that might be introduced and readily mixed with the waters of the estuarine system.

MODEL TESTING

It is anticipated that during the next 25 years, continued growth and industrial development within the Columbia River basin, including construction and completion of many water development and conservation projects, will have a marked effect on the quality as well as characteristics of Columbia River flows. In order that the Columbia model may be a useful tool during this critical phase of development, the model has been constructed to have a useful life of at least 25 years. During the early portion of its life the model will serve to solve problems of present-day urgency, after which it will be available to lend guidance to the solution of future estuarine problems as they develop and affect the welfare of the lower Columbia Estuary and Entrance area. Having been successfully verified, tests now proposed for the model are outlined in the following paragraphs.

Entrance Relocation - The threat of a channel relocation through the shore end of the South Jetty resulting from the loss of shore material in that area poses an extremely difficult and challenging problem to those charged with maintenance

of a usable and satisfactory entrance channel for navigation. Considering the enormous build-up of materials immediately offshore and north of the present entrance, the attrition of the shore and offshore areas immediately south thereof, and the continuing growth of the Clatsop Spit shoals, it is not difficult to perceive that this threat is quite imminent, particularly when the destructive effects of storms experienced at the Columbia Entrance are directed toward such an eventuality. Recognizing the possibility that such a relocated entrance, if developed in accordance with careful planning, could possess merit over the present entrance, insofar as channel maintenance is concerned, the model offers an opportunity for careful and complete engineering analyses of the problems associated with the development of such a new channel. In the model the factors now producing the large shoals in the present entrance can be evaluated as they would effect conditions along the relocated channel, and permit engineers to investigate all phases of the potential problem before it occurs, thus saving much time, money and effort which might otherwise be expended. Considering the dislocation to established navigation which would occur by a sudden relocation of the entrance channel, one of the initial model tests will be to explore the consequences of such a relocation and to determine the courses of action to be taken.

Jetty Rehabilitation - As previously mentioned, jetties at the Columbia Entrance have been rehabilitated on several occasions to restore portions of these structures which have been damaged or destroyed by destructive storms. Rehabilitation undertaken in the past has largely been directed toward restoration and increasing the height and sections of those portions of the structures lying above mean sea level on the assumption that the portion below this level, if not in satisfactory condition, would make itself evident by complete failure of the jetty structure. This assumption has been proved correct as subsidence of the structures, particularly after their initial construction, revealed the fact that a certain amount of consolidation was required to effect a stable jetty foundation. Such a foundation has been secured over the years until now rehabilitation is confined to restoration of those portions of the structures damaged by wave action. Notwithstanding the limited nature of rehabilitation, the work involved is costly and must be conducted during the relatively calm season of the year. Its cost and the construction difficulties involved, together with experience gained at other river entrances, have raised question among

engineers as to the value of such limited rehabilitation insofar as maintenance of project depths are concerned. Although completely rehabilitated jetties undoubtedly provide some benefit to small craft against heavy seas as long as these craft remain in the lee of these structures, these particular benefits are seldom of sufficient magnitude to justify the large rehabilitation costs involved. Further, if sea conditions beyond the jetty are such as to preclude safe operation of small craft, there is little reason to expect that the prudent operator of such a vessel would have need for any protection a rehabilitated jetty might provide. Despite the deteriorated condition of the South Jetty at the entrance to Grays Harbor, Washington, just north of the Columbia Entrance, depths in the authorized entrance channel to that harbor are more than twice those for which the jetties were designed to maintain. Although early rehabilitation of that jetty is now being considered, this work is required to preserve its structural integrity against attack by currents which threaten to undermine the jetty foundation. Aside from work of such emergent nature, there appears to be sound basis for question as to the actual value of rehabilitation for the sole purpose of preserving the upper portions of jetties. Certainly area exists for exploration of the most economical time interval for conducting such rehabilitation operations, taking into consideration the construction problems involved and the actual benefits to be expected. The Columbia model, in its initial testing phase, will provide an opportunity to demonstrate the value of recent rehabilitation work and such further work as may be proposed for the immediate future.

Entrance Channel Realignment - As may be noted from recent condition surveys, generally as shown on Figure 9, the authorized entrance channel takes a southwesterly course through the outer bar as it proceeds seaward through the Columbia jetties. Although dredging on the outer bar on this alignment is not now significant, heavy dredging is required to maintain the adopted channel through the inner bar within the jetties. Just west of the authorized channel hydrographic surveys reveal a natural parallel channel of even greater depth which appears to offer a possibility of decreasing dredging requirements if, through some means, advantage might be taken of the greater depths afforded, without introducing an undesirable risk to navigation. In connection with model studies of different channel alignments at the

Southwest Pass entrance to the Mississippi River, it was found that the introduction of a degree of sinuosity into the channel alignment took advantage of the prevailing river and ocean forces to secure a more satisfactory entrance channel. Such an expedient, in combination with realignment of the entrance channel, might have definite merit at the Columbia Entrance and will be tested in the comprehensive model.

Salinity Intrusion and Shoaling - The model will accurately define the extent of salinity intrusion in the Columbia Estuary under the different conditions of tide and upland discharge and will show the part such intrusion plays in the development of the shoaling regime of the estuary and entrance. The movable-bed tests will show the mechanism responsible for the formation of Clatsop Spit, the forces involved in the great imbalance of offshore materials to the north and south of the present entrance, and the role which alongshore littoral forces play in the formation of these large shoal and attrition areas. Once these forces are clearly understood and their interrelationships evaluated in the model, tests can be made of structural measures designed to take advantage of these forces in the development of an entrance channel that will be easier and less costly to maintain.

Reduction of Entrance Width - Although early engineers were guided by observations of existing bank-to-bank widths in the estuary in determining the present width between the ends of the jetties, approximately two miles, it has long been felt by the present-day engineers that these structures were too far apart to efficiently guide the forces at work to produce an easily maintained entrance channel. In the model it will be possible to test the value of more confining structures, such as would result from extension of the alignment of the original South Jetty past the "knuckle". Other confining works, such as groins constructed perpendicular to the South Jetty, could also be tested and evaluated.

Jetty "B" - One of the early tests in the model will evaluate the merit of Jetty "B" as presently authorized by the 48-foot entrance project. The 1959 prototype measurement program revealed the existence of generally upstream currents at all times along the bottom of the "cul-de-sac" in which Jetty "B" would be located. Such a structure could possibly tend to cause undermining of the existing North Jetty through

reflection of the prevailing bottom upstream currents toward that structure. The merits as well as the possible adverse effects of Jetty "B" will be explored fully in the model.

Other Tests - The above brief discussion outlines some of the early tests proposed for the comprehensive Columbia Estuary and Entrance model. Doubtlessly, numerous other tests will be made as new problems arise through increased growth and development of the Columbia Basin. Not the least of these will be that caused by increased pollution of Columbia River waters through domestic and industrial waste disposal. It may be expected that the Columbia model, like models of estuaries elsewhere, particularly along the heavily developed Eastern Seaboard, will define the flushing pattern peculiar to the Columbia Estuary and will point the way to solution of this problem as well as other problems not now envisioned by engineers of this day.

SUMMARY OF PRESENT KNOWLEDGE

The vastness of the lower Columbia Estuary and Entrance area is only one characteristic that belies the complexity of the problem of achieving and maintaining a reasonable degree of permanence insofar as navigation is concerned. The problem is further complicated by the dynamic forces of ocean salinity, littoral drift, river flow, and storm waves which are primarily responsible for the geographical formation of the area and the interactions taking place therein. These characteristics, together with the extremely large and variable range of diurnal tidal action prevailing along the Oregon and Washington coasts, give to the Columbia Estuary and Entrance a uniqueness beyond compare. The tremendous amounts of energy expended by these out-sized forces in the entrance and estuary area exceed those expended in any similarly improved area anywhere in the world today. Past efforts to regulate these forces in the interest of navigation have led to construction of massive and long, stone training structures, the North and South Jetties, which confine the ship channel to a relatively limited area but do not assure adequate depths for navigation without continual dredging year after year. Comparison of depths shown by hydrographic surveys undertaken since the beginning of improvement reveal that the estuary is gradually becoming shallower, being filled with bottom materials carried by the river and transported from adjacent ocean areas. Clatsop Spit shoals, which

continually encroach on the present entrance channel, constitute the most striking evidence of this process. Other evidence, although less spectacular, such as the changes occurring immediately upstream from these shoals, confirm this trend. Measurements of current direction and velocity, as well as salinity and temperature, at different depth levels throughout the estuary reveal the existence of a salinity block or salt-water wedge action along the bottom through the entrance, which not only prevents the movement of bottom materials to the sea but encourages the movement of ocean materials into the estuary. This intrusion of salinity into the estuary, an incidental by-product of improvement, now controls the regimen of the estuary area. Another incidental effect of improvement, interception of the predominately north to south alongshore littoral drift by the North Jetty, has created a severe imbalance of materials immediately offshore the entrance. This imbalance threatens not only to pinch off the present entrance channel by the accumulation of littoral material from the north but, with the assistance of storm waves, also threatens to produce a major relocation of the river outlet to the south, where attrition of the shore and offshore area has weakened the confining influence of the South Jetty. The comprehensive hydraulic model of the Columbia Estuary and Entrance, now undergoing verification tests at the Waterways Experiment Station, offers the sole means of developing an engineering analysis and evaluation of the forces responsible for the pending cataclysm in this area and of determining the action which might be taken to prevent such an eventuality.

CONSIDERATIONS FOR THE FUTURE

Achievement of all feasible storage in the Columbia River headwater areas in the primary interests of flood control, hydroelectric power and irrigation will alter materially the pattern of river flows in the lower estuary. As shown on Figure 28, these flows have in the past ranged from a minimum of 59,000 cfs to a maximum of about 1,300,000 cfs. Regulation by such storage will reduce the future range of these flows by lowering extreme discharges to not more than 600,000 cfs and by increasing minimum flows to about 150,000 cfs. This alteration of the river flow pattern may be expected to eliminate any possible flushing of bottom sediments from the estuary to the sea by extreme river discharges of the magnitude that has been experienced in the past. On the other hand

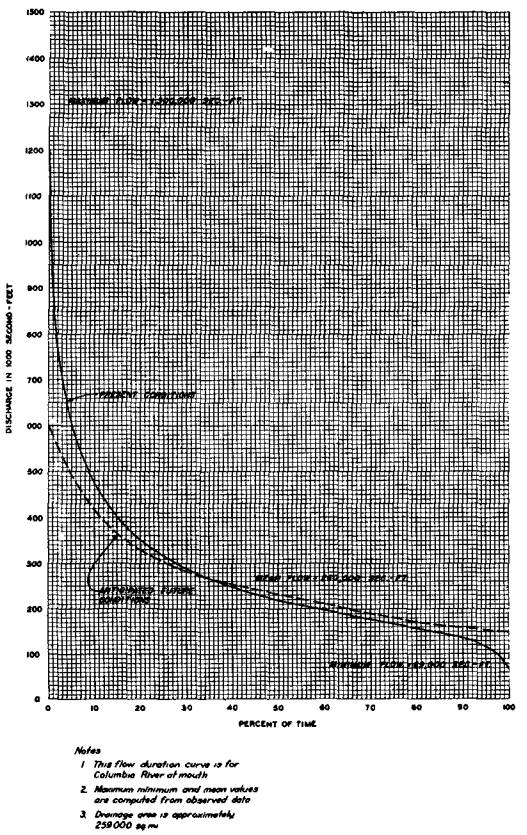

Fig. 28. Flow-duration curve.

the increase in low river flows may, to a small degree, reduce the extent of salinity intrusion in limited portions of the lower estuary. While this regulation of river flow is not expected to appreciably modify the total amount of fresh water entering the estuary, it will, by reduction of extremely high discharges, tend to maintain the permanency and quite likely increase the degree of salinity intrusion into the estuary. Also, as revealed by experience gained at the Savannah Estuary, such regulation of upland flows may tend to concentrate shoaling to a much more limited length of the Columbia Estuary.

History of the Pacific Northwest reveals that channels of greater and greater depth are required to support the increase in ocean commerce attending the continued growth and economic development of this region. Due to the geography of the entrance area and the severe wave and weather conditions which prevail in that area during the winter months, depths of 48 feet are necessary for safe passage

through the Columbia Entrance, while the main Columbia channel inland now provides only a depth of 35 feet. Recent increases in the size and draft of the world fleet of ocean carriers have revealed a need for increasing the minimum depth of the main river channel above the entrance to Portland and Vancouver from 35 to 40 feet, and plans to effect such further deepening of the main channel are now under way. Although no corresponding deepening of the entrance channel is planned at present, due to the fact that elimination of delays caused by the 48-foot entrance channel to prospective traffic will not now justify such further deepening, it is obvious that eventually, as the region continues to grow, greater entrance depths will be required. Provision of the contemplated 40-foot channel in the river above the entrance is expected to extend the effect of salinity intrusion farther into the estuary, causing changes in shoaling patterns and increased dredging to maintain the larger channel dimensions. Any further deepening of the present entrance channel will intensify saline conditions within the estuary and certainly modify, and quite likely aggravate, the shoaling problem.

As previously mentioned, pollution of estuarine waters is not now a serious problem facing those charged with maintaining the quality of Columbia River water. However, with the expected growth in population and industrial development in the area tributary to this great river, experience elsewhere, particularly along the Atlantic Seaboard, points to the eventual need for strict control of pollutants disposed in the Columbia River. The extent of such control will largely be governed by the flushing characteristics of the Columbia Estuary as affected by improvements designed primarily for the sole benefit of navigation. It does not appear unreasonable that the degree of pollution induced into the river may some day exceed the flushing capacity of the estuary.

All these problems are susceptible to study, analysis and evaluation in the comprehensive hydraulic model of the lower Columbia Estuary and Entrance and there is little doubt that the model will contribute greatly to the solution of these and other problems of an unforeseeable nature at this time. In the event the model demonstrates the merit of a planned major relocation of the entrance channel through the South Jetty, it appears probable that many of the problems created by salinity intrusion into the estuary may also be solved or greatly alleviated. Such a planned relocation

would involve construction of a navigation canal in the Point Adams area of the dimensions required by ocean commerce connecting the estuary at that point with the deep ocean area just south of the present South Jetty. A lock might be required in this canal at Point Adams to eliminate or reduce the intrusion of salinity into the estuary from the canal. Also, a new but substantially shorter South Jetty may be required to firmly fix the entrance channel between this new structure and the enrockment forming the present South Jetty. With such a relocated entrance channel and salt-water lock, the present entrance would be abandoned, closed to navigation, and allowed to shoal naturally. If shoaling in the present entrance channel reduces controlling depths to the equivalent of those prevailing prior to 1885, it may be expected that the intrusion of salinity into the estuary will be correspondingly reduced until it is no longer a controlling factor in the estuarine regime. With the reduction of depths created by shoaling it may be expected that, even with the minimum regulated flow of about 150,000 cfs, river flows will completely usurp the entire channel section at all times and there will no longer prevail the marked density currents which are now so characteristic of the intrusion of salinity into the estuary. At that time, except for the modification of the river flow pattern resulting from upstream storage, the restored flushing characteristics of the river would move the bottom sediments to the sea in a manner similar to that which prevailed prior to man's attempt to improve the entrance. The fresh-water estuary thus obtained will be capable of more complete flushing of pollutants and it is reasonable to expect that dredging requirements for navigation will be considerably less demanding. Along with such achievement there would be restored the uninterrupted predominately north to south littoral drift past the present entrance which would nourish and restore the starved shoreline immediately to the south. Although restoration of the natural littoral regime may eventually require dredging of the relocated entrance channel this work will not be required for many years due to the depths now existing in that area. Thus, with restoration of conditions which largely prevailed prior to improvement, the strategic value of the Columbia Estuary and Entrance area may be assured throughout the foreseeable future at reasonable costs.

ACKNOWLEDGMENT

The discussion and data presented herein were obtained from research conducted under the Engineer Planning Program of the United States Army Corps of Engineers. The permission granted by the Chief of Engineers to publish this information is appreciated.

REFERENCES

1. Report of the Board of Engineers, dated 13 October 1882, printed as part of Senate Executive Document No. 13, 47th Congress, 2d Session.

2. Report of the Board of Engineers, dated 24 January 1903, printed as part of Appendix XX of Annual Report, Chief of Engineers, U. S. Army, 1903, Part 3, Volume 3.

3. Mouth of Columbia River Current Survey, 1932, on file in the Office of the District Engineer, U. S. Army Engineer District, Portland, Oregon.

4. Simmons, H. B. and Schultz, E. A., "Fresh Water - Salt Water Density Currents, a Major Cause of Siltation in Estuaries," Technical Bulletin No. 2, April 1957, Committee on Tidal Hydraulics, Corps of Engineers.

5. Ippen, Arthur T. and Harleman, Donald R. F., "One-Dimensional Analysis of Salinity Intrusion in Estuaries," Technical Bulletin No. 5, June 1961, Committee on Tidal Hydraulics, Corps of Engineers.

6. Report of the District Engineer, U. S. Army Engineer District, Portland, "Interim Report on 1959 Current Measurement Program, Columbia River at Mouth, Oregon and Washington," dated 1 September 1960.

7. National Marine Consultants, Inc., Santa Barbara, California, "Wave Statistics for Twelve Most Severe Storms Affecting Three Selected Stations off the Coasts of Washington and Oregon, During the Period 1950-1960," January 1961; "Oceanographic Study for Columbia River Entrance," March 1961; "Wave Statistics for Three Deep Water Stations Along the Oregon-Washington Coast," May 1961.

CHAPTER 41

SOME CHARACTERISTICS OF THE DUTCH COAST

Ir. T.Edelman and Drs. D.N.Eggink
Coastal Research Division
Rijkswaterstaat, The Hague, Netherlands.

1. INTRODUCTION

The Dutch coast is over its whole length a sandy coast. Along such a coast the changes in shape of the coast-line are determined by transport of sediments, in casu sand, along the coast. This transport is brought about by water and by air. The latter, the eolian transport, though it may have some importance, has been neglected in this study. The marine transport along the Dutch coast is caused by currents and by waves; we do not know which is the most important.

In this study the transport by waves is considered to be the effect of waves, moving in one predominant direction; the transport by currents is taken into account as a transport by tidal currents only.

We should like to underline here the very general character of the following considerations.

2. GENERAL TRANSPORT-FORMULAE

From the continuity-condition it follows that

$$\frac{\partial y}{\partial t} = A \frac{\partial Q}{\partial x}$$

where Q = the quantity of transported material per unit of time
t = the time
A = a constant.
The x-axis has been taken along the coast-line.

The factor $\frac{\partial y}{\partial t}$ is the velocity, with which the coast-line moves. Erosion will occur if $\frac{\partial y}{\partial t}$ is positive, accretion if $\frac{\partial y}{\partial t}$ is negative.

If $\frac{\partial y}{\partial t} = 0$, the coast-line will not alter its situation.
The equilibrium-condition of the coast-line, therefore is:

$$\frac{\partial Q}{\partial x} = 0$$

or: the coast-line is in equilibrium if in every cross-section of the coast the same quantity of material is transported.

If the quantity transported increases in the transport-direction, $\frac{\partial Q}{\partial x}$ is positive, and thus $\frac{\partial y}{\partial t}$ is positive, so erosion occurs. If the quantity transported decreases in the transport-direction, there will be accretion.

It may be allowed to suppose that along a non-disturbed coast

(i.e. a coast without inlets, groins, jetties etc.) in each cross-section the quantity Q transported equals the transport-capacity Q_c. In that case the changes in the shape of the coast-line depend only on the changes in the transport-capacity along the coast, i.e. on changes in wave-direction or wave-intensity, or on changes in the tidal capacity.

This does not hold good along a disturbed coast, where in some parts a difference may exist between the quantity actually transported and the transport-capacity. A certain stretch (the length of which we do not know) is needed to bring Q into accordance with Q_c. If $Q > Q_c$ accretion occurs, if $Q < Q_c$ there will be erosion along the stretch of disturbance. The erosion stretch may be relatively longer than the accretion stretch, since a surplus may be deposited quicker than a deficit is supplied.

We assume that it is allowed to superimpose the $\frac{\partial y}{\partial t}$ curves of the disturbances linearly on the general $\frac{\partial y}{\partial t}$ curve of Q_c.

3. EFFECT OF A TIDAL CURRENT ON A NON-DISTURBED COAST

The transport-capacity of a tidal current will increase with the tidal range. If, therefore, the tidal range increases along the coast in the direction of propagation of the tidal wave the coast will be eroded. A decreasing tidal range in that direction will cause an accretion.

4. EFFECT OF WAVES ON A NON-DISTURBED COAST

Along large stretches of a coast the average intensity and the average dominant direction of the waves will not change very much. The angle α, between the wave direction and the perpendicular on the coast-line, however, does change if the coast-line is not a straight line. Therefore, Q_c will be a function of α.

$$Q_c = Q_m \; f(\alpha) \quad .$$

If we put $f(\alpha) = \sin 2\alpha$, then

$$Q_c = Q_m \sin 2\alpha \quad .$$

$Q_c = Q_m$ if $\alpha = \frac{\pi}{4}$. $Q_c = 0$ if $\alpha = 0$ and if $\alpha = \frac{\pi}{2}$.

Along a concave coast (see figure I^A) $Q_c = Q_m$ in M_1 and M_2; $Q_c = 0$ in A, B_1 and B_2, Therefore, the waves will cause an erosion along the stretches $B_1 M_1$ and $B_2 M_2$ and an accretion along M_1 A M_2.

Along a convex coast (see figure I^B) it is the opposite. Along $B_1 M_1$ and $B_2 M_2$ accretion occurs and M_1 A M_2 will be eroded.
We see that waves tend to straighten a curved coast-line.

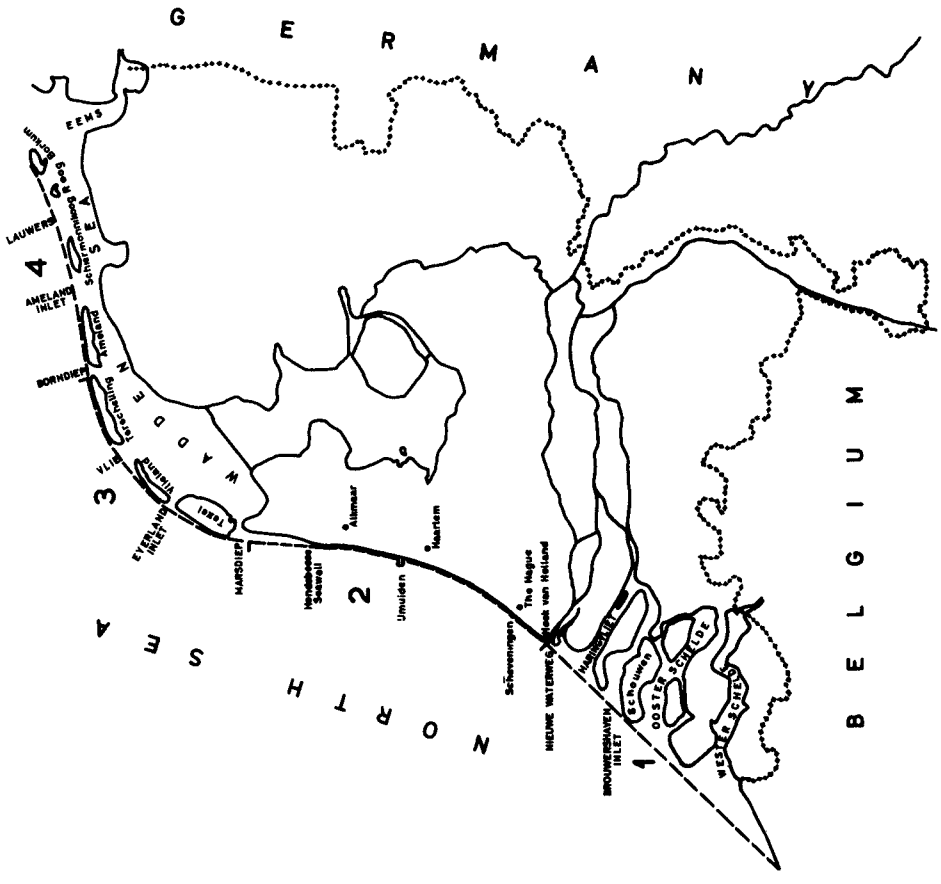

Fig. 2. The Dutch coast-line.

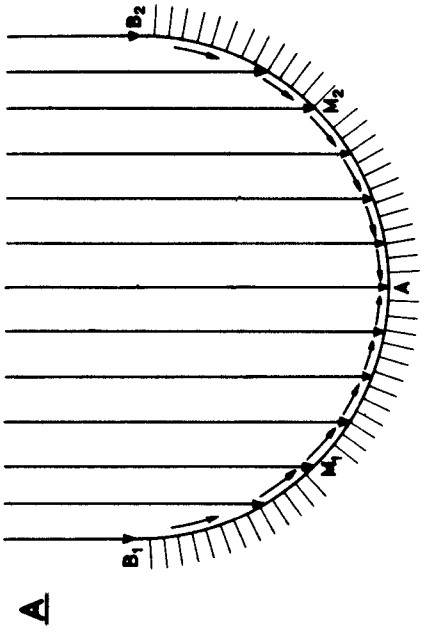

Fig. 1. Effect of waves on a concave and on a convex coast.

5. EFFECT OF DISTURBANCES

Tidal currents mostly cause erosion on both sides of a disturbance. The eroded material moves into deeper water, where shoals are formed.

The effect of waves on both sides of an inlet is similar. Jetties, groins and such disturbances, however, mostly show an accretion on the lee-side and an erosion on the windwardside.

6. THE DUTCH COAST-LINE

As a whole, the Dutch coast-line consists of four parts (see figure II).

1. A straight line, from the Belgian frontier to Hoek van Holland.
2. A concave part between Hoek van Holland and the Marsdiep-inlet.
3. A convex part from Marsdiep to Borndiep.
4. A faintly curved concave part from Borndiep towards Germany.

Part 1 is disturbed by 5 inlets: Westerschelde, Oosterschelde, Brouwershaven-inlet, Haringvliet and Nieuwe Waterweg. A real coast-line hardly exists here.

Between Hoek van Holland and Marsdiep there are no inlets, but some disturbances are caused by the harbour jetties of Scheveningen and IJmuiden, and by the bulwark (groins) of the Hondsbosse Seawall.

The curves of the Wadden-islands (part 3 and 4) are disturbed by large inlets: Marsdiep, Eyerland-inlet, Vlie, Borndiep, Ameland-inlet, Lauwers and Ems.

7. EFFECT OF TIDAL CURRENTS

The tidal range decreases from the Belgian frontier until the Marsdiep-inlet and increases from Marsdiep to Germany. Since the direction of propagation of the tide is from Belgium towards Germany, the tidal currents tend to bring about an accretion along part 1 and 2, and an erosion along part 3 and 4.

8. EFFECT OF WAVES

The effect of waves on the Dutch coast depends mainly on what may be considered as the dominant wave direction with regard to the transport of sediments. In figure III we have constructed the effect of waves if the dominant wave direction would be N.W. and W., respectively.

9. EFFECT OF DISTURBANCES

By the simplified and general method applied, it will be impossible to analyse the changes of the coast-line in part 1 and part 4, since on these parts of the coast the disturbances caused by the many large inlets will surpass by far the normal effects of waves and tidal currents.

On the islands Texel, Vlieland or Terschelling perhaps some stretches may be found on which the influence of the tidal inlets may be neglected.

With the disturbances along the concave part between Hoek van Holland and Marsdiep we are dealing in more detail in paragraph 12.

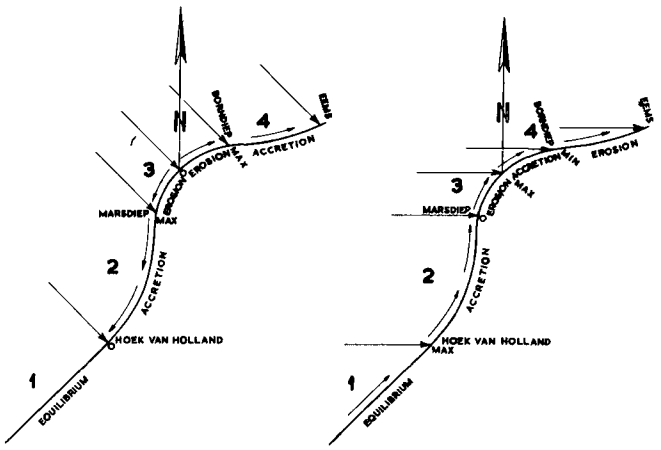

Fig. 3. Effect of waves on the Dutch coast-line.

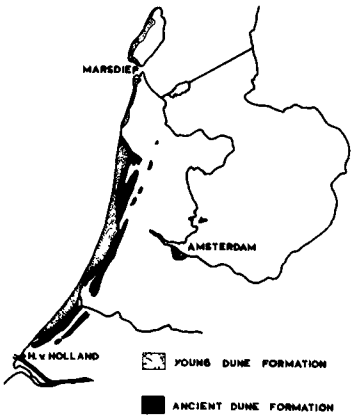

Fig.4. The "ancient dune formation" between Hoek van Holland and Marsdiep.

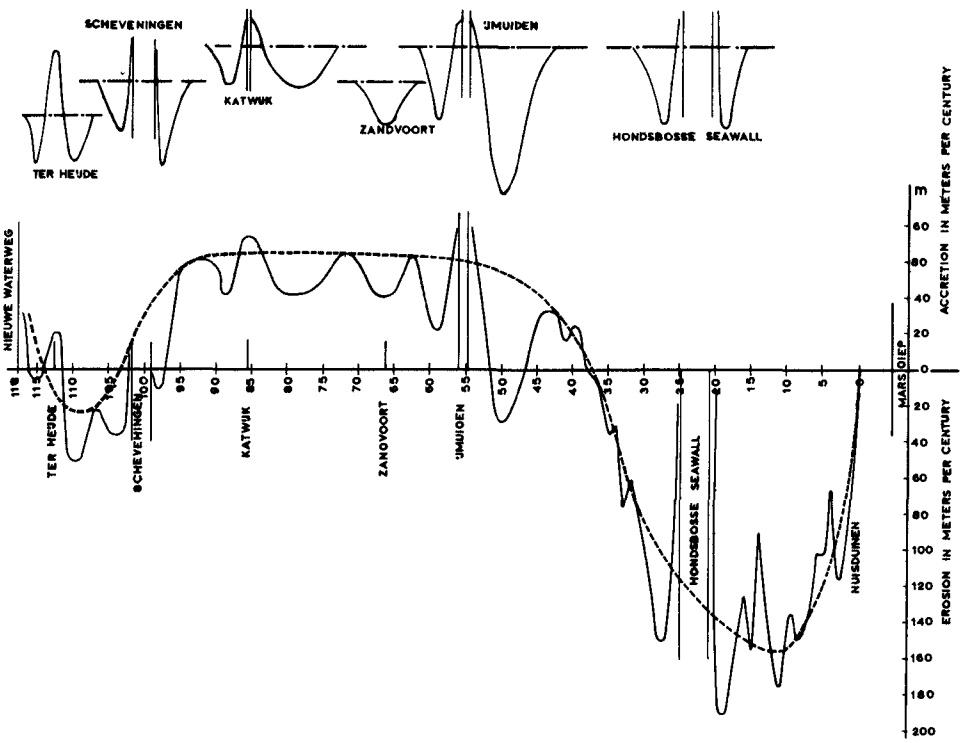

Fig. 5. Analysis of dune-foot movements between Hoek van Holland and Marsdiep.

10. EFFECTS TO BE EXPECTED

1. Belgian frontier - Hoek van Holland.
Accretion by tidal currents; equilibrium by waves (straight line); heavy disturbances by many large inlets, which probably will prevent a proper analysis.

2. Hoek van Holland - Marsdiep.
Accretion by tidal currents; accretion by wave action; disturbances by jetties and groins which will probably not prevent an analysis.

3. Marsdiep - Vlie.
Erosion by tidal currents; erosion by waves; heavy disturbances by inlets.

4. Vlie - Borndiep.
Erosion by tidal currents; erosion by waves from N.W., accretion by waves from W., perhaps a stretch where the influence of the inlets may be negligible.

5. Borndiep - Ems.
Erosion by tidal currents; light accretion by waves from N.W., light erosion by waves from W., heavy disturbances by large inlets, which probably will prevent a proper analysis.

This is, in a general way, what may be expected from theoretical considerations. We turn now to the facts and we will see in how far they affirm our expectations.

11. GEOLOGICAL DATA

In former times, probably, a sandy coastal barrier existed along the whole Dutch coast. This coastal barrier must have been interrupted by inlets, through which the rivers debouching into the lagune behind the barrier brought their water into the sea. This ancient barrier showed a weak surface relief, that may be described best as a series of low dune ridges, parallel to the coast-line, with oblong coastal plains between them. Afterwards (perhaps during the ninth century) this "ancient dune formation" has been partly covered by high dunes, the "young dune formation". These young dunes do not show a clear morphology; they have not been deposited in longitudinal ridges.

Between Hoek van Holland and the Marsdiep the ancient dune formation still exists. At the sea-side it is partly covered by the young dunes, but behind this region the uncovered ancient dune formation reaches landwards over one kilometre and more. Cities as The Hague, Haarlem and Alkmaar have been founded on the ancient dune ridges; the famous bulb-fields are situated nearly exclusively upon this ancient formation.

From figure IV it may be seen, that in the neighbourhood of the inlets (i.e. between The Hague and Hoek van Holland, and south of the Marsdiep) the uncovered ancient dune formation tends to disappear. The morphology of the coastal barrier as a whole suggests a coast, which is

accruing since very remote times and which only at both its ends has been eroded under the influence of the bordering inlets. This is in accordance with the expectations, stated in paragraph 10.

Along the coast south of Hoek van Holland, only very few remains of the ancient dune formation are present. If extant (as for instance on the island of Schouwen) the ancient formation is always covered by young dunes. This gives the impression, that this coastal section, since centuries, is subject to erosion. Without any doubt, this erosion is caused by the large inlets.

It is a remarkable fact, that along the Belgian coast the uncovered ancient dune formation is still in existence, from which we may perhaps conclude, that the average dominant wave direction is more likely to be N.W. than W.

In sharp contrast with the above mentioned parts of the coast, there are no traces of an ancient dune formation along the Dutch coast North of the Marsdiep. Even on the island of Texel, the southern part of which consists of a very resistent boulder clay, an ancient dune formation does not exist. We are dealing here with an eroding coast, its coastal barrier must always have been whirled up and thrown back by waves and currents.

So far, geological and morphological data are in good accordance with our theoretical derivations.

12. COASTAL MEASUREMENTS

Since more than one hundred years the position of the L.W.-line, the H.W.-line and the dune foot, once a year, has been measured every one thousand metre along the Dutch coast. Especially between Hoek van Holland and the Marsdiep a beautiful series of data results, from which the movements of the coast-line during the last century can be studied in detail.

The data about the dune foot provide the most regular series. From this series, therefore, we derived figure V, in which the resulting movement of the dune foot from ± 1850 till ± 1950 is plotted. At first we obtained a rather irregular curve in which, however, the disturbances caused by the jetties of IJmuiden and Scheveningen, by the Hondsbosse Seawall and a few others, can be clearly distinguished. After subtraction of the disturbances and after some flattening, the dotted curve of figure V emerges. The outer parts of this curve represent the border-disturbances due to the southern system of inlets and to the northern inlet of the Marsdiep. The southern disturbance extends to about km 90; the northern one is longer and extends to about km 55 (IJmuiden). Between km 55 and km 90 there are no border- disturbances present; in this section the undisturbed coast-line proves to have migrated seawards over about 60 m (as an average) during the last one hundred years.

Thus, by studying the measured data, we have been able to estimate quantitatively an accretion, the existence of which we derived qualitatively from theoretical considerations.

Similar data of the Wadden-islands yield only a very confused picture. No clear evidence of a permanent tendency of a landward movement of the coast-line could be found. The measured data of the islands of Ameland and Schiermonnikoog rather seem to indicate an accretion of their northern coasts.

13. HISTORICAL DATA

Historical data throw some more light on the behaviour of the Wadden-islands. It is known, for instance, that formerly the western part of Vlieland was situated far more northwards than to-day. This part, with high dunes upon it, has been destroyed by the sea during the 17th and 18th centuries; from the remaining sand the sea built up a flat sand-bank, without any dunes: the present-day southwestern part of the island. Since that time, the eastern part of Vlieland was so heavily attacked by the sea, that the coast had to be protected by 54 groins in order to stop the ever increasing erosion.

During the last centuries the coast of Terschelling has not shown very great alterations. The island has been lengthened in easterly direction and the northwestern point has shown a slow accretion. A tendency of landward movements of the coast-line is not evident.

From ancient sea-charts it can be derived that the islands of Ameland and Schiermonnikoog move in eastward direction (erosion at the western end; accretion at the eastern end). Archaeological data point in the same direction. As an average over many centuries, the eastbound velocity may have been some hundred metres per century. Again, there is no evidence of a movement in a southerly direction.

The behaviour of the little island of Rottumeroog, especially during the last 150 years, is well-known. The island moves in easterly direction at a rate of 10 or 20 metres per year. Every 25 or 30 years the house of the guardian has to be rebuilt upon the eastern side; after due time it finds itself standing on the western shore, where it is attacked by the sea.

The available data suggest, that during the last centuries the Dutch coast between Vlie and Ems, in sharp contrast with the coast between Marsdiep and Vlie, has not endured an accretion or an erosion of any importance. After all, the coast-line in this part is nearly a straight line, so that the waves are hardly able to cause an important accretion or erosion. Material, however, is transported to a large amount along this section. So we tend once more to the conclusion, that the average dominant wave direction is more likely to be N.W. than W.

14. CONCLUSION

From the continuity-condition it follows, that the changes of the transport-capacity are responsible for erosion or accretion along a sandy coast.

The transport-capacity of tidal currents depends on the tidal range. The transport-capacity of waves changes with the direction in which the waves approach the coast. This means that, if a dominant wave-direction exists, the curvature of the coast must be responsible for erosion or accretion by wave action.

Since the pattern of the tidal range along the Dutch coast is well-known, as well as the curvature and the general shape of this coast, a general and qualitative prediction could be given about the behaviour of the coast-line.

Disturbances by inlets, groins, jetties, etc., however, spoil the picture and have even prevented in some cases a proper prediction.

However, investigation of available geological, morphological and historical data and an analysis of data from coastal measurements prove, that such data are in good accordance with predictions derived as mentioned above. Our simple theory, therefore, may perhaps be considered to give a rough explanation of the behaviour of the Dutch coast-line.

CHAPTER 42

THE NATURAL DEVELOPMENT OF THE WADDEN SEA AFTER THE ENCLOSURE OF THE ZUIDER SEA

C.F.W.Rietveld
Engineer, Zuiderzee Works,
Sweelinckplein 14, The Hague, The Netherlands

ABSTRACT

The Wadden Sea and Zuider Sea used to form an internal sea which was parated from the North Sea by a chain of islands. In 1932 the Zuider Sea w enclosed by a dam 32 km in length. Owing to this, the Wadden Sea experienc changes in the normal tidal movement, the storm-surge levels and the confi guration of the bed. This article discusses the movement of water and sand the Wadden Sea and its natural development since the enclosure of the Zuid

I.INTRODUCTION

The formation of the Wadden Sea and Zuider Sea commenced about the be ginning of the Christian era when the sea broke through the coastal barrie as a result of a rising sea level. The peat and clay areas lying behind th coastal barrier where either drowned or eroded away. In this way an interr sea was created, surrounded by a low-lying clay and peat area and bounded the sea side by an intermittent line of coastal dunes. Some tidal inlets m have appeared where the coast was already broken by the mouths of rivers.

As the area of the internal sea increased, the capacity of the tidal lets also increased. This caused increased erosion and so the process was celerated. In the course of the Middle Ages the inhabitants began to stabi lise the coast-line by means of dykes. In this way a dynamic equilibrium w established between the rise in sea level and the configuration of the bec the internal sea. The transport of water and sand takes place chiefly in a system of channels which branch out strongly landwards of the tidal inlets. Between these channels lie flats and banks called the Wadden. The height c the Wadden is determined among other factors by the transport of material the sea and the level of high-water. At high-water the Wadden-flats are cc ed by water and some of the suspended material which has been brought in s to the bottom. As the water ebbs, not all the material which has settled c is carried back again, so the flats are gradually increasing in level. Thi increase slows down as the level of the Wadden approaches high-water level If the sea-level were to remain constant and the amount of material brough in were sufficient, new land would be created. Vegetation would take root the Wadden would come to lie above high-water level. The reservoir capacit of the sea would become smaller, resulting in a decrease in the size of th channels. However, if the sea-level is continually rising, the level of th Wadden will show a certain delay in response which is dependant on the qua tity of material available and the rate of rise in sea-level.

If the increase in sea-level shows fluctuations, an alternate accreti and erosion of the Wadden can occur. By "increase in sealevel" is meant th relative increase in sea-level, consisting of the absolute movement of the sea-level and the movement of the land, which may be susceptible to tector movement of the earth's crust and to consolidation of the sediments.

The geological structure of the Wadden area can be broadly described follows. Westwards of the Vlie Inlet, boulder clay has often been found at depth varying from a few meters to about 20 m under N.A.P. (Dutch Ordnance Level = mean sea level). Boulder clay at depths of less than 20 m under NA means that this area was an island during the Riss-Würm interglacial. In t

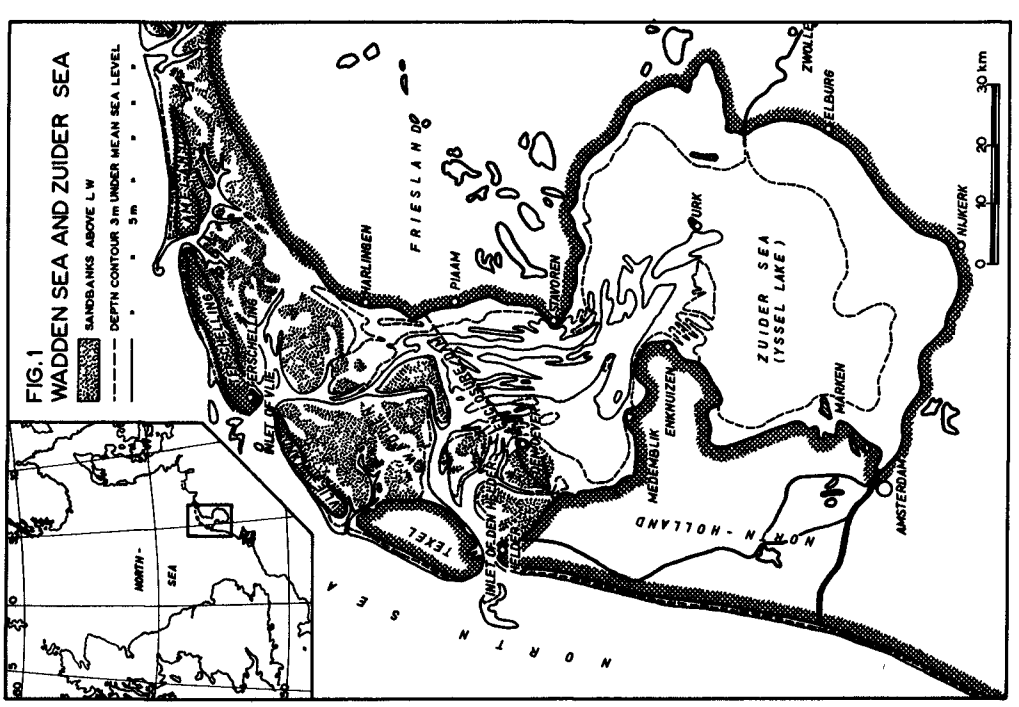

Fig. 1. Wadden Sea and Zuider Sea.

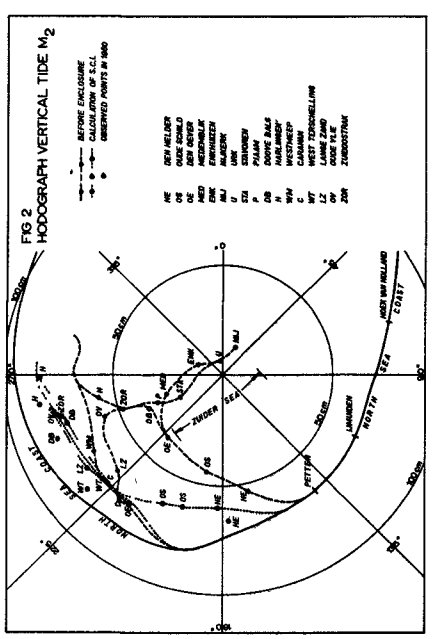

Fig. 2. Hodograph vertical tide M_2.

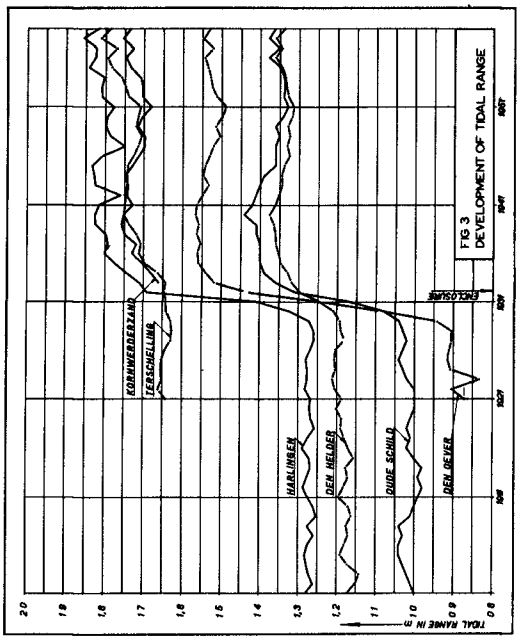

Fig. 3. Development of tidal range.

case, marine Eem deposits are not present. During the Würm glacial, low-terrace sand was deposited on the boulder-clay. At the beginning of the holocene, about 10.000 years ago, a peat layer was formed on this sand. This peat layer is referred to as "peat at greater depth". On top of the peat a early holocene Wadden deposits and old marine clay (5.000 - 2.000 B.C.). A present the old marine clay extends to 2 -2,5 m under NAP and in places it has a very low chalk content, indicating that this marine clay has at some time lain above high-water. On the old marine clay, the great Dutch peat l er was formed. In the Wadden Sea this layer has now an average thickness o about 1 m. About at the beginning of our era, erosion of the peat layer st ed. The great loss of land took place in the 13th and 14th centuries. Perh this was assisted by the digging of canals and the excavation of peat. On parts of the peat layer which were left, new marine clay or new marine san was deposited, a process which is still taking place.

Thus after the Würm glacial there were two periods with peat formatio Then the relative rise in sea-level was retarded or even changed into a te porary fall, so that the Wadden had the capacity for accretion, using the m terial available.

From about the 1st century onwards, the Wadden, which had previously creted by peat formation, were flooded and largely eroded away as a result the relative rise in sea-level.

In this way the Zuider Sea was formed. It was surrounded by land whic was protected by dykes, but which suffered from repeated flooding. During storms, the North Sea water surged through the inlets and high water level could occur as a result of the local wind effect on this shallow sea. Brea in the dykes were common and raising the level of the dykes was very expen as a result of the very long coast-line.

After the storm surge disaster of 1916, the plans for the reclamation a part of the Zuider Sea became definite and an integral part of these pla was the enclosure of the Zuider Sea. The enclosure would prevent high wate levels in the Zuider Sea and reduce the coast-line from a length of c. 250 to 30 km. The remaining part of the internal sea, the Wadden Sea, would re in open connection with the North Sea. Work on the enclosing dam began in and in May 1932 the last gap was closed. The area of the internal sea was by reduced from c. 5200 km^2 to 1500 km^2. The movement of water in the rema part would experience important alterations, chief of which would be that storm surge levels along the coast would be changed. Because of this, a co mission was set up whose task was to determine how much the enclosure woul raise storm surge levels along the coast outside the enclosing dam above w would have previously occurred (State Commission Lorentz 1918 - 1926). Thi commission, hereafter referred to as S.C.L., published a comprehensive rep on the changes which would occur in the normal tidal movement and in the s surge levels in the Wadden Sea after enclosure of the Zuider Sea.

As a result of the changes in the movement of water, the topography c the Wadden Sea would experience alterations.

In the paragraphs which follow, the normal tidal movement, the storm surges and the topography of the bed will be described.

II. NORMAL TIDAL MOVEMENT.

In the Wadden Sea and the former Zuider Sea (now the IJssel lake) tid effects are chiefly dependent on the diurnal lunar tide M_2. The amplitude the tide is not everywhere the same. See fig 2, in which the amplitude and phase of the M_2 tide are represented graphically.

Before calculating the increase in storm surge levels due to enclosur of the Zuider Sea, it was first necessary to compute the influence of the enclosure on normal tidal movement.

For this purpose the Wadden Sea and Zuider Sea were schematically represented as a network of flowing channels, separated by flats and banks, which were considered to provide storage capacity.

As tide, the sinusoidal diurnal lunar tide M_2 was considered. The cal culation was made following the single harmonic method with linear frictio In comparison with the tidal flow, fresh water flow could be neglected.

The boundary conditions were the vertical tide in the North Sea which would not be influenced by the enclosure, and the condition of zero flow a the ends of dead-end channels.

The result of the calculations for the vertical tide in a number of points is shown in fig 2. The amplitude of the vertical tide would increas landwards and in the region of the enclosing dam it would even be doubled places. The capacity of the inlets would increase considerably. The latter be clarified schematically as follows.

Without friction a standing wave would occur with a node at a 1/4 wav length λ from the closed end and an antinode at $1/2\lambda$. The "length" of the internal sea is reduced from $0,6\lambda$ to $0,2\lambda$ by the enclosure of the Zuider S This causes the flow in the inlets to increase. If friction is taken into count, the ratio of the amplitudes of the vertical tidal movement and the at the open end of a uniform channel can, for a sinusoidal tide, be descri by:

$$\frac{a_s^2}{a_h^2} = \frac{4\pi^2 b^2 u^2}{4\pi^2 + r^2\lambda^2} \cdot \frac{e^{2r\ell} + e^{-2r\ell} - 2\cos\frac{4\pi\ell}{\lambda}}{e^{2r\ell} + e^{-2r\ell} + 2\cos\frac{4\pi\ell}{\lambda}} \qquad (1$$

(see litt. 1, p. 113)

in which

a_s = amplitude of the flow
a_h = " " " vertical tide
u = velocity of propogation of the tide
λ = wave-length of the tidal wave
r = damping factor resulting from linear friction
ℓ = length of the channel
b = width " " "

The first factor in (1) is independent of the length of the canal. The sec factor is a damped oscillation about the value 1 . In the interval between $\ell = 1/2\lambda$ and $\ell = 1/4\lambda$ the value increases with decreasing ℓ. Between $\ell = 1/4\lambda$ and $\ell = 0$ the reverse is true. The "lengths" of the Wadden Sea and Z der Sea are respectively $0,2\lambda$ and $0,4\lambda$. By the enclorues of the Zuider

Sea the length is reduced from $0,6\lambda$ to $0,2\lambda$. Hereby, the ratio a_s^2/a_h^2 increases.

From the comprehensive tidal calculation it appeared that the increase was so great that it was feared that the tidal inlets would come into a dar gerous situation. This was one of the considerations which led to the enclosing dam being constructed somewhat to the north of where it was originally designed. By this means the danger to the inlets could to some extent be reduced. The length of the Wadden Sea then comes further under the $1/4\lambda$ so that the ratio a_s/a_h becomes smaller.

The increase in the capacity of the Inlet of Den Helder was reduced fi 30 % to about 25 % in this way.

During and after the enclosure, the development of the tidal movement was carefully observed. The results of the calculations of the S.C.L. appe ed to be in very good agreement with the actual development. In fig 2 the ual vertical M_2 tide has been drawn for several observation stations.

The adaptation of the tide to the new situation in some parts of the Wadden Sea took place more quickly than in others. This is partially depen on the adaptation of the channel system. As an illustration, fig 3 shows t tidal range before, during, and after enclosure for a number of observatio stations.

In this figure can also be seen the influence of the variation in the inclination of the moon's orbit to the equator. The period of the variatio is 18 2/3 years. Maxima occur in 1922, 1941 and 1960 and the influence on tidal range amounts to 1 1/2 - 2 %.

Correction of the observations since 1933 results in a tidal range wh decreases for Den Oever and Oude Schild, increases for Harlingen and Tersc ling and is almost unchanged for Den Helder and Kornwerderzand. This will referred to in chapter IV.

The regular flow measurements have also largely confirmed the results the tidal calculations.

Another important consequence of the enclosure was the formation of a watershed between the two main inlets of Den Helder and The Vlie.

With an open Zuider Sea, the tidal streams coming from these inlets w directed towards the Zuider Sea. Since the enclosure, the streams meet eac other in a region near Harlingen, and a watershed has been formed. Because shoaling usually takes place at a watershed, it was important to know whet and, if so, where, there was a chance of shoaling which could be a hindrar to navigation. The tidal calculation gave useful information about this tc The position of the watershed is very much dependent upon the slowly devel ing system of channels. The situation in this area has still not come to r and the development is regularly surveyed by means of water-level recorder soundings and flow measurements.

The work of the S.C.L. has thus proved that even for such a complicated ar as the Wadden Sea and Zuider Sea tidal calculations can be performed with success.

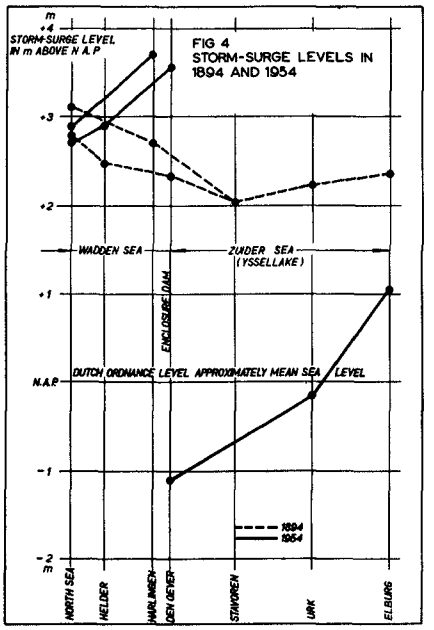

Fig. 4. Storm-surge levels in 1894 and 1954.

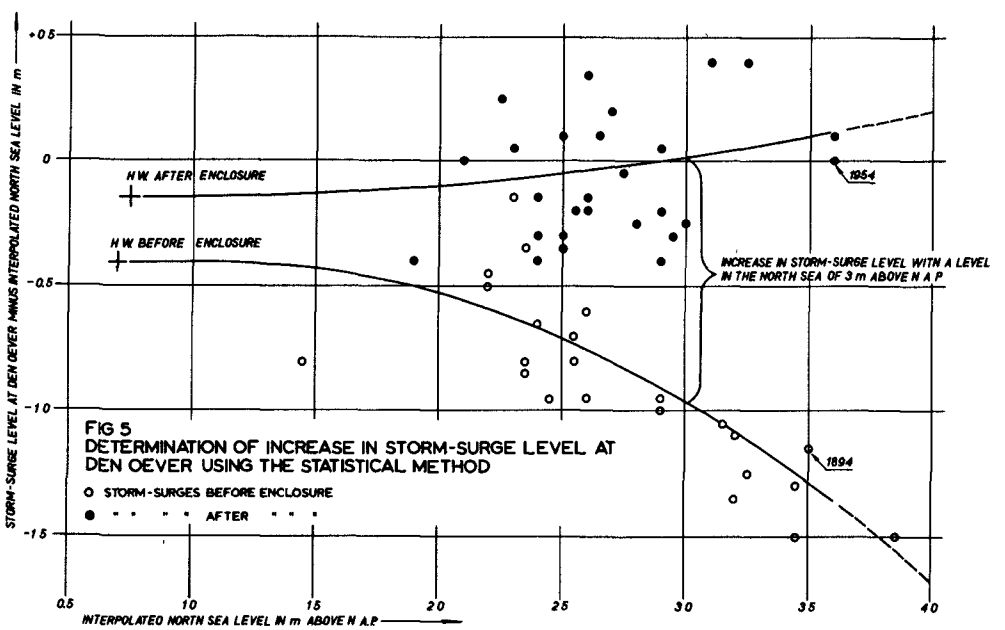

Fig. 5. Determination of increase in storm-surge level at Den Oever using the statistical method.

THE NATURAL DEVELOPMENT OF THE WADDEN SEA AFTER THE ENCLOSURE OF THE ZUIDER SEA

III. THE STORM SURGES

Northwesterly gales increase the water levels along the Dutch coast. As a result of the difference in head and the action of the wind, water flows through the inlets into the Wadden Sea and formerly also into the Zuider Sea. If the storm lasts for long enough, a state of equilibrium is reached between the force of the wind and the slope of the water surface. If the state of equilibrium is not reached, the maximum water level is not only dependent on the gale-force but also on the degree to which the basins behind the inlets are filled. The area of the Wadden Sea and Zuider Sea together was so big relative to the capacity of the tidal inlets, that even prolonged storms usually fail to produce complete filling right up to the equilibrium condition. In this way the Zuider Sea helped to reduce the highest water levels in the Wadden Sea.

After the enclosure the area was reduced from 5200 to 1500 km^2 and the capacity of the inlets is sufficient to cause complete filling of the Wadden Sea if the storm is prolonged. This can be shown by means of fig 4 in which the storm surge levels in the Wadden Sea (and Zuider Sea) are represented for the storms of 1894 and 1954, which were similar. It is clear from the slope of the lines that the situation in 1894 was still far from equilibrium. In 1954 equilibrium was almost attained. As illustration, several water levels in the IJssel Lake have been drawn in for 1954 to demonstrate the influence of enclosure in lowering the storm surge levels in the IJssel Lake (former Zuider Sea).

From fig 4 it also appears that the levels at Den Helder and Den Oever in 1954 were respectively 0,4 and 1,1 m higher than in 1894.

The task of the S.C.L. was now to predict how much the known storm surge levels would be raised as a result of the enclosure. It calculated the rise to be expected by various methods. In all cases the observations made of previous storms were used. There was no question of extrapolation of frequencies of storm surges because the aim of the enquiry concerned only the rise in known storm surge levels. The sea defences could then be raised so that the same degree of safety against breaching would exist as before the enclosure. The height required for the enclosing dam could also be determined from the enquiry. At the time of the S.C.L. the heights of dykes were not determined by using frequencies, but were based on the highest known storm surge level at that point.

The storm of 1894 was taken as the design condition, as it caused the greatest flow from Wadden Sea into Zuider Sea. For this storm very extensive stationary calculations were made, again using a Wadden Sea schematized as a network of channels. In addition, some trial calculations were performed using a method of integration by power series. It was not necessary to base this latter calculation on a permanent condition so that, in addition to the forces due to friction and hydraulic gradient, the momentum could also be taken into account. The calculation was, however, very cumbersome and could only be applied to a very much simplified network of channels. It was used to make corrections to the results of the stationary calculation. In general, the results of the non-stationary calculation were higher than those of the stationary, especially near the inlets.

After the storm surge disaster of 1953, the "Delta Commission" was set up, which in 1955 had to construct the frequency lines for the storm flood surges along the Dutch coast. These frequency lines had to show what water level was attained with a certain frequency at all points along the coast. The aim of this was to be able to design a height for a sea-defence which

would guarantee a degree of safety suited to the value of the area lying hind. For this, the frequency lines of the observation stations in the W Sea had also to be used. Because the period of observation since the enc ure of the Zuider Sea amounted to only 23 years and was therefore too sh for estimating very infrequent levels, the data from before 1932 had to treated in such a way that it fitted into the frequency lines found afte closure.

At the same time, it was possible to use this research to test the diction of the S.C.L. against actual conditions. Until then this had only done approximately for individual storms.

For the frequency lines, all storms from before the enclosure had t considered; it was not sufficient to calculate the rise for a few chosen storms.

The following methods were used for this:

1. STATISTICAL METHOD.

For each storm, the North Sea level "N" is derived from observation coastal stations which lie sufficiently far from the region influenced b enclosure. This derived North Sea level is therefore independent of the closure of the Zuider Sea.

The difference between N and the observed storm surge level at a ce station is plotted graphically against N. Two lines are then drawn; one through the points representing storms before the enclosure and one thro points from after the enclosure. The ordinate between these two lines gi the rise in storm surge level at a certain station as a function of the surge level in the North Sea outside the inlets.

In this fashion, all observations from before the enclosure can be verted to the situation after enclosure.

2. LINES OF RELATIONSHIP.

In this method each of the stations influenced by the enclosure is pared with a station not subject to such influence. The storm surge leve the two stations are plotted graphically, one against the other. As befo lines are drawn through points which represent levels before and after e closure. The ordinate between the two lines gives the rise at a certain ion as a function of the storm surge level at the other station. A Wadde station can of course be compared with more than one uninfluenced statio

Both methods have rather serious disadvantages. One of the most ser is that in this analysis, the duration of the storm is neglected and it this duration which is so important in connection with the filling of th Zuider Sea. At a station in the neighbourhood of the enclosing dam a pro ed storm before the enclosure can lead to the same water levels as a sho storm after the enclosure. In the analysis described above, no rise in s level would be noticed.

The points in the graphs therefore show a rather large scatter. It only the more or less uniform behaviour of the storms which prevents the scatter from being even greater. Fig 5 has been appended as an example o such a graph. In it, the rise in storm surge level for Den Oever has bee determined by the statistical method.

Finally, a hydraulic calculation was made for one particular storm usir a semi-permanent iteration method. This calculation served to give a better understanding of the course of the storm surge and to verify the results of the above mentioned methods for this particular storm.

Some results of the various calculations for three stations are given i Table 1.

TABLE 1.

Station	Rise in storm surge level in meters for a design storm as defined by the S.C.L.			
	S.C.L.	Statistical method	Lines of relationship	Hydraulic computation
Den Helder	0,42	0,7	0,95	0,55
Den Oever	1,08	1,4	1,15	-
Harlingen	0,64	0,75	0,7	1,0

The values given by the S.C.L. are in general too low. In the correctic of the stationary calculation incomplete account has been taken of the resul of the exact calculation. The latter gave deviations from the stationary cal culations which were much bigger in the inlets than along the coast of the Wadden Sea.

Afterwards, it appeared that the behaviour of the 1894 storm was such that it caused relatively high levels in the inlets so that the rise predict ed for the 1894 storm agrees, but for most other storms with the same North Sea level, the predicted rises would be too low. This is not a consequence c the method of calculation used but is dependent on which storm is chosen to define design conditions. The corrections which were applied to the final results with regard to other storms are wrong. The values found by means of the statistical method and the lines of relationship will deviate from reali for a certain storm, but they give a good approximation when it is a questic of correcting a large number of storm surge levels.

The hydraulic method is not capable of being applied to a great number of storms because of the great amount of work required.

Research in a hydraulic model, although possible in principle, would al so become too protracted to be applied in practice.

IV.TOPOGRAPHY OF THE BED.

GENERAL CONDITIONS.

A possible explanation of the mechanism of the Wadden Sea is as follows Before the enxlosure of the Zuider Sea, there existed in the Wadden Sea a certain relationship between the height of the Wadden, the rise in sea level and the transport of sand from the North Sea. The system of channels was adapted to the storage capacity of the region. If the transport of sand were to decrease, the increase in bed-level would be delayed with respect to the rise in sea-level, or in other words the delay in response would be greater. The storage reservoir would increase and thereby also the capacity of the in

lets and the system of channels behind, and this would continue until a r equilibrium was reached. The delay in response of the Wadden need not be same at every point. There are reasons for believing that the build up ir region of the inlets takes precedence over that further back in the Wadc Sea. Material which is brought in through the inlet will settle out in tl direct neighbourhood rather than further back. Furthermore, the wave move further back in the Wadden Sea is stronger than in the lee of the islands The height of the Wadden with respect to H.W. therefore decreases landwar from the inlet.

The bed of the Wadden Sea consists chiefly of fine sand. Silt hardly settles out at all; the Wadden are too exposed to the action of wind waves for this to occur. Only in sheltered corners and with artificial means, s as the reclamation works along the Frisian and Groningen coast, can the s settle out. Also the digestive processes of shell-fish cause some silt tc settle.

All sediments have their origin in the North Sea, as has been shown petrographic research. River sand or river silt is not found. Silt can al originate in clay layers in the Wadden Sea itself which become exposed anc eroded through the movement of channels.

The material for building up the bed must therefore come into the Wa Sea through the inlets. It may come from littoral drift, by erosion of tl North Sea coast and perhaps also directly from the bed of the North Sea. littoral drift alone is, according to van Bendegom (litt. 2), insufficier satisfy the sand hunger of the Wadden Sea.

During the last 50 years the relative rise in sea level amounted to 2 mm per year. For an area of 1500 km^2, the amount of sand required is 3×10^6 m^3 per year.

The stretch of coast on the North Sea which is influenced by the Wac Sea loses, owing to erosion, an amount of sand roughly estimated at about 1×10^6 m^3 per year. The amount of material which enters the Wadden Sea t the inlets is unknown. With the present day instruments and measurement t niques, it has proved impossible to measure a resultant sand- and silt-tr port with sufficient accuracy.

The amount of silt which arrives by discharge from the IJssel Lake i relatively insignificant, about 0.5×10^6 m^3 per year.

The enclosure of the Zuider Sea has had a big influence on the proce described above. As a result of enclosure, over almost the whole of the v Wadden Sea (as far as the Terschelling watershed), high water level has r from 0,1 - 0,3 m. This has the same effect as a sudden rise of a similar in the sea level. The sand hunger of the Wadden Sea has increased strongl a result.

Since the enclosure, bed-levels have been regularly sounded, especia in a strip 10 km wide along the enclosing dam.

A calculation of the difference in bed-level for this area over the period since enclosure, shows that, after correcting for the rise in sea level, an average of $9 - 10 \times 10^6$ m^3 per year of sand and silt is laid dc this is equivalent to 2 cm per year. The greater part of this material ha been deposited in the channels which have been blocked by the enclosing c

(7 - 8 x 10^6 m^3 per year). The sand flats, in so far as they are found in this area, have even become lower - about 1 cm per year. It must however be noted that a great proportion of the flats considered lie in the region of the Dove Balg, where the movement of water has increased considerably since the enclosure. The enlargement of the cross-sectional area available for fl may perhaps be sought outside the limits of the Dove Balg and extending ove the flats on either side.

There is also a possibility that material is disturbed by wave action and transported to the dead-end channels where it settles out and is thus taken out of circulation.

Since enclosure the transport of sand and silt to the 10 km strip considered has been greater than that which would correspond with the rise in sea level. Actually, it is even greater than would be necessary to keep up with the rise in sea level over the whole Wadden Sea. The origin of the material is not clear. It may be partly derived from the rest of the Wadden S but a large part must have come from the North Sea.

An approximate survey of the height of the flats behind Texel and Vlie land has shown that since the enclosure, these flats are becoming lower by an average of 2 - 3 mm per year. From this, a quantity of sand would be released of about 0,5 x 10^6 m^3 per year. If the other flats in this area beh similarly, then about 10^6 m^3 of sand per year can be taken up.

An attempt to establish a sand and silt balance for the western Wadde Sea gives the following result:

Settling in the strip c. 10 km wide, north of enclosing dam	10 x 10^6 m^3/year	
Taken up from the flats to the north of this area		1 x 10^6 m^3/year
Transport along the North Sea coast, according to van Veen (litt.8) amounts to 1 - 2 x 10^6 m^3 per year. If almost all of this enters the Wadden Sea, then we have		1 x 10^6 m^3/year
Coastal erosion can supply a maximum of		1 x 10^6 m^3/year
From erosion of the external deltas, maximum		1 x 10^6 m^3/year
IJssel Lake silt		0,5 x 10^6 m^3/year
Directly from the North Sea, errors in the above estimates and unknown sources		5,5 x 10^6 m^3/year
	10 x 10^6 m^3/year	10 x 10^6 m^3/year

From the above data and assumptions, about 8 x 10^6 m^3/year enters the western Wadden Sea through the inlets. The capacity of the inlets of Den Helder and the Vlie together amount to 2 x 10^9 m^3. If it is assumed that half of the transport takes place over the bed and the other half in suspe ion, then a difference in concentration of 4 - 5 mg/l would be sufficient carry 4 x 10^6 m^3/year of suspended solids into the Wadden Sea. As the aver content is 40 mg/l, the accuracy of measurement would have to be better th 10 % to be able to show this resultant transport. Bed transport measuremen are even less accurate than measurements of transport in suspension. The c clusion is therefore that in the western Wadden Sea a large amount of mate is deposited, the origin of more than half of which is unknown. Measuremen of transport in the inlets cannot provide any information because of the r

Table 2

Hydrographical data of Wadden Sea

nr	station name	mean tidal conditions: max.velocity in m/sec flood	max.velocity in m/sec ebb	max.discharge in 10^3 m^3 flood	max.discharge in 10^3 m^3 ebb	tidal priem in 10^6 m^3 flood	tidal priem in 10^6 m^3 ebb	area of cross-section in m^2	C $m^{\frac{1}{2}}$/sec	τ_{max} N/m^2	$u_{*\,max}$ m/sec	bed material 1)	development of cross-section 2)
1	Marsdiep	1,8	1,6	72,0	64,0	930	1020	54.000	53	6,4	0,08	I, II	1,04
2	Texelstroom W	1,4	1,4	46,0	43,0	615	710	44.500	53	3,8	0,06	II, III	0,88
3	Wisrbalg	0,8	0,6	-	-	-	-	3.200	50	3,9	0,05	II, III	0,48
4	Dove Balg O	1,2	0,8	16,0	10,8	170	170	15.200	50	4,4	0,06	I	1,26
5	Inschot	0,8	1,0	8,4	7,0	120	125	10.700	50	2,5	0,05	II	0,67
6	Blauwe Slenk	1,0	0,9	8,2	5,9	130	100	9.000	50	3,3	0,06	I, II	1,16
7	Pannengat	"	-	7,0	7,5	115	135	8.000	50	3,5	0,06	I	
8	Vlietstroom	1,3	1,2	31,5	25,5	475	425	25.000	52	5,9	0,07	I, II	1
9	West Meep	1,6	1,1	21,0	22,0	350	375	18.500	52	5,2	0,07	II	1,28
10	Vlierede bij Caranan	1,3	1,1	-	-	-	-	40.000	53	6,0	0,08	I	1,20

1) Classification - I - coarse sand, often with gravel and shell remains
II - sand with very little or no silt
III - half sand - half silt to sand with little silt

2) Development of cross-section = $\frac{\text{area in 1950-1960}}{\text{area before enclosure}}$

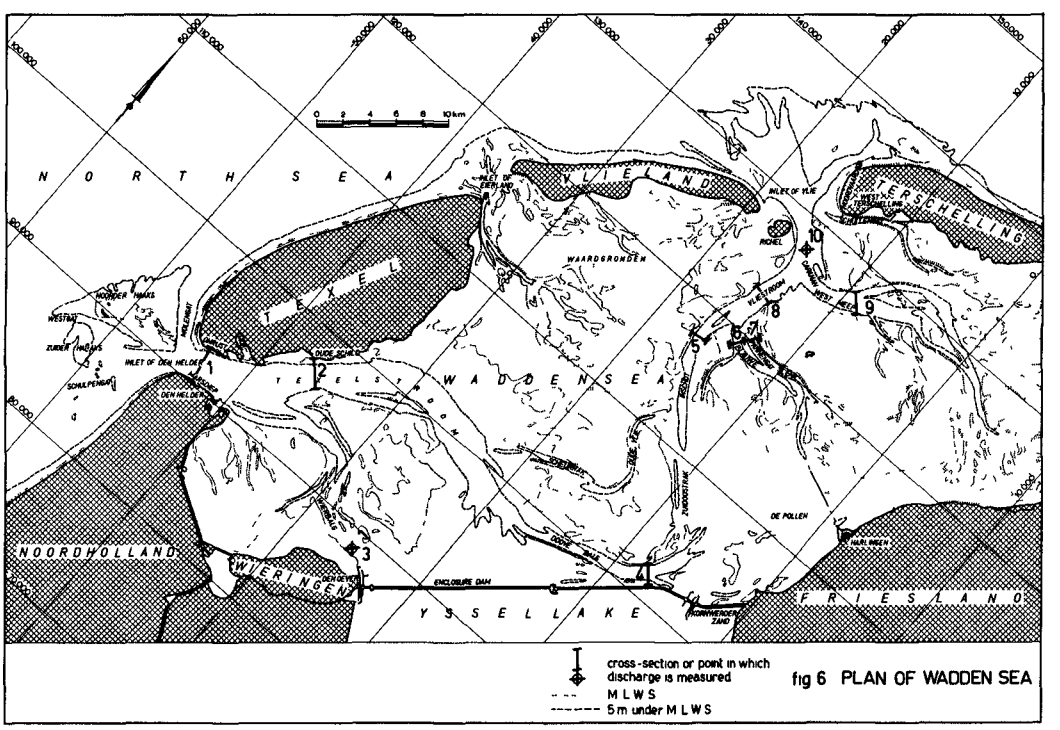

fig 6 PLAN OF WADDEN SEA

Fig. 6. Plan of Wadden Sea.

quired accuracy of measurement. The only available method appears to be t establishment of sand and silt belances over long periods using soundings beach measurements over the whole area which is influenced.

Special considerations (see fig 6).

The systems of channels running from the Inlet of Den Helder and the let of Vlie meet each other in an extensive area of zero horizontal tide the neighbourhood of Harlingen. Formerly, both systems ran approximately rallel to the Zuider Sea. A resultant water transport from the Inlet of D Helder to the Inlet of Vlie hardly occurs. For both inlets, the volume of ebb is almost equal to that of the flood.

The connections between the two channel-systems originated in the ph lag between the tide in the inlets of Den Helder and Vlie.

After the enclosure, two connections remained north of the enclosing namely the Dove Balg and the Scheurrak - Oude Vlie channel.

The tide comming from the Inlet of Den Helder is so much earlier tha that coming from the Inlet of Vlie that both connections are entirely und the influence of the former inlet. The flood in the Scheurrak meets that the Vlie near the confluence of the Oude Vlie with the Inschot. Because o this, the flows in the former channel have somewhat decreased.

The Dove Balg however, at present, carries a large quantity of water the direction of Harlingen and the cross section of this channel has incr appreciably since enclosure.

This growth in cross section causes the tide on the east side to arr earlier, so that the area of influence is still increasing. Moreover, beca of this, the tidal range in the area round Harlingen is still increasing slightly. From fig 3 it is seen that for Harlingen, after correction for influence of the inclination of the lunar orbit, there is an average incr in the tidal range of 3 cm in 20 years. Because of the growth of the Dove the tidal range at Oude Schild is decreasing, as also can be seen in fig The earlier appearance of the tide at both stations is in agreement with

The channels to the north and east of Wieringen, which formerly carr water to the Zuider Sea, now cater for the filling of only a small area r Wieringen. Their dimensions are therefore rapidly diminishing. As a resul this, the tidal range at Den Oever has somewhat decreased since the enclo (see fig 3).

The Texelstroom remains almost unchanged, except for the eastern par The discharge here has also varied little since the enclosure.

The Marsdiep, the throat of the Inlet of Den Helder, also hardly var in cross section, although the max. discharge here has increased by about The southern shore has been stabilised and the depth is very great, in pl 45 m. The bed consists of coarse sand. It is not known why the cross sect area remains practically constant.

The channels which are influenced by the Inlet of Vlie are, with the exception of the Inschot, becoming larger. This is a consequence of the i creased tidal movement in this area, which was predicted by the S.C.L.

The tide at Terschelling has been increasing rather rapidly since en-

closure (about 7 cm in 20 years). This would indicate an influence of the i let between Terschelling and Ameland in which the tidal movement is stronge than in the Inlet of Vlie. Since enclosure, the tide at Terschelling arrive earlier. This is in contradiction to the assumption made above. The actual cause of the behaviour of the tide at Terschelling is unknown.

The Inschot has not grown because the discharge here has not increasec as a result of the watershed which has formed near by.

An interesting area is the Pollen. This is a basin with an almost hori zontal bed with several very shallow channels. The explanation of the origi of this area (where actually a rather high flat might have been expected) i possibly as follows. The area was formed by erosion of the upper peat laye and/or by transgression. The supply of material from the North Sea was not sufficient to keep up wich the rise in sea level over the whole of the Wadc Sea and the flats in the neighbourhood of the inlets received the greater p of the material. The shortage was felt chiefly in the area lying farthest landwards, that is the Pollen. The build up of the bed or formation of flat therefore lags far behind the increase in sea level. In addition, wave atta can be playing a part. With SW to N winds (the direction of gales) the area lies the farthest behind the sheltering row of islands so that the waves hea are high. Fine sediment (other sediment never settles in this area) is there fore easily brought into suspension and is then carried further by the curr This process does not occur exclusively at times of storm surges, because t bed is at 2 - 3 m below mean sea level and is soon disturbed by the movemer of waves.

In general, the behaviour of the channels corresponds quite clearly tc the movement of the water. In table 2 the results of flow measurements in a number of channels are presented. The lines along which discharge is measur are shown in fig 6. The measurements were performed in 1957 - 1959. By mear of this data and from measurements of hydraulic gradient, several factors h been calculated such as Chézy's coefficient C, the bed shear stress τ_{max}, the shear-velocity $u_{*\,max}$. These last two factors were calculated using the following formulae:

$$\tau = \rho g \frac{Q^2}{A^2 C^2} \qquad \text{Newtons/m}^2 \qquad (1)$$

$$u_* = \frac{\sqrt{g}}{C} \cdot \frac{Q}{A} \qquad \text{m/sec} \qquad (2)$$

where C = Chézy's coefficient in $m^{\frac{1}{2}}/sec$
A = cross sectional area in m^2
τ = bed shear stress in Newtons/m^2
ρ = density of water in kg/m^3
g = acceleration due to gravity in m/sec^2
Q = max. discharge in m^3/sec
u_* = shear velocity in m/sec

Further, at the end of the table, the type of bed material and the behaviour of the cross sectional area are described.

The influence of the external deltas.

The existence of an external delta at an inlet which is subject to strong tidal movement, is a common phenomenon. The external delta provides bridge for the littoral drift across the perpendicular flow in the inlet. I the transport takes place in the form of banks which erode on one side and accrete on the other and transplant themselves in their entirety across the

external delta. A cyclic process of this type can be observed in the delt the Inlet of Den Helder. However, the Noorder Haaks is here exeptional. T is presumably a very resistant bank which maintains almost the same posit The banks moving up from the south unite with the Noorder Haaks and from a flat makes the crossing of the northern channel of the delta and joins i self to the island of Texel.

To the south of the Noorder Haaks lie two channels: Schulpengat and Westgat. At the moment, the Westgat is being pushed against the Noorder H by the Zuider Haaks and is sanding up. The Schulpengat is therefore begin to take over the function of the Westgat and a new Schulpengat is being f along the coast of North Holland.

To the north of the Noorder Haaks lies one channel, the Molengat. Thi too is moving from south to north, under influence of the pressure of the bank which is moving from the Noorder Haaks to Texel. A former Molengat c be discerned in the Mok on Texel. The Onrust is a bank which has crossed c This course of events was shown by Ir.Grijm at the congress in Scheveninge in a film which was made by means of successive sounding charts.

The development of the Inlet of Vlie is much less clear. If it exist cycle here apparently takes much longer to complete.

However, the pressure of the eastern part of Vlieland is quite evide Because of this pressure, the inlet is being driven eastwards.

The western end of Terschelling, the "Noordvaarder", is a flat which united with Terschelling in about the 17th century. Old publications menti a navigable channel which connected with the North Sea directly to the we of the harbour of Terschelling.

The swinging of the channels in the external delta influences the ori ation of the channels on the inside of the inlet. The transport of sand is probably not the same during the various phases of the development.

The Eierlandse gat, between Texel and Vlieland experiences a similar course of events as the Inlet of Den Helder. Here there is only one main channel.

The cross-section of this inlet is increasing quite rapidly, probably a result of the shortage of sand in the external delta and a relatively sm littoral drift.

The development has apparently been influenced by the enclosure of th Zuider Sea. From 1911 to 1930, the cross sectional area oscillated about a value of 10.000 m^2; after 1930 it increased to 15.500 m^2 in 1960.

Future development.

The most important factors here are:
- the relative rise in sea level
- the transport of sand to the Wadden Sea
- coastal engineering

There is little known about the future movement of the sea level. Thi is dependent upon the climate on the earth and upon many other factors whe by the ratio of water to ice is altered. Observations over the whole earth indicate both rising and falling sea levels.

However, seeing that an important part of the relative rise in sea le is caused by consolidation of sediments and subsidence of the earth, it ca be assumed that the present movement will continue for the next few centur although perhaps at a different rate.

The amount of sand arriving will decrease because the Dutch and Belgi coasts are being increasingly protected against erosion by means of groyne In some places, harbour piers are being built far out into the sea (IJmuid Europoort) whereby the littoral drift is interrupted, at least for some tim

As long as the North Sea does not become shallower, no increased tran port of material from the sea bottom is to be expected.

The expectation is therefore that, if the present rise in sea level c tinues, the Wadden Sea as a whole will undergo little change. Owing to the shortage of sand, it is possible that the delay in response of the Wadden increase. The relative lowering and diminution of the flats which will acc pany this, can cause an increase in the capacity of inlets.

Local changes will continue to occur, especially in the area which is fluenced by the enclosing dam.

It is conceivable that in the distant future all the Wadden or a larg part of it will disappear and a region will be created similar to the pres day Pollen.

There are various reasons for wanting to terminate the existence of t Wadden Sea.

By closing the inlets, the coast line would be appreciably shortened. This would yield greater safety as well as economic advantages. The closur is technically possible especially now that in the Rhine delta so much ex perience will be gained in large closures.

The removal of the sand hunger of the Wadden Sea would cause the coas erosion along the North Sea to decrease. The external deltas would disappe and a clear coast would arise such as that of North and South Holland. Bec of this, it is possible that the heads of the Wadden islands, which now pr into the sea because they are sheltered behind the external deltas, would attacked and serious local erosion would occur.

Owing to the build up of the bed, the clay and peat layers of the Hol cene which still exist will be buried to increasing depths under new sea l If it is the intention to use the Wadden for agricultural purposes in the future, the closure of the inlets must not be delayed for too long.

A study of the soils in 1950 - 1952 showed that by means of deep plo on the flats between Den Helder and Wieringen, 64 % or 50 km^2 of clayey s heavier soil can be reclaimed and on the flats behind Texel and Vlieland or 120 km^2. If the sand were to continue covering the flats, these areas decrease.

At the moment there are no concrete plans for large civil works in t western Wadden Sea. Activity is temporarily diverted to the south, to the urgent closures in the Rhine delta.

The future will doubtless see the closure of the inlets of the Wadde Sea. This closure may be partial and may or may not be accompanied by wo

of reclamation.

REFERENCES

1. Staatscommissie Zuiderzee (1918 - 1926). Report of the State Commission for the Zuider Sea. Algemene Landsdrukkerij. The Hague, 1926

2. Various authors (1950). Waddensymposium. Reprint from the Tijdschrift Koninklijk Nederlandsch Aardrijkskundig Genootschap. May 1950.

3. Postma, H. (1954). Hydrography of the Dutch Wadden Sea (thesis).

4. Wemelsfelder, P.J. (1960). On the use of frequency curves of stormflood Proceedings 7th Conference Coastal Engineering, The Hague, Netherl Aug. 1960.

5. Wiggers, A.J. (1952). De bodemgesteldheid van het westelijke Waddengebi Rapport van de Directie van de Wieringermeer - Landbouwkundige afd (The nature of the bed in the western Wadden Sea. Report of the Bc of the Wieringermeer - Agricultural Department).

6. Vlam, A.W. (1936). Resultaten van een onderzoek naar de kaarten van het zeegat van het Vlie van de 16e eeuw tot 1800. (Results of research to the maps of the Inlet of Vlie from the 16th century until 1800) Tijdschrift Koninklijk Nederlandsch Aardrijkskundig Genootschap, 1 pp. 202 - 209.

7. Burght, J.H.van der (1936). Veranderingen in de zeebodem van het zeegat het Vlie en in de kustlijn der Waddeneilanden Vlieland en Terschel ling. (Changes in the sea bed of the Inlet of Vlie and in the coas line of the Wadden islands, Vlieland and Terschelling). Tijdschrif Koninklijk Nederlandsch Aardrijkskundig Genootschap, 1936, Volume pp. 212-237.

8. Veen, J.van (1936). Onderzoekingen in de Hoofden in verband met de gest heid van de Nederlandsche kust. (Research in the English Channel i connection with the condition of the Dutch coast), The Hague, Alge mene Landsdrukkerij.

9. Bruun, P. and Gerritsen, F. (1960). Stability of Coastal Inlets. North Holland Publishing Company, Amsterdam.

10. Dillo, H.G. (1960). Sandwanderung in Tideflüssen. Mitteilungen des Fran Instituts für Grund- und Wasserbau der TechnischeHochschule, Heft Hannover. (The movement of sand in tidal streams. Report of the Franzius Institute for Civil Engineering of the Technical Universi of Hannover, Volume 17).

11. Horst, H. (1960). Die Geschwindigkeitsverteilung in offenen Gerinnen be turbulenter Strömung und ihre Beziehungen zum Geschiebetransport. Deutsche Gewässerkundliche Mitteilungen, Jahrgang 4, Heft 3 und 6. (Velocity distribution in open channels with turbulent flow and it effect on the bed load).

CHAPTER 43

THE INFLUENCE OF SHORE PROTECTION WORKS ON GULLIES

T. Groot
Engineer, Rijkswaterstaat
Research Division Vlissingen

When studying charts showing the bottom-topography of estuaries in the South-West of Holland, it is striking that in the longitudinal development of gullies local depths occur, which are much greater than the average depth. From a closer consideration it appears that the deepest points are always situated near protective works against erosion of the shore.

The connection between the shore protection works and the deep scourholes and its influence on the gully-system will be dealt with in this paper.

INTRODUCTION

It appears that on sandy shores the construction of shore-protection often causes rapid erosion, which gradually develops more or less parallel to the shore. Thus unprotected nearby parts of the shore are often attacked with increasing force, necessitating an extension of the shore protection works. This will lead to further scouring of both the unprotected part of the shore and the gully in front of it; the result of the latter will be a trough of considerable length. The location of the gully will as a consequence be fixed for a long time.

THE DEVELOPMENT OF SOME SCOUR-HOLES

The gullysystem in the south-west of the Netherlands has been reproduced on figure 1, on which depths greater than N.A.P. - 10 m have been shaded, while scour holes are indicated as black spots. (The Netherland ordnance datum N.A.P. is practically equal to mean sea level). Shore-protection works are shown as fat parts on the shoreline. The connection between shore protectionworks and scour-holes is clearly visible.

In case of erosion of the shore the construction of shore protection works is generally thought necessary. An unsuitable shape of those constructions often causes progressive erosion.
This statement will be supported by a number of examples. The areas dealt with in detail are indicated on figure 1.

JONG BRESKENS POLDER

In past century the tidal-channel Wielingen has changed its location. The section near Nieuwe Sluis advanced to the shore. The eastern and (especially) the western reaches moved to the north. See figures nos. 2, 3, 4 and 5 with the situations of 1825, 1865, 1875 and 1952/1958.

The changing of the adjoining gully system and (for the western section) the sanding of the Zeeuwsch Vlaanderen coast influenced the displacement of the Wielingen. It is surprising however that the gully near Nieuwe Sluis moved southward instead of northward.

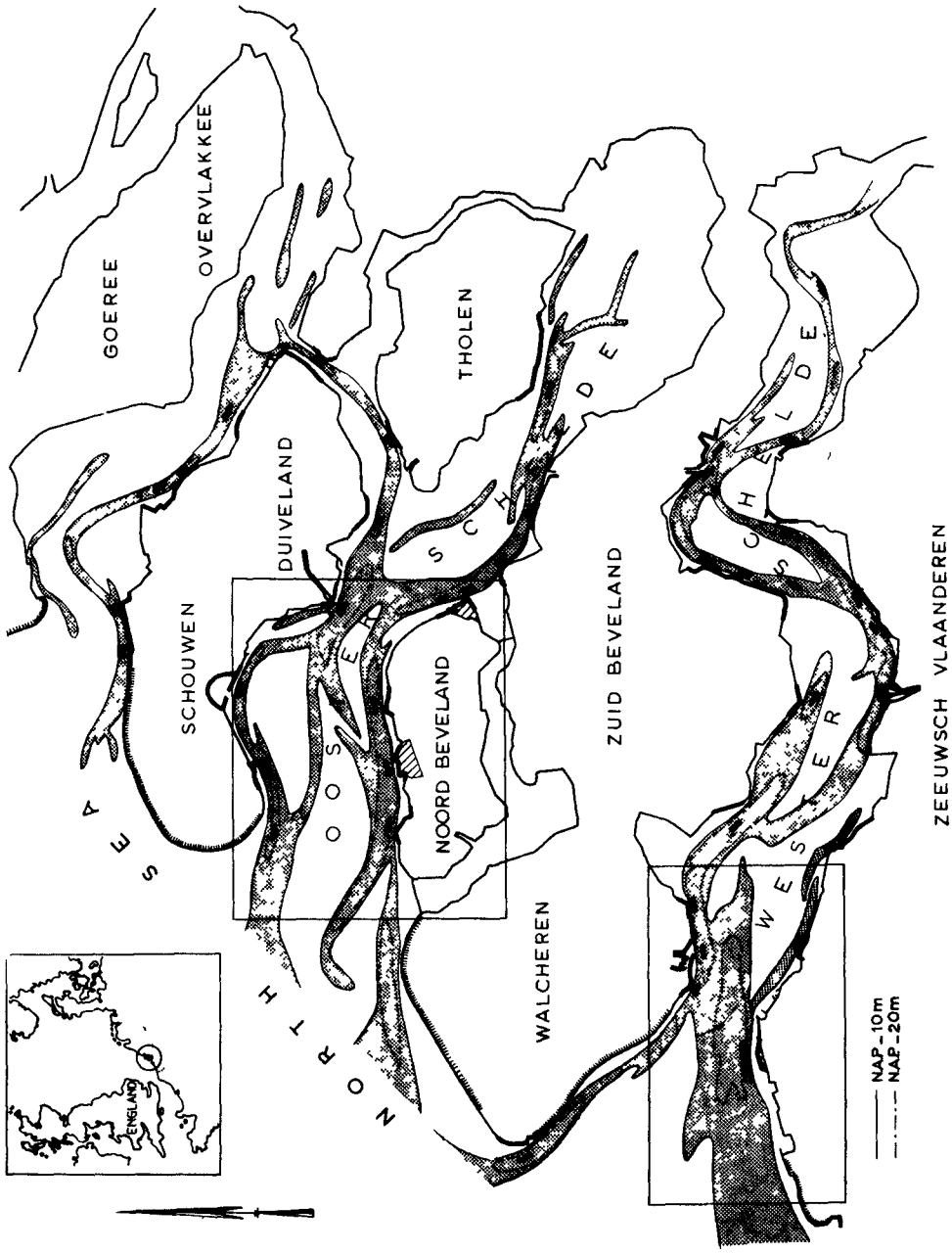

Fig. 1. Shore-protection works and scourholes in the south-west of the Netherlands.

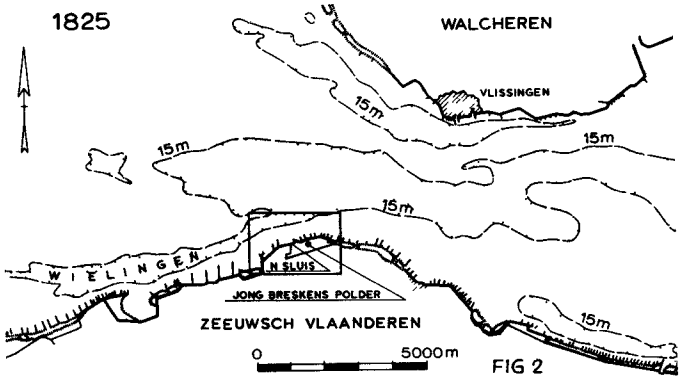

Fig. 2. Depth-contours in the Westerschelde-mouth (1825).

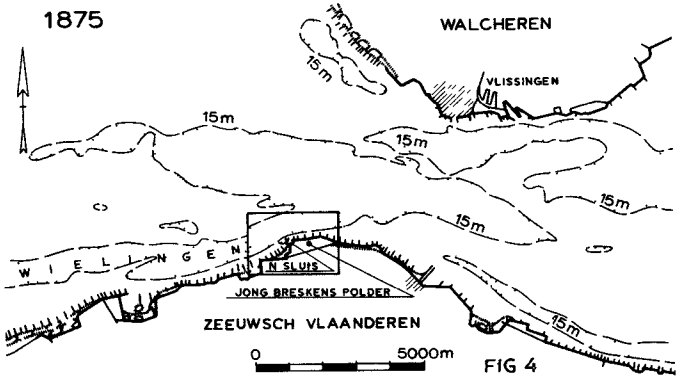

Fig. 4. Depth-contours in the Westerschelde-mouth (1875).

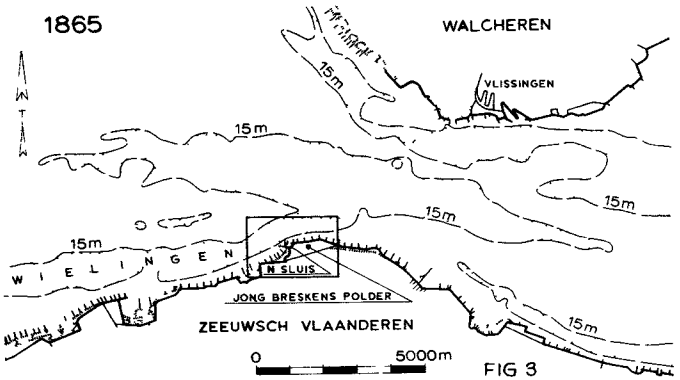

Fig. 3. Depth-contours in the Westerschelde-mouth (1865).

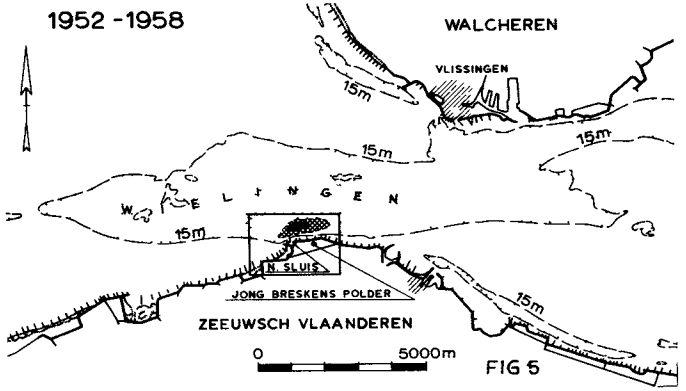

Fig. 5. Depth-contours in the Westerschelde-mouth (1852-1958).

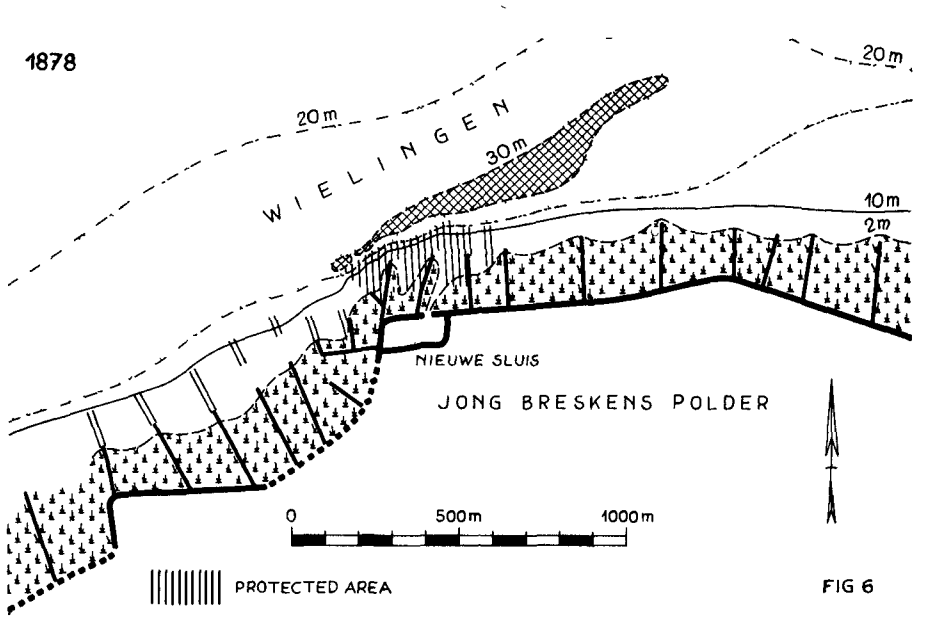

Fig. 6. Early-development near Nieuwe Sluis (1878).

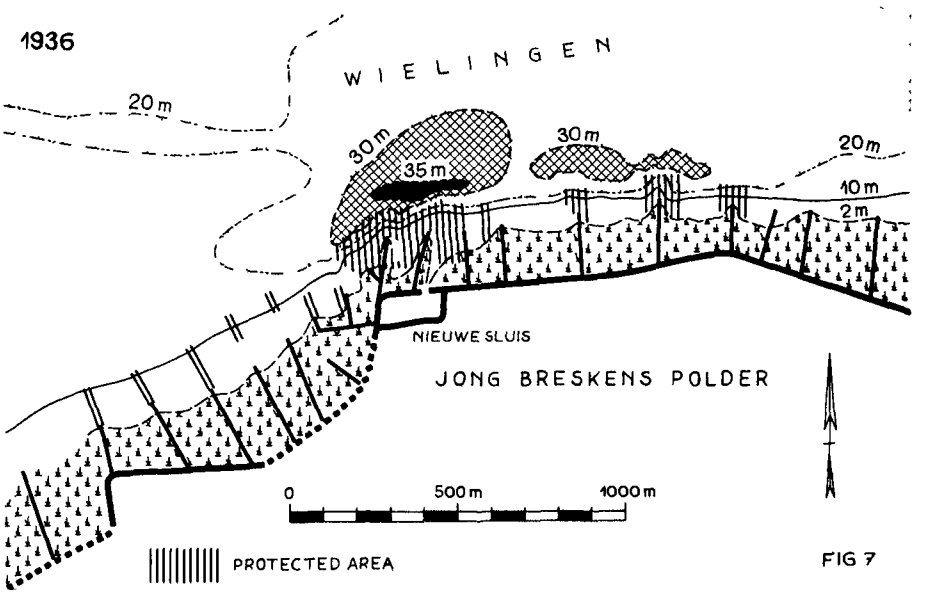

Fig. 7. Scourholes near Nieuwe Sluis caused by badly shaped shore-protection works (1936).

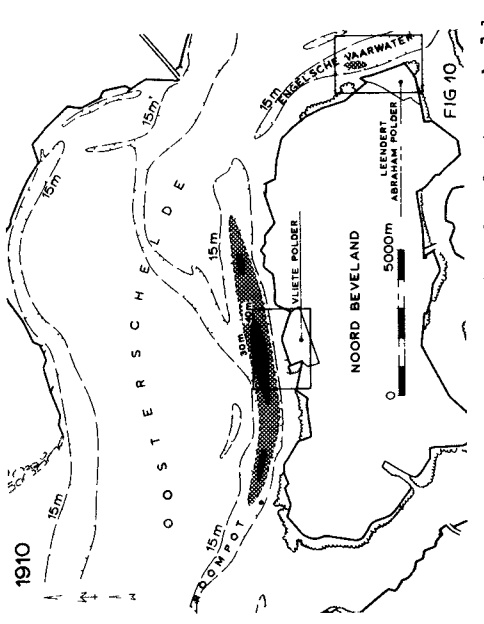

Fig. 10. Depth-contours in the Oosterschelde (1910).

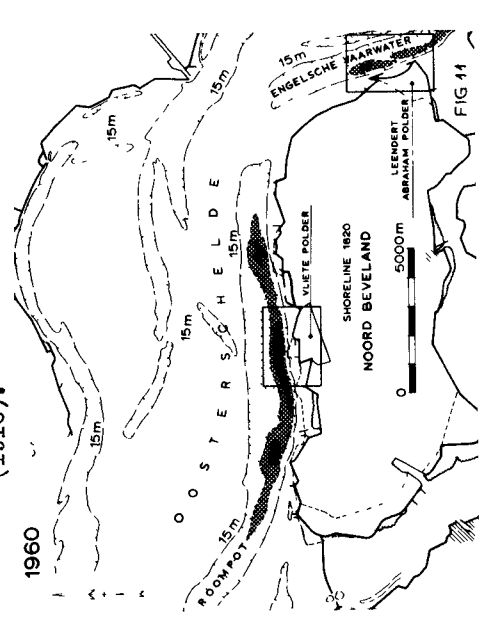

Fig. 11. Depth-contours in the Oosterschelde

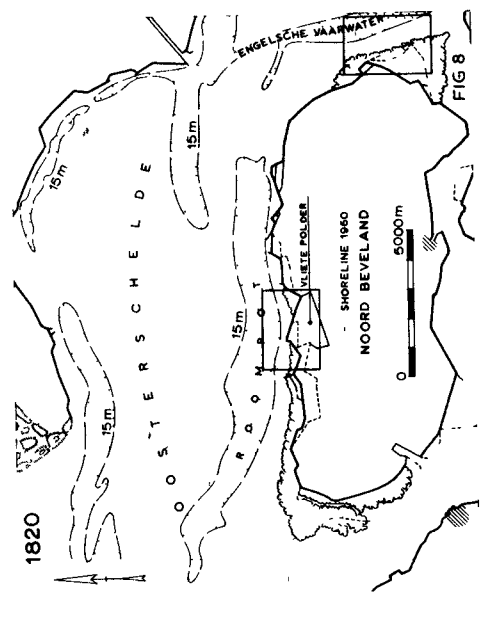

Fig. 8. Depth-contours in the Oosterschelde (1820).

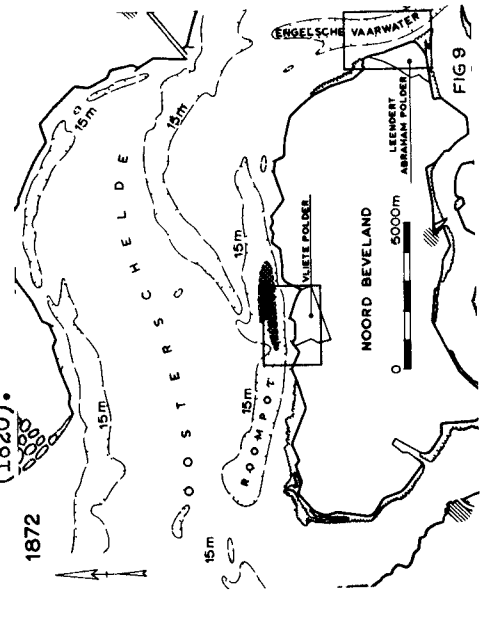

Fig. 9. Depth-contours in the Oosterschelde

THE INFLUENCE OF SHORE PROTECTION WORKS ON GULLIES

At the end of the 18th and at the beginning of the 19th century some polders west of Nieuwe Sluis were flooded. Owing to this Nieuwe Sluis got a relatively more advanced situation with probably some contraction of the stream.

Before 1830 the shore was already protected at some points by means of rip-rap. At several points mattresses (willow mattings) have since then been placed. They are indicated on the figures nos. 6 and 7.

Because of the irregular shape of these constructiόns the currentpattern was unfavourably influenced, causing considerable deepenings to the adjacent unprotected shore, which were attended with dozens of falls and slides. Parts of the protectionworks were thus lost. Extension proved to be necessary.

About 1880 an uninterrupted protection was reached. Some 90.000 m2 of the underwatershore had been covered with matresses and with 65.000 tons of rip-rap.

This bastion has influenced the stream in the gully. Local scouring of the sand-bed occurred; see the figures nos. 6 and 7 with the situations of 1878 and 1936. The bottom topografy shows that the scourholes are due to turbulence and not to the normal tidal stream.

VLIETE POLDER

Early in the 19th century some parts of the northern shore of Noord Beveland were affected partly because of the irregular shore line; see figure no. 8.

The first protection was introduced about 1820 in front of the Vlietepolder, where some attacked places were protected with small mattresses covered with rubble-stone. Later on these constructions were connected to the shore by means of submerged rubble-dams. This way of protecting the shore caused considerable erosion up to N.A.P. - 40 m, where formerly a depth of 15 m was sounded.

After some time 60.000 m2 of the underwater shore was covered with mattresses and with 80.000 tons of rip-rap. Also because the mattresses were placed over the existing constructions (so far as still present) a very irregular and unequal topography of the protection works developed.

The gully in front, the Roompot, moved to the shore, causing local depths of N.A.P. - 45 to 50 m; these pits enlarged in the longitudinal direction of the gully; see the figures nos. 8, 9, 10 and 11 with the situations of 1820, 1872, 1910 and 1960.

Owing to the southward movement of the gully many falls and slides occurred, through which the shoreline drew back; see the figures nos. 12, 13 and 14.

LEENDERT ABRAHAM POLDER

The above mentioned development led to the enlargement of the Roompot's profile. This may have caused an increasement of the gully's capacity which will have influenced the development of the adjacent gullies by changing the distribution of the tidal-water in the different gullies of the sea-arm. The changing of the slope of

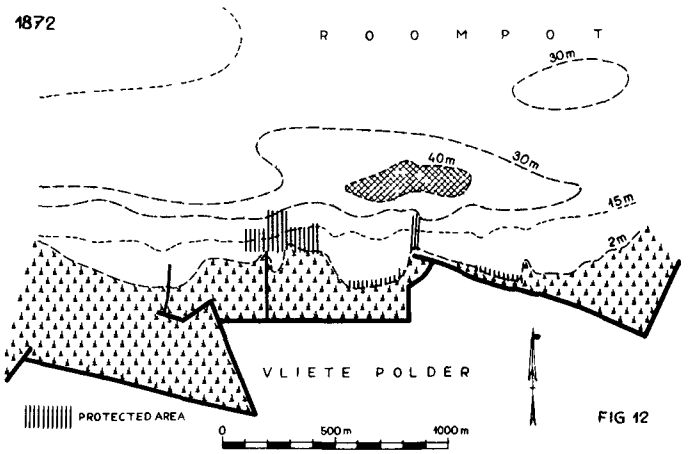

Fig. 12. Early development near Vliete Polder (1872).

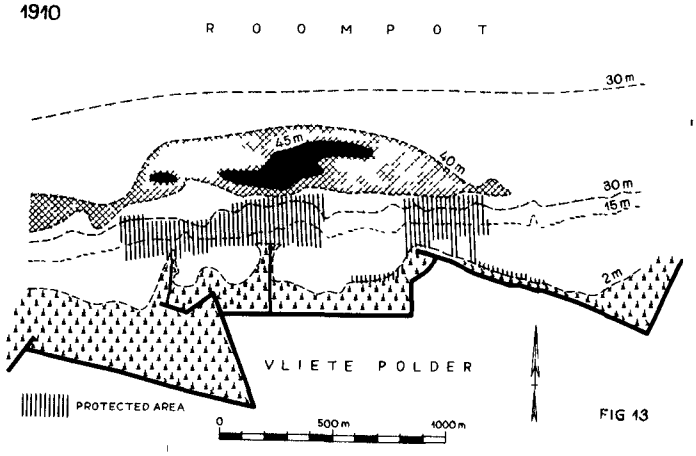

Fig. 13. Protection-works-caused erosion near Vliete Polder (1910).

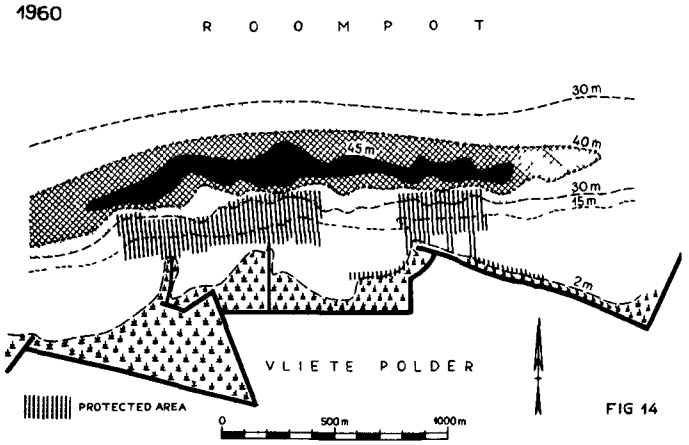

Fig. 14. Further erosion near Vliete Polder (1960)

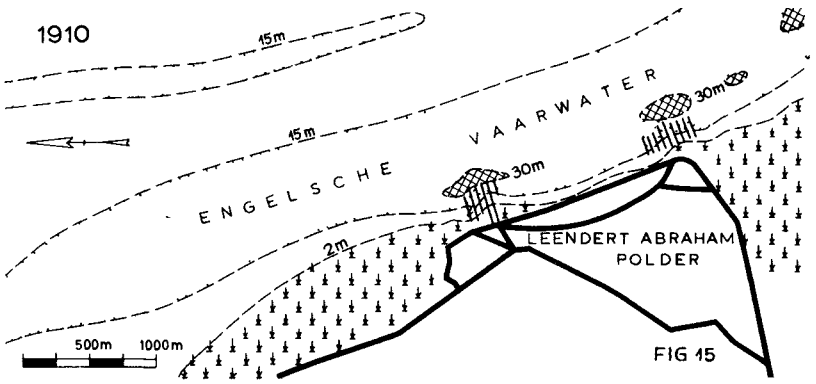

Fig. 15. Early development near Leendert Abraham Polder (1910).

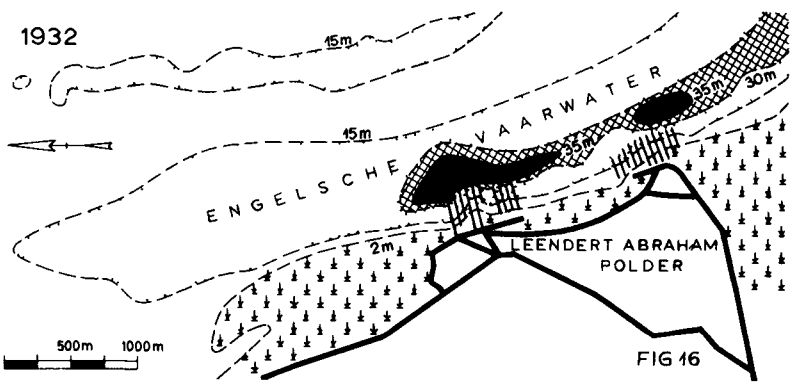

Fig. 16. Protection-works-caused erosion near Leendert Abraham Polder (1932).

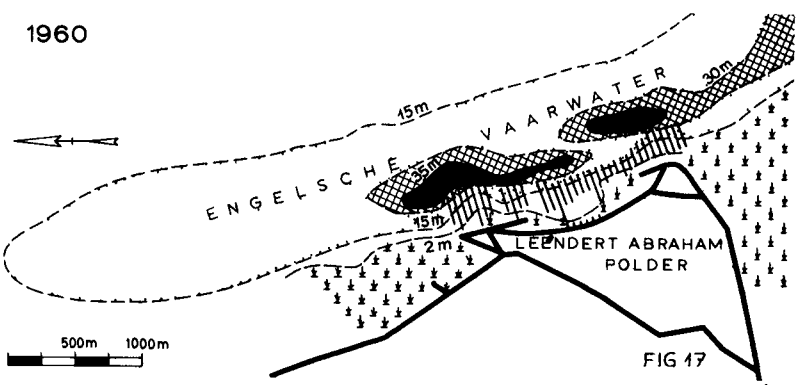

Fig. 17. Further erosion near Leendert Abraham Polder (1960).

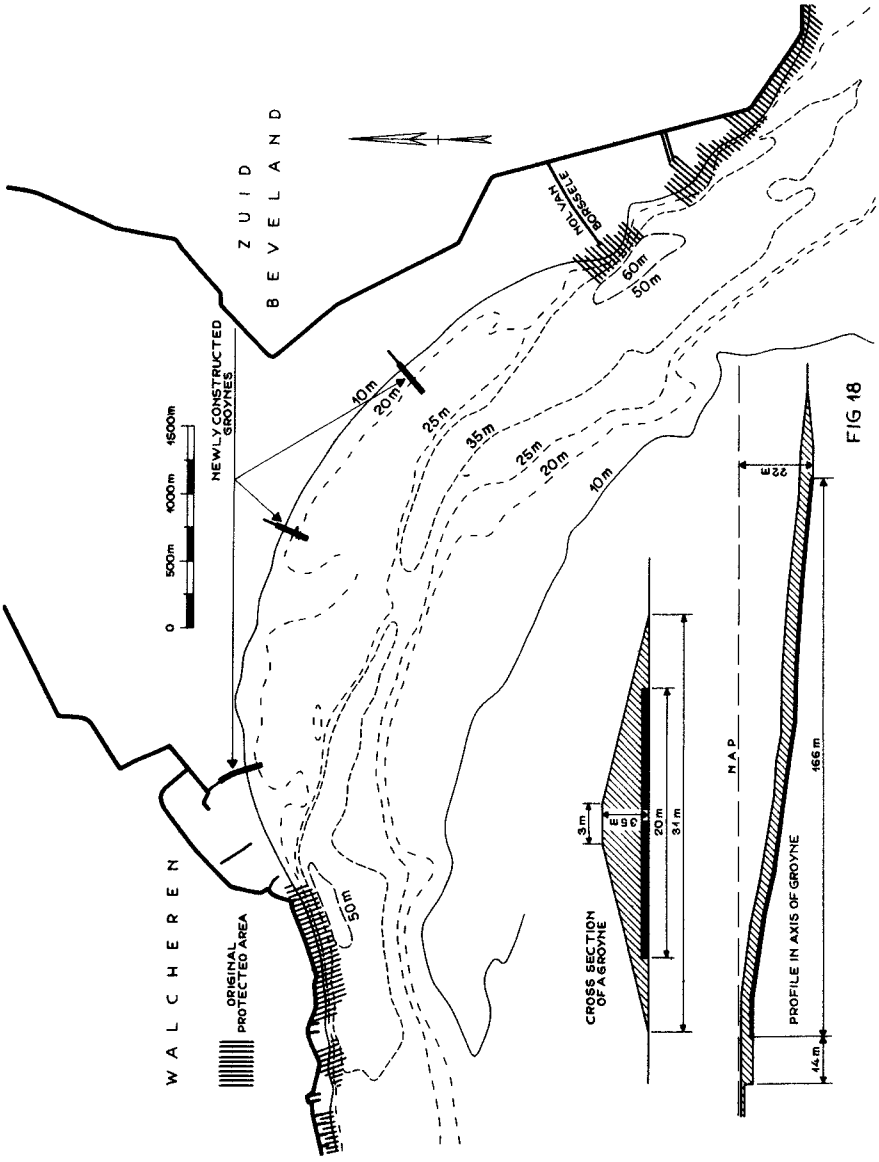

Fig. 18. Protection-works between Walcheren and Zuid-Beveland.

the watersurface between the gullies Roompot and Engelsche Vaarwater forced the latter to move westward, though some curve-effect cannot be neglected; see the figures 8, 9, 10 and 11. Other developments may be noticed too, which will not be dealt with in this paper.

The Engelsche Vaarwater moved to the west, attacking the most eastern part of Noord-Beveland, the so-called Leendert Abraham Polder.

About 1880 it was thought necessary to protect the shore. Two extensive shore protection works were built.

Near these works scourholes were formed, necessitating an expansion of the protection: 300.000 m2 of the shore were covered with mattresses and with 300.000 tons of rip-rap.

After this local scouring up to N.A.P. - 45 m took place. The gully moved to the shore and was held there.

A picture of the development is given by the figures nos. 15, 16 and 17, which also show the retiring of the shoreline, owing to numerous falls and slides, causing the destruction of the initial dike.

SUPPLEMENTARY REMARKS

Shore protection works are built to divert the stream from an attacked shore or to reduce the effect of the stream.

With the construction of a shore protection work of rip-rap with of without mattresses the watermovement next to the work will be disturbed by turbulence near the bottom.

By the building of groynes moreover the velocity gradient in a cross-section of a stream will increase.

In both cases the result is erosion of the unprotected parts of the shore. After some time these parts will have to be protected too. In this way a bastion of rip-rap or an extended series of groynes will be obtained in due course.

In front of both such a bulwark and such groynes the velocity-gradient will be so great that deep pits will be formed. By the turbulent stream these pits will be eroded to troughs in the direction of the stream.

A great part of the discharge which passes through the total cross-section of the sea-arm will take its way via this deepened gully which will in general develop into a main gully at the expense of the by-gullies.

The influence of shore-protectionworks appears to be effective even when built in deteriorating gullies.

The developments described are due to an imperfect design of the defenceworks. A badly shaped construction causes a strongly turbulent currentpattern, as a result of which powerfull erosive forces come into being. This can be prevented by giving a better design to the defence-works.

A protection made of rip-rap will have to be constructed in such a way that it doesn't show high and irregular elevations.

When the shore is not steep yet, it will be best to build groynes under a mild slope, equal to the slope of the shore, through which in fact a submerged stoneridge is created.

Laboratory-tests proved that with a slope of 1 : 8 the deepening in front of the groyne is small, while little regression of the shore between the groynes takes place. Steeper slopes than 1 : 8 are not to be recommended. This subject is treated in detail in (1) and (2).

Recently the slightly eroding shore between Walcheren and Zuid-Beveland has been fixed over a length of about 5 km between the existing protective works by means of three groynes, sloping under 1 : 8 from the lowwaterline to a depth of N.A.P. - 20 m; see figure no. 18. The results seem satisfactory.

The bastion to the east of this, called Kol van Borssele (a spurdike, i.e. a remainder of a former dike), has caused a very deep scourhole of more than N.A.P. - 60 m. In the laboratory it was found possible to get a sanding-up of the scour-hole up to a depth of N.A.P. - 40 m by reconstructing the bastion. To this end the originally high bastion was bevelled in the laboratory to 1 : 8 from N.A.P. - 20 m upwards.

CONCLUSIONS

It may be said that on sandy shore the design of a shore protection work is of the greatest importance for the erosion of the shore, for the generation of deeply scoured troughs and for the development of the gully-system. The influence of these constructions is by no means restricted to the immediate vicinity.

Groynes constructed under a slope of 1 : 8 will reclaim the shore, while the current-pattern is hardly disturbed.
This will also have a favourable influence on the stability of slopes in areas which are sensitive to slides.

Rip-rap defenceworks extending over a large area are expensive and should therefore be avoided. If nevertheless constructed they should have a regular surface.

Some existing shoreworks had rather be reconstructed, to which a milder slope is generally recommended. Further studies and especially detailed laboratory-tests are in most cases necessary to solve these problems

ACKNOWLEDGEMENT

The assistance of C. de Swit (Rijkswaterstaat Research Division Vlissingen) in providing general information and detailed data for use in this paper is gratefully acknowledged.

REFERENCES

1. Vergelijking van het stroombeeld en de uitschuring bij verschillende kribvormen, report H 610 Delft Hydraulic Laboratory.
2. A number of reports concerning the protection of the shore between Walcheren and Zuid-Beveland; Delft Hydraulic Laboratory (in Dutch).
3. Scour around obstructions, mrs Garde, Subramanya and Nambudripad; Irrigation and Power nr. 18. 1961, nr. 7.
4. Local scour in rivers, Tison; Journal of Geophys. Res. 66, 1961, nr. 12.

CHAPTER 44

ARTIFICIAL BEACH BUILDING ON THE CROISETTE WATERFRONT AT CANNES

LOUIS TOURMEN
Engineer, Sogréah
Grenoble

OBJECT OF THE REPORT

In view of the persistent increase in traffic density on the Croisette and the restrictions caused by a one-way system which had to be introduced, the Cannes municipality decided to ease the situation by widening the road to handle two-way traffic.

Numerous schemes for widening the road on the seaward side were proposed but none were satisfactory for the resulting gains were minimal, and the beach, which is at present very narrow and even non-existent at certain places (see fig. 2), would have suffered accordingly. Consulted on this problem, Sogréah decided to examine the possibility of rebuilding the beach to start with, to be followed by the construction of a new, wide promenade, the net effect being a wider beach than the existing one. Since the beach could not be expected to extend naturally, this involved the construction of a completely man-made beach. This artificial beach building is extremely attractive from a technical point of view, since it presents no snags but it was nevertheless considered advisable to verify that this method could be applied to the Croisette beach.

The Cannes Council Technical Department commissioned Sogréah to do a study, the aim of which was to discover whether the artificial beach would be sufficiently stable without extensive maintenance.

This report is a record of these studies and the practical achievements they made possible.

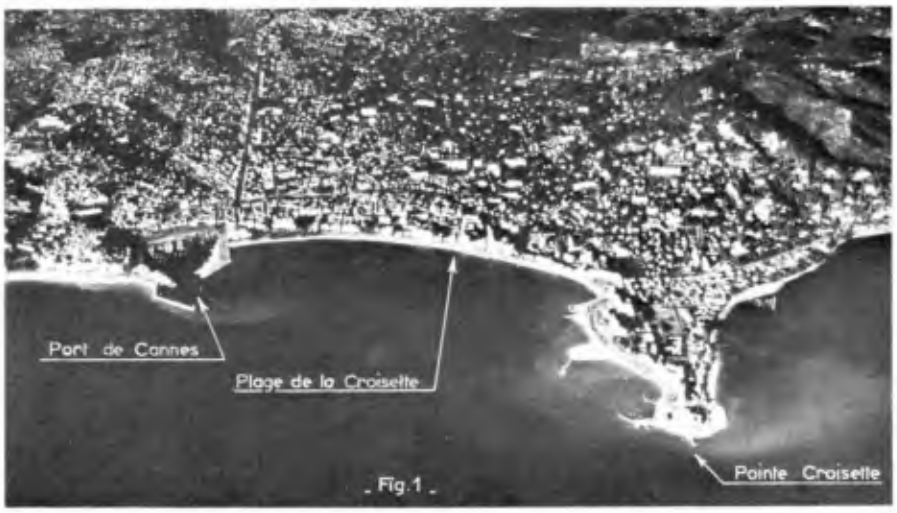

_ Fig.1 _

Fig.2

La playa antes del acandicianamienta,
durante un temporal

La plage avant aménagement,
par gros temps

The beach before improvement,
in heavy weather

ARTIFICIAL BEACH BUILDING ON THE CROISETTE WATERFRONT AT CANNES

STABILITY OF THE SHORE ALONG THE CANNES ROADSTEAD

The shore of the Cannes roadstead stretches between two protecting arms which make it a separate entity, cut off from the rest of the adjoining coastline. These two limits are as follows (see fig. 1) :

1) Eastwards

The Croisette point, presumably underlain by rock, of which the Iles de Lérins may be considered to be a prolongation seawards.

2) Westwards

The port, whose west jetty springs from the Saint-Pierre rock and whose east jetty protects the fill on which the Casino is built.

For more than a century this shore has been undergoing profound changes. A plan dating from 1823 shows that there was no man-made interference with its natural development at this time. It seems likely that quantities of sand were brought into the bay to the east of the Saint-Pierre rock, on the present site of the harbour. Sedimentation in varying degrees also took place owing to the influence of numerous small streams spread out along the coast, emptying a small catchment area down their gullies.

Subsequent and numerous development schemes have seriously cut down the natural sedimentation of the area.

In the first place the harbour protection works form an impenetrable barrier to material coming from the beaches of the Gulf of La Napoule. Moreover, the quantity of such material has been drastically reduced by the commercial exploitation of the river Siagne sand deposits, to the west of Cannes.

In the same way the sedimentation due to the gullies has been largely stopped by works carried out in their upper sections.

On can therefore state that natural sedimentation in the Cannes roadstead, and settling one the beach, is at the present moment minimal.

At the same time various kinds of artificial deposits were brought on to this beach, mainly in the form of waste products from constructional work. When the foundations were being dug for the big hotels the resulting rubble etc. was dumped directly on the beach. This form of tipping was banned in 1926 and since then no artificial deposits have been placed on the Croisette.

The above survey shows that the Croisette at the present moment receives no form of deposits, whether natural or artificial. This is a first piece of evidence as to its being in a state of stable equilibrium.

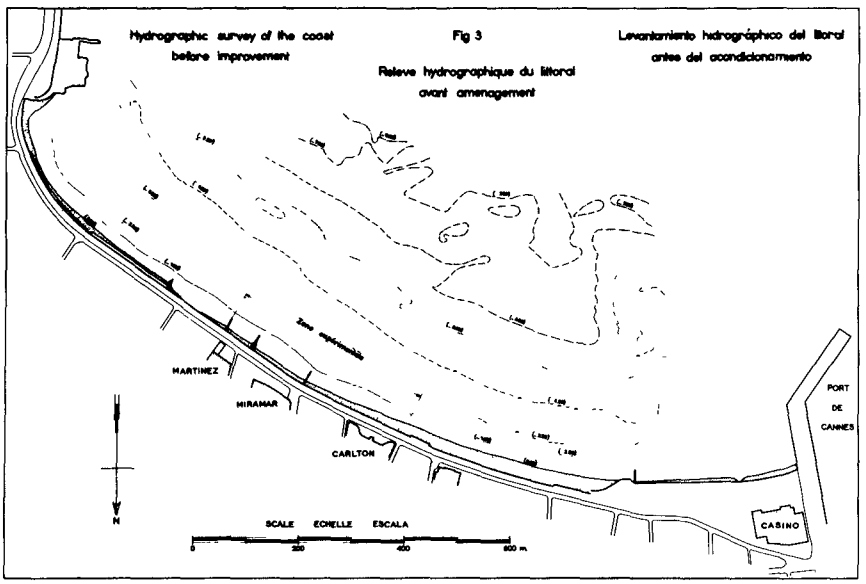
Hydrographic survey of the coast before improvement
Fig 3
Releve hydrographique du littoral avant amenagement
Levantamiento hidrográphico del litoral antes del acondicionamento
MARTINEZ
MIRAMAR
CARLTON
PORT DE CANNES
CASINO
N
SCALE ECHELLE ESCALA
0
200
400
600 m.

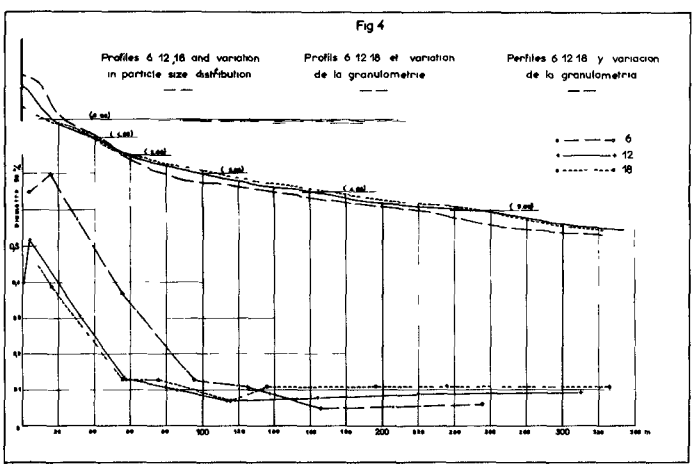
Fig 4
Profiles 6 12 18 and variation in particle size distribution
Profils 6 12 18 et variation de la granulometrie
Perfiles 6 12 18 y variacion de la granulometria
6
12
18

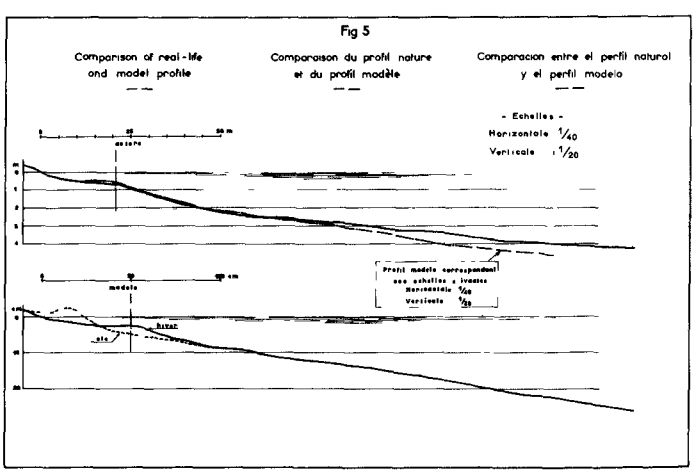
Fig 5
Comparison of real-life and model profile
Comparaison du profil nature et du profil modèle
Comparacion entre el perfil natural y el perfil modelo
- Echelles -
Horizontale 1/40
Verticale 1/20
nature
modèle
RIVAGE

Further evidence in support of this statement is provided by a comparison between the French Navy Hydrographical Service survey in 1897 and that carried out by Sogréah in 1960. This reveals that only very limited development has taken place, with no large-scale movement of materials. It is probable, moreover, that what little change has taken place has been due to the building of the Palais des Sports, at the eastern end of the roadstead, since it is in this area that development is most obvious.

Other factors also tend to confirm this stability. The sea-bed, for example, is covered by vegetation down to a depth of 4 m, which is always a certain pointer to stability. Finally, the water-tight jetties on the beach do not reveal any noteworthy deposits in any one direction, and this denotes the absence of a prevailing movement of sand. All these factors tend to demonstrate that the beach is in fact in a state of stable equilibrium, generally speaking, at least over a fifty-year period. This conclusion is the prerequisite for successful beach building, as artificial accretion is able to last only on a beach in a state of dynamic equilibrium.

CHARACTERISTICS OF THE CROISETTE BEACH

Examination reveals that the profiles chosen along the whole length of the beach resemble each other fairly closely. This fact is seen at once by looking at a sea chart of the roadstead, the contours of which are parallel and show a regular concave shape. The typical profile at the basis of our study is extremely representative. It is n° 12, fig. 3 and was taken from midway along the shore. It was used for all the general studies. This profile, is to be found among others, in fig. 4 drawn with a 5 to 1 distortion.

The profile from the beach down to the 2 m mark has a gradient of about 5 %. Afterwards the slope flattens out to between 1 and 2 %. This second section goes as far as the vegetation. Simultaneously with the plotting of profiles, sediment samples were taken from the sea-bed at the same points. Particle-size analysis showed a certain correlation between levels and gradients on the one hand, and the 50 % sample diameter on the other.

Fig. 4 gives this correlation for three profiles taken at random along the beach. At this point it is worth noting that for a 5 % gradient a 50 % particle diameter represents approx. 0.2 to 0.3 mm whereas for a 1 to 2 % gradient the figure is from 0.05 to 0.1 mm. These granulometric studies were of great help in determining choice of material for beach building.

Qualitatively speaking, the range of material found on the Croisette beach is very wide and of fairly recent date, which is after all normal since the original beach was composed of a wide range of materials tipped in recent times.

Also worth noting is a characteristic change in profile of the upper section of the beach during the December to July period, caused by seasonal variation in the standard profile.

PRELIMINARY STUDIES OF POSSIBLE WAYS OF DEVELOPING THE BEACH

The problem was to build up the profile, basically similar to those in fig. 4, with sand, so as to create a new, stable beach, thirty metres or so in front of the previous one. The Cannes Municipal Council Technical Department accepted an increase of 20 to 30 metres as sufficient.

NATURE OF SAND TO BE USED

Right from the start an over-riding consideration was the particle-size of the sand available for beach building.

The particle-size of the added sand had first of all to be compared with that of the existing beach, to determine whether the work would be successful or not and to reject any unsuitable material.

Generally speaking, on a given beach, the added sand to be really stable, should be much coarser than that already in position. Proof of this is to found on the Croisette beach, which is really an artificial beach composed of widely-varying materials but where nevertheless the largest particles have remained in position at the head of the beach (see fig. 4).

If beach building is carried on by depositing sand of a finer grade on top of the existing beach there is a strong chance that it will progres sively slip downhill into the sea. It is thus impossible (without taking special precautions) to transform a pebble beach into a stable sandy beach merely by dumping material on the head of the beach. One may attempt to hold this sand in place by artificial means, but this always increases the cost of the undertaking very considerably.

The above remarks are practically always valid but especially so in areas where tides are very weak and waves are mostly the result of local winds, i.e. as at Cannes. The erosion produced by such waves is far greater than that of swell coming in from far distances ; on account of the absence of tides, the bed materials are more evenly sorted at least in relatively shallow waters.

Simultaneously with our studies, the Cannes Council Technical Department were surveying for possible sources of good quality sand, preferably in the region. Certain deposits were in fact found on the sea-bed near the Croisette point and the Lérins islands but both quantity and quality were deficient. Analysis revealed up to 40 % of crushed shells in the samples, which is much to high, owing to the low density of crushed shells.

An attempt was therefore made to find other deposits and at the time of these preliminary studies it seemed that medium quality sand of rather fine grade would have to be accepted.

The study continued based on these assumptions ; the added deposits were assumed to have the same granulometric characteristics as the existing sand on the beach. The a priori solution therefore seemed to favour an underground retaining barrier which, although perhaps not essential, would nevertheless improve the stability of the added material.

The problem was reduced to the study of the stability of the proposed beach extension based on a profile using the same particle-size as the existing ones. The simplification of the problem to these terms made it much more accessible to experimental study.

After the conclusion of the preliminary studies, it should be noted that the Cannes Council Technical Department managed to find a deposit of excellent sand, with the required granulometric qualities. This discovery had a most beneficial effect on subsequent operations, and will be commented on subsequently.

EXPERIMENTAL SCALE-MODEL STUDIES

A few tests were carried out in a glass-walled flume in order to find out what would happen during beach building.

This flume was able to produce waves either by the classical wave-paddle method or by a stream of air blown across the surface, the speed of which could be varied.

In the above flume the beach was reconstructed by building up the head of the foreshore. The wave amplitude was set at an average value corresponding to an air-speed of 4 metres per sec. The material used was ground pumice of density 1.4.

We must make it quite clear that this model was never intended to be an exact reproduction of the actual phenomenon. It was merely an analogy which helped to clarify the problems but could not provide solutions.

The beach reconstructed in the flume gradually settled down and when this process was practically completed, the resulting profile was compared with the typical profile of the Cannes beach. This comparison was satisfactory, provided that the horizontal scale and scale distortion were properly selected.

Fig. 5 shows the experimental profile superposed on the typical profile drawn to a horizontal scale of 1:40 and a vertical scale of 1:20, i.e. a distorsion of 2. Various tests were carried out on this profile to study the artificial building-up of the beach. The tests fall into three groups :-

1) Study of the behaviour of material identical to the basic profile material, dumped on the beach and subject to wave action.

2) With the same lay-out, the effect of a toe-mound placed about a hundred metres from the beach was studied.

3) In the final group a study was made of the influence of dumping methods on the final equilibrium of the beach.

Without going into detail we shall give the results which we were able to obtain. The first two groups of tests in the wave flume revealed that artificial beach building was possible but would involve constant maintenance, since when not protected by a toe-mound the beach offers low resistance to wave action in storms and the extension obtained is reduced every winter owing to loss of material swept out to sea during heavy weather. These losses would have to be replaced from time to time. These tests are only valid for material identical to that constituting the original beach.

On the other hand, the extension can be protected successfully even during very heavy seas by the construction of a water-tight sand toe-mound about a hundred metres from the shore.

The third group of tests demonstrated, at least experimentally, that dumping methods had no effect on the final result. We have nevertheless recommended that the actual building-up of the beach be done as progressively as possible.

CONCLUSIONS FROM THE PRELIMINARY STUDIES

The conclusions of the above preliminary studies are that beach building with materials of the same particle-size as on the original beach was not an economic proposition without the addition of a toe-mound to check loss of material in the sea, unless the necessity of periodic replacement of material were accepted.

With a toe-mound an estimated 25 m of beach would be gained at a cost of 200 cu.m. per metre run of shore.

EXPERIMENTAL BEACH BUILDING ON SITE

The relatively favourable conclusions of the preliminary studies and the discovery of deposits of sand of coarser grade than that previously available prompted the Technical Department of Cannes Council to consent to the building of an experimental section on the beach of the Croisette.

NATURE OF SAND USED

The sand finally chosen came from Fréjus, 40 km from Cannes. Its particle-size and general appearance were eminently suitable.

Transport from the source was carried out by heavy lorries.

Fig. 6 gives the average granulometric curve of the sand chosen and also the granulometric curves corresponding to samples taken at various depths on profile 12, before starting the development work. It is thus obvious that the added sand was much coarser than the original at all points along the profile.

The quality of the sand available for the tests made it possible to decrease the amount used and the final figure was about 100 cu.m per metre run.

EXPERIMENTAL SITE

Fig. 3 gives the exact site of the experimental area, which extended over a distance of 330 m and included profile 12, described below.

The limits of the area were marked by dikes to prevent lateral spreading of the sand. An experimental toe-mound of sand-filled nylon sacks was placed along a distance of about 80 m situated in the centre of the area, at about 100 m from the low water mark. Given the grade of sand used it is questionable whether such a mound was really necessary. The experimental nature of the project seemed to recommend one but the subsequent course of events showed that it was superfluous.

The test revealed some loss of sand at the edges of the area, except in the case of the eastern dike, which was a masonry construction.

This loss of sand modifies the information provided by the experiments only by affecting the results obtained in a conservative sense.

SAND DUMPING

Total mount dumped : 29,550 cu.m, at a daily rate of 850 cu.m.

It is worth noting that the above figures for daily and total amounts were measured in lorry-loads. We were interested in finding out, by means of a comparison with profiles constructed before and after dumping, the actual volume of sand mesured in situ. This comparison would seem to reveal a certain ratio assumed by us as constant, between the amount given by measuring lorry-loads and that given by comparing bed surveys.

This ratio is in the region of 2/3.

From now on volumes measured by the lorry-load method will be marked by an asterisk. The average amount placed along the 330 m of the experimental area was :

$$\frac{29{,}550^{*} \text{ cu m}}{330 \text{ m}} \neq 90^{*} \text{ cu m per metre run}$$

Fig.6

Variation de la largeur utile de la plage — Variation of the useful width of the beach — Variación del ancho útil de la playa

Fig.6

Granulométrie de la plage — Granulometría de la playa

Sand granulometer used in construction of the experimental beach

Fig.6

Granulométrie du sable utilisé pour l'ensablement expérimental

Granulometría de la arena utilizada para el enarenado experimental

Placing the sand — Mise en place du sable — Distribución de la arena

ARTIFICIAL BEACH BUILDING ON THE CROISETTE WATERFRONT AT CANNES

Sand was tipped directly at the head of the beach at specially-prepared points along the Promenade de la Croisette, and afterwards levelled by bulldozer, so as to ensure proper spreading out.

It was laid in two successive operations, each layer measuring 50 cu.m per metre run. For the second operation the extension was taken 20 m beyond the former shore-line. Simultaneously with the dumping operations the eastern and western boundaries and the experimental toe-mound were also placed in position.

No difficulties were experienced during dumping.

Fig. 7 gives an oblique aerial view of the area during dumping operations.

COASTAL DEVELOPMENT DURING AND AFTER DUMPING

Various measurements and surveys were carried out at intervals during and after the beach building operations.

In particular :

Wave observations ;
Level variation observations ;
Surveys of the useful width of the beach ;
Survey of beach profiles.

Fig. 8 gives the results obtained during two periods :

(1) 25 Nov. to 29 Dec. 1960, when the average rate of dumping was 850 cu m per day.

(2) 2 Jan. to July 1961.

Also shown on the figures are :

Wave characteristics, e.g. amplitude, periodicity ;
Levels observed ; and
Variations in the useful width of the beach for six profiles.

This figure reveals the considerable increase in the width of the beach by means of a comparison between the starting (25.11.1960) and finishing (11.7.1961) ordinates.

It must be noted, however, that the increases are not completely valid and that the following two points must be borne in mind in interpreting the results :

a) A seasonal change in slope takes place between November 1960 and July, 1961. It is therefore difficult to compare increases for this period.

b) Since the very beginning of the dumping operations the western boundary of the area was leaking sand. It was in fact removed in the spring of

Fig.9

Modification of profile 12 after addition of sand

Modification du profil 12 après apport de sable

Modificación del perfil 12 después del aporte de arena

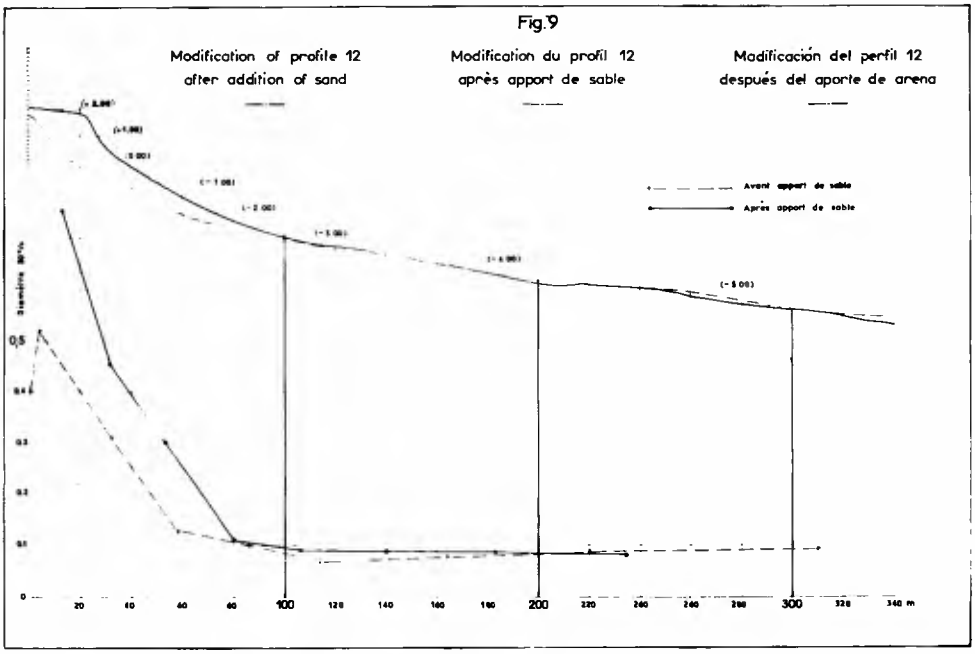

Fig.10

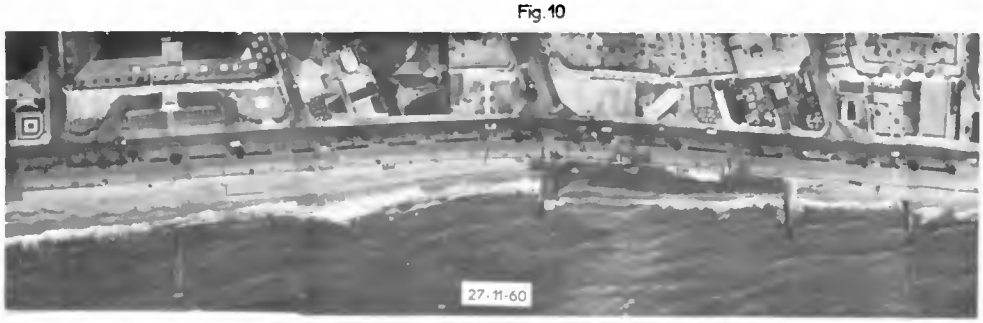

Aerial views of the experimental zone

Vues aériennes de la zone expérimentale

Vistas aéreas de la zona experimental

1961.

The movement of the sand was not simply lateral but also lengthways, a tendency which increased in the areas nearest the western boundary.

The eastern boundary being much more solid, movement of sand in this direction was very slight.

It is therefore safe to state that, owing to the leakage at the western limit, the June 1961 survey was no longer valid for the beach which had been built up by 88* cu.m per metre run since this figure had been reduced by lateral losses.

These reservations having been made, the increase in effective width of the beach between November 1960 and July, 1961 may be given in the following table :

Profile	Increase in effective width between November, 1960 and July, 1961.
6	11 metres
8	12 "
10	15 "
12	18 "
14	18 "
at the dike near to 16	19 "

Profiles were drawn on four occasions after completion of the experimental beach building project.

It is instructive to compare these with the profiles drawn before the start of the project. Owing to loss of sand towards the west, no useful purpose is served by study of the variations in depth of sand for a given profile over any considerable length of time, since the amount per metre run was not constant, even showing a decrease on the average.

In our opinion the two most interesting surveys were those of November 1960 and March, 1961 since the sideways spreading of the sand had not reached proportions large enough to produce inaccurate results. Furthermore this period includes the few days of heavy weather recorded during the winter of 1960 - 1961. Fig. 9 gives profile 12 in Nov. 1960 and March 1961. This figure also reveals that the extension was in the region of some 20 m and that the sand was not spreading seaward beyond a depth

of -3m. The figure also gives the graphs of the median diameter of samples from profile 12 before and after beach building. The points at which both profiles meet and the intersections of the grain size curves agree very well.

This diagram also demonstrates the irrelevance of the toe-mound.

The development of the coast was also recorded by vertical aerial photography.

Fig. 10 gives two such aerial views.

CONCLUSIONS FROM THE EXPERIMENTAL BEACH BUILDING PROJECT

They are essentially as follows :

1) The addition of material in the experimental area (100 cu m per metre run) led to an extension of approx. 20 m.

2) The particle-size of the sand used was perfectly suitable for artificial beach building in the case of Cannes. Particle-size was seen to be a basic principle largely determining the success or failure of the project.

3) The toe-mound described above did not serve any useful purpose, since the sand did not reach it.

Therefore it may be said that such a mound is not necessary for the complete and final extension of the Croisette beach, provided that the materials used have the correct grading.

Summing up, it may be said that the experiments carried out on the site helped to confirm the results of the preliminary studies.

From this point on the projected total building up of the beach could be faced with confidence, since the basic factors of a successful scheme had been established.

FINAL EXTENSION OF THE CROISETTE BEACH

NATURE OF SAND USED

The grading of the sand used was similar to those employed in the experimental section.

ARTIFICIAL BEACH BUILDING ON THE CROISETTE WATERFRONT AT CANNES

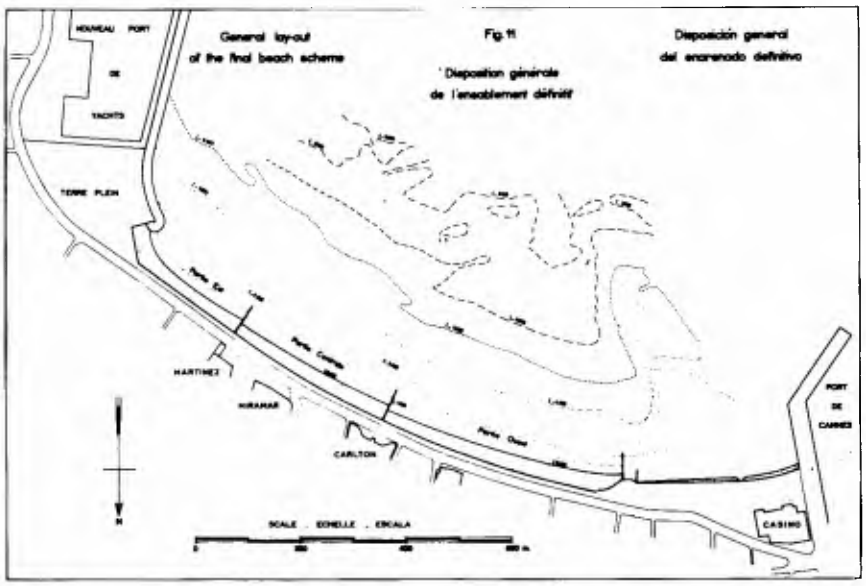

General lay-out of the final beach scheme

Fig. 11

Disposition générale de l'enrochement définitif

Disposición general del encarenado definitivo

Partitioning jetty (West end)

Epi de cloisonnement (limite Ouest)

Espigón limitando la zona acondicionada (límite oeste)

The beach after improvement

La plage après aménagement

La playa después del acondicionamiento

GENERAL LAY-OUT OF THE ARTIFICIAL BEACH

Any plan or aerial photograph of the Croisette beach before development immediately reveals that the shore-line is not parallel to the Promenade.

This is explained by the fact that the Promenade was built to follow the original shore-line existing before the construction of the Albert Edouard Jetty and the Casino foundation fill. Their construction modified the development of the beach to give it the form it presented before the artificial extension works began.

It seems logical to presume that any such extension work undertaken without special precautions will lead to uniformity of outline, since all projections due to beach building will be smoothed away by wave action. Such an extension would be inflexible and unsuited to requirements at particular sections.

If it were desired to extend the narrowest part of the beach by, say, 30 m, this would involve a generalised extension of the whole beach, whereas in the western area there is certainly no need for any such extension. The uneconomic nature of this method led us to envisage a partitioning system. If, in fact, the beach is divided into several sections, the extension of each one can be pursued independently of the others and the shore-line is stepped. Obviously the number of these partitions should be kept to a minimum, since the cost of the work should not exceed that of the sand economised. Aesthetic considerations also prohibit an excess of these structures.

An adequate solution seemed to be three partitions and this was adopted, with the agreement of the Cannes Council Technical Department. The partitions take the form of jetties built of a double row of metal sheeting-piles (see fig. 11).

Rainwater has been led away to drain off inside the jetty.

Fig. 12 gives a general plan view of the final lay-out.

TOTAL VOLUME OF SAND TO BE USED

A break-down of the total volume (which it is estimated will be needed is as follows :

ARTIFICIAL BEACH BUILDING ON THE CROISETTE WATERFRONT AT CANNES

Section	Length in metres	Amount measured "in situ" cu m	Amount measured in lorry loads cu m
West	420	23,400	35,000*
Centre	320	24,600	37,000*
East	300	22,000	33,000*
TOTAL	1,040	70,000	105,000*

PRESENT STATE OF ARTIFICIAL BEACH

At the moment 60,000 cu m of sand have been laid on the Croisette beach. The rest, some 105,000 cu m will have been laid by the end of the year. The partitions are wholly or partly finished.

The widening of the Promenade has been partly carried out in the form of a reinforced concrete structure overhanging the beach, the form of which shelters the bathing huts and places them out of sight from the Croisette. Sogréah was also responsible for the design of this structure, built on piers and therefore independent of all changes taking place in the beach.

The photograph in Fig. 13 gives some idea of this achievement which has allowed Cannes to resolve two frequently incompatible problems:

The widening of a coast road

The widening of the beach separating this road from the sea.

oOo

CHAPTER 45

EL TRANSPORTE DE LOS SEDIMENTOS MARINOS DE LITORAL

Luis Blasquez L.
Instituto de Geologia, U. N. A. M.

RESUMEN

Se considera el oleaje como producido por la transmisión sin desplazamiento, de vibraciones moleculares que participan tanto del movimiento ondulatorio longitudinal como del transversal, y tienen las características principales explicables con la teoría trocoidal de Gerstner modificada y movimiento orbital cercano al concebido por Stokes y desarrollado por Levi-Civita. El autor propone una nueva teoría que llama de la multiondulación coincidente.

El poder de transporte en cualquier sitio del oceano, no contradice la teoría trocoidal ni la multiondulatoria, proque es debido a esfuerzos locales del viento que pueden impulsar dentro y fuera del fech en determinado momento, las crestas de las olas y producir efectos de turbulencia y corrientes hidrodinámicas, distintas a las vibraciones, que cambian también localmente sus propiedades.

El transporte anual de sedimentos marinos, por su complejidad, no puede aun ser calculado directamente a partir de las características de las olas. Estadísticamente, se valora basándose en numerosas observaciones y mediciones directas. Se propone un estudio previo de las áreas terrestres y marinas que pueden afectar las obras portuarias, por medio de fotogeología, mineralogía, petrografía, estratigrafía, tectónica y morfología de costas, litorales y zonas marinas de la playa y anteplaya y en seguida el levantamiento de cartas batimétricas antes y después de las tempestades, en las calmas y en alta y baja marea. La batimetría será acompañada con el muestreo sistemático inicial de los sedimentos y posteriormente, empleando postes testigos y numerosos trazadores del transporte, consistentes en minerales y arenas de rocas peculiares, fácilmente identificables y adquiribles, colocados a partir del primer muestreo, en los accidentes positivos, barras y prominencias de los fondos y en los negativos, hondonadas y depresiones.

Valorizados los cambios locales de volumen y la topografía submarina durante el tiempo mas largo posible, y con las indicaciones de los trazadores, podrá conocerse la dirección general y cuantía media del acarreo de sedimentos, a lo largo de las playas y anteplayas, para determinar de antemano cual será el comportamiento de las obras de defensa que se pretenda construir, según los datos que aporten estos estudios.